University of Agronomic Sciences
and Veterinary Medicine of Bucharest
Faculty of Land Reclamation
and Environmental Engineering

SCIENTIFIC PAPERS

Series E

LAND RECLAMATION, EARTH OBSERVATION & SURVEYING, ENVIRONMENTAL ENGINEERING

Volume XII

2023
BUCHAREST

SCIENTIFIC PAPERS

Series E

LAND RECLAMATION, EARTH OBSERVATION &
SURVEYING, ENVIRONMENTAL ENGINEERING

Volume XII

University of Agronomic Sciences
and Veterinary Medicine of Bucharest
Faculty of Land Reclamation
and Environmental Engineering

SCIENTIFIC PAPERS

Series E

LAND RECLAMATION, EARTH OBSERVATION & SURVEYING, ENVIRONMENTAL ENGINEERING

Volume XII

2023
BucharesT

PUBLISHERS:
University of Agronomic Sciences and Veterinary Medicine of Bucharest, Romania - Faculty of Land Reclamation and Environmetal Engineering
Address: 5 9 Marasti Blvd., District l, Zip code 011464 Bucharest, Romania
Phone: + 40 213 1830 75, E-mail: conference@fifim.ro, Webpage: www.fifim.ro

CERES Publishing House
Address: 29 Oastei Street, District 1, Bucharest, Romania
Phone: + 40 21 317 90 23, E-mail: edituraceres@yahoo.com, Webpage: www.editura-ceres.ro

To be cited: Scientific Papers. Series E. LAND RECLAMATION, EARTH OBSERVATION & SURVEYING, ENVIRONMENTAL ENGINEERING, Vol. XII, 2023

Print ISSN 2285-6064, CD-ROM ISSN 2285-6072, Online ISSN 2393-5138, ISSN-L 2285-6064

International Database Indexing:
Web of Science Core Collection (Emerging Sources Citation Index)
Index Copernicus; Ulrich's Periodical Directory (ProQuest); PNB (Polish Scholarly Bibliography); Scientific Indexing Service; Cite Factor (Academic Scientific Journals) Scipio; OCLC; Research Bible

SCIENTIFIC & REVIEW COMMITTEE

SCIENTIFIC CHAIRMAN
Prof. univ. dr. Sorin Mihai CÎMPEANU

MEMBERS*

**alphabetically ordered by family name*

CONTENTS

ENVIRONMENTAL SCIENCE AND ENGINEERING

SUSTAINABLE DEVELOPMENT OF RURAL AREA

DISASTER MANAGEMENT

WATER RESOURCES MANAGEMENT

POLLUTION CONTROL, LAND PLANING

TOPOGRAPHY AND CADASTRE

EARTH OBSERVATION AND GEOGRAPHIC INFORMATION SYSTEMS

MISCELLANEOUS

Scientific Papers. Series E. Land Reclamation, Earth Observation & Surveying, Environmental Engineering. Vol. XII, 2023
Print ISSN 2285-6064, CD-ROM ISSN 2285-6072, Online ISSN 2393-5138, ISSN-L 2285-6064

MONITORING OF "DEALUL MARIA" MARBLE PERIMETER, RUSCHIȚA, CARAȘ-SEVERIN COUNTY

Ovidiu Marcel SÎRBU[1], Clara-Beatrice VÎLCEANU[2], Anca Maria MOSCOVICI[2], Alexandru-Iulian ILIESCU[3], Remus CHENDEȘ[2], Otilia-Maria ANDERCA[2]

[1]Politehnica University Timisoara, Faculty of Management in Production and Transportation, 14 Remus Street, Timisoara, Romania
[2]Politehnica University Timisoara, Civil Engineering Faculty, 2 Traian Lalescu Street, Timisoara, Romania
[3]University of Agronomic Sciences and Veterinary Medicine of Bucharest, Faculty of Land Reclamation and Environmental Engineering, 59 Marasti Blvd, District 1, Bucharest, Romania

Corresponding author email: beatrice.vilceanu@upt.ro

Abstract

Soil excavation represents a fundamental step in the construction and development of infrastructure. Despite the widespread application of best practices and regulations, accidents in the construction industry are comparatively higher than those in other industries. Deep excavations have the potential to cause adverse effects on the stability of the soil and nearby structures. Thus, in addition to ensuring safety, it is necessary to assess and monitor the environmental impact of deep excavations during construction processes. An eloquent example is represented by monitoring the marble resources exploitation from the quarry located in the "Dealul Maria" perimeter, in the town of Ruschița, through topographical surveys realized with a view to determine volumes, carried out quarterly, for a period of 5 years. The achieved 3D modeling highlights the differences between the initial shape of the natural land before the start of exploitation, the resulting shape of the land at different stages of the exploitation and the final shape as well as supports a proposal to green the exploited area by restoring the exploited land to a form as close as possible to the original one.

***Key words**: 3D modeling, deep excavations, environmental impact, BIM, topographic survey.*

INTRODUCTION

Building Information Modeling (BIM) involves a working methodology that uses digital models of a building to record and consistent manage the spatial information and data relevant to its life cycle and the exchange between the specialists involved (Pescari et al., 2022).
BIM aims to provide improved visualization of project variants, a significant reduction in planning errors, and easier construction based on collaboration and computer-aided simulation. The BIM concept (Figure 1) emerged as a need to improve the way buildings are designed, constructed and operated (Wu et al., 2015). The main problems that this concept solves are: reducing design time, eliminating the need for redesign, improving coordination between disciplines, the possibility of exploration and simulation within the model in order to detect design problems at a low cost, increasing the quality and level of trust for deliverables (they are uniquely connected to the 3D model, and the risk of inconsistencies is practically null) (https://bimmda.com/en/what-is-bim).

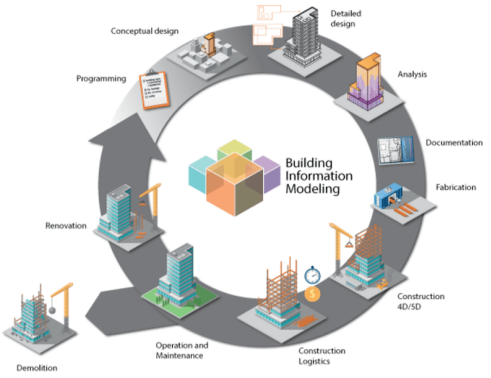

Figure 1. BIM definition (https://bimmda.com/en/what-is-bim)

The main advantage of BIM is to increase the level of coordination and collaboration between the members of all the teams involved in the project (architects, specialized engineers, manufacturers, executors, beneficiaries) throughout its duration (concept, technical design, execution details, manufacturing, construction, maintenance) (Badea, A.C. & Badea, G., 2022).

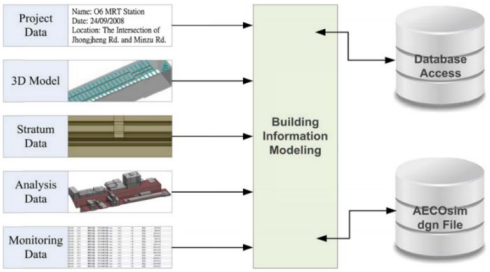

Figure 2. Data sources to be integrated in BIM (Wu et al., 2015)

For the industry to converge to the use of three-dimensional, object-oriented models such as BIM, three essential elements need to work together: computational power, a platform for a common database, and a network with sufficient bandwidth (Figure 2). The system shown in Figure 2 is based on commercial hardware and software comprising the Bentley AECOsim Building Designer, which supports visualization of a 3D model with some capabilities for 3D object manipulation and information query with Application Programming Interfaces (API) for functionality extensions (Wu et al., 2015). BIM can be interpreted through the aspects that define it.

A first aspect concerns conceptual design as it is commonly perceived. The conceptual design is the most creative part of the design work and brings into focus all aspects of the project in terms of function, cost, construction methods and materials, environmental impact, cultural and aesthetic considerations and more. During it, the entire knowledge and experience of the members of the design team is activated and put to use (Oprea et al., 2014).

A second aspect concerns the use of BIM for the design and analysis of building systems. Analysis means, in this case, the operations of simulating and measuring the fluctuations of the physical parameters that are expected from the real construction (Kim et al., 2012).

The third aspect is the classical one, regarding the use of BIM for the development of construction information at the level of execution details (Marcuta et al., 2020).

BIM provides detailed 3D visualization and the ability to organize large volumes of building-related data for management. Different scientist (Hsieh & Lu, 2012) demonstrated that a visualization system allows users to interpret monitoring data effectively and intuitively, reduces misinterpretation, improves communication efficiency, and facilitates effective decisions that are supported by collected monitoring data. On the other hand, other researchers (Kim et al., 2012) focused on monitoring and visualizing aggregated and real-time states of various energy uses represented by location-based sensor data collected within the city, in particular referring to building.

Design representations are no longer 2D drawings. Instead, designers use 3D BIM models that are assembled in the same manner a building is constructed. BIM can be used in construction companies to better reuse accumulated management information (Oprea et al., 2014) (Figure 3).

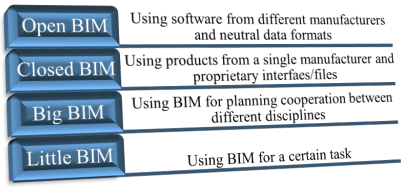

Figure 3. Different types of BIM

Employing spatial information within the BIM model (Figure 4) enables everyone on the project team to make better and more informed decisions throughout the entire lifecycle of construction and infrastructure projects.

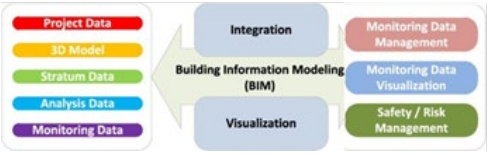

Figure 4. Logical diagram of a BIM-based monitoring system development project (Wu et al., 2015)

In terms of understanding the current state of safety planning in built-up areas, an in-depth understanding of previous research studies is summarized as safety planning practices related to excavation pits in the construction industry. Inadequacies in contemporary safety planning have been addressed with advanced BIM-based design for safety concepts. Research works on rule-based safety planning and BIM are thoroughly reviewed and the need for the proposed safety rule-based automated excavation modeling approach is established (Buza et al., 2001).

An eloquent example is represented by automatic modeling of safety excavation, regulatory compliance and safety best practices, using visual programming and BIM technologies for the safety management process. The more specific objective of the study was to develop an automated BIM-based safety planning tool specific to construction excavation that can identify potential hazards related to falls, pits and safety exits together with a 3D model visualized with a built-in prevention solution for hazard recognition. As a limitation it is mentioned that this solution does not take into account the whole hazard related to geotechnical activities. Therefore, the scope of the study is limited to the major types of potential hazards, including but not limited to fall and exit hazards (Khan et al., 2019).

Thus, academic researchers as well as industry professionals are currently paying vital attention to ensuring construction safety even from the project stage. To this end, various algorithms to increase safety in the pre-construction phase have been developed. These algorithms focus on analysing potential risks, checking the BIM model for fall risks and limiting access to areas where masonry wall constructions are being carried out. Using programming languages, such algorithms automatically generate geometric conditions in BIM and visualize potential risks and adoption of safety measures, along with quantity calculation and optimized locations.

This paper presents the monitoring process of the marble resources exploitation from the quarry located in the "Dealul Maria" perimeter, Caraş-Severin County, Romania. This objective represents an eloquent example of assessing and monitoring the environmental impact of excavations which have the potential to cause adverse effects on the stability of the soil and nearby structures and could be successfully further integrated into BIM. By implementing such an approach, it brings added value to the entire process of safety planning in construction (Sălăgean et al., 2017).

MATERIALS AND METHODS

The purpose of environmental impact assessment is to highlight both the negative, as well as the positive effects of a planned activity or an ongoing one (in the case of development or modernization projects of existing capacities) on the environment.

From an administrative point of view, "Dealul Maria" exploitation perimeter is located outside the built-up areas of Ruşchiţa locality, Rusca Montană commune, Caraş-Severin County, 2 km from Ruşchiţa locality and 25 km northeast of Oţelul Roşu town (Figure 5). Access to the exploitation perimeter is realized from Caransebeş - Haţeg national road, on the partially modernized county road Voislova - Rusca Montană - Ruschiţa, then on an industrial road to the exploitation perimeter "Dealul Maria", at an elevation of +800 m above Black Sea 1975 level.

Figure 5. Location of the “Dealul Maria” exploitation perimeter (© Google Earth)

The exploitation activity in the "Dealul Maria" quarry was expected to be in progress over a period of 11 years (2010-2021). Thus, a concession license for exploitation has been

issued by the National Agency for Mineral Resources, as well as additional documents 2 and 3 to this license. The key deciding element in what concerns the granting of the exploitation licence is represented by the accomplishment of the planned production during the validity period of the license through the systematization of the quarry in the perspective of the continuation of the exploitation beyond the year 2021.

Marble exploitation from "Dealul Maria" deposit will be carried out on all 12 levels, starting with level 1 and up to the last level +780 m elevation, level 12, partially.

The total expected production for the period of validity of the exploitation license will be 3,224,215 tons, respectively 39,401 tons of industrial extraction in the first year of exploitation, reaching 279,696 tons per year of industrial extraction at the end of the license, in the last year of exploitation (S.C. Omya Calcita S.R.L. Bucureşti, Report, 2010).

The following types of waste result from the activities that have been carried out within the objective:

- plant (organic) waste, sawdust, plant residues etc. derived from forest vegetation clearing works;
- topsoil and technological waste resulting from the deposit discovery works and exploitation losses;
- household waste.

Vegetable waste from vegetation clearing works consisting of sawdust, wood scraps etc. will be completely collected, ground and utilized.

The topsoil will be stored separately from the sterile rocks, in a temporary topsoil dump, so that at the end of the exploitation license period, respectively at the end of the exploitation activity, it will be used for environmental restoration works (Herbei et al., 2021). The dump will be located in the northern area of the exploitation perimeter, between elevations +890 m and +910 m. The amount of topsoil from "Dealul Maria" perimeter that is to be stored in the landfill until the end of the validity of the exploitation license is 20,000 m^3 (1,176 m^3/year).

The hydrographic network of the area is represented by "Valea Morii" stream and "Raci" stream, the left tributary of the "Padeşului" valley. The rugged relief in the area with steep slopes and narrow valleys, with relatively poor vegetation, contributes to the oscillating flow of the "Padeş" River. The closest watercourse to the site is "Valea Morii", about 400 m away.

From a hydrogeological point of view, the geological research carried out did not indicate the existence of permanent or temporary aquifer layers, holes or underground voids with possible accumulations of water.

Forest soils are spread in the areas where forest vegetation develops, the dominant type being the Preluvosol, as a subtype-the typical Preluvosol that appears on the highest, well-forested ridges. Because of these soils' weaker physical and biochemical properties, compared to chernozems and faeozems, they are much more exposed especially to physical and chemical degradation. Located in regions with higher slopes, when the forest is cleared, these lands are exposed to intense erosion. On large areas, on steep slopes, due to the marked degradation of the land, regosols-class protosols (unevolved soils) developed on a parent material originating from unconsolidated rocks and maintained close to the surface by slow and long geological erosion, but especially the erodisols, are also found caused by accelerated erosion.

From a geotechnical point of view, the land shows no indications of geodynamic phenomena existence that could affect the stability of the site.

The final slopes of the quarry will have an established slope so that, under normal conditions, landslides will not occur.

The quarry is located far from towns, in an area without traffic or permanent activity, without industrial objectives or networks (electricity, gas, water, roads) to protect.

Under these conditions, for 5 years monitoring of the definitive slopes of the quarry, the following measures have been taken:

- placement of levelling benchmarks at the base of the definitive slopes;
- semi-annual monitoring by precision levelling of slope stability combined with GNSS planimetric measurements;
- recording the measurement results in a special register.

RESULTS AND DISCUSSIONS

In this section, the geodesy-specific methodology and technology used for monitoring the marble resources exploitation from the quarry located in the "Dealul Maria" perimeter in the town of Ruschița, are presented. The topographic surveys have been realized quarterly, over a period of 5 years, with a view of determining the volumes and creating the 3D models of the terrain. The 3D modeling will highlight the differences between the initial shape of the natural land before the start of exploitation, the resulting shape of the land at different stages of the exploitation, the final shape and a proposed model to green the exploited area by restoring the land to a form as close as possible to the original one.

The first measurements session was carried out in October 2016 on the new area proposed for exploitation. The measurements were performed after clearing of the mentioned area initially covered by forest vegetation and represent the basis for realizing the layout plan and the 3D model of the terrain, which will be considered as the reference for future calculations. The equipment used for the topographic surveys consists in a GNSS receiver, STONEX S10A, using the RTK (Real Time Kinematics) method; the services of the ROMPOS (Romanian Position Determination System) RTK system were used to determine the detail points.

Topographic surveys have been realized in adequate temperature and environmental conditions. Processing of the measurements with a view of obtaining the 3D model and volume calculation of the exploited marble implied using TopoLT and AutoCAD software.

The reference measurement included representation of forced slope change lines required for 3D terrain modelling (Figure 6) using the TopoLT software, consisting of existing topographical details on the quarry site such as: slopes, determined by slope shoulder and slope foot, roadsides, ditches etc.

In addition to the studied area for the marble exploitation, the area in the vicinity where dust pollution from the cutting and sectioning process could occur was also identified during the first session of measurements.

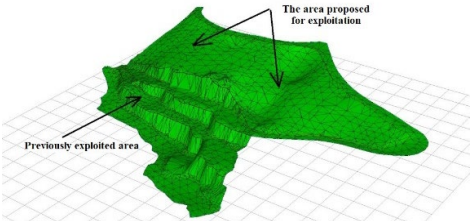

Figure 6. The 3D model of the terrain resulting from processing of the first measurement session carried out on 30.10.2016

The preparation of the levelling plan (Figure 7) necessary for the specialized works related to the exploitation is based on generating the contour lines with TopoLT software.

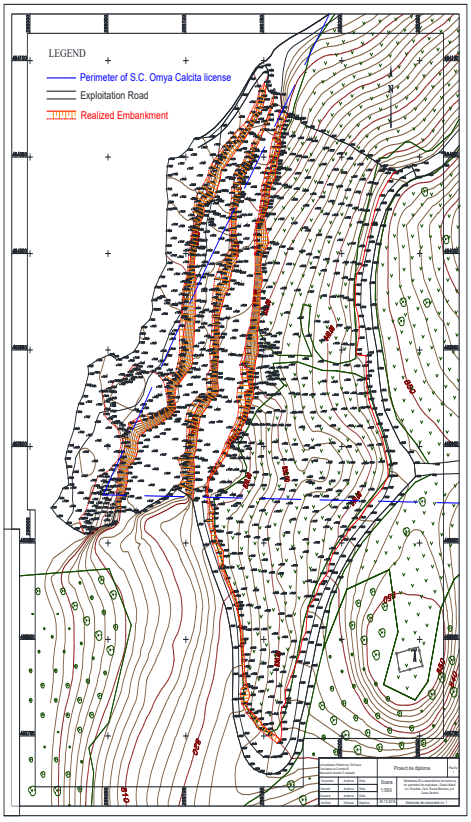

Figure 7. Layout plan of the marble quarry in the "Dealul Maria" perimeter (First session of measurements)

Analysing the levelling plan, one can see that the maximum elevation reaches 850 m starting from 780 m, in the area where exploitations have been previously realized. Also, another

conclusion is that terraces are formed in the exploited area with a 10 m level difference between. In this measurement, the three terraces are at an elevation of 800 m, 810 m, respectively 820 m.

From the measured coordinates, we also studied the positioning of the first locality near the marble exploitation, which is less than 4 km from the first inhabited houses. We have identified the areas where air monitoring sensors will be installed. The interest in this aspect is increased and the results are centralized to find solutions to reduce pollution.

Next, from all the quarterly measurement sessions, session number 10 realized on 29.12.2018, respectively the last measurement session, namely session 20 on 30.05.2021, have been selected to be discussed in this paper.

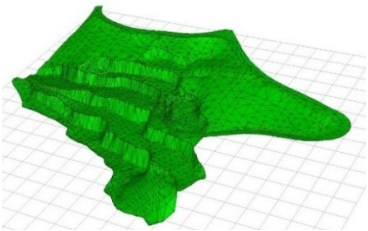

Figure 8. The 3D model of the terrain resulting from processing of measurement session no.10 carried out on 29.12.2018

Data processing has been performed in the same manner as for the first measurements session, realizing both the 3D models (Figure 8 and 11) and the layout plans (Figure 9 and 12).

Analysing Figure 9, one can identify the new areas where marble exploitations have been carried out. We noticed that the exploitation on the 830 m contour line were expanded and the topographic surveys were realized for the 840 m contour line. At this elevation (840 m), the transverse profiles were made and the slope of the ramp was identified. It was also found that, in the northern part, the transition from the contour line 820 m to 830 m was made without keeping the buffer zone.

The volume calculation of the exploited marble was carried out using the TopoLT software. This application allows users to calculate the volume between different measurement sessions by computing the difference between 3D models.

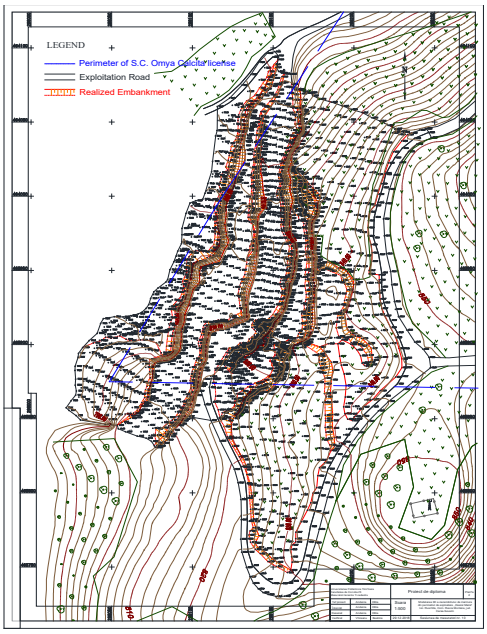

Figure 9. Layout plan of the marble quarry in the "Dealul Maria" perimeter (measurement session no.10)

Figure 10 shows the volume calculation between measurement session 1 and session 10.

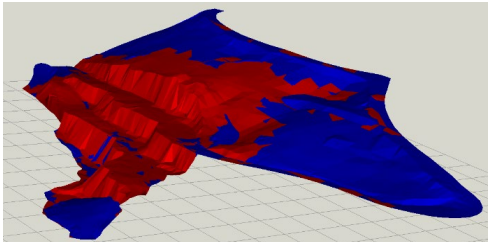

Figure 10. Volume calculation between measurements session 1 and session 10 and representation of the exploited area

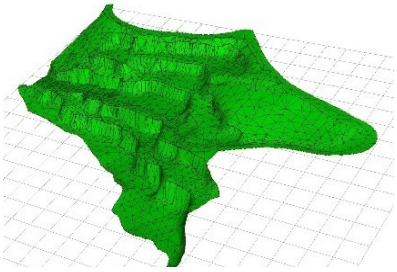

Figure 11. The 3D model of the terrain resulting from processing of measurement session no.20 carried out on 30.05.2021

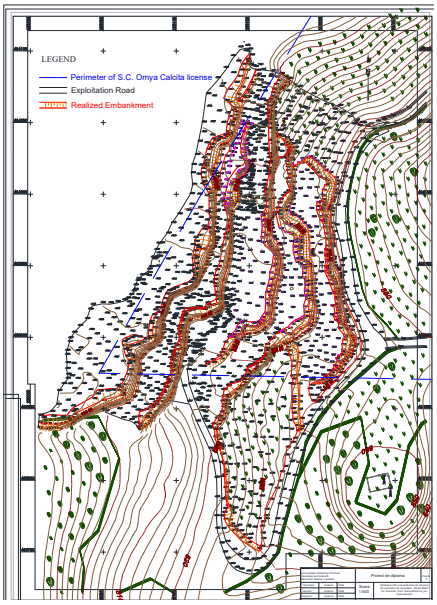

Figure 12. Layout plan of the marble quarry in the "Dealul Maria" perimeter (measurement session no.20)

Figure 12 shows the exploited area at 840 m elevation. From the resulting plan, the five benches of exploitation and their interval by elevation were also identified. The first step is between +785 and 800 m, the second step between 800 and 815 m, the third step starts from 815 to 825 m, the 4th step is between 825 and 835 m, and the last step is identified at +835 m to 845 m.

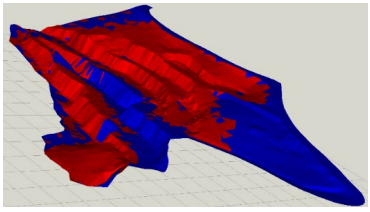

Figure 13. Volume calculation between measurements session 10 and session 20 and representation of the exploited area

In Figure 13 the volume calculation between measurement sessions 10 and 20 is represented. Table 1 summarizes the volume calculation between the 3 surveying sessions which spread over a 5-year period. As it can be seen, the value of the exploited marble is lower than the initial estimated value of 279,696 tons per year of industrial extraction.

Table 1. Volume calculation of the exploited marble

Measurement session	Volume calculation [m³]	Volume calculation [tons]
Session 1 Session 10	+93,427.87	252,255.249
Session 10 Session 20	+80,928.88	218,507.976

A future exploitation is proposed for the final period of the license, in the sense of greening the area simultaneously with the marble excavation process. Slope excavation is established between the slope foot lines of the existing steps, in order to avoid filling works in view of minimal greening costs. In other words, following the proposed exploitation, the quarry will be directly greened (Figures 14 and 15).

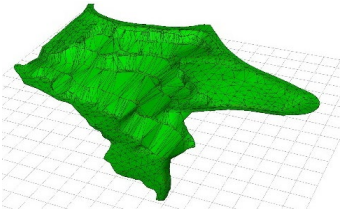

Figure 14. 3D model after greening the exploited area

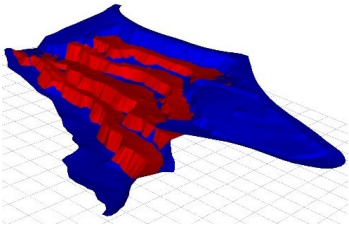

Figure 15. Marble volume calculation remaining to be exploited according to the greening proposal

CONCLUSIONS

Despite the vital development of BIM technologies for construction safety planning, the current practice of excavation safety planning is still manual and based on conventional methods. To address this problem, both internationally and in Romania, automatic excavation safety planning tools must be developed and tested.

The topicality of this research is given by the fact that assessing and monitoring the environmental impact of excavations which have the potential to cause adverse effects on the stability of the soil and nearby structures can be successfully further integrated into BIM.

The implementation of such an approach also brings added value to the construction process, as optimal decisions can be adopted with regard to streamlining time and costs.

The potential of BIM for excavation safety planning and modelling in the pre-construction stage has been ascertained and confirmed through real case studies (Herbei et al., 2022).

Various studies have demonstrated the usefulness of a BIM of deep excavation projects to integrate a 3D model and relevant spatial information regarding the retaining walls, excavation and adjacent buildings; and then visualized all the analysis and assessment results to present the likely locations and degrees of risk and safety in different situations. These facilities enable users to interpret monitoring data effectively and intuitively, reduce misinterpretations, improve communication efficiency, and facilitate effective decisions that are supported by the collected monitoring data.

As regards "Dealul Maria" objective, its exploitation consisted in carrying out the activity of extracting the marble reserves from the quarry fronts, loading the material into dump trucks and transporting it to the primary crushing plant located outside the exploitation perimeter. At the end of the activity, works will be carried out to close the objective in order to return to the initial environmental conditions, which will consist of: evacuation of machinery and equipment, proper evacuation and storage of any waste, correcting the slopes and covering the horizontal surfaces of the quarry with topsoil and seeding with grass the surfaces covered with vegetable soil, applying fertilizer.

ACKNOWLEDGMENTS

This paper was financially supported by the Project "Network of excellence in applied research and innovation for doctoral and postdoctoral programs/InoHubDoc", project co-funded by the European Social Fund financing agreement no. POCU/993/6/13/153437.

REFERENCES

Badea, A.C. & Badea, G. (2022). Open Geospatial Data and Tools for Sustainable Cities - Advantages and Disadvantages Open Geospatial Data and Tools for Sustainable Cities, Volunteering for the future - Geospatial excellence for a better living, Poland.

Buza, M., Dimen, L., Pop, G., Turnock, D. (2001). Environmental protection in the Apuseni Mountains: The role of Environmental Non-Governmental Organisations (ENGOs). *GeoJournal, 55.* 631–653. https://doi.org/10.1023/A:1021757431777.

Herbei, M.V., Herbei, R.C., Filip, L.O. (2021). Spatial Representation of Useful Minerals Deposits, *Mining Revue/Revista Minelor, 27(2).* 84-92, DOI: 10.2478/minrv-2021-0019.

Herbei, M.V., Herbei, R. C., Sala, F., (2022). Assessment of the Tilt Phenomenon and the Tilt Distance of the Land as an Effect of Coal Mining, Jiu Valley Basin, Romania, *Mining Revue/Revista Minelor, 28(3).* 28-38.

Hsieh, YM & Lu, YS. (2012). Visualization system for field monitoring data and its effectiveness. *Automation in Construction*, *26.* 54–68

Khan, N., Ali, A. K., Skibniewski, M. J., Lee, Do Y., Park, C. (2019). Excavation Safety Modeling Approach Using BIM and VPL, *Advances in Civil Engineering Journal*, Article ID 1515808.

Kim, SA, Shin, D, Seibert, T, & Walz, SP. (2012). Integrated energy monitoring and visualization system for Smart Green City development: Designing a spatial information integrated energy monitoring model in the context of massive data management on a web-based platform. *Automation in Construction*, *22.* 51–59.

Marcuta, L., Marcuta, A., Iagaru, P., Iagaru, R., Dimen, L. (2020). The relationship between demography and the development of smart city. Case study - Bucharest, *Scientific Papers Series Management, Economic Engineering in Agriculture and Rural Development, 20(1).* ISSN 2284-7995.

Oprea, L., Ienciu, I., Popescu, C., Vorovencii, I. (2014). Urban Conversion and Topographic Extension of Residential Land in View of Building New Housing Complexes, *Proceedings of the 14th SGEM GeoConference, 2.* 623-628.

Pescari, S., Pitroaca, A., Merea, M., Vilceanu, C.B. (2022). A Particular Case of Urban Sustainability: Comparison Study of the Efficiency, *Sustainability 14(23).* DOI: 10.3390/su142316283.

Sălăgean, T., Moscovici, A., Păunescu, V., Călin, M., & Şuba, E.E. (2017). Research on vertical displacements analysis of concrete dams. *Proceedings of the 17th SGEM GeoConference,* 555-560.

Wu, I-Chen, Lu, Siang-Rou, Hsiung, Bin-Chen, (2015). A BIM-based monitoring system for urban deep excavation projects, *Visualization in Engineering Journal*, *3.* 2.

https://bimmda.com/en/what-is-bim

***S.C. Omya Calcita S.R.L. Bucureşti (2010). Report on the environmental impact for the objective of opening and commissioning the marble deposit in the exploitation perimeter Dealul Maria, Ruschiţa, Rusca Montana, Caraş-Severin County.

Scientific Papers. Series E. Land Reclamation, Earth Observation & Surveying, Environmental Engineering. Vol. XII, 2023
Print ISSN 2285-6064, CD-ROM ISSN 2285-6072, Online ISSN 2393-5138, ISSN-L 2285-6064

5 METHODS OF DETERMINING THE CHARACTERISTIC VALUES OF SHEAR STRENGTH PARAMETERS

Ernest Daniel OLINIC[1], Tatiana OLINIC[2], Adrian ANDRONIC[1]

[1]Technical University of Civil Engineering Bucharest, Faculty of Hydrotechnics,
122-124 Lacul Tei Blvd, District 2, Bucharest, Romania
[2]University of Agronomic Sciences and Veterinary Medicine of Bucharest,
Faculty of Land Reclamation and Environmental Engineering,
59 Marasti Blvd, District 1, Bucharest, Romania

Corresponding author email: olinictatiana@gmail.com

Abstract

The shear strength parameters, internal friction angle (φ [°]) and cohesion (c [kPa]) represent derived values, according to the methodology of Eurocode 7 and NP 122. They are determined by processing the pairs of normal stress (σ) - tangential stress (τ) values resulted from direct shear or triaxial compression tests. The paper presents 5 methods of determining the characteristic values, following the direct processing of φ and c values or indirectly, by processing pairs of σ-τ values, resulted from direct shear tests. The characteristics values of shear strength parameters are required for the geotechnical design in the case of various geohazards and for foundation solution. A series of conclusions are drawn based on the legislation in force.

Key words*: characteristic values, cohesion, derived values, internal friction angle, shearing strength parameters.*

INTRODUCTION

From a geotechnical engineering perspective, there are two types of parameters which are essential in analysing the mechanical behaviour of soils: the parameters governing the relation between stresses and strains (compressibility and consolidation parameters) and the parameters governing the development of plastic strains which lead to failure.
Prästings et al. (2019) said that the lack of harmonisation between reliability-based design and the partial factor method in Eurocode 7 is preventing the widespread introduction of a risk-based concept in geotechnical design.
The current paper deals with the determination of the values to be used for design, namely the inferior characteristic values of the shearing resistance parameters, as used in Mohr-Coulomb constitutive model.
The choosing of the characteristic values is anything but trivial, due to the highly heterogeneous nature of soils and the variation of the parameters with respect to the method used for analysing the shearing resistance, in particular.
Another particular property of soils that increase the difficulty in choosing the parameters is the dependence on the state of stress in which the soil is at a particular moment and more than that, on the history of the loading states.
The current paper analyses the fit of usage for five methods of computing the characteristic values of the shearing resistance parameters, by analysing the current technical norms in use and prior methods prescribed by the legislation in Romania. For that, several direct shearing tests have been employed, analysing the results from the point of view of the safety the five methods provide.
The methods used in this paper are based only on the stochastic approach, without using any other numerical methods for analysing the fitness of the methods.

MATERIALS AND METHODS

Using following notations:
X_i - measured values, with $i \in [0,n]$;
X_m - average of the measured values X_i;
s_x – standard deviation of the measured values X_i;
V_x - coefficient of variation;

X_k - characteristic value (there will be a superior value and an inferior value);
t_α - statistical coefficient derived from STAS 3300/1-1985.

Computation procedures considered are:

- According to NP 122-2010

The average of the measured values is computed using equation (1):

$$X_m = \frac{\sum_{i=0}^{n} X_i}{n} \quad (1)$$

The standard deviation of the measured values is computed using equation (2):

$$s_x = \sqrt{\frac{\sum_{i=0}^{n}(X_i - X_m)^2}{n-1}} \quad (2)$$

The coefficient of variation is computed using equation (3)

$$V_x = \frac{s_x}{X_m} \quad (3)$$

The superior and inferior characteristic values are computed using equation (4). The statistical coefficient k_n is determined using Table 3.2 from NP 122-2010.

$$X_{k\_sup} = X_m(1 + k_n V_x) \quad (4)$$
$$X_{k\_inf} = X_m(1 - k_n V_x)$$

The previous computation procedure was applied in two different hypotheses. The first hypothesis determined the values of the shear resistance parameters for each of the direct shearing tests performed and applied the previously described procedure to compute the characteristic values of the shear resistance parameters.

The second hypothesis considered the maximum shearing stress determined from the direct shearing tests (the normal stress for each test was imposed). The characteristic values for maximum shearing stresses were determined for each of the imposed normal stresses and the shearing resistance parameters were determined using the pairs of the characteristic shearing stresses and the imposed normal stresses.

- According to NP 122-2010 Appendix A.4

In appendix A.4 of NP 122-2010 certain values are recommended for the coefficient of variation V_x, depending on the analysed parameters. For the current case, the recommended coefficient for the internal friction angle ϕ', applied on the tangent of the angle is 0.1. Similar, the recommended value for the drained and undrained cohesion is 0.4.

- According to NP 122-2010 Appendix A.5

The procedure uses a regression line, having the equation $\tau=\sigma \tan \phi + c$ and the characteristic values are obtained based on the statistical coefficient t_α.

$$y_k = a_k x + b \pm t_\alpha s_c \quad (5)$$
$$t_\alpha = f(n-1)$$

As a result, the correlation that gives the characteristic value is parallel to the regression line calculated by the least squares method. Therefore, only the cohesion value is underestimated, and a characteristic value is provided, while the internal friction angle has the same value, from the regression line.

- According to the procedure from STAS 3300/1-1985 Appendix A

Before the entry into force of Eurocode 7 and NP 122, the calculation values of the geotechnical parameters are determined according to STAS 3300-1/85 which contains distinct procedures for independent parameters (ρ, w, E_{oed}) and correlated parameters (φ and c).

The procedure described in STAS 3300/1-1985, that can be fully applied because it uses mathematical statistics relationships, is based on the following equations:

$$y_k = a_k x + b_k \quad (6)$$
$$a_k = a_m\left(1 \pm \frac{t_\alpha s_{x,a}}{a_m}\right)$$
$$b_k = b_m\left(1 \pm \frac{t_\alpha s_{x,b}}{b_m}\right)$$
$$t_\alpha = f(n-2)$$

As a result, both the internal friction angle and the cohesion are underestimated (inferior characteristic values are obtained).

The coefficient of variation, through the recommended maximum values for physical characteristics of soil, underlies the delimitation of geological strata (Olinic, 2014).

RESULTS AND DISCUSSIONS

For obtaining the input data for the current paper, 36 direct shearing tests were performed. The tests were conducted with imposed normal stress (12 tests with an imposed value of 121.37 kPa, 12 tests with an imposed value of 216.75 kPa, and 12 tests with an imposed value of 312.12 kPa). The maximum shearing stress was recorded for all the 36 tests and presented in the Table 1.

Table 1. Measured maximum shearing stresses for the performed direct shearing tests [kPa]

Measured values	σ_1	σ_2	σ_3
	121.37	216.75	312.12
	τ_1	τ_2	τ_3
X_1	132.66	159.12	187.23
X_2	155.00	194.10	228.12
X_3	148.92	201.91	242.62
X_4	130.56	172.90	208.00
X_5	148.92	166.29	212.50
X_6	132.22	172.34	223.10
X_7	141.13	186.67	231.66
X_8	161.19	199.12	228.12
X_9	125.00	168.44	207.48
X_{10}	151.70	177.92	200.23
X_{11}	112.22	163.42	198.56
X_{12}	167.88	198.00	243.74
Minimum values, X_{min}	112.22	159.12	187.23
Maximum values, X_{max}	167.88	201.91	243.74
Average values, X_m	142.28	180.02	217.61

The measured results were plotted in an σ-τ coordinates graph, presented in Figure 1.

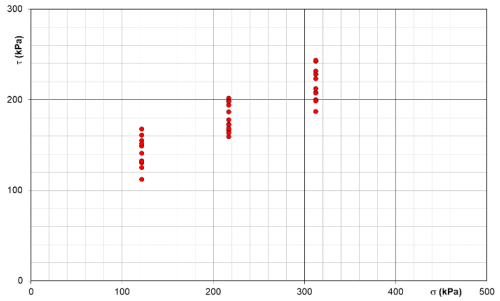

Figure 1. Measured values plotted in σ-τ coordinates.

From the measured stresses, the shearing resistance parameters were derived. The obtained values are presented in Table 2.

Table 2. Derived values of the shearing resistance parameters

Derived values	ϕ_{CU}	tan ϕ_{CU}	c_{CU}
	°	-	kPa
X_1	15.96	0.286	97.67
X_2	20.96	0.383	109.39
X_3	26.16	0.491	91.34
X_4	22.25	0.409	82.01
X_5	18.44	0.333	110.31
X_6	25.47	0.476	72.62
X_7	25.39	0.475	83.63
X_8	19.34	0.351	120.08
X_9	23.38	0.432	73.25
X_{10}	14.27	0.254	121.48
X_{11}	24.35	0.453	59.96
X_{12}	21.69	0.398	117.01
Minimum values, X_{min}	14.27	0.254	59.96
Maximum values, X_{max}	26.16	0.491	121.48
Average values, X_m	21.47	0.395	94.90

The obtained values were plotted in a ϕ-c coordinate graph presented in Figure 2.

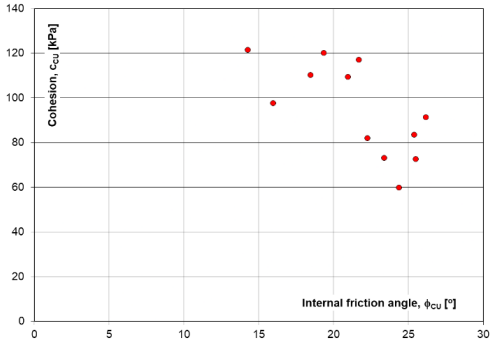

Figure 2. Derived shear resistance values plotted in ϕ-c coordinates.

Following the computation procedure described in the previous section, using the provisions of NP 122-2010, the following characteristic values were derived (Table 3).

Table 3. Derived values of the characteristic shearing resistance parameters

Number of selected X_i values, n	12	12	12
Standard deviation, s_x	3.84	0.0767	20.8
Coefficient of variation, V_x	0.179	0.194	0.220
k_n for $V_{xunknown}$	0.51	0.51	0.51
$X_{k\ sup} = X_m(1+k_n V_{x\ unknown})$	23.44	0.434	105.55
$X_{k\ inf} = X_m(1-k_n V_{x\ unknown})$	19.51	0.356	84.24
$\phi_{CU\ k\ inf}$		19.59	

The derived values were plotted in a σ-τ graph, together with the measured values for stresses, showed in Figure 3.
The same computation procedure was applied for the values of the measured stresses. The characteristic values that were obtained are presented in Table 4.

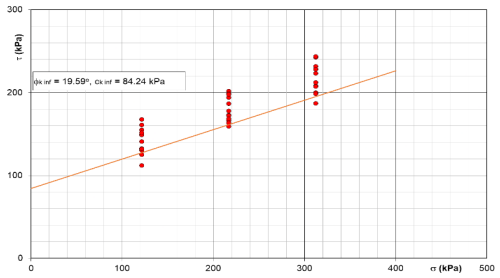

Figure 3. Derived characteristic values for the shearing resistance parameters using NP 122-2010 together with the measured values plotted in σ-τ coordinates.

Table 4. Characteristic values of the shearing stresses using NP 122-2010 and derived characteristic shearing resistance parameters

Number of selected X_i values, n	12	12	12
Standard deviation, s_x	16.20	15.25	18.00
Coefficient of variation, V_x	0.114	0.085	0.083
k_n for $V_{xunknown}$	0.51	0.51	0.51
$X_{k\_sup} = X_m(1+k_n V_{x\ unknown})$	150.57	187.82	226.82
$X_{k\_inf} = X_m(1-k_n V_{x\ unknown})$	134.00	172.22	208.40
$\phi_{CU\ k\ inf}$		21.31	
$c_{CU\ k\ inf}$		87.00	

The derived characteristic values of the shearing resistance parameters were plotted in a σ-τ graph, together with the measured stresses (Figure 4).

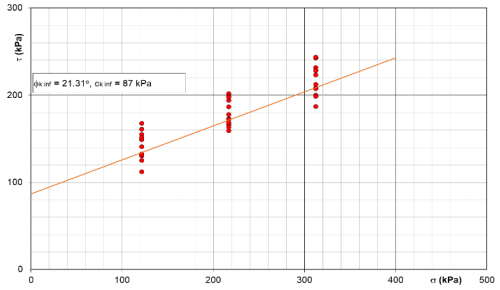

Figure 4. Derived characteristic values for the shearing resistance parameters from the characteristic derived stresses using NP 122-2010 together with the measured values plotted in σ-τ coordinates

Using the computation procedure described in NP 122-2010 Appendix A.4, the coefficients of variation V_x for the tan(ϕ) and c were considered 0.1 and 0.4 respectively. With these values, the derived characteristic values for the shearing resistance parameters were computed, using the values presented in Table 2. The results are presented in Table 5.

Table 5. Derived characteristic values of the shearing stresses using NP 122-2010 Appendix A.4

Number of selected X_i values, n	12	12	12
Standard deviation, s_x	3.84	0.0767	20.8
Coefficient of variation, V_x	0.179	0.100	0.400
k_n for $V_{xunknown}$	0.51	0.51	0.51
$X_{k\_sup} = X_m(1+k_n V_{x\ unknown})$	23.44	0.415	114.31
$X_{k\_inf} = X_m(1-k_n V_{x\ unknown})$	19.51	0.375	75.48
$\phi_{CU\ k\ inf}$		20.55	

The characteristic shearing resistance parameters obtained using the appendix A.4 were plotted in a σ-τ graph, together with the measured stresses (Figure 5).

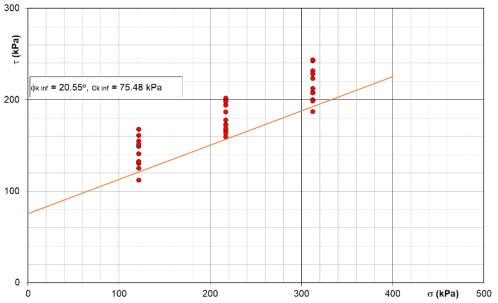

Figure 5. Derived characteristic values for the shearing resistance parameters using NP 122-2010 Appendix A.4 together with the measured values plotted in σ-τ coordinates

Following the computation procedure described in NP 122-2010 A.5, the trendline was derived from the measured stresses. The trendlines and values obtained are presented in Figure 6.
Applying the procedure described in STAS 3300/1 - 1985 to improve the results obtained from NP 122-2010 Appendix A.5, new trendlines are obtained. The results are presented in Figure 7.

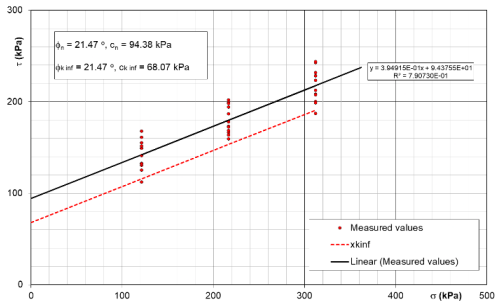

Figure 6. Derived characteristic values for the shearing resistance parameters using NP 122-2010 Appendix A.5 together with the measured values plotted in σ-τ coordinates

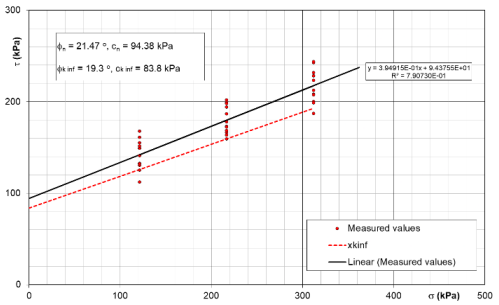

Figure 7. Derived characteristic values for the shearing resistance parameters using NP 122-2010 Appendix A.5, improved with the procedure from STAS 3300/1-1985 together with the measured values plotted in σ-τ coordinates

Table 6. The characteristic inferior values of the shearing resistance parameters obtained through the five methods described in the current paper

Characteristic inferior values of the shearing resistance parameters	NP 122-2010 - derived values – Method 1	NP 122-2010 - inferior values for stresses - Method 2	NP 122-2010 - App A.4 - Method 3	NP 122-2010 App A.5 - Method 4	NP 122-2010 Appendix A.5+STAS 3300/1 -1985 - Method 5
$\phi_{CU\ k\ inf}$	19.6 °	21.3 °	20.6°	21.5 °	19.3 °
$c_{CU\ k\ inf}$	84.2 kPa	87.0 kPa	75.5 kPa	68.1 kPa	83.8 kPa

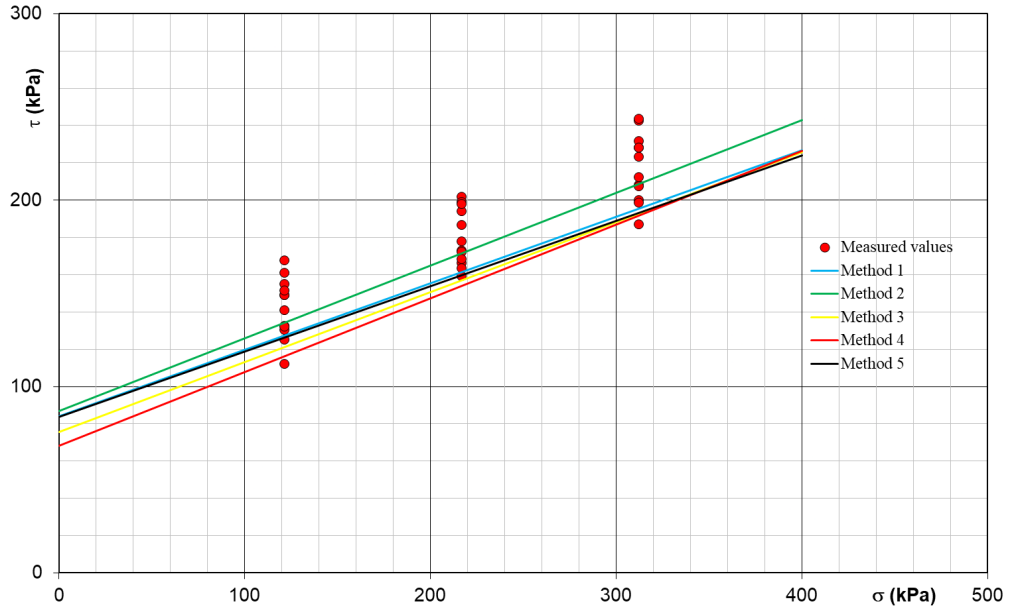

Figure 8. Mohr-Coulomb failure lines plotted using the inferior characteristic values of the shearing resistance parameters determined using the five methods described in the paper

CONCLUSIONS

The current paper analyses the use of five different methods of computing the inferior characteristic values of the shearing resistance parameters (Table 6), using the Mohr-Coulomb constitutive model formulation. If considering the results plotted in Figure 8, the first conclusion is that Method 2 doesn't provide sufficient reliability to be used.

On the other hand, considering that Mohr-Coulomb constitutive model is highly dependent on the normal stress applied, and considering that all the other methods (except for Method 2, of course) provide results that are inferior to most of the measured stresses – smaller than 95% of the obtained results, the choice of the method used relies rather on the designer.

The recommendation of the authors is to choose the usage of Method 4 for the situations where the normal stresses are low enough (up to 200 kPa) and Method 5 for normal stresses higher than 200-250 kPa.

Methods 1, 3 and 4 are prescribed by the current design norms and choosing any of them will be in accordance with the laws in use. As one can observe in Figure 8, all of them provide sufficient reliability.

More tests on more types of materials can provide with a better understanding of the methods for determining the characteristic values, considering that different types of materials might provide improved results.

ACKNOWLEDGEMENTS

This research was financed by the University of Agronomic Sciences and Veterinary Medicine of Bucharest (Grant number: 1068/15.06.2022, Acronym: GeoRoots).

REFERENCES

NP 122 - 2010. "Normativ privind determinarea valorilor caracteristice si de calcul ale parametrilor geotehnici".

Olinic, E. (2014). The influence of geotechnical investigations magnitude on characteristic values of soils parameters. *International Multidisciplinary Scientific GeoConference: SGEM, 2*, 915.

Prästings, A., Spross, J., Larsson, S. (2019). Characteristic values of geotechnical parameters in Eurocode 7. *Proceedings of the Institution of Civil Engineers - Geotechnical Engineering, 172*(4), 301–311, https://doi.org/10.1680/jgeen.18.00057.

STAS 3300/1 - 1985. "Teren de fundare. Principii generale de calcul".

SR EN 1977-1:2004. Eurocode 7: Geotechnical design - Part 1: General rules, Romania, 2004.

Scientific Papers. Series E. Land Reclamation, Earth Observation & Surveying, Environmental Engineering. Vol. XII, 2023
Print ISSN 2285-6064, CD-ROM ISSN 2285-6072, Online ISSN 2393-5138, ISSN-L 2285-6064

BIO-REINFORCEMENT OF SLOPES

Tatiana OLINIC[1], Ana Maria STANCIU[2], Ana Cornelia BUTCARU[3], Vasilica LUCHIAN[4]

[1]University of Agronomic Sciences and Veterinary Medicine of Bucharest,
Faculty of Land Reclamation and Environmental Engineering,
59 Marasti Blvd, District 1, Bucharest, Romania
[2]University of Agronomic Sciences and Veterinary Medicine of Bucharest,
Faculty of Agriculture, 59 Marasti Blvd, District 1, Bucharest, Romania
[3]University of Agronomic Sciences and Veterinary Medicine of Bucharest,
Research Centre for Studies of Food and Agricultural Products Quality,
59 Marasti Blvd, District 1, Bucharest, Romania
[4]University of Agronomic Sciences and Veterinary Medicine of Bucharest,
Faculty of Horticulture, 59 Marasti Blvd, District 1, Bucharest, Romania

Corresponding author email: olinictatiana@gmail.com

Abstract

The influence of vegetation on mechanical soil behaviour represents a significant factor to be considered in erosion control. This type of erosion control process is named bio-reinforcement and it is an environmentally friendly engineering method for shallow slope stabilization. The mechanical reinforcement made by roots has effect in shallow soil, where the most root biomass exists. Vegetation plays an important role in stabilizing settlements and infrastructures from hazards produced by water energy. The new trend named sustainability has forced engineers to rediscover vegetation as an engineering solution for shallow slope protection. This review paper presents various species of plants with an important role in slope stabilization applications. The need for a sustainable future creates a new engineering discipline, named Eco-geotechnics, which integrates knowledge from soil mechanics, botanics, engineering geology and atmosphere science.

Key words*: slope stability, bio-reinforcement, vegetation, roots tensile.*

INTRODUCTION

In order to prevent soil erosion on slopes it is very efficient to use bio-reinforcement using living plants. The utilization of vegetation as an environmentally friendly method to increase the stability of natural and artificial slopes is well known all over the world. In the scientific literature there are many papers on this topic, especially papers with authors from Asia (China, Indonesia, Malaysia, India, etc), Europe (Italy, Spain, France) and South America (Brazil, Peru).

The erosion process occurs when rainfall appears, especially on steep slopes that have a poor cover of vegetation or on non-vegetated slopes (Figure 1) besides the rainfall intensity, the erosion process depends on: relief, soil erodibility, water flows, climatic area and vegetation cover. Erosion produced by water (which presents interest for our paper) can occur by: splash erosions (or raindrop erosion), sheet erosion, rill erosion and gully erosion.

Sheet erosion is the soil particles movement from the upper part of the soil mass or topsoil produced by raindrop impact; along the slope and close to the base water will detach sheets and layers of soil from all the surface area.

Rill erosion represents small channels produced by runoff water concentrated down a slope. If the channel is up to 0.30 m it is rill erosion; if it is deeper, it is about gully erosion.

Gully erosion appears when the water flow is strong and can detach and move the soil particles. Gully erosion is visible on site and has a negative effect on soil productivity, roads, buildings, land and fences.

Splash erosion or raindrop erosion is caused by the splash of falling raindrops; and appears due to the rough splashes of water.

According to Touze-Foltz and Zanzinger (2016), an important achievement when we speak about surface erosion control on

construction sites (steep slopes human made, fences, embankments, slopes around roads) is to stabilize soil and seed on slopes until the seed can germinate and fix in the topsoil.

MATERIALS AND METHODS

This paper it is a review article, which present the influence of bio-reinforcement made by vegetation on shallow slope stability applications, it was used some conclusions from a series of experiments from the scientific literature. The materials and methods used in various papers are presented below.

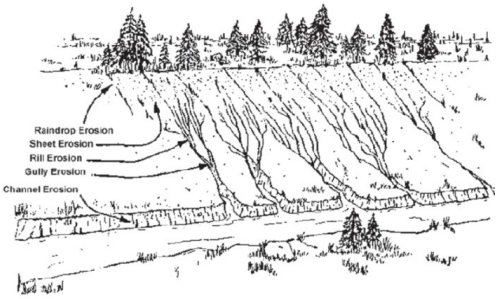

Figure 1. Types of soil erosion (Rimoldi, 2016)

The type of vegetation

Singh et al. (2021) studied trees and woody shrubs stabilization by their reinforcing properties and they concluded that the root systems transmit stability to slopes, subjected to mitigate soil erosion or landslides. The heart-root system of the shrubs and grass-roots provide a more significant increase in soil cohesion than tap-root system; the grass-roots protect the topsoil and reduce shallow landslides.

For a right solution of bio-stabilisation, it is important to take into account natural vegetation which can be found on site. These plants are naturally adjusted to the climate and soil from the region.

Woody plants used in studied papers are: *Chimonobambusa* sp. (it is a small bamboo of about 1.10 m height), *Pseudosasa japonica* (a type of bamboo, perennial, with a height of about 1.00 m), *Indigofera amblyantha* (a perennial deciduous shrub with a horizontally developed root system), *Ligustrum vucaryi* (a shrub with roots of 0.50-0.70 m), *Fumana thymifolia* (a shrub, medicinal plant which can grow to 30 cm tall), *Tamarix canariensis* (a shrub or small tree up to 4 m tall), etc.

Grass used in studied papers are: *Cymbopogon* sp. (Lemongrass - a tropical perennial grass with a length of roots of 0.35 m), *Chrysopogon zizanioides* (Vetiver grass is a common used plant in bio-stabilisation; it is a graminaceous plant, the roots can grow to 1.00 m in 3 months), *A fruticosa* (a plant used for ecological restoration for tailing ponds), *Limonium supinum* (it is a perennial herb, very common in saline areas from Iberian Peninsula; it is a plant used for the restoration of arid zones*), Stipa tenacissima* (it is a common plant from Mediterranean countries; it is very efficient in ecological domain because prevents desertification), etc.

The most common plant used for bio-reinforcement is *Medicago sativa*, also called alfalfa. It is a widespread perennial flowering plant; it is a forage crop in many countries from the world. Once it is established, this plant doesn't require cultivation, being a sustainable solution on slopes where it is difficult to reach with agricultural machinery. The root system reaches a depth of 3.00-5.00 m. According to Wang et al. (2022), the deep and root system of *Medicago sativa* go into the soil; the root system creates spaces and channels in depth allowing water infiltration.

Figure 2. The climatic areas in Romania (GE 027-1997)

In Romania, the bio-reinforcement of slopes with different plant is made depending on the climatic areas. In National Guide 027-1997, the surface of Romania is divided into 3 main areas; for each area it is proposed a mixture of perennial plants in order to protect the slopes for erosion (Figure 2).

The proposed mixtures for vegetalization of slopes are composed by the following plants: *Bromus inermis, Agropyrum cristatum, Medicago sativa, Dactylis glomerata, Festuca pratensis and Trifolium pratense*. These plants are known to have beneficial effects in erosion control, but unfortunately *Bromus inermis* and *Agropyrum cristatum* seeds are no longer produced and sold in Romania.

According to De Baets et al. (2009), in a study from Mediterranean part of Spain, the root characteristics to predict the erosion-reducing potential of vegetation depend both on the site conditions and on the erosion process of interest. In order to prevent rill and gully erosion it is mandatory to prevent the initiation of concentrated flow erosion.

Soil used in studies

In many laboratory studies, the soil was chosen in order to be a very erodible one or a difficult foundation soil. In the category of very erodible soil are coarse sands, fine sands, silty sands or silty soils. Difficult foundation soils used in analyzed scientific papers are: loessoid soils and expansive soils.

Preparing the samples

A series of studies were carried out on samples remodelled in the laboratory, samples in which vegetable fibbers were added (Figure 3).

Figure 3. Samples remodelled in laboratory (Badhon et al., 2021; Guo et al., 2020)

The most relevant studies are those carried out on soil samples where the plants grew, where the roots are naturally distributed in the soil mass (Figure 4). The relation between roots and soil can be schematic view in Figure 5.

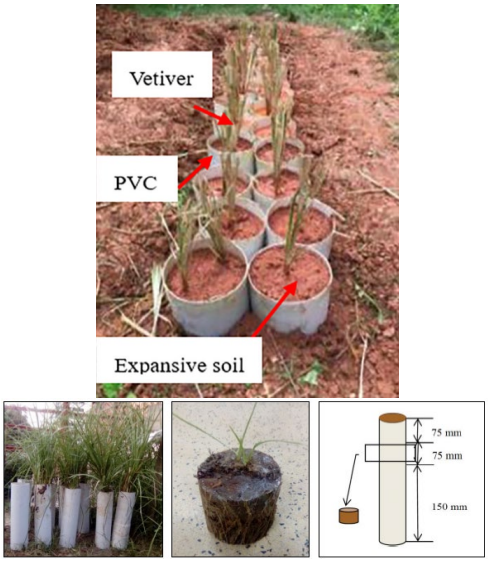

Figure 4. Preparation of undisturbed rooted soil samples (Badhon et al., 2021; Wang et al., 2020)

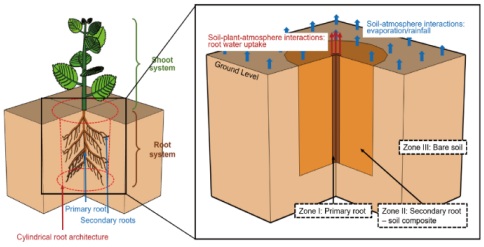

Figure 5. A schematic 3D root system (Ng et al., 2022)

Rainfall tests

In laboratory studies, have been used rainfall simulator with nozzles in order to apply various rainfall intensities for different period of time.

In the case of field experiments, rainfall was measured using automatic weather stations installed in the vicinity of the experimental plots.

Strength parameters

Researchers Waldron (1977) and Wu (1979) made the first attempts to quantify soil reinforcement due to roots using a simple perpendicular root model. This model in well known as Wu/Waldon Model - WWM and show that the increase in soil shear strength

appears as an increase in soil cohesion, c_r (kPa). The roots cohesion it is expressed as:

$$c_r = 0.4 (\sin\delta + \cos\delta * \tan\varphi') * T_r * RAR$$

where: δ - shear distortion angle of roots, φ' - effective friction angle of soil; T_r - root tensile strength and RAR - root is ratio.
In a simple manner, the effect of root reinforcement on slope stability can be measured directly in terms of the additional shear strength given by plant roots in reinforced soil (Gao et al., 2020).
According to Wu (2013), for woody plants it can be measured the Young's modulus (E) and tensile strength. The tensile strength provided by the roots in soil mass (σ_{rt}) can be measured by performing a tension test on a root segment.

RESULTS AND DISCUSSIONS

A study from South-East part of Spain, made by De Baets et al., in 2009, presents a visual interpretation on the impact of 25 species of grass, forbs, reeds, rushes, shrubs and trees on slope stabilisation, erosion control, sediment obstruction potential or bending by water flow. They grouped the plant species into 8 categories; depending on the bio-stabilizing function they perform (Table 1).

Table 1. Plant species grouped according to their effect on bio-stabilization (De Baets et al., 2009)

Plants used in tests	Bio-stabilization effect
Fumana thymifolia *Teucrium capitatum*	Concentrated flow erosion - low resistance Sediment obstruction potential - low Bending by water flow - not resistant Improve slope stability - no potential
Nerium oleander *Rosmarinus officinalis*	Slope stabilization - low potential Prevent erosion by concentrated runoff - medium potential Bending by water flow - high resistance Sediment obstruction potential - medium
Anthyllis cytisoides *Retama sphaerocarpa* *Salsola genistoides* *Tamarix canariensis* *Atriplex halimus*	Slope stabilization - high potential Bending by water flow - very resistant Sediment obstruction potential - low Potential to prevent concentrated flow erosion - medium to high
Thymus zygis *Artemisia barrelieri* *Lygeum spartum* *Avenula bromoides* *Piptatherum miliaceum*	Prevent erosion by concentrated runoff - medium to high Slope stabilization - low Sediment obstruction potential - medium Bending by water flow - low
Stipa tenacissima *Thymelaea hirsuta* *Dittrichia viscosa* *Ononis tridentata* *Dorycnum pentaphyllum*	S lope stabilization - low Prevent incision by water flow - low Bending by water flow - medium to high Sediment obstruction potential - low
Plantago albicans *Limonium supinum* *Helictotrichon filifolium* *Brachypodium retusum*	Prevent concentrated flow erosion - medium to high Slope stabilization - low Sediment obstruction potential - high
Juncus acutus	Prevent concentrated flow erosion - high sediment obstruction potential - high Bending by water flow - medium
Phragmites australis	Bending by water flow - medium Sediment obstruction potential - medium Prevent concentrated flow erosion - low

The effect of the root characteristics in the reinforced soil according to Guo et al. (2020) shows that the values of cohesion of the soil-root system increase under consolidated - drained and consolidated - undrained condition, under unconsolidated - undrained condition it presents a complicated change. By the fact that the plant roots can be fully in contact to the soil particles it is registered an increase of the contact area while the root content increases. Some studies have shown that for an optimal root content the shear strength increases with root content until a peak value is achieved. When the root content continues to increase, the plant roots are not effectively connected with the soil particles and plant roots are in contact to each other's; in this case, the lateral restraint of the root system in the soil is no longer strengthened.
Studies on tree roots shows that the tensile strength reaches values of 5 to 60 MPa and the Young's modulus is between 200 to 600 MPa (Wu, 2013). In the same time, experiments made on woody roots shows that root tensile strength decrease exponentially with increasing root diameter.
A relation between shear strength and shear deformation is shown by Meijer et al. (2022). The experiments show that peak root reinforcements occurred at large shear deformations; this has a significant indication for the definition of the root reinforcement peak value. Peak root reinforcement is always defined as the difference between the peak shear strengths of rooted and bare soils and is named "apparent reinforcement". If the root reinforcement is calculated by WWM, it is called "actual reinforcement" and the author's shows in Figure 6 that it is a major difference between apparent and actual reinforcement (measured vs. estimated).
Experiments performed in direct shear test made by Badhon et al. (2021), on samples with and without *Vetiver* roots, shows that adding

roots increases the shear strength of soil (Figure 7). The used soil in tests was a sandy soil, known as a very erodible soil.

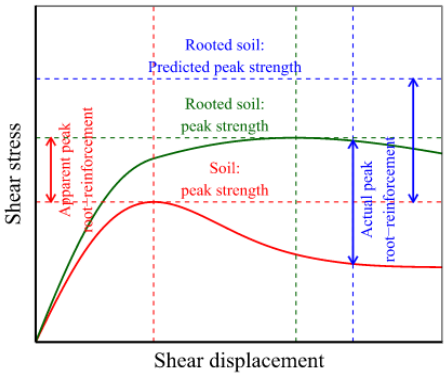

Figure 6. Different definitions of root-reinforced shear strength (Meijer et al., 2022)

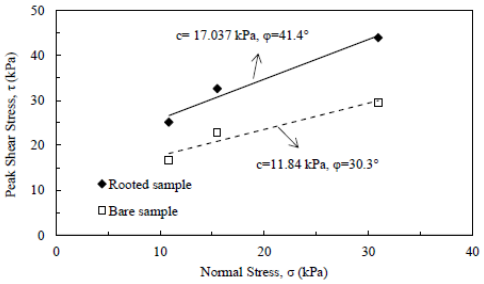

Figure 7. Shear strength parameters on bare soil and rooted soil sample (Badhon et al., 2021)

CONCLUSIONS

The aim of this review paper was to make a synthesis on the existing data in the field of stabilization by using living plants, plants known for their erosion control benefits.

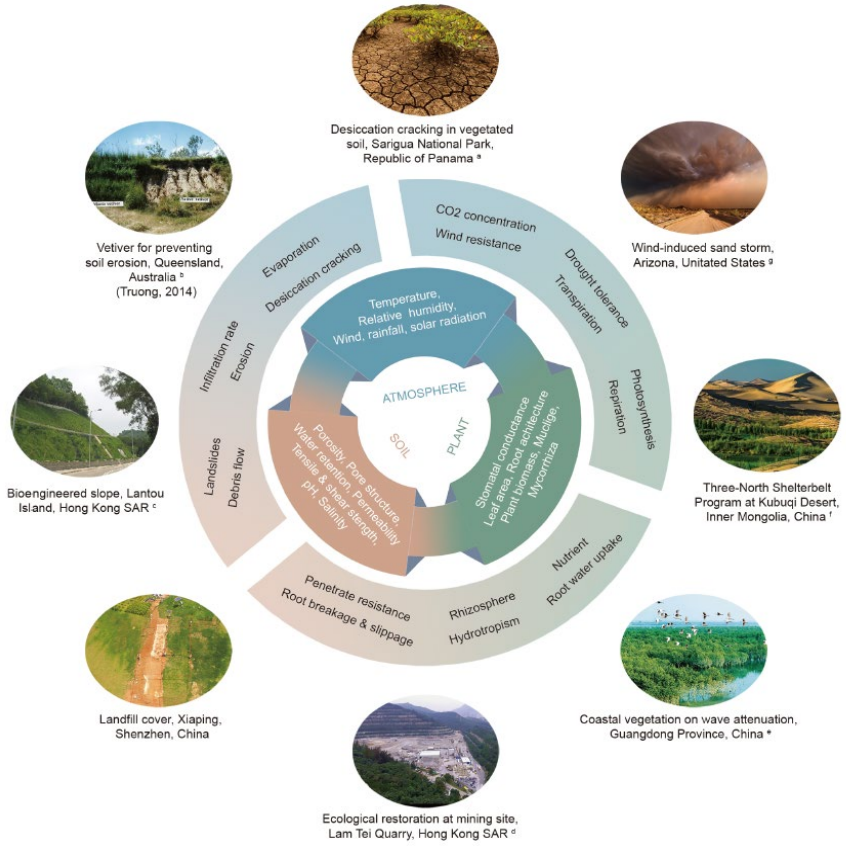

Figure 8. Eco-geotechnics - a sustainable discipline (Ng et al., 2022)

Using vegetation for shallow slope stability application is a sustainable method and creates a new discipline in Geotechnical Science. According to Ng et al. (2022), Eco-geotechnics is an emerging discipline and has gained recognition in the field of sustainable development in recent years. Eco-geotechnics should integrate knowledge from soil mechanics, ecology, rock mechanics, botanic, engineering geology and atmosphere science (Figure 8). In this context, geotechnical processes and ecological behaviour are inter-related to achieve overall sustainability.

For an efficiency of bio-reinforcement it is recommended to use geosynthetic materials for erosion control. These materials provide a protection for the topsoil cover, until the germination process occurs. According to Rimoldi (2016), some of geosynthetics are biodegradable materials or photodegradable; other geosynthetics remain in place for an extended period, or even permanently, and work in concert with the vegetation that grows up through them.

ACKNOWLEDGEMENTS

This research was financed by the University of Agronomic Sciences and Veterinary Medicine from Bucharest (Grant number: 1068/15.06.2022, Acronym: GeoRoots).

REFERENCES

Badhon, F.F., Islam, M.S., Islam, M.A. (2021). Contribution of *Vetiver* Root on the Improvement of Slope Stability. *Indian Geotech Journal, 51*, 829–840 https://doi.org/10.1007/s40098-021-00557-0

De Baets, S., Poesen, J., Reubens, B., De Baerdemaeker, J., Meersmans, J. (2009). Methodological framework to select plant species for controlling rill and gully erosion: application to a Mediterranean ecosystem, *Earth Surface Processes and Landforms, 34*, 1374-1392, doi: 10.1002/esp.1826.

GE 027-1997. Guide for the design and execution of slope protection and consolidation works at canals and dikes.

Guo, P., Xia, Z., Liu, Q., Xiao, H., Gao, F., Zhang, L., Yang, Y., Xu, W. (2020). The mechanism of the plant roots' soil-reinforcement based on generalized equivalent confining pressure. *PeerJ., 8:e10064*. https://doi.org/10.7717/peerj.10064.

Meijer, G.J., Knappett, J.A., Bengough, A.G., Bull, D.J., Liang, T., Muir Wood, D. (2022). DRAM: A three-dimensional analytical model for the mobilisation of root reinforcement in direct shear conditions, *Ecological Engineering, 179*, 106621, ISSN 0925-8574, https://doi.org/10.1016/j.ecoleng.2022.106621.

Ng, C.W.W., Zhang, Q., Zhou, C. (2022). Eco-geotechnics for human sustainability. *Science China Technological Sciences, 65*, 2809–2845 https://doi.org/10.1007/s11431-022-2174-9.

Rimoldi, P. (2016). Design of geosynthetics for erosion control on slopes. *Proceedings of 6thEuroGeo 6 Conference Ljubljana - Slovenia*, 339-360.

Singh, T.J., Ibotombi, S. and Singh, M.P., (2021). Influence of Plant Roots on Slope Stabilization: A Geotechnical Investigation. https://doi.org/10.21203/rs.3.rs-623966/v1

Touze-Foltz, N., Zanzinger, H. (2016). Laboratory tests for evaluating the performance of geosynthetics for surface erosion control. *Proceedings of 6th European Conference on Geosynthetics*, 329-338.

Wang, Q., Fuchun, L., Xiaole, Z., Wucheng Z., Dengkui Z., Xujiao Z., David J., Xiaoyun W., Qinglin L., Xiaoling L., Guang L., Heling W., Kai Z., Jin C. (2022). Runoff and nutrient losses in alfalfa (*Medicagosativa L*) production with tied-ridge-furrow rainwater harvesting on sloping land, *International Soil and Water Conservation Research, 10(2)*, 308-323, ISSN 2095-6339, https://doi.org/10.1016/j.iswcr.2021.09.005.

Wang, G., Huang, Y., Li, R., Chang, J., Fu, J. (2020). Influence of *Vetiver* root on strength of expansive soil-experimental study. *PLOS ONE 15(12)*: e0244818. https://doi.org/10.1371/journal.pone.0244818

Wu, T.H., (2013). Root reinforcement of soil: review of analytical models, test results and applications to design. *Canadian Geotechnical Journal, 50*, 259-274.

Scientific Papers. Series E. Land Reclamation, Earth Observation & Surveying, Environmental Engineering. Vol. XII, 2023
Print ISSN 2285-6064, CD-ROM ISSN 2285-6072, Online ISSN 2393-5138, ISSN-L 2285-6064

THE INFLUENCE OF FORESTS FROM LUNCA MUREŞULUI NATURAL PARK ON GREENHOUSE GASES LEVELS

Nicolae CADAR[1], Diana PITAR[2], Carmen IACOBAN[3], Ilie-Cosmin CÂNTAR[1]

[1]"Marin Dracea" National Research and Development Institute in Forestry, Timisoara Reserach Station, 8 Padurea Verde Street, Timisoara, Romania
[2]"Marin Dracea" National Research and Development Institute in Forestry, Simeria Research Station, 1 Biscaria Street, Simeria, Romania
[3]"Marin Dracea" National Research and Development Institute in Forestry, Campulung Moldovenesc Research Station, 73BIS Calea Bucovinei, Campulung Modovenesc, Romania

Corresponding author email: nicu_cadar@yahoo.com

Abstract

The paper aims to analyze the influence of the stand characteristics in two areas of the Lunca Mureşului Natural Park, on the main greenhouse gases in the atmosphere (O_3, NH_3, NO_2). In the first part, an extensive bibliographic study was carried out, regarding similar research referring to greenhouse gases in generally and O_3, NH_3 and NO_2 in specially, and the relation of these greenhouse gases to forest vegetation. The working method regarding data collection in the period 2014-2019, the types of gases analyzed, the types of collection pads used, the exposure times of the collection pads were presented, together with the working method for data processing. The results were obtained by analyzing relation of certain characteristics of the stand (age, volume, stand density) with concentration of studied greenhouse gases on vegetation season from the period 2014-2019. The obtained results were discussed in the context of other current research in the field and the most important aspects were presented as conclusions at the end of the paper.

Key words*: atmosphere, stand composition, forest age, height of trees.*

INTRODUCTION

Atmospheric emissions of greenhouse gases have increased dramatically in recent decades, compared to the last century, due to technological development (George et al., 2021). This leads to climate change and global warming, which affects people's living standard (Jeffry et al., 2021). The greenhouse effect has two aspects: the main effect that has existed for thousands of years and gives the planet Earth its hospitable temperature, and the secondary effect that has existed for only 250-300 years and is caused by the increase in the concentration of greenhouse gases (Tucket et al., 2019).

Ozone is the air pollutant of major concern for forests and is also recognized as a significant greenhouse gas. Current O_3 levels in the Northern Hemisphere have increased approximately 2-4.5 times since pre-industrial times (Paoletti, 2008). Currently, tropospheric ozone (O_3) is the third most important greenhouse gas after carbon dioxide (CO_2). (Ehhalt, 2001). Ozone (O_3) together with infrared active gases (IR) - mainly water vapor, naturally present in the atmosphere, they absorb the radiation, the atmosphere being heated by this mechanism. (Ledlez et al., 1999).

At the global scale, NH_3 (ammonia) and their deposition on vegetation is considered the most important, among all N (nitrogen) gases in the atmosphere (Krupa, 2003). Among others, agriculture is a significant contributor to emissions of NH_3 in the atmosphere (Duxbury 1994). NH_3 can contribute to the formation of atmospheric aerosols, particles that decrease the amount of light available for plant photosynthesis (Templer et al., 2012).

Nitrogen dioxide (NO_2) is a concern pollutant in the urban areas, related to fossil fuel burning, including transportation, generation of electricity and residential and industrial activities (Restrepo, 2021). Although NO_2 is not actually a greenhouse gas, it is in fact a precursor for formation of a greenhouse gas - tropospheric ozone (Paraschiv et al., 2020).

Forests and woodlands represent a substantial stock of carbon that is contained in soil, trees

and other vegetation (Morison et al., 2012). Management of forests for mitigation of greenhouse gas emissions assumed conservation management options as slowing deforestation, protection and conservation of forests (Brown, 2012).

Relevant changes of the balance of greenhouse gases in the forest sector are related to forest management. To have a sink of carbon, increment of wood need to exceed harvested timber volume (Baritz and Strich, 2000), but it needs to be considered that mechanized operations on forest harvesting activities are sources of greenhouse gas emissions (Berg and Karjalainen, 2003).

The paper aims to analyse the relation between some stand characteristics in two areas of the Lunca Mureşului Natural Park, and the content of some greenhouse gases in the atmosphere (O_3, NH_3, NO_2).

MATERIALS AND METHODS

This paper analyzes the relation of stand characteristics of forest and greenhouse gases from Lunca Mureşului National Park on two points in the vicinity of forest administrated by Iuliu Moldovan Forest department (Figure 1):

- Point A - Bezdin: located in U.P. (production unit) I, near management units 54A, 54B, 54C, 54D, 54E, 54F, 54G, 54H, 55A, 55B, 55C, 55D, 55E, 55F - close to Munar village, Secusigiu community;
- Point B - Ceala: located in U.P. V, near management units 18A, 18B, 18C, 18D, 18E, 18F, 18G, 18H, 18I, 18 J, 18K, 21A, 21B, 21C, 21D, 21E - close to Arad municipality.

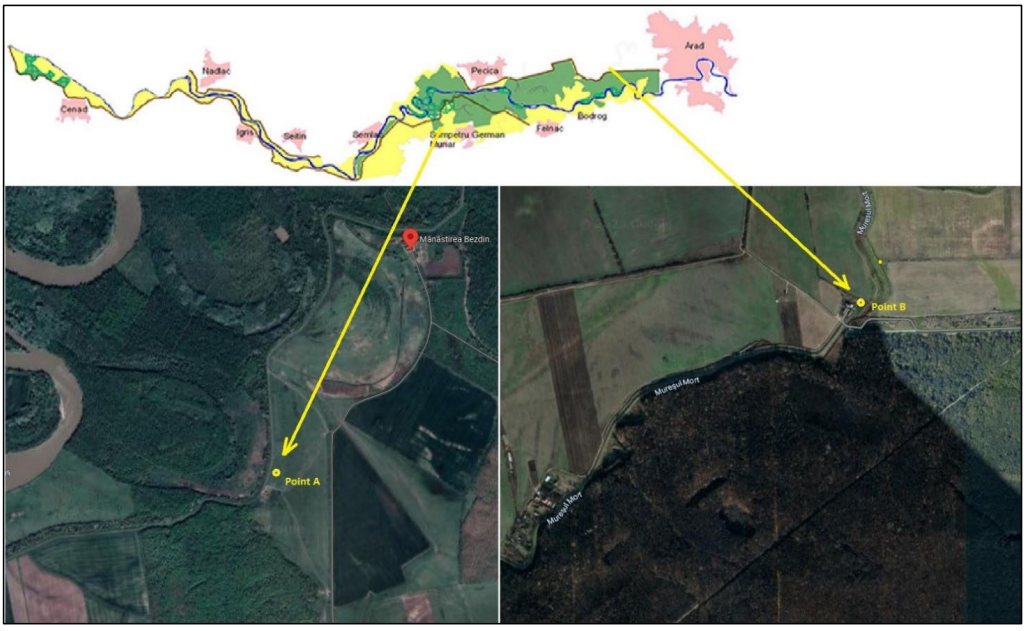

Figure 1. Location of Point A and B where greenhouse gases concentration was measured (Google Maps)

In the above-mentioned points, O_3, NH_3 and NO_2 concentration was measured using passive samplers (Ogawa & CO): O_3 (PS-114), NH_3 (PS-154), NO_2 (PS-134) monthly exposed in the field, in the vegetative season, in the period July 2014 - September 2019. Each month measurement was duplicated in the field, results of the monthly analyses being obtained by the average of the results for the two duplicates samples. For each year, result of O_3, NH_3 and NO_2 analyses was obtained using the average for the entire sample period on the year.

The concentrations of the greenhouse gases mentioned above and captured in the passive samplers during the specified period, were determined in the chemistry laboratory of INCDS "Marin Dracea" - Câmpulung Moldovenesc Research Station. Results of

analyses for the ozone, ammonia and nitrogen dioxide concentrations were expressed in parts per billion (ppb).

Management units considered in this study, from vicinity of A and B points (Figure 1) are the closest forest area delimited by parcel lines, being part of Bezdin and respectively Ceala forest. Based on a bibliographic data, stand characteristics were analysed using data from management plan of production units 1 and 5 from Iuliu Moldovan Forest department, namely data corresponding for management units from vicinity of point A and B - greenhouse gases passive sampler location. For each stand, elements from each management unit, and the following stand characteristics were considered for analyses: age, species, diameter, height, stand density, volume.

The relationship between the above mentioned characteristics and the concentration of O_3, NH_3 and NO_2 was studied in the period 2014-2019.

RESULTS AND DISCUSSIONS

The determinations expressed in ppb regarding the concentrations of O_3, NH_3 and NO_2 in the Bezdin and Ceala locations were made by analyzing the passive samplers exposed monthly in these locations (Figure 1). The results of the analysis, summarized by each analyzed period, and standard deviation for the analyzed samples, are shown for Point A - Bezdin in Table 1.

Table 1. O_3, NH_3 and NO_2 content on collection pads exposed on Point A - Bezdin

Analysed period (month, year)	O_3 content (ppb)	Standard deviation (%)	NH_3 content (ppb)	Standard deviation (%)	NO_2 content (ppb)	Standard deviation (%)
Jul. 2014	33.38	2.20	1.87	4.42	1.46	0.36
Aug. 2014	38.48	5.79	1.82	1.23	1.85	6.45
Sept. 2014	28.15	0.83	1.26	4.85	0.26	5.47
Apr. 2015	29.55	0.00	2.16	5.04	1.39	0.12
May 2015	42.71	0.00	3.09	11.12	1.91	3.13
Jun. 2015	38.94	0.00	3.19	0.90	1.83	3.98
Jul. 2015	31.46	0.12	3.86	0.14	1.25	0.13
Aug. 2015	43.54	0.14	3.05	2.01	1.82	2.31
Sept. 2015	37.74	0.30	5.25	0.14	2.80	0.17
Apr. 2016	39.17	1.87	2.13	6.98	1.57	1.68
May. 2016	40.59	3.53	1.98	1.97	1.24	3.12
Jun. 2016	38.39	0.53	2.89	1.42	1.12	4.86
Jul. 2016	36.69	5.22	2.54	3.55	1.35	2.46
Aug. 2016	31.64	30.11	3.52	0.97	1.77	5.84
Sept. 2016	23.36	5.22	11.20	14.45	1.97	9.07
Apr. 2017	35.18	2.18	3.10	8.49	1.81	15.03
May. 2017	30.73	0.54	4.03	10.08	1.23	0.54
Jun. 2017	44.44	1.28	2.66	0.20	1.64	1.55
Jul. 2017	22.45	2.08	3.87	0.36	1.39	11.16
Aug. 2017	26.51	0.99	2.23	14.76	1.67	0.00
Sept. 2017	26.86	1.90	4.11	5.70	3.62	1.60
Apr. 2018	40.66	1.97	2.43	8.51	1.62	78.61
May 2018	37.34	1.61	2.12	7.23	2.18	77.42
Jun. 2018	33.13	3.32	2.73	0.91	1.86	71.02
Jul. 2018	33.96	0.66	2.10	8.99	1.95	87.81
Aug. 2018	35.19	0.38	2.31	4.17	2.48	40.69
Sept. 2018	28.91	1.03	3.16	5.52	2.53	38.40
Oct. 2018	25.55	1.71	2.23	2.06	3.16	5.67
Apr. 2019*	-	-	5.13	1.85	2.10	0.14
May 2019	23.99	5.41	2.30	13.63	6.66	0.90
Jun.2019	28.90	0.77	4.72	0.65	1.31	12.32
Jul. 2019	23.61	0.76	3.31	4.33	1.22	1.88
Aug. 2019*	-	-	1.30	7.04	1.79	0.95
Sept. 2019	20.65	2.07	0.12	11.69	1.98	0.84

*Data are missing due to filter contamination

For Point B - Ceala, the results of greenhouse gases analyses in vegetation seasons from the period July 2014 - September 2019 are shown on Table 2.

Table 2. O_3, NH_3 and NO_2 content on collection pads exposed on Point B - Ceala

Analysed period (month, year)	O_3 content (ppb)	Standard deviation (%)	NH_3 content (ppb)	Standard deviation (%)	NO_2 content (ppb)	Standard deviation (%)
Jul. 2014	33.16	1.89	3.81	1.27	1.90	2.15
Aug. 2014	36.56	7.04	3.15	0.46	2.61	4.20
Sept. 2014	30.37	1.40	3.01	2.44	3.05	4.73
Apr. 2015	30.72	0.00	3.79	0.12	2.09	2.52
May 2015	43.20	0.00	6.50	1.38	2.96	2.24
Jun. 2015	40.95	0.00	5.12	1.17	2.25	0.29
Jul. 2015	30.75	0.13	4.12	0.15	1.87	6.35
Aug. 2015	47.18	0.13	3.98	0.40	2.81	0.19
Sept. 2015	40.88	0.28	3.19	1.74	3.82	3.24
Apr. 2016	39.34	2.46	3.13	0.04	2.49	0.17
May 2016	40.30	2.11	3.61	2.96	2.27	4.54
Jun. 2016	41.12	2.71	5.54	9.23	2.20	6.18
Jul. 2016	38.17	3.19	5.77	6.20	2.76	0.63
Aug. 2016	51.66	21.39	6.32	0.12	2.75	7.79
Sept. 2016	24.05	7.03	6.26	0.46	2.93	0.57
Apr. 2017	32.19	4.98	4.62	0.36	3.02	0.20
May 2017	31.78	9.00	5.09	2.04	1.99	0.09
Jun. 2017	47.86	3.88	6.37	8.79	2.91	0.06
Jul. 2017	24.13	3.22	6.06	9.80	2.32	0.38
Aug. 2017*	-	-	-	-	2.71	0.30
Sept. 2017*	-	-	-	-	3.85	0.57
Apr. 2018	38.37	5.24	3.88	3.94	3.02	0.45
May 2018	36.07	2.13	5.01	12.30	3.34	1.88
Jun. 2018	28.09	1.02	8.85	0.82	1.98	1.50
Jul. 2018	31.12	0.04	4.12	1.42	2.88	0.47
Aug. 2018	35.03	2.14	3.41	8.11	3.82	0.31
Sept. 2018	27.67	1.13	3.76	5.67	4.71	1.89
Oct. 2018	23.41	3.42	4.20	4.19	4.96	2.17
Apr. 2019*	-	-	5.92	4.17	2.76	1.59
May. 2019	25.04	0.56	6.24	1.77	1.82	1.76
Jun. 2019	24.82	9.34	11.10	0.52	2.36	4.21
Jul. 2019	22.94	0.49	7.90	5.95	2.35	5.54
Aug. 2019	30.75	1.79	9.45	0.32	3.20	0.14
Sept. 2019	19.02	4.28	4.26	2.71	3.07	1.80

*Data are missing due to filter contamination

As it can be seen in Figure 2, O_3 concentration is similar for the entire period between the two analyzed points, showing that between the two points from the vicinity of stands with different characteristics there are not differences on O_3 concentration. This fact leads to the hypothesis that the different characteristics of the stand, such as the age and the volume of woody mass, do not lead to differences in terms of the O_3 concentration in the immediate vicinity.

Regarding NH_3 it can be observed a higher concentration in Point B – Ceala in the majority of analyzed periods (Figure 2). The same situation can be observed also in the case of NO_2 where in almost all the analyzed periods the concentration of this greenhouse gases is higher in the Point B - Ceala compared to Point A - Bezdin (Figure 2).

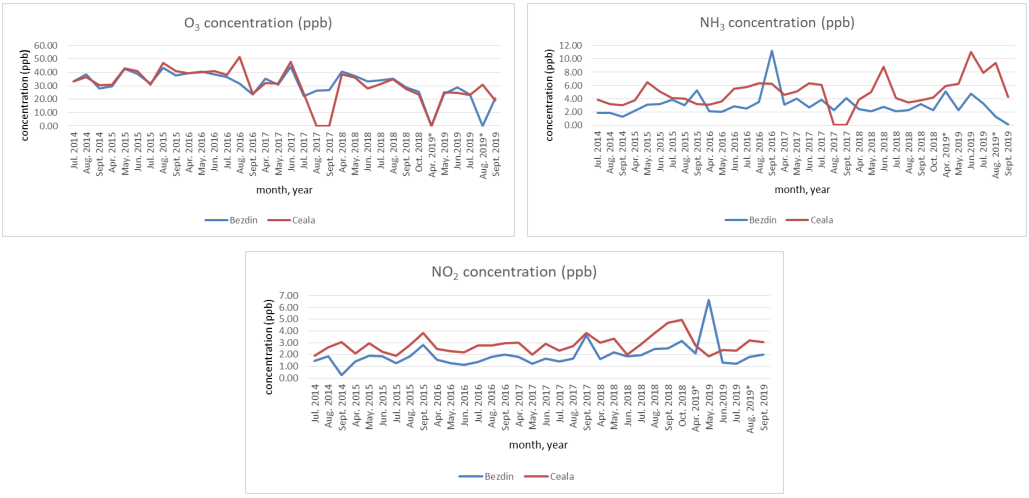

Figure 2. Greenhouse gases (O_3, NH_3, NO_2) concentration in Point A - Bezdin (blue) and Point B - Ceala (red)

The two forests from vicinity of greenhouse gases sample points are similar in terms of specific composition, the main forest species being Pedunculate oak, Turkey oak, European ash, Field maple, Poplar.

In terms of age, the forest from vicinity of Point B - Ceala is older than the forest from vicinity of Point A - Bezdin. Also, the younger forest (Bezdin) has a greater stand density in comparison to the older (Table 3).

Table 3. Stand characteristics in the vicinity of Point A - Bezdin and Point B - Ceala, where analyzed greenhouse gases has been gathered

Monitoring point	UP, management unit	Age (years)	Stand density (%)	Volume per ha (m^3)	Monitoring point	UP, management unit	Age (years)	Stand density (%)	Volume per ha (m^3)
A - Bezdin	I, 54A	35	90	229	B - Ceala	V, 18A	80	70	244
	I, 54B	5	50	1		V, 18B	80	70	266
	I, 54C	25	90	151		V, 18C	25	60	107
	I, 54D	30	90	189		V, 18D	60	70	195
	I, 54E	35	90	210		V, 18E	80	70	244
	I, 54F	20	80	51		V, 18F	20	90	68
	I, 54G	25	80	81		V, 18G	80	70	250
	I, 54H	15	80	45		V, 18H	10	60	2
	I, 55A	35	80	217		V, 18I	80	80	280
	I, 55B	70	80	463		V, 18J	5	70	1
	I, 55C	10	90	46		V, 18K	5	60	1
	I, 55D	20	80	64		V, 21A	70	80	269
	I, 55E	10	90	33		V, 21B	20	100	105
	I, 54F	20	80	64		V, 21C	60	70	181
Total/ Average		**25**	**80**	**132**		V, 21D	5	60	1
						V, 21E	80	70	307
					Total/ Average		**48**	**72**	**158**

As it can be seen, in term of stand age, forest from the vicinity of point A – Bezdin have an average of 25 years old, being younger than the others which have an average age of 48 years (Table 3, Figure 3).

In terms of stand density and volume per ha, relations between the two areas are shown a higher stand density for the youngest forest and a higher volume for the older one.

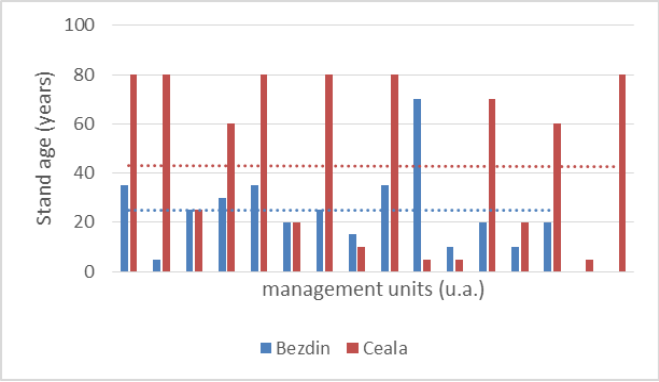

Figure 3. Stand age on the management units from the vicinity of points where analyzed greenhouse gases has been gathered

Based on Figure 2, Table 3 and Figure 3, we can observe similarities between NH_3 and NO_2 greenhouse gases concentration and forest age. Concentration of these greenhouse gases is higher on areas where forest age is higher. This fact shows that the low age of the stands and the increased growth capacity could lead to the reduction of these greenhouse gases.

Regarding stand density, it can be observed that high density of the youngest forest area (Bezdin) can lead to a reduction of NH_3 and NO_2 greenhouse gases concentration. High NH_3 losses from soil are possible in condition of high temperature, forest floor and soil with pH between 5 and 6 and air steadily moving on the soil surface (Watkins et al., 1972). High stand density can contribute to temperature reduction and reduction of air circulation and by these mechanisms, NH_3 from the atmosphere are reduced.

The contribution of high stand density to NO_2 reduction is also confirmed by other studies that show that Absorption of NO_2 into plant leaves contribute to improving urban air quality (Yli-Pelkonen et al., 2020).

CONCLUSIONS

There are not differences on O_3 concentration regardless the differences between age, stand density and volume per ha between the two areas from the vicinity of greenhouse gases gathering points.

Similarities between NH_3 and NO_2 greenhouse gases concentration and forest age, have been observed, concentration of these greenhouse gases being higher on areas where forest age is higher.

Low age of the stands and an increased growth capacity of stand could lead to the reduction of NH_3 and NO_2 on the atmosphere.

High stand density can lead also to a reduction of NH_3 and NO_2 greenhouse gases concentration.

ACKNOWLEDGEMENTS

This paper was carried out with the support of the Ministry of Research, Innovation and Digitization (MCID), through "Programul 1 - Dezvoltarea sistemului naţional de cercetare - dezvoltare, Subprogram 1.2 - Performanţă instituţională - Proiecte de finanţare a excelenţei în CDI" - project "Creșterea capacității și performanței instituționale a INCDS "Marin Drăcea") în activitatea de CDI -CresPerfInst" (Contract no. 34PFE./30.12.2021) and Nucleu BIOSERV Programme (Ctr. 12N/2019), project PN19070101.

REFERENCES

Baritz, R., Strich, S. (2000). Forests and the national greenhouse gas inventory of Germany. COST E21 Workshop. Contribution of forests and forestry to mitigate greenhouse effects. Joensuu (Finland). 28-30 Sep 2000. *Biotechnologie, Agronomie, Société et Environnement, 4.*

Berg, S., Karjalainen, T. (2003). Comparison of greenhouse gas emissions from forest operations in Finland and Sweden. *Forestry, 76*(3), 271-284.

Brown, S. (1996). *Management of forests for mitigation of greenhouse gas emissions*. pp. 773-797. ISBN 0521564379.

Duxbury, J.M. (1994). The significance of agricultural sources of greenhouse gases. *Fertilizer research, 38,* 151-163.

Ehhalt, D., Prather, M., Dentener, F., Derwent, R., Dlugokencky, E., Holland, E., Isaksen, I., Katima, J., Kirchhoff, V., Matson, P., Midgley, P., Wang, M. (2001). *Atmospheric chemistry and greenhouse gases*. pp. 239-288. Cambridge University Press. ISBN 9780521807678.

George, A., Shen, B., Craven, M., Wang, Y., Kang, D., Wu, C., Tu, X. (2021). A Review of Non-Thermal Plasma Technology: A novel solution for CO_2 conversion and utilization. *Renewable and Sustainable Energy Reviews, 135,* 109702.

Jeffry, L., Ong, M.Y., Nomanbhay, S., Mofijur, M., Mubashir, M., Show, P.L. (2021). Greenhouse gases utilization: A review. *Fuel, 301*, 121017.

Krupa, S.V. (2003). Effects of atmospheric ammonia (NH_3) on terrestrial vegetation: a review. *Environmental pollution, 124*(2), 179-221.

Ledley, T.S., Sundquist, E.T., Schwartz, S.E., Hall, D.K., Fellows, J.D., Killeen, T. L. (1999). Climate change and greenhouse gases. Eos, *Transactions American Geophysical Union, 80*(39), 453-458.

Morison, J., Matthews, R., Miller, G., Perks, M., Randle, T., Vanguelova, E., White, M., Yamulki, S. (2012). Understanding the carbon and greenhouse gas balance of forests in Britain. Research Report-Forestry Commission, UK, (018).

Paoletti, E. (2008). Ozone impacts on forests. Cabi Reviews: Perspectives in agriculture, veterinary science. *Nutrition and Natural Resources, 2.*

Paraschiv, S., Barbuta-Misu, N., Paraschiv, S.L. (2020). Influence of NO_2, NO and meteorological conditions on the tropospheric O_3 concentration at an industrial station. *Energy Reports, 6*, 231-236.

Restrepo, C.E. (2021). Nitrogen dioxide, greenhouse gas emissions and transportation in urban areas: lessons from the Covid-19 pandemic. *Frontiers in Environmental Science, 9*, 689985.

Templer, P.H., Pinder, R.W., Goodale, C.L. (2012). Effects of nitrogen deposition on greenhouse-gas fluxes for forests and grasslands of North America. *Frontiers in Ecology and the Environment, 10*(10), 547-553.

Tuckett, R. (2019). Greenhouse gases. In Encyclopedia of Analytical Science, 362-372. Elsevier.

Watkins, S.H., Strand, R.F., DeBell, D.S., Esch Jr.J. (1972). Factors influencing ammonia losses from urea applied to northwestern forest soils. *Soil Science Society of America Journal*, *36*(*2*), 354-357.

Yli-Pelkonen, V., Viippola, V., Kotze, D.J., & Setälä, H. (2020). Impacts of urban roadside forest patches on NO_2 concentrations. *Atmospheric environment*, *232*, 117584.

***Google Maps – https://maps.google.ro.

***Parcul Natural Lunca Mureşului - https://luncamuresului.ro

Scientific Papers. Series E. Land Reclamation, Earth Observation & Surveying, Environmental Engineering. Vol. XII, 2023
Print ISSN 2285-6064, CD-ROM ISSN 2285-6072, Online ISSN 2393-5138, ISSN-L 2285-6064

COMPLEX ORGANO-MINERAL FERTILIZERS BASED ON SEWAGE SLUDGE WITH MINERAL ADDITIVES AND THEIR EFFECTIVENESS IN GROWING CORN FOR SILAGE IN THE FODDER CROP ROTATION CHAIN IN THE NORTHERN FOREST-STEPPE OF UKRAINE

Vitaliy DYSHLYUK

National Scientific Center "Institute for Soil Science and Agrochemistry Research named after O.N. Sokolovsky", 4 Chaikovska Street, Kharkiv, Ukraine

Corresponding author email: dyshlyuk_ve@ukr.net

Abstract

It was determined that the sewage sludges of the sewage treatment facilities of a million-plus city and the industrial center in the north of Ukraine, after the final aging on sludge sites, according to agroecological indicators, are suitable for their use as a local organic raw material to produce innovative types of complex organo-mineral fertilizers. The composition of complex organo-mineral fertilizers based on sewage sludge with mineral additives of various origins was developed and new types of organo-mineral fertilizers of prolonged action for multi-purpose use were obtained. When studying the effectiveness of new types of organo-mineral fertilizers in a field experiment, it was established that on gray forest soil under the conditions of the northern Forest-Steppe of Ukraine, fertilizers of the first type were not inferior to traditional and non-traditional organic fertilizers in terms of effectiveness in the year of direct action when the main application was made in optimal doses under corn for silage and complete mineral fertilizer in equivalent doses. New organo-mineral fertilizers of the second type were not inferior to organic fertilizers in terms of direct-action efficiency.

Key words: *effectiveness, organic-mineral, mineral additives, sewage sludge; Ukraine.*

INTRODUCTION

At the present time, a serious problem in megacities, large cities and industrial centers is the rational disposal of sewage sludge (hereinafter - SWS) of municipal sewage treatment plants.

Among the organic wastes, SWS of sewage treatment facilities (hereinafter - SWTF) of these cities, belongs to a special category, it is contaminated with toxic substances and harmful microorganisms and therefore is mostly not suitable for direct use as non-traditional organic fertilizers in agriculture.

The main volumes of such SWS after technological treatment at the SWTF as a waste of IY–Y hazard classes (low-toxic substances) are placed at waste storage facilities (GOST 12.1.007-76).

Storage of SWS in sludge storage facilities is a dangerous method of its disposal and causes significant economic and ecological losses for society due to environmental degradation, violation of the natural state of large areas, loss of useful substances, negative impact on the health of the population (Dregulo et al., 2012; Ospanov et al., 2014; Nasirov et al., 2015).

At the current rates of urbanization and agglomeration and the lack of innovative methods of final disposal of SWS, there is a threat of significant accumulation of these multi-tonnage organic wastes and catastrophic environmental pollution.

Some scientists believe (Merzla, 2006) that it is possible to stabilize the situation with the final disposal of SWS only by implementing new technologies for wastewater treatment, sediment treatment and processing them into complex organic-mineral fertilizers of the new generation (hereinafter - OMF), which will ensure a decrease in energy consumption and a sharp reduction of land areas for the arrangement of storage facilities for the disposal of SWS.

At the same time, in connection with the low efficiency and danger of the assortment of mineral tuks, the urgency of creating a new generation of OMF with increased agroecological value and efficiency is increasing.

The work (Melnikov, 2007) proposed a concept that substantiates the need to revise the existing fertilizer policy in favor of the production and use of ecologically safe organic, organo-mineral fertilizers using for this purpose mineral-raw resources, waste, and substances of humus nature. Agricultural scientists predict (Bambalov et al., 2020) that in the XXI century, there will inevitably be a gradual replacement of fast-dissolving forms of mineral fertilizers by fertilizers with a prolonged effect, including OMF, and in the second half of the century, fertilizers with a programmed release of nutrients will become the dominant forms.

In the literature (Doroshkevich et al., 2002; Stepanova et al., 2003; Pyndak et al., 2010) there are data on the creation of new complex OMF based on the SWS of large cities and industrial centers of the Russian Federation (Volgograd, Ulan-Ude, Orla) with mineral additives (mineral tuks, natural sorbents - zeolites, glauconites, etc.).

In Ukraine, technology and a technological line for the production of organo-mineral mixtures (hereinafter - OMM) have been developed on the basis of SWS of large cities (Zaporizhia, Dnipropetrovsk) with industrial waste-lignin and phosphogypsum (Shevchuk et al., 2001). New complex OMF were created on the basis of the SWS of the megacityand municipal solid waste (Malyuga et al., 2005), as well as on the basis of the SWS of the megacity with mineral additives (mineral tuks, natural sorbents - agroperlite, expanded vermiculite) (Patents, 2017; Dyshlyuk, 2022) and others. New types of OMF have higher agronomic, ecological, energy and economic efficiency indicators than standard complex mineral fertilizers, which indicates the prospects of using man-made organic raw materials for the production of new generation of fertilizers.

In Ukraine, the problem of the final disposal of accumulated SWS in cities with a population of more than 1 million inhabitants, primarily in the capital, industrial centers, etc., has not been solved. bridge. For more than 30 years, there has been an acute problem of disposing of the accumulated SWS of the million-plus city in the north of Ukraine (hereafter - the megalopolis), which threatens the country's largest city with an ecological disaster, as well as all the settlements adjacent to the Dnipro. Every day, 3,000 tons of liquid SWS are produced at the city's SWTF, which are placed on sludge sites (area 272 hectares). Their capacity has already exceeded three times - instead of the 3.5 million tons provided, they hold 10 million tons of SWS (dry matter - hereinafter DM).In 2013, there was a breach of the dam, but then it was possible to prevent an environmental disaster that could have occurred due to the spill of liquid sewage into the Dnipro (Bortnytsky Aeration Station Problem..., 2018). The problem of utilization of the accumulated SWS of the megacity is one of the important environmental tasks that requires an immediate solution.

The goal of the work:

- to study the quality indicators of the SWS of a megacity in the north of Ukraine and to find out the feasibility of using them as a local organic raw material for the production of a new generation of OMF;
- to create new OMF for use in agriculture on the basis of the SWS of the megacity;
- to evaluate the effectiveness of new OMF based on the specified SWS in the year of their direct action on soils of the eluvial type of soil formation.

MATERIALS AND METHODS

The object of the study: megacity SWS of the long-term storage, formed under the conditions of technogenesis in the pre-crisis period.

The study of the effectiveness of non-traditional organic fertilizers (SWS) and their processing products (new OMF) was carried out in a temporary field experiment located at the experimental site of the State Institution "Central Scientific Research Laboratory of Water and Soil Quality" of the Institute of Water Problems and Land Reclamation of the National Academy of Sciences, in the conditions of the northern Forest-steppe of Ukraine.

The experiment studied the effectiveness of the direct action of non-traditional organic fertilizers in the form of SWS at different rates of their application per unit area of arable land (in a dose of N_{total}, equivalent to 220 and 300 kg/ha), of the above-mentioned fertilizers in combination with mineral fertilizers (respectively in a dose of N_{total}, equivalent to

150 kg/ha + $P_{90}K_{90}$) to balance the ratio of the main nutrients in the soil, processing products of SWS - 4 types of experimental fertilizer composites (OMM), in particular, mixtures of the first type, which are based on the organic matter of anthropogenic origin (SWS) and mineral fats and natural sorbents (OMM 1 and 2 in a dose, equivalent to $N_{150}P_{90}K_9$) and, accordingly, the second type, which is based on SWS and only mineral additives (natural sorbents) (OMM 3 and 4 in a dose of N_{total}, equivalent to 150 kg/ha).

The rates of application of the studied substrates into the soil were established based on the content of total nitrogen in them. The following plots of the experiment were accepted as control options: without fertilizer (control 1), with the application of traditional organic fertilizer (cattle manure) (in a dose of N_{total}, equivalent to 150 kg/ha) (control 2) and complete mineral fertilizer (in a dose N_{150} P_{90} K_{90}) (control 3).

Experiment scheme:

1 - without fertilizers (control 1);

2 - SWS in a dose of N_{total} 300 kg/ha;

3 - SWS in a dose of N_{total} 220 kg/ha;

4 - SWS in a dose of N_{total} 150 kg/ha + $P_{90}K_{90}$;

5 - Cattle manure in a dose of N_{total} 150 kg/ha (control 2);

6 - Complete mineral fertilizer in a doseN_{150} P_{90} K_{90} (control 3);

7 - OMM 1 based on the dose $N_{150}P_{90}K_{90}$;

8 - OMM 2 based on the dose $N_{150}P_{90}K_{90}$;

9 - OMM 3 based on the dose on $N_{tot.}$ 150 kg/ha;

10 - OMM 4 based on the dose on $N_{tot.}$ 150 kg/ha.

The following fertilizers were used in the experiment: semi-rotted cattle litter manure, SWS of long-term storage (8-10 years), mineral fertilizers: nitrogen (ammonium nitrate), phosphoric (simple superphosphate) and potash (potassium-magnesium), 4 types of new fertilizer mixtures: OMM 1 (SWS + mineral tuks (nitrogen, phosphorus, potassium) + natural sorbent (agro perlite), OMM 2 (SWS + mineral tuks (nitrogen, phosphorus, potassium) + natural sorbent (vermiculite), OMM 3 (SWS + natural sorbent (agro perlite), OMM 4 (SWS + natural sorbent (vermiculite).

The experimental group of OMM was obtained by mixing the specified components in certain ratios and the subsequent physical and physicochemical interaction of activated organic matter and the elemental composition of SWS with mineral components. Protection documents from Ukraine were obtained for the method of production of OMM based on SWS with mineral additives (Patents, 2017).

The study of the effectiveness of fertilizers and the rates of their application was carried out in the chain of fodder crop rotation: corn for silage - winter wheat - annual grasses. The area of the sown plot is 10.8 square meters (3.6 m x 3.0 m). The location of options is single-tiered, and the repetition of options is four times with randomized placement of plots.

Agrotechnics of growing crops is zonal, with the exception of the studied factors. Fertilizers were applied to the soil in one application in a continuous way (scattered) under the main tillage for the first crop of the crop rotation chain - maize for silage (hybrid Kolektivny 205). The soil of the research area is gray forest light loam. When establishing the experiment and conducting research, generally accepted methods were used. Soil samples for research were taken from the 0-20 cm layer in the spring and at the end of the growing season. Agrochemical, physicochemical, and ecological-toxicological parameters were determined in the samples of cattle manure, SWS, and OMM 1-4 according to regulatory documents.

The assessment of the degree of contamination of SWS and OMV 1-4 with toxicants was carried out according to DSTU (2013), the level of provision of soil with microelements according to the Methodological Guidelines (1976), the level of soil contamination with toxicants and the suitability of plant products for feeding farm animals on the content of heavy metals according to Departmental Regulatory Documents (1999).

This report presents the results of research on establishing the effectiveness of OMM 1-4 in a year of a direct action of fertilizers in a field of corn on silage.

RESULTS AND DISCUSSIONS

It has been established that SWS of long-term storage is characterized by sufficiently high fertilizing properties. Their composition

contains a high content of total nitrogen and phosphorus, but the content of potassium is insignificant.

Among the mobile nutrient forms, P_2O_5 (0.35% per DM) prevails in SWS, the content of mineral forms of nitrogen (N-NH_4+ N-NO_3) is 0.21% per DM, K_2O is contained in an insignificant amount (0.02% per DM). The agrochemical indicators of SWS meet the requirements of the regulatory document (DSTU, 2013) (Table 1).

Table 1. Agrochemical composition of SWS (average data)

Indicators	Content[1]	Norm[2]
Mass fraction of dry matter	50.94	-
Mass fraction of organic matter	39.30	not>40
Mass fraction of total carbon, C total	19.12	-
Mass fraction of total nitrogen, N	2.84	not>1.5
Mass fraction of total phosphorus, P_2O_5	4.90	not>0.7
Mass fraction of total potassium, K_2O	0.29	-
pH_{H2O}	6.5	6.5-7.5
Correlation C: N	8.2	-

1 - in % per DM
2 - norms of agrochemical indicators of SWS according to DSTU 7369.

SWS is characterized by a high content of total carbon (19% per year). The SWS has a narrower C:N ratio (8 units vs. 12 in cattle manure) and a higher total nitrogen content (2.84% vs. 2.16% in cattle manure), which indicates a higher fertilizing effect of SWS than cattle manure.

SWSis characterized by high remedial indicators. Thus, the content of water-soluble calcium in SWS varies between 17.00 and 25.44 meq/100 g of substrate (compared to 1.02 meq/100 g in cattle manure), the Ca:Na ratio in the salt composition of SWS is 75-77 units, (in cattle manure - 0.5 units). SWS contains a significant amount of organic matter (39% per DM).

The carbon content of humic acids in the composition of organic matter of SWS prevails over the carbon content of fulvic acids (respectively, 1.58% versus 0.93% per DM). The type of humus formation in SWS is fulvate-humate. In the granulometric composition of the SWS, the content of physical clay is in the range of 38-48%, including silt (coarse and fine) and colloids - 23-29%. The number of fractions with a particle size > 0.05 mm (fine, medium, and coarse sand) varies between 14 and 30%. The number of fractions participating in soil structuring as passive material (coarse, medium and fine dust) is 46-57%. According to the classification of soils according to the granulometric composition of SWS with a physical clay content of 38-48%, it can be conditionally equated to a soil characterized by medium, and heavy loam granulometric composition.

As a result of the assessment of the quality indicators of the SWS and its properties, we came to the conclusion that these wastes can be characterized as organic raw materials with a complex of agronomically valuable features. The substrate has high fertilizing and ameliorative properties (high soluble calcium content, high calcium activity), which is important for soil improvement, reducing the acidic reaction (pH of the soil - 5.3-5.6) and enriching the soil-absorbing complex with calcium. SWS can be used as a material, capable of performing the functions of a geochemical barrier in the path of toxicants. However, SWS has an unbalanced ratio of the main nutrients (N:P:K = 1:1.70:0.10), and increased concentrations of certain heavy metals (hereafter HM), which according to their systematic agriculture application may cause soil contamination by HM.

It should be noted that at the present time, newly formed SWS contains permissible values of HM in connection with the decrease in the share of industrial wastewater in the city-wide runoff, which conditions the prospects of their agricultural application (Delalio et al., 2003). Therefore, due to the indicated disadvantages of long-term storage, from an ecological point of view, it is more appropriate to use it as a local organic raw material for the production of new OMF.

New OMM 1-4 are characterized by high fertilizing properties (especially OMM 1-2), high cation exchange capacity, and prolonged action, as well as the ability to transfer mobile forms of HM into a fixed state.

OMM 1-2 differ from the original SWS by a more optimal ratio of the main nutrients (OMM 1, ratio N:P:K = 1:1.20:0.90; OMM 2, ratio N:P:K = 1:1.10:0.70), a higher content of

mobile nutrients and their longevity, a wide range of macro- and microelements, better physicochemical properties. Agrochemical indicators of OMM 1-2 generally meet the requirements of the normative document (DSTU, 2013) (Table 2).

Table 2. Agrochemical composition of OMM 1 and 2 (average data)

Indicators	OMM 1	OMM 2
	Content[1]	
Mass fraction of dry matter	75.14	71.93
Mass fraction of organic matter	34.00	34.50
Mass fraction of total nitrogen, N	4.74	4.64
Mass fraction of total phosphorus, P_2O_5	5.58	5.12
Mass fraction of total potassium, K_2O	4.18	3.14
pH_{H2O}	5.60	5.70
Correlation C: N	3.6	4.6

1 - in % per dry matter

The new OMM 3-4 differ from the original SWS by a more balanced ratio of the main nutrients (OMM 3, ratio N:P:K = 1:1.30:0.40; OMS 4, ratio N:P:K = 1:1.50:0.50), a higher content of mobile nutrient elements and their prolongation, the presence of a wide range of macro-and trace elements and better physicochemical properties, but they are inferior to OMM 1-2 in terms of the content of general and mobile forms of NPK. Agrochemical indicators of OMM 3-4 generally meet the requirements of the normative document (DSTU, 2013) (Table 3).

Table 3. Agrochemical composition of OMM 3 and 4 (average data)

Indicators	OMM 3	OMM 4
	Content[1]	
Mass fraction of dry matter	87.31	82.02
Mass fraction of organic matter	35.61	36.90
Mass fraction of total nitrogen, N	2.23	2.29
Mass fraction of total phosphorus, P_2O_5	2.88	3.44
Mass fraction of total potassium, K_2O	0.87	1.23
pH_{H2O}	6.0	6.1
Correlation C: N	8.1	7.2

1 - in % per DM

Samples of new fertilizers (OMM 1-4) have low moisture content (25-28%), which is important for saving costs for their transportation, and reduces technological costs for application to the soil and storage.

In a field experiment, we established that the main application of OMM 1-2 under corn in the fodder crop rotation chain provided an increase in plant production of standard quality in the range of 27.1-29.5 t/ha (silage mass) in the year of direct action of fertilizers compared to the control without fertilizers (yield on control - 28.5 t/ha) and in terms of efficiency were not inferior to organic fertilizers (traditional, non-traditional) and full mineral fertilizer in equivalent doses.

OMM 3-4 were inferior to OMM 1-2 in terms of efficiency, but also provided an increase in plant production within the range of 15.5-16.5 t/ha of silage mass and were not inferior to organic fertilizers in terms of efficiency.

CONCLUSIONS

New OMM 1-4 based on SWS with mineral additives are characterized by increased agrochemical and agroecological value compared to sewage sludge.

The use of 1-4 natural sorbents in the composition of OMM, thanks to their high exchange and sorption capacity, makes it possible to consider them as an effective means for optimizing the fertilizing and reclamation properties of fertilizers, reducing non-productive losses of nutrients (nitrogen) of plants, preventing toxicant contamination of plant products and environmental components.

New OMM 1-2 on the basis of SWS with mineral additives for the main application under corn for silage in the year of their direct effect was not inferior in effectiveness to complete mineral fertilizer, organic fertilizers (traditional, non-traditional) in equivalent doses.

With a science-based approach, the SWS of urbanized areas can become a constantly renewable source of local raw materials for the production of qualitatively new, highly efficient OMF.

REFERENCES

Alikbaeva, L.A., Sidorin, G.A., Lukovnikova, L.V., Ryzhkov, A.L., Fomin, F.M., Beck, A.V. (2009). Toxicity and danger of waste treatment facilities of

urbanized areas. *Kazan Medical Journal, 90.* 513-517.

Bambalov, N.N., Sokolov, G.A. (2020). A new generation of complex organo-mineral fertilizers of prolonged action. *Agriculture and crop production, 4.* 28-33.

Delalio, A., Goncharuk, V.V., Kornilovich, B.Yu., Pshinko, G.N., Spasenova, L.N., Krivoruchko, A.P. (2003). Utilization of urban sewage sludge. *Chemistry and technology of water, 25*(5), 458-464.

Departmental Regulatory Documents 33-5.5-06-99. Protection of water, soil and plant resources from contamination by heavy metals under irrigation conditions. K.: Derzhvodhosp of Ukraine. 26.

Doroshkevich, S.G., Ubugunov, L.L., Mangataev, Ts.D., Badmaev, A.B. (2002). Productivity and qualitative composition of potatoes when using organic-mineral fertilizer mixtures based on sewage sludge and zeolites. *Agrochemistry, 8,* 42-49.

Dregulo, A.M., Panova, N.E. (2012). Assessment of the negative impact of landfills for storing sediments from biological treatment facilities on the environment. *Ecology and Industry of Russia, 8,* 43-45.

Dyshlyuk, V.Ye. (2022). Efficiency of new fertilizers based on sewage sludge of urbantreatment facilities in the fodder crop rotation in the Western Forest-Steppe of Ukraine [Electronic resource]. *Scientific Papers. Series E. Land Reclamation, Earth Observation & Surveying, Environmental Engineering, XI.*, 120-125 – Access mode: https://landreclamationjournal.usamv.ro/pdf/2022/Art14.pdf

DSTU 7369:2013 Wastewater. Requirements for wastewater and its sediments for irrigation and fertilization [Valid from 2013-08-22]. K.: Ministry of Economic Development of Ukraine. 8 p. (National Standard of Ukraine).

GOST 12.1.007-76 The system of labor safety standards. Harmful substances. Classification and general safety requirements. Date of adoption: 01.01.1977. Moscow: USSR State Committee for Standards, 1977.

Malyuga, Yu.E., Tarnopilsky, Yu.B., Ustsky, I.M., Boltenkov, Yu.A., Torosov, A.S., Smolyaninov, I.I., Mostepanyuk, A.A., Degtyarev, V.V., Chekar, E.Yu., Shaporev, V.P., Zinchenko, M.G., Zhaber, M.A., Vepritsky, S.S. (2005). Ways to solve the recycling of SBW and SWS into a complex organo-mineral fertilizer: environmental and economic aspects of the problem. Ecology and human health: Sat. scientific tr. XIII *International scientific and technical conferences* (June 13-17, 2005, Alushta), 1, 765-772.

Melnikov, L.F. (2007). *Organo-mineral fertilizers. Theory and practice of their production and application.* St. Petersburg: Publishing House of the Polytechnic University, 302.

Merzlaya, G.E. Use of organic waste in agriculture (2006). *Resource-saving technologies, 10*, 21-31.

Nasyrov, I.A., Mavrin, G.V., Shaikhiev, I.G. (2015). Problems of utilization of silt sediments of treatment facilities. *Bulletin of the Kazan Technological University, 2*, 42-47.

Ospanov, K.T., Kuldeeva, E.M., Tamabaev, O.P. (2014). Assessment of the current state of treatment of sewage sludge from the aeration station in Almaty, Republic of Kazakhstan. *Water and Ecology: Problems and Solutions, 1,* 26-34.

Patent of Ukraine No. 114648 (2017). Method of production of organic-mineral fertilizer based on sewage sludge for soil cultivation / V.E. Dyshlyuk, E.G. Dehodyuk, V.L. Kurylo, L.V. Ostapchuk. *Bulletin "Industrial Property"*, 5, 5 p.

Patent of Ukraine No. 114649 (2017). Method of production of organic-mineral fertilizer based on sewage sludge for fertilizing plants of agricultural crops / V.E. Dyshlyuk, E.G. Dehodyuk, V.L. Kurylo, L.V. Ostapchuk. *Bulletin "Industrial Property"*, 5, 6 p.

Pyndak, V.I., Pomogaev, E.F., Stepkina, Yu.A. (2010). Non-traditional complex fertilizers for growing potatoes with drip irrigation. *Reclamation and water management, 3,* 29-30.

Shevchuk, V.Ya., Chebotko, K.O., Razgulyaev, V.M. (2001). *Biotechnology of obtaining organo-mineral fertilizers from secondary raw materials.* Kyiv: "Phoenix" Publishing House, 203.

Stepanova, L.P., Nozdrina, S.I. (2003). Agroecological efficiency of fertilizer properties of sewage sludge and zeolites. Ecology of the Central Black Earth Region of the Russian Federation, 1, 25-27.

The problem of the Bortnytsk aeration station needs an immediate solution at the national level [Electronic resource].// Voice of Ukraine dated February 22, 2018, No. 1390. - Access mode: http://www.golos.com.ua/article/300149.

Vazhenin, I.G. (1976). *Guidelines for agrochemical survey and mapping of soils for the content of trace elements*. M.: Publishing house of VASKHNIL, 27.

Scientific Papers. Series E. Land Reclamation, Earth Observation & Surveying, Environmental Engineering. Vol. XII, 2023
Print ISSN 2285-6064, CD-ROM ISSN 2285-6072, Online ISSN 2393-5138, ISSN-L 2285-6064

PREDICTIONS ABOUT SESSILE OAK FOREST ECOSYSTEMS FROM BANAT MOUNTAINS IN THE NEXT 80 YEARS

Vlad CRISAN[1], Lucian DINCA[1], Virgil SCARLATESCU[2], Cosmin BRAGA[1], Gruita IENASOIU[1], Carmen CRISAN[3]

[1]"Marin Dracea" National Research and Development Institute in Forestry, 13 Closca Street, Brasov, Romania
[2]"Marin Dracea" National Research and Development Institute in Forestry, Principala Street, Mihaesti, Romania
[3]"Nicolae Titulescu" College, 125 December 13th Street, Brasov, Romania

Corresponding author email: vlad_crsn@yahoo.com

Abstract

The climate impact on sessile oak ecosystems may be measured by means of the HYPE climatic software. The climatic modelling software is employed to predict future temperatures and precipitations across the studied teritory. After interpreting the data provided by the software, we can predict how forest ecosystems will be influenced by climate change in the future. Different plots across the Banat Mountain range have been studied in order to determine the future existence of oak forest ecosystems. Consequently, two simulations have been designed, leading to two different future climatic scenarios. To begin with, the first scenario there is a moderate increase in green house gases (rcp-4.5) whilst in the second scenario there is an accentuated increase (rcp-8.5). The analysis which resulted from the data processing from within all three sessile oak stands reveals the fact that the Moldova-Noua and Paltinis stands will be the most vulnerable ones and the Bocsa-Romana stand the less vulnerable one. The importance of these results is closely related to how local forest administrators can use such findings in order to apply the best management measures.

Key words*: climate change, forest ecosystems, sessile oak, Banat Mountains.*

INTRODUCTION

Intergovernmental Panel on Climate Change (IPCC) made climatic projections with increased seasonal temperatures and decreased amounts of summer rainfall in certain regions across the temperate zone (Christensen et al. 2007). There is recent scientific research in Europe in which authors studied effects of climate change on species distribution for beech (*Fagus sylvatica*) and silver fir (*Abies alba*) (Baumbach et al., 2019; Garcia-Duro et al., 2021).

For the next decades changes of temperature and precipitation patterns will reshape forest ecosystems as well as future forest management (Allen et al., 2010; Bonan, 2008; Lindner et al., 2010).

In Romania climate changes affected forest ecosystem of pines (Constandache & Dincă, 2019; Silvestru-Grigore et al., 2018; Vlad et al., 2019) and Norway spuruce (Murariu et al., 2021; Dincă et al., 2019). Beside trees (Dincă et al., 2020; Ducci et al., 2021; Kutnar et al., 2021), there is also a negative impact regarding region landscape (Fedorca et al., 2020), wildlife (Fedorca et al., 2021) or even logging (Cantar et al., 2022).

In this article we used a software "HYPE" wich is a climatic model developed by the Swedish Meteorological and Hydrologic Institute because it has a high resolution for estimating data in areas where no data are available.

The program has good results and easy in use unlike older models (Harper, 2008) wich they were generated errors (Dickinson et al., 1989) or being time consuming (Edwards, 2010).

The present research paper aims to analyze 3 sessile oak forest ecosystems which are representative for the Banat mountains regarding the future climate changes in the next 80 years. (Figure 1).

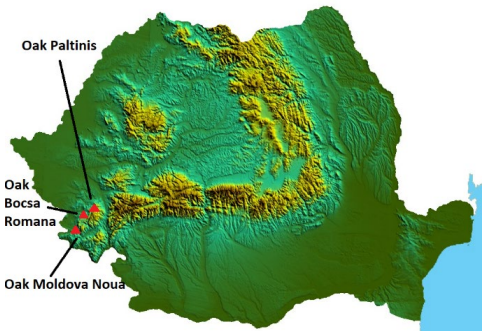

Figure 1. Location of oak plots in Banat Mountains

MATERIALS AND METHODS

The "HYPE" model and its software menus have been used in the current study with the purpose of introducing entrance parameters. Therefore the coordinates of points, the indicator type as well as the wanted climatic scenario have been introduced.

As a result, global warming is estimated to vary between 1 and 3.7°C, by means of the representative concentration pathway (RCP). Subsequently, simulations show that the database (present day 1986-2005) will be exceeded with values between 1.0 (RCP 2.6) and 3.7°C (RCP 8.5) by the end of the 21st century (Quante and Colijn, 2016).

There is a number of three scenarios that the HYPE software offers: there is a low growth in greenhouse gases ("Low - RCP 2.6"), there is a moderate growth ("Moderate - RCP 4.5") or a high growth ("High - RCP 8.5") (Figure 2).

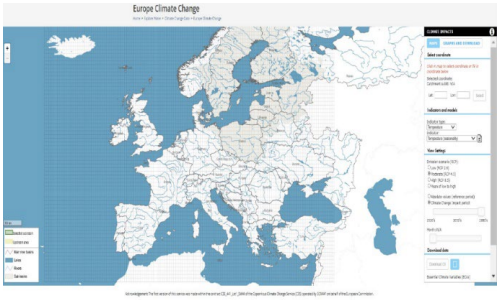

Figure 2. "HYPE" program menu

Following the choice of the scenarios, a convenient timeframe needed to be established (in our case 2100) and then we had to download the file from the "Download data" submenu.

Microsoft Excel was used to transform the obtained data into table form in order to represent monthly values. There are three sessile oak stands situated in the Banat Mountains that have been used to extract the data.

The HYPE Software belongs to a family of regional climatic models. The name REMO 2009 is related to a regional atmospheric model (REgional MOdel) which was originally developed by the Max Planck Institute for Meteorology (MPI-M) in Hamburg.

The reason for which the REMO 2009 model was chosen is because it is the most recent hydrostatic version (Jacob & Podzun, 1997; Jacob, 2001). To obtain average monthly values for the studied period (1971-2100) Microsoft Excel was used to process data.

RESULTS AND DISCUSSIONS

The results provided by the HYPE modelling program have been introduced in Microsoft Excel. The data processing shows both the mean annual precipitations and the mean annual temperatures for each stand up to the year 2100. Each scenario is represented in a graphical form: i.e. an average growth of greenhouse gasses (rcp-4.5) and a high growth of greenhouse gases (rcp-8.5). Also, there is a set of values for precipitations and for temperatures corresponding to each installed stand.

A problem that we have also faced in the analysis of the stands in the Transylvanian area (Crisan et al., 2021a; Crisan et al., 2021b) as well as in the area of the Moldavian plateau (Crisan et al., 2022) will be the productivity of the stands within the conditions of changing climatic factors.

In order to better explain the effects that these changes in climate data values have on the species and implicitly the forest ecosystems, we will refer to the ecological data sheets of the species taken from the Dendrology textbook (Șofletea and Curtum, 2008) (Table 1).

Thus, the sessile oak is not very particular about the summer heat, preferring a transitional climate from the Atlantic to the continental. It is a mesothermal, mesophytic species and its

ecological optimum in terms of precipitation is between 600-800 (850) mm/year. Sessile oak are located in the ecological optimum at the age of 100 years reach a productivity of 6 m³/year/ha (Stănescu et al., 1997 in Șofletea & Curtu, 2008).

Table 1. Ecologic card (Stănescu et al., 1997) *Quercus petraea* (Matt.) Liebl.

Ecologic factors	Values or states of ecologic factors													
	Variation of the species' biologic potential based on ecologic factors													
Average annual temperature (°C)	-2	-1	0	1	2	3	4	5	6	7	8	9	10	11
								l	s	s	o	o	o	s
Average annual precipitations (mm)	400	500	600	700	800	900	1000	1100	1200	1300	1400	1500		
		s	o	o	o	s	l	l						

where "l" represents the limit, "s" the suboptimum and "o" the optimum

The data from Table 1 represents the time period in which the annual average level of temperature and precipitation is representative for oak species. According to the future climatic scenarios there will be periods of time when the annual averages will exceed the species existence interval.

The first sessile oak stand under study in the area of the Banat Mountains is the one from Bocșa Română Forest District from Caras Severin County. It can thus be seen in Figure 3 the arrangement of the trees inside the sample surface.

Even if the basic species in this area is the sessile oak that forms the floor of the dominant and codominant trees, the existence of a sub-floor of vegetation corresponding to the trees and shrubs of several species can be observed as well. In this case, the hornbeam has a fairly consistent presence of approximately 34% (Figure 4) and this can give us an indication of how the composition of this forest ecosystem could evolve in increasingly limiting climatic conditions for the existence of the main species, namely the sessile oak.

Also, this composition represents a challenge for the management of this stand, as it is necessary to maintain a balance between the optimal development of the dominant trees, valuable from the forestry and economic point of view, and the gradual extraction of the less valuable trees, avoiding the sudden reduction of the stand's consistency.

For the sessile oak area installed at Bocșa Română Forest District, the annual average temperature shows an increasing trend in the case of both climate scenarios (Figure 5).

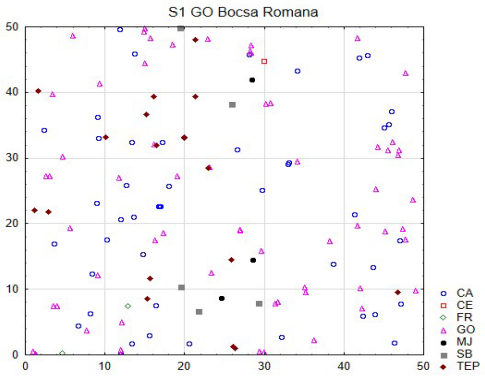

Figure 3. Tree positions for Bocsa Romana plot

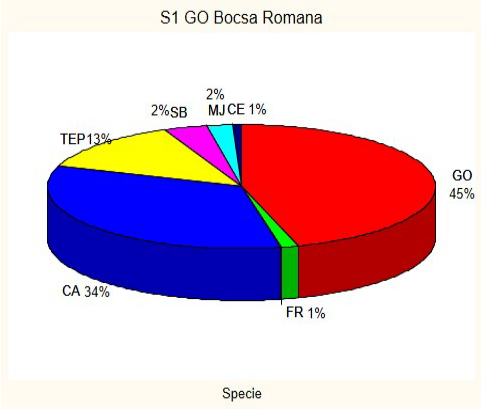

Figure 4. Forest composition for plot Bocsa Romana

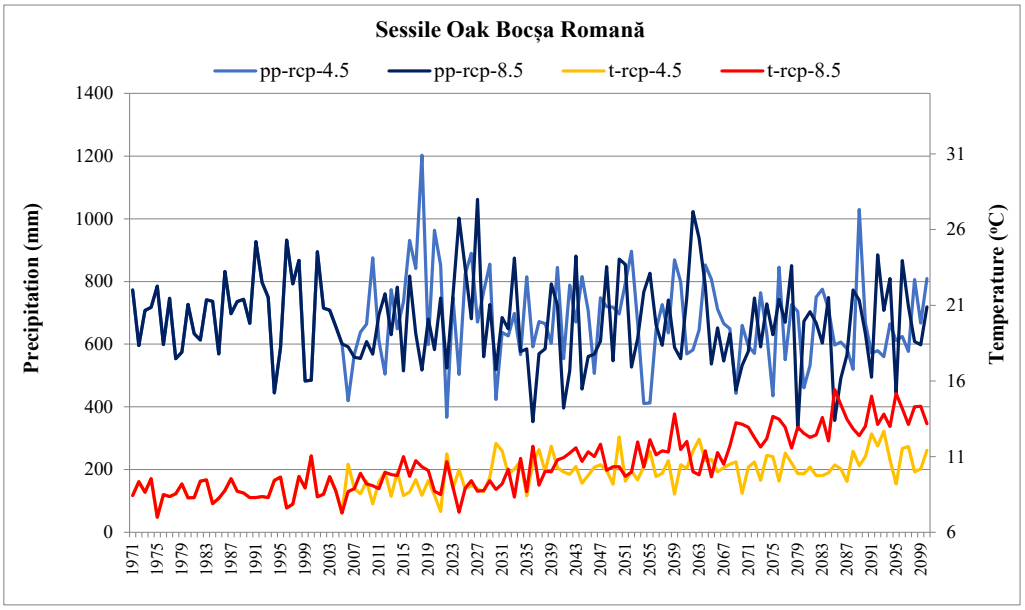

Figure 5. Climatic scenarios for the sessile oak plot from Bocsa Romana

For this location, in terms of annual mean precipitations in both rcp 4.5 and rcp 8.5 scenarios there does not appear to be any major problems in the future time frame, with most values falling between the extremes of the species range, for both climate scenarios. These stands will be less impacted in the next 80 years.

In the case of the annual average temperature in the first climate scenario rcp-4.5 there will be years in which stands will suffer from the increase in annual average temperatures.

In the case of the rcp-8.5 scenario in which greenhouse gases increase significantly from the year 2068, problems begin to appear, the average values of temperatures exceeding the endurance limit of the species and this will not change before the end of the analyzed time interval, namely the year 2100 .

The second experimental area was installed within the Păltiniș Forest District, forest unit V-111 C and represents the second area studied where the sessile oak is found as the main species in the Banat mountains. The layout of the trees can be seen in Figure 6.

It can be observed within this surface the small proportion of secondary species of the South European flowering ash and the European hornbeam (Figure 7).

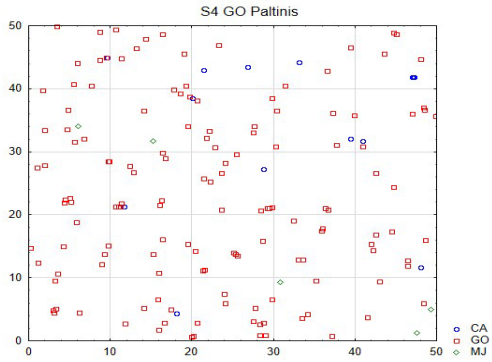

Figure 6. Tree positions for Paltinis plot

The sessile oak tree located in the area of Păltiniș Forest District seems to encounter higher temperatures and precipitation values with a negative effect on the growth and development of the trees than the one in Bocșa Română Forest District.

The prediction of the program for both climate scenarios (rcp-8.5 and rcp 4.5) in the case of precipitations shows us that the sessile oak stands in this area will be slightly impacted with only 6 predicted exceedances of the lower thresholds in the next 80 years in the case of the rcp 4.5 and rcp scenarios 8.5 (Figure 8).

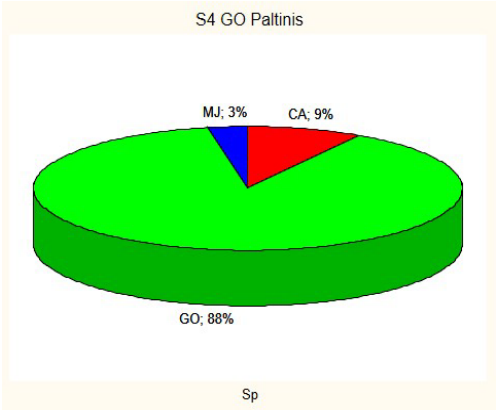

Figure 7. Forest composition for plot Paltinis

From the point of view of the evolution of the average annual temperatures, there will be very serious problems for the trees that grow in this area. Thus, in the case of both climate scenarios, there are more than 70 years in which these trees will be subjected to temperature stress. This situation is all the more worrying since towards the end of the time interval the average annual temperatures will exceed by 6°C or even 7°C the limit value of the existence of the species (as the stands are very strongly impacted).

The experimental area 7 was installed within the Moldova Nouă Forest District, IV-7B united forest and represents the last sessile oak area within the Banat Mountains. The layout of the trees can be seen in Figure 9.

Even if the basic species in this area is the sessile oak that forms the floor of the dominant and codominant trees, the existence of a sub-floor of vegetation corresponding to the trees and shrubs of several species can be observed. In this case, the sorbus is present in a proportion of 12%, field maple 10%, hornbeam 7% and ash 2% (Figure 10). This can give us an indication of how the composition of this forest ecosystem could evolve in increasingly limiting climatic conditions for the existence of the main species, namely the sessile oak.

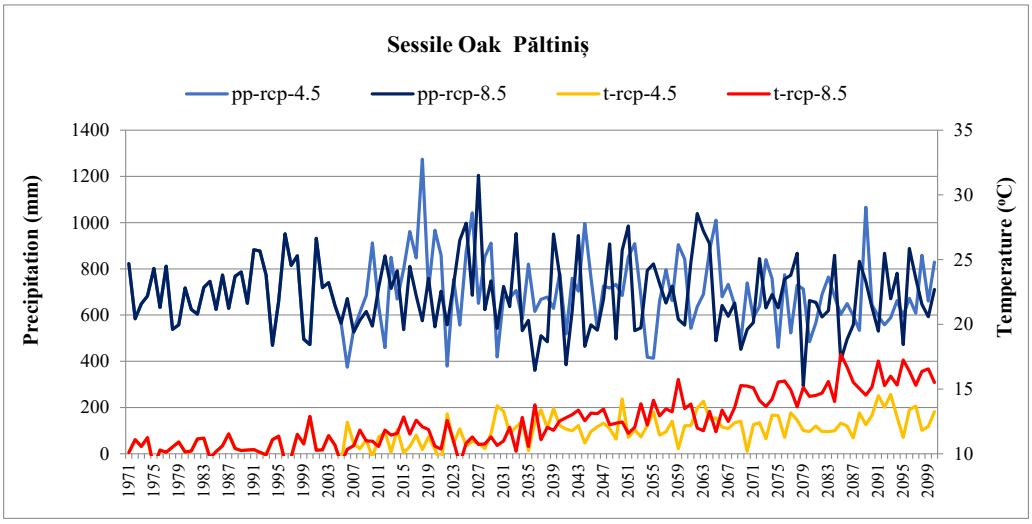

Figure 8. Climatic scenarios for the sessile oak plot Paltinis

The surface located within the Moldova Nouă Forest District is the last surface analyzed in the Banat Mountains area, being made up of almost 70% of sessile oak (Figure 10).

It can be seen that the arboretum will have problems not so much because of the lack of precipitation as because of the increase in average temperatures throughout the half of the 21st century (Figure 11).

Thus, the sessile oak from Moldova Nouă Forest District will be very strongly impacted unlike (Bocșa Română forest plot) the first stand analyzed (the one from Bocșa Română) and like the stand from OS Păltiniș, having 75

and 74 values that will exceed the heat tolerance threshold of the species.

In the case of both climate scenarios, rcp-4.5 and rcp-8.5, from the point of view of average annual precipitations, the sessile stands will be slightly affected, so in this area there will be no problems in the water supply from precipitations even if the darkest scenarios of climate change are met.

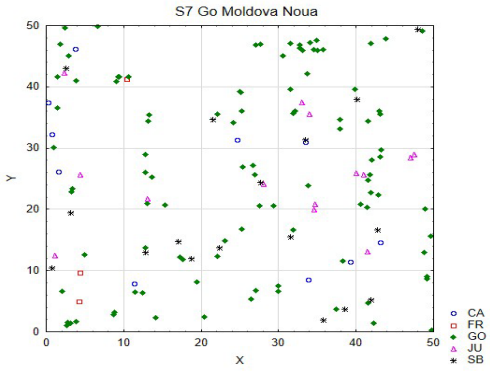

Figure 9. Tree positions for Moldova Noua plot

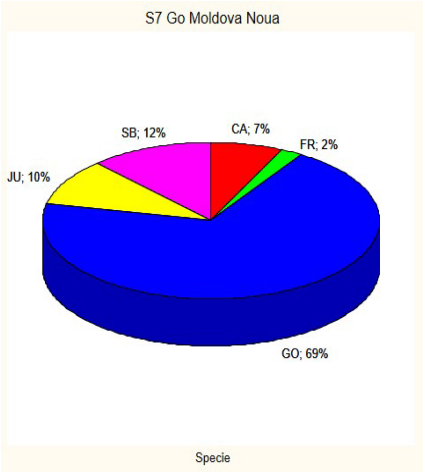

Figure 10. Forest composition for plot Moldova Noua

In the case of the rcp-4.5 climate scenario, the impact of average annual temperatures will be medium and very strong in the case of sessile oak stands. In the case of the rcp-8.5 climate scenario, the impact of average annual temperatures will be strong and very strong in the case of the sessile oak.

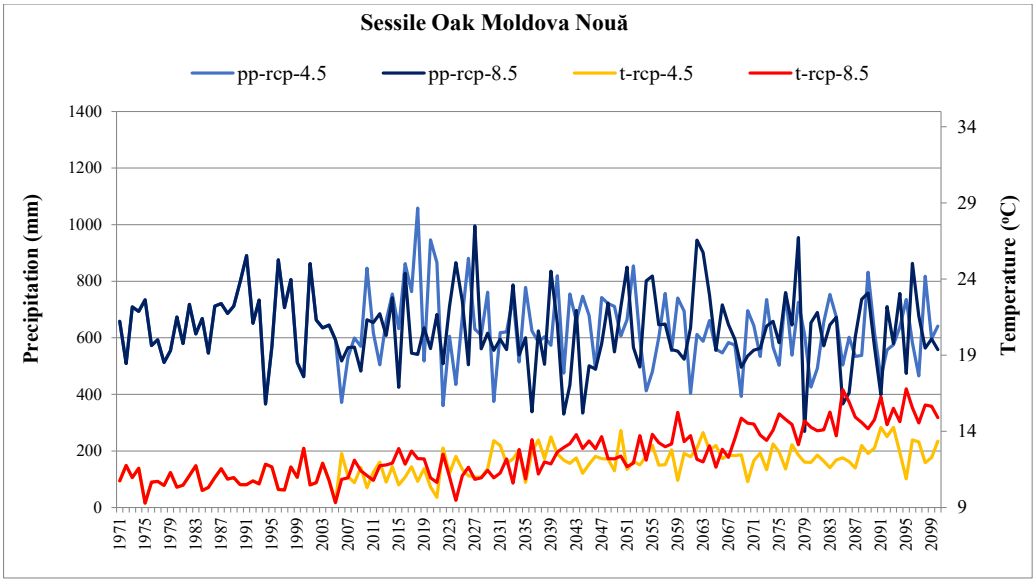

Figure 11. Climatic scenarios for the sessile oak plot from Moldova Noua

CONCLUSIONS

The research study analyzed three oak forest ecosystems from the Banat mountains in future climatic scenarios characterized by the increasing effects of greenhouse gas concentrations. Over the next 80 years, the climatic scenarios have been analyzed in the context of moderate and significant changes. Depending on the changes that can be anticipated regarding changes in temperature and precipitation regimes on ecological indicators, periodic evaluations and studies are needed to determinate their spatio-temporal variability. At the same time, by capitalizing on and improving a database, forecasts of the impact of destabilizing climate factors on forest ecosystems can be issued.

Moreover, forestry must take into account the future changes in the ecological conditions of the species so that, through the accumulation of silvotechnical works, decision-makers can intervene promptly and efficiently.

At the same time, a rethinking of both regeneration solutions and the choice of species for afforestation can significantly contribute to the creation of stands much more resistant to future climate changes.

ACKNOWLEDGEMENTS

This research work was funded by the Romanian Ministry of Research, Innovation and Digitization, within National Institute of Research and Development in Forestry „Marin Dracea" through the Nucleu National Programme BIOSERV, Project-PN-19070506/Contract no. 12N/2019 and Project number PN 23090301 (contract no 12N/2023), within FORCLIMSOC program (Sustainable forest management adapted to climate change and societal challenges).

REFERENCES

Allen, C.D., Macalady, A.K., Chenchouni, H., Bachelet, D., McDowell, N., Vennetier, M., Kitzberger, T., Rigling, A., Breshears, D.D., Hogg, E.H., Gonzalez, P., Fensham, R., Zhang, Z., Castro, J., Demidova, N., Lim, J.H., Allard, G., Running, S.W., Semerci, A., Cobb, N. (2010). A global overview of drought and heat-induced tree mortality reveals emerging climate change risks for forests. *Forest Ecology and Management*, *259(4),* 660–684. https://doi.org/10.1016/j.foreco.2009.09.001.

Baumbach, L., Niamir, A., Hickler, T., Yousefpour, T. (2019). Regional adaptation of European beech (Fagus sylvatica) to drought in Central European conditions considering environmental suitability and economic implications. *Regional Environmental Change, 19,* 1159-1174. https://doi.org/10.1007/s10113-019-01472-0.

Bonan, G.B. (2008). Forests and climate change: forcings, feedbacks, and the climate benefits of forests. *Science 320(5882),* 1444–1449. https://doi.org/10.1126/science.1155121.

Cântar, I.C., Ciontu, C.I., Dincă, L., Borlea, G.F., Crișan, V.E. (2022). Damage and Tolerability Thresholds for Remaining Trees after Timber Harvesting: A Case Study from Southwest Romania. *Diversity, 14,* 193.

Christensen, J.H., Hewitson, B., Busuioc, A., Chen, A., Gao, X., Held, I., Jones, R., Kolli, R.K., Kwon, W.-T., Laprise, R., Magaña Rueda, V., Mearns, L., Menéndez, C.G., Räisänen, J., Rinke, A., Sarr, A., Whetton, P. (2007). Regional Climate Projections et al In: Solomon S, Qin D, Manning M (eds) *Climate change: the physical science basis.* Contribution of working group I to the Fourth Assessment Report of the Intergovern-mental Panel on Climate Change. Cambridge University Press, Cambridge, 747–845

Constandache, C., Dincă, L. (2019). The management of pine stands situated outside their habitat. *Scientific Papers: Management, Economic Engineering in Agriculture & Rural Development*, *19(4),* 59-65.

Crisan, V., Dinca, L., Braga, C., Deca, S. (2022). Oak reaction to future climate changes in central and eastern Romania. *Scientific Papers. Series E. Land Reclamation, Earth Observation & Surveying, Environmental Engineering*, *11,* 107-114.

Crisan, V., Dinca, L., Breaban, I.G., Deca, S. (2021a). Analysing Pine Forest Ecosystems from Transylvania in the Context of Future Climatic Changes. *Present Environment and Sustainable Development*, *15(2),* 199-208.

Crisan, V., Dinca, L., Deca, S., Ienasoiu, G., Scarlatescu, V. (2021b). Sessile oak forest ecosystems from Transylvania in the context of climatic changes. *Current Trends in Natural Sciences. 10(19),* 48-57.

Dickinson, R.E., Errico, R.M., Giorgi, F., Bates, G.T. (1989). A regional climate model for the western United States. *Climatic change*, *15(3),* 383-422.

Dincă, L., Murariu, G., Enescu, C.M., Achim, F., Georgescu, L., Murariu, A., Timiș-Gânsac, V.,

Holonec, L. (2020). Productivity differences between southern and northern slopes of Southern Carpathians (Romania) for Norway spruce, silver fir, birch and black alder. *Notulae Botanicae Horti Agrobotanici Cluj-Napoca*, *48(2),* 1070-1084. doi.org/10.15835/nbha48211824.

Dincă, L., Murariu, G., Iticescu, C., Budeanu, M., Murariu, A. (2019). Norway spruce (*Picea abies* (L.) Karst.) smart forests from the Southern Carpathians. *International Journal of Conservation Science*, *10*(4), 781-790.

Ducci, F., Rogatis, A.D., Proietti, R., Curtu, L.A., Marchi, M., Belletti, P. (2021). Establishing a baseline to monitor future climate-change-effects on peripheral populations of Abies alba in central Apennines. *Annals of Forest Research*, *64*(2), 33-66. doi:10.15287/afr.2021.2281

Edwards, P.N. (2010). *A vast machine: Computer models, climate data, and the politics of global warming.* Cambridge: MIT Press. pp. 518. ISBN 9780262013925.

Fedorca, A., Popa, M., Jurj, R., Ionescu, G., Ionescu, O., Fedorca, M. (2020). Assessing the regional landscape connectivity for multispecies to coordinate on-the-ground needs for mitigating linear infrastructure impact in Brasov - Prahova region. *Journal for Nature Conservation, 58,* 1-11.

Fedorca, A., Fedorca, M., Ionescu, O., Jurj, R., Ionescu, G., Popa, M. (2021). Sustainable landscape planning to mitigate wildlife-vehicle collisions. *Land*, *10(7),* 737.

García-Duro, J., Ciceu, A., Chivulescu, S., Badea, O., Tanase, M.A., Aponte, C. (2021). Shifts in Forest Species Composition and Abundance under Climate Change Scenarios in Southern Carpathian Romanian Temperate Forests. *Forests. 12(11),* 1434. https://doi.org/10.3390/f12111434

Harper, K.C. (2008). *Weather by the Numbers: The Genesis of Modern Meteorology*. Cambridge, MA and London: MIT Press. pp. xii+308. ISBN 978-0-262-08378-2.

Jacob, D. (2001). A note to the simulation of the annual and inter-annual variability of the water budget over the Baltic Sea drainage basin. *Meteorol. Atmos. Phys.*, *77,* 61–73.

Jacob, D., Podzun, R. (1997). Sensitivity studies with the regional climate model REMO. *Meteorol. Atmos. Phys.*, *63,* 119–129.

Kutnar, L., Kermavnar, J., Pintar, A.M., (2021). Climate change and disturbances will shape future temperate forests in the transition zone between Central and SE Europe. *Annals of Forest Research*, *64(2),* 67-86.

Lindner, M., Maroschek, M., Netherer, S., Kremer, A., Barbati, A., Garcia-Gonzalo, J., Seidl, R., Delzon, S., Corona, P., Kolström, M., Lexer, M.J., Marchetti, M. (2010). Climate change impacts, adaptive capacity, and vulnerability of European forest ecosystems. *Forest Ecology and Management, 259(4),* 698–709. https://doi.org/10.1016/j.foreco.2009.09.023

Murariu, G., Dinca, L., Tudose, N., Crisan, V., Georgescu, L., Munteanu, D., Dragu, M.D., Rosu, B. Mocanu, G.D. (2021). Structural Characteristics of the Main Resinous Stands from Southern Carpathians, Romania. *Forests*, *12(8),* 1029.

Quante, M., Colijn, F. (2016). *North Sea Region Climate Change Assessment*; Publisher: Springer, Cham, 153-160. https://doi.org/10.1007/978-3-319-39745-0

Silvestru-Grigore, C.V., Dinulică, F., Spârchez, G., Hălălișan, A.F., Dincă, L., Enescu, R., Crișan, V. (2018). The radial growth behaviour of pines (*Pinus sylvestris* L. and *Pinus nigra* Arn.) on Romanian degraded lands. *Forests, 9(4),* 213. doi.org/10.3390/f9040213.

Stanescu, V., Sofletea, N., Popescu, O. (1997). *Romanian woody forest flora.* Editura Ceres, Bucuresti, 451 (in romanian).

Șofletea, N., Curtu, L. (2008). *Dendrology.* Editura Pentru Viață, Brașov, Romania, 418 (in romanian).

Vlad, R., Constandache, C., Dincă, L., Tudose, N.C., Sidor, C.G., Popovici, L., Ispravnic, A. (2019). Influence of climatic, site and stand characteristics on some structural parameters of scots pine (*Pinus sylvestris*) forests situated on degraded lands from east Romania. *Range Management and Agroforestry*, *40(1),* 40-48.

Scientific Papers. Series E. Land Reclamation, Earth Observation & Surveying, Environmental Engineering. Vol. XII, 2023
Print ISSN 2285-6064, CD-ROM ISSN 2285-6072, Online ISSN 2393-5138, ISSN-L 2285-6064

EMBEDDING LOW CARBON EMISSION INTO THE WATER INFRASTRUCTURE

Mirela-Alina SANDU[1], Adela-Constanta VLADASEL (PASARESCU)[2], Adriana-Magdalena PIENARU[1]

[1]University of Agronomic Sciences and Veterinary Medicine of Bucharest,
Faculty of Land Reclamation and Environmental Engineering,
59 Marasti Blvd, District 1, Bucharest, Romania
[2]Stantec, CF23 8HA, Cardiff, United Kingdom

Corresponding author email: apienaru@gmail.com

Abstract

Climate change is the biggest global challenge of our times. If, at all levels of society and organisation, we can work together to reduce carbon emissions while also planning how to adapt to change, we can prevent climate change from making our planet uninhabitable. Romania is committed to fighting climate change and pursuing low carbon development. Therefore, the Government of Romania, through the Ministry of Environment and Climate Change (MECC), has requested the World Bank to provide advisory services to help meet this commitment. To reduce the carbon footprint of the infrastructure is essential to assess the carbon embodied in the materials and construction methods, plus the operational carbon emissions of the resulting asset.
Carbon Management in Infrastructure provides a national framework for these assessments and can be directly applied to the water industry as it needs to engage the whole value chain to achieve the net zero commitments.

Key words*: Carbon Management, climate change, emissions, net zero carbon.*

INTRODUCTION

Some of the global problems humanity is facing are water scarcity, water quality degradation and changes in the water cycle in the context of climate change. Human activities and economic development exert pressure on water resources, which are unevenly distributed over the Earth's surface. In addition, rapid urbanisation, the development of municipal water supply and sewerage facilities plus climate change are all contributing to increased consumption, making water ever scarcer. In general, in the context of water scarcity, socially and politically, wastewater management receives less attention compared to the water sector, although the two are intrinsically linked. Wastewater has a negative impact on the sustainability of the water supply system, human health, the environment and economy. Increased discharges of improperly treated industrial wastewater, untreated municipal wastewater and sewage seepage have led to water quality degradation worldwide. Thus, Wastewater Treatment Plants (WWTPs) are an important part of the water cycle and in achieving the concept of circular sustainability by integrating the three dimensions: environmental, economic and social.

The primary objective of the WWTPs is to remove pollutants from wastewater to ensure the protection of the receiving water body (Fighir et al., 2019). In Europe, urban wastewater treatment is regulated by the Council Directive 91/271/EEC concerning urban wastewater treatment (UWWTD). Limited importance is attached to the ways in which these pollutants have been removed or the energy used to remove pollutants from wastewater or the number of emissions of greenhouse gases (GHG) produced. Research has shown that sewage treatment plants are an undeniable source of man-made greenhouse gas emissions that lead to global warming and climate change (Larsen, 2015; Sweetapple et al., 2014). Wastewater treatment can account for about 1-2% of total global greenhouse gas emissions to the atmosphere (Lanqing et al., 2022). Another important issue is the management of sludge from the treatment process, which comprises most of the pollutants present in wastewater (Shao et al., 2019).

Today, a different vision of sewage treatment plant design based on multiple criteria is needed and GHG emissions produced in the treatment process, can no longer be ignored.
Wastewater treatment plants have the potential to be an integral component of circular sustainability through embedding both resource and energy capture during safe water production. The transition to the circular economy embraces all areas of the economy, even the water (Sandu & Virsta, 2021) and wastewater sectors (Smol, 2023).
Climate change is forcing us to place carbon management at the forefront of every approach to water solutions (e.g. reducing carbon footprint to net neutrality and ultimately to zero net carbon emissions). These measures shape the circular economy, the heart of a sustainable future.
The primary aim of the paper is to provide an overview regarding the importance of the carbon emissions concept in wastewater treatment plants.

MATERIALS AND METHODS

The methodology applied to achieve the goals of the research incorporated a mapping to theoretical frameworks (specific elements of sewage treatment plant carbon emissions) of interest. In the initial stage of this study, the importance of WWTPs was highlighted. This comprised a review and assessment of the different levels of wastewater treatment processes and an analysis of urban wastewater production and treatment in Romania. In the second phase of this research, carbon emissions from wastewater treatment plants were correlated with GHG emissions from the municipal wastewater treatment plants during operation.
This study was conducted using the documentary research method, which implied collecting information from available resources accessible in existing published scientific databases, websites and libraries. Primary research literature has been retrieved from full-text academic databases like Elsevier, Web of Knowledge, Wiley Online, Google Scholar, Multidisciplinary Digital Publishing Institute and European Union statistics (Eurostat).

RESULTS AND DISCUSSIONS

Wastewater Treatment Plants

The mixture of municipal wastewater, runoff from streets and paved surfaces as well as industrial wastewater is called urban wastewater. Untreated, this wastewater contaminates rivers, lakes, groundwater, seas and can create serious public health risks. In Europe, most wastewater ends up in the sewer system from where it is transported to a wastewater treatment plant to reduce the concentration of pollutants The treated water is then released into the environment, usually into lakes and rivers. When pollution control at source fails, urban wastewater treatment is the ultimate opportunity to prevent pollutants from entering the environment, is an "end-of-pipe" measure.
Wastewater treatment refers to the physical, chemical, and biological processes used to eliminate pollutants from wastewater. It also includes the transformation of water into an effluent that can be cycled back into the water system. Once the effluent is returned to the water cycle, it has an acceptably low impact on the environment or is used for other applications. Different levels of processing can be carried out, usually covering the following (Figure 1).
Urban wastewater treatment UWTPs produces sewage sludge, which is usually processed to meet the sludge's suitability for its intended use or disposal (Figure 2). Wastewater carries valuable resources. These include not just water alone, but also heat, nutrients like phosphorus and nitrogen, as well as energy as well and other valuable resources which may be obtained from sewage sludge. In some areas of Europe, processed sewage sludge is prized for the nutrients and organic matter it contains in agriculture, although worries regarding contamination, mostly chemical, limit its application potential. From this point of view, the most efficient plants can fulfil the environmental thresholds for discharge and producing at minimum enough energy for their own energy demands. Through imposing requirements on the quality of incoming effluent until resource recovery, these "resource centres" could support a circular economy.

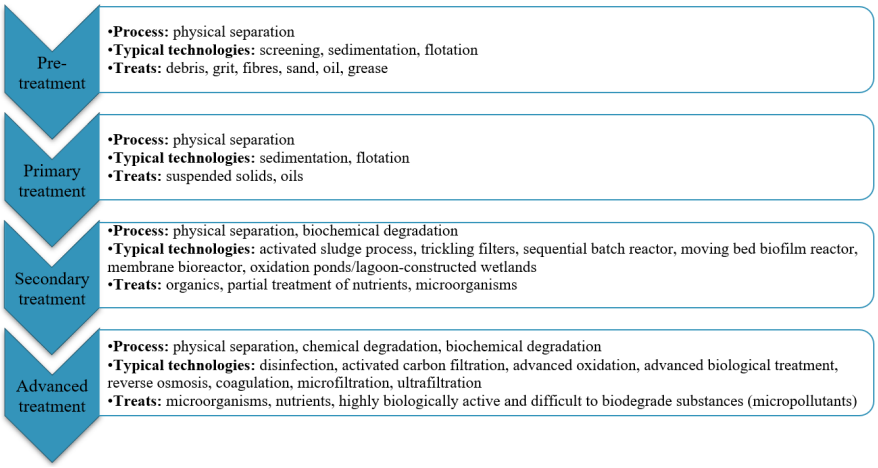

Figure 1. Wastewater treatment processes

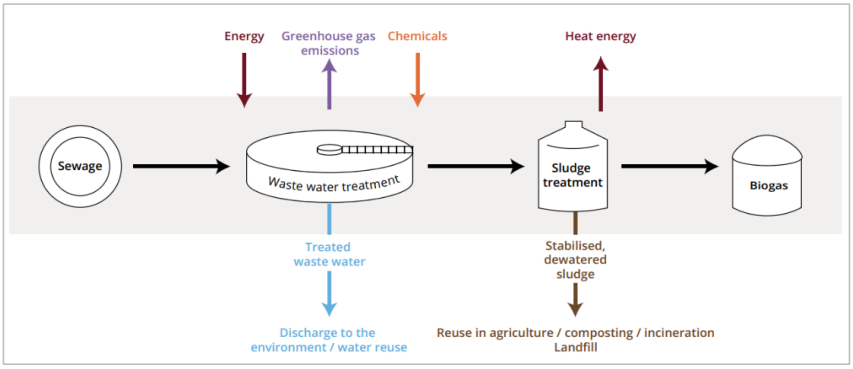

Figure 2. Urban wastewater treatment plan (EEA, 2022)

Carbon emissions in the WWTPs

It is mandatory to know the carbon emissions of the WWTPs, as measures to reduce GHG emissions are linked to measures to improve the energy efficiency of plants and lead to better plant management. Carbon emissions from wastewater treatment plants are emissions related to the collected, treated and final disposal of treated wastewater and the resulting sludge (Figure 3).

The main sources of emissions from wastewater treatment plants include "energy consumption and biological, chemical and biochemical processes to achieve effluent quality" (IPCC, 2014).

According to Parravicini et al. (2016), GHG emissions can be classified into two major categories: direct and indirect emissions. Wastewater treatment plants' direct greenhouse gas emissions refer to emissions generated at wastewater collecting and discharging points. Indirect greenhouse gas emissions result from the consumption of electricity, the use and transfer of chemicals, sludge handling and stabilisation processes. Total GHG emissions are the sum of direct and indirect emissions (Parravicini et al., 2016; Masuda et al., 2015).

Greenhouse gases of concern from wastewater treatment plants are:

- carbon dioxide (CO_2),
- methane (CH_4),
- nitrous oxide (N_2O) (Shahabadi et al., 2009).

CO_2 emissions are linked to two major drivers: the treatment process and electricity consumption. In the anaerobic treatment process, BOD_5 from wastewater is embedded in biomass or transformed into CO_2 and CH_4. Part of the biomass is transformed into CO_2 and

CH_4 by endogenous respiration. Additional CO_2 emissions are from sludge digesters and digester gas flaring. During the aerobic phase, carbon dioxide is generated by the decomposition of organic matter in the activated sludge phase and, in part, by primary clarifiers (Taşeli, 2017).

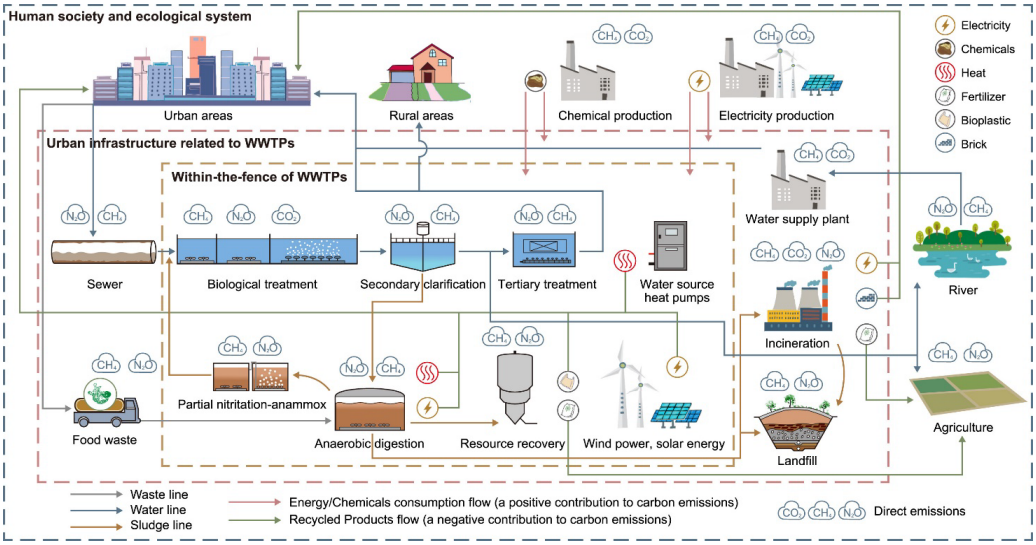

Figure 3. Carbon accounting in wastewater treatment
(Lanqing et al., 2022)

Wastewater together with sludge constituents are capable of generating CH_4 if they degrade in an anaerobic manner. About 72% of these CH_4 emissions occur in the anaerobically digested sludge line (Campos et al., 2016). According to Gupta & Singh (2015), the amount of CH_4 production depends in the first place on the type of treatment system, the amount of degradable organic matter and the temperature of wastewater. As the temperature rises, so the rate of CH_4 generation increases. This is especially important in non-controlled systems and a warmer climate.

N_2O is linked to the nitrogen constituent's degradation in wastewater (proteins, nitrates and urea). Household wastewater comprises human wastewater combined with other domestic wastewater, possibly containing effluent from washing machines, sinks, shower drains, etc. Wastewater treatment facilities can incorporate a variety of technologies, starting with lagoons to tertiary treatment technologies to remove nitrogen constituents. Once processed, the effluent treated usually is released into receiving water. Nitrous oxide generation is related to biological nitrogen removal from wastewater, as it is a by-product of both nitrification and denitrification processes (Wu et al., 2009; Fighir et al., 2019).

Because water and other resources are withdrawn for reuse from wastewater, these operations generate costs associated with energy consumption and greenhouse gas emissions. There is no other part of water infrastructure that is considered to be more energy intensive per unit of treated water than wastewater recovery, and it is the sector with the greatest capacity to become carbon neutral. Carbon footprint may be reduced to a minimum through energy and chemical inputs into treatment processes and maximising wastewater energy generation through carbon and heat capture (Pagilla, 2022).

The embedded carbon or embodied carbon footprint of WWTPs includes the total amount of greenhouse gas emissions from their construction, maintenance and disposal (Nayeb et al., 2019).

At a basic scale, the energy contained in wastewater and its extraction in a utilizable form creates possibilities for reductions in the carbon footprint of WWTPs. Inputs of energy

for treatment represent costs that contribute to the carbon footprint. Maximising opportunities and minimising inputs by optimisation are the formula for achieving net zero carbon in WWTPs (Pagilla, 2022).

Net zero refers to the balance between the quantity of greenhouse gases produced by a company and the quantity removed from the atmosphere through mitigation measures. Net zero is reached when the amount we add will not be greater than the amount removed.

Improvements in urban wastewater treatment have been made since the 1990s. These have led to the prevention of significant methane emissions due to efficient and centralised wastewater collection and treatment (EC, 2020). As a result, emissions have steadily decreased reaching 17,351 kt CO_2 equivalent (CO_2e) in 2019. This reduction is seen only in CH_4 emissions, which have fallen by more than half from 1989. Nitrous oxide emissions decreased very slightly from 2000, to 6,100 kt CO_2e per year (EEA, 2023b). The fossil fuel use for electricity generation and for drying and transportting sewage sludge represent indirect emissions from UWWTPs (Zheng & Ma, 2019).

Greenhouse gas emissions from wastewater treatment may be minimised in a number of ways, starting with optimising operation and ending with modifications to the plant.

In European countries, improvements have been made to sanitation systems in recent years. Today, municipal wastewater is treated at the tertiary level in most EU countries. Still, there are countries where less than 80% of the population is connected to public municipal wastewater treatment systems (EEA, 2022). Countries with high percentages of population hooked up to wastewater treatment plants are Luxembourg, Netherlands, Malta, with Croatia and Romania at the opposite end (Smol, 2023).

Different tools have been developed in order to identify and reduce GHG emissions from WWTPs.

A first tool is called the *Energy Performance and Carbon Emissions Assessment and Monitoring* (ECAM), which is an open-source software. This tool has been developed to collect essential information for energy performances of installations at operational level within a WWTP, with main purpose to identifying critical areas for GHG emission reduction, for increasing energy savings where possible, and improving the overall efficiencies for costs reduction. This tool can be applied and useful for all key stakeholders involved in the water and wastewater sector, for service management and planning regarding GHG emission and energy performance assessments and resulting suitable and operative perspectives for limitation of the overall carbon dioxide emissions (http://wacclim.org/ecam/v1/).

Another tool for calculating the carbon footprint for wastewater treatment plants has been developed in the project "Calculation of the carbon footprint from Swedish wastewater treatment plants" (SVU 12-120). This tool is an Excel file, containing 13 sheets, in each sheet different data and information are saved and calculated, grouped on different categories, such as:

- Group 1: input data (important information regarding the process within the selected WWTP, chemicals used, energy data, information on basic transports of the sludge, destination routes, resulted waste, etc.)
- Group 2: represents results of the simulation and calculations;
- Group 3: emission factors for electricity production, heat production, biogas use, etc. Global Warming Potentials (GWP) and different conversion factors, as well as constants used for the calculation; and the last group is
- Group 4: includes appropriate references and input data for the use of the tool.

It is a complex tool offering interesting and solid results for the carbon footprint of a WWTP.

Urban wastewater production and treatment in Romania

In households and certain industries in Romania, 20.0 million p.e. of wastewater are generated every day. This amount of wastewater is treated in 642 plants before being discharged. Thus, depending on the type of treatment applied there are 434 biological treatment plants, 174 biological treatment plants with nitrogen and phosphorus removal and 34 primary treatment plants.

Only 12% of urban wastewater in Romania is treated in accordance with UWWTD requirements and this is well below the EU average of 76% (Figure 4).

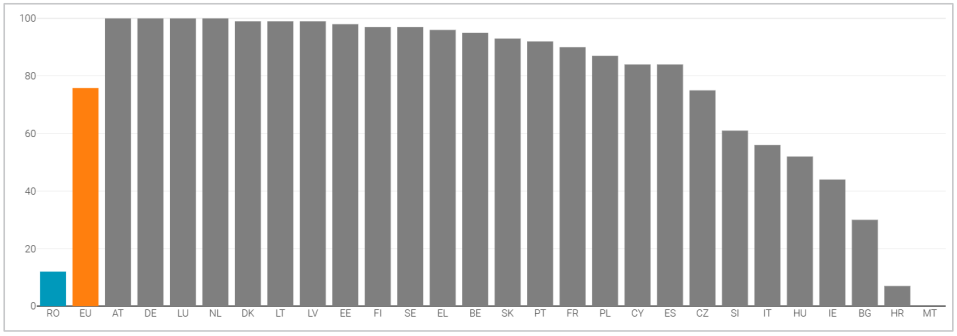

Figure 4. The proportion of urban wastewater that meets all requirements of the UWWTD [Romania (europa.eu)]

According to the latest report by the specialists of the National Administration "Romanian Waters" on the "Status of urban wastewater treatment works and capacities in execution and put into operation for human agglomerations in 2020", a level of connection to collection systems (sewerage networks and appropriate individual systems) of 66.15% and to treatment systems (treatment plants and appropriate individual systems) of 63.58% was assessed for urban agglomerations with more than 2,000 inhabitants equivalent.

The annual production of wastewater sludge in Romania was over 247,760 tons in 2018. Based on data reported up to 2018, Figure 5 shows a significant range in the uses of sewage sludge: 53.5% were landfilled, 18.7% of sewage sludge was used in agriculture, 0.3% was incinerated, and 27.5% was disposed of in other ways (EEA, 2023a).

According to EEA greenhouse gases - data viewer (2023b), emissions of greenhouse gases by the urban wastewater treatment sector in Romania have decreased by 25.9% between 2010 and 2019 (Figure 6).

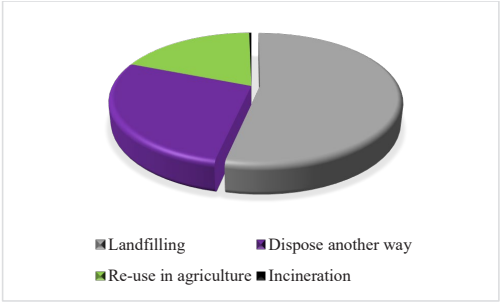

Figure 5. The proportion of wastewater sludge from treatment plants reused or disposed (EEA, 2023a)

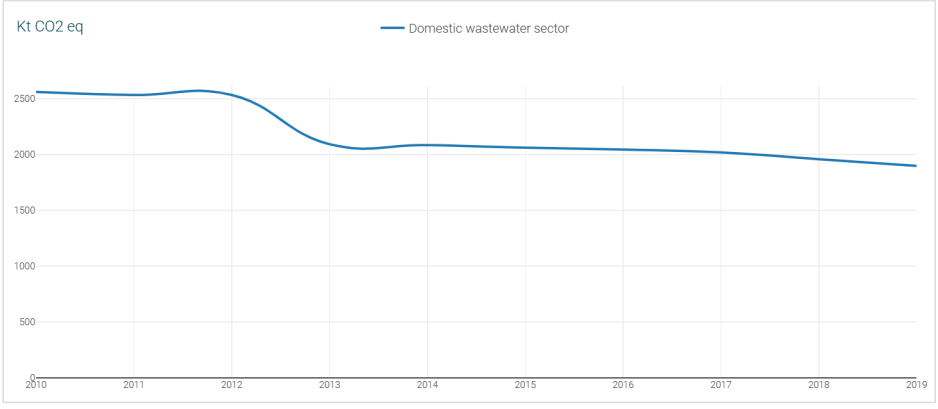

Figure 6. Greenhouse gases emissions generated by the urban wastewater treatment sector in Romania (EEA greenhouse gases - data viewer, 2023)

CONCLUSIONS

In 2021, 36 billion tons of carbon dioxide were emitted globally. As the amount of carbon dioxide increases, the planet continues to warm. Thus, devastating effects such as increased flooding, extreme heat, drought and worsening forest fires are increasingly being felt by millions of people around the world. In 2020, Romania emitted 71.48 million tons of CO_2, according to Our World in Data (*Romania: CO2 Country Profile - Our World in Data*). The figure represents 0.21% of the total issued globally. In the same year, Romania registered 3.72 metric tons of CO_2 emitted per capita. CO_2 emissions from industrial processes in Romania are relatively high, even if they decreased by 64% between 1989 and 2011, due to the reduction of industrial activity after the communist period. In the same interval, transport emissions (17% of the total) increased by 67%, exceeding a 55% increase in greenhouse gas emissions, according to Climate Analytics (*Romania - 1.5ºC Pathways for Europe: Achieving the highest plausible climate ambition - Oct 2021 (climateanalytics.org)*). Romania has ratified and transposed into national legislation two of the most important international treaties regarding climate change: the United Nations Framework Convention on Climate Change and the Kyoto/Japan Protocol. In order to achieve the goal of the Paris Agreement (*The Paris Agreement | UNFCCC*), the EU is working to achieve "net zero" emissions by 2050. The goal of the agreement is to limit global warming to less than 1.5 degrees Celsius compared to pre-industrial levels. The Earth is already approaching this value, with temperatures already reaching the threshold of 1 degree Celsius.

Regarding the necessary measures to achieve the goal of "net zero" by 2050, the European Commission recommended that Romania increase the level of ambition for 2030. Among these necessary new measures is a plan to decarbonize the environment by increasing the share of energy from renewable sources by at least 34%.

Wastewater treatment plants have the capacity to generate valuable water resources, energy, and new secondary raw materials, which can be utilized across various sectors such as municipalities, industries, and agriculture. In a world where the demand for fresh water is continuously increasing, and existing water resources face growing pressures from over-extraction, pollution, and climate change, it would be imprudent to overlook the opportunities that arise from improved wastewater management. Successful resource recovery from wastewater contributes to the principles of the circular economy and fosters long-term sustainable development. However, achieving a shift from merely removing pollutants to actively recovering resources necessitates a paradigm shift. Resource recovery should be a strategic objective incorporated into the earliest planning stages of new investments whenever feasible. Recent developments in EU regulations indicate an increasing support for resource recovery and a growing momentum for change, although a comprehensive approach has yet to be fully embraced.

Wastewater treatment plants, which consume significant amounts of energy and produce high carbon emissions, have the potential to transition into substantial energy producers and generators of recycled organic and metallic materials. This transformation can effectively contribute to broader sustainable development objectives, the circular economy, and the interconnected systems of water, energy, sanitation, food, and carbon.

The WWTPs plant operations and process optimization role is essential not just to meet water requirements and plant quality goals, but also to achieve resource and sustainability recovery goals or outcomes. The carbon footprint for an existing plant is the operational activities and therefore the potential to achieve net zero carbon.

Understanding the carbon footprint of WWTPs is essential to comprehending their environmental impact. Through quantification of emissions, plants can identify areas for improvement and implement specific strategies to reduce their carbon footprint.

ACKNOWLEDGEMENTS

This paper was carried out with the financial support of University of Agronomic Sciences

and Veterinary Medicine of Bucharest – Romania, Research Project 1059/15.06.2022, acronym HybridPraxisLab in the competition IPC 2022.

REFERENCES

Campos, J.L., Valenzuela-Heredia, D., Pedrouso, A., Val del Rio, A., Belmonte, M., Mosquera-Corral, A. (2016). Greenhouse Gases Emissions from Wastewater Treatment Plants: Minimization, Treatment, and Prevention. *J. Chem., 2016*, 1–12.

EC (2020). Communication from the Commission to the European Parliament, the Council, the European Economic and Social Committee and the Committee of the Regions on an EU strategy to reduce methane emissions.https://ec.europa.eu/energy/sites/ener/files/eu_methane_strategy.pdf

European Environment Agency - EEA (2022). Beyond Water Quality-Sewage Treatment in a Circular Economy. ISBN 9789294804785, ISSN 1977-8449, doi:10.2800/897113

European Environment Agency - EEA (2023a). Waterbase - UWWTD: Urban Waste Water Treatment Directive - reported data https://www.eea.europa.eu/en/datahub/datahubitem-view/6244937d-1c2c-47f5-bdf1-33ca01ff1715.

European Environment Agency - EEA (2023b). EEA greenhouse gases - data viewer. https://www.eea.europa.eu/data-and-maps/data/data-viewers/greenhouse-gases-viewer.

Fighir, D., Teodosiu, C., Fiore, S. (2019). Environmental and Energy Assessment of Municipal Wastewater Treatment Plants in Italy and Romania: A Comparative Study. *Water, 11*(8), 1611. https://doi.org/10.3390/w11081611

Gupta, D. &Singh, S.K. (2015). Energy use and greenhouse gas emissions from wastewater treatment plants. *International Journal of Environmental Engineering, 7*(1), 1–10.

IPCC (2014). Climate change 2014: mitigation of climate change. summary for policymakers and technical summary.

Lanqing Li, Xiuheng Wang, Jingyu Miao, Aliya Abulimiti, Xinsheng Jing, Nanqi Ren, (2022). Carbon neutrality of wastewater treatment - A systematic concept beyond the plant boundary, *Environmental Science and Ecotechnology, 11*, https://doi.org/10.1016/j.ese.2022.100180.

Larsen, T.A. (2015). CO_2 neutral wastewater treatment plants or robust, climate friendly wastewater management? A system perspective. *Water Res., 87*, 513–521.

Masuda, S., Suzuki, S., Sano, I. (2015). The seasonal variation of emission of greenhouse gases from a full-scale sewage treatment plant. *Chemosphere, 140*, 167–173. https://doi.org/10.1016/j.chemosphere.2014.09.042.

Nayeb, H., Mirabi, M., Motiee, H., Alighardashi, A., Khoshgard, A. (2019). Estimating greenhouse gas emissions from Iran's domestic wastewater sector and modeling the emission scenarios by 2030. *Journal of Cleaner Production, 236*, 2019.

Pagilla, K.R. (2022). Book chapter. Pathways to Water Sector Decarbonization, Carbon Capture and Utilization. *Chapter 4: Operational optimization and control strategies for decarbonization in WRRFs*. IWA Publishing. doi: https://doi.org/10.2166/9781789061796_0051

Parravicini, V., Svardal, K., Krampe, J. (2016). Greenhouse gas emissions from wastewater treatment plants. *Energy Procedia, 97*, 246–253. https://doi.org/10.1016/j.egypro.2016.10.067.

Romania (europa.eu)

Sandu, M.A. & Virsta, A. (2021). The water footprint in context of circular economy. *AgroLife Scientific Journal, 10*(2), 170-177.

Shahabadi, M.B., Yerushalmi, L., Haghighat, F. (2009). Impact of process design on greenhouse gas (GHG) generation by wastewater treatment plants. *Water Res., 43*(10), 2679–2687.

Shao, S., Mu, H., Yang, F., Zhang, Y., Li, J. (2019). Application of energy analysis to the sustainability evaluation of municipal wastewater treatment plants. *Sustainability, 9*, 8.

Smol, M. (2023). Circular Economy in Wastewater Treatment Plant-*Water, Energy and Raw Materials Recovery. Energies, 16,* 3911. https://doi.org/10.3390/en16093911.

Sweetapple, C., Fu, G., Butler, D. (2014). Identifying sensitive sources and key control handles for the reduction of greenhouse gas emissions from wastewater treatment. *Water Res., 62*, 249–259.

Taşeli, B.K. (2017). Point source pollution and climate change impact from sequential batch reactor wastewater treatment plant. *Global NEST Journal, 20*(1), 33–41.

UNFCCC https://unfccc.int/process-and-meetings/the-paris-agreement

Wu, J., Zhang, J., Jia, W., Xie, H., Gu, R., Li, C., Gao, B. (2009). Impact of COD/N on Nitrous Oxide Emission from Microcosm Wetlands and Their Performance in Removing Nitrogen from Wastewater. *Bioresour. Technol., 100*, 2910–2917.

Zheng, M., & Ma, Y. (2019). *Energy use and challenges in current wastewater treatment plants*. A-B Processes: Towards Energy Self-sufficient Municipal Wastewater Treatment, IWA Publishing https://doi.org/10.2166/97817890 60089_0001.

http://wacclim.org/ecam/v1/.

https://climateanalytics.org/media/romania.pdf

https://ourworldindata.org/co2/country/romania#per-capita-how-much-co2-does-the-average-person-emit

https://rowater.ro/wp-content/uploads/2022/09/Stadiul-implementarii-Directivei-ape-uzate-in-anul-2019.pdf - "Status of urban wastewater treatment works and capacities in execution and put into operation for human agglomerations in 2020".

Scientific Papers. Series E. Land Reclamation, Earth Observation & Surveying, Environmental Engineering. Vol. XII, 2023
Print ISSN 2285-6064, CD-ROM ISSN 2285-6072, Online ISSN 2393-5138, ISSN-L 2285-6064

PROCESS AUDIT AT A GRINDING PLANT (CEMENT MILL) AT A CEMENT FACTORY - A CASE STUDY IN ROMANIA

Cristian-Bogdan CIOBANU[1], Gheorghe VOICU[2], Irina-Aura ISTRATE[2], Paula TUDOR[2], Bianca-Stefania ZABAVA[2]

[1]CEPROCIM SA Bucharest, 6 Preciziei Blvd, District 6, Bucharest, Romania
[2]University Politehnica of Bucharest, Department of Biotechnical System, 313 Splaiul Independentei, District 6, Bucharest, Romania

Corresponding author emails: ghvoicu_2005@yahoo.com, paula.tudor@upb.ro

Abstract

The process audit is an analysis for the operation of an equipment, to establish its performance and to make proposals for measures to increase production, decrease consumption and improve product quality. The objective of the process audit is to establish the actual state of operation for the cement grinding plant (the degree of loading with grinding bodies, the air speed in the mill, the granulation of the material at the entrance and the exit, the wear of the shields, energy consumption) and is the basis for proposing measures for optimization. The audit from a grinding plant is carried out in the following situations: upon commissioning (to record the initial condition of the equipment) after modernization/modifications of the equipment in the composition of the grinding plant whenever there are deviations from the expected performance as a routine test, at least once a year, to appreciate the real condition of the equipment. The paper presents some determinations made at a cement mill from a Romanian cement factory, the sampling method to carry out analyses and recommendations for improving production.

Key words*: grinding ability, grinding chart, grinding efficiency, process audit, particle size analysis.*

INTRODUCTION

The audit process is intended to estimate whether the process requirements specified in operating instructions, procedures, and rules for the conduct of the manufacturing process are suitable for achieving quality objectives.
The audit can be performed by a person or team, depending on the complexity of the operation under examination and the need for skills outside the training of the technical staff on the production flow.
The technical audit is more important as it is one of the effective tools for reducing production costs (Ciobanu et al., 2020; Engin & Arı, 2005; Krishnamoorthy et al., 2018; Ramesh et al., 2013).
Cement plants and process technical managers are often asked to examine, "the big picture" in a production/operations environment.
The audit process is a procedure that helps technical staff determine not only what is wrong, but also what is right in an industrial activity.
The cement plant audits assess its performance against a criterion of corresponding reference, and after a detailed assessment, recommendations are made to optimize the plant through capital investments.
For example, an energy audit of the dry rotary kiln system operating in a cement factory in Turkey showed that approx. 40% of the total input energy is lost through the hot flue gases (19.15%), the cooling stack (5.61%), and the furnace casing (15.11%, convection plus radiation). Following the audit, some ways to recover heat losses were presented, and the findings noted that approx. 15.6% of the total input energy can be recovered (Engin & Arı, 2005; Garba et al., 2010).
The methods of carrying out the technical audit involve the monitoring of working, electrical and maintenance practices in different sectors of the cement factory, as well as of the exploitation operations, the condition of the instrumentation, environmental pollution control techniques, etc. (Khan et al., 2012; www.cementequipment.org).
For example, for the assessment of ball mills, maximum production, energy consumption, system air flow and material flow, separator performance, and the operational variables to be monitored include: temperature, at the inlet

and outlet of the mill, the inlet pressure in the mill, the differential pressure, energy consumption, mill vibrations and other process parameters. In the paper are presented some determinations made at a cement mill from the formation of a cement factory in Romania, the method of sampling to carry out analyses and recommendations for improving production.

MATERIALS AND METHODS

The following methodologies and measuring devices were used to perform the mill audit:
a) The method was chosen to determine the specific surface area (SSB) of the grinding material (https://thecementinstitute.com).
The Blaine procedure is applicable to all cements defined in the standard SR EN 196-6: 2019.
The fineness of the cement shall be measured in the form of a specific surface, expressed in cm^2/g, which is based on determining the time of a fixed volume of air at known temperature to cross a layer of compacted cement, using the Blaine device.
b) A TESTO 920 type of device was used to measure the temperature at the main points of the installation.
c) The relative static pressures and flow rates at the main points of the grinding system were performed with the TESTO 400 to which a Pitot tube and a pressure transducer were connected.
d) For the chemical and granulometric analysis of the clinker, limestone + slag, gypsum and cement samples taken from the cement mill, an apparatus was used to perform the chemical analysis of the NovAA 400 grinding material.
The spectrometer is fully controlled by the PC for the flame and graphite technique, with transversely heated graphite furnace, single and double beam mode, and automatic turret with 6 lamps. Precise measurement of trace elements over a wide range of concentration is achieved by high precision at the high-performance optical drive, high-sample speed, and nucleus – transversely heated graphite furnace.
e) For the analysis of clinker granulometry, Mastersizer 2000E and CILAS - Delcita 715 are used (https://www.n8equipment.org.uk/).
There are three distinct ways to measure a sample with the Mastersizer 2000E:
1) The sample is prepared and dispersed to the correct concentration and then sent to the optical drive. Sample preparation is the most important step in making a measurement. If the sample is poorly prepared (unrepresentative or poorly dispersed) then the basic data will be incorrect.
2) Capture the spreading pattern from the prepared sample - measurement. The detector machine has a "snapshot" of the spreading pattern. Obviously, this snapshot only captures the scattering pattern in the particles passing through the analyser beam at that time. Taking a single snapshot may not get a representative view of the spreading pattern. Mastersizer takes many snapshots (known as snaps) and averages the result. Typically, more than 2000 snapshots are taken per measurement at a 1 ms interval.
3) Once the measurement is complete, the raw data is analysed by the machine's Malvern Software. After the data has been analysed, the information can be displayed in various ways.
The possibilities of investigation of the equipment are: Measuring the granulometric classes in the range of 1 ÷ 192 μm in a wet environment on any type of powdery material.
Interpretations of analyses:

- graphical presentation of the weight on 16 granulometric classes located in the range 1 - 192 μm;
- tracing the granulometric curve of the analysed powder;
- determination of the average diameter.

f) Optical microscopy apparatus Carl Zeiss AXIO IMAGER A1m and component determination by mineralogical analysis on natural raw materials: clay, marne, limestone, tiles, bushes and synthetic products such as cement clinker. It allows examination, both with transmitted light and reflected light (current 220 V, 15 A and frequency 50 Hz).

RESULTS AND DISCUSSIONS

The sampling and measurements necessary for the audit were carried out according to the schedule of determinations agreed with the factory representatives.
The cement produced was CEM II/A-LL 42.5R, with clinker, limestone, gypsum and dust from the furnace electrofilter (CKD). The grinding additive GTA 140 (dosage 300 g/t)

was used for grinding, for increasing production, and SYNCRO 206 (dosage 600 g/t) for reducing chromium.
The cement mill was stopped for the purpose of evaluating the interior equipment and taking samples for drawing the grinding diagram.
The audit includes information about the main process parameters recorded in the factory control room and measurement results (sampling for chemical analysis, granulometric analysis of materials introduced in the cement mill, determination of the grinding fineness of the cement expressed by specific surface Blaine and determinations in the air flow of the ball mill).
The stages of the process audit are as follows:
1. Submission of observations on the process parameters of the ball mill;
2. Presentation of observations on grinding efficiency;
3. Measurements in the air flow of the ball mill (measurements of temperatures, pressures and flows), as well as observations from the measurements made;
4. Determinations on materials (clinker, slag and limestone, gypsum, mixture, cement);
5. Inspection of the interior of the mill (interior equipment of the mill) for determining the filling degrees and specific consumption of electricity;
6. Tracing and analysis of the grinding diagram;
7. Separation efficiency by sampling points of the dynamic separator: Separator supply, separator fine output, separator output grid, and Tromp selectivity curve drawing based on laser granulometric distributions.
The main process parameters, recorded in the control room, are summarized in Table 1, and the grinding efficiency is synthesized by the parameters expressed in Table 2.

Table 1. Process parameters in the control room

Characteristic	Value
Assortment of cement produced	II AS 32.5
Raw mixture, Dosage (wet), %	
Clinker	69.52
Slag + limestone	23.63
Gypsum	6.85
Moisture mixture at the entrance to the mill, %	1.29
Mill production: wet/dry	75.2/74.2
Specific electricity consumption (dry), kwh/t	
cement mill	32.5
factory	41.6
Cement characteristics	
specific surface, cm^2/g	3,174*
SO_3 content, %	3.33

*determinations mean in CEPROCIM laboratory

***Remarks**:*
- the mill production and the dosage of the mixture were calculated based on the hourly indications of the component meters (clinker, limestone + slag, gypsum);
- the moisture of the mixture was calculated weighted, based on the moisture of the components, determined in the factory laboratory;
- the specific surface of the cement represents the average of the determinations made by the CEPROCIM laboratory.

Table 2. Milling efficiency

Parameter	Val.	Observations
Production (dry), t/h	74.2	- low production
Cement grinding finesse, cm^2/g	3174	- appropriate finesse
Finesse filter dust, cm^2/g	3598	- possibility of increasing the air speed through mill
Electricity consumption (dry), kwh/t factory cement mill	 32.6 41.6	- relatively good consumption
Recirculation coefficient	1.51*	- low value
Air speed above the charge, m/s	0.78	- speed outside the usual range (1-1.5 m/s)
Diameter max/min balls, mm, CI	90/60	- appropriate structure
CII	50/18	
Degree of filling, % CI	29.27	- degrees of filling calculated from H measured with material in the mill
CII	27.08	
Average ball weight in CI, kg	1.40	- relatively low weights
Average ball weight in CII, g	48.44	
Grinding chart, % $R_{2,5\ mm}$ at the mill wall	1.99	- good value (with a mill insufficiently loaded with material)
Mill speed, % of critical speed	76.40	- appropriate speed

*calculated from feed and grit flows

Determinations in the air flow

Using the portable equipment of CEPROCIM, measurements of temperatures, pressures and flows were made in the air flow. Thus, Table 3 shows the air temperatures and relative static pressures measured at the main points of the grinding plant, respectively the average air flow values, calculated based on dynamic pressure and temperature measurements.

Table 3. Process parameters on air flow

Measurement point	Air temperature, °C	Relative static pressures, mm H_2O	Air flow, Nm^3/h
Mill outlet pipe	87-95	111-127	24,042
Fan inlet of separator	78-80	223-233	114,301
Entrance to the mill dedusting fan	78-80	242-212	33,315
Filter basket and attachments	64-65	0.2-2.6	25,489

***Remarks**:*
- for the air flow of 24,042 Nm^3/h measured at the mill outlet, the maximum air speed through the mill (0% false air) is 0.97 m/s. Considering the false air infiltration at the exit of the mill of ca. 20%, the actual air speed through the mill becomes 0.78 m/s, value outside the range (1-1.5 m/s);
- the value of air infiltration on the mill outlet - mill deburnout filter basket is 9,273 Nm^3/h and represents approx. 27% of the air discharged to the basket.

Determinations on materials

During the audit, clinker, limestone + slag, gypsum and cement samples were taken, on which the following determinations were made:

✓ ***Clinker determinations (CEPROCIM determinations)***

The chemical analysis of clinker performed in the CEPROCIM laboratory is presented in Table 4.

Table 4. Chemical composition of materials

Chemical and modular composition	Clinker	Slag + limestone	Gypsum
Humidity*, %	0.01	4.06	4.72
Constitution water, %	0.72	4.02	13.6
SiO_{2total}, %	20.03	33.11	14.38
CaO, %	65.37	47.61	25.57
Al_2O_3, %	5.48	10.34	4.34
Fe_2O_3, %	3.83	1.18	1.26
MgO, %	1.41	2.0	1.6
SO_3, %	1.34	0.22	28.23
CaO_{free}, %	1.0	-	-
Insoluble residue, %	0.18	0.77	-
M_{Si}	2.13	-	-
M_{Al}	1.43	-	-
LSF	99.74	-	-
C_3S, %	65.02	-	-
C_2S, %	9.07	-	-
C_3A, %	8.04	-	-
C_4AF, %	11.65	-	-
CO_2, %	-	-	4.56
$CaSO_4 \cdot 2H_2O$, %	-	-	60.69
$CaCO_3$, %	-	-	10.37
Clay substances, %	-	-	23.22

*determination carried in the factory laboratory

***Remarks**:*
- potential alite and belite contents favourable to obtaining cements with low energy consumption.

The granulometric analysis of the mean clinker sample, respectively slag + scale, is shown in Table 5.

Table 5. Granulometric characteristics of the materials

Parameter	Clinker	Slag + limestone	Gypsum	Mixture
R_{25mm}, %	14.87	0.8	32.85	12.77
$d_{80\%}$, mm	22.0	4.0	31.00	19.50
$d_{50\%}$, mm	11.9	2.5	16.50	6.50

***Remarks**:*
- the particle size of clinker, gypsum and mix is well above the recommended value, while the particle size of the slag is very good compared to the recommended value (R_{25mm} < 5%).

Determination of cement

The grinding fineness of the cement expressed by the specific surface of Blaine, $R_{90\mu m}$, $R_{64\mu m}$ was determined in the CEPROCIM laboratory, and the results are presented in Table 6.

Table 6. Grinding finesse of cement

Hour	CEPROCIM residues		Specific surface area Blaine, cm^2/g	
	$R_{90\mu m}$,%	$R_{64\mu m}$,%	Factory	CEPROCIM
10	2.04	8.36	3,250	3,270
11	2.04	8.40	3,250	3,250
12	2.28	8.56	3,020	3,040
13	1.88	7.48	3,100	3,120
14	2.12	8.16	3,230	3,220
15	2.04	8.52	3,080	3,280
16	2.12	8.48	3,000	3,150
17	2.16	8.44	2,850	3,060
Average	**2.09**	**8.30**	**3,098**	**3,174**

***Remarks**:* the specific surface values of the cement determined in the CEPROCIM laboratory are like those determined in the factory laboratory.

The proportion of limestone (dry) in cement was estimated by selective component determination on the average cement sample. The scale ratio is approx. 2.15%.

The proportion of slag in the cement was determined by optical microscopy on the Hourly samples.

The proportion of slag + scale calculated from the counters was 23.63% (wet) and 22.97% (dry), respectively. CEPROCIM determinations indicate an average slag value of 21.9% (dry) and 2.15% (dry), with total slag + limestone being 24.05% (dry), higher than the one calculated based on the metering of the supply flows of the mill. The measurements were made from hour to hour between 10:00 ÷ 17:00.

Temperature measurements on the mill input/output material are shown in Table 7.

Table 7. Mill inlet/outlet temperature

Temperature, ºC	Value
Clinker at mill inlet	80.0-86.5
Slag + limestone al mill inlet	27.6-33.0
Gypsum at mill inlet	7.7-8.4
Cement belt conveyor	73.0-78.5

Inspection of the interior of the mill

The inspection of the interior of the cement mill was aimed at:
- free height measurement (H), for determining the degree of filling with grinding bodies;
- assessment of the condition of the interior equipment of the mill;
- sampling to draw the grinding diagram; the samples were taken in three directions from 0.5 to 0.5 m.

The measurement of the free height (H) above the load with grinding bodies was done without emptying the material mill, and the initial structure of the load with grinding bodies is shown in Table 8.

Table 8. Cement mill - loading and filling grades (Cement II AS 32.5)

Mill	Production, t/h	Speed, rpm	Length, m	Inner diameter, m	Blaine, cm^2/g
MC	74	16.0	10.5	4.2	3174

Chamber	Length, m	Inner diameter, m	Balls density, $/m^3$	Critical speed, rpm	Mill speed, % of critical speed	H* measured, m
I	3.81	4.08	4.31	20.94	76.40	2.717
II	6.04	4.08	4.80	20.94	76.40	2.792

**measured with material in mill*

Based on the measurements of free H, the filling degree and the specific electricity consumption were calculated (relation Slegten), Table 9.

Table 9. The filling degree and the specific electricity consumption

Parameter	Chamber I	Chamber II	Total mill
Degree of filling, %	29.27	27.08	-
Specific electricity consumption, kWh/t	12.7	19.8	32.6

***Remarks**:* the specific electricity consumption of the mill is relatively good.

The internal equipment of the mill - Chamber I

Figure 1. Aspects at the entrance to the mill - material level and cascade armours for chamber I

***Remarks**:* armours in good condition.

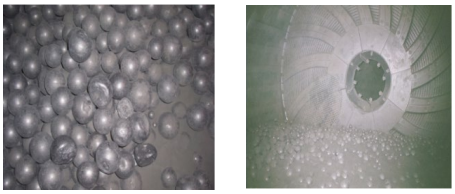

Figure 2. Broken balls, deformed balls (detail), respectively the partition wall, the ventilation ring, the material level and the cascade shields - chamber I

***Observation**:* Material below the ball level, missing material on the left side of the mill and broken and deformed grinding bodies and the presence of grinding bodies from chamber II.

Figure 3. Cascade shields (detail) and slots in the partition wall with ventilation ring (detail) - chamber I

***Observation**:* Field armour in good condition.

The internal equipment of the mill - Chamber II

Figure 4. Partition wall, self-sorting shields, the material level and the slots in partition wall (detail) - chamber II

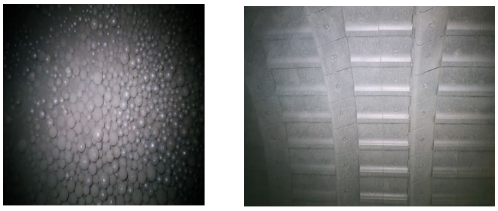

Figure 5. Balls distribution and self-sorting shields (detail) - chamber II

Figure 6. The slots in the mill outlet wall (detail) and mill outlet grate (detail) - chamber II

***Remarks**:* the shields in the partition wall and those at the mill outlet are in good condition, but the material is below the level of the balls. In addition, there are balls wedged between armours and slots partially blocked with balls.

The grinding diagram

To perform the grinding diagram, the cement mill was instantly switched off. Material samples were taken from 0.5 m in 0.5 m, in three directions along the mill, by CEPROCIM personnel. On the material samples, the residences were determined on the 5 mm, 2.5 mm, 1 mm, 200 µm, 90 µm sides of the eye, 64 µm and 32 µm and specific Blaine surfaces (room II) in the CEPROCIM laboratory and then the grinding diagram was drawn. The results are shown in Figures 7 and 8.

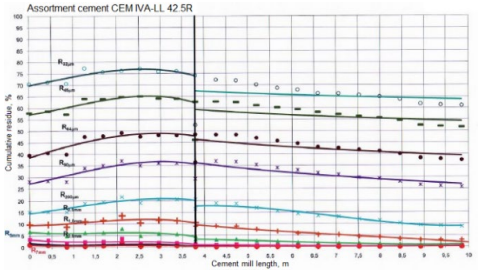

Figure 7. Cement mill. Milling diagram. Three-way sample average

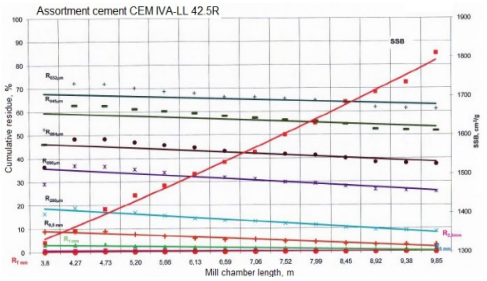

Figure 8. Cement mill. Residues evolution and Blaine specific surface area (SSB) in chamber II

The analysis of the grinding diagram highlights the following aspects:

Chamber I:

- ✓ well prepared material in room I - $R_{2.5mm}$ = 1.99% at the partition wall, in conditions of a mill insufficiently loaded with material.

Chamber II:

- ✓ active grinding along the entire length of the chamber;
- ✓ $R_{90\mu m}$ when leaving the mill (separator supply) cca 8%.

Efficiency of separation

For the characterization of the separation efficiency, samples were taken from the following grinding plant points:

- ✓ mill output material (separator supply);
- ✓ separator output for fine material;
- ✓ separator output for grout.

The following determinations were made on the materials taken:

- ✓ resided ($R_{90\mu m}$ and $R_{64\mu m}$);
- ✓ specific Blaine surfaces;
- ✓ laser granulometric distributions.

The values of the residuum and characteristic parameters of the grinding-separation process are shown in Table 10.

Table 10. Grinding-separation process parameters

Characteristics	Value
Recirculation coefficient, -	1.48
Fine material volume, %	67.65
Grit volume, %	32.35
Degree of fine material separation, %	75.34
Degree of grit separation, %	13.17
Separation eficiency, %	62.17

***Remarks**:*

- R_a - the separator feed material resin – on the 90 µm and 64 µm sieve, %;

- R_g - the semolina resin - on the 90 μm and 64 μm sieve, %;
- R_F - the fin resin on the 90μm and 64μm sieve, % respectively;
- k - the recirculation coefficient;
- V_f - the volume of fine resulting from separation, %;
- V_G = the volume of semolina resulting from separation, %;
- f - the degree of separation of the fin (fine to fine), %;
- g - the degree of separation of the semolina (fine to fine), %;
- E - separation efficiency (f - g), %.

Have been found: good separation of the fin; poor separation of the semolina; relatively good separation efficiency; low value of recirculation coefficient.

The efficiency parameters of the separator were also calculated based on the laser granulometric distributions; the Tromp selectivity curve being drawn (Figure 9).

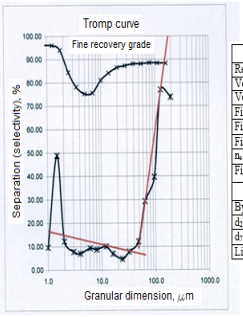

Separation characteristics			
Recirculation coefficient	1.24		
Volume of fine, %	80.7		
Volume of grist, %	19.3		
Fine efficiency at 30 μm, %	92.2	Grist in fine at 30 μm, %	65.1
Fine efficiency la 64 μm, %	89.7	Grist in fine at 64 μm, %	48.0
Fine efficiency la 90 μm, %	87.6	Grist in fine at 90 μm, %	34.9
α_k	0.90	$d_{R64.8\%}$, μm	25.4
Fine recovery grade, %	88.35		
Tromp curve characteristics			
Bypass, %	8.1		
d_{25}, μm	60.2	d_{55}, μm	97.7
d_{75}, μm	135.1	Imperfection, %	0.38
Limit of acuity, μm	34.8	Accuracy	2.2

Figure 9. Tromp curve. Characteristics of separation at the cement mill

It was found that the recirculation coefficient, calculated from the results of the laser granulometric analysis, was within the recommended range (2-2.5), with positive implications on production, but the degree of recovery of the fin (f) was relatively low (approximately 42%). However, the degree of wheat recovery (g) was very good (99.5%). Also now, the efficiency parameter values are characteristic of the third generation of separators.

Compared to the 2nd and 3rd generation separators, the WEDAG mill separator is presented in Table 11.

Table 11. Parameters of the cement factory separator

Separator parameters	Generation III	Generation II	WEDAG Separator
Coefficient of recirculation	>2	>2	1.23
Tromp curve characteristics			
By-pass, %	<10	10 - 35	8.30
imperfection, -	<0.310	0.30 - 0.45	0.40
acuity limit, μm	<15	15 -20	33.3
The slope of the RRS line, -	>1	0.85 - 1.0	0.90

It can be said that the efficiency parameters of the separator are favourable, located between those specific to the second and third generations of separators, under the conditions of low recirculation coefficients.

CONCLUSIONS

Following the audit of the mill, the following recommendations were proposed:

At the grinding:

- increasing the load of the mill with material, respectively increasing the degree of recirculation;
- increasing the degree of filling of the mill with grinding bodies to the maximum level allowed in both chambers, in order to increase productivity;
- increasing air speed through the mill by increasing aeration;
- increasing the weight of the average ball in room I;
- periodic inspection of the interior of the mill and intervention at the slots, diaphragm, wall exit mill, armour, etc.
- periodic cleaning of the bulkhead slots and the wall at the outlet of the stuffed ball mill, as well as the exhaust screen around the spray nozzle.

At the separation:

- periodic inspection of the interior of the separator;
- the value of the by-pass is within the range specified by the literature for the manufacture of this type of cement (5-15%);
- the slope of the RRS right indicates a narrower distribution of particle sizes in cement, which may be beneficial for the final strength of the cement. For this type of manufactured cement, the literature mentions the range of 0.85-1.15 for the slope of the RRS right.

ACKNOWLEDGEMENTS

This research paper was carried out, among others, through the Human Capital Operational Program, the Project 'Scholarships for entrepreneurial education among doctoral students and postdoctoral researchers (Be Antreprenor!)', no. 51680/ 07.09.2019.

REFERENCES

Ciobanu, C., Tudor, P., Constantin, G.A., Musuroi, G. (2020). Determination of granulometrical composition of the clinker by grinding in a ball mill to determine the specific consumption of additional energy*, 9th Int. Conference on Thermal Equipment, Renewable Energy and Rural Development*, E3S Web of Conferences, 180, 04007, https://doi.org/10.1051/e3sconf/202018004007

Engin, T., Arı, V. (2005). Energy auditing and recovery for dry type cement rotary kiln systems - A case study. *Energy Conversion and Management, 46(4),* 551-562.

Garba, K., Abubakar, A.I., El-Nafaty, U.A. (2010). Energy audit and conservation opportunities for pyroprocessing unit of a typical dry process cement plant, *Energy*, *35(3),* 1237-1243, doi: 10.1016/j.energy.2009.11.003.

Khan, S.N.M., Sethi, Y.P., PatiShow, S.N., Singh, R., Saxena, A., Shah, K.A., Dubey A.K. (2012). Technical audit of an Indian cement plant, Cement International, No.3 (10).

Krishnamoorthy, K., Amarnath, P., Roshan, V., Thangavel Pandi, M. (2018). Investment Grade Energy Auditing in Cement Industry, International *Journal for trends in Engineering and Technology*, *30(1),* 47-51.

Ramesh, A., Akkarapattiakkal, L.A.J., Madhu G. (2013). Energy audit of thermal utilities in a cement plant, *International Journal of Mechanical Engineering (IJME) 2(2),* 11-22.

***SR EN 196-6:2019, Metode de încercare a cimenturilor. Partea 6: Determinarea fineții (Cement test methods. Part 6: Determination of fineness) (asro.ro)

***Mastersizer 2000E equipment, https://www.n8equipment.org.uk/equipment/detail/mastersizer-2000e

***Cement mill audits - Infinity for cement equipment, https://www.cementequipment.org/home/cement-grinding-system/cement-mill-audits/

***Performing a cement plant operations audit, https://thecementinstitute.com/performing-a-cement-plant-operations-audit/

Scientific Papers. Series E. Land Reclamation, Earth Observation & Surveying, Environmental Engineering. Vol. XII, 2023
Print ISSN 2285-6064, CD-ROM ISSN 2285-6072, Online ISSN 2393-5138, ISSN-L 2285-6064

LAND DEGRADATION AND CLIMATE CHANGE

Mihai Teopent CORCHEȘ

"1 Decembrie 1918" University of Alba Iulia, 5 Gabriel Bethlen Street, Alba Iulia, Romania

Corresponding author email: corchesmihai@yahoo.com

Abstract

Land degradation is a worrisome phenomenon that is closely related to climate change, contributing to the accentuation of climate change and at the same time being caused by it. Land degradation is mainly caused by human activities that lead to soil pollution or degradation, by agricultural practices, by forestry management, urbanization but also by extreme weather phenomena such as floods and droughts. Desertification is also a land degradation phenomenon that is caused by climate change and that contributes to intensifying climate change. This study aims to summarize the main causes leading to land degradation and which have a major contribution to the exacerbation of climate change, but also to identify the appropriate measures to avoid, reduce and reverse land degradation. At the same time, this study identifies the main direct and indirect impacts of land degradation on people's way of life. Regarding the impact of climate change on land degradation, the study identifies ways in which climate change accentuates land degradation processes.

Key words*: climate change, land degradation, impact.*

INTRODUCTION

Land degradation is a global problem that threatens economic and social development all over the world. Land degradation is a rather complex process, caused by various anthropogenic activities but also by climatic conditions that reduce the productive potential of the land, at the same time reducing much-needed agricultural production in the context of the continuous increase in the global population. At the same time, in certain areas where agriculture is the main occupation of the people, land degradation increases the vulnerability of farmers to food shortages, possibly jeopardizing even the possibility of people's survival. Land degradation is a complex process to define, with results that are difficult to quantify, but which represents in general terms a permanent or temporary loss or reduction of the productivity of natural capital in various forms, followed by a loss or reduction of the economic value of the land. According to the study carried out by UN Environment, in partnership with the Global Environment Facility (GEF), one-third of the Earth's land surface is degraded, affecting more than 2.6 billion people and costing us as much as $10.6 trillion every year in lost ecosystem services. The pressure on agricultural land will increase significantly in the next period, until the year 2050 an increase in the need for food is presumed to increase by approximately 50 percent, and ensuring this need will represent a major challenge. (United Nations et al., 2017).
During the Conference of the Parties to the United Nations Convention to Combat Desertification (UNCCD), held on 9-10 September 2019 in New Delhi, it was emphasized that desertification/land degradation and drought undermine health, development and prosperity in all regions and the effects of degradation of land and drought are felt most by vulnerable people. Also, within this conference organized under the United Nations Decade on Ecosystem Restoration (2021-2030), it was proposed as a Sustainable Development Goal to achieve the neutrality of land degradation by promoting practices that conserve and restore land and soil affected by desertification/land degradation, drought and floods. (United Nations et al., 2017).

MATERIALS AND METHODS

The purpose of this study was to summarize the main causes of land degradation and how climate change contributes to land degradation, but also how degraded land exacerbates climate change. In order to carry out this study, a

literature review was carried out to provide a better understanding of these phenomena and the intensity of them at a global level. At the same time, the research also focused on how land degradation affects people's livelihoods, but also on an identification of the main measures that could be taken to prevent land degradation and to restore degraded land.

RESULTS AND DISCUSSIONS

Land degradation leads to a temporary or permanent loss of the productive capacity of the land, manifested by a reduction in biomass, a loss of current or potential productivity of the land, a loss of biodiversity and even a loss of organic soil content (Kemalo et al., 2021)
Anthropogenic activities that cause land degradation are the following:
- ***Deforestation*** leads to the degradation of forest land and is considered the main cause leading to the loss of biodiversity (loss of habitats and species).
According to the data presented by FAO, forests have an uneven global distribution and occupy over 31 percent of the global land surface, and represent 4.06 billion hectares, or approximately 5000 square meters per person. Forests are not equally distributed around the globe, the first 10 countries with the largest areas covered by forests at the global level owning two-thirds (66 percent) of global forests (Table 1) (FAO and UNEP, 2020).

Table 1. Global distribution of forests showing the ten countries with the largest forest area, 2020 (FAO and UNEP, 2020)

Country	Forest area (million hectares)	% of world forest
Russian Federation	815	20.1
Brazil	497	12.2
Canada	347	8.5
United States of America	310	7.6
China	220	5.4
Australia	134	3.3
Democratic Republic of Congo	126	3.1
Indonesia	92	2.3
Peru	72	1.8
India	72	1.8

Deforestation to convert land to agricultural land or other uses can lead to land degradation. Since 1990, it is estimated that approximately 420 million hectares of forest have been lost through conversion to other land uses, with the expansion of agriculture continuing to be the main cause of deforestation and forest degradation, being large-scale agriculture. (FAO and UNEP, 2020)
The average annual rate of forest area change, which considers forest expansion and deforestation (Figure 1), decreased from -7.84 million ha/year in the period 1990-2000 to -4.74 million ha/year in the period 2010-2020 (FAO and UNEP, 2020).

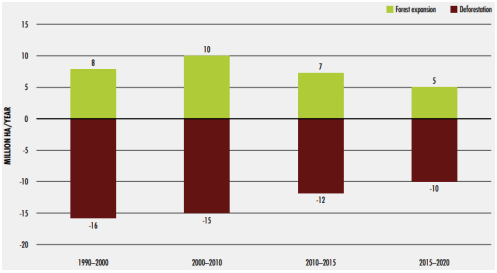

Figure 1. Global forest expansion and deforestation, 1990-2020 (FAO and UNEP, 2020)

- ***Land use changes*** - are accelerated by economic development and population growth in certain areas, especially in developing countries. Thus, a permanent pressure is exerted on agricultural lands in the vicinity of human agglomerations, by converting them into buildable land for residential areas, industrial areas or for the development of infrastructure. As a result of these pressures, arable land is decreasing dramatically, representing a major threat to food security. (Yuzhe et al., 2011).
Agricultural land refers to the share of land area that is arable, under permanent crops, and under permanent pastures. In 2020, globally, agricultural land occupied an area of approximately 47,388,929 sq. kilometres according to the World Bank collection of development indicators. This area represents around 36.5 percent of the world's land area. (The World Bank Group, 2023)
- ***Unsustainable land management***, includes agricultural over-exploitation that reduces the supply of soil organic matter as well as its resistance to erosion.
- ***Soil erosion*** - is a major problem faced by the land under the action of various environmental factors. Erosion and transport of soil material is mainly caused by water through precipitation or erosion due to runoff or seawater erosion.

Along with the eroded soil, the water also picks up various residues of pesticides and organic or inorganic fertilizers applied to the soil. Other causes are wind erosion and various human activities. Erosion reduces soil fertility and implicitly its economic value, and the intensity of the phenomenon is proportional to the degree of vegetation coverage of the soil. Soil erosion is also accentuated on recently deforested sloping land where the vegetal carpet is not sufficiently developed (Figure 2). Wind erosion is a phenomenon that cannot be neglected. According to some studies, during a storm, up to 15 tons of soil can be lost from one hectare, which represents a decrease in the thickness of the soil layer by up to 1 mm (Alam, 2014).

Figure 2. Soil erosion after deforestation
(Poiana Horea, Cluj County, Romania, 2021)

Land degradation through erosion also has an impact on other long-distance environmental factors, such as the aquatic and marine environment, and on human health (through wind erosion). Eroded soil is not only a loss of resources but can also be a source of pollution, especially of air and water (Alam, 2014).

- ***Desertification*** - is a phenomenon of extreme long-term land degradation in arid, semi-arid, and dry sub-humid areas, known as drylands, produced by human activities and climatic conditions, which leads to the loss of at least one of the characteristics of the land: biological productivity, ecological integrity, or economic value. Invasive plants also contribute to the phenomenon of deforestation (Assennato, 2020; Mirzabaev, 2019).
- ***Land salinization*** - occurs naturally in drylands regions of the world, as a result of hydrological changes in the soil, by increasing the mineralized groundwater level, which leads to an increase in the salt content of the soil. This phenomenon also occurs due to anthropogenic causes because of improper irrigation of the land (Mirzabaev, 2019).
- ***Land compaction*** - occurs because of agricultural works carried out with heavy equipment that change the structure of the soil leading to its compaction, the reduction of soil porosity and its hydraulic properties resulting in the reduction of plant root growth followed by the reduction of soil productivity by up to 50 percent (Shaheb, 2021).
- ***Urbanization*** - is an important trend especially in developing countries. The expansion of residential areas around cities reduces the areas occupied by agricultural land, produces changes in the vegetation that naturally occupies the soil, changes the degree of soil compaction and aero-hydric properties of the soil. The topsoil is mixed with the lower organic matter-poor layers and is often mixed with various building material scraps and waste. Microclimatic conditions in urbanized areas often change and the level of pollutants in the soil increases.
- ***Grazing*** is also associated with soil compaction depending on its intensity (heavy, moderate, or light) and overgrazing. A study published in 2020 showed that compared to un-grazing, the heavy and moderate grazing significantly increased soil bulk density and penetration resistance and reduced soil organic carbon and total nitrogen. Heavy grazing significantly decreased nitrate (NO_3^-), water content, and microbial biomass carbon. All this study concluded that light grazing significantly increased soil organic content and NH_4^+ (Lai et al., 2020).
- ***Agricultural practices*** have an impact on soil degradation. Inadequate agricultural practices can lead to the reduction or elimination of the vegetal cover, reducing the ability of the soil to store water, which thus becomes vulnerable to erosion if measures are not taken to reduce the rate of water runoff on these lands (Alam, 2014).
- ***Industrial land use*** can lead to an impact on environmental factors, especially by increasing the areas occupied by various types of waste, but also by increasing the level of air pollution,

which is a vector for the transfer of pollutants into the soil.

- ***Natural disasters*** such as earthquakes, volcanic eruptions, landslides, floods, avalanches and tsunamis are direct causes of land degradation, leading to land deformation and topsoil degradation (Sharma, 2019).

Climate change exacerbates land degradation in the following ways:

- ***Increasing global temperature*** intensifies land degradation processes. As global temperatures increase, the hydrological cycle also intensifies, thus producing more intense precipitation, which is an important factor in the intensification of erosion phenomena (Olson et al., 2019; Sandu et al., 2014). The increase in global temperature increases the risk of wildfires, which are also responsible for intensifying the phenomena of desertification.
- ***Thermal stress*** is accentuated because of climate change that produces more intense and more frequent heat waves, which lately most often coincide with periods of soil drought, increasing the temperature and decreasing the air humidity. The decrease in air humidity can modify human heat stress which sometimes produces serious effects on human health (Wouters et al., 2022).
- ***Sea level rise*** because of climate change affects coastal areas by intensifying erosion, but also by intensifying the salinization of groundwater through seawater intrusion. (Mirzabaev et al, 2019). Sea level rise can lead to the permanent loss of large areas of land.
- ***Changing precipitation patterns*** caused by climate change play an important role in a multitude of processes occurring at ground level. Agricultural and ecosystem productivity is closely related to soil moisture levels, soil biogeochemical processes are influenced by temperature and soil moisture (Roque-Malo et al., 2017). Changing the precipitation regime can distort the distribution of precipitation globally, intensifying erosion phenomena in some areas, substantially changing the water supply of the soil in other areas, all these effects leading to land degradation. Changing rainfall patterns may lead to more frequent and more intense flooding. At the same time, the change in the rainfall regime can have an impact on agriculture, which will be affected by the lack of water in the soil in some areas of the world and which will develop in other areas where the rainfall regime will be higher. The intensification of drought phenomena in some areas diminishes the vegetation of the land, intensifying the phenomena of erosion and leading to the depletion of nutrients in the soil.

The impact of climate change on agriculture can manifest itself differently globally by decreasing agricultural productivity in some areas and intensifying agriculture in other areas, which can cause soil degradation in areas not affected by such phenomena in the past (Olson et al., 2019).

- ***Intensification of cyclones*** is a likely cause of climate change, leading to intensification of rainfall and wind intensity along coastal regions associated with increased relative air humidity in these areas, as well as intensification of flooding and land erosion phenomena in coastal areas (Sarkar, 2022).
- ***Permafrost thawing*** is also considered a threat to the integrity of polar and subpolar infrastructure. This impact is often linked to anthropogenic global warming. Infrastructure damage was observed in up to 80 percent of buildings in some cities in Russia and about 30 percent of some road surfaces in the Qinghai-Tibet Plateau. It is estimated that these damages will continue in the next period, until 2050, 30-50 percent of critical circumpolar infrastructure thought to be at high risk (Hjort et al., 2022).

How land degradation affects people's livelihoods:

- ***Affect the standard of living***

The number of people whose livelihood depends directly on natural resources for subsistence, food security and income, and who depend on degraded land is estimated at 1.5 billion worldwide. Land degradation reduces the productivity of the land and increases the workload of managing the land, leaving people vulnerable to extreme climatic events, with consequences such as poverty and food insecurity, and in some cases to migration, conflicts and the loss of cultural heritage (Olson et al., 2019).

- ***Problems at the political level***

Public decision-making authorities in areas affected by land degradation are often held responsible for making wrong decisions or not making certain decisions in time. All of them

are subject to pressure from the public who are increasingly aware and concerned about the causes and effects of climate change and are also responsible for integrating climate change adaptation and mitigation measures into national, regional and local level plans and programs. As the effects of climate change become more evident and natural disasters become more intense and frequent, causing major effects especially on agriculture, people will suffer, especially in poor countries, all of which may cause riots and political instability.

- ***Social and economic***

The social and economic consequences of land degradation are associated with the low economic development of the areas occupied by such lands but also with the high environmental costs for adaptation to present and future conditions. Economic instability and the reduction of the means of subsistence of the local community can lead to the migration of the population from the traditional lands from which they will no longer be able to secure their daily livelihood.

To reduce the areas affected by land degradation, the following measures can be taken:

- ***Land restoration*** has the main purpose of accelerating the natural recovery rate of degraded lands. Reforestation of deforested areas can reverse the trend of biodiversity loss, but it is also an effective method of capturing carbon from the atmosphere, but it can also bring economic advantages. Some researchers have shown that investments in environmental protection can lead to an increase in Gross Domestic Product per capita over time (Todea, 2018).
- ***Land revegetation*** prevents erosion and desertification, also leading to the improvement of soil quality over time. Agricultural management measures based on agroforestry can also be promoted because it is well known that agroforestry improves soil conditions.
- ***Conservation tillage*** and replenishment of soil organic matter can restore poor soils.
- ***Restoring the natural hydrology of rivers*** can increase the frequency of floods in river floodplains, the deposited silt increasing soil fertility.
- ***Public involvement in decision-making***. In large brownfield restoration projects, it is absolutely necessary to involve the local community from the early stages of planning, to identify and resolve potential conflicts, to take into account possible conflicting points of view and to present to them the main objectives of the restoration project. The local community, which has a key role in the sustainable and long-term restoration of degraded land, can often be composed of the local population, public government authorities, NGOs, the academic community, and may have different interests, goals and knowledge about local ecosystems, which must be taken into account (Santini, 2022).

CONCLUSIONS

Land degradation is a worrying phenomenon, closely related to climate change, which manifests itself over large areas worldwide, the effects of which are not fully quantified economically in terms of lost productivity. Land degradation is mainly caused by anthropogenic activities, but also by natural causes, the phenomenon of degradation being accentuated by climate change, but in turn, degraded land contributes to intensifying the intensity of climate change. Land degradation affects people's well-being but can also cause political, economic and social disturbances in areas strongly affected by these phenomena.

In the context of the intensification of climate change, for the well-being of future generations, it is necessary to identify and preserve lands unaffected by degradation phenomena, and to apply management measures in order to preserve their productivity. At the same time it is vital that we restore our degraded land, and prevent further damage, by adopting sustainable management practices now.

REFERENCES

Alam, A. (2014). Soil Degradation: A Challenge to Sustainable Agriculture, *International Journal of Scientific Research in Agricultural Sciences, 1(4),* 50-55.

Assennato, F., Di Leginio, M., d'Antona, M., Marinosci, I., Congedo, L., Riitano, N., Luise, A., Munafò, M. (2020). Land degradation assessment for sustainable soil management. *Italian Journal of Agronomy, 15*, 1770.

FAO and UNEP (2020). *The State of the World's Forests 2020. Forests, biodiversity and people.* Rome.

Hjort, J., Streletskiy, D., Doré, G. (2022). Impacts of permafrost degradation on infrastructure. *Nature Reviews Earth & Environment, 3,* 24–38.

Kemalo, A., Isreal, Z. (2021). Effect of Land Degradation on Livelihood. *Asian Journal of Plant Science and Research, 2021, 11 (5), 149-153*.

Lai, L., Kumar, S. (2020). A global meta-analysis of livestock grazing impacts on soil properties. *PLoS ONE, 15(8).*

Mirzabaev, A., Wu, J., Evans, J., García-Oliva, F., Hussein, I.A.G., Iqbal, M.H., Kimutai, J., Knowles, T., Meza, F., Nedjraoui, D., Tena, F., Türkeş, M., Vázquez, R.J., Weltz, M. (2019). *Desertification. In: Climate Change and Land: an IPCC special report on climate change, desertification, land degradation, sustainable land management, food security, and greenhouse gas fluxes in terrestrial ecosystems* [P.R. Shukla, J. Skea, E. Calvo Buendia, V. Masson-Delmotte, H.-O. Pörtner, D.C. Roberts, P. Zhai, R. Slade, S. Connors, R. van Diemen, M. Ferrat, E. Haughey, S. Luz, S. Neogi, M. Pathak, J. Petzold, J. Portugal Pereira, P. Vyas, E. Huntley, K. Kissick, M. Belkacemi, J. Malley, (eds.)].

Olsson, L., Barbosa, H., Bhadwal, S., Cowie, A., Delusca, K., Flores-Renteria, D., Hermans, K., Jobbagy, E., Kurz, W., Li, D., Sonwa, D.J., Stringer, L. (2019). *Land Degradation. In: Climate Change and Land: an IPCC special report on climate change, desertification, land degradation, sustainable land management, food security, and greenhouse gas fluxes in terrestrial ecosystems* [P.R. Shukla, J. Skea, E. Calvo Buendia, V. Masson-Delmotte, H.-O. Pörtner, D. C. Roberts, P. Zhai, R. Slade, S. Connors, R. van Diemen, M. Ferrat, E. Haughey, S. Luz, S. Neogi, M. Pathak, J. Petzold, J. Portugal Pereira, P. Vyas, E. Huntley, K. Kissick, M. Belkacemi, J. Malley, (eds.)].

Roque-Malo, S., Kumar Praveen. (2017). Patterns of change in high frequency precipitation variability over North America, *Scientific reports, 7*, 10853.

Sandu, M.A., Virsta, A., Petrescu, N., Mocanu, P. Ivanescu, V. (2014). Deforestations impact on extreme hydrological phenomenon. *SGEM 2014 Conference Proceedings, 1, 177-182.*

Santini, N.S., Miquelajauregui, Y. (2022). The Restoration of Degraded Lands by Local Communities and Indigenous Peoples - *Frontiers in Conservation Science, 3,* 873659.

Sarkar, Debajit (2022). *Intensification of Tropical Cyclones due to climate change: A case study from Bay of Bengal (2001-2020)*, DO - 10.13140/RG.2.2.22584.62728.

Shaheb, M.R., Venkatesh, R., Shearer, S.A. (2021). A Review on the Effect of Soil Compaction and its Management for Sustainable Crop Production. *J. Biosyst. Eng., 46,* 417–439.

Sharma, A. (2019). *The Social and Economic Impact of Soil Degradation in India: A Survey of Literature*, doi 10.13140/RG.2.2.28629.17128.

The World Bank Group (2023). *Agricultural land (% of land area) - https://data.worldbank.org/indicator/*

Todea, N., Cioca, C. (2018). The analysis of the correlation between environmental protection expenditure and gross domestic product in EU countries, *Journal of Environmental Protection and Ecology, 19(4),* 1947-1954.

United Nation Environment, Global Environment Facility (GEF) (2017). *Land degradation - factsheet*

Wouters, H., Keune, J., Petrova, I.Y., van Heerwaarden Chiel C., Adriaan J., Teuling, J., Pal, S., Vilà-Guerau de Arellano, J., Miralles, D.G. (2022). *Science advances, 8.*

Yuzhe Wu, Xiaoling Zhang, Liyin Shen (2011). The impact of urbanization policy on land use change: A scenario analysis (2011). *Cities, 28(2),* 147-159.

Scientific Papers. Series E. Land Reclamation, Earth Observation & Surveying, Environmental Engineering. Vol. XII, 2023
Print ISSN 2285-6064, CD-ROM ISSN 2285-6072, Online ISSN 2393-5138, ISSN-L 2285-6064

WORKS SPECIFIC TO THE INTRODUCTION OF SILVOPASTORAL SYSTEMS IN THE FOREST FUND

Ghiţă Cristian CRAINIC, Florin COVACI, Nicu Cornel SBĂU, Silviu Ioan SICOE, Flavia IRIMIE (CIOFLAN), Marinela Florica BODOG, Călin Ioan IOVAN

University of Oradea, 1 University Street, Oradea, Romania

Corresponding author email: calin_iovann@yahoo.com

Abstract

The introduction of areas with a different use into the forest fund is relevant for several reasons considering the area of the forest fund in our country which is below the European average. In recent decades, silvo-pastoral systems, represented by common pastures with partially afforested meadow, have undergone a series of transformations. In a great measure they have been abandoned, which is why successions of pioneer species, with low ecological and economic value, have been triggered on these surfaces. As a result, the utility of these silvo-pastoral systems has been reduced considerably, in some cases their introduction into the forest fund being opportune or even necessary. The current legislation regulates the possibility of introducing into the forest fund some areas occupied by forest vegetation in compliance with some functional and administrative conditions - the consistency index > 0.4, the necessity to prepare a forestry management plan, the observance of the forestry regime, etc. The works necessary for the introduction of the silvo-pastoral systems into the forest fund involve a series of specific activities, namely precise delimitation and spatial positioning of the related areas, their mapping and evaluation, the establishing of the complexity of necessary silvotechnical interventions and, last but not least, the ensuring of their ecosystem stability. As a consequence, these works will be executed in stages, depending on the complexity of the conditions characteristic to these activities.

Key words: *forest fund, forest vegetation, silvopastoral systems, silvotechnical interventions, succession of pioneer species.*

INTRODUCTION

The agroforestry and silvopastoral systems represent complex land exploitation systems that are suitable simultaneously for agricultural crops, horticultural crops, forest crops and, respectively, for raising animals (Nair, 1993).

As a result, these complex systems of vegetable crops (Crainic & Stamate, 2009) and animal production, present a series of peculiarities, depending on the geographical area on the world map, thus highlighting a series of such systems, for the specific conditions of all continents (Cubbage et al., 2012).

The silvo-pastoral systems represent complex opportunities for diversified exploitation of the productive potential of the land, respectively the cultivation of trees from forest species of national and local interest, and the raising of animals. Although the agroforestry, agrosilvopastoral and silvo-pastoral systems present a series of advantages, after 1989, in many areas in Romania, their maintenance and promotion were unjustifiably abandoned. As a result, a series of such land exploitation systems were abandoned, unjustifiably, by the owners, and currently, for their optimal exploitation, a series of mapping works are needed (Bodog & Crainic, 2016) and maintenance (Crainic, 2017), correlated with the specifics of the land exploitation system.

This category also includes a series of partially wooded pastures (pastures on which biogroups with forest vegetation are installed), which were used especially for raising animals, and from the biogroups of trees, the wood had various uses for the proprietary communities from the area.

In the last three decades, the interest in raising animals in individual households has considerably reduced, and silvopastoral holdings have largely degraded, as a result, successive processes related to forest vegetation (successions between pioneer and fundamental forest species) have been highlighted on the respective surfaces.

In Romania, the area of the forest fund related to the number of inhabitants (population) is

0.27 ha and is below the European average (Florescu & Nicolescu, 1996; Nicolescu, 2009). In this context, for a series of lands, which are not used in accordance with the category of use, in the case of pastures undergoing afforestation, the necessary steps are taken to introduce them into the forest fund, private or state property, depending on the situation.

In the last two decades, in Romania, the area of land that has been forested has increased significanthly (Abrudan et al., 2003; Willoughby et al., 2008). As a result, a series of degraded and/or unsuited lands for agriculture were included in the national forest fund (Abrudan et al., 2003).

A particular situation is the introduction into the forestry fund of the Dobreşti Territorial Administrative Unit (municipality), administered by the Codrii Cămării Forestry of the Autonomous Management (A.M.) of an area of 7.60 ha, which comes from a silvopastoral system, respectively a wooded pasture.

The necessary administrative acts (documents) were drawn up for this area, to be included in the forest fund, and respectively for the change of the use category.

The introduction of this area of 7.60 ha into the forest fund requires a mapping, an analysis and an elaborate study, regarding the situation on the ground (the actual state) of it, in order to be able to establish on a scientific basis the complex of necessary measures, which they will impose.

For the various works specific to the forestry sector, technical norms are currently being developed, depending on their specificity. In the case of lands with a different category of use than forestry, namely wooded pastures (degraded silvopastoral systems), a series of works to introduce them into the forest fund, present different particularities, mostly transitory. As a result, the design, implementation and completion of these specific - transitory works must be carried out professionally, in some situations requiring particular solutions, based on local experience.

Currently, on a European level, a series of studies have been carried out regarding the forest management model, which would satisfy the requirements of the current society regarding forest products and services (Duncker et al., 2012). In this context, several models of forest management have been proposed, which satisfy certain requirements, very clearly established, depending on the geographical area and, respectively, the silvoproductive potential of the habitat.

Consequently, the process of introducing into the forest fund some areas from similar use categories (areas related to agroforestry, silvopastoral, agrosilvopastoral systems), must include a series of legal, technical and economic aspects.

Currently, in Romania, as part of the National Recovery and Resilience Program (P.N.R.R.), on December 12, 2022, the Guide to financing afforestation through the P.N.R.R. was launched, thus creating legal and technical codes, for the introduction into the forest fund, of lands that are not suitable for agriculture, or that have been abandoned and on which complex systems of exploitation, with specific agroforestry or silvopastoral, functioned in the past.

As a result, by introducing into the forest fund some areas on which complex exploitation, agroforestry and/or silvopastoral systems have been organized, the importance of these complex land exploitation systems is not diminished, but the introduction into the productive system within the forestry sector is aimed at, of these areas, which are not suitable for high-performance agriculture, with all the advantages that arise from this complex process (carbon storage, environmental protection, increase in the area of the forest fund, etc.).

MATERIALS AND METHODS

The present study was carried out on an area of 7.60 ha, from the property of the Territorial Administrative Unit (T.A.U.) Dobreşti, Bihor County (Figures 1 and 2), which was included in the forest fund administered by the private Forest District of Codrii Cămării Autonomous Management (A.M.). This surface was used as wooded pasture, and was introduced into the forest fund, based on a land exchange, carried out by National Agency Romanian Watershed Crişuri Oradea with T.A.U. Dobreşti, in compliance with the legislation in force.

The research and studies started in the spring of 2013 and continue partially even today.

As research methods were used: bibliographic documentation, analysis and study of the forest management and forest map in the areas adjacent to the location, analysis of acts, documents and records within the forestry unit that will manage the respective area, observation on the itinerary, stationary observation, experiment, comparison, simulation, spatial positioning, mapping, digital recording of representative images.

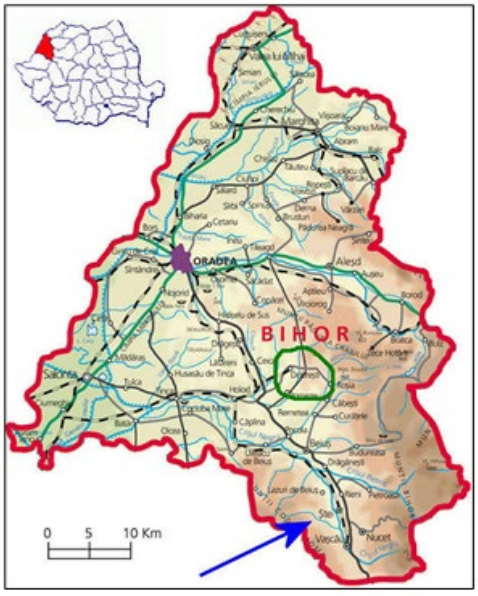

Figure 1. General location of the study
(https://pe-harta.ro/bihor/)

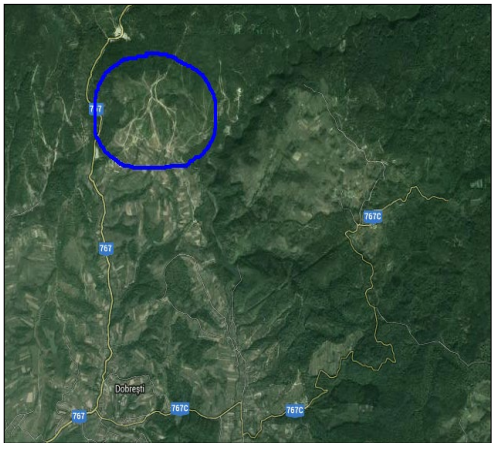

Figure 2. Location of the studied area
(https://maps.google.ro/maps?hl=ro)

To establish the type of forest resort, the type of soil, the type of indicator flora and respectively the type of forest, maps were carried out on the ground and a comparative analysis was carried out, taking as a reference the forest ecosystems in the immediate vicinity, which are even adjacent to the analyzed and studied surface.

The positioning of the characteristic contour points of the surface that will be the subject of the introduction into the forest background and the respective case study, the GPS system was used, within the G.N.S.S. technology, using dual frequency receivers, model TRIMBLE R10 (Crainic, 2011; Pica et al., 2022) (Figure 3).

Figure 3. Positioning of details with the GPS system through the RTK method

The working method used was R.T.K. - respectively kinematic positioning in real time, with obtaining the coordinates of the points positioned on the ground, in real time. The Trimble Controller program was used to collect field data and process it (Crainic, 2011).

The MapSys 10 program was used to report the coordinates of the contour points. The orthophoto plan of the work area was also used, for appropriate information regarding the spatial position of the studied surface (Crainic, 2011).

The work of mobilizing the soil, making the terraces, and digging the pits in which the saplings with bare roots were planted, was done with the mountain hoe (Figure 4).

Figure 4. The mountain hoe used for mobilizing the soil and building the terraces (original photo)

Chainsaws, power tools and tools were used to carry out the land preparation works, depending on their specifics. The woody vegetation was removed using the "STIHL" MS 180 mechanical chainsaw, and the Stihl F.S. 310, and Strauss motor tool (Figure 5).

Figure 5. The cutter Straus

The sequence of works was staggered by vegetation seasons, depending on the state of the forest crops and the biogroups of the pre-existing usable seedbed, respectively on their rate of growth and staged development.

RESULTS AND DISCUSSIONS

The area of 7.60 ha that will be included in the forest fund, and is the subject of this case study, was positioned with the GPS system, and the coordinates of its characteristic contour points, which were determined in real time, were reported in the plan with the MapSys 10 program and superimposed on the orthophoto plane related to the respective area (Figure 6).

Figure 6. Spatial location of the study area

Also, a series of biogroups with usable pre-existing seed from the *Quercus cerris* species, which will be included in the future arboretum, were positioned, and mapped (Figure 7).

Figure 7. Biogroups with specimens of the *Quercus cerris* species, which were integrated in the artificial regeneration, in the plot that will be introduced into the forest fund

The research, studies and analyzes carried out in the plot of the silvopastoral system, with an area of 7.60 ha, which was included in the forest fund, led to the obtaining of some results regarding the soil, habitat, and vegetation, which are presented below.

The identified soil type is luvic brown, with the code 240, which occurs on substrates poor in calcium and ferromagnesian minerals, respectively on clays, silicic shales, quartzites, mica shales, alternations of sandstones with clays, on gently sloping slopes or plateaus. The acidity varies between 5.3-5.8. It is intensely humiferous on the surface, with a humus content of 11.3-4.5% per 10 cm thickness. It shows the degree of saturation in bases of 59% in the El horizon and 72-76% in Ao and Bt is a mesobasic soil.

The creditworthiness is superior for beech, oak and hornbeam - on a soil with a large edaphic volume and shaded slopes, and medium in the other cases.

The type of resort that was identified in the area where the studied area is located is 5132 - Hilly of oaks Bm, medium edaphic luvosol, with mesophytic flora with grasses +/- *Luzula*. The relief is represented by a moderately undulating slope, with South-West exposure, sunny.

The identified forest type is 5131 - Coastal oaks with *Graminee* and *Luzula luzuloides*, of medium productivity (m), on the border with forest type 7112- Hill oaks (with *Quercus cerris*) of medium productivity (m).

Because the studied location is positioned in the phytoclimatic floor corresponding to the stands that have in their composition the species *Quercus cerris* L., *Quercus petraea* (Matt), Liebl., *Fagus sylvatica* L., *Fraxinus excelsior* L., *Acer pseudoplatanus* L., *Prunus avium* L., in the forest culture that will be installed on the surface of 7.60 ha, which is introduced into the forest fund, the future arboretum will have these species in its composition.

As a result, the afforestation formula, which was used for the installation of forest vegetation on the studied and analyzed surface, in accordance with the type of soil, the type of forest, the type of habitat and the technical norms in force, is the following: 60%*Quercus petraea* + 20%*Fagus sylvatica* + *20Acer pseudoplatanus/Fraxinus excelsior/Prunus avium.*

Also, the use of forest vegetation that has settled naturally, in biogroups, belonging to the species *Quercus cerris*, *Quercus petraea*, *Fagus sylvatica*, and various mixed deciduous species, characteristic of the respective habitat, will be considered.

The works required for the introduction of a plot of 7.60 ha into the forest fund, from a silvopastoral system, are similar to a series of silvotechnical works, but the working conditions are specific to agroforestry and/or silvopastoral systems. As a result, these works must be established, designed, executed and received rigorously, in order to obtain very good results, with minimal expenses.

After the spatial positioning and respectively the mapping of the surface that will be introduced into the forest fund, the works were established and carried out, staged, depending on the dynamics of the installation process, growth and development of the artificial and natural regeneration (where it is installed).

The proposed and executed works are represented by:

-cleaning the land of grassy and woody species;

-manual cutting of bushes, shrubs and thin trees without removing the root;

-the mobilization and preparation of the soil in order to establish the forest vegetation;

-the installation of forest vegetation, through plantations, in previously prepared land;

-completion of artificial regeneration through plantations;

-removing the overwhelming grassy vegetation from and between the rows of saplings, mechanized, with a power tool, using the disc as an active organ;

-removal of the overwhelming grassy vegetation on and between the rows of saplings, mechanized, with a power tool, using mechanical shears as the active organ.

These works are presented in detail, with the specific peculiarities of the time and production norms, related to the forestry sector (Table 1).

To prepare the land to mobilize the soil and install forest vegetation, the land was cleared of grassy and woody species, by mechanized cutting of bushes, shrubs and thin trees without removing the roots. As a result, light power saws, disc power tools and power shears were used.

To avoid the reduction of the area to be introduced into the forest fund, the plant material that resulted from the soil preparation works was removed from this area, and later it was used differently. After the removal of the grassy and woody plant remains, the mobilization of the soil became relatively easy.

The mobilization and preparation of the soil for the installation of forest vegetation was done manually, with a mountain hoe, in continuous strips, having a width of approximately 70-80 (100) cm and a depth of 10-15 cm respectively.

For a good location on the field of the prepared and mobilized bands, they are materialized on the field, by stretching some strings between the stakes (stakes) which are placed on alignments of approx. 50 m.

The mobilized strips were oriented on the level curves, to prevent water runoff from precipitation along the line with the highest slope (Figure 8). In 2013, an area of 4.00 ha was mobilized, and in 2014, the difference in surface area of 3.60 ha.

Table 1. Evidence of the works carried out in 2013, for the introduction into the forest fund, of the parcel analyzed and studied related to the silvopastoral system

Work done				
Code (standard symbol)	The specifics of the work	Unit	Time norm N.T..	Production standard N.P.
C.1.III.B	Cleaning the land of grassy and woody species;	100 square meters	0.68	11.83
C.4.A.b	Manual cutting of bushes, shrubs and thin trees without removing roots;	100 square meters	2.63	3.04
C.18.A.I.a.2	Prepared land in simple terraces 70-80 cm wide, with skeleton content below 25% (50-60 cm)	meter of terrace	0.17	46.39
C.18.A.I.b	Prepared land in simple terraces with a width of 70-80 cm, with a skeleton content of 25-50% (50-60 cm)	meter of terrace	0.26	30.20
C.24.I.b.1	Ditch storage of three-year-old deciduous saplings;	1000 pieces	0.21	38.84
C.28.I.A.b	Planted seedlings in prepared soil in pits of 30x30x30 cm in medium conditions - grouped norm;	1000 pieces	45.55	0.176
C.58.I.b	The discovery of forest species of herbaceous and woody species	100 square meters	1.16	6.90

Figure 8. Orientation of the mobilized bands on the level curves

The forest vegetation installation works on the studied surface were carried out by planting forest saplings with bare roots, started in the spring of 2013, and were staggered over a period of five years. In the spring of 2013, integral plantations were carried out on an area of 4.0 ha, and in the spring of 2014, the area difference of 3.6 ha was completed with integral afforestation works (Tabel 2). Also, from the spring of 2014 until 2017, works were carried out to supplement the forest vegetation, through plantations, on the surfaces where the artificial regeneration was not carried out (installed) in optimal conditions.

The seedlings were planted in previously prepared land, in pits of 30 x 30 x 30 cm, in a rectangular device, using 5,000 seedlings per hectare at 1.0 m per row and respectively at 2.0 m between rows (Figure 9). The working conditions were average, and for the economic evaluation of the work done, the use of the grouped norm was considered.

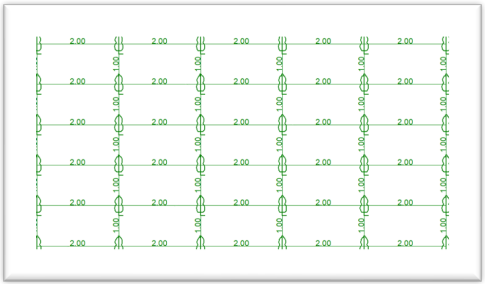

Figure 9. Placement of the saplings that will be planted in a regular device - the shape of a rectangle

Fagus sylvatica saplings were procured from the Codrii Cămării Forestry District A.M. the village of Dobreşti, from a tree registered as a source of seeds, following the agreement of the

Territorial Inspectorate of Forestry and Hunting (I.T.R.S.V.) Oradea, based on the regulations in force. The saplings from the other species were purchased against cost, based on official offers, from authorized nurseries, which had available the necessary biological regeneration material.

Table 2. Record of the surfaces on which integral afforestation works and additions were carried out, for the introduction into the forest fund, of the analyzed and studied parcel related to the silvopastoral system

Year	Surface (ha)		
	with integral afforestation works (I)	with aditions to afforestation works (C)	total with afforestation works
2013	4.0	0.0	4.0
2014	3.6	0.8	4.4
2015	0.0	1.5	1.5
2016	0.0	0.9	0.9
2017	0.0	0.4	0.4
Total	7.6	3.6	11.2

In 2013, 12,000 seedlings of the *Quercus petraea* species, 4,000 of the *Fagus sylvatica* species (Figure 10), 2,000 of the *Prunus avium* species (Figure 11) and 2,000 of the *Fraxinus excelsior* species were planted (Table 3). In total, in 2013, a number of 20,000 saplings on an area of 4.00 ha were planted in the form of biogroups of approximately 25 - 50 specimens of the same species.

In 2014, saplings were planted on the surface difference of approx. 3.6 ha. As a result, a number of 11,000 saplings of the *Quercus petraea* species, 3,000 saplings of the *Acer pseudoplatanus* species, and 4,000 saplings of the *Fagus sylvatica* species were planted.

On the area planted in 2013, part of the planted saplings was displaced (pulled out) by the *Sus scrofa attila* L. species, and it was necessary to complete the artificial regeneration. As a result, a number of 4,000 *Quercus petraea* saplings were planted. In total, in 2014, a number of 22,000 saplings were planted on an area of 4.40 ha.

In 2015, works were carried out to complete the artificial and natural regeneration, on an area of 1.50 ha. Thus, a number of 5,000 saplings of the *Quercus petraea* species were planted, and respectively 2,500 saplings of the *Acer pseudoplatanus* species. In total, in 2015, a number of 7,500 saplings were planted on an area of 1.50 ha.

In 2016, works were carried out to complete the artificial and natural regeneration, on an area of 0.90 ha. A number of 3,000 seedlings of the *Quercus petraea* species, 0,500 seedlings of the *Fraxinus excelsior* species, 0,500 seedlings of the *Acer pseudoplatanus* species, and 0,500 seedlings of the *Larix decidua* Mill species were planted. The species *Larix decidua* was introduced (planted) in the upper part of the slope - where the wind frequently blows, with the main objective of strengthening the ecosystem stability of the future stand, under the action of the dominant wind. In total, in 2016, a number of 4,500 saplings were planted on an area of 0.90 ha.

In 2017, works were carried out to complete the artificial and natural regeneration, on an area of 0.40 ha. A number of 1,000 *Quercus petraea* saplings and 1,000 *Quercus rubra* saplings were planted. In total, in 2017, a number of 2,000 saplings were planted on an area of 0.40 ha.

The surfaces on which there are biogroups with natural regeneration, from the species *Quercus cerris*, *Fagus sylvatica*, *Prunus avium*, *Fraxinus excelsior*, *Acer pseudoplatanus*, *Malus sylvestris*, *Pirus piraster*, etc., have been integrated into the artificial regeneration currently being installed, and which will form the future arboretum.

The total number of saplings, which were planted between 2013 and 2017, in the plot that will be included in the forest fund, is 56,000, on an efectiv total area of 1120 ha, seven species being used (Tables 3 and 4).

Table 3. Records of saplings by species and years, which were planted, for the introduction into the forest fund, of the analyzed and studied parcel related to the silvopastoral system

Year	Species (thousands of pieces)							Total (thousands of pieces)
	Quercus petraea	*Fagus sylvatica*	*Prunus avium*	*Fraxinus excelsior*	*Acer pseudoplatanus*	*Quercus rubra*	*Larix decidua*	
2013	12.0	4.0	2.0	2.0	-	-	-	20.0
2014	15.0	4.0	-	-	3.0	-	-	22.0
2015	5.0	-	-	-	2.5	-	-	7.5
2016	3.0	-	-	0.5	0.5	-	0.5	4.5
2017	1.0	-	-	-	-	1.0	-	2.0
Total	36.0	8.0	2.0	2.5	6.0	1.0	0.5	56.0

Table 4. Evidence of saplings by species, specific to afforestation works and years, which were planted, for the introduction into the forest fund, of the analyzed and studied parcel related to the silvopastoral system

Year	Planted seedlings of the species (thousands of pieces)														Total seedlings planted (thousands of pieces)
	Quercus petraea		*Fagus sylvatica*		*Prunus avium*		*Fraxinus excelsior*		*Acer pseudoplatanus*		*Quercus rubra*		*Larix decidua*		
	Saplings planted, specific to afforestation works, Integral afforestation, C-completions (thousands of pieces)														
	I	C	I	C	I	C	I	C	I	C	I	C	I	C	
2013	12	-	4	-	2	-	2	-	-	-	-	0	0	0	20
2014	11	4	4	-	-	-	-	-	3	-	-	0	0	0	22
2015	-	5	-	-	-	-	-	-	-	2,5	-	0	0	0	7,5
2016	-	3	-	-	-	-	-	0,5	-	0,5	-	0	0	0,5	4,5
2017	-	1	-	-	-	-	-	-	-	-	-	1	0	0	2
Total	23	13	8		2	-	2	0,5	3	3	0	1	0	0,5	56

Figure 10. Specimen (seedlings) of the *Fagus sylvatica* species, planted in the spring of 2013

Figure 11. *Prunus avium* specimen, planted in the spring of 2013

The percentage distribution of saplings planted, by species, for introduction into the forest fund, of the analyzed and studied parcel related to the silvopastoral system, is shown in the Figure 12. From the analysis of the data in the diagram presented in Figure 12, the *Quercus petraea* species has the highest share, over 60%.

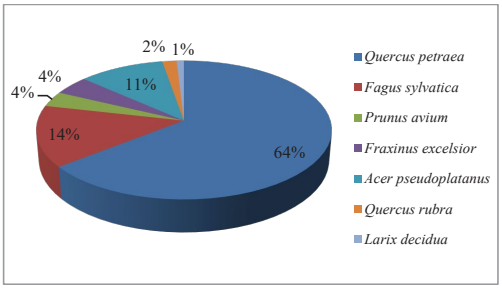

Figure 12. The percentage distribution of saplings planted, by species, for introduction into the forest fund, of the analyzed and studied parcel related to the silvopastoral system

The regeneration maintenance works installed in the plot are presented below.

An opportune work to be carried out within the experimental device is represented by the removal of overwhelming woody and grassy vegetation, respectively the uncovering of the seedbed.

This intervention aims to protect the seed immediately after its installation, against weeds that endanger its existence or that can prevent its development.

The work is carried out only on the portions on which there is a danger of overwhelming the seed, establishing the effective surface through observations and the placement of test squares.

The removal of the overwhelming vegetation will be carried out once or twice a year, the first intervention being done one month after the

beginning of the vegetation season - that is, the end of May, the beginning of June, so that the saplings can be fortified before the arrival of the hot season.
The second clearing is carried out at the end of September - the beginning of October, only if there is a danger that the grasses, weeds, shrubs, shoots due to their height and density will cause the saplings to lie down under the impact of snow. The vegetable mass resulting from the clearing is stored so that it does not disturb the installed seed.
In the present case study, the overwhelming grassy vegetation is represented by the fern *Dryopteris filix-mas* (L.) Schott, which shows a very active vigor of growth and development, in some places even luxuriant. Also, the mulberry species - *Rubus fruticosus* L., is present on some surfaces, overwhelming the biogroups with artificial and natural regeneration.
Considering the particularities of the season and of the grassy and woody vegetation related to the studied site, the following intervention options were proposed:
-removing the overwhelming vegetation from and between the rows of saplings with a motor tool, using the disc as an active organ (Figure 13);
-removing the overwhelming vegetation from and between the rows of saplings with the power tool, using the mechanical scissors as the active organ (Figure 14).
On the reception of the completed works, the specificity, quality and quantity of the completed works were checked and respectively analyzed, in the plot that was included in the forest fund.

Figure 13. Removal of overgrown vegetation from planted seedling rows with a Strauss disc harrow

Figure 14. Biogroups with regeneration from the species *Fagus sylvatica*, overwhelmed by the species *Dryopteris filix-mas*

The reception of the soil preparation and mobilization works was carried out following the passage of the surface on which these works were carried out, thus verifying compliance with their characteristic elements (the way in which unwanted grassy, shrubby and woody vegetation was removed, the way of placing mobilized strips, their width and depth, the distance between them, the degree of soil fragmentation). Following the receptions, it was found that the works were carried out properly, in accordance with the technical rules in force, for the activities in the forestry sector, and as a result, these works were settled (paid) to the executor.
For the reception of the afforestation works and the completion of the regeneration, it is necessary to place some trial areas in this sense. In accordance with the Technical Norms for carrying out the annual control of regenerations, for the regenerations in the II stage (natural, mixed and artificial), a series of common aspects are considered with the activity of performing the reception of the forest vegetation installation works on the road natural, artificial and/or mixed.
For the area of 4.0 hectares, which was planted in 2013, 16 test areas of 200 sqm were placed, which represents 8% of the culture area under control (for areas under 5 ha), totaling 3,200 sqm, in accordance with the technical rules in force.
For the area of 3.60 hectares, which was planted in 2014, 13 test areas of 200 sqm were

placed (which represents 8% of the culture area under control, for areas under 5 ha), totaling 2600 sqm, in accordance with the technical rules in force.

The shape of these test areas is rectangular, with dimensions of 20 m x 10 m, and the practical location on the ground is made using an imaginary rectangular grid of rectangles, with the large side on the contour line. The establishment of this network is carried out in relation to the first control surface, which is fixed in a corner of the regenerated surface.

Since the control surfaces are permanently maintained in the initial location, until the massive state is achieved, it is necessary that they be materialized on the ground, through terminals. In the case of quadrangular surfaces, the terminal is located in a corner that remains the same for all control surfaces, the other corners materializing through stakes firmly driven into the ground.

The bollard is made of wood, having a thickness of 8-10 cm, and a length of 1.20 m - 1.50 m (of which 0.6 - 0.8 m is buried in the ground). For easy identification, the upper head of the bollard will be painted red over a length of 10-15 cm and will bear an order number that will correspond to the registration in the field book (Figure 15).

Figure 15. Sample area made for the reception of afforestation works, and respectively for the annual control of regenerations, stage II, on the area of 4.00 ha

The test areas, which were placed in the field at the end of the afforestation action, are used for the technical reception of the afforestation works, and will also be used as annual control areas, for the regenerations carried out by artificial and/or mixed means.

On the reception of the afforestation works and the completion of the regeneration, it was found that they were properly carried out, and the payment of their consideration to the executor was accepted.

The reception of the works to remove the overwhelming vegetation was carried out at the completion of the work, checking the entire surface that was covered with this work (Figures 16 and 17). After the completion of the reception, it was found that the works were carried out properly, and as a result the settlement of these works was ordered the executor.

Figure 16. Removal of the overwhelming vegetation near the specimens from *Quercus petraea* species, which were planted in the spring of 2013

Figure 17. Removal of the overwhelming vegetation near the specimens from *Quercus petraea* species, which were planted in the spring of 2014

Starting with 2018, the plot on which it was planted, and on which regeneration maintenance works were carried out, was included (included) in the forest management (management plan), being numbered number 60.
Also, based on the analysis of the data from the field, it was found that the mixed regeneration tends towards biological independence on at least 80% of the plot surface, and as a result, it is considered that the conditions for the achievement of the massif status are met. As a result, a series of care works specific to young stands were established and proposed, generically called care cuts or typical cultural operations.

CONCLUSIONS

The introduction of some land surfaces, belonging to the silvopastoral systems in the forest fund, presents a series of peculiarities, due to the specific seasonal (vegetation) conditions and the way of exploitation of these complex exploitation systems.
The preservation and introduction of biogroups with usable regeneration, installed on the surface of silvopastoral systems, in the future arboretum, ensures regeneration in an optimal period, and determines the outline of a diversified structure, which can contribute to the consolidation of its ecosystem stability.
The species used for the installation of a stand, on the surface that will be introduced into the forest fund, must correspond to the fundamental natural type of forest, which was identified in the bordering (neighboring) stands, to properly use the silvoproductive potential of the station (of the conditions of environment).
To carry out the works to complete the natural regeneration, the species that were used were available at the time of planting, thus ensuring, from a technical point of view, all the prerequisites for their complete success.
The use of the *Larix decidua* species, in the upper part of the slope, was justified by the fact that this species develops a deep rooting system, which confers an increased (increased) resistance to the action of the dominant, destabilizing winds.
To ensure a suitable protection of the arboretum that has been installed in plot 40, it is necessary to make a suitable fence of it, especially to avoid the negative impact produced by the fauna of hunting interest, represented by the species *Sus scrofa attila*, *Capreolus capreolus* and *Cervus elaphus*.

ACKNOWLEDGEMENTS

The case study and the related research were carried out within the service provision contract made by S.C. ECOPROD FOREST S.R.L. from Oradea, Bihor County, with private Forestry District Codrii Cămării Autonomous Management (A.M.) from the village of Dobreşti, Bihor County, since 2013.
It also benefited from the collaboration and support of the Codrii Cămării Autonomous Management (A.M.) Private Forestry District collective, starting from 2013 and until now.

REFERENCES

Abrudan, I.V., Blujdea, V., Brown, S., Kostyushin, V., Pahontu, C., Phillips, H., Voicu M. (2003). Prototype carbon fund: afforestation of degraded agricultural land in Romania. *Revista Pădurilor, 1,* Yar 118. Bucharest, 5-17.

Abrudan, I.V., Pahonţu, C., Negruţiu, F., Florescu, G. (2003). *Aspects related to the afforestation works carried out in Romania in the period 1991-2001*. The forest and the future. Transilvania University Publishing House from Braşov, Brasov, 97-100.

Bodog, M.F., & Crainic, G.C. (2016). *Some Specific Characteristics of the Geomatic Applications in the Agro-Forestry Sector*. Annals of the University of Oradea, Environmental Protection Fascicle, University of Oradea Publishing House, XXVII. 337-346. ISSN - 1224-6255.

Crainic, G.C. (2011). *Research on the modernization of topographical works in the forestry sector*. Ministry of Education, Research, Youth and Sports, Transilvania University of Brasov, Faculty of Forestry and Forestry, Department of Forestry, Forest Management, Land Surveys, Brasov, PhD Thesis.

Crainic, G.C. (2017). *Specific Works for The Maintenance of Agroforestry Systems*. Annals of the University of Oradea, Environmental Protection Fascicle, University of Oradea Publishing House, XXIX, 153-164. ISSN - 1224-6255.

Crainic, G.C., & Stamate, G. (2009). Agro-Forestry Systems - a Possible Valorization Alternative of the Forestry Potential in Some Extreme Sites. *Bulletin of University of Agricultural Sciences and Veterinary Medicine Cluj-Napoca. Horticulture, 66*(1). 572-577. ISSN - 1843-5394.

Cubbage, F., Balmelli, G., Bussoni, A., Noellemeyer, E., Pachas, A.N., Fassola, H., Colcombet, L., Rossner, B., Frey, G., Dube, F., Lopes de Silva, M.,

Stevenson, H., Hamilton, J., & Hubbard, W. (2012). Comparing silvopastoral systems and prospects in eight regions of the world. *Springer Science+Business Media B.V., Agroforest System, 86*. 303 - 314. doi 10.1007/s10457-012-9482-z.

Dorog, L.S., & Crainic, G.C. (2015). Shrubs and trees regeneration in silvopastorale systems in the counties of bihor and arad. *Jurnal of Agriculture Science, 47(4).* 64-69. University of Agriculture Sciences and Veterinar Medicine of the Banat, Timişoara. https://www.cabdirect.org/cabdirect/abstract/20163022043.

Duncker, P.S., Barreiro, S.M., Hengeveld, G.M., Lind, T., Mason, W.L., Ambrozy, S., & Spiecker, H. (2012). Classification of Forest Management Approaches: A New Conceptual Framework and Its Applicability to European Forestry. *Ecology and Society, 17*(4). 51. http://dx.doi.org/10.5751/ES-05262-170451.

Environmental Protection (MAPPM), *Technical norms regarding compositions, schemes and technologies for forest regeneration and afforestation of degraded lands No. 1.*

Florescu, I.I., & Nicolescu, N.V. (1996). *Forestry*, I, Forest Study, Lux-Librix Publishing House, Brasov.

Nair Ramachandran, P.K. (1993). *An Introduction to Agroforestry*. Kluwer Academic Publishers, Dordrecht/Boston/London in Cooperation with International Centre for Research in Agroforestry.

Nicolescu, N.V. (2009). *Forestry*, Aldus Publishing House, Brasov.

Pica, A., Boja, F., For a, C., Moatar, M., & Boja, N. (2022). Advantages of using gnss technology and QGIS software in inventory stands exploiters. *Series E. Land Reclamation, Earth Observation & Surveying, Environmental Engineering, XI.* 434 -443.

Popa, B. (2022). *The Role of Forest Ecosystem Services for the Forest-based Bioeconomy in Romania*. In: The Plan B for Romania's Forests and Society, Transilvania University Publishing House from Brasov, 89-97.

Willoughby, I., Scott Bentsen, N., McCarthy, N., & Claridge J., eds (2008). *Forest vegetation management in Europe. Current practices and future needs.* COST Office, Brussels.

***(1997). Ministry of Water, Forests and Environmental Protection (MAPPM), National Forest Management (RNP), *Unified time and production norms for works in Forestry*.

***(2000), Ministry of Water, Forests and Environmental Protection (MAPPM), *Technical norms for the care and management of the stand No. 2.*

***(2000), Ministry of Water, Forests and Environmental Protection (MAPPM) *Technical rules regarding the annual control of regenerations, No. 7.*

***(https://maps.google.ro/maps?hl=ro).

****Forest management of Production Unit I Dobreşti, Bihor County*. (2018).

****Forestry map of Production Unit I Dobreşti*, Bihor County. (2018).

***https://pe-harta.ro/bihor/.

***https://www.primaimpadurire.ro/ghid-impaduriri-pnrr/.

***The guide to financing afforestation through PNRR, 12 XII 2022, Bucharest.

Scientific Papers. Series E. Land Reclamation, Earth Observation & Surveying, Environmental Engineering. Vol. XII, 2023
Print ISSN 2285-6064, CD-ROM ISSN 2285-6072, Online ISSN 2393-5138, ISSN-L 2285-6064

HEAVY METALS ACCUMULATION IN THE TISSUES OF THE COMMON REED (*PHRAGMITES AUSTRALIS*)

Marcel Daniel POPA[1], Ira-Adeline SIMIONOV[2], Stefan-Mihai PETREA[2], Floricel Maricel DIMA[2], Neculai PATRICHE[2], Catalina ITICESCU[2], Elena-Cristina OANCEA[2], Marilena-Florentina LACATUS[2]

[1]Research and Development Institute for Aquatic Ecology, Fisheries and Aquaculture, 54 Portului Street, Galați, Romania
[2]REXDAN Research Infrastructure, "Dunarea de Jos" University of Galati, 98 George Cosbuc Street, Galati, Romania

Corresponding author email: popa.marceldaniel@gmail.com

Abstract

The aim of the present study was to provide a comparative analysis related to the concentration of heavy metals (Cd, Pb, Ni, Cr) in the tissues (stem, leaves, panicle) of the common reed (Phragmites australis). The reed samples were collected from 10 different sampling stations located in Danube Delta Reservation Biosphere, 2 sampling station from Lake Brateș and 2 sampling station situated on a tributary of the Danube River (Chineja River), Romania. The concentration of heavy metals varied depending on the location, the lowest values were found in plants located on the course of the Chineja River. As well, depending on the plant structure, was observed that the panicle contained the lowest concentrations of the chosen heavy metals for the experiment.

Key words*: bioaccumulation, common reed, heavy metals.*

INTRODUCTION

Reed is a perennial plant that can be found in temperate and tropical regions, especially in areas with high humidity. It spreads in all environments with water levels close to the soil surface (irrigated and drained agricultural or non-agricultural areas, swamps, ponds) (Vymazal, 2013).

The plant is dominant mainly in Europe, but also widespread in North America and various regions of South America and Australia (Srivastava et al., 2014; Mykleby et al., 2016).

Common reed (*Phragmites australis* (Cav.) Trin. ex Steud.), has a resistant rhizome system with high propagation capacity and long growth period, increased adaptability to different environmental conditions and strong resistance to pollution (Fraser et al., 2004; Liu et al., 2012).

The reed stem can grow up to 6 m with the ability to survive in high concentrations of toxic contaminants (Bragato et al., 2009).

The way in which reed adapts to environmental conditions (water depth, pH, salinity, pollutants, extreme climate) is through changes in the physiological, morphological, and behavioural characteristics. With diverse patterns in regard to the reproductive and physiological adaptations, *Phragmites australis* can be used successfully in phytoremediation of depredated wetland ecosystems (Qin et al., 2022)

Heavy metals and other pollutants end up in the Danube Delta, after being collected from the entire hydrographic basin, which represents over 800,000 km^2. The reed is an integral part of the ecology and economy of the Danube Delta by creating an important habitat and by phytoremediation of the Danube waters.

Phytoremediation represents the remediation of contaminated soil, sediments, or water using plants. Compared to other chemical and physical methods of cleaning up, phytoremediation is more environmentally friendly.

Depending on the mechanism of heavy metals removal, phytoremediation can be classified into:

- phytoextraction - heavy metals are stored in the leaves of plants (Lee, 2013);
- phytostabilization - toxic pollutants are transformed into nontoxic or less toxic substances (McSorley et al., 2016);

♦ phyto immobilization - the mobility of heavy metals is reduced by sequestering them within the rhizosphere (Yadav et al., 2018).

The species selected for phytoremediation must have the ability to accumulate a vast range of heavy metals, a high tolerance and a high growth rate (Darajeh et al., 2017; Kushwaha et al., 2018).

Phragmites australis is a macrophyte well known for the capacity to uptake, translocate, and accumulate heavy metals in the plant tissues, both from water and sediments (Bonanno & Giudice, 2010; Huang et al., 2018).

Southichak et al., 2016, reported that reed biomass is an effective biosorbent with high sorption performance even if the heavy metals are found in low concentrations.

The current study presents the heavy metals (Cd, Pb, Ni, Cr) concentrations measured in the leaves, stems and panicles of Phragmites australis, sampled from the Danube Delta, Brateș Lake and Chineja River.

MATERIALS AND METHODS

In order to evaluate the concentration of heavy metals from reed, plant samples were collected from 10 locations in the Danube Delta, 2 locations were in the Brateș Lake, and 2 locations were on the course of a tributary river, Chineja River (near the villages of Tulucești and Folteștii), that flows in the Brateș Lake and connects it to the Danube.

The coordinates of the sampling points and the codes used to identify them are presented in Table 1. In Figure 1, the sampling points are represented on the map, to present their spatial distribution.

Reed stems, leaves and panicles were collected from the selected sampling points, during the autumn harvest campaign of October 2022.

Plant material was harvested from a 100 m × 100 m area in each location, and homogenous samples were obtained from randomly selecting stems, leaves, and panicles from each location.

In order to assess the heavy metals quantity in the organs of common reed, the samples digestion is done beforehand. The digestion process is achieved using the digestion oven Topwave Analytikjena Germany. Teflon containers with the samples were subjected to a digestion protocol specific to plants.

Heavy metals were determined from the matrix resulted after the samples digestion. An ANALYTIK JENA ContrAA 700® was used, which is an atomic absorption spectral photometer. Samples were analysed in triplicate and the results are express as average ± standard deviation.

One-way classification variance analysis and ANOVA tests were used, to highlight statistical differences. When differences were statistically significant ($p \leq 0.05$), Tukey's post hoc test was applied to identify which group differs.

Table 1. The coordinates of the sampling points and the codes used to identify them

Nr.	Coordinates Danube Delta		Code	Coordinates Brateș Lake		Code	Coordinates Chineja River		Code
	Latitude	Longitude		Latitude	Longitude		Latitude	Longitude	
1	45°09'32.4"N	29°30'57.6"E	DDa	45°27'45.0"N	28°05'52.5"E	BLa	45°34'19.7"N	28°03'15.2"E	CRa
2	45°09'00.0"N	29°25'55.2"E	DDb	45°30'17.0"N	28°02'30.3"E	BLb	45°43'59.9"N	28°04'27.7"E	CRb
3	45°10'48.0"N	29°25'22.8"E	DDc	-	-	-	-	-	-
4	45°07'55.2"N	29°31'22.8"E	DDd	-	-	-	-	-	-
5	45°10'26.4"N	29°28'22.8"E	DDe	-	-	-	-	-	-
6	45°19'45.7"N	29°24'28.8"E	DDf	-	-	-	-	-	-
7	45°03'06.0"N	29°29'42.4"E	DDg	-	-	-	-	-	-
8	45°06'07.9"N	29°38'31.2"E	DDh	-	-	-	-	-	-
9	44°59'57.9"N	29°24'08.7"E	DDi	-	-	-	-	-	-
10	45°15'14.9"N	29°12'47.9"E	DDj	-	-	-	-	-	-

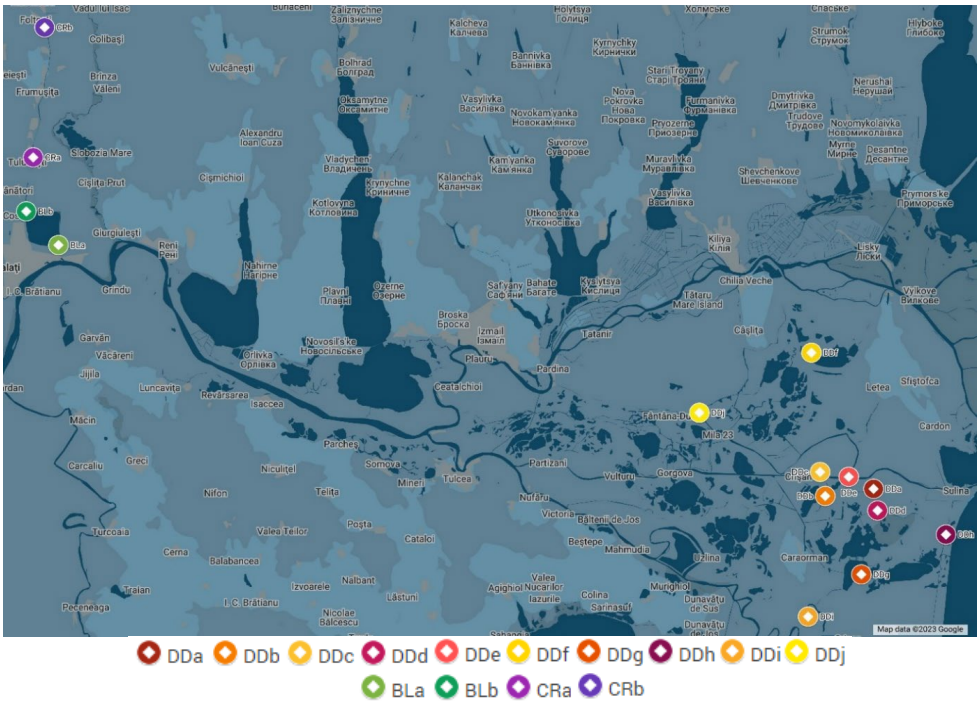

Figure 1. Map representation of the sampling points and their spatial distribution

RESULTS AND DISCUSSIONS

Cadmium was found, generally, in the highest quantity in the reed leaves, followed by stems and panicles. The highest concentration of cadmium was present in the samples from the Brateș Lake (BLa and BLb), with the lowest concentration in the samples from the Chineja River (CRa and CRb).

This trend is observed in all the vegetal parts of the reed. In the Danube Delta, the highest concentrations of cadmium were found in the sampling points closest to the river flow (DDe>DDb>DDc>DDj>DDa>DDd>DDi>DDh>DDf>DDg).

There were no significant differences between the locations from Chineja River, or the locations from Brateș Lake ($p \geq 0.05$).

In the Danube Delta, there were significant differences between all locations for all plant organs ($p \leq 0.05$), phenomenon explained by the considerable distance between some of the locations, the flow regime of the river, proximity to human settlements or transportation lanes. Table 2 presents the data obtained following the analysis for cadmium.

Table 2. Cadmium concentrations in the organs of common reed, *Phragmites australis*, present in the sampling locations of the experiment

µg/g	Cadmium		
	Stems	Leaves	Panicles
DDa	0.70399±0.00018	1.07435±0.00087	0.64935±0.00025
DDb	0.56465±0.00046	1.27301±0.00074	0.74599±0.00030
DDc	0.42208±0.00033	1.12328±0.00038	0.68247±0.00042
DDd	0.78989±0.00051	1.00977±0.00050	0.52130±0.00054
DDe	0.97810±0.00020	1.28461±0.00044	0.75758±0.00023
DDf	0.39432±0.00011	0.84665±0.00055	0.19883±0.00031
DDg	0.48828±0.00037	0.70770±0.00029	0.17904±0.00053
DDh	0.44479±0.00017	0.89962±0.00038	0.30804±0.00025
DDi	0.45650±0.00026	0.95462±0.00011	0.35827±0.00019
DDj	0.78449±0.00040	1.08430±0.00068	0.68019±0.00022
BLa	1.02389±0.00032	1.49960±0.00057	0.86777±0.00049
BLb	1.08836±0.00026	1.52588±0.00033	0.93618±0.00010
CRa	0.29314±0.00037	0.45532±0.00044	0.25523±0.00072
CRb	0.27168±0.00039	0.42615±0.00056	0.21535±0.00081

Data is presented as average ± standard deviation

Lead presented a similar trend of phytoaccumulation as cadmium (leaves>stems>panicles), presented in table 3. The highest concentrations were found in the samples from Danube Delta (DDe>DDd>DDc), even though the samples from the Brateș Lake had higher concentrations of lead than some locations from the Danube Delta. The lowest concentrations of lead were found in the samples from the Chineja River, for all the plant organs.

Table 3. Lead concentrations in the organs of common reed, *Phragmites australis*, present in the sampling locations of the experiment

µg/g	Lead		
	Stems	Leaves	Panicles
DDa	2.01140±0.00044	2.98431±0.00076	1.49850±0.00025
DDb	2.04583±0.00034	3.13357±0.00086	1.77173±0.00029
DDc	3.46320±0.00055	5.61640±0.00028	2.39464±0.00031
DDd	4.42338±0.00021	6.35179±0.00064	1.95976±0.00025
DDe	3.65075±0.00036	6.60013±0.00033	1.61186±0.00019
DDf	1.57729±0.00030	3.03514±0.00094	0.66278±0.00036
DDg	1.67411±0.00041	3.94997±0.00061	1.30208±0.00022
DDh	2.30061±0.00011	4.26136±0.00055	1.13489±0.00030
DDi	2.64638±0.00027	3.87382±0.00077	1.57638±0.00025
DDj	2.77918±0.00036	5.95602±0.00024	1.70474±0.00031
BLa	2.50954±0.00022	4.02576±0.00050	1.65289±0.00035
BLb	2.55138±0.00029	4.06382±0.00085	1.79135±0.00029
CRa	1.46570±0.00017	1.95137±0.00066	0.55050±0.00019
CRb	1.32943±0.00013	1.89554±0.00019	0.48392±0.00017

Data is presented as average ± standard deviation

There were no statistical differences between the samples from Chineja River (CRa and CRb), or the samples from Brateș Lake (BLa and BLb), $p \geq 0.05$. There were significant differences between all locations for all plant organs in the Danube Delta ($p \leq 0.05$).

Nickel is the metal with the highest concentration, from the analysed 4 heavy metals, measured in the biological samples. The Brateș Lake has the highest concentration of nickel in the tissues of common reed, more than twice the amount measured in the Chineja River. There were no significant differences between the locations from the Chineja River (CRa and CRb, $p \geq 0.05$), and significant differences for nickel found in the reed leaves and panicles from the locations in the Brateș Lake ($p \leq 0.05$). In the Danube Delta, the differences varied greatly with statistical significance, $p \leq 0.05$.

Table 4. Nickel concentrations in the organs of common reed, *Phragmites australis*, present in the sampling locations of the experiment

µg/g	Nickel		
	Stems	Leaves	Panicles
DDa	3.60375±0.00055	7.33288±0.00059	2.59740±0.00046
DDb	5.31915±0.00068	7.63807±0.00046	3.82320±0.00022
DDc	4.87013±0.00081	8.84583±0.00019	3.35249±0.00047
DDd	4.26540±0.00063	8.30619±0.00031	2.48236±0.00096
DDe	4.86766±0.00044	9.65873±0.00032	1.77305±0.00055
DDf	2.99685±0.00071	5.91054±0.00048	1.59067±0.00025
DDg	2.37165±0.00040	5.43120±0.00017	1.62760±0.00033
DDh	2.45399±0.00033	5.99747±0.00019	1.29702±0.00043
DDi	4.96196±0.00040	6.64084±0.00044	2.14961±0.00055
DDj	4.29510±0.00028	8.70495±0.00088	3.06853±0.00018
BLa	5.11945±0.00013	9.86312±0.00093	7.85124±0.00010
BLb	5.18659±0.00027	10.11699±0.00077	8.00593±0.00066
CRa	2.83369±0.00009	4.25298±0.00006	0.90081±0.00028
CRb	2.77594±0.00042	4.01019±0.00011	0.84668±0.00031

Data is presented as average ± standard deviation

Chromium was found with the lowest concentration in the samples from the Chineja River (CRa and CRb), with no significant differences between locations, for all reed organs ($p \geq 0.05$). The leaves of *Phragmites australis* accumulated the highest concentration of chromium, followed by stems and panicles. The highest value measured for the concentration of chromium was in the leaves of common reed from the location BLb. The highest concentrations of chromium from stems and panicles were also measured in the same location BLb. Data collected from the Danube Delta presented significant differences between locations, for all the vegetal organs ($p \leq 0.05$).

Table 5. Chromium concentrations in the organs of common reed, *Phragmites australis*, present in the sampling locations of the experiment

µg/g	Chromium		
	Stems	Leaves	Panicles
DDa	2.34663±0.00049	3.49591±0.00082	1.39860±0.00011
DDb	1.39116±0.00057	3.81904±0.00076	0.65274±0.00011
DDc	1.29870±0.00066	3.36984±0.00093	0.59866±0.00024
DDd	2.05371±0.00022	3.42020±0.00021	1.17586±0.00019
DDe	2.58594±0.00035	3.86349±0.00050	1.12830±0.00005
DDf	1.89274±0.00041	3.67412±0.00068	0.79533±0.00038
DDg	1.39509±0.00021	3.29164±0.00034	0.81380±0.00019
DDh	1.22699±0.00010	2.99874±0.00028	0.64851±0.00016
DDi	1.32319±0.00061	2.49032±0.00071	0.85985±0.00024
DDj	1.38959±0.00013	3.35980±0.00015	0.85237±0.00011
BLa	2.60992±0.00022	3.92512±0.00025	1.85950±0.00029
BLb	2.75292±0.00010	4.16285±0.00033	1.90047±0.00021
CRa	1.17256±0.00011	2.40168±0.00048	0.25023±0.00009
CRb	1.16014±0.00017	2.37629±0.00061	0.24012±0.00009

Data is presented as average ± standard deviation

Heavy metals decreased in the order leaves > stems > panicles, in all the locations selected for the experiment. This trend was also observed by Vymazal and Březinová (2016), Parzych et al. (2016), Rzymski et al. (2014), Ganjali el al. (2014).

The heavy metals uptake by the organs of P. australis were: stems Ni>Pb>Cr>Cd, leaves Ni>Pb>Cr>Cd and panicles Ni>Pb>Cr>Cd.

Bonanno, 2013, found more Pb and Cr than Ni in the stems and the same order in leaves, when comparing the capacity of heavy metals removal by P. australis.

These results are like those obtained by Astel et al. (2014), Jiang et al. (2018), Dan et al. (2017).

The strategies used for the uptake of heavy metals are dependent on several factors: pH, metal type, temperature, and depth of the contamination (Ashraf et al., 2017; da Conceição et al., 2016).

Phragmites australis is a valuable plant that can be used successfully for the phytostabilization of trace metals due to the high bioaccumulation capacity, the ability to translocate these metals, and limited mobility. This is because of the different accumulation levels and transport systems, with very specific metal-affinity patterns (Klink, 2017; Pérez-Sirvent et al., 2017).
The capacity of P. australis to bioaccumulate is also dependent on the season, as observed by Grisey et al., 2012.

CONCLUSIONS

The present study confirms that *P. australis* is a suitable candidate for biomonitoring of heavy metals pollution in aquatic environments. As well, the capacity to bioaccumulate heavy metals in the tissues above the ground and the resistance to metal toxicity, makes this plant a perfect solution for phytoremediation of contaminated environments.
The heavy metals uptake by the organs of *P. australis* were: stems Ni>Pb>Cr>Cd, leaves Ni>Pb>Cr>Cd and panicles Ni>Pb>Cr>Cd.
Further studies should be conducted in an integrated manner, considering different biotic and abiotic components of aquatic environments to obtain a clear view on heavy metals accumulation, transfer and dispersion in water systems.

ACKNOWLEDGMENTS

The present research was supported by the project An Integrated System for the Complex Environmental Research and Monitoring in the Danube River Area, REXDAN, SMIS code 127065, co-financed by the European Regional Development Fund through the Competitiveness Operational Programme 2014-2020, contract no. 309/10.07.2021.

REFERENCES

Ashraf, M.A., Hussain, I., Rasheed, R., Iqbal, M., Riaz, M., Arif, M.S. (2017). Advances in microbe-assisted reclamation of heavy metal contaminated soils over the last decade: a review. *Journal of Environmental Management, 19.* 132–143.

Astel, A., Obolewski, K., Skorbiłowicz, E., Skorbiłowicz, M. (2014). An assessment of metals content in *Phragmites australis* (Cav.) Trin. ex Steudel grown in natural water reservoirs according to climate zone and salinity. *Desalination and Water Treatment, 52.* 3928–3937.

Bonanno, G., Lo Giudice, R. (2010). Heavy metal bioaccumulation by the organs of *Phragmites australis* (common reed) and their potential use as contamination indicators. *Ecological Indicators, 10.* 639–645.

Bonanno, G. (2013). Comparative performance of trace element bioaccumulation and biomonitoring in the plant species *Typha domingensis*, *Phragmites australis* and *Arundo donax*. *Ecotoxicology and Environmental Safety, 97.* 124–130.

Bragato, C., Schiavon, M., Polese, R., Ertani, A., Pittarello, M., Malagoli, M. (2009). Seasonal variations of Cu, Zn, Ni and Cr concentration in *Phragmites australis* (Cav.) Trin ex Steudel in a constructed wetland of North Italy. *Desalination, 246.* 35–44.

da Conceição, G., Maria, A., Hauser-Davis, R.A., de Souza, A.N., Vitória, A.P. (2016). Metal phytoremediation: general strategies, genetically modified plants, and applications in metal nanoparticle contamination. *Ecotoxicology and Environmental Safety, 134.* 133–147.

Dan, A., Oka, M., Fujii, Y., Soda, S., Ishigaki, T., Machimura, T., Ike, M. (2017). Removal of heavy metals from synthetic landfill leachate in labscale vertical flow constructed wetlands. *Science of the Total Environment, 584.* 742–750.

Darajeh, N., Idris, A., Fard Masoumi, H.R., Nourani, A., Truong, P., Rezania, S. (2017). Phytoremediation of palm oil mill secondary effluent (POMSE) by *Chrysopogon zizanioides* (L.) using artificial neural networks. *International Journal of Phytoremediation, 19.* 413–424.

Fraser, L.H., Carty, S.M., Steer, D. (2004). A test of four plant species to reduce total nitrogen and total phosphorus from soil leachate in subsurface wetland microcosms. *Bioresource Technology, 94.* 185–192.

Ganjali, S., Tayebi, L., Atabati, H., Mortazavi, S. (2014). *Phragmites australis* as a heavy metal bioindicator in the Anzali wetland of Iran. *Toxicological & Environmental Chemistry, 96.* 1428–1434.

Grisey, E., Laffray, X., Contoz, O., Cavalli, E., Mudry, J., Aleya, L. (2012). The bioaccumulation performance of reeds and cattails in a constructed treatment wetland for removal of heavy metals in landfill leachate treatment (Etueffont, France). *Water Air Soil Pollut., 223.* 1723–1741.

Huang, X., Wang, L., Zhu, S., Ho, S.-H., Wu, J., Kalita, P.K., Ma, F. (2018). Unraveling the effects of arbuscular mycorrhizal fungus on uptake, translocation, and distribution of cadmium in *Phragmites australis* (Cav.) Trin. ex Steud. *Ecotoxicology and Environmental Safety,149.* 43–50.

Jiang, B., Xing, Y., Zhang, B., Cai, R., Zhang, D., Sun, G. (2018). Effective phytoremediation of low-level heavy metals by native macrophytes in a vanadium mining area, China. *Environmental Science and Pollution Research, 25.*

Klink, A. (2017) A comparison of trace metal bioaccumulation and distribution in Typha latifolia and *Phragmites australis*: implication for phytoremediation. *Environmental Science and Pollution Research, 24.* 3843–3852.

Kushwaha, A., Hans, N., Kumar, S., Rani, R. (2018). A critical review on speciation, mobilization and toxicity of lead in soil-microbe-plant system and bioremediation strategies. *Ecotoxicology and Environmental Safety, 147.* 1035–1045.

Lee, J.H. (2013). An overview of phytoremediation as a potentially promising technology for environmental pollution control. *Biotechnology and Bioprocess Engineering, 18.* 431–439.

Liu, X., Huang, S., Tang, T., Liu, X., Scholz, M. (2012). Growth characteristics and nutrient removal capability of plants in subsurface vertical flow constructed wetlands. *Ecological Engineering, 44.* 189–198.

McSorley, K., Rutter, A., Cumming, R., Zeeb, B.A. (2016). Phytoextraction of chloride from a cement kiln dust (CKD) contaminated landfill with *Phragmites australis*. *Waste Management, 51.* 111–118.

Mykleby, P.M., Lenters, J.D., Cutrell, G.J., Herrman, K.S., Istanbulluoglu, E., Scott, D.T., Twine, T.E., Kucharik, C.J., Awada, T., Soylu, M.E. (2016). Energy and water balance response of a vegetated wetland to herbicide treatment of invasive *Phragmites australis*. *Journal of Hydrology, 539.* 290–303.

Parzych, A., Sobisz, Z., Cymer, M. (2016). Preliminary research of heavy metals content in aquatic plants taken from surface water (Northern Poland). *Desalination and Water Treatment, 57.* 1451–1461.

Pérez-Sirvent, C., Hernández-Pérez, C., Martínez-Sánchez, M.J., García- Lorenzo, M.L., Bech, J. (2017). Metal uptake by wetland plants: implications for phytoremediation and restoration. *Journal of Soils and Sediments, 17.* 1384–1393.

Qin, H., Jiao, L., Li, F., Zhou, Y. (2022). Ecological adaptation strategies of the clonal plant *Phragmites australis* at the Dunhuang Yangguan wetland in the arid zone of northwest China, *Ecological Indicators, 141*. https://doi.org/10.1016/j.ecolind.2022.10910

Rzymski, P., Niedzielski, P., Klimaszyk, P., Poniedziałek, B. (2014). Bioaccumulation of selected metals in bivalves (Unionidae) and *Phragmites australis* inhabiting a municipal water reservoir. *Environmental Monitoring and Assessment, 186.* 3199–3212.

Southichak, B., Nakano, K., Nomura, M., Chiba, N., Nishimura, O. (2006). *Phragmites australis*: a novel biosorbent for the removal of heavy metals from aqueous solution. *Water Research, 40.* 2295–2302.

Srivastava, J., Kalra, S.J., Naraian, R. (2014). Environmental perspectives of *Phragmites australis* (Cav.) Trin. ex. Steudel. *Applied Water Science, 4.* 193–202.

Vymazal, J. (2013). Emergent plants used in free water surface constructed wetlands: a review. *Ecological Engineering, 61.* 582–592.

Vymazal, J., Březinová, T. (2016). Accumulation of heavy metals in aboveground biomass of Phragmites australis in horizontal flow constructed wetlands for wastewater treatment: a review. *Chemical Engineering Journal, 290*. 232–242.

Yadav, K.K., Gupta, N., Kumar, A., Reece, L.M., Singh, N., Rezania, S., Khan, S.A. (2018). Mechanistic understanding and holistic approach of phytoremediation: a review on application and future prospects. *Ecological Engineering,* 120. 274–298.

Scientific Papers. Series E. Land Reclamation, Earth Observation & Surveying, Environmental Engineering. Vol. XII, 2023
Print ISSN 2285-6064, CD-ROM ISSN 2285-6072, Online ISSN 2393-5138, ISSN-L 2285-6064

SPATIAL DISTRIBUTION OF PHARMACEUTICALS IN THE LOWER DANUBE RIVER WATER

Valentina Andreea CALMUC, Madalina CALMUC, Maxim ARSENI, Ira-Adeline SIMIONOV, Alina ANTACHE, Stefania-Adelina MILEA, Catalina ITICESCU, Puiu Lucian GEORGESCU

REXDAN Research Infrastructure, "Dunarea de Jos" University of Galati, 98 George Cosbuc Street, Galati, Romania

Corresponding author email: valentina.calmuc@ugal.ro

Abstract

Pharmaceuticals are part of the emerging pollutants class found in aquatic ecosystems. The presence of these contaminants in the aquatic ecosystem can have harmful effects on living organisms due to their toxicity and ability to accumulate in tissues. In this study, water samples taken from stations located in the Lower Danube River Basin were analysed in order to identify and quantify some classes of pharmaceuticals. To confirm the presence of pharmaceutical traces in surface water samples, a High-resolution UHPLC-MS/MS was used. The obtained results demonstrated that the most frequently identified pharmaceutical residues in the water samples were: caffeine > carbamazepine > metformin > sulfamethoxazole > trimethoprim > clindamycin > ketoprofen > diclofenac > clarithromycin. The highest recorded concentration was 118.52 ng/L for caffeine possibly due to the presence of this compound especially in drinks and food and to a lesser extent also in medicines and the lowest value was 0.36 ng/L for trimethoprim.

Key words*: surface water, pharmaceuticals, emerging pollutants, Danube river.*

INTRODUCTION

The pollution of the Danube River Basin is a topic of interest especially for scientists, governments and residents of the riverside cities, because it is the second longest river in Europe, has a wide variety of fauna and flora and is an important source of drinking water (Popescu et al., 2022; Woitke et al., 2003). Pharmaceutical substances (PhACs) are considered emerging pollutants that are continuously discharged into the aquatic environment (Hejna et al., 2022). Until now, this class of pollutants is not regulated by law, but some of these compounds are on the Watch List adopted by the European Commission (EU) 2020/1161. The latest version of the "Watch List" was revised in 2020 and contains the following pharmaceutical compounds for human use: amoxicillin, ciprofloxacin, sulfamethoxazole, trimethoprim, venlafaxine and o-desmethylvenlafaxine (*Commission Implementing Decision (EU) 2020/1161*).

The main sources of surface water pollution with this class of contaminants are: the pharmaceutical industry, wastewater from hospitals and homes, surface runoff from agricultural land and animal farms (Gaw et al., 2014; Vatovec et al., 2021).

The presence of pharmaceutical residues in aquatic ecosystems has toxic effects on aquatic biota. Depending on the class to which they belong and the concentration in which they are found, pharmaceutical substances can cause the physiological and behavioural disorders in certain fish species. For example, contraceptives can cause feminisation of fish (Gross-Sorokin et al., 2006), antidiabetics have potential effects of disrupting the endocrine system in fish, antibiotics determine the development of antibiotic resistance and analgesics cause damage to some organs in fish (Khan et al., 2020; Patel et al., 2019).

The main aim of this study is to determine the occurrence of some classes of pharmaceuticals in the Danube River Lower Basin water.

MATERIALS AND METHODS

In order to determine the presence of pharmaceutical residues in the water of the Danube River Lower Basin, 500 mL of water were collected from 6 sampling stations located near the Galati city in 2021 (Figure 1).

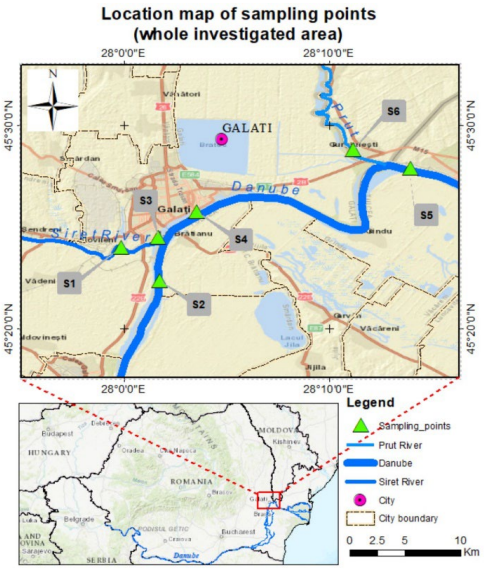

Figure 1. Map of sampling stations

Extraction of target compounds was performed using the Dionex AutoTrace 280 Thermo Scientific automated solid phase extraction instrument (Figure 2). After conditioning the Branchia C18 cartridges, 500 mg/ 6 mL with 5 mL methanol followed by 5 mL water, loading of 100 mL water sample adjusted to pH 3. Elution of the analytes was performed with 6 mL methanol. The eluate was concentrated by evaporation in a nitrogen atmosphere of purity 5.0, at a temperature of 42°C using the Reacti-Therm Heating Thermo Scientific equipment (Figure 3). The eluate was redissolved with 25 µl of methanol and 225 µl of water (Chitescu et al., 2015).

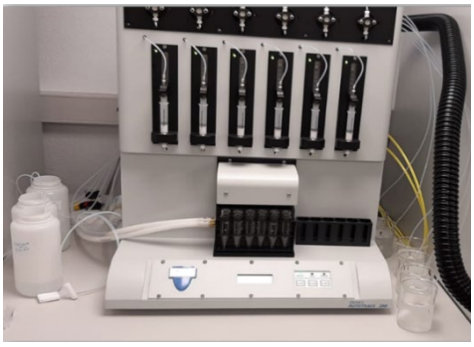

Figure 2. Extraction of pharmaceuticals from water samples

Figure 3. Concentration of eluate under a N_2 flow

Analytical standards purchased from Sigma-Aldrich were used for the identification and quantification of pharmaceutical residues in the analysed water samples for the following compounds: caffeine, ketoprofen, diclofenac, carbamazepine, metformin, clindamycin, sulfamethoxazole, trimethoprim and clarithromycin.

The identification and quantification of the compounds was carried out with the Vanquish Flex UHPLC Systems equipment coupled to the Orbitrap Exploris 120 mass spectrometer - Thermo Fisher Scientific (Figure 4).

Figure 4. Identification and quantification of analytes

The column used to separate the compounds was Accucore C18 (100 x 2.1 mm, 2.6 µm).

The mobile phase consisted of 2 solvents A - ultrapure water with 0.1% formic acid (98% - 100% LC-MS grade) and B - methanol (LC-MS grade) with 0.1% formic acid (98-100% LC-MS grade).

The detection of the compounds was carried out with the Orbitrap Exploris 120 mass spectrometer at a high resolution of 120,000 (FWHM) at m/z 200. To confirm the presence of the compounds in the water samples, MS/MS analysis were performed.

RESULTS AND DISCUSSIONS

In order to identify and quantify the pharmaceutical compounds present in the water samples, the standards of the compounds tracked in the samples were analysed. Table 1 and Figure 5 show the retention times and chromatograms obtained for each analysed compound.

Table 1. Retention time of analyzed pharmaceuticals

Compound	Formula	Adduct	m/z	RT Time (min)
Metformin	$C_4H_{11}N_5$	+ H	130,1087	0.44
Trimethoprim	$C_{14}H_{18}N_4O_3$	+ H	291,1452	3.21
Caffeine	$C_8H_{10}N_4O_2$	+ H	195,0877	3.38
Sulfamethoxazole	$C_{10}H_{11}N_3O_3S$	+ H	254,0594	3.69
Clindamycin	$C_{18}H_{33}ClN_2O_5S$	+ H	425,1871	4.91
Carbamazepine	$C_{15}H_{12}N_2O$	+ H	237,1022	5.72
Clarithromycin	$C_{38}H_{69}NO_{13}$	+ H	748,4842	6.50
Ketoprofen	$C_{16}H_{14}O_3$	+ H	255,1016	6.65
Diclofenac	$C_{14}H_{11}Cl_2NO2$	+ H	296,024	8.03

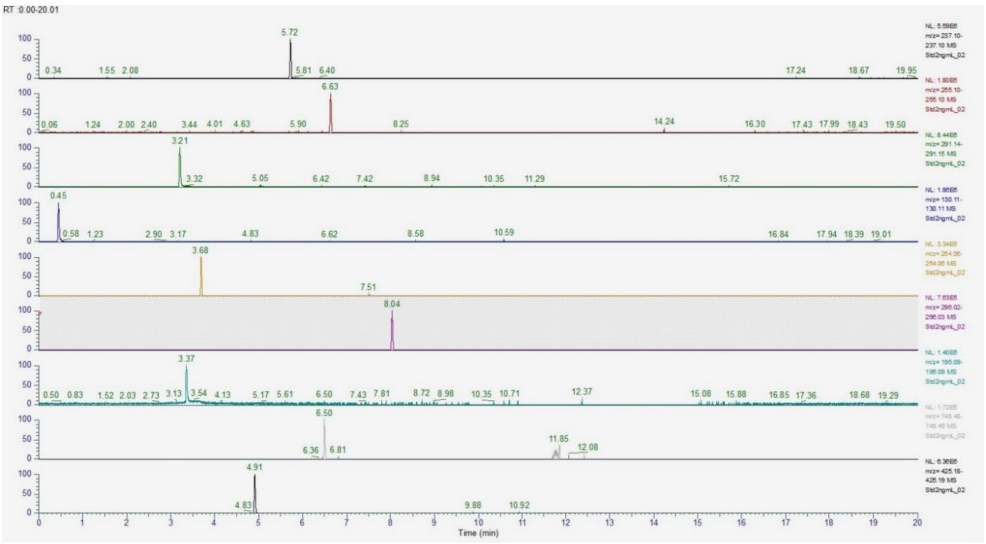

Figure 5. Chromatograms of analyzed pharmaceutical residues

Metformin is an anti-diabetic drug used by people with type 2 diabetes (Oosterhuis et al., 2013). This compound was registered in 5 sampling stations. The lowest value was 0.74 ng/L (S2) and the highest value was recorded for station 1.83 ng/L (S3) (Figure 6).

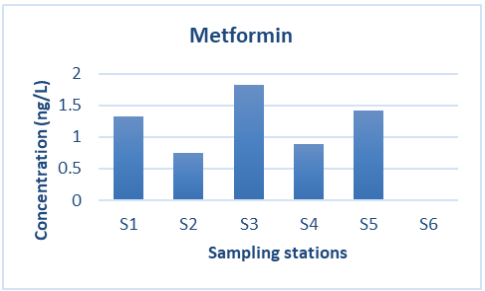

Figure 6. Spatial distribution of metformin concentration concentration

Trimethoprim is an antibiotic that belongs to the diaminopyrimidine class (Straub, 2013). The values of trimethoprim concentrations are in the range of 0.36 ng/L - 9.17 ng/L (Figure 7).

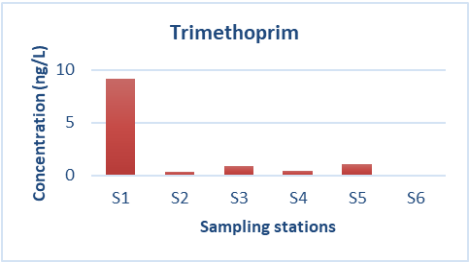

Figure 7. Spatial distribution of trimethoprim

For the caffeine, values were recorded in all 6 sampling stations. This alkaloid is one of the most consumed psychoactive substances worldwide. It is found in food, drinks and medications (Edwards et al., 2015). The highest concentration was 118.52 ng/L, in station S3 (Figure 8).

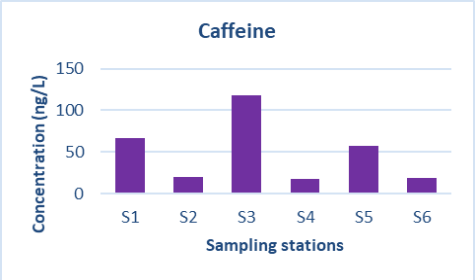

Figure 8. Spatial distribution of caffeine concentration

Sulfamethoxazole is part of the sulfonamides class and is one of the most prescribed antibiotics (Patrolecco et al., 2018). The concentrations of sulfamethoxazole in surface waters were detected in the range 3.57 ng/L - 4.36 ng/L (Figure 9).

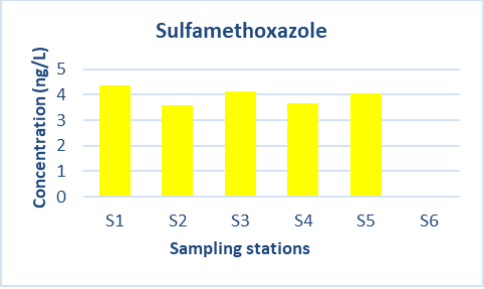

Figure 9. Spatial distribution of sulfamethoxazole concentration

Clindamycin is an anti-bacterial drug used to treat various acute and chronic infections (Koba et al., 2017). This compound was detected in 4 of the 6 sampling stations, the lowest value was 3.32 ng/L (S4), and the highest concentration was 3.54 ng/L (S3) (Figure 10).

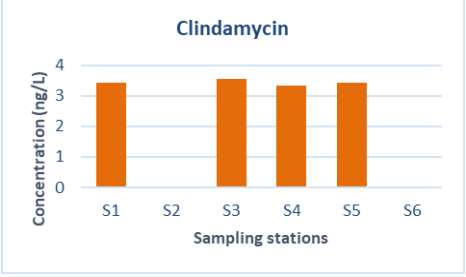

Figure 10. Spatial distribution of clindamycin concentration

Carbamazepine is an anticonvulsant used especially as a treatment for epilepsy (Cunningham et al., 2010). Based on the results obtained, it was observed that this compound was detected in all 6 sampling stations. Carbamazepine concentrations varied from 0.16 ng/L in station S2 to 9.07 ng/L in station S1 (Figure 11).

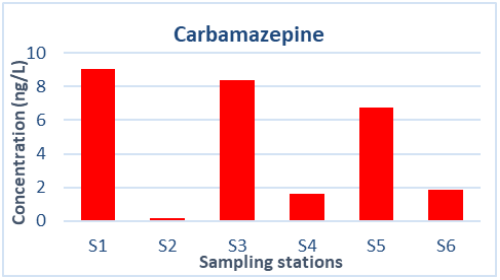

Figure 11. Spatial distribution of carbamazepine concentration

Ketoprofen is a non-steroidal anti-inflammatory drug (NSAIDs) used especially to relieve inflammation and pain (Alkimin et al., 2020). Figure 12 illustrates that only 2 values were obtained for this pharmaceutical residue, respectively 5.55 (S3) ng/L and 5.37 ng/L (S5).

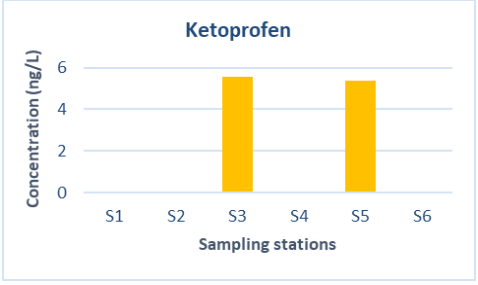

Figure 12. Spatial distribution of ketoprofen concentration

Diclofenac belongs to the category of non-steroidal anti-inflammatory drugs (Peters et al., 2022). For this pharmaceutical compound, only one value was recorded, in the water sample taken from station S3 (Figure 13).

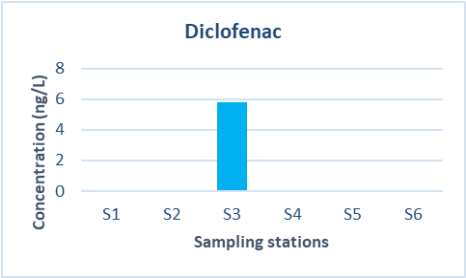

Figure 13. Spatial distribution of diclofenac concentration

The macrolide antibiotic clarithromycin (Baumann et al., 2015) was also analyzed in the water samples, but was not detected at any sampling station.

CONCLUSIONS

The method applied to determine the pharmaceutical compounds tracked in the analyzed water samples proved to be suitable for their identification and quantification.
The most frequently detected compounds in the water samples were caffeine and carbamazepine, while the antibiotic clarithromycin was not detected in any of the 6 sampling stations.
Also, the obtained results highlight the fact that the fewest pharmaceutical compounds were identified in sampling station S6. Considering the fact that one of the major sources of pollution with pharmaceutical substances is municipal waste water, the most pharmaceutical compounds were identified in the stations that are located near the urban agglomeration of the Galati city (S1, S3, S5).
To confirm the identity of each analysed compound, at least two fragment ions with the appropriate ion-ratio were detected.

ACKNOWLEDGEMENTS

The technical support was provided by the Rexdan Research Infrastructure, created through the project An Integrated System for the Complex Environmental Research and Monitoring in the Danube River Area, REXDAN, SMIS code 127065, project co-financed by the European Regional Development Fund through the Competitiveness Operational Programme 2014-2020, contract no. 309/10.07.2020.

REFERENCES

Alkimin, G.D., Soares, A.M.V.M., Barata, C., Nunes, B. (2020). Evaluation of ketoprofen toxicity in two freshwater species: Effects on biochemical, physiological and population endpoints. *Environmental Pollution, 265.* 114993. https://doi.org/10.1016/j.envpol.2020.114993.

Baumann, M., Weiss, K., Maletzki, D., Schüssler, W., Schudoma, D., Kopf, W., Kühnen, U. (2015). Aquatic toxicity of the macrolide antibiotic clarithromycin and its metabolites. *Chemosphere, 120.* 192–198. https://doi.org/10.1016/j.chemosphere.2014.05.089.

Chitescu, C.L., Kaklamanos, G., Nicolau, A.I., Stolker, A.A.M. (Linda) (2015). High sensitive multiresidue analysis of pharmaceuticals and antifungals in surface water using U-HPLC-Q-Exactive Orbitrap HRMS. Application to the Danube River basin on the Romanian territory. *Science of the Total Environment, 532.* 501–511. https://doi.org/10.1016/j.scitotenv.2015.06.010.

Commission Implementing Decision (EU) 2020/1161 of 4 August 2020 establishing a watch list of substances for Union-wide monitoring in the field of water policy pursuant to Directive 2008/105/EC of the European Parliament and of the Council. (2020). OJL.

Cunningham, V.L., Perino, C., D'Aco, V.J., Hartmann, A., Bechter, R. (2010). Human health risk assessment of carbamazepine in surface waters of North America and Europe. R*egulatory Toxicology and Pharmacology, 56.* 343–351. https://doi.org/10.1016/j.yrtph.2009.10.006.

Edwards, Q.A., Kulikov, S.M., Garner-O'Neale, L.D. (2015). Caffeine in surface and wastewaters in Barbados, West Indies. *SpringerPlus, 4.* 57. https://doi.org/10.1186/s40064-015-0809-x.

Gaw, S., Thomas, K.V., Hutchinson, T.H. (2014). Sources, impacts and trends of pharmaceuticals in the marine and coastal environment. Philos. *Regulatory Toxicology and Pharmacology, 369.* 20130572. https://doi.org/10.1098/rstb.2013.0572.

Gross-Sorokin, M.Y., Roast, S.D., Brighty, G.C. (2006). Assessment of Feminization of Male Fish in English Rivers by the Environment Agency of England and Wales. Environ. *Health Perspect., 114.* 147–151. https://doi.org/10.1289/ehp.8068.

Hejna, M., Kapuścińska, D., Aksmann, A. (2022). Pharmaceuticals in the Aquatic Environment: A Review on Eco-Toxicology and the Remediation Potential of Algae. *International Journal of Environmental Research and Public Health, 19.* 7717. https://doi.org/10.3390/ijerph19137717.

Khan, H.K., Rehman, M.Y.A., Malik, R.N. (2020). Fate and toxicity of pharmaceuticals in water environment: An insight on their occurrence in South Asia. *Journal of Environmental Management, 271.* 111030. https://doi.org/10.1016/j.jenvman.2020.111030.

Koba, O., Golovko, O., Kodešová, R., Fér, M., Grabic, R. (2017). Antibiotics degradation in soil: A case of

clindamycin, trimethoprim, sulfamethoxazole and their transformation products. *Environmental Pollution, 220*. 1251–1263. https://doi.org/10.1016/j.envpol.2016.11.007.

Oosterhuis, M., Sacher, F., Ter Laak, T.L. (2013). Prediction of concentration levels of metformin and other high consumption pharmaceuticals in wastewater and regional surface water based on sales data. *Science of the Total Environment, 442.* 380–388. https://doi.org/10.1016/j.scitotenv.2012.10.046.

Patel, M., Kumar, R., Kishor, K., Mlsna, T., Pittman, C.U.Jr., Mohan, D. (2019). Pharmaceuticals of Emerging Concern in Aquatic Systems: Chemistry, Occurrence, Effects, and Removal Methods. *Chemical Reviews, 119.* 3510–3673. https://doi.org/10.1021/acs.chemrev.8b00299.

Peters, A., Crane, M., Merrington, G., Ryan, J. (2022). Environmental quality standards for diclofenac derived under the European water framework directive: 2. Avian secondary poisoning. *Environmental Sciences Europe, 34.* 28. https://doi.org/10.1186/s12302-022-00601-7.

Popescu, F., Trumić, Milan, Cioabla, A.E., Vujić, B., Stoica, V., Trumić, Maja, Opris, C., Bogdanović, G., Trif-Tordai, G. (2022). Analysis of Surface Water Quality and Sediments Content on Danube Basin in Djerdap-Iron Gate Protected Areas. *Water, 14.* 2991. https://doi.org/10.3390/w14192991.

Straub, J.O. (2013). An Environmental Risk Assessment for Human-Use Trimethoprim in European Surface Waters. *Antibiotics, 2.* 115–162. https://doi.org/10.3390/antibiotics2010115.

Vatovec, C., Kolodinsky, J., Callas, P., Hart, C., Gallagher, K. (2021). Pharmaceutical pollution sources and solutions: Survey of human and veterinary medication purchasing, use, and disposal. *Journal of Environmental Management, 285.* 112106. https://doi.org/10.1016/j.jenvman.2021.112106.

Woitke, P., Wellmitz, J., Helm, D., Kube, P., Lepom, P., Litheraty, P. (2003). Analysis and assessment of heavy metal pollution in suspended solids and sediments of the river Danube. *Chemosphere, 51.* 633–642. https://doi.org/10.1016/S0045-6535(03)00217-0.

Scientific Papers. Series E. Land Reclamation, Earth Observation & Surveying, Environmental Engineering. Vol. XII, 2023
Print ISSN 2285-6064, CD-ROM ISSN 2285-6072, Online ISSN 2393-5138, ISSN-L 2285-6064

AN AUTOMATED METHOD FOR FORESTRY DETERMINATION USING A UAV LIDAR-MOUNTED PLATFORM

Maxim ARSENI, Octavian ROMAN, Madalina CALMUC, Valentina-Andreea CALMUC, Adrian ROSU, Stefan-Mihai PETREA, Catalina ITICESCU, Lucian-Puiu GEORGESCU

REXDAN Research Infrastructure,
"Dunarea de Jos" University of Galati, Faculty of Sciences and Environment,
98 George Cosbuc Street, Galati, Romania

Corresponding author email: maxim.arseni@ugal.ro

Abstract

LiDAR is one of the most promising technologies in the forestry industry. The LiDAR scanning methods help to improve and to drive sustainable forest management. The main purpose of this paper is to apply the UAV LiDAR scanning method, to identify and measure the tree volume calculation along a road section. The flight was made using a UAV octocopter and a LiAir LiDAR system. To determine the forestry volume several steps of postprocessing were applied. Therefore we create a 3D point cloud reconstruction of large forest areas. After the preliminary post-process, we apply a segmentation for the study area and track individual trees, to create an inventory for the detected trees. Determining the tree volume helps to make a correct financial estimation of the elimination of this from a new road or area that changes its destination. On the overhand, automated methods like LiDAR scanning of forestry and terrain, and automated tree volume calculation helps to improve the time spent confronted with traditional taxation methods.

Key words*: LiDAR, UAV, Forestry segmentation, Point cloud classification.*

INTRODUCTION

The essence of the technology reveals its name: LiDAR from English Light Identification Detection and Ranging - light detection and range determination. It works as follows: the optical system sends a light signal, and based on it receives and processes information about distant objects - and, using this data, creates a three-dimensional image of the scanned object (Burt et al., 2019). The history of the technology began in the 1960s of the 20th century - LiDAR was used to track satellites and military targets(Fryskowska & Stachelek, 2018). Over time, technology has improved and its scope has expanded. For example, today the LiDAR scanner, among other things, is built into the latest iPad Pro model.

One of the most widespread laser scanning technologies has found its way into the forestry industry. Since the early 2000s, LiDAR has been used worldwide as an alternative to traditional forest inventory methods. The advantages of laser taxing over traditional approaches are obvious: the method saves time and therefore money.

Most importantly, laser surveying makes it possible to obtain the most accurate and objective data on the condition of forests, down to tree height and trunk diameter (Kukkonen et al., 2021). The process consists of several stages. The first is information gathering: an aircraft or drone, with a LiDAR scanner installed, flies over a certain territory, scanning it. Penetrating through the forest canopy to the ground, the laser beam encounters many surfaces along the way and is reflected from them. This reflection is captured by the scanner receiver installed on the board of the UAV. Since the scanner is capable of generating from 100 up to 500 thousand laser pulses per second, depending on the used LiDAR model, and also it can provide a very large amount of information that is generated at the end of the scan(Wang et al., 2020).

The next step is decryption. The data collected by the LiDAR scanner is a so-called "point cloud" - a dense field of points located in a three-dimensional coordinate system. Each point in the cloud has its class: soil; undersized vegetation; vegetation of medium height; tall vegetation; noise; water surfaces. To view this

information and build 3D terrain models based on it, special programs are used. The most accurate results are provided by the additional use of information from external geolocation systems, terrain maps, and GNSS. The data taken from them about roads, lakes, and rivers serve as a kind of reference point for the creation of accurate digital models of the relief, terrain, and canopy of plantations.

The study area was chosen so that there are areas sufficiently covered with trees.

The study area is situated in the western part of Romania, rather than between $22^0 38' 30"$ to $22^0 40' 30"$ East longitude and $45^0 88' 20"$ to $45^0 88' 67"$ (Figure 1).

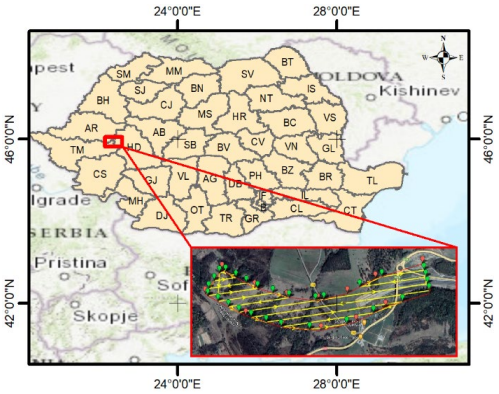

Figure 1. The mission flight path inside the study area

MATERIALS AND METHODS

To obtain point cloud data from aerial scanning an octocopter UAV with a LiAir V70 LiDAR sensor was used. The LiDAR sensor generates up to 240 000 points for the first strongest return and a total of 720 000 points for a triple return. Additionally, the LiAir sensor has an optical Sony A5100 camera with a 24-megapixel. The range accuracy of the LiDAR unit is ± 2 cm with an 70.4^0 (horizontal) field of view (Figure 2).

The flight plan has 1.7 km long with a 300 m corridor width. The maximum speed allowed for this data collection was 6 m/s. The total flight time was above 50 minutes (Figure 3).

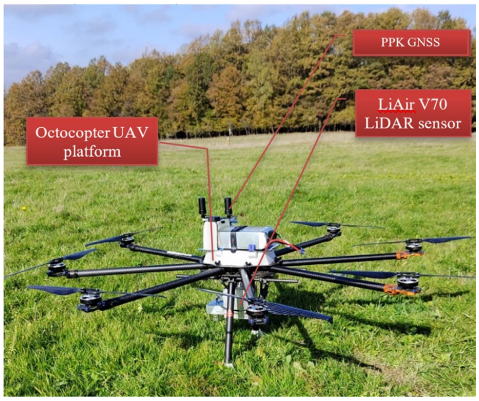

Figure 2. UAV platform and LiDAR sensor used for flight and point cloud data collected

Figure 3. Image footprint and flight path mission created for the aerial survey

Additionally to the UAV platform, in the field was made statical GNSS determinations of ground control points (GCPs). The GCPs were used for the point cloud georeferencing and model calibration. The PPK technology was used to align all the cloud points and trajectory adjustments. The PPK GNSS observation post-processing involves a process of differential correction, which involves comparing the raw GNSS data collected by the receiver with the precise ephemeris data and carrier phase measurements to obtain highly accurate positioning information (Figure 4). The GCP's point was surveyed with a Hiper HR GNSS, produced by Topcon.

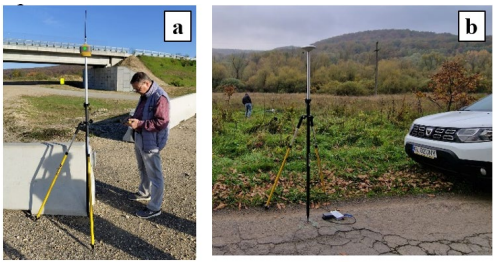

Figure 4. The precision GNSS static survey - image (a). PPK equipment for trajectory adjustment linked to PPK GPS mounted on UAV platform - image (b)

The overlapping of flight paths was 60 x 80%, to have the best accuracy in point cloud coordinate determination (Figure 5) (Arseni et al., 2016). In this case, approximately all the study area was scanned twice, and the confidence level of the data was very high. The UAV flight survey was performed in parallel paths, trying to maintain a constant altitude, by inputting a predefined Digital Elevation Model (DEM) inside the UAV pilot memory. The altitude of the flight was 80 m above the ground.

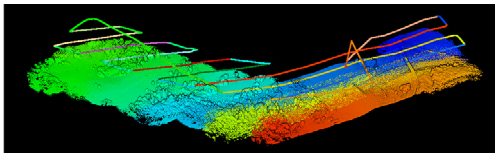

Figure 5. The UAV flight path with 60 x 80 overlapping and displayed by GNSS time mode with applied shading technique to enhance the visual contour effects

Thus, it was collected a dataset having an average point density of 196 points/m². The total covered area was 55.8 hectares with an amount of 191 million points.

To post-process the surveyed point cloud data was made with LiGeoreference software, produced by Green Valley company (Liu et al., 2022). The optional software LiDAR360, also produced by Green Valley was used for the point cloud classification and forestry determination. The ground classification of the point cloud from the collected UAV LiDAR data involves separating the points that correspond to the ground surface from other points such as trees, buildings, and other objects (Zeybek & Şanlıoğlu, 2019). This can be achieved through several techniques, like height thresholding, slope-based filtering, Canopy height model (CHM), or machine learning algorithms. For this study, the ground classification was made by a combination of the height thresholding combined and slope filtering method (Figure 6).

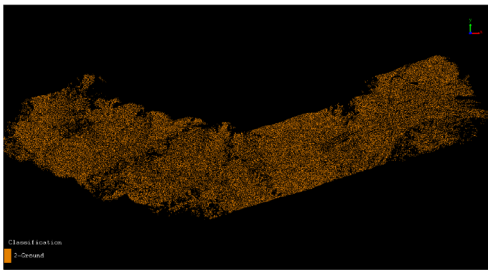

Figure 6. The classification of point cloud data depends on ground points to create a DTM model

To achieve the main purpose of this study, namely to determine the forestry from a point cloud database a flowchart was followed. If we analyze the workflow from Figure 7 the proposed approach includes two main phases: the first step is the flight planning and LiDAR scanning, and the second one is the post-process step and Canopy Height Model (CHM) derivation and extraction of tree parameters.

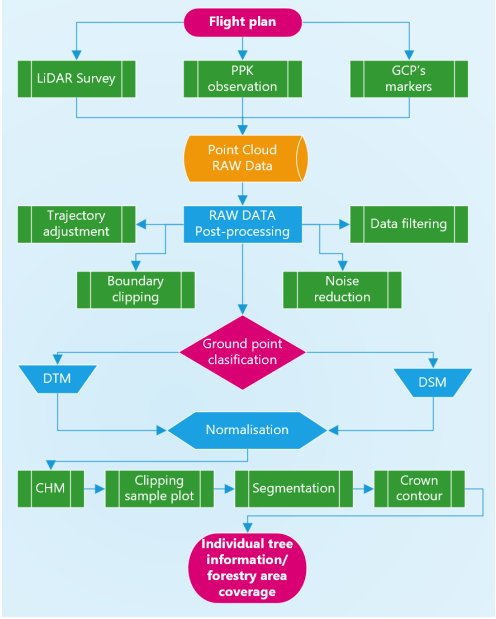

Figure 7. The flowchart of the main steps to automated segmentation and forestry determination from UAV LiDAR data

RESULTS AND DISCUSSIONS

To achieve the main purpose of this research is necessary to resolve some problems of DTM and DSM creation. These two results serve to estimate the over parameters such as canopy height, individual trees, or crown volume and area. All these data are based on the collected LiDAR measurements. The collected RAW data was pre-processed, by trajectory adjustment, elevation adjustment, and data filtering to obtain a projected point cloud model (Figure 9).
The final result of the point cloud was cleared by removing the outliers. It helps eliminate high-level gross errors and low-level gross errors.

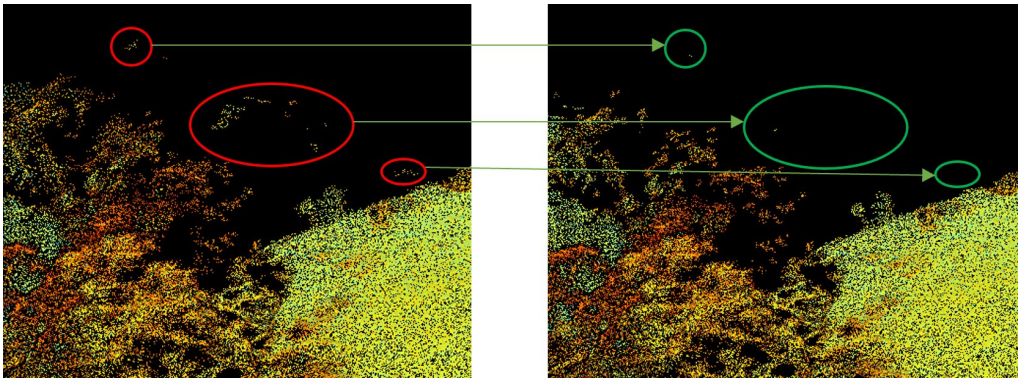

Figure 8. Example of a result obtained by removing the outliers from pre-processed point cloud data

After the point cloud classification by ground point with 20 m maximum building height and 88^0 maximum terrain angle, the DTM model was created with 0.5x0.5 m pixel dimension. The TIN interpolation method was used to create the DTM model.
Digital Surface Model (DSM) created for the study area refers to the digital representation of the height of the surface including the buildings, bridges, roads, and trees (Selim et al., 2022). Compared to a DEM, a DSM contains more elevation information for buildings, bridges, forests, and other surface objects that don't exist in the DEM. The DSM was created with the same pixel size, by using the TIN interpolation method. DSM is based on DEM and further covers the elevation of surface information other than the ground. As is shown in Figure 9 the DTM profile has only terrain points, while the DSM has forestry information.
An important step for forestry determination from point cloud data is to obtain the canopy height model (CHM) by the subtraction of the DTM from the DSM. Both digital models at 0.5 m spatial resolution will derive to CHM with the same spatial resolution. This resolution is optimal for tree crown delimitation and statistical parameter calculation.

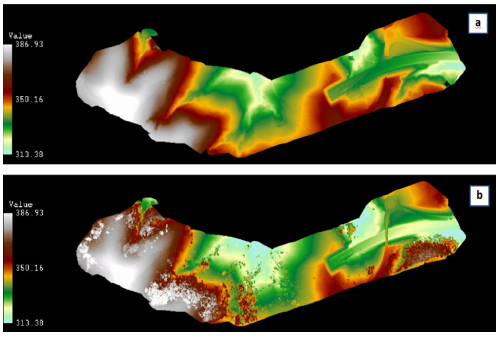

Figure 9. The DTM (a) and DSM (b) at 0.5 m spatial resolution with height variation between 313.38 to 386.93 m reference to the Black Sea Elevation Datum

To eliminate some negative values, the CHM model was normalized by DEM (Figure 10). By normalization, we remove the influence of terrain relief on the elevation value of the point cloud data.
This process is performed by subtracting the corresponding terrain elevation of the DEM from each point's Z value. The height of the CHM model varies between 0 to 35.85 m

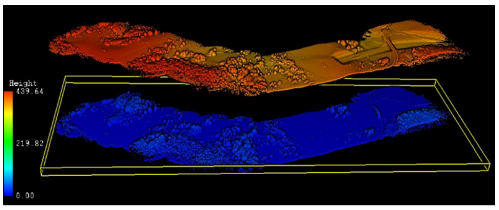

Figure 10. The normalization by DEM of point cloud data makes it easier to identify and separate the ground points from other features in the scene

Extracting forestry information from LiDAR point cloud data involves processing the data to identify and analyze different features of the forest. To make it possible is a need to make a tree segmentation. Tree segmentation from point cloud data is a process of identifying and extracting the point cloud data related to trees in a given environment. It is a crucial task in many fields such as forestry management, urban planning, and environmental monitoring. For this research, it was used a canopy-based segmentation. This method segments trees based on their canopy shape. It assumes that trees have a well-defined canopy shape that can be detected using geometric or statistical methods. The method uses algorithms such as region growing, clustering, or graph-based methods to segment points within the canopy as trees. Canopy-based segmentation step was based on dividing the point cloud data set into tree-like objects based on the characteristics of their canopies (Jakovljevic et al., 2019; Zeybek & Şanlıoğlu, 2019). These basis algorithms used for point cloud segmentation are described by the next equation:

$$P_d x \left(\frac{H_c}{W_c}\right) > T \quad (1)$$

where:
P_d - the number of points per unit area within the canopy;
H_c - the height of the canopy, typically measured as the vertical distance between the highest and lowest points within the canopy;
W_c - the average width of the canopy, typically measured as the horizontal distance between the leftmost and rightmost points within the canopy;
T - a defined threshold value that determines whether a given cluster of points represents a single tree or not.
To achieve more accurate results is indeed apply the above formula by first identifying clusters of points that represent individual trees based on their proximity to each other. For each cluster, the point density, canopy height, and canopy width are calculated. The formula then evaluates whether the combination of these factors meets a user-defined threshold value. If the threshold is exceeded, the cluster is considered to represent a single tree or tree-like object and is segmented from the rest of the point cloud data (Dai et al., 2022; Nasiri et al., 2021). For point cloud segmentation in this research, a 2 m distance threshold value was used, and a 1.5 m height above ground value was applied to avoid the influence of low vegetation (e.g., grass and shrubs). The result of point cloud segmentation is shown in Figure 11.

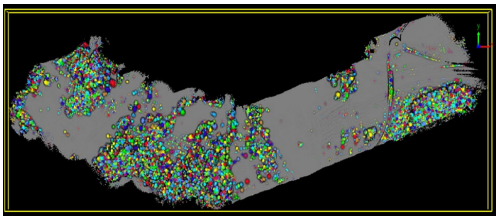

Figure 11. The point cloud segmentation and display by height mode, the grey color represents the above the tree area, under 1.5 m height

To visualize better the obtained segmentation result the crown circle mode representation was run. Each circle represents the crown tree size diameter. Crown diameter is an important metric for assessing the size and growth of individual trees, as well as for estimating forest canopy structure and biomass. Figure 12 shows the result of the crown size diameter classification.

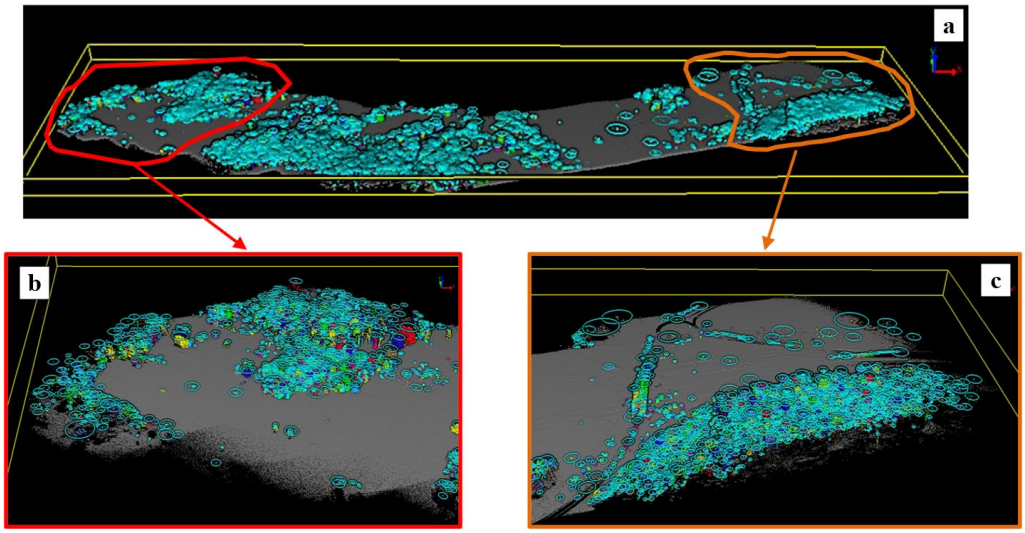

Figure 12. The crown tree representation of the entire area (a - image) and zoom-in clipped sample data from the left (b - image), and the right part (c - image), to visualize the crown size distribution

To identify and adjust the tree segmentation the manual seed identification method was used, The seed point allows selection points within the point cloud that represent the tops of trees and adjust if necessary. Once the seed points have been identified, the ALS seed point editor was used to delineate the individual tree crowns within the lidar data. This is accomplished using algorithms that connect the seed points with neighboring lidar points to create a three-dimensional representation of the tree crown (Schmohl et al., 2022) (Figure 13). The resulting tree crown delineation can be used for a variety of applications, including forest inventory and management, biodiversity assessments, and carbon accounting.

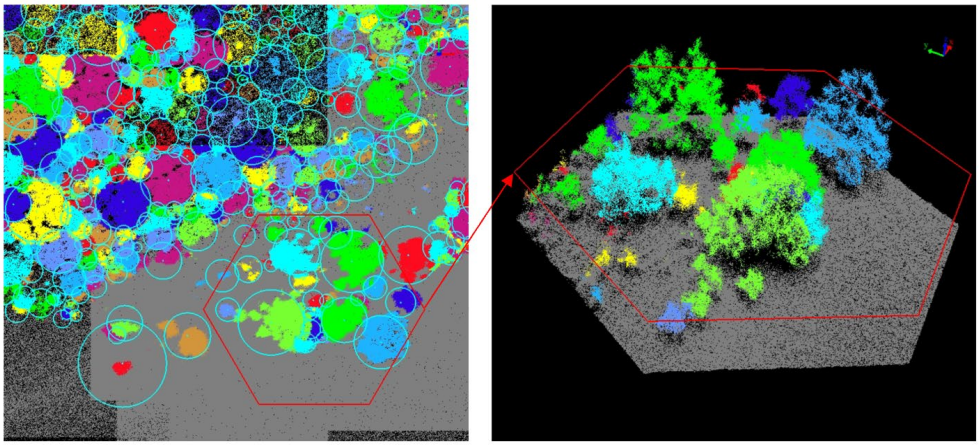

Figure 13. The seed points tool application to represents the 3D model of the tree crown

The total volume of tree crown calculated by point cloud segmentation for the entire surveyed area was amount 300 thousand tons. By applying the segmentation algorithm it was identified 12160 trees. The histogram of height shows that the average tree height is 13.73 m (Figure 14).

The maximum height of the tree was 35.855 m and the minimum was 1.73 m.

Height and crown diameter are two important metrics for characterizing the size and structure of individual trees. The positive and significant results are given by Pearson statistic correlation. The linear relationship between crown diameter and tree height shows that taller trees tend to have medium or smaller crown diameters. Different research studies describe this result as an anomaly, given by the sun missing in the forestry area. So, where the light of the sun is missing the end of the trees is to grow up straight and with minimum crown diameters (Figure 15).

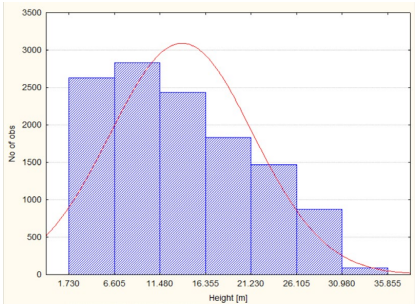

Figure 14. The histogram representation of the height of the tree distributed into 7 classes

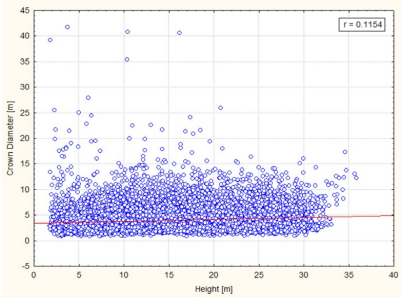

Figure 15. The Pearson correlation between crown diameter and trees height for the entire scanned area

A 3D statistical surface plot is used to represent a three-dimensional graphical surface that is constructed using the crown diameter, crown area, and crown volume parameters. The plot was created by fitting a linear mathematical function to this set of data and then using this function to generate the 3D surface that represents the relationship between the variables in the data set. In Figure 16 can be observed the relationship between the 3 variables. If a tree has a larger diameter then the area and volume also are bigger, and vice versa.

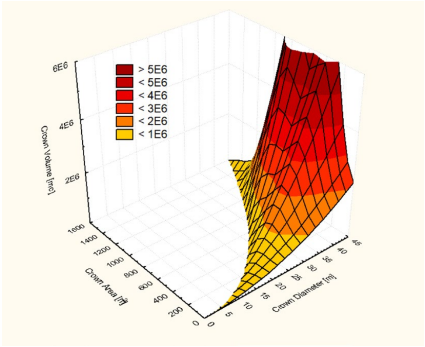

Figure 16. The 3D surface plot representation of dependence between forestry parameters

The forest metrics indicator shows the results of the quantitative measures. This indicator is important to assess various aspects of forest ecosystems, such as their structure, composition, and function. These metrics are used to evaluate the health and condition of forests and to inform management and conservation decisions. The result of the more than 1.5 m canopy cover is presented in Figure 17.

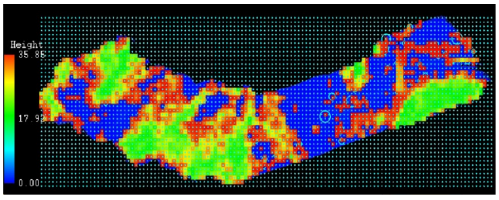

Figure 17. 15 m x 15 m pixel raster representation of canopy cover from the study area

Table 1 shows the summary statistics about the forest from the LiDAR-scanned study area.

Table 1. Summary statistics about forest parameters processed by the CH model

	Valid N	% Valid obs.	Mean	Sum	Minimum	Maximum
Tree Height [m]	12160	100.0000	13.7	166968	1.7	35.9
Crown Diameter [m]	12160	100.0000	3.9	47527	0.8	41.7
Crown Area [sqm]	12160	100.0000	17.1	207335	0.5	1367.9
Crown Volume [cm]	12160	100.0000	69.1	839830	0.6	5498.8

CONCLUSIONS

The practice shows that data collected based on LiDAR not only provides a more accurate estimate of wood stocks but is very useful for statistical assessment and different prediction models for forestry management. The information also allows us to better plan the harvest work, right down to selecting the necessary equipment and its placement. However, LiDAR inventory of forest areas is only one of the applications of laser forest scanning.

Today, the possibilities of LiDAR are increasingly discussed in the context of sustainable forestry. With the help of LiDAR scanning, it is possible to track the growth dynamics of tree trunks, crowns, and their undergrowth, and detect outbreaks of pests and forest diseases promptly. In addition, researchers use LiDAR to measure the amount of carbon that forests in a given area can absorb. Crown diameter is an important metric for assessing the size and growth of individual trees, as well as for estimating forest canopy structure and biomass. Lidar (Light Detection and Ranging) is a remote sensing technology that can provide high-resolution, 3D point cloud representations of the forest canopy, including the crown of individual trees.

The main purpose of this research was to estimate crown diameter from a lidar point cloud, several methods have been applied, like DEM computation, CH model, or Point Cloud Segmentation. One common approach was to use a point cloud segmentation algorithm to identify individual tree crowns in the point cloud. Once the crown segments have been identified, the diameter can be calculated from various metrics, such as the maximum or average width of the crown segment.

By accurately identifying and measuring individual tree crowns, the ALS seed point editor can help improve our understanding of forest ecosystems and their response to environmental change.

For statistical analysis, the Pearson correlation was used. The R factor shows that the correlation between tree height and crown diameter is ($r = 0.1154$). It shows that the forest from the study area was of high density and the crown is smaller overwise the tree height. However, as mentioned earlier, tree crowns can have different shapes, such as irregular or multi-stemmed, and different formulas or methods may be needed to estimate their volumes accurately. Additionally, tree volume can be affected by many factors such as the tree's age, health, and site conditions, so accurate measurement and estimation of tree volume require careful consideration of these factors. Overwise, the result shows that the canopy coverage is 25% reported to the entire study area.

Overall, lidar point cloud representations offer a powerful tool for accurately and efficiently estimating crown diameter and other important forest metrics. These estimates can be used to inform forest management decisions and assess the health and productivity of forest ecosystems.

ACKNOWLEDGEMENTS

The present article was supported by the project *An Integrated System for the Complex Environmental Research and Monitoring in the Danube River Area, REXDAN*, SMIS code 127065, co-financed by the European Regional Development Fund through the Competitiveness Operational Programme 2014-2020, contract no. 309/10.07.2021.

REFERENCES

Arseni, M., Georgescu, L. P., & Murariu, G. (2016). Photogrammetric aplications using UAV systems. *Annals of the University Dunarea de Jos of Galati: Fascicle II, Mathematics, Physics, Theoretical Mechanics*, *39*(1).

Burt, A., Disney, M., & Calders, K. (2019). Extracting individual trees from lidar point clouds using treeseg. *Methods in Ecology and Evolution*, *10*(3). 438–445.

Dai, W., Guan, Q., Cai, S., Liu, R., Chen, R., Liu, Q., Chen, C., & Dong, Z. (2022). A Comparison of the Performances of Unmanned-Aerial-Vehicle (UAV) and Terrestrial Laser Scanning for Forest Plot Canopy Cover Estimation in Pinus massoniana Forests. *Remote Sensing*, *14*(5). 1188.

Fryskowska, A., & Stachelek, J. (2018). A no-reference method of geometric content quality analysis of 3D models generated from laser scanning point clouds for hBIM. *Journal of Cultural Heritage*, *34*. 95–108.

Jakovljevic, G., Govedarica, M., Alvarez-Taboada, F., & Pajic, V. (2019). Accuracy assessment of deep learning based classification of LiDAR and UAV points clouds for DTM creation and flood risk mapping. *Geosciences*, *9*(7). 323.

Kukkonen, M., Maltamo, M., Korhonen, L., & Packalen, P. (2021). Fusion of crown and trunk detections from airborne UAS based laser scanning for small area forest inventories. *International Journal of Applied Earth Observation and Geoinformation*, *100*. 102327.

Liu, H., Cao, F., She, G., & Cao, L. (2022). Extrapolation Assessment for Forest Structural Parameters in Planted Forests of Southern China by UAV-LiDAR Samples and Multispectral Satellite Imagery. *Remote Sensing*, *14*(11). 2677.

Nasiri, V., Darvishsefat, A. A., Arefi, H., Pierrot-Deseilligny, M., Namiranian, M., & Le Bris, A. (2021). Unmanned aerial vehicles (UAV)-based canopy height modeling under leaf-on and leaf-off conditions for determining tree height and crown diameter (case study: Hyrcanian mixed forest). *Canadian Journal of Forest Research*, *51*(7). 962–971.

Schmohl, S., Narváez Vallejo, A., & Soergel, U. (2022). Individual tree detection in urban ALS point clouds with 3D convolutional networks. *Remote Sensing*, *14*(6). 1317.

Selim, S., Demir, N., & Şahin, S. O. (2022). Automatic detection of forest trees from digital surface models derived by aerial images. *International Journal of Engineering and Geosciences*, *7*(3). 208–213.

Wang, X., Pan, H., Guo, K., Yang, X., & Luo, S. (2020). The evolution of LiDAR and its application in high precision measurement. *IOP Conference Series: Earth and Environmental Science*, *502*(1). 012008.

Zeybek, M., & Şanlıoğlu, İ. (2019). Point cloud filtering on UAV based point cloud. *Measurement*, *133*. 99–111.

Scientific Papers. Series E. Land Reclamation, Earth Observation & Surveying, Environmental Engineering. Vol. XII, 2023
Print ISSN 2285-6064, CD-ROM ISSN 2285-6072, Online ISSN 2393-5138, ISSN-L 2285-6064

ANALYSIS REGARDING THE INCREASE IN THE RESISTANCE OF CEMENTITIOUS SELF-HEALING COMPOSITES TO THE ACTION OF MICROORGANISMS BY INDUCED PHOTOACTIVATION CAPACITY

Elvira GREBENIȘAN, Andreea HEGYI, Adrian-Victor LĂZĂRESCU

NIRD URBAN-INCERC Cluj-Napoca Branch, 117 Calea Floresti, Cluj-Napoca, Romania

Corresponding author email: andreea.hegyi@gmail.com

Abstract

The development of biofilms of micro-organisms on the surface of buildings, in addition to the negative impact and risk to the health of the population, leads to their degradation and the need for continuous sanitation operations. Inducing superhydrophilicity and self-cleaning performance of cement surfaces by adding TiO_2 nanoparticles to the composite matrix, as a result of photoactivation reactio. This method, can become an effective for the production of new materials in order to increase the durability of buildings and to increase the degree of hygiene, due to the ability of these new materials to inhibit the growth of microorganisms. Experimental results have shown that in case of contamination with two types of moulds (Aspergillus niger, Penicillium notatum) and four types of bacteria (Escherichia Coli, Pseudomonas Aeruginosa, Staphylococus Aureus, Streptococus Pyogenes) respectively, the development of harmful biofilm is inhibited. This performance was monitored using the dimensional development of the specific inhibition halo as a quantifiable indicator. It can be said that it is influenced by the type of contaminant and the nanoparticle content of the cementitious composite matrix, but is manifested in all cementitious composites containing TiO_2 nanoparticles photoactivated under laboratory conditions.

Key words*: biocidal effect, photocatalysis, self-cleaning cementitious composites, TiO_2 nanoparticles.*

INTRODUCTION

Today, worldwide, especially in developed countries, but not exclusively, there is a change in people's lifestyles, with more and more activities taking place inside buildings. Micro-organisms such as moulds, bacteria, viruses, algae, lichens or mites, have a negative impact on building surfaces. This is known to have negative effects on the health of the population if the growth occurs on the surfaces of indoor living spaces. Also, the growth of micro-organism films on the built surface has a negative effect on the durability and operational safety of buildings, accelerating their degradation and contributing on the degree of environmental pollution. Each tonne of manufactured cement (the main raw material used in the construction industry) is responsible for the release of 0.8-1.1 tons of CO_2 into the atmosphere because of fuel combustion and limestone calcination (International Energy Agency, 2009). "Sick building syndrome (SBS)" (Farrag et al., 2021; Gawande et al., 2020; Sarkhosh et al., 2021; Wang et al., 2022; Gao et al., 2021; Huo et al., 2020) is known as having negative impact on the health of users and is recognized worldwide as, manifesting itself in people who work, partially or totally, inside buildings. They can be affected by deposits of microorganisms, as a result of the degradation of indoor air quality through contamination with spores and toxins emanating (Andersen et al., 2011; Baxter et al., 2005; Żukiewicz-Sobczak et al., 2013; Haverinen-Shaughnessy, 2012; Giannantonio et al., 2009; Sökmen et al., 2001; Sökmen et al., 2008). These mould spores, toxins emanating in the normal life cycle of micro-organisms, or even the micro-organisms themselves, reach the human body both through the air breathed in and through direct contact with contaminated surfaces.

Cheap and handy antibacterial methods can become a very important method for the development of simple, new types of materials. This issue is actual and very important because, in recent years, damage caused by harmful microorganisms has become a serious social problem (Yandav et al., 2016; Wang et al., 2017). Exterior surfaces act as reservoirs for the development of microorganisms that could, in turn, lead to the spread of infections or

become the main cause of various health conditions (Kühn et al., 2003). The conceptually, simple and promising technology, in which applications of the photocatalytic process of TiO_2 nanoparticles (NT), generate an inhibition in the growth of some microorganisms, moulds or bacteria, becomes an alternative to the use of chemical disinfectants (Drugă et al., 2018; Machida et al., 2005; Watts et al., 1995; Jakubickova et al., 2020; Khannyra et al., 2022; Wang et al., 2022). In general, NT is found as a mixture of rutile and anatase (both being crystallographic forms of TiO_2). There is also the situation where the crystallographic form anatase is predominant (over 90%), and, according to the literature, TiO_2 nanoparticles could be added dry, by direct mixing with cement powder, followed by the addition of hydration water. Water does not chemically react with any crystallographic form of titanium dioxide, nor does a chemical reaction occur between the photosensitive nanoparticles. The hydration-hydrolysis phases of the cement and the hydration-hydrolysis reactions are not chemically influenced by the chemical reaction (Quagliarini et al., 2012). The major influence of these nanoparticles on the performance of cementitious composites is to induce a superhydrophilicity of the surface, with a sustained self-cleaning capacity and also increased resistance to the action of microorganisms The developed materials could also present an imparting a biocidal effect.

Under the action of UV rays, as a semiconductor with a band gap of about 3.0 eV and by absorbing energy, titanium dioxide generates electrons (e^-) and holes (h^+). Ti (IV) cation to the Ti (III) ion is reduced by the above mentioned and holes oxidize O_2^- anions. This process will release oxygen, creating vacancies on the surface of the titanium dioxide. This vacancies will allow the water molecules to bind with the release of hydroxyl groups (OH^-). Literature indicates that, in the case of TiO_2-containing cementitious composite surfaces (Jakubickova et al., 2020; Khannyra et al., 2022; Wang et al., 2022; Matsunaga et al., 1988; Drugă et al., 2018) that photogenerated (h+) voids (holes) cause the bond length within the TiO_2 structure to increase bringing the surface into a metastable state. Simultaneously with the formation of new hydroxyl groups and the release of a proton, this allows the adsorption of molecular water (Figure 1) (Zhang et al., 2010; Matsunaga et al., 1988).

Using the energy provided by UV radiation, simultaneously with the development of superhydrophilicity, which is greater than the valence band gap of TiO_2, electron pairs (e^-) and holes (h^+) are generated. Those react with O_2 and H_2O forming anionic radicals (O_2^-) and (OH). These oxidative species (h^+,$\cdot O_2^-$) and (OH) are all highly reactive and participate to the destruction of microorganism cells (Haleem Khan & Mohan Karuppayil, 2012). Research to date has led to a number of hypotheses regarding the biocidal effect indicating that the cell membrane is photocatalytically destroyed (Sunada et al., 2003). This is also supported by reports by Oguma et al. (Oguma et al., 2002) who propose a destruction mechanism explained by both cell wall destruction and induction of disruption at the cellular level following contact of the microorganism with TiO_2, while Saito et al. (Saito et al., 1992) propose the hypothesis of a destruction mechanism explained by the inhibition of the bacterial cell's respiratory function once in contact with TiO_2.

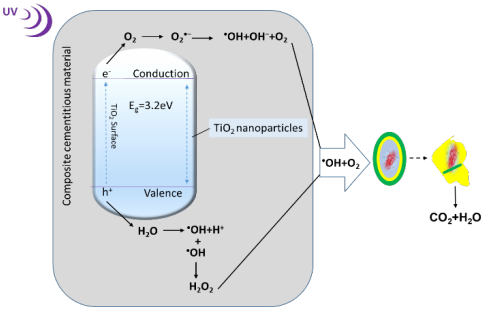

Figure 1. Sequential representation of the biocidal mechanism

The aim of this paper is to analyse the biocidal capacity of cementitious composites containing with TiO_2 nanoparticles (NT).

MATERIALS AND METHODS

The samples were produced using NT-added cement paste, with AEROXIDE® TiO_2 P25. The TiO_2 nanoparticles were characterized by

an average particle size of 21 nm, a specific surface of 35-65 m^2/g and 99.5% purity, containing more than 70% anatase, were prepared for the experimental tests. The composite cementitious paste was prepared and conditioned as shown in Figure 2, with mixture P1 as a control sample (0% NT).

According to literature references (Hope, 2013; Rosen & Heseltine, 2009; Fisk et al., 2007; Mudarri & Fisk, 2007; Jaakkola et al., 2005) and based on preliminary research, since NT has a low density and a necessity for water, it was not possible to maintain a constant amount of preparation water without affecting the consistency and workability of the fresh material. In order to determine the standard consistency of the paste, the Tetmayer probe was chosen as a constant parameter and the mixing water was determined for each individual cement/TiO_2 nanoparticles ratio. The mix design ratio is presented in Figure 2, with a water/cement ratio ranging of 0.45-0.5.

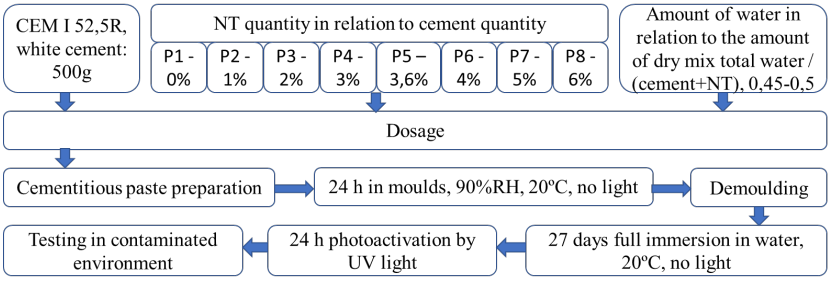

Figure 2. Methodology for the production of the test specimens

Cementitious composite specimens, made in the form of 17.4 mm diameter discs and 24 mm x 30 mm plates respectively, were photoactivated by holding them for 24 hours under UV light using a light source within the range of 400-315 nm UVA band. The lights were displaced at a distance of 10 cm above the specimen surface, resulting in a light flux intensity of 860 lux.

For each contaminating microorganism (mould/bacteria) an experimental stand was constructed to eliminate the risk of cross-contamination. For each case, the repeatability of the results was demonstrated by repeating the tests for at least 3 similar specimens.

The final result is expressed as the average of the individual results. The contamination material used consisted of pure cultures of *Penicillium notatum* (Fag19002) and *Aspergillus niger* (FAg18003), obtiained from USAMV Cluj-Napoca, respectively, *Streptococcus pyogenes* (ATCC 19615), *Pseudomonas aeruginosa* (ATCC 27853), *Escherichia coli* (ATCC 25922) and *Staphylococcus aureus* (ATCC 25923) commonly used in laboratory medicine practice. Exposure to contaminants was affected by applying solutions prepared from mold/bacterial reference cultures and introducing 2 colonies (2 loops of 1µl) biological material into 1 ml saline.

Since there is no generally accepted standard of analysis for evaluating the behaviour of cementitious composites in the presence of mould/bacteria, the antibiogram method was taken as the starting point for testing. This method is a common method, mainly used in medicine. Consequently, the test specimens were made, taking as indicative sizes the samples used in laboratory medical practice (Hernandez-Carnerero et al., 2021).

Petri dishes, φ 90 mm, were prepared for each case analysed, in which nutrient substrate was placed to grow bacterial cultures (agar for *Escherichia coli*, *Pseudomonas aeruginosa*, *Staphylococus aureus*, respectively blood agar for *Streptococcus pyogenes*), or mould cultures (Potato Dextrose Agar - PDA, 39 g/l) which were also sterilised under UV light. In each Petri dish the nutrient substrate was contaminated uniformly over the entire surface with 1 ml of the solution prepared as described above. Then, the light-activated cementitious composite specimen was placed centrally and 0.5 ml of biological material - mould/bacteria suspension - was applied directly to the surface of the specimen, after which the whole system was closed and isolated. For each type of

mould or bacteria used samples were produced and, subsequently, control samples (P0). The control sample was considered as the sample for demonstrating the viability of the mould/bacteria spores in the suspensions used, following the development of the culture, which was also confirmed by rapid and intense growth.

The growth systems prepared for testing were placed under laboratory conditions at (30±2)°C, constant temperature and (55±2)% relative humidity. The systems were examined visually and microscopically, at regular intervals, for signs of growth/development of biological material (colonies) and the existence/development of the inhibition halo was observed. Quantification of the resistance of cementitious composites to the action of microorganisms was achieved by identifying the existence and measuring the inhibition halo in the case of specimens exposed to a mould-contaminated environment, and by assessing the microbiological load of the system, respectively, according to STAS 12718/1989 in the case of specimens exposed to the action of bacteria. The degree of development of bacterial material in the system was recorded in agreement with STAS 12718/1989 where the following classes are specified: Class 0(-) indicating no growth (sterile); Class 1(+) indicating 1-10 colonies of microorganisms; Class 2(++) indicating over 10 colonies of micro-organisms; Class 3(+++) indicating areas with confluent colonies and Class 4(++++) indicating growth over the entire area.

The entire experimental testing process, i.e. preparation of the cementitious composite with/without the addition of NT, production of test specimens (casting in moulds, demoulding after 24 h, storage for 27 days in water for maturation), 24 h UV photoactivation, creation of a contaminated environment system in Petri dishes (creation of specific substrate for mould or bacteria growth, soaking with solution containing contaminating microorganism, placing photoactivated cementitious composite test tube, applying solution containing contaminating microorganism on the surface of the test tube, closing and sealing the system), were carried out once for each test tube in the test batch. As specified, for each cementitious composite and for each type of microorganism (2 types of mould and 4 types of bacteria) three test specimens were made. Therefore, the test batch was composed of: 8 types of cementitious composite x 6 types of contaminant medium x 3 test specimens for each situation, i.e. 144 test specimens, each of them contained in an individual, closed, sealed test system (Petri dish). After sealing the individual test system, no additional photoactivation of the specimens in the cementitious composite was performed and the contaminant medium was not altered by enrichment with additional volumes of solution containing mould spores or bacteria. For the identification and measurement of the inhibition halo and for taking the example photographs, the individual, closed, sealed system was not opened, as these operations may have been performed through the transparency of the Petri dish lid. This mode of operation allowed the same specimen to be followed over time, in the same contaminant environment, without inducing possible elements of additional variation. Also, the monitoring of the size of the halo of indifference was carried out each time by the same operator, with the same calibrated measuring instrument. Therefore, it can be appreciated that the uncertainty of measurement remained constant throughout the experimental test, for all the cases analysed.

The durability of the biocidal effect was examined by analysing the maintenance of the inhibition halo for 7 days under constant temperature and humidity conditions and natural lighting (natural day-night cycles), without intervening with a new dose of UV radiation.

Additionally, in order to compare the production cost of the cementitious composites with NT with that of the control cement composite, based on the raw material mixture, the cost/m^3 was calculated. Based on this cost price, it was assumed that panels, with dimensions 50 cm x 50 cm x 2 cm, are made of concrete with NT content, class C20/25. These panels will be used for wall cladding of a building. In this hypothesis, it was calculated how much the cost of making the coating would increases for the use of cementitious composite with the addition of NT, compared to the situation of using a classic concrete. For testing to demonstrate the biocidal effect of NT

under laboratory conditions, a UV photoactivation plant was used. Given the intended use of these materials, i.e. outside buildings, this photoactivation will take place naturally, either from sunlight. If these materials will be used inside buildings, literature (Khannyra et al., 2022; Machida et al., 2005; Kühn et al., 2003; Matsunaga et al., 1988) indicates that indoor light sources such as neon bulbs, for example, or natural lunation incident on the cement surface during the period of ventilation of spaces by opening windows, provide sufficient light radiation to achieve this photoactivation process. Therefore, the cost of electricity used by the photoactivation system in the laboratory was not included in the calculated cost. Furthermore, the literature (Khannyra et al., 2022; Machida et al., 2005; Kühn et al., 2003; Matsunaga et al., 1988) indicates that, in cementitious composites, so, in the present SiO_2, NT photoactivation, once performed under UV, is kept active for several days without the need for a new UV dose.

RESULTS AND DISCUSSIONS

The results of the experimental investigations, as shown in Figure 3 to Figure 8, showed a number of aspects proving the biocidal ability of NT-containing cementitious composites.

In the case of exposure of the cementitious composite in an environment contaminated with *Penicillium notatum*, Figure 3a). the existence of the inhibition halo is observed in all specimens of cementitious composite material, including the control sample (P1-0% NT). However, with regard to the test system carried out with the control sample, a reduced size of the inhibition halo is identified and, after 3 days of exposure, its disappearance.

Regarding the behaviour of the photoactivated NT-containing cementitious composite material (P2-P8) in *Penicillium notatum*-contaminated environment, the appearance and maintenance of the inhibition halo throughout the test is identified, even if, over time, this inhibition halo undergoes reductions in diameter, which means a reduction in the inhibition power of the biological film development. After 4 days of testing, it can be said that there is a tendency for the phenomenon to stabilise, from a kinetic point of view (Figure 3a), since the decrease in the diameter of the inhibition halo is much smaller between two consecutive days (measurements), compared to the situation during the first 3 days of testing.

In the case of exposure of the cementitious composite in an environment contaminated with *Aspergillus niger*, Figure 3b) the existence of the inhibition halo is observed in all specimens of cementitious composite material, including the control sample (P1-0% NT).

The maintenance of the inhibition halo, in the case of this mould species, occurs during the first 4 days of testing in all specimens, including the control specimen, after which its disappearance is observed both for the control and for the cement composite specimens prepared with the addition of 1% NT and 2% NT. Even in the case of the 3% NT cement composite, the mould film develops on the nutrient substrate, covering it completely after the 5th day of testing, but without any signs of mould growth on the surface of the cement specimen. Also, similarly to the behaviour of specimens exposed to *Penicillium notatum* contaminated medium, a tendency of stabilization of the inhibition halo diameter is observed in the last 3 days of testing, which would suggest a stabilization of the phenomenon from a kinetic point of view.

At the same time, by comparing the results presented in Figure 3a) and 3b), it can be said that *Aspergillus niger* species shows a higher aggressiveness than *Penicillium notatum* species. Both were based on the inhibition diameters values and as a result of the ability of this species to grow even when there are composites with 1%, 2% and even 3% NT in the system.

It is therefore considered that, in the case of these mould species, frequently encountered in everyday life, good protection could be obtained by using quantities of at least 3% NT as an addition to the cementitious composite, in relation to the quantity of cement, provided, of course, that a good cost/benefit ratio is maintained. Based on the calculation made by the simplified methodology, presented above, under the current price conditions, it can be said that the costs of cladding with concrete panels increase by 6-20 euro/m^2 for the use of a quantity of 1-3% NT in the cementitious

composite, respectively by over 25 euro/m^2 if the amount of NT used is at least 4% (relative to the quantity of cement). The frequency and complexity of decontamination, washing, maintenance, etc. of surfaces will of course vary from case to case, depending on the characteristics of the construction, location, intended use, etc. However, it is considered that reducing the frequency with which these maintenance operations are required will result in a cost/benefit balance in favour of the use of cementitious composites with added NT. Despite this increase in the cost of the initial investment, in the case of using NT-enhanced material, as a result of biocidal capacity, the costs of washing, sanitizing and surface maintenance will decrease. Moreover, it is appreciated that thus, indirectly, the impact on the health of the population will improve, so that possible treatment costs in the medical system will be reduced. No signs of mould growth were observed on the surface of the composite specimens for any of the species used as biological aggressors (*Penicillium notatum*/*Aspergillus niger*).

Significant examples in terms of inhibition halo evidence are shown in Figure 9a) and 9b) for for cases of exposure to mold, respectively, Figure 9c) for the case of exposure to the *Escherichia coli* bacteria.

Microscopic analysis revealed, for all test systems in which the specimen was made of cementitious composite with NT, 3 circular areas of contamination and growth of biological material (Figure 10 and Figure 11). In the immediate vicinity of the specimen, the inhibition halo is formed, with variable diameter (D) depending on the amount of NT in the composite and the type of contaminant (mould/bacteria).

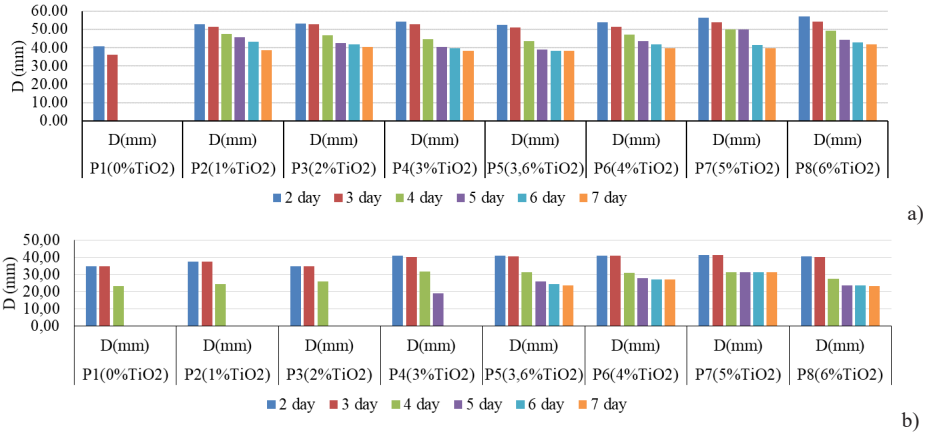

Figure 3. Variation of inhibition halo diameter during 7 days of testing for specimens exposed to *Penicillium notatum* (a) and *Aspergillus niger* (b) contaminated medium

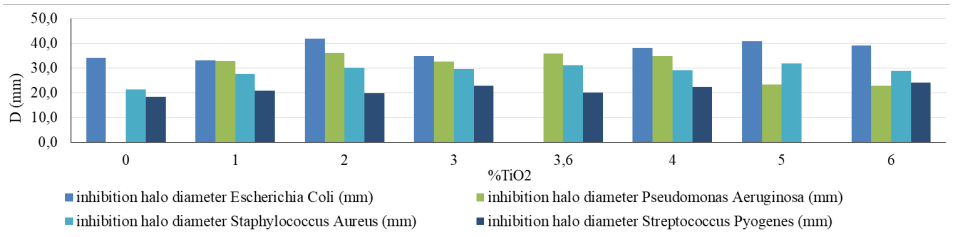

Figure 4. Inhibition halo diameter for specimens exposed 2 days in medium contaminated with *Escherichia coli*, *Pseudomonas aeruginosa*, *Staphylococcus aureus*

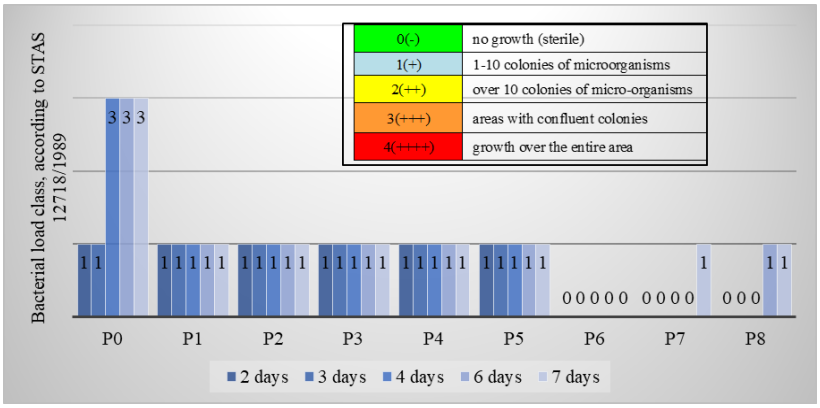

Figure 5. The degree of development of bacterial material (Class acording to STAS 12718/1989) in case of environment contaminated with *Escherichia coli*

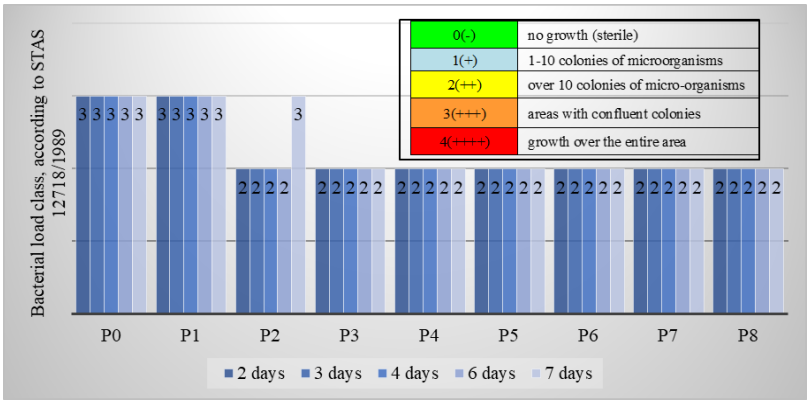

Figure 6. The degree of development of bacterial material (Class acording to STAS 12718/1989) in case of environment contaminated with *Pseudomonas aeruginosa*

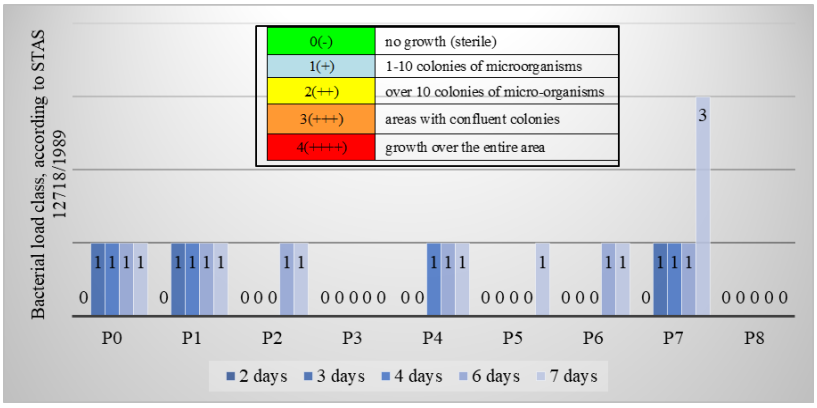

Figure 7. The degree of development of bacterial material (Class acording to STAS 12718/1989) in case of environment contaminated with *Staphylococus aureus*

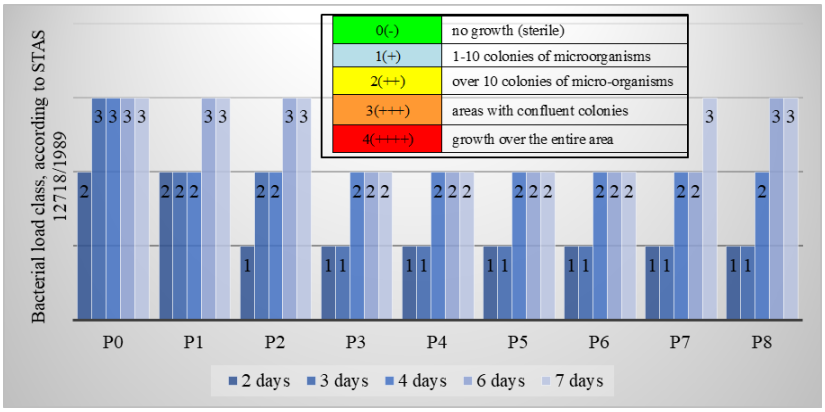

Figure 8. The degree of development of bacterial material (Class acording to STAS 12718/1989) in case of environment contaminated with *Streptococus pyogenes*

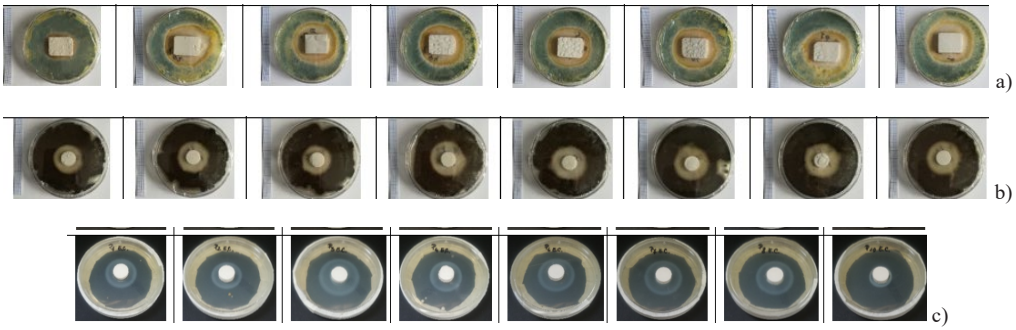

Figure 9. Evidence of inhibition halo - example for sample exposed 3 days in medium contaminated with *Penicillium notatum* (a), *Aspergillus niger* (b) *Escherichia Coli* (c) (P1 - P8, from left to right)

The inhibition halo is characterized, according to STAS 12718/1989, corresponding to a growth of maximum 1-10 colonies, or "sterile". Subsequently, a transition zone is identified in which biological growth begins to intensify, reaching a maximum of intense growth, in which independent units of biological material can no longer be identified and reach confluence.

As regards the behaviour of the photoactivated NT-containing cementitious composite material (P2-P8) in a bacterially contaminated environment, some similarities and some differences can be observed compared to the behaviour in the presence of moulds. Thus, the appearance of inhibition halos is identified (Figure 4), which are much smaller in diameter than in the cases of the two mould species, but remain constant throughout the test.

Microscopic analysis shows the appearance of bacterial colonies on the surface of the nutrient substrate, but not on the surface of the cementitious specimen. As shown in Figures 5-8, the biological load was quantified for each test system (Petri dish with nutrient substrate, with cementitious composite specimen and with biological contaminant material) separately. Each type of bacteria has a different degree of aggressiveness and a different strength of resistance and growth in the presence of the control or NT-enriched cementitious composite. Thus, a graded classification of bacterial aggressiveness can be appreciated, with the most aggressive behaviour exhibited by *Pseudomonas aeruginosa* bacteria and the least aggressive by *Staphylococus aureus* and *Escherichia coli.*

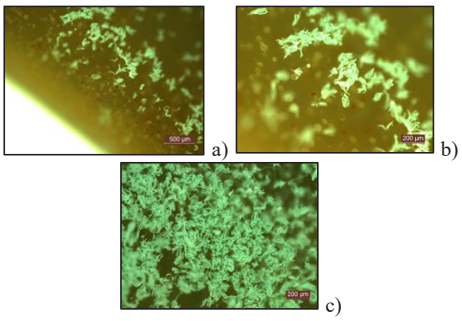

Figure 10. Sample captures for microscopic analysis in which the following can be identified: a). inhibition halo; b). transition zone; c). zone of intense growth - sample exposed 7 days in *Penicillium notatum* contaminated medium

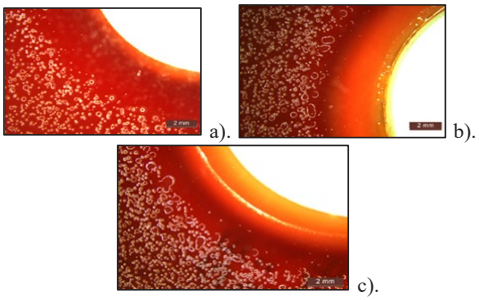

Figure 11. Sample captures for microscopic analysis in which the following can be identified a) inhibition halo; b) transition zone; c) zone of vigorous growth - sample exposed 7 days in *Streptococcus pyogenes* contaminated medium

Analysing the evolution of the biological load in the system during the 7 days of analysis, Figures 5-8, together with the fact that the inhibition halo, although small, is also maintained throughout the evaluation period, it can be appreciated that the biocidal effect is maintained over time and that an amount of min. 1% NT, in relation to the amount of cement, as an addition to the cementitious mixtures, is sufficient. However, if this range of concentration of photoreactive material (NT) were to be analysed in conjunction with the behaviour against mould aggressiveness, it is estimated that the minimum NT required would be 3%, relative to the amount of cement.

CONCLUSIONS

The aim of the work was to investigate the ability of TiO_2 nanoparticle-enriched photoactivated UV-enriched cementitious composites to reduce the risk of mould and bacteria growth on building surfaces. Thus, eight cementitious mixtures were designed, based on white cement, to which TiO_2 nanoparticles were added in an amount of 0-6% of the cement. For each of these situations, test specimens were made and, after UV photoactivation, exposed to media contaminated with *Aspergillus niger*, *Penicillium notatum*, *Escherichia coli*, *Pseudomonas aeruginosa*, *Staphylococcus aureus* or *Streptococcus pyogenes* for a period of 7 days.

Based on the above, it can be considered that the biocidal effect induced by the addition of nanoparticles in the composite cement matrix under UV photoactivation is manifested for all cases analysed. However, the effectiveness of this effect is influenced by the type of contaminant and the species to which it belongs. Also, this effect of increasing the resistance of cementitious composite materials to the action of microorganisms is influenced by the amount of nanoparticles used as additive. Although in the case of bacteria an addition of 1% NT would be sufficient, as the inhibition haloes would be maintained throughout the evaluation, in the case of mould species, a minimum of 3% NT would be required, relative to the amount of cement.

Among the bacteria used as contaminants, *Pseudomonas aeruginosa* was found to be more resistant and aggressive, *Staphylococcus aureus* and *Escherichia coli* were found to be less resistant in the presence of NT-added cementitious composites, and *Aspergillus niger* was found to be more aggressive than *Penicillium notatum*.

In terms of the durability of this effect over time, it was found that, in the absence of other influencing factors, under constant temperature conditions and under daylight exposure conditions corresponding to day-night cycles, the growth of microorganism films is inhibited without the need for additional surface photoactivation over and above the initial one.

The experimental results obtained are encouraging arguments for further research in this area. At this stage of the research, the number of experimentally obtained data is insufficient to start a statistical analysis, which is one of the directions for further research.

Also, the encouraging experimental results lead to a new research direction, namely a cost/benefit analysis applied to the concrete case of an existing building for which it is proposed to finish the exterior with cladding panels based on cementitious composite with added NT, under specific climatic and environmental contaminant exposure conditions.

ACKNOWLEDGEMENTS

This work was carried out within *Nucleu Programme* of the National Research Development and Innovation Plan 2022-2027, supported by MCID, "ECODIGICONS" project no. PN 23 35 05 01: "Innovative sustainable solutions to implement emerging technologies with cross-cutting impact on local industries and the environment, and to facilitate technology transfer through the development of advanced, eco-smart composite materials in the context of sustainable development of the built environment".

REFERENCES

Andersen, B., Frisvad, J.C., Søndergaard, I., Rasmussen, I.S., & Larsen, L.S. (2011). Associations between Fungal Species and Water-Damaged Building Materials. *Applied and Environmental Microbiology*, *77(12)*. 4180–4188.

Baxter, D.M., Perkins, J.L., McGhee, C.R., & Seltzer, J.M. (2005). A Regional Comparison of Mold Spore Concentrations Outdoors and Inside "Clean" and "Mold Contaminated" Southern California Buildings. *Journal of Occupational and Environmental Hygiene*, *2*. 8–18.

Drugă, B., Ukrainczyk, N., Weise, K., Koenders, E., & Lackner, S. (2018). Interaction between wastewater microorganisms and geopolymer or cementitious materials: Biofilm characterization and deterioration characteristics of mortars. *International Biodeterioration & Biodegradation*, *134*. 58–67.

Farrag, N., Abou El-Ela, M. A., & Ezzeldin, S. (2022). Sick building syndrome and office space design in Cairo, Egypt. *Indoor and Built Environment*, 568–577.

Fisk, W.J., Lei-Gomez, Q., & Mendell, M.J. (2007). Meta-analyses of the associations of respiratory health effects with dampness and mold in homes. *Indoor Air*, *17(4)*. 284–296.

Gao, X., Jali, Z. M., Aziz, A. A., Hizaddin, H. F., Buthiyappan, A., Jewaratnam, J., & Bello, M. M. (2021). Inherent health-oriented design for preventing sick building syndrome during planning stage. *Journal of Building Engineering*, *44*. 103285.

Gawande, S., Tiwari, R. R., Narayanan, P., & Bhadri, A. (2020). Indoor air quality and sick building syndrome: Are green buildings better than conventional buildings? *Indian Journal of Occupational and Environmental Medicine*, *24(1)*. 30.

Giannantonio, D.J., Kurth, J.C., Kurtis, K.E., & Sobecky, P.A. (2009). Effects of concrete properties and nutrients on fungal colonization and fouling. *International Biodeterioration & Biodegradation, 63(3)*. 252–259.

Haleem Khan, A.A., & Mohan Karuppayil, S. (2012). Fungal pollution of indoor environments and its management. *Saudi Journal of Biological Sciences*, *19*. 405–426.

Haverinen-Shaughnessy, U. (2012). Prevalence of dampness and mold in European housing stock, *Journal of Exposure Science and Environmental Epidemiology*, *22*. 461–467.

Hegyi, A., Szilagyi, H., Grebenișan, E, Sandu, A.V., Lăzărescu, A.-V., & Romila, C. (2020), Influence of TiO_2 Nanoparticles Addition on the Hydrophilicity of Cementitious Composites Surfaces. *Applied Sciences, 10*. 4501-4515.

Hernàndez-Carnerero, À., Sànchez-Marrè, M., Mora-Jiménez, I., Soguero-Ruiz, C., Martínez-Agüero, S., & Álvarez-Rodríguez, J. (2021). Antimicrobial resistance prediction in intensive care unit for pseudomonas aeruginosa using temporal data-driven models. *IJIMA*I, *6(5)*. 119-133.

Hope, J. (2013). A review of the mechanism of injury and treatment approaches for illness resulting from exposure to water-damaged buildings, mold, and mycotoxins. *Scientific World Journal,* 767482.

Huo, X., Sun, Y., Hou, J., Wang, P., Kong, X., Zhang, Q., & Sundell, J. (2020). Sick building syndrome symptoms among young parents in Chinese homes. *Building and Environment*, *169*. 106283.

Jaakkola, J.J.K., Hwang, B.F., & Jaakkola, N. (2005). Home dampness and molds, parental atopy, and asthma in childhood: a sixyear population-based cohort study. *Environmental Health Perspectives*, *113(3)*. 357–361.

Jakubickova, M., Petrzilkova, M., Amartuvshin, B., Kejzlarová, L., & Kejzlar, P. (2020). The effect of NPs addition on the photocatalytic and antibacterial effectivity of composite TiO_2/SiO_2 paint. *IOP Conference Series: Materials Science and Engineering*, *723(1)*. 012010.

Khannyra, S., Luna, M., Gil, M. A., Addou, M., & Mosquera, M. J. (2022). Self-cleaning durability assessment of TiO_2/SiO_2 photocatalysts coated concrete: effect of indoor and outdoor conditions on the photocatalytic activity. *Building and Environment*, *211*. 108743.

Kühn, K.P., Chaberny, I.F., Massholder, K., Stickler, M., Benz, V.W., Sonntag, H.G., & Erdinger, L. (2003). Disinfection of surfaces by photocatalytic oxidation with titanium dioxide and UVA light. *Chemosphere*, *53(1)*. 71–77.

Machida, M., Norimoto, K., & Kimura, T. (2005). Antibacterial Activity of Photocatalytic Titanium Dioxide Thin Films with Photodeposited Silver on

the Surface of Sanitary Ware. *Journal of the American Ceramic Society*, *88*. 95–100.

Matsunaga, T., Tomoda. R., Nakajima, T., Nakamura, N., & Komine, T. (1988). Continuous-sterilization system that uses photosemiconductor powders. *Applied and Environmental Microbiology*, *54(6)*. 1330–1333.

Mudarri, D., & Fisk, W.J. (2007). Public health and economic impact of dampness and mold. *Indoor Air*, *17(3)*. 226–235.

Oguma, K., Katayama, H., & Ohgaki, S. (2002). Photoreactivation of Escherichia coli after Low- or Medium-Pressure UV Disinfection Determined by an Endonuclease Sensitive Site Assay. *Applied and Environmental Microbiology*, *68*. 6029–6035.

Page, K., Wilson, M., & Parkin, I.P. (2009). Antimicrobial surfaces and their potential in reducing the role of the inanimate environment in the incidence of hospital-acquired infections. *Journal of Materials Chemistry A*, *19*. 3819.

Quagliarini, E., Bondioli, F., Goffredo, G.B., Cordoni, C., & Munafò, P. (2012). Self-cleaning and de-polluting stone surfaces: TiO_2 nanoparticles for limestone. *Construction and Building Materials*, *37*. 51–57.

Rosen, E., & Heseltine, J. (2009). *WHO guidelines for indoor air quality: dampness and mould*. World Health Organization, Geneva, Switzerland.

Saito, T., Iwase, T., Horie, J., & Morioka, T. (1992). Mode of photocatalytic bactericidal action of powdered semiconductor TiO_2 on mutans streptococci. *Journal of Photochemistry and Photobiology B: Biology*, *14*. 369–379.

Sarkhosh, M., Najafpoor, A. A., Alidadi, H., Shamsara, J., Amiri, H., Andrea, T., & Kariminejad, F. (2021). Indoor Air Quality associations with sick building syndrome: An application of decision tree technology. *Building and Environment*, *188*. 107446.

Sökmen, M., Candan, F., & Sümer, Z. (2001). Disinfection of E. coli by the Ag–TiO_2/UV system: lipidperoxidation. *Journal of Photochemistry and Photobiology A: Chemistry*, *143(2–3)*. 241–244.

Sökmen, M., Degerli, S., & Aslan, A. (2008). Photocatalytic disinfection of Giardia intestinalis and Acanthamoeba castellani cysts in water. *Experimental Parasitology*, *119(1)*. 44–48.

Sunada, K., Watanabe, T., & Hashimoto, K. (2003). Bactericidal Activity of Copper-Deposited TiO2 Thin Film under Weak UV Light Illumination. *Environmental Science & Technology*, *37*. 4785–4789.

Vohra, A., Goswami D.Y., Deshpande, D.A., & Block, S.S. (2005). Enhanced photocatalytic inactivation of bacterial spores on surfaces in air. *Journal of Industrial Microbiology and Biotechnology*, *32*. 364–370.

Wang, L., Hu, C., & Shao, L. (2017). The antimicrobial activity of nanoparticles: Present situation and prospects for the future. *International Journal of Nanomedicine*, *12*. 1227–1249.

Wang, M., Li, L., Hou, C., Guo, X., & Fu, H. (2022). Building and health: Mapping the knowledge development of sick building syndrome. *Buildings*, *12(3)*. 287.

Wang, X., Ding, H., Lv, G., Zhou, R., Ma, R., Hou, X., & Li, W. (2022). Fabrication of superhydrophilic self-cleaning SiO_2–TiO_2 coating and its photocatalytic performance. *Ceramics International*, *48(14)*. 20033-20040.

Watts, R.J., Kong, S., Orr, M.P., Miller, G.C., & Henry, B.E. (1995). Photocatalytic inactivation of coliform bacteria and viruses in secondary wastewater effluent. *Water Research*, *29*. 95–100.

Yadav, H.M., Kim, J.S., & Pawar, S.H. (2016). Developments in photocatalytic antibacterial activity of nano TiO_2: A review. *Korean Journal of Chemical Engineering*, *33*. 1989–1998.

Zhang, S.M.-H., Tanadi, D., & Li W. (2010) *Effect of photocatalyst TiO_2 on workability, strength, and self-cleaning efficiency of mortars for applications in tropical environment*. 35th Conference on Our World In Concrete & Structures, Singapore.

Żukiewicz-Sobczak, W., Sobczak, P., Krasowska, E., Zwoliński, J., Chmielewska-Badora, J., & Jolanta Galińska, E.M. (2013). Allergenic potential of moulds isolated from buildings. *Annals of Agricultural and Environmental Medicine*, *20(3)*. 500–503.

Scientific Papers. Series E. Land Reclamation, Earth Observation & Surveying, Environmental Engineering. Vol. XII, 2023
Print ISSN 2285-6064, CD-ROM ISSN 2285-6072, Online ISSN 2393-5138, ISSN-L 2285-6064

MANAGEMENT OF MANURE

Paula COJOCARU, Gabriela BIALI

"Gheorghe Asachi" Technical University of Iasi,
Faculty of Hydrotechnics, Geodesy and Environmental Engineering,
63-65 Prof. dr. docent Dimitrie Mangeron Blvd, Iasi, Romania

Corresponding author email: paula.cojocaru@academic.tuiasi.ro

Abstract

In this paper, we aimed to achieve the management of the manure taken from five localities near the county of Iași, Romania. For this, two manure storage platforms with an area of 500 square metres will be built for its temporary storage. The platforms will serve the small farmers in this area, consisting of the platform itself and a collection basin located next to the platform, where the water from precipitation, animal urine and water for sanitising the platform reaches. Thus, this paper describes the constructive elements of the platforms, calculates the volumes of water collected from its surface and sizes the collection basin. The collection basin will have a volume of 120 m^3 and has been sized to ensure a storage capacity for a period of 30 days of precipitation and all liquid fractions resulting from the composting process.

Key words*: collection basin, manure, management, storage platform.*

INTRODUCTION

Manure is not only an agricultural waste but also anorganic fertiliser resource. Applying organic fertilisers is a feasible practice for mitigating soil degradation caused by excessive use of chemical fertilisers, which can affect bacterial diversity and soil composition (Zhang S. et al., 2020).

It is used on unstructured land, consisting of humus-poor soils, improves water retention, stimulates soil microbial activity, adds genetic and functional diversity to soils, and improves soil chemical and physical properties (Das et al., 2019; Wang J. et al., 2019; Yost J.L. et al., 2023; Köninger J. et al., 2021).

An important amount of the micro and macro elements taken from the plants used in fodder is returned to the soil through manure.

Applying manure and other organic fertilisers is important both for the nutrients that are embedded into the soil and for improving the conditions for the growth and development of plants (Wang J. et al. 2023). Since manure results gradually, applying it is not done as such. It is collected in platforms and composted.

Manure composting can be done by several methods. Commonly used methods are aerobic composting, anaerobic composting, and mixed composting.

Applying manure before a minimum rainfall period and applying manure by embedding reduces the risks associated with nutrient loss through surface runoff (Saha A. et al., 2023).

Manure can also cause pollution by introducing toxic elements, for example, heavy metals, antibiotics, pathogens and contributes to nutrient losses.

Another additional risk of pollution from manure results from the massive use of food supplements for animals (for example, copper and zinc supplements in raising pigs and poultry) for the purpose of their intensive breeding, supplements that end up in manure (Moral et al., 2008; Provolo et al., 2018).

Soil organisms play an essential role in the transformation of manure into soil and in the degradation of any potentially toxic constituents (Köninger J. et al., 2021).

Thus, manure is stored as far as possible from households and water sources, at least 50 metres, to avoid air and water pollution. It is recommended to place a platform specially arranged for this purpose, on a higher ground, so that rainwater does not collect at the base of the material.

Through the controlled storage of manure, nutrient losses resulting there from are mitigated and the product obtained can support soil fertility and increase crop productivity (Basit A. et al., 2019).
The purpose of this paper is to organise the management of manure collected from an area belonging to Iași county and to size the constructive elements of the platforms necessary for its controlled storage.

MATERIALS AND METHODS

The temporary storage of manure will be done on two storage platforms. The first platform will serve three localities, whereas the second one will serve two localities.
The platforms will have the same surface and will be located at least 500 m from the first household in the locality.
The sizing of the collection basin located next to the storage platform will be done considering the types of water collected from the surface of the platform. Thus, water from precipitation, animal urine produced, drinking water wasted by animals and/or people and water for sanitation will be captured.
This volume is determined by the formula 1.

$$V_t = V_u + V_p, \text{ (year)} \quad (1)$$

where:
V_u is the volume given by animal urine, drinking water wasted by animals and/or humans and water for sanitation; according to the provisions of the Code of Good Agricultural Practices, 4-5 m^3 for every 100 tons of fresh manure (Integrated Nutrient Pollution Control Project, 2016) and the amount of 81 tons/year of manure produced by the 5 UVM held by the owner result:

$$Vu = 5 \cdot \frac{81}{100} (m^3/\text{year}) \quad (2)$$

where: $Vu = 4.05$ (m^3/year)
V_p is the volume of water originating from precipitation during the period of one year.
The volume of water from precipitation (V_p) to be captured during a year, from the surface of the manure platform, will be calculated by the following calculation equation (Cojocaru et al., 2021):

$$V_p = 10000 \cdot \sum_{i=1}^{Ts} (P_i - E_i) \cdot (1 - \delta) \cdot \sigma \cdot S_p \ (1) \quad (3)$$

where:
Pi is the height of precipitation dropped in month *i* of the storage period, in an average climatic year, (mm/month *i*);
i - the month in the manure storages pan;
Ei - the value of evaporation from month *i* of the storage period, in an average year;
σ - the coefficient of leachate drainage from the storage facility; we propose $\sigma = 0.95$;
δ - the coefficient of precipitation retention in manure; we propose $\delta = 0.7$;
S_p - the area of the manure platform (ha).
Considering a degree of filling of 90% for the drainable basin, the total volume of the drainable basin is calculated by the equation:

$$Vbv = \frac{Vp}{0.9} (m^3) \quad (4)$$

where:
Vp is the volume of water from precipitation.

RESULTS AND DISCUSSIONS

Considering the amounts of manure obtained for the studied area, it is necessary to place two manure storage platforms, each with an area of 500 square metres.
These platforms will be located on the public sector and the distances from the last households can be seen in the Figures 1 and 2.
The main elements that make up the two manure platforms are: the concrete storage platform, the semi-buried collection basin and the water drainage system with gutters.

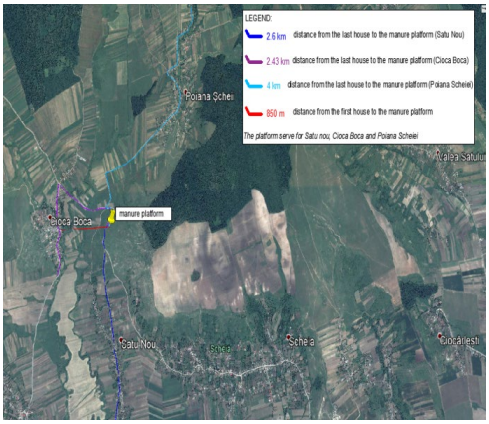

Figure 1. Location area of platform 1

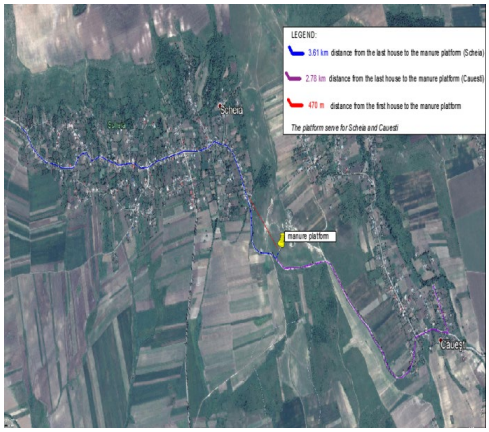

Figure 2. Location area of platform 2

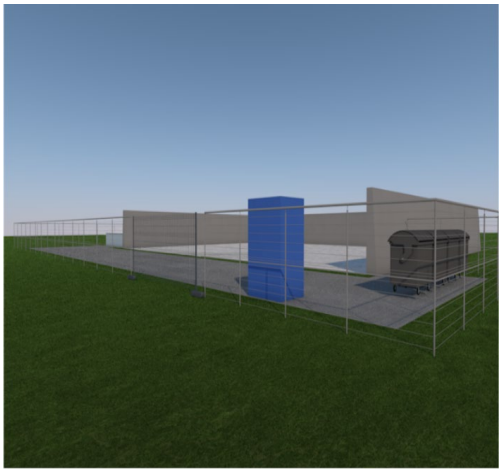

Figure 3. Manure storage platform

The platform will be made of road concrete and the walls of reinforced concrete. All elements of the construction will be sized in such a way as to withstand the specific load exerted by the volumes of stored manure, machinery, external forces as well as the accidental touching of the walls by the machinery.

The platform will not have internal dividing walls in order not to disturb the handling of the machines and to allow the free disposal of the manure piles.

The characteristics of the platform are rectangular shape, walls on 3 sides (no front side), top view dimensions: L x W x h = 20 x 25 x 2 m.

In Figures 4-5, the main elements of the two manure platforms can be seen.

When checking the sizing of the platform, the maximum amount of stored manure must be considered.

In Figure 3, a frontal view of the future platform can be seen.

At the front of the platform, a concrete scraper will be provided, necessary to ensure an area for the movement and handling of machinery and for the unloading/loading of manure from the means of transport.

Along the entire length of the front plate between the platform and the scraper, there is an effluent collection channel covered with a metal or reinforced concrete grate that discharges into the basin.

Sections through the two platforms are shown below.

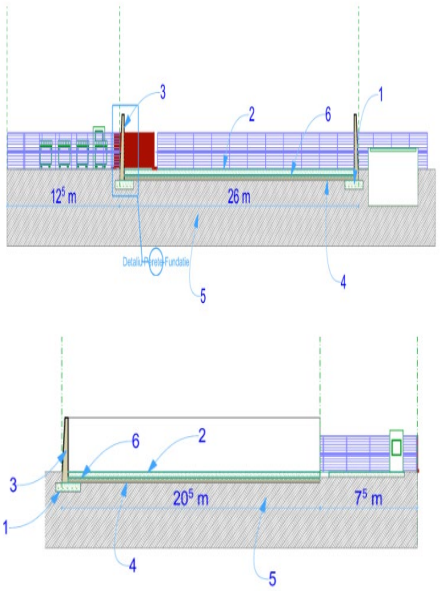

1 - Reinforced concrete foundation
2 - Manure platform
3 - Reinforced concrete wall
4 - Ballast layer
5 - Natural land
6 - Membrane for waterproofing.

Figure 4. Sections through concrete storage platform 1

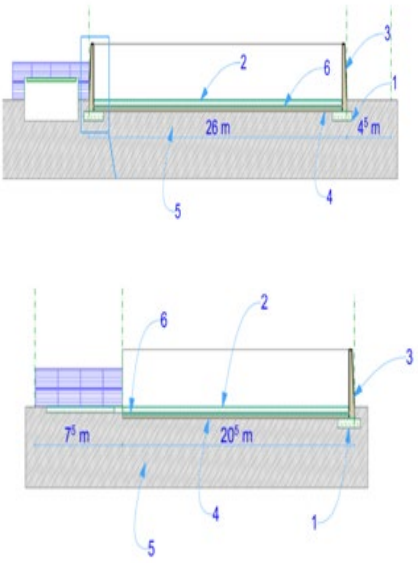

1 - Reinforced concrete foundation
2 - Manure platform
3 - Reinforced concrete wall
4 - Ballast layer
5 - Natural land
6 - Membrane for waterproofing.

Figure 5. Sections through concrete storage platform 2

A semi-buried basin of reinforced concrete with a volume of 120 useful cubic metres will be built, located in the immediate vicinity of the platform with the role of collecting effluents and rainwater. It has been sized to ensure a storage capacity for a period of 30 days. The collection basin will be waterproofed to prevent any possible infiltration of the liquid fraction from the manure into the soil. For the drainage of rainwater from the road surface inside the composting platform, a unique slope of 2% towards the sewer was provided.
There will be an empty tank trailer that serves to handle the liquid fraction that accumulates in the storage basin by turning it over the rows of manure on the platform to maintain the moisture required in the composting process.

A view of the collecting basin is shown in Figure 6.

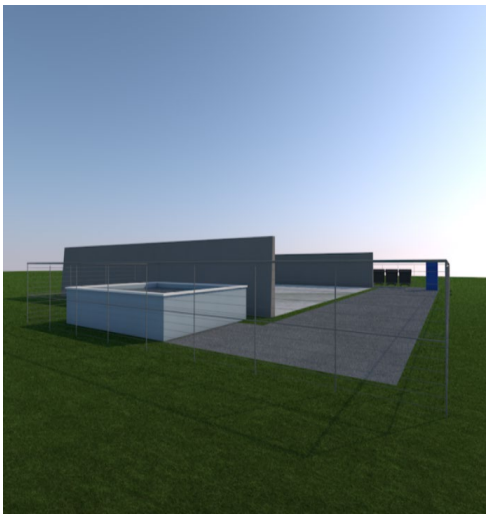

Figure 6. View of the collecting basin

In order to prevent pollution and to constantly monitor the quality of the underground water, the inner surfaces of the walls and floor of the platform as well as the collecting channel will be waterproofed. Also, a waterproofing membrane will be placed on the layer of earth on which the platform is built to prevent the infiltration of effluents from the manure storage into the ground and into the groundwater in case of damage to the platform.
In order to periodically monitor the quality of underground water, two piezometers will be installed both downstream and upstream of the storage platform to be built.
The volume of water from precipitation during a year that reaches the surface of the platform was calculated by means of equation (3) and the results obtained are presented in Table 1.
By then substituting in equation (4), it follows that the drainable basin must have a minimum volume Vbv=79.28 m^3.

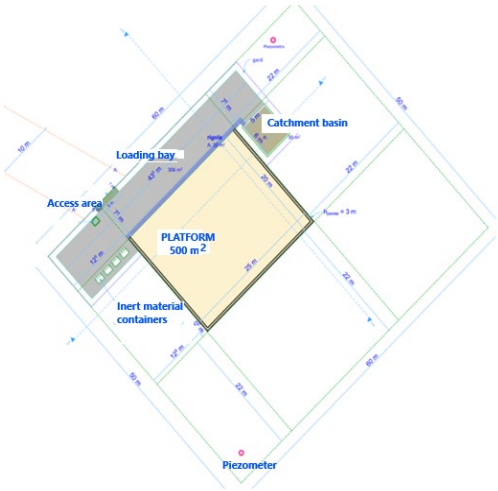

Figure 7. Elements of manure platform 1

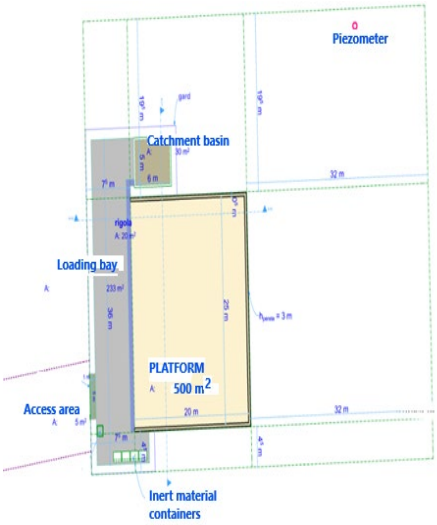

Figure 8. Elements of manure platform 2

Table 1. Calculation of the volume of water from precipitation (Vp)

Month	I	II	III	IV	V	VI	VII	VIII	IX	X	XI	XII
P (mm)	32	31	31	53	63	101	83	56	48	25	35	31
E (mm)	0	0	13.66	57.44	90.09	96.81	95.5	79.61	58.94	35.55	13.5	0
Pi-Ei	32	31	17.34	-4.44	-27.09	4.19	-12.5	-23.61	-10.94	-10.55	21.5	31
σ	0.95	0.95	0.95	0	0	0.95	0	0	0	0	0.95	0.95
δ	0.7	0.7	0.7	0	0	0.7	0	0	0	0	0.7	0.7
Sp (ha)	0.0783	0.0783	0.0783	0.0783	0.0783	0.0783	0.0783	0.0783	0.0783	0.0783	0.0783	0.0783
Vi (mc)	16.66	16.14	9.03	0	0	2.18	0	0	0	0	11.19	16.14
Vu (mc/year)	**71.35 mc/year**											

Considering the volume obtained, a standard drainable basin with a volume of 120 m^3 will be chosen, a sufficient volume if the platform is expanded in the future.

CONCLUSIONS

Through the management of the manure in the five localities, the quality of life will be improved, the risk of affecting the citizens' health will be reduced and the air hygiene will be maintained in a suitable state of comfort. Also, the soil will not be affected by pollution, because the storage platform will be waterproofed with a waterproofing membrane to prevent the infiltration of effluents from the manure storage.

And by collecting effluents and rainwater in the collection basin located next to the platform, possible infiltration into the soil is thus prevented.

REFERENCES

Basit, A., Abbas Shah, G., Traore, B., Abbas Shah, S.A., Shah, S.S., Mohammad Al-Solaimani, S.G., Hussain, Q., Ali, N., Shahzad, K., Shahzad, T., Ahmad, A., Muhammad, S., Shah, G.M., Arshad, M., Hussain, R.A., Shah, J.A., Anwar, A., Amjid, M.W., Rashid, M.I. (2019). Manure storage operations mitigate nutrient losses and their products can sustain soil fertility and enhance wheat productivity. *Journal of Environmental Management, 241,* 468-478.

Cojocaru, P., Statescu, F., Biali, G. (2021). Contributions on the centralized collection of manure. *Environmental Engineering and Management Journal, 20(3),* 371-375.

Das, R., Purakayastha, T.J., Das, D., Ahmed, N., Kumar, R., Biswas, S., Walia, S.S., Singh, R., Shukla, V.K., Yadava, M.S., Ravisankar, N., Datta, S.C. (2019). Long-term fertilization and manuring with different organics alter stability of carbon in colloidal organo-mineral fraction in soils of varying clay minetalogy. *Science of the Total Environment, 684*, 682-693.

Integrated Nutrient Pollution Control Project (2016). World Bank Group, Washington D.C., On line at: http://documents.worldbank.org/curated/en/106441468197929345/Romania-Integrated-Nutrient-Pollution-Control-Project-additional-financing.

Köninger, J., Lugato, E., Panagos, P., Kochupillai, M., Orgiazzi, A., Briones, M.J.I. (2021). Manure management and soil biodiversity: Towards more sustainable food systems in the EU. *Agricultural Systems, 194,* 103251.

Moral, R., Perez-Murcia, M., Perez-Espinosa, A., Moreno-Caselles, J., Paredes, C., Rufete, B. (2008). Salinity, organic content, micronutrients and heavy metals in pig slurries from South-eastern Spain. *Waste Management, 28,* 367-371.

Provolo, G., Manuli, G., Finzi, A., Lucchini, G., Riva, E., Sacchi, G.A. (2018). Effect of pig and cattle slurry application on heavy metal composition of maize grown on different soils. *Sustainability*, *10,* 2684-2692.

Saha, A., Cibin, R., Veith, T.L., White, C.M., Drohan, P.J. (2023). Water quality benefits of weather-based manure application timing and manure placement strategies. *Journal of Environmental Management, 333,* 117386.

Wang, J.,Wu, L., Xiao, Q., Huang, Y., Liu, K., Wu, Y., Li, D., Duan, Y., Zhang, W. (2023). Long-term manuring enhances soil gross nitrogen mineralization and ammonium immobilization in subtropical area. *Agriculture, Ecosystems & Environment*, *348,* 108439.

Wang, J., Sun, N., Xu, M., Wang, S., Zhang, J., Cai, Z., Cheng, Y. (2019). The influence of long-term animal manure and crop residue application on abiotic and biotic N immobilization in an acidified agricultural soil. *Geoderma*, *337,* 710-717.

Yost, J.L., Leytem, A.B., Bjorneberg, D.L., Dungan, R.S., Schott, L.R. (2023). The use of winter forage crops and dairy manure to improve soil water storage in continuous corn in Southern Idaho. *Agricultural Water Management, 277,* 108074.

Zhang, S., Sun, L., Wang, Y., Fan, K., Xu, Q., Li, Y., Ma, Q., Wang, J., Ren, W., Ding, Z. (2020). Cow manure application effectively regulates the soil bacterial community in tea plantation. *BMC Microbiology*, *20(190)*, 2-11.

Scientific Papers. Series E. Land Reclamation, Earth Observation & Surveying, Environmental Engineering. Vol. XII, 2023
Print ISSN 2285-6064, CD-ROM ISSN 2285-6072, Online ISSN 2393-5138, ISSN-L 2285-6064

STUDY OF AIR POLLUTION LEVEL IN AN URBAN AREA USING LOW-COST SENSOR SYSTEM ONBOARD MOBILE PLATFORM

Adrian ROSU[1], Maxim ARSENI[1], Daniel-Eduard CONSTANTIN[1], Bogdan ROSU[2], Stefan-Mihai PETREA[3], Mirela VOICULESCU[1], Catalina ITICESCU[1], Lucian-Puiu GEORGESCU[1]

[1]REXDAN Research Infrastructure, "Dunărea de Jos" University of Galati, Faculty of Sciences and Environment, 111 Domneasca Street, Galati, Romania
[2]"Dunărea de Jos" University of Galati, Faculty of Automation, Computer Sciences, Electronics and Electrical Engineering, 47 Domneasca Street, Galati, Romania
[3]"Dunărea de Jos", University of Galati, Faculty of Food Science and Engineering, 111 Domneasca Street, Galati, Romania

Corresponding author emails: rosu_adrian_90@yahoo.ro, adrian.rosu@ugal.ro

Abstract

The paper aims to assess the air pollution level using one mobile low-cost measurement system versus in situ sensing data from local air quality network stations. The measurements were performed during the winter of 2022 on the main streets of Galați city, one of the largest cities in Romania. The main purpose of the measurements is to use mobile measurements to capture the spatial and temporal distribution of important air pollutants such as NO_2+O_3, CO, SO_2, and PM_{10} in large urban areas. For this study used a mobile air quality monitoring system Sniffer 4Dv1 to record spatial and temporal data on air pollutants on the street of Galati City. The data sets from local RNAQMN (Romanian National Air Quality Monitoring Network) are compared with Sniffer 4Dv1 data to infer various limitations for each of the two data sets.

Key words*: air pollution, air quality, AQS in situ measurements, mobile measurements.*

INTRODUCTION

Over the past few decades, air pollution has become a major environmental concern on a global scale. The most significant sources of air pollution are man-made and include industrial activities, transportation, and energy generation. In general, air pollutants are defined as significant levels of trace gases or particulate matter (PM) compared to natural ones, which can be detected using a variety of methods and tools, each with pros and cons.

Stationary in-situ measurements, such as air quality stations (AQS), can be utilized as a measuring method since they can measure the local variation of air contaminants (Guerreiro, Foltescu and De Leeuw, 2014; Iorga, 2016; Maftei, Muntean and Poinareanu, 2022; Năstase et al., 2018; Voiculescu et al., 2020). Another way of monitoring air pollution is to use mobile measurements to cover broad regions and capture the spatial distribution of pollutants as well as the location of their sources (Constantin et al., 2017; Elen et al., 2012; Roşu et al., 2020; Roșu et al., 2021; Samad and Vogt, 2021).

The most important air pollutants monitored in urban areas are particulate matter (PM) (Hamanaka and Mutlu, 2018; de Miranda et al., 2012), nitrogen dioxide (NO_2) (Meier et al., 2017; Roşu et al., 2020; Roșu et al., 2022), sulfur dioxide (SO_2) (Constantin et al., 2020; Schwela, 2000; Zhao et al., 2018), ozone (O_3) (Bishoi, Prakash and Jain, 2009; Manes et al., 2016), and carbon monoxide (CO) (Al-Ali, Zualkernan and Aloul, 2010; Brienza et al., 2015; Liu et al., 2012).

In recent years a more thorough and up-to-date data about air pollution are required to support policy and public health decisions. This practice led to a grow into the usage of low-cost sensors to monitor air pollution in urban areas. Low-cost sensors are used today to measure air pollutants such as particulate matter, nitrogen dioxide, and ozone for a fraction of the cost of standard air monitoring equipment (including AQS). Research in Delhi, India, for example, discovered that using low-

cost sensors helped to detect high-pollution locations and assess the success of pollution-reduction strategies (Gulia et al., 2020). Similarly, research carried out in Los Angeles, California, USA, showed how low-cost sensors may be used to monitor pollution trends and pinpoint their origins, offering useful data to decision-makers and neighbourhood organizations. (Lu, 2022; Lu et al., 2022).

The main objective of the study is to test a low-cost sensor monitoring system in the quantification of the amount and distribution of several air pollutants (NO_2+O_3, SO_2, CO, and PM_{10}) in a large urban area in South East of Romania. Also, we aim to identify the hot spots of the concentration of these air pollutants and identify the emissions sources. Another objective is to evaluate the concentration values recorded with the low-cost air quality system with respect to the measured concentrations for the same air pollutants provided by the national air quality stations located in the same area.

MATERIALS AND METHODS

1.1. Study area and localization

For our study, we performed mobile air quality measurements in the fifth largest city in Romania Galati City (GL), with a population of 217851 (Anon n.d.-b). We choose Galati City because the main emissions sources include local industry, moderate car traffic, and household heating (Roșu et al., 2020; Roșu et al., 2022). The mobile measurements were performed in the afternoon, from 12 -15 local time (LT) on 19 January 2022 on the main streets of Galati city by mounting the low-cost air quality monitoring system Sniffer 4Dv1(SN) on the top of a car (Figure 2).

The measured data were compared with the local AQS data to verify the measurement values. The route of the mobile air quality system is presented in Figure 1 along with the location of the local AQS.

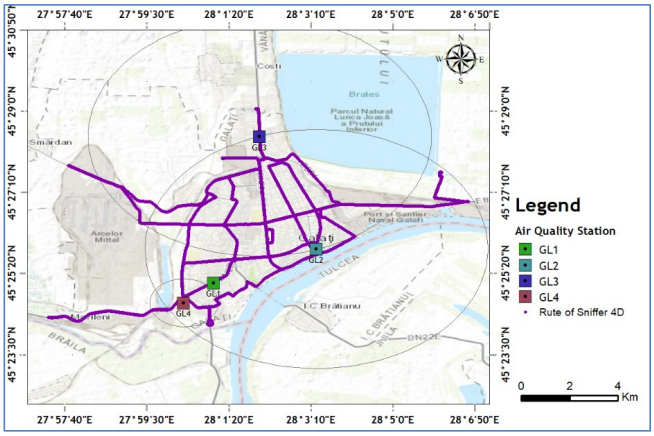

Figure 1. The track of the mobile measurements performed on 19 January 2022 in Galati city with the air quality system Sniffer 4D v1 and the location of the AQS

1.2. Equipment and data used

1.2.1. Air quality stations from Galati City (AQS)

The local air quality monitoring network in Galati City is administrated by the local administrative office of the Environmental Protection Agency from Galati (Agenția de Protecția Mediului din Galați - APM GL). The Galati city monitoring network consists of 4 stationary AQS that are located in different parts of the city (Figure 1). Each AQS is composed of a container that houses monitors and sensors that continuously measures individual pollutants. The list of the parameters measured by each AQS in Galati City includes a large list of air pollutants and meteorological data. The ones that interest us in our study are (including the determination method): particulate matter (PM_{10} - Light Scattering Particle), nitrogen dioxide (NO_2 - chemiluminescence), sulfur dioxide (SO_2 - UV fluorescence analyser), carbon monoxide (CO - Non-Dispersive Infrared), and ozone (O_3 - ultraviolet photometric analyser) (Anon, 2008).

The measurements are made in real time and are transmitted to a central database that is free to use (Anon n.d.-a). Details of the AQS from Galati City are presented in Table 1. In Figure 1 and Table 1 it is presented graphically and numerically the spatial extent of the maximum spatial detection limit buffer of each AQS.

Table 1. Specifications of AQS network from Galati city

AQS type	AQS code	Limit of detection maximum (km)	Limit of detection minimum (km)	Latitude (decimal degrees)	Longitude (decimal degrees)
Traffic	GL1	0.1	0.01	45.41868	28.016577
Urban	GL2	5	1	45.43146	28.054877
Suburban	GL3	5	1	45.47377	28.033728
Industrial	GL4	1	0.01	45.41117	28.005526

1.2.2. Air quality system Sniffer 4Dv1 (SN)

The air quality system Sniffer 4Dv1 is a very lightweight (>350 g), compact, and portable air quality system that uses various determination methods via several sensors that can measure up to nine air quality parameters, including temperature and humidity. The system works using pomp to bring external air to the sensors via the frontal inlet. The sensors can be mounted inside the main body of the monitor in several combinations depending on applications, this include personal exposure monitoring, urban air quality monitoring, and industrial emissions monitoring (Anon n.d.-d). The sensor combination used for this study is presented in Table 2 along with the technical specifications of each sensor.

Table 2. Specifications of sensors of the air quality system Sniffer4D v1 used for the measurements performed on 19 January 2022 in Galati city (Anon n.d.-c)

Sensor type	High-resolution NO_2+O_3	Inhalable Particulate Matter (PM_{10})	High-resolution CO	High-resolution SO_2
Pollutant	NO_2+O_3	PM 10 (particle size 0.3~10 µm)	CO	SO_2
Measurement Range	0-11 (ppm)	0-1000 (µg/m3)	0-10 (ppm)	0 -15 (ppm)
Detection Limit:	5 (ppb)	1 (µg/m3)	10 (ppb)	5 (ppb)
theoretical resolution	1 (ppb)	1 (µg/m3)	0.7 (ppb)	0.5 (ppb)
Sensor type	Electrochemical	Laser scattering/Light scattering	Electrochemical	Electrochemical

The air quality system Sniffer 4Dv1 was developed to be used on-board mobile platforms, specifically for UAVs (unmanned aerial vehicles), but for our study we adapted it, so it was mounted on top of our mobile laboratory (Figure 2). In Figure 2 the inlet of the equipment is pointing in the forward direction, so the system will not measure the direct emissions of our auto-laboratory. In Figure 2 it can be noticed that we powered the system via a 6S1P drone Li-Po battery. Also, it can be observed the telemetry antenna which is mounted on the back of the air quality system Sniffer 4Dv1, is used for real-time data transfer, settings, and measurements startup from a maximum distance of 2 km in urban areas (Anon n.d.-c).

Our system houses a combination of several sensors that can simultaneously collect real-time data for NO_2+O_3, SO_2, PM_{10}, and CO.

The data from these sensors is collected and processed using advanced algorithms to provide real-time measurements of air quality. The data is transferred via a 433MHz radio telemetry system to a laptop where the data is recorded, analysed, and visualized in real-time using the software Sniffer4D Mapper (Figure 3).

The general specification of data sampling from AQS and details of the track and sampling specification for the air quality system Sniffer 4Dv1 are presented in Table 3.

Table 3. Sample specifications for AQS and air quality system Sniffer 4Dv1 during the measurements performed between 12 -3 PM on 19.01.2022 in Galati city

Instrument/ AQS Sampling specifications	Sniffer track and measurements characteristics	AQS GL1	AQS GL2	AQS GL3	AQS GL4
Number of Samples	10309	240	240	240	240
Average Size of the Grid (km2)	0.019	0.031	78.5	78.5	3.1
The total detected area (km2)	11.252	0.00031	78.5	78.5	3.1

a) b)

c)

Figure 2. The setup of the air quality system Sniffer 4Dv1 mounted on top of the auto laboratory: a) Positioning the system, the power cable, and telemetry antenna b) Connection to the 6SP1 Li-Po battery used as the power source. c) The laptop is used for real-time data visualization and recording

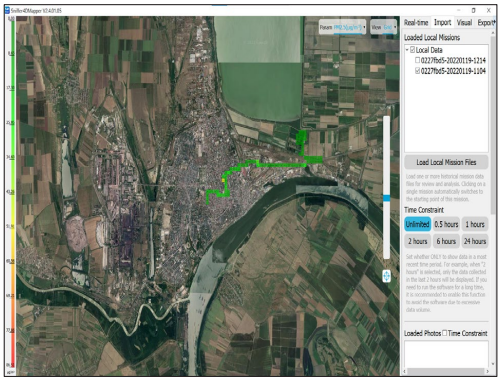

Figure 3. Print screen of the software Sniffer4D Mapper interface during the real-time data recording and visualization for the measurements performed in Galati city on 19.01.2022

For the comparison of AQS with the data from the Sniffer 4Dv1, we summed up the concentration values for O_3 and NO_2 recorded at each AQS from Galați City. Also, we excluded data from Sniffer 4D data for $PM_{2.5}$ because no data was available from all AQS at the time we performed the measurement.

RESULTS AND DISCUSSIONS

Using the coordinates embedded in the Sniffer 4 Dv1 data set we produced maps using Geographic Information System (GIS) software. All the maps of the concentration's distribution of each air pollutant PM_{10}, NO_2+O_3, SO_2, CO, alongside with AQS average hourly mean of the same air pollutant are presented in Figures 4 to 7. The AQS value was produced from all the hourly mean values of each pollutant during the whole time we performed mobile measurements (from 12:00 - 3:00 PM).

Firstly, we can observe in Figures 4 to 7 there is a high difference between the values of SN versus AQS and that could be a cause of the sampling rates of the Sniffer 4Dv1, one determination per second, and the AQS sampling rate of one determination each minute (the result is expressed in hourly mean value). The Sniffer 4Dv1 has a higher temporal resolution and probably this influences the results of the measurements into obtaining more values and thus a higher overestimation of the air pollution. Another cause of the high differences is the determination method but some of the studies presented that for similar sensors the differences between the measured values measured with chemiluminescence and electrochemical sensors are small, especially for CO, NO_2+O_3 (Afshar-Mohajer et al., 2018; Lin et al., 2015; Mead et al., 2013; Spicer et al., 1994).

If we discuss on the area of the sampling of the air pollution detection (pixel sampling size), on the one hand, we can observe in Table 3 that the SN has a sampling area of 0.019 km^2 per measurement(pixel), on the other hand, the AQS sampling area of detection ranges from very narrow pixels (0.031 km^2) to very wide ones (~78.5) km^2. Thus, GL1 and GL4 will detect more localized emissions whereas GL2 and GL3 will detect far-away emissions and will mediate them on the entire surface of the detection limit as we can observe in the pollutants values the maps presented in Figures 4 to 7.

Also, the fact that we capture with our SN more localized hot spots during the mobile measurements could help us understand what the major emissions sources for each air pollutant are and where is concentrated spatially within the Galati city boundary.

The circles represented with the black line in Figures 4 to 7 represent the maximum limit of detection of each AQS (Table 1). For AQS GL1 the spatial buffer (radius around the AQS) is 100 m, that's the reason it is not visible on the map.

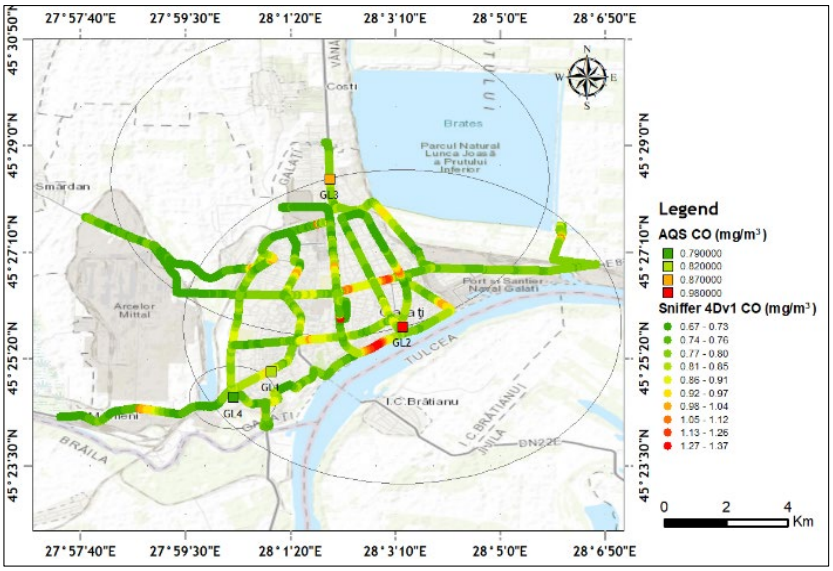

Figure 4. Distribution map of CO concentrations measured with SN and recorded by AQS between 12-15 LT on 19.01.2022 in Galati city

In Figure 4 is observed that CO higher concentrations measured by SN are concentrated in the eastern part of Galati city with values between 1.04-1.37 mg/m^3. The high values can be a cause of traffic agglomeration on the main roads of the city, or we believe it's the wind-driven plume of an oil factory that is located in that part of the city (Roşu et al., 2020).

The fact that we believe it's the oil factory is that a similar value is recorded by the AQS GL2 0.98 mg/m^3 which is located in the same part of the city. Also, we should consider that the AQS GL2 value has resulted from averaging all the concentration values recorded inside its buffer of the detection limit, and this could explain the difference between SN, with most of the lower values along the track and more localized for higher values. We could notice that the value of 0.98 mg/m^3 recorded by AQS GL2, even if it is an average hourly value for the entire period when the mobile SN measurements were performed, is similar to the high values recorded close by the SN system. This could mean that at each passing by the SN, the system measured instantaneous values of the plume that was passing that area and produced the value recorded by AQS GL2.

A similar averaging effect can be seen in the measured hourly value of CO concentrations from all AQS where it can be observed that practically the values measured by each AQS can be described by the SN mobile measurements inside each stations limit of detection buffer trough a spatial mediation effect of the mobile recorded values.

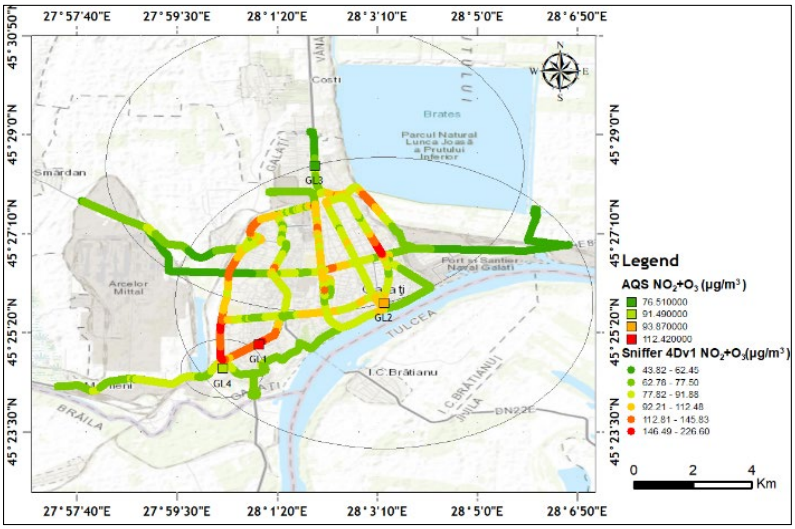

Figure 5. Distribution map of $NO_2 + O_3$ concentrations measured with SN | and recorded by AQS between 12-15 LT on 19.01.2022 in Galati city

Figure 5 presents the measured values for the sum of nitrogen dioxide and ozone concentrations values recorded by SN and AQS on 19.01.2022 in Galati City. As we can observe the variation of the recorded values is higher than in the case of CO. High values between 92.21-226.60 µg/m³ were measured in the centre of the city and on the main roads with an intensified car or heavy truck traffic, e.g. the ring roads of the city or the highly circulated roads that cross the entire city from one side to another. The AQS GL1 recorded averaged hourly values to a value of 112 µg/m³, a value that is like the ones that SN recorded instantaneously in the same area. The explanation for recording a very similar value is that the AQS averaged all the NO_2+O_3 values within its buffer of the maximum range of detection of 0.01 km. Also, the high values could be explained by the fact that the plume of pollutants NO_2+O_3 remained in the same area, or the area pollution is being caused by high constant car traffic. If we look at the spatial limit of the detection buffer (black line circle) for the AQS GL2 and the average value for 12-3 PM of 93.87 µg/m³we could say that the value is similar to the ones that were recorded by the SN inside the buffer of AQS GL2, most of the value recorded are between 43.82-91.88 µg/m³, followed by the high values between 112.81-226.60 µg/m³, which are less localized and were detected alongside a small portion of the main roads. This could only strengthen the idea that the main source of the recorded values are cars and heavy traffic. In Figure 5 it can be observed that the AQS GL3 recorded a smaller hourly average value of 71.51 µg/m³ since it's a suburban station and as we can observe the extent of the buffer it's more likely to measure the emissions outside the urban agglomeration and only a small portion of buffer covers the city. This can be explained also if we observe the values recorded by the SN we can say that the AQS GL3 only detects the emissions sources (car traffic) that reside in the Northern part of Galati city and the suburban area. The same thing can be noticed for the industrial AQS GL 4 which measured an hourly averaged value of 91.49 µg/m³, where high values measured by SN ranged between 112.81 – 146.40 µg/m³ and covered a small portion of the buffer of the AQS GL4 and most of the buffer was spatially covered by SN instantaneous measured values ranged between 62.78-91.88 µg/m³.

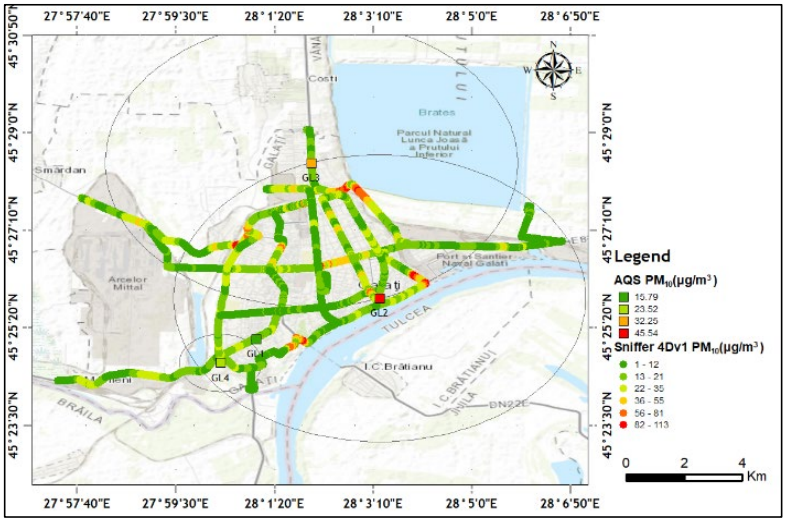

Figure 6. Distribution map of PM_{10} concentrations measured with SN and recorded by AQS between 12-15 LT on 19.01.2022 in Galati city

The values for the measured concentrations of PM_{10} by the SN system along the main streets of Galati City are presented in Figure 6. The values measured ranged from 1-113 µg/m³. High values between 56-113 µg/m³ were measured close to important crossroads or in the areas where heavy traffic is usually present (the North and North-East of Galati City). Similar values of PM_{10} concentrations were recorded by each of the AQS if we consider the spatial limit of the detection buffer and the location of each AQS. Values that are sustained by the measured values with the SN system. The highest hourly average value of 45.54 µg/m³ was recorded by AQS GL2. Also, all high values recorded by the SN system ranged between 36-113 µg/m³ and were measured inside the AQS GL2 buffer. The emissions were measured at the cross of the main roads. This could only indicate that the emissions of PM_{10} are most likely produced by car traffic and heavy traffic.

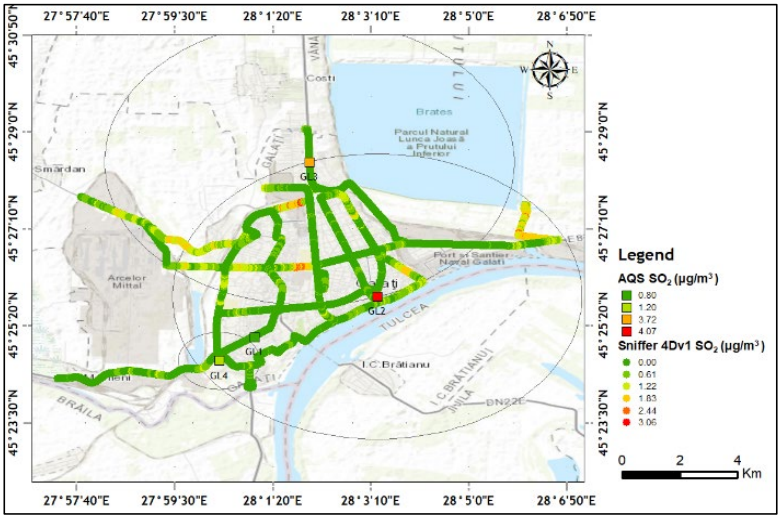

Figure 7. Distribution map of SO_2 concentrations measured with SN and recorded by AQS between 12-15 LT on 19.01.2022 in Galati city

In the case of sulphur dioxide (SO_2), we can observe in Figure 7 that measured concentrations with SN are very low and ranges from 0.00 – 3.06 µg/m³. Similar averaged hourly concentration values of SO_2 were recorded by all AQS. This could only underline that the SN measured values are real and comparable with AQS data if we take into account the spatial distribution of measured values of the SN system concerning the detection limit range of each AQS. Also, it can be noticed that hot spots of SO_2 measured by the SN system are localized in the central area and the north part of Galati City, near rural areas or where more houses with household heating based on fossil fuel burning (wood or coal) are present. Anomalies of measured values can be observed in the remote east part of Galati City, where we believe measured values of SO_2 are errors caused by the presence of high concentrations of H_2S due to a marshy area (Khan, Rao & Li 2019). This finding needs to be further analysed and studied with a sensor of SN that can measure concomitantly the H_2S and SO_2 (Anon n.d.-c).

CONCLUSIONS

The results of the study showed that the Sniffer 4Dv1 is a very complex and useful instrument that can be used for air quality monitoring in urban areas, as we presented in the results of the measurements performed on January 19, 2022, on the main roads of Galati. The main advantage of the SN is that it can detect and measure real-time and simultaneous data for a wide range of air pollutants, including nitrogen oxides, sulfur dioxide, ozone, and particulate matter, which were the main subject of this work. By capturing instantaneous values of the concentration of each air pollutant, we can better observe the dynamics of air pollutants and indicate the main sources, which we found based on SN measurements to be industrial for CO, industrial and car traffic for NO_2 and O_3, car traffic and heavy traffic PM_{10}, and household heating for SO_2.

The comparison with the average hourly data from AQS, for the entire period we performed mobile measurements with SN, showed that the SN system measured more localized concentration values (hot spots) around emissions sources, while the AQS measures values from wide areas to narrow areas (0.031 km^2), integrating and averaging all the values recorded within its detection buffer. However, the spatially compared data recorded at each AQS for each air pollutant showed similar values to those recorded by our SN system inside the buffer of each AQS.

Overall, we believe that the Sniffer 4Dv1 represents an advancement in air quality measurement technology, enabling us to better understand the complex dynamics of air pollution in our urban environments. The Sniffer 4Dv1 is a valuable tool for understanding the sources and impacts of air pollution and for developing effective strategies to reduce exposure and improve public health.

We propose doing more comparative studies to identify the sensibility of the system by measuring each air pollutant in different conditions and with different equipment and different measuring methods. Further studies need to be done to say to validate the data obtained with Sniffer 4Dv1 compared to data from the best available technologies (BAT) implemented at each AQS or by other standardized instruments for air quality measurements. The next studies will include an analysis of time series variation using local long-time measurements near AQS with a long-range spatial limit of detection and AQS with a narrow spatial limit of detection for the same pollutants, this will give us an idea of data consistency over time and on the evaluation of error of detection for each pollutant (factory versus experimental).

ACKNOWLEDGEMENTS

The present study was supported by the project An Integrated System for the Complex Environmental Research and Monitoring in the Danube River Area, REXDAN, SMIS code 127065, co-financed by the European Regional Development Fund through the Competitiveness Operational Programme 2014-2020, contract no. 309/10.07.2022.

REFERENCES

Afshar-Mohajer, N., Zuidema, C., Sousan, S., Hallett, L., Tatum, M., Rule, A.M., Thomas, G., Peters, T.M., Koehler, K. (2018). Evaluation of Low-Cost Electro-

Chemical Sensors for Environmental Monitoring of Ozone, Nitrogen Dioxide, and Carbon Monoxide. *Journal of Occupational and Environmental Hygiene, 15*(2). 87–98.

Al-Ali, A.R., Zualkernan, I., Aloul, F. (2010). A Mobile GPRS-Sensors Array for Air Pollution Monitoring. *IEEE Sensors Journal, 10*(10). 1666–1671.

Anon. (2008). *Directive 2008/50/EC of the European Parliament and of the Council of 21 May 2008 on Ambient Air Quality and Cleaner Air for Europe*, 152.

Anon. n.d.-a. Disclaimer. Retrieved April 14, 2023 (https://www.calitateaer.ro/public/monitoring-page/reports-reports-page/?__locale=ro).

Anon. n.d.-b. *RECENSAMANTUL POPULATIEI SI LOCUINTELOR – 2021 date provizorii – DJS-GALAȚI*.

Anon. n.d.-c. Sniffer4d 4d v1 Spec - Google Search. Retrieved April 14, 2023 (https://shorturl.at/cHW78).

Anon. n.d.-d. "Sniffer4D V2 Multi-Gas Detection Hardware | Soarability." Retrieved April 14, 2023 (https://www.soarability.tech/sniffer4dV2_hardware_en).

Bishoi, B., Prakash, A., Jain, V.K. (2009). A Comparative Study of Air Quality Index Based on Factor Analysis and US-EPA Methods for an Urban Environment. *Aerosol and Air Quality Research, 9*(1). 1–17.

Brienza, S., Galli, A., Anastasi, G., Bruschi, P. (2015). A Low-Cost Sensing System for Cooperative Air Quality Monitoring in Urban Areas. *Sensors, 15*(6). 12242–12259.

Constantin, D.E., Merlaud, A., Voiculescu, M., Van Roozendael, M., Arseni, M., Rosu, A., Georgescu, P.L. (2017). NO_2 and SO_2 Observations in Southeast Europe Using Mobile DOAS Observations. *Carpathian Journal of Earth and Environmental Sciences*, *12*(2). 323-328.

Constantin, D.-E., Bocăneala, C., Voiculescu, M., Roşu, A., Merlaud, A., Van Roozendael, M., Georgescu, P.L. (2020). Evolution of SO_2 and NOx Emissions from Several Large Combustion Plants in Europe during 2005–2015. *International Journal of Environmental Research and Public Health, 17*(10). 3630.

Elen, B., Peters, J., Poppel, M.V., Bleux, N., Theunis, J., Reggente, M., Standaert, A. (2012). The Aeroflex: A Bicycle for Mobile Air Quality Measurements, *Sensors 13*(1). 221–240.

Guerreiro, Cristina B.B., Foltescu, V., De Leeuw, F. (2014). Air Quality Status and Trends in Europe. *Atmospheric Environment, 98*. 376–384.

Gulia, Sunil, Prasad, P., Goyal, S.K., Kumar, R. (2020). Sensor-Based Wireless Air Quality Monitoring Network (SWAQMN)-A Smart Tool for Urban Air Quality Management. *Atmospheric Pollution Research, 11*(9). 1588–97.

Hamanaka, R.B., Mutlu, Gökhan M. (2018). Particulate Matter Air Pollution: Effects on the Cardiovascular System. *Frontiers in Endocrinology, 9.* 680.

Iorga, Gabriela. (2016). Air Pollution Monitoring: A Case Study from Romania. *Air Quality–Measurement and Modeling*.

Khan, M.A.H., Rao, M.V., Li, Q. (2019). Recent Advances in Electrochemical Sensors for Detecting Toxic Gases: NO_2, SO_2 and H_2S. *Sensors, 19*(4). 905.

Lin, C., Gillespie, J., Schuder, M.D., Duberstein, W., Beverland, I.J. Heal, M.R. (2015). Evaluation and Calibration of Aeroqual Series 500 Portable Gas Sensors for Accurate Measurement of Ambient Ozone and Nitrogen Dioxide. *Atmospheric Environment, 100.* 111–16.

Liu, J., Chen, Y., Lin, T., Chen, C., Chen, P., Wen, T., Sun, C., Juang, J. & Jiang, J. (2012). An Air Quality Monitoring System for Urban Areas Based on the Technology of Wireless Sensor Networks. *International Journal on Smart Sensing and Intelligent Systems, 5*(1). 191–214.

Lu, T., Liu, Y., Garcia, A., Wang, M., Li, Y., Bravo-Villasenor, G., Campos, K., Xu, J., Han, B. (2022). Leveraging Citizen Science and Low-Cost Sensors to Characterize Air Pollution Exposure of Disadvantaged Communities in Southern California. *International Journal of Environmental Research and Public Health, 19*(14). 8777.

Lu, Yougeng. (2021). Beyond Air Pollution at Home: Assessment of Personal Exposure to PM2. 5 Using Activity-Based Travel Demand Model and Low-Cost Air Sensor Network Data. *Environmental Research, 201*. 111549.

Maftei, C., Muntean, R., Poinareanu, I. (2022). The Impact of Air Pollution on Pulmonary Diseases: A Case Study from Brasov County, Romania. *Atmosphere, 13*(6). 902.

Manes, Fausto, Marando, F., Capotorti, G., Blasi, C., Salvatori, E., Fusaro, L., Ciancarella, L., Mircea, M., Marchetti, M., Chirici, G. (2016). Regulating Ecosystem Services of Forests in Ten Italian Metropolitan Cities: Air Quality Improvement by PM10 and O_3 Removal. *Ecological Indicators, 67*. 425–40.

Mead, M.I., Popoola, O.A.M., Stewart, G.B., Landshoff, P., Calleja, M., Hayes, M., Baldovi, J.J., McLeod, M.W., Hodgson, T.F., Dicks, J. (2013). The Use of Electrochemical Sensors for Monitoring Urban Air Quality in Low-Cost, High-Density Networks. *Atmospheric Environment, 70*. 186–203.

Meier, A.C., Schönhardt, A., Bösch, T., Richter, A., Seyler, A., Ruhtz, T., Constantin, D.-E., Shaiganfar, R., Wagner, T., Merlaud, A. (2017). High-Resolution Airborne Imaging DOAS Measurements of NO_2 above Bucharest during AROMAT. *Atmospheric Measurement Techniques, 10*(5). 1831–57.

de Miranda, R.M., de Fatima Andrade, M., Fornaro, A., Astolfo, R., de Andre, P.A., Saldiva, P. (2012). Urban Air Pollution: A Representative Survey of PM 2.5 Mass Concentrations in Six Brazilian Cities. *Air Quality, Atmosphere & Health, 5.* 63–77.

Năstase, G., Șerban, A., Năstase, A.F., Dragomir, G., Brezeanu, A.I. (2018). Air Quality, Primary Air Pollutants and Ambient Concentrations Inventory for Romania. *Atmospheric Environment,* 184. 292–303.

Roşu, A., Constantin, D.-E., Voiculescu, M., Arseni, M., Merlaud, A., Van Roozendael, M., Georgescu, P.L. (2020). Observations of Atmospheric NO_2 Using a

New Low-Cost MAX-DOAS System. *Atmosphere, 11*(2). 129.

Roșu, A., Constantin, E.-D., Voiculescu, M., Arseni, M., Roșu, B., Merlaud, A., Van Roozendael, M., Georgescu, P.G. (2021). Assessment of NO_2 Pollution Level during the COVID-19 Lockdown in a Romanian City. *International Journal of Environmental Research and Public Health, 18*(2). 544.

Samad, A., Vogt, U. (2021). Mobile Air Quality Measurements Using Bicycle to Obtain Spatial Distribution and High Temporal Resolution in and around the City Center of Stuttgart. *Atmospheric Environment, 244*. 117915.

Schwela, D. (2000). Air Pollution and Health in Urban Areas. *Reviews on Environmental Health, 15*(1–2). 13–42.

Spicer, C.W., Kenny, D.V., Ward, G.F., Billick, I.H., Leslie, N.P. (1994). Evaluation of NO_2 Measurement Methods for Indoor Air Quality Applications. *Air & Waste*,*44*(2). 163–168.

Voiculescu, M., Constantin, D.-E., Condurache-Bota, S., Călmuc, V., Roșu, A., Dragomir Bălănică, C.M. (2020). Role of Meteorological Parameters in the Diurnal and Seasonal Variation of NO_2 in a Romanian Urban Environment. *International Journal of Environmental Research and Public Health, 17*(17). 6228.

Zhao, S., Liu, S., Hou, X., Cheng, F., Wu, X., Dong, S., Beazley, R. (2018). Temporal Dynamics of SO_2 and NO_X Pollution and Contributions of Driving Forces in Urban Areas in China. *Environmental Pollution, 242*. 239–248.

Scientific Papers. Series E. Land Reclamation, Earth Observation & Surveying, Environmental Engineering. Vol. XII, 2023
Print ISSN 2285-6064, CD-ROM ISSN 2285-6072, Online ISSN 2393-5138, ISSN-L 2285-6064

THE IMPACT OF LOGGING ACTIVITY ON RESIDUAL TREES - A CASE STUDY FROM SOUTHWEST ROMANIA

Ilie-Cosmin CÂNTAR, Nicolae CADAR, Cătălin-Ionel CIONTU

"Marin Dracea" National Research and Development Institute in Forestry, Timisoara Research Station, 8 Padurea Verde Street, Timisoara, Romania

Corresponding author email: nicu_cadar@yahoo.com

Abstract

The paper aims to analyze the impact of logging activity on residual trees from logging yards from southwest Romania, located in plain, hill and mountain area and covered with a large variety of silvicultural works-first-intervention cuttings, preparatory and seed-cutting (shelterwood systems or selection systems), cuttings to increase light availability for regeneration (shelterwood systems), final cuttings (shelterwood systems). The impact of logging activity on the residual trees was analyzed based on the data obtained from the measurements made at the end of the vegetation season of 2019 and the beginning of the vegetation season of 2020. Based on the data obtained, the total number of tree damages in the variants studied on relief forms, the relationship between the number of tree damages and different stand characteristics, and the damages distribution by their types in the studied variants, were analyzed. Trees damage evaluation was done by determining damage indexes calculated as a ratio between the volume of damages found and the volume of damaged trees. The most important conclusions have been discussed in the context of other researches in the field.

Key words*: tree damage, logging yard, barking wound, trees wound.*

INTRODUCTION

Logging technologies must be correlated with treatments that are adequate to the essential characteristics of stands in order to preserve the protection potential of forests. This correlation is mandatory for harvesting wood material as well as for fulfilling the necessary conditions for natural regeneration and for creating healthy and valuable economically stands (Dămăceanu & Gava, 1991). Logging works leads to soil compaction and damage to saplings and trees (Whitman et al., 1997). Soil compaction caused by logging machines has an important influence on seedling growth and/or mortality (Picchio et al., 2019).

Logging damage to residual trees is one of the potential difficulties of logging works in any stand (Clatterbuck, 2006). In this process, when harvested trees are moved and the residual stand is dense, damage to residual trees are inevitable (Picchio et al., 2012). In order to remove harvested timber from the stand, repeated entries of machines in the stand are necessary, but this activity increase the risk of damages to residual trees (Ficklin et al., 1997).

However, in terms of serious injury, feeling of trees are the major source of this type of damages (Fairweather, 1991). Stand damages from this category can be reduced by a prior planning of felling direction (Tavankar et al., 2013). Frequency of felling damage is increasing with the level of timber removals and skidding damage is higher when the number of trees in adjacent area of skid trails is high (Hartsough, 2003).

Regarding damages resulting from timber transportation from harvesting place to the loading point, most of them are within the root collar and in the lower part of tree trunk (Cudzik et al., 2017).

The technique of timber harvesting can result to important damages to residual trees and seedlings, and also to timber products and soil, but the logging damages can be minimized by using a proper technique for harvesting (Eroğlu et al., 2009). For a feasible harvesting system, the machinery used in logging should be chosen based on their impact on ecosystem, not only based on productivity rate (Akay et al., 2006).

The paper aims is to analyze the impact of logging works on residual trees on logging yards where different silvicultural works were applied and to assess tree damages on considered variants.

MATERIALS AND METHODS

The studied logging yards were chosen in different relief areas to reduce the influence of the geomorphological and vegetation conditions and at different managers of the forest fund, to reduce the influences given by the logging technology, the machine system available to a certain agent in the respective area, the mode and working habits of the logging teams. The layout of research in variants and logging yards is presented as follows:

• Variant V1 - logging yards where thinning works were applied from the plains (OS (Forest departmant) Bocşa Română - UP (production unit) II, u.a. (management unit) 58A and UP III, u.a. 49), hill (OS Bocşa montană - UP VI, u.a. 95A and OS Moldova Nouă - UP III, u.a. 15B) and mountain (OS Băile Herculane - UP II, u.a. 23 and BE (Experimental base) Caransebeş - UP VI, u.a. 99A);

• Variant V2 - logging yards with first-intervention cuttings, preparatory and seed-cutting within shelterwood systems or selection systems, from the plain (OS Bocşa Română - UP I, u.a. 11C and UP II, u.a. 55), hill (OS Bocşa Montană - UP IV, u.a. 62B and OS Moldova Nouă - UP III, u.a. 212A) and mountain (OS Văliug - UP VI, u.a. 15A and u.a. 16A);

• Variant V3 - logging yards where cuttings to increase light availability for regeneration where applied within shelterwood system at the plain (OS Bocşa Română - UP III, u.a. 28B and 76A), hill (BE Caransebeş - UP II, u.a. 30B and OS Moldova Nouă - UP III, u.a. 176A) and mountain (OS Băile Herculane - UP II - u.a. 99A and 100A);

• Varianta V4 - logging yards where final cutting within shelterwood system were applied at plain (OS Bocşa Română - UPI, u.a. 1E şi 14A), hill (BE Caransebeş - UP I, u.a 46D şi OS Moldova Nouă - UP III, u.a. 162B) and mountain (OS Băile Herculane – UP IV, u.a. 98A and BE Caransebeş – UP V, u.a. 16A).

Along the collection paths, in each logging yard, the research was carried out in three sample areas of a 100 m long section along the most representative collection path, arranged in the upstream part, in the middle and respectively in its downstream part (Figure 1). Inside each logging yard, the research was carried out in the initially installed surfaces, namely for each parquet, in a circular sample area of 2500 m^2 located in the middle area of the logging yard in such a way that it does not include areas of collection paths.

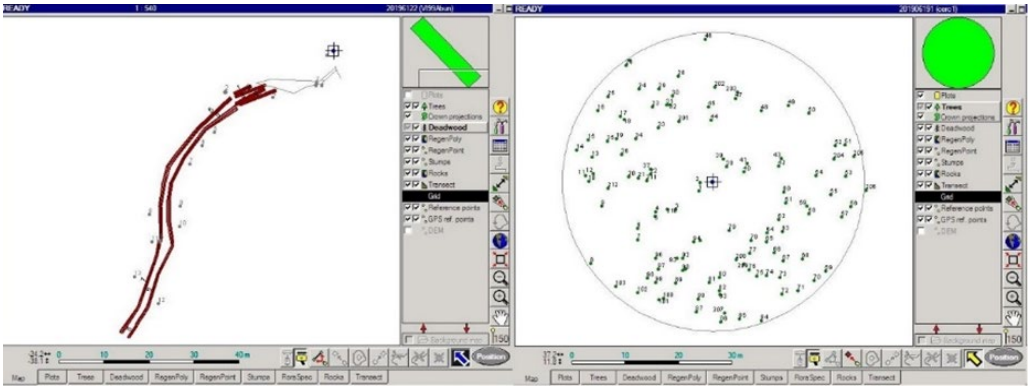

Figure 1. The location of the sample areas (along the collection trails - left, inside the logging yard - right) (FieldMap System)

The impact of logging works on the residual trees was analysed based on the data obtained from the measurements made at the end of the vegetation season of 2019 (in logging yards from mountain area) and the beginning of the vegetation season of 2020 (in logging yards

from plain and hill area) in the previously presented sample areas.

The carried out field work followed: identification of the tree, observation of the status of the tree (dead/alive), identification of each damage previously found based on its type (galling (bark removed partially without cambial lesions.) barking (areas with bark removed up to the wood), splintering (areas with bark and wood removed), breaking (the trunk or the branches), uprooting (total or partial), according to Knežević et al. (2018)).

Based on the data obtained, the total number of tree damages in the studied variants on relief, the relationship between the number of tree damages and the different characteristics of the stand, as well as the distribution of damages by their types in the variants studied, were analysed.

The evaluation of wound and damages caused to trees through logging works was done by determining damages indexes calculated as a ratio between the volume of damage found and the volume of damaged trees. Tree damage indexes were determined for each type of damage, for total trees and for each variant separately, based on the relationship 1:

$$i = \frac{V_v}{V_{av} \times 1000} \quad (1)$$

where:

i - damage index;

V_v - damage volume (cm^3);

V_{av} - damaged tree volume (m^3).

In the formula 1, the volume of the damages was determined based on their dimensional characteristics as the product of the length, width, and depth of each damage. In order to determine the damage indexes, it was necessary to relate the volume of damages at the volume of damaged trees. The latter was calculated using formula 2 (Giurgiu et al., 2004):

$$\log V = a_0 + a_1 \log d + a_2 \log^2 d + a_3 \log h + a_4 \log^2 h \quad (2)$$

where:

a_0, a_1, a_2, a_3, a_4 - the values of the regression coefficients on species;

d - tree diameter (dbh) (cm);

h - tree height (m);

V - tree volume (m^3).

RESULTS AND DISCUSSIONS

Results regarding the impact of logging activity on trees

A total number of 1,237 damaged trees were identified in all the sample areas of the logging yards, distributed as follows: 537 trees in the V1 variant, 254 trees in the V2 variant, 215 trees in the V3 variant, 231 trees in the V4 variant. Regarding the type of damages compared to their total number, 1945 damages were identified - many trees have multiple damages - most of them being barking (78.9%), followed in descending order by splintering (11%), galling (7.7%), broken trees (1.8%) and uprooting in a very small percentage (0.6%).

Analyzing the total number of damages in the studied variants by categories of relief, the most damages were recorded in the hills and mountains in all the variants, with a maximum of them in variant V1 - Thinning (Figure 2). In the plain, the fewest damages were found in all the variants. Here, relief energy plays an important role in producing damages to trees.

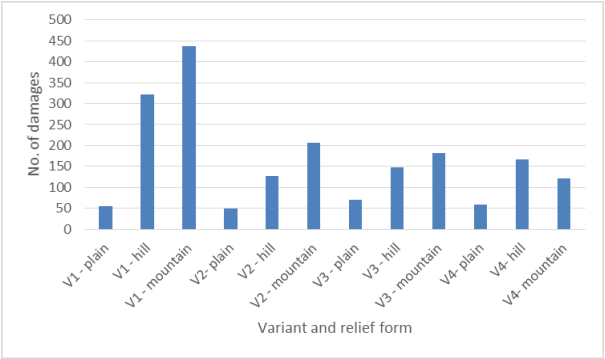

Figure 2. The total number of tree damages in the studied variants, on relief forms

There is a proportional relationship between the total number of damages identified for each logging yard and certain logging yard or stand characteristics (Figure 3).

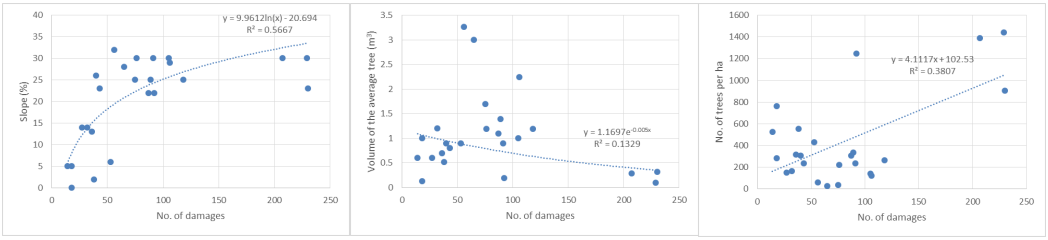

(a) (b) (c)

Figure 3. The relationship between the number of tree damages and different stand characteristics: (a) - the relationship between the total number of damages and the slope; (b) - the relationship between the total number of damages and the volume of the average tree; (c) - the relationship between the total number of damages and the number of trees per ha

The slope in the logging yards directly proportionally influences tree damages number (Figure 3a). The increase in the damages number with the increase of the slope is logarithmic, the slope in the logging yards leading to a higher number of damages. The slope makes it difficult to gather and caring the wood material, it changes the trajectory of the loads, inevitably leading to damage to the trees.

Large values of the volume of the average logged tree led to a lower number of damages (Figure 3b), registering an exponential increase in the number of damages with the decrease in the volume of the average tree. At high values of volumes of the average logged tree, the number of loads is lower and including machine passes, skidder tractors are lower. At low volumes, the loads are more, requiring more runs to collect, thus resulting in a higher number of damages.

The number of trees per hectare influences directly and proportionally the number of damages (Figure 3c). A large density of the stands makes it difficult to collect and remove the wood material, inevitably leading to damage to the trees.

As previously analyzed, the negative impact of logging activity on trees is related to the slope of the land, the average tree volume and the number of trees per ha. By analyzing the number of damages for each variant separately, it is observed that the most damages, both in terms of their types and in total number, are those in variant V1 - Thinning (Figure 4), where the number of trees is the highest, this being decisive for the occurrence of damages.

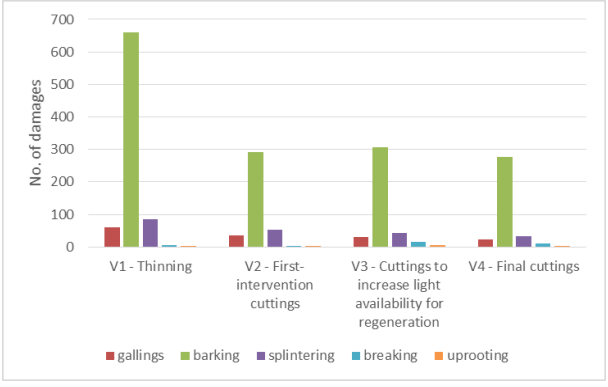

Figure 4. The distribution of damages by their types in the studied variants

The most frequently identified damage, barking (78.9% of the total number of damages) (Figure 4), shows the same trend as the total number of damages, influencing it directly. The number of

barking and also damages of other types, found in thinning, is much higher than that of the other variants, the dynamics of their production being influenced by the same variables that influence the production of all damages, mentioned and discussed previously.

As for the galling, it can be seen (Figure 4) that they are relatively evenly distributed in the studied logging yards with a slight increase in the thinning where the most damages are recorded.

Splintering register an almost identical trend to barking, and more serious damages (breaking, uprooting) are found in all the studied variants studied and in most of the logging yards.

The fewest braking and uprooting were observed in variant V2 - First intervention cuttings, and the most in variant V3 - Cuttings to increase light availability for regeneration, where the extracted volumes are larger and the remaining trees are still in significant numbers compared to the variant V4 - Final cuttings.

Assessment of tree damages

The method used to assess the impact of logging activities on the trees, is based on damage indexes, by damage types and total damages, calculated as a ratio between the volume of each tree damages and the volume of injured trees based on the formula presented in the material and method chapter. Considering that the number of broken or uprooted trees is very small and that most of them were extracted from the logging yard, their diameter and height not being able to be measured, the calculations below refer only to galling, barking and splintering. Tree damage indexes were calculated for each damage type, for total trees and for each logging yard. Damage indexes thus calculated, are shown in Table 1.

Table 1. Indexes of tree damage by types of damage in the studied variants

Variant	Relief form	Damage index			
		Galling	Barking	Splintering	Total
V1 - Thinning	Plain	0.490	0.726	0.720	0.708
	Hill	1.630	2.191	5.509	2.235
	Mountain	0.035	1.318	0.889	1.218
Total V1		1.289	1.619	1.528	1.585
V2 - First intervention cuttings	Plain	0	18.327	45.370	20.535
	Hill	0.0396	22.778	29.795	19.199
	Mountain	0.019	1.894	4.419	2.217
Total V2		0.033	10.863	13.913	10.255
V3 - Cuttings to increase light availability for regeneration	Plain	0.0006	10.972	12.297	10.987
	Hill	0.0278	17.962	0.089	14.504
	Mountain	0.011	0.837	1.440	0.843
Total V3		0.019	9.080	3.380	7.711
V4 - Final cuttings	Plain	0.011	28.378	15.775	26.222
	Hill	0.0771	28.101	20.096	24.272
	Mountain	0.024	3.196	5.860	3.289
Total V4		0.058	19.038	15.528	17.317
TOTAL		0.533	8.006	7.125	7.313

As can be seen in Figure 5a and in Table 1, galling has the highest values of the damage index in the logging yards from the plain where thinning works were applied. In this variant, the impact of logging is minimal, galling being the lightest damage produced by logging activities. In these logging yards where thinning works were applied, the loads formed by trees with small volumes, light but with little potential for damages, led to a large number of damages in this category.

The barking has the highest values of the damage index in logging yards where final cuttings were applied, where residual trees

were subjected to the impact of loggings works during relatively recent previous works (Figure 5b).

Splintering dislodges the largest volumes of wood at the level of the damages, compared to the volume of the trees, in the logging yards from the V2 variant where first intervention cuttings were applied (Figure 5c). Here, the exploited volumes are significant, and the number of trees during the cutting for opening the regeneration areas is still high.

Analyzing the damage index for all damages in the studied variants (Figure 5d), high values are observed in the case of variant V4 - Final cuttings, for all three types of analyzed damages. This a fact is determined by the small number of trees remaining in the logging yard, or that have reached the necessary diameter to be included in the research, most of them collecting damages from all the cuts within the shelterwood system, that have taken place in the last period.

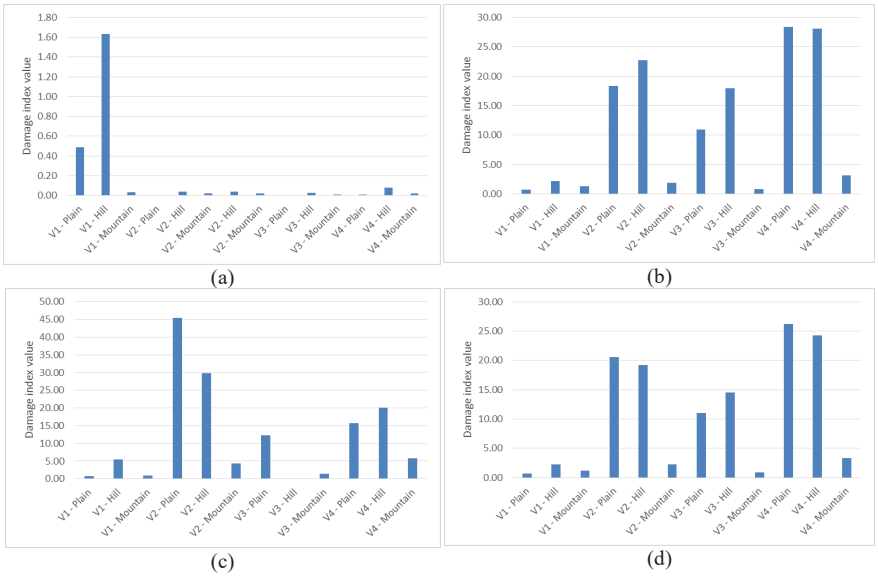

Figure 5. Damage indexes for trees by types of damage (a - galling; b - barking; c - splintering; d - total damages)

CONCLUSIONS

Barking is the most common damage identified in the repetitions from the studied versions (78.9% of the total number of damages), followed by splintering (11%) and galling (7.7%). Ruptured and uprooted trees are present only in a very small percentage. Results from similar studies that were focused however on animal logging, have also placed barking on the first place (61.5%), followed by light damages such as squashed bark (23.1%) and small percentages for debarked and damaged tree (15.4%). Unlike our study, the higher percentage of light damages is caused by using animal logging, an exploitation technology from the reduced impact logging category (Knežević et al., 2018). Other studies have shown that, on average, logging damage affected 40% of residual trees, with 21% being injured and 19% being dead trees (Bertault & Sist, 1997).

The most damages were recorded in the hills and mountains in all the variants, with a maximum of them in variant V1 - Thinnings. As for subsequent growths for trees damaged through logging in thinning, Norway spruce forests from nordic countries was applied the whole-tree harvesting process that has caused a significant decrease in volume growth, especially in the following 10 years (Helmisaari, 2011). Even though trees in logging yards where thinning were applied are young, some authors mentioned that the cambial tissue never survives exposure. In this way, even if some small bark pieces are removed, the xylem is open to an invasion of pathogen agents. Closing bark lesions varies on

the quantity of removed bark, as well as on the vigor and the species, while all damaged trees will maintain rot pockets even after minor damages and regardless of age. Heavier damages will result in the following decades inside the stem's interior rot (Putz et al., 2008).
In order to protect the forest ecosystem, some studies show that applying specific measures can reduce with 25-33% the damages on residual trees (Johns et al., 1996). These measures must be feasible from a technical perspective and acceptable from an economic one (Jonkers, 2000).
The fewest damages found in all the variants from the plain, lead to conclusion that the relief energy plays an important role in producing damages to trees. The slope in the logging yards directly proportionally influences tree damages number. Large values of the volume of the average logged tree lead to a lower number of damages. The number of trees per hectare influences directly and proportionally the number of damages. Similar results were found in other studies, showing that residual tree damage level is correlated to terrain slope, density of stand and logging intensity (Tavankar et al., 2015).
The barking have the highest values of the damage index in logging yards where final cuttings were applied and splintering dislodge the largest volumes of wood at the level of the damages, compared to the volume of the trees, in logging yards where first intervention cuttings were applied.

ACKNOWLEDGEMENTS

This paper was carried out with the support of the Ministry of Research, Innovation and Digitization (MCID), through "Programul 1 - Dezvoltarea sistemului național de cercetare - dezvoltare, Subprogram 1.2 - Performanță instituțională - Proiecte de finanțare a excelenței în CDI" - project "Creșterea capacității și performanței instituționale a INCDS „Marin Drăcea") în activitatea de CDI - CresPerfInst" (Contract no. 34PFE./30.12.2021) and Nucleu BIOSERV Programme (Ctr. 12N/2019), project PN19070507. The paper was carried out also, with the support of National Institute for Research and Development for Forestry "Marin Drăcea" through the Program of Research in own Bases – project P1/2022.

REFERENCES

Akay, A.E., Yilmaz, M., & Tonguc, F. (2006). Impact of mechanized harvesting machines on forest ecosystem: Residual stand damage. *Journal of applied sciences*, *6(11)*. 2414-2419.

Bertault, J.G., Sist, P. (1997). An experimental comparison of different harvesting intensities with reduced-impact and conventional logging in East Kalimantan, Indonesia. *Forest ecology and management*, *94*(*1-3*). 209-218.

Clatterbuck, W.K. (2006). Logging damage to residual trees following commercial harvesting to different overstory retention levels in a mature hardwood stand in Tennessee. In *13th Biennial Southern Silvicultural Research Conference, Gen. Tech. Rep. SRS–92, Asheville*, 591-594.

Cudzik, A., Brennensthul, M., Białczyk, W., Czarnecki, J. (2017). Damage to soil and residual trees caused by different logging systems applied to late thinning. *Croatian Journal of Forest Engineering: Journal for Theory and Application of Forestry Engineering*, *38*(*1*). 83-95.

Dămăceanu, C., Gava, M. (1991). Research on the Determination of Tree, Seed and Soil Damage Thresholds by Logging Operations. *ROMSILVA, Institutul de Cercetări și Amenajări Silvice, Seria a II-a, Centrul de Material Didactic si Propaganda Agricola*, Redactia de Propaganda Tehnica Agricola: Bucharest, Romania. (in romanian).

Eroğlu, H., Öztürk, U.Ö., Sönmez, T., Tilki, F., & Akkuzu, E. (2009). The impacts of timber harvesting techniques on residual trees, seedlings, and timber products in natural oriental spruce forests. *African Journal of Agricultural Research*, *4*(*3*). 220-224.

Fairweather, S.E. (1991). Damage to residual trees after cable logging in northern hardwoods. Northern *Journal of Applied Forestry*, *8*(*1*). 15-17.

Ficklin, R.L., Dwyer, J.P., Cutter, B.E., & Draper, T. (1997). Residual tree damage during selection cuts using two skidding systems. In *Proc. of the 11th Central Hardwood Forest Conf., Univ. of Missouri*, 36-46.

Hartsough, B. (2003). Economics of harvesting to maintain high structural diversity and resulting damage to residual trees. *Western journal of applied forestry 18*(*2*). 133-142.

Helmisaari, H.S., Hanssen, K.H., Jacobson, S., Kukkola, M., Luiro, J., Saarsalmi, A., Tamminen, P., Tveite, B. (2011). Logging residue removal after thinning in Nordic boreal forests: long-term impact on tree growth. *Forest Ecology and Management*, *261*(*11*). 1919-1927.

Johns, J.S., Barreto, P., Uhl, C. (1996). Logging damage during planned and unplanned logging operations in the eastern Amazon. *Forest ecology and management*, *89*(*1-3*). 59-77.

Jonkers, W.B.J. (2000). Logging damage and efficiency: a study on the feasibility of reduced impact logging in Cameroon. *Tropenbos-Cameroon Programme*.

Knežević, J., Gurda, S., Musić, J., Halilović, V., Sokolović, D., Bajrić, M. (2018). The Impact of Animal Logging on Residual Trees in Mixed Fir and Spruce Stands. *South-east European forestry*, *9*(*2*). 107-114.

Picchio, R., Magagnotti, N., Sirna, A., & Spinelli, R. (2012). Improved winching technique to reduce logging damage. *Ecological Engineering*, *47*. 83-86.

Picchio, R., Tavankar, F., Nikooy, M., Pignatti, G., Venanzi, R., Lo Monaco, A. (2019). Morphology, growth and architecture response of beech (*Fagus orientalis* Lipsky) and maple tree (*Acer velutinum* Boiss.) seedlings to soil compaction stress caused by mechanized logging operations. *Forests*, *10*(*9*). 771.

Putz, F.E., Sist, P., Fredericksen, T., Dykstra, D. (2008). Reduced-impact logging: challenges and opportunities. *Forest ecology and management*, *256*(*7*). 1427-1433.

Tavankar, F., Majnounian, B., Bonyad, A.E. (2013). Felling and skidding damage to residual trees following selection cutting in Caspian forests of Iran. *Journal of forest science*, *59*(*5*). 196-203.

Tavankar, F., Bonyad, A.E., & Majnounian, B. (2015). Affective factors on residual tree damage during selection cutting and cable-skidder logging in the Caspian forests, Northern Iran. *Ecological Engineering*, *83*. 505-512.

Whitman, A.A., Brokaw, N.V., Hagan, J.M. (1997). Forest damage caused by selection logging of mahogany (*Swietenia macrophylla*) in northern Belize. *Forest Ecology and Management*, *92*(*1-3*), 87-96.

Scientific Papers. Series E. Land Reclamation, Earth Observation & Surveying, Environmental Engineering. Vol. XII, 2023
Print ISSN 2285-6064, CD-ROM ISSN 2285-6072, Online ISSN 2393-5138, ISSN-L 2285-6064

THE RISK ASSESSMENT FOR THE MANAGEMENT OF PETROLEUM PRODUCT STORAGE & DISTRIBUTION SITE

Ana Maria PETRUTA[1], Dragoș DRĂCEA[2]

[1]Technical University of Civil Engineering Bucharest, 122-124 Lacul Tei Blvd, District 2, Bucharest, Romania
[2]University of Agronomic Sciences and Veterinary Medicine of Bucharest, 59 Marasti Blvd, District 1, Bucharest, Romania

Corresponding author email: petrutaanamaria@yahoo.com

Abstract

The paper presents a risk assessment for the management of contaminated sites. For defining the solutions for management of petroleum products storage and distribution sites there were developed two main activities. The first one consists in a detailed site investigation using a conceptual model to define its geological, hydrogeological characteristics and surely the contamination level. The second activity is dedicated to the assessment of risk generated by the soil, subsoil, air and groundwater contamination, by using a professional software applied to a real case study. The results showed that for carcinogenic and non-carcinogenic compounds the risk is above the thresholds according to the legislation. The conclusions of this analysis allow establishing the measures to mitigate this risk, based on a feasibility study and on the best solutions for site remediation (soil and groundwater).

Key words*: assessment, contaminated, deposits, risk.*

INTRODUCTION

The management of contaminated zones is a tool that prevents and reduces the negative effects generated by these areas to the environment and surely to human health (Bica & Petruta, 2021). Among the analysis criteria used to establish the management solution of a contaminated area must be included two general principles deriving from resource management: minimizing future maintenance needs, respectively regulatory requirements to ensure the safe use of the area and reducing to a reasonable level the constraints of the use of the area (Bica & Petruta, 2021).

For contaminated areas, the risk assessment defines the procedure by which the hazards generated by contamination to the health of the population or to the ecosystem are estimated qualitatively or quantitatively (Bica & Petruta, 2021).

The qualitative assessment of the risk can be subjective, based on the evaluator's experience and with a high degree of generalization.

The quantitative assessment requires a high degree of knowledge of the area, by collecting information from the field, investigations necessary to define the contaminated site.

In the case of quantitative risk assessment numerical data are used and provide the results having an objective character.

In order to perform a quantitative risk assessment, a detailed soil and subsoil investigation plan was prepared of the product storage and distribution site (warehouse), taking into account the potential sources of pollution and define the geological and hydrogeological characteristics of the site, the size of hot spot areas and the specific contaminants.

The lithological section (Figure 1) of the analysed site describes the fact that, down to the depth of approximately 0.7 m, a non-homogenous filling layer develops, consisting of a clayey-sandy layer mixed with sands and gravels (Petruta & Bica, 2021). Under these layers, down to depths of 6.70-7.40 m, a slightly cohesive formation develops, consisting of clayey sandy dusts, plastically consistent (Petruta & Bica, 2021). Starting from depths ranging between 6.70-7.40 m down to depths of 9.30-9.60 m, a non-cohesive formation develops, consisting mainly of wet sands, and down to the depth of 10 m a dusty clay layer, plastically hard, is identified (Petruta & Bica, 2021).

The phreatic aquifer is surrounded by the non-cohesive formation, consisting of sands (Figure 1) and this aquifer is supplied particularly from rainfall and from the nearby river (Petruta & Bica, 2021).

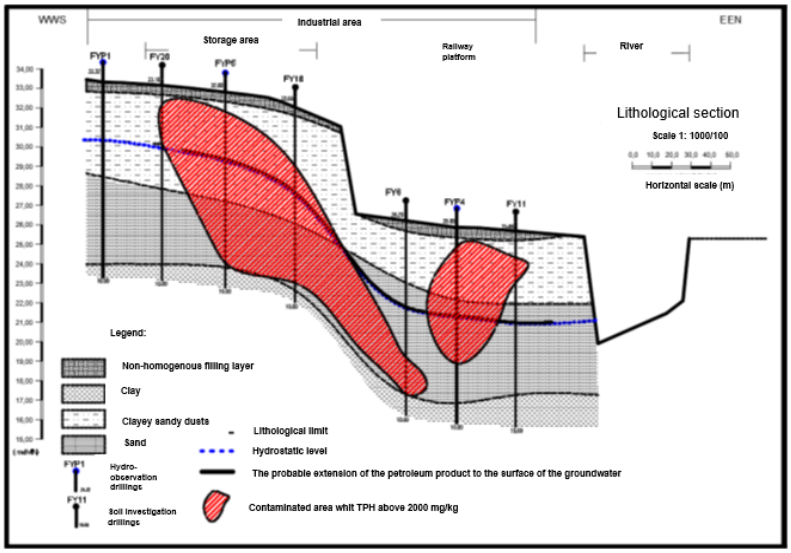

Figure 1. Lithological section

The general flowing direction of the phreatic aquifer is from NV towards SE, more particularly from the monitoring well FYP1, located upstream of the facilities that have a polluting potential, towards the wells FYP2 and FYP3, located downstream of the specified facilities, near the river course (Petruta & Bica, 2021). The phreatic aquifer surrounded by the terrace deposits is supplied from rainfall, whereas the one embedded in the plain is supplied as much from the terrace discharge as from rainfall and from the river (Petruta & Bica, 2021).

MATERIALS AND METHODS

The physical and chemical properties of contaminants was determined with the investigation plan in terms of establishing the sampling points, collecting the samples, and establishing the methods to measure them. Also, these properties control the transport of pollutants into the underground environment, determining the size of the polluted area (Bica, 2014). As regards the types of pollutants specific to the distribution and storage oil industry, it is important to know and assess the characteristics of chemicals, such as: water solubility, density, boiling point, steam pressure, volatilization of pollutants, biodegradability (ARCADIS, 2019).

To assess the degree of horizontal and vertical contamination of the site, 20 soil/subsoil investigation drillings were conducted, out of which 5 drillings (FYP1, FYP2, FYP3, FYP4, FYP5) were turned into hydro-observation drillings to assess the ground water quality evolution in time (Figure 2) (Petruta & Bica, 2021). The drillings were placed in such a way as to cover the entire site, but mainly focalised on the potential pollution sources (judgmental and systematic sampling designs) (Bica, 2014).

Following the investigations and the results of laboratory tests, besides the soil pollution with TPH, soil pollution with aromatic hydrocarbons and concentrations of benzene, respectively, was also identified, which exceed the alert threshold in the drillings made in the tanks park area and the railway platform towards the southern part, FY16 and FY18, as well as the intervention threshold in drillings FYP2, FY7, FY18 (Petruta & Bica, 2021).

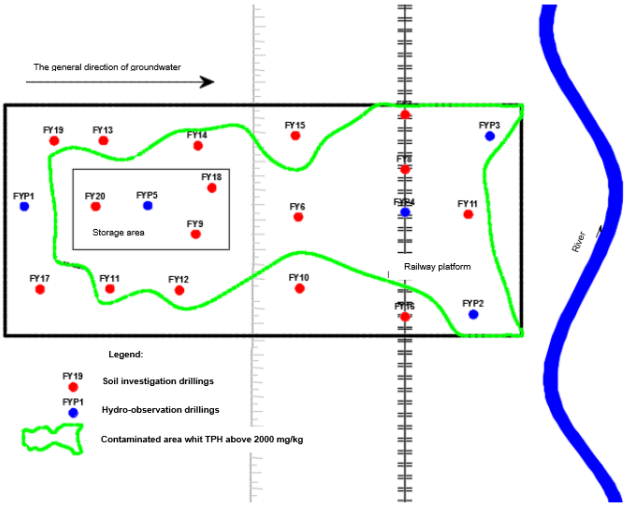

Figure 2. Master plan of the warehouse, with location of technological items

After analysing the laboratory test results and the isolines with the TPH and BTEX (particularly benzene, ethylbenzene and xylene) concentrations, it follows that there is a contamination of the soil, especially at the former facilities: pumping station, tanks and vehicle platform in the northern part of the site, settling tank, the railway platform spot and the scavenge oil storage area (Petruta & Bica, 2021). Following the investigation stage, it was identified a contamination of the soil down to the depth of 4.5-5.0 m and, considering the presence of the hydrostatic level of the underground water at these depths, an active influential and interdependence connection is noticed between soil and groundwater (Petruta & Bica, 2021).

The contamination of the soil on the specific site represents approximately 67% of its total area and the estimated pollution of the groundwater covers approximately 82% of the total specific site (Petruta & Bica, 2021).

Considering the soil permeability, the groundwater was also investigated by using the monitoring wells (Figure 3), following which a significant contamination was noticed (according to Romanian legislation, Ministerial Order no.756/1997 for the approval of the Regulation on the assessment of environmental pollution).

It can be noted that the areas with significant pollution are within the perimeter of the storage tanks, of the petroleum product unloading platform and in the area between the railway platform and the river (Petruta & Bica, 2021).

Significant pollution with petroleum products was confirmed at site level for the aquifer, and such contamination with petroleum products tends to migrate beyond the site.

Considering the detailed investigation stage, the potential exposure pathways taken into account in the quantitative risk assessment are: dermal contact with surface soil during the execution of on-site works; dermal contact with groundwater (thickness NAPLs), this pathway is specific to people who could swim in the river in the immediate vicinity of the site, but this has a low probability of being achieved because the river water is not contaminated in this specific case; soil or water ingestion (accidental); inhalation of particles/dust, on medium and long term exposure route, during the on-site construction works; inhalation of volatile compounds during the on-site works, in which the affected receivers could be the permanent or occasional workers on the site and residents in the proximity of the site (up to 25 m distance), especially in the dominant direction of the wind; solubilization from the soil in the groundwater, considering the results of the water samples.

Also, we mention the fact that both the population and the industrial area do not use the water from the aquifer, there is a centralized

water supply system, so the risk of using underground water is reduced.
Below are presented the measurements performed in the soil drillings and the observation and control drillings (piezometers) with whose help we obtained the input data values of the investigated site.

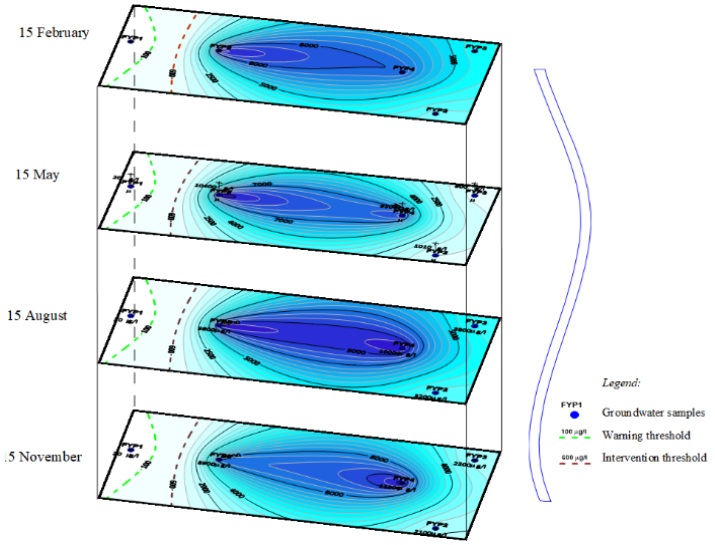

Figure 3. TPH concentrations in the groundwater samples during the monitoring period

The quantitative risk assessment modelling program RBCA Toolkit and RISC5 software were used to run the input data, with the hydraulic gradient value of the water-bearing unit being 0.01.
The thickness of surface soil (outdoor air volatilization factor) zone was set at 1 m and the predominant wind direction is East South - West East and the average annual speed was 2.5 m/s.
The hydraulic conductivity value entered in software is 5.0E-1 (0.5) m/day; the maximum value identified was used, considering it to be the most unfavourable according to the principle of data use.
Effective porosity of the soil varies from 37.5% to 40%. The value of 0.38 was used in the programs.
The flow rate of the aquifer water varies with the hydraulic conductivity; for the risk assessment process, the value of the groundwater velocity was 5.0E-3 m/day. The predominant direction of water flow is West-East, but there are also local variations given by the presence of buildings in the residential area, by the physical characteristics of the soil that drain the water in randomly oriented secondary directions.
The phreatic aquifer is contained in the non-cohesive formation made up of sands. This aquifer is fed mainly by precipitation and by the nearby river. The water level in the site is interdependent with the water level in the river, according to the measurements during the monitoring period of the water level in the monitoring wells.

RESULTS AND DISCUSSIONS

The RBCA Toolkit for Chemical Releases is a comprehensive modelling and risk characterization software package (RBCA Toolkit for Chemical Releases, 2007). The RBCA combines contaminant transport models and risk assessment tools to calculate baseline risk levels and derive risk-based clean-up standards for a full array of soil, groundwater, surface water, and air exposure pathways (Bica & Petruta, 2021).
Similar to the RBCA Toolkit, the RISC 5 software allows determining the values of pollutant concentrations at the source to obtain

a level of risk imposed on receptors; in this way, the remediation levels that should be obtained for the contaminated area are defined.
Similarly, the two RISC 5 and RBCA Toolkit software have the same threshold values, in accordance with international practice and specialized literature; the cancer risk threshold value used will be 10-5, and the threshold value for non-cancer risk will be 1.
The RISC 5 software contains contaminant transport models for estimating their concentrations in various points of contaminated area.
Based on the introduction of the input data, namely the definition of the pollution source, the exposure routes and the way in which the receptors could be affected, the source-path-receptor relationship was defined.
In the first stage, are identified the chemical substances of interest (constituent of concern in each source area, soil and groundwater) and they are chosen according to the database of each program.
The RISC 5 software calculates the risk to human health, separately for the unsaturated zone and groundwater as output data.
In the first part of the software, the conceptual model is defined by choosing the source, respectively the unsaturated zone, this being the main source of contamination on the site (Figure 4).

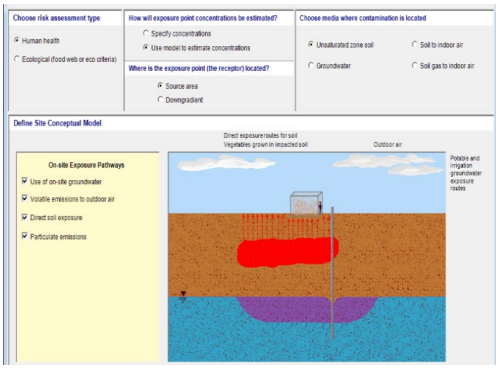

Figure 4. Exposure pathways identified for risk assessment on human health – RISC 5 software

In the following, geological and hydrogeological parameters are characterized, specific pollutants are defined, the contaminated area of the site according to those requested to be completed at the software level and adapted to the real conditions in the specific terrain of the site. Within both programs, RBCA Toolkit and RISC 5, the most unfavourable scenario was considered, having the highest concentrations of pollutants on the entire site.
Considering the input data in the RISC 5 program, the estimated value of the risk on the health of the population (Figure 5) highlights a non-cancerous risk for the soil, as an environmental factor, through the following exposure routes: soil ingestion and dermal contact, in the case of contact with the contaminated soil.

SUMMARY OF HAZARD QUOTIENTS
Receptor 1:
Construction Worker - Upper Percentile

Chemical	Ingestion of Soil	Dermal Contact with Soil	Ingestion of Irrigation Water	Dermal Contact with GW	Inhalation of GW Spray	Inhalation of Outdoor Air	Inhalation of Particulates	TOTAL
Benzene	5.9E-02	1.9E-01	0.0E+00	4.5E-31	5.9E-32	4.9E-04	2.6E-15	2.5E-01
Ethylbenzene	1.5E-02	4.8E-02	0.0E+00	0.0E+00	0.0E+00	1.6E-05	4.9E-16	6.3E-02
TPH Aliphatic C10-12	2.4E+00	7.0E+00	0.0E+00	0.0E+00	0.0E+00	5.3E-09	7.8E-14	1.0E+01
Xylenes (total)	1.9E-03	6.0E-03	0.0E+00	0.0E+00	0.0E+00	4.7E-05	1.2E-15	8.0E-03
TOTAL	2.5E+00	8.0E+00	0.0E+00	4.5E-31	5.9E-32	5.6E-04	8.2E-14	1.1E+01

Figure 5. Non-carcinogenic risk assessment in the unsaturated zone - RISC 5 software

Regarding the carcinogenic risk generated by the concentrations of the compounds identified following the site investigation, namely benzene, ethylbenzene, xylene, the risk does not exceed the standardized limit value according to Romanian legislation. The risk generated for contaminated groundwater based on the input data in the RISC 5 program, demonstrates a carcinogenic and non-cancerous risk through exposure to dermal contact with contaminated groundwater (THP concentrations exceed the intervention threshold limit according to the current legislation).
The following figures show some captures from the RBCA Toolkit software used, showing its working mode, respectively the data used for the risk assessment.
Figure 6 shows the identified exposure routes: groundwater exposure (commercial receptors on the site), surface soil exposure (commercial receptors, workers on site) and air exposure in open spaces (commercial receptors outside the site, at 25 m).
Exposure factors are volatilization, leakage/infiltration of polluting waters and wind erosion (Figure 7). Exposure routes for contaminated soil are dermal contact, ingestion,

inhalation; the ways of exposure to air are: volatilization and/or contaminated particles; the exposure routes for contaminated groundwater are: ingestion of groundwater or drinking water.

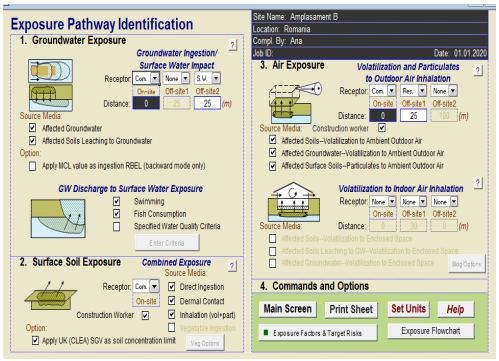

Figure 6. Exposure pathways - RBCA Toolkit software

The specific indicators of the soil pollutants on the site (risk factors) are: THP, benzene, ethylbenzene and xylene, and in the case of groundwater, the pollutants identified following the investigation are THP and benzene. In the risk assessment, the sample with the maximum concentration was considered without thickness of the free phase of the oil product identified during the measurements in monitoring periods.

Benzene is a complex compound of BTEX and difficult to degrade, with volatile properties and high solubility in water, so it presents a significant risk to human health (carcinogenic risk) and to the environment.

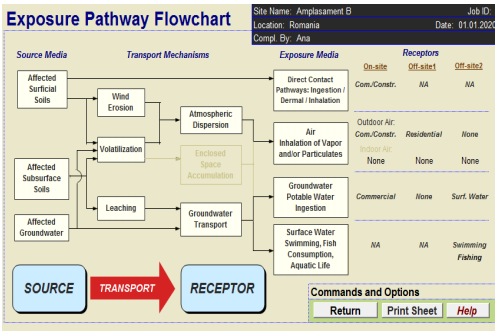

Figure 7. Exposure Pathway Flowchart - RBCA Toolkit software

The type of soil was chosen with specific parameters defined according to international literature, similar to the type of soil related to the specific site, and in the case of geological and hydrogeological data, the parameters was defined through in situ measurements.

The next figure (Figure 8) shows the results of the risk assessment for the warehouse.

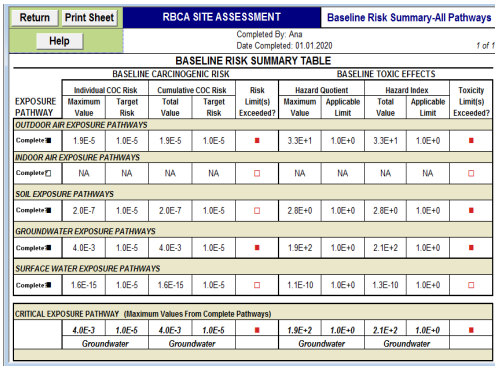

Figure 8. Carcinogenic and non-carcinogenic risk assessment using RBCA Toolkit software

The results are structured by risk categories, namely carcinogenic risk and non-carcinogenic risk, and by exposure routes. The output data highlight the following aspects:

- carcinogenic risk is identified for exposure by air (in open spaces, outdoor air) and for exposure through groundwater;
- the risk generated by toxicity (non-carcinogenic risk) is identified for the air exposure route (in open spaces, outdoor air), for the soil exposure route and for the groundwater exposure route.

As a result of the risk assessment, it is required that soil and groundwater to be decontaminated on the specific site to reduce the concentrations of pollutants to the acceptable levels for the human health and for environment.

CONCLUSIONS

The quantification of the risk is represented by the average daily dose that reaches the human body (receiver) through the pathways exposure (ingestion, dermal contact, inhalation, etc.) and by the daily tolerance coefficient, present at the level of the program in the database, established by the WHO (World Health Organization).

Considering the modelling results, a risk level above the admissible limits can be predicted for

the receptors identified and presented at the level of the conceptual model site.

Carcinogenic and non-carcinogenic risk assessment is carried out by the two software, RBCA Toolkit and RISC 5, and the results of the risk assessment were different.

In the case of the site, the carcinogenic and non-carcinogenic risk is significant in several pathways' exposure calculated by the RBCA software compared to the carcinogenic and non-carcinogenic risk calculated by RISC 5 software.

In order to explain this situation, the similarities and differences between the two software are presented below, starting from the characteristic input data and output data.

From the point of view of the source of contamination and of the transport routes, the RBCA Toolkit software allows the assessment of the risk when we have contamination in the soil and in the groundwater and considering the migration and infiltration of pollutants from the unsaturated zone to the saturated zone. In the case of the RISC 5 software, the risk assessment is different, such that the risk is calculated separated for the unsaturated zone (soil) and the saturated zone (groundwater).

In terms of similarities, both software is using almost the same types of chemical substances / constituents of concern and allowed the introduction the same concentrations. Also, each software considers the homogeneous conditions in the field, and have a database of the properties of chemical substances, toxicity, geological, hydrogeological conditions, etc.

The differences between the software are also indicated at the level of the exposure pathways for the unsaturated zone and saturated zone. In the case of the RBCA Toolkit software, the important routes of exposure for soil (which could be selected as input data from the software) are: ingestion, inhalation of particles, volatilization and dermal contact; the routes of exposure for groundwater, if they are discharged into surface water: swimming and consumption of fish from contaminated water.

In the case of the RISC 5 software, the exposure routes for soil, specific for the site, are: ingestion, inhalation of particles, dermal contact, and in the case of groundwater, they are ingestion, dermal contact, and inhalation of particles.

The RBCA software allows entering the distance from the contaminated area to the receivers (2 receivers outside the site) but also mentions the receivers located at the site level, such as the workers during the remedial stage of the works.

The RISC 5 software allows entering the type of receivers without defining the distance to them; in this software, the sensitive receptors are also included separately, children for which the carcinogenic and non-carcinogenic risk calculation is performed separately. In the case of the RBCA Toolkit, the receivers are generically residential, including adults, children, adolescents, without making a difference between them, children for example.

Also, there are same differences between the software in the case of geological, hydrogeological and hydraulic parameters, for which in RBCA ToolKit parameters are defined for certain types of soil, while in the RISC 5 software, they are not defined.

To explain this situation, I present one such example, for which the RBCA software includes data on geological and hydrogeological parameters in the case of the dusty-sandy soil specific to the warehouse; in the case of the RISC 5 software this type of soil was not found and a sandy soil was considered. The RISC 5 software allows modifying the parameters already defined by the program depending on the need to reproduce the real situation in the field as faithfully as possible.

Another difference is the fact that each software presents risk assessment models and implicitly somewhat different calculation parameters considering the ways of exposure and transport of pollutants in the geological environment.

ACKNOWLEDGEMENTS

This research work was carried out with the support of Technical University of Civil Engineering Bucharest, Department of Hydraulics and Environmental Protection and University of Agronomic Sciences and Veterinary Medicine of Bucharest, the Faculty of Land Reclamation and Environmental Engineering.

REFERENCES

ANZECC (1999). Guidelines for the assessment of on-site containment of contaminated soil. Australia and New Zeeland Environment and Conservation Council.

ARCADIS (2019). Manual for managing potentially contaminated and contaminated sites pertaining to the petrochemical industry in Romania.

Bica, I. (2014). Remediation of contaminated sites. Orizonturi Universitare, Timisoara.

Bica, I., Petruta, A.M. (2021). The risk assessment, a decision-making tool for the management of contaminated sites. *E3S Web of Conferences 265*, 04001.

Ministry for the Environment (2004). Contaminated Land Management Guidelines No.5: Site Investigation and Analysis of Soils.

Petruța, A.M. (2021). PhD Thesis Risk. Analysis a deposit management tool from decommissioned industrial warehouses.

Petruta, A.M., Bica, I. (2021). Analysis of the pollution degree of the geological environment on a petroleum product storage and distribution site. The *7th Conference of the Sustainable solutions for energy and environment*, Sci.664 012070.

RBCA ToolKit for Chemical Releases (2007). Software Guidance Manual RBCA ToolKit for Chemical Releases.

Scientific Papers. Series E. Land Reclamation, Earth Observation & Surveying, Environmental Engineering. Vol. XII, 2023
Print ISSN 2285-6064, CD-ROM ISSN 2285-6072, Online ISSN 2393-5138, ISSN-L 2285-6064

MACHINE LEARNING-BASED MODELING FRAMEWORK FOR IMPROVING ROMANIAN RESILIENCE STRATEGY TO GREENHOUSE GAS EMISSIONS IN RELATION TO VISEGRAD GROUP

Stefan-Mihai PETREA, Ira-Adeline SIMIONOV, Alina ANTACHE, Aurelia NICA, Cristina ANTOHI, Dragos Sebastian CRISTEA, Maxim ARSENI, Madalina CALMUC, Catalina ITICESCU

REXDAN Research Infrastructure, "Dunarea de Jos" University of Galati,
98 George Cosbuc Street, Galati, Romania

Corresponding author emails: ira.simionov@gmail.com, dragoscristea@yahoo.com

Abstract

The present research reveals the difference between Romania and V4 in terms of the Greenhouse Gas Emissions Strategy and establishes a machine learning (ML) - based modeling framework for improving the ability to reach zero GHG by the mid-21st century. The ML tree-based algorithms, based on dual dimension environmental-economic nexus, revealed that net greenhouse gas emissions (NGHGE) are mostly conditioned by greenhouse gases from agriculture (GHGA), a fact valid both in the case of Romania (feature importance - FI = 0.41) and V4 (FI = 0.86). However, for V4, the 2nd important predictor is identified as greenhouse gases from waste management (FI = 0.26), while in the case of Romania, the national expenditure on environmental protection has a limited impact (FI =0.02) on NGHGE. Both integrated models have good prediction accuracy (Rsq. 0.70, RMSE 0.53 for the model associated with the Romania database and Rsq. 0.76, RMSE 0.47 for the V4 model). It can be concluded that in terms of integrated GHG emissions management strategy, Romania can merge with V4 to increase the environmental efficiency towards achieving the EU environmental goals.

Key words*: machine learning, environmental modeling, GHG, environmental strategy, tree-based models.*

INTRODUCTION

It is a reality that climate change impacts the world's environmental heritage, a fact revealed by extreme weather conditions such as heat waves of rapidly changing climate. Thus, the European Union Commission responded to this environmental challenge by adopting European Green Deal and Intergovernmental Panel for Climate Change suggested a carbon neutrality target by 2050 (*EUR-Lex - 52021DC0240 - EN - EUR-Lex*, n.d.; Von Der Leyen, n.d.). Greenhouse gas emissions (GHG) are a major concern nowadays and new EU joint countries are making efforts to align with the established desideratum. Thus, regional groups have been created, such as Visegrad Group (V4), to encourage and sustain optimum cooperation between the countries, for the successful accomplishment of common goals, such as GHG reduction.

The European Union has been a leader in addressing climate change and reducing greenhouse gas emissions. In 2019, the EU set a target to achieve net-zero greenhouse gas emissions by 2050 (*Virtual Workshop - UNFC Europe: Ensuring Sustainable Raw Material Management to Support the European Green Deal | UNECE*, n.d.). To achieve this goal, the EU has implemented various policies and initiatives.

One of the most important initiatives in this area is the EU Emissions Trading System (EU ETS), which is the world's largest carbon market. It covers more than 11000 power stations and industrial plants in the EU and regulates the emissions of carbon dioxide (CO_2) and other GHGs. The EU ETS works by allocating a limited number of permits to each participating company, which allows them to emit a certain amount of CO_2. Companies that emit less than their allocated amount can sell their unused permits to companies that exceed their allocation. Another important directive is the Renewable Energy Directive (RED), which aims to increase the share of renewable energy in the EU's energy mix. It sets binding targets for each EU member state to increase the share of renewable energy in their final energy consumption by 2030. The RED also establishes sustainability criteria for biofuels and bioliquids,

ensuring that only those with a high degree of greenhouse gas emission savings can be counted towards the targets. In addition, the Energy Efficiency Directive (EED) sets binding energy efficiency targets for EU member states, with the aim of reducing energy consumption by 20% by 2020 and 32.5% by 2030. The EED requires member states to establish energy-saving schemes for households, businesses, and public buildings, and to carry out energy audits on large companies. The EU has also adopted the Effort Sharing Regulation (ESR), which sets binding national GHG reduction targets for sectors not covered by the EU ETS, such as transport, buildings, and agriculture. The ESR requires each member state to reduce its GHG emissions by a certain percentage compared to 2005 levels. The targets for 2030 range from 0% to 40%, depending on the country's wealth and emissions level. Finally, the EU has recently proposed the Fit for 55 packages, a set of legislative proposals aimed at achieving the EU's climate neutrality goal. The package includes revisions to existing directives such as the EU ETS, RED, and EED, as well as new initiatives such as the Carbon Border Adjustment Mechanism (CBAM), which aims to ensure that the carbon cost of imports into the EU is equivalent to the cost paid by EU companies under the EU ETS. Overall, the EU's environmental policies aim to reduce GHG emissions, promote renewable energy, increase energy efficiency, and achieve climate neutrality by 2050. The directives discussed above are some of the key tools the EU is using to achieve these goals.

As a member state of the EU, Romania is also subject to these policies and initiatives. In 2019, Romania's greenhouse gas emissions were 181 million tons of CO_2 equivalent, which is a decrease from 2005 levels but still above the country's emissions reduction target. Romania has implemented several measures to reduce its greenhouse gas emissions, including promoting energy efficiency and renewable energy sources, improving public transportation, and reducing methane emissions from landfills. On the other hand, Visegrad Group (Poland, Czech Republic, Slovakia, Hungary) was subject to infringement proceedings by EC for failing to implement emissions reduction targets under the Effort Sharing Regulation. The Czech Republic had first considered that the EU Green Deal is a huge threat to the country. It is considered that Bioeconomy GHG emissions make up 11.99% of GHG emissions in Slovakia, 15.15% in Czechia, 21.69% in Poland and 24.63% in Hungary (Lazorcakova et al., 2022). Slovakia, the Czech Republic and Hungary have already achieved the level of emission reductions required by the Paris Agreement and can contribute to the achievement of the EU target (Tucki et al., 2021). In December 2020, Poland announced its intention to achieve net-zero greenhouse gas emissions by 2050, a significant shift in its previous stance on climate change. Overall, EU greenhouse gas policies and climate change initiatives are closely linked, with the aim of achieving net zero emissions by 2050 and mitigating the impact of climate change. Romania and the Visegrad Group are subject to these policies, but there are varying levels of commitment and progress among the member states. The European Union (EU) has set a goal to become climate neutral by 2050, which means that the net greenhouse gas (GHG) emissions will be reduced to zero. To achieve this goal, the EU has implemented several environmental policies, including European directives, aimed at reducing GHG emissions and promoting renewable energy sources.

The aim of the present study is to emphasize the difference between Romania and V4 in terms of GHG and to support decision management in achieving the zero GHG goal by mid-21st century, considering dual dimension environmental-economic nexus, by using a machine learning (ML) tree-based algorithm framework. Therefore, the framework will be used as a support tool for building a strategy which will target to maximize the efficiency of the decision process by using artificial intelligence (AI) methodology. Also, the study will reveal the main trend in GHG research in association with both area of study and AI methodology used to achieving the main goals.

MATERIALS AND METHODS

Bibliographic analysis

The analysis was performed using R code - Bibliometric and Scientometric Python Library, considering the following dimensions, within WoS databse: GHG Emissions Romania, GHG Emissions Visegrad, Environment - economics

nexus, GHG machine learning, GHG economic policies, GHG agriculture modeling, GHG waste modeling, GHG industry modeling, GHG energy modeling, GHG modeling, GHG neural networks, GHG deep learning. Thus, during the 2011-2023 timespan, a number of 93 research articles, 3 book chapters, 1 data paper, 45 proceeding papers and 4 review articles were considered and analysed, counting 571 authors with a collaboration index of 29.45. The repartition of all analysed scientific papers, by year publishing year, is presented in Table 1.

Table 1. Annual scientific production considering the keywords-based, already established, analytical framework

Annual scientific production	
Year	No. of articles
2011	3
2012	6
2013	8
2014	9
2015	7
2016	15
2017	11
2018	11
2019	23
2020	10
2021	18
2022	19
2023	6

Database descriptiton

Data provided by Eurostat, related to a number of 10 indicators, between the years 2010-2022, were taken into consideration for the analytical framework: National expenditure on environmental protection (mil. euros) *NEEP*; Environmental protection investments of total economy (mil. euros) *EPITE*; Total environmental taxes (mil. euros) *TET*; Taxes on Pollution/Resources (mil. euros) *TPR*; Net greenhouse gas emissions (tonnes per capita) - *NGHG*; Greenhouse gases from agriculture (thousand tons) *GHGA*; Greenhouse gases from waste management (thousand tons) *GHGWM*; Greenhouse gases from industrial processes and product use (thousand tons) *GHGIPP*; Greenhouse gases from energy sector (thousand tons) *GHGES*; Research and development expenditure (*% of GDP*). The indicators were divided, firstly, into 2 groups: dependent variable (NGHG) and predictors (the rest of the indicators). Moreover, the predictors' group was divided into 2 dimensions, as follows: economic dimension (NEEP, EPITE, TET, TPR, RDE) and environmental dimension (GHGA, GHGWM, GHGIPP, GHGES). The dependent variable was firstly analyzed considering each dimension parameters, separately, as the independent variables.

Machine learning algorithms

Two machine learning supervised techniques were used to develop the analytical frameworks within the present study, as follows: random forest tree-based algorithms (RF) and generalized additive models (GAM). The RF represents a machine-learning algorithm, consisting of many decision trees, each being a regressor for the input data. Sampled data is used as input, based on a subset of features randomly selected. Therefore, RF involves bagging and random selection of features, generating a certain number of regression trees. The input data is selected through bootstrap sampling, while the features represent a random subset of the original features.

Boosting and bagging are important concepts for random forest models. Boosting represents the combination of several weak learners into one accurate prediction algorithm, while bagging means that only a random subset of samples is independently drawn from the training sample. The randomly selected samples are used to grow weak learners, dealing well with the overfitting situation, the average prediction value being chosen as the final prediction value. Random forest is a very popular algorithm (Liu et al., 2021; Wang et al., 2016) as it is accurate, robust against noise and outliers, fast, and able to perform feature selection. The parameter feature importance is measured by calculating how the overall score decreases when a feature is not available. Thus, the predictor variables will be ranked in terms of relative significance, by calculating the decrease in node impurity weighted by the probability of reaching that node, probability that is calculated by the number of samples that reach the node, divided by the total number of samples. When the value is high, the feature is more important (eq. 1) (*Random Forest Feature Importance Computed in 3 Ways with Python | MLJAR*, n.d.).

$$n_{ij} = w_j C_j - w_{left(k)} C_{left(j)} - w_{right(j)} C_{right(j)} \quad (1)$$

where:

w_j = weighted number of samples reaching node j;

right (j) = child node from right split on node *j*;
n_{ij} = represents the importance of node *j*;
C_j= the impurity value of node *j*;
left(j) = child node from left split on node *j*;
It is possible to calculate the importance for each feature on a decision tree by using the following formula:

$$fi_i = \frac{\sum_{j:node\ j\ splits\ on\ feature\ i} ni_j}{\sum_{k \in all\ nodes} ni_k} \quad (2)$$

where:
fi_i is the importance of feature *i*;
ni_j = the importance of node *j*.
The values obtained from the above equation are normalized (*normfij*), obtaining values between 0 and 1 by dividing by the sum of all feature importance values:

$$normfi_i = \frac{\sum_{j \in all\ trees} normfi_{ij}}{T} \quad (3)$$

The feature importance is the average over all the trees. The sum of the feature's importance value on each tree is calculated and divided by the total number of trees:

$$RFfi_i = \frac{\sum_{j \in all\ trees} normfi_{ij}}{T} \quad (4)$$

where:
T = total number of trees;
normfi$_{ij}$ = normalized feature importance for *i* in tree *j*;
$RFfi_i$ = the feature *i* importance, calculated from all the trees in the RF model.
The GAM is represented by the sum of different functions specific to each feature, the relationship between the dependent variable and the predictors being different from the simple weighted sum. The Thus, the linear regression coefficients are replaced by spline functions allowing the description of nonlinear relationships. The GAM's advantage is its interpretability, as each predictor's contribution can be clear.

RESULTS AND DISCUSSIONS

Bibliographic analysis

The top journals revealed by the bibliographic analysis that published papers related to the search dimensions presented in the material and methods section of the present research paper are as follows: Energies - MDPI (17 publications), Environmental Engineering and Management Journal, Journal of Environmental Protection and Ecology, Sustainability - MDPI (each with 6 research papers) and Journal of Cleaner production (4 research papers considered). Most relevant keywords are GHG (30 appearance), followed by renewable energy (13 appearance) and climate change - energy (within 10 appearance each) (Figure 1).

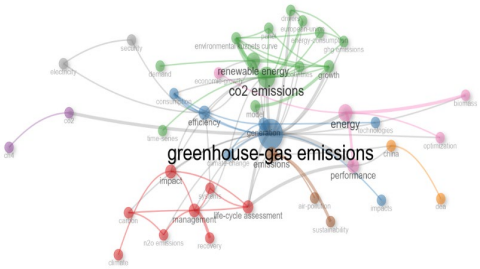

Figure 1. Keywords occurrences network

Considering the keywords conceptual structure (Figure 2) it can be stated that 3 main dimensions are distinguished, as follows: the environmental dimension (blue), the economic dimension (red) and the environmental economics impact dimension (green). However, the red and green dimensions explain almost 40% of the data variance (Figure 2). Therefore, it is necessary to include the 3rd dimension in order to identify a trend within keywords usage in order to elaborate a bibliometric framework which will support the decision process.

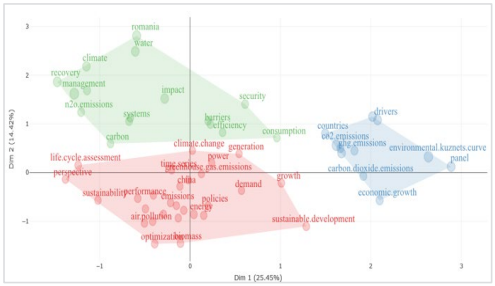

Figure 2. Keyword's conceptual structure map

However, low search results are encountered when AI concepts such as machine learning or autoregression models are included in the search structure. This reveals that there is a gap within the scientific literature related to the use of new, innovative techniques for generating decision-support tools related to GHG emissions for both Romania and V4 group. However, the if analysing the total citations per country, it can

be observed that Romania is on the second position, after Italy, with a number of 551 total citations - TC (average article citations - AAC 6.5) while the V4 is mostly represented by Slovakia (4th place) with 80 TC and 16 AAC, followed by Poland (6th place) with 78 TC and AAC 7.71, Hungary (17th place) with TC21 and ACC 7 and the Czech Republic (25th place).

Most cited paper in the area of the study presented in the present article is *EDGAR v4.3.2 Global Atlas of the three major greenhouse gas emissions for the period 1970-2012* (Janssens-Maenhout et al., 2019) with 250 citations, followed by *Agroforestry creates carbon sinks whilst enhancing the environment in agricultural landscapes in Europe* (Kay et al., 2019) with 79 citations and *Oxy-combustion of coal, lignite and biomass: A techno-economic analysis for a large scale Carbon Capture and Storage (CCS) project in Romania* (Cormos, 2016) with 68 citations.

In terms of countries' collaboration for the elaboration of research articles in the area of interest for the present paper, Romania mostly collaborates with Germany and Austria, while from V4, it can be distinguished 3 clusters as follows: Czech Republic - Slovakia, Hungary (connected with Portugal, Greece and Finland) and Poland (connected with France, Portugal and Germany) (Figure 3).

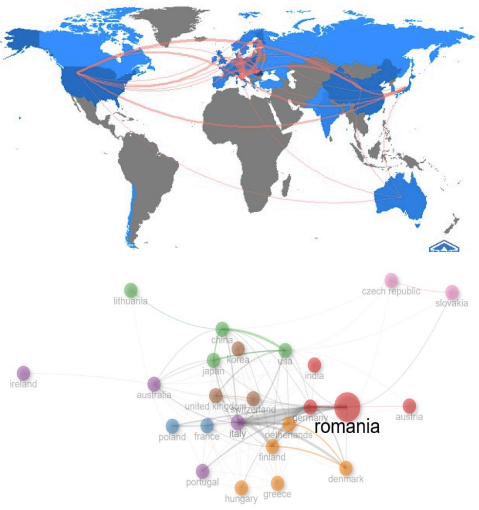

Figure 3. Countries' collaboration in the area of study

GAM modelling framework

The environmental economics dimension generates a prediction of NGHG related to RDE, TET and MEEP (Figure 4A, 4C, 4D) revealing that research and development spendings are directly dependent on GHG emissions, therefore, the increase of emissions generating a similar increase of RDE, TET and MEEP in Romania. Also, in terms of the NGHG-EPITE relation, it can be observed (Figure 4B) that the share of environmental protection investment will increase as the NGHG increases, but with a slower dynamic - however, the EPITE will continue its increase more over the NGHG will decrease to values. The TPR - NGHG relation in Romania has a certain cyclicity as an increase of TPR (between 9 -11 mil. euros) generates positive effects on NGHG, while the variation of TPR outside this interval is promoting high values of NGHG in Romania (Figure 4E).

The Romania environmental dimension emphasizes that the energy sector does not impact the NGHG since an increase of GHGES will generate a continuous decrease of the predicted variable (Figure 5A). However, the situation is different in the case of the waste management sector where an increase in GHGWM generates a direct and proportional increase in NGHG (Figure 5B), a fact that reveals the necessity of applying an optimized waste management strategy in order to increase the sustainability related to GHG emissions in Romania.

The agriculture sector can be considered one of the sectors where *green* measurements can generate an increase of sustainability related to NGHG, revealing its crucial importance, at least in the first stages, in decreasing emissions by acting as a substitute for other industries. However, practising more intensive agriculture (increasing productivity) as well as maximizing production can generate a negative effect on NGHG (Figure 5D).

Industrial processes are also an important source of GHG and can influence NGHG especially if the industry overcomes a maximum sustainable production capacity point (Figure 5C). However, if variated within the optimal range, the industry can be a proper tool for controlling the NGHG in the case of Romania.

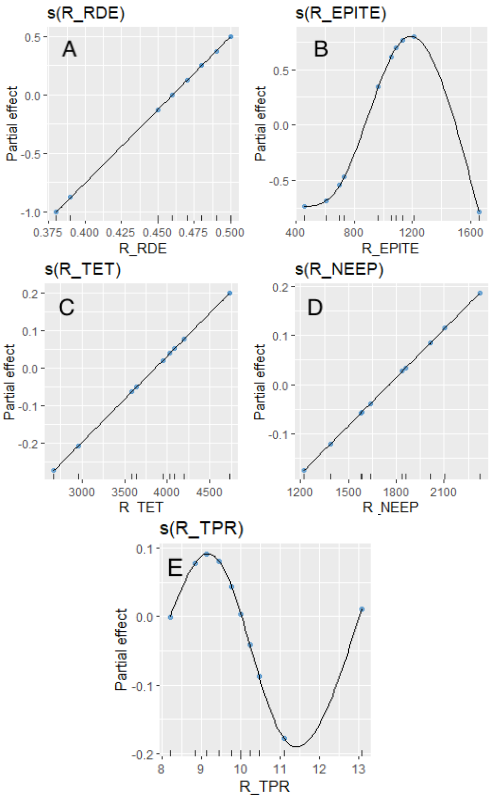

Figure 4. Romania GAM prediction models for the NGHG dependent variable, based on several predictors from environmental economics dimension
(A - RDE; B - EPITE; C - TET; D - NEEP; E - TPR)

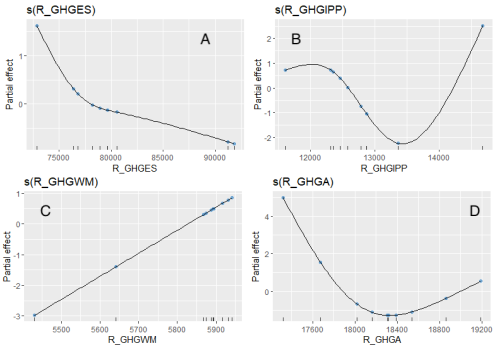

Figure 5. Romania GAM prediction models for the NGHG dependent variable, based on several predictors from the environmental economics dimension
(A - GHGES; B - GHGIPP; C - GHGWM; D - NEEP; E - GHGA)

The environmental economics dimension for V4 generates a prediction of NGHG related to RDE (Figure 6A) and reveals that research and development in the environment can be used in order to decrease NGHG, at least during the first layers of a resilience plan. However, RDE cannot offer a linear relation in association with NGHG and overusing this tool can have a boomerang effect. However, TET and EPITE can be used as efficient tools for decreasing NGHG in V4 (Figure 6B, 6C) since their increase will generate a decrease in the predicted variable.

The NEEP can be an indicator that can be used for monitoring the NGHG in the first steps of the expansion of emissions since it has high sensitivity (Figure 6D), a fact valid also is considering TPR (Figure 6E). However, if the increase in NEEP can be associated with a slower increase in NGHG (Figure 6D), the situation of TPR differs - a decrease in the predicted variable is associated with the increase in TPR.

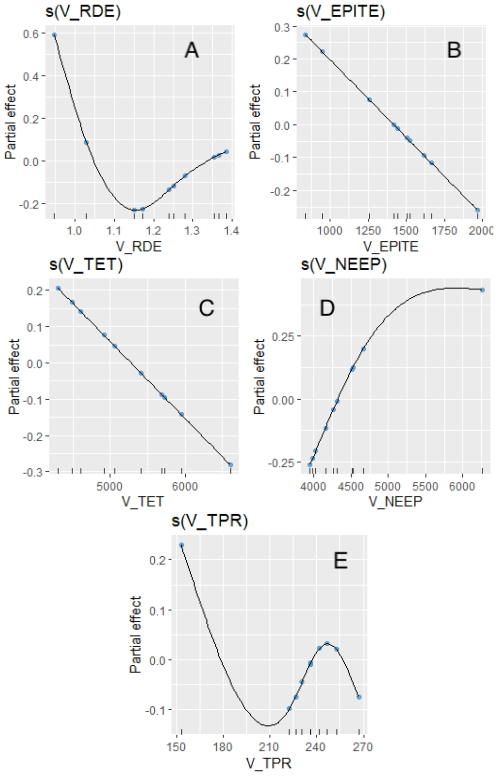

Figure 6. V4 GAM prediction models for the NGHG dependent variable, based on several predictors from environmental economics dimension
(A - RDE; B - EPITE; C - TET; D - NEEP; E - TPR)

The V4 environmental dimension emphasizes that the energy sector and agricultural sector can be used as tools for decreasing the NGHG (Figure 7A, 7D) since an increase of GHG within these two economic sectors can lead to a decrease of NGHG. However, the situation is different in the case of GHGIPP (Figure 7B) since this parameter can be used as a monitoring tool in NGHG dynamics, being directly correlated with the predicted parameter. The waste management sector can be used as a tool for decreasing the NGHG only if GHGWM variates within an optimum interval (5600-5900 thousand tons) (Figure 7C).

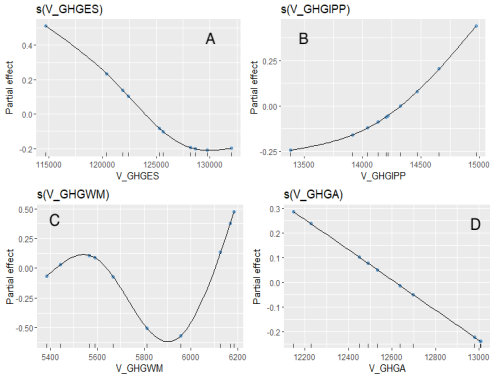

Figure 7. V4 GAM prediction models for the NGHG dependent variable, based on several predictors from the environmental economics dimension (A - GHGES; B - GHGIPP; C - GHGWM; D - NEEP; E - GHGA)

Similar to other studies, also this study is subject to several limitations. The main limitation is related to the dataset time period since it covered a period of 10 years. Thus, although the accuracy of the prediction was high, increasing the time associated with dataset collection will explain better the complex relations between the analytical framework parameters.

CONCLUSIONS

Summarizing the findings, it can be concluded that in terms of integrated GHG emissions management strategy, Romania can merge with V4 to increase the environmental efficiency towards achieving the EU environmental goals. This can be due to similarities between several relations which characterize NGHG within the environmental economics dimension (NGHG - TPR, NGHG - NEEP), but especially within the environmental dimension, where Romania is closely align with the V4 strategy.

Future studies are recommended to be performed in order to widen the number of dimensions involved in the present analytical framework and to perfect the decision support tool based on in-depth observations.

ACKNOWLEDGEMENTS

The present research was supported by the project: "An Integrated System for the Complex Environmental Research and Monitoring in the Danube River Area", REXDAN, SMIS code 127065, co-financed by the European Regional Development Fund through the Competitiveness Operational Programme 2014-2020, contract no. 309/10.07.2021.

The present research was supported by the project "Integrated research and sustainable solutions to protect and restore Lower Danube Basin and coastal Black Sea ecosystems, (ResPonSE) ", 760010/30.12.2022, component C9. PRIVATE SECTOR SUPPORT, RESEARCH, DEVELOPMENT AND INNOVATION, Investment "I5. Establishment and operationalization of Competence Centers".

REFERENCES

Cormos, C.C. (2016). Oxy-combustion of coal, lignite and biomass: A techno-economic analysis for a large scale Carbon Capture and Storage (CCS) project in Romania. *Fuel*, *169*, 50–57. https://doi.org/10.1016/J.FUEL.2015.12.005

EUR-Lex - 52021DC0240 - EN - EUR-Lex. (n.d.). Retrieved October 8, 2022, from https://eur-lex.europa.eu/legal-content/EN/TXT/?uri=COM:2021:240:FIN

Janssens-Maenhout, G., Crippa, M., Guizzardi, D., Muntean, M., Schaaf, E., Dentener, F., Bergamaschi, P., Pagliari, V., Olivier, J. G. J., Peters, J. A. H. W., Van Aardenne, J. A., Monni, S., Doering, U., Roxana Petrescu, A. M., Solazzo, E., & Oreggioni, G. D. (2019). EDGAR v4.3.2 Global Atlas of the three major greenhouse gas emissions for the period 1970-2012. *Earth System Science Data*, *11*(3), 959–1002. https://doi.org/10.5194/ESSD-11-959-2019

Kay, S., Rega, C., Moreno, G., den Herder, M., Palma, J. H. N., Borek, R., Crous-Duran, J., Freese, D., Giannitsopoulos, M., Graves, A., Jäger, M., Lamersdorf, N., Memedemin, D., Mosquera-Losada, R., Pantera, A., Paracchini, M. L., Paris, P., Roces-Díaz, J. V., Rolo, V., … Herzog, F. (2019). Agroforestry creates carbon sinks whilst enhancing the environment in agricultural landscapes in Europe.

Land Use Policy, *83*, 581–593. https://doi.org/10.1016/J.LANDUSEPOL.2019.02.025

Lazorcakova, E., Dries, L., Peerlings, J., & Pokrivcak, J. (2022). Potential of the bioeconomy in Visegrad countries: An input-output approach. *Biomass and Bioenergy*, *158*, 106366. https://doi.org/10.1016/J.BIOMBIOE.2022.106366

Liu, J., Murshed, M., Chen, F., Shahbaz, M., Kirikkaleli, D., & Khan, Z. (2021). An empirical analysis of the household consumption-induced carbon emissions in China. *Sustainable Production and Consumption*, *26*, 943–957. https://doi.org/10.1016/J.SPC.2021.01.006

Random Forest Feature Importance Computed in 3 Ways with Python | MLJAR. (n.d.). Retrieved July 12, 2023, from https://mljar.com/blog/feature-importance-in-random-forest/

Tucki, K., Krzywonos, M., Orynycz, O., Kupczyk, A., Bączyk, A., & Wielewska, I. (2021). Analysis of the Possibility of Fulfilling the Paris Agreement by the Visegrad Group Countries. *Sustainability 2021, Vol. 13, Page 8826*, *13*(16), 8826. https://doi.org/10.3390/SU13168826

Virtual Workshop - UNFC Europe: Ensuring sustainable raw material management to support the European Green Deal | UNECE. (n.d.). Retrieved July 12, 2023, from https://unece.org/sustainable-energy/events/virtual-workshop-unfc-europe-ensuring-sustainable-raw-material-management

Von Der Leyen, U. (n.d.). *A Union that strives for more My agenda for Europe*.

Wang, Y., Ge, X. ling, Liu, J. liang, & Ding, Z. (2016). Study and analysis of energy consumption and energy-related carbon emission of industrial in Tianjin, China. *Energy Strategy Reviews*, *10*, 18–28. https://doi.org/10.1016/J.ESR.2016.04.002

Scientific Papers. Series E. Land Reclamation, Earth Observation & Surveying, Environmental Engineering. Vol. XII, 2023
Print ISSN 2285-6064, CD-ROM ISSN 2285-6072, Online ISSN 2393-5138, ISSN-L 2285-6064

PREDICTION MODELS FOR IMPROVING WASTE DECISION SUPPORT MANAGEMENT IN ROMANIA IN ASSOCIATION WITH V4 MEMBER COUNTRIES

Stefan-Mihai PETREA[1, 2, 3], Ira-Adeline SIMIONOV[1, 2, 4], Alina ANTACHE[1, 2, 6], Aurelia NICA[2], Cristina ANTOHI[3], Dragos Sebastian CRISTEA[3], Adrian ROȘU[1, 5], Valentina CALMUC[1, 5], Bogdan ROȘU[4]

[1]"Dunarea de Jos" University of Galati, REXDAN Research Infrastructure, 98 George Cosbuc Street, Galati, Romania
[2]"Dunarea de Jos" University of Galati, Faculty of Food Science and Engineering, 11 Domneasca Street, Galati, Romania
[3]"Dunarea de Jos" University of Galati, Faculty of Economics and Business Administration, 59-61 Nicolae Balcescu Street, Galati, Romania
[4]"Dunarea de Jos" University of Galati, Faculty of Automation, Computers, Electrical Engineering and Electronics, 47 Domneasca Street, Galati, Romania
[5]"Dunarea de Jos" University of Galati Faculty of Sciences and Environment, Department of Chemistry, Physics and Environment, 47 Domneasca Street, Galati, Romania
[6]"Alexandru Ioan Cuza" University, Faculty of Biology, Iasi, Romania

Corresponding author email: ira.simionov@gmail.com

Abstract

The present study results are based on the application of XGBoost machine-learning algorithms and indicate that total waste, as a dependent parameter, can be accurately evaluated considering plastic wastes (feature importance-FI = 1.53, Rsq.= 0.75, RMSE = 0.47) in the case of V4 group, while for Romania, the dependent parameters identified as most reliable are chemical wastes (FI = 0.58) and industrial effluent sludges (FI = 0.04), with lower accuracy metrics (Rsq. = 0.46, RMSE = 0.75). In terms of waste treatment (WT), the portable batteries and accumulators' market (FI=0.45) presents high reliability to be used as the main predictor (Rsq. = 0.80, RMSE=0.42) for V4 support tool, while for Romania, the waste generation (FI = 1.57, Rsq.= 0.85, RMSE=0.36) highly explains the variability of WT. However, batteries and accumulators waste (FI = 0.77, Rsq. = 0.82, RMSE=0.39) can be used as a reliable predictor for WT variation in a more extended analytical framework, in the case of Romania. It can be concluded that waste decision support management can be supported based on ML models which are different in the case of Romania, compared to V4, emphasizing the regional importance when developing environmental modeling-based tools.

Key words*: prediction models, waste treatment, waste decision support models, XGBoost, waste framework.*

INTRODUCTION

The expansion of waste footprint is both environmentally and economically unsustainable. As a response, the European Union (EU) has set a Waste Framework Directive which regulates a series of concepts related to waste management, considering risks linked to human health, water – air – plants – animals pollution, as well as noise and odour pollution. In order to improve the capacity to respond to different social, economic and environmental challenges, regional interest groups have been created, such as the Visegrad Group (V4). A demonstrated increase in efficiency associated with already establish regional groups could encourage their extension and could optimize the environmental strategies, considering the regional specificity.

Waste management is a critical issue in the EU, and the EU has implemented several environmental policies to manage waste in a sustainable and environmentally friendly way. These policies aim to promote a circular economy, reduce waste, and improve resource efficiency (*Single-Use Plastics Directive - European Bioplastics e.V.*, n.d.). Some of the key European directives related to waste management in the EU are, as follows: Waste

Framework Directive (WFD) (*Implementation of the Waste Framework Directive*, n.d.), Packaging and Packaging Waste Directive (PPWD) (*Packaging Waste*, n.d.), Waste Electrical and Electronic Equipment Directive (WEEE) (*EUR-Lex - 02012L0019-20180704 - EN - EUR-Lex*, n.d.), Landfill Directive (LD) (*Landfill Waste*, n.d.)and Circular Economy Package (CEP) (*Circular Economy Policy - Library*, n.d.). The WFD establishes the basic concepts and definitions related to waste management and lays out a hierarchy of waste management options that prioritize prevention, reuse, and recycling over landfilling and incineration. The directive requires member states to take measures to reduce waste generation and to ensure that waste is managed without endangering human health or harming the environment. The PPWD aims to reduce the environmental impact of packaging and packaging waste by setting targets for the recovery and recycling of packaging waste. Member states are required to establish systems for the collection and recovery of packaging waste and to ensure that a certain percentage of the waste is recycled. The WEEE establishes rules for the collection, treatment, and disposal, which include electronic devices such as computers, televisions, and refrigerators. The directive requires member states to establish collection systems and to ensure that the waste is treated and disposed of in an environmentally sound manner. The LD aims to reduce the amount of biodegradable waste that is sent to landfills, which are a significant source of methane emissions. The directive establishes strict standards for the operation and closure of landfills and requires member states to reduce the amount of biodegradable waste that is landfilled. The CEP consists of several legislative proposals aimed at promoting a circular economy in the EU. The package includes new initiatives such as the Circular Economy Action Plan and the EU Strategy for Plastics in a Circular Economy. The package aims to increase the recycling and reuse of waste, reduce waste generation, and promote resource efficiency. Overall, the EU's waste management policies aim to reduce waste, promote recycling and reuse, and protect the environment and human health (Virsta, 2020). The directives discussed above are some of the key tools the EU is using to achieve these goals.

In the Visegrad Group, waste management policies vary among the member states. Poland and Slovakia, for instance, have been criticized for their lack of progress in waste reduction and recycling compared to other EU member states (Mišík, 2019). Hungary has implemented measures to promote recycling and improve waste treatment facilities (Buczkó, 2018), while the Czech Republic has focused on waste reduction and reuse (Fialová, 2019).

The EU's waste management policies continue to evolve, with a focus on reducing waste generation and promoting a circular economy. Romania and the Visegrad Group are subject to these policies, and while progress has been made, some member states, particularly Poland and Slovakia, face criticism for their lack of progress in waste reduction and recycling.

Therefore, the aim of the present study is to develop a series of prediction models which target improving waste decision support management, considering the specificity of Romania, in association with V4 member countries.

MATERIALS AND METHODS

Bibliographic analysis

The analysis was performed using R code - Bibliometric and Scientometric Python Library, considering the WoS database and the following dimensions, within WoS database: waste management modeling, waste management machine learning, waste management neural networks, waste management deep learning, waste management Romania, waste management Visegrad, waste treatment modeling, households waste modeling and recycling modeling. Thus, during the 2008-2022 timespan, a number of 101 research documents (64 articles, 1 book and 36 proceedings papers) were considered and analysed, with an annual growth rate of 8.78%, counting 285 authors with an international co-authorship percentage of 9.90%.

The scientific papers publishing dynamics (Figure 1) reveal a considerable increase in the last 4 years of the analysed period, emphasizing the upward interest trend related to the analysed scientific areas.

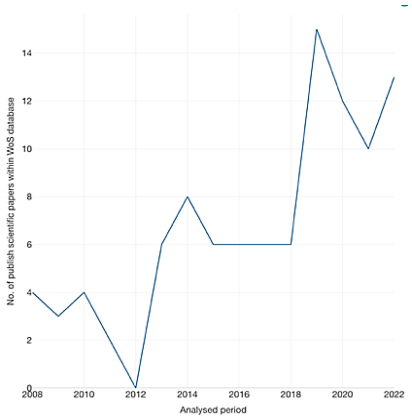

Figure 1. Annual scientific production dynamics considering the keywords-based, already established, analytical framework

Database descriptiton

Data provided by Eurostat, related to a number of 14 indicators, between the years 2004-2020, were taken into consideration for the analytical framework: used oils wastes (tons) OUW; chemical wastes (tons) CW; industrial effluent sludges (tons) IES; health care and biological wastes (tons) HCBW; plastic wastes (tons) PW; textile wastes (tons) TW; batteries and accumulators wastes (tons) BAW; household and similar wastes (tons) HSW; total waste (tons) TW; waste treatment (kg per capita) WT; waste generated (kg per capita) WG; recycling rates of packaging waste RRPW; portable batteries and accumulators market (tons) PBAM; wastes collected - Portable batteries and accumulators (tons) WCPBA.

The dependent variables were considered as being TW and WT. However, for TW, the OUW, CW, IES, HCBW, PW, BAW and HSW are considered predictors, while for WT, two dimensions were considered as follows: D1 (including WG, RRPW, PBAM, WCPBA as predictors) and D2 (including OUW, CW, IES, HCBW, PW, TW, BAW, HSW as predictors).

Machine learning algorithms

For creating an in-depth machine learning-based analytical framework, firstly, generalized additive models (GAM) algorithms were used. The generalized additive models (GAM) extend the linear model with nonlinear functions of each variable. Therefore, for GAM, the linear component b_jX_j is replaced with a non-linear $f_j(X_j)$ function associated with feature j, according to eq. 1. The functions are calculated for each predictor having the contributions added to the result. Based on dispersion diagrams and by using cubic spline functions, the f_i functions are evaluated through interpolation (eq. 2).

$$g^{-1}(E[Y]) = a + f_1(X_1) + f_2(X_2) + \cdots + f_n(X_n) + \varepsilon \quad (1)$$

where:
ε - minimized error;
$E[Y]$ - the arithmetic mean of the dependent variable Y;
a - point of origin of the trajectory;
g^{-1} is the inverse of the function g, called the link function;
$f_1(X_1),\ldots, f_n(X_n)$ - spline functions associated with independent variables.

$$S(x) = a_i + b_i x + c_i x^2 + d_i x^3, for\ \forall x \in [x_{i-1}, x_i] \quad (2)$$

where:
$S: [a, b] \to \mathbb{R}$;
$f: [a, b] \to \mathbb{R}$;
$(x_i) = S(x_i),\ i = \overline{0, n}$.

According to underlying patterns in the data, generalized additive models can provide an understanding of the impact of the predictive variables through linear or non-linear smooth functions. Some of the best reasons for using GAM in predictive problems (Murphy et al., 2019) are, as follows: interpretability, regularization and flexibility/automation. Thus, GAM models provide a good balance between the interpretable linear model and the "black box" learning algorithms. For additive models, the marginal impact interpretation of a single variable is not related to the values of the other variables. As a consequence, the model can provide various insights into the effects of the predictive variables.

For a GAM, it is possible to control the smoothness of the predictor functions, avoiding too many inflexion points, by adjusting the level of smoothness (Khamma et al., 2020). Also, even if the dataset contains noisy relationships, a prior belief that predictive

relationships are inherently smooth in nature can be imposed.

The XGBoost algorithm was applied in order to create prediction models based on a strong classifier, using data from weak classifiers (accuracy under 20-30%). The applied data analysis framework is presented in Figure 2.

Sampled data is used as input, based on a subset of features randomly selected. The XGBoost - extreme gradient boosting uses boosting for merging and combining several models with low prediction accuracy in order to generate a core model with high accuracy. The algorithm target to set target outcomes for the next models for minimizing the errors. Among the unique features of XGBoost it can be mentioned the following ones: regularization, handling spare data, weighted quantile sketch, block structure for parallel learning, cache awareness and out-of-core computing. The application of the algorithm provides several advantages, as follows: high accuracy, scalability, efficiency, flexibility, regularization, interpretability and open source.

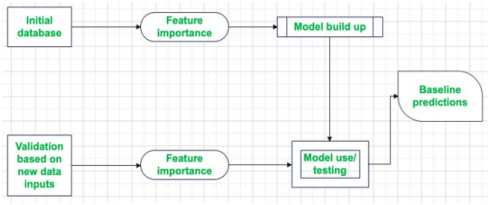

Figure 2. Data analysis framework

Also, since the database is structured, the XGBoost is considered to perform better, compared to the random forest tree-based algorithm (RF). Therefore, the XGBoost represent an important background which can be used in correlation with GAM in order to develop a predictable analytical framework which can be used, further on as bases for the development of decision support systems.

RESULTS AND DISCUSSIONS

Bibliographic analysis

The bibliometric analysis revealed that the top journals which had published articles framed into the search profile described in the material and methods section are Environmental Engineering and Management Journal (15 publications) and Sustainability - MDPI (10 publications), respectively. Most relevant keywords are wastes management (18 appearance), followed by the waste model (9 appearances), waste systems (8 appearances), followed by waste impact, municipal solid-waste and solid waste management (each with 6 appearances) (Figure 3). Waste management appears mostly linked to waste recycling and circular economy, within the first keywords cluster (blue cluster within Figure 3), while waste related to management, recovery, sustainability, environmental economics and households defines the 2nd resulted keywords cluster (the red cluster emphasized in Figure 3). However, considering the keywords' conceptual structure map presented in Figure 4, it can be observed that it explains over 65% of the data variance. However, most of the red dimension revealed by the conceptual structure map is widened and, together with the green dimension, can be used in order to create the necessary roadmap for developing multiples frameworks which can be used as a baseline for developing high accuracy decision support tools.

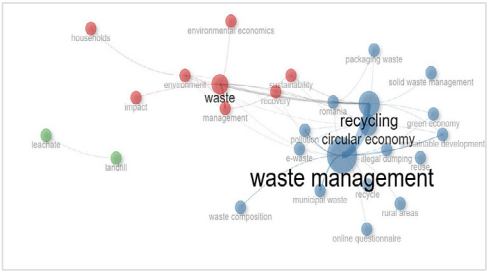

Figure 3. Keywords occurrences network

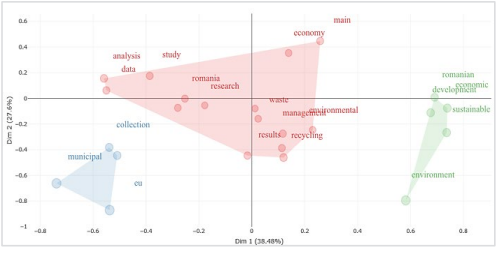

Figure 4. Keywords conceptual structure map

No search resmethodologieslink waste and waste management within Romania or V4 to artificial intelligence methodology were

identified, a fact which confirms the novelty of the present research structure and desideratum. However, if analysing the total citations per country, it can be observed that Romania is in the 1st position (total citations - TC 815, average article citation AAC 9.2), followed by Italy (173 TC, 57.7 AAC) and Portugal (149 TC, 149 AAC). Reported to the V4, the geopolitical group is mostly represented by Poland (5th place) with 8 TC and 8 AAC, followed by Slovakia (6th place) with 5 TC and AAC 5 and the Czech Republic (7th place,) with 3 TC and 3 AAC.

Most cited paper in the area of the study presented in the present article is *Synthesis and characterization of new zeolite materials obtained from fly ash for heavy metals removal in advanced wastewater treatment with* 200 citations, followed by *Packaging waste recycling in Europe: Is the industry paying for it?* with 149 citations, *Introduction of the circular economy within developing regions: A comparative analysis of advantages and opportunities for waste valorisation* with 145 citations and *Forecasting municipal solid waste generation using prognostic tools and regression analysis* with 115 citations. In terms of countries' collaboration for the elaboration of research articles in the area of interest for the present paper, Romania mostly collaborates with Italy (Figure 5).

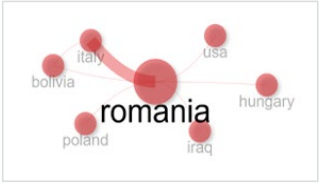

Figure 5. Countries' collaboration in the area of study

XGBoost prediction models

The results are based on the application of XGBoost machine-learning algorithms and indicate that total waste, as a dependent parameter, can be accurately evaluated considering plastic wastes (feature importance-FI = 1.53, Rsq. = 0.75, RMSE = 0.47) in the case of V4 group, while for Romania, the dependent parameters identified as most reliable are chemical wastes (FI = 0.58) and industrial effluent sludges (FI = 0.04), with lower accuracy metrics (Rsq. = 0.46, RMSE = 0.75).

In terms of waste treatment (WT), the portable batteries and accumulators' market (FI = 0.45) presents high reliability to be used as the main predictor (Rsq. = 0.80, RMSE = 0.42) for V4 support tool, while for Romania, the waste generation (FI = 1.57, Rsq. = 0.85, RMSE = 0.36) highly explains the variability of WT. However, batteries and accumulators waste (FI = 0.77, Rsq. = 0.82, RMSE = 0.39) can be used as a reliable predictor for WT variation in a more extended analytical framework, in the case of Romania.

GAM modelling framework

The GAM prediction models are made in order to assist the decision-support process in selecting the correct mechanisms for limiting both the total wastes (TW), and also maximizing and encouraging waste treatment (WT).

The present study analysis both indicators in various analytical framework scenarios, based on supporting databases from a multitude of relevant predictors, in order to reveal the controlling mechanisms for both Romania and V4 geopolitical group and to identify to which degree the two analysed entities can merge in a future globalization taskforce for improvement of the resilience against the wastes in the Eastern part of European Union (EU). Therefore, if TW is targeted to be predicted, and UOW, CW, HCBW, PW and BAW are considered independent parameters, it can be stated that used oil wastes, chemical wastes and plastic wastes all significantly influence the total wastes production and can be successfully used as tools for minimizing the TW (Figures 6A, 5B, 5D). Thus, targeting to decrease the quantity of the nexus *used oils-chemical-plastic wastes* could be the solution for controlling the TW in the case of Romania. However, it seems that healthcare and biological wastes have a reverse impact on TW since their increase creates premises for the decrease of TW in Romania (Figure 6C).

The batteries and accumulator's wastes increase until 38000 tonnes generate an increase in TW, while a further increase, over the previously mentioned value generates a reverse effect on TW, decreasing the value of

the predicted indicator (Figure 6E). This can be because increasing BAW could represent the beginning of a long-term strategy of increasing the sustainability of several industries by shifting to alternative sources which are more sustainable (i.e., adoption of electric vehicles powered by batteries and decreasing the number of conventional engine vehicles). Thus, the results of this strategy, in relation to TW, will be visible after a long-term period, therefore, explaining the prediction dynamics presented in figure 6E.

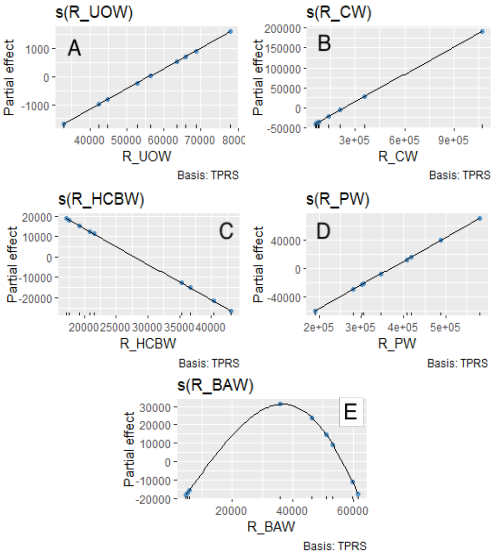

Figure 6. Romania GAM prediction models for the TW dependent variable, based on several predictors (A - OUW; B - CW; C - HCBW; D - PW; E - BAW)

The waste treatment indicator, in the case of Romania, is predicted to increase as both the waste generation and portable batteries and accumulators market increase (Figure 7A, 7C). Therefore, it can be observed that the Romanian mechanism of waste treatment is highly responsive to any increase in waste generation due to the increase in the waste generation products market, enhancing the opinion according to which Romania has the capacity to handle difficult scenarios which could appear in the future, in terms of waste management. Also, both recycling rates of packaging wastes and wastes collected quantity associated with portable batteries and accumulators emphasize a Gaussian shape prediction in relation to TW in Romania (Figure 7B, 7D). This completes the finding previously mentioned for WT prediction, according to which the shifting to more sustainable tools for accomplishing the desideratum targeted by the EU Green Deal (GD) had already started in Romania and this will not imply immediate effects on WT, instead, will induce positive long-term effects.

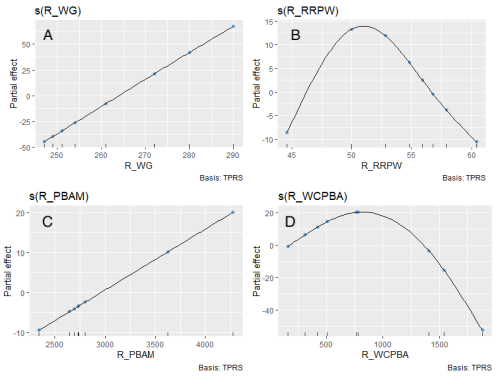

Figure 7. Romania GAM prediction models for the WT dependent variable, based on several predictors (A - WG; B - RRPW; C - PBAM; D - WCPBA)

If targeting to develop a wider analytical framework in order to predict the WT in Romania, based mainly on the waste sources, indicators such as OUW, CW, HCBW, BAW, TW, IES and PW are to be considered. Thus, it seems that after the application of GAM algorithms, two groups were identified, as follows: 1st group includes OUW, CW, TW, PW and IES, while the 2nd group includes HCBW and BAW (Figure 8). Therefore, waste treatment is highly responsive both to the variation of total waste quantitative parameters, but also to oil, chemical, plastics and industrial-based wastes (Figures 8A, 8B, 8E, 7F and 8G), an increase of these predictors generating a relatively similar response in the evolution of WT in Romania. However, the healthcare and biological wastes and the batteries and accumulators' wastes confirm their reverse impact on WT (Figure 8C, 8D), similar to what they had done in relation to TW (Figure 6C, 6E).

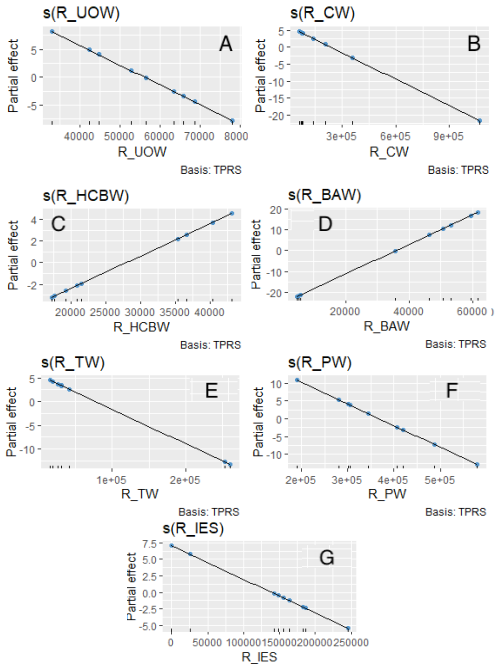

Figure 8. Romania GAM prediction models for the WT dependent variable, based on several predictors (A - UOW; B - CW; C - HCBW; D - BAW; E - TW; F - PW; G - IES)

In the case of V4, the prediction relation between TW, as a predicted variable, and UOW, CW and HCBW as predictors, is similar to that described in the case of Romania (Figure 9A, 9B, 9C). However, if PW, IES and HSV are considered predictors for predicting the TW dependent variable, it can be stated that their impact is the opposite, compared to the Romania case (Figure 9D, 9E, 9G). Thus, an increase in plastic waste and industrial effluent sludges generates a decrease in TW, revealing that in the case of V4 the industry sector is more environmentally sustainable, compared to Romania and the plastics wastes management is more efficient, so the control of TW can be done in a more generous way which can also mean the increase of plastic wastes as a low impact substitute of other high environmental impact types of wastes which mostly compose TW value within the analysed geopolitical group. However, household wastes can be used as a tool for detecting the TW as their increase also generates an increase in predicted values of this dependent parameter (Figure 9G). The batteries and accumulators waste increases are related to TW decrease (Figure 9F), a fact which can be associated with the green technologies' implementation status in V4 - thus, if V4 had overcome the 1st state of transition towards the extended use and implementation of green technologies, this could indicate that the initial investments for shifting to EU GD desideratum were efficient in achieving their goal.

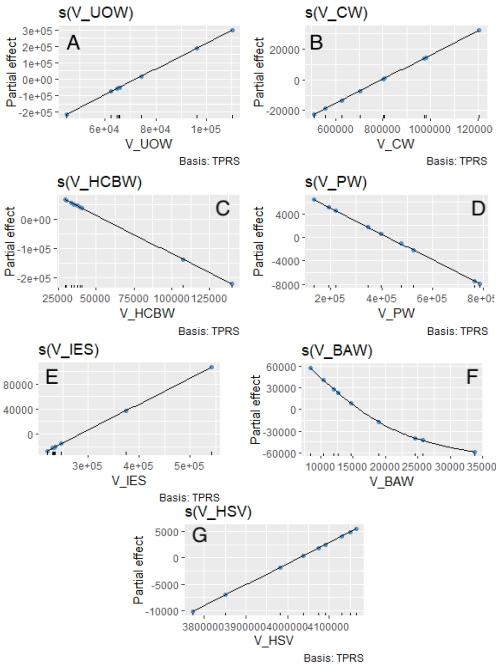

Figure 9. The V4 GAM prediction models for the TW dependent variable, based on several predictors (A - OUW; B - CW; C - HCBW; D - PW; E - IES; F - BAW; G - HSV)

The WT prediction by considering the WG, RRPW, PBAM and WCPBA as predictors reveal some similarities between V4 and Romania. Thus, in terms of using WG and PBAM as predictors for predicting WT, the situation between Romania and V4 is relatively similar since an increase of both predictors can relate to an upward trend of WT (Figures 10A, 10C, 7A, 7C). However, if considering RRPW and WCPBA, the situations are different, both indicating a Gaussian variation of WT predicted values, revealing that V4 has not yet reached maturity when it comes to recycling and packaging wastes management, as well as portable batteries and accumulators waste

collection management (Figure 10B, 10D). Predicting the WT in relation to a wide range of predictors as revealed in Figure 11, concluded some similarities between V4 and Romania if considering UOW, CW, HCBW, IES and BAW (Figures 11A, 11B, 11C, 11G, 11H, 8A, 8B, 8C, 8D, 8G).

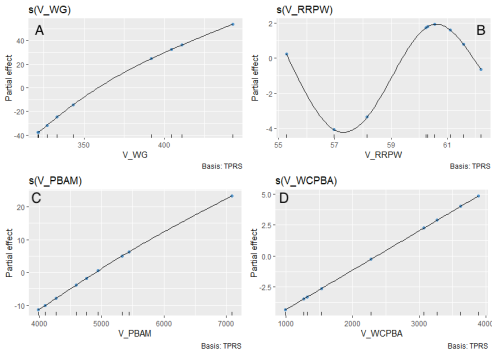

Figure 10. The V4 GAM prediction models for the WT dependent variable, based on several predictors (A - WG; B - RRPW; C - PBAM; D - WCPBA)

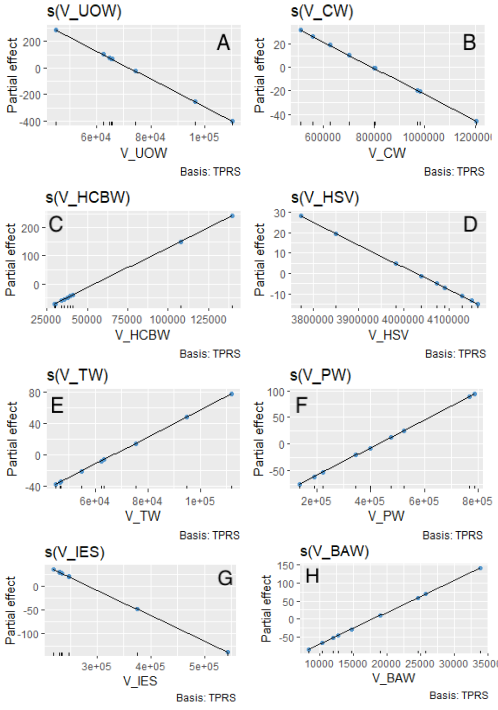

Figure 11. The V4 GAM prediction models for the WT dependent variable, based on several predictors (A - UOW; B - CW; C - HCBW; D - HSV; E - TW; F - PW; G - IES; H - BAW)

However, some indicators have a reverse impact, such as PW (Figures 11F, 8F) on WT, most probably due to the more advanced level of V4 in terms of implementing sustainable measurements in some waste-generating areas. In accordance with other studies, also this study is subject to several limitations. The main limitation is related to the dataset structure and time frame.

Widening the database by including other relevant synthetic indicators, corresponding to subgroups attached to the main waste management indicators, can offer new mechanisms for improving the management of waste. Also, a time-series data frame could offer the possibility of generating several forecasting analytical frameworks, using algorithms such as recurrent neural network LSTM.

CONCLUSIONS

The analytical framework of both Romania and V4, in terms of predicting the total waste production and total waste treatment, reveals several similarities, as follows: the total wastes can be predicted, with similar outputs, by using oil, chemical, healthcare and biological, as well as portable batteries and accumulators market size as main predictors; predictors as total wastes, oil, plastics and industry wastes, as well as healthcare and biological wastes can be used for predicting the waste treatment indicator, with similar results between Romania and V4. However, there are several peculiarities which can be associated with each of both analytical frameworks, and which reveal that V4 is more advanced in certain areas involving the shift to EU Green Deal desideratum, compared to Romania, in terms of waste management. Future studies should target widening the number of analytical framework dimensions to assure a more holistic approach.

ACKNOWLEDGEMENTS

The present research was supported by the project: "An Integrated System for the Complex Environmental Research and Monitoring in the Danube River Area", REXDAN, SMIS code 127065, co-financed by the European Regional Development Fund through the

Competitiveness Operational Programme 2014-2020, contract no. 309/10.07.2021.
The present research was supported by the project "Integrated research and sustainable solutions to protect and restore Lower Danube Basin and coastal Black Sea ecosystems, (ResPonSE)", 760010/30.12.2022, component C9. Private Sector Support, Research, Development and Innovation, Investment "I5. Establishment and operationalization of Competence Centers".

REFERENCES

Buczkó, K. (2018). Municipal solid waste management in Hungary:A review. *Waste management & research, 36*(3), 195-204.

Circular Economy Policy - Library. (n.d.). Retrieved July 12, 2023, from https://circabc.europa.eu/ui/group/6e9b7f79-da96-4a53-956f-e8f62c9d7fed/library/37e8e207-6222-4212-ad7c-e809e64df72c; accessed on 12.03.2023.

EUR-Lex - 02012L0019-20180704 - EN - EUR-Lex. (n.d.). Retrieved July 12, 2023, https://eur-lex.europa.eu/legal-content/EN/TXT/?uri=CELEX:02012L0019-20180704; accessed on 17.03.2023.

Fialová, J. (2019). Waste management in the Czech Republic and its comparison with selected European Union countries. *Polish Journal of Environmental Studies*, *28*(6), 3759–3769.

Implementation of the Waste Framework Directive. (n.d.). Retrieved July 12, 2023, from https://environment.ec.europa.eu/topics/waste-and-recycling/implementation-waste-framework-directive_en; accessed on 23.04.2023.

Khamma, T. R., Zhang, Y., Guerrier, S., & Boubekri, M. (2020). Generalized additive models: An efficient method for short-term energy prediction in office buildings. *Energy*, *213*, 118834.

Landfill waste. (n.d.). Retrieved July 12, 2023, from https://environment.ec.europa.eu/topics/waste-and-recycling/landfill-waste_en; accessed on 02.05.2023.

Mišík, M. (2019). Waste management policy in Slovakia and its European context. *E3S Web of Conferences, 92*, 02001.

Murphy, R. R., Perry, E., Harcum, J., & Keisman, J. (2019). A Generalized Additive Model approach to evaluating water quality: Chesapeake Bay case study. *Environmental Modelling & Software*, *118*, 1–13.

Packaging waste. (n.d.). Retrieved July 12, 2023, from https://environment.ec.europa.eu/topics/waste-and-recycling/packaging-waste_en; accessed on 05.03.2023.

Single-Use Plastics Directive - European Bioplastics e.V. (n.d.). Retrieved July 12, 2023, from https://www.european-bioplastics.org/policy/single-use-plastics-directive/; accessed on 25.03.2023.

Virsta, A., Sandu, M.A., Daraban, A.E. (2020). Dealing with the transition from in line economy to circular economy - public awareness investigation in Bucharest. *AgroLife Scientific Journal, 9*(1), 355-361.

Scientific Papers. Series E. Land Reclamation, Earth Observation & Surveying, Environmental Engineering. Vol. XII, 2023
Print ISSN 2285-6064, CD-ROM ISSN 2285-6072, Online ISSN 2393-5138, ISSN-L 2285-6064

DATA COLLECTION IN THE WILD: CHALLENGES AND SOLUTIONS

Peter UDVARDY[1], Levente DIMEN[2], Gergely VAKULYA[1]

[1]Obuda University, Alba Regia Technical Faculty, 45 Budai, Szekesfehervar, Hungary
[2]University of Alba Iulia, 5 Gabriel Bethlen, Alba Iulia, Romania

Corresponding author email: udvardy.peter@uni-obuda.hu

Abstract

Extensive monitoring plays a key role in environmental protection. This task, however, has many issues to solve, communication and data collection being a difficult one. This paper focuses on the challenges of observing hard-to-access areas, such as forests and wetlands. The performance of the possible solutions for this problem are compared, focusing to sensor networking and Low-Power Wide-Area Network (LPWAN) technologies, and a drone-based solution will be proposed. The presented method offers a robust, and reliable, yet simple data collection solution. The hardware and software architecture, the communication protocol will be described, and the estimated performance of the system is analysed.

Key words*: data collection, environment, LPWAN, UAV.*

INTRODUCTION

Sensor networks in environmental monitoring

Sensor networks consist of nodes with sensing, processing, and communication capabilities. Their main application area is data collection, especially on large areas or with large number of points. In most applications the power sources of the devices are batteries, since the mains current is not an option. Since the required lifespan of such a network is at least 2-3 years, the power budget must be highly optimized.

One of the most promising classic sensor networking applications was the monitoring of remote, non-accessible areas (Corke et al., 2010), such as rainforests (Wark et al., 2008; Cama et al., 2013), volcanos (Werner-Allen et al., 2006; Song et al., 2009) or glaciers (Martinez et al., 2004; Martinez et al., 2005).

Most conventional sensor network-based monitoring systems use a mesh routing protocol to send all measurement messages to a dedicated base station. In a typical setup the sensor nodes have a limited amount of power (most commonly batteries), while the power source of the base is practically unlimited (mains power or solar energy). These protocols often apply Time Division Multiple Access (TDMA), which relies on a tight time synchronization. In such a system each message is relayed through multiple subsequent nodes, which means extra energy consumption each time. Another less obvious disadvantage is, that nodes closer to the base relay more packets, thus they consume more energy.

Another possible approach is to use one of the modern Low-Power Wide-Area Network (LPWAN) protocols (e.g., Long Range (LoRa) (Ertürk et al., 2019; Migabo et al., 2017) or Narrowband Internet of things (NBIoT)). Firstly, these solutions obviously requite a working infrastructure. Secondly, they are typically not designed to transfer large amount of (measurement) data.

Wetlands

Wetlands are usually considered as a specific biotope with high biodiversity potential located on the edge of the solid surface and the permanent or seasonal water covered areas. The presence of the water causes saturation into the soil due to the proximity of the water table. The periodic oxygen-free status of the ground results in anoxic hydric soils. Wetlands occur in different forms such as swamps, marches, estuaries, mangrove swamp, marsh, moorland, or peatland. Wetlands play vital role in biodiversity of vegetation and animal species all over the world and maintain stable ecosystems. There are many types of water in wetland soils such as freshwater, seawater or brackish water depending on the habitat's

location. The vegetation of the wetlands can be woods, trees, shrubbery, reeds, cattails, or sedges. Climate zones classified by Trewartha define the type of wetlands (Belda et al., 2014). Beside the importance in habitat protection wetlands can be seen as natural water filters which collect sediment and pollutants and release almost pure water to the surrounding areas. Furthermore, wetlands regulate water floodings, climate change effects and can be considered also as recreational areas and cultural heritage (Mitsch et al., 2013).

Wetland are threatened by many effects, such as eutrophication, pollution, sewage and drainage problems, toxic contamination, acidification or salinisation. These effects are mainly caused by human factors and urban development.

Wetlands are protected by 'Ramsar convention on Wetlands of International Importance Especially as Waterfowl Habitat' since 1971 in which legal and institutional framework of the wetland areas' protection, conservation and sustainable use was established (Belda et al., 2014). The convention defined the list of wetlands of international importance, for instance Velence and Dinnyés Nature Conservation Area, which is located in the same geographical area as the Sóstó natural reserve (Figure 1), is also on the Ramsar list.

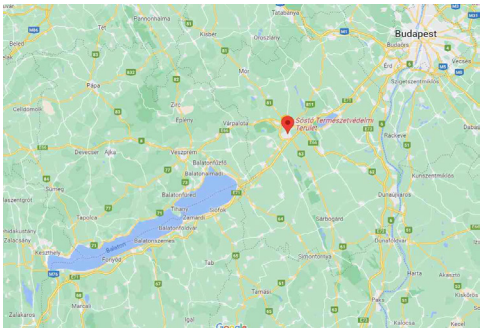

Figure 1. The location of Sóstó natural reserve in the Northen-West part of Hungary relative to Budapest and Lake Balaton (Source: Google Maps)

The Sóstó natural reserve

The Sóstó natural reserve (Figure 2) is located only two and a half kilometres in the southern direction from the downtown of Székesfehérvár and can be considered as an organic part of the city ("Sóstó Természetvédelmi Terület és Sóstó Látogatóközpont", n.d.). Székesfehérvár is located halfway between Budapest and lake Balaton. The wetland is located on 218 hectares of which 121 hectares are nationally and the rest is locally protected area. The visitor centre is in the vicinity of the local football arena.

Figure 2. The map of the Sóstó natural reserve (Source: https://sostoszekesfehervar.hu/turak)

In historic times Székesfehérvár was surrounded by deep swamps until the middle of the 19th century, since then the Sóstó area was partly drained and used as a recreational area. Two deep wells were used as water supply but after the Second World War 600 m^3 sewage sludge were deposited yearly which caused fast eutrophication and decay. The rehabilitation of the Sóstó area was started in the 1990's and in 2003 the area got a naturally protected status. New educational trail was formed for recreational and training purposes. The Sóstó biotope gives various possibilities to the flora and fauna, many protected species can be found there. The water supply of the wetland is provided by local purified wastewater source,

500 m^3 clear water feeds the lakes arrived by a 4 kilometres long pipeline.

MATERIALS AND METHODS

System architecture

The architecture of the monitoring system consists of several independent measuring nodes and a base station, which is attached to an Unmanned Aircraft System (UAS), flying over the measurement area at regular times, allowing to download the collected data (Figure 3). The sensor nodes do preprogramed measurements and store the collected data in flash memory.

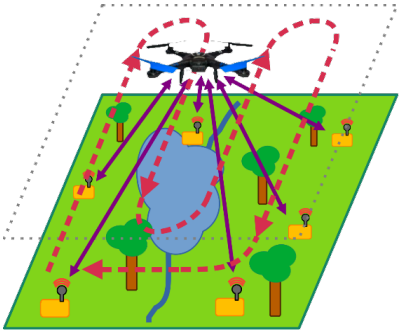

Figure 3. The architecture of the proposed system (own image)

The proposed communication protocol

In the proposed monitoring system, the data collector nodes have limited energy (they are powered by batteries) similarly to regular sensor networking applications. Using a mesh protocol to collect the measured data, each message would be sent by possibly many sensor nodes. The proposed protocol uses a star topology instead, which requires to send each message only once, but on the other hand it assumes direct connection (i.e., line of sight). The speciality of the system is, that the base station is absent in the huge majority of the time and present only occasionally.

The goal of the proposed communication protocol is to detect the presence of the base station and transfer the collected data when the conditions are given. The sensor nodes don't necessarily hear each other; therefore, collision avoidance is the task of the base station.

The protocol utilizes the fast acknowledgements of the 802.15.4 MAC layer. Instead of listening for some kind of beacon messages transmitted by the base station, the sensor nodes emit hello messages regularly and wait for an ACK message. The time interval of the hello messages is a design parameter of the protocol.

The 802.15.4 ACK packet has 3 unused bits (Figure 4), which are used to sign, when the actual data transfer process is possible. Each of the 8 combinations can sign different waiting times. This way the base station can spread the time slots of the nodes. The nodes turn off their radio during waiting. Note that the nodes do not need to maintain tight time synchronization, for this task.

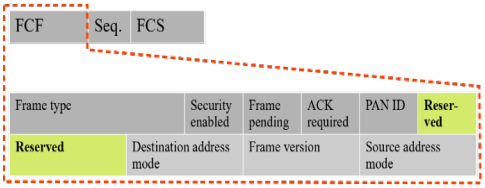

Figure 4. The format of the 802.15.4 ACK packet with the 3 reserved bits highlighted in the frame control field (FCF)

During the actual data transfer each node send the previously collected data divided into packets. Each packet is sent tightly next to each other, with acknowledgements by the base station.

Sensor nodes

The hardware of the sensor node is based on an Unicomp UCMote Proton B mote (Figure 5). The base board has an 8-bit ATmega128RFA1 Soc as the main controller. The microcontroller core is running at 16 MHz, with an approx. 4 mA current consumption from 3.3 V. The microcontroller has different sleep modes, and can be stopped from program execution. When stopped, the current consumption is reduced to the approx. 0.1 mA range. Another important parameter is the wakeup time, which is in the range of microseconds. The SoC contains a 2.4 GHz radio unit, that supports the 802.15.4 range standard for low-power low-range communication. This communication channel is used only during testing for debug purposes only, for two reasons. First the 2.4 GHz band is not suitable for the proposed monitoring system because of the high absorption of. Second, the

board has only a low gain chip antenna connected of the Soc.
The main board contains an additional AT86RF212 radio chip, which operates in the 868 MHz ISM band. This radio chip can be configured to use different communication speeds from 20 to 1000 kbps according to the link conditions. Depending on the communication bandwidth the receiver sensitivity can be as good as -110 dBm. With the +10dBm maximum power output the achievable link budget can reach 120 dB, which is well suits to the proposed system. This radio is connected to an MMCX RF connector, which allows to connect a high gain external antenna.
Since the UAS is located above the sensor nodes during the data download process the usual quarter wave vertical antennas are not a good choice for this purpose, given they have very low gain in axial direction. QFH antennas (Adams et al., 1974), however have good overhead gain, therefore they are much more suitable for the proposed system. The power source of the proposed sensor node consists of 4 D type non-rechargeable lithium batteries, providing 76000 mAh capacity at 3.6 V.

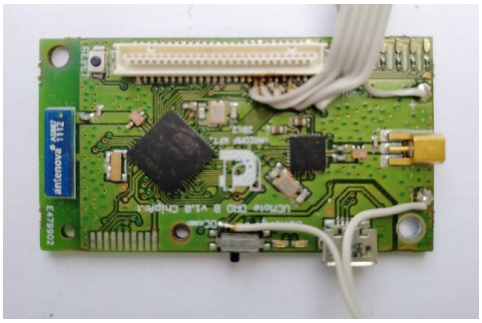

Figure 5. The UCMote Proton B mote

The software of the sensor nodes is built around the TinyOS. It is a component based real-time operating system, especially tailored for low-power applications. It has support for different types of microcontrollers, radios and sensors and the uniform interfaces make adding new device drivers and communication protocols possible.
TinyOS already supported the ATmega128RFA1 SoC with its microcontroller core and automatically put it in low-power mode, when it has no task to run and no event to process. The 2.4 GHz radio is also supported and 802.15.4 standard packets can be sent and received with a simple CSMA/CA MAC protocol. The other radio chip (AT86RF212, 868 MHz) is also supported with the standard CSMA/CA protocol, although the special low-power mode had to be implemented.
To achieve this, the header, which contains the source address, must be intercepted and the time-critical background lookup must be processed in parallel with the reception of the remaining part if the packet, before the full packet arrives (Figure 6) (Vakulya and Simon, 2013). Based on the result of the lookup one of the reserved bits of the acknowledgement packet is set of cleared, signalling the presence or the absence of a pending packet.

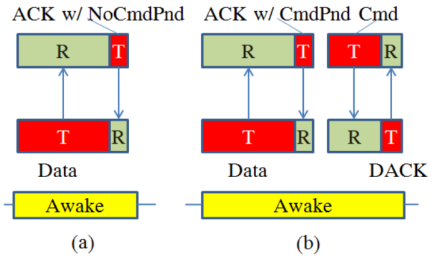

Figure 6. The timing diagram of the ACK piggybacking protocol (Vakulya et al., 2013)

UAS technology

The Chinese DJI company can be considered as one of the leading UAV manufacturers in the world. The DJI Phantom 3 Advanced UAV is available since 2015 and beside its good features cannot be considered as the latest techniques (Udvardy et al., 2019).
The UAV weighs 1280 grams and has a 15.2V 4480mAh battery which allows maximum 23 minutes' flight time. The onboard Sony EXMOR 1/2.3" camera has 12 million pixels and has a FOV of 94° with 20 millimetres focal length. The ISO value changes between 100 and 3200 for video recording and 100 and 1600 for photographs. The shutter speed varies between 8 and 1/8000 seconds. The resolution of the video caption is 2.7K (30fps).
The camera is hanged on-board with the help of a 3-axis gimbal which helps to stabilize the camera during flight.

For navigation DJI Phantom 3 UAV uses GPS/GLONASS system outdoor and has a vision positioning system for indoor positioning. The hover's horizontal accuracy is between 0.3 and 1.5 meters and the vertical accuracy is between 0.1 and 0.5 meters depending on the positioning method.
This UAV can reach approximately 3 kilometres distance outdoor from the home point which is marked before the flight starts. The 'Go home' function helps to find the hover in case of being lost or invisible.

RESULTS AND DISCUSSIONS

Using the proposed system, several different monitoring applications can be implemented. The following 3 demonstrative examples show measurement scenarios related to environment monitoring and calculations to communication settings and for the projected lifetime. Such a system has to be designed taking into account not only physical limitations but also legal requirements. The last two subchapters discuss these equally important aspects in terms of frequency usage and UAV regulations.

Low density environmental data collection

In this scenario, slowly changing environmental parameters are monitored. The sensor modalities are:

- Soil temperature with 16 bit resolution, one measurement every 5 minutes;
- Air temperature with 16 bit resolution, one measurement every 5 minutes;
- Ambient light intensity with 16 bit resolution, one measurement every 5 minutes;
- Relative humidity with 8 bit resolution, hourly;
- Soil moisture with 8 bit resolution, hourly.

A total of 15 sensor nodes are installed in the system. In each node a total number of 1776 bytes are generated each day. If the data is collected every two months, approx. 100 kBytes of data is fetched from each node. With a pessimistic 20 kbps bandwidth approx. 1 minute is necessary to download this data amount from each node. A 1-minute beacon interval for the sensor nodes would give a good balance between latency and power consumption. With these parameters the average flight time can be estimated to approx. 20 minutes.
The 802.15.4 packet has a 13 byte header (including the preamble, physical and MAC headers) and a 2 byte footer. The length of a hello message with a 5 byte payload is 20 bytes, which requires 8 ms to send with 20 kbps. The length of the ACK packet is 11 bytes, which requires 4.4 ms of time. Another approx. 1 ms is required to turn on and off the radio and approx. 2 ms of gap time is required between the two packets. This adds up to 15.4 ms. The actual data transfer requires approx. 60 seconds of time. The on time of the radio can be calculated as follows for a year.

$$T_{on,annual} = 60 \cdot 6 + 365 \cdot 24 \cdot 60 \cdot \frac{15.4}{1000} = 8454[s] \quad (1)$$

Now the annual power consumption of the radio can be calculated as follows:

$$C_{annual} = T_{on,annual} * I_{radio,on} = \frac{8454[s]}{3600} \cdot 20[mA] = 47[mAh] \quad (2)$$

Considering only the radio communication, one D type cell would last for several years (practically the self-discharge limits the lifespan).

Pollution related monitoring

In this scenario, the focus is on pollution related monitoring, specifically air quality parameters. The sensor modalities and data collection parameters are as follows:

- Particulate Matter ($PM_{2.5}$) concentration with 16-bit resolution, one measurement every minute;
- Carbon Monoxide (CO) concentration with 16-bit resolution, one measurement every minute;
- Nitrogen Dioxide (NO_2) concentration with 16-bit resolution, one measurement every minute;
- Ozone (O_3) concentration with 16-bit resolution, one measurement every minute;
- Ambient Temperature with 16-bit resolution, one measurement every minute;
- Relative Humidity with 8-bit resolution, one measurement every minute.

In this scenario, a monthly data collection is scheduled. Each day, 15840 bytes of data is generated on each sensor, which means approx. 500 kBytes monthly. With 20 kbps bandwidth the net data transfer time is 190 s. Now let's choose a 30 s beacon time. The annual on time can be calculated as follows:

$$T_{on,annual} = 190 \cdot 12 + 365 \cdot 24 \cdot 60 \cdot 2 \cdot \frac{15.4}{1000} = 18468[s] \quad (3)$$

Now the annual power consumption of the radio can be calculated as follows:

$$C_{annual} = T_{on,annual} * I_{radio,on} = \\ = \frac{8454[s]}{3600} \cdot 20[mA] = 102[mAh] \quad (4)$$

In this case, the overall annual power consumption is twice as much as the previous case, but the same D type battery would also last for several years in this case. Note that only the radio communication was taken into account for the calculations. Powering the sensors take additional energy.

Fine grain seismic monitoring

In this scenario a demonstrational example for a fine grain environmental parameter (seismic activity) is presented. Here the sensor modality is a triaxial accelerometer with 16 bit resolution and 12.5 Hz sample rate. A total number of 6 nodes are required for this experiment.

This measurement setup generates much more data, than the previous example. Let's use a one-week interval for the data collection. The total data amount during a week is 2.1 MB in each node. In this case a higher data rate (250 kbps) is more suitable, which is only achievable when the distance between the nodes and the base station is smaller (the altitude of the UAS is lower) and when no significant obstacles (i.e. large trees) are present.

We can here choose similar beacon interval to the previous example (1 minute). Note that the nodes can use different data rates for the beaconing and for the data transfer. The calculated data transfer time is 472 seconds. Based on the calculations the annual on-time is:

$$T_{on,annual} = 52 \cdot 472 + 365 \cdot 24 \cdot 60 \cdot \frac{15.4}{1000} = 510198[s] \quad (5)$$

Now the annual power consumption of the radio can be calculated as follows:

$$C_{annual} = T_{on,annual} * I_{radio,on} = \\ = \frac{510198[s]}{3600} \cdot 20[mA] = 1822[mAh] \quad (6)$$

Considering a 19000 mAh battery capacity, the lifespan of the system would be approx. 10 years. Note that only the radio communication was taken into account.

Frequency usage

Although several frequency bands are referred as unlicensed, they are under legal control as well. The most well-known groups are the ISM (Industrial, Scientific and Medical) bands and the SRDs (Short Range Devices) (Loy, 2005). Our case is focused to the former one.

ISM bands are regulated by the International Telecommunication Union. Depending on the geographical region, different bands are allocated with different conditions. In several cases, more different services share the same band and, in general they either must tolerate each other or priorities are defined.

The compliance with the regulations is officially tested and validated as the part of the Certification Process. Only certified commercial off the shelf parts can be distributed. In case of custom-built devices, the certification is the task of the builder.

The 2.4 GHz band (from 2.4 to 2.5 GHz) is generally available worldwide as ISM band. The regulation of the UHF (specifically the 434 MHz, 868 MHz and 915 MHz) bands is different between the regions. In Europe, both the 433 and 868 MHz bands are allowed, with different conditions (e.g. bandwidth, power and duty cycle).

UAV regulations

In Hungary, the Unmanned Aerial Vehicle (UAV) and Unmanned Aircraft System (UAS) flight is regulated by strict law which is harmonised with the European legislations (Table 1), (EU Regulation 2019/947 on the rules and procedures for the operation of unmanned aircraft) (EUR-Lex – Access to European Union Law, n.d.).

Table 1. UAS requirements and limitations (https://www.easa.europa.eu/en/faq/116452)

UAS		Operation		Drone Operator/pilot		
Class	MTOM	Subcategory	Operational restrictions	Drone Operator registration	Remote pilot competence	Remote pilot minimum age
Privately built	< 250 g	A1 (can also fly in subcategory A3)	- may fly over uninvolved people (should be avoided when possible) - no fly over assemblies of people	No, unless camera / sensor on board **and** a drone is not a toy	- no training needed	No minimum age
0					- read user's manual	16*, no minimum age if drone is a toy
Legacy drones (art. 20)						16*
1	< 900 g		- No expected fly over uninvolved people (if happens, should be reduced) - no fly over assemblies of people	Yes	- read user's manual - complete online training - pass online theoretical exam	16*
2	< 4 kg	A2 (can also fly in subcategory A3)	- no fly over uninvolved people - keep horizontal distance of 30 m from uninvolved people (it can be reduced to 5 m if low speed function is activated)	Yes	- read user's manual - complete online training - pass online theoretical exam - conduct and declare a self-practical training - pass a written exam at the CAA (or at recognized entity)	16*
3	< 25 kg	A3	- fly away from people - fly outside of urban area (150 m distance)	Yes	- read user's manual - complete online training - pass online theoretical exam	16*
4						
Privately built						
Legacy drones (art. 20)						

Each UAS of which the weight exceeds 120 grams or has onboard data recording equipment (i.e., camera) must be registered online first. In the following step, the UAS operators also must be registered together with their valid third-party liability insurance linked to their UAS at the Traffic Authority. The insurance must cover between 12-15 thousand EURO damage for a year (Légtér.hu Kft., n.d.) UAS operators must get the so-called flight licence and as a drone operator they get a unique registration number which is valid in all EASA (European Union Aviation Safety Agency) member state. This flight open category licence is available for those UAS's which are less than 25 kilograms of maximum take-off mass (MTOM), the maximum flight height is 120 meters from the above ground level (AGL), the UAS must remain in visual line of sight (VLOS) and the UAS cannot fly over assembly people and cannot transport dangerous materials and cannot spread any materials to the ground. This category contains A1-A3 and A2 subcategories with the difference in UAS weight, the minimum distance from and overfly time of uninvolved persons and the horizontal flight speed (Drónpilóták Országos Egyesülete, n.d.).

The competence exam is available and valid in every EU states. In Hungary, the Austrian A1-A3 exam is very popular as it is online and free.

After the fulfilment of the legislative background, the GoodID application for identification purposes and MyDroneSpace ny Hungarocontrol application right before flight must be used. UAS operators must ask for airspace usage permission for the exact time. The official administrative deadline for the permission is 30 days before flight but for special stakeholders there is a simplified procedure with 5 days lead time.

CONCLUSIONS

Monitoring physical or natural parameters in harsh environments (e.g., forests and wetlands) has several challenges, getting the collected data being one of the hardest one. Both individual data loggers or classic wireless sensor networks have major flaws. The former requires frequent physical access to the devices, while in case of the latter, communication is the main issue. In this paper, a novel data collection approach was presented, using drone technology. The system design with the sensor nodes' hardware, software, the communication protocol and the UAS technology was presented.

The measuring devices are similar to the nodes of a wireless sensor network, but instead of a continuously maintained mesh topology communication they use a direct connection to an infrequently appearing base station. The line of sight is provided by UAV technology, which, at the same time results in low path loss, high possible bandwidth, quick data transfer and consequently a longer lifetime.

Three different demonstrative examples with different data density were chosen to show the applicability of the proposed system.

The first scenario is general, where most useful application of the collected data is climate research. Either long-term data analysis or comparing different points in the same period would be interesting. The title of the second example can be misleading. Although the word "seismic" is related to the motion of tectonic plates, the vibrations, which can be detected by accelerometers are most likely caused by animals or vehicles. Monitoring both animal and (forbidden) vehicle activity can be interesting in such a protected area. The third measurement scenario is related to the monitoring of air pollution, the importance of which cannot be overstated. Since this system enables the simultaneous and long-term data collection, it may facilitate locating the sources.

REFERENCES

Adams, A, R Greenough, R Wallenberg, Ada Mendelovicz, and C Lumjiak (1974). "The Quadrifilar Helix Antenna." IEEE Transactions on Antennas and Propagation 22 (2): 173–78.

Belda M, Holtanová E, Halenka T, Kalvová J (2014) Climate classification revisited: from Köppen to Trewartha. Clim Res 59:1-13. https://doi.org/10.3354/cr01204

Cama, Alejandro, Francisco G Montoya, Julio Gómez, José Luis De La Cruz, and Francisco Manzano-Agugliaro (2013). "Integration of Communication Technologies in Sensor Networks to Monitor the Amazon Environment." *Journal of Cleaner Production* 59: 32–42.

Corke, Peter, Tim Wark, Raja Jurdak, Wen Hu, Philip Valencia, and Darren Moore (2010). "Environmental Wireless Sensor Networks." *Proceedings of the IEEE* 98 (11): 1903–17.

Drónpilóták Országos Egyesülete, n.d. https://www.doe.hu.

Ertürk, Mehmet Ali, Muhammed Ali Aydın, Muhammet Talha Büyükakkaşlar, and Hayrettin Evirgen (2019). "A Survey on LoRaWAN Architecture, Protocol and Technologies." *Future Internet* 11 (10): 216.

EUR-Lex - Access to European Union Law, n.d. https://eur-lex.europa.eu.

Légtér.hu Kft., n.d. https://www.legter.hu.

Loy, Matthew (2005). "ISM-Band and Short Range Device Regulatory Compliance Overview." In.

Martinez, Kirk, Royan Ong, and Jane Hart (2004). "Glacsweb: A Sensor Network for Hostile Environments." In 2004 First Annual IEEE Communications Society Conference on Sensor and Ad Hoc Communications and Networks, 2004. IEEE SECON 2004., 81–87. IEEE.

Martinez, Kirk, Paritosh Padhy, Alistair Riddoch, Royan Ong, and Jane Hart (2005). "Glacial Environment Monitoring Using Sensor Networks." In Proceedings of the Workshop on Real-World Wireless Sensor Networks (REALWSN'05), Stockholm, Sweden, 20–21. Citeseer.

Migabo, Emmanuel, Karim Djouani, Anish Kurien, and Thomas Olwal (2017). "A Comparative Survey Study on LPWA Networks: LoRa and NB-IoT." In Proceedings of the Future Technologies Conference (FTC), Vancouver, BC, Canada, 29–30.

Mitsch, W.J., Bernal, B., Nahlik, A.M. et al. (2013). Wetlands, carbon, and climate change. Landscape Ecol 28, 583–597. https://doi.org/10.1007/s10980-012-9758-8

Song, Wen-Zhan, Renjie Huang, Mingsen Xu, Andy Ma, Behrooz Shirazi, and Richard LaHusen (2009). "Air-Dropped Sensor Network for Real-Time High-Fidelity Volcano Monitoring." In Proceedings of the 7th International Conference on Mobile Systems, Applications, and Services, 305–18.

Sóstó Természetvédelmi Terület és Sóstó Látogatóközpont, n.d. https://www.sostoszekesfehervar.hu.

Udvardy, P, T Jancsó, and B Beszédes (2019). "3D Modelling by UAV Survey in a Church." In 2019 New Trends in Aviation Development (NTAD), 189–92. IEEE.

Vakulya, Gergely, and Gyula Simon (2013). "Low-Power Communication Protocol for Low Duty Cycle Data Acquisition Applications." In 2013 IEEE

International Workshop on Measurements & Networking (m&n), 58–62. IEEE.

Wark, Tim, Wen Hu, Peter Corke, Jonathan Hodge, Aila Keto, Ben Mackey, Glenn Foley, Pavan Sikka, and Michael Brunig (2008). Springbrook: Challenges in Developing a Long-Term, Rainforest Wireless Sensor Network. In 2008 International Conference on Intelligent Sensors, Sensor Networks and Information Processing, 599–604. IEEE.

Werner-Allen, Geoff, Konrad Lorincz, Jeff Johnson, Jonathan Lees, and Matt Welsh (2006). "Fidelity and Yield in a Volcano Monitoring Sensor Network." In Proceedings of the 7th Symposium on Operating Systems Design and Implementation, 381–9.

Scientific Papers. Series E. Land Reclamation, Earth Observation & Surveying, Environmental Engineering. Vol. XII, 2023
Print ISSN 2285-6064, CD-ROM ISSN 2285-6072, Online ISSN 2393-5138, ISSN-L 2285-6064

ADAPTATION STRATEGIES TO CLIMATE CHANGE WITH SUSTAINABLE IRRIGATION

Öner ÇETİN[1], Kıvanç Hayri DOĞANAY[1], Jovana BEZDAN[2]

[1]Dicle University, Faculty of Agriculture, Dept. of Agricultual Structures and Irrigation, Diyarbakır, Turkiye
[2]University of Novi Sad, Faculty of Agriculture, Department of Water Management, 21000, Novi Sad, Serbia

Corresponding author email: oner_cetin@yahoo.com

Abstract

Global warming and climate change are the biggest problems of the world today. Agricultural irrigation plays a very important role in both increasing production and reducing the potential risk of drought. However, excessive use of water in agriculture (>10 000 m^3 ha^{-1}), very low irrigation efficiency (35-50%) and the effect of climate change cause a rapid decrease in water resources.In adaptation to climate change, efficient use of water resources in agricultural production, irrigation water productivity (kg m^{-3}), economic productivity of water ($ m^{-3}), farmers' net income ($ ha^{-1}) and total water use (m^3ha^{-1}) should be considered for each irrigated area. Thus, both the farmers, the irrigation authority and the decision makers can choose to implement possible deficit irrigation strategies and/or the most effective water use strategies according to these parameters. Thus, the main categories might be identified under the sustainable resource management, water management, technological developments, farm management, and farm production practices. Adaptation strategies to climate change can be implemented, but the costs and benefits of these practices need to be well understood.

Key words*: climate change, irrigation, irrigation efficiency, sustainability, water productivity.*

INTRODUCTION

Global warming and climate change are the biggest problems of the world today. Climate change also accelerates more frequent and severe droughts, floods and extreme precipitation, melting of glaciers, reduction of groundwater and deterioration of water quality (Sidhu, 2022).

On the one hand, there is uncertainty about the effect of increasing CO_2 on plant physiology and its effects on agricultural production with climate change. Therefore, the impact of global climate change on agricultural production cannot be measured precisely at present (Gornall et al., 2010).

Agriculture is an important sector in arid and semi arid regions. The rain-fed crop systems are, thus, highly dependent on climatic conditions. For this reason, the rain-fed farming is sensitive to changes in precipitation and temperature that change or intensify due to global warming (Gornall et al., 2010; Rosa et al., 2020). Thus, climate change is expected to affect agriculture differently in different parts of the world and in different ecosystems (Olesen and Bindi 2002; Parry et al., 2004; Finger et al., 2011).

The most important sectors using water are agriculture, industry and domestic use. In the near future, both competition and water demand among these sectors will increase. Moreover, climate change will cause also increasing water demand (Bates et al., 2008; OcCC, 2007; 2008; Finger et al., 2011). Similarly, climate change will bring along many economic and social problems faced by water management in agricultural areas (IPCC, 2008; Iglesias & Garroteb, 2015).

On the other hand, water management in agriculture is very complex. Options in agricultural water management include a wide range of technical, economic, social and infrastructure factors (Iglesias & Garroteb, 2015).

Aforementioned negativities caused by climate change can only be met with adaptation and sustainable use of resources. It is, thus, inevitable to take some precautions or adaptation strategies to reduce the negative effects of climate change, especially on soil and water resources and agricultural production. In this article, the relationship between climate

change and irrigation and adaptation strategies to climate change are discussed.

CLIMATE CHANGE AND IRRIGATION

The increase in population also demands more food production. This gives irrigation an important role in increasing land use. For this reason, it is expected that irrigated agriculture will increase rapidly in the future to provide more production from irrigated agriculture since irrigation provides higher yields than rain-fed agriculture (Chartzoulakis & Bertaki, 2015).
On the other hand, the expansion of irrigation areas increases the pressure on global freshwater resources and often leads to their unsustainable use. In order to meet food needs in the future, it is necessary to adapt to climate and socio-economic changes as well as to manage sustainnably soil and water resources in arid and semi-arid regions (Harmanny & Malek, 2019). A majority of countries have a priority for adaptation in their climate change plans. For that reason, climate change adaptation strategies have over 80% were water-related (Sidhu, 2022).
Adaptation is needed to ensure the sustainability, resilience and reliability of soil and water resources in agriculture. Irrigation water demand and consumption are significantly affected by climate condition, irrigation system efficiency and crop type (Zhao & Boll, 2022).
Under climate projections, low water availability is a challenge water supply for agricultural activities. Clearly, new management strategies and water conservation are required to overcome the effects of climate change on agriculture, especially in arid and semi-arid regions. In this issue, adoption and adaptation are key factors. Adoption of innovative approaches for future uncertainties, supportive policies and financial support for stakeholders can be considered as preventive actions (Zhao & Boll, 2022).
As a result, food demand and safety will increase in the near future and these will become more complex. Increasing temperatures due to climate change will increase water demand in places where precipitation decreases. Therefore, more irrigation will be required for food security and a sustainable life. In connection with these issues, the effects of reduction in irrigation water requirements will be significant in the near future so that further water conservation should be considered at both a regional and global level (Turral et al., 2011).

ADAPTATION STRATEGIES TO CLIMATE CHANGE WITH IRRIGATION

The main user of fresh water resources on earth is globally the agriculture sector. Because irrigation significantly increases crop yield, water productivity (irrigation water use efficiency) and maximizing the farmer's economic return.
Agricultural irrigation plays a very important role in both increasing production and reducing the potential risk of drought. Irrigation can increase crop yield 1 to 5 times depending on crop variety, soil characteristics and other agricultural practices in arid and semi-arid regions although there are many different applications in adaptation strategies to climate change. On the other hand, increasing water demand for domestic and industrial use and environmental sustainability puts pressure on the irrigated agriculture sector.
Figure 1 shows the relationships between crop yield and irrigation water and other inputs. The farmers often aim to achieve maximum yield. This situation may require the use of excessive irrigation water (Figures 1 and 2). In this case, water use efficiency or irrigation water productivity decreases. Therefore, considering possible drought and decreasing water resources, the water-yield relationship of crops should be known so that irrigation water savings, yield and economic losses in possible irrigation water shortages can be known (Figure 1).

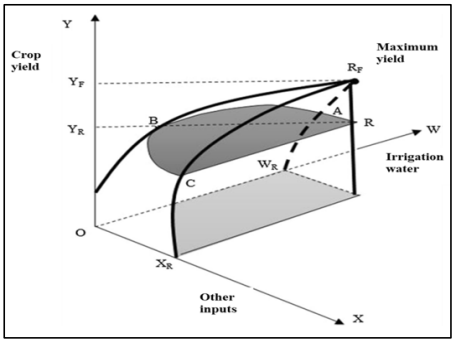

Figure 1. Relationships between crop yield and irrigation water together with other inputs
(Reinhard et al., 1999; Hong and Yabe, 2017)

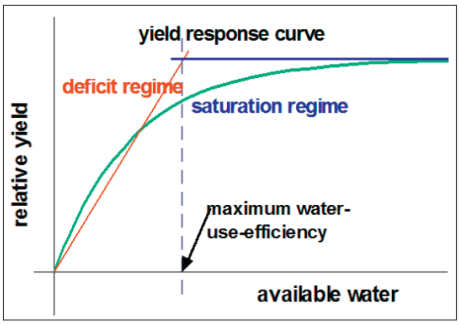

Figure 2. Yield response curve to irrigation (Chartzoulakis & Bertaki, 2015)

The most countries have considered importance to irrigation infrastructures and made significant investments in the 1980s. However, use of mainly surface irrigation methods and ignoring the necessary technical applications for this caused both excessive water use and environmental problems (salinity, alkalinity and drainage etc.). In the last quarter century, the use of pressurized irrigation systems (drip and sprinkler) has increased rapidly depending on the developing technologies. These systems, which are called modern irrigation systems, have provided water saving about 20-40%, an increase in yield and quality, and much less negative environmental effects (Çetin, 2019).

For our future, the most important way of good management of water used both in agriculture and for other purposes is its sustainable use. In addition, economic efficiency should be a priority in water use and soil conservation. As in the past, technological developments and innovation will continue to be critical factors.

Water is a physically scarce resource. This is particularly evident in North Africa, Central and Western Asia, and the Middle East. Moreover, the irrigation efficiency is quite low (35-50%) (SUEN, 2022). Existing water management systems have significant problems due to increasing water demand, complexity of regulations, and excessive consumption of resources. For this, sustainable management strategies based on environmental sustainability in the management of scarce resources should be applied.

In agricultural water use, increasing water use efficiency, increasing the quality and quantity of water source, and digitizing and optimizing localized water management processes on a large scale should be the main objectives. Some adaptation options, such as shifting sowing dates, can be implemented by farmers at no cost. In other options, the application of irrigation technologies requires a certain cost and, in this case, economy should be considered (Finger et al., 2011).

Three categories, infrastructure, management and agronomic issues, are important for adaptation and risk reduction (Iglesias and Garroteb, 2015).

Accordingly, sustainable water management requires appropriate allocation between competing water sector demands and balancing the financial and social resources needed to support the required water systems.

In addition, methods of evaluating water management practices should be, first, based on the complexity of the problem and the efficient and balanced use of resources for agricultural, urban and natural systems.

Varela-Ortega et al. (2016) stated that water availability may decrease and the impact of drought will be more visible in severe climate change projections. In this case, farmers will have to adapt to lower yields and lower incomes. For that reason, the various adaptation measures should be considered such as modern irrigation technologies and new crop varieties.

Some traditional and/or surface/flood irrigation methods are still the mostly used in most of counties, especially Middle East and Asian countries.

However, the modern irrigation systems (pressurized irrigation systems such as drip and sprinkler) have increased year by year. Because, these systems ensured higher irrigation efficiency, less water use, no water erosion and uniformity compared to surface irrigation methods. For this, the Turkish government has subsidized 50% of the total cost of pressurized irrigation systems for the farmers who want to use them.

One of the adaptation strategies is deficit irrigation (DI) which is a strategy for optimizing under yield reduction and some degree of water deficit conditions.

During deficit irrigation, crops are exposed to less amount of water required in a certain period or the throughout growing period. The main objective of DI is to water productivity of the

crop by eliminating irrigations that have little impact on yield.

Smart or precious irrigation can improve yield and water productivity and save irrigation water, consequently leading to improved food security for the increasing population (Bwambale et al., 2022).

Subsidization of pressurized irrigation systems by governments, if well controlled and used appropriately, is important for efficient and sustainable use of irrigation water. However, this subsidization should not adversely affect other less costly irrigation water-saving practices (Finger et al., 2011).

The problems and challenges in agricultural irrigation related to climate change and some solution suggestions are given in Table 1.

Table 1. Solutions and recommendations for climate change and irrigation related problems

Climate change and irrigation related problems	Solutions and recommendations
Drought	Drought resistant plant breeding, deficit irrigation
Water scarcity	Use of drip irrigation and treated waste water, water harvesting
Excessive water use	Pressurized irrigation systems, use of water based on volumetric measurement, smart irrigation, digitization, training,
Erosion in irrigation	Contour sowing-planting on sloping lands, use of pressure irrigation system (especially drip irrigation)
Monoculture	Polyculture
Evaporation from the soil	Mulching, subsurface drip irrigation
Salinity-Drainage	Prevention of excessive water use, installation of drainage systems
Inter-institutional cooperation	Increasing cooperation
Sanctions are insufficient	Imposing new regulations and sanctions
Lack of infrastructure	Improving irrigation infrastructures
Insufficient technical capacity	Increasing capacity building

CONCLUSIONS

Basic issues related to irrigation in adaptation to climate change are; to increase water use efficiency, water productivity and capacity building, reuse of marginal waters (reclaimed or brackish) for irrigation, regulation of water pricing, adoption of innovative irrigation techniques and wider and more effective participation. In addition, use of modern technologies such as smart irrigation and fertigation are also important. Extension and training should be also associated with other factors and applications.

In adaptation to drought and climate change, efficient use of water resources in agricultural production, irrigation water productivity (kg m^{-3}), economic productivity of water ($ m^{-3}), farmers' net income ($ ha^{-1}) and total water use (m^3 ha^{-1}) should be calculated and considered for each region and all these data and recommendations should be presented to users as a guidebook. Thus, both the farmer, the irrigation authority and the decision makers can choose to implement possible deficit irrigation strategies and/or the most effective water use strategies according to these parameters.

The use and dissemination of these modern irrigation systems have been necessary for the sustainable use of water resources, which are declining due to the increasing population demand and climate change. However, in sustainable water use and adaptation to climate change, besides the use of modern irrigation systems, effective and continuous management, raising awareness among users, education and support policies are at least as important. In addition, purification and reuse of domestic wastewater and water harvesting are also important in this respect.

As a result, Harmanny & Malek (2019) identified some main adaptation categories such as farm production practices, water management, sustainable resource management, technological developments, and farm management strategies. The results showed that farmers have greater potential to adapt in rural areas where have low rainfall and high temperature. This is evidence that the socio-economic effects of adaptation strategies may also be different as spatial. On the other hand, adaptation strategies to climate change can be implemented, but the costs and benefits of these

practices need to be well understood (Sidhu, 2022).

REFERENCES

Bates, B.C., Kundzewicz, Z.W., Wu, S., Palutikof, J.P. (2008). Climate change and water. *Technical paper of the Intergovernmental Panel on Climate Change. IPCC Secretariat*, Geneva, 210.

Bwambale, E., Abagale, F.K., Anornu, G.K. (2022). *Smart Irrigation for Climate Change Adaptation and Improved Food Security,* doi: 10.5772/intechopen.106628, from https://www.intechopen.com/online-first/83182.

Çetin, Ö. (2019). Sustainable water saving and water productivity using different irrigation systems for cotton production. *In Proceedings of 3rd World Irrigation Forum*, 1-7 September 2019, Bali, Indonesia, ST-1-3, W.1.3.31.

Chartzoulakis, K., Maria Bertaki, M. (2015). Sustainable water management in agriculture under climate change. *Agriculture and Agricultural Science Procedia, 4.* 88–98. doi: 10.1016/j.aaspro.2015.03.011,

Finger, R., Hediger, W., Stéphanie-Schmid, S. (2011). Irrigation as adaptation strategy to climate change—a biophysical and economic appraisal for Swiss maize production. *Climatic Change, 105*, 509–528. doi: 10.1007/s10584-010-9931-5.

Gornall, J., Betts, R., Burke, E., Clark, R., Camp, J., Willett, K., Wiltshire, A. (2010). Implications of climate change for agricultural productivity in the early twenty-first century. *Philosophical Transactions of the Royal Society of London. Series B, Biological Sciences, 365*, 2973–2989. doi:10.1098/rstb.2010.0158.

Harmanny, K.S., Malek, Z. (2019). Adaptations in irrigated agriculture in the Mediterranean region: an overview and spatial analysis of implemented strategies. *Regional Environmental Change, 19*, 1401–1416. doi:10.1007/s10113-019-01494-8.

Hong, N.B., Mitsuyasu Yabe, M. (2017). Improvement in irrigation water use efficiency: a strategy for climate change adaptation and sustainable development of Vietnamese tea production. *Environment, Development and Sustainability, 19*, 247–1263. doi: 10.1007/s10668-016-9793-8.

Iglesias, A., Garroteb, L. (2018). Adaptation strategies for agricultural water management under climate change in Europe. *Agricultural Water Management, 15*, 113–124. doi: 10.1016/j.agwat.2015.03.014.

IPCC (2008). *Technical Paper on Climate Change and Water*, June 2008. IPCC, Cambridge, United Kingdom/New York, NY, USA.

Molle, F., Mollinga, P.P., Wester, P. (2009). Hydraulic bureaucracies and the hydraulic mission: Flows of water, flows of power. *Water Alternatives, 2*(3), 328-349.

OcCC (2007). *Klimaänderung und die Schweiz* 2050. OcCC-Organe consultatif sur les changements climatiques, Bern.

OcCC (2008). *Das Klima ändert-was nun?* Der neue UN-Klimabericht (IPCC 2007) und die wichtigsten Ergebnisse aus Sicht der Schweiz.

Olesen, J.E., & Bindi, M. (2002). Consequences of climate change for European agricultural productivity, land use and policy. *European Journal of Agronomy, 16*, 239–262.

Parry, M.L., Rosenzweig, C., Iglesias, A., Livermore, M., Fischer, G. (2004). Effects of climate change on global food production under SRES emissions and socio-economic scenarios. *Global Environmental Change, 14*, 53–67.

Reinhard, S., Lovell, C.A.K., Thijssen, G. (1999). Econometric estimation of technical and environmental efficiency: An application to Dutch dairy farms. *American Journal of Agricultural Economics, 81*(1), 44-60.

Rosa, L., Chiarelli, D.D., Sangiorgio, M., Beltran-Peña, A.A., Rulli, M.C., D'Odorico, P., Inez Funga, I. (2020). Potential for sustainable irrigation expansion in a 3 °C warmer climate. *Proceedings of the National Academy of Sciences of the United States of America*, 117:47, 29526 - 29534, from www.pnas.org/cgi/doi/10.1073/pnas.2017796117.

Sidhu, B.S. (2022). *Half the world is facing water scarcity, floods and dirty water - Large Investments Are Needed for Effective Solutions*. IPCC REPORT, from https://www.preventionweb.net/news/ipcc-report-half-world-facing-water-scarcity-floods-and-dirty-water-large-investments-are.

SUEN (2022). *Improving agricultural water use efficiency and productivity in the Middle East: Pressures, status, impacts and responses*. Lead Author: M. Kay. Contributed authors: Ö. Çetin, G. Çapar, Y. Ahi, T. Pilevneli. Turkish Water Institute (SUEN), ISBN: 978-625-8451-33-7.

Turral, H., Burke, J., Faurès, J.M. (2011). *Climate change, waterand food security*. Food And Agriculture Organization of The United Nations, Rome.

Varela-Ortega, C., Blanco-Gutie´rrez, I.., Esteve, P., Bharwani, S., Fronzek, S., Thomas, E. (2016). How can irrigated agriculture adapt to climate change? Insights from the Guadiana Basin in Spain. *Regional Environmental Change*, *16*, 59–70, doi: 10.1007/s10113-014-0720-y.

Zhao, M., & Boll, J. (2022). *Adaptation of water resources management under climate change. Frontiers in Water* 4:983228. 1-21, doi: 10.3389/frwa.2022.983228.

Scientific Papers. Series E. Land Reclamation, Earth Observation & Surveying, Environmental Engineering. Vol. XII, 2023
Print ISSN 2285-6064, CD-ROM ISSN 2285-6072, Online ISSN 2393-5138, ISSN-L 2285-6064

THE SOIL FERTILITY IMPROVEMENT OF THE MARGINAL LANDS DEPENDING ON KIND OF AMENDMENTS

Mykola KHARYTONOV[1], Mykhailo BABENKO[1], Nadia MARTYNOVA[2]

[1]Dnipro State Agrarian and Economic University, 25 Seghii Yefremov Street, Dnipro, Ukraine
[2]Dnipro National University, 72 Gagarin Avenue, Dnipro, Ukraine

Corresponding author email: kharytonov.m.m@dsau.dp.ua

Abstract

The major goal of this case study was to estimate the impact of two soil amendments on soil fertility, grain crops yield, and quality. The greatest effect of increasing sweet sorghum biomass produced in loess like loam has been obtained using sewage sludge (SS) at the rate of 80t/ha. Such a reaction has become appropriate to the introduction of nutrients into the "young" soil. The SS applying by rate of 60 t/ha had little effect on the increase in the content of zinc and copper in sunflower seeds in the experiment managed on black soil. Trace concentrations of lead and cadmium are recorded. The addition of vermicompost and a solid fraction of digestate at a rate of 40 t/ha led to an increase in the corn grain yield obtained on black soil at the 20.1 and 35.0%, respectively. The greater starting effect on urease activity was recorded from the introduction of vermicompost compared to the solid fraction of the digestate. The application of the solid fraction of the digestate had a positive effect on the activity of phosphatase in the topsoil in the first part of the season of vegetation.

Key words*: amendments, crops yield, heavy metals, marginal land, soil fertility.*

INTRODUCTION

Increasing urbanization has led to a dramatic rise in the amount of wastewater generated globally (Wang et al., 2008). In the European Union the policy framework for wastewater management is based on the Water Framework and the Urban Waste water Treatment Directives (EC., 1991; Directive 2000/60/EC, 2000). The use of biosolids for fertilizer manufacture can decrease sewage sludge disposal costs and reduce reliance on mineral fertilizers (Mtshali et al., 2014). The Circular Economy principle can be implemented in the wastewater sector aiming at a green and eco-efficient community, by reusing and cycling materials and creating a "closed loop" approach (Sandu & Virsta, 2021). The sludge from municipal wastewater processing includes compounds of agrochemical value (nitrogen, potassium, phosphorus, organic matter and small quantities of magnesium, calcium, and sulphur) as well as pollutants, including heavy metals, pathogens, and toxic organic substances (Iticescu et al., 2021). According to Amir et al. (2010), sewage sludge is "rich in aliphatic and aromatic acids, polysaccharides, proteinaceous material, and organic sulfonates". In agricultural soils, it is necessary to treat sewage sludge with a blend of dolomite and calcite to increase the pH and prevent it from falling. Such countries as France, Belgium, Denmark, Ireland, UK, and Sweden use from 35 to 60% of the collected sewage sludge directly on agricultural land (Maisonnave et al, 2002; Bondarczuk et al., 2016; Ekane et al., 2021). It was shown that a 25 t/ha sewage sludge application rate provided the highest productivity of the wheat crop, while Cd and Pb concentration levels in soil and wheat grains were below the maximum values allowed by regulation (Cocarta et al., 2017). Maximum maize grain yield was achieved when the soil was fertilized with 60 t/ha of slurry incorporation (Elsalam et al., 2021). It was recommended that application of 37.5 t/ha of dewatered with calcium oxide sewage sludge can be repeated each two years to get best corn yield in low fertile soil (Delıbacak & Ongun, 2016). It should be taken into consideration that 20, 10 and 5% of the organic N in the sewage sludge is mineralized in the first, second and

third year respectively (Gilmour & Skinner, 1999). It was showed also that sewage sludge application 80 t/ ha yielded even higher than those obtained with the equivalent NPK rate applied as chemical fertilizer (Khan et al., 2007). The recommendable rate is 40 t/ ha to avoid the possible risk of metals uptake and accumulation in the soil.

Large volumes of manure applied directly to the soil as fertilizer cause odor releases and soil pathogen contamination. (Ogunwande et al., 2008; Mortola et al., 2019). It was estimated that up to 1.0 billion tons of manure from chickens, whereas pigs and cattle were produced every year between 2016 and 2019. within EU-27 countries (Kovacic et al., 2022). This is why the Nitrates Directive has set a limit of 170 kg/ha/year of N from organic manure, to give farmers exemptions if manure disposal does not harm ecosystems.

The digestate is a by-product remaining after the anaerobic digestion of biodegradable feedstock (Simon et al., 2015). Recycling organic matter and nutrients from digestate back into the soil is seen as a low-cost means of disposal and nutrient recovery for agricultural systems. (Alburquerque et al., 2012).

The digester and media (soil) interaction overlap the larger yield variations induced by differences in composition between digestates (Hafner et al., 2022). Increased concentrations of Cu, Zn and Mn in digestates resulting from co-digestion of pig and cattle manure raw materials endanger the sustainability of agricultural soils after repeated applications (Nkoa, 2014).

Nitrogen use efficiency improved for chicken manure digestate and cow manure digestate compared to the first year of implementation (Doyeni et al., 2021). The application of digestate as an organic nutrient versus granulated chicken manure led to positive effects (Soleymani et al., 2022). Chicken manure demonstrated the highest increase in soil P content among the other manure types (Afriyie et al., 2013). At the same time, the dry fermented digestate vermicompost raised the soil pH and consequently turned the soil much more basic than manure and cow dung.

The major goal of this study was to estimate the impact of two soil amendments on soil fertility, grain crops yield and quality.

MATERIALS AND METHODS

Field experiments on determining the reaction of maize, sunflower and sweet sorghum (Medovy hybrid) were laid in the spring of 2021 at the DDAU research station to determine the effect of the treated with a flocculant municipal sewage sludge (MSS).

Experiments with sunflower (SUR variety) and maize (Duncan hybrid) were laid on two types of soils: black soil and phytomeliolated loess like- loam. Sweet sorghum reaction on sewage sludge application was determined only on the phytomeliorated loess like - loam. Otherwise, the option of experiment with phytomeliorated loess like - loam can be equated with an eroded soil, which has a lower transitional horizon. The humus content in the black soil was 3%, in the phytomeliorated loess like - loam -1.3%. That is why in the experiment on the phytomeliorated loess like - loam, two doses of MSS (40 and 80 ton/ha) were brought under three grain crops.

The dose of sewage sludge 60 ton/ha in the experiments on the black soil was recognized as maximum, referring to the amount of humus more than 2 times.

The effect of vermicompost and the solid fraction of digestate on maize at a dose of 40 t/ha has been investigated. Solid fraction of poultry litter digestate was obtained from MHP Oril-Leader farm situated in Dnipropetrovsk province in the south-eastern part of Ukraine. Preparation of plant samples for chemical analysis was made by conventional methods. Analysis of concentrations of heavy metals was performed by the method of atomic absorption spectrophotometry. Soil enzymes (urease and phosphatase) activity was determined for 2 pooled depths: 0-20, 20-40 cm.

The results obtained were processed by statistical methods at a significance level 95%.

RESULTS AND DISCUSSIONS

The accounting data of field experiments obtained on plots with a phytomeliorated loess like loam to determine the impact of sewage sludge application (at rates 40 and 80 t/ha) on the yield of sweet sorghum and maize are shown in Figure1.

Adding sewage sludge at doses of 40 and 80t/ha led to an increase in maize grain yield by 18.6 and 31.1% and sweet sorghum - by 34.80% and 56.50%.

The results of determining the impact of the introduction of two doses of SS on the productivity of aboveground biomass of sweet sorghum and maize are shown in Figure 2.

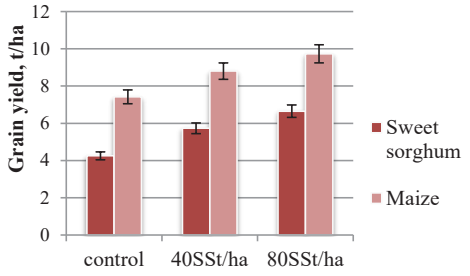

Figure 1. Sweet sorghum and maize grain yield in an experiment with sewage sludge made on a phytomeliolated LLL

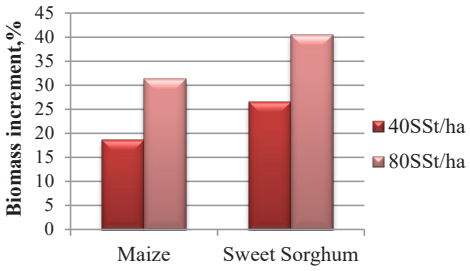

Figure 2. Sweet sorghum and maize biomass increment in an experiment with sewage sludge settled on a phytomeliorated LLL

The greatest effect of increasing sweet sorghum biomass obtained from the addition of sewage sludge has obtained at the rate of 80 t/ha. Such a reaction has become appropriate to the introduction of nutrients into the "young" soil (Shewangizaw et al., 2018).

The accounting data of the field experiments managed to determine the effect of sewage sludge application in black soil at doses of 60t/ha on maize and sunflower seeds yield are shown in Figure 3.

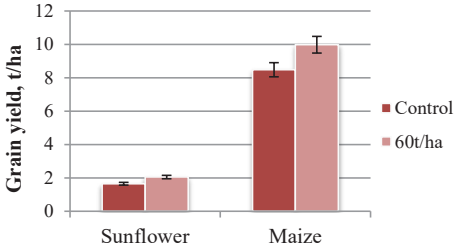

Figure 3. Sunflower and maize grain yield in an experiment with sewage sludge laid on black soil

It is obviously that sewage sludge impact on maize in dose 60t/ha inferior to the results obtained in the experiment with the introduction of 80 t/ha to the LLL.

The results of determining the content of four heavy metals in the grain, leaves and stems of maize in the field experiment with SS added to LLL are shown in the Figures 4 to 7.

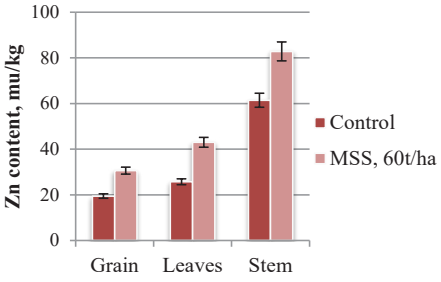

Figure 4. Zinc content in grain, leaf and stem of maize in experiment with the introduction of sewage sludge into LLL

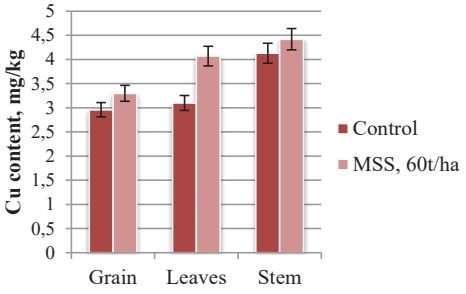

Figure 5. Copper content in grain, leaf and stem of maize in experiment with the introduction of sewage sludge into LLL

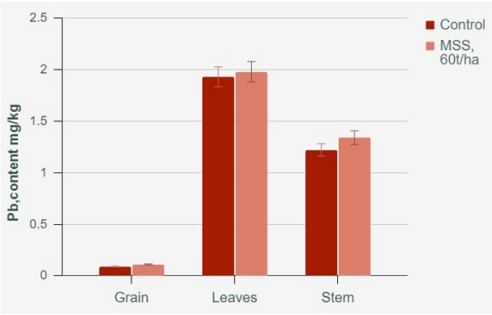

Figure 6. Lead content in grain, leaf and stem of maize in experiment with the introduction of sewage sludge into LLL

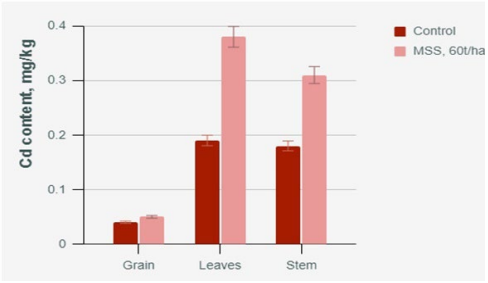

Figure 7. Cadmium content in grain, leaf and stem of maize in experiment with the introduction of sewage sludge into LLL

The results of the evaluation of the content of heavy metals in sunflower seeds in the field experiment with sewage sludge are shown in Figure 8.

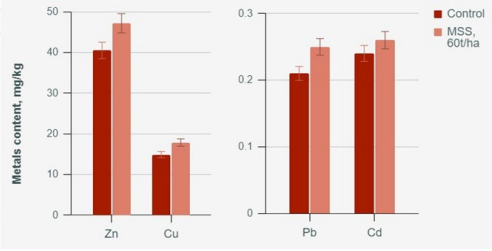

Figure 8. The content of Zn, Cu, Pb and Cd in sunflower grain in experiment with 60t/ha of MSS laid on black soil

The MSS applying by rate of 60 t/ha had little effect on the increase in the content of zinc and copper in sunflower grains in the experiment managed on black soil.

Trace content of lead and cadmium are recorded.The data obtained can be explained with black soil high level buffer capacity to the heavy metals (Kharytonov et al., 2007).

The addition of vermicompost and solid fraction of digestate at a dose of 40 t/ha led to an increase in the of maize grain yield obtained on black soil up to 20.1 and 35.0%, respectively (Figure 9).

The dynamics of two soil enzymes (urease and phosphatase) activity depending on kind and rate of soil amendment (digestat and vermicompost) are shown in Figures 10 to 13.

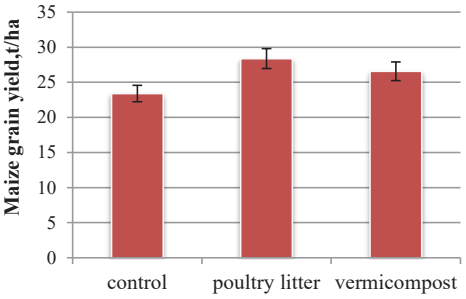

Figure 9. Maize grain yield in experiment with digestat and vermicompost laid on black soil

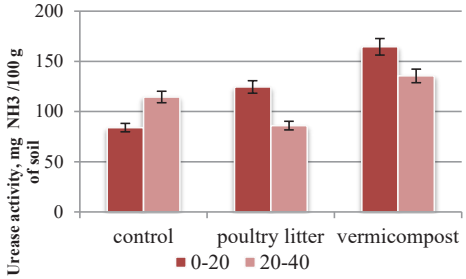

Figure 10. Urease activity in top and subsoil in June

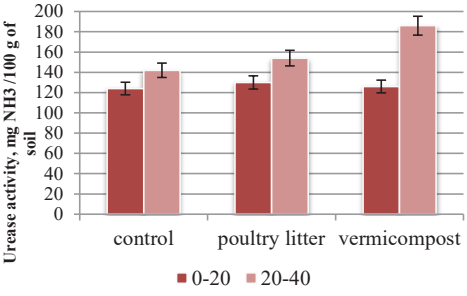

Figure 11. Urease activity in top and subsoil in September

The greater starting effect on urease activity was recorded after the introduction of

vermicompost compared to the solid fraction of the digestate.

The application of the solid fraction of the digestate had a positive effect on the activity of phosphatase in the topsoil in June.

It was fixed low impact of the emissions of CO_2 and CH_4 from the field fertilized with digestate from biogas plant on total emission from agriculture (Czubaszek & Wysocka-Czubaszek, 2018).

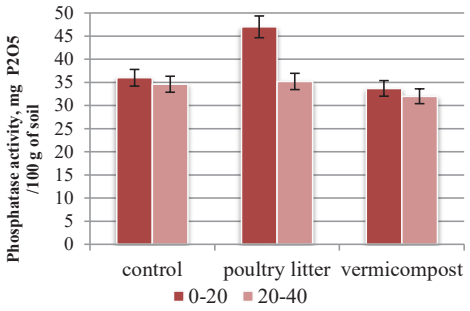

Figure 12. Phosphatase activity in top and subsoil in June

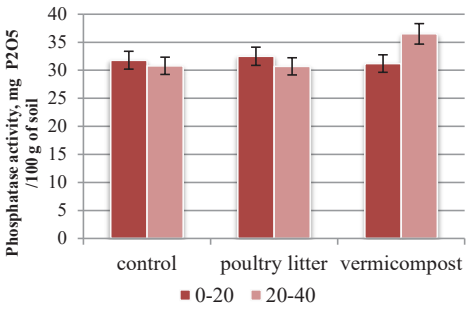

Figure 13. Phosphatase activity in top and subsoil in September

There are prospects to cultivate maize and (or) sweet sorghum as biomass for anaerobic treatment in biogas complexes and to continue restore low organic marginal lands by adding organic matter and facilitating microbial activity. Municipal sewage sludge can be used also as soil amendment to get high grain crops yields for bioethanol production (Kharytonov et al., 2019).

The possibility of municipal and agri-waste nutrients applying as fertilizer could become an alternative to the use of conventional fertilizers after forthcoming ecotoxicological and hygienic investigations.

CONCLUSIONS

The MSS applying by rate of 60 t/ha had little effect on the increase in the content of zinc and copper in sunflower grains in the experiment managed on black soil.

Trace concentrations of lead and cadmium are recorded in seeds. The addition of vermicompost and solid fraction of digestate at a rate of 40 t/ha led to an increase in the maize grain yield obtained on black soil at the 20.1 and 35.0%, respectively. The greater starting effect on urease activity was recorded from the introduction of vermicompost compared to the solid fraction of the digestate. The application of the solid fraction of the digestate had a positive effect on the activity of phosphatase in the topsoil in first part of season of vegetation.

ACKNOWLEDGEMENTS

This research work was carried out with the support of Ministry of Education and Science of Ukraine

REFERENCES

Alburquerquea, J.A., de la Fuente, C., Campoy, M., Carrasco, L., Nájera, I., Baixauli, C., Caravaca, F., Roldán, A., Cegarra, J., Bernal, M.P. (2012). Agricultural use of digestate for horticultural crop production and improvement of soil properties. *Eur. J. Agron. 43*, 119–128.

Amir, S., Jouraiphy, A., Meddich, A., El Gharous, M., Winterton, P., Hafidi, M. (2010). Structural study of humic acids during composting of activated sludge-green waste. *Elemental analysis, FTIR and 13C NMR. J. Hazard. Mater. 177*, 524–529.

Baize, D. (2009). Cadmium in soils and cereal grains after sewage-sludge application on French soils. A review. *Agron. Sustain. Dev., 29,* 175–184.

Bondarczuk, K.; Markowicz, A.; Piotrowska-Seget, Z. (2016) The urgent need for risk assessment on the antibiotic resistance spread via sewage sludge land application. *Environ. Int., 87*, 49–55.

Bozkurt, M.A., Akdeniz, H., Keskin, B., Yilmaz, I.H. (2006). Possibilities of using sewage sludge as nitrogen fertilizer for maize, *Acta Agriculturae Scandinavica Section B-Soil and Plant Science*, *56*(2), 143-149. doi: 10.1080/0906471051003113.

Cocarta, D.M., Subtirelu, V.R., Badea, A. (2017). Effect of sewage sludge application on wheat crop productivity and heavy metal accumulation in soil and wheat grain. Environmental *Engineering and Management Journal*, *16*(5), 1093-1100, from http://omicron.ch.tuiasi.ro/EEMJ/.

Czubaszek, R., Wysocka-Czubaszek, A. (2018). Emissions of carbon dioxide and methane from fields fertilized with digestate from an agricultural biogas plant. *Int. Agrophys*., *32*(1), 29-37, from https://doi.org/10.1515/intag-2016-0087.

Delıbacak, S. and Ongun, A.R. (2016). Influence of treated sewage sludge applications on corn and succeeding wheat yield and on some properties of sandy clay soil. *Turkish Journal Of Field Crops*, *21*(1), 1-9. doi: 10.17557/tjfc.88475.

Directive 2000/60/EC of the European Parliament and of the Council of 23 October 2000 Establishing a European Commission, (1991). Council Directive of 21 May 1991 concerning urban waste water treatment. *Off. J. Eur. Communities, 135*, 40–52.

Doyeni, M.O., Stulpinaite, U., Baksinskaite, A., Suproniene, S., Tilvikiene, V. (2021). The Effectiveness of Digestate Use for Fertilization in an Agricultural Cropping System. *Plants 10*, 1734, from https://doi.org/ 10.3390/plants10081734.

Ekane, N, Barquet, K., Rosemarin, A. (2021). Resources and Risks: Perceptions on the Application of Sewage Sludge on Agricultural Land in Sweden, a Case Study. *Front. Sustain. Food Syst*., 5:647780. doi: 10.3389/fsufs.2021.647780.

Elsalam, H.E.A., El Sharnouby, M.E., Mohamed, A.E., Raafat, B.M., El-Gamal, E.H. (2021). Effect of Sewage Sludge Compost Usage on Corn and Faba Bean Growth, Carbon and Nitrogen Forms in Plants and Soil. *Agronomy, 11*, 628, from https:// doi.org/10.3390/agronomy11040628.

Framework for Community Action in the Field of Water Policy. Off. J. Eur. *Union* 2000, *327*, 1–73.

Gilmour, J.T., Skinner, V. (1999). Predicting Plant Available Nitrogen in Land-Applied *Biosolids. Journal of Environmental Quality, 28*(4), 1122-1126, from https://doi.org/10.2134/jeq1999.00472425002800040010x.

Hafner, F., Hartung, J., Moller, K. (2022). Digestate Composition Affecting N Fertiliser Value and C Mineralisation. *Waste and biomass valorization, 13*, no. 8: 3445-3462. doi: 10.1007/s12649-022-01723-y.

Iticescu, C., Georgescu, P.-L., Arseni, M., Rosu, A., Timofti, M., Carp, G., Cioca, L.-I. (2021). Optimal Solutions for the Use of Sewage Sludge on Agricultural Lands. Water, *13*, 585, form https://doi.org/ 10.3390/w13050585.

Kharytonov, M., Martynova, N., Babenko, M., Rula, I., Sytnyk, S., Bagorka, M., Gavryushenko, O. (2019). Bioenergetic assesment of sweet sorghum grown on reclaimed lands. *Acta Technica Corviniensis-Bulletin of Engineering*., *12*(3), 89-92.

Kharytonov, M.M., Kroik, A.A., Shupranova, L.V. (2007). Steppe Soils Buffer Capacity and the Multipollution Impact of Industrial Enterprises in Ukraine. In: Mothersill, C., Mosse, I., Seymour, C. (eds) Multiple Stressors: A Challenge for the Future. NATO *Science for Peace and Security Series. Springer, Dordrecht. Chapter 27*, 373-380, from https://doi.org/10.1007/978-1-4020-6335-0_27.

Kovacic, D., Loncaric, Z., Jovic J., Samac D., Popovic, B., Tisma M. (2022). Digestate Management and Processing Practices: A Review. *Appl. Sci*., *12*, 9216, from https:// doi.org/10.3390/app12189216.

Maisonnave, V., Montrejaud-Vignoles, M., Bonnin, C., Revel, J.C. (2002). Impact on crops, plants and soils of metal trace elements transfer and flux, after spreading of fertilizers and biosolids, *Water Sci. Technol*., *46*, 217– 224.

Mortola, N., Romaniuk, R., Cosentino, V., Eiza, M., Carfagno, P., Rizzo, P., Bres, P., Riera, N., Roba, M., Butti, M., Sainz, D., Brutti , L. (2019). Potential use of a poultry manure digestate as a biofertiliser: Evaluation of soil properties and *Lactuca sativa* growth. *Pedosphere*. *29*(1), 60–69.

Mtshali, J.S., Tiruneh, A.T., Fadiran, A.O. (2014). Characterization of Sewage Sludge Generated from Wastewater Treatment Plants in Swaziland in Relation to Agricultural Uses, *Resources and Environment*, *4*(4), 190-199. doi: 10.5923/j.re.20140404.02.

Nkoa, R. (2014). Agricultural benefits and environmental risks of soil fertilization with anaerobic digestates: a review. *Agronomy for Sustainable Development*, *34*(2), 473-492. ff10.1007/s13593- 013-0196-zff. ffhal-01234816.

Ozyazici, M.A., (2013). Effects of sewage sludge on the yield of plants in the rotation system of wheat-white head cabbage-tomato. Eurasian J. *Soil Sci*., *2*(1), 35-44.

Sandu, M.A. & Virsta, A. (2021). The water footprint in context of circular economy. *AgroLife Scientific Journal*, *10*(2), 170-177.

Shewangizaw, B. (2022). Yield response of barley to the application of mineral fertilizers containing major nutrients on Cambisols and Vertisols in Ethiopia. *Experimental Agriculture*, *58,* E1. doi:10.1017/S0014479721000223.

Simon, T., Kunzova, E., Friedlova, M. (2015). The effect of digestate, cattle slurry and mineral fertilization on the winter wheat yield and soil quality parameters. *Plant Soil Environ*., 61(11), 522–527. doi: 10.17221/530/2015-PSE.

Soleymani, M., Mirzaii, A., Bahrami, H., Masir, M.N. (2022). Study of the Use of Chicken Manure Digestate as Organic Fertilizer in Comparison with Fresh Chicken Manure. *Biomechanism and Bioenergy Research*, *1*(1), 47-54.

Wang X, Chen T, Ge Y, Jia Y. (2008). Studies on land application of sewage sludge and its limiting factors. *J Hazard Mater*., 1*60*(2-3), 554-8. doi: 10.1016/j.jhazmat.2008.03.046

Scientific Papers. Series E. Land Reclamation, Earth Observation & Surveying, Environmental Engineering. Vol. XII, 2023
Print ISSN 2285-6064, CD-ROM ISSN 2285-6072, Online ISSN 2393-5138, ISSN-L 2285-6064

THE POSSIBILITY OF ESTABLISHING A GOJI CULTURE AND ITS EFFICIENCY THROUGH ADAPTATION TO THE PEDOCLIMATIC CONDITIONS OF GORJ COUNTY

Irina-Ramona PECINGINA, Roxana-Gabriela POPA

"Constantin Brancusi" University of Targu Jiu, 30 Eroilor Street,
Targu Jiu, Gorj, Romania

Corresponding author email: pecingina2016@gmail.com

Abstract

In the current agro-economic context, for the rural development of Gorj County, it is important to identify new, attractive, but also economically efficient businesses. Starting from the fact that the interest in Goji fruits has increased significantly, along with their use in organic food and in traditional medicine, and the adaptation of this shrub to the pedoclimatic conditions in Gorj County, if the culture technology is respected, this study present the possibility of establishment and capitalization of a culture that is not specific to the area, but which, through its characteristics, can adapt to the pedoclimatic conditions in Gorj County. Following the economic analysis, it is demonstrated that this business has a positive impact on the sustainable development of the rural area of Gorj County, on the economy, on the social life and on the environment, by capitalizing of agricultural land, creating jobs, promoting the area and increasing the income of entrepreneurs.

Key words*: culture, economic efficiency, Goji.*

INTRODUCTION

Goji berries have been known for over 2000 years, but interest in them has increased significantly with their use in organic food and traditional medicine due to their antioxidant content.

Goji shrub has the advantage, being not pretentious to environmental conditions, it adapts easily, but it is preferable to plant it in a sunny place and with enough space to grow.

The growth of the goji plant does not involve difficulties, resisting low temperatures of -25°C in the first two years and of -30°C in the following years, as well as to peaks of up to +40°C. (Bordes, 2008; Kourdi, 2011).

Goji has the scientific name *Lycium chinese* and *Lycium barbarum*, being a shrub of the *Solanaceae* family, originally from Tibet, belonging to the same family as tomatoes, potatoes and eggplants.

Both species produce many ellipsoidal fruits with a bright red-orange colour.

The flowers are small, purple in colour and appear in the summer between june and september (Babuc, 2012; Sharamon, 2009) (Figure 1).

Figure 1. *Lycium barbarum*

The composition of dried goji berries/100 *g* is as follows:

- energy 1461 kJ (17%);
- protein 12.1 g (24% more than cereals);
- carbohydrates 57.82 g (60%);
- fat 0.73 g (1%);
- fibres 7.78 g (43%);
- vitamin C (400 times more than oranges);
- vitamins A (role in improving vision), B1 (thiamine), B2 (riboflavin), B3, B6 (necessary for the biochemical processes of

transforming food into energy, helps metabolism), B12, E (prevents the occurrence and evolution of atherosclerosis) (Şengün & Kadakal, 2021);

- different amino-acids (L-glutamine and L-arginine, important in improving growth hormone levels and gluten, important in the fight against free radicals, which turn in the body into gluten peroxidase, a very powerful antioxidant);
- 21 minerals (Ca, P, Zn, K);
- 21 microelements (Fe, Mg, K, With, like, P, Zn, Ge, Se);
- antioxidants (goji berries are the most effective fruits);
- 29 fatty acids;
- beta carotene (can be compared with carrots, antioxidant and sun-protective effect);
- phytonutrients;
- betaine (beneficial in depression and anxiety; protects the liver), zeaxanthin (with protective effect on the retina), beta-sitosterol (treating impotence and prostate diseases; anti-inflammatory effect and significant role in lowering cholesterol levels), physalin (active compound that fights the main forms of leukaemia), lutein (regeneration of DNA and all body cells; antiviral effect), solavetivone (strong antifungal and antibacterial effect), cyperone (in cases of cervical cancer; blood pressure control), anthocyanins and saccharides (Donno et al., 2015).

The aspects for which account is taken in setting up a Goji culture are as follows:

- soil type (sandy, calcimorphic, luteous or brown soils);
- soil pH = 7.1-7.5;
- soil fertility (to determine the level and type of fertilizers and the fertilization plan);
- timing of the plantation care work;
- technology of culture;
- possibility of accessing European funds to cover part of the expenses (since 2018, the goji culture is eligible for financing with European funds);
- geographical area in which the plantation is established (on flat or sloping land, with rows oriented on the level curves);
- location in an area with at least 8 hours of sun/day, because the goji plant develops best in the presence of the sun (avoiding shady areas or with too much moisture);
- establish an efficient irrigation system (to increase the yield of goji berry crop and plant resistance);
- surrounding the area (to ensure and prevent investment safety issues);
- market insurance (in Romania there is only one collection centre for the members of the association).

Goji blooms at the earliest in May and bears fruit between June and November, with buds, flowers, green fruits and ripe fruits on the same branch. (Kulczyński & Gramza-Michałowska, 2016).

Production of 2-3 kg/plant occurs in plants over 3 years of age. The bearing fruit period of Goji berries in plants obtained from seeds is after 2-3 years, but from cuttings, from the first year. For a production-efficient, qualitative and quantitative culture with high yields, emphasis is placed on spraying, watering, cutting, fertilizer use and pesticide use. Cutting and structuring the shrub is paramount for the appearance, development and qualitative and quantitative production. The traditional way of shaping Goji shrub is in the form and structure of canopy, through which the sun and wind can pass, on 1, 2 or 3 floors. In this regard, cutting is done in winter or early spring, when the plant is in the vegetative rest period (Koçyiğit & Sanlier, 2017) (Figure 2).

Figure 2. Cutting the Goji shrub

MATERIALS AND METHODS

In order to highlight the economic efficiency regarding the establishment and capitalization of a Goji plantation in Gorj County, a plot with

an area of 7,100 m^2 was identified, in the extra village area, with the category of arable use. Regardless of the planting scheme applied, it is taken into account that the goji shrub needs a distance between plants of minimum 1.5 m in order to develop well, and the compliance with the recommendations contained in the goji shrub cultivation technology leads to an increase in the quality and quantity of production.

The technology for the establishment and cultivation of Goji berries is based on the following steps:

Land choosing

- the soil related to the land intended for the establishment of the Goji plantation must comply with the following conditions: good fertility, medium texture, clayey, sandy or loamy soil, permeable, pH = 6.1-8.1;
- existing water source nearby, for phytosanitary treatments and irrigation in case of excessive drought, during the months of july-august.

To carry out the pedological study, soil samples were collected from the land area and it was demonstrated that the land identified for planting has the following characteristics:

- texture = clayish on the surface (0-24 cm, horizon A0) and clayey alluvial and colluvial lutum, (in horizon Bt1, W, 58-75 cm);
- structure = finely porous;
- degree of compaction = medium;
- fertility = medium to low;
- pH = 5.4 (moderately acidic reaction);
- degree of saturation in bases (V%) = moderately mesobasic;
- content in humus = small;
- mobile phosphorus content = medium = 8.86 ppm;
- mobile potassium content = low = 112 ppm.

Land preparation

The technological works carried out for the establishment of the Goji plantation in semi-intensive system are as follows:

- delimitation of the land allocated to the plantation;
- land levelling (modelling of areas of land that favour water accumulation) (Figure 3);
- application of pesticides, with a role in combating diseases, insects and nematodes (Figure 4);
- fertilization with manure (in the amount of 40 to 60 t/ha, given the low fertility of the soil);
- basic fertilization with P and K (250 + 250 kg/ha or by the use of complexes);
- soil mobilization (50-60 cm deep, by unclogging or by scarification, through two perpendicular passes);
- plowing (at 27-30 cm);
- ploughing + levelling (two, perpendicular ways) (Figure 5).

Figure 3. Levelling and fertilizing with manure

Figure 4. Application of pesticides and soil scarification

Figure 5. Soil plowing and ploughing

Soil fertilization is carried out by correlating agrochemical indicators with the requirements of the goji plant, compared with the fertility indicators for achieving an efficient production qualitatively and quantitatively:

- correction of moderately acidic pH = 5.4, when the crop is set up under plowing, with 4 t/ha calcareous amendments;
- organic fertilization, with 30-40 t/ha manure and repeat at 4 years, with 20 t/ha fermented manure applied on the plants row;
- annual fertilization with complex fertilizers of type N, P, K, at N80 P80 K120 kg/ha level, which is 400 kg/ha complex of type N20 P20 K20;
- foliar fertilization, with a foliar fertilizer, simultaneously with a treatment.

Land parcelling and marking

Land marking is necessary before planting, to respect row and row distances and to have a perfect alignment.

It is carried out using 2 m long rollers, painted to be visible, 50 m long roulette and 0.5 m long pickets (Figure 6).

Figure 6. Marking and planting Goji shrubs, autumn

Plant purchasing

Seedling materials are purchased from authorized and experienced producers, who can provide information and guarantees for the administration of a Goji plantation; the plantation with good quality Goji berry bushes can form the genetic basis for their rooting and multiplication (Figure 7).

Figure 7. Certification label of the of Goji seed material

Shrubs planting

- being a plant little spread in Romania, the breeders did not work on the creation of varieties, the species introduced in the country are only of foreign origin: Ninxia NQ1, Goji berry, *Lycium chinese* species and *Lycium barbarum;*
- the optimal planting period is autumn (the plant enters vegetation in spring, directly in the field and time is gained in development) or early spring (when the soil is moist); the advantages of autumn plantings are: by spring, the roots of the trees make close contact with the ground, the shrubs start in vegetation 10 to 15 days earlier than those planted in spring, and achieve growth by 20 to 30%;
- the young plants should be 45-50 cm tall, and the stem should grow straight, up to a height of 1.5-2 cm;
- planting distance depends on the crop system: intensive (planting distance between plants in row = 1.5 m and between rows = 2 m) or semi-intensive (planting distance between plants in row = 2 m and between rows = 2.5 m);
- the specific planting works are as follows: digging holes at 30 x 30 x 30 cm; preparing seedlings, by removing from stratification; protecting seedlings, to avoid dehydration, until planting, from sun and wind; root shaping and crown reduction; mud soaking of roots; laying the young plant in the pit, laying the ground in successive layers by foot compaction; watering with 10-15 L water, if there is not enough moisture in the ground (Figure 8).

Figure 8. Planting Goji berries and mounting the dripping system

Maintenance of culture throughout the year

- the culture should be cleaned of weeds and unproductive shoots, which grow from the root of the shrubs;
- early spring and late autumn, shrubs sprinkle with copper-based substances to protect the plant from pests;
- during summer and during flowering, can be stimulated the development of plants, by foliar sprinkle with various nutrients, which must comply with a fertilization plan made by specialists based on the carried-out soil tests;
- depending on the variety, Goji berries begin to bloom in May and bear fruit from June to October-November; after they begin to bear fruit, there are flowers, buds, unripe fruits and ripe fruits on the plant; in the first year of cultivation, emphasis should be placed on the formation and development of shrubs and not on fruiting; profit from the sale of Goji berries is obtained from the third year of cultivation;
- the soil maintenance system can be: black field (the soil is kept free of weeds and loose throughout the period, by digging dig through the plants) or grazing (on the interval between rows and black field on the row of plants, by manual weeding and weeding with Roundoup, Glifogan herbicides);
- maintenance works in the crown are aimed at suppressing the main stem in the first 2 years at 1 m height and in the following years at 1.5-2 m, suppressing the side branches by maintaining a maximum of 4-5 shoots and removing the shoots from the base that develop very quickly but do not bear fruit.

Fruit harvesting

- Goji berries are harvested manually and staggered, depending on ripening of the fruits and can be consumed fresh or dry;
- Goji berries are perishable and require increased attention to handling, because they can easily oxidize;
- a shrub of over 4 years of cultivation produces 3-4 kg of fresh fruit;
- fruiting begins in the second year, but production is obtained after the fourth year of planting (Figure 9).

Figure 9. Harvesting Goji berries

RESULTS AND DISCUSSIONS

The investment required to set up 1 ha of Goji plantation is about 10,000-15,000 euros, which covers the purchase of the shrubs, the preparation of the land and the actual planting, taking into account that 3,000-3,500 shrubs are required for 1ha. The cost for obtaining the bio certification is 500-600 euros, which also covers laboratory tests that prove that the land is not polluted, and for shortening the conversion period, another application is submitted to the certification entity and new soil tests will be carried out, which cost another 500 euros.

In order to highlight the economic efficiency of initiating a business regarding the establishment and capitalization of a Goji plantation in Gorj County, on a land area of 7,100 m^2, are presented:

- the expenditure on setting up the Goji plantation (Table 1);
- the expenditure on the materials necessary for the establishment of the Goji plantation (Table 2);

- the expenditure on the maintenance of the Goji plantation, up to the entry on the start bearing fruit period (year I and II) (Table 3);
- the expenditure on the necessary materials for the maintenance of the Goji plantation in year I and II since its establishment (Table 4);
- the total expenditure on the establishment and maintenance of the Goji plantation in year I and II of growth, up to the bearing fruit period (type of expenditure on establishment and maintenance and total expenditure) (Table 5).

Table 1. Expenses for the establishment of the Goji plantation

Name of the agrarian work	Value workmanship (lei)	Value workmechanical (lei)	Value materials (lei)	Total costs (lei)
soil mobilization (unclogging or by scarification)	-	400	-	400
Plowing	-	300	-	300
fertilization with manure (30-40 t/ha)	-	100	3,000	3,100
application of pesticides (fighting diseases and pests)	-	50	150	200
soil plowing twice (levelling + incorporation of fertilizers and pesticides)	-	300	-	300
land marking (for planting)	60	-	598	658
digging holes (30 x 30 x 30)	125	-	50	175
distribution of tutors to pits	55	-	1,136	1,191
root shaping	67	-	30	97
mud preparation + mud soaking of roots	54	-	20	74
distribution of propagating material to pits	49	-	-	49
planting seedlings + watering	135	-	13,682	13,817
tying the shrubs to the tutors	56	-	50	106
spilling of the stems	54	-	35	89
sowing herbs on the interval between shrubs	-	150	750	900
TOTAL	**655**	**1,300**	**19,501**	**21,456**

Table 2. Expenditure on materials necessary for the establishment of the Goji plantation

Name of the material	UM	Amount	Value (lei)	
			UM	Total on the material
Goji seedlings	pieces	1,136	12	13,632
Wooden pickets	pieces	1,136	0.5	568
Manure	t	30	100	3,000
Wooden tutors	pieces	1,136	1	1,136
Binding foil	kg	1	50	50
Barracks	pieces	5	10	50
Hoes	pieces	7	10	70
Scissors for trees	pieces	2	15	30
Lime	kg	4	5	20
Paint brush	pieces	1	15	15
Roulette 50 m	pieces	1	30	30
Pesticides	pieces	2	75	150
Seed herbs (for grassing on intervals)	kg	15	50	750
TOTAL				**19,501**

Table 3. Expenditure for maintenance of the Goji plantation until the first and second year of growth

Name of the agrarian work	Workmanship value (lei)	Value of mechanical works (lei)	Material value (lei)	Total costs (lei)
Chemical fertilization (NPK = 300 kg/ha)	55	150	618	823
cutting (for crown forming)	180	-	100	280
phytosanitary treatments (at the vegetative resting period)	60	150	200	410
digging on the row of plants (2 works/year)	1,800	-	100	1,900
mechanical mowing (3-4 work between rows)	240	400	-	640
phytosanitary treatments (5-6 treatments during vegetation)	300	750	1,000	2,050
irrigation (400-600 m^3/ha, 2-3 watering /year)	180	100	100	380
binding and driving of the stems and skeleton branches (2 works/year)	567	-	150	717
TOTAL				**7,200**

Table 4. Expenditure on materials necessary for the maintenance of the Goji plantation in year I and year II of its establishment

Name of the material	UM	The amount	Value (lei)
NPK complex fertilizers	K	215	618
Different tools	buc	10	200
Pesticides		-	1,200
Materials for binding			150
TOTAL			**2,168**

Table 5. Total expenditure on the establishment and maintenance of the Goji plantation in the first and second year of growth, until entering on the fruit phase

Type of expenditure	Value (lei)
Establishment of the Goji plantation	21,456
Materials necessary for the establishment of the Goji plantation	19,501
Maintenance of the Goji plantation until the first and second year of growth	7,200
The necessary materials for the maintenance of the Goji plantation in the first and second year of its establishment	2,168
TOTAL	**50,325**

For the expenses related to the establishment and maintenance of the Goji plantation in the first and second years after its establishment, are presented for each type of agricultural work carried out, its position in the normative, the category of works, the value of the labour for each work, the value of the mechanical works carried out, the cost of the materials and total expenditure on the establishment and maintenance of the Goji plantation up to the entry on the start bearing fruit period, i.e. the first and second year of growth (Table 1 and Table 3).

For the expenditure on materials necessary for the establishment and maintenance of the Goji plantation in year I and II of its establishment, Table 2 and Table 4 present the name of the materials, the unit of measurement, the quantity required, the value per unit of measure, Total value for each material and total expenditure on the materials necessary for the establishment and maintenance of the Goji plantation in year I and II since its establishment.

Analysing the data presented, regarding all types of expenses necessary for setting up a Goji plantation, on an area of 7,100 m^2 in the Gorj County, it is noted that the initiation of this business has economic efficiency, contributes to the rural development of the commune and to the promotion and development of agro tourism in the area.

Goji plants enter on the fruit phase since the third year of planting, but the economic efficiency is achieved after the 4th-5th year.

- Production potential = 2-4 kg/fruit/plant
- Estimated production = 1,600 plants/ha x 3 kg/plant = 4,800 kg fruits
- Price of valorisation = 50 lei/kg of fresh fruits
- Production value/ha = 240,000 lei
- Value of production at cultivated area of 7,100 m^2 = 170,400 lei
- Profit starting with year 4 = income – expenses = 170,400 – 50,325 = 120,075 lei

CONCLUSIONS

Goji berries have been known for over 2000 years, but interest in them has increased significantly with their use in organic food and traditional medicine due to their antioxidant content

Goji berries can be eaten fresh or dried or can be used in various food industry preparations.

The initiated business has a positive impact on the sustainable development of the rural area of Gorj County, on the economy, social life and environment, by capitalizing on agricultural land, creating jobs, promoting the area and increasing the income of the entrepreneur.

REFERENCES

Babuc, V. (2012). *Pomiculture*, State Agrarian University of Moldova, Practical Institute of Horticulture and Food technologies, Central Printing House, Chişinău, ISBN 978-9975-53-067-5.

Bordes, J.P. (2008). *Goji, a genuine food for well-being*, Agen, Je médite.

Donno, D., Beccaro, G.L., Mellano, M.G., Cerutti, A.K., Bounous, G. (2015). Goji berry fruit (*Lycium* spp.): antioxidant compound fingerprint and bioactivity evaluation, *Journal Funct Food, 18*, 1070-1085.

Koçyiğit, E., Sanlier, N. (2017). A Review of Composition and Health Effects of *Lycium* barbarum*, International Journal of Chinese Medicine, 1*(1), 1-9. doi: 10.11648/j.ijcm.20170101.11.

Kulczyński, B., Gramza-Michałowska, A. (2016). Goji Berry (*Lycium barbarum*): Composition and Health Effects - a Review, *Polish Journal of Food and Nutrition Sciences, 66*(2), doi:org/10.1515/pjfns-2015-0040.

Kourdi, J. (2011). *100 Brilliant business ideas*, pp. 234. Adevărul Holding, Bucharest. ISBN: 978-0-462-09960-6.

Şengün, P., Kadakal, C. (2021). Effect of Ripening Stages and Oven Drying on the Carotenoid Composition of Goji Berry (*Lycium barbarum* L.) Fruits, *Türk Tarım ve Doğa Bilimleri Dergisi*, *8*(4), 1130–1138. https://doi.org/10.30910/turkjans.976116

Sharamon, S. (2009). *La Baie de Goji*, Paris, Médicis. ISBN 978-2-8532-7395-4.

Scientific Papers. Series E. Land Reclamation, Earth Observation & Surveying, Environmental Engineering. Vol. XII, 2023
Print ISSN 2285-6064, CD-ROM ISSN 2285-6072, Online ISSN 2393-5138, ISSN-L 2285-6064

ARE THERE OPPORTUNITIES OF USING SOLAR ENERGY IN IRRIGATION SYSTEMS?

Dragoș DRĂCEA, Augustina Sandina TRONAC, Sebastian MUSTAȚĂ

University of Agronomic Sciences and Veterinary Medicine of Bucharest,
Faculty of Land Reclamation and Environmental Engineering,
59 Marasti Blvd, District 1, Bucharest, Romania

Corresponding author email: augustina.tronac@yahoo.com

Abstract

The paper aims to have a look over the energy production over the time, and its specific nowadays, with the desire to find alternative solutions, but taking into account the specifics of the way in which irrigation systems and schemes in Romania are structured and used, and watering methods are distributed according to the plants, over the territory. Analysing the Romanian Energy System for 2 different periods (winter and summer) and the distribution the energy sources, there are comparisons between the evolution of energy production and energy needed for irrigation. In that manner it is possible to conclude if and when solar energy has efficient utilization.

Key words*: energy, solar, irrigation, consumption-demand balance, storage.*

INTRODUCTION

Social and economic development implies an increase in the energy need. Industrial evolution was based, in its first phase, on fossil energy resources (that have the advantage of a high energy density): coal was the main source of energy, quickly followed by oil (Figure 1).

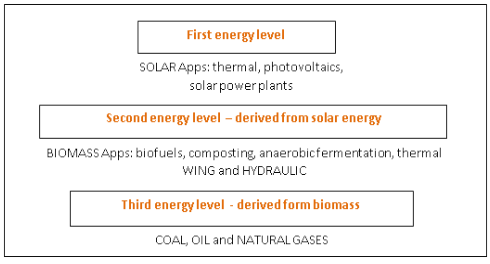

Figure 1. Energy levels depending on generation mode and historical time

The primary energy received from the sun is converted in a short time into wind, hydraulic and biomass energy. The third level of energy was due to natural biomass transformation processes.

The energy density increases from the first level to the last one, high efficiency applications being made throughout the period of industrial development. Hydraulic energy has developed throughout the entire mankind development period due to the multiple advantages related to efficiency and the possibility of storage.

The technology transfer and the society development have led to the continuous increase of the energy requirement with an unfavourable effect on the environment.

The main ways of environmental impairment caused by energy production are:

- natural resources overexploitation, deforestation, change of land use, water resources extensive and intensive use;
- mining, oil extraction and processing;
- tailings - associated land and water pollution;
- carbon emissions, powders, other combustion gases, atmospheric pollution.

In recent period, climatic changes were highlighted, the measured values show temperature increases and precipitation regime changes, these effects being closely related to the greenhouse effect produced by carbon and powders high concentrations in atmosphere.

In this context, a plan was proposed to modify the energy field and re-technologically the entire society, whereby the energy sources from level 3 (Figure 1) are gradually abandoned and the necessary provision is made through the resources mentioned at level 2 and 1, as seen in the energy production evolution between 2010 and 2020 graph by source type (Figure 2).

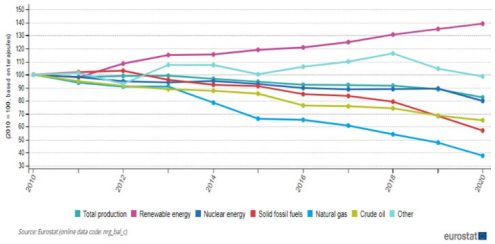

Figure 2. Production of energy by source type, EU, 2010-2020 (Source: Eurostat, 2021)

The directions of action are:
- increasing energy efficiency in all activity fields;
- giving up coal and oil (level 3);
- energy provision from renewable sources (level 1 and 2);
- consumption and transport based on electricity and hydrogen;
- balancing the demand-supply stages based on natural gas and electricity storage systems (through hydropower methods, hydrogen production, integrated production-storage-consumption systems) and intelligent consumption systems.

The energy system transformation involves a considerable volume of investments in which both producers and consumers will have to be engaged, through following methods:
- changing the type of used energy, investments in electricity production, storage and transport units;
- car fleet replacement, entire transport system restructuring;
- processes optimization and automation.

THE CURRENT SITUATION OF ENERGY IN ROMANIA

Nowadays, in Romania the main activities that involve energy consumption are (INSS, 2018; 2019; 2020; 2021; 2022):

- transport consumption: derived from oil (diesel, petrol and LPG): 300 l/year.consumer ≈ 2,400 kWh/year.consumer = 6.6 kWh/ day.consumer (average values, considering the reduced fuel consumption during the Covid pandemic period);
- total electrical energy consumption: 5,000-8,000 MWh/hour ≈ 150 GWh/day = 8 kWh/ day consumer;
- consumption for heating in the cold period: 50-150 W/m^2 ≈ 50 kWh/day consumer;
- consumption for domestic hot water preparation: 50 l/day = 1.5 kWh/ day consumer.

Romanian data show that the largest share of consumption is found in the heating sector, the consumption of electricity and for transport being at a low level.

In order to reduce energy consumption in Romania, in accordance with the European plan for reducing carbon dioxide emissions, the following projects are underway:
- buildings insulation and thermal rehabilitation;
- conversion to electric transport;
- electricity production from renewable sources;
- increasing the processes energy efficiency;
- biomass and biofuels projects development;
- capture and recovery of thermal energy using heat pumps.

Overall, the energy system modification and the predominant of electricity use implies the increase of this system by approx. 200-300 % in all sections: production, transport, distribution.

To characterize the national electricity system current situation, an analysis of production and consumption was carried out for two periods: June 18-25, 2022 (the longest day of the year) and December 18-25, 2022 (the shortest day of the year), resulting:
- production-consumption- balance and the share of each category of energy in production (Table 1);
- hourly evolution of solar and wind energy production.

Table 1. Production-consumption balance for the analysed periods

Period		18-25 jun. 2022		18-25 dec. 2022	
		GWh	%*	GWh	%*
Consumption	GWh	1175.09	100.00	1250.65	100.00
Production	GWh	1141.07	97.11	1333.40	106.62
Coal	GWh	250.70	21.33	217.05	17.35
Hydrocarbs	GWh	208.42	17.74	284.04	22.71
Hydro	GWh	361.16	30.73	412.40	32.97
Nuclear	GWh	131.55	11.20	268.51	21.47
Wind	GWh	130.20	11.08	129.74	10.37
Photovoltaic	GWh	48.45	4.12	10.71	0.86
Biomass	GWh	10.61	0.90	10.97	0.88
Sold	GWh	34.04	2.90	-82.74	-6.62

*percentage-weight of the total consumption

For the analysed periods, it turns out that the share of renewable energy produced in the national energy system is about 16% in the hot

season and 10% in the cold season. The differences are due to climatic factors that especially affect solar energy, 4% weight in the warm period and only 0.9% in the cold period (Figure 3).

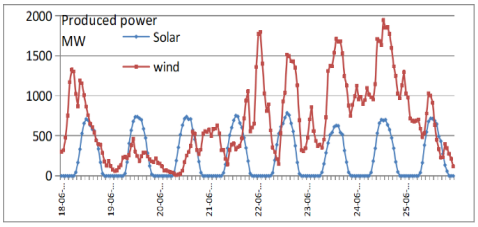

Figure 3. Evolution of solar and wind sources energy production - period (18-25).06.2022 (processed data, Transelectrica, 2023)

It can be seen that on the 19th and 20th of June the production of photovoltaic energy was higher compared to wind energy. For the period analysed it is found productions close for solar energy, making predictable this category of energy, depending on the weather forecast and the evolution.

There are periods with low consumption and high production originating from the wind component. For these reasons, wind energy sources require energy storage systems, while predictable photovoltaic energy can be used in the national distribution and consumption system without the need for storage in compensation, especially with hydraulic energy.

Figure 4 shows significant variations in the two energy categories and the possibility of correlation: large day-to-day differences in solar energy can change wind energy production due to changes in weather conditions, differential heating and local or regional generation of air mass movements in atmosphere.

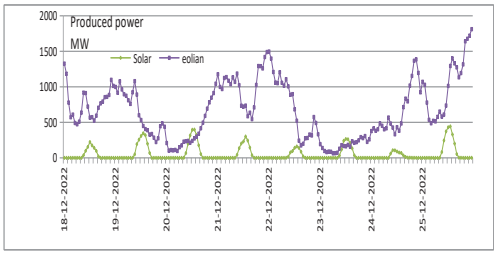

Figure 4. Evolution of solar and wind sources energy production - period (18-25).12.2022 (processed data, Transelectrica, 2023)

Figure 5 shows the significant production variations within the winter period and reduced values compared to the summer period; the values produced in winter days can be of the order of percentages compared to warm season production.

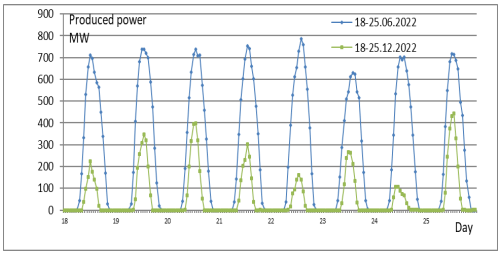

Figure 5. Comparative evolution of summer-winter photovoltaic energy production (processed data, Transelectrica, 2023)

The production evolution shown in Figure 6 indicates significant variations and the need for compensation in the national system or the creation of storage systems.

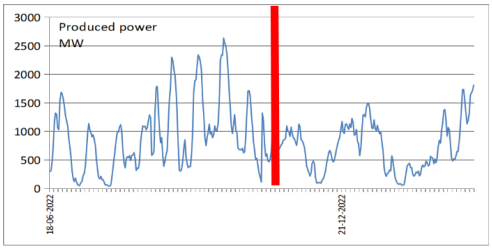

Figure 6. Evolution of solar and wind sources energy production - periods (18-25).06.2022 and (18-25).12.2022 (processed data, Transelectrica, 2023)

Figure 7 shows the relatively constant daily production but also the significant hourly variations: about 4 hours/day the production is at a level of over 90% of the maximum value and about 7 hours/day at a production of over 70% of the maximum value. The obtained graph shape coincides with the one described by Victor, 2011.

The production uniformity during this period makes predictable this type of energy production, depending on the weather conditions.

The overlapping of the production during the period of high consumer demand means that this type of energy does not require storage units if the introduction into the national energy system is ensured.

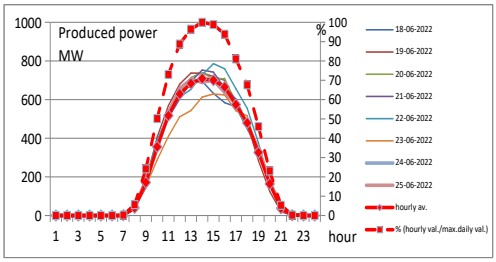

Figure 7. Hourly evolution of photovoltaic energy production- period (18-25).06.2022 (processed data, Transelectrica, 2023)

Figure 8 shows the significant hourly and daily variations of the photovoltaic energy production during the analysed winter period.

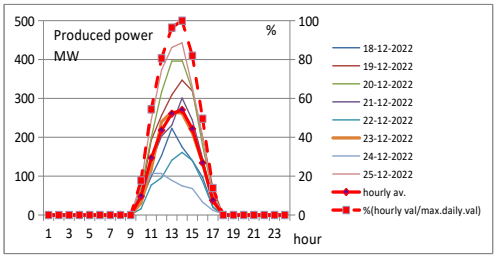

Figure 8. Hourly evolution of photovoltaic energy production- period (18-25).12.2022 (processed data, Transelectrica, 2023)

The average value of the maximum daily production at a value of 270 MWh is about 2.5 times lower than that obtained in the summer period analysed in Figure 5, where the average production at the maximum of the day was 700 MWh.

SOLAR-PHOTOVOLTAIC ENERGY USE FOR IRRIGATION

The irrigation systems are large energy consumers; for example, the U.S. agricultural irrigation consumed 60.6 TWh in 2018 and there is an acute interest to diminish the energy footprint of this activity (Sow & Dicataldo, 2022).
Climate changes affect the energy consumption of irrigation systems, major adaptation needed cause the fact that increasing water use efficiency means intensifying energy use through increasing pumping head (Daudin & Weber, 2020).
The irrigation systems in Romania were created to ensure the water requirements for large areas, in the context of the state ownership of the respective areas. The plan for the irrigation systems development envisaged investments for 3 million ha, an area that represents approximately 20% of the country's agricultural area.
The irrigation technology for these extensive systems involves watering with high rates at a time interval calculated or resulting from the water balance for each irrigated plot.
Practically, the volume of active soil is considered as the storage volume between the minimum and maximum humidity (field capacity), the technology involves soil irrigation.
The energy requirement for pumping water for large surfaces is high and optimization measures are adopted in operation:

- pumps high efficiency operation;
- reduction of water losses form transport channels and pipelines networks;
- watering installations function at minimum pressures

The transition to a new society organization led to labour force reduction, which migrated to the industry, more economically efficient, so the irrigation systems were equipped with hydraulic displacement equipment that requires higher pressures at the pumping station (about 6-7 bar). In these conditions, considering an irrigated surface of 1 million ha with an average rate of 1500 m^3/ha/month, the energy requirement only for the pressurized stations is 570 MWh/h, which represents approx. 10% of the current capacity of the national energy system (Burchiu et al, 2004):

$$P(kW) = \frac{\gamma QH}{\eta.pX\eta.me} = \frac{9.81X\dfrac{1500}{30X20X3600}X60}{0.8X0.9} = 0.57kW$$

where:
P - power of the pumping unit, Kw;
Q - pumped flux rate, m^3/s;
H - pumping head, mCA;
η.p - pump efficiency;
η.me- electric motor efficiency.

The estimated value in this case is optimistic, the energy consumption being higher due to:

- energy losses during the transport and transformation of electricity (approx. 10%);
- infiltration and evaporation water losses in transport systems;
- energy consumed by pumping and

repumping stations (different, specific value for each irrigation system and plot);
- ensuring the necessary irrigation norms in dry periods (reaching values of 3000 m^3/ha/month).

The previous analysis shows that for extensive irrigation systems it is impossible to provide energy from solar energy sources, the main incompatibilities being:
- high energy requirement for irrigation throughout the day including during the night (when watering is recommended to ensure higher efficiencies);
- high energy requirement for irrigation and low solar energy density, the use of the variant involving investments in photovoltaic parks on large areas;
- large hourly variations in the photovoltaic energy production and the impossibility of ensuring the necessary power on a constant basis;
- the lack of overlapping of the energy production period with the efficient irrigation application period;
- the need to over-equip irrigation systems or the use of other complementary energy sources;
- the high production price of photovoltaic energy.

For agricultural production systems on small areas, specific to horticultural farms, efficient irrigation systems "at the plant", through drip or similar systems, the option of using photovoltaic energy can be adapted. On the same calculation assumptions, the result for 1 ha is a photovoltaic system of 0.57 kW x 20 hours = 12 kWh/day with an area of 15- m^2.

The watering norms application can be ensured by oversizing the irrigation installation or by storing energy in the form of electricity or hydraulic, the last option requiring the oversizing of the photovoltaic system depending on the additional pressures required.

CONCLUSIONS

Photovoltaic energy production is variable both seasonally and hourly, which makes it impossible to ensure the necessary for domestic and industrial consumers. To compensate for hourly production, storage systems for high production capacity are not justified; the overlapping of production over demand implies the injection of this photovoltaic energy directly into the energy transport systems. Low-capacity storage systems for the isolated individual consumer can be considered cost-effective.

The advantage of solar energy is that it is predictable in terms of production depending on weather conditions and can be easily compensated in the national energy system. In the cold season, the production is variable in a wide range, the share within the national energy system being reduced.

Variable wind energy production requires storage systems or extreme compensation measures within the national energy system.

Photovoltaic energy can provide the necessary for small surfaces irrigation systems with plant watering, oversizing the watering system or storing the energy in hydraulic form. For extensive irrigation systems, photovoltaic solar energy is not suitable due to the hourly non-uniformity energy production and the reduced production time.

REFERENCES

Burchiu, V., Mocanu, P., Gheorghiu, L. (2004). *Machines and installations for environmental protection*, Atlas Press Publishing House, Bucharest, pp. 16.

Daudin, K., Weber, C. (2020). Energy consumption of irrigation systems: a functional perspective, *Conference Water Energy Nexus*, from https://www.researchgate.net/publication/355171899_Energy_consumption_of_irrigation_systems_a_functional_perspective/link/616405f40bf51d48176ce7e2/download.

Sow, R.B., Dicataldo, E. (2022). The energy footprint of U.S. irrigation: A first estimate from open data, *Energy Nexus, 6*, https://doi.org/10.1016/j.nexus.2022.100066.

Victor, E.L. (2011). *Alternative energy sources*, MatrixRom Publishing House, Bucharest, pp. 79.

Eurostat (2021), from https://ec.europa.eu/eurostat/statistics-explained/index.php?title=Energy_production_and_imports.

INSSE (2023), from http://statistici.insse.ro:8077/tempo-online/#/pages/tables/insse-table.

Transelectrica (2022), from https://www.transelectrica.ro/widget/web/tel/sen-grafic/-/SENGrafic_WAR_SENGraficportlet.

Scientific Papers. Series E. Land Reclamation, Earth Observation & Surveying, Environmental Engineering. Vol. XII, 2023
Print ISSN 2285-6064, CD-ROM ISSN 2285-6072, Online ISSN 2393-5138, ISSN-L 2285-6064

SPATIAL DATA RESULTING FROM THE AUTOMATION OF THE PERMANENT SEISMIC MONITORING SYSTEM

Claudiu-Sorin DRAGOMIR[1, 3], Iolanda-Gabriela CRAIFALEANU[2, 3], Daniela DOBRE[2, 3], Emil-Sever GEORGESCU[3]

[1]University of Agronomic Sciences and Veterinary Medicine of Bucharest,
59 Marasti Blvd, District 1, Bucharest, Romania
[2]Technical University of Civil Engineering Bucharest,
122-124 Lacul Tei Blvd, District 2, Bucharest, Romania
[3]National Institute for Research and Development URBAN-INCERC,
266 Pantelimon Rd, District 2, Bucharest, Romania

Corresponding author email: dragomirclaudiusorin@yahoo.com

Abstract

The stations from the INCD URBAN-INCERC network are distributed throughout the country, including Bucharest, and are located either in free-field conditions, in small buildings, in medium-height buildings or in boreholes. The interactive map representation of the seismic stations and the automatic monitoring of their operation, based on the analysis of received data, are currently carried out with the SeisComP software. The paper exemplifies, as performance benchmarks, some data processing obtained in 2022 within the permanent seismic monitoring system.

Key words*: seismic data, seismic network, spatial analysis, semi-automatic generation of PGA maps.*

INTRODUCTION

In a general context, the main objective of the automation of the permanent seismic monitoring system is to improve the understanding of the structural behaviour of buildings and their damage potential under the dynamic action of earthquakes or of other vibration sources.
The capacity of the seismic network of INCD URBAN-INCERC was developed in this direction and a significant amount of data was obtained through the permanent monitoring of buildings such as that of the General Inspectorate of Emergency Situations, IGSU, the Ministry of Research, Innovation and Digitalization, MCID, the Faculty of Biotechnologies, BTH (USAMVof Bucharest), the University Emergency Hospital, the VENUS and the APATEL buildings, but also through the temporary seismic instrumentation of a number of 14 research and development institutes premises.
This is an important step in the research for increasing public safety, given that the obtained records obtained will provide, in time, important data for the:

- systematic and efficient verification of the performance of the structures and the identification of potential prerequisites for future damage;
- overall vulnerability assessment of instrumented/monitored buildings;
- evaluation of dynamic characteristics as reference data for the future instrumentation of the same buildings, or for informing retrofitting interventions;
- identification of the level of ambient vibrations in some urban areas and of the peculiarities of recorded signals;
- comparison and selection among different operational modal analysis techniques for identifying the structural behaviour from the response analysis in the time and frequency domains under low-amplitude ambient vibrations;
- semi-automatic generation of PGA maps and highlighting of various patterns and trends revealed by the recorded data;
- enriching the existing records database by acquiring real-time data transmitted through the Romanian Special Telecommunications Service network etc.

BUILDING RESPONSE MONITORING

Some aspects of advanced seismic monitoring are presented in the following. The automatic monitoring of seismic stations operation, the generation of maps with the seismic stations that transmit in real-time and, the advanced spatial analysis of the seismic data and the calculation of various parameters of specific earthquake engineering significance represent some of the main activities conducted in support to and within the broader context of the assessment of seismic risk in case of major earthquakes.

The interactive mapping, based on the analysis of the data received from the stations, is carried out using the SeisComP *scmv* module (gempa.de). Figure 1 shows a map, generated by the SeisComP system, with stations from the INCD URBAN-INCERC seismic network. The stations are distributed throughout the entire territory of the country, including Bucharest, devices/sensors being placed either in free-field conditions, in small buildings, in medium-rise buildings (for seismic monitoring) or in boreholes.

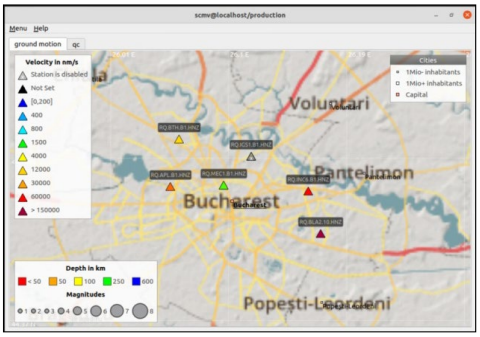

Figure 1.Representation in SeisComP of the seismic stations from the INCD URBAN-INCERC network, with the reference channels (vertical - HNZ) - detail for Bucharest (with also BTH station)

Figure 2 shows the waveforms recorded at some seismic stations of the network during the earthquakes of July 16 and 18, 2022, using the SeisComP scolv module. The waveforms show the automatic identification of the primary ("P") waves and, respectively, the secondary ("S") wave's arrivals. The advanced spatial analysis of seismic data can be performed with the SIGMA program, also developed by gempa.de (Germany), as the SeisComP system. The program performs: interactive or automatic analysis of seismic motions; generates maps of modified Mercalli Intensity (MMI), peak ground acceleration (PGA) and peak ground velocity (PGV); computes earthquake engineering-specific parameters such as, for example, the Arias intensity and duration and allows the selection, mapping and validation of ground motion prediction equations (GMPE). The computed values are stored in a database that can be accessed report generation.

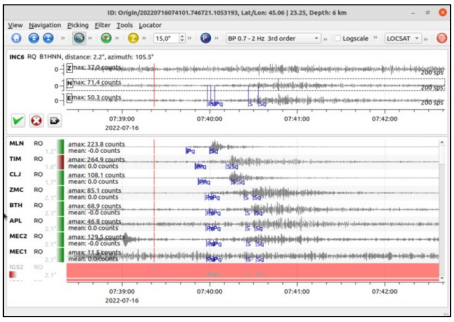

Figure 2. Waveforms recorded at the stations of the INCD URBAN INCERC network during the seismic event of 16.07.2022. Representation generated by using the *scolv* module of SeisComP

The waveforms in Figure 2, displayed for the earthquake on 07/16/2022 (M_L=4.1), show various times of arrival of P- and S-waves for stations in Bucharest, including those recorded at the Faculty of Biotechnologies (USAMV of Bucharest) seismic station, code BTH.

In Figure 3, a map is displayed for another earthquake, that of November 3, 2022 (M_L = 5.4), with the recorded peak accelerations of the soil (as resulting from the countrywide seismic monitoring).

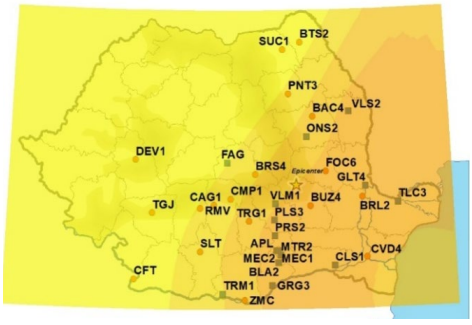

Figure 3. PGA map for the earthquake of 11/03/2022

RESULTS AND DISCUSSIONS

Processing of data recorded by seismic stations. For each of the recordings, the desired components can be selected and the response spectrum, phase spectrum and power spectrum can be computed and displayed, using different options related to axes, corrections etc. Wave forms recorded at the seismic stations can be also represented using the *scolv* module of SeisComP.

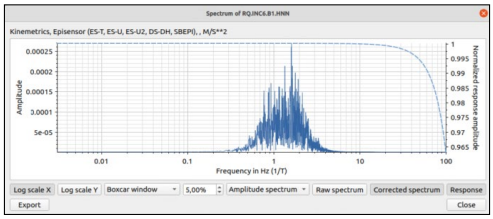

Figure 4. Response spectrum of the earthquake recording from 16.07.2022, INC6 station (INCERC Bucharest branch), N-S component. Representation made with the *scolv* module of SeisComP

Spatial analysis and advanced processing of seismic data. In the following figures (5 to 8), the application of the SIGMA program for the Vrancea subcrustal earthquake of 17/18.07.2022is presented for illustration.

Figure 5. Waveforms (corrected accelerations) recorded in the pilot stations of the seismic network of INCD URBAN-INCERC during the earthquake of 17/18.07.2022

The recorded amplitudes have important applications in earthquake early warning, which can be performed directly at station level, thus gaining time in case of the exceedance of the preset levels (Marmureanu et al., 2021; Tiganescu et al., 2022).

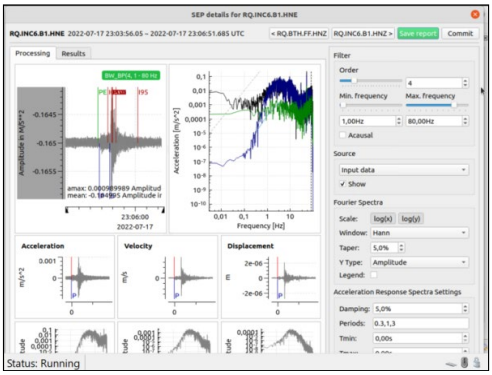

Figure 6. Detailed processing carried out with the SIGMA program for a pilot station of the seismic network of INCD URBAN-INCERC, for the earthquake of 17/18.07.2022

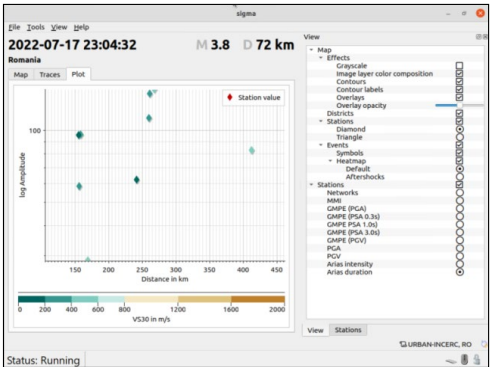

Figure 7. Chart of amplitudes as a function of epicentral distance

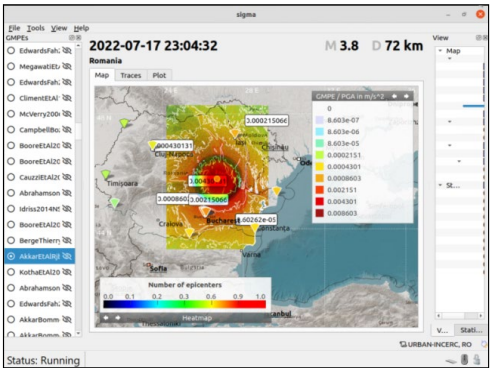

Figure 8. Testing of Ground Motion Prediction Equations (GMPEs) with SIGMA

The role of seismic instrumentation. Up to 2022, 14 research and development institutes have been instrumented by INCD URBAN-INCERC, apart from another set of permanently monitored buildings. The obtained results contribute to the development of the existing database and to the analysis of the differences between the structural dynamic properties determined by measurements and the results from the application of the simplified formula from the Romania seismic design code P100-1/2013 (Figures 9, 10, 11).

Also, as the dynamic properties evaluated by seismic instrumentation (under low-intensity excitations) will likely not coincide with the dynamic properties recorded under severe earthquakes, arrange of frequently recorded accelerations, is considered (Dragomir et al., 2017; 2018; 2020).

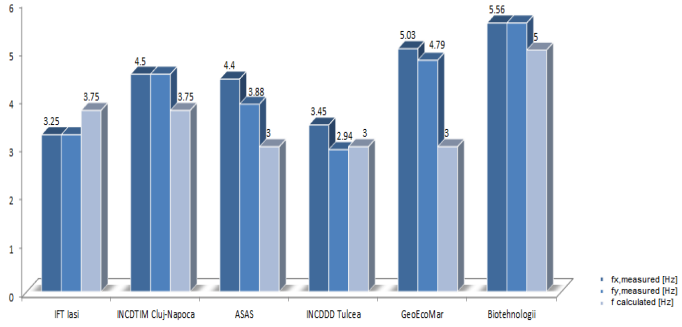

Figure 9. Average level of frequencies recorded from ambient vibrations and computed according to the P100-1/2013 code, for 3-story buildings (including the BTH_USAMV station)

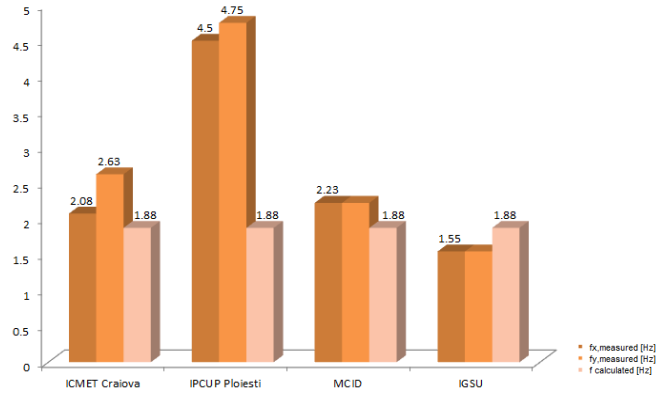

Figure 10. Average level of frequencies recorded from environmental vibrations, compared to those computed according to P100-1/2013, for 7-story buildings

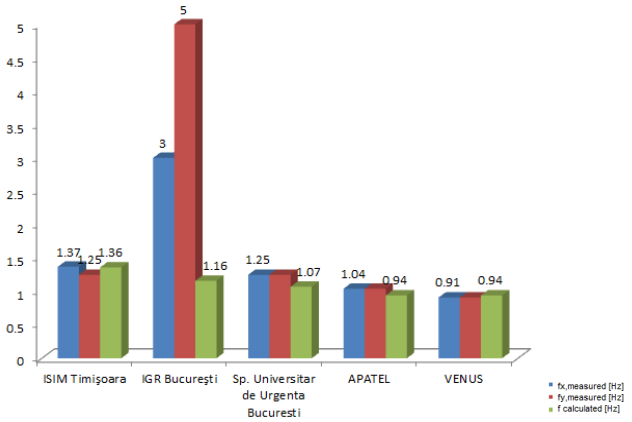

Figure 11. Average level of frequencies recorded from environmental vibrations, compared to those calculated according to P100-1/2013, for 10, 12, 13 and 15-story buildings

CONCLUSIONS

In the context of the applications of the seismic instrumentation/monitoring activity, the possibility of its integration into the new BIM-Building Information Modelling approach, in a multidimensional and multidisciplinary relationship, for a new type of evaluation and mitigation of seismic risk, should also be mentioned, through the following aspects:

- data of interest can be provided on the characteristics of both the structural elements and the non-structural elements of a building, from the BIM model, correlated with the structural instrumentation/ monitoring data;
- the structural health monitoring before and after an earthquake can provide information for a self-diagnosis in BIM;
- structural instrumentation/monitoring to can support the creation of an earthquake emergency management hub within a building management system;
- estimation of structural seismic losses by going through a few successive stages:
- measurement of the structural dynamic response from environmental vibrations and subsequent identification of the characteristics of the structural system only from output data (operational modal analysis);
- experimental and/or analytical structural analysis;
- automatic analysis of seismic losses through implementation in the existing BIM application.

Regarding the semi-automatic generation of PGA maps from seismic actions or other vibrational sources and the rapid assessment of the vulnerability of instrumented buildings, a series of software modules necessary for the automation of the permanent seismic monitoring system, based on the use of the specialized SeisComP software package, were previously prepared, configured and implemented. Thus, the following stages were completed in this process:

- installation and configuration of the program core;
- initial population of the database;
- creation of the inventory of seismic stations;
- definition of the seismic network characteristics;
- import of the characteristics of the seismic recording instruments from the Nominal Response Library database of the Incorporated Research Institutes for Seismology, IRIS;
- definition of data related to the seismic stations (general characteristics of the stations, device locations - geographical coordinates, location within the seismic station, characteristics of the channels);
- generation and import of the XML file with the data on the seismic network into the SeisComP database;

- configuration of online communication, in real time, with the seismic stations in the territory;
- configuration of connections with network stations;
- configuration of local archiving of seismic records;
- graphic representation of data recorded in real-time (waveforms);
- representation of recorded data in real-time, in a special format;
- real-time verification of the quality of the operation of the seismic stations;
- access to files from the SDS archive;
- management of the station metadata file.

Shake maps can be also generated based on the ground motion attenuation equations (laws) selected by the user from a list provided by SIGMA. Attenuation laws can be dependent on PGA, PGV, or on the pseudo-spectral amplitude (PSA) expressed at various period values (0.3s, 1.0s, 3.0s).

ACKNOWLEDGEMENTS

This research work was carried out within the Project PN 19 -33 01 01: "Research on the development of an integrated system to ensure the security of the built space, with semi-automatic generation of PGA maps originating from seismic actions or other vibrational sources and rapid assessment of the vulnerability of instrumented buildings" financed by Ministry of Research, Innovation and Digitalization.

REFERENCES

Dragomir, C.S., Dobre, D. (2017). Selection criteria for investigation of microseismic and ambient vibrations. Case studies. *17th International Multidisciplinary Scientific Geoconference & Expo SGEM, Albena, Bulgaria*. doi: 10.5593/sgem2017/14/S05.049.

Dragomir, C.S., Craifaleanu, I.G., Dobre, D., Georgescu, E.S. (2018). Prospective studies for the implementation of a remote access earthquake damage detection system for high-rise buildings in Romania". *Proceedings of the World Multidisciplinary Earth Sciences Symposium/WMESS*, Prague, Czech Republic. doi:10.1088/1755-1315/221/1/012036.

Dragomir, C.S., Dobre, D. (2020). Improvements in a smart monitoring system for buildings. *XXth International Multidisciplinary Scientific GeoConference Surveying, Geology and Mining, Ecology and Management - SGEM 2020*. doi: 10.5593/sgem2020/1.2/s05.075.

Dragomir, C.S., Dobre, D., Iliescu, V. (2020). A comprehensive approach for the seismic vulnerability of a building of public utility. *The 5th World Multidisciplinary Civil Engineering-Architecture-Urban Planning Symposium WMCAUS*. doi:10.1088/1757-899X/960/4/042073.

Marmureanu, A, Ionescu, C., Grecu, B., Toma-Danila, D., Tiganescu, A., Neagoe, C., Toader, V., Craifaleanu, I.G., Dragomir, C.S., Meita, V., Ivanovich Liashchuk, O., Dimitrova, L., Ilies, I. (2021). From National to Transnational Seismic Monitoring Products and Services in the Republic of Bulgaria, Republic of Moldova, Romania, and Ukraine. *Seismological Research Letters, 92*(3), 1685–1703.

Tiganescu, A., Craifaleanu, I.G., Aldea, A., Grecu, B., Vacareanu, R., Toma-Danila, D., Balan, S.F., Dragomir, C.S. (2022). Evolution, Recent Progress and Perspectives of the Seismic Monitoring of Building Structures in Romania. *Frontiers in Earth Science*, *10*, 819153. doi: 10.3389/feart.2022.819153.

Scientific Papers. Series E. Land Reclamation, Earth Observation & Surveying, Environmental Engineering. Vol. XII, 2023
Print ISSN 2285-6064, CD-ROM ISSN 2285-6072, Online ISSN 2393-5138, ISSN-L 2285-6064

ANALYSIS OF SEISMIC DATA FROM MODERATE INTENSITY EVENT OF 2022.11.03 RECORDED ON INSTRUMENTED STRUCTURES

Stefan Florin BALAN, Bogdan Felix APOSTOL, Anton DANET

National Institute of R-D for Earth Physics, 12 Calugareni Street, Magurele, Ilfov, Romania

Corresponding author email: sbalan@infp.ro

Abstract

There is a need for safer constructed medium in order to respond to the constant necessity for raising the security level of human society to earthquakes impact. In this respect the buildings monitoring in areas subjected to seismic site effects provides the possibility of getting immediate and reliable information on the status of certain structures, which enables decision makers to better allocate resources and to direct rescue operations. A procedure is implemented, which allows to perform real-time data acquisition, data exchange and data analysis from structures exposed to seismic excitation or under ambient vibration. The processed recordings are used to deliver information in real time about the seismic event. Engineering seismology parameters are computed: maximum acceleration, spectral acceleration, corresponding oscillation periods, etc., on both structures and free field. The output is conceived as a standard report on the characteristic response of the instrumented building. In the paper such an approach is described in an extended and thoroughly version, for two instrumented buildings, located in different areas, under the last year's strongest seismic event of 2022.11.03, $M_w = 5$ that hit the Romanian territory.

Key words*: near-real time seismic analysis, moderate Vrancea earthquakes, structures monitoring performance.*

INTRODUCTION

Vrancea seismic region is the most important source of the seismic hazard for almost the entire country territory through its intermediate-depth earthquakes activity. There are also many superficial focal-depths seismic zones which, along with the Vrancea crustal one has their local area of influence. The seismic events belonging to the former location are the strongest that hit the Romanian territory during centuries. Their hypocentres roughly located deeper than 90 km, to 150 km or even more are confined to a certain volume recently described as consisting in an upper mantle seismic nest (Ismail-Zadeh et al. 2012).

Traditionally the main attention was given to the influence of the ground motion characteristics, its amplitude, duration and frequency content, on the potentially damage induced upon the constructed medium (Trifunac & Todorovska, 2000). With the more developing of the urban centres the interest was focused also on dynamic soil-structure interaction and soil-building resonance, important features being brought by new development of earthquake engineering regarding nonlinear behaviour of soils, dynamic of buildings and resonance implications (Apostol, 2017; Bratosin et al., 2017; Lomnitz, 1999; Takewaki, 2001; Todorovska, 2000; Wolf & Song, 2002; Balan et al., 2020a). Other studies are also focused on evolution of dynamic characteristics of buildings during and after earthquakes (Trifunac et al., 2001a; Trifunac et al., 2001b; Gallipoli et al., 2003a; Balan et al., 2019; Balan et al., 2022a,b) with impact to urban risk mitigation.

The aim has a many fold character, pursuing: - to contribute at enabling a system of both integrate observational and results in earthquake engineering and seismological data to issue warnings (alerts); - to assess near-real-time (i.e., right after a potentially damaging event and/or during its aftershock sequence) structure response-based status; - to give a contribution to seismic risk assessment, based on data acquired from buildings network, in cities exposed to different/various site effects.

These aims are to be accomplished by rapidly processing the recorded parameters of the earthquake in order to generate useful information about the seismic response, for civil protection needs and earthquake engineering purposes. This will also contribute at rising the security level in densely populated cities to the earthquakes impact and enable authorities to better allocate resources and to direct rescue operations.

SEISMOGENIC FEATURES OF THE INVOLVED AREAS

In this paper two urban areas are considered, both strongly affected by the previous damaging earthquakes generated by Vrancea-intermediate seismic source, hence with a quite high level of seismic hazard. The first town, Bucharest, the capital of Romania, is located at distances between ~120 and ~170 km from the epicentres zone, is a highly urbanized metropolitan area with a high risk posed by the constructed medium, which suffered a lot of damage and many human losses in the previous century as a consequence of last destroying earthquakes (Dilley et al., 2005; Bonjer et al., 2010; Kronrod et al., 2013). The second city, Focsani is located much closer to the epicentres, also exposed at crustal earthquakes generated by the neighbouring seismically active area.

Apart from the highly seismic risk of the two cities, they are experiencing quite important site effects, along with other seismic hazard exposed areas, during last medium-to-strong seismic events. The recordings, as well as data processed and spectral characteristics, show large values for the ground motion parameters and amplifications (Marmureanu, 2016; Marmureanu et al., 2021a; 2022).

A comprehensive background analysis was previously undertaken using strong motion data from earthquakes corroborated with observational damage and considering the evolution of the three generations of code-based spectral levels for the two cities (Balan et al., 2019). Herein a case-study for two densely populated Romanian cities (Focsani and Bucharest) is presented, using data from a 5 M_W earthquake (November 03, 2022, see Figure 1a). Its characteristics were as follows: triggered time 06.50:25 local time, lat. 45.4949 N, long. 26.5166 E, focal depth 148.8 km, 122 km and 48.33 km epicentre distances for Bucharest and Focsani respectively. The earthquake belongs to the intermediate-depth Vrancea seismic region and was felt with intensities about V on MSK scale in the epicentre area and III-IV in both cities, as well as in other cities over the country (Figure 1b). This seismic area has generated 11 earthquakes above 5 M_W in the last 23 years. The earthquake was recorded with high quality data at 132 accelerometers with North-East South-West directivity of the highest values, as well as in the Eastern part of the epicentre with maximum PGA = 48 cm/s^2 (INCDFP internal seismic report, www.infp.ro, ROMPLUS, 2022).

BUILDINGS SEISMIC NETWORK AND MONITORING PERFORMANCE

The improvement of the National Seismic Network (RSN) was a constant concern at National Institute of R-D for Earth Physics (INCDFP). An increase of the performance of seismic instruments was pursued, in order to record in the wide range of frequencies from very strong seismic movement to very weak vibrations.

In the last couple of decades, RSN has seen a remarkable development, so that currently, Romania has one of the largest and most modern seismic networks in Europe. Data recorded from 163 stations (Marmureanu et al., 2021b; Neagoe et al., 2011) which cover the entire country territory are transmitted in real-time to the main location (Magurele).

In the last decade, the National Institute for Earth Physics has deployed permanent instrumentation with accelerometers at key stories of six buildings in metropolitan cities areas that recorded the seismic motion. This activity was carried out and supported through different scientific projects, cooperation activities and research contracts (see, for example: URban Seismology Project CRC461, 2003; Ritter et al., 2005; NATO Project 981882, 2008; TURNkey Project, 2019; Balan et al., 2020b; Balan et al., 2022b). Within the Department of Engineering Seismology structures behaviour was studied, to better understand the influence of seismic movements on constructions. The recorded data are transmitted in real time to the National Data Centre (NDC) (BRTT, 2018).

The monitored buildings are Institute of Atomic Physics (TURN tower building, IFA), located in Magurele area, a locality near Bucharest city, completed in 1974 and partially damaged by the 1977 earthquake being retrofitted twice, and Hotel Unirea from Focsani (FOCR), Vrancea County, near to the Vrancea seismic source. Both are tall reinforced concrete structures.

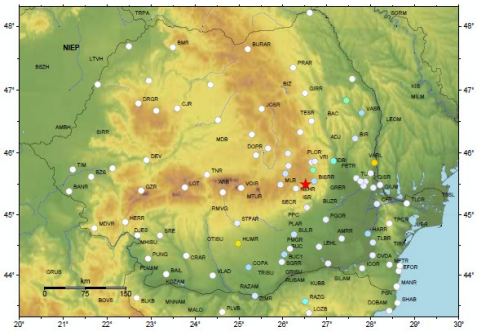

Figure 1a. Epicentre location and recorded velocities stations of 5 M_W earthquake, 2022.11.03 (after ROMPLUS, 2022 and INCDFP internal seismic report, 2022)

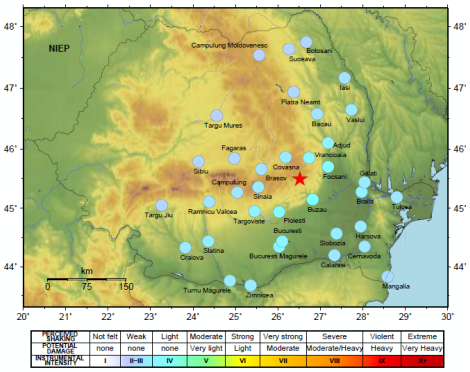

Figure 1b. Estimated intensities (MSK) of 5 M_W earthquake, 2022.11.03 (after ROMPLUS, 2022 and INCDFP internal seismic report, 2022)

The monitoring is achieved at building TURN with 3 accelerometers placed at underground (TURN1), 6th floor (TURN2) and 10th floor (TURN3), and at building FOCR with 3 accelerometers placed at basement (FOCR1), 4th floor (FOCR2) and 8th floor (FOCR3).
The TSA-100S tri-axial accelerometers and a 24-bit Digitizer (iDAS) transmitted data in real-time to the INFP' National Data Centre (NDC), for the purposes of archiving and post-processing.

The instrumented buildings of different design and at different epicentral distances have the following structural characteristics:
- TURN tower, a structure situated in the Southern part of the Bucharest city (10 floors high), on office building, of reinforced concrete with shear walls, built in 1974, retrofitted after 1990 (Figure 2, left).
- FOCR, Hotel Unirea, a tower structure in Focsani, located near the epicentral area, suits (8 floors high), of reinforced concrete frames, built in 1971 (Figure 2, right).

Figure 2. The instrumented buildings, TURN in Bucharest city (left) and Hotel Unirea in Focsani city (right)

The data recorded by free-field seismic stations located in Bucharest were used as reference motion, in order to assess the amplification or decreasing of the seismic waves when propagating in the structure. Acceleration and velocity data were previously analysed, both in time domain and in frequency domain, for selected frequency ranges (Balan et al., 2020b; 2021). In the framework of the previous studies on data recorded on buildings located in

Bucharest, this study adds new valuable information and contributes to a better understanding of seismic response of buildings.

MATERIALS AND METHODS

One of the important activities of the engineering seismology is the evaluation of the site's response, and of the earthquake engineering, structure response at seismic loads and buildings response as overall. These characteristics and information can be used further to carry out seismic risk analyses, which must include (besides exposure data) the vulnerability of the structures.

It is important to ensure the data flow and make them available in a shorter time after the earthquake, to the authorities, civil protection, decision makers. Following the most accurate and rapid evaluation of the engineering parameters, information is obtained about the behaviour of the respective structure, certain type of buildings, or of group of buildings in the area under the respective seismic demand. Nowadays in Bucharest there are more than 40000 buildings erected before 1940, which is an alarming fact. The recorded acceleration time histories are pre-processed: baseline corrected and filtered using a 4^{th} order Butterworth bandpass (0.2-25 Hz) filter. The limits were set for obtaining a good signal to noise ratio, and a taper function was applied on the data to allow the Fourier spectra calculation.

In Figure 3 are shown the recordings for the studied earthquake in terms of acceleration and corresponding computed velocity and displacement, at the underground or basement of the buildings, on the horizontal directions, i.e., N-S and E-W. In the case of a medium or strong earthquake, the seismic recordings sent in real-time to the processing centre underpin a standard report which is generated based on regular procedure for the buildings seismic instrumentation.

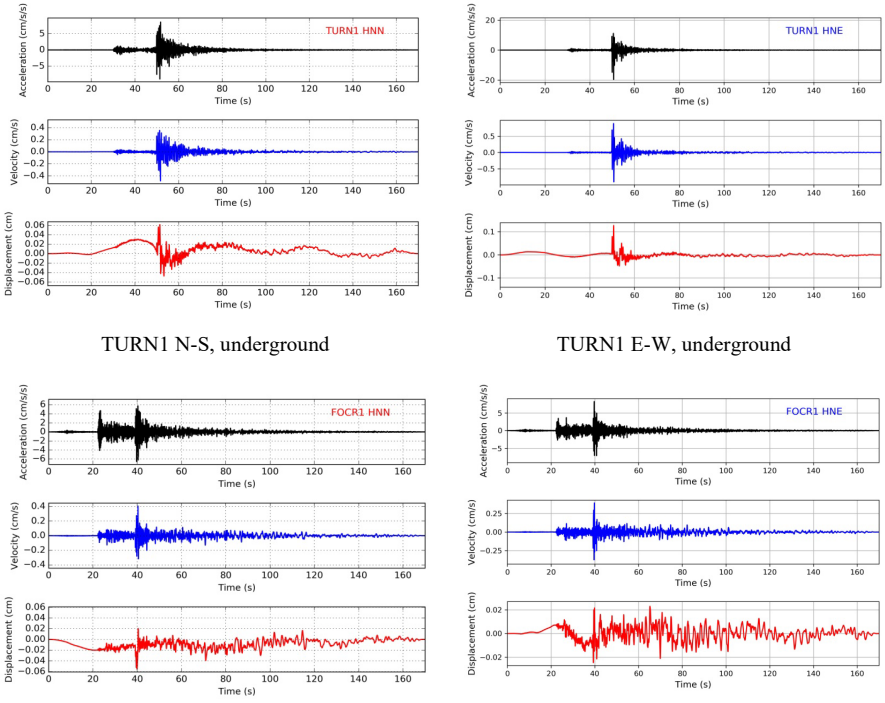

TURN1 N-S, underground

TURN1 E-W, underground

FOCR1 N-S, basement

FOCR1 E-W, basement

Figure 3. Recordings on two buildings, at the underground TURN1 (up) and basement FOCR1 (down) sensors, on two horizontal components (N-S, left, and E-W, right)

It consists mainly in seismic, engineering and damage related parameters such as maximum recorded acceleration, spectral acceleration, corresponding fundamental and oscillation periods belonging to elastic response spectra, Fourier spectra and acceleration recordings waveform. This information is of concern mainly for civil protection purposes and a possible spatial distribution and degree of expected damages are assessed where is the case. Once this spectrum is computed, it is compared with the code spectrum used to design that building or for the area. The received data are processed and integrated for a quick assessment of the structural situation in a given area. The Antelope software package, from Boulder Real-Time Technologies (BRTT, 2018) is undertaking the analyses, archive and exchange of the seismic data. It is the main tool for collecting and exchanging seismic data. The Bighorn module is an extension module of the Antelope package, performing real-time computations of spectral acceleration exceedance and issues alarms accordingly (Skolnik et al., 2014). The main program can continuously compute strong motion response spectra for sets of 3-component waveforms for many stations and then release parameter file spectra packets. These packets are fed to a strong motion response spectra alarm detector, which compares the actual response spectra to a set of exceedance limit spectra and displays them (more precisely: near-Real-time calculation of pseudo-spectral acceleration - PSA exceedance and alarm dissemination).

RESULTS AND DISCUSSIONS

Near-real time analysis and results

The Fourier Spectra analysis reveals approximately same ranges for frequency amplification for both buildings, as well as for the amplitude peaks. Only one peak differs in amplitude, on EW component at TURN1 being the highest value (Figures 4a and 4b). From these data one can conclude there are some similarities between buildings response in frequency domain, especially in amplification range, including corresponding amplitude peaks and even amplitudes level for three out of four spectra.

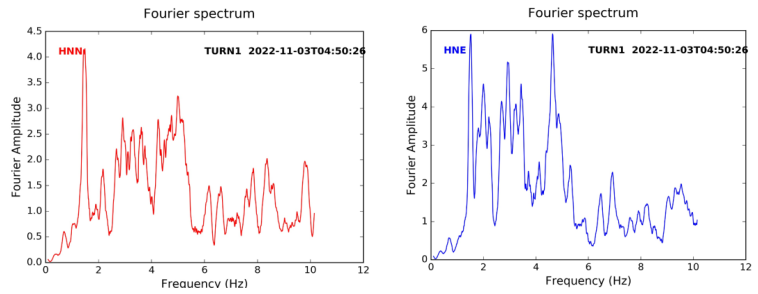

Figure 4a. Fourier spectra at building TURN, underground sensor TURN1, on NS (left) and EW (right) components

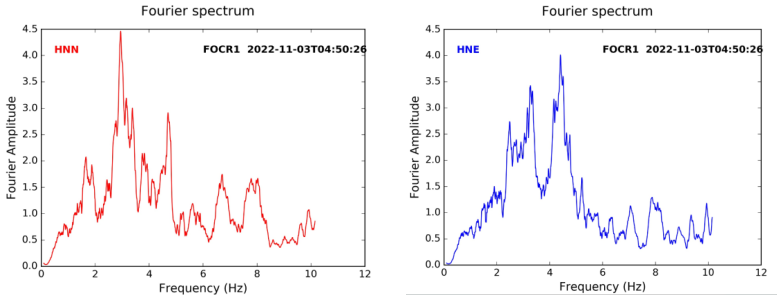

Figure 4b. Fourier spectra at building FOCR, basement sensor FOCR1, on NS (left) and EW (right) components

The processing of the data releases elastic response spectra in terms of spectral pseudo-acceleration, with 5% damping. In Figures 5a and 5b the information is presented as engineering parameters, that are maximum acceleration a_{max} recorded on three directions (two horizontal, NS, EW, and one vertical Z), maximum spectral acceleration (SA_{max}) from elastic response spectra, and corresponding oscillation periods T_0.

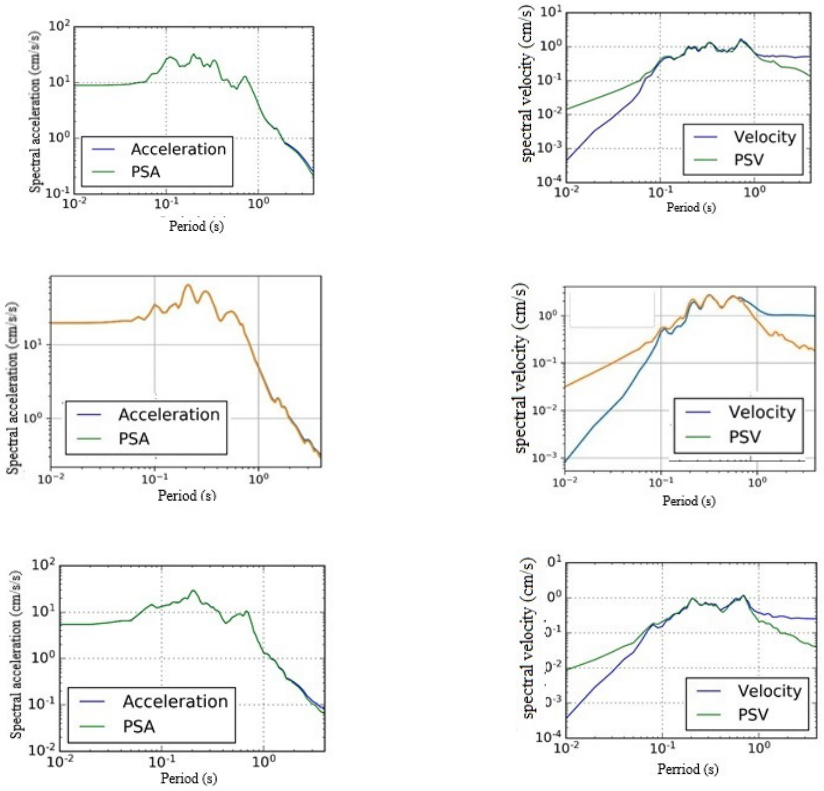

Figure 5a. Acceleration (left) and velocity (right) spectra at the underground sensor TURN1, on NS (up), EW (middle), Z components (down)

The sensors that yield these parameters are located at the underground or basement of the two buildings (TURN1 and FOCR1) located in Magurele, a town near Bucharest, being part of its metropolitan area, and Focsani city. From Table 1 could be observed that maximum accelerations in two buildings are spanning on a low values interval, between ~5-20 cm/s^2, therefore one could not imply differences due to the focal localization or epicentral distances.

However, for the Focsani city the highest value is on vertical component (Z, 13.38 cm/s^2), the other two horizontal ones having lower values (6.55 cm/s^2 on NS and 8.22 cm/s^2 on EW). The same situation is valid for spectral acceleration too, as oscillation periods are higher for the horizontal components, with 0.23 s the higher on EW direction.

In the case of the other building (TURN1), the situation is quite the opposite, with higher values of acceleration on horizontal directions, the stronger 19.63 cm/s^2 and on EW component. This value is however stronger than those in Focsani, which is closer to the epicenter. The same for SA_{max} with 65.08 cm/s^2 (EW). The spectral characteristics display oscillation period value in a restricted range for building TURN1, with much closer values around 0.21 s. For the building FOCR1 the values are much disperse, between 0.07 s (Z) and 0.23 s (EW).

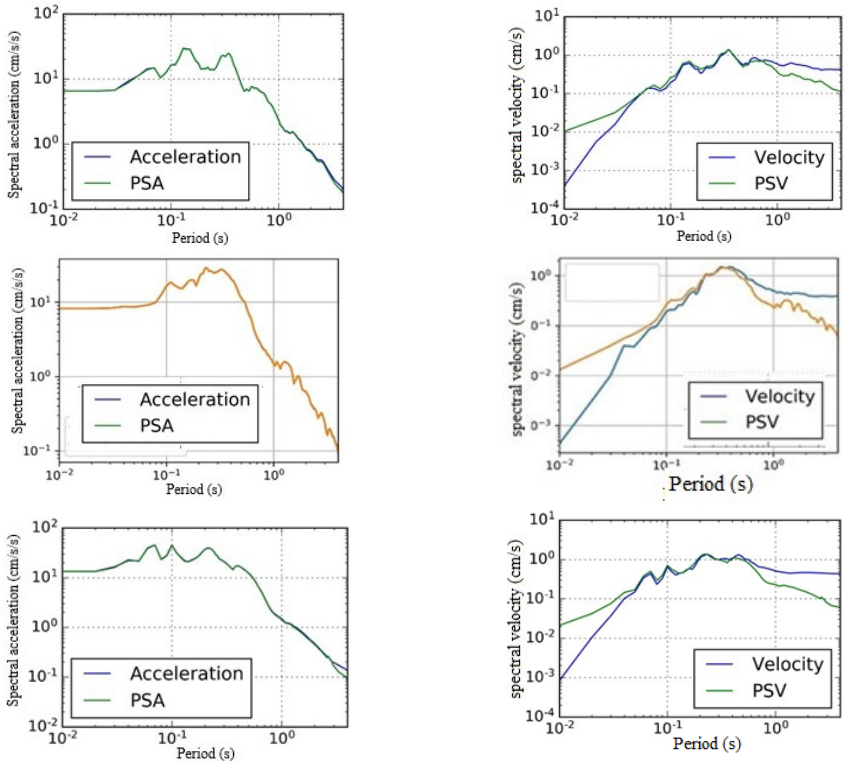

Figure 5b. Acceleration (left) and velocity (right) spectra at the basement sensor FOCR1, on NS (up), EW (middle), Z components (down)

Table 1. Engineering parameters (maximum recorded acceleration, maximum spectral acceleration, oscillating period) for three components at both buildings

Date/ Magnitude M_W/ Depth	Station	Component								
		N-S			E-W			Z		
		a_{max} (cm/s^2)	SA_{max} (cm/s^2)	T_0 (s)	a_{max} (cm/s^2)	SA_{max} (cm/s^2)	T_0 (s)	a_{max} (cm/s^2)	SA_{max} (cm/s^2)	T_0 (s)
2022.11.03 M_W=5, 148.8 km	TURN1	8.95	32.53	0.2	19.63	65.08	0.21	5.41	28.92	0.2
	FOCR1	6.55	29.43	0.13	8.22	28.65	0.23	13.38	45.30	0.07

Considering higher median value for the former, one can assume strictly the two buildings design specificity, though they are of almost same high, construction material, being typical representatives of structures build under seismic codes in the Romania `70s.

Moreover, building TURN1 is twice retrofitted, as it suffered damages under two strong seismic event of 1977 and 1986, hence one may substantiate the success of these interventions.

CONCLUSIONS

In the aftermath of the 2022.11.03 earthquake the developed methodology was validated through a robust procedure for an impact analysis of the involved systems (near-real time) toward improvement of the community resilience to earthquakes. The application was implemented and proved for two risk-endangered cities.

The network consisting in structures or free-field deployed sensors has undertaken an appropriate integration of its data in the national seismic network thus improving local and regional seismic monitoring. It secures and demonstrates the real-time streaming of various seismic markers in a consistent data format to the central server through continuously feed parametric data from the buildings' sensors to the platform that enables a consistent approach to improved post-Earthquake Warning and Rapid Response to Earthquakes. The present study is focused on two tower buildings presenting structural similarities, i.e., TURN1 and FOCR1 located in different cities, built at the same time. For the purpose of this work are basically used recordings from three-component accelerometers, installed on 3 levels at each building (see Figure 3, upper panels, black). The accelerations recorded on the analysed structures were a result of Vrancea medium magnitude earthquake of 2022.11.03, with magnitudes Mw 5, and focal depth 148.8 km (ROMPLUS, 2022). An analysis of structural response was made concerning each building, and acceleration response spectra, Fourier spectra at the underground (TURN1) or basement of buildings (FOCR1) are calculated. The recorded data and subsequent analysis aim to contribute to a better understanding of the structure's responses, even subjected to medium magnitude seismic events, and to the mitigation of seismic risk for densely populated areas.

Fourier amplitude spectra data show highest level of amplification, with amplitude around 6 for EW component at building TURN1, therefore at longer epicentral distance. The corresponding frequency range is between 1.5 and 4.5 Hz, with ordinate peaks at its limits. The first peak corresponds on the NS component too, but at a lower amplitude level, slightly above 4, as well as amplification on frequency range (~1.5-5 Hz). At closer epicentral distance, the building FOCR1 the peaks are observed at 4.2 Hz on EW direction and ~3 Hz on NS, as the amplitudes are in the range 4-4.5 for both components. The response spectra analysis suggests that the amplitudes values, ranges and structural behaviour are not quite different from the previous studies in respect with this earthquake-type characteristics, i.e. Vrancea intermediate-depth source, localization, magnitude range (moderate), epicentral distances, for the instrumented buildings located in both cities, including their design characteristics (Balan et al., 2018; 2019; 2021; 2022a, 2022b).

At the same time with the National Seismic Network development the buildings monitoring network has been designed and implemented – for pursuing the main objective of an acceleration network that is to provide, information to calculate the event parameters (BRTT, 2018). The procedure implemented by INCDFP relying on an automatic near-real-time report provides valuable information for the decision making authorities (Balan et al., 2019; 2021; 2022a, 2022b; Tiganescu et al., 2021).

Further developments of this application at larger scale implies a continuously enhancing of the equipment quality for seismic shaking monitoring, especially at buildings, data processing and sensing level performance enabled for permanent surveillance and temporarily experiments assessing.

ACKNOWLEDGEMENTS

This paper was carried out within Nucleu Program SOL4RISC, supported by Ministry of Research, Innovation and Digitization, project no. PN23360201, PN23360101.

REFERENCES

Apostol, B.F. (2017). A resonant coupling of a localized harmonic oscillator to an elastic medium. *Romanian Reports in Physics*, *69*, 116.

Balan, S.F., Tiganescu, A., Apostol, B.F. (2018). Seismic Monitoring of Structures Subjected to Medium Intensity Earthquakes. *18th International Multidisciplinary Scientific Conference Earth & GeoScience, SGEM 2018*, Albena, Bulgaria, June 30 - July 9.

Balan, S.F., Tiganescu, A., Apostol, B.F., Danet, A. (2019). Post-earthquake warning for Vrancea seismic source based on code spectral acceleration exceedance. *Earthquakes and Structures, an International Journal*, *17*(4), 365-372. doi: 10.12989/eas.2019.17.4.365

Balan, S.F., Tiganescu, A., Apostol, B.F. (2020a). Structure response analysis of the seismic isolated buildings in Bucharest city. I*OP Conf. Ser.: Earth Environ. Sci. 609 012080, WMESS 2020*, Praga, September 7–11. doi:10.1088/1755-1315/609/1/012080

Balan, S.F., Apostol, B.F. (2020b). Urban Researches for Risk Mitigation in Bucharest City Area. *Scientific*

Papers. Series E. Land Reclamation, Earth Observation & Surveying, Environmental Engineering, 9, 98–105, Bucharest.

Balan, S.F. Apostol, B.F., Tiganescu, A. (2021). Soil Conditions and Structural Typologies for Seismic Isolation of Buildings, in Cities Exposed to Strong Earthquakes Hazard. *Scientific Papers. Series E. Land Reclamation, Earth Observation & Surveying, Environmental Engineering, 10*, 128–134, Bucharest. (Print ISSN 2285-6064, ISSN-L 2285-6064).

Balan, S.F. Apostol, B.F., Tiganescu, A. (2022a). The Impact of TURNEY Seismic Monitoring Network in Bucharest. *Scientific Papers. Series E. Land Reclamation, Earth Observation & Surveying, Environmental Engineering, 11*, 281-288, Bucharest. (ISSN 2285-6064, ISSN-L 2285-6064, Online ISSN 2393-5138)

Balan, S.F. Apostol, B.F., Tiganescu, A., Danet, A. (2022b). Monitoring buildings at INFP for seismic vulnerability mitigation. *3rd European Conference on Earthquake Engineering & Seismology*, Bucharest, Romania (3ECEES), September 2022, 4381-4386.

Bratosin, D., Apostol, B.F., Balan, S.F. (2017). Avoidance strategy for soil-structure resonance by considering nonlinear behaviour of the site materials. *Rom. J. Phys*., *62*, 5-6, 808.

BRTT (2018). *Boulder Real Time Technologies*, Boulder, CO, USA, from www.brtt.com

Bonjer, K.-P., Glavcheva, R., Drumea, A., Paskaleva, I., Radulian, M., Radovanovich, S., Gribovszki, K., Weisbrich, W. (2010). Destructive Vrancea (Romania) intermediate depth earthquakes: intensity distribution and isoseismals. *Geophysical Research Abstracts, 12*, EGU2010-6159, EGU General Assembly.

Dilley, M., Chen, R.S., Deichmann, U., Lerner-Lam, A.L., Arnold, M. with Agwe, J., Buys, P., Kjekstad, O., Lyon, B., Yetman, G. (2005). Natural disaster hotspots: A global risk analysis. *The World Bank Hazard Management Unit*, Washington, D.C.

EN 1998-1. (2004). Eurocode 8: Design of structures for earthquake resistance - Part 1: General rules, seismic actions and rules for buildings, European Committee for Standardization; Brussels, Belgium.

Gallipoli, M.R., M. Mucciarelli, R.R. Castro, G. Monachesi Contri, P. (2003). Structure, soil-structure response and effects of damage based on observations of horizontal-to-vertical spectral ratio of micro-tremors. *Soil Dyn. Earthquake Eng*., *24*, 487–495.

Internal seismic report (2022). National Institute for Earth Physics (INCDFP).

Ismail-Zadeh, A., Matenco, L., Radulian, M., Cloetingh, S., & Panza, G. (2012). Geodynamics and intermediate-depth seismicity in Vrancea (the south-eastern Carpathians): Current state-of-the art. *Tectonophysics*, 530-531, 50–79. https://doi.org/10.1016/J.TECTO.2012.01.016

Kronrod, T., Radulian, M., Panza, G.F., Popa, M., Paskaleva, I., Radovanovich, S.L, Gribovszki, K., Sandu, I., & Pekevski, L. (2013). Integrated transnational macroseismic data set for the strongest earthquakes of Vrancea (Romania). *Tectonophysics*, *590*, 1–23.

Lomnitz, C. (1999). The end of earthquake hazard. *Seism. Res. Lett*., *70*, 387–388.

Marmureanu, G., Moldoveanu, C.L., Cioflan, C.O. Apostol, B.F. (1999). The seismic earth response by considering nonlinear behavior of the soils at strong Vrancea earthquakes. *In: Vrancea Earthquakes: Tectonics, Hazard and Risk Mitigation, Wenzel F., Lungu D., Novak O. (Eds.)*, Netherlands, Kluwer Academic Publishers, Dordrecht, 175–185.

Marmureanu, G. (2016). *Certainties/Incertainties in Vrancea hazard and seismic risk evaluation,* Romanian Academy Publishing House, Bucharest, Romania.

Marmureanu, G., Borcia, I-S. Marmureanu, A., Cioflan, C.O., Toma-Danila, D., Ilies, I., Craiu, G.M. Stoian, I. (2020). Larger peak ground accelerations in extra-Carpathian area than in epicentre. *Romanian Journal of Physics*, *5-6*(65), 1-10.

Marmureanu, G., Cioflan, C.O., Apostol, B.F. (2021a). Seismic response analysis for Romanian extra-carpathian sedimentary areas. *Territorium*, *28*(II), 83–92.

Marmureanu, A., Ionescu, C., Grecu, B., Toma-Danila, D., Tiganescu, A., Neagoe, C. (2021b). From National to Transnational Seismic Monitoring Products and Services in the Republic of Bulgaria, Republic of Moldova, Romania, and Ukraine. *Seismol. Res. Lett., 92*(3), 1685–1703. doi:10.1785/0220200393

NATO SfP Project 981882 (2008). Site-effect analyses for the earthquake-endangered metropolis. *Final Report NATO SfP Project 981882*, 2006-2008, Bucharest, Romania.

Neagoe, C., Manea, L.M., Ionescu, C. (2011). Romanian complex data center for dense seismic network. *Annals of Geophysics*, *54*(1), 9–16.

P 100-1/2013 (2013). Seismic Design Code - Part I: Earthquake Resistant Design of buildings, Ministry of Regional Development and Public Administration (M.D.R.A.P.); Bucharest, Romania (in Romanian) from https://doi.org/10.1016/j.tecto.2020.228688.

Ritter, J.R.R., Balan, S.F., Bonjer, K.-P., Diehl, T., Forbinger, T., Marmureanu, G., Wenzel, F., Wirth, W. (2005). Broadband Urban Seismology in the Bucharest Metropolitan Area. *Seismological Research Letters*, *76*, 5.

ROMPLUS (2022). *Romanian earthquake catalogue*, National Institute for Earth Physics, Magurele, Romania, from www.infp.ro/romplus.

Skolnik, D.A., Ciudad-Real, M., Franke, M., Harvey, D. and Lindquist, K. (2014). Post-earthquake alarm system based on real-time continuous response spectra exceedance. *Proceedings of the 10th U.S. National Conference on Earthquake Engineering*, Anchorage, Alaska.

Takewaki, I. (2001). Resonance and criticality measure of ground motions via probabilistic critical excitation method. *Soil Dyn. Earthquake Eng*., *21*, 645–659.

Tiganescu, A., Toma-Danila, D., Grecu, B., Craifaleanu, I.G., Florin Balan, S., and Sorin Dragomir, C. (2021). Current Status and Perspectives on Seismic Monitoring of Structures and Rapid Seismic Loss Estimation in Romania. *In: Proc. of the 1st Croatian Conference on Earthquake Engineering*, S. Lakušić

and J. Atalić (Eds.), 81–91 *1CroCEE*, Zagreb, Croatia. doi:10.5592/CO/1CroCEE.2021.120.

Trifunac, M.D., Todorovska, M.I. (2000). Long period microtremors, microseisms and earthquake damage: Northridge, CA, earthquake of 17 January 1994. *Soil Dyn. Earthquake Eng*., *19*, 253–267.

Trifunac, M.D., Ivanovic, S.S., Todorovska, M.I. (2001a). Apparent period of a building. I. Fourier analysis. *J. Struct. Eng*., *27*(5), 517–526.

Trifunac, M.D., Ivanovic, S.S., Todorovska, M.I. (2001b). Apparent period of a building. II. time-frequency analysis. *J. Struct. Eng*., *27*(5), 527–537.

TURNKey Project. (2019). Towards more Earthquake-resilient Urban Societies through a Multi-sensor-based Information System enabling Earthquake Forecasting, Early Warning and Rapid Response Actions, Contract 821046, European Union's Horizon 2020.

Urban Seimology Project. (2003). URS Collaborative Research Centre 461 (CRC461), at the University of Karlsruhe, Geophysical Institute, and the National Institute of R-D for Earth Physics (NIEP), 2003-2004.

Scientific Papers. Series E. Land Reclamation, Earth Observation & Surveying, Environmental Engineering. Vol. XII, 2023
Print ISSN 2285-6064, CD-ROM ISSN 2285-6072, Online ISSN 2393-5138, ISSN-L 2285-6064

THE STATE AND BEHAVIOR OF SOME FORESTRY CULTURES INSTALLED ON DEGRADED LANDS IN THE FOREST-STEPPE SITE

Cristinel CONSTANDACHE, Ciprian TUDOR, Laurenţiu POPOVICI, Vlad RADU

"Marin Drăcea" National Institute for Research and Development in Forestry,
Romania, 128 Eroilor Street, Voluntari, Ilfov County

Corresponding author email: cipriantudor210@gmail.com

Abstract

The research carried out aimed at capturing the structural and qualitative changes, the overall evolution of forest ecosystems on degraded lands and highlighting the types of effective cultures on different categories of degraded land. The researches were carried out in the period 2017-2018 in research plots located in perimeters for the improvement of degraded lands, in representative situations. In the paper are presented synthetically the data regarding on the characteristics of forestry cultures in the forest-steppe site, realized in different compositions on lands with various forms of degradation.
On very strongly eroded and ravenous lands, the forestry cultures made with black pine in intimate mixture with xerophytic species and shrubs, gave good results. On moderately to heavily eroded lands, mixed cultures with oak and different species, gave good results, in association them in biogroups or grouping at least 2 rows of oak interleaved with accessory species and shrubs. The obtained results offer particularly valuable information for the scientific substantiation of future afforestation compositions and of the silvotechnical works for the installation and tending of forestry cultures on degraded lands.

Key words*: afforestation, degraded lands, forest-steppe, forestry cultures.*

INTRODUCTION

In the current international circumstances, when more and more emphasis is placed on increasing the role of the forest in environmental protection and mitigating climate change, but also as a renewable natural resource, the management (tending and management) of stands becomes a primary concern of the forester.
On this line, the latest researches take into account the issues of stability, structure, regeneration, the dynamics of the development of stands on degraded lands (Vlad et al, 2019). Nowadays, the stands are affected by abiotic factors (drying, breaks, ruptures), following climate changes (Constandache et al., 2016; Dincă & Achim, 2019; Dinulică et al., 2015; Merlin et al., 2015; Silvestru-Grigore et al., 2016). Protective forestry cultures were installed on degraded lands in order to improve and exploit them (Constandache, 2003; Traci, 1985). The types of forestry cultures with an ameliorative role, the compositions and planting schemes, the techniques of land preparation and afforestation of degraded lands constituted an object of concern for a large number of researchers from the forestry and agricultural domains (Constandache et al., 2006; Ciortuz, 1981; Ciortuz, 2004; Nistor & Nistor, 2002). The afforestation actions carried out in the past, for the most part, had the expected improvement effects. It is estimated that in our country there are approximatively 300,000 hectares of degraded lands, mostly afforested with pine and locust (Enescu & Dănescu, 2015; Lukić et al., 2015; Untaru et al., 2012; Untaru et al., 2013). Many of these were damaged due to some abiotic factors (drought, wind, etc.), in the conditions of climate changes but also in situations where they were not covered in time or properly with tending works, being currently destructured (Constandache et al., 2020). Others have exceeded the age of 60 where silvotechnical measures are required for their regeneration and succession (Cenușa, 1992).
The evolution of cultures takes place in the most difficult pedo-climatic conditions, under the influence of a complex of abiotic (drought, wind, snow, etc.) and biotic (mushrooms, insects, etc.) disturbing factors whose action has

intensified in the last time and which can generate strongly imbalances at certain moments, their behavior and evolution being unpredictable (Cenuşă, 2002; Constandache, 2003; Giurgiu, 1987; 2004). Very important, in the current conditions, are the state of health of the stands, given by the biological particularities of the species of trees and shrubs in the composition, in relation to the environmental conditions (Ganatsas, 2011; Chazdon, 2008; Onet et al, 2019).

The state and evolution of forestry cultures on degraded lands were monitored periodically (intervals of 5 years) starting from 1981, when permanent research plots were placed in perimeters for the improvement of afforested degraded lands (Traci & Untaru, 1986; Traci & Costin, 1966). In addition to the existing research plots, it was necessary to expand the network of permanent research plots and in forestry cultures installed on degraded lands after 1980 (especially in the forest-steppe site, where the effect of climate change is more obvious- PN 305, 2016). The monitoring of these cultures is important in the current conditions, the surface of the stands affected by drying or other harmful factors, being in a continuous increase. Assessing the state and their evolution are important for ensuring an adaptive management of forest ecosystems on degraded lands (Badea, 1998; Badea et al., 2004; Badea, 2008; Mînza & Mamai, 2010). Thus, in order to be able to create the conditions for maintaining ecological functionality and stability in forestry cultures on degraded lands, it will be necessary to take into account the effect of harmful factors, in addition to monitoring the structural parameters (consistency, thickness and so on) both directly influence stability (biotic, abiotic) and indirectly influence individual and group stability, in the context of climate change (Martín-Benito et al., 2013; Mérian & Lebourgeois, 2011; Zang et al., 2012; Vlad & Constandache, 2014). In the conditions of climate change, the increase in average annual temperatures by more than 1-2ºC will have as a first consequence, the aridification of the southern and south-eastern, plain, but also hilly areas, causing major changes in environmental conditions and the emergence of limiting conditions for vegetation forestry, according to the specifications published in the *"Guidelines on adaptation to the effects of climate change"* (Stocker et al., 2013).

The effects of forestry cultures consist in the improvement, stabilization and valorization of inefficient lands for other uses (Constandache et al., 2010) but also in mitigating the effects of global warming through the high storage capacity of atmospheric CO_2 (Dincă et al., 2015), stopping land degradation due to the ability to fix and improve soils (Nicolescu et al., 2018), reducing anthropogenic pressure on natural forestry ecosystems and using them as an alternative for obtaining fossil fuels (Spîrchez & Lunguleasa, 2016).

The research carried out was aimed at analyzing the current state of forest crops and structural characteristics in specific environmental conditions.

MATERIALS AND METHODS

The researches were carried out in 27 research plots, located in 7 improvement perimeters (PA) from Romania, afforested in the period 2002-2006, located in the east and south-east of the country, in representative situations (compositions and environmental conditions of degraded lands). At the establishment of the research plots there was in view of tracking the main species and formulas used in afforestation in relation to the intensity of degradation. After the establishment of the research plots, the measurements and observations in forestry cultures from forest-steppe site were made (Figure 1), on lands affected by complex degradation, respectively: moderate to very strongly erosion in the surface associated with excessive dryness, in the following improvement perimeters (PA):

- A. Buznea, Iloaiei Bridge Forest District-Iaşi County, (*47°11'29.41" N; 27°02'11.69" E*);
- B. Gropana and Hulubăţ, Epureni Forest District-Vaslui County (*46°19'52.22" N, 28°02'28.72" E*);
- C. Lozoviţa, Hanu Conachi Forest District, Galaţi County (*45°37'7.03" N, 27°53'12.12" E*);
- D. Agighiol I and Agighiol III, Babadag Forest District-Tulcea County (*45°7'30.82" N, 28°50'36.70" E; 45°8'39.74" N, 28°52'2.92" E*);
- E. Releu-Vâlceaua-Negureni, Baneasa Forest District Constanța County (*44˚03'46.2" N, 27˚44'32.1" E*).

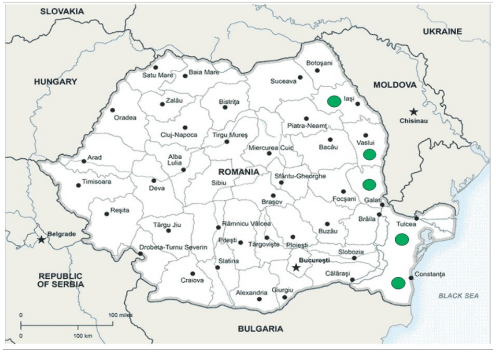

Figure 1. Location of improvement perimeters (PA) on the geographical map of Romania

The current state, biometric characteristics (average diameter-Dm; average height-hm), structural and diversity parameters of the stands in different environmenal conditions were analyzed and highlighted (Giurgiu et al, 2004; Giurgiu & Drăghiciu, 2004). To evaluate the structural diversity, a series of indexes were calculated: the basal surface (G), the average diameter (Dm) and its coefficient of variation (cv%-), the Hart-Becking (s%), Camino (H) and Gini (G). The Hart-Becking index (s%) expresses the density state of the stand. It was calculated according to the following formula:

$$s\% = \frac{a}{hdom} \cdot 100 \quad (1)$$

where: *a* - distance between trees; *hdom* - dominant height of the stand. The Camino (H) index were calculated in ratio with the basal surface, with the following formula:

$$H = \frac{\sum_{i=1}^{n-1} SN\%}{\sum_{i=1}^{n-1} SN\% - SG\%} \quad (2)$$

where: *SN%* - the cumulative number of trees until the i category; *SG%* - the cumulative basal surface until i category; n- maximum category of diameters in which SN% = 1.

According to Camino (1976), the homogeneity of stands can be expressed as a percentage ratio between the number of trees and the basal surface by category of diameters, expressed by a certain Lorenz curve. The degree of structural homogeneity is defined as a deviation of the Lorentz curve from the diagonal, in the sense that the value 10 indicates a high homogeneity, and the value 2 shows the lack of homogeneity. The Gini index (G) determined according to the basal surface is calculated as the ratio between the area determined by the Lorentz curve and the reference line. On the other hand, the area of the triangle is formed by the reference line with the abscissa and parallel to the ordinate through the point of intersection between the Lorentz curve and the right landmark. The values of the Gini coefficient are between 0 and 1, meaning maximum homogeneity and maximum heterogeneity. The more homogeneous a population is, the closer the value of the Gini index will be to 0.

The general calculation formula is:

$$G = 1 - 2 \cdot \int_0^1 f(x)dx \quad (3)$$

where *f(x)* - the function of the Lorentz curve in relation to the considered variable.

The comparative analysis of afforestation compositions and cultures establishment techniques used on lands affected by various forms of degradation provides valuable information regarding the viability of various forestry species in certain enviromental conditions, as well as regarding the planting scheme, the type of mixture, the silvotechnical works applied. Thus, the forestry species capable of enhancing different categories of degraded land were highlighted, as well as the most suitable techniques for the installation of forestry cultures.

Thus, on moderately eroded lands, research areas were installed in plantations with greyish oak (Stb) or common oak (St) in an intimate, grouped mixture or strips with different mixed deciduous species (linden-Te, ash-Fr, sweet cherry- Ci, maple-Ml, elm-Ul, sycamore-Pa, wild pear-Pă, mahaleb cherry-Vit, oleaster-Sl) and with locust (Sc). On strongly eroded lands, research plots were installed in plantations of: locust (pure or mixed); of greyish/common oak, mixed with Siberian elm or elm, ash, oleaster, honey locust or mahaleb cherry (50-67%) mixed with oleaster. On highly eroded lands, mixed crops of different deciduous species were identified (oleaster, manna ash-Mj, wild pear, cherry plum-Cd, sycamore or black pine mixed with wild pear, oleaster, mahaleb cherry, manna

ash with shrubs; on slippery lands with excess moisture- Pennsylvania ash and those without moisture- locust). The analyzed forestry cultures are between 10 and (15) years old and offer particularly valuable information for the scientific substantiation of afforestation compositions, mixing schemes, silvotechnical works (tending and management) of future forestry cultures on degraded lands.

RESULTS AND DISCUSSIONS

The afforestation works on the degraded lands were carried out by applying special techniques for the installation of forestry vegetation, different from those used in forestry lands, due to the harsh environmental conditions and the lack of shelter provided by the neighboring stands. As a result, the saplings were exposed to intense stress conditions (insolation and increased evapotranspiration, weed competition, limited access to nutrients, determined in particular by the accentuated shortage of water in the soil), requiring special measures for the establishment of the plantation, as well as for the maintenance of the cultures. Added to this is the fact that the soils in the degraded lands are beaten up by grazing and strongly sodded. The results obtained by afforestation of degraded lands are good, the forestry vegetation covering the entire area on which plantations were made (Figure 2).

Figure 2. Agighiol III improvement perimeter (Tulcea County Forest Administration, Babadag Forest District)

On moderately to heavily eroded land (E_1 - E_2), the forest crops have oak and acacia as the base species, being made through plantations both on simple terraces or on land prepared by strip plowing and on unprepared land (in pits etc.). In the compositions with oak (in a proportion of 10-30%, sometimes 70%), mixed species (linden, elm, cherry, palin, ash) were introduced as well as helpful xerophytic species: Turkish cherry, willow, Turkestan elm.

On moderately to heavily eroded lands (E_1 - E_2), the forestry cultures have common oak and locust as the base species, being made through plantations both on simple terraces or on land prepared by strip plowing and on unprepared land (in pits, hearths). In the compositions with common oak (in a proportion of 10-30%, sometimes 70%), mixed species (linden, elm, sweet cherry, sycamore, ash) were introduced as well as helpful xerophytic species: Mahaleb cherry, oleaster, Siberian elm.

The low proportion of common oak in the composition (<20%) and the intimate mixture with the other species are not favorable, especially on lands with more difficult conditions (sun exposure, higher slope, stronger erosion), where the common oak is overwhelmed and has reduced growths and the mixture/accessory species register an almost double increase in the number of exemplars compared to the normal number extracted from the production tables, a phenomenon that calls for the urgent application of silvicultural interventions to regulate thinning and especially to open some access roads in some places. It can be observed a large growth in the height of the greyish oak in the grouped mixture (Figure 3).

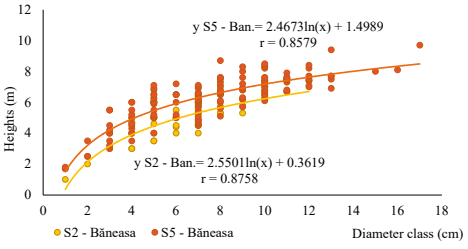

Figure 3. Height distribution on diameter classes at greyish oak (S2, S5-PA Releu-Vâlceaua-Negureni)

Regarding on the biometric characteristics of the stands analyzed: for common oaks, aged between 10-13 years, the average diameter (Dm) is between 2.88 cm (S1, PA Lozovița) and 6.47 cm (S3, PA Agighiol I), and the average height

(hm), between 3.53 m (S1, PA Lozovița) and 5.04 m (S3, PA Agighiol I). These results lead to the conclusion that the oaks maintain their development growth even in the case of strongly eroded lands, but it is still distinguishable from this phase, the highlighting and the larger growths of the arborescent species of the III size and with xerophytic character: the Siberian elm, mahaleb cherry, tartarian maple, oleaster and so on (Figure 4).

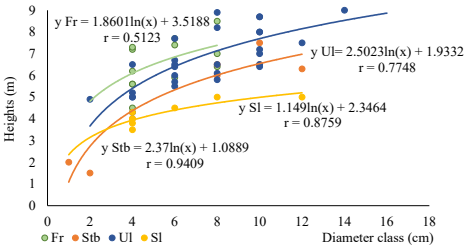

Figure 4. The distribution of the heights on diameter classes and on stand elements (S3, PA Agighiol I)

The oak is maintained and develops very well if the mixture is grouped or in rows grouped at least 2-3 and is surrounded, having lateral protection created by accessory and shrub species. Locust in pure cultures behaves very well achieving growths comparable to the higher production classes (II). The number of high trees is concentrated in the middle diameter classes and the curve of experimental frequencies follows the normal law of even-aged stands (Figure 5).

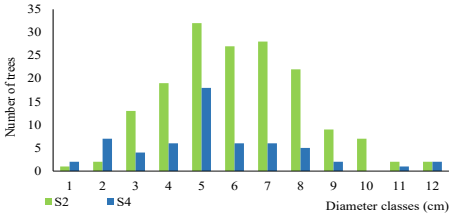

Figure 5. The structure of the stands in ratio with the diameter class at locust species

Locust cultures show different characteristics in different environmental conditions.

On lands with shaded and semi-shaded exposures, inferior slopes with a slight slope, without carbonates (S2, PA Lozovița), the locust cultures achieve values of the biometric characteristics (Dm, hm) significantly higher compared to the plantations of the lands with sunny exposures, with kneaded soils, with carbonates (S4, PA Lozovița) (Figure 6).

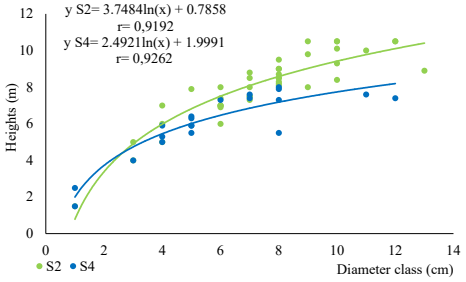

Figure 6. The relashionship between height and diameter at the stands constituted by locust species (S2, S4-PA Lozovița)

The biometric characteristics (number of trees, average diameter, average height) of the locust at the age of 10-12 years are superior to those of the common oak and the other species, both on moderately eroded and heavily eroded lands (Figure 7). The maximum number of trees belonging to the locust species falls into diameter class 6 (64 trees)-S2 PA Agighiol.

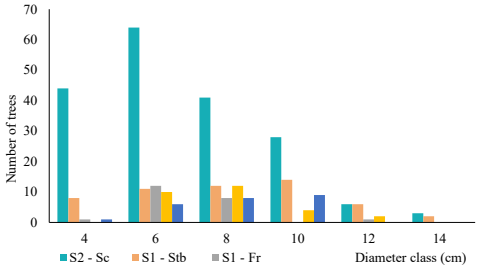

Figure 7. The distribution of the number of trees by diameter classes in pure cultures of locust and in mixed cultures of greyish oak and ash

On such lands, plantations of black pine (Pin) and/or Scots pine (Pi), (25%, in an intimate mixture with auxiliary species (manna ash, cherry plum, wild pear, mahaleb cherry) and xerophytic shrubs (blackthorn, dog rose, hawthorn and oleaster) at the age of 10 years, have both a state of vegetation and growth active, achieving average diameters between

8.84 and 9.78 cm and average heights between 4.61 and 5.06 m (Figure 8).
Such culture consisting of pines mixed with the mentioned auxiliary and shrub species, makes optimal use of environmental conditions and achieves higher biomass accumulations (in relation to the average basal area per stand) which represents 75% of the total.

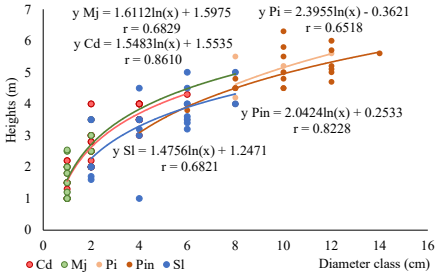

Figure 8. The distribution of heights on diameter classes for component species of forestry cultures from S4- PA Hulubăț (Vaslui) on very highly eroded lands (E_3)

Structural and diversity parameters of forestry cultures on degraded lands

When analyzing the structural diversity of forestry cultures, the grouping of individuals in space, their functional relationships and size variability were taken into account, highlighting the stability and ability to adapt to enviromental conditions, of forestry cultures with different compositions.
In the forestry cultures aged between 10-13 years from the 7 improvement perimeters investigated in the forest-steppe site, the dimensional variability of the exemplars is directly influenced both by the environmenal conditions specific to each improvement perimeter and by the nature of the species and their adaptability to the existing conditions. In addition, there are determining factors resulting from the constructive elements of the plantation, especially from the shape and dimensions of the planting device, the development space of each exemplar being often strongly influenced by the degree of development, especially in horizontal structure, of the neighboring exemplar of the adjacent species from device.

On heavily eroded lands, in the case of the mixture of xerophytic deciduous species (e.g., mahaleb cherry, oleaster, S1, PA Buznea), high variability was recorded both for diameters 35.36% and for heights (55.1%) due to the specificity of these species to form several stems on the same stump (bushes), with large diameters, which overwhelm each other, but which cover and stabilize the ground very well.
An optimal variability was registered by the pine cultures made on very strongly eroded lands, where the pine growths are distinguishable from the rest of the mixed species (S4, PA Hulubăt). The variability of the heights follows the distribution corresponding to the diameters. Also on very strongly eroded land, but also with sliding phenomena, with excess water on the surface (S4, PA Buznea), the Pennsylvania ash culture proved to be a viable solution in such situations, registering a normal variability of diameters (31.2%), but a low variability of heights (11.9%).
On moderately to strongly eroded lands, common oak and greyish oak cultures in intimate mixture with different deciduous species (ash, S3, PA Gropana; S3, PA Agighiol I); Siberian elm, oleaster, S1, PA Lozovița) shows a higher variability of diameters (42.1-54.2%) and a low variability of heights (<30%), determined by the intimate mixture of some species with different bioecological parcularities.
On moderately to strongly eroded lands, in common oak cultures mixed with deciduous species, the variability of diameters (37.7%) and heights (31.6%) are high (S5, PA Hulubăț), as a result of the diversification of species still forming the structure from the planting, an optimal balance between all the component elements, the main species: common oak, ash with the mixed species: linden, sweet cherry and Siberian elm and the accessory and xerophytic shrubs: cheery-plum, hawthorn, mahaleb cherry and so on. It is considered to be the most appropriate compositional formula among the cultures analyzed (Figure 9).

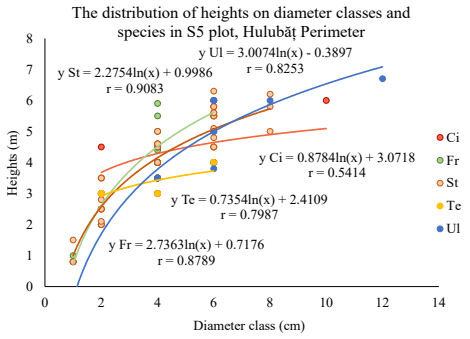

Figure 9. The relationship between quantitative variables (diameter class and height)

In the case of locust or honey locust cultures on heavily eroded land, the coefficients of variation for heights and diameters indicate normal distributions and variability, highlighting that the adopted solutions were appropriate to environmental conditions. The thickness (I_N) and density (I_G) indexex in some cases exceed the value of 1, due to the competitiveness and the very high number of trees (Table 1). The Hart-Becking spacing factor (s%) expresses in minimum percentages the connection that exists between the arrangement in the horizontal structure and the height of the trees, the maximum being reached in PA Releu-Vâlceaua-Negureni (S1).

Table 1. The indexes of thickness and spacing of the stands from analyzed improvement perimeters

PA	DEG	S	I_N	I_G	h_{dom}	s% Hart-Becking
Buznea	E_1	2A	2.07	1.82	10.01	14.84
	E_2	1	1.66	0.75	5.09	26.49
	E_2+Al	2B	1.99	2.07	8.94	16.28
		3	1.27	0.86	7.12	19.23
Gropana	E_1	1	1.51	1.34	8.65	15.53
	E_1-E_2	2	1.01	0.89	9.41	18.88
Hulubăț	E_1-E_2	5	1.07	0.56	5.67	25.82
		6	2.26	1.53	8.65	15.54
	E_3+R	4	1.02	1.06	5.43	28.18
Lozovița	E_1	2	1.36	1.27	9.75	17.80
	E_2	4	0.96	0.70	7.28	28.28
	E_1-E_2	1	1.42	0.45	5.16	27.91
Releu-Vâlceaua-Negureni	E_1	1	0.78	0.33	5.44	34.37
		2	0.63	0.69	6.46	29.41
		5	0.98	1.23	7.66	23.91
Agighiol I	E_1	2	1.70	1.36	10.69	15.34
	E_1-E_2	1	0.88	1.30	9.17	21.64
	E_2	3	0.96	0.79	7.95	20.25
		10	0.89	1.08	7.53	24.49

Note: DEG- degradation form; S-permanent experimental plot; I_N-density index by the number of trees; I_G-density index by the basal area; $s\%_{Hart-Becking}$- spatial index; R-ravenous land; Al-landslide.

The Gini (G) and Camino (H) indexes indicate a moderate to high degree of diversity for most of the analyzed mixed stands, which shows that these stands tend to evolve towards diversified structures on structural elements (classes of diameters, heights, number of trees, spacing index and so on) and tend to form relatively even-aged and relatively plurien structures from a juvenile stage of development. In relation to the Camino index (H), the structure of the stands varies from relatively even-aged (H between 3.25 and 4.71), to relatively plurien (H between 2.12 and 3.49), due to the diversified complexity of the species, competition ratios and dependence on ecological factors (Table 2). The homogeneity is represented by values of the Gini index close to the maximum homogeneity value (G = 0), which indicates that the frequency of the cumulative base areas (SG%) is distributed according to a Lorentz curve very close to the line of equality.

Table 2. Indexex of structural diversity and population variability

PA	DEG	S	cv% -D_m	H	G
Buznea	E_1	2A	35.70	4.02	0.37
	E_2	1	35.36	4.23	0.35
	E_2+Al	2B	34.80	4.32	0.35
		3	31.20	4.75	0.31
Gropana	E_1	1	46.30	3.49	0.47
	E_1-E_2	2	35.60	3.30	0.47
Hulubăț	E_1-E_2	5	44.32	5.86	0.44
		6	38.61	4.71	0.38
	E_3+R	4	26.86	2.33	0.59
Lozovița	E_1	2	35.30	4.52	0.36
	E_2	4	46.50	2.91	0.45
	E_1-E_2	1	56.10	3.23	0.52
Releu-Vâlceaua-Negureni	E_1	1	86.50	2.12	0.61
		2	56.20	3.25	0.36
		5	41.90	4.53	0.38
Agighiol I	E_1	2	34.50	4.36	0.36
	E_1-E_2	1	33.60	3.50	0.35
	E_2	3	45.10	3.95	0.45
		10	26.94	4.45	0.29

Note: cv%-D_m-coefficient of variation, H-Camino index; G-Gini index.

CONCLUSIONS

The forestry cultures made on degraded lands in the forest-steppe site for the most part, have achieved the purpose for which they were made and their follow-up over time will provide new scientific information particularly useful for the appropriate substantiation of the afforestation compositions of degraded lands from the forest-steppe site.

The results obtained from the research carried out are particularly useful in the management of stands on degraded lands, in establishing the type of silvotechnical interventions starting with the implementation of appropriate afforestation technologies and continuing with the application of tending and management works.

Diversification of afforestation compositions can sometimes present a disadvantage for valuable species (oaks), which in intimate mix with other species, can be embarrassed due to the high frequency of competition ratios.

This phenomenon calls for the urgent application of silvicultural interventions to regulate the thickness and density of cultures to optimize the multimodal structures.

For the best possible development, it is recommended that the xerophytic species of oaks to be introduced in grouped mixtures or in at least 2-3 grouped rows and ensure the planting of auxiliary species around them, to confer lateral protection.

The association of common oak mixed with deciduous species (linden, sweet cherry and Siberian elm) and with xerophytic accesory species and shrubs (cherry-plum, hawthorn, mahaleb cherry) proved to be the most appropriate compositional formula adapted to heavily eroded lands.

The behavior of locust proves to be beneficial in pure cultures, where it registers superior production classes (II).

Pine cultures, mixed with accesory species and shrubs species, make optimal use of environmental conditions and achieve superior biomass accumulations.

The installation of pines by association with a varied range of xerophytic species leads to obtaining multi-storey and multimodal structures, with higher resistance over time and with high anti-erosional efficiency.

In relation to Camino and Gini structural diversity indexed, most cultures show relatively even-aged to relatively plurien structures, homogeneous from the point of view of the Gini index.

In the future, resistant forms of the species used in afforestation or even other species that respond to the new complex challenges must be sought, respectively efficient ecological methods of management of the destabilizing factors.

ACKNOWLEDGEMENTS

This research work was carried out with the support of INCDS "Marin Drăcea", within the studies required for the assurance of sustainable management of the stands located on degraded lands in forest-steppe site (PN 16330305, 2016). The present work represents a starting point towards new directions and visions regarding the long-term research of the particularities of forestry cultures located on degraded lands from internal and external forest-steppe (PN 23090203, 2023).

REFERENCES

Badea, O. (1998). Forest Condition monitoring in Romania: results on optimization of the national permanent plot network for the assessment of forest health status. *Imprimerie ONF, Fontaibleau*, 15-17.

Camino, R. (1976). Zur Bestimmung der Bestandes homogenitat. *A*.F.J.Z., 147, 2/3, 54-58.

Cenuşă, R. (1992). Research on the structure, ecological volume, and succession of forest ecosystems at the altitudinal limit in the Northern Carpathians (Călimani and Giumalău), PhD Thesis. ASAS Bucharest. (in Romanian).

Constandache, C., Nistor, S., Ivan, V. (2006). Afforestation of the degraded lands unsuitable for agriculture in the southeast of the country (in Romanian). *Analele ICAS, 49*, 187-204.

Constandache, C., Dincă, L., Tudor, C. (2020). The bioproductive potential of fast-growing forest species on degraded lands. *Scientific Papers. Series E. Land Reclamation, Earth Observation & Surveying, Environmental Engineering. IX*, 87-93.

Constandache, C., Peticila, A., Dinca, L., Vasile, D. (2016). The usage of Sea Buckthorn (*Hippophae rhamnoides* L.) for improving Romania's degraded lands, *AgroLife Scientific Journal, 5(2),* 50-58.

Chazdon, R. L. (2008). Beyond Deforestation: Restoring Forests and Ecosystem Services on Degraded Lands. *Science, 1155365(1458),* 320.

Dincă, L., Achim, F. (2019). The management of forests situated on fields susceptible to landslides and erosion from the Southern Carpathians. *Scientific papers series Management, Economic Engineering in Agriculture and Rural Development*, *19*(3).

Dincă, L., Dincă, M., Vasile, D., Spârchez, G., Holonec L. (2015). Calculating Organic Carbon Stock from Forest Soils, *Notulae Botanicae Horti Agrobotanici Cluj-Napoca, 43(2),* 568-575.

Enescu, C.M., Dănescu, A. (2015). Black locust (Robinia pseudoacacia L.) - an invasive neophyte in the conventional land reclamation flora in Romania. *Bulletin of the Transilvania University of Braşov Series II: Forestry • Wood Industry • Agricultural Food Engineering, 6*(55) No. 2, 23-30.

Ganatsas, P., Tsitsoni, T., Tsakaldimi, M., Zagas, T. (2011). Reforestation of degraded Kermes oak shrublands with planted pines: effects on vegetation cover, species, diversity and community structure. *New Forests 43*, 1–11.

Giurgiu, V. (1987). Condition of forests with protective functions. The volume, "Optimal structures for protective forests" (in Romanian).

Giurgiu, V. (2004). *Silvology,* vol III B, Sustainable management of Romania's forests. Romanian Academy Publishing House, Bucharest, 320 (in Romanian).

Giurgiu, V., Drăghiciu, D., Decei, I. (2004). *Dendrometric methods and tables.* In Romanian. Bucharest, RO: Ceres Publishing House.

Giurgiu, V., Drăghiciu, D. (2004). *Mathematical-auxological models and production tables for stands.* In Romanian. Bucharest, Romania: Ceres Publishing House.

Lukić, S., Pantić, D., Simić, S.B., Borota, D., Tubić, B., Djukićand, M., Djunisijević-Bojović, D. (2015). Effects of black locust and black pine on extremely degraded sites 60 years after afforestation - a case study of the Grdelica Gorge (southeastern Serbia). *Forest, 9*. 235–243.

Nicolescu, V.N., Hernea, C., Bakti, B., Keser, Z., Antal, B., Rédei, K. (2018). Black locust (Robinia pseudoacacia L.) as a multi-purpose tree species in Hungary and Romania: a review. *Journal of Forestry Research*, *29(6).* 1449-1463.

Nistor, D., Nistor D., (2002). Land Degradation by Erosion and Its Control in Romania. *12th ISCO Conference, Beijing*. 621-626.

Onet, A., Dincă, L.C., Grenni, P., Laslo, V., Teusdea, A.C., Vasile, D.L., Enescu, R.E., Crisan, V.R. (2019). Biological indicators for evaluating soil quality improvement in a soil degraded by erosion processes. *Journal of Soils and Sediments*, *19(5).* 2393-2404.

Silvestru-Grigore, C.V., Spârchez, G., Dinulică, F. (2016). The health condition of pine stands installed on degraded lands in Buzau Subcarpathians. *Forest magazine*, *131(3/4)*. 7-18.

Spîrchez, Gh. C., Lunguleasa, A. (2016). Wood biomass, an important source of renewable energy. *AGIR Bulletin, 1*. 40-42 (in Romanian).

Stocker, T.F., Qin, D., Plattner, G.-K., Tignor, M., Allen, S.K., Boschung, J., Nauels, A., Xia, Y., Bex, V., Midgley, P.M. (2013). *The Physical Science Basis. Contribution of Working Group I to the Fifth Assessment Report of the Intergovernmental Panel on Climate Change (IPCC report).* Cambridge, United Kingdom and New York, USA: University Press.

Traci, C. (1975). The effects of the 1973 drought on the conifer plantations on eroded sites in the Cheia-Macin area in the forest-steppe of N. Dobruja. *Revista Padurilor - Industria Lemnului, Celuloza si Hirtie, Silvicultura si Exploatarea Padurilor, 90, (1).* 25-30.

Untaru, E. (1976). Reforestation a means of reclaiming degraded soils in the Vrancea area [Romania]. *Buletinul-Academiei-de-Stiinte-Agricole-si-Silvice (Romania), 4.* 43-52.

Untaru, E., Constandache, C., Nistor, S. (2012 & 2013). Status and projections for the future of ecological reconstruction through afforestation of degraded land in Romania (I & II). *Revista Pădurilor, 6/2012.* 28-34*; 1/2013*. 16-26 (in Romanian).

Traci, C., Untaru, E. (1986). Behavior and enhancement and consolidation effect of forestry plantation on degraded lands in experimental perimeters. *ICAS, 2nd series,* 70.

Traci, C., Costin, E., (1966). *Degraded lands and their valorification on forestry way*. Bucharest, RO: Agro-forestry Publishing House.

Vlad, R., Constandache, C., Dincă, L., Tudose, N.C., Sidor, C.G., Popovici, L., Ispravnic, A. (2019). Influence of climatic, site and stand characteristics on some structural parameters of scots pine (Pinus sylvestris) forests situated on degraded lands from east Romania. *Range Mgmt. & Agroforestry 40 (1)*. 40-48.

***PN 16330305 report, 2016. Analysis of the structural-functional dynamics of forest ecosystems installed on degraded land to support methods for their ecological regeneration/reconstruction. (in Romanian).

***PN 23090203 report, 2023. New scientific contributions for sustainable management of torrential watersheds, degraded lands, forest canopies and other agroforestry systems in the context of climate change (in Romanian).

Scientific Papers. Series E. Land Reclamation, Earth Observation & Surveying, Environmental Engineering. Vol. XII, 2023
Print ISSN 2285-6064, CD-ROM ISSN 2285-6072, Online ISSN 2393-5138, ISSN-L 2285-6064

THE PARTICULARITIES OF THE ECOLOGICAL REHABILITATION WORKS OF THE SESSILE OAK STANDS (*Quercus petraea* (Matt.) Liebl.), FROM THE SEED RESERVE

Ghiţă Cristian CRAINIC[1], Silviu Ioan SICOE[1], Flavius IRIMIE[2], Flavia IRIMIE (CIOFLAN)[1], Călin Ioan IOVAN[1], Marinela Florica BODOG[1]

[1]University of Oradea, 1 University Street, Oradea, Romania
[2]"Stefan cel Mare" University of Suceava, 13 University Street, Suceava, Romania

Corresponding author email: marinelabodog@gmail.com

Abstract

The sessile oak stands within the seed reservation that were affected by the extreme weather phenomena (windthrown and windsnapped trees) on the 17th of September 2017, from the forest fund of the U.P. VII Văratec, the Forest District Sudrigiu, County Forest Administration Bihor, presents a relatively low ecosystem stability, considering the impact suffered. After the identification of the sessile oak stands affected (by extreme weather phenomena), the assessment of the affected wood material was carried out and implicitly, its extraction and superior valorization. The necessary works, proposed for the ecological rehabilitation of the sessile oak stands that have been examined and studied, take into account their actual state, the regulations of the forestry management plan for the current decade, the provisions of the technical norms in force at the date of implementation of the study, and last but not least, the necessary logistical and financial possibilities.
Surfaces from which the wood material was extracted, will be delimited in separate management units, which will regenerate naturally from the seed coming from the remaining stands, thus preserving their provenance in-situ.

Key words*: ecological rehabilitation, extreme weather phenomena, natural regeneration, sessile oak, seed reservation.*

INTRODUCTION

Since 2007, when our country became a member of the European Union, we have had the obligation to implement and comply with the provisions of EU Directive 1999/105/CE and other related regulations regarding the production, use and sale of reproductive forest materials (Pârnuţă et al., 2012).
As a result, in the new national and international context in this field, the complete revision of the 2001 edition Catalog was mandatory, and its completion, through new actions to identify and describe new source units for obtaining forest biological material, necessary for reproduction it introduces all the main basic, main mixed, main auxiliary and exotic forest species into the national forest fund (Pârnuţă et al., 2012).
The development of the National Catalog of the basic materials for obtaining forest biological reproduction materials by categories, species and regions of origin, was one of the main objectives of the EU directive, for the forestry sector.
Also, a set of 30 maps were made in the GIS system, at a scale of 1:3200000, for the location of the source units of reproductive genetic material, which were established for all species and artificial hybrids, by category of forest biological materials of reproduction and regions of origin by species, in accordance with MO No. 1028/2010 (Pârnuţă et al., 2012).
From the analysis of the data from the National Catalog of basic materials for the production of reproductive forest materials, 2012, it can be seen that in 2011 in our country there were 458 stands selected from the *Quercus petraea* (Matt.) Liebl. ssp. *petraea* (Liebl.) species, with an area of 8,341.41 ha, of which 15 stands, with an area of 285.10 ha, were tested (Pârnuţă et al., 2012).
Within the U.P. VII Văratec, O.S. Sudrigiu, D.S. Bihor, the *Quercus petraea* stands that are part of the S.U.P. "K" - respective seed reserves, occupy an area of 119.69 ha (Figure 1).

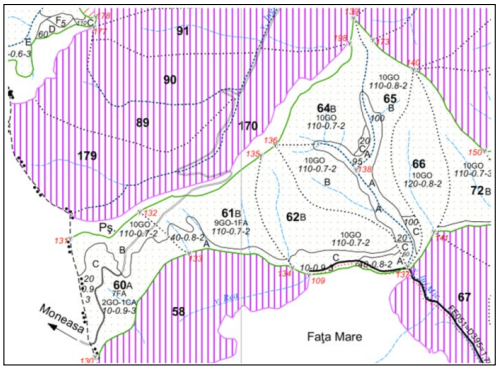

Figure 1. The location of *Quercus petraea* groves included in the seed reservation, from Production Unit VII Văratec, Forest District Sudrigiu, Forest Regional Board Bihor (extract from the forest map)

As a result, these stands aim to produce genetically controlled seeds, being included in the active type II. Consequently, these stands were excluded from the regulation of the wood production process (Table 1). Considering these aspects, silvotechnical interventions for these stands are represented by hygiene cuts and extracting accidental products when appropriate (when they are produced).

Table 1. Establishment of the management unit in which *Quercus petraea* stands are included in the seed reserve (extract from the forestry management in force)

Sub-unit production (S.U.P.)	Plots	
K	60B, 61B, 62B, 63B, 64B, 65B, 66	
Total	Surface: 119.69 ha	Number of plots: 7

Stand from plot 60B occupies an area of 8.11 ha, is a pure *Quercus petraea* species, 110 years old, production class II - a, with consistency k = 0.7, being obtained from natural regeneration. Accidental products were extracted from the tree in 2011, and hygiene products in 2013.

Stand from plot 61B occupies an area of 19.63 ha, is a practically pure *Quercus petraea* species, aged 110 years, production class II - a, with consistency k = 0.7, being obtained from natural regeneration. Accidental products were extracted from the tree in 2011, and hygiene products in 2013.

Stand from plot 62B occupies an area of 24.07 ha, is a pure *Quercus petraea* species, 110 years old, production class II, with consistency k = 0.7, being obtained from natural regeneration. Accidental products were extracted from the tree in 2011, and hygiene products in 2013.

Stand from plot 63B occupies an area of 13.63 ha, it is a pure *Quercus petraea* species, 110 years old, production class II - a, with consistency k = 0.7, being obtained from natural regeneration. Accidental products were extracted from the tree in 2011, and hygiene products in 2013.

Stand from plot 64B occupies an area of 18.69 ha, is a pure *Quercus petraea* species, aged 110 years, production class II - a, with consistency k = 0.7, being obtained from natural regeneration. Accidental products were extracted from the tree in 2012, and hygiene products in 2013.

Stand from plot 65B occupies an area of 15.00 ha, is a pure *Quercus petraea* species, aged 110 years, production class II, with consistency k = 0.8, being obtained from natural regeneration. Accidental products were extracted from the tree in 2012, and hygiene products in 2013.

Stand from plot 66 occupies an area of 20.56 ha, is a pure *Quercus petraea* species, 120 years old, production class II, with consistency k = 0.8, being obtained from natural regeneration. Accidental products were extracted from the tree in 2008 and 2012.

On September 17.2017, the western part of the country was affected by a very strong storm, which lasted less than an hour and caused numerous damages. Strong gusts of wind reached nearly 100 km per hour and uprooted trees, snapped power lines, and destroyed roofs from a number of buildings

The wind, due to its destabilizing and destructive effect on forest ecosystems, is considered to be the most important and dangerous (harmful) abiotic factor, with a destabilizing character. This can cause significant damage to forests, resulting in the uprooting and/or breaking of tree trunks, which causes imbalances at the ecosystem level and respectively considerable financial losses for forest administrators and owners (Ní Dhubhain & Farrelly, 2018).

Depending on the intensity and extent of the extreme meteorological phenomenon (the storm produced by the wind), two large

categories of downfalls produced by the wind can be identified: catastrophic downfalls or mass downfalls. Due to, extreme meteorological conditions, with very high intensity winds, which affects a large area (at least 0.25 ha of the stand) and respectively isolated fellings - which occur frequently every year, as a result of the impact on forest ecosystems of medium-intensity winds, in which case the damage produced has economic effects reduced, but if repeated periodically, through accumulation they can become very important (Mitchell, 2013).

The factors that condition and respectively influence the evolution of windfalls can be classified into two categories: seasonal factors favoring falls (lithological substrate, soil, relief, slope, exposure) and respectively seasonal triggering factors, which are represented by climatic conditions - the variety of hydrometeors, temperature variations, wind speed and direction (Crainic et al., 2003).

To assess the risk of falls and/or wind breaks, three large categories of methods can be used, as follows: observational methods - which involve the analysis of specific risk indicators (Crainic & Dorog, 2003), mechanical experimental methods - which refer to testing the resistance of trees to the action of the wind, either through mechanical modeling and simulation techniques of the behavior of trees to the action (loading) of the wind or through specific experiments (Peltola et al., 2000). These specific experiments are mathematical methods, based on the principles of statics and material resistance (Fetea et al., 2003), and statistical methods, namely regression analysis in estimating the probability associated with windfalls, depending on stationery and tree factors (Popa, 2005).

Leaving aside the assessment methods used to assess the risk of windfalls, a number of other factors are of particular importance, such as: tree species (due to the type of rooting), soil type, lithological substrate and respectively the loads from wind, which acts on the trees and can cause them to topple. Also, an important influence is the relief, the slope and the altitude. They act synergistically, through their common resultant within the climatic elements, influencing the initiation and development of the falls (Coates et al., 2018). A product of the windfalls in the mountain area is the specific microrelief, known as the microrelief of the downfalls (Geambașu, 1984), an aspect that can also be frequently encountered in the hilly area. In storms with high intensity, the root system of forest species with trailing roots gives way, being dislodged from the soil together with a disk of earth retained between the roots, thus forming the slough. When the trees are overturned in the upstream to downstream direction, a characteristic micro-depression remains in the disc separation area, which fades over time but does not disappear definitively, as depicted in Figure 2.

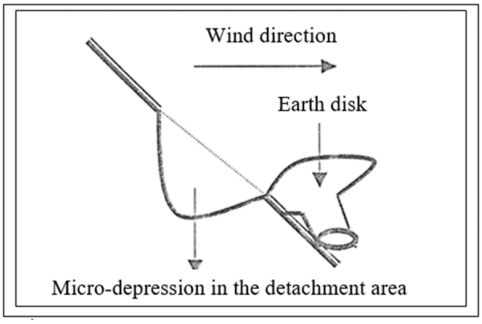

Figure 2. The appearance of a dislocated stump in the upstream-downstream direction, side view (from Crainic, 2002, after Geambașu, 1984)

Since the effects of landslides on the soil and relief are long-lasting, the microrelief of landslides can constitute a seasonal indicator (element), with a special indicative value, related to the frequency of wind landslides. The presence of the micro-relief of falls has a special importance for the station study, turning it into a real tool (indicator, coupon) for assessing (evaluating) the risk of the station in the event of falls.

Wind, on the European continent, is considered a major factor (the main factor) of destabilization and destruction of forest ecosystems, which produces consistent damage - more than half of the volume of all damage to forests (Gardiner, 2013). The increase in the frequency and intensity of storms caused by wind is currently considered to be influenced by climate change, including the number and intensity of these extreme weather phenomena, recently being on the rise (Sabău & Iovan, 2018; Constandache et al., 2018). The

increasing trend in the frequency and intensity of storms caused by wind in Europe has been highlighted since 1950, being also characterized by the quantification of the increasing damages produced in the forest fund. Between 1970 and 2010, damage caused by windstorms in the European forest fund doubled, increasing from about 50 million m^3 to about 100 million m^3 (Chirici et al., 2017).

The negative effects of windfall are also felt in Romania, especially in the mountainous area. The catastrophic windfalls, from November 1995, produced calamities on an area of over 140.000 ha, resulting in a total volume of approximately 7.9 million m^3 of accidental wood products. Also, the natural calamities, which occurred in March 2002, in Suceava county, resulted in the felling produced by the wind, estimated at over 7 million m^3 of accidental wood products (Popa, 2005).

The trees within Forest District Sudrigiu, Forest Regional Board Bihor, were affected by these extreme weather phenomena, namely a devastating storm, which produced the felling by uprooting and the breaking of trees on thousands of hectares. Within the Production Unit VII Vărătec, a number of trees from the group of deciduous species were affected, including the seven gorun trees, which are included in the seed reserve. As a result, the total area of the affected trees is approx. 920 ha, of which 119.69 ha is represented by the surface of the seven *Quercus petraea* groves, from the seed reserve.

The gorun trees within the seed reservation were affected by the uprooting and breaking of the trees by the wind that reached speeds of over 28 m/s (100 km/h), thus resulting in a considerable volume of accidental wood products and respectively a series of surfaces on which quantities of soil and rock fragments were dislodged.

Also, access to the affected stands was blocked, and the natural landscape in that area was radically changed, becoming a desolate one.

MATERIALS AND METHODS

The case study was carried out in the gorun groves belonging to the seed reservation (plot 60B, 61B, 62B, 63B, 64B, 65B and 66) within the Production Unit VII Vărătec, administered by the Sudrigiu Forest District, subordinate to the Forest Regional Board Bihor.

For the characterization of the gorun stands, from the seed reserve, which were affected by the extreme weather phenomena of 17.09.2017, the forestry management, the management map, and a series of documents (inventory, valuation documents, centralizers, situations, etc.) within the Sudrigiu Forest District, regarding the affected stands, belonging to Production Unit VII Vărătec. Also, observations were made on the itinerary, stationary observations, statistical-mathematical inventories, integral inventories and image recordings, with the objective reality from the field, on magnetic media.

The period in which the study was carried out was 2017-2022.

For the correct assessment of the state of the affected stands, observations were made successively, in different periods of the growing season and/or outside the growing season, in the plots analyzed and studied, thus analyzing all the identified peculiarities.

The recorded data were processed using appropriate work technologies, and the obtained results were interpreted accordingly, for the rigorous documentation of the technical solutions that will be proposed.

The establishment and respectively the adoption of appropriate (effective) technical solutions for the ecological rehabilitation of the analyzed and studied gorun groves, involves the evaluation (calculation) of their affected surface, the analysis of the respective groves's stability and the identification (establishment) of the necessary works (silvotechnical interventions).

In order to determine the affected area of the stands where the accidental products I were identified, the degree of damage of these stands was used - I_a, as a ratio between the volume of the accidental products and the volume of the stand, respectively, before their production, for the entire landscaping unit, the volume that was taken from the arrangement.

$$I_a = \frac{V_e}{V_a} \quad (1)$$

where:

I_a - the degree of damage to the trees;

V_e - the volume of accidental products, to be extracted, from the affected tree, from the plot analyzed and studied;
V_a - the volume of the arrangement related to the affected stand from the analyzed and studied plot.
The degree of damage to the stands (I_a) was applied to the area of the landscaping unit - the one presented in the arrangement, thus obtainning the theoretical area related to the volume of accidental products that were inventoried, generically called the affected area.

$$S_{af} = S_a \cdot I_a \quad (2)$$

where:
S_{af} - the affected surface, related to the volume of accidental products evaluated, from the landscape unit analyzed and studied;
S_a - the landscaped surface, related to the affected trees in the plot (landscape unit) analyzed and studied.
For the calculations, the volume from the arrangement was used, for each affected tree, which was analyzed and studied.
For the analysis of the stability of the stands to the destabilizing action of the dominant (or accidental) winds, the slenderness coefficient values related to these stands were calculated.
The slenderness coefficient was determined as the ratio between the average height and the average diameter of the stand (Florescu & Nicolescu, 1996) relation 3.

$$Z_{\%} = \frac{\bar{h}}{\bar{d}} \cdot 100 \quad (3)$$

where:
Z - slenderness coefficient;
$\bar{h}$ - the average height of the stand, in meters;
$\bar{d}$ - the average diameter of the stand, in centimeters.
The values of the slenderness coefficients were determined for the values of the heights and diameters from the acts of valuing the accidental products, but also for the values presented in the forestry management in force, for the affected stands, which were analyzed and studied. In this context, the slenderness coefficient values obtained for the data from the field (experimental data) and respectively for those from the forestry management, for the same trees, will be analyzed comparatively.
As a result, Z_a- represents the slenderness coefficient determined with the height (h_a) and diameter (d_a) of the arrangement;
Z_t- represents the slenderness coefficient determined with the height (h_t) and diameter (d_t) recorded in the field, which can be found in the valuation act.
The silvotechnical interventions corresponding to the stands included in the seed reserves are relatively restrictive, accepting the works necessary to improve and/or maintain an appropriate phytosanitary state (hygiene works/cuts) and, where appropriate, regeneration works, which ensures the in-situ conservation of the gene pool. As a result, the interventions that need to be analyzed in order to be implemented as technical solutions refer to the extraction of hygiene products, the removal of the negative effects of their exploitation process and, last but not least, the natural regeneration of the affected stands.

RESULTS AND DISCUSSIONS

The data recorded in the field, on the occasion of the complete inventories of the accidental products that occurred as a result of the extreme weather phenomena of 17.09.2017, in the *Quercus petraea* groves of the seed reservation within the Production Unit VII Văratec, were properly processed, with specialized work programs (FOND, SUMAL), obtaining the volume of the affected wood.
Table 2 shows the results obtained after processing the data from the affected stands, included in the seed reserve, within the Production Unit VII Văratec.

Table 2. The records of the affected stands, included in the seed reserve, within the Production Unit VII Văratec

Plot	Volume (m^3/u.a.)		Surface (ha)			
	$V_{arrangement}$	$V_{extract}$	$S_{arrangement}$	S_{affect}	$S_{to\ regenerate}$	$S_{regenerate}$
60B	2984	390	8.11	1.06	0.36	0.70
61B	7655	802	19.63	2.06	0.56	1.50
62B	9460	634	24.07	1.61	0.31	1.30
63B	5016	317	13.63	0.86	0.16	0.70
64B	7345	2266	18.69	5.77	1.20	4.57
65B	6735	2664	15.00	5.93	1.93	4.00
66	9231	2855	20.56	6.36	1.36	5.00
Total	48426	9928	119.69	23.65	5.88	17.77

From the analysis of the results presented in Table 2, from the surface, the total surface of the *Quercus petraea* seed reserve within the Production Unit VII Văratec of 119.69 ha, an area of 23.65 ha was affected by the extreme weather phenomena on September 17, 2017.

Of the affected area of 23.65 ha, natural regeneration is being installed on an area of 17.77 ha, and on an area of 5.88 ha, completion works and/or installation of forest vegetation are needed.

Analyzing the data presented in Figure 3, of the surface of the seven affected trees, included in the seed reservation, 80% is unaffected, 15% is undergoing regeneration, and 5% requires works to install forest vegetation.

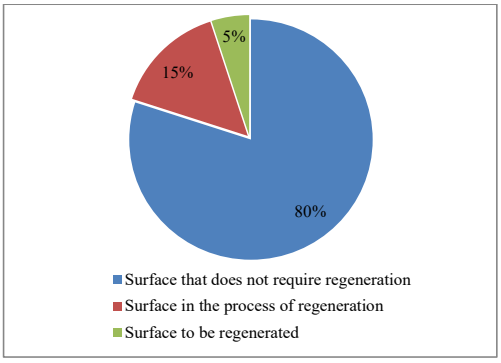

Figure 3. The situation of the affected areas and in the process of regeneration from the analyzed stands, which are included in the seed reservation within the Production Unit VII Văratec

The values of the slenderness coefficients of the gorun stands, within the seed reservation, which were analyzed, are presented in Table 3.

Table 3. The slenderness coefficient values for the gorun stands in the seed reserve, which were analyzed and studied

Plot	Capitalization act		H (m)		D (cm)		Z (%)	
	Nr.	V_{act} (m^3)	H_a	H_t	D_a	D_t	Z_a	Z_t
60B	500	390	27	26	40	46	68	57
61B	500	802	28	27	40	44	70	61
62B	500	634	28	26	42	38	67	68
63B	537	215	27	25	40	36	68	69
64B	537	1574	28	25	42	36	67	69
65B	570	2664	28	25	42	36	67	69
66	567	1800	28	25	44	40	64	63

The values of the slenderness coefficient Z, in stands with high ecosystem stability under the action of destabilizing dominant winds and with optimal thicknesses, are generally in the range of 60-90% (Florescu & Nicolescu, 1996).

From the analysis of the data presented in Table 3, the values of the slenderness coefficients, which were calculated for the studied gorun stands, fall within the range of 64-70% for the data from the forestry management, and respectively in the range of 57-69% for experimental (field) data.

Although the affected *Quercus petraea* stands have a corresponding thickness and slenderness coefficients with values that indicate a high ecosystem stability, they were nevertheless differently affected by wind blows, on compact surfaces of different sizes.

The possible cause of these windfalls, (disregarding meteorological conditions) as a predisposing factor, can be represented by the relatively low thickness of the soil and the presence of rock on the surface, on considerable surfaces.

The objective reality on the ground (situation on the ground) of the *Quercus petraea* stands in the seed reservation, which were affected, presents itself relatively differently, as the affected area and respectively, as the state of the remaining stands.

From the analysis of the data in Table 4, it is found that the cumulative surface, on which ecological rehabilitation works were proposed, in the affected stands, is 83.49 ha.

Table 4. Evidence of technical solutions, proposed in the affected stands, which are included in the reservation of gorun seeds

The proposed work		S (ha)
The symbol of the norm	The specifics of the work	
C.1	Land clearing for afforestation	5.88
C.2	Cleaning the land of stones and pebbles	5.88
C.51	Manual soil mobilization around seedlings in plantations, direct sowing and natural regeneration	0.78
C.46	Review of plantations and direct sowing	23.65
C.56	Reception of natural and artificial seeds	17.77
C.58	The discovery of forest species of herbaceous and woody species	23.65
C.75	Supplementing natural regeneration through direct seeding	5.88
Total		**83.49**

It is worth noting that in 2019, there was abundant fruiting of the *Quercus petraea* species in the Production Unit VII Văratec, and as a result, there are premises for the installation of a natural regeneration, from the seed, ensuring in this way the in-situ

conservation of the respective provenance and implicitly of the gene pool, for the affected gorun stands from the seed reservation, which were studied (Figure 4).

Figure 4. Abundant fruiting in the gorun species, in the stand in plot 64B (Crainic, 11.X. 2019, Production Unit VII Văratec)

Proposed works in the affected stands included in the gorun seed reservations - S.U.P. K
In the stand in plot 60B, the surface on which it is necessary to install forest vegetation, by direct sowing, was approx. 0.36 ha.
In the image from Figure 5, we can see the presence of the regeneration of the gorun species and respectively the presence of the black bilberry - *Vaccinium myrtillus* L., a species that indicates a relatively acidic soil. It should be noted that this species is not specified in the plot description, under the indicator flora heading.

Figure 5. Surface affected by felling and wind breaks, on which it is necessary to install regeneration, in the stand of u.a. 60B (Crainic, 11.X.2019, Production Unit VII Văratec)

For plot 60B we recommend the following regeneration composition: 70% *Quercus petraea* +20% *Fagus sylvatica +10% Prunus avium*.
The necessary works are represented by: C.1 on an area of 0.36 ha, C.2 on an area of 0.36 ha, C.75 on an area of 0.36 ha (because in the current year there is abundant fruiting of the *Quercus petraea* species), C.46 on an area of 1.06 ha, C.51 on an area of 0.05 ha, C.56 on an area of 0.70 ha and C.58 on an area of 1.06 ha.
In the stand in plot 61B the surface on which it is necessary to install forest vegetation: by direct sowing approx. 0.56 ha (Figure 6).

Figure 6. Biogroups with regeneration from the *Quercus petraea* species, with black bilberry, which settled on the surface affected by felling and wind breaks, in the stand of plot 60B (Crainic, 11.X.2019, Production Unit VII Văratec)

For plot 61B we recommend the following regeneration composition: 70% Go + 20% Fa + 10% Ci.
The necessary works are represented by: C.1 on an area of 0,56 ha, C.2 on an area of 0.56 ha, C.75 on an area of 0.56 ha, because in the current year there is abundant fruiting of the *Quercus petraea* species, C.46 on an area of 2.06 ha, C.51 on an area of 0.10 ha, C.56 on an area of 1.50 ha, C.58 on an area of 2.06 ha (Figure 7).
In the stand in plot 62B, the surface on which it is necessary to install forest vegetation: by direct sowing approx. 0.31 ha.
For plot 62B we recommend the following regeneration composition: 70% *Quercus petraea* + 20% *Fagus sylvatica* + 10% *Prunus avium*.
The necessary works are represented by: C.1 on an area of 0.31 ha, C.2 on an area of 0.31 ha, C.75 on an area of 0.31 ha, C.46 on an area of

1.61 ha, C.51 on an area of 0.08 ha, C.56 on an area of 1.30 ha, C.58 on an area of 1.61 ha (Figure 8).

Figure 7. Biogroups with regeneration from the gorun species, which settled on the surface affected by felling and wind breaks, in the stand of plot 61B (Crainic, 11.X.2019, Production Unit VII Văratec)

Figure 8. Surface affected by felling and wind breaks, on which it is necessary to install regeneration, in the stand of u.a. 62B (Crainic, 11.X.2019, Production Unit VII Văratec)

In the stand in plot 63B, the surface on which it is necessary to install forest vegetation: by direct sowing approx. 0.16 ha.

For plot 63B we recommend the following regeneration composition: 70% *Quercus petraea* + 20% *Fagus sylvatica* + 10% *Prunus avium*.

The necessary works are represented by: C.1 on an area of 0.16 ha, C.2 on an area of 0.16 ha, C.75 on an area of 0.16 ha, C.46 on an area of 0.86 ha, C.51 on an area of 0.05 ha, C.56 on an area of 0.70 ha, C.58 on an area of 0.86 ha (Figure 9).

In the stand in plot 64 B, the surface on which it is necessary to install forest vegetation: by direct sowing approx. 1.20 ha. For plot 64 B we recommend the following regeneration composition: 70% *Quercus petraea* + 20% *Fagus sylvatica* +10% *Prunus avium* (Figure 10).

Figure 9. Biogroups with regeneration from the gorun species, which settled on the surface affected by felling and wind breaks, in the stand of plot 63 B (Crainic, 11.X.2019, Production Unit VII Văratec)

Figure 10. Surface affected by felling and wind breaks, on which it is necessary to install the regeneration, in the stand of u.a. 64B (Crainic, 11.X.2019, Production Unit VII Văratec)

The necessary works are represented by: C.1 on an area of 1.20 ha, C.2 on an area of 1.20 ha, C.75 on an area of 1.20 ha, C.46 on an area of approx. 5.77 ha, C.51 on an area of 0.15 ha, C.56 on an area of approx. 4.57 ha and C.58 on an area of approx. 5.77 ha (Figures 11 and12).

In the stand in plot 65B, the surface on which it is necessary to install forest vegetation: by direct sowing approx. 1.93 ha. For plot 65B we recommend the following regeneration composition: 70% *Quercus petraea* + 20% *Fagus sylvatica* + 10% *Prunus avium*.

The necessary works are represented by: C.1 on an area of 1.93 ha, C.2 on an area of 1.93 ha, C.75 on an area of 1.93 ha, C.46 on an area of approx. 5.93 ha, C.51 on an area of 0.15 ha, C.56 on an area of approx. 4.00 ha, C.58 on an area of approx. 5.93 ha (Figure 13).

Figure 11. Surface affected by felling and wind breaks, on which it is necessary to mobilize the soil, to facilitate the regeneration process, in the stand in plot 64B (Crainic, 11.X.2019, Production Unit VII Văratec)

Figure 12. Biogroups with regeneration of the *Quercus petraea* species, overwhelmed by shrubby vegetation, in the stand of plot 64B (Crainic, 11.X.2019, Production Unit VII Văratec)

Figure 13. Compact area affected by windthrow and windthrow breakage, on which soil mobilisation and regeneration is required, in the stand of plot 65 B (Crainic, 11.X.2019, plot 65B, Production Unit VII Văratec)

In the stand in plot 66, the surface on which it is necessary to install forest vegetation: by direct sowing approx. 1.36 ha.
The necessary works are represented by: C.1 on an area of 1.36 ha, C.2 on an area of 1.36 ha, C.75 on an area of 1.36 ha, C.46 on an area of approx. 6.36 ha, C.51 on an area of 0.20 ha, C.56 on an area of approx. 5.00 ha, C.58 on an area of approx. 6.36 ha (Figures 14 and 15).
For plot 66 we recommend the following regeneration composition: 70% *Quercus petraea* + 20% *Fagus sylvatica* +10% *Prunus avium*.

Figure 14. Blowdowns and wind breaks on compact surfaces, in the stand in plot 66 (Crainic, 08.VIII.2020, Production Unit VII Văratec)

Figure 15. Compact surface affected by felling and wind breaks, on which it is necessary to mobilize the soil and install regeneration, in the stand of plot 66 (Crainic, 08.VIII.2020, Production Unit VII Văratec)

The cumulative area on which ecological rehabilitation works have been proposed for each gorun tree within the seed reservation is different, varying depending on the affected fence and implicitly depending on the affected area (Figure 16). As a result, it can be seen that that the gorun groves in plots 66, 65B and 64B have the highest degree of damage, and the stands in plots 63B and 60B show a relatively low degree of damage.
Due to the fact that in the gorun stands within the seed reservation, the consistency at the time

of applying the current forestry management, respectively at the beginning of 2014, had values in the range of 0.7-0.8, on a series of portions of the surface of the plots, was installed usable seed, due to the fruitings prior to 2014 and, respectively, the conditions created for the initiation and development of this ecosystem level process.

As a result, a series of silvotechnical interventions is necessary for these surfaces, specific to the stage and respectively the stage of development of biogroups with usable seeds.

Although in the seed reserves the silvotechnological interventions recommended by the technical norms in force and proposed by the forestry management are represented only by the hygiene works and the extraction of accidental products, for the regeneration of the surfaces from which the trees were extracted for justified reasons, a series of specific works.

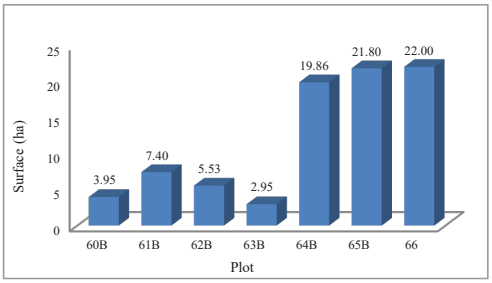

Figure 16. The cumulative surface area of the proposed ecological rehabilitation works on plots

Table 5. The centralizer of the proposed technical solutions, specific to works, surfaces and landscaping units, in the affected stands included in the seed reservation within the Production Unit VII Văratec

Nr. crt.	u.a.	The work (the symbol of the norm)							
		C.1	C.2	C.75	C.46	C.56	C.58	C.51	Total
1	60B	0.36	0.36	0.36	1.06	0.70	1.06	0.05	**3.95**
2	61B	0.56	0.56	0.56	2.06	1.50	2.06	0.10	**7.40**
3	62B	0.31	0.31	0.31	1.61	1.30	1.61	0.08	**5.53**
4	63B	0.16	0.16	0.16	0.86	0.70	0.86	0.05	**2.95**
5	64B	1.20	1.20	1.20	5.77	4.57	5.77	0.15	**19.86**
6	65B	1.93	1.93	1.93	5.93	4.00	5.93	0.15	**21.80**
7	66	1.36	1.36	1.36	6.36	5.00	6.36	0.20	**22.00**
Total		**5.88**	**5.88**	**5.88**	**5.88**	**17.77**	**23.65**	**0.78**	**83.49**

From the analysis of the data presented in Table 5, we find that the works that have the highest weight, depending on the surface on which they are recommended, are represented by C.46 and C.58, followed by C.56, C.1, C.2 and C.75. Works C.51 have the lowest weight.

CONCLUSIONS

From the analysis of the results obtained in the research carried out in the gorun stands affected by extreme meteorological phenomena, it can be concluded that the wind is the main natural factor, with a destabilizing character, in the forest ecosystems, in the hill and mountain areas.

The negative effects of extreme weather phenomena, on the forest ecosystems in the researched location, influence the structure and stability of the stands, as well as the possibilities of higher utilization of wood, due to the losses of value recorded in the process of utilization of accidental products.

The defective exploitation of the wood from accidental wood products, in the affected stands, especially the way in which the parquets (exploited surfaces) were cleaned, represents a limiting factor in the research and ecological rehabilitation processes in these stands.

Also, due to the fact that in the period from the occurrence of ruptures and windfalls until the year 2022, the meteorological conditions favored the growth and development at an alert rate of grassy, shrubby, subshrubby and woody vegetation, the collection of data from the field, the analysis and study of the affected stands, as well as a series of works necessary for the installation and management of natural and/or mixed regeneration, was relatively difficult.

In 2019 within the Production Unit VII Văratec there was abundant fruiting of the gorun species, and in 2020, abundant fruiting of the beech species was also reported. As a result, thanks to these abundant fruiting, the premises for natural and artificial regeneration are

ensured - especially through direct sowing, in the stands that were affected by the extreme weather phenomena of September 2017.
The works to complete the natural regeneration through direct sowing, in the gorun calamitate groves, from the seed reservation, are much more effective compared to plantations with seedlings, due to their superior technical and economic efficiency, if the acorns harvested from these groves are used, preserving - thus the local origin of the gene pool, in situ.
It is necessary to carry out these works in the spring, because during the winter, the direct sowing can be affected and even destroyed by the herds of wild boars and/or by the rodents.

ACKNOWLEDGEMENTS

The case study and the related research were carried out within the framework of the research contract with the socio-economic environment: Ecological rehabilitation of the stands affected by the storm of 17.09.2017 in the area of the Forest District Sudrigiu, Forest Regional Board Bihor - Contract no. 12395/ 23.07.2019, University of Oradea - Forest Regional Board Bihor, carried out within the University of Oradea, Faculty of Environmental Protection, Department of Forestry and Forestry Engineering, with the collaboration and support of the Forest Regional Board Bihor, Forest District Sudrigiu.

REFERENCES

Chirici, G., Bottalico, F., Giannetti, F., Del Perugia, B., Travaglini, D., Nocentini, S., Kutchartt, E., Marchi, E., Foderi, Cr., Fioravanti, M., Fattorini, L., Bottai, L., McRoberts, R.E., Næsset, E., Corona, P. & Gozzini, B. (2017). *Assessing forest windthrow damage using single-date, post-event airborne laser scanning data*. Forestry, *91*, 27-37.

Coates, K.D., Hall, E.C. & Canham, Ch.D. (2018). Susceptibility of trees to windthrow storm damage in partially harvested complex - structured multi-species forests, *Forests, 9*, 199, 1-14.

Constandache, C., Dinca, L., Popovici, L., Braga, C. & Blaga, T. (2018). The effect of climatic changes over some Romanian forest ecosystems. *18th International Multidisciplinary Scientific Geoconference SGEM 2018. Conference proceedings*, 18, Water resources, Forest, Marine and ocean ecosystems, Issue 3.2. Soils, Forest Ecosystems, Marine and ocean ecosystems, 941-948.

Crainic, G.C., Dorog, S., Geambaşu, N., Cristea, M. & Sotoc, H. (2003). *The permanent particularities which favorized tree overthrow at Production Unit III Vârciorog Forestry District Dobreşti in January 2003*. Annals of the University of Oradea, Forestry Fascicle, University of Oradea Publishing House, Vol. VIII, Year 8, ISSN - 1453-9489.

Crainic, G.C. & Dorog, S. (2003). *Some Aspects that Consider the Stability of the Trees from Production Unit III Vârciorog Forestry District Dobreşti*. Annals of the University of Oradea, Forestry Fascicle, University of Oradea Publishing House, Vol. VIII, Year 8, ISSN - 1453-9489.

Crainic, G.C. (2017). *Aspects Relating to The Evaluation Of Accidental Wood Products, In The Period 17 09-06 11 2017, In The Forestry District Sudrigiu, Bihor Forestry Department*. Annals of the University of Oradea, Forestry Fascicle, University of Oradea Publishing House, Vol. XXVIII, 189-196.

Crainic, G.C., Sicoe, S., Curilă, M. & Curilă, S. (2020). *The influence of structural characteristics on the stability of stands affected by windfalls and windbreaks*. Annals of the University of Oradea, Forestry Fascicle, University of Oradea Publishing House, Vol. XXXV, 153 – 164.

Fetea, M., Crainic, G.C., Dorog, S. & Cheregi, G. (2003). *The verification to bending solicitation of trees in a forest due to the loadings caused by the wind*. Annals of the University of Oradea, Forestry Fascicle, University of Oradea Publishing House, Vol. VIII, Year 8, ISSN - 1453-9489, 93-102.

Florescu, I.I. & Nicolescu, N.V. (1998). *Forestry, Vol. II, Silvotechnics*. Transilvania University Publishing House from Braşov.

Geambaşu, N.M. (1984). Research on the soils and forestry stations in the Rarău massif in order to optimally exploit their silvoproductive potential - doctoral thesis. University of Braşov, Faculty of Forestry and Forestry Exploitations.

Gardiner, B., Schuck, A., Schelhaas, M.J., Orazio, C., Blennow, K. & Nicoll, B. (2013). *Introduction. In Living with storm damage to forests*. What Science Can Tell Us 3. European Forest Institute, 123.

Mitchell, S.J. (2013). Wind as a natural disturbance agent in forests: a synthesis. *Forestry: An International Journal of Forest Research, 86*(2), 147-157.

Ní Dhubhain, A. & Farrelly, N. (2018). Understanding and managing windthrow. *Silviculture/Management 23*, 1-4.

Peltola, H., Kellomaki, S., Hassinen, A. & Granander, M. (2000). *Mechanical stability of Scots pine, Norway spruce and birch: an analysis of tree-pulling experiments in Finland*. Forest Ecology and Management, *135*, 143-153.

Pârnuță, G. (2011). *National catalog of forest genetic resources.* Forest Publishing House, Bucharest, 5-522.

Pârnuță, G., Lorent, A., Tudoroiu, M., Petrila, M. (2010). *The regions of origin for the basic materials from which the reproductive forest materials in Romania are obtained*. Forest Publishing House, Bucharest, 5-122.

Pârnuță, G. (2010). *Genetics and tree improvement*. Forest Publishing House, Bucharest.

Popa, I. (2005). *Windthrow - Risk factorr in mountainous forest ecosystems*, Annals of ICAS, 48, 3-28.

Sabău, N.C. & Iovan, C.I. (2018). *The influence of climate and pedological droughts on the hydrological drought of the small hydrographic basins from the Northen part of Codru-Moma Mountains, Bihor County*. Natural Resources and Sustainable Development, 8(2), doi: 10.31924/nrsd.v8i2.011, 87-104.

Sicoe, S.I., Crainic, G.C., Iovan, C.I. & Sabău, N.C. (2019). Changes in the common beech stand micro-relief due to windfalls in the Management Unit VII Văratec, Sudrigiu Forest District, Bihor County, Romania, *Natural Resources and Sustainable Development*, *9*(2), eISSN 2601-5676, Print ISSN-L 2066-6276, doi: 10.31924/nrsd.v9i2.037, 203 – 220.

***Arrangement U.P. VII Văratec, Forest District Sudrigiu, Bihor Forestry Directorate

***Development map of VII Văratec, Forest District Sudrigiu, Bihor Forestry Directorate

***(1997). Ministry of Water, Forests and Environmental Protection (MAPPM), National Forest Management (RNP), *Unified time and production norms for works in Forestry*.

***(2000). Ministry of Water, Forests and Environmental Protection (MAPPM), *Technical norms regarding compositions, schemes and technologies for forest regeneration and afforestation of degraded lands No. 1.*

***(2000). Ministry of Water, Forests and Environmental Protection (MAPPM), *Technical rules regarding the annual control of regenerations, No. 7.*

***(2019). *Ecological rehabilitation of the stands affected by the storm of September 17, 2017 in the radius of Forest District Sudrigiu, Bihor Forestry Directorate*, Research contract with the socio-economic environment, Partial report.

***(2020). *Ecological rehabilitation of the stands affected by the storm of September 17, 2017 in the radius of Forest District Sudrigiu, Bihor Forestry Directorate*, Research contract with the socio-economic environment, Final report.

***(2020). *Centralizer regarding the downfalls and wind breaks produced due to special meteorological phenomena recorded in the period 2017-2020, Forest District Sudrigiu, Bihor Forestry Directorate,* No. 1467/06.05. 2020.

***https://www.capital.ro/furtuna-puternica-in-vestul-romaniei-cinci-persoane-au-decedat.html, 2017.

Scientific Papers. Series E. Land Reclamation, Earth Observation & Surveying, Environmental Engineering. Vol. XII, 2023
Print ISSN 2285-6064, CD-ROM ISSN 2285-6072, Online ISSN 2393-5138, ISSN-L 2285-6064

SEISMO-ARCHAEOLOGY IN ROMANIA: THE ANCIENT EARTHQUAKES AS A PATH TO FUTURE KNOWLEDGE

Emil-Sever GEORGESCU

National Institute for Research and Development in Constructions, Urbanism and Sustainable Spatial Development URBAN-INCERC, 266 Pantelimon Road, District 2, Bucharest, Romania

Corresponding author email: emilsevergeorgescu@gmail.com

Abstract

The earliest chronological data on seismic events in the history of Romania date from the 10th century, but the data on strong earthquakes from the intermediate depth source Vrancea are limited to the 19th and 20th centuries. To compensate for this gap, we can turn to seismic archaeology or archaeoseismology, an interdisciplinary science based on archaeological and engineering methods and data. In this context, we present data for the initiation of the study of the possible impact and seismic damage to sites and settlements, castra, forts and Roman vallums in Dacia. These were located in seismic zones of southeastern Dacia/Moesia Inferior, southwestern Dacia - Dacia Malvensis. Of interest is the line of forts on the Limes Alutanus and Limes Transalutanus, the Danubian Limes - in Dacia Malvensis, as well as in Moesia (beyond the Danube), areas exposed to strong accelerations of 0.20-0.25 g. As a result, the research should prove the years of impact and damage or destruction of some constructions by earthquakes, so that we have an extended basis for future hazard and seismic risk assessments.

Key words*: earthquake archaeology, Roman Limes, Vrancea seismic source.*

INTRODUCTION

Archaeoseismology is an interdisciplinary science, based on archaeological methods and data, in combination with seismology and engineering approaches, able to prove and to interpret damage or destruction of artifacts by the earthquakes of the past (buildings, public works, heritage etc.), with disorganization of public life etc. (Galadini et al., 2006).

Seismicity in Romania is strongly dominated by the Vrancea source, in the curvature area of the Carpathian Mountains. Earthquakes with magnitudes over 7 and with depth of foci between 60-70 km and 170-220 km, give strong shaking on some 50% of the territory in the eastern and southern Romania and causes transboundary damage at, in north of Bulgaria, in R. of Moldova and S of Ukraine (Bălan et al., 1982). Some other sources exist, as superficial (with depth of foci less than 5 km) and crustal (or normal), with depth of foci between 5 and 30-60 (?) km. In Dobrudja, there is an exposure to local crustal sources and northern Bulgaria and Black Sea crustal sources. Scientists need more data about the seismicity in the first millennium, because the Romanian Catalogue of earthquakes gives scarce historical information, only since 984 (NIEP Romplus Catalogue, 2021).

The lack of instrumental data gathered on Romanian territory was a cause of long-term under evaluation of seismic loads in buildings design. The unique accelerogram of March 4, 1977, Vrancea earthquake, obtained in INCERC Bucharest, allowed a huge progress in code evolution (Bălan et al., 1982; Berg et al., 1980; Georgescu & Sandi, 2018; Georgescu et al., 2022). However, there is still a need of complementary data for a better probabilistic assessment of seismic hazard.

MATERIALS AND METHODS

The methodological concept for identifiing the date of damaging earthquakes by archaeoseismology includes the following main steps (Galadini et al., 2006):

- identification of damage in a site/stratigraphy and try to associate/dissociate causes of damage from accidents, invasions or other hazards versus earthquakes;

- evaluation of possible causal seismic sources and local geological factors; find other sites where earthquakes of the same source have caused damages simultaneously;
- finding chronology - year/period of such damages; providing dating with coins, pottery, C 14 etc.

We may be thus concerned about where to search for impact of ancient Vrancea earthquakes in Dacia (actual Romania) and Moesia/Thracia (actual Bulgaria)?

The 1802 Vrancea earthquake produced a large area of IX to VII degrees MSK intensities in Romania, while in Bulgaria cover an important area of VII degree (Sagalova, 1968). Other authors, as Radu & Utale (1992), give MSK intensities in Bulgaria on a greater area of VII degree, including Sofia (Figure 1a).

Figure 1a. The isoseismal map of Great Vrancea 14/26 October 1802, Mw 7.9 earthquake, after Sagalova, 1968

In 1838 the MSK intensities in Bulgaria were from VII (near Danube) to VI and V in rest, while strongly felt in Vratsa, Trojan, Veliko Tarnovo, Drianovo (Rogozea et al., 2014) (Figure 1b).

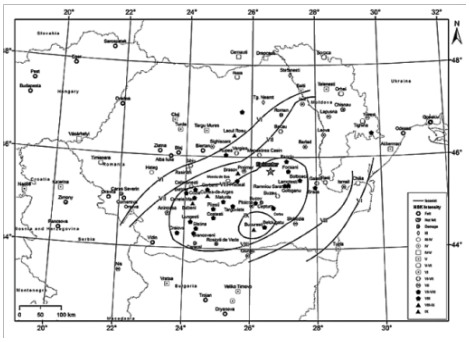

Figure 1b. The isoseismal map of Vrancea, January 23, 1838, Mw 7.5 earthquake. Seismic intensity map on MSK scale based on revised data of Rogozea et al., 2014

In the November 10, 1940 Vrancea earthquake (Figure 2a), caused a large area of VII and VIII degrees MSK intensities in Romania, with peaks of IX in epicentral zone; in Bulgaria, there is an area of VI intensity degrees MSK in northeast (Leydecker et al., 2008).

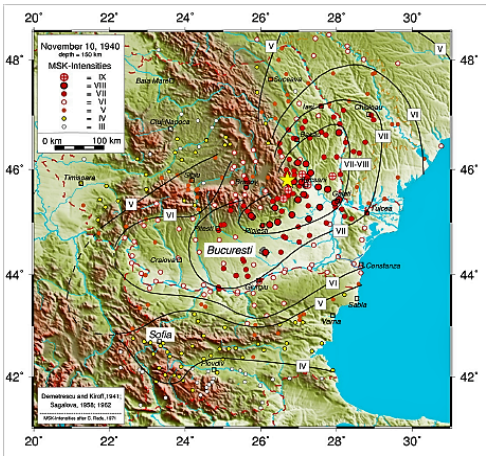

Figure 2a. Macroseismic maps in MSK intensity - Vrancea, November 10, 1940, Mw 7.7 earthquake (Leydecker et al., 2008. CC BY-SA 3.0 license) (Accessed April 2021)

In the March 4, 1977, earthquake (Figure 2b), the directivity towards S and SW of Romania was obvious, with intensities of VII and sites of heavy damage as over VIII MSK.

The shaking almost destroyed the Romanian town of Zimnicea and caused collapse of three high-rise buildings in Bulgarian town of Svishtov, both on Danube banks. In Bulgaria, many places with VIII degrees MSK occurred in

north, up to 50 km south of Danube, with large areas of VII intensity degrees MSK spread towards Sofia (Leydecker et al., 2008; Solakov and Simeonova, 2012).

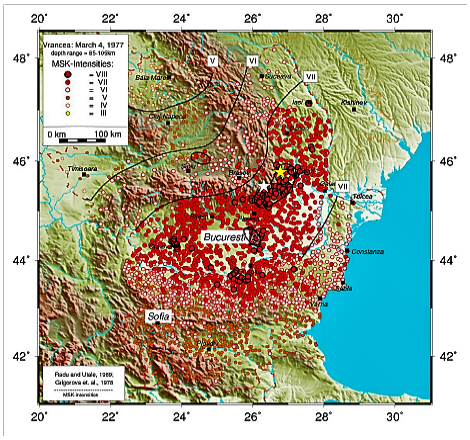

Figure 2b. Vrancea, March 4, 1977, Mw 7.5 earthquake (Leydecker et al., 2008. CC BY-SA 3.0 license) (Accessed April 2021)

It is important to emphasize that in 1977 Vrancea earthquake, the INCERC Bucharest Seismic Network recorded a unique accelerogram, proving a long-period pattern of Vrancea motions waves with potential of damage for tall and slender structures, also at large distances (Bălan et al., 1982; Berg et al., 1980; Georgescu & Sandi, 2018; Georgescu et al., 2022). Although the general directivity of Vrancea earthquake is NE-SW, the May 31, 1990 Vrancea earthquake (Mw 6.4) INCERC records proved a directivity towards S-E, in Dobrudja/Scythia Minor (Borcia, 2006; Georgescu & Sandi 2018). In other terms, concerning the Vrancea source, there are some specific questions:

- earthquake catalogue data (NIEP Romplus Catalogue, 2021) with data since 984 allowed the study of sometime-magnitude regularities expressed in years spans of possible great magnitude events, as 3 great earthquakes for an average of 100 years (Enescu, Marza & Zamarca, 1974). Other assessments revealed some statistical cycles of 100 year as well as of some quasi-cycles of 300 years (Purcaru, 1979). These patterns were detailed later (e.g., a refined exponential model by Enescu, Struzik & Kiyono, 2008).
- the challenging question is if we may assume that the seismicity was statistically the same in previous 1000 years, in terms of recurrence and/or directivity towards S-W and/or S-E, and the if the archaeological data may give answers?

Thus, we assume the premise that the archaeological surveys may give more chances to find simultaneously affected sites and to confirm the patterns of recurrence, energy release and low attenuation, i.e. impact at remote sites, of Vrancea deep source.

It is very important that the seismological knowledge gathered after 1977 proves that crustal earthquakes that happens at hundreds of kilometres (e.g. events of Constantinople 477 or 583 or Skupi 518) cannot cause strong shaking and damages on Danube Limes or Moesia Inferior sites. Only Vrancea greater and deeper earthquakes have this capacity.

RESULTS AND DISCUSSIONS

The ancient Dacian local culture and architecture was based on wood and earth, while stone was available only near hills or Carpathian Mountains. The Roman conquest of Dacia since 2-nd century covered mainly the western and Central area (Dacia Superior/Apulensis and Porolissensis), north of Danube only the south/southwest area (Dacia Inferior/Malvensis). In south-west the stone was used only in some Roman defense castra, while most of military watch towers were made of wood and earth, along the Alutanus Limes and Transalutanus Limes (Teodor, 2015). The current data from excavations do not indicate seismic causes of damage. The earth and wood do not preserve the traces of damage and this is the reason of lack of testimonies in excavations on Dacian or Roman Dacia constructions that existed between Danube and Carpathian Mountains.

There are promising data of Bulgarian and Polish archaeologists about traces of earthquake damage in Moesia/Thrace on Danubian Limes. East of Danube there was a Roman Moesia/Scythia Minor, where stone was used in most of defence and civil constructions and Romanian archaeologists were able to found more data about earthquake impact. In Figure 3, there is a seismic zoning map of Romania.

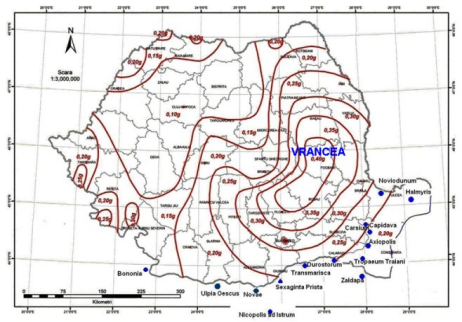

Figure 3. Seismic zoning map of Romania for IMR-mean interval of recurrence (return period) of 225 years, used for seismic design, indicating values of peak ground acceleration-PGA (Romanian Seismic Design Code 2013, UTCB-MDRT), having added the ancient Roman castra on Danube Limes, and eastern part of Moesia Inferior

Figure 4. Map of Roman Limes in Dacia. https://ro.wikipedia.org/wiki/Limes#/media/. File: Roman_Byzantine_Gothic_Walls_Romania_Plain. svg. CC BY-SA 3.0. Derivative work: Cristian Chirita (talk) Roman_Dacia.svg: Andrei_nacu, uploaded at Commons by El_Bes - Roman_Dacia.svg (Accessed April 2021)

The map shows the zones with great peak ground accelerations of 0.15-0.25 g, visible on the S-W direction in Romania, where it was Dacia Inferior/Malvensis, with impact in south all over Danubian Limes and in Moesia/Thracia. Archaeological research on Roman castra, fortifications and municipia is necessary in south/southwest of Romania in order to recover data on damage, at least in I-st to VII-th centuries, until the Danube Limes existed.

The places of Roman castra, forts and vallums on Limes Alutanus and Limes Transalutanus are depicted in Figure 4 (Chirita, 2021). In correlation with Figure 3 it results an exposure in the seismic zones with strong PGA - peak ground acceleration of 0.20-0.25 g. In fig. 4 we see on Limes Alutanus - on Alutus/Olt River 11 castra / citadels / municipia, defense stone and earth vallums, while on Limes Transalutanus - east of Alutus/Olt River there are 18 forts of earth and stone, earth vallums, in south many forts were in timber and earth.

Timber and earth structures are less vulnerable to earthquakes. Remnants and traces of seismic damage possibly to find only in case of some larger stone constructions. Many sites not yet excavated.

Castrum Arutela on Limes Alutanus (on River Alutus/Olt, near Calimanesti, in Vrancea impact zone) was erected in 138 during Hadrian Emperor reign, in the Roman province of Dacia on the Limes Alutanus by a unit of Syrian archers (Suri Sagittari). It was destroyed by a flood of Alutus/Olt in 3-rd century.

In Figure 5 it is shown the reconstruction of Porta Praetoria done in 1982-1983 (https://ro.wikipedia.org/wiki/Castrul_roman_Arutela).

Figure 5. Castrum Arutela. Porta Praetoria (reconstruction) as seen from the River Olt (Photo Georgescu, E.S., 2022)

Castrum Jidava on Limes Transalutanus (near Campulung-Muscel, exposed to Vrancea and local crustal seismic source) was erected in 190-211, under Emperors Commodus and Septimius Severus.

It is the only stone castrum of Limes Transalutanus. It was destroyed by fire at 244-245 after Carps invasion, when all forts of Limes Transalutanus were destroyed. Excavations were done after 1962 with consolidation and partial reconstruction of 1970 (Petolescu & Cioflan, 1995; Popescu & Popescu, 1968, 1970) (Figure 6) https://ro.wikipedia.org/wiki/Castrul_roman_Jidava).

Figure 6. Castrum Jidava on Limes Transalutanus. Reconstruction of castrum main gate/Porta Praetoria, view from inside (Photo Georgescu, E.S., 2018)

As cities and citadels in Dacia Malvensis, the first glance gives:

- Romula/Malva (Resca)–Capital of Dacia Malvensis, Municipium during Hadrian reign, Colonia during Septimius Sever, inhabited until IV-th to VI-th century (https://ro.wikipedia.org/wiki/Romula);
- Sucidava (Corabia-Celei) on Danube, in front of Ulpia Oescus (Moesia)-fortified with 8 towers in IV-VIth century; it was devastated by Huns in 443 or 447? (https://ro.wikipedia.org/wiki/Sucidava).

Concerning the seismic exposure in Dobrudja/Scythia Minor/Moesia Inferior, the crustal Pontic seismic sources impact is known for some sites, as the Roman edifice with mosaic in Constanta (in VI-th century), also a presumable seashore settlement in Callatis and traces of possible earthquake in Histria.

Vrancea source was considered too remote, but the Triumphal Monument Tropaeum Traiani in Scythia Minor suffered the collapse of its upper part, sometime, between 3-rd and 6-th century. Trophy pieces were found fallen in NW-SE of the ruin, just in Vrancea source zone direction (Tocilescu, Benndorf & Niemann, 1895; Georgescu 2014; Georgescu 2015).

The Civitas Tropaeensium/Municipium Tropaeum Traiani: excavation data of east tower A prove some cracks of foundations towards the end of III-rd century and large construction works in of citadel at the beginning of IV-th century (findings based on field works of Ioana Bogdan Cătăniciu in http://www.cimec.ro/arheologie/tropaeum/cetatea/index.html), the works could be related to the Licinius and Constantine “de fundamentis” reconstruction. Such damage and reconstruction were caused by an earthquake or a landslide? It was Vrancea or a crustal neighboring source?)

Concerning the seismic exposure on the right bank of Danube Limes, Moesia/Thrace, we may refer to some areas beyond the Danube Limes in present Bulgaria as a part of Thrace, for some historical periods, while for later periods some territories changed their administrative allocation from the province of Thrace to Moesia Inferior, probably in the last decade of the 2nd century (cf. Boteva 1996, 173). The maps of seismic zoning from Romania and Bulgaria show for Danubian Limes and Moesia - exposure to Romania Vrancea intermediate earthquakes with PGA - peak ground accelerations of 0.15-0.25 g taller or greater buildings existed in ca. 70 places at S and S-E of Danube (colonia, municipia, castra, castella and vici) in present Serbia, Bulgaria and Romania.

In Moesia/Thrace there is also exposure to crustal earthquakes of north Bulgaria, to Gorna Oryahovitsa source zone PGA - peak ground accelerations of 0.11-0.15 g (Bulgaria’s seismic hazard map for 475 years return period, 2012). In Bulgaria - south Dobrudja there are sources of Cape Shabla - Kaliakra and Dulovo.

As castra and municipia with confirmed earthquake traces in Moesia/Thrace, we identified: Svishtov-Novae legionary fortress headquarters and episcopal complex, Ulpia Oescus/Gigen with Fortuna Temple, Nicopolis ad Istrum/Nikyup-with important buildings, Sextaginta Prista/Durostorum with a basilica etc.

The synthesis of existing archaeological data provides a preliminary attempt to a chronological summary of damaging earthquakes. At a first glance, as a result of a literature review, a chronological summary of years of earthquakes and damages on Danubian Limes and adjacent zones during I-st - VII-th centuries AD, resulted as follows:

- in 80-damage and ground faults by a very strong earthquake. Dating with coins and

Carbon 14 at Novae (Svistov) - legionary bath (Dyczek, 2011; Kolendo & Kowal, 2011; Lemke, 2009-2010)
- in 170-great destruction at Civitas Tropaeensium-Costoboci invasion;
- at ca. 170-repairs at Sanctuary in Sextaginta Prista (Russe), caused by Costoboci invasion or an earthquake (Varbanov, 2013);
- in 204-disturbing or destructive unknown event, hiding of a coin heard treasure - imperial denars in Civitas Tropaeensium, final of Severians (Barnea, 2011) (could it have been Vrancea earthquake ?? and/or invasion?);
- in 238 p. Chr.-Histria was destroyed (Black Sea earthquake?);
- in 251...269-Gots destroy Civitas Tropaeensium;
- in II-nd-III-rd century-damaging earthquake at Novae (Sarnowski, 2015)
- in III-rd century-Capidava baths were destroyed by an earthquake (R. Florescu cited in Opriș, Rațiu & Potârniche, 2018);
- in III-rd century-distructions and reconstructions at Nicopolis ad Istrum (Rizos, 2013);
- in 316-the reconstruction of Civitas Tropaeensium by Licinius and Constantin, after invasions? could it be related also to earthquake damages ??;
- in 326-327 a Durankulak–Shabla-Kaliakra source earthquake;
- after III-rd century-Nicopolis ad Istrum–building 7 destroyed by an earthquake with directivity of Vrancea; Dikov (citing Tsarov) 2018, excavations confirm that after III-rd century there was a very damaging earthquake;
- at the end of IV-th century or early V-th century–two warehouses destroyed by earthquakes at Nicopolis ad Istrum (?? Vrancea ??), (Rizos, 2013);
- in 370-380's Novae Center Sector XII - strong earthquake well dated with coins (Dyczek, 2018);
- in the late IV-th/early V-th century - two buildings destroyed at Nicopolis ad Istrum (Rizos, 2013);
- in 544/545 or 543 Earthquake of M 7.5 - tsunami at Kavarna, Cape Kaliakra–Temple of Cybele of Dionysiopolis (Balcik) and the harbour of Greek colony Bisone (Kavarna) destroyed by an earthquake and tsunami, with landslides. Similar Odessos and Afrodision; 544/545 (Guidoboni, 1989; Ranguelov et al., 2008);
- in 488, 515, 557-damaging earthquakes at Novae (??) (Biernacki, 2013);
- until first half of IV-th century - a disaster event at Novae (Gots or earthquake?) (Zakrjewski, 2015);
- in the first third of V-th century until beginning of VI-th century–damaging earthquake at Novae (Sarnowski et al., 2018; Sarnowski, 2015; Sarnowski, T., Kovalevskaja, L., & Tomas, A., 2008; Sarnowski et al, 2016);
- to the end of V-th century-beginning of VI-th century - Roman edifice with mosaic of Tomis destroyed by a Black Sea earthquake;
- to the end of V-th century-beginning of VI-th century-earthquake (?? from Vrancea ??), heavy damaging of basilica in Durostorum (Atanasov/Russev, 2009);
- in the second half of VI-th century-devastating earthquake at Nicopolis ad Istrum;
- in late 5th early 6th centuries the Durostorum Christian Basilica survived a considerable destruction, probably caused by an earthquake, and it was restored later (Atanasov & Russev, 2009);
- to the end of VI-th century-Ulpia Oescus (Gigen, vis-a-vis Corabia, Romania) - Temple of Fortuna-height 22 m! was destroyed by an earthquake, not by Christians! (Kabakchieva, 2015, http://archaeologyinbulgaria.com/2015/06/07/ancient-thracian-and-roman-city-ulpia-oescus-in-bulgarias-gigen-deserves-greater-publicity-archaeologist-says/), also Farkov & Kolarov, 2016, consider Vrancea earthquake as a causal event!
- to the end of VI-th century-Zaldapa decades and disappears at a decade after Avars invasion of 585 (Torbatov, 2000). Could it have been also because of earthquakes? From Shabla source? From Vrancea source?
- end of VI-th century-Capidava building C 1 destroyed by an earthquake (R. Florescu cited by Opriș & Rațiu, 2017); alternatively, some data may prove that at the beginning of VII-th century at Capidava a great earthquake (?? from Vrancea??) destroys the

Citadel, after the Avars invasion of 586 (http://cimec.ro/Arheologie/Capidava/descrie.htm);
- in the VII-th century-the Danubian Limes is considered out of function; how many other earthquakes struck in the VIII-th century ?? the IX-th century?? What may happen later?

CONCLUSIONS

Although the research is still at the beginning, the preliminary attempt to establish a framework able to facilitate finding/recovery of archaeological data about the Vrancea earthquakes impact in southern Roman Dacia proves to be fruitful.
Few oral presentations on preliminary issues on this subject were done by the author in last years (Georgescu, 2018; 2021; 2022) and the audience proved an increasing interest. The earthquake exposure is high, but the impact along the Limes Alutanus and Limes Transalutanus and in Dacia Malvensis is not yet identified in published archaeological data. However, the reevaluation of existing excavation reports may reveal and ascertain the traces of great Vrancea events in the recorded physical damage, if the archaeologists will cooperate with engineers and architects to a larger extent. Since there are many sites to search, this approach may have a potential of triggering new evaluations and producing results after further investigations and/or recovery of data.
The earthquake impact along Danubian Limes and on its influence area, as well as in Moesia/Thrace/Scythia Minor (Dobrudja), is proved by archaeological data. The impact of Romanian earthquakes is quite important in Bulgaria from Danube up to Stara Planina Mountains (some data prove that the March 4, 1977 Vrancea earthquake caused damage in Sofia, where some crustal earthquakes striking West of Romania in February 2023 were also felt!). The concurrent impact of local seismic sources, as well as the impact of other catastrophes must be ascertained.
The range of dating intervals for earthquakes causing damage/collapses, as given by existing historical/archaeological reports, is still in large range of years. Although the archaeological data are insufficient, the damage in many places is a proof of some simultaneous impact of large earthquakes along Limes and in Moesia strongly indicates the Vrancea source. After the III-rd century AD, the available data also seems to confirm a pattern of 3 great events per century. The issue of considering the earthquake damages of defence works as a favouring factor for the invasions impact, needs further investigation. The archaeoseismology has a larger potential to give more results and needs detailing and additional data gathering and recovery in all considered Dacia and Danubian Limes areas. The research should prove the years of impact and damage or destruction of some constructions by earthquakes, so that we have an extended basis for seismic risk assessments.

ACKNOWLEDGEMENTS

The author is grateful to Prof. Dr. Ana Vîrsta, Dean, for the generous invitation to be a keynote speaker.
The work was done within the "NUCLEU" PROGRAMME in PNCDI 2022-2027 with the support of MCDI, Project PN 2335.

REFERENCES

Atanasov, G.G., & Russev, N.D., (2009). An Early Christian Basilica of Durostorum. *Stratum plus, 2009.* No 5, 602-615, from https://www.e-anthropology.com/English/Catalog/History/STM_DWL_TwYn_aD4Ssz7t8rwj.aspx (Accessed April 2021).

Bălan, Șt., Cristescu, V., Cornea, I. (Coordinators) (1982). *The Romania Earthquake of March 1977* (in Romanian, with English abstract). Romanian Academy Press, Bucharest.

Barnea, A. (2011). *Tropaeum Traiani. Vol. 3. Imperial Roman denarius hoard.* (in Romanian) Romanian Academy Press, Bucharest, ISBN 978-973-27-2099-8.

Berg, G.V., Bolt, B.A., Sozen, M.A., & Rojahn, C. (1980). *Earthquake in Romania March 4, 1977. An Engineering Report.* National Research Council and Earthquake Engineering Research Institute. National Academy Press, Washington D.C., USA.

Biernacki, A.B. (2013). The Bishopric of Novae (Moesia Secunda, 4th-6th cent.): History, Architecture, Daily Life. in: *Acta XV Congressus Internationalis Archaeologiae Christianae,* Toleti 8-12.9.2008, Episcopus, Civitas,Territorium, Pars I, Citta de Vaticano 2013, pp.895-914.

Borcia, I.S. (2006). *Data processing of strong motion records obtained during Romanian earthquakes* (in Romanian), PhD. Thesis, TUCEB, Bucharest, Romania.

Boteva, D. (1996). The south border of Lower Moesia from Hadrian to Septimius Severus. In: Petrović, P. (ed.). *Roman Limes on the Middle and Lower Danube*. Belgrade, 173-176.

Chirita, C. (2021). Map of Roman Limes in Dacia, from https://ro.wikipedia.org/wiki/Limes#/media/ (File: Roman_Byzantine_Gothic_Walls_Romania_Plain.svg. CC BY-SA 3.0. Derivative work: Cristian Chirita (talk) Roman_Dacia.svg: Andrei_nacu, uploaded at Commons by El_Bes - Roman_Dacia.svg).

Dikov, I. (2018). Tsarov, I. cited in the paper "Gladiator fight relief discovered in ancient roman city of Nicopolis ad Istrum near Bulgaria's Veliko Tarnovo", *Archaeology in Bulgaria*, September 6, 2018, interview by Ivan Dikov, from http://archaeologyinbulgaria.com/2018/09/06/gladiator-fight-relief-discovered-in-ancient-roman-city-of-nicopolis-ad-istrum-near-bulgaria s-veliko-tarnovo/ (Accessed April 2021).

Dyczek, P. (2011). Observations on marks on rooftiles, bricks and ceramic tiles from sector iv in novae (Moesia Inferior). *NOVENSIA 22. Studia i materiały pod redakcją naukową Piotra Dyczka*. Warszawa 2011, ISBN: 978–83–928330–9–3 ISSN: 0860–5777, 85-107.

Dyczek, P. (2018). Novae - Western Sector (Section XII), 2011–2018 Preliminary Report on the excavations of the Center for Research on the Antiquity of Southeastern Europe, University of Warsaw. *NOVENSIA 29. Studia i materiały pod redakcją naukową Piotra Dyczka*, 27-71.

Enescu, B., Struzik, Z., Kiyono, K. (2008). On the recurrence time of earthquakes: insight from Vrancea (Romania) intermediate-depth. *Geophysical Journal, 172*(1), 395-404.

Enescu, D., Marza, V., Zamarca, I. (1974). Contributions to the statistical prediction of Vrancea earthquakes, *Rev. Roum. Geophys*., *18,* 67-79.

Farkov, J. & Kolarov, V. (2016). Colonia Ulpia Oescensium /Oescus/ Temple of Fortuna–Anastiloza, Recovery of Architectural Memory. Международна Научна Конференция Бани'2016. *International Scientific Conference BASA Proc., 18*.

Galadini, F., Hinzen, K.G., Stiros, S. (2006). Archaeoseismology: Methodological issues and procedure. *J Seismol*, 10, 395–414 doi 10.1007/s10950-006-9027-x,395-414.

Georgescu, E.S. (2014). Seismic response of Tropaeum Traiani monument, Romania, between history and earthquake engineering assessments. doi: 10.13140/2.1.3271.9041. *Proc. Second European Conference on Earthquake Engineering and Seismology (2ECEES),* Istanbul, Turkey.

Georgescu, E.S. (2015). Seismic response of Tropaeum Traiani monument, Romania, between history and earthquake engineering assessments. *Construction Magazine*, *1*.

Georgescu, E.S. (2018). Challenges of earthquake archaeology in Romania. Case study of Tropaeum Traiani. *Pontica International Scientific Session, 51st edition: History and Archaeology in the Western Pontic Space.* Constanta 3–5 oct. 2018. (in romanian).

Georgescu, E.S. (2021). The potential of earthquake archaeology in Romania. Case study: Roman Dacia, the Danubian Limes and Lower Moesia. *ARA 21-2021, Symposium Architecture, Restoration, Archaeology,* 22-24.04.2021. (in romanian).

Georgescu, E.S. (2022). Seismic archaeology of Roman buildings in southern Dacia. *Meeting of the National Commission on the In Situ Behaviour of Buildings*, Caciulata, Romania. (in romanian).

Georgescu, E.S. & Sandi, H. (2018). Recalling and revising the experience and the INCERC- Bucharest studies on the 1977.03.04 Vrancea earthquake. *Proc. European Conference on Earthquake Engineering,* Thessaloniki, Greece, 18-21 June 2018.

Georgescu, E.S., Craifaleanu, I.G., Dragomir, C.S. & Dobre, D. (2022). The INCERC record of the March 4, 1977 Vrancea earthquake: unique features and relevance for the six decades of modern earthquake engineering in Romania. Paper no. 3369, *Proceedings of the Third European Conference on Earthquake Engineering and Seismology - 3ECEES:* September 5-September 9, 2022, Bucharest, Romania/Editors: Cristian Arion, Alexandra Scupin, Alexandru Ţigănescu. - Bucureşti: Conspress, 2022. ISBN 978-973-100-533-1, 3184.

Guidoboni, E. (Editor) (1989). *I Terremoti prima del Mille in Italia e nell'area mediterranea.* ING Roma-SGA Bologna, Storia - Geofísica - Ambiente, Italia.

Kolendo, J. & Kowal, T. (2011). Stamps on ceramic pipes from Novae (Moesia Inferior). *NOVENSIA 22. Studia i materiały pod redakcją naukową Piotra Dyczka.* Warszawa 2011, ISBN: 978–83–928330–9–3 ISSN: 0860–5777, 67-76.

Lemke, M. (2010). Fieldwork at Novae (Bulgaria) in 2009 and 2010 (PLS. 199–201). *Światowit. VIII (XLIX)/*A, 191-194.

Leydecker, G., Busche, H., Bonjer, K.P., Schmitt, T., Kaiser, D., Simeonova, S., Solakov, D. & Ardeleanu, L. (2008). Probabilistic seismic hazard in terms of intensities for Bulgaria and Romania – updated hazard maps. *Nat. Hazards Earth Syst. Sci.*, 8, 1431–1439, from www.nat-hazards-earth-syst-sci.net/8/1431/2008/ Work distributed under the Creative Commons Attribution 3.0 License.

NIEP (2021). *Romplus Catalogue*. http://www.infp.ro/index.php?i=romplus (Accessed April 2021).

Opriș, I.C. & Rațiu, A. (2017). Capidava II Building C1 - Contributions to the history of annona militaris in the 6th century. With contributions by: Andrei Gândilă, Tomasz Ważny, Peter I. Kuniholm, Charlotte L. Pearson, Adriana Rizzo and Choi Mak. Roman Frontiers in Romania. Mega Publishing House. Cluj-Napoca 2017, ISBN 978–606–543–912–2, 209.

Opriș, I.C., Rațiu, A. & Potârniche, A. (2018). The Roman baths of Capidava. Preventive archaeological research report. *Cercetari arheologice*, *XXV*, 3-28. (in romanian).

Petolescu, C.C. & Cioflan, T. (1995). The Roman Stone Castles of Câmpulung (Pescăreasa, Argeş County) - Research from 1978-1989, *Argessis*, *VII.* (in romanian).

Popescu, Em., Popescu, Eug. (1968). Jidava-Cîmpulung Roman Castle (Preliminary remarks), *Studies and communications, I, Pitesti Museum.* (in romanian).

Popescu, Em., & Popescu, Eug. (1970). Preliminary report on the excavations carried out in 1962-1967 in the Roman castrum near Cîmpulung Muscel, *Archaeological Materials and Research, IX.* (in romanian).

Purcaru, G. (1979). The Vrancea, Romania, earthquake of March 4, 1977-a quite successful prediction. *Planetary Interiors*, *18*(4), 274-287.

Radu, C. & Utale, A. (1992). The Vrancea (Romania) earthquake of October 26, 1802. *Proc. XXIII ESC General Assembly,* Prague, 110-113.

Ranguelov, B. & Bojkova, A. (2008). Archaeoseismology in Bulgaria. Geoarchaeology and Archaeomineralogy (Eds. R. I. Kostov, B. Gaydarska, M. Gurova). 2008. *Proceedings of the International Conference*, 29-30 October 2008 Sofia, Publishing House "St. Ivan Rilski", Sofia, 341-346.

Ranguelov B., Mircheva, E., Lazarenko, I. & Encheva, R. (2008). The archaeological site–possible evidence about multihazard ancient events, *Proc. Conf. Geoarchaeology and Archaelomineralogy*, 347-352.

Rizos, E. (2013). Centres of the late Roman military supply network in the Balkans: a survey of horrea. *Jahrbuch des Römisch - Germanischen Zentralmuseums, 60*, 659-696.

Rogozea, M., Marmureanu, Gh., Radulian, M., & Toma, D. (2014). Reevaluation of the macroseismic effects of the 23 January 1838 Vrancea. Earthquake. *Romanian Reports in Physics, Earth Physics*, *66*(2), 520–538.

Romanian Seismic Design Code P100-1/2013. (2013). Design provisions for buildings. Published in *Official Monitor* Part I, No. 558 bis/3.09.2013, Bucharest, Romania (in Romanian).

Sagalova, E.A., 1968, cited in Medvedev, S.V. *Seismic Zoning of the USSR*, 1968, in Russian; English Edition, Israel (1976).

Sarnowski, T., Kovalevskaja, L. & Tomas, A. (2008). Novae-Castra Legionis, 2006-2009. Preliminary Report on the Excavations of the University of Warsaw Archaeological Expedition (Pl. XXI - XXV). *Archeologia 59*, 2008, 153-172, plus plates XXI - XXV. © Tadeusz Sarnowski, Ludmila Kovalevskaja, Agnieszka Tomas, 2010.

Sarnowski, T. (2015). In medio castrorum legionis I Italicae at Novae. Preserved remains, 3D virtual modelling and full-size visualization on the original site. C. Sebastian Sommer, Suzana Matešic´ (Hrsg.) *Limes XXIII Sonderband 4 / I Proceedings of the 23rd International Congress of Roman Frontier Studies,* Ingolstadt 2015. Akten des 23. Internationalen Limeskongresses in Ingolstadt 2015. Limes XXIII. Kapitel 8. Session 7 – Reconstructions of Roman Fortified Sites and their Surroundings, 350-359.

Sarnowski, T. (2018). Novae in Lower Moesia building the Early Christian episcopal complex with inscribed pagan stones from the roman legionary headquarters. Novae, Moesia and Thracia. 2018, Sacrum et profanum. Haec studia amici et collegae A.B. Biernacki septuagennio dicant. *Novae. Studies and Materials* VI, Poznań.

Sarnowski, T., Tomas, A., Kovalevskaja, L., Zakrzewski, P., Dziurdzik, T. & Jęczmienowski., E. (2014). Novae-Castra, Canabae, Vicus, 2013-2015. Preliminary Report on the excavations and prospection surveys of the University of Warsaw Archaeological Expedition. *Archeologia 65*, 177–203. © IAE PAN and Tadeusz Sarnowski.

Solakov, D. & Simeonova, S. (2012). Seismicity and seismic hazard modeling for Bulgaria. Bulgaria seismic hazard map. National Institute of Geophysics, Geodesy and Geography, from https://drmkc.jrc.ec.europa.eu/Portals/0/Partnerships/Seminars/3_Scientific_Seminar_DRMKC/Presentations/session_3b/pdf/4_dimcho_solakov-seismicity_and_seismic_hazard_modelling_for_bulgaria.pdf, 23 p. Accessed April 2021.

Teodor, E.S. (2015). *The Invisible Giant: Limes Transalutanus. An overview south of Argeş River. Târgovişte.* Cetatea de Scaun Publishing House, 2015. ISBN 978-606-537-298-6, 249, from www.academia.edu/16837823/The_Invisible_Giant_Limes_Transalutanus_An_overview_south_of_Argeş_River (Accessed April 2021), 15.

Tocilescu, G., Benndorf, O. & Niemann, G. (1895). *Monumentul de la Adamklissi, Tropaeum Traiani.* Wien, A. Hoelder, 1895, Romanian Edition, 182.

Torbatov, S.B. (2000). *The late antique city of Zaldapa*. 2000 (Торбатов, С.Б. Късноантичният Град Залдапа). Publishing House ALEA, Sofia, ISBN 454-4450-03-5, 113. (in Bulgarian, with English summary).

Varbanov, V. (2013). A Roman sanctuary in Sexaginta Prista. In Jupiter on your side. Gods and humans in antiquity in the Lower Danube area. *Accompanying publication for the thematic exhibitions in Bucharest, Alba Iulia and Constanţa.* May-September 2013. Editor Cristina-Georgeta Alexandrescu. Bucharest, 55-60.

Zakrzewski, P. (2015). The Gates of The Legionary Fortress at Novae (Lower Moesia). *Archeologia, 66*, 7-26.

Scientific Papers. Series E. Land Reclamation, Earth Observation & Surveying, Environmental Engineering. Vol. XII, 2023
Print ISSN 2285-6064, CD-ROM ISSN 2285-6072, Online ISSN 2393-5138, ISSN-L 2285-6064

ASSESSMENT OF THE SAFETY OF URBAN GREEN AREAS USING GIS

Peter UDVARDY[1], Levente DIMEN[2], Tudor BORSAN[2]

[1]Obuda University Alba Regia Technical Faculty, 45 Budai, Szekesfehervar, Hungary
[2]"1st December 1918" University of Alba Iulia, 5 Gabriel Bethlen Street, Alba Iulia, Romania

Corresponding author email: ldimen@uab.ro

Abstract

This paper aims to present a GIS-aided safety map related to the non-invasive assessment of trees in urban green areas. The goal is to create an urban GIS-based evidence of the green areas focused on hidden tree pathology, in order to increase the safety of urban parks and provide an instrument for decision-making to eliminate trees that pose a danger to citizens due to hidden pathology. This is especially important in light of the tremendous physical destruction, injury, loss of life, and economic damage caused by wind disasters, as well as concurrent heavy rains and flooding, which have become increasingly common in recent decades. Improved observational capabilities and recordings of such events have led to greater public awareness of severe weather events.

Key words*: Urban safety, Urban Green, GIS.*

INTRODUCTION

Climate change is an undeniable reality that is transforming the world as we know it. Among its wide-ranging consequences, one of the most concerning is the intensification and increased frequency of wind disasters. Wind patterns are intricately linked to climate systems. The alteration of climate patterns due to global warming has resulted in shifts in wind intensity, direction, and distribution. Warmer oceans, for instance, provide the fuel for tropical storms to develop into more powerful hurricanes and typhoons. Additionally, changes in temperature gradients and atmospheric conditions can influence the formation and behaviour of tornadoes. These alterations in wind patterns have led to an increased occurrence of extreme wind events across the globe. Climate change has contributed to a rise in extreme weather events having serious effects in the urban green areas.

This paper explores the application of Geographic Information System (GIS) in establishing a comprehensive database for managing green spaces in urban areas. It discusses the responsibility of local governments to conduct inventories of public green spaces and create an evidence registry for efficient management (Grecea, C. et al., 2012). The focus is on auditing the green areas within administrative boundaries, considering factors such as area coverage, vegetation quality, accessibility, and safety. By adopting an individualized approach for each green space entity, a more accurate understanding of the entire green infrastructure within territorial administrative units can be achieved, enabling effective measures for maintenance and management (Muntean et al., 2016).

THE URBAN GREEN AREAS

In 2015, the total area of urban green spaces in Romania was 25,778 hectares. This represents an increase of 4,145 hectares compared to 1991. This information is provided by the National Institute of Statistics (2017) Figure 1 and refers to the area of green spaces developed in the form of parks, public gardens, squares, plots with trees and flowers, forests, cemeteries, grounds of sports grounds and facilities that are located in the buildable perimeters of the localities, i.e. public green spaces. These figures reflect an increase in urban green spaces in Romania over some 24 years. It is important to note that these data refer only to green spaces officially developed and recognised as public green spaces. Other forms of green spaces, such as undeveloped natural areas or agricultural land in or near

localities, may not be included in these statistics.

This increase in the amount of urban green space may reflect the efforts of authorities and communities to promote and develop green areas to improve the quality of life in the urban environment and conserve biodiversity. However, it is important to continue efforts to conserve and sustainably develop green spaces within cities to ensure a healthy and balanced urban environment for residents.

Looking at the county scale, according to Figure 1, 27 counties in Romania show an increase in the amount of urban green space. This indicates that efforts have been made in these counties to develop and expand green spaces in urban areas. These increases may be the result of local initiatives and policies promoting environmental protection, improved quality of life and sustainable development of cities. County and local authorities can implement programs and projects aimed at developing parks, public gardens and other green spaces within communities (Oprea, L., 2018). It is gratifying to see that there is interest and commitment to increasing the amount of urban green space in most counties in Romania. This can contribute to healthier, more pleasant and sustainable urban environments, providing recreational and leisure opportunities for communities and promoting biodiversity (Marulli, J., 2005). However, it is important to continue to monitor and support the development of urban green spaces in all counties to ensure an appropriate balance between the needs of urban development and environmental conservation.

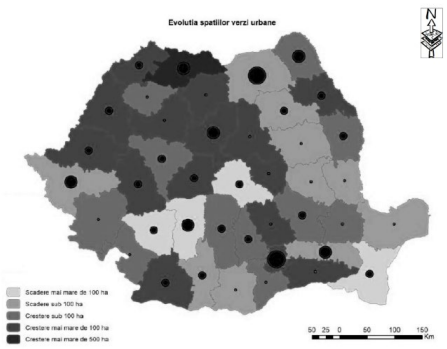

Figure 1. Evolution of the area of urban green infrastructure between 1991 and 2015 (INS, 2017)

Creation of GIS databases related to green cadastre

Today, Geographic Information Systems (GIS) are one of the main tools used to analyse green spaces and vegetation in urban areas. These systems are used for green cadastre databases, integrated management plans and the establishment of intervention phases for urban vegetation (Coppock, 1991).

One of the major advantages of GIS systems is their ability to produce complex, geo-referenced databases that can be dynamically revised and updated (Wade, T., 2006). These databases offer the possibility to manage detailed information about green spaces and urban vegetation, facilitating informed decision-making and appropriate planning of interventions. Another important advantage of GIS systems is their versatility, allowing direct communication with specific technologies for top-down approaches to green cadastre as well as bottom-up mapping methods (Gavrilidis et al., 2015). This means that data from a variety of sources can be integrated, from satellite images and orthophotos to locally collected user data. The system can therefore be used to get a complete and detailed picture of green spaces and vegetation in the urban environment.

In addition, modern technology allows the use of UAVs to collect GIS data. These UAVs can be equipped with various instruments such as high-performance cameras, temperature and humidity sensors, infrared sensors and others. This allows much more complex and comprehensive databases to be obtained than with traditional methods.

To register trees in a GIS database, an approach is used to include different attributes relevant to each group/entity (Norme Tehnice pentru aplicarea Legii nr. 24/2007).

- Unique ID - each tree can have a unique identifier to allow individual identification and management of each tree in the database.
- Species - attribute indicating the species of the tree (e.g. oak, spruce, acacia, etc.).
- Trunk diameter - the attribute that records the diameter of the tree trunk, either at the base or at the height of 1.3 metres from the ground. Useful for assessing tree maturity and for planning appropriate care.

- Trunk girth - the attribute that records the girth of the trunk of the tree measured at a given height above the ground (e.g. 1.3 metres above the ground). This quantification is relevant for assessing tree size and maturity.
- Trunk height - the attribute that records the height of the tree trunk, measured from the base of the tree to the first quarter or main branch. This can be useful for determining the structure of the tree and its vertical dimension.
- Crown diameter - the attribute that records the diameter of the crown of the tree, usually measured at the widest part of the crown. This can be useful for assessing the horizontal size of the tree and the area the crown occupies.
- Shaft deviation - the attribute that records the deviation of the shaft axis from the vertical. It can be expressed in degrees and indicates whether the tree is vertical or inclined to the vertical. This information is important for assessing shaft stability and determining potential structural problems.
- Health status - an attribute that indicates the overall health of the tree, including assessment of possible disease, damage or other problems.
- Geographic location - the attribute that contains the tree's geographic/geographic/ rectangular coordinates (latitude and longitude) to allow accurate positioning of the tree on the map within the GIS database.
- Year planted - attribute that records the year the tree was planted or established to allow the age and history of the tree to be tracked.

When designing the database, specific codes will be assigned to each attribute, depending on the type of information it will contain.

- Text - this data type is used to store textual information, such as tree species name, street name or any other textual description. In general, a maximum length is specified for the text field as needed.
- Integer - is used to store whole numbers, such as trunk circumference or trunk height. A minimum and maximum value is specified to limit the range of values accepted.
- Real number - is used to store real numbers such as crown diameter or crown height. A precision (number of digits after the decimal point) is also specified to control the detail of the real values.
- Date - is used to store calendar dates, such as the date of planting or the date of the last record. It allows chronological operations and comparisons to be made.
- Boolean - this data type is used to store logical values, such as tree health status (yes/no, true/false). It allows the representation of binary information.

MATERIALS AND METHODS

Hidden tree pathologies

Rotting of trees refers to the natural decay process that occurs when a tree's organic matter breaks down over time. It is a natural part of the life cycle of trees and is primarily caused by fungi and bacteria. When a tree dies or is injured, the process of decomposition begins, leading to the breakdown of the tree's structural components.

The rotting process typically starts from the inside of the tree and progresses outward (Figure 2). Fungi, especially wood-rotting fungi, play a crucial role in decomposing the tree's wood fibers. These fungi secrete enzymes that break down the complex molecules in the wood into simpler compounds, such as carbon dioxide and water. This process helps recycle nutrients back into the ecosystem.

Figure 2. Internal rotting

The rotting process can also pose risks and challenges. Trees that are extensively decayed may become structurally weak and more prone to falling, posing a safety hazard. This is particularly concerning in urban areas where falling trees can damage property or endanger

people. Therefore, regular tree inspections and maintenance are important to identify and address potential risks associated with rotting.
It's worth noting that not all rotting is visible from the outside. Trees may appear healthy and robust on the surface while experiencing significant internal decay. Thus, the use of specialized tools and techniques, such as sonic tomography or resistograph, can help arborists and tree experts assess the internal condition of trees and make informed decisions regarding their management and safety (Fote, K.E., 1995).

NON-INVASIVE ASSESSMENT

The speed of sound measured perpendicular to the fiber can serve as a diagnostic tool for detecting various anomalies that affect the path of sound waves (Divós et al., 2015). Such abnormalities can include internal cavities, rot, or long cracks within the material. In healthy and intact wood, the speed of sound traveling perpendicular to the fiber typically ranges from 1800 to 2000 m/s.
However, when a fiber run crack is present, the speed of sound is significantly reduced, leading to an increase in the measured propagation time. This change in propagation time can indicate the presence of defects within the wood. Additionally, this measurement technique can also be utilized to determine the depth of a crack. While the depth of a crack on the surface can be estimated by observing the penetration depth of a thin plate, the crack path is not always linear. Consequently, the obtained measurement may not accurately represent the actual crack depth.
To calculate the crack depth (C), the propagation time over the crack and the propagation time over the same distance in an unaffected area without a crack are compared. The formula for determining the crack depth is described by Divós & Szalai (2002) and can be employed for this purpose:

$$C = \frac{D}{2}\sqrt{\left(\frac{Tcrack}{Tsolid}\right)^2 - 1} \quad (1)$$

where:
- D is the length of the propagation path;
- T crack is the Propagation time in the cracked surface;
- T solid is the propagation time in the crack free surface.

It works based on sound velocity measurements between several sensors around the trunk (Figure 3). The basic measurement principle is that sound velocity drops if there is a hole or density difference occur between sensors.

Figure 3. Sound velocity measurement

RESULTS AND DISCUSSIONS

The detection of defects through measurements conducted perpendicular to the fiber has proven to be effective. This method is particularly useful when the sound waves propagate along an alternative path between the sensors. However, when aiming to identify defects that are not visible externally, it may be necessary to utilize more than two sensors. This technique, known as acoustic tomography, has been successfully employed in the examination of urban trees and is valuable for studying large cross-section timber and living trees, using the Arbosonic 3D software (www.fakopp.com/en/product/arbosonic).
Acoustic tomography relies on measuring the speed of sound between multiple sensors placed around the trunk or structure. By comparing the sound velocity measurements, valuable insights can be obtained. Specifically, if there is a void or hole between two sensors, the sound velocity will decrease. This principle forms the basis of the measurement technique

and offers a powerful approach for detecting hidden defects. By employing multiple sensors and measuring sound velocities, this technique proves beneficial for studying large cross-section timber and living trees, as well as examining urban tree health and integrity.

By tapping the sensors, we can measure the propagation speed on all possible routes, for N = 12 sensors on N (N-1)/2 = 66 routes. From this 66 sound speed measurements, the 3D device restores the speed map of the examined cross-section. This is seen in Figure 4 showing the time passing data through the trunk between the sensors and Figure 5 the imaging expression of the processing of physical data obtained from the sensor. It only contains example text and proper formatting.

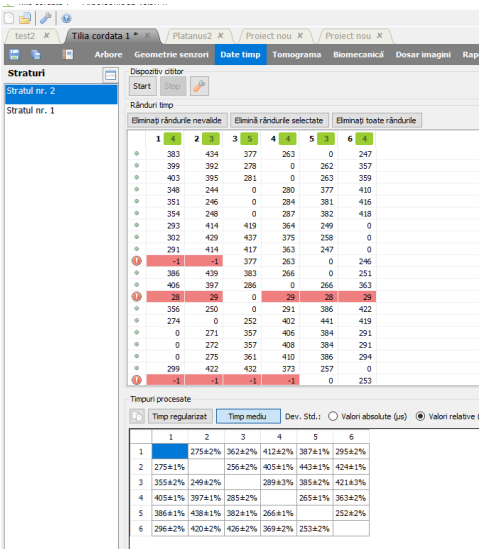

Figure 4. Get the time passing data through the trunk between the sensors

The colours indicate the condition of the tree. Red areas indicate damaged areas and blue indicates a cavity.

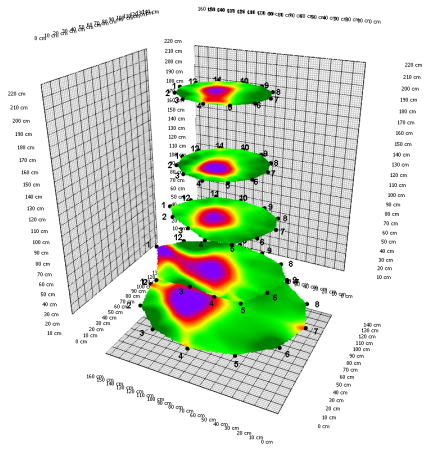

Figure 5. Example of internal assessment on different heights

In Figure 6 we can see the *Platanus acerifolia* sound velocity measurement and processed data.

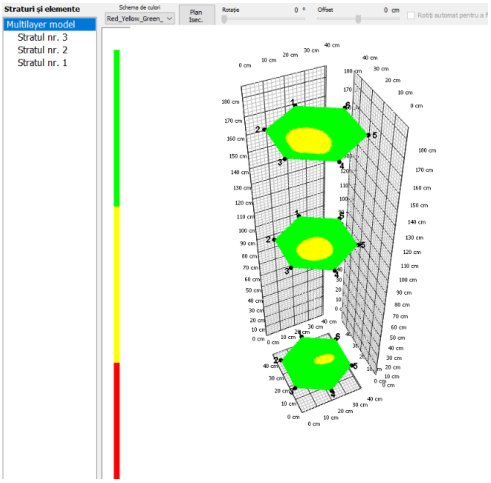

Figure 6a. *Platanus acerifolia* data processed

Figure 6b. *Platanus acerifolia*

CONCLUSIONS

The acoustic tomography technique was applied at urban green areas to evaluate its probability in detecting internal decay in high-value trees. Based on the preliminary analysis of acoustic tomograms, we conclude that:

- Acoustic tomography proved to be an effective tool for detecting internal structure change in urban trees,
- The tomogram can show the location and the relative size and shape of internal rotten areas,
- Green cadastre should record special data in green cadaster related to the hidden pathology of the trees.
- the concept of Urban Green Safety must be considered in any assessment and data recordings related to the urban green/forest.

ACKNOWLEDGEMENTS

This research work was carried out with the support of project: "Improvement of the educational infrastructure in the D and H buildings of the University 1 December 1918 in Alba Iulia" SMIS code 120779, financed by P.O.R. 2014-2020

Reference number and date of the Financing Contract: Financing Contract no. 4159/06.05.2019 SMIS 120779

REFERENCES

Coppock, J.T., Rhind, D.W. (1991). The history of GIS, Grossmont College paper, pp. 25-40. http://www.grossmont.edu/judd.curran/History_of_GIS.pdf.

Divós, F. (1999). *Fahibák, bélkorhadás feltárása a hangsebesség mérésével,* In: DIVÓS, F. (szerk.): Roncsolásmentes faanyagvizsgálat, Mérési útmutató, Soproni Egyetem, 1-5. old

Divós, F., Németh, L., Major, B. (2015). Új technológiák bemutatása a faszerkezetek felülvizsgálata területén, Magyar Mérnőki Kamara.

Divos, E., Szalai, L. (2002). Tree evaluation by acoustic tomography. *Proc. of the 13th International Symp. on Nondestructive Testing of Wood*, Aug. 19-21, Berkeley, CA., 251-256.

Gavrilidis, A., Gradinaru, S., Ioja, C., Carstea, E., Stupariu, I. (2015). Land use and land cover dynamics in the periurban area of an industrialized East-European city an overview of the last 100 years. *Carpathian journal of earth and environmental sciences, 10*. 29-38.

Grecea, C., Ienciu, I., Dimen, L., Bala, A.C., Oprea, L. (2012). Impact of Surveying Engineering on the Environmental Protection Problems. *J. Environ. Prot. Ecol., 13*(1), 352.

Foote, K.E., Lynch, M. (1995). *Database Concepts. The Geographer's Craft Project*, Department of Geography, The University of Colorado at Boulder. http://www.colorado.edu/geography/gcraft/notes/sources/sources_f.html.

Marulli, J., Mallarachet, J.M. (2005). A GIS methodology for assessing ecological connectivity: application to the Barcelona Metropolitan Area. *Landscape and Urban Planning, 71*(2-4), 243-262. https://doi.org/10.1016/j.landurbplan.2004.03.007.

Muntean, L., Arghiuş, V., Mihăiescu, R., Baciu N., Maloş, C. (2016). Strategic environmental assessment (a case study: Transylvania motorway project, Romania), *International Multidisciplinary Scientific GeoConference, SGEM, 3*, 436-470.

Oprea, L. (2018). Green Cadastre of Romania - Between Necessity and Realisation, *Journal of Environmental Protection and Ecology, 19*(1), 208–215.

Wade, T., Sommer, S. (2006). A to Z GIS, ESRI Press, Redlands, California. https://www.fakopp.com/en/product/arborsonic/

***National Institute of Statistics - INS. (2017). Baza de date TEMPO - Date teritorial-administrative si date asupra dinamicii spatiilor verzi;

***Norme Tehnice pentru aplicarea Legii nr. 24/2007 privind reglementarea şi administrarea spaţiilor verzi din zonele urbane (Elaborarea Registrului Local al Spaţiilor Verzi).

***www.fakopp.com/en/product/arbosonic

Scientific Papers. Series E. Land Reclamation, Earth Observation & Surveying, Environmental Engineering. Vol. XII, 2023
Print ISSN 2285-6064, CD-ROM ISSN 2285-6072, Online ISSN 2393-5138, ISSN-L 2285-6064

IMPROVING THE SYSTEM OF LOGISTICS MANAGEMENT AND SIGNALING, IDENTIFICATION, CLASSIFICATION OF NONCOMPLIANCE IN THE WATER BOTTLING INDUSTRY

Maria POPA[1], Mirel GLEVITZKY[1], Gabriela-Alina DUMITREL[2], Dorin POPA[1], Ana VIRSTA[3]

[1]"1 Decembrie 1918" University of Alba Iulia, 11-13 Nicolae Iorga Street, Alba Iulia, Romania
[2]University Politehnica of Timișoara, Faculty of Industrial Chemistry and Environmental Engineering, 6 Vasile Parvan Street, Timisoara, Romania
[3]University of Agronomic Sciences and Veterinary Medicine of Bucharest, Faculty of Land Reclamation and Environmental Engineering, 59 Marasti Blvd, District 1, Bucharest, Romania

Corresponding author email: mirel_glevitzky@yahoo.com

Abstract

Starting from the Kaizen approach which aims at continuous improvement, the study synthesizes the information regarding the classification, identification and reporting of defects and all types of non-compliance encountered during the manufacturing process in the food industry, particularizing on a water bottling process. Starting from an optimized logistic system model within the organization, the article deals with the non-conformities on the material and informational flow system, or for technological equipment (machines, equipment and installations). A chi-square test was performed to evaluate the occurrence of defects in different equipment of the technological process. The study is a tool to keep under control the problems that appear and can be constituted in a standard or an internal procedure of the company applicable when a non-compliance is identified. The analysis is carried out to show how to facilitate the signalling, identification, classification, isolation and evaluation of the non-compliant product or service in order to prevent non-quality. The methodology is an effective and efficient tool in preventing non-conformities.

Key words*: defects, industry, non-compliance, quality, statistics, water bottling.*

INTRODUCTION

Definitions of quality improvement are based on the concepts formulated by J.M. Juran in the 50s (Ionescu Luca, 2007), according to which quality improvement processes are carried out in parallel with quality control processes, constituting an additional component of quality control and does not replace it. It focuses on human resources, in the sense of organization, communication and coordination of functions within the company (Achim et al., 2008).
Masaaki Imai developed the guide "Kaizen, the key to Japanese competitive success" which highlights the main specific techniques of Kaizen management, namely: strategic thinking of profit on activities, management of customer needs, visionary control strategies at the level of processes in the organization and management of the supply chain etc. (Imai, 1986). The Kaizen policy is based on the process oriented towards the development of continuous improvement techniques and strategies, with the help of all the organization's staff from all departments and hierarchical levels (Imai, 2013).
Total Quality Management (TQM) combines the philosophy and principles of Deming and Juran on probabilistic/statistical process control. TQM is defined as an ongoing effort of the management and employees of an organization to ensure customer loyalty and satisfaction, as Fornell says: "one happy and satisfied customer brings with him ten new customers, while one disappointed individual it will spread word of mouth and spoil more of your existing customers as well as potential customers" (Fornell, 2007).
Quality can be measured in several terms, such as: durability, reliability, usability. Total quality management is a structured effort of employees to continuously improve the quality of products and services through appropriate feedback and research. Ensuring the superior quality of a product or service is not the responsibility of a

single member (Oprean, 2006), requiring the involvement of all employees. "Kaizen" philosophy means continuous improvement involving everyone without spending a lot of money (Imai, 1997).
TQM is among the key tools that are often used to facilitate the implementation of the Kaizen process, being a form of management policy that can be used to work alongside these principles (Stoller, 2015).
In present, in food industry, according to article 5(1) of Regulation (EC) No 852/2004 of the European Parliament and of the Council of 29 April 2004 on the hygiene of foodstuffs requires that all food business operators implement and maintain a procedure based on the HACCP principles (EC Regulation 852/2004). The HACCP system is a program for managing the quality and safety of food products that uses techniques to control the stages considered critical points in the process. The system is based on data from specialized literature and has as a priority the prevention of non-compliance related to their food safety and sanitary security. Through its implementation, the dangers, and corrective measures to ensure their control are reviewed (Glevitzky et al., 2019). HACCP programs include measures aimed at preventing and reducing the number of inspections, respectively the number of analyses of finished products.
The signalling, identification, documentation, isolation, evaluation, treatment of the non-compliant product or service aims to reduce the exposure to losses (Bhatti, 2020).
The research carried out within the company confirms the need to analyse the existing problems within the organization in a centralized form and with a certain frequency, namely the notification of the involved functions and the rechecking after the removal of the non-compliance. To resolve non-compliance of any kind in the entire organization (material, informational or technological), there is the self-quality matrix tool (Self-Quality Matrix - SQM, or Auto-Quality Matrix - AQM) to keep under control the problems that have arisen, and for the product there are standards for verification and quality assurance.
The paper presents a useful tool for reporting, identifying and documenting non-compliance in the bottled water industry that can be extrapolated and adapted to any organization, from any field of activity. The aim of the study is to identify and report the problems arising on the material, informational or technological flow in order to be able to establish the levels of competence, the working tools and the methods of solving and preventing them. It can constitute a standard, an internal procedure of the company applicable when non-compliances are identified.

DESIGN AND OPERATION OF A LOGISTICS SYSTEM

The operation of logistic systems within the organization must be permanently optimized along with the quality of the products and services offered. This is only possible through the continuous improvement of all processes in the company. In this sense, an important role also belongs to the employees involved in the organization of the logistics system, starting from supply to sales based on the optimization of the flow of information and material (Bulat, 2018; Cernăianu, 2015).
The study includes logistics management methods that can serve as examples and possible high-quality tools or solutions as part of the continuous improvement process. The logistic system is a cohesive system that contains the material flows and all the elements that accompany them (Turcov et al., 2005).
In Figure 1, an adaptive logistic system is proposed with interconnections between its subsystems and the relationships developed with the external environment.
On the external input flow, we have the suppliers and logistics, and on the other side there are the customer orders. From a qualitative point of view, product admissibility criteria are imposed on suppliers, they are being accepted following an evaluation and selection through questionnaires or audits.
Quality barriers on products, whether they are raw materials, semi-finished products or finished products, are imposed from the reception of the products, in production and to the control of the finished product.
In order to solve non-compliances of any kind, (material or informational), there is the self-quality matrix tool to keep the problems under control, and for the product there are standards for verification and quality assurance.

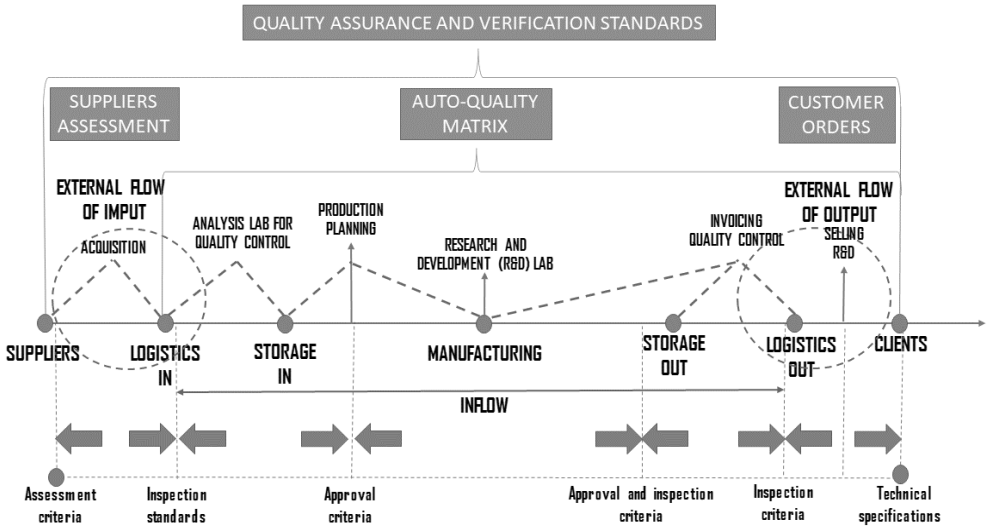

Figure 1. The micrologistics system within the company

The micrologistics system proposes the organization of activities aimed at optimizing material and informational flows. Currently there is a wide range of logistic management methods specific to modern production systems, which aim to reduce costs. Among the logistic progress mechanisms and techniques used in industrial engineering, we mention: Enterprise Resource Planning (ERP), Supply Chain Management, supply - delivery strategies, manufacturing cells, Supplier Relationship Management, business and strategic development operations, Continuous Improvements (Kaizen, Lean Manufacturing, Six Sigma, Total Quality Management), Customer Relations Service. An adaptive logistic system with interconnections was set up, simplifying the organization of activities with the aim of directing and optimizing material and information flows.

THE DESIGN AND SCOPE OF THE SELF-QUALITY MATRIX

The Self-Quality Matrix is a "tool" that helps to visualize the quality level of each section/ service in part and its evolution. Self-Quality Matrix is a technique to identify where the defect is created and detected in the manufacturing process. SQM is based on the visual inspection of the quality level of the product, service, or production line. At the same time, it helps to identify non-conformities as close as possible to the section/area that generates them and makes staff aware of the concept of self-quality. Also, non-conformities are dealt with directly in GEMBA, together with the staff involved.

For the continuous improvement of self-quality in the company, the self-quality matrix was built on the material flow (SQM Gemba Productive), on the information flow (SQM Gemba Services), respectively the self-quality matrix for technological equipment (equipment, machinery and work installations)/per department.

The Self-Quality Matrix is built on the kaizen principle: "Don't receive, don't do, don't pass on!". The Self-Quality Matrix not only shows the formation and detection of defects, but also provides a visual basis for acting on them. A company using SQM for every defect/non-compilances they encounter will not only help gain deeper insights, but also by forcing them to map or model their processes and value streams. To create the Self-Quality Matrix, the main "suppliers" of non-conformities, of the departments involved in the material flow, must be identified on the supplier-client relationship ("Where did the non-compliance occur?"). They can be identified depending on the place where the non-conformity is generated.

Table 1. Internal or external source of non-conformities

External suppliers	Internal suppliers	DMP	Production	Bottling	DPF	Source
Suppliers of non-conformities from outside the company	Indirect internal suppliers of non-conformities	Raw materials warehouse	PET preform blowing section	Bottling section	Finished products warehouse	Water source

Regarding the identification of the main "suppliers" of non-conformities, of the departments involved in the material flow, on the supplier-client relationship ("Where did the non-compliance occur?"), they can be:
- External suppliers - suppliers of non-conformities from outside the company;
- Internal suppliers - indirect internal suppliers of non-conformities (Table 1).
At the same time, the main "clients" of the non-conformities can be identified, by asking: "Where was the non-compliance found?".
Table 2 shows the structure by areas/ departments of the spring water bottling unit and the possible areas/sources where non-compliances can be identified.

Table 2. Structure/areas within the organization

DMP	Raw and auxiliary materials warehouse
Production	PET preform blowing section
Bottling	Bottling section
DPF	Finished products warehouse
QC	Quality control department
Internal customer	Research and development, logistics, and others
External customer	The end customer

Table 3 presents the classification of the main types of SQM non-compliances, which can be identified on the material and informational flow.

Table 3. Types of non-compliance at SQM material and informational flow

Nr.	Material flow non-compliances	Non-compliances for technological equipment	Non-compliances on information flow
1	Product loss	Blow Molding Machine - PET	Basic information is missing
2	Non-compliant documents	Water Pump	Missing atypical information/ incomplete information
3	Product with foreign taste and smell	Filling Machine	Incorrect information
4	Product with impurities	Capping Sealing Corking Machine	Unclear information
5	Contaminated product	Labeling Machine	Delayed information
6	Non-compliant product due to the machine	Sealing Shrink Wrapping Machine	Back order/out of stock
7	Sufficiently non-carbonated/non-zoned product	Pallets Wrapping Machine	Order late/finished product missing/raw material in stock
8	Non-compliant packaging	Tracee / conducted	Order late/finished product missing/raw material missing
9	Non-compliant labels	Bottle Conveyors	Back order for raw material/back order
10	Different color product	Ozone generator (Air Tree-Ozone Technology)	Missing documents
11	Lack of quality documents	Plate filter	Missing customer information
12	Non-conformity when making boxes, palletizing	-	Delayed customer information
13	Missing in management	-	Various
14	Missing labels/double labeling	-	Information overload
15	Failure to meet admissibility criteria	-	Erroneous services
16	Technical non-compliance	-	Unsatisfactory service quality
17	Other defects	-	Delayed services
18	-	-	No Services
19	-	-	Errors in operation

The Self-quality matrix per material flow involves the daily collection by operators of data related to the identified non-compliances, by completing the "Self-quality matrix (SQM)" sheets and mentioning the non-compliances in the "Material flow SQM column". Later, the non-co compliance can be selected and analyzed together with the operators involved in the flow, and the weekly analysis of the non- compliances is carried out together with the heads of sections/departments.

The Self-Quality matrix per information flow works similarly through the daily collection by employees of data related to the identified non-conformities entered in the "SQM" files in the "SQM information flow/per department" column. A weekly or bimonthly analysis of the data collected on the Self-Quality Matrix informational flow is carried out, along with the selection of problems that repeatedly generate non-conformities, their analysis, together with the operators involved.

The Self-quality matrix per flow of technological equipment (equipment, machinery, and work installations) on each section works in a similar way. The non-conformities related to the technological equipment are entered in the revision sheets of the machines and analyzed periodically, depending on their severity.

The operating stages of the Self-Quality Matrix are represented by the daily collection by operators of data related to the identified non-compliances, the daily transcription of the non-conformities reported on the SQM panel, the selection of the "problem of the day", the analysis of the "problem of the day" together with the operators involved in the flow and training, together with the weekly or bimonthly analysis of non- compliances together with the heads of departments.

The self-quality matrix tool is designed with the aim of keeping the problems under control by identifying and signaling problems in the material, informational or technological flow, establishing competence levels, work tools and methods for solving and preventing them. It can constitute a standard, an internal procedure of the company applicable when a non-conformity (problem) of any nature is identified.

The research can be applied in all departments involved in material flow (production, storage, logistics, but also in support services: technical, quality, laboratory, research and development), as well as in those involved in information flow (support services for material flow: technical , quality, laboratory, research and development, along with support services within the company: procurement, logistics, economic, financial, back-office sales, human resources, IT, administrative). Subsequently, the analysis and resolution of problems can be carried out within each department of the company where a non-compliance was reported, at the departmental or general meeting.

STATISTICAL ANALYSIS OF THE EQUIPMENT FAILURE INCIDENCE

The maintenance of machines and equipment involves the control of noncompliance related to the functioning problems that may arise in production. In the manufacturing process, the good operation of the machinery is essential to achieving the objectives of production and to obtaining safe, quality products. Thus, in a competitive economy, safety management is a critical component for quality and safe production (Glevitzky et al., 2019).

In the production process, the proper functioning of machinery and equipment is essential for achieving production goals and for obtaining quality and safe products.

Defects and their history are good indicators of equipment maintenance. The antecedents of equipment failure can cost a lot; therefore, it is necessary to anticipate them or find their causality (coincidental or which justifies a more detailed investigation) for corrective or preventive actions in the company.

Using the chi-squared test (χ^2 test), it was checked whether the calculated probability of occurrence of noncompliance (defects) in production equipment differs significantly from the theoretical probability of their presence. So, the chi square test (χ^2) can be used to assess a relationship between two of these categorical variables, that is, to determine whether there is an association between them (Greenwood & Nikulin, 1996).

The technical equipment of the factory were about 18 years old; they were purchased from the same supplier and being used under the same conditions. Is the lower number of equipment

failures in the technological process real and natural? Or failures with a higher frequency are caused by faults in the use or design of the machines. It should be noted that the appearance of several defects in other machines can be determined by a piece of equipment on the production line before it or is caused by other factors and is not accidental. All the noncompliance encountered appeared in the context of the normal annual use and maintenance of the machines used in the process. The question is whether there is a need for a higher frequency of interventions related to equipment maintenance.

From the total of 25 defects in the last 5 years, the results for each type of technical equipment are shown in Table 4.

Table 4. The results of the calculation of the chi-squared test for the occurrence of technological equipment defects in the process

Machinery (Equipment)	PET Bottle Blowing Machine	Water Pump	Filling Machine	Capping Sealing Corking Machine	Labeling Machine	Sealing Shrink Wrapping Machine	Pallets Wrapping Machine	Total
Number of defects	2	2	9	4	5	3	0	25
$F - n \times p$	-1.5725	-1.5725	5.4275	0.4275	1.4275	-0.5725	-3.5725	-0.0075
$(F-n\times p)^2/n\times p$	0.6922	0.6922	8.2457	0.0512	0.5704	0.0917	3.5725	13.9158

F - the frequency of defects; n - the sum of incidence of defects.

If, according to the hypothesis, all seven technological equipment from the production process that operate simultaneously under the same conditions, the probability that one of them will be out of order is p = 0.1429. The mathematical expectation related to the presence of the number of defects is M (n) = n·p = 3.5725. For ν = 6 degrees of freedom and the value χ^2 computed = 13.916 we find a significance level (α or p-value) less than 0.50, but greater than 0.25 (Gluck, 1971). This means that the chi-square value would occur simply by chance between 25% and 50% of the time. We can conclude that the variables are not independent of each other and that there is a statistical relationship between the categorical variables.

These results can lead to rejection of the null hypothesis, and we will admit that the difference between the number of defects is not accidental. So, we have enough arguments to support the need for a detailed analysis of all the causes that lead to such many defects, especially in the filling machine, capping-sealing-corking machine and labelling machine.

CONCLUSIONS

The Self-Quality Matrix can be a standardized process that takes on real potential in the context of implementation within organizations that emphasize the remediation of non-compliances and continuous improvement. The Self-Quality Matrix tool focuses on quality, respectively the importance for customer satisfaction and evaluates robustness. At the same time, it evaluates the manufacturing and inspection processes against the potential or actual severity of the problem. This tool allows a real positive impact on customer satisfaction by acting to identify and signal problems arising on the material, informational or technological flow. At an advanced level of implementation, the self-quality matrix becomes an effective and efficient tool in preventing non-conformities.

The chi-square test was performed to evaluate the occurrence of defects in different equipment of the technological process of the water bottling industry, meaning there is a definite, consequential relationship between the occurrence of defects in production equipment reported to the theoretical probability of their presence.

REFERENCES

Achim, I.M., Arcadie, H., Bele, I. (2008). *General management of the enterprise*, Cluj Napoca, RO: Risoprint Publishing House.

Bhatti, M. (2020). Managing Shariah Non-Compliance Risk via Islamic Dispute Resolution. *Journal of Risk and Financial Management*, *13*(1), 2.

Bulat, V. (2018). Integrarea fluxului material în activitatea sistemului logistic, *Conferința Științifică Internațională Jubiliară „Paradigme moderne în*

dezvoltarea economiei naționale și mondiale", Chișinău, Moldova, 2-3 noiembrie, 309-313.

Cernăianu, A. (2015). *Logistică: teorie, aplicații și simularea fluxurilor logistice*, Craiovam RO; Universitaria Publishing House.

EC Regulation No. 852/2004 on the *Hygiene of Foodstuffs*, L 139. In Official Journal of the European Union; The European Parliament and the Council of the European Union: Brussels, Belgium, 2004, 1–54.

Fornell, C. (2007). *The Satisfied Customer, Winners and Losers in the battle for Buyer Preference*, New York: Palgrave MacMillan.

Glevitzky, I., Sârb, A., Popa, M. (2019). Study Regarding the Improvement of Bottling Process for Spring Waters, through the Implementation of the Occupational Health and Food Safety Requirements. *Safety*, *5*(2), 32.

Gluck, A. (1971). *Metode Matematice în Industria Chimică*. Bucuresti, RO: Tehnică Publishing House.

Greenwood, P. E., Nikulin, M. S. (1996). *A Guide to Chi-Squared Testing* (Wiley Series in Probability and Statistics) 1st Edition, New York, USA: Wiley-Interscience Publisher House.

Imai, M. (1986). *Kaizen: The Key to Japan's Competitive Success*. New York; McGraw-Hill Education Publishing House.

Imai, M. (1997). *An interview with Masaaki Imai. Interview in the Quality-Digest.* Retrieved from http://www.qualitydigest.com/ june97/html/imai.html.

Imai, M. (2013). *Gemba Kaizen: A Practical Approach to Continuous Improvement Strategy*, ed. II, Bucharest, RO: Kaizen Institute.

Ionescu, L. C. (2007). *Legislation and auditing of quality systems*. Iasi, RO: Performantica Publishing House.

Oprean, C. (2006). *Methods and techniques of scientific knowledge*, Sibiu, RO: "Lucian Blaga" Sibiu University Publishing House.

Stoller, J. (2015). *Leaders Kaizen-Lean. The road to world-class excellence*, Bucharest, RO: Kaizen Institute Romania.

Turcov, E., Petrovici, S., Petrovici, A. (1966). *Tehnologiile comerciale și logistica*, Chișinău: ASEM Publishing House.

Scientific Papers. Series E. Land Reclamation, Earth Observation & Surveying, Environmental Engineering. Vol. XII, 2023
Print ISSN 2285-6064, CD-ROM ISSN 2285-6072, Online ISSN 2393-5138, ISSN-L 2285-6064

STATUS, PROBLEMS AND SOLUTIONS CONCERNING SURFACE WATER MANAGEMENT IN BULGARIA

Krasya KOLCHEVA, Marian VARBANOV, Kristina GARTSIYANOVA

National Institute of Geophysics, Geodesy and Geography - Hydrology
and Water Management Tesearch Center, Bulgarian Academy of Sciences,
Acad. G. Bonchev Street, Sofia, Bulgaria

Corresponding author email: kolchevakrasi@abv.bg

Abstract

Water resource conservation and management is vital as well for humankind, as for nature and economy, and is exposed to anthropogenic and climatic pressures, transcends national boundaries. The EU Water Framework Directive 2000/60/EC establishes a legal framework to protect and restore clean water in the EU and to secure its long-term sustainable use and mitigate the effects of floods and drought. In this regard, EU member-states are developing river basin management plans based on current characteristics and water status and programs with measures. In the planning process were identified different types of pressures on the surface waters, defining the significant management issues, such as pollution with biogenic substances, organic and chemical pollution, pressure from water intake and climate pressure. These problems solutions require both science-based approaches and specific target measures definitions to improve the water resources status and the level of their management.

Key words*: chemical pollution, ecological status, scientific approaches, water intake.*

INTRODUCTION

To protect the water resources from the diverse anthropogenic impact in the conditions of global climate change is one of the main tasks for society to solve today at global, national and a local level. The main document implemented in the European Union countries is the European Framework Directive (Water Framework Directive, WFD) adopted in 2000 and regulating the integrated water management policies.

Among the WFD most important goals and tasks are the achievement by 2027 of good ecological and chemical status of all surface and underground waters through the river basin management plans (RBMPs), including analysis and assessment of the water current state, assessment of the pressure on water quality, and six years program of measures to limit the anthropogenic impact on water.

Given the territorial and climatic specifics, the internal flow of Bulgaria is relatively limited, but with the external inflow from the Danube River it increases several times.

Thus, the total fresh water resources, both in absolute volume and per capita, significantly exceed those, in a number of European countries.

The pressures of diverse nature on surface water identified in the planning process determine significant management problems in terms of quantitative and qualitative specifics among which in 2021 are identified: surface waters pollution with biogenic substances; organic and chemical pollution; pressure from water intake and physical modifications; and climate pressure. Solving these problems requires science-based approaches to improve the level of planning, including the selection of adequate measures for the current state of waters. These actions aim to achieve environmental goals and will generally improve water management.

This paper presents the evaluated based on the available methodologies state of the surface waters in the process of planning, highlighting the gaps and the important management issues. The upgrading of the methodological basis and the resolution of the problems require science-based approaches and mitigating measures.

MATERIALS AND METHODS

Territorial scope and main specifics of the area studied

Bulgaria has an area of 110912 km^2 located in the east Balkan Peninsula. It borders Romania in

the north, Serbia and North Macedonia in the west, Greece and Turkey in the south, and the Black Sea in the east. The National Statistical Institute (NSI) published data for 2021 indicate that the Bulgarian population is about 6.8 million people, with 73% living in urban areas. According to data by the Institute for market economy for 2019, the gross domestic product amounts is 67% for services, 28% for industry, and only 5% of agriculture.

The implementation of water management according to the basin principle pursuant the Water Resources Act and the provisions of Art. 3 of WFD Bulgaria is divided into four basin management regions (BMRs), distinguished by the natural location of the watersheds between the catchment areas of one or several main rivers (Table 1), namely:

- Danube River Basin District (DRBD),
- Black Sea River Basin District (BSRBD), - East Aegean River Basin District (EARBD),
- West Aegean River Basin District (WERBD).

In Figure 1 is represented the territorial scope of the basin regions, and on Figure 2 - their respective share of the area of Bulgaria.

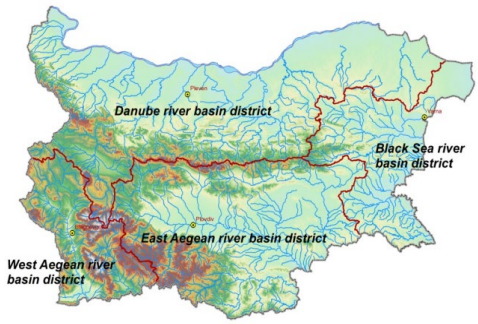

Figure 1. River Basin Districts in Bulgaria

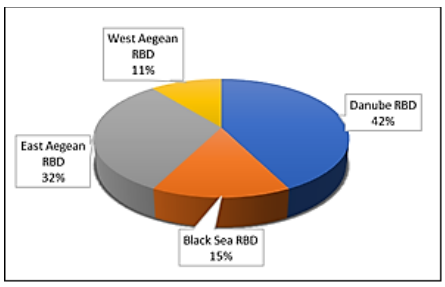

Figure 2. Share of the respective region from the total area of Bulgaria

Table 1. River Basin Districts (RBD) - main characteristics

RBD	Main river basins	Ecoregion
Danube River Basin District	Erma and Nishava, River west to Ogosta, Ogosta, Vit, Osam, Iskar, Yantra, Rusenski Lom, Danube and Dobrudjanski rivers	12 - Pontic province
Black Sea River Basin District	Black Sea Dobrudjanski rivers, Kamchia, Provadiiska, North Burgas rivers, Manderski rivers, South Burgas rivers, Veleka and Resovska rivers, Preseltsi-Chernomoretz gullets	7 and 12 - Eastern Balkan and Pontic province
East Aegean River Basin District	Maritsa, Tundja, Arda and Byala reka	7 - Eastern Balkan
West Aegean River Basin District	Struma, Mesta and Dospat	7 - Eastern Balkan

The Bulgarian climate most specific feature is the transition between the temperate and the Mediterranean (subtropical) climate with a slow but positive trend of growth in air temperature over the last century, unevenly distributed precipitation throughout the year, and frequent extreme events such as droughts and floods.

The year 2020 is the second warmest year since 1930 with an average annual temperature for Bulgaria of 12.4°C or 1.9°C above the climate average for the period 1961-1990, while in 2021 the average annual temperature is 11.8°C or 1.3°C higher than the climate average for the same period. The country average annual precipitation in 2020 is 594 mm or 93% of the norm, and that in 2021 is 766 mm or 20% above the norm (NIMH, 2020). Multi annual fluctuations in precipitation amounts are used as a regional climate change indicator and assessment of such economic sectors impact, specifically on agriculture (Alexandrov & Shopova, 2020), as well as a factor in the formation of national water resources.

The available renewable water resources of Bulgaria, excluding the external inflow from the Danube, the multiannual average for the period 1981-2020 are estimated to 15.8 billion m^3 distributed within the four basin areas, according to Figure 3 (NSI, EEA, 2020).

The average multi annual river runoff varies widely, most often at 50% supply at between 18.0 and 20.8 billion m^3/year, and at 95% supply it is 8.0-9.5 billion m^3/year. The volume of registered surface runoff for Bulgaria in 2020 was 10.1 billion m^3 and compared to the average multi-annual data for 1961-1990, 1971-2000, and 1981-2010, data indicate decrease by 45.2, 37.7%, and 35.0% respectively, thus being the smallest for the last five years (EEA, 2020). The participation in surface runoff for 2020 share is

respectively for: Danube catchment basin - 38.2%, Eastern Aegean basin - 37.6%, West Aegean basin - 19.1% and Black Sea - 5%.

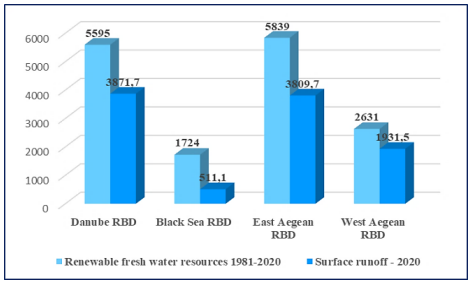

Figure 3. Available renewable fresh water resources without external inflow (1981-2020) and Surface runoff (2020) by the RBDs, mil. m^3

Within the current RBMPs 2016-2021, 955 surface water entities are defined (natural - 77%, highly modified - 21% and artificial - 2%), divided into four classes - rivers - 89%, lakes - 6.5%, with those specifics only for the RBRMs - transitional and coastal waters. Out of the identified types for Bulgaria under System B (Appendix No. 1 to Art. 2 of Ordinance H-4/14.09.2012 concerning the surface water characterization), considering multiple indicators - geomorphological, hydro morphological, biological, geological, hydraulic, the largest number water entities being of R3 - mountain type, followed by R4 - semi-mountainous rivers in the Pont province, and R5 - semi-mountainous type.

Assessment methods concerning surface waters pressure and condition, and the measures planning

Surface water management is based on an assessment of their ecological and chemical status adequate to the identified anthropogenic pressure, and the results of the monitoring and the potential risk of not achieving the goals, together with the harmful impact of the waters, determine the degree of significance.

The RBMPs conceptual model 'Drivers - Pressure - Status - Impact – Response' (DNSVO)' proposed in Guideline No. 3 'Analysis of Pressure and Impacts' of the General Strategy for the Implementation of the Water Framework Directive 2000/60/EC (WFD) has been applied as based on causal relationships and interaction between society, its economic activity, and the environment.

Driving forces (natural and anthropogenic) define the category and type of pressure which, as significant alone or in combination with other types of pressure, may negatively affect the ecological objectives of a water body (WB). The significant pressure is based on an assessment of monitoring data and how much they account for a change in condition from a certain impact with a potential risk of not achieving good condition. The ecological status/potential assessment of surface water entities for (natural, WWTP and artificial) in accordance with the requirements in Annex V of the WFD and Guideline No. 6, is carried out according to the following quality elements: biological (BEC), physical and chemical (FHEC - general indicators and specific pollutants) and hydro morphology as accepted scales specified in Table 2.

Table 2. Classification and designations of ecological status

Ecological status				
High	Good	Moderate	Poor	Bad
1	2	3	4	5

The BEC leading assessment is based on selected indices/metrics for the following elements - phytoplankton (lakes/dams), phytobenthos (rivers), macrophytes, macrozoobenthos (rivers) and fish fauna (rivers), and that of the main physical and chemical indicators (10 per number) - dissolved oxygen (DO), biochemical oxygen demand (BOD_5), ammonium (NH_4^+- N), nitrite (NO_2^--N) and nitrate (NO_3^--N) nitrogen, total nitrogen, phosphates (PO_4^{3-}-P), total phosphorus, electrical conductivity and pH of their average annual concentrations. This is regulated in points A and B of Appendix No. 6 in the above-mentioned Ordinance No. H-4/14.09.2012. Due to lack of an approved analysis methodology the hydro morphological state analysis is expert and based on monitoring data.

The excellent condition is determined with unobserved or minor deviations from the natural conditions and in all other cases good condition is defined (Table 3), as for the water bodies with a significant impact on BEK, indicative of hydro morphological pressure, a test is conducted to determine highly modified water bodies.

Table 3. Groups of indicators to evaluate the quality elements

Ecological status		
Biological elements	Physico-chemical elements	Hydromorphological elements
High	High	High
Good	Good	Good
Moderate	Moderate	
Poor		
Bad		
U	Unknown	

The chemical state of assessment surface waters is carried out based on the concentrations of priority substances and some other pollutants established during monitoring in accordance with the list and standards in Directive 2008/105/EC on setting environmental quality standards (EQS), transposed into Ordinance from 2010 on environmental quality standards for priority and other pollutants of the Bulgarian legislation.

A good chemical status is defined with average annual value (AAV) for each monitored priority substance does not exceed the AAV-EQS, and a bad one when the average value is greater than the AAV-AQS, according to Appendix 2 of the Ordinance on EQS (Table 4). In 2016 National methodology for assessing the chemical state of surface waters was adopted, which will be applied during the implementation period of the second RBMP.

Table 4. Assessment of chemical status of surface water bodies

Chemical status	Good	
	Bad	
	U	unknown

To preserve or improve the surface waters condition is developed a Program of Measures (PoM) as part of the RBM. The minimalist approach adopted in the first RBMP in PoM development is built on in the second plan with national approach that considers the interactions of driving force - pressure - impact - condition - environmental objectives - measures. The approach aims to ensure the planning of measures focused at specific type and sources of pressure, thus identifying significant problems in water management according the specific conditions and state of individual water entities. Each measure is related to concerned water entity and its determined driving force: urbanization, agriculture, energy, flood protection, industry, climate change, etc.

The measures (main, complementary, and additional) in the second program are drawn from a national catalog and may apply to more than one water entity or to an entire basin area. The main measures focus on compliance with the WFD minimum mandatory requirements and the Water Resources Act, while the complementary ones are enforced in cases where the main one's implementation is not sufficient for the good status.

If the main and the complementary measures do not produce the required result in the stipulated period, new "additional" measures are envisaged within the current RBMP with respect to the established anthropogenic pressure on a given water body. These measures are foreseen within the implementation of the RBMP should monitoring or other data indicate that the environmental protection objectives for a specific water entity cannot be achieved through planned measures and/or within the period set.

RESULTS AND DISCUSSIONS

Water conditions

Based on the assessment of the surface water state by the applied in the RBMP methods, the results from the monitoring in 2020 and the analysis of the National Report on the State and Protection of the Environment in Bulgaria for 2020, the following generalizations can be made:

- In 2020 the number of water entities in excellent and moderate conditions increased by 39.6% and 26.6%, respectively, and those in good conditions decreased by 90.6% compared to the second planning period 2016-2021, while keeping the positive trend for the main physical and chemical indicators (Table 5, Figure 4).
- The monitoring results for 2020 regarding the biological quality elements indicate that in 74% of surface water points in category *rivers* and 63% in category *lakes* the objectives for good conditions are not fulfilled, while the assessment of main physical and chemical indicators shows that most examined points are in excellent and good conditions. During 1996-2020 is registered a decrease in the concentrations of O_2, NH_4-N, N-NO_3, BOD_5 and PO_4^{3-}-P (EEA, 2020);

- The chemical state improvements for surface water entities are insignificant, with 64% being not assessed due to missing monitoring data and laboratory analysis methods for some priority substances (Table 6).

Table 5. Ecological status of the surface water bodies by the RBDs - RBMP 2016-2021 - Annual report 2020

Ecological status/potential / River Basin District	Danube		Black Sea	
	RBMP 2016-2021	Annual report 2020	RBMP 2016-2021	Annual report 2020
1 (high)	19	27	5	10
2 (good)	94	83	72	32
3 (moderate)	59	79	83	97
4 (poor)	22	14	25	10
5 (bad)	11	8	20	6
U (unknow)	51	1	0	33
no monitoring	0	44	0	17
Total	**256**	**256**	**205**	**205**
Ecological status/potential / River Basin District	**East Aegean**		**West Aegean**	
	RBMP 2016-2021	Annual report 2020	RBMP 2016-2021	Annual report 2020
1 (high)	18	4	11	33
2 (good)	105	112	103	69
3 (moderate)	112	143	51	67
4 (poor)	26	37	8	9
5 (bad)	12	14	5	2
U (unknow)	38	1	5	0
no monitoring	0	0	0	3
Total	**311**	**311**	**183**	**183**

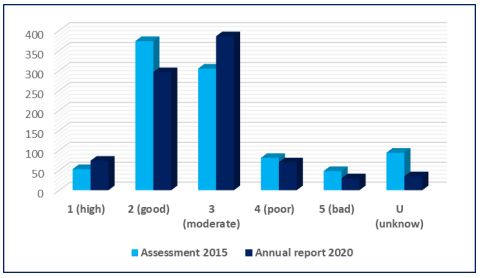

Figure 4. Total ecological status of the surface water bodies in Bulgaria

Table 6. Chemical status of the surface water bodies by the RBDs - RBMP 2016-2021

River Basin District/Chemical status	Danube	Black Sea	East Aegean	West Aegean
High	165	45	49	63
Good	6	9	7	3
U	85	11	255	117
no data	0	140	0	0
Total	**256**	**205**	**311**	**183**

Significant management issues

The significant pressures delineated by the above-mentioned conceptual method in RBMP and the third Mid-term review of significant water management issues - 2021 identify among the water management important problems the following ones depicted below.

- Contamination with biogenic elements

Main causes of this pollution are: *Erosion* - in Bulgaria 1.7 million ha are affected by erosion, out of which 0.4 million ha - to a high and very high degree; *Farming* - during the last decade agricultural production in Bulgaria has increased by over 50%, and meat production by 48%. Cultivated land is treated with artificial fertilizers and preparations for plant protection. During the period 2010-2019 the average nitrogen mineral fertilizers used dose in DRBD is 120 kg/ha, in BSRBD - 123 kg/ha, in EARBD - 75 kg/ha, and in WERBD - 31 kg/ha, so that the treated area increased respectively by 56%, 67%, 112%, and 55% compared to 2010.

The average dose of mineral phosphorus fertilizers used for the same period is: DRBD - 11.4 kg/ha, in BSRBD - 12 kg/ha, in EARBD - 7 kg/ha, and WERBD - 3 kg/ha, so that the treated area increase is respectively by 120%, 137%, 201%, and 119% compared to 2010. Significant agricultural pressure on the quality and quantity of surface waters in Bulgaria exerts animal husbandry - raising birds, pigs and cattle in farms, which produce significant amounts of waste water; *Wastewater from settlements and industry* - the share of the population connected to sewage and wastewater treatment plants (WWTPs) is an indicator, refer to Figure 5. The population in Bulgaria connected to public sewage is 76.3% with relatively small regional differences, while those connected to WWTPs are 66.7% with the Danube and Black Sea RBDs leading the way. Pursuant the provisions of Directive 91/271/EEC, the construction of WWTPs for another 123 agglomerations for 2000 units/population is planned as follow: in DRBD, 53, in BSRBD, 119, in EARBD, and 37 in WERBD. Tourism exercises significant pressure in RBRM, as well as intensive cultivation of aquaculture in fishponds mainly in EARBD and WERBD.

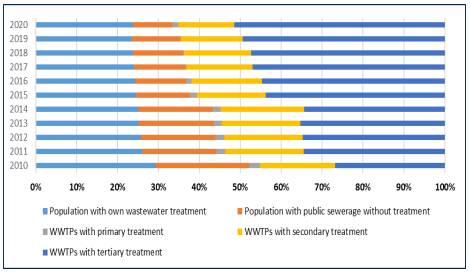

Figure 5. Population with public sewerage without treatment and wastewater treatment plants (WWTPs) in the period 2010-2020

- ***Organic pollution*** - the monitoring of BOD_5 results analysis indicates excesses in a relatively large number of SWBs in Bulgaria, with slight decrease trend in the multi annual values. The analysis of issued permits indicates that in BSRBD over 82%, in EARBD over 79% and in WERBD over 99% of catchment permits of BOD_5 are due for domestic wastewater. The situation is similar for the DRBD, where biogenic pollution exceeds organic pollution.
- ***Chemical pollution*** *(priority substances, specific and other pollutants)* due to such sources as farm related pesticides and plant protection preparations; industrial and household atmospheric emissions; wastewater discharge from industrial sources, waste landfills, old industrial areas and mine waters with contamination risks with specific pollutants (including radiation pollution) and with priority substances. As far as *the category river* in DRBD is concerned, specific pollutants affected 29% of the surface waters (the river beds of rivers Iskar, Ogosta, and Yantra being the most affected) and out of 13% of EARBD and WERBD. While of *category lake* - 4% in EARBD and 13% in WERBD.
- ***Water intake pressure*** is determined by the permits regime to secure the water users needs which may have a negative impact on the available surface runoff and, in particular, on water ecosystems. The trend of water intake from surface water sources in Bulgaria for the period 2010-2020 is presented in Figure 6.

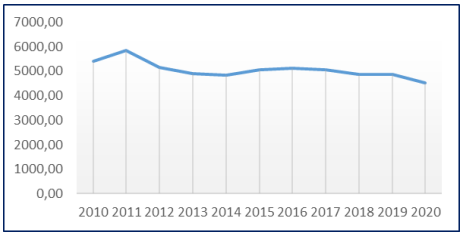

Figure 6. Surface water withdrawal in Bulgaria during the period 2010-2020

The largest share of granted permits for water consumption in Bulgaria are those for electricity production and cooling, while in relation to other sectors the leading one is fish aquaculture farming with 33.7%, followed by irrigation with 29%, drinking - domestic water supply with 18.2%, and industry with 14.2% (Figure 7).

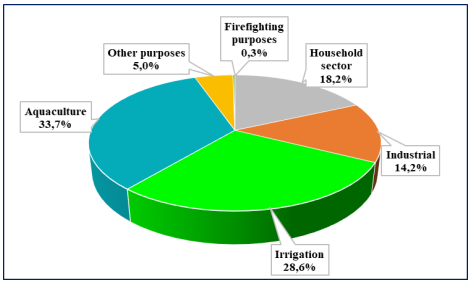

Figure 7. Permitted limits for water withdrawal from surface water sources in Bulgaria by 2022

The pressure from water intake on surface water in RBMP is based on a research report by the National Institute of Meteorology and Hydrology (NIMH) on the annual average national and regional (basin) resources, as well as data from the Basin Directorates on abstraction at the water body level. The pressure is classified in the following categories - from 0 to 3%; from 3 to 15%; from 15 to 20%; from 20 to 25%; from 25 to 30% and over 30%.
According to the second RBMPs, a total of 549, or 57.5%, of the surface water entities are exposed to water intake pressure, which according to the RBDs are shown in Figure 8.

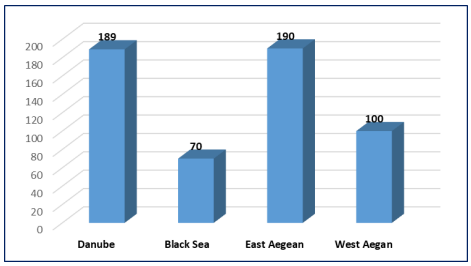

Figure 8. Surface water bodies under pressure from water withdrawn

The RBMPs 2016-2021 lack water user's security assessment and the water shortages, for which a summary assessment was produced in 2022 by calculating the Falkenmark Index for dry year. The index values varying from 543 for the Black Sea River Basin District to 1135 m^3/person/year for the Aegean Sea basin and total for Bulgaria - 842 m^3/person/year, are below the indicative water shortage norm of 1700 m^3/person/year (Seymenov, 2022).

- ***Climate pressure*** - With the applied in the second RBMPs "Approach to Assessing the Pressures and Impacts on Surface and Groundwater from Climate Change and Assessing the Availability of Water for Economic Sectors" climate change is integrated into the process of determining the risk of climate pressures by assessing the effect of changes under RCP 8.5 (pessimistic) and RCP 4.5 (moderate) climate scenarios. The model results for both scenarios indicate trends for increasing autumn precipitation in Bulgaria and decreasing summer precipitations. Concerning the RCP 8.5 climate change scenario for steadily increasing greenhouse gas emissions in time, the projected runoff change trends in the long term are strongest for the period 2071-2100. The Figures 9 to 11 present the climate change intensity for each of the three periods (2013-2042; 2021-2050, and 2071-2100) within the RCP 8.5 scenario.

The established significant positive trends in the air temperature in Bulgaria and modified hydrothermal conditions in the agricultural areas (Shopova et al., 2022) are increasingly becoming the subject of scientific research, given the pressure from the water resources use.

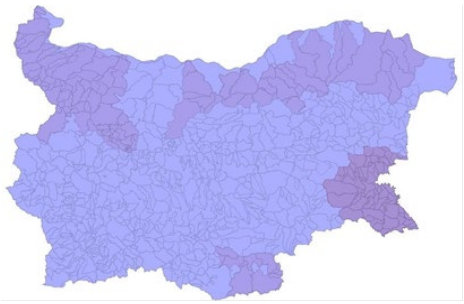

Figure 9. Intensity of expected climate changes for the period 2013-2042

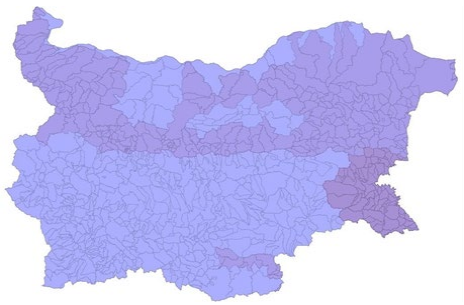

Figure 10. Intensity of expected climate changes for the period 2021-2050

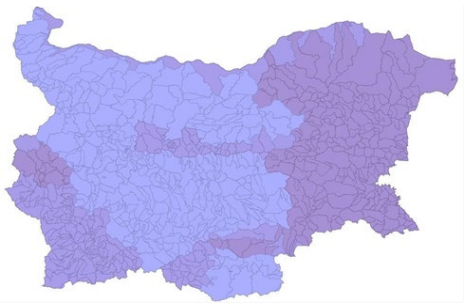

Figure 11. Intensity of expected climate changes for the period 2071-2100

Planned measures

Given the above approach, the updated PoM driving forces include the following key core measures to:

- ***urban territories*** - construction of new or modernization of existing WWTPs, protection of drinking and domestic water sources with introduction of secured zones and prevention of urban areas, transport and existing infrastructure pollutions;
- ***industry*** - construction of new or modernization of existing industrial WWTPs;

- ***agriculture*** - reduction agriculture generated biogenic elements and pesticides pollution, reduction of soil erosion and surface runoff deposits;
- ***energetics*** - improving the water entities hydrology morphological conditions (restoration of rivers, improvement of coastal areas, removal of hard embankments, restoration of the connection between rivers and floodplains, etc.), runoff regime improvement and/or determination of the minimum ecological runoff in rivers.

An extremely important measure is the implementation of efficient water use in irrigation, industry, energy and households. Complementary measures usually concern the implementation of monitoring, control and additional research, as well as the implementation of good agricultural practices, some prohibitions (e.g. for the construction of hydroelectric power stations) and the construction of facilities such as fish passages. The largest share is for the urban zones planned measures. For example, in the EARBD the measures share in urbanization is 50%, those planned for more than one driving force - 20% and for agriculture - 13%.

CONCLUSIONS

In Bulgaria, although with successfully introduced and applied methods and practices for integrated basin water management, there are still a number of gaps in the planning process.

The indicated management issues focus on surface water pollution and under-estimated water intake pressures in drought periods and require above all science-based approaches.

First of all, in order to boost the assessment credibility for pollution sources and relevant pollutants, and select appropriate measures, it is necessary to coordinate the scientific research results with available methodologies and upgrade them.

Since the quantitative status is an integral part of the water general state, in sake for planning objectivity and completeness, the European Commission requires actions in this field. It requires available water resources management assessment to find out the assurance degree for water users in different water supply periods in connection with climate scenarios. Based on existing scientific developments in Bulgaria, and considering changing conditions and water users' requirements, an approach for water balance assessments at the basin/sub-basin level with the definition of water efficiency targets should be both justified and applied. Considering the climate change pressure, independently or as part of the next RBMPs, is of particular importance the development of a management plan for water resources in drought conditions, a challenge for the scientific research community in Bulgaria.

Finally, the achievement of the WFD and the RBMP targets depends directly on the implementation of planned measures. In Bulgaria, this is generally hindered by: unsecured or delayed funding for investment measures (for example: for basic structure measures such as construction/upgrading of sewage systems), insufficient administrative capacity to control the measures implementation and non-implementation by the managing authority for investments or administrative measures (for example, non-fulfillment of permit conditions for surface water withdrawal).

ACKNOWLEDGEMENTS

This work has been carried out in the framework of the National Science Program "Environmental Protection and Reduction of Risks of Adverse Events and Natural Disasters", approved by the Resolution of the Council of Ministers № 577/17.08.2018 and supported by the Ministry of Education and Science (MES) of Bulgaria (Agreement № Д01-271/09.12.2022).

REFERENCES

Alexandrov, V., & Shopova, N. (2020). Analysis of precipitation during the autumn-winter period in agricultural regions of Bulgaria. In: *Proceedings of the Climate, atmosphere and water resources in the face of climate change, 2,* 15 - 16 October 2020, 191-197.

Black Sea River Basin Directorate (2020). Assessment of the current state of waters in the Black Sea River Basin District for 2020.

Black Sea River Basin Directorate (2021). Mid-term review of significant water management issues in the Black Sea River Basin District.

Danube River Basin Directorate (2020). Analysis of the state of surface water bodies, located on the territory of the Danube River Basin District for the period 2019-2020, by individual quality elements.

Danube River Basin Directorate (2021). Mid-term review of significant water management issues in the Danube River Basin District.

East Aegean River Basin Directorate (2020). Report on the state of waters in the territory of the East Aegean River Basin District - 2020.

East Aegean River Basin Directorate (2021). Mid-term review of significant water management issues in the East Aegean River Basin District.

Executive Environment Agency (EEA). (2020). National report on the state and protection of the environment in the Republic of Bulgaria.

National Institute of Meteorology and Hydrology (2020, 2021). Annual Hydrometeorological Bulletin 2020 and 2021.

River Basin Management Plan for the Black Sea District (2016-2021).

River Basin Management Plan for the Danube River Basin District (2016-2021).

River Basin Management Plan for the East Aegean District (2016-2021).

River Basin Management Plan for the West Aegean District (2016-2021).

Seymenov, K. (2022). Geographical aspects of water scarcity in Bulgaria during 2001. "Climate, atmosphere and water resources in the face of climate change", *4*, 79-84. ISSN 2683-0558.

Shopova, N., Alexandrov, V. & Tsaikin, N. (2022). Hydrothermal conditions in the agricultural areas of Bulgaria expressed by the indices of Ped and De Martonne. In: *Proceedings of the Climate, atmosphere and water resources in the face of climate change, Sofia, 4*, 85-92. ISSN: 2683-0558.

West Aegean River Basin Directorate (2020). Bulletin on the state of surface and underground water bodies in the West Aegean River Basin District - 2020.

West Aegean River Basin Directorate (2021). Mid-term review of significant water management issues in the West Aegean River Basin District.

Scientific Papers. Series E. Land Reclamation, Earth Observation & Surveying, Environmental Engineering. Vol. XII, 2023
Print ISSN 2285-6064, CD-ROM ISSN 2285-6072, Online ISSN 2393-5138, ISSN-L 2285-6064

DRAMATIC REDUCTION OF THE WATER AND SEDIMENT FLUXES IN A HUMAN MODIFIED MEANDERING ECOSYSTEM FROM THE DANUBE DELTA, ROMANIA

Florin DUȚU, Laura TIRON DUȚU, Irina CATIANIS

National Institute for Research and Development for Marine Geology and GeoEcology (GeoEcoMar), 23-25 Dimitrie Onciul Street, Romania

Corresponding author email: florin.dutu@geoecomar.ro

Abstract

The pressure control of the anthropogenic factors has consequences on the fluvial systems, generating structural changes. The hydrology, hydraulics and sediment load of the rectified meandering systems depend on the hydrologic connectivity with the main stem of the river. The former meanders can be permanently, temporarily disconnected with the main channel producing interruptions in the transfer of fresh water and thus affecting the morpho-sedimentological processes and the biodiversity. This paper aims to investigate the distribution of the water and suspended sediment fluxes between the former meanders and the artificial man-made canals along the St. George distributary and thus, the hydrological connectivity. Understanding these complex human pressures are of high importance for reaching/ maintaining the ecological status of the Danube. Herein, we made investigations along the St. George branch on many sub-systems river-channel-lake site type, formed by cutoff meanders, connective channels and lakes to observe how much the water and sediment inputs to the delta depressions is affected by the structural changes of the meander's physiography.

Key words*: ADCP, cut-off meander, Danube Delta, hydrologic connectivity, human pressure.*

INTRODUCTION

The good functionality of a deltaic system is represented by the hydrological connectivity developed by hydrologists to better understand the importance for water quantity and quality (Pringle, 2001; Bunn & Arthington, 2002; Karim et al., 2015). The water hydrology and hydraulics and the sediment load characteristics of river-channels- floodplain lakes from deltas depend on several natural coupled with human factors; however, the main driver of these characteristics is represented by the hydrologic connectivity with the main stem of the river (Junk et al., 1989; Pringle, 2003; Bracken et al., 2013; Covino, 2017). The reduction of the sediment load is generally due to the human activities, such as landscape engineering, construction of reservoirs, hydrotechnical works, dredging (Zaharia et al., 2011; Habersack et al., 2016; Nistor et al., 2021).

Since the 16th century, people have been changing the natural course of the rivers in the Danube River Basin, mainly for flood defence, hydropower generation and navigation. More than four-fifths of the Danube is regulated for flood protection, while approximately 30% of its length is additionally impounded for hydropower generation. Over 700 dams and weirs have been built along the main tributaries of the Danube (ICPDR, 2008; 2015). Moreover, to the upstream anthropogenic changes along the Danube River are added the downstream ones localized in the delta itself (Pacioglu et al., 2022a). The decrease of the sedimentary discharge started before the construction of the Iron Gates dams, and has been accelerated after their construction (1972, 1984, respectively). Since the middle of the 19th century, the direct anthropic changes within the Danube Delta began, after the establishment of the Danube Commission in 1856. The works consists in meander bends cut-offs, construction of dikes, jetties, groins, construction of a very large network of canals, river bank stabilization, substitution of natural ecosystems into large polders (Vădineanu, 2001). Along the St. George branch six free meanders were rectified between 1984 and 1994 diminishing the length by 32 km from the previous 108 km. Such river training works caused a change in the distribution of the solid as well as the streamflow in the whole delta, enhancing fluxes through the rectified channels (Bondar & Panin, 2000; Pojar et al., 2021; Vasiliu et al., 2021;

Tiron Duţu et al., 2022). Inside the meander systems, strong modifications were developed by acceleration of the liquid and solid fluxes through the artificial canals combined with sedimentation of the former meanders, as demonstrated by Popa (1997), Duţu et al. (2022a); Tiron Duţu et al. (2022); Trifanov et al. (2022). The changes of the river bed morphology, water and sediment fluxes produce a decrease of the fresh water and sediment fluxes to the former meanders and forward, to the interdistributary depressions, affecting the hydrological connectivity (Pacioglu et al., 2022b). This leads to the lake's eutrophication by the low intake of fresh oxygenated water, and thus, to habitat changes or even their loss (Trifanov et al., 2022).

This paper aims to investigate the distribution of the water and suspended sediment fluxes between the former meanders and the artificial man-made canals along the St. George distributary and thus, the hydrological connectivity between the branch and the former meanders and interdistributary depressions. Understanding theses complex human pressures are of high importance for reaching/ maintaining the ecological status of the Danube. Herein, we made investigations along the Saint George branch on many sub-systems river-channel-lake site type, formed by cutoff meanders, connective channels, and lakes to observe how much the water and sediment inputs to the delta depressions is affected by the structural changes of the meander physiography.

Figure 1. The St. George branch with the position of the investigated cross-sections. The lines in red represent the artificial canals of the rectified meanders (Global Mapper v17)

MATERIALS AND METHODS

The hydrological data were acquired in September 2020, with a powered boat-mounted acoustic Doppler current profiler (ADCP, RiverRay 600 kHz, manufactured by Teledyne Marine). Reported water depths are expressed in local values. During the field campaign, 55 transverse ADCP profiles were completed (Figure 1), distributed in key locations such as bifurcations, junctions and apex, in order to observe the water fluxes distribution along the rectified systems. In addition to the bottom-track reference used for ADCP velocity and path measurements, the data were continuously georeferenced by a vessel-mounted DGPS. The bathymetry, water velocity, and discharge were handled by means of WinRiver II Teledyne RDI software.

Suspended sediment concentrations were measured in 55 locations in laboratory using the filtration methods. In all the selected cross-sections, water samples were taken using a 5 L horizontal Niskin-types bottle. The water samples were filtered with a Millipore filtration unit, using 4.7 cm acetate cellulose filter membranes of 0.45 µ porosity, according to STAS 6953-81.

RESULTS AND DISCUSSIONS

The upstream rectilinear sector (between P01 and P06) had relatively constant flow rates, between 1382 and 1330 $m^3.s^{-1}$, mainly due to the presence of the lateral canal Litcov, on the left bank, linking the branch with the Gorgova, Isac, and Isacel lakes. Generally, the velocities are homogenously distributed along the cross-sections (0.48 and 0.54 $m \cdot s^{-1}$) (Figure 2).

Along the first large meander (Mahmudia meander, M1) the water flow is unequally

distributed between the former meander (receiving a very small part of the upstream flow, 14 $m^3 \cdot s^{-1}$, representing 1% of the upstream flow of 1330 $m^3 \cdot s^{-1}$). At the junction (P13) very low velocities are found (between 0.01 and 0.04 $m \cdot s^{-1}$ on the natural channel of the former meander and between 0.52 and 0.58 $m \cdot s^{-1}$ along the artificial canal) (Figure 3).

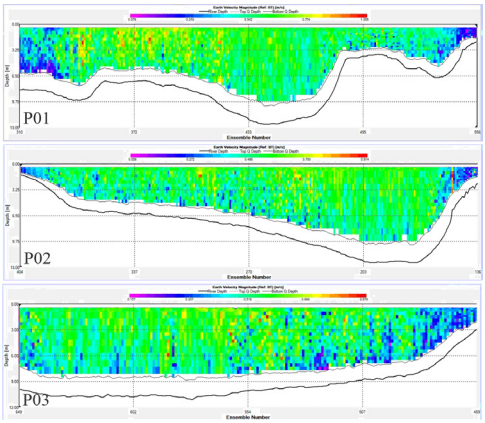

Figure 2. The velocity distribution on cross sections situated along the upstream rectilinear sector of the St. George branch

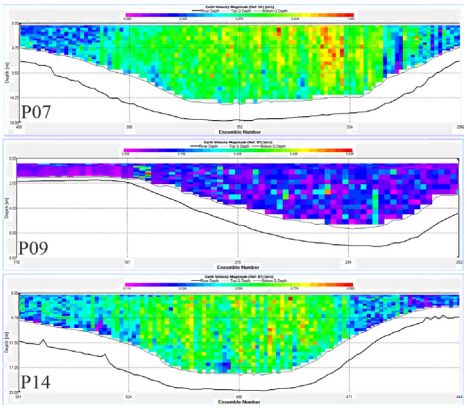

Figure 3. The velocity distribution on cross sections situated along the Mahmudia meander (M1), on the natural channel (P08 and P10) and on the artificial canal (P07 and P14)

On the Dunavăț de Sus meander (M2), the water flow circulates mainly on the natural channel of the cutoff (1025 $m^3 \cdot s^{-1}$ i.e. 76% on the P19 profile), with mean velocities between the values of 0.31 and 0.46 $m \cdot s^{-1}$ on the natural channel and between 0.50 and 0.62 $m.s^{-1}$ on the artificial canal; the velocities are uniformly distributed on the cross section (Figure 4) except for the profile located in the apex (P20) where a more pronounced dynamic is observed in the area of the convex bank.

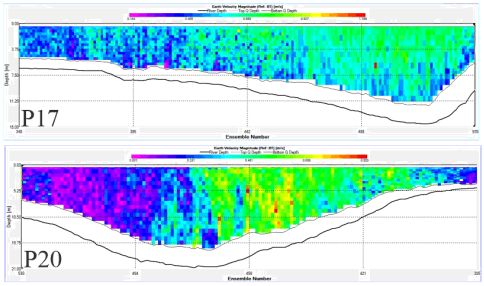

Figure 4. The velocity distribution on the cross sections situated along the Dunavăț de Sus meander (M2)

Along the Dunavăt de Jos meander (M3), the water flow has a different/opposite distribution comparing with the previous meander, with a preponderance on the artificial canal (99%, 1294 $m^3 \cdot s^{-1}$); the natural former meander transported approximately 0.8% (11.5 $m^3 \cdot s^{-1}$) from the total upstream flow (Figure 5). The average speeds were situated between the values of 0.08-0.19 $m \cdot s^{-1}$ on the natural channel and between 0.64 and 0.66 $m \cdot s^{-1}$ on the artificial canal.

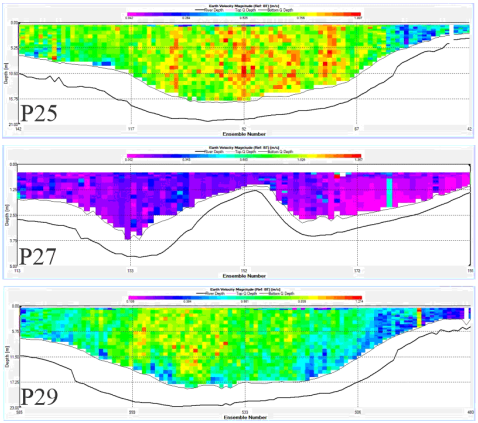

Figure 5. The velocity distribution on the cross sections situated along the Dunavăț de Jos meander (M3)

Going downstream, on the Dranov de Sus meander (M5), the main water flow passes mainly on the artificial canal (1069 $m^3 \cdot s^{-1}$, i.e. 86% on the P33 profile) to the detriment of the

natural channel with approximately 14% (204 $m^3.s^{-1}$ on the P34 profile) of total upstream flow. The average speeds ranged between the values of 0.29 - 0.35 $m \cdot s^{-1}$ on the natural channel and between 0.65 and 0.66 $m \cdot s^{-1}$ on the artificial canal (Figure 6). On the profiles situated on the artificial canal, high current speeds can be observed in the central part of the cross-sections.

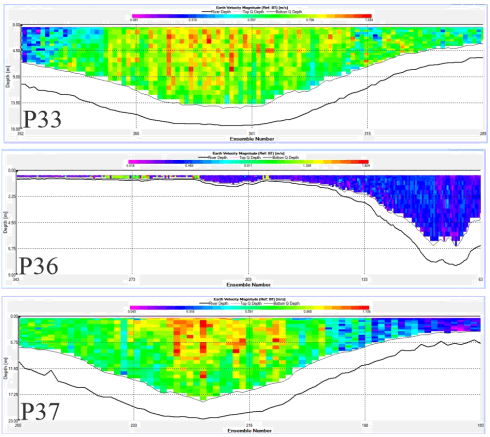

Figure 6. The velocity distribution on the cross sections situated along the Dranov de Sus meander (M5)

Along the Dranov de Jos meander (M6), the main water flow is taken by the the artificial canal (95%, 1237 $m^3.s^{-1}$) while the natural former meander transported approximately 5% (62 $m^3.s^{-1}$) of total upstream flow (Figure 7). The average speeds were very low along the natural channel of the former meander (between the values of 0.06 - 0.26 $m \cdot s^{-1}$) and higher along the artificial canal (between 0.57 and 0.61 $m \cdot s^{-1}$).

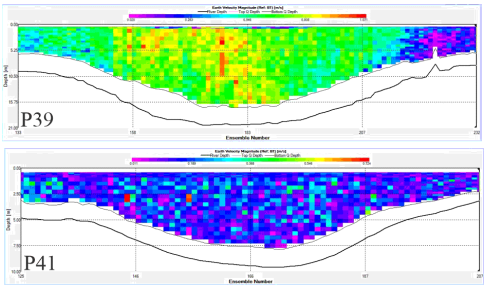

Figure 7. The velocity distribution on the cross sections situated along the Dranov de Jos meander (M6)

On the Ivancea meander (M7), situated near the distributary mouth, the distribution of water between the two channels is approximately equal (with 46% from the total upstream discharge passing through the natural channel) (Figure 8). The average speeds ranged between the values of 0.23-0.36 $m \cdot s^{-1}$ on the natural channel and between 0.49 and 0.60 $m \cdot s^{-1}$ on the artificial canal. High current velocities can be observed in the central areas of the investigates profiles.

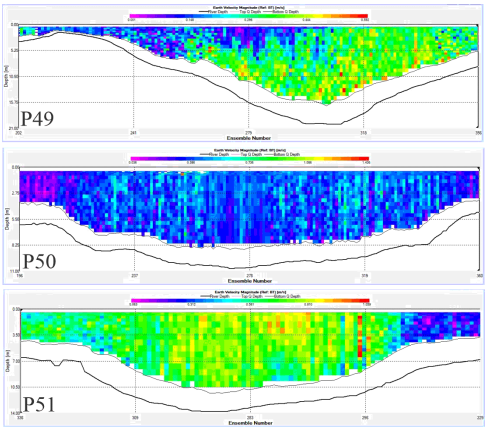

Figure 8. The velocity distribution on the cross sections situated along the Ivancea meander (M7)

Downstream, along the rectilinear sector of the branch, the discharge remained constant between 1215 and 1229 $m^3 \cdot s^{-1}$, without significant water flow losses to the Gârla Turcească canal, located on the right bank. The speeds are homogeneously distributed on the cross-sections, with the average between the values of 0.42 and 0.48 $m \cdot s^{-1}$) (Figure 9).

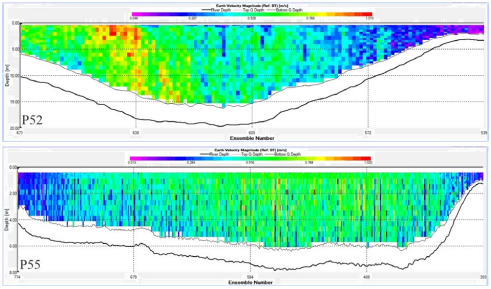

Figure 9. The velocity distribution on the cross sections situated along the downstream rectilinear sector of the St. George

Table 1 presents the evolution of the percentages of liquid flows taken over by the artificial canals

after the rectification works (performed between 1984 and 1994).
The changing of water fluxes distribution between the natural channels of the former meanders and the artificial canals between 1993 and 2020 has been accelerated on M1, M3, and M6, and currently some of these canals take more than 95% of the upstream water flow.

Table 1. Long-term evolution of the percentages of liquid flows taken over by the artificial canals after the rectification works

Year	M1	M2	M3	M5	M6	M7
1993	39.3	8.3	13	21.7	14.7	14.5
1994	54	13	24	27	28	27
2006	82	15	56	-	-	-
2016	96	22	97	-	-	-
2020	99	24	99	86	95	54

The role of cut-off canals depends mainly on how much the slope of the water free surface has been increased due to the cut-off canal and, in even greater extent, on the angle between the natural course and the cut-off canal at its beginning (Tiron Duţu et al., 2022).
Previous research studies mentioned the importance of the channel bed slope ratio, the sinuosity, the bottom sediments grain size, the water surface elevation at the bifurcation areas, the diversion angle, on the flows taken over by the artificial canals after rectification works (Law & Reynolds, 1966; Hager, 1984; Duţu et al., 2022a; Duţu et al, 2022b). Along the cutoffs of the St. George branch three former meanders (Mahmudia, Dunavăţ de Jos, and Dranov de Jos meanders) are dramatically affected by the changes of the physiography and express an obvious inequality in the repartition of the liquid fluxes between the natural and artificial channels that obviously explain the infilling processes. It is a certitude that the meandering system is very sensitive to the meanders cut-off programme, by acceleration and fast response in decreasing of its water discharges and in the changes of hydro-morphological and sedimentological processes.
To better understand the impact of the human pressure along this complex meandering system, the suspended sediment discharge was calculated using a common formula based on correlating the sedimentary concentration in suspension with water velocity and section area (Carvalho et al., 2000):

$$Qs = SSC \cdot v \cdot A$$

where:
- Qs is the suspended sediment discharge ($kg \cdot s^{1}$),
- SSC is the mean concentration of suspended sediment for the considered section ($mg \cdot l^{-1}$),
- A is the area of the section (m^2),
- v is the average water velocity per cross-section ($m \cdot s^{-1}$).

The concentrations of suspended sediments (SSC) measured on the investigated sections range between 7.0 and 36.0 $mg \cdot l^{-1}$ (Figure 10).

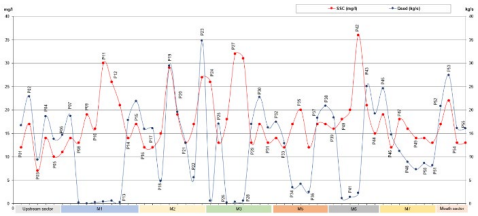

Figure 10. SSC ($mg \cdot l^{-1}$) mean values within cross-sections of the St George branch meanders (red line) and the SS fluxes (kg·s-1) (blue line)

At the bifurcation of the St. George branch, at Ceatal St. George (on profile P01) the suspended sediment discharge of the St. George distributary was of approximately 16.7 $kg \cdot s^{-1}$. Downstream, to the mouth (on profile P55) the suspended sedimentary discharge was estimated at 16.1 $kg \cdot s^{-1}$. At the scale of the entire branch the difference is not significant, but, along the former meanders, the accumulation of sediments and erosion of the riverbed occur locally as follows:
On the Mahmudia meander, from the sedimentary discharge of 14.7 $kg \cdot s^{-1}$ at the upstream bifurcation (cross-section P06), a very small part, 0.2 $kg \cdot s^{-1}$ passes through the natural course of the meander. On the cut-off channel (between P06 and P15) the sedimentary flow in suspension is significantly enriched (from 14.7 $kg \cdot s^{-1}$ to 21.9 $kg \cdot s^{-1}$) showing erosion processes along the artificial canal. Within the meander natural course, the suspended sediment discharge is low until the confluence with the cut-off canal (0.3 $kg \cdot s^{-1}$ on P13). At the exit of the meander a part of the discharge measured on P15 is settled down immediately downstream,

the sedimentary discharge in P16 was 15.9 $kg \cdot s^{1}$.

On Dunavăţ de Sus meander, the most part of the suspended sedimentary discharge is taken over by the meander natural course. Additionally, at the bifurcation area, a supplementary volume of suspended sediments (18 $kg \cdot s^{-1}$) are locally eroded and deposed just downstream on P20. In the second half of the former meander, the sedimentation is dominant, expressed by a lower sediment discharge, of 13.9 $kg \cdot s^{-1}$ on P21. At the exit from the cut-off canal (P23) the discharge is higher than the sum of the sedimentary fluxes P22 + P21 indicating erosion at the junction area.

Downstream, on Dunavăţ de Jos meander the situation is reversed, but similar as for Mahmudia meander. The sedimentary discharge captured by the cut-off canal is around 99% of the total discharge of the distributary. Along the former meander the sedimentary discharge is maintain with a very low value (between 0.21 $kg \cdot s^{-1}$ and 0.6 $kg \cdot s^{-1}$). Along the artificial canal the sedimentary discharge in maintain constantly around the value of 17 $kg \cdot s^{-1}$.

Downstream, the two meanders of Dranov de Sus and de Jos have the same behavior, the most part of the sedimentary discharge (95-99 %) is taken by the artificial canals. The sedimentary discharge is very low along the former meanders (between 1.1 and 4.8 $kg \cdot s^{-1}$), while along the artificial canals the values are situated between 18.3 and 20.0 $kg \cdot s^{-1}$).

As for the Ivancea meander the sedimentary discharge is distributed almost equally between the two canals (11.3 $kg \cdot s^{-1}$ on the artificial canal and 8.6 $kg \cdot s^{-1}$ on the natural channel).

Downstream, going to the branch mouth area, (between P52 and P55), the sedimentary discharge is reduced from 20.1 $kg \cdot s^{-1}$ to 16.1 $kg \cdot s^{-1}$.

The distribution of SS concentrations and fluxes varies and depending on the local morphology and water dynamics. It is a clear disparity between the sections situated on the former meanders and those situates near the bifurcations /confluences characterised by steep slopes and most intense hydrodynamic activity.

The concept of hydrological connectivity was widely employed in different environments and defines the water-mediated transfer of matter, energy and organism within the hydrological cycle (Pringle, 2001; 2003; Zhang et al., 2021). Human activities have generally altered hydrological connectivity (Pringle, 2001) by small to large interventions that can disturb the entire ecosystems. Loss of the connectivity will diminish the fresh transfer between upstream and downstream. The longitudinal connectivity is important for the nutrients transport and the migration of aquatic organism (Zhang et al., 2021).

The reduction/interruption of the fresh water transfer influence the biogeochemical fluxes. The consequences on the ecological equilibrium of the delta territory are various with important influences on a variety of aquatic ecosystem processes (Covino, 2017) including: solute transport (Ren & Packman, 2005), nutrient (Mulholland et al., 1997), carbon (Wagner & Beisser, 2005), streamflow dynamics (McGlynn & Seibert, 2003), aquatic biota and biological habitat (Stanford & Ward, 1988), and water resource management (Oxtobee & Novakowski, 2002).

The hydrotechnical works carried out along the St. George branch to improve navigation produced negative effects on the exchange of water and sediments with the lakes in the delta through the connecting channels (Figure 11). Most of the natural channels of the above-mentioned rectified meanders are currently heavily clogged and the sediments accumulated in the bed create sediment blockages.

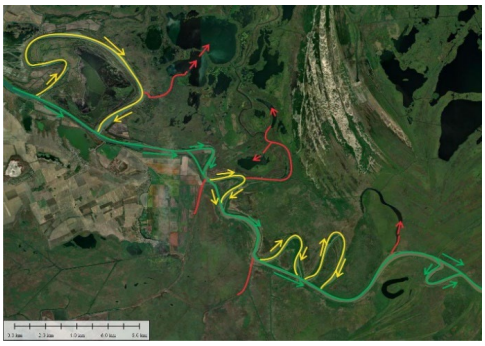

Figure 11. The rectified meanders of the St. George branch and the areas affected by the interruption of the hydrological connectivity (with green is the main stream, with yellow are the natural channels of the former meanders, with red are the areas disconnected when the hydrological connectivity is lost

Therefore, at low water levels, these areas are isolated from the main distributary producing interruptions of the liquid fluxes transfer with consequences on the hydrological connectivity.
Over time, this process tends to separate the former meander channel from the main branch and isolate the interdistributary areas. As in a chain processes/effect, the partial or complete disconnection of the lateral natural channels from the former meander (red line on Figure 11) will produce the physically separation of the interdistributary depressions (deltaic lakes).

CONCLUSIONS

River-floodplain hydrologic connectivity is important to be maintained to facilitate the exchange of water, sediment and nutrients between streams and floodplains.
The results shows that the water circulation along the study area is very complex. The hydrological changes are related to the human interventions, mainly by shortening the length of natural river courses, producing an increase of the water-free surface slope and therefore the water flow velocity along the artificial canals. The most dramatic situation is on Mahmudia meander (M1), Dunavăţ de Jos meander (M3) and Dranov de Jos meander (M6), where the cut-off canals take over 95-99 % of the upstream water and sediment flows, while the natural courses of the rectified meanders suffer infilling process, with the almost complete stopping of the water circulation on them therefore compromising the hydrological connectivity with the interdistributary depressions.
Efforts to rehabilitate the ecosystem must be assumed to maintain the restoration, and the redevelopment of the affected areas, based on the principle of sustainable development and ensuring 4D connectivity. One suggestion for future research is to investigate and monitor with specific equipment the water transfer and how storage of water occurs in different catchments to produce (dis)connected flow.

ACKNOWLEDGEMENTS

This research was financially supported by the Romanian Ministry of Research, Innovation and Digitization in the framework of the projects: PN19200401 (Contract no. 13N/08.02.2019), PN23300304 (Contract no. 4N/30.12.2022), and Project AMBIACVA (Contract no. 23PFE/30.12.2021).
The authors thank Gabriela Vlad and Naliana Lupaşcu from GeoEcoMar for collecting and analysing the suspended sediments samples.

REFERENCES

Bondar, C., & Panin, N. (2000). The Danube Delta Hydrologic Database and Modeling. *Geo-Eco-Marina, 5-6*, 5–53.

Bracken, L/J, Wainwright, J., Ali, G.A., Tetzlaff, D., Smith, M.W., Reaney, S.M. & Roy, A.G. (2013). Concepts of hydrological connectivity: research approaches, pathways and future agendas. *Earth-Scrience Reviews, 119*, 17–34.

Bunn, S. E. & Arthington, A. H. (2002). Basic principles and ecological consequences of altered flow regimes for aquatic biodiversity. *Environmental Management 30*, 492–507.

Carvalho, N.O., Filizola, N., dos Santos, P.M.C., & Lima, J.W. (2000). Guia de Práticas Sedimentométricas. *Ed.ANEEL/PNUD/ OMM, Brasília*, pp. 154.

Covino, T. (2017). Hydrologic connectivity as a framework for understanding biogeochemical flux through watersheds and along fluvial networks. *Geomorphology*, *277*, 133–144.

Duţu, F., Duţu, L., Catianis, I., & Ispas, B-A. (2022a). Sediment dynamics and hydrodynamical processes in the Danube Delta (Romania): A response to hydrotechnical works. *Zeitschrift fur Geomorphologie, 64*(4), 365–378.

Duţu, L., Duţu, F. & Iordache, G. (2022b). Intensive infilling processes of a cutoff meander in the Danube Delta. *Transylv. Rev. Syst. Ecol. Res., 24*(3), 1–10.

Habersack, H., Hein, T., Stanică, A., Liska, I., Mair, R., Jager, E., Hauer, C., & Bradley, C. (2016). Challenges of river basin management: Current status of, and prospects for, the River Danube from a river engineering perspective. *Science of the Total Environment, 543*, 828–845.

Hager, W.H. (1984). An approximate treatment of flow in branches and bends. *Proceedings of the Institute of Mechanical Engineers, 198*, 63–69.

ICPDR (2008). Joint Danube Survey 2, Final Scientific Report, pp. 242.

ICPDR (2015). Joint Danube Survey 3, A Comprehensive Analysis of Danube Water Quality, pp. 369.

Junk, W. J., P. B. Bayley & R. E. Sparks. (1989). The flood pulse concept in river-floodplain systems. *Canadian Special Publication of Fisheries and Aquatic Sciences 106*, 110–127.

Karim, F., D. Dutta, S. Marvanek, C. Petheram, C. Ticehurst, J. Lerat, S. Kim & A. Yang. (2015). Assessing the impacts of climate change and dams on floodplain inundation and wetland connectivity in the wet-dry tropics of northern Australia. *Journal of Hydrology Elsevier 522*, 80–94.

Law, S.W. & Reynolds, A.J. (1966). Dividing flow in an open channel. *Journal of the Hydraulics Division*, *American Society of Civil Engineers, 92*, 207–231.

McGlynn, B.L. & Seibert, J. (2003). Distributed assessment of contributing area and riparian buffering along stream networks. *Water Resour. Res. 39*(4).

Mulholland, P.J., Marzolf, E.R., Webster, J.R., Hart, D.R. & Hendricks, S.P. (1997). Evidence that hyporheic zones increase heterotrophic metabolism and phosphorus uptake in forest streams. *Limnol. Oceanogr. 42*(3), 443–451.

Nistor, C., Savulescu, I., Mihai, B-A., Zaharia., L., Virghileanu, M. & Cacablaisa, S. (2021). The impact of the large dams on fluvial sedimentation; the Iron gates reservoir on the Danube River. *Acta geographica Slovenia, 61(*1), 41–55.

Oxtobee, J.P.A. & Novakowski, K. (2002). A field investigation of groundwater/surface water interaction in a fractured bedrock environment. *J. Hydrol. 269* (3-4), 169–193.

Pacioglu, O., Duţu, F., Pavel, A.B., & Tiron Duţu, L. (2022a). The influence of hydrology and sediment grain-size on the spatial distribution of macroinvertebrate communities in two submerged dunes from the Danube Delta (Romania), *Limnetica, 41*(1), 85–100.

Pacioglu, O., Duţu, L., Duţu, F., & Pavel, A.B. (2022b). Habitat preferences and trophic interactions of the benthic invertebrate communities inhabiting depositional and erosional banks of a meander from Danube Delta (Romania). *Global Ecology and Conservation, 38*, e02213.

Pojar I., Tiron Duţu L., Pop C.I., & Duţu F. (2021). Hydrodynamic observations on microplastic abundances and morphologies in the Danube delta, Romania. *Agrolife Scientific Journal, 10*(2), 142–149.

Popa, A., (1997). Environment changes in the Danube Delta caused by the hydrotechnical works on the St. George branch. *Geo-Eco-Marina, 2*, 135–147.

Pringle, CM. (2001). Hydrologic connectivity and the management of biological reserves: a global perspective. *Ecol Appl., 11*(4), 981–998.

Pringle, C. (2003). What is hydrologic connectivity and why is it ecologically important?. *Hydrological processes, 17*. 2685-2689.

Ren, J.H. & Packman, A.I. (2005). Coupled stream-subsurface exchange of colloidal hematite and dissolved zinc, copper, and phosphate. *Environ. Sci. Technol. 39*(17), 6387–6394.

Stanford, J.A. & Ward, J.V. (1988). The hyporheic habitat of river ecosystems. *Nature 335*(6185), 64–66.

Tiron Duţu, L., Panin, N., Duţu, F., Popa, A., Iordache, G., Pojar, I., & Catianis, I. (2022). The Danube Delta Environment Changes Generated by Human Activities. *Chapter 1 in The Danube River Delta, Springer - Earth and Environmental Sciences Library,* 3-32. ISBN 978-3-031-03982-9. doi: https://doi-org.am.e-nformation.ro/10.1007/978-3-031-03983-6_1.

Trifanov, C., Dumitriu, D., Mihu-Pintilie, A., Stoleriu, C. & Mierlă, M. (2022). Some morphodynamic aspects concerning the meandred river section of the Sf. Gheorghe's arm from the Danube Delta Biosphere Reserve. *Scientific Annals of the Danube Delta Institute, 27*, 129–138.

Vasiliu, D., Tiron Duţu, L., Bucşe, A., Lupaşcu, N., & Duţu, F. (2021). Geochemical characteristics of riverbed sediments in the Danube delta, Romania. *Scientific Papers. Series E. Land Reclamation, Earth Observation & Surveying, Environmental Engineering, X*, 258–264.

Vădineanu, A. (2001). Lower Danube Wetlands System (LDWS). *Observatorio Medioambiental, 4*, 373-402.

Wagner, F.H. & Beisser, C. (2005). Does carbon enrichment affect hyporheic invertebrates in a gravel stream? *Hydrobiologia, 544*, 189–200.

Zaharia, L., Grecu, F., Toroimac, I.G. & Neculau, G., (2011). Sediment Transport and River Channel Dynamics in Romania - Variability and Control Factors. In: Manning, A. J., editor. *Sediment Transport in Aquatic Environments*. London: IntechOpen. doi: 10.5772/21416.

Zhang, Y., Huang, C., Zhang, W., Chen, J., & Wang, L. (2021). The concept, approach, and future research of hydrological connectivity and its assessment at multiscales. *Environmental Science and Pollution Research, 28*, 52724–52743.

Scientific Papers. Series E. Land Reclamation, Earth Observation & Surveying, Environmental Engineering. Vol. XII, 2023
Print ISSN 2285-6064, CD-ROM ISSN 2285-6072, Online ISSN 2393-5138, ISSN-L 2285-6064

EFFICIENCY OF A RADIAL PRIMARY CLARIFIER FOR MUNICIPAL WASTEWATER

Bianca-Ștefania ZĂBAVĂ, Gheorghe VOICU, Gabriel-Alexandru CONSTANTIN, Paula TUDOR, Sorin CĂNĂNĂU

University POLITEHNICA of Bucharest, 313 Splaiul Independentei, District 6, Bucharest, Romania

Corresponding author email: ghvoicu_2005@yahoo.com

Abstract

The prime method to combat water pollution, and a means to improve the quality of wastewater, is the wastewater treatment process, which is now widely used. The common method of mechanical (primary) treatment is (conventional) sedimentation at rest. Decanters (also called sedimentation tanks or clarifiers) are an integral part of every wastewater treatment plant. The present work aims to determine the performance of a radial primary clarifier in an urban wastewater treatment plant in Romania for the year 2020. The determinations were carried out for one winter month (January) and one summer month (July), and for the other calendar months the average inlet and outlet concentrations of the clarifier were determined. For each day of January and July, the concentrations of impurities (mg/L) in the wastewater at the inlet of the decanter (ci) and in the clarified water at the outlet of the decanter were recorded, based on which the separation efficiency of decanter could be determined. To improve the primary settling efficiency, the use of coagulating agents (iron and aluminium solutions) is recommended.

Key words*: efficiency, radial clarifier, sedimentation wastewater.*

INTRODUCTION

The biggest problem facing humankind right now is extreme environmental pollution. The natural environment is progressively getting worse and that ecological systems cannot respond to the pressure from anthropogenic factors, making the ecosphere's ability to regulate itself, impossible.

As infrastructure and regulatory development has been left behind by population expansion and urbanisation, urban wastewater management has become difficult in many countries (Saravanane et al., 2014).

Large cities started to realize they needed to decrease the number of pollutants found in the water that needed to be released into the environment in the 19th century, which is when wastewater treatment industries first emerged. Even though fresh water sources were abundant, and the water had an inherent ability to naturally purify itself over time, communities were so closely knit by 1850 that deadly disease outbreaks were blamed on bacteria in the contaminated water (Phumelele & Kallon, 2021). Since then, the most advanced biological, physical, chemical, and mechanical techniques have been used to establish and enhance wastewater collection and treatment practices. The public's health and the water's cleanliness are thus better safeguarded than ever.

Wherever people live, there is a continuous need for fresh drinking water and a constant production of waste. Thus, drinking water supply and wastewater management have been essential to the success of human society (Holger et al., 2006).

Advanced technologies and some conventional industrial facilities are used to satisfy food and basic human demands (physical, social, and psychological). Whether food factories or other industrial establishments, these entities emit waste into the environment, continuously discharging colossal quantities of wastewater, pumped straight into rivers and oceans. The consequences are dramatic - besides damaging the marine environment and fisheries, little is being done to conserve water at a moment when so many predict that global water scarcity is about to take its toll (Anjum et al., 2016). One of the biggest barriers to a sustainable future for the entire globe is the rising demand for clean water.

The best methods for environmental preservation are being sought after at the European level. Wastewater treatment, currently the most common technique, is the main way to stop water pollution.

A major strategy for protecting water sources is wastewater management, understood as the collection, treatment and reuse of wastewater. Perhaps the most important piece of infrastructure, the wastewater collection network, can face several problems due to unwanted behaviour. Since wastewater treatment is a procedure that depends on a multitude of physical and chemical aspects, it is imperative to predict the variables in wastewater treatment plants. Treated urban wastewater has some restrictions but is an appropriate resource for distribution to various industries and uses like agriculture (Roozbahani, 2021).

Figure 1 illustrates the various processes or operating components that make up a WWTP, including: pre-treatment, primary and secondary treatment, sludge and tertiary treatment.

Particulate pollutants like solids, grit, and greases are primarily targeted for elimination during pre-treatment and primary treatment. Through biological and chemical mechanisms, secondary treatment removes phosphorus, nitrogen, and organic matter from sewage (Rashid, 2023). In some WWTPs, tertiary treatment is used to get rid of any last-minute tiny particles and pathogens.

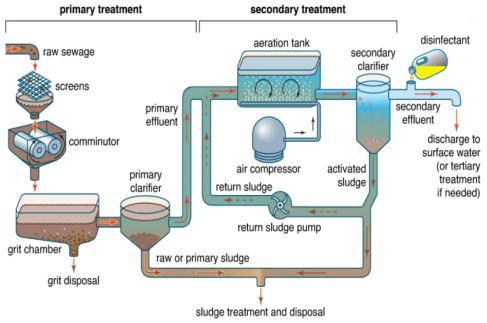

Figure 1. Flow diagram of the wastewater treatment process
(https://www.britannica.com/technology/wastewater-treatment/Primary-treatment#/media/1/666611/19281)

Because most industries rely on water and having restricted access to clean water resources can affect both production capacity and profits, water management is a crucial component of any economy. The circular economy (CE), which implies sustainable management of raw materials (including water) and waste, emphasizes the importance of water problems (also wastewater) (Smol, 2002; Sandu et al., 2021).

Every strategy must now be created with consideration for the environment's global influence; if this factor is overlooked, environmental loads will change or have an effect, and no reduction will be made. Due to the integration of energy production and resource recovery during the production of clean water, urban wastewater treatment facilities can be a significant component of circular sustainability. Facilities for wastewater treatment will soon need to use "environmentally sustainable" technical solutions. Global nutrient requirements as well as water and energy recovery from wastewater are currently the primary forces driving the development of the wastewater industry (Neczaj & Grosser, 2018).

Particle separation plays a significant role in wastewater purification. This is because most pollutants in wastewater are particulate or colloidal in nature or change to these forms during the cleaning process. This has caused the wastewater treatment approach to first remove particulate and colloidal matter, and then deal with soluble compounds that need to be converted to particulate and colloidal matter. Traditionally, settling is used to perform particle separation in the first stage (Ødegaard, 1998).

The first experimental studies concentrated on the overall separation performance and efficiency of decanters. Therefore, the effectiveness of removing suspended solids relies on both the flow regime in the decanter and the physical characteristics of the solids (type and nature, particle size, density, and sedimentation velocity).

The separation of the liquid-solid mixture is dependent on many parameters linked to the solid component, the liquid component, and the design parameters of the decanter.

Andral et al. (1999) and Roger et al. (1998), show in their studies that particles with a diameter smaller than 50 μm made up 70-80% of the total amount of solid suspensions, and in 2002, Furumai and colleagues showed that particles with a diameter smaller than 20 μm

made up more than 50% of the total amount of solid suspensions for experiments with total solid suspension concentrations lower than 100 mg/L. Wakeman (2011) noted that particles with a diameter of order a few microns decant very slowly and advised that they be coagulated for a while to increase effective dimension and, consequently, a while increase sedimentation rate (Wakeman, 2011). McNown et al. (1952) carried out one of the first studies to ascertain the impact of solid particle concentration on sedimentation velocity. Despite being qualitatively incompatible, their findings demonstrate that a decrease in particle settling velocity is caused by a rise in particle concentration (McNown & Lin, 1952).

Following research, Kinnear discovered that excess suspended solids in effluents rise as air temperature falls in 2004 (Kinnear, 2004).

According to Goula et al. (2008), a temperature differential of just 1°C is enough to reduce settling efficiency.

Throughout the settling process, a particle's sedimentation velocity increases until its own weight, which acts as a settling force, matches the opposing pressures. Due to the balance of the forces acting on the particle in this instance, $(dvp/dt) = 0$. Sedimentation velocity, an essential hydrodynamic quantity, plays an important role in both the technical design of the equipment used for the separation of heterogeneous systems by sedimentation and the characterization of particle motion (Gavrilă, 2001).

Sewage contains polluting substance in a variety of forms, which is complicated. The mixture also contains a heterogeneous dispersion of various substances (organic and inorganic), in colloidal, pseudo colloidal, and basic suspension forms, in addition to the dissolved impurities.

Most of the insoluble inorganic matter and the gross solid material are removed during the initial screening and grit removal processes, but the suspended matter, which is primarily organic and heavily polluting, continues to flow through the liquid. Processes for removing pollutants from wastewater frequently employ physical settling methods.

The first stage of wastewater purification traditionally uses primary settling to separate particles. According to Stokes law, particles down to about 30-50 μm will settle out at the usual velocity rates (around 2 m/h) and typical wastewater particle densities.

Primary settling removes about 50% of the suspended solids and 30% of the organic debris. A significant increase would be made if particles smaller than one micron could be removed (Ødegaard, 1998).

Primary settling tanks are an essential component of the biological wastewater and sludge treatment process (Patziger, 2016) and have been used widely to remove suspended solids (SS) by gravitational settling that are not removed by preliminary treatment (Christoulas, et al., 1998). The need for primary settling tanks, which are now required for both wastewater treatment and the production of renewable energy in the wastewater treatment plant in the form of biogas and electrical energy, is one of the factors affecting the overall construction costs of wastewater treatment facilities (WWTP).

The main objective of sedimentation is to separate sewage into the two components of settled sewage and sludge so that each can be treated separately, usually more successfully and affordably. Most of the time, sedimentation reduces the sewage's total polluting load by up to 50% (The Institute of Water Pollution Control, 1980).

In many unit processes in wastewater treatment plants, settling is a crucial process (WWTPs). Primary settling tanks (PSTs), which are treatment units before the biological reactor, and secondary settling tanks (SSTs), which are a clarification stage before discharge into a receiving water, are the two most well-known of these unit processes.

Additionally, settling is crucial in the development of novel technologies like granular sludge reactors (Torfs, 2016). The current study seeks to estimate the 2020 efficiency of a radial primary clarifier in a Romanian urban wastewater treatment facility.

The typical inlet and outlet concentrations of the clarifier were calculated for the remaining calendar months, and the measurements were made for one winter month (January) and one summer month (July).

MATERIALS AND METHODS

To assess the primary clarifier's efficiency in the winter (January) and the summer (July) of 2020, measurements were taken at one of the radial main clarifiers in the wastewater treatment facility.

The determinations were carried out for one winter month (January) and one summer month (July), and for the other calendar months the average inlet and outlet concentrations of the clarifier were determined. For each day of January and July, the concentrations of impurities (mg/L) in the wastewater at the inlet of the decanter (c_i) and in the clarified water at the outlet of the decanter were recorded, based on which the separation efficiency of decanter could be determined.

The radial clarifier has a structure comparable to that in Figure 2 and measures 55 meters in diameter, 8000 m^3, 7% invert slope, 0.8 meters in width, and 29 meters in length. Its peripheral velocity is 1.8 meters per minute.

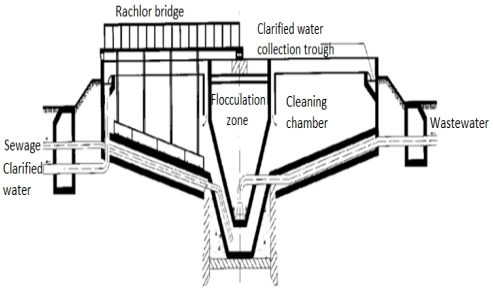

Figure 2. Radial clarifier

The separation efficiency of decanter E (%) was determined using the relation:

$$E = \frac{c_i - c_f}{c_i} \cdot 100$$

where:
- E is the separation efficiency (%);
- c_i - initial concentration (%);
- c_f - final concentration (%).

RESULTS AND DISCUSSIONS

Table 1 displays the values obtained from the measurements and includes the accompanying notations: T - wastewater temperature (ºC); c_i - concentration of the suspension at the inlet to the decanter (mg/L); c_f - suspension concentration decanter outlet (mg/L); E -separation efficiency (%).

For both January and July, M. Excel was used to process the data and show the efficiency variation over 31 days (Figure 3).

Table 1. Decanter inlet and outlet concentration values for January and July 2020

January				July			
T, ºC	c_i, mg/L	c_f, mg/L	E, %	T, ºC	c_i, mg/L	c_f, mg/L	E, %
≈ 10	159	79	50.31	≈ 23	179	85	52.51
	128	69	46.09		147	76	48.29
	227	87	61.67		161	83	48.44
	261	105	59.77		167	67	59.88
	209	101	51.67		182	87	52.19
	175	87	50.86		266	92	65.41
	145	85	41.38		167	98	41.31
	179	86	51.96		255	78	69.41
	228	108	52.63		187	56	70.05
	192	79	58.85		218	59	72.93
	201	86	57.21		153	77	49.67
	377	115	69.49		137	79	42.33
	289	93	67.82		208	95	54.32
	187	87	53.47		157	87	44.58
	195	91	53.33		145	83	42.75
	176	94	46.59		239	87	63.59
	209	87	58.37		185	105	43.24
	287	85	70.38		175	85	51.42
	199	76	61.80		173	93	46.24
	197	89	54.82		276	94	65.94
	346	98	71.67		138	82	40.57
	222	104	53.15		195	87	55.38
	227	107	52.86		195	73	62.56
	182	115	36.81		202	72	64.35
	261	102	60.91		157	79	49.68
	189	89	52.91		279	81	70.96
	168	75	55.35		167	86	48.50
	209	97	53.58		186	71	61.82
	189	106	43.91		185	69	62.70
	227	119	47.57		279	65	76.70
	194	108	44.32		199	77	61.30

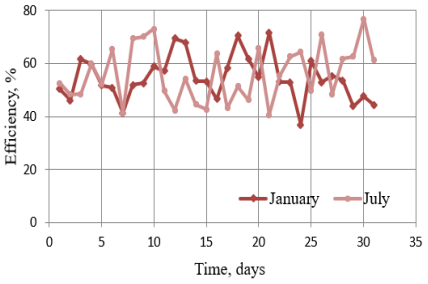

Figure 3. Efficiency variation for January and July, 2020

As can be seen, the higher the value of the solid particle concentration, the more efficient the settling process is (> 60%). The accumulation of particulate could be the cause of this. Uncontrolled discharges and abundant rains both contribute to higher settler inlet concentration levels. In January, efficiency was 54.56%, and in July, output was 56.10%.

The monthly decanter efficiency was determined based on the monthly average of the

inlet and outlet concentrations for 2020. Table 2 displays the values that were found.

Table 2. Monthly average values for inlet concentration, outlet concentration and decanter efficiency

Month	Monthly average concentration c_i, mg/L	Monthly average concentration c_f, mg/L	Monthly decanter efficiency E, %
January	209.74	95.28	54.57
February	198.65	115.50	41.86
March	217.55	117.50	45.99
April	250.14	129.40	48.27
May	240.22	118.95	50.48
June	215.74	108.52	49.70
July	199.94	81.49	59.24
August	194.28	97.35	49.89
Septem-ber	195.87	105.45	46.16
October	222.25	118.75	46.57
Novem-ber	205.25	109.78	46.51
Decem-ber	235.40	127.45	45.86

Figure 4 illustrates the decanter efficiency forecast for 2020, which is predicted to be 48.75%.

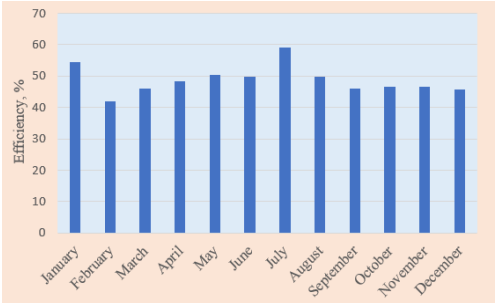

Figure 4. Efficiency of the decanting process for year 2020

Coagulating agents (solutions of iron and aluminium) are suggested to increase the effectiveness of the main settling process.
From the foregoing, decanter efficiency does not inherently correlate with atmospheric temperature, although mean efficiency in summer months is marginally greater than in lower temperature months.

CONCLUSIONS

One of the biggest barriers to a sustainable future for the entire globe is the rising demand for clean water. Wastewater treatment, currently the most common technique, is the main way to stop water pollution.
The main objective of sedimentation is to separate sewage into the two components of settled sewage and sludge so that each can be treated separately, usually more successfully and affordably. Most of the time, sedimentation reduces the sewage's total polluting load by up to 50%.
The higher the value of the solid particle concentration, the more efficient the settling process is (> 60%). In January, efficiency was 54.56%, and in July, output was 56.10%.
To improve the efficiency of the primary settling procedure, coagulating agents (solutions of iron and aluminium) are advised.

ACKNOWLEDGEMENTS

This work has been funded by the European Social Fund from the Sector al Operational Programme Human Capital 2014-2020, through the Financial Agreement with the title "Training of Ph.D. students and postdoctoral researchers in order to acquire applied research skills - SMART", Contract no. 13530/16.06.2022 - SMIS code: 153734.

REFERENCES

Andral, M.C., Roger, S., Montréjaud-Vignoles, M., &Herremans L. (1999). Particle size distribution and hydrodynamic characteristics of solid matter carried by runoff from motorways, *Water Environ. Res.,71*(4), 398-407.

Anjum, M.N., Rasheed, H.U., &Ahmed, W. (2016). Impact of Waste Water Treatment on Quality of Influent & Effluent Water, *IJIR, 2*(11).

Christoulas, D.G., Yannakopoulos, P.H., & Andreadakis, A.D. (1998). An empirical model for primary sedimentation of sewage. *Environ. Int.*, *24*, 925–934.

Gavrilă, L. (2001). Unit operations in the foodindustry and biotechnology, Universitatea din Bacău.

Goula, A.M., Kostoglou, M., Karapantsios, T.D., & Zouboulis, A.I. (2008). A CFD methodology for the design of sedimentation tanks in potable water treatment, *Chem. Eng. J. 140*, 110–121.

Goula, A.M., Kostoglou, M., Karapantsios, T.D., &Zouboulis, A.I. (2008). The effect of influent temperature variations in a sedimentation tank for potable water treatment - a computational fluid dynamics study, *Water Res.*, *42*(13), 3405–3414.

Holger, D., Taylor, M.W., &Wagner, M. (2006). Wastewater treatment: a model system for microbial ecology, *Trends in Biotechnology*, *24*(11), 483-489.

Kinnear, D.J. (2004). Littleton Englewood *Wastewater Treatment Facility*, Personal communication.

McNown, J.S., & Lin P.N. (1952). Sediment concentration and fall velocity. Proc. 2nd. Midwest. *Conf. Fluid Mech.,* Ohio State Univ., 401-411.

Neczaj, E., &Grosser, A. (2018). Circular Economy in Wastewater Treatment Plant–Challenges and Barriers. *Proceedings*, *2*. 614. 10.3390/proceedings2110614.

Ødegaard, H. (1998). Optimised particle separation in the primary step of wastewater treatment, *Water Science and Technology*, *37*(10), 43-53.

Patziger, M., Günthert, F.W., Jardin, N., Kainz, H., & Londong, J. (2016). On the design and operation of primary settling tanks in state of the art wastewater treatment and water resources recovery. *Water Sci. Technol.*

Phumelele, M., & Kallon, D.V.V. (2021). Review of Clarifier Technologies *Proceedings of the International Conference on Industrial Engineering and Operations Management* Sao Paulo, Brazil, April 5-8.

Rashid, S.S., Harun, S.N., Hanafiah, M.M., Razman, K.K., Liu, Y.-Q., & Tholibon, D.A. (2023). Life Cycle Assessment and Its Application in Wastewater Treatment: A Brief Overview. *Processes*, *11*, 208.

Roger, S., Montréjaud-Vignoles, M., Andral, M.C., Herremans, L., & Fortuné, J.P. (1998). Mineral, physical and chemical analysis of the solid matter carried by motorway runoff water, *Water Res., 32* (4), 1119–1125.

Roozbahani, A. (2021). Chapter 6 - *Application of Bayesian Networks Modelling in Wastewater Management*, Editor(s): Rama Rao Karri, GobinathRavindran, Mohammad HadiDehghani, Soft Computing Techniques in Solid Waste and Wastewater Management, *Elsevier*, 111-130.

Sandu, M. A. & Vîrsta, A. (2021). The water footprint in context of circular economy. *AgroLife Scientific Journal, 10*(2), 170-177.

Saravanane, R., Ranade, V.V.,Bhandari, V.M., & Seshagiri Rao, A.S. (2014). Chapter 7 - Urban Wastewater Treatment for Recycling and Reuse in Industrial Applications: Indian Scenario, Editor(s): Vivek V. Ranade, Vinay M. Bhandari, *Industrial Wastewater Treatment, Recycling and Reuse*, Butterworth-Heinemann, 283–322,

Smol, M. (2022). Chapter 1 - *Circular economy approach in the water and wastewater sector*, Editor(s): Alexandros Stefanakis, Ioannis Nikolaou, Circular Economy and Sustainability, *Elsevier*, 1-19.

The Institute of Water Pollution Control Ledson House, 53 London Road. Manuals of British Practice in Water Pollution Control bQl< 9 Unit Processes Primary Sedimentation First edition 1973, Reprinted 1980.

Torfs, E. (2016). Experimental Methods in Wastewater Treatment. Edited by M.C.M. van Loosdrecht, P.H. Nielsen, C.M. Lopez-Vazquez and D. Brdjanovic. ISBN: 9781780404745 (Hardback), ISBN: 9781780404752 (eBook). Published by *IWA Publishing*, London, UK.

Wakeman, R.J. (2011). Sedimentation, Thermopedia A-to-Z Guide to Thermodynamics, Heat & Mass Transfer, and Fluids Engineering.

https://www.britannica.com/technology/wastewater-treatment/Primary-treatment#/media/1/666611/19281

Scientific Papers. Series E. Land Reclamation, Earth Observation & Surveying, Environmental Engineering. Vol. XII, 2023
Print ISSN 2285-6064, CD-ROM ISSN 2285-6072, Online ISSN 2393-5138, ISSN-L 2285-6064

THE EFFICIENCY OF HYDROTECHNICAL WORKS IN THE GURGHIU HYDROGRAPHIC BASIN

Iulia Diana ARION[1], Felix ARION[2], Irina Maria MORAR[1]

[1]University of Agricultural Sciences and Veterinary Medicine of Cluj-Napoca, Department of Forestry, 3-5 Manastur Street, Cluj-Napoca, Romania
[2]University of Agricultural Sciences and Veterinary Medicine of Cluj-Napoca, Department of Economic Sciences, 3-5 Manastur Street, Cluj-Napoca, Romania

Corresponding author email: felixarion@usamvcluj.ro

Abstract

The characterisation and knowledge of the Gurghiu drainage basin represents a realistic analysis of the current state of the drainage basin. This analysis led to the obtaining of information on morphometric parameters specific to the drainage basin and the Orşova, Fâncel and Sirod sub-drainage basins; the current state, together with the effects and efficiency of torrent correction works in these sub-drainage basins and the knowledge of the grain size of the alluviums accumulated behind the hydrotechnical works. To analyse the profitability of the hydrological management work in the sub-drainage basin Fâncel, a series of specific indicators were used: specific investment, duration of the recovery of the investment, updated net value, internal rate of return and profitability index. The total amount of alluvium retained in the valleys of the Gurghiu hydrographic basin is 24,960.3 m^3, with direct retention accounting for 6,774.55 m^3 and consolidation for 8,185.8 m^3. The analysis reveals that the costs associated with extracting torrential alluvium would have been roughly 1,859.55 thousand lei. Recommendations are to urgently restore essential repairs to damaged, broken, or detached parts of the work, to cover infiltrations and cracks and to complete masonry in places affected by degradations.

Key words*: forest management, rural development, sustainable development.*

INTRODUCTION

The study starts from the assumption, that, the management of water resources will soon involve planning and constructing new water supply systems as well as analysing the financial performance of the current ones. The instability and lack of the predictability of the water amount in time and space will cause more and more efforts to be focused on solving water scarcity and reducing water conflicts. In such an assumption, the hydro-economic models depict integrated systems that consider the infrastructure already in place and management choices based on economic values (Turner et al., 2000). The processes for allocating and managing water within these integrated tools are to be determined either by the known economic value of water or by its estimation based on economic value.

Within these integrated tools, the processes of water allocations and management are to be determined either by the known economic value of water or by its estimation based on economic value on specific time and place. A basic concept considers that water demand is not uniform, and therefore, it depends on the quantities of water used at a given time, so its total and marginal economic value can differ greatly (Harou et al., 2009).

The increase in disaster-related losses is slower than the increase in wealth, according to research cited in a 2012 World Bank Policy Research Working Paper by Hallegatte (Hallegate, 2012). A straightforward model demonstrates that this trend can outweigh the impact of risk reduction measures in many countries where rising incomes have also contributed to increased migration and investment in high-risk areas. This assessment may be understated because it ignores the production losses brought on by the destruction of assets, which are indirect losses brought on by natural disasters. In the case of major disasters, indirect losses may be comparable in size to direct losses.

In Romania, research on how the hydrological disturbances generate, as an inevitable effect,

the reduction of the area's natural potential has also been carried out. The information on water management in Wallachia dates to 1576, and the oldest writing reference about flood protection is known as the "Canalul Ipsilantis", dating from 1774 (Mititelu, 2010). Currently, other scholars (Hâncu & Nițescu, 2016) think that, overall, the water management must be considered a distinct branch of the economy and it must be approached accordingly, and it has not to be integrated within other branches, such as environmental economics or forestry economics.

It is undeniable that traditional engineering and hydrological models of water management issues are integrating more and more economic and social concepts and methods (Toscani et al., 2020). For better results and information for decisions and policies regarding water management, economic management concepts and performance indicators should be combined with an adequate engineering level of understanding of a hydrological system (Sun & Vose, 2016). Such models can serve as a basis for a common understanding of water issues as a foundation for management solutions and negotiated public policies when they are created and used with stakeholder involvement. Integrated hydro-economic models can offer creative solutions that decision-makers can take into account when they are put into practice using optimization software. Their applications to watershed management problems are constantly being reviewed. The economic and integrated modeling of the economy-engineering-hydrology triplet is then discussed in relation to the European Water Framework Directive (Heinz et al., 2007). Cost recovery and water pricing, the effectiveness of water management strategies in terms of cost, and public participation in decision-making are all pertinent factors.

In a situation where there is competition for scarce water resources, combined hydro-economic models of river basins are essential tools for assessing management and infrastructure strategies to increase the economic effectiveness of water use. The physical behaviour of the system must be accurately modeled in integrated hydro-economic models, including interactions between the various surface and groundwater resources as well as the spatial and temporal variability of resource availability. However, according to Pulido-Velazquez et al., these models must consider the value of water for various urban, agricultural, and industrial uses and users (Pulido-Velazquez et al., 2008). Economic values for water use are established in accordance with the marginal residual value of water for production (for agricultural and industrial uses) or the accessibility of payment for urban supply and other end uses of water.

The current inability to provide pertinent information required to achieve the necessary coherence in various government policies can be partially resolved by integrated research on hydrological aspects combining the social and natural sciences. A comprehensive framework for watershed research has been developed (Lindroth et al., 1994) contends that combining economic analysis with integrated modelling, stakeholder analysis, multi-criteria assessment, and stakeholder analysis can yield complementary insights into wetland management, policy optimization, and welfare maximization. Each part of this integrated wetland research is then examined and connected to wetland management strategy.

Constructions utilizing hydrotechnical methods have a wide range of significant environmental effects, both good and bad. Because of this, they should be examined using a sophisticated tool that incorporates techniques unique to economic sciences. That is a prerequisite (Mititelu, 2010) for them to agree with those established at the Conference of Nations United of June 1972 from Stockholm, which defined environmental impact as any impact that human activity has on the environment, including the safety and health of wildlife, plants, soil, water, climate, landscapes, and historical structures like monuments.

The direct protection of the objectives threatened by torrential floods, as well as an important ecological effect, can be ensured by the retention of alluvium, both directly by the transverse hydrotechnical works, and indirectly by covering the beds by all types of hydrotechnical works used (Bremer et al., 2021; Clinciu et al., 2008).

The article is addressing the scientific gap related to the estimation of the efficiency of hydrotechnical works, especially on forests.

There are recent studies (Arion et al., 2023) proposing the use of cost-benefit analysis based on real-cost methodology, so, for the purpose of this study, it was used the determination of the amount of alluvium retained due to retention and consolidation. Two significant indicators were used: direct retention and retention through consolidation, as proposed by scholars in Romania (Gaşpar et al., 1979; Clinciu, Gaşpar, 2005; Lupaşcu, 2009).

MATERIALS AND METHODS

On the following torrential valleys - on the right side, Fâncel, Sirod, Fătăciunița, and Pârâul Negru - which are situated on the direct slopes of the Gurghiu River and its tributaries-research on the efficacy of hydrotechnical works have been conducted. The areas under study are covered with projects to stabilize torrents, safeguard banks, and safeguard forest roads.

The Gurghiu hydrographic basin, which is a part of the Gurghiu Mountains' volcanic region, the Reghin Subcarpathians' hilly unit, and the Mureș Terraced Corridor, is situated in the Eastern portion of the Transylvanian Depression. In the hydrographic basin of the Mureș River, it is situated in the northeastern region of Mureș County. It is, also, part of the Eastern Carpathians, the North-Western part of the Gurghiu Mountains, part of the Gurghiu-Călimani-Harghita volcanic mountains and, the area with lower altitudes, is part of the Transylvanian Plateau.

The delimitation of the Gurghiu Basin and the sub-basins where torrent correction works were carried out was done with the ArcHydro9 application through a sequence of operations, the surface of the basin automatically resulting.

The surface of the hydrographic basin is 655 km^2 - 65,500 ha calculated as a result of the delimitation of the hydrographic basin by drawing the water balance on the Topographic maps 1:25,000, being included into the category of very large basins, so the effect of heavy precipitation and sudden melting of upstream snow is felt with a delay.

In the Orșova, Fâncel and Sirod sub-basins, in order to reduce the effects of torrential floods, since 1970, a large-scale development of the torrential hydrographic basins was started. This action mainly had in mind the protection of localities and public and forest roads by reducing the transport of alluvium and strengthening the torrential hydrographic basin.

The location of the hydrographic basins where works were carried out was done starting from the existing documentation and records at the Mureș Forestry Directorate (Figure 1).

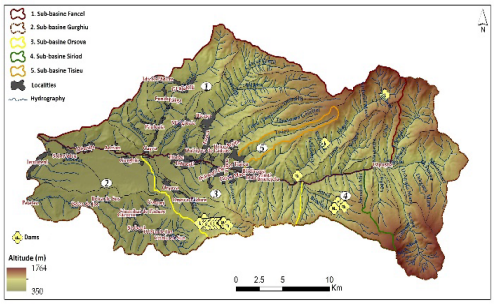

Figure 1. Location of hydrotechnical works on studied area

Estimation of Consolidated length, Consolidated Area and Volume of Alluvium

The consolidated length by covering the beds by the landings (Lat), the consolidated surface (Sat) and the volume of alluvium stored by the landings (Wat) are the studied indicators. They were quantified according to the methods proposed by scholars (Lupaşcu, 2009; Colişar, 2011), as follow:

- the SilvaClinoMaster hypsometer was used to measure the slope of the landing that had formed or was in the process of forming;
- Lat was measured using the 50 m tape;
- Sat was calculated as the product between the length of the landing and its width in the hydro-technical work location area;
- Wat was determined with the simplified formula proposed by Gaşpar (Gaşpar et al., 1979) for cases where the bed slopes and cross sections are constant:

$$Wat = 0.167 \cdot Yat \cdot Lat \cdot (2b + B) \qquad (1)$$

where:

- Yat - the blocked height of the transverse hydrotechnical work;
- b - the width of the riverbed thalweg in the area where the work is located;
- B - the width of the valley at the level of the landing formed or in the process of formation.

In order to verify the results obtained regarding the volume of the landing, the volume of alluvium estimated in the projects developed by Institute of Forestry Research and Management in Romania (I.C.A.S.) was compared with the volume of alluvium landed behind the hydrotechnical works.

Estimation of Direct retention (RD)

The direct retention (RD) is represented by the transverse works, dams and thresholds, constituted by the volume of the landing formed or in the process of formation.

Estimation of Retention through Consolidation (RC)

The action of correcting the torrents through the landscaping works stops the erosion of the banks and riverbeds during the operation of the works. Retention through consolidation constitutes the volume of alluvium fixed by these works and can be expressed by the following parameters (Lupaşcu, 2009):

- retention by consolidation, originating from formed landings, evaluated separately for dams and clogged thresholds;
- retention by consolidating the beds by the works themselves, considered separately for each work.

Reinforcement by capping the banks was calculated considering the length covered by the flood drainage channels, which supports the defence of the banks against lateral erosion and other mass transport phenomena.

Retention by consolidation was analysed and calculated on torrential valleys and on each work separately, using the following calculation formula:

$$RC = N \cdot Waa \qquad (2)$$

where:

- N - the number of years of the period of operation of the works;
- Waa - the volume of alluvium, which in the assumption of the non-application of the works would have been transported from the bed sectors covered with the landings of the works.

Waa was determined according to the Gaspar-Apostol method (Gaspar et al., 1995), which forecasts the approximate amount that could have been transported from the torrential network.

$$Waa = 0.0175 \cdot (0.5 \cdot H) \cdot (0.125 \cdot F) \cdot \left(\frac{Lv}{La} \cdot 0.15\right) \cdot f \cdot \sum \left(L \cdot qa \cdot c \cdot \left(\frac{ia}{is}\right) \cdot 0.5\right) \qquad (3)$$

where:

- H (mm) - average annual rainfall;
- F(ha) - basin surface;
- Lv (m) - the length of the slopes;
- La (m) - the length of the main bed;
- Ia - the average slope of the main bed;
- Iv - the average inclination of the slopes;
- F - coefficient established according to the textural class of the substrate;
- L (km) - the length of each bed sector;
- qa (mc/year/ha) - specific standard erosion;
- c (mc/year/ha) - the average erodibility coefficient on the sector of length L;
- ia - the real average slope of the considered bed secto;r
- is - the average slope of the considered bed sector.

It must be specified that some of the elements introduced in the calculations were measured or assessed during the field survey phase, others were taken from the forestry plans, while others were taken from the situation plans at the scale 1:5,000 and 1:10,000, and others being taken with the help of the GIS application.

The precipitation retention potential was determined by land use category and subsequently the period of operation of the hydrotechnical works executed was established.

Estimation of the economic effects produced by reducing the transport of alluvium

Torrential alluvium causes damage to various objectives and lands inside and outside the basins, such as clogging of forest roads, agricultural and forestry lands, civil, industrial and household buildings.

The volume of flood alluvium transported from the basins is determinable as (25-75)% of alluvium causes damage (Grudnicki & Ciornei, 1997). The assessment of these damages is done by determining both the costs of reflate, removal of alluvium, and the costs of repairing the damage. The estimation of the partial economic effects of the development works is calculated by adding up the values of direct retention and retention through consolidation, and only the

expenses that would have been occasioned by the excavation, transport and storage of alluvium are considered torrential (Lupașcu, 2009; Ciornei, 2000). It is considered that the extraction of coarse alluvium is carried out mechanized and manual, the transport would have been done over 5 km, with unit costs updated from the 1984 Design Standard.

RESULTS AND DISCUSSIONS

Direct retention

In the Fâncel and Sirod hydrographic subbasins, all the levees and dams executed fulfilled their role of retaining the alluvium, at the date of the inventory of the works, the retention capacities of the works were exhausted (Figure 2).

Figure 2. Direct retention, Fâncel and Sirod sub-basins

The surface, length and volume of the landings formed in the Fâncel, Sirod and Orșova hydrographic subbasins

Based on the measurements and calculations carried out, the landings that are formed behind the transverse works on the torrential streams in the basin under study extend over a length of 424 m, having a total area of 6,770.11 m^2 and forming a volume of alluvium of 6,774.55 m^3 (Table 1).

It is found that the largest volume of alluvium stored behind the works is in the Orșova valley with 5301.98 m^3, the reasons being the greater number of works, the works are much larger and the torrential valley has a much wider opening large in relation to the other two sub-basins. The Fâncel subbasin has the lowest values for the elements considered, because of the number of fewer works, although the works in this basin have exhausted their retention capacity to the maximum.

Table 1. The area, the length and the volume sediments behind dams of the Orșova, Fâncel and Sirod sub-basins

No	Torrential valley/Transversal work	Length (Lat) (m)	Area (Sat) (m^2)	Volume (Wat) (m^3)
1	Orșova dam 1	25.0	480.00	881.76
2	Orșova dam 2	31.0	654.1	1,009.51
3	Orșova dam 3	17.0	266.9	202.70
4	Orșova dam 4	25.0	417.5	508.93
5	Orșova dam 5	23.0	478.4	304.21
6	Orșova dam 6	23.5	472.35	486.64
7	Orșova dam 7	17.0	277.1	182.60
8	Orșova dam 8	16.8.0	231.84	432.06
9	Orșova dam 9	18.0	304.2	292.18
10	Orșova dam 10	23.0	333.5	232.69
11	Orșova dam 11	24.0	439.2	427.739
12	Orșova dam 12	23.2	392.08	340.95
	Total Orșova	266.5	4,747.17	5,301.98
13	Fâncel dam 1 Pr. Porcul de Jos borna 22	18.9	217.35	138.88
14	Fâncel dam 2 Pr. Tarcea de Sus borna 80	26.3	433.95	494.11
15	Fâncel traversă 3 Pr. Buneasa	11.8	171.1	39.45
	TOTAL Fâncel	57.0	822.4	672.44
16	S.1 prag Pr. Borna 51/VIII	13.6	108.8	66.77
17	S.1 dam Pr. Borna 52/VIII	23.4	210.6	200.08
18	S.1 dam Pr. Borna 54/VIII	25.1	238.45	251.50
19	S.1 prag Pr. Borna 104/VIII	18.3	270.84	124.69
20	S.1 prag Pr. Borna 106/VIII	20.1	371.85	157.09
	Total Sirod	100.5	1,200.54	800.14

(source: own calculations)

Length, area and volume of landings on transverse works

The three previously mentioned indicators and their frequency were analysed separately for each work, according to Figures 3 and 5.

Analysing the length of the landings formed or in the process of formation behind the transversal works, it can be seen in Figure 3 that the longest length is recorded in the Orșova sub-basin at dam 2 (Lat = 31 m), followed by the dam on Pr. Tarcea de Sus, and the shorter length is recorded at the threshold of Pr. Buneasa (Lat = 11.8 m) in the Fâncel sub-basin.

Looking at the frequency of works by Lat classes (Figure 4) most landings, in number of 9, have a length between 20 and 25 m, 6 landings

have a length between 15-20 m, only 2 landings have a length between 25 and 30 m.

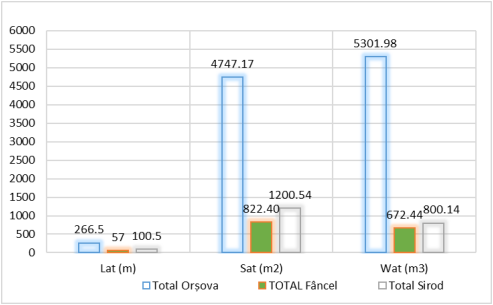

Figure 3. The length, the area and the volume of sediments behind dams

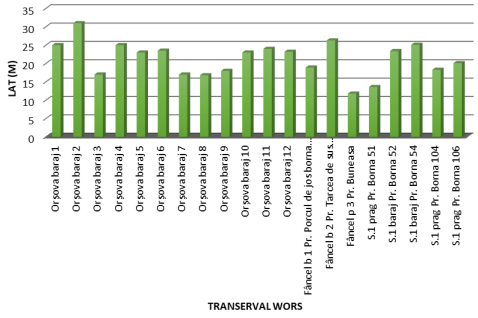

Figure 4. The length of the transversal works sediments behind dams

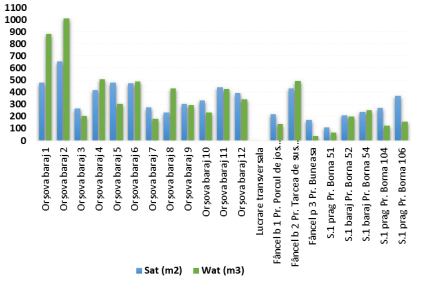

Figure 5. Distribution of area and volume of sediments behind dams on transverse works

The area of landings (Sat) was determined as a product between Lat and the width of the landing formed in the hydrotechnical work location area. Sat may vary depending on the width of the valleys.

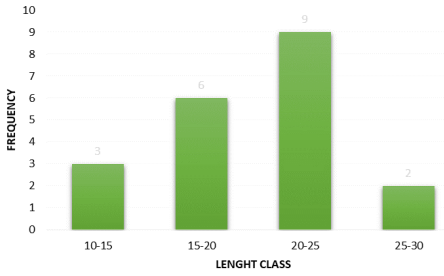

Figure 6. The frequency of transversal works on length classes

The landed surface of the transverse works is larger on the Orșova valley, because the valley is wider than the other two valleys. Also, it is observed that only dams 1 and 2 in the Orșova sub-basin have a large volume of stored alluvium, namely 1009 m^3 and 881 m^3, respectively, due to the total blocked height. Although the length of the landings on Orșova is longer, it can be seen that the surface and the volume landed is not that big, the reason being: some dams are filtering and others have not yet reached their maximum retention capacity.

Regarding the distribution of the terms Lat, Sat, Wat by classes of height of transverse works, for the variables Lat and Sat, the distributions of the values are similar. The best representation for the length and surface of the landing is the class 2.0-2.5 m, followed by in order of classes 4.0-4.5 m and 3.0-3.5 m. In the case of the variable Wat, the class with the highest value is 4.0-4.5, followed by classes 3.0-3, 5 m and 2.0-2.5 m (Figure 7).

The fact that in the category of low height works further demonstrates the impact of the height of the works, up to 2.5 m, Sat predominates over Wat, while at heights greater than 2.5 m, Wat predominates over Sat. Not only the height of the work, but also the elements that define the morphology of the subbasins leave their mark on these terms. The volume of alluvium retained is directly proportional to the height of the works and the width of the valleys and inversely proportional to the landing length.

The retention of alluvium from the landings led to a storage of amounts of alluvium that caused problems for the transport facilities in hydrographic basin Gurghiu, stabilized the banks of the beds in the area where the works are located and reduced their slope.

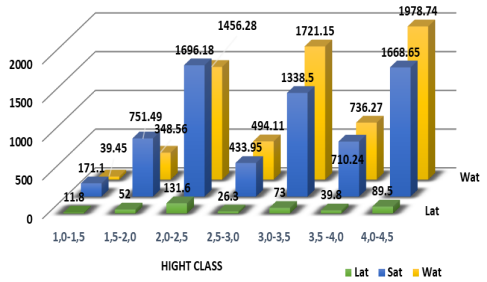

Figure 7. The length, the area and the volume distribution on works height classes

Retention through Consolidation

Analysing the retention values obtained through consolidation, it is observed that the highest value appears at the dam on Pr. Tarcea de Sus with a percentage of 27.52%, followed by the B2 dam on the Orșova River with 15.26%, followed by the dams from Orșova and then Fâncel.

Through the execution of the works on the three basins studied, the following retention values were achieved: direct retention in landings is 6,774.5 m^3, retention through consolidation has a volume of alluvium of 18,185.8 m^3 (Table 2), and the total amount of alluvium retained in the valleys of hydrographic basin Gurghiu is 24,960.3 m^3.

Consolidation retention for works that have fully formed landings has a weight of 62.5% of the total value of consolidation retention due to landings. One cause would be an overly optimistic forecast of the transport of alluvium within these sub-basins, a characteristic that will have to be considered in the choice of future technical solutions for the arrangement of the torrential hydrographic network, and a knowledge of the evolution of the effects of the works would be needed.

A reason that leads to the consumption of the alluvium retention capacity by the transversal works would be the intensive exploitation of the trees in the top of the streams and the setting up of the installations to remove and close the woody material.

It can be said that the greater the volume of alluvium retained directly by the transversal works, the greater the volume of alluvium consolidated on the torrential streams, an aspect for this situation would be the number of hydrotechnical works built.

Table 2. Distribution of the sediments volume of the Orșova, Fâncel and Sirod sub-basins

No	Works on torrential valleys	The year of execution/no. of years	Waa (m^3/year)	Total Waa (m^3)
1	Orșova dam 1	1970/48	19.2	921.6
2	Orșova dam 2	1970/48	57.8	2,774.4
3	Orșova dam 3	1970/48	10.3	494.4
4	Orșova dam 4	1970/48	36.9	1,771.2
5	Orșova dam 5	1970/48	11.5	552
6	Orșova dam 6	1970/48	15.7	753.6
7	Orșova dam 7	1970/48	8.1	388.8
8	Orșova dam 8	1970/48	10.6	508.8
9	Orșova dam 9	1970/48	9.3	446.4
10	Orșova dam 10	1970/48	11.2	537.6
11	Orșova dam 11	1970/48	17.9	859.2
12	Orșova dam 12	1970/48	14.1	676.8
13	Fâncel b 1 Pr. Porcul de jos Borna 22	2008/10	84.2	842.0
14	Fâncel b 2 Pr. Tarcea de sus Borna 80	2008/10	500.4	5,004.0
15	Fâncel p 3 Pr. Buneasa	2008/10	93.5	935.0
16	S.1 prag Pr. Borna 51	2009/10	6.0	60.0
17	S.1 dam Pr. Borna 52	2009/10	11.0	110.0
18	S.1 dam Pr. Borna 54	2009/10	35.0	350.0
19	S.1 prag Pr. Borna 104	2009/10	6.0	60.0
20	S.1 prag Pr. Borna 106	2009/10	14.0	140.0
	Total			18,185.8

(source: own calculations based on preliminary studies to substantiate the need for hydrological works in the small hydrographic Fâncel watershed)

The economic effects produced by reducing the transport of alluvium

The value of direct retention is 6,774.55 m^3 and retention through consolidation is 18,185.8 m^3, and the total amount of alluvium retained in the valleys of hidrographic basin Gurghiu is 24,960.3 m^3.

The unit cost of manual extraction of coarse alluvium is estimated at 80 lei/m^3 and the cost of mechanized extraction of coarse alluvium is estimated at 69 lei/m^3 updated. Having in mind the geography of the area, it can be estimated that 50% could mechanized extracted and 50% manually, which implies an average cost of 75 lei/m^3. The costs were established by consulting the local economic operators that provide such services, considering that, by the Emergency Ordinance no. 85/2018 for the repeal of some legal provisions in the field of investments financed from public funds, dated 13/09/2018, thus repealing the cost standards for investment

objectives financed from previously existing public funds, the beneficiaries returning the obligation to update and approve on his own responsibility the updated value of the works from the intervention works (Table 3).

Table 3. Estimative costs of sediments excavation

No	Indicator	Measurement unit	RC	RD
1	Volume	m^3	18,185.8	6,774.55
2	Unitary cost	lei/m3	74,5	74.5
3	Estimated value	thousand lei	1,354.84	504.70
5	Estimated Total	lei/m3	1,859.55	

The analyse shows that the expenses that would have been necessary for the excavation of torrential alluvium would have been approximately 1,859.55 thousand lei.

CONCLUSIONS

The results are in the line with the recommendations formulated by The World Bank Group (Darghouth et al., 2008). These recommendations highlight the relevance of using of economic and financial analysis when an investment on watershed is planned. Also, its emphases the "cost of inaction", by estimating the externalities at their real-value costs (Bhaduri et al., 2016).

The retention of alluvium in the landings led to the storage of quantities of alluvium which caused problems for the transport facilities in hydrographic basin Gurghiu, stabilized the banks of the beds in the area where the works are located and reduced their slope.

A weight of 62.5% of the total consolidation retention due to landings is assigned to consolidation retention for works with fully formed landings.

The following retention values were reached through the execution of the works on the three basins under study: direct retention in landings is 6774.5 m^3, retention through consolidation has a volume of alluvium of 18,185.8 m^3, and total alluvium retention in the valleys of hydrographic basin Gurghiu is 24,960.3 m^3. The higher the volume of alluvium obtained by RD from the transverse hydrotechnical works, the higher the volume of RC.

The watershed management works help to lessen how destructive torrential events are as well as the risk of flooding on nearby communities and socioeconomic goals.

The limit of the study includes the insufficient similar studies to allow an in-depth comparison of the result, so the need for further studies is obvious.

ACKNOWLEDGEMENTS

Some of the mentioned studies are the result of P.h.D. thesis of Dr. Iulia Diana Arion, named "Studies regarding the efficiency of hydrotechnical works from hydrographic Basin 10Gurghiu (Cercetări privind eficiența lucrărilor hidrotehnice din Bazinul Hidrografic al Gurghiului), " coordinated by Prof. Dr. Marcel Dirja, in the framework of the Doctoral School Agricultural Engineering Sciences of the University of Agricultural Sciences and Veterinary Medicine of Cluj-Napoca.

REFERENCES

Arion, I.D., Arion, F.H., Tăut, I., Mureșan, I.C., Ilea, M., Dîrja, M. (2023). Investment in Forest Watershed—A Model of Good Practice for Sustainable Development of Ecosystems. *Water, 15*, 754

Bhaduri, A., Bogardi, J., Siddiqi, A., Voigt, H., Vörösmarty, C., Bunn, S.E., Shrivastava, P., Lawford, R., Foster, S., Kremer, H., Renaud, F.G., Bruns, A., Osuna, V.R. (2016). Achieving Sustainable Development Goals from a Water Perspective. *Front. Environ. Sci.*, 4, 64. doi: 10.3389/fenvs.2016.00064.

Bremer, L.L., DeMaagd, N., Wada, C.A., Burnett, K.M. (2021). Priority watershed management areas for groundwater recharge and drinking water protection: A case study from Hawai'i Island. *J. Environ. Manag., 286*, 111622.

Ciornei, I. (2000). *Eficienţa economică a investiţiilor pentru amenajarea bazinelor hidrografice torenţiale*. *Bucovina Forestieră, 8*(2), 23-29.

Clinciu, I., Gaspar, R. (2005). Comportarea lucrărilor hidrotehnice de amenajare a torenților, o problem de actualitate a cercetării științifice. *Revista Pădurilor, 5*, 36-45.

Clinciu, I., Păcurar, V.D., Petriţan, I.C., Vasilescu M.M. (2008). Cercetări privind vegetația forestieră instalată pe rețeaua torențială amenajață în bazinul superior al Târlungului. *Revista Pădurilor, 6*, 13-20.

Colișar, A. (2011). *Cercetări privind comportarea lucrărilor de corectarea torenților din Bazinul Hidrografic al Râului Strei.* Teza de doctorat. Elaborată în cadrul Școlii Doctorale de Științe Agricole Inginerești, Cluj-Napoca.

Darghouth, S., Ward, C., Gambarelli, G., Styger, E., Roux, J. (2008). *Watershed Management Approaches, Policies, and Operations: Lessons for Scaling Up.* Paper No. 11; Water Sector Board Discussion Paper

Series 2008; The World Bank: Washington, DC, USA, 2008; https://documents1.worldbank.org/curated/en/142971468779070723/pdf/442220NWP0dp111Box0327398B01public1.pdf

Gaşpar, R., Costin, A., Clinciu, I., Lazăr, N. (1995). *Amenajarea bazinelor hidrografice torenţiale. Protejarea şi dezvoltarea durabilă a pădurilor României*, Editura Arta Grafică, Bucureşti.

Gaşpar, R., Munteanu, S.A., Costin, A. (1979). Cu privire la metodologia de determinare a ficienței hidrologice și antierozionale a lucrărilor de amenajare a bazinelor hidrografice torențiale. *Buletinul A.S.A.S., 8*, Bucharest.

Grudnicki, F., Ciornei, I. (1997). Contribuții la evaluarea efectelor lucărilor de amenajare a bazinelor hidrografice torențiale. *Analele Universității "Ștefan cel Mare" Suceava- Secțiunea Silvicultură, III*, 33-40.

Hallegatte, S. (2012). A Cost-Effective Solution to Reduce Disaster Losses in Developing Countries: Hydro-Meteorological Services, Early Warning, and Evacuation. *World Bank Policy Research Working Paper 6058*.

Hâncu, C.D., Nițescu, C. (2016). Amenajări hidrotehnice, Ovidius University Press – Constanța, ISBN 978-973-614-897-2.

Harou, J.J., Pulido-Velazquez, M.; Rosenberg, D.E.; Medellín-Azuara, J., Lund, J.R., Howitt, R.E., (2009). Hydro-economic models: Concepts, design, applications, and future prospects. *Journal of Hydrology, 375*(3–4), 627-643.

Heinz, I.R., Pulido-Velazquezj, Lund J., Andreu, J. (2007). Hydro-economic Modeling in River Basin Management: Implications and Applications for the European Water Framework Directive. *Water Resour Manage, 21*, 1103.

Lindroth, A., Verwijst, T., Halldin, S. (1994). Ecological-economic analysis of wetlands: scientific integration for management and policy. *Journal of Hydrology, 156*(1–4), 1-19.

Lupaşcu, F. (2009). *Cercetări privind comportarea şi efectele lucrărilor de amenajare a reţelei hidrografice torenţiale din bazinul superior al Someşului Mic*, Teză de doctorat, Universitatea Transilvania din Braşov.

Mititelu, L.A. (2010). Impactul amenajărilor hidrotehnice asupra mediului pe Valea Argeşului (până la Goleşti). *Lakes reservoirs and ponds, 4*(2), 152-166, ISSN: 1844-6477

Pulido-Velazquez, M., Andreu, J., Sahuquillo A., Pulido-Velazquez, D. (2008). Hydro-economic River basin modelling: The application of a holistic surface–groundwater model to assess opportunity costs of water use in Spain. *Ecological Economics, 66*(1), 51-65.

Sun, G., Vose, J. (2016). Forest management challenges for sustaining water resources. *Anthropocene. Forests, 7*, 68.

Toscani, P., Sekot, W., Holzleitner, F. (2020). Forest Roads from the Perspective of Managerial Accounting-Empirical Evidence from Austria. *Forests, 11*, 37.

Turner R.K., Van den Bergh, J.C.J.M., Söderqvist, T., Barendregt, A., Van der Straaten, J., Maltby, E., Van Ierland, E.C. (2000). Ecological-economic analysis of wetlands: scientific integration for management and policy. *Ecological Economics, 35*(1), 7-23.

Scientific Papers. Series E. Land Reclamation, Earth Observation & Surveying, Environmental Engineering. Vol. XII, 2023
Print ISSN 2285-6064, CD-ROM ISSN 2285-6072, Online ISSN 2393-5138, ISSN-L 2285-6064

HEAVY METALS ACCUMULATION IN PROCESSED FISH PRODUCTS AND RISK ASSESSMENT ANALYSIS ON HUMAN HEALTH

Ira-Adeline SIMIONOV, Alina ANTACHE, Madalina CALMUC, Nina CONDURACHE, Miruna CODREANU, Adeline MILEA, Catalina ITICESCU, Puiu-Lucian GEORGESCU

"Dunarea de Jos" University of Galati, REXDAN Research Infrastructure,
98 George Cosbuc Street, Galati, Romania

Corresponding author email: ira.simionov@ugal.ro

Abstract

The present study aimed to evaluate the concentration of heavy metals (aluminium - Al, beryllium - Be, cadmium - Cd, arsenic - As, nickel - Ni, chromium - Cr, copper - Cu, lead - Pb, zinc - Zn, and mercury - Hg respectively) in several processed fish foods (canned tuna, sardines, herring, salmon, and mackerel respectively) and assess the risks manifested on human health due to products consumption in Romania. In this context, the estimated daily intake (EDI) and target hazard quotient (THQ) was calculated based on the concentration of elements analysed by using the ICP-MS technique, the average fish products consumption in Romania and the average weight of Romanian consumers. The registered values for EDI and THQ were below 1, fact that indicates there is no risk on consumer's health. However, continuous screening of heavy metals contamination of food products is needed, due to the on-going risk for elements accumulation.

Key words*: fish products, heavy metals, risk assessment.*

INTRODUCTION

Animal protein is a major component of human diets, due to their high content in essential amino acids (Langyan et al., 2022). The availability of proteins for human consumption is necessary to ensure food security (Boyd et al., 2022). Today, almost 20% of the global animal-based protein destined for human consumption is ensured by fish meat and fish products derived from aquaculture or fisheries practices (Boyd et al., 2022).

Even more, fish meat and fish products are also a great source of long chain omega-3 polyunsaturated fatty acids such as eicosapentaenoic acid (EPA) and docosahexaenoic acid (DHA) (Leroy et al., 2023). At the same time, given the increased anthropogenic pressures exercised on aquatic ecosystems, fish meat and fish products have been observed to accumulate different contaminants which can cause toxicity if transferred in humans via consumption. Hazardous substances such as heavy metals can counteract the health benefits generated by fish consumption due to their lack of biodegradability and accumulation tendency (Djedjibegovic et al., 2020). Exposure and accumulation of heavy metals in the human body has been linked to a series of brain pathologies such as Parkinson's and Alzheimer's disease, Wilson disease, as well as multiple sclerosis (Mitra et al., 2022).

In this context, to protect the health of citizens, the European Union has established maximum permitted levels of heavy metals in fish meat and fish products through the regulation (EC) No 1881/2006. The regulation also calls for constant and continuous monitoring of heavy metals concentration levels in food products in order to detect and prevent possible threats posed to human health.

Therefore, the aim of the present study was to evaluate the concentration levels of aluminium (Al), beryllium (Be), cadmium (Cd), arsenic (As), nickel (Ni), chromium (Cr), copper (Cu), lead (Pb), zinc (Zn), and mercury (Hg) respectively, in several processed fish foods (canned tuna, sardines, herring, salmon, and mackerel respectively), commercialised in the Romanian market. Further on, a risk assessment analysis was conducted according to Kin order to identify if there are any potential health problems generated by the consumption of the aforementioned fish products.

MATERIALS AND METHODS

Canned fish products were purchased from the local stores in Galati city, Romania. Samples of processed fish products (*n=42*) were collected as it follows: canned tuna in brine, canned herring in vegetable oil, canned sardines in vegetable oil, canned tuna pate, canned salmon pate and canned mackerel pate (Figures 1 and 2).

Figure 1. Sample collection of canned tuna in brine

Figure 2. Sample collection of canned tuna pate

The samples were analysed within the Rexdan Research Infrastructure. Thus, each sample was digested with nitric acid and hydrogen peroxide and further analyzed by ICP-MS technique (Figure 3).

The final aqueous solution was analysed by inductively coupled plasma with mass spectrometry (ICP-MS) with the Perkin Elmer NexION 2000 equipment. The following heavy metals were quantified in saples: Be, Zn, Cu, Al, As, Cr, Hg, Cd, Pb, Ni, respectively.

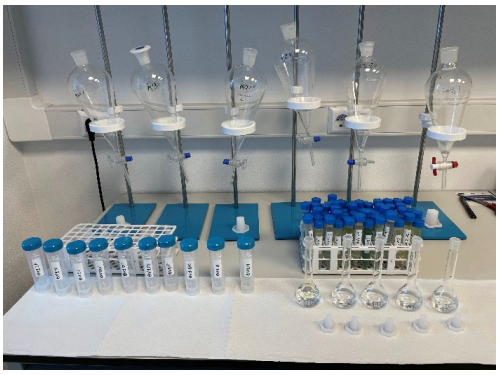

Figure 3. Digested samples

Risk assessment analysis

The estimated daily intake (EDI) and the target hazard quotient (THQ) were calculated to highlight potential risks posed on human health by the consumption of processed fish products. EDI and THQ were computed according to Kowalska et al. (2020) as it follows:

$$EDI\ (mg/kg/day) = \frac{EF\ x\ ED\ x\ IR\ x\ C}{WAB\ x\ ATn}$$

where:
- EF = Exposure frequency (365 days/year);
- ED = Exposure duration – average lifetime in Romania (74.2 years);
- IR = Fish and seafood ingestion rate (kg person/day) - 17.26 g per person/day;
- C = metal concentration in fish muscle (mg/kg);
- WAB = average body weight (kg) - 78.65 kg for adults (85.1 kg for males and 72.2 kg for females;
- ATn = Average exposure time for non-carcinogen (365 days/year x ED).

$$THQ = \frac{EF\ x\ ED\ x\ IR\ x\ C}{RfD\ x\ WAB\ x\ ATn}\ x\ 10^{-3}$$

where:
- EF = Exposure frequency (365 days/year);
- ED = Exposure duration - average lifetime (74.2 years);
- IR = fish and seafood ingestion rate (g/day);
- C = metal concentration in edible tissue muscle (mg/kg);

- RfD = oral reference dose for each metal (mg/kg/day);
- WAB = average body weight (kg);
- ATn = average exposure time for non-carcinogen (365 days/year x ED).

RESULTS AND DISCUSSIONS

The analysis revealed that Be was below the detection limit in all analysed samples.
Further on, the following heavy metals accumulation trend in the canned tuna in brine was identified: Zn>Cu>Al>As>Cr>Hg>Cd>Pb>Ni (Figure 4). Zn had the highest concentration (2.798± 0.543 µg/g), while the lowest concentration was observed in case of Ni (0.018±0.002 µg/g

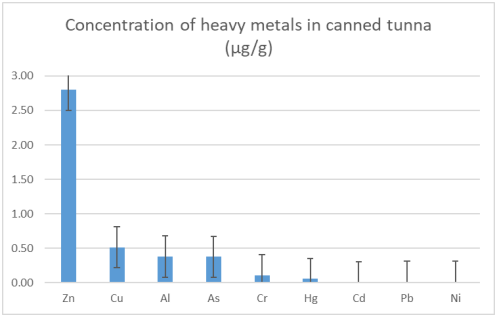

Figure. 4. Concentration of heavy metals in canned tuna in brine

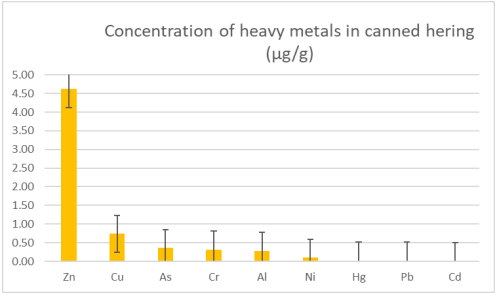

Figure. 5. Concentration of heavy metals in canned herring in vegetable oil

In case of heavy metals accumulation in canned herring in vegetable oil, the following trend was identified: Zn>Cu>As>Cr>Al>Ni>Hg>Pb>Cd (Figure 5). As previously observed the highest concentration level is in case of Zn (4.621±0.145 µg/g), while the lowest is observed in case of Cd concentration (0.002±0.001 µg/g).

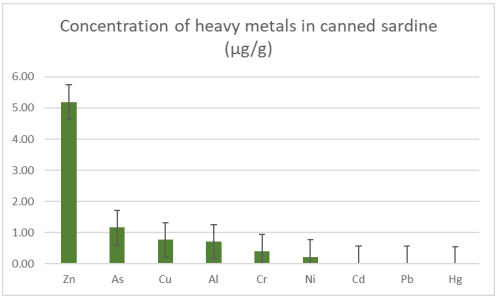

Figure. 6. Concentration of heavy metals in canned sardines in vegetable oil

In case of heavy metals accumulation in canned sardines in vegetable oil, the following accumulation trend was registered: Zn>As>Cu>Al>Cr>Ni>Cd>Pb>Hg. Zn had the highest concentration level (5.191±0.027 µg/g), while Hg registered the lowest concentration level (0.011±0.001 µg/g).

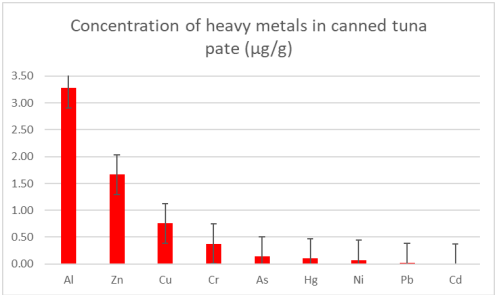

Figure. 7. Concentration of heavy metals in canned tuna pate

The accumulation trend of heavy metals in canned tuna pate is as it follows: Al>Zn>Cu>Cr>As>Hg>Ni>Pb>Cd (Figure 7). It can be observed that the highest concentration level was obtained in case of Al (3.275±0.205 µg/g). This can be due to poor quality of can material and transfer of Al from the packaging to the food inside. The lowest concentration level was registered in case of Cd (0.0042±0.0001 µg/g), as previously observed in canned herring.
Further on, in case of heavy metals accumulation in canned salmon pate, the following trend was identified: Al>Zn>Cu>Cr>As>Ni>Pb>Hg>Cd (Figure 8). As previously observed, the highest concentration level was in case of Al (3.803±0.159 µg/g), while the lowest

concentration level was registered in case of Cd (0.0030±0.000 µg/g).

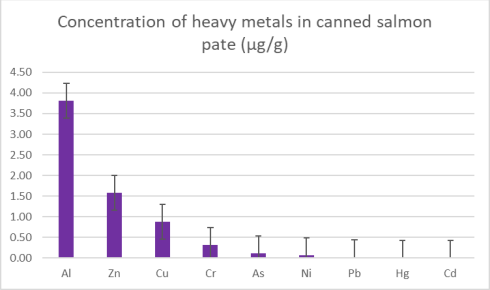

Figure. 8. Concentration of heavy metals in canned salmon pate

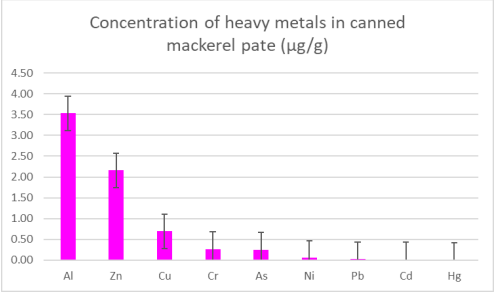

Figure. 9. Concentration of heavy metals in canned mackerel pate

The accumulation trend of heavy metals in canned mackerel pate was as it follows: Al>Zn>Cu>Cr>As>Ni>Pb>Cd>Hg (Figure 9). The highest value was registered in case of Al concentration (3.533±0.177 µg/g), while the lowest value was registered in case of Hg concentration (0.011±0.000 µg/g).

The results highlight that Zn had the tendency to accumulate in canned fish products conserved in vegetable oil or in brine. These results are in accordance with the study conducted by Islam et al., in which canned tuna, sardines and mackerel had the highest concentration levels in case of Zn, after magnesium (Islam & Mustafa, 2023). In all studied canned fish pates, the highest tendency of heavy metals accumulation was observed in case of Al.

Heavy metals with the lowest accumulation tendency were Cd, Hg and Ni.

As well, the concentrations of heavy metals in the canned fish samples registered values below the maximum permitted level set by the European Union in the (EC) No 1881/2006, which are 0.3 mg/kg in case of Pb, 0.05 mg/kg in case of Cd and 0.5 mg/kg in case of Hg.

In the study conducted by Miedico et al., the authors highlighted that 11% of the canned tuna samples exceeded the maximum permitted level in terms of Hg content and one tuna can exceed the maximum permitted levels in case of Cd content (0.22 mg/kg) (Miedico et al., 2020).

As well, El-Dahman et al. (2019) showed that canned tuna had higher Hg concentrations compared to other type of preserved fish (salted or frozen fish) (El-Dahman et al., 2019).

In Table 1, the values of the computed estimated daily intake (EDI) are represented. As it can be observed, the estimated intake of Al from consuming canned fish pates is above the tolerable limits specified by World Health Organization, which can lead to chronic toxicity in the human body.

The same phenomenon was observed in case of Cd, which registered values of EDI above the tolerable limit, except for herring in vegetable oil and salmon pate. The intake of Ni was also above the tolerable limit in herring and sardines conserved in vegetable oil, and in tuna and salmon pates respectively. The intake of Hg is above the tolerable limit in all studied canned fish products. The most concerning heavy metal intake is registered in case of Pb, because the EDI values in all canned fish products were above the 0.0006 mg/kg/day, which is the intake that generated the loss in IQ by 1 point in children (Joint FAO/WHO, 2011).

The registered values for EDI are in accordance to the ones registered by (Djedjibegovic et al., 2020).

In Table 2 are represented the values of the computed target hazard quotient (THQ), which are significantly lower than 1. Scores of THQ lower than 1 indicate that there are no risks on the exposed population via the consumption of canned fish products. This is due to the low fish products consumption in Romania.

Table 1. Estimated daily intake (EDI) of heavy metals (mg/kg/day)

	Tuna in brine	Herring in oil	Sardines in oil	Tuna pate	Salmon pate	Mackerel pate	Tolerable limits
Al	0.0835	0.0624	0.1571	0.7189	0.8347	0.7754	0.28
As	0.0833	0.0782	0.2564	0.0302	0.0251	0.0548	-
Cd	0.0026	0.0005	0.0060	0.0009	0.0007	0.0035	0.00089
Cr	0.0241	0.0685	0.0886	0.0827	0.0706	0.0592	-
Cu	0.1128	0.1628	0.1695	0.1662	0.1935	0.1523	0.5
Ni	0.0040	0.0216	0.0496	0.0162	0.0163	0.0121	0.013
Pb	0.0040	0.0044	0.0056	0.0047	0.0049	0.0051	0.0006
Zn	0.6141	1.0140	1.1392	0.3655	0.3475	0.4738	1
Hg	0.0129	0.0046	0.0024	0.0224	0.0007	0.0024	0.00057

Table 2. Target hazard quotient (THQ)

	Tuna in brine	Herring in oil	Sardines in oil	Tuna pate	Salmon pate	Mackerel pate
Al	8E-08	6E-08	2E-07	7E-07	8E-07	8E-07
As	3E-04	3E-04	8E-04	1E-04	8E-05	2E-04
Cd	3E-06	5E-07	6E-06	9E-07	7E-07	3E-06
Cr	8E-06	2E-05	3E-05	3E-05	2E-05	2E-05
Cu	3E-06	4E-06	4E-06	4E-06	5E-06	4E-06
Ni	4E-07	2E-06	4E-06	1E-06	1E-06	1E-06
Pb	1E-06	1E-06	2E-06	1E-06	1E-06	1E-06
Zn	2E-06	3E-06	4E-06	1E-06	1E-06	2E-06
Hg	1E-04	5E-05	2E-05	2E-04	7E-06	2E-05

CONCLUSIONS

The main conclusion of the present study is that the concentrations of the studied heavy metals (Al, As, Cd, Cr, Cu, Ni, Pb, Zn, Hg) in canned fish products from Galati, Romania did not exceed the maximum permitted levels imposed by the European Union legislation.

Zn had the tendency to accumulate in canned fish products conserved in vegetable oil or in brine, while all studied canned fish pates, had the highest tendency to accumulate Al.

The estimated daily intake factor revealed that the consumption of canned fish products from Galati, Romania can contribute to the exposure of human population through diet to Al, Hg, Ni and Cd.

The target hazard quotient was significantly below 1, which indicates that there are no risks posed on the health of human consumers of canned fish products.

Continuous and constant monitoring of heavy metals in food products is recommended in order to ensure food safety and to protect the health of EU citizens.

ACKNOWLEDGEMENTS

The present research was supported by the project An Integrated System for the Complex Environmental Research and Monitoring in the Danube River Area, REXDAN, SMIS code 127065, co-financed by the European Regional Development Fund through the Competitiveness Operational Programme 2014–2020, contract no. 309/10.07.2021.

This work was supported by the Fondo Proserpina S.R.L., grant number 2506/2022, "The impact of heavy metals and microplastics from aquatic organisms on human health".

REFERENCES

Boyd, C.E., McNevin, A.A., & Davis, R.P. (2022). The contribution of fisheries and aquaculture to the global protein supply. *Food Security*, *14*(3), 805–827. https://doi.org/10.1007/s12571-021-01246-9.

Djedjibegovic, J., Marjanovic, A., Tahirovic, D., Caklovica, K., Turalic, A., Lugusic, A., Omeragic, E., Sober, M., & Caklovica, F. (2020). Heavy metals in commercial fish and seafood products and risk assessment in adult population in Bosnia and Herzegovina. *Scientific Reports*, *10*(1), Article 1. https://doi.org/10.1038/s41598-020-70205-9.

El-Dahman, D., Hassan, M., & Eleiwa, N. (2019). Assessment of heavy metal residues in some fishery products. *Benha Veterinary Medical Journal*, *36*(2), 49–56. https://doi.org/10.21608/bvmj.2019.13841.1024.

Islam, M.S., & Mustafa, R.A. (2023). Assessment of trace elements in canned fish and health risk appraisal. *Foods and Raw Materials*, 43–56. https://doi.org/10.21603/2308-4057-2023-1-554.

Joint FAO/WHO. (2011). *Safety evaluation of certain food additives and contaminants: Prepared by the Seventy-third meeting of the Joint FAO/WHO Expert Committee on Food Additives (JECFA)*. https://apps.who.int/iris/handle/10665/44521.

Langyan, S., Yadava, P., Khan, F.N., Dar, Z.A., Singh, R., & Kumar, A. (2022). Sustaining Protein Nutrition Through Plant-Based Foods. *Frontiers in Nutrition*, *8*. https://www.frontiersin.org/articles/10.3389/fnut.2021.772573.

Leroy, F., Smith, N.W., Adesogan, A.T., Beal, T., Iannotti, L., Moughan, P.J., & Mann, N. (2023). The role of meat in the human diet: Evolutionary aspects and nutritional value. *Animal Frontiers*, *13*(2), 11–18. https://doi.org/10.1093/af/vfac093.

Miedico, O., Pompa, C., Moscatelli, S., Chiappinelli, A., Carosielli, L., & Chiaravalle, A. E. (2020). Lead, cadmium and mercury in canned and unprocessed tuna: Six-years monitoring survey, comparison with previous studies and recommended tolerable limits. *Journal of Food Composition and Analysis*, *94*, 103638. https://doi.org/10.1016/j.jfca.2020.103638.

Mitra, S., Chakraborty, A.J., Tareq, A.M., Emran, T.B., Nainu, F., Khusro, A., Idris, A.M., Khandaker, M.U., Osman, H., Alhumaydhi, F.A., & Simal-Gandara, J. (2022). Impact of heavy metals on the environment and human health: Novel therapeutic insights to counter the toxicity. *Journal of King Saud University - Science*, *34*(3), 101865. https://doi.org/10.1016/j.jksus.2022.101865.

Scientific Papers. Series E. Land Reclamation, Earth Observation & Surveying, Environmental Engineering. Vol. XII, 2023
Print ISSN 2285-6064, CD-ROM ISSN 2285-6072, Online ISSN 2393-5138, ISSN-L 2285-6064

EVALUATION OF HEAVY METALS CONCENTRATIONS IN THE BLACK SEA TURBOT AND ELEMENTS CORRELATION ANALYSIS

Ira-Adeline SIMIONOV[1, 2], Valentina CALMUC[1], Stefan-Mihai PETREA[1, 2], Alina ANTACHE[1, 2], Aurelia NICA[1, 3], Catalina ITICESCU[1, 3], Puiu-Lucian GEORGESCU[1, 3], Victor CRISTEA[4]

[1]"Dunarea de Jos" University of Galati, REXDAN Research Infrastructure, 98 George Cosbuc Street, Galati, Romania
[2]"Dunarea de Jos" University of Galati, Faculty of Food Science and Engineering, 47 Domneasca Street, Galati, Romania
[3]"Dunarea de Jos" University of Galati, Faculty of Sciences and Environment, 47 Domneasca Street, Galati, Romania
[4]"Dunarea de Jos" University of Galati, Cross-Border Faculty of Humanities, Economics and Engineering, 47 Domneasca Street, Galati, Romania

Corresponding author email: ira.simionov@gmail.com

Abstract

The Black Sea Turbot (BST) is one of the most valuable fish species exploited within the fisheries activities conducted in the Black Sea, due to market demand and high selling prices. However, due to the anthropogenic pressure exercised on the Black Sea, BST is prone to accumulate different contaminants such as heavy metals. The risk of heavy metals transfer to the human consumer, through fish consumption, is possible. Thus, constant evaluation of the biomass is needed in order to avoid consumer intoxication. It is well known that different metals manifest competing behaviour for binding spots when accumulating in biota. Therefore, the present study aims to evaluate the concentration of macro- (Ca, Mg, K, Na) and micro-elements (Fe, Zn, Cu, Ni, Cr, Mn, Co, Cd, Pb) in BST muscle tissue collected from the Romanian Black Sea sector and to determine the correlation relationship between them (Pearson coefficient). The following accumulation trend in BST muscle was identified: Na>K>Ca>Mg>Zn>Fe>Cu>Mn>Ni>Cd>Pb>Cr>Co.

Key words*: Black Sea, correlation, heavy metals, turbot.*

INTRODUCTION

The high economic value of the marine flatfish turbot (*Scophthalmus maximus*, Pallas, 1814) is generally acknowledged due to market demand and its meat high nutritional value (Turan et al., 2019; Ivanova et al., 2021; Liu et al., 2021). Globally, the turbot is a target species for both the fisheries and the aquaculture sector (Khanaychenko & Giragosov, 2019; Ma et al., 2021; Massa et al., 2021).

In the Black Sea, the turbot represents one of the most valuable fish stocks for the fisheries activities conducted in all riparian countries (Giragosov & Khanaychenko, 2012; Firidin et al., 2020; Hulak et al., 2021). As well, from all riparian countries, it has been highlighted that Romania and Bulgaria have the most abundant turbot stocks, which are influenced by the presence of sandy habitats and rich prey items (Ulman et al., 2020). The nutritional value of turbot meat is assessed based on protein content, essential fatty acids, and also, macro- and microelements (Manthey-Karl et al., 2016).

The macro- and microelements profile of turbot meat depends heavily on the feeding regime of the fish (Pouil et al., 2016). In aquaculture production systems, the nutritional value of reared turbot meat can be easily controlled by using specialised pelleted fish feeds. However, in case of specimen obtained from fisheries activities, hence from natural and uncontrolled marine environments, the meat nutritional value depends on food availability and quality. Besides the uptake of essential elements from food, the turbot is prone to accumulate elements with toxic potential such as heavy metals with no essential role in fish metabolism (cadmium - Cd and lead - Pb). At the same time, it is well known that metals considered essential nutrients in living cells such as calcium (Ca), magnesium (Mg), potassium (K) and sodium (Na) can

inhibit the uptake of heavy metals in fish by competing for binding spots when accumulating in biota (Marchetti, 2013). Therefore, the aim of the present study was to evaluate the macro- (sodium - Na, potassium - K, magnesium - Mg, calcium - Ca) and microelements with toxic potential (iron - Fe, zinc - Zn, copper - Cu, nickel - Ni, chromium - Cr, manganese - Mn and cobalt - Co) , and toxic trace elements lead - Pb, cadmium - Cd) profile of the Black Sea turbot meat - *Scophthalmus maeoticus* (Pallas, 1814).

MATERIALS AND METHODS

The BST specimen (*n=21*) were caught by commercial fishing, using specialized gillnets, in the Romanian coastal waters of the Black Sea, Sf. Gheorghe, Tulcea county.

Figure 1. Sample collection from the studied biological material (*Scophthalmus maeoticus)*

The biological material was stored in polyethylene bags and kept on ice until transportation to the laboratory within the REXDAN Research Infrastructure, where samples of muscle tissue were processed in triplicate (Figure 1).
The biometric measurements were determined for each fish specimen and the results are presented as average ± standard deviation in Table 1.
All the extracted samples were subjected to the digestion process with suprapure reagents (nitric acid and hydrogen peroxide) and the final aqueous solution was analysed by inductively coupled plasma with mass spectrometry (ICP-MS) with the Perkin Elmer NexION 2000 equipment (Figures 2 and 3).

Table 1. Biometric measurements of the biological material

Indicator	Value
Total length (cm)	37 ± 2.75
Total weight (g)	1.4 ± 0.12

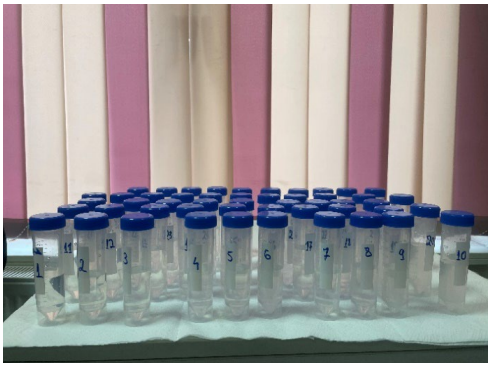

Figure 2. Sample preparation through microwave digestion

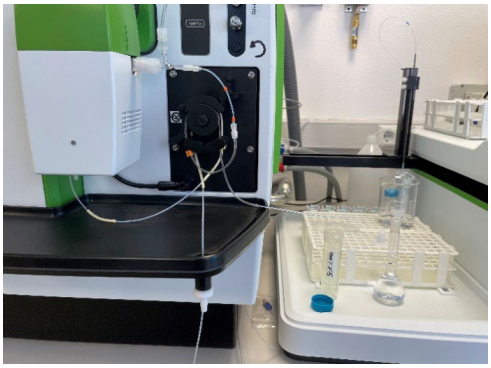

Figure 3. Sample analysis through ICP-MS technique

The following elements were quantified in the muscle tissue of the Black Sea turbot: Na, K, Mg, Ca, Fe, Zn, Cu, Ni, Cr, Mn, Pb, Cd and Co.

RESULTS AND DISCUSSIONS

The concentration of macroelements in the turbot muscle registered the following decreasing trend Na>K>Ca>Mg (Figure 4). As it is expected, the highest concentration was registered in case of the macroelement Na (735.96 ± 115 µg/g fresh weight). Na is involved in the normal function of the muscle by maintaining an adequate blood pressure (Din et al., 2015; Stoyanova, 2018).

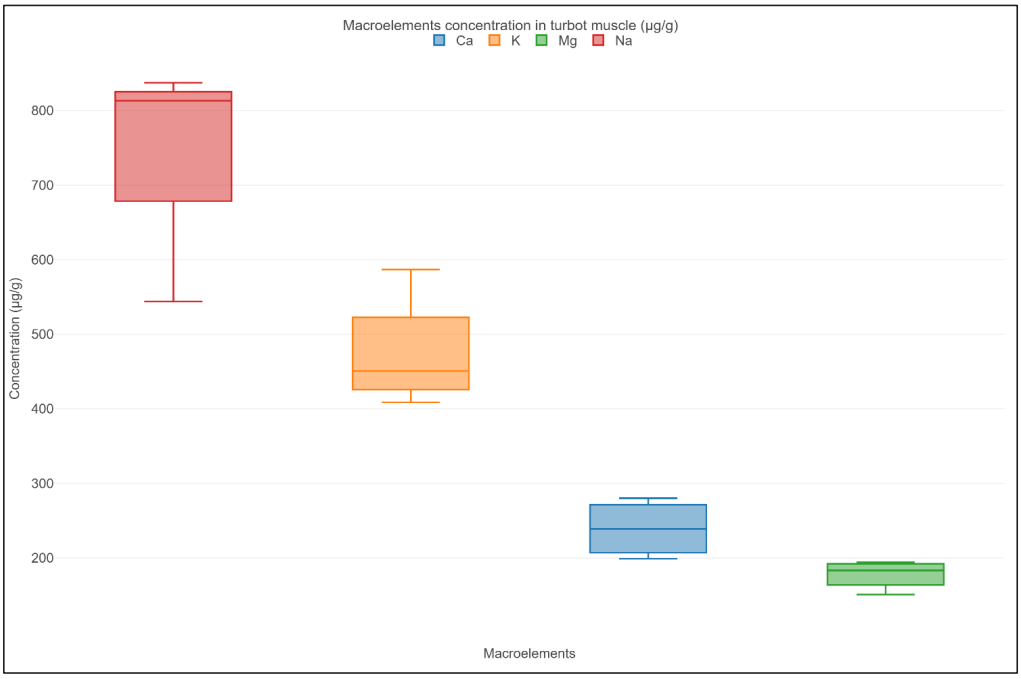

Figure 4. Boxplot representation of macroelements concentration in turbot muscle

Following, the second highest concentration was registered in case of K concentration (474.29 ± 67 µg/g fresh weight). As well as Na, K is involved in the contraction of the muscles, and at the same time, in responsible for maintaining the fish osmoregulation balance (Lall & Kaushik, 2021; Wen et al., 2021; Presas-Basalo, 2022).

Further on, the Ca concentration in the muscle of Black Sea turbot registered an average value of 239.22 ± 33 µg/kg. According to (Hrynevych et al., 2022), there is a positive correlation between Ca accumulation in fish muscle and water temperature.

The Zn concentration in the muscle tissue of the studied biological material registered an average value of 9.01 ± 0.4 µg/g fresh weight (Figure 5). Considering Fe concentration, the analysis of muscle tissue of Black Sea turbot indicated a value of 1.93 ± 0.33 µg/g fresh weight (Figure 5).

Fe and Zn are essential elements involved in fish metabolism. For instance, Fe is part of the haemoglobin protein, which is responsible for the transport of oxygen, while Zn is part of several metalloenzymes in fish (Zhao et al., 2014; Silva et al., 2019; Abd-Elhamed et al., 2021.

The concentration of Cu registered an average value of 0.21 ± 0.06 µg/g fresh weight in the muscle tissue of the studied biological material, while Mn registered a mean value of 0.13 ± 0.01 µg/g fresh weight (Figure 6). As well as Fe, Cu is an essential element of fish erythrocytes (Kamunde et al., 2002; Malhotra et al., 2020).

At the same time, Mn is involved in enzymatic activities and anti-oxidant processes (Antony Jesu Prabhu et al., 2019; Zhou et al., 2022).

Regarding the concentration of Ni, the mean registered value in the muscle of the Black Sea turbot was 0.07 ± 0.02 µg/g fresh weight. In case of Cd and Pb concentrations, the average value in the muscle was 0.02±0.001 µg/g fresh weight and 0.01 ± 0.001 µg/g fresh weight respectively. Ni essentiality in fish has been speculated, however no evidence has been found to support that hypothesis (Muyssen et al., 2011; Blewett & Leonard, 2017). Therefore, it could be considered that trace amounts of Ni, Cd and Pb, which have no biological role in the fish organism can negatively influence fish growth and welfare.

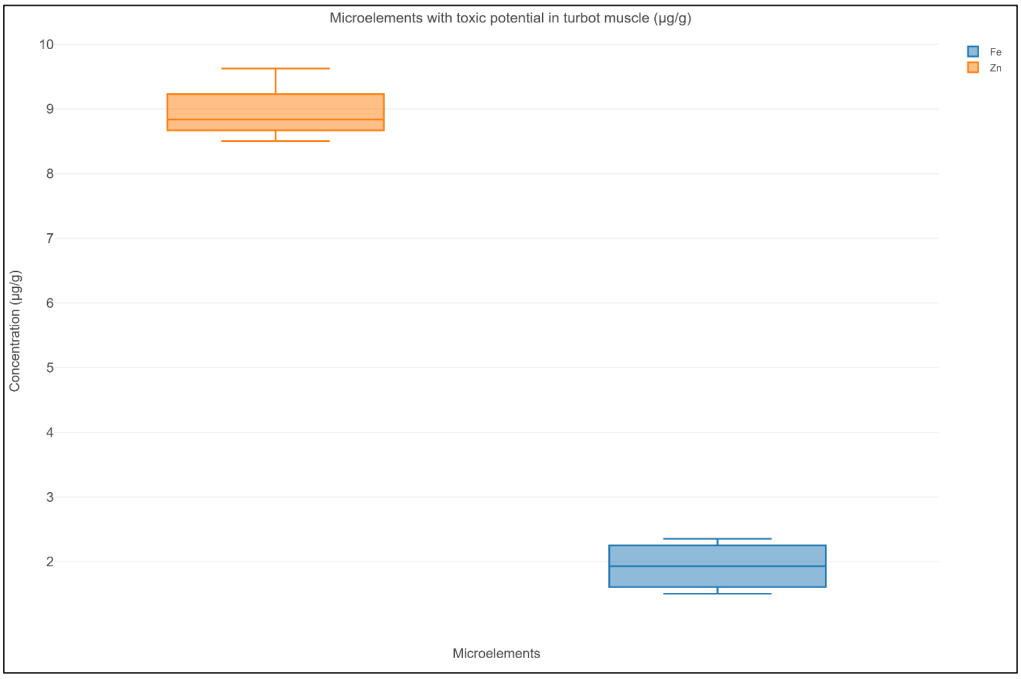

Figure 5. Boxplot representation of microelements concentration in turbot muscle

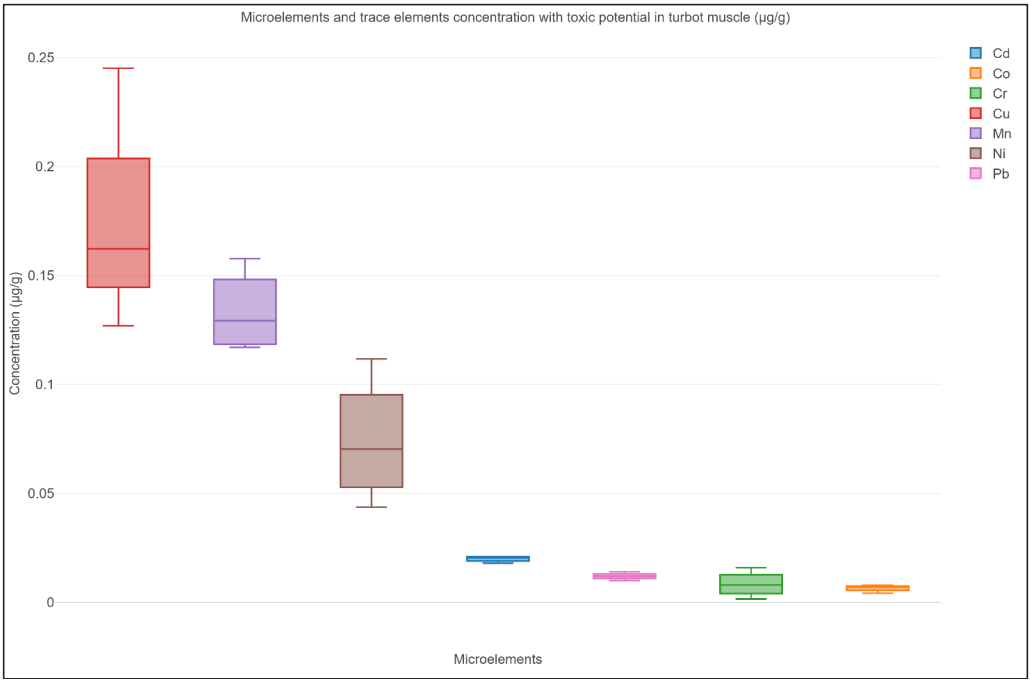

Figure 6. Boxplot representation of microelements concentration in turbot muscle

The lowest concentrations of elements in the muscle tissue of the Black Sea turbot were registered in case of Cr and Co respectively, with mean values of 0.008 ± 0.00 µg/g fresh weight and 0.007 ± 0.00 µg/g fresh weight respectively (Figure 6).

Chromium is boots insulin activity and holds an essential role in the glucose metabolism, whilst cobalt is part of B_{12} vitamin (Blust, 2011; Zhang et al., 2022).

The correlation matrix (Figure 7) highlights the positive relationship between the following elements: Cr-Co (0.57), Ni-Mn (0.59), Ni-K (0.97), Cu-K (0.8), Zn-Cr (0.81), Fe-Cr (0.81), Cu-Cr (0.63), Cu-Ni (0.74), Zn-Ca (0.75), Na-Ca (0.87), Fe-Ca (0.54), Fe-Cu (0.9), Na-Cu (0.57), Zn-Cu (0.73), Ca-Zn (0.75), Zn-Fe (0.95), Na-Fe (0.71).

As well, in Figure 7 it can be observed the following negative correlations between elements in the muscle tissue of the Black Sea turbot:

Mn-Co (-0.87), K-Cd (-0.93), K-Mg (-0.89), Cr-Pb (-0.64), Cr-Mn (-0.68), Ca-Pb (-0.86), Ca-Co (-0.6), Cu-Pb (-0.66), Cu-Cd (-0.91), Cu-Mg (-0.9), Zn-Pb (-0.97), Na-Pb (-0.9), Fe-Pb (-0.89), Fe-Cd (-0.66), Fe-Mg (-0.66).

Further on, as it can be observed in Figure 8, the PCA matrix confirms the positive and negative correlations between elements. Withal, the PCA analysis explains 77.1% of the data, which are distributed in 2 groups.

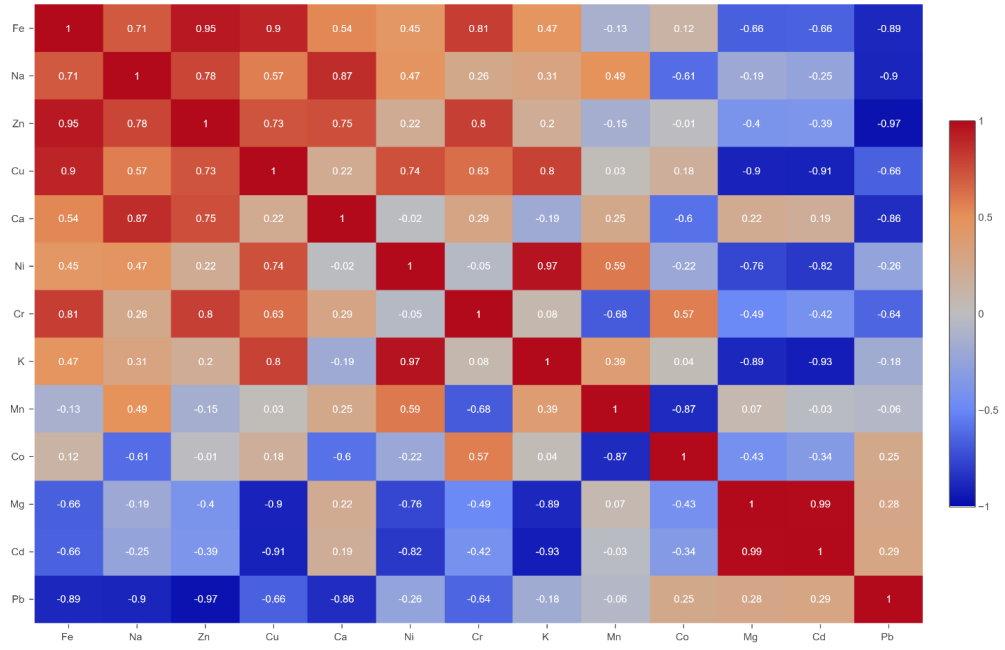

Figure 7. Correlation matrix of elements in the muscle tissue of the Black Sea turbot

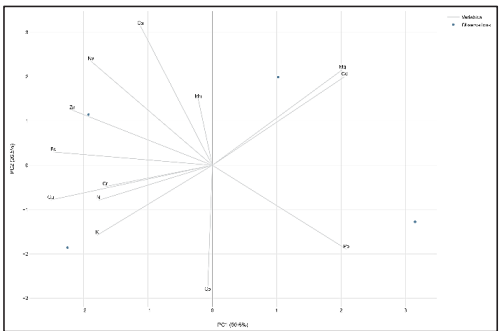

Figure. 8. Principal component analysis of elements in the Black Sea turbot

CONCLUSIONS

The main conclusion of this research is that the Black Sea turbot is an important source of essential macronutrients such as Ca, Mg, K, Na and micronutrients such as Fe, Zn, Cu, Mn, Cr and Co. At the same time, the Black Sea turbot can also be a source of non-essential elements, with toxic potential in the human diet, such as Ni, Cd and Pb.

The following accumulation trend in Black Sea turbot muscle was identified: Na>K>Ca>Mg>Zn>Fe>Cu>Mn>Ni>Cd>Pb> Cr>Co.

Competition between elements has been identified through correlation and PCA analysis, especially between K and Cd, Mg and Cu, Ca and Pb, Na and Pb.

ACKNOWLEDGEMENTS

The present research was supported by the project An Integrated System for the Complex Environmental Research and Monitoring in the Danube River Area, REXDAN, SMIS code 127065, co-financed by the European Regional Development Fund through the Competitiveness Operational Programme 2014-2020, contract no. 309/10.07.2021.

This work was supported by the Fondo Proserpina S.R.L., grant number 2506/2022, "The impact of heavy metals and microplastics from aquatic organisms on human health".

REFERENCES

Abd-Elhamed, M. (2021). Applying Nano-technology in tilapia Nutrition: Influence of Iron and Zinc nanoparticles as dietary supplementary on biological performance and body composition of Oreochromis niloticus fry. *Mediterranean Aquaculture Journal*, *8*(1), 30–41. https://doi.org/10.21608/maj.2021.225673

Antony Jesu Prabhu, P., Silva, M. S., Kröeckel, S., Holme, M.-H., Ørnsrud, R., Amlund, H., Lock, E.-J., &Waagbø, R. (2019). Effect of levels and sources of dietary manganese on growth and mineral composition of post-smolt Atlantic salmon fed low fish meal, plant-based ingredient diets. *Aquaculture*, *512*, 734287. https://doi.org/10.1016/j.aquaculture.2019.734287

Blewett, T. A., & Leonard, E. M. (2017). Mechanisms of nickel toxicity to fish and invertebrates in marine and estuarine waters. *Environmental Pollution*, *223*, 311–322. https://doi.org/10.1016/j.envpol.2017.01.028

Blust, R. (2011). 6—Cobalt. In C. M. Wood, A. P. Farrell, & C. J. Brauner (Eds.), *Fish Physiology* (Vol. 31, pp. 291–326). Academic Press. https://doi.org/10.1016/S1546-5098(11)31006-0

Din, N., Nazeer, N., Masood, Z., & Ullah, A. (2015). *The Levels of Some Selected Metals in Muscle's Tissues of Three Commercially Important Edible Fishes Collected from the Fish Market of Quetta City in Balochistan Province*.

Firidin, S., Ozturk, R. C., Alemdag, M., Eroglu, O., Terzi, Y., Kutlu, I., Duzgunes, Z. D., Cakmak, E., & Aydin, I. (2020). Population genetic structure of turbot (*Scophthalmus maximus* L., 1758) in the Black Sea. *Journal of Fish Biology*, *97*(4), 1154–1164. https://doi.org/10.1111/jfb.14487

Giragosov, V., &Khanaychenko, A. (2012). The State-of-Art of the Black Sea Turbot Spawning Population off Crimea (1998-2010). *Turkish Journal of Fisheries and Aquatic Sciences*, *12*(5), 377–383.

Hrynevych, N., Svitelskyi, M., Solomatina, V., Ishchuk, O., Matkovska, S., Sliusarenko, A., Khomiak, O., Trofymchuk, A., Pukalo, P., &Zharchynska, V. (2022). Acclimatization of fish to the higher calcium levels in the water environment. *Potravinarstvo Slovak Journal of Food Sciences*, *16*, 101–113. https://doi.org/10.5219/1732

Hulak, B., Leonchyk, Y., Maximov, V., Tiganov, G., Shlyakhov, V., &Pyatnitsky, M. (2021). The current state of the turbot, (Linnaeus, 1758), population in the northwestern part of the Black Sea. *Fisheries & Aquatic Life*, *29*(3), 164–175. https://doi.org/10.2478/aopf-2021-0018

Ivanova, P., Dzhembekova, N., Atanassov, I., Rusanov, K., Raykov, V., Zlateva, I., Yankova, M., Raev, Y., &Nikolov, G. (2021). Genetic diversity and morphological characterisation of three turbot (*Scophthalmus maximus* L., 1758) populations along the Bulgarian Black Sea coast. *Nature Conservation*, *43*, 123–146. https://doi.org/10.3897/natureconservation.43.64195

Kamunde, C., Grosell, M., Higgs, D., & Wood, C. M. (2002). Copper metabolism in actively growing rainbow trout (Oncorhynchus mykiss): Interactions between dietary and waterborne copper uptake. *Journal of Experimental Biology*, *205*(2), 279–290. https://doi.org/10.1242/jeb.205.2.279

Khanaychenko, A. N., &Giragosov, V. E. (2019). Morphological features of the Black Sea turbot (*Scophthalmus maeoticus*) during the period of embryonic development. *Marine Biological Journal*, *4*(4), Article 4. https://doi.org/10.21072/mbj.2019.04.4.06

Lall, S. P., & Kaushik, S. J. (2021). Nutrition and Metabolism of Minerals in Fish. *Animals : An Open Access Journal from MDPI*, *11*(9), 2711. https://doi.org/10.3390/ani11092711

Liu, W., Wang, Q., Mei, J., &Xie, J. (2021). Shelf-Life Extension of Refrigerated Turbot (*Scophthalmus maximus*) by Using Weakly Acidic Electrolyzed Water and Active Coatings Containing Daphnetin Emulsions. *Frontiers in Nutrition*, *8*. https://www.frontiersin.org/articles/10.3389/fnut.2021.696212

Ma, A., Huang, Z., Wang, X., Xu, Y., & Guo, X. (2021). Identification of quantitative trait loci associated with upper temperature tolerance in turbot, *Scophthalmus maximus*. *Scientific Reports*, *11*(1), Article 1. https://doi.org/10.1038/s41598-021-01062-3

Malhotra, N., Ger, T.-R., Uapipatanakul, B., Huang, J.-C., Chen, K. H.-C., & Hsiao, C.-D. (2020). Review of Copper and Copper Nanoparticle Toxicity in Fish. *Nanomaterials*, *10*(6), 1126. https://doi.org/10.3390/nano10061126

Manthey-Karl, M., Lehmann, I., Ostermeyer, U., &Schröder, U. (2016). Natural Chemical Composition of Commercial Fish Species: Characterisation of Pangasius, Wild and Farmed Turbot and Barramundi. *Foods*, *5*(3), Article 3. https://doi.org/10.3390/foods5030058

Marchetti, C. (2013). Role of Calcium Channels in Heavy Metal Toxicity. *ISRN Toxicology*, *2013*, 184360. https://doi.org/10.1155/2013/184360

Massa, F., Aydın, I., Fezzardi, D., Akbulut, B., Atanasoff, A., Beken, A. T., Bekh, V., Buhlak, Y., Burlachenko, I., Can, E., Carboni, S., Caruso, F., Dağtekin, M., Demianenko, K., Deniz, H., Fidan, D., Fourdain, L., Frederiksen, M., Guchmanidze, A., Yücel-Gier, G. (2021). Black Sea Aquaculture: Legacy, Challenges & Future Opportunities. *Aquaculture Studies*, *21*(4). https://www.aquast.org/abstract.php?lang=en&id=524

Muyssen, B. T. A., Brix, K. V., DeForest, D. K., & Janssen, C. R. (2011). Nickel essentiality and homeostasis in aquatic organisms. *Environmental Reviews*. https://doi.org/10.1139/a04-004

Pouil, S., Warnau, M., Oberhänsli, F., Teyssié, J.-L., Bustamante, P., &Metian, M. (2016). Influence of food on the assimilation of essential elements (Co, Mn, and Zn) by turbot *Scophthalmus maximus*. *Marine Ecology Progress Series*, *550*, 207–218. https://doi.org/10.3354/meps11716

Presas-Basalo, F. X. (2022). Potassium Homeostasis and Fish Welfare in Coupled Aquaponic Systems. *Fisheries and Aquaculture Journal*, *13*(2), 1–5.

Silva, M. S., Sele, V., Sloth, J. J., Araujo, P., &Amlund, H. (2019). Speciation of zinc in fish feed by size exclusion chromatography coupled to inductively coupled plasma mass spectrometry – using fractional factorial design for method optimisation and mild extraction conditions. *Journal of Chromatography B*, *1104*, 262–268. https://doi.org/10.1016/j.jchromb.2018.11.010

Stoyanova, S. (2018). *Investigation of macroelements in the muscle of four marine fish species*. *6*(2), 219–222.

Turan, C., Ivanova, P. P., Raykov, V. S., Gurlek, M., Erguden, D., Yaglioglu, D., Karan, S., Dogdu, S. A., Uyan, A., Ozturk, B., Nikolov, V., Dobrovolov, I., Khanaychenko, A., &Giragosov, V. (2019). Genetics Structure Analysis of Turbot (Scophthalmus maximus, Linnaeus, 1758) in the Black and Mediterranean Seas for Application of Innovative Management Strategies. *Frontiers in Marine Science*, *6*. https://www.frontiersin.org/articles/10.3389/fmars.2019.00740

Ulman, A., Zengin, M., Demirel, N., & Pauly, D. (2020). The Lost Fish of Turkey: A Recent History of Disappeared Species and Commercial Fishery Extinctions for the Turkish Marmara and Black Seas. *Frontiers in Marine Science*, *7*. https://www.frontiersin.org/articles/10.3389/fmars.2020.00650

Wen, Z.-Y., Qin, C.-J., Lv, Y.-Y., Li, Y.-P., Zou, Y.-C., Guo, S.-T., & Shi, Q. (2021). Homeostasis Regulation by Potassium Channel Subfamily K Member 3 (KCNK3) in Various Fishes. *Frontiers in Marine Science*, *8*. https://www.frontiersin.org/articles/10.3389/fmars.2021.816861

Zhang, Y., Luo, J., Zhu, T., Zhang, X., Jin, M., Jiao, L., Meng, F., Figueiredo-Silva, C., Hong, Y., & Zhou, Q. (2022). Dietary chromium could improve growth, antioxidant capacity, chromium accumulation in tissues and expression of genes involved into glucose and lipid metabolism in juvenile mud crab *Scylla paramamosain*. *Aquaculture Reports*, *23*, 101088. https://doi.org/10.1016/j.aqrep.2022.101088

Zhao, L., Xia, Z., & Wang, F. (2014). Zebrafish in the sea of mineral (iron, zinc, and copper) metabolism. *Frontiers in Pharmacology*, *5*. https://www.frontiersin.org/articles/10.3389/fphar.2014.00033

Zhou, M., Zhang, Y., Wang, J., Shi, Y., & Puig, V. (2022). Water Quality Indicator Interval Prediction in Wastewater Treatment Process Based on the Improved BES-LSSVM Algorithm. *Sensors*, *22*(2), Article 2. https://doi.org/10.3390/s22020422

Scientific Papers. Series E. Land Reclamation, Earth Observation & Surveying, Environmental Engineering. Vol. XII, 2023
Print ISSN 2285-6064, CD-ROM ISSN 2285-6072, Online ISSN 2393-5138, ISSN-L 2285-6064

STUDY ON MICROPLASTICS OCCURRENCE IN THE LOWER DANUBE RIVER WATER

Madalina CALMUC, Valentina Andreea CALMUC, Nina Nicoleta CONDURACHE, Maxim ARSENI, Ira-Adeline SIMIONOV, Mihaela TIMOFTI, Puiu-Lucian GEORGESCU, Catalina ITICESCU

"Dunarea de Jos" University of Galati, REXDAN Research Infrastructure,
98 George Cosbuc Street, Galati, Romania

Corresponding author email: madalina.calmuc@ugal.ro

Abstract

Microplastics are considered emerging pollutants of growing concern due to their ubiquitous presence and toxic potential in the aquatic ecosystem. However, there are few studies assessing the occurrence of microplastics in freshwaters, most articles are focused rather on the marine environment. Due to the lack of standardized protocols for separating and analyzing microplastics, different methods are described in the literature data. In this paper, FT-IR spectrometry coupled with microscopy (micro-FT-IR) was applied to identify the presence of microplastics in the Predeltaic sector of the Danube River. Based on the morphological classification, the microplastics collected were fragments, films, and fibers. The results of micro-FT-IR analysis confirmed the majority presence of polyethylene and polypropylene-based microplastic particles in water.

Key words*: emerging pollutant, freshwater, micro-FT-IR, Lower Danube water.*

INTRODUCTION

Microplastics (MPs) are plastic fragments smaller than 5 mm classified based on their origin into primary and secondary microplastics (Eerkes-Medrano et al., 2015; Li et al., 2018; Wagner et al., 2014).

Primary MPs are manufactured at the microscale for use in various industrial applications such as personal care products and plastic pre-production pellets.

Secondary MPs result from the degradation of larger plastic waste (meso and macro) under the influence of environmental conditions (e.g. UV radiation, high temperatures, mechanical and biological factors) (Cera et al., 2020; Horton et al., 2017).

Due to their ubiquity and toxicity in the aquatic ecosystem, MPs are considered to be emerging contaminants (Lambert and Wagner, 2018). According to Ding et al., 2021, the toxic potential of microplastics in freshwater is given by the following two behaviours:

a) Size and shape of MPs can cause physical and histophysiological injury;
b) MPs are transport vectors for other types of organic and inorganic pollutants. MPs in combination with these contaminants cause synergistic effects in organisms.

Regarding the microplastics assessment protocol in freshwaters, there are no standardized methods of sampling, isolation, identification, and quantification of microplastics. To this end, it is required to develop a standardized protocol that allows an objective comparison and evaluation of the results from various places and times (Rios Mendoza & Balcer, 2019; Razeghi et al., 2022). Although the first studies on the presence of microplastics in marine environments were published in the 1970s, research on microplastic occurrence in freshwaters began about 15 years ago (Talbot & Chang, 2022). This subject should not be ignored given that rivers are now known to play a crucial role in microplastic transport in marine ecosystems (Sarijan et al., 2021).

The main aim of this paper is to evaluate the occurrence of microplastics in the second longest river in Europe, namely the Danube River. More specifically, the Predeltaic sector of the Danube, which is the transport pathway of microplastics into the Black Sea, was investigated.

MATERIALS AND METHODS

The microplastics were taken from the following three stations located on the Romanian Lower Danube sector (Figure 1):

- P1 - the confluence of the Siret River with the Danube;
- P2 - the confluence of the Prut River with the Danube;
- P3 - the riverside sector of the city of Isaccea.

Figure 1. Microplastic sampling stations

The samples were collected from the surface layer of the water (0-15 cm) using a sampling equipment consisting of a pump with a flow rate of 5 litres/second and a net with 125 µm mesh (Figure 2). The total volume of filtered water was 10 m^3. The main advantages of this type of sampling equipment are that samples can be taken from different depths of the water column and the filtered water volume is known.

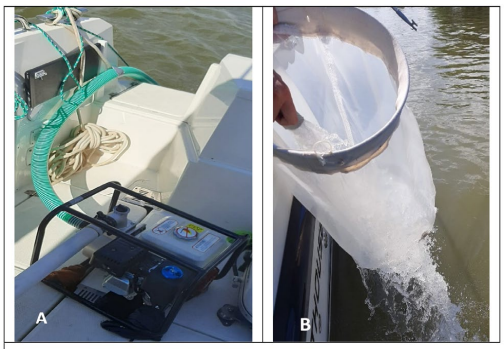

Figure 2. Microplastics sampling equipment
(A - pump and B - net)

After the samples were taken, they were transported to the laboratory to isolate the microplastics. The organic matter was removed using KOH 10M and H_2O_2 30%. The separation from the other impurities was carried out in the separation funnel with zinc chloride ($ZnCl_2$) 60-70% (Pojar et al., 2021; Călmuc et al., 2022). The microplastic supernatant was filtered using a vacuum pump filtration system on a glass fibre filter paper with a diameter of 47 mm and pore size of 2 µm (Figure 3).

Figure 3. Collection of microplastics on filter paper

In order to identify and confirm the occurrence of the microplastics, the Spotlight 400 FT-IR Imaging System (micro-FT-IR), PerkinElmer from the Spectrometry laboratory of the REXDAN Research Infrastructure, "Dunarea de Jos" University of Galati, Romania was used (Figure 4).

The parameters of the micro-FT-IR analysis method applied in this study were as follows:

- Spectral range: 4000 -750 cm^{-1};
- Resolution: 16 cm^{-1};
- Scans per pixel: 2;
- Interferometer speed:1 cm/s;
- Pixel size: 25 µm.

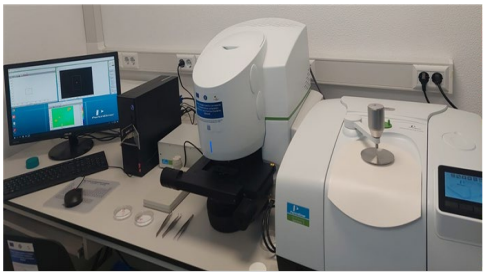

Figure 4. Micro-FT-IR analysis of microplastics

RESULTS AND DISCUSSIONS

Figures 5, 6, and 7 illustrate the microplastics isolated from the three samples collected. The abundance of microplastics in station P1 was 9 particles per 10 m^3 of which, based on the morphological characteristics (Rosal, 2021; Xu et al., 2021), 8 were fragments and one fiber (Figure 8).

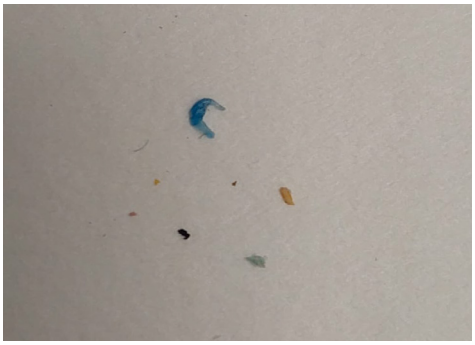

Figure 5. Microplastics collected from P1 sampling station

Most microplastics were collected from site P2, respectively 20 microplastics per 10 m^3 were extracted, the majority being fragments (15), and the rest fibers (3) and films (2). This sampling station is located at the confluence of the Prut River with the Danube, which has an important contribution to the Danube quality as it crosses many urban agglomerations on both the Romanian and Moldavian territory.

Figure 6. Microplastics collected from P2 sampling station

From station P3, 12 microplastics were sampled including 10 fragments, one film and one fiber. Information on the shape of microplastics is essential since they can suggest their origin, implicitly the sources of pollution. For example, the fragments are produced by the breakage of plastic waste in the presence of UV radiation and mechanical forces. The films are the result of the fragmentation of plastic bags and vinyl used in agriculture. Also, the fibers can be originated from de fishery field (nets and ropes) and municipal sewage discharge (laundry washing) (Kye et al., 2023).

Figure 7. Microplastics collected from P3 sampling station

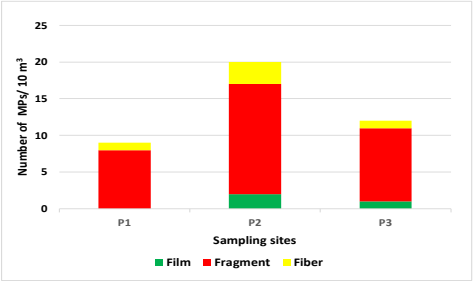

Figure 8. Abundance and morphological classification of MPs

Regarding the colour of the microplastics, they had different colours such as: blue, red, black, yellow, green, transparent. Also, the colour of microplastics can be an important indicator in terms of establishing pollution sources (Li et al., 2021).

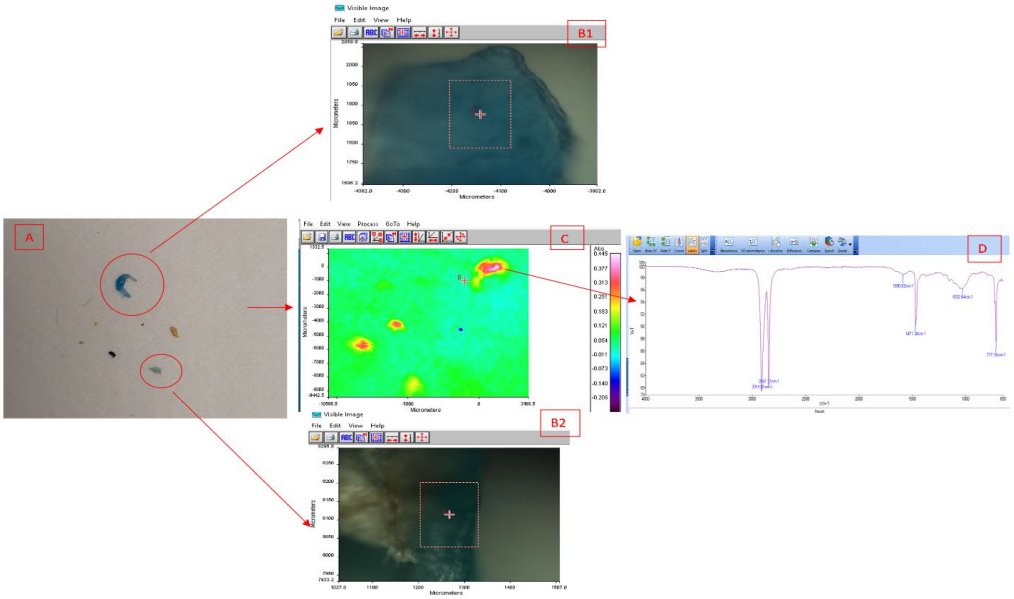

Figure 9. Micro-FT-IR microplastics analysis results (A - P1 microplastic sample, B1 and B2 - Visible images of MP, C - micro FT- IR spectral image of the sample, D - FT-IR spectrum of MP)

Figure 9 shows the diagram regarding the stages of microplastics analysis using the micro-FT-IR equipment. the filter paper with microplastics (A) was placed on microscope stage and was preliminarily investigated in the visible spectrum.

Visible images of MPs (B1 and B2) were analysed to establish the morphological characteristics such as shape, colour, size of the MP. Then, the sample was scanned in the IR range to confirm the presence of microplastics and to determine their composition. At the end of the analysis, the spectral image of the sample was obtained (C) and the IR spectra were extracted (D) for the areas where changes in absorbance were detected.

IR spectra were compared with Spectra Databases for polymers - S.T. Japan Europe GmbH to identify the type of polymers in the MPs composition (Figure 11).

Polypropylene (PE) and polyethylene (PP) polymers were mostly found in all three sampling stations (Figure 10). Sporadically, polystyrene (PS) was also identified.

The PE, PP and PS polymers are commonly used to manufacture different packaging materials (bags, bottles), films, building materials, and coatings (Andrady, 2011; Uurasjärvi et al., 2020).

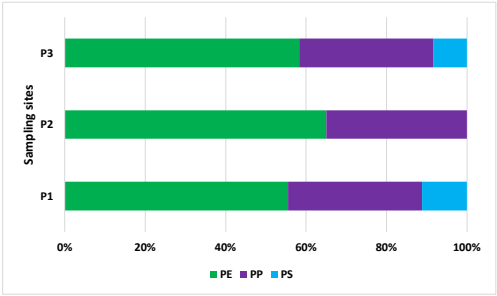

Figure 10. The type of polymers identified

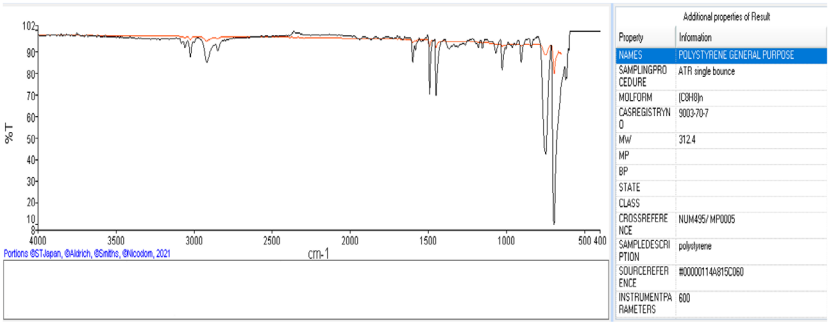

Figure 11. IR spectra of polystyrene

CONCLUSIONS

The microplastics occurrence in the Predeltaic sector of the Lower Danube was studied in this paper. A pump-type equipment was used to collect the microplastics from the surface of the water in three sampling stations.

Regarding the abundance of microplastics, most were taken from the P2 site (20 microplastic per 10 m^3), which was located at the confluence of the Prut River with the Danube River. Based on the morphological criteria, most MPs were fragments.

Micro-FT-IR spectroscopy was applied in this study to confirm the presence of microplastics and identify the type of polymers in their composition. The most identified polymers were polyethylene and polypropylene.

According to the results obtained in this study, it can be concluded that the methods applied were suitable in assessing the occurrence of microplastics in the investigated Danube sector.

ACKNOWLEDGEMENTS

The present article was supported by the project An Integrated System for the Complex Environmental Research and Monitoring in the Danube River Area, REXDAN, SMIS code 127065, co-financed by the European Regional Development Fund through the Competitiveness Operational Programme 2014-2020, contract no. 309/10.07.2021.

REFERENCES

Andrady, A.L. (2011). Microplastics in the marine environment. *Mar. Pollut. Bull., 62*, 1596–1605. https://doi.org/10.1016/j.marpolbul.2011.05.030

Călmuc, M., Călmuc, V.A., Arseni, M., Simionov, I.A., Antache, A., Apetrei, C., Georgescu, P.L., Iticescu, C. (2022). Identification and characterization of plastic particles found in the Lower Danube River. *Scientific Papers. Series E. Land Reclamation, Earth Observation & Surveying, Environmental Engineering, XI., 332 - 337.*

Cera, A., Cesarini, G., Scalici, M. (2020). Microplastics in Freshwater: What Is the News from the World? *Diversity, 12*, 276. https://doi.org/10.3390/d12070276

Ding, R., Tong, L., Zhang, W. (2021). Microplastics in Freshwater Environments: Sources, Fates and Toxicity. *Water. Air. Soil Pollut., 232*, 181. https://doi.org/10.1007/s11270-021-05081-8

Eerkes-Medrano, D., Thompson, R.C., Aldridge, D.C. (2015). Microplastics in freshwater systems: A review of the emerging threats, identification of knowledge gaps and prioritisation of research needs. *Water Res., 75*, 63–82. https://doi.org/10.1016/j.watres.2015.02.012

Horton, A.A., Walton, A., Spurgeon, D.J., Lahive, E., Svendsen, C. (2017). Microplastics in freshwater and terrestrial environments: Evaluating the current understanding to identify the knowledge gaps and future research priorities. *Sci. Total Environ., 586*, 127–141. https://doi.org/10.1016/j.scitotenv.2017.01.190

Kye, H., Kim, J., Ju, S., Lee, J., Lim, C., Yoon, Y. (2023). Microplastics in water systems: A review of their impacts on the environment and their potential hazards. *Heliyon, 9*, e14359. https://doi.org/10.1016/j.heliyon.2023.e14359

Lambert, S., Wagner, M. (2018). Microplastics Are Contaminants of Emerging Concern in Freshwater Environments: An Overview, in: Wagner, M., Lambert, S. (Eds.), Freshwater Microplastics, The Handbook of Environmental Chemistry. Springer International Publishing, Cham, pp. 1–23. https://doi.org/10.1007/978-3-319-61615-5_1

Li, C., Gan, Y., Zhang, C., He, H., Fang, J., Wang, L., Wang, Y., Liu, J. (2021). "Microplastic communities" in different environments: Differences, links, and role of diversity index in source analysis. *Water Res., 188*, 116574. https://doi.org/10.1016/j.watres.2020.116574

Li, J., Liu, H., Paul Chen, J. (2018). Microplastics in freshwater systems: A review on occurrence, environmental effects, and methods for microplastics

detection. *Water Res., 137*, 362–374. https://doi.org/10.1016/j.watres.2017.12.056

Pojar, I., Kochleus, C., Dierkes, G., Ehlers, S.M., Reifferscheid, G., Stock, F. (2021). Quantitative and qualitative evaluation of plastic particles in surface waters of the Western Black Sea. Environ. *Pollut., 268*, 115724. https://doi.org/10.1016/j.envpol.2020.115724

Razeghi, N., Hamidian, A.H., Mirzajani, A., Abbasi, S., Wu, C., Zhang, Y., Yang, M. (2022). Sample preparation methods for the analysis of microplastics in freshwater ecosystems: a review. *Environ. Chem. Lett., 20*, 417–443. https://doi.org/10.1007/s10311-021-01341-5

Rios Mendoza, L.M., Balcer, M. (2019). Microplastics in freshwater environments: A review of quantification assessment. T*rAC Trends Anal. Chem., 113*, 402–408. https://doi.org/10.1016/j.trac.2018.10.020

Rosal, R. (2021). Morphological description of microplastic particles for environmental fate studies. *Mar. Pollut. Bull., 171*, 112716. https://doi.org/10.1016/j.marpolbul.2021.112716

Talbot, R., Chang, H. (2022). Microplastics in freshwater: A global review of factors affecting spatial and temporal variations. *Environ. Pollut., 292*, 118393. https://doi.org/10.1016/j.envpol.2021.11839.

Uurasjärvi, E., Hartikainen, S., Setälä, O., Lehtiniemi, M., Koistinen, A. (2020). Microplastic concentrations, size distribution, and polymer types in the surface waters of a northern European lake. *Water Environ. Res., 92*, 149–156. https://doi.org/10.1002/wer.1229

Wagner, M., Scherer, C., Alvarez-Muñoz, D., Brennholt, N., Bourrain, X., Buchinger, S., Fries, E., Grosbois, C., Klasmeier, J., Marti, T., Rodriguez-Mozaz, S., Urbatzka, R., Vethaak, A.D., Winther-Nielsen, M., Reifferscheid, G. (2014). Microplastics in freshwater ecosystems: what we know and what we need to know. *Environ. Sci. Eur., 26*, 12. https://doi.org/10.1186/s12302-014-0012-7

Xu, X., Zhang, L., Xue, Y., Gao, Y., Wang, L., Peng, M.,Jiang, S., Zhang, Q. (2021). Microplastic pollution characteristic in surface water and freshwater fish of Gehu Lake, China. *Environ. Sci. Pollut. Res., 28*, 67203–67213. https://doi.org/10.1007/s11356-021-15338-8

Scientific Papers. Series E. Land Reclamation, Earth Observation & Surveying, Environmental Engineering. Vol. XII, 2023
Print ISSN 2285-6064, CD-ROM ISSN 2285-6072, Online ISSN 2393-5138, ISSN-L 2285-6064

PRELIMINARY REPORT ON THE WATER QUALITY, ICHTHYOFAUNA AND BIOMETRIC INDICES FOR PRUSSIAN CARP FROM IEZERUL MOSTIȘTEA LAKE, ROMANIA

Mala-Maria STAVRESCU-BEDIVAN[1], Mirela Alina SANDU[2], Gina VASILE SCĂEȚEANU[1], Ana VÎRSTA[2], Roxana Maria MADJAR[1], Ștefania BAICU[1]

[1]University of Agronomic Sciences and Veterinary Medicine of Bucharest, Faculty of Agriculture, 59 Marasti Blvd, District 1, Bucharest, Romania
[2]University of Agronomic Sciences and Veterinary Medicine of Bucharest, Faculty of Land Reclamation and Environmental Engineering, 59 Marasti Blvd, District 1, Bucharest, Romania

Corresponding author email: rmadjar@gmail.com

Abstract

*Summarizing so far personal observations dated April 2023 and knowledge among anglers concerning the ichthyofauna of Iezerul Mostiștea located in Călărași County, was established that this ecosystem host 18 edible species. This paper analyzes for the first-time weight-length relationships, Fulton's condition factor and the size structure for Prussian carp in relation to water quality from Mostiștea Lake. A positive allometric growth pattern was estimated for Carassius gibelio: $TW = 0.0148TL^{3.3097}$ (coefficient of determination $R^2 = 0.9803$), $TW = 0.0046SL^{3.4855}$ ($R^2 = 0.977$). The values for length ranged between 7.8 and 21.1 (average 11) cm for TL, 6 and 17.4 (average 8.77) cm for SL, while total weight varied from 5 to 174 (average 23.76) grams. Condition factor ranged between 1.05 and 1.86. Eustrongylides spp. and Philometroides sanguineus were also recorded. Water samples collected from three sampling points were subjected to physico-chemical characterization and based on results water was classified in quality classes. Total hardness values present very significant correlations with electrical conductivity (r=0.8814***) and pH (r=0.9183***). The determined parameters indicated that the water quality is optimal for the development of aquatic organisms.*

Keywords*: Carassius gibelio, fish species, Mostistea, water quality, weight-length relationship.*

INTRODUCTION

Iezerul Mostiștea is an artificial lake, part of a rich network of reservoirs with multiple functions, e.g., water supply, fishing ponds, irrigation, recreation, created in the Mostiștea hydrographic basin located in the Eastern Romanian Plain (Ghiță, 2008). In a technical paper regarding the inland fisheries of Europe, Dill (1993) mentioned "Mostiștea" from Călărași County among principal River lagoons from Romania.

Previous approaches of Mostiștea Valley have emphasized the importance of this micro-region in terms of archeological discoveries and cultural heritage (Covătaru et al., 2022), wetland for protected bird species (Tanislav, 2014) or mapping hydrogeomorphological hazard (Grecu et al., 2013).

Even though Mostiștea Lake was included in Natura 2000 site ROSPA0105 Valea Mostiștei (Mostiștei Valley), providing the framework for practicing water sports, fishing and wildlife observing (https://ceddu.ro/), few data have been published about its ichthyofauna until now. Thus, in an integrated diagnostic study of the socio-economic development potential of the Dorobanțu commune in Călărași County (2015), it is mentioned that there are numerous fish farms on the Mostiștea reservoirs, including common carp *Cyprinus carpio* and Prussian carp *Carrasius auratus gibelio* (https://primariadorobantu.ro/).

Most available information regarding the names of the bony fish species inhabiting Iezerul Mostiștea comes from Romanian fishing forums or websites that promote tourist attractions and accommodation, which suggest the presence of bleak, common carp, rudd, roach, Prussian carp, Silver carp (https://www.desprepescuit.ro/), freshwater bream, sichel, Wels catfish, Northern pike,

pike-perch, European perch, gobies (https://www.pescuitul.ro/), tench and Crucian carp (https://www.infopensiuni.ro/). As for European bitterling *Rhodeus sericeus amarus*, this fish was mentioned for Iezerul Mostiștea fauna between April 2018 and March 2019 in a final report about the inventory and mapping the species and habitats from ROSCI0131 Oltenița-Mostiștea-Chiciu (https://www.natura2000oltenita-chiciu.ro/wp-content/uploads/).

Weight-length relationships (WLRs) and Fulton's condition factor (K) are essential tools to provide the growth pattern of fishes and interactions between biotic and abiotic environmental factors in fishery research (Jin et al., 2015; Stavrescu-Bedivan et al., 2016; Stavrescu-Bedivan et al., 2018; Khan et al., 2020).

Previous studies have highlighted before the importance of monitoring the physico-chemical parameters of the water (Scăeţeanu et al., 2012; Stavrescu-Bedivan et al., 2022) and length frequency distribution within of a fish population (Stavrescu-Bedivan et al., 2016), to evaluate the ecosystem health.

The present report aims to update the inventory of ichthtyofauna and to provide first data on some biometric features of *Carassius gibelio* in relation to water quality parameters of Iezerul Mostiștea from Mostistea Valley, an important tourist attraction and fishery resource from Romanian Plain.

In the case of collected water samples were determined the following physico-chemical parameters: turbidity (**T**), **pH**, electrical conductivity (**EC**), chloride (**Cl^-**), total hardness (**TH**), dissolved oxygen (**DO**), chemical oxygen demand (**COD**), biochemical oxygen demand (**BOD**), phosphate-phosphorus (**$P\text{-}PO_4^{3-}$**) nitrate-nitrogen (**$N\text{-}NO_3^-$**), nitrite-nitrogen (**$N\text{-}NO_2^-$**), ammonium nitrogen (**$N\text{-}NH_4^+$**). Based on the results and according to Order 161/2006 water was classified in quality classes.

MATERIALS AND METHODS

Study area

Iezerul Mostiștea (Figure 1), also known as Ezerul Mostiștea (Moștiștei) is placed in Călărași County, Romania (44°15'0" N, 26°54'0" E) (https://www.mindat.org/; https://ro.getamap.net/).

Located on the lower course of the Mostiștea River, it is a fluviatile liman mainly used for fish farming and irrigation, where sport fishing can be practiced all year round (https://www.skytrip.ro/). Iezerul Mostiștea is considered the largest water accumulation in Bărăgan with an area of 1860 ha. The increase in water level by raising the dikes led to the reduction of the surface of the reeds and other swamp plants that emerged around this lake (https://primariadorobantu.ro/).

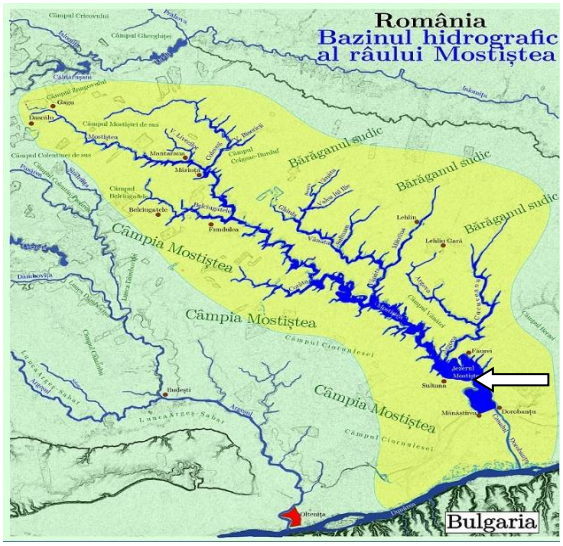

Figure 1. Iezerul Mostiștea (arrow) in the hydrographic basin of Mostiștea River (https://commons.wikimedia.org/wiki/)

Fish inventory, collection and measurements

An inventory of fish species living in Iezerul Mostiștea was performed using data provided by grey literature (fishing websites, reports on mapping the species and habitats from Natura 2000 sites, brochures about biodiversity conservation management planning) and personal catches dated April 2023. In Results and Discussions section (Table 2) is presented scientific classification according to FishBase (Froese & Pauly, 2023) of each fish species with both English and Romanian common names.

Some fish species were collected from Mostiștea Lake in the spring of 2023 (Figure 2), outside the prohibition season, using fishing rods and nets.

Considering Directive 2010/63/EU (2010) and recommendations of AVMA (2020) concerning ethical issues regarding fish welfare, as quickly

as possible after collection the fishes were subjected to rapid cooling, then sorted, labeled, and transported to the laboratory (Figure 3), in order to record the biometric characteristics and investigate for the presence of parasites under a Krüss Optronic stereomicroscope.

Figure 2. Aspects of Mostiștea Lake (April 2023)

Figure 3. Fish samples from Mostiștea Lake in laboratory

A total of 101 fish individuals belonging to nine teleost fish species (Table 3) were measured for total length (TL ± 0.1 cm), standard length (SL ± 0.1 cm) and weighted to the nearest 0.01 g total body weight (TW) with a A PS 2100.R2.M precision balance.

The weight-length relationships were calculated as $TW=aTL^b$ and $TW=aSL^b$, where intercept *a* describes the rate of change of weight with length of fish and slope *b* gives information about the type of growth (Froese, 2006). The relationships between the weight and the length were also expressed through linear regression (Log W= Log a + b Log L) (Stavrescu-Bedivan et al., 2018; Stavrescu-Bedivan et al., 2022).

A positive allometric pattern of growth is suggested when b > 3, while b < 3 indicates a negative allometric or hypoallometric growth type (Karachle & Stergiou, 2012).

The Fulton's condition factor (K) was calculated as $K= (TW/TL^3)*100$ to assess the well-being of fishes in their habitat (Nehemia et al., 2012; Stavrescu-Bedivan et al., 2018; Khan et al., 2020).

Size frequency distribution of fish is another important parameter, therefore size intervals for total length and total weight distribution of fish samples were established (Innal, 2012; Stavrescu-Bedivan et al., 2015).

Water sampling and analyses

Water samples were collected from three different points (**SP**) (Figure 4), as it follows:

(**SP1**) 44°13'26.2"N, 26°55'59.1"E 6WFM+H6G Dorobanțu;

(**SP2**) 44°13'07.7"N, 26°55'14.7"E 6W9C+G7H Mânăstirea;

(**SP3**) 44°12'51.6"N, 26°54'28.4"E 6W75+P5J Mânăstirea.

Figure 4. Water sampling points from Mostiștea Lake (map source: Google Earth)

Sampling campaign was conducted in April 2023 and samples were collected by manual grab from 0.5 m depth in polyethylene bottles

that were labelled and transported in a cold box (4°C) in laboratory. All samples were allowed to stay until they reached room temperature before analysis which was performed in triplicates. The analyses were conducted as previously reported (Stavrescu et al., 2015) by using methods like those recommended for drinking water (Mănescu et al., 1994) and briefly listed in Table 1.

Table 1. Performed analyses, analytical techniques and instrumentation

Analysis	Analytical technique	Instrumentation
Turbidity (**T**)	Nephelometric	HI-88703-02 Turbidity Meter
pH	Potentiometry	InolabWTW pH-meter
Electrical conductivity (**EC**)	Conductometry	Hach SensIon7
Chloride ($\mathbf{Cl^-}$)	Volumetry (Mohr's procedure)	Digital burette
Total hardness (**TH**)	Complexometric titration	-
Dissolved oxygen (**DO**)	Potentiometry	HI98193 - Portable Dissolved Oxygen Meter and BOD Meter
Chemical oxygen demand (**COD**)	Manganometry	-
Biochemical oxygen demand (**BOD**)	Manometric	BOD Sensor + BOD Incubator
Phosphate phosphorus ($\mathbf{P\text{-}PO_4^{3-}}$)	Spectrophotometry	MetertekSP830 Plus spectrophotometer
Nitrite nitrogen ($\mathbf{N\text{-}NO_2^-}$)		
Nitrate nitrogen ($\mathbf{N\text{-}NO_3^-}$)		
Ammonium nitrogen ($\mathbf{N\text{-}NH_4^+}$)		

RESULTS AND DISCUSSIONS

1. Ichthyofauna composition of Mostiștea Pond

Overall, a list comprising 18 fish species was compiled for the ichthyofauna of Iezerul Mostiștea Lake located in Călărași County (Table 2). Of these, nine fish species were identified in the fish sampled in April 2023 and their biometric measurements are shown in Table 3.

Seven species were encountered both in literature survey and present report, namely: *Carassius gibelio* and *Cyprinus carpio* (Order Cypriniformes, Family Cyprinidae); *Abramis brama*, *Rutilus rutilus* and *Alburnus alburnus* (Order Cypriniformes, Family Leuciscidae) (Figure 5 a-c); *Perca fluviatlis* and *Sander lucioperca* (Order Perciformes, Family Percidae).

Gymnocephalus cernua (Perciformes: Percidae) and *C. carpio* var. *specularis* (Cypriniformes: Cyprinidae) were mentioned for the first time in the present report for the ichthyofauna of Mostiștea Lake (Figure 5 d, e).

Figure 5. Some fish species caught from Mostiștea Lake: **a.** *Abramis brama*; **b.** *Rutilus rutilus*; **c.** *Alburnus alburnus*; **d.** *Gymnocephalus cernua*; **e.** *Cyprinus carpio* var. *specularis*

2. Prussian carp sample and biometric analysis

The biometric data for *Carassius gibelio* (N=50, unsexed) were registered as follows: TL (min. 7.8 - max. 21.1 cm, with an average of 11 cm); SL (min. 6 – max.17.4 cm, with a mean of 8.77 cm); TW (min. 5 – max. 174 g, with average of 23.76 g).

The weight-length relationships (Figure 6) were calculated as:

$\text{Log(TW)} = 3.4855\text{Log(TL)}-2.3391$ (r^2= 0.9803, 95% confidence intervals for the intercept and the slope); $\text{TW}=0.0046\text{TL}^{3.4855}$; $\text{Log(TW)} = 3.3097\text{Log(SL)}-1.8298$ (r^2= 0.977,

95% confidence intervals for the intercept and the slope); $TW = 0.0148SL^{3.3097}$.

The values for slope were within the expected range of 2.5-3.5 for all *C. gibelio* analyzed individuals. Since $b > 3$, the growth type for Prussian carp sampled in April 2023 was estimated as positive allometric, which means that fish grows faster in weight than in length (Karachle & Stergiou, 2012).

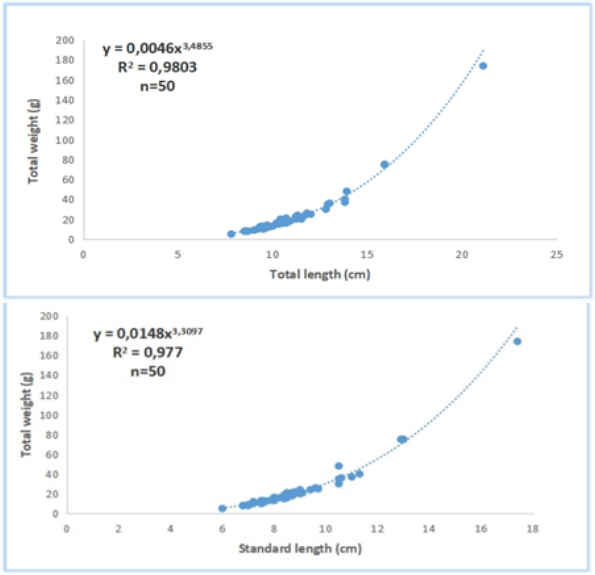

Figure 6. WLRs of *C. gibelio* in Mostiștea Lake (April 2023)

With values higher than 1 (min. 1.05 - max. 1.86, average 1.46), Fulton's condition factor K indicates favorable growth conditions (Şimşek & Kale, 2022) for Prussian carp in Iezerul Mostiștea.

As previous research mentioned, the fish condition and parameters of length-weight relationship in fish could be influenced by various factors such as sample size, size of captured specimens, sexual maturity age, food, environmental conditions, or sampling methods (Stavrescu-Bedivan et al., 2016; Famoofo & Abdul, 2020).

More biologically relevant than age was considered the determining the length of the fish (Rosli and Isa, 2012; Stavrescu-Bedivan et al., 2016; Stavrescu-Bedivan et al., 2022). According to FishBase, the common total length for *C. gibelio* is 20 cm (Kottelat & Freyhof, 2007).

In April 2023, the TL value of most (82%) Prussian carp individuals collected in Mostiștea Lake ranged between 7.8 and 12 cm, while 84 % of *C. gibelio* registered values of TW ranging between 5 and 30 grams (Figure 7).

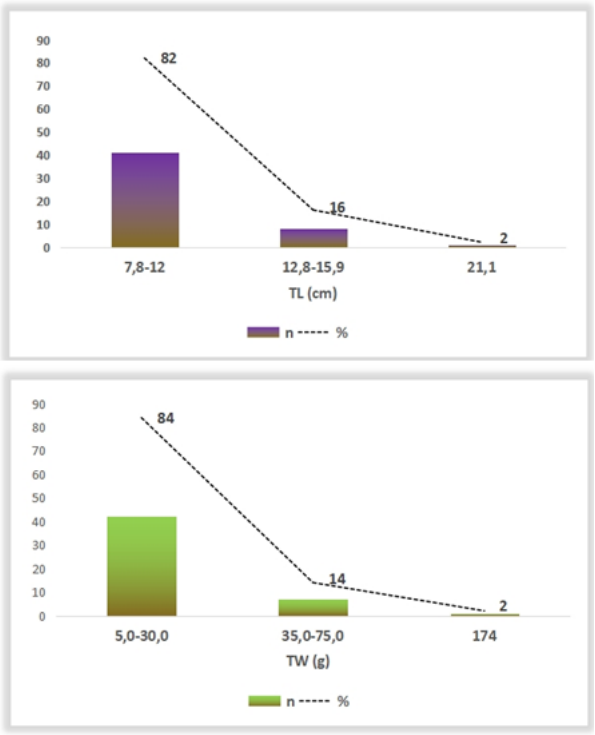

Figure 7. Length and weight distribution among size groups of *C. gibelio* (Mostiștea Lake, April 2023)

3. Parasites recorded in fishes from Mostiștea Lake

Following the parasitological examination of fish species sampled in Mostiștea Lake in April 2023, the parasites *Eustrongylides* spp. (Nematoda: Dioctophymatidae) and *Philometroides sanguineus* (Nematoda: Philometridae) were collected from the perch and Prussian carp, respectively.

Thus, infection with *Eustrongylides* spp. was noticed analyzing the external surface and internal organs of both individuals of *Perca fluviatilis* sampled among the fishes from Mostiștea Lake: 98 parasites removed from one perch (TL=17.5 cm; TW= 77.3 g) and 28 parasites removed from the second perch (TL= 18 cm; TW= 80 g) (Figure 8 a, b).

Figure 8. *Eustrongylides* spp. in *Perca fluviatlis* (**a, b**) and *Philometroides sanguineus* (**c-e**) in *Carassius gibelio* from Mostiștea Lake

As for *Philometroides sanguineus*, female of this nematode species was identified in the caudal fins of each of the four *Carassius gibelio* parazited individuals in the fish sample (TL ranging from 10.2 to 21.1 cm; SL ranging from 8 to 17.4 cm; TW ranging from 16 to 174 grams) (Figure 8 c-e).

In Romania, the nematode *Philometroides sanguineus* was registered before in the caudal fin of *Carassius gibelio* individuals (Cojocaru, 2010; Stavrescu-Bedivan & Vasile Scăețeanu, 2020; Stavrescu-Bedivan et al., 2021).

Table 2. Ichthyofauna of Mostiștea Lake
(☑ = encountered; n/a = data not available; C. name = common name; Ro.c.name= Romanian common name)

Fish species and classification	C. name	Ro. c. name	Literature survey	Present report
Abramis brama (Linnaeus, 1758) (Cypriniformes: Leuciscidae)	Freshwater bream	plătică	☑	☑
Alburnus alburnus (Linnaeus, 1758) (Cypriniformes: Leuciscidae)	Bleak	oblete	☑	☑
Carassius carassius (Linnaeus, 1758) (Cypriniformes: Cyprinidae)	Crucian carp	caracudă	☑	n/a
Carassius gibelio (Bloch, 1782) (Cypriniformes: Cyprinidae)	Prussian carp	caras	☑	☑
Cyprinus carpio Linnaeus, 1758 (Cypriniformes: Cyprinidae)	Common carp	crap	☑	☑
Cyprinus carpio var. specularis Lacepède, 1803 (Cypriniformes: Cyprinidae)	Mirror carp	crap oglindă	n/a	☑
Esox lucius Linnaeus 1758 (Esociformes: Esocidae)	Northern pike	știucă	☑	n/a
Gymnocephalus cernua (Linnaeus, 1758) (Perciformes: Percidae)	Ruffe	ghiborț	n/a	☑
Hypophthalmichthys molitrix (Valenciennes, 1844) (Cypriniformes: Xenocyprididae)	Silver carp	fitofag	☑	n/a
Pelecus cultratus (Linnaeus, 1758) (Cypriniformes: Leuciscidae)	Sichel	sabiță	☑	n/a
Perca fluviatilis Linnaeus, 1758 (Perciformes: Percidae)	European perch	biban	☑	☑
Rhodeus sericeus amarus (Bloch, 1782) (Cypriniformes: Acheilognathidae)	European bitterling	boarță	☑	n/a
Rutilus rutilus (Linnaeus, 1758) (Cypriniformes: Leuciscidae)	Roach	babușcă	☑	☑
Sander lucioperca (Linnaeus, 1758) (Perciformes: Percidae)	Pike-perch	șalău	☑	☑
Scardinius erythrophthalmus (Linnaeus, 1758) (Cypriniformes: Leuciscidae)	Rudd	roșioară	☑	n/a
Silurus glanis Linnaeus, 1758 (Siluriformes: Siluridae)	Wels catfish	somn	☑	n/a
Tinca tinca Linnaeus, 1758 (Cypriniformes: Tincidae)	Tench	lin	☑	n/a
n/a (Gobiiformes: Gobiidae)	goby	guvid	☑	n/a

Table 3. Fish species caught in Mostiștea Lake in April 2023 (C. name = common name; Ro.c.name= Romanian common name; n = number of individuals; TL and SL = total and standard length, in cm; TW = total weight, in grams)

Fish species	C. name	Ro. c. name	n	TL (min.-max.)	TL average	SL (min.-max.)	SL average	TW (min.-max.)	TW average
Sander lucioperca (Linnaeus, 1758)	Pike-perch	șalău	1	48.3	-	-	-	1094	-
Cyprinus carpio var. *specularis* Lacepède, 1803	Mirror carp	crap oglindă	1	13	-	-	-	27	-
Alburnus alburnus (Linnaeus, 1758)	Bleak	oblete	2	15.7-16.9	16.3	12.5-13.8	13.5	34-37	35.5
Perca fluviatilis Linnaeus, 1758	European perch	biban	2	17.5-18	17.75	15.2-15.3	15.25	77.3-80	78.65
Gymnocephalus cernua (Linnaeus, 1758)	Ruffe	ghiborț	4	10.4-12	11.35	8.4-10	9.4	14-21	18.75
Rutilus rutilus (Linnaeus, 1758)	Roach	babușcă	12	13.5-16.7	14.72	10.7-13.3	11.7	25-54	32.42
Abramis brama (Linnaeus, 1758)	Freshwater bream	plătică	13	9.9-32.3	27.09	7.5-27	22.42	8-414	314.46
Cyprinus carpio Linnaeus, 1758	Common carp	crap	16	8.5-23.6	14.44	6.8-19.5	11.87	10-182	51.12
Carassius gibelio (Bloch, 1782)	Prussian carp	caras	50	7.8-21.1	11	6-17.4	8.77	5-174	23.76

4. Water quality analyses

The obtained data resulted from analyses were grouped into three categories: physico-chemical parameters (Table 4), oxygen regime data (Table 5) and nutrient levels (Table 6) and the significance of them is presented in sections below.

Table 4. Values of physico-chemical parameters for water samples collected from Mostiștea Lake

Sampling point	T	Cl^-	pH	EC	TH
	NTU	mg/L		µS/cm	mg CaO/L
SP1	11.30	30.80	8.32	1134.67	17.62
SP2	11.70	28.50	8.62	1240.67	19.07
SP3	12.80	24.90	8.56	1242	18.74
Average±SD	**11.93±0.776**	**28.06±2.973**	**8.50±0.158**	**1205.78±61.58**	**18.48±0.760**
Limits/Quality classes*	NA	II	6.50-8.50	NA	NA

SD = standard deviation; *according to Order 161/2006 for the approval of the Normative concerning the classification of surface water quality to establish the ecological status of water bodies; **NA** = not available.

Table 5. Results concerning oxygen regime for water samples collected from Mostiștea Lake

Sampling point	DO	COD	BOD
	mg O_2/L		
SP1	8.30	15.43	4.20
SP2	8.27	15.59	4.51
SP3	8.62	15.43	3.91
Average±SD	**8.39±0.193**	**15.48±0.092**	**4.20±0.300**
Limits/Quality classes*	II	III	II

SD = standard deviation; *according to Order 161/2006 for the approval of the Normative concerning the classification of surface water quality to establish the ecological status of water bodies.

Table 6. Results concerning nutrient levels for water samples collected from Mostiștea Lake

Sampling point	$P\text{-}PO_4^{3-}$,	$N\text{-}NO_2^-$	$N\text{-}NO_3^-$	$N\text{-}NH_4^+$
	mg P/L	mg N/L		
SP1	BDL	BDL	BDL	BDL
SP2	BDL	BDL	BDL	BDL
SP3	BDL	BDL	BDL	BDL
Limits/Quality classes*	I	I	I	I

*According to Order 161/2006 for the approval of the Normative concerning the classification of surface water quality to establish the ecological status of water bodies; **BDL** = below detection limit of the used method for quantification.

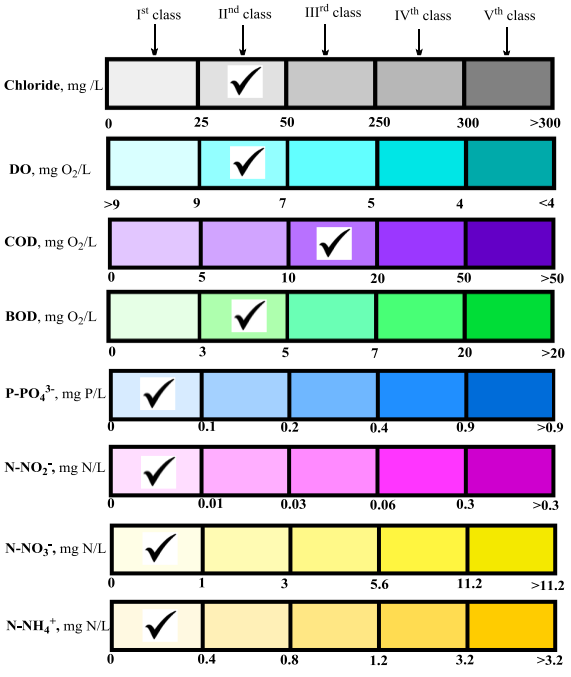

Figure 9. Quality classes for surface water according to legislation and assigned quality classes for water from Mostiștea Lake

a) Results concerning turbidity and chloride

Turbidity is associated with cloudiness of water, and it is determined by the presence of suspended matter (clay, mud, algae, silica, microorganisms) (Jagaba et al., 2020). Beside decrease of aesthetic quality of lakes, high turbidity levels are associated with negative effects on aquatic organisms the more so as decrease the water oxygen levels.

Water samples collected from Mostiștea Lake present turbidity slightly higher than 10 NTU (11.93 NTU, as average) (Table 4) much lower than values identified for Moara Domnească pond (58.43 NTU) (Sandu et al., 2023) but higher than those reported for Cuteţchi lake (5.06 NTU) (Catianis et al., 2018).

According to literature (DataStream Initiative, 2021), turbidity values below 10 NTU are considered low, 50 NTU correspond to moderately turbid water and values over 100 NTU are associated with very high turbidity (DataStream Initiative, 2021).

Chloride levels in water samples from Mostiștea allow to frame the water in IInd quality class (Figure 9) with an average of 28.06 mg/L (Table 4). According to some authors (Dugan et al., 2017) the presence of chloride in lakes is benign, levels higher of 100 mg/L posing ecological impact. Similar values as those determined in this study were reported for Mogoşoaia and Pantelimon lakes (Ionescu et al., 2015).

b) Results concerning pH, EC, TH and correlations between them

The **pH** values of all samples are at the upper limit of the interval imposed by legislation for surface waters (Order 161/2006) (Table 4), with an average of 8.50. As it is presented in the literature, **pH** is an important parameter for aquatic organisms and its' monitoring is recommended for aquaculture systems the more so as extreme values affect fish life and

productivity. Therefore, some authors (Stone & Thomforde, 2004) state that pH values below 6.50 reduce fish reproduction and newly hatched fish are affected by pH values above 9.00 to 9.50. Generally, an optimum range for fish is between 6.50-9.00, values above 9.00 being responsible of conversion of ammonium ion into ammonia, toxic chemical specie for fish (https://www.epa.gov/caddis-vol2/ph). pH values for water collected from different ponds and lakes located in Bucharest and vicinity are reported in several studies (Ionescu et al., 2015; Scăețeanu Vasile et al., 2020; Mihai C. et al., 2022).

EC is a measure of water ability to conduct electricity and is related with concentration of dissolved ions in the analysed sample. According to literature (Austin et al., 2016), desirable range for most fish species is 60-2000 µS/cm but some aquaculture species (channel catfish) can live in water with EC as high as 30000 µS/cm. Concerning this parameter, the analyses indicated close values for each sampling points, with an average of 1205.78 µS/cm, higher than those reported for different fishing ponds (Stavrescu-Bedivan et al., 2015; Scăețeanu Vasile et al., 2019; Stavrescu-Bedivan et al., 2021).

Ions responsible of **TH** level are calcium and magnesium and with a small contribution other divalent ion that usually are encountered in insignificant amounts. Different fish species have various hardness requirements, but desirable range is between 28-84 mg CaO/L, meanwhile acceptable range is above 5.6 mg CaO/L (Stone & Thomforde, 2004). In addition, calcium and magnesium are important for fish biological processes and are absorbed directly from water (Wurts & Durborow, 1992).

The average **TH** value (18.48 mg CaO/L) for analyzed samples corresponds to very soft water (Adey & Loveland, 2007).

Between **EC** (µS/cm) and **TH** (mg CaO/L) and between **pH** and **TH** (mg CaO/L) values were evidenced very significant correlations with correlation coefficient r=0.8814*** and r=0.9183***, respectively (Figure 10).

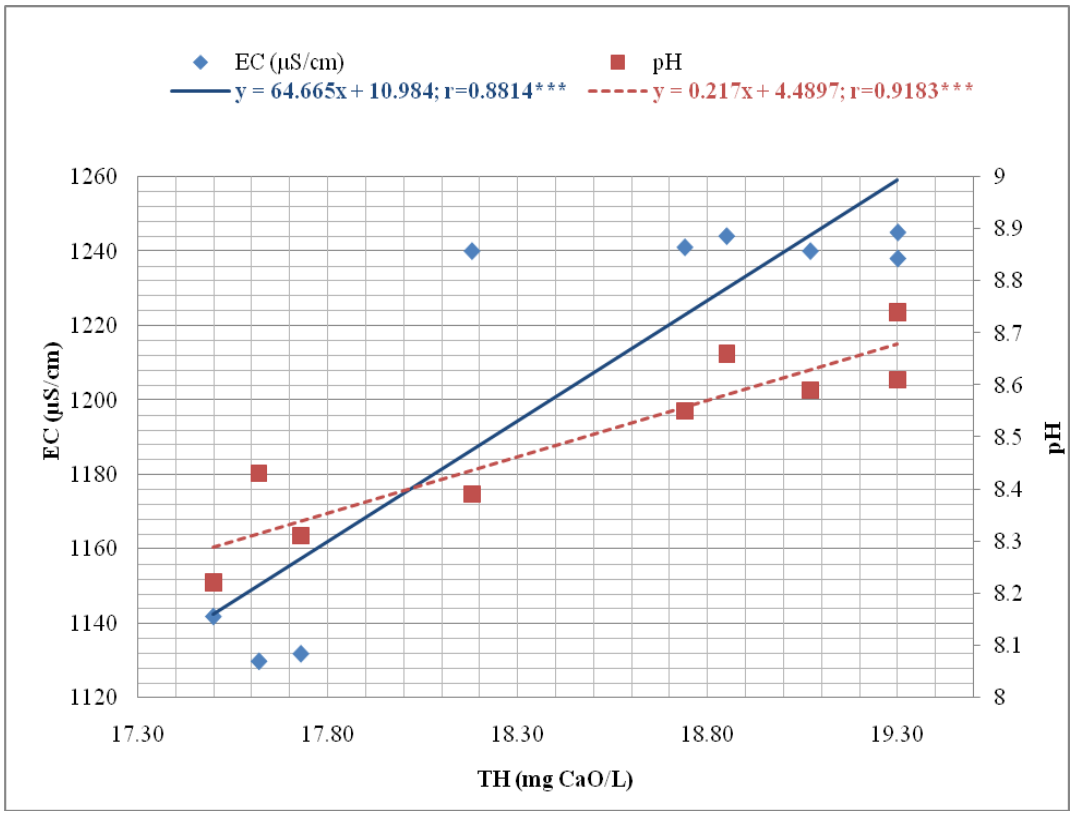

Figure 10. Correlations between conductivity and pH values with TH of water samples from Mostiștea Lake

c) Results concerning oxygen regime

Amount of oxygen dissolved in water that is available for aquatic life is represented by dissolved oxygen (**DO**). Generally, it is produced during photosynthesis of aquatic plants and algae. Related to fish requirements

there are data that sustain that warm water fishes need at least 5 mg O_2/L in comparison with cold water fishes which require 6-7 mg O_2/L (Hudson, 1998). In addition, values lower than 3-4 mg O_2/L favour anaerobic bacteria activity which will generate methane and hydrogen sulphide (Sallenave, 2012). Also, low levels are associated with hot cloudy weather, algae die-offs (Francis-Floyd, 2003).

As concerning our study, the analyses indicated an average value of 8.39 mg O_2/L for **DO (**Table 5**)** this suggesting IInd quality class according to Order 161/2006 (Figure 9). Average values for **DO** of 8.87 mg O_2/L was reported by Dunea et al. (2020) for Ialomița River Basin.

BOD and **COD** parameters indicate the level of contamination of water. **BOD** is the amount of dissolved oxygen needed for microorganisms to decompose organic matter. In contrast, **COD** is the given by the amount of oxygen used to chemical break down the organic molecules from water. **COD** is usually high in contrast with **BOD**.

Based on the obtained results for **COD** (15.48 mg O_2/L, as average) and **BOD** (4.20 mg O_2/L, as average) (Table 5) it could be assumed that water corresponds to IIIrd and IInd quality classes, respectively (Figure 9).

Related to **COD**, already published data indicate that water from Comana pond is framed in IIIrd quality class, also (Stavrescu-Bedivan et al., 2021). Similar values **BOD** was reported by Ionescu et al (2015) for Ialomița River Basin, Mogoșoaia, Herăstrău and Pantelimon lakes.

d) Results concerning nutrient species

Phosphorus and nitrogen species are encountered naturally in water but due to human activities as use of fertilizers, runoff from use of detergents and animal wastes or unproper wastewater management these species have risen unwanted levels. Among negative effects, it could be mentioned eutrophication that generates algal growth, large daily fluctuation of dissolved oxygen, poor water clarity, unpleasant odours.

For water samples collected from Mostiștea Lake, it has been found that nitrogen species (nitrate, nitrite, ammonium) and phosphorus (as phosphate) are below detection limit of the used method for quantification (spectrophotocolorimetry) (Table 6). These results allowed us to assign Ist quality class to analysed water (Figure 9). In contrast with this result, for Moara Domnească pond, it has been reported (Sandu et al., 2023) high levels of nutrient species based on which water was categorized in the Vth quality class.

CONCLUSIONS

On the one hand, this research reported novel information on fish species and on size frequency distribution, condition factor and parameters of weight-length relationship in *Carassius gibelio* inhabiting Iezerul Mostiștea, an important water resource from Romanian Plain, located in Călărași County. On the other hand, the adaptation of Prussian carps in their environment was assessed in relation to physico-chemical analysis of water samples.

The Ruffe *Gymnocephalus cernua* and Mirror carp *Cyprinus carpio* var. *specularis* are new records for the ichthyofauna of the studied ecosystem.

Fulton' condition factor K factor revealed the well-being of Prussian carps in the ecosystem, with values greater than 1.

The results obtained by physico-chemical analyses were used to frame the water to quality classes according to standards imposed by Order 161/2006. Hence, based on nutrient species levels water is classified as Ist quality class. Chloride, **DO** and **BOD** values sustain association with IInd quality class, meanwhile COD values indicate IIIrd quality class. **TH** values present very significant correlation with **EC** (r=0.8814***) and with **pH** (r=0.9183***), respectively. Based on the obtained results and analysis with literature data it could be assumed that water from Mostiștea Lake meets the requirements for optimal development of aquatic organisms. This study evidenced that maintaining water parameters within acceptable specific limits of species worth primary consideration and it is important for fish life.

ACKNOWLEDGEMENTS

This paper was carried out with the financial support of University of Agronomic Sciences and Veterinary Medicine of Bucharest –

Romania, Research Project 1059/15.06.2022, acronym HybridPraxisLab in the competition IPC 2022.
The authors are grateful to I. Baicu and Gh. Baicu for providing fish samples, to N. Crăciun and C.F. Alistar for their suggestions and to E.C. Velicu, C. Dincă and I.C. Sfetcu for assistance during the laboratory procedures.

REFERENCES

Adey, W.H. & Loveland, K. (2007). Water Composition. *Dynamic Aquaria*, 61–74.

Austin, B.J., Sinha, A., Stone, N., Green,W.R., Daniels, M. & Haggard, B.E. (2016). How to Collect Your Water Sample and Interpret the Results for the Fish Pond Analytical Package, Arkansas Water Resources Center, Fayetteville, AR, FS-2016-02.

Catianis, I., Pojar, I., Grosu, D., Scrieciu, A., Secrieru D., Vasiliu, D. & Pavel, A.B. (2018). The investigation of the water quality and bed-sediment conditions in Cutetchi Lake, Danube Delta, Romania. *Scientific Annals of the Danube Delta Institute*, *23*, 13-22.

Cojocaru, C.D. (2010). Fish Parasites of Romania-An Update. Sixth International Symposium on Aquatic Animal Health. Global Strategies for a changing environment, Tampa, Florida, USA. Volume Proceedings, doi: 10.13140/RG.2.1.1779.7204.

Covataru, C., Stal, C., Florea, M., Opriș, I., Simon, C., Radulescu, I., Călin, R., Ignat, T., Ghiță, C. & Lazăr, C. (2022). Human Impact Scale on the Preservation of the Archaeological Sites from Mostiștea Valley (Romania). *Frontiers in Environmental Science*, *10*, 1065.

DataStream Initiative (2021). A water monitor's guide to water quality. Turbidity. Available from: https://datastream.org/en/guide/turbidity#content [18.05.2023].

Dill, W.A. (1993). Inland fisheries of Europe. EIFAC Technical Paper. No. 52 Suppl. Rome, FAO. 281 p.

Dugan, H.A., Bartlett, S.L., Burke, S.M., Doubek, J.P., Krivak-Tetley, F.E., Skaff, N.K., Summers, J., Farrell, K., McCollough, I., Morales-Williams, A., Roberts, D., Ouyang, Z., Scordo, F., Hanson, P. & Weathers, K.C. (2017). Salting our freshwater lakes. *Proceedings of the National Academy of Sciences*, *114*(17), 4453–4458. doi:10.1073/pnas.1620211114.

Dunea, D., Bretcan, P., Tanislav, D., Şerban, G., Teodorescu, R., Iordache, S., Petrescu, N. & Tuchiu, E. (2020). Evaluation of water quality in Ialomița River basin in relationship with land cover patterns. *Water*, *12*, 735. https://doi:10.3390/w12030735.

Famoofo O.O. & Abdul W.O. (2020). Biometry, condition factors and length-weight relationships of sixteen fish species in Iwopin fresh-water ecotype of Lekki Lagoon, Ogun State, Southwest Nigeria. *Heliyon*, *6*(1), e02957.

Francis-Floyd, R. (2003). Dissolved oxygen for fish production. University of Florida, Institute of Food and Agricultural Sciences. Fact Sheet FA-27.

Froese, R. (2006). Cube law, condition factor and weight-length relationships: history, meta-analysis and recommendations. *Journal of Applied Ichthyology*, *22*(4), 241-253.

Froese, R. & Pauly, D. (Eds.), (2023). FishBase. World Wide Web electronic publication. Retrieved from www.fishbase.org.

Ghiță, C. (2008). Antropizarea pe Valea Mostiștei, *Lucrări și Rapoarte de Cercetare*, II(1), 85-96 (in Romanian).

Grecu, F., Ghiță, C. & Budileanu, M. (2013). Vulnerability map to hydrogeomorphological processes (Romanian Plain), *Journal of Geomorphology*, *15*, 5-12.

Hudson, H. (1998). Lake Notes. Common lake water parameters. Available from: https://www3.nd.edu/~aseriann/Water_Parameters.pdf [19.05.2023].

Innal, D. (2012). Age and growth properties of *Carassius gibelio* (Cyprinidae) living in Aksu River Estuary (Antalya-Turkey). *Review of Hydrobiology*, *5*(2), 97-109.

Ionescu, P., Radu, V.M., Diacu, E. & Marcu, E. (2015). Assessment of water quality in the lakes along Colentina river. *Advanced Engineering Forum*, *13*, 194-199.

Jagaba, A.H., Kutty, S.R.M. & Hayder, G., (2020). Water quality hazard assessment for hand dug wells in Rafin Zurfi, Bauchi State, Nigeria. *Ain Shams Engineering Journal*, *11*, 983-999.

Jin, S., Yan, X., Zhang, H. & Fan, W. (2015). Weight–length relationships and Fulton's condition factors of skipjack tuna (*Katsuwonus pelamis*) in the western and central Pacific Ocean. *PeerJ*, *3*, e758.

Karachle, P.K. & Stergiou, K.I. (2012). Morphometrics and allometry in fish. In: Wahl C.M., 2012. Morphometrics. New York: Cornell University, 65-68. (Agricultural and biological science). doi: 10.5772/34529.

Khan, M.S., Hayat, S., Ishtiaq, A., Malik, A., Akhtar, M.N., Khan, G.Z., Khan, Z.I. & Ali, Q. (2020). Length-Weight relationships of *Cyprinus carpio* from the Indus River at Chashma Lake, District Mianwali, Punjab, Pakistan. *Journal of Wildlife and Biodiversity*, *4*(4), 72-80.

Kottelat, M. & Freyhof J. (2007). Handbook of European freshwater species. Cornol, Switzerland: Berlin, Germany.

Mănescu, S., Cucu, M. & Diaconescu, M.L. (1994). Chimia sanitară a mediului. Editura Medicală București.

Mihai, C., Erghelegiu, B., Nițu, C.C., Mihalache C.E., (2022). Monitoring the physicochemical parameters of water quality from lake Herăstrău Bucharest - 2015 -2020. *AgroLife Scientific Papers. Series E. Land Reclamation, Earth Observation & Surveying, Environmental Engineering, XI, 350-357.*

Rosli, M.N.A. & Isa, M.M. (2012). Length-weight and Length-length Relationship of Longsnouted Catfish, *Plicofollis argyropleuron* (Valenciennes, 1840) in the Northern Part of Peninsular Malaysia. Tropical Life Sciences Research, 23(2), 59–65.

Sallenave, R. (2012). Understanding water quality

parameters to better manage your pond. Guide W-104. Cooperative Extension Service. College of Agricultural, Consumer and Environmental Sciences.

Sandu, M.A., Virsta, A., Vasile Scăeţeanu, G., Iliescu, A.-I., Ivan, I., Nicolae, C.G., Stoian, M. & Madjar, R.M., (2023). Water quality monitoring of Moara Domnească pond, Ilfov County, using UAV-based RGB imaging. *AgroLife Scientific Journal*, *12*(1), 191- 201, doi:10.17930/AGL2023122.

Scăeţeanu, G., Manole, M.S., Stavrescu-Bedivan, M.M., Penescu, A. & Pele, M. (2012). Evaluation of water quality in lakes from Bucharest. *Scientific Papers. Series E. Land Reclamation, Earth Observation & Surveying, Environmental Engineering, I*, 113-116.

Scăeţeanu Vasile, G., Madjar, R.M., Silvestro, A., Dulea, C. & Stavrescu-Bedivan, M.-M. (2019). Water quality monitoring and assessment of the ecological status of Tătaru fish pond, Călăraşi County. 19th International Multidisciplinary Scientific GeoConferenceSGEM 2019, *SGEM 2019 Conference Proceedings*, *19*(1.4), 309-316.

Scăeţeanu Vasile, G., Madjar, R.M. & Stavrescu-Bedivan, M.-M. (2020). A comparative evaluation of surface water quality standards for lakes and fish ponds from Bucharest and vicinity. *Romanian Journal of Ecology & Environmental Chemistry*, *2*(2), 30-37.

Şimşek, E. & Kale, S. (2022). Length-Weight Relationship and Condition Factor of Prussian Carp (*Carassius gibelio*, Bloch, 1782) from Asi River. *Journal of Agricultural Production*, *3*(2), 69-77.

Stavrescu-Bedivan, M.M., Scăeţeanu Vasile, G., Madjar, R.M., Matei, P.B. & Tobă, G.F. (2015). Comparative study of length-weight relationship, size structure and Fulton's condition factor for Prussian carp from different Romanian aquatic ecosystems. *Agrolife Scientific Journal*, *4*(2), 132–139.

Stavrescu-Bedivan, M.M., Vasile Scăeţeanu G., Madjar R.M., Manole M.S., Staicu A. C., Aioanei F.T., Plop E.F., Tobă G.L. & Nicolae C.G. (2016). Interactions between fish well-being and water quality: a case study from Morii Lake area, Romania. *Agriculture and Agricultural Science Proceedia*, *10*, 328-339.

Stavrescu-Bedivan, M.M., Vasile Scaeteanu G., Madjar R.M. & Manole M.S. (2018). Investigation of length-weight relationship and condition factor of *Carassius gibelio* related to water quality in Pantelimon II Lake. *AgroLife Scientific Journal*, *7*(1), 123-130.

Stavrescu-Bedivan, M.M. & Vasile Scăeţeanu, G. (2020). A note on the presence of philometrid fish parasites in Romania, with emphasis on *Philometroides sanguineus* (Rudolphi, 1819). *AgroLife Scientific Journal*, 9(2), 313-318.

Stavrescu-Bedivan, M.-M., Săndulescu, E.M., Croitoru, C.M., Madjar, R.M., Boiu-Sicuia, O.-A. & Scăeţeanu Vasile, G. (2021). A preliminary evaluation of water quality related to aquatic organisms in Comana pond. *AgroLife Scientific Journal*, *10*(2), 178-188.

Stavrescu-Bedivan, M.M., Madjar, R.M., Sion, A. & Scăeţeanu Vasile, G. (2022). Assessment of water quality and biometric analysis for common carp *Cyprinus carpio* L., 1758: a case study from Biţina Pond (Ilfov County, Romania). *AgroLife Scientific Journal*, *11*(2), 191-200.

Stone, N.M. &Thomforde, H.K. (2004). Understanding your fish pond water analysis report, cooperative extension program. University of Arkansas at Pine Bluff, United States Department of Agriculture, 1–4.

Tanislav, D. (2014). Protected wetlands in Romania. 2nd In International Conference-Water resources and wetlands, Tulcea-Romania, 469-474. Available online: http://www.limnology.ro/water2014/proceedings.html

Wurts, W. & Durborow, R. (1992). Interactions of pH, carbon dioxide, alkalinity and hardness in fish ponds. SRAC Publication No.464.

***content/uploads/2019/08/RF_inventariere_ROSCI0131.pdf

***https://ceddu.ro/documente/Situl_Natura_2000_Valea_Mostistei.pdf

***https://primariadorobantu.ro/wp-content/uploads/2017/04/Analiza-Diagnostic-comuna-Dorobantu-varianta-finala.pdf

***https://www.epa.gov/caddis-vol2/ph.

***https://www.fishbase.se/

***https://www.getamap.net/maps/romania/romania_(general)/_mostistea_ezerul/

***https://www.infopensiuni.ro/cazare-frasinet/obiective-turistice-frasinet/lacul-mostistea_4546

***https://www.mindat.org/feature-672789.html

***https://www.natura2000oltenita-chiciu.ro/wp-

***https://www.pescuitul.ro/pescuit-mostistea-344

***https://www.pescuitul.ro/subiect-Lacul-Iezer-Mostistea-72671

***https://www.skytrip.ro/lacul-mostistea-din-judetul-calarasi-ob-953.html

***AVMA Guidelines for the euthanasia of animals, (2020). American Veterinary Medical Association, Schaumburg, IL 60173.

***Directive 2010/63/EU on the European Parliament and of the Council of 22 September 2020 on the protection of animals used for scientific purposes.

***Order 161/2006 for the approval of the Normative concerning the classification of surface water quality to establish the ecological status of water bodies.

Scientific Papers. Series E. Land Reclamation, Earth Observation & Surveying, Environmental Engineering. Vol. XII, 2023
Print ISSN 2285-6064, CD-ROM ISSN 2285-6072, Online ISSN 2393-5138, ISSN-L 2285-6064

HEAVY METAL ACCUMULATION AND CHEMICAL COMPOSITION OF ESSENTIAL OILS OF COSTMARY (*TANACETUM BALSAMITA* L.) CULTIVATED ON HEAVY METAL CONTAMINATED SOILS

Maria IHTYAROVA, Violina ANGELOVA

Agricultural University - Plovdiv, 12 Mendeleev Blvd, Plovdiv, Bulgaria

Corresponding author email: vileriz@abv.bg

Abstract

Comparative research has been conducted to determine the content of heavy metals and chemical composition of costmary oils, as well as to identify the possibility of costmary (Tanacetum Balsamita L.)| growth on soils contaminated by heavy metals. Costmary is a plant tolerant of heavy metals and can be grown on contaminated soils. Heavy metals do not affect the development of costmary and the quality of oil obtained from it. Twenty-three components were identified, accounting for 98.26-98.99% of the total oil components. The major components (> 1.0%) contained in costmary oil are carvone (42.66-44.12%), alpha-thujone (29.81-30.07%), beta-bisabolene (5.51-6.24%), 1,8-cineole (2.71-3.58%), beta-thujone (2.47-2.60%), cis-para-mentha-1(7),8-dien-2-ol (1,63-1,72%), trans-para-mentha-2,8-dienol (1.34-1.41%), cis-carveol (1.20-1.74%), and gamma-muurolene (1.69-1.78%). The content of oxygen-containing monoterpenes (88.75-89.41%) is the highest in costmary oil, followed by sesquiterpene hydrocarbons (7.74-8.35%), oxygen-containing sesquiterpenes (1.0-1.06%) and monoterpene hydrocarbons (0.58-0.61%). The analysed costmary oils belong to the carvone - α-thujone chemotype.

Key words*: contaminated soils, costmary, essential oil composition, heavy metals.*

INTRODUCTION

Costmary (*Tanacetum balsamita*), also called balsam chrysanthemum, is a herbaceous perennial plant that belongs to the Asteraceae family. The balsam chrysanthemum reaches a height of 45-60 centimetres and blooms in summer with yellow flowers. In spring, it begins its growth with the growth of a leafy rosette and a flower stalk. The leaves are oval, and the flowers are basket-shaped and are grouped in an umbel-like inflorescence.

The species is widespread in southeastern Europe and southwestern Asia but has been naturalised and cultivated in various parts of the world (Hassanpouraghdam et al., 2008a; Hassanpouraghdam et al., 2008b; Oberprieler et al., 2009). It occurs in the botanical gardens of most European countries (Philips and Foy, 1992). It is cultivated in Asia, America, Iran, Turkey and Romania, Germany, Italy, Spain, and England (Bylaite et al., 2000; Marculescu et al., 2001a; Marculescu et al., 2001b; Gallori et al., 2001; Hassanpouraghdam et al., 2008a).

The plants are cold-tolerant. It prefers full sun and well-drained soil but grows well under most conditions (Hassanpouraghdam et al., 2008b). Propagation of this plant is by division or by root cuttings, while propagation by seed is not satisfactory (Marculescu et al., 2001b).

The aboveground part of the plant (leaves and flowers) is used in the Mediterranean, Balkans, South America, and Asia (Bylaite et al., 2000; Abad et al., 2006; Hassanpouraghdam et al., 2008a). Costmary contains biologically active substances (essential oil, phenylpropane derivatives, flavonoids (flavonols, apigenin derivatives, scutellarin derivatives and luteolin derivatives potent antioxidants), tannins and oligo elements (Ca, K, Mg, P and Fe), vitamin C (ascorbic acid). For this reason, it is used as a spice, herbal tea, and to produce essential oil (Hassanpouraghdam et al., 2008a; Venskutonis, 2016). The fresh and dried leaves of the costmary possess a lemon-myrrh solid aroma and a sweet, astringent taste. Fresh leaves can be added to salads, pasta and various beverages. Dried leaves are used as flavourings in soups and meats, sausages and pastries, and refreshing tea (Bylaite et al., 2000; Abad et al., 2006). The flowers can be added to jams, sweets and preserves. Costmary leaves have been used as a hepatoprotective, tonic, sedative, painkiller and astringent

(Hassanpouraghdam, 2009). The oils can be used as natural additives in many foods due to their antibacterial, antifungal, antioxidant and anticarcinogenic properties (Juknevicine et al., 1973; Hüsnü et al., 2001; Jaimand & Rezaee, 2005), and to alleviate inflammatory diseases (Bagci et al., 2008; Yousefzadi et al., 2009; Venskutonis, 2016; Ivashchenko, 2017).

The essential oil is extracted by steam distillation of the aerial parts (leaves and flowers) and is a colourless to pale yellow liquid (Hassanpouraghdam et al., 2008a). The oil is secreted in the glandular trichomes, with the highest essential oil content in the leaves before flowering. For the essential oil of the costmary to be of high quality, the plants must be harvested at the beginning of flowering (Bylaite et al., 2000; Gallori et al., 2001; Hassanpouraghdam et al., 2008a, 2008b). The essential oil contains up to 186 compounds (Bylaite et al., 2000), which are dominated by monoterpenes and sesquiterpenes. The oil greatly affects skin diseases such as eczema, rashes, pimples, and acne. The essential oil is used in medicine, pharmacology, food, perfume and confectionery industries. The essential oil can also be used in aromatherapy.

It is known that some medicinal plants, such as mint, St. John's wort, sage, and others, can accumulate large amounts of toxic heavy metals in their tissues, be used for phytoremediation, and replace food crops grown under the same conditions. The concentrations of various plant by-products are highly dependent on the growing conditions and affect the metabolic pathways responsible for synthesising associated natural products. Metals can significantly alter the chemical composition of secondary metabolites in aerial parts of plants and thus seriously affect the quality, safety and efficacy of natural plant products (Akula & Ravishankar, 2011).

Although there is data on the composition of costmary oil, there needs to be more information on the heavy metal content of the aerial mass and oil when costmary is grown on soils contaminated with heavy metals.

The present work aims to conduct a comparative study that will allow us to determine the amounts and deposition of Pb, Zn, Cd and Hg accumulation in the vegetative organs of costmary, the quality of costmary oil, as well as to establish the feasibility of growing costmary on soils contaminated with heavy metals.

MATERIALS AND METHODS

The experiment was performed on an agricultural field contaminated by Zn, Pb, and Cd, situated at different distances (0.5 and 15.0 km) from the source of pollution, the NFMW (Non Ferrous Metal Works) near Plovdiv, Bulgaria.

The study was conducted with a costmary test plant. Costmary seedlings were purchased and planted in spring on areas located at different distances (0.5 km and 15 km) from the source of contamination NFMW-Plovdiv. In the second and third years after planting, samples of plant material (roots, stems, leaves, and flowers) were taken for analysis from each experimental plot. Costmary was hand-harvested at the flowering stage in June. After transporting the plants to the laboratory, scissors were used to divide them into their individual organs (roots, stems, leaves and inflorescences). Samples of the roots, stems, leaves and flowers were dried at room temperature until an air-dry mass was obtained, after which they were dried at 45ºC. The content of heavy metals in different parts - roots, stems, leaves and flowers were determined. The essential oil of the costmary was obtained in laboratory conditions from the flowers by steam distillation for 2 h using a Clevenger-type apparatus.

The pseudo-total content of metals in soils was determined in accordance with ISO 11466. The available (mobile) heavy metal contents were extracted by ISO 14870 by a solution of DTPA. The contents of Pb, Zn, Cd and Hg in the plants and in the costmary's essential oil were determined by microwave mineralisation method. The quantitative measures were carried out by ICP (Jobin Yvon Emission - JY 38 S, France). The Hg content of the samples was determined without preliminary sample preparation with a Hg analyser. Digestion and analytical efficiency of ICP and Hg analyser were validated using a standard reference material of apple leaves (SRM 1515, National Institute of Standards and Technology, NIST). The chemical composition of the oils in hexane

(1:1000) was analysed on Agilent 7890A Gas Chromatography system equipped with FID detector and Agilent 5975C mass spectrometer. The oil's chemical constituents were determined on a 7890A gas chromatograph (Agilent Technologies) and a 5975C mass spectral detector (Agilent Technologies). Compounds were identified by comparing retention times and Kovacs relative indices (RI) with those of standard substances and mass spectral data from the NIST'08 library (National Institute of Standards and Technology, USA).

RESULTS AND DISCUSSIONS

Soils

To elucidate the extent of soil contamination with heavy metals and their localisation in the vegetative organs of costmary, soil samples were collected from the areas at different distances from the NFMW (0.5 and 15 km). The physical and chemical properties of the soil samples are presented in Table 1. The soils are characterised by a slightly alkaline reaction, medium organic carbon content and medium to high nutrient (N, P, K) availability.

Table 1. Characterization of soils sampled from NFMW-Plovdiv

Parameter	Soil 1 (S1) 0.5 km from NFMW	Soil 2 (S2) 15 km from NFMW
pH	7.6	7.5
Organic content,%	5.4	1.5
N Kjeldal,%	0.29	0.12
P, mg/kg	703.1	387.3
K, mg/kg	7782.5	6780.0
Ca, mg/kg	22746	7927.3
Mg, mg/kg	14046	8428.4
Cu, mg/kg	307.4	35.2
Fe, mg/kg	32340	25282
Mn, mg/kg	957.6	879.0
Pb, mg/kg	2966.9	24.6
Zn, mg/kg	3196.1	177.9
Cd, mg/kg	92.0	2.7
Hg, ng/g	488.1	41.0

MPC (pH >7.4) - Pb -100 mg/kg, Cd - 3.0 mg/kg, Zn -400 mg/kg, Hg - 1.5 mg/kg

The results presented in Table 1 show that with distance from NFMW-Plovdiv, there is a well-defined trend of decreasing total heavy metal content in the soil. In the soil samples taken from the area 0.5 km away from KCM (S1), values for Pb exceeding the MPC (maximum permissible concentrations, approved for Bulgaria) (100 mg/kg) were recorded - 2966.9 mg/kg. In the area 15 km away, the Pb content decreased significantly to 24.6 mg/kg. Similar results were obtained for Cd and Zn. In the area 0.5 km away from the NFMW, 3196.1 mg/kg Zn and 92.0 mg/kg Cd were recorded, with values significantly exceeding the MPC. In the more distant area (15 km from NFMW), 177.9 mg/kg Zn and 2.7 mg/kg Cd were detected. The Hg content in soils from both regions was lower than the MPC.

The results for the mobile forms of the metals determined by DTPA show that the mobile forms of Cd in the contaminated soils are the most significant portion of its total content and reached to 67.2%, followed by Pb with 42.0%, Zn with 10.6% and Hg to 1.3%.

In the uncontaminated soils, the mobile forms of Cd were the most significant fraction of its total content and reached 24.8%, followed by Pb at 8.5%, Zn at 7.1% and Hg at 2.7% (Table 2).

Table 2. DTPA-extactable Pb, Zn, Cd (mg/kg) and Hg (ng/g) in soils sampled from NFMW

Soils		S1	S2
Pb	mg/kg	1244.7	21.5
	%*	42.0	43.5
Cd	mg/kg	61.9	0.7
	%	67.2	70
Zn	mg/kg	339.1	40.0
	%	10.6	22.5
Hg	ng/g	6.3	1.1
	%	1.3	2.7

*DTPA -extractable/total content

Costmary

To elucidate the uptake, accumulation and distribution of heavy metals in the vegetative organs of the costmary, samples of roots, stems, leaves and flowers were analysed.

In Table 3 are presented the results obtained for the heavy metal content in the organs of the studied essential oil crop. Significant differences were found in the elemental contents of the different parts of the costmary. The main part (Pb, Cd, Zn and Hg) accumulated in the aerial parts of the costmary (leaves and flowers).

The content of Pb in the roots of costmary grown on contaminated soils (S1) reached up to 648.0 mg/kg, Zn - up to 500.7 mg/kg, Cd - up to 67.3 mg/kg, and Hg - up to 365.4 ng/g. The values obtained for the heavy metals (Cd, Pb and Zn) in the roots were much higher than the values considered toxic to plants by Kabata Pendias (2001) (0.1 mg/kg Cd, 30 mg/kg Pb,

100 mg/kg Zn). Significantly lower values were found in the roots of the costmary grown on uncontaminated soil (S2). The Pb content in the roots reaches 1.1 mg/kg, Zn - 30.7 mg/kg, Cd - 0.08 mg/kg and Hg - 81.8 ng/g. Costmary is distinguished by a shallow root system, with many thin horizontally arranged feeding roots (Philips & Foy, 1992). This is probably the reason why it accumulates significant amounts of heavy metals in the roots.

Table 3. Element contents in costmary grown 0.5 and 15 km from NFMW-Plovdiv

Element	Roots	Srems	Leaves	Flowers	Oils
S1 Pb, mg/kg	648.0	217.0	566.0	244.0	2.7
S1 Cd, mg/kg	67.3	18.7	83.1	23.9	0.08
S1 Zn, mg/kg	500.7	121.1	768.0	190.0	1.7
S1 Hg, µg/kg	365.4	215.3	412.2	348.6	nd
S2 Pb, mg/kg	1.1	1.5	2.7	0.8	0.03
S2 Cd, mg/kg	0.08	0.1	0.3	0.1	0.005
S2 Zn, mg/kg	30.7	13.6	11.5	62.4	0.16
S2 Hg, µg/kg	81.8	54.5	99.3	76.3	nd

nd-not detecable

The Pb content in the stems of costmary grown on contaminated soil (S1) reaches 217.0 mg/kg, Zn up to 121.1 mg/kg, Cd up to 18.7 mg/kg, and Hg up to 215.3 ng/g. Significantly lower values were found in the stems of costmary grown on uncontaminated soil (S2). The content of Pb in stems reached up to 1.5 mg/kg, Zn - 13.6 mg/kg, Cd - 0.1 mg/kg, Hg - 54.5 ng/g. The anatomical structure of the stems of the tested plant can explain the higher values found in the costmary grown on the contaminated soil. Costmary is distinguished by a stem covered with hairs, contributing to the fixation of aerosol pollutants and their accumulation.

The content of heavy metals is higher in the aboveground mass of the costmary than the roots, indicating uptake and movement of metals along the conducting system. The results obtained were similar to Jasion et al. (2013), who found that metal accumulation in leaves, were higher compared to roots.

The Pb, Zn, Cd and Hg contents in the leaves of costmary from the contaminated soil reached 566.0 mg/kg, 768.0 mg/kg, 348.6 mg/kg and 412.2 ng/g, respectively. Despite high concentrations of Cd and Pb in the leaves, there was no evidence of Cd and Pb toxicity. Significantly lower values were found in the leaves of costmary grown on uncontaminated soil (S2), where Pb reached up to 2.7 mg/kg, Zn up to 11.5 mg/kg, Cd up to 0.3 mg/kg and Hg up to 99.3 ng/g.

The higher accumulation of heavy metals in the leaves of the costmary is probably due to the fact that the leaves of the costmary are mossy, which contributes to the fixation of aerosol pollutants and their accumulation there. A characteristic feature of the costmary is the presence of trichomes (hairs) on the plant's surface, a typical morphological part of the Asteraceae family.

The accumulation of heavy metals in the flowers is high but lower than in the leaves. The Pb content in the flowers of costmary grown on contaminated soil reaches up to 244.0 mg/kg, Zn - up to 190 mg/kg, Cd - up to 23.9 mg/kg and Hg - 348.6 ng/g. Significantly lower values were found in the flowers of costmary grown on non-contaminated soil (S2): Pb - up to 0.8 mg/kg, Zn - up to 62.4 mg/kg, Cd - up to 0.1 mg/kg, Hg - up to 76.3 ng/g.

The content of heavy metals in the essential oils of costmary was also determined. The obtained results show that the main part of heavy metals contained in the flowers of the costmary does not pass into the oil during the processing of the flowers. Therefore their content in the oil is significantly lower. When the oils are obtained by distillation, the heavy metals remain in the plant residues, so the heavy metals in oils remains low.

Pb in the essential oil of costmary grown on contaminated soil (S1) reaches up to 2.7 mg/kg, Zn up to 1.7 mg/kg and Cd up to 0.08 mg/kg. Significantly lower values were found in costmary essential oil grown on uncontaminated soil (Pb up to 0.03 mg/kg, Zn up to 0.16 mg/kg and Cd up to 0.005 mg/kg). The Hg content of the oil is below the limits of the method used.

The results obtained strongly indicate that most of the Pb, Cd, Zn and Hg contained in the flowers of a costmary grown 0.5 km from the NFMW do not pass into the resulting oil. The amounts of Pb, Cd and Hg in the costmary oil are lower than the accepted maximum values and meet the requirements for an environmentally friendly product (5 mg/kg Pb, 1 mg/kg Cd, 0.1 mg/kg Hg) (Council of

Europe, 2021). The results of previous studies by Angelova et al. (2015) are confirmed, according to which the heavy metal content of the essential oil is very low and is not affected by the level of soil contamination with heavy metals. Essential oils contain only trace amounts of heavy metals in distilled oils because these metals have molecules too heavy and oversized to volatilise and concentrate in the distillation process sufficiently.

In order to provide a definitive answer to the question of the mudflat's ability to absorb heavy metals from the soil and assess its potential for phytoremediation, the Bioconcentration Factor (BCF), and Translocation Factor (TF) were calculated.

The results obtained for BCF and TF are presented in Figure 1.

Transport factor (TF) gives information on the ability of plants to uptake heavy metals through the roots and move them to the aboveground mass (leaves). TF values more significant than 1 indicates that the plant is a potential accumulator of heavy metals and can translocate metals efficiently from the roots to the aboveground mass. For Pb, Zn, Cd and Hg, TF values are greater than 1, regardless of the degree of soil contamination.

Bioconcentration factor (BCF) is the ratio of heavy metal content in plant organs to that in soil. Depending on this value, plants can be classified as hyperaccumulators (BCF > 1) or exclusion (BCF < 1).

For Pb and Zn, all coefficients (root BCF, aboveground BCF and plant BCF) are <1, indicating that the elemental content in the mudflat does not exceed the amount in the soil. For Cd, the BCF root values were <1, while BCF aboveground mass and BCF plant reached 1.37 and 2.09.

In terms of Hg, BCF aboveground mass and BCF plant were >1, while BCF roots were <1 (Fig. 1). The Hg content of the studied soils was relatively low, suggesting that the primary source of soil and plant contamination was the aerosol deposition of Hg.

The bioconcentration factor (BCF) and translocation factor (TF) values of Cd and Hg indicate that these elements accumulate in the aboveground part of the costmary. Considering the TF values for the capacity of costmary to move pollutants out of the soil and the BCF value, costmary can be referred to indicator plants for Hg and Cd and partially for Pb where the heavy metal content is similar to that in soil. Similar results were obtained by Jasion et al. (2013), who found that T. vulgare can be used as a bioindicator of Cd, Mn, and Zn in areas of lignite industry.

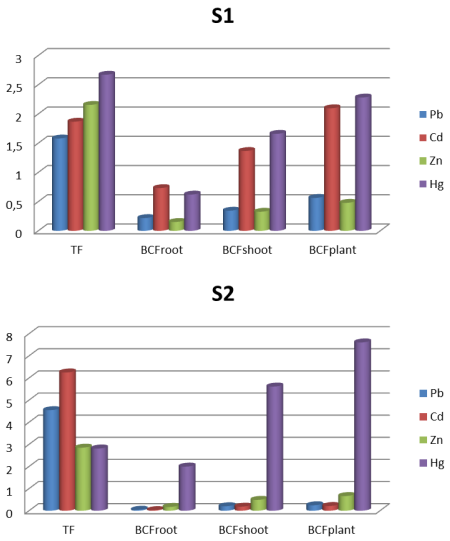

Figure 1. Translocation and bioconcentration factors for costmary

The results show that the distribution of heavy metals in the costmary organs is selective and depends primarily on the parts of the plant under study and their surface area. The distribution of heavy metals in the organs of costmary has a selective character, which decreases in the following order: Pb - roots≥ leaves>flowers>stems, Cd, Zn and Hg - leaves>roots>flowers>stems (Figure 2).

There is a distinct pattern in the accumulation of heavy metals in the vegetative organs of the costmary. The costmary accumulates heavy metals through its root system, much of which the roots retain. However, most of the metals move and get in the aboveground parts (stems, leaves and flowers). The results show that costmary can be successfully grown in areas contaminated with heavy metals.

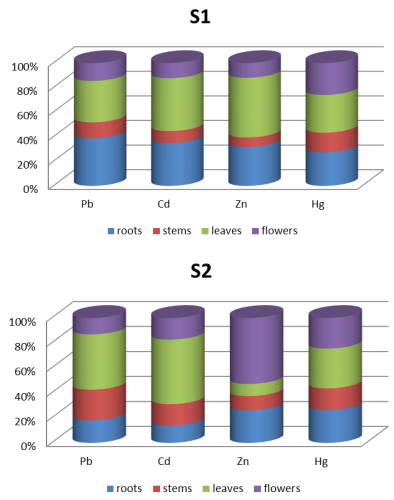

Figure 2. Distribution of heavy metals in the vegetative and reproductive organs of costmary

Oil

The yield of essential oil from the costmary is presented in Table 4. The oil yield depends on the origin of the plants, the anatomical part used to obtain the oil and the harvesting period. The oil content has been found to vary from 0.05% in stems to 2.2% in flowers (Jukneviciene et al., 1973), while in leaves from 0.31 to 1.25% (Bylaite et al., 2000). Significantly lower scores were found by Jaimand & Rezaee (2005) in the essential oil of leaves (0.25%), flowers (0.15%) and stems (0.05%) of costmary. During intense flowering, the yield decreases from both leaves and flowers (Bylaitė et al., 2000).

According to some authors, the oil content of flowers is higher than that of leaves (Jukneviciene et al., 1973; Bylaitė et al., 2000), while according to others it is lower (Jaimand & Rezaee, 2005).

The results obtained in this experiment showed that the essential oil content of costmary ranged from 1.28% to 1.45%, with higher contents in costmary grown on uncontaminated soil. Some heavy metals have been reported to affect essential oil yield from aromatic medicinal plants. The decrease in oil content with increasing soil heavy metal content may be due to the inhibition of photosynthetic rate by the toxic concentration of heavy metals which adversely affect plant growth.

Das (1997) reported that the heavy metals Cr, Pb and Cd move to the aboveground mass and negatively affect the plant metabolism, resulting in decreased plant biomass. The decrease in essential oil yield is due to the reduction of biomass of the plant, as the oil yield is calculated by the formula (biomass yield x oil in biomass).

The results of the chromatographic analysis of the essential oils obtained from the processing of the flowers of costmary grown at different distances from the NFMW are presented in Table 4. The volatiles identified in the essential oil of *T. balsamita*, their retention indices and percentages are presented in Table 4. Table 4 also shows the detailed distribution for each class of organic compounds.

Twenty-three components were identified in the costmary oil samples belonging to the monoterpenes and sesquiterpenes classes, which accounted for 98.68-98.82% of the total number of oil components (Table 4).

The major components (>1.0%) present in the costmary oil are carvone (42.66-44.12%), α-thujone (29.81-30.07%), β-bisabolene (5.51-6.24%), 1,8-cineole (2.71-3.58%), β-thujone (2.47-2.60%), cis-para-mentha-1(7),8-dien-2-ol (1.63-1.72%), trans-para-mentha-2,8-dienol (1.34-1.41%), cis-carveol (1.20-1.74%), gamma-muurolene (1.69-1.78%). Trace minor components (in the range < 1.0 and > 0.10%) myrtenol (0.80-0.85%), cis-para-mentha-2,8-dienol (0.77-0.81%), α-cadinol (0.62-0.65%), p-cymene (0.58-0.61%), delta-cadinene (0.43-0.45%), trans-pinocarveol (0.42-0.44%), cis-verbenol (0.32-0.50%), eudesm-7(11)-en-4-ol (0.39-0.41%), trans-verbenol (0.36-0.38%), cis-carvyl acetate (0.37-0.39%), pinocarvone (0.35-0.3%), cis -chrysanthenyl acetate (0.33-0.35%), and terpinen-4-ol (0.27-0.29%). The predominant class of compounds in the costmary oil is oxygenated monoterpenes, whose content ranges from 88.75% in the oil from S1 oil to 89.41% in the oil from S2.

Of the oxygenated monoterpenes, the highest content was monoterpene ketones, which ranged from 75.29 to 77.14%, consistent with the results of Bylaite et al. (2000) (71.6%). Carvone (monoterpene ketone) is the significant component identified in the oils of costmary grown in the NFMW area. Its content ranged from (42.66-44.12%), with higher

content in the costmary from the uncontaminated area. It is known that carvone is an antiseptic, central nervous system stimulant, antitumor agent, and insecticide.

Table 4. Composition of costmary oil (%)

	Component	RI	S1	S2
1	p-cymene	1025	0.58	0.61
2	1,8-cineole	1030	3.58	2.71
3	alfa-thujone	1103	29.81	30.07
4	beta-thujone	1115	2.47	2.60
5	trans-para-mentha-2,8-dienol	1124	1.34	1.41
6	cis-para-mentha-2,8-dienol	1139	0.77	0.81
7	trans-pinocarveol	1141	0.42	0.44
8	cis-verbenol	1143	0.50	0.32
9	trans-verbenol	1145	0.36	0.38
10	pinocarvone	1166	0.35	0.36
11	terpinen-4-ol	1177	0.27	0.29
12	trans-para-mentha-1(7),8-dien-2-ol	1190	1.35	1.42
13	myrtenol	1197	0.80	0.85
14	cis-carveol	1230	1.74	1.20
15	cis-para-mentha-1(7),8-dien-2-ol	1232	1.63	1.72
16	carvone	1244	42.66	44.12
17	cis-chrysanthenyl acetate	1265	0.33	0.35
18	cis-carvyl acetate	1370	0.37	0.39
19	gamma-muurolene	1480	1.69	1.78
20	beta-bisabolene	1507	6.24	5.51
21	delta-cadinene	1525	0.43	0.45
22	alfa-cadinol	1653	0.62	0.65
23	eudesm-7(11)-en-4-ol	1702	0.39	0.41
Monoterpene hydrocarbons (MH)			0.58	0.61
Oxygenated monoterpenes (eters)			3.58	2.71
Oxygenated monoterpenes (ketones)			75.29	77.14
Oxygenated monoterpenes (alcohols)			9.19	8.83
Oxygenated monoterpenes (esters)			0.70	0.73
Sesquiterpene hydrocarbons (SH)			8.35	7.74
Sesquiterpene alcohols			1.01	1.06
Total			98.68	98.82

Carvone has been found to be a significant component in the essential oil of costmary from Lithuania (56-80%, Bylaite et al., 2000), Turkey (52%) and Spain (57%) (Basher et al., 2001; Perez Alonso et al., 1992; Hassanpouraghdam, 2009), with no significant difference between the carvone content of the leaf (52.1%) and flower oils (54.2%) (Bylaite et al., 2000; Vukic et al., 2022). Carvone, camphor and α-thujone predominate in oils from Romania, Poland, Germany and Russia (Gallori et al., 2001). In oils from Iran, the main components are bornyl acetate, pinocarvone, camphor and terpineol (Jaimand & Rezaee, 2005). The content of monoterpene ketone α-thujone was high (29.81-30.07%) in oils studied, with a higher content in the oil from the non-polluted area (S2). The content of β-thujone was significantly lower (2.47-2.60%) in the oil. Many studies have found that the highly toxic monoterpenes α-thujone and β-thujone are present in costmary oil. The content of α-thujone and β-thujone in costmary oil varies widely: α-thujone 1% (Serbia, Vutic et al., 2022), 15.93% (Gallori et al., 2011), 24.6% (Iran, Hassanpouraghdam, 2009); β-thujone - 2.68% (Iran, Hassanpouraghdam, 2009), 6.4% (Serbia), 9.0 to 16.1% (Bylaite et al., 2000), 84% (Baczek et al., 2017). Although, thujone has antibacterial, pesticidal, and insecticidal effects. care should be taken in the internal use of α-thujone and β-thujone rich essential oils of costmary (Bylaite et al., 2000; Hassanpouraghdam et al., 2008). The EMA (European Medicines Agency) and the EC (European Commission) recommend a maximum intake of between 3 and 7 mg of thujone/day (EMA, 2012).The second class of compounds identified in the oil are the monoterpene alcohols (9.19- 8.83%), of which cis-carveol (1.74-1.20%), cis-p-mentha-1(7),8-dien-2-ol (1.63-1.72%) and trans-p-mentha-1(7),8-dien-2-ol (1.35-1.42%) predominate.

The essential oil also contains the monoterpene ether 1,8-cineole (3.58-2.71%). Significantly lower below 1% is the content of the monoterpene hydrocarbon p-cymene (0.58-0.611%) and the monoterpene esters (cis-hrysanthenyl acetate, 0.33-0.35% and cis-carvyl acetate, 0.37-0.39%).

The next class of compounds identified in the oil were sesquiterpene hydrocarbons (SH) (8.35-7.74%) of which gamma-muurolene (1.69-1.78%) and β-bisabolene (6.24-5.51%) predominated.

The content of sesquiterpene alcohols was significantly lower (1.01-1.06%), with the amount of alpha-cadinol (0.62-0.65%) and eudesm-7(11)-en-4-ol (0.39-0.41%) being less than 1%.

The composition of the oil is affected by heavy metal contamination of the soil. Of the oxygenated monoterpenes, the content of alcohols, ethers, and sesquiterpene hydrocarbons is higher in the costmary oil from the contaminated soil. In comparison, the content of ketones, esters, and monoterpene hydrocarbons is higher in the oil from the non-contaminated soil (S2). No significant difference was observed between the contents of sesquiterpene alcohols.

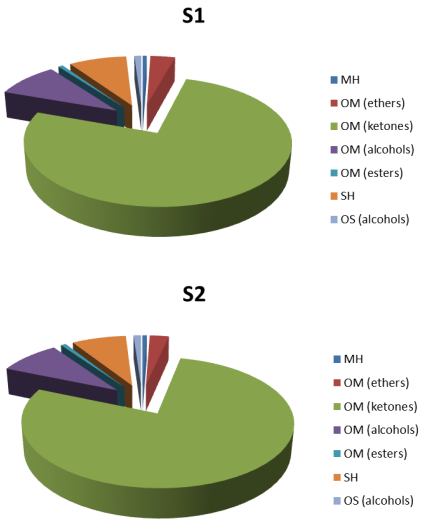

Figure 3. Example text to describe to figure above that should be replaced with your information

The composition of costmary essential oil varies depending on genetic, geographical and climatic factors (Pengelly, 2004). This phenomenon is called chemical polymorphism (Pengelly, 2004).

According to the predominant terpenes in the essential oil, 5 chemotypes have been identified in calophyllum:

1) Carvone type,
2) Camphor type,
3) Camphor-Tunion type,
4) Carvone - α-Tunion chemotype (Bylaite et al., 2000; Marculescuet al., 2001),
5) Bornyl acetate-Pinocarvone chemotype (Jaimand & Rezaee, 2005).

So far, no data are available for the carvone-α-thujone chemotype. The costmary oils analysed in this study belong to the carvone - α-thujone chemotype.

Costmary can be used as a rich source of carvone-like monoterpenes, similar to carvone-containing plants such as peppermint (*Mentha spicata* L.), caraway (*Carum carvi* L.) and fennel (*Anethum graveolens* L.).

CONCLUSIONS

It was found that:

1. There is a distinct pattern in the accumulation of heavy metals in the vegetative organs of costmary. The distribution of heavy metals in the organs of costmary grown on a highly polluted area has a selective character which decreases in the order: Pb–roots>leaves>flowers>stems, Cd, Zn and Hg–leaves>roots>flowers>stems, Zn-leaves>roots>stems>flowers.
2. Costmary is a heavy metal tolerant plant that can be grown on soils heavily contaminated with heavy metals and shows no symptoms of toxicity (chlorosis and necrosis) at a soil content of 92 mg/kg Cd, 2966.9 mg/kg Pb and 3196.1 mg/kg Zn.
3. Costmary can be referred to as indicator plants and used for monitoring soil and aerosol heavy metal pollution.
4. The content of heavy metals Pb, Cd and Hg in costmary essential oil is lower than the accepted maximum values and meets the requirements for an environmentally friendly product.
5. The content of oxygen-containing monoterpenes (88.75-89.41%) is the highest in costmary oil, followed by sesquiterpene hydrocarbons (7.74-8.35%), oxygen-containing sesquiterpenes (1.0-1.06%) and monoterpene hydrocarbons (0.58-0.61%).
6. Soil contamination affects the individual components in the oil of costmary. The monoterpene ethers, monoterpene alcohols are higher, while the concentration of monoterpene ketones and esters as well as monoterpene hydrocarbons is higher in the oil from costmary than the uncontaminated soil. No significant difference was observed with respect to sesquipropane alcohols.
7. This is the first report of a costmary oil with a mixed carvone-α-thujone chemotype.

ACKNOWLEDGEMENTS

This research work was carried out with the support of Bulgarian National Science Fund and also was financed from Project KP-06-H54/7.

REFERENCES

Abad, M.J., Bermejo, P, Villar, A. (2006). An approach to the genus *Tanacetum* L. (Compositae): Phytochemical and pharmacological review. *Phytotherapy Res*., *9*(2), 79-92.

Akula, R., Ravishankar, G.A. (2011). Influence of abiotic stress signals on secondary metabolites in plants. Plant Signal. *Behav., 6* (11), 1720–1731.

Angelova, V., Grekov, D., Kisyov, V., Ivanov, K. (2015). Potential of lavender (*Lavandula vera* L.) for phytoremediation of soils contaminated with heavy metals. *International Journal of Agricultural and Biosystems Engineering*, *9* (5), 522-529.

Baczek, K.B., Kosakowska, O., Przybył, J.L., Pióro-Jabrucka, E., Costa, R., Mondello, L., Gniewosz, M., Synowiec, A., Weglarz, Z. (2017). Antibacterial and antioxidant activity of essential oils and extracts from costmary (*Tanacetum balsamita* L.) and tansy (*Tanacetum vulgare L.*). *Ind. Crops Prod*., *102,* 154–163.

Bagci, E. Kursat, M. Kocak, A. Gur, S. (2008). Composition and antimicrobial activity of the essential oils of *Tanacetum balsamita* L. subsp. *balsamita* and *T. chiliophyllum* (Fisch. et Mey.) Schultz Bip. var. chiliophyllum (Asteraceae) from Turkey. *J. Essent. Oil-Bear Plants*, *11*, 476–484.

Basher, H.C.K., Demirci, B., Tabanca, N., Ozek, T., Goren, N. (2001). Composition of the essential oils of *Tanacetum armenum* (DC.) Schultz Bip., *T. balsamita* L., *T. chiliophyllum* (Fisch. & Mey.) Schultz Bip. var. *chiliophyllum* and *T. haradjani* (Rech. fil.) Grierson and the enantiomeric distribution of camphor and carvone. *Flav Fragr J*., *3*, 195-200.

Bylaitė, E., Venskutonis, R., Roozen, J.P., Posthumus, M.A. (2000). Composition of essential oil of costmary [*Balsamita major* (L.) Desf.] at different growth phases. *J. Agric. Food Chem*., *48*, 2409–2414.

Council of Europe (2021). European Pharmacopoeia 10th Edition (with supplements 10.6-10.7-10.8). Strasbourg.

Das, P., Samantaray, S., Rout, G.R. (1997). Studies on cadmium toxicity in plants: a review. *Environmental pollution*, *98* (1), 29-36.

EMA (European Medicines Agency) (2012). Public Statement on the Use of Herbal Medicinal Products Containing Thujone EMA/HMPC/732886/2010. 22 May 2012. Available online: https://www.ema.europa.eu/en/documents/scientific-guideline/public-statement-use-herbal-medicinal-products-containing-thujone-revision-1_en.pdf (accessed on 24 November 2022).

Gallori, S., Flamini, G., Bilia, A.R., Morelli, I., Landini, A., Vincieri, F.F. (2001). Chemical Composition of Some Traditional Herbal Drug Preparations: Essential Oil and Aromatic Water of Costmary (*Balsamita suaveolens* Pers.). *J. Agric. Food Chem*., *49*, 5907–5910.

Hassanpouraghdam, M.B., Tabatabaie, S.J., Nazemiyeh, H., Vojodi, L., Aazami, M.A., Shoja, A.M. (2008a). *Chrysanthemum balsamita* (L.) Baill.: A forgotten medicinal plant. *FU Med. Biol*., *15*, 119–124.

Hassanpouraghdam, M.B., Tabatabaie, S.J., Nazemiyeh, H, Aflatuni, A. (2008b). N and K nutrition levels affect growth and essential oil content of costmary (*Tanacetum balsamita* L.). *J Food Agricult Environ*., *6*(2), 150-154.

Hassanpouraghdam, M.B. (2009). Flowerhead Volatile Oil Composition of Soilless Culture-Grown *Chrysanthemum balsamita* L. *Nat. Prod. Res*., *23*, 672–677.

ISO 11466. (1955). Soil quality - Extraction of trace elements soluble in aqua regia.

ISO 14870. (2001). Soil quality - Extraction of trace elements by buffered DTPA solution.

Ivashchenko, I. (2107). Antimicrobial properties of *Tanacetum balsamita* L. (Asteraceae) introduced in Ukrainian Polissya. *Ukr. J. Ecol*., *7*, 52–57.

Jaimand, K., Rezaee, M.B. (2005). Chemical constituents of essential oils from *Tanacetum balsamita* L. ssp. *balsamitoides* (Schultz-Bip.) Grierson. from Iran. *J Essent Oil Res*., *17*, 565-566.

Jasion, M., Samecka-Cymerman, A., Kolon, K., Kempers, A.J. (2013). *Tanacetum vulgare* as a Bioindicator of Trace-Metal Contamination: A Study of a Naturally Colonized Open-Pit Lignite Mine. *Arch Environ Contam Toxicol*., *65*, 442–448.

Juknevicine, G., Morkunas, A., Stankeviciene, N. (1973) Some biological characteristics and essential oil content of costmary. In: Useful plants in Baltic countries and Belarus. Proceedings of the 2nd science conference (Russian): Vilnius. Lithuania, 299-303.

Kabata-Pendias, A. (2011). *Trace elements in soils and plants.* 4th ed. CRC Press.Taylor & Francis Group, Boca Raton. London, New York.

Marculescu, A., Hanganu, D., Kinga, O.N. (2001a). Qualitative and quantitative determination of the caffeic acid and chlorogenic acid from three chemovarieties of *Chrysanthemum balsamita* L. *Romanian Biotechnological Letter*, *6*(6), 477-484.

Marculescu, A., Sand, D., Barbu, C.H., Bobit, D., Hanganu, D. (2001b). Possibilities of influencing the biosynthesis and accumulation of the active principles in *Chrysanthemum balsamita* L. species. *Romanian Biotechnological Letter*, *7*(1), 577-584.

Oberprieler, C., Himmelreich, S., Kallersjo, M., Valles, J., Vogt, R. (2009). *Anthemideae*. In: Funk V, Susanna A, Stuessy TF, Bayer R (eds) Systematics evolution and biogeography of the Compositae. IAPT, Vienna, pp. 631–666.

Pengelly, A. (2004). *The constituents of medicinal plants: An introduction to the chemistry and therapeutics of herbal medicine*. 2nd edition. Allen and Unwin, Australia, 86-87.

Perez-Alonso, M., Velasco-Negueruela, A., Burzaco, A. (1992). *Tanacetum balsamita* L.: A Medicinal Plant from Guadalajara (Spain). *Acta Hortic*., *306*, 188–193.

Philips R, Foy, N. (1992). *Herbs*. Pan Books Ltd, UK, 151-152.

Venskutonis, P.R. (2016). *Costmary* (*Chrysanthemum balsamita*) Oils. In Essential oils in food preservation, Flavor and Safety; Elsevier: Amsterdam, The Netherlands, 365–375.

Vukic, M.D., Vukovic, N.L., Obradovic, A.D., Galovicova, L., Cmikova, N., Kacaniova, M., Matic, M.M. (2022). Chemical composition and biological activity of *Tanacetum balsamita* Essential Oils Obtained from Different Plant Organs. *Plants*, *11*, 3474.

Yousefzadi, M., Ebrahimi, S.N., Sonboli, A., Miraghasi, F., Ghiasi, S., Arman, M., Mosaffa, N. (2009). Cytotoxicity, antimicrobial activity and composition of essential oil from *Tanacetum balsamita* L.subsp. balsamita. *Nat. Prod. Comm*., *4*, 1934578X0900400126.

Scientific Papers. Series E. Land Reclamation, Earth Observation & Surveying, Environmental Engineering. Vol. XII, 2023
Print ISSN 2285-6064, CD-ROM ISSN 2285-6072, Online ISSN 2393-5138, ISSN-L 2285-6064

USE OF WASTE SLUDGE IN THE IMPROVEMENT OF THE QUALITY OF SOILS CONTAMINATED WITH PETROLEUM PRODUCTS

Cristian Mugurel IORGA[1], Maria Cătălina ŢOPA[1], Mihaela Marilena STANCU[2]

[1]"Dunarea de Jos" University of Galati, REXDAN Research Infrastructure,
98 George Cosbuc Street, Galati, Romania
[2]Institute of Biology Bucharest of Romanian Academy,
296 Splaiul Independentei, Bucharest, Romania

Corresponding author email: cristian.iorga@ugal.ro

Abstract

The ecological reconstruction of the sites contaminated with petroleum products is necessary to restore the geological environments affected by the economic activities specific to the petroleum industry. The purpose of ecological reconstruction is for the site to be returned to the environment for the resumption of economic and landscape functions, without presenting risks to the environment and human health. Decontamination technologies are based on various bioremediation methods. In many cases, significant amounts of soil are required to fill the resulting excavations and to systematize the land to complete the ecological reconstruction work. In the present study, the possibility to use sludge collected from a municipal wastewater treatment plant in the ecological reconstruction is presented. Both, the presence of hydrocarbon-degrading bacteria and the geotechnical characteristics make it possible to use the waste dehydrated sludge for the ecological reconstruction of the sites contaminated with petroleum products.

Key words*: contaminated site, decontamination, ecological reconstruction, sewage sludge.*

INTRODUCTION

It is well known that the oil and gas industry play an important role in the world economy. Its products represent both an important source of energy and a source for raw materials needed in other fields of activity. Large areas of land are occupied by the activities of this industry. In the entire technological chain for the exploitation of oil there is a risk of contamination of the marine and terrestrial environment, both with oil and with the products obtained from its processing. Oil spills affect large areas of land and have a negative impact on ecosystems and human health. Lands affected by oil pollution can no longer be used (Poliak et al., 2018).

The decontamination, remediation of the soil, the subsoil and the ecological reconstruction of a site contaminated with petroleum products appeared as a necessity to reduce the negative effects on the environment, eliminate any risk to the health of the population and return the land to the natural circuit for the resumption of ecological, economic and landscape functions. Agricultural lands that have been polluted with oil products, forest areas, pastures must resume their productive functions, and the most difficult mission in ecological reconstruction is to restore the soil. Pollution with petroleum products affects soil quality by modifying microbial activity (Li et al., 2007; Silva-Castro et al., 2015), but certain microorganisms can metabolize petroleum hydrocarbons.

The use of microorganisms for the decontamination of soils polluted with hydrocarbons has started to be a method used on a large scale as an ecological and versatile solution (Bento et al., 2005; Silva-Castro et al., 2013). For the bioremediation of soils contaminated with hydrocarbons it is necessary creating a favorable environment that provides the nutrients and the carbon source necessary for the development of microorganisms.

It is known from specialized literature that sewage sludge contains nutrients, microorganisms, many beneficial substances and can be used in agriculture as a natural fertilizer (Iticescu et al., 2021). All these characteristics could make sewage sludge play an important role in the bioremediation of soils contaminated with petroleum hydrocarbons. Sewage sludge results from wastewater treatment and is continuously increasing due to

investments in new treatment plants (Iticescu et al., 2021).

Presently, the management of sewage sludge is an enormous challenge in the field of environmental engineering (Rorat et al., 2019). The increase of sewage sludge produced by wastewater treatment plants around the world needs their proper disposal (Duan et al., 2017). After sewage sludge discarding in the sea, land use of dehydrated sludge for soil bioremediation of the contaminated sites or as fertilizers in agriculture becomes a common disposal way, due to the abundance of valuable components like organic matter and nutrients (e.g., nitrogen, phosphorus, potassium) (Duan et al., 2017; Rorat et al., 2019). In several European Union countries, more than 50% of the sludge is used in several applications. It is well-known, that land application of sewage sludge can improve soil properties (e.g., pH, organic matter, nutrients, porosity, moisture, stability) and finally increase plant growth (Duan et al., 2017). However, sewage sludge can also contribute to soil pollution since they contain organic and inorganic contaminants, as well as pathogens that pose a potential danger to human and animal health and the quality of ecosystems, if used as a fertilizer (Iticescu et al., 2021).

The aim of this study was to investigate the presence of several bacterial groups, including hydrocarbon-tolerant and hydrocarbon-degrading bacteria, in two sewage sludge samples taken from a municipal wastewater treatment plant. The presence of heterotrophic bacteria and enterobacteria was also investigated in the present work.

MATERIALS AND METHODS

Sampling. The sewage sludge samples, named sludge 1, and dehydrated sludge 2 were taken from the Galati wastewater treatment plant (Galati County, Romania).

Microbiological analysis of the sludge samples. Samples were mixed (1:2 v/v or g/v) with phosphate buffer saline (PBS, Sambrook and Russel 2001) and incubated at room temperature on a rotary shaker (200 rpm) for one hour. Then, serial dilutions (10^{-1}-10^{-12}) were done in PBS. The pH of the samples was determined using a Hanna pH 213 (Woonsocket, Rhode Island, USA).

In the **plate count agar** (PCA) method, serial dilutions of each sample were inoculated onto different culture media: LB agar (Sambrook and Russel 2001) for heterotrophic bacteria account, LB agar added with diesel fuel (5% v/v) for hydrocarbon-tolerant bacteria, minimal agar (Stancu, 2022) added with diesel (5% v/v) for hydrocarbon-degrading bacteria, and EMB agar (Levine agar) for enterobacteria account. Petri plates were incubated at 30°C, for 1-5 days. Then, the number of bacteria present per ml or g (CFU ml^{-1} or CFU g^{-1}) of the sample was determined.

In the **most probable number** (MPN) method, serial dilutions of each sample were inoculated (as described previously by Stancu & Grifoll, 2011) onto 96-multiwall plates containing different culture media: LB broth (Sambrook and Russel 2001) for heterotrophic bacteria account, LB broth added with diesel (5% v/v) for hydrocarbon-tolerant bacteria, and minimal broth (Stancu, 2022) added with diesel (5% v/v) for hydrocarbon-degrading bacteria account. Multiwall plates were incubated at 30°C, for 1-14 days. The bacterial population growth was determined using triphenyl tetrazolium chloride (TTC 0.3% w/v) dye as an indicator of cellular respiration (Stancu & Grifoll, 2011). The multiwall plates were incubated at room temperature for one more day in the dark. When red color was developed (because of the TTC reduction) wells were considered positive for bacterial growth (cel. ml^{-1} or cel. g^{-1}).

Isolation of hydrocarbon-tolerant, hydrocarbon-degrading bacteria. The bacteria were isolated by the enrichment culture method (Stancu and Grifoll, 2011; Stancu, 2020). Each sample (5% v/v) was used to initiate enrichment cultures in LB broth added with diesel (5% v/v), as well as in minimal broth added with diesel (5% v/v) as the sole carbon source. Tubes were incubated at 30°C, on a rotary shaker (200 rpm) for 14 days. The enrichment cultures (5% v/v) were transferred into fresh LB broth added with diesel for hydrocarbon-tolerant bacteria isolation, and minimal broth added with diesel for hydrocarbon-degrading bacteria isolation. Then, the tubes were incubated in the same conditions for another 14 days. The isolated bacteria were stored frozen in 25% (v/v) glycerol at -80°C.

The growth of the isolated bacteria in the presence of diesel was confirmed by the

measurement of the optical density at 660 nm (OD_{660}), as well as by the spot method (as described by Stancu, 2020). In the spot method, the cultures (25 µl) were inoculated onto LB agar, and then the Petri plates were incubated at 30°C, for 1-3 days. The diesel biodegradation by the isolated bacteria was confirmed by fragmenting the oil film on the surface of the growth medium and by monitoring the carbon dioxide production (CO_2 mg l^{-1}) (as described by Stancu, 2022).

RESULTS AND DISCUSSIONS

In the sewage sludge samples, sludge 1 and dehydrated sludge 2 it was revealed, by the plate count agar method, the presence of the following groups of bacteria: heterotrophic, hydrocarbon-tolerant, hydrocarbon degrading, and enterobacteria. The number of these four bacterial groups varied from one sample to another (10^3-10^7 CFU ml^{-1} or g^{-1}) (Table 1).

The heterotrophic bacteria were present in higher numbers (10^5, 10^7 CFU ml^{-1} or g^{-1}) in the two samples, as compared to the number of hydrocarbon-tolerant bacteria (10^4, 10^5 CFU ml^{-1} or g^{-1}). The enterobacteria were present in higher numbers in the dehydrated sludge 2 sample (10^7 CFU g^{-1}), as compared to their numbers in the sludge 1 sample (10^3 CFU ml^{-1}). When the LB agar and MM agar were supplemented with diesel, we observed diffuse bacterial colonies or cloth bacterial growth on the plates (Table 1, Figure 1). For these two groups of bacteria, as well as for the heterotrophic bacteria we also used the most probable number (MPN) method for more precise quantification of the viable bacteria that can tolerate and/or degrade petroleum hydrocarbons that exist in the composition of diesel.

Through the MPN method, the existence of the following groups of bacteria was detected in the sludge samples: heterotrophic, hydrocarbon-tolerant, and hydrocarbon-degrading bacteria (Table 1), and like in the previous assay, their number varied from one sample to another (10^4-10^{12} cells ml^{-1} or g^{-1}). One of the most important factors for the presence of bacteria in petroleum-polluted environments is frequently represented by their ability to adapt to new and changed environmental conditions (Stancu, 2019).

The heterotrophic bacteria were present in higher numbers (10^9, 10^{12} cells ml^{-1} or g^{-1}) in the two sludge samples.

Table 1. Microbiological analysis of the waste sludge samples

Sample	Number of bacteria by						
	PCA method (CFU ml^{-1} or g^{-1})				MPN method (cel. ml^{-1} or g^{-1})		
	Heterotrophic	Hydrocarbon-tolerant	Hydrocarbon-degrading	Enterob.	Heterotrophic	Hydrocarbon-tolerant	Hydrocarbon-degrading
Sludge 1	1.8×10^5	4.0×10^4, CBG	DBG	1.0×10^3	1.7×10^9	2.0×10^8	2.0×10^4
Sludge 2	2.4×10^7	1.8×10^5, CBG	DBG	1.6×10^7	2.5×10^{12}	2.5×10^{12}	2.0×10^6
The plate count agar (PCA) method; most probable number (MPN) method; enterobacteria (Enterob.); diffuse or cloth bacterial growth (DBG).							

Most of the bacteria present in the sludge 1 and dehydrated sludge 2 sample proved to be hydrocarbon-tolerant bacteria (10^8, 10^{12} cells ml^{-1} or g^{-1}). As observed (Table 1), the hydrocarbon-degrading bacteria were present in lower numbers in both sludge samples (10^4, 10^6 cells ml^{-1} or g^{-1}) proving that only some of them have the ability to degrade petroleum hydrocarbons which are commonly very toxic for most of the bacteria (Stancu, 2018; Stancu, 2019).

The enriched culture method was further used for the isolation of hydrocarbon-tolerant and hydrocarbon-degrading bacteria from the two sludge samples, sludge 1 and dehydrated sludge 2.

As previously reported, the enriched culture method is a very effective technique for the isolation of bacteria that exist in environments polluted with petroleum and petroleum products (Stancu & Grifoll, 2011; Stancu, 2020; Stancu, 2022). The growth of hydrocarbon-tolerant and hydrocarbon-degrading bacteria was revealed by the opalescence of the culture media and by the formation of black or brown sediment in the growth tubes (Figure 1). Most petroleum hydrocarbons faced in the environment are degraded by indigenous bacteria that use these

toxic organic compounds for their growth. There are over 70 bacterial genera capable to degrade petroleum hydrocarbons, and several of them, as are the bacteria from the genera *Achromobacter, Acinetobacter, Alcaligenes, Arthrobacter, Bacillus*, *Burkholderia*, *Corynebacterium*, *Enterobacter*, *Flavobacterium, Micrococcus*, *Mycobacterium*, *Pseudomonas*, *Rhodococcus, Vibrio*, etc. has a significant role in petroleum hydrocarbons degradation (Xu et al., 2018).

As expected, the growth of the hydrocarbon-tolerant and hydrocarbon-degrading bacteria in the presence of diesel (5%) varied from one sample to another (OD_{660} 0.46-1.87) (Table 2). In the case of hydrocarbon-tolerant bacteria, we observed higher growth (OD_{660} 1.61, 1.87), compared with the growth of hydrocarbon-degrading bacteria (OD_{660} 0.46, 0.77). The results were confirmed by the fact that the isolated bacteria showed good viability (25-100%) when they were grown in the presence of diesel (5%).

The fragmentation of the diesel film (Table 2), as a result of the hydrocarbon biodegradation, was observed both in the case of hydrocarbon-tolerant, as well as in the case of hydrocarbon-degrading bacteria. We observed that the amount of CO_2 released varied from one sample to another (704-770 mg l^{-1}), indicating petroleum hydrocarbon degradation. Since the sludge samples were contaminated with petroleum hydrocarbons (TPH 1370 mg l^{-1}), the isolation of hydrocarbon-tolerant and hydrocarbon-degrading bacteria from sludge 1 and dehydrated sludge 2, was not a surprise. From the hydrocarbon-tolerant and hydrocarbon-degrading bacterial cultures obtained, six isolates were purified through repeated passages on LB agar (Figure 1).

It was reported that certain physiological properties of the bacteria isolated from the petroleum-polluted environments can increase the availability and degradation of toxic hydrocarbons.

It is well-known that the bacteria which exist in petroleum-polluted environments have the ability to produce biosurfactants. These bacterial metabolites can emulsify petroleum hydrocarbons increasing the attack surface of bacteria and the accessibility of its enzymes (Stancu, 2015; Stancu, 2018; Stancu, 2020; Stancu, 2022).

CONCLUSIONS

In the sewage sludge samples, sludge 1 and dehydrated sludge 2 it was revealed by using the plate count agar method and MPN method, the presence of heterotrophic, hydrocarbon-tolerant, hydrocarbon-degrading, and enterobacteria.

All these four groups of bacteria were detected in higher numbers (10^5-10^{12} CFU or cells) in the dehydrated sludge 2, as compared to their numbers in the sludge 1 sample (10^3-10^9 CFU or cells).

The isolation of hydrocarbon-degrading, as well as hydrocarbon-tolerant bacteria from these two sludges, was not unexpected since the sewage samples were contaminated with petroleum hydrocarbons because of human activities.

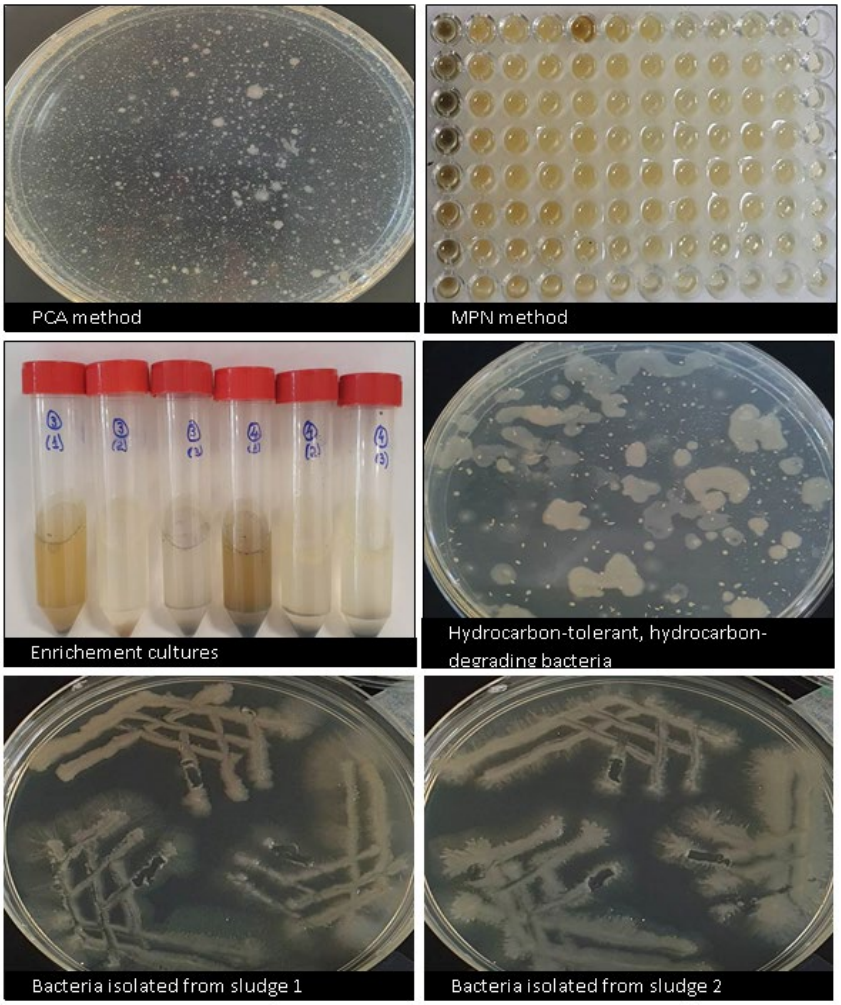

Figure 1. Enumeration and isolation of hydrocarbon-tolerant, hydrocarbon-degrading bacteria
Plate count agar (PCA) method; most probable number (MPN) method

Table 2. Characterization of the isolated bacterial populations

Sample	Bacteria							
	Hydrocarbon-tolerant				Hydrocarbon-degrading			
	Growth (OD_{660})	Viability	Diesel fragm.	CO_2 (mg l^{-1})	Growth (OD_{660})	Viability	Diesel fragm.	CO_2 (mg l^{-1})
Sludge 1	1.61	75	+	704	0.46	100	+	1100
Sludge 2	1.87	25	+	770	0.77	100	+	1230
Diesel film fragmentation (diesel fragm.), positive reaction (+); CO_2 production (CO_2 mg l^{-1}).								

ACKNOWLEDGEMENTS

The study was funded by project no. 769/2022 from the "Dunărea de Jos" University of Galați and project no. RO1567-IBB05/2022 from the Institute of Biology

REFERENCES

Bento, F.M., Camargo, F.A.O., Okeke, B.C., Frankenberger, W.T. (2005). Comparative bioremediation of soils contaminated with diesel oil by natural attenuation, biostimulation and

bioaugmentation. *Bioresourse Technol., 96*(9), 1049-1055.

Duan, B., Zhang, W., Zheng, H., Wu, C., Zhang, Q., Bu, Y. (2017). Disposal situation of sewage sludge from municipal wastewater treatment plants (WWTPs) and assessment of the ecological risk of heavy metals for its land use in Shanxi, China. *International Journal of Environmental Research and Public Health*, *4*(7), 823. doi:10.3390/ijerph14070823.

Iticescu, C., Georgescu, L.P., Gurau, G., Murarescu, M., Dima, D., Murariu, G., Gheorghies, C. (2015). Methods to reduce environmental impact of municipal wastewater sewage sludge. *Environmental Engineering and Management Journal*, 14(10), 2457 – 2463.

Iticescu, C., Georgescu, L.P., Murariu, G., Cîrciumaru, A., Timofti, M. (2018). The Characteristics of Sewage Sludge Used on Agricultural Lands*, AIP Conference Proceedings 2022, 020001*; doi: 10.1063/1.5060681*,* 02001 – 1 – 02001 – 8.

Iticescu, C., Georgescu, P.L., Arseni, M., Rosu, A., Timofti, M., Carp, G., Cioca, L.I. (2021). Optimal Solutions for the Use of Sewage Sludge on Agricultural Lands, *Water, 13*, 585. https://doi.org/10.3390/w13050585

Li, H., Zhang, Y., Kravchenko, I., Xu, H., Zhang, C. (2007). Dynamic changes in microbial activity and community structure during biodegradation of petroleum compounds: a laboratory experiment. *J. Environ. Sci., 19,* 1003-1013.

Polyak, Y.M., Bakina, L.G., Chugunova, M.V., Mayachkina, N.V., Gerasimov, A.O., Bure, V.M. (2018). Effect of remediation strategies on biological activity of oil-contaminated soil–A field study. *International Biodeterioration & Biodegradation 126,* 57-68 https://doi.org/10.1016/j.ibiod.2017.10.004

Rorat, A., Courtois, P., Vandenbulcke, F., Lemiere, S. (2019). Sanitary and environmental aspects of sewage sludge management. *Industrial and Municipal Sludge*, 155-180. doi:10.1016/B978-0-12-815907-1.00008-8.

Sambrook, J., Fritsch, E.F., Maniatis, T. (1989). Molecular Cloning, A Laboratory Manual. 2nd ed. Cold Spring Harbor Laboratory Press, Cold Spring Harbor, New York.

Stancu, M.M. (2015). Solvent tolerance mechanisms in *Shewanella putrefaciens* IBB_{Po6}. *Water, Air, and Soil Pollution, 226*(39). doi:10.1007/s11270-015-2328-3.

Stancu, M.M. (2018). Production of some extracellular metabolites by a solvent-tolerant *Pseudomonas aeruginosa* strain. *Waste and Biomass Valorization, 9*(10), 1747-1755.

Stancu, M.M. (2019). Bioremediation of petroleum contaminated environments by *Pseudomonas* species. *Journal of Biotechnology & Bioresearch, 2*(1), JBB.000530.2019.

Stancu, M.M. (2020). Kerosene tolerance in *Achromobacter* and *Pseudomonas* species. *Annals of Microbiology, 70*(8). doi:10.1186/s13213-020-01543-2.

Stancu, M.M. (2022). Characterization of new diesel-degrading bacteria isolated from freshwater sediments. *International Microbiology, 25*(4). doi:10.1007/s10123-022-00277-2.

Stancu, M.M., Grifoll, M. (2011). Multidrug resistance in hydrocarbon-tolerant Gram-positive and Gram-negative bacteria. *The Journal of General and Applied Microbiology, 57*, 1-18.

Xu, X., Liu, W., Tian, S., Wang, W., Qi, Q., Jiang, P., Jiang, P., Gao, X., Li, F., Li, H., Yu, H. (2018). Petroleum hydrocarbon-degrading bacteria for the remediation of oil pollution under aerobic conditions: a perspective analysis. *Frontiers in Microbiology, 9*, 2885. doi:10.3389/fmicb.2018.0288.

Scientific Papers. Series E. Land Reclamation, Earth Observation & Surveying, Environmental Engineering. Vol. XII, 2023
Print ISSN 2285-6064, CD-ROM ISSN 2285-6072, Online ISSN 2393-5138, ISSN-L 2285-6064

RESEARCH ON THE HEAVY METALS CONTENT IN SOILS FROM VARVOR LOCALITY, DOLJ COUNTY

Gilda-Diana BUZATU, Ana Maria DODOCIOIU

University of Craiova, Faculty of Horticulture, 13 A.I. Cuza Street, Craiova, Romania

Corresponding author email: anadodocioiu@gmail.com

Abstract

In the current research, heavy metals content (Zn, Ni, Cd, Cu, Pb) was analysed in soil and corn cobs samples to determine if the soil and corn plants are polluted with these heavy metals, corroborated with the humus content, total nitrogen, mobile forms of phosphorus and potassium, soil reaction, clay, sand and silt. Soil samples were collected from 9 parcels located in the Varvor area. Varvor is situated in the SW of Dolj County, 18 km from Craiova, and positioned in the northeast part of the Desnatui Plain, on the border with the high Balacita Plain. Following the results, was found that all values obtained for these parameters are falling below the established normal values by Order 756/1997, for sensitive soils. Only concerning Cu content of the analysed soil samples, the limit value of 20 mg kg $^{-1}$ was exceeded for 6 of the 9 samples, the variation range being between 19.1-35.8 mg kg $^{-1}$. Heavy metals content in corn cobs were within the acceptable limits according to Codex Alimentarius, except for cadmium, which exceeded the limit value established by Commission Regulation no. 1881/2006.

Key words*: chemical, heavy metals, physical, properties, soil.*

INTRODUCTION

Among the pollutants, heavy metals have a recognized toxic potential on all living organisms, each of these metals being dangerous outside a certain range of values.

Due to soil's ability to store heavy metals over the years, the soil can be considered a repository for them (Buzatu & Dodocioiu, 2015).

Sources of heavy metals can be both natural (lithogenetics, pedogenetics) and anthropogenic: fertilizers and amendments, manure, urban sludge, irrigation water, pesticides, non-ferrous industry, residues from coal combustion, vehicle emissions etc.

These can contribute to greater or lesser loading of the soil and, implicitly, of the plants with these chemical elements (Dodocioiu & Mocanu, 2009; Buzatu & Dodocioiu, 2017).

In Romanian soils are predominant the following heavy metals: manganese, copper, zinc, boron, molybdenum, lead, nickel, chromium and sometimes beryllium, vanadium, zirconium, scandium (Davidescu & Davidescu, 1988).

Most of the agricultural soils in our country are formed on sediments with a medium and fine texture, with reserves of trace elements inherited from the parent material. Naturally high levels in the soil can result from geological processes, but mostly result from agriculture and industrial activity.

Heavy metals are elements that exist in nature and that can create a complete biological cycle, i.e. from soil - plant - animal - man.

Among these heavy metals, copper, zinc and nickel are essential for plant growth, entering the active zone of some enzymes, thus being co-factors or co-enzymes (Sungur et al., 2014).

The absorption of nutrients by plants disturbs the balance in the soil solution, which leads to the passage of some elements from the adsorbed state into the soil solution. The organic matter in the soil, on one hand, retains a series of elements, and on the other hand, following the microbiological activity, it releases a series of elements, for this reason it could be considered a dynamic balance. The intensity of the absorption process of heavy metals from the soil into the plant differs depending on the soil and plant type, fertilizers, irrigation and the interaction between these factors (Milačič & Štupar, 1995; Banks et al., 2006).

Workplace and food are main routes of human exposure to the action of heavy metals. Higher plants are very sensitive to climate changes: zinc reduces biological activity in the soil, modifies its physicochemical properties, acts on microorganisms by disrupting the transformation

process of organic matter in the soil and slows down physiological processes. In addition, cadmium (often present in phosphate fertilizers) produces the blocking of microbiological processes.

The toxic effect of heavy metals also manifests itself on the microorganisms in the soil, which further leads to the modification of the activity of all the microorganisms in the soil (Ashraf & Ali, 2007).

Cadmium and lead compete with minerals such as calcium, magnesium or iron for absorption but can also bind to structural proteins, enzymes and nucleic acids, so they can interfere with their functioning (Andrade et al., 2017).

In order to reduce the mobility of some heavy metals (i.e. cadmium) from the soil to cereals is considered the utilization of organic fertilizers and liming (Zhao et al., 2015).

Maize is considered the basic grain in animal and human food (Lu et al., 2015).

Because complete removal of heavy metals from grains can rarely, if ever, be achieved; prevention is more effective than treatment (Thielecke & Nugent, 2018).

Some heavy metals such as cadmium and lead have no physiological role in plants and as a result, they are considered not essential for plants growth (Singh, 2011). But others such as copper, nickel and zinc are considered essential for normal growth and metabolism of plants and have toxic effects when found in larger quantities than the plants need (Garrido et al., 2002; Rascio & Izzo, 2011).

Occurrence of cancer, cardiovascular, neurological and other diseases are some negative effects resulted after consuming vegetal products with heavy metals, as reported by different authors (Jarup, 2003; Baghaie & Fereydoni, 2019).

Considering the maintenance of human and animal health, it is necessary to monitor the content of heavy metals in plants and to consider Directive no. 86/278/CEE, regarding the use of sludge from sewage treatment plants as fertilizer in agriculture, and for crops known to have a content of these elements, they must be excluded from animal and human feed.

The main objectives of this research were: (1) to determine the physical and chemical characteristics of the analyzed soil; (2) to determine the content of heavy metals in soil and corn cobs; (3) to evaluate the relationship between the uptake of heavy metals by corn cobs and the content of heavy metals in soil.

MATERIALS AND METHODS

Experimental site

The study was carried out in Varvor locality on a stagnant, vertic, moderately pseudo-glazed, bathycalcaric preluvosol with loamy/clayey texture, generated by disaggregation-alteration material consisting of medium-fine and fine material stratifications, in the year 2021, the area where wheat and corn are cultivated. Varvor is situated in the SW of Dolj County, 18 km from Craiova, and positioned in the northeast part of the Desnatui Plain, on the border with the high Balacita Plain, temperate continental climate, with precipitation of 551.4 mm/year.

Soil and plant sampling

We collected 9 paired soil - corn samples. The soil samples were collected from 0-20 cm surface layer. Corn cobs samples (*Zea mays, Gramineae* family) were taken from the 9 plots from which soil samples were taken. All the samples were transported to the laboratory where they were analyzed. Soil samples were dried at the room temperature, grounded with an agate mortar and sieved.

Soil analysis

Soil diagnosis and inclusion in the soil classification system was carried out in accordance with the Romanian Soil Taxonomy System (SRTS, Florea & Munteanu, 2012).

Determination of the granulometry composition of the soil was achieved by treating the soil samples in order to obtain the dispersion according to the Kacinski method. The separation of the particle size fractions was carried out by sieving for particles smaller than 0.02 mm and by pipetting for particles with a diameter equal to or greater than 0.02 mm. The results were expressed in percentages compared to the material remaining after pre-treatment, the sum of the fractions being 100%.

The determination of the pH value was carried out by the potentiometric method, using a Mettler Toledo, MP 220 pH-meter, at a soil: water ratio of 1:2.5.

The humus content (%) was determined by wet oxidation according to the Walkley-Black method modified by Gogoasa.

The total N content (%) was determined by Kjeldahl method, using Raypa MBC-6 digester and Pro-Nitro-1, I.C.T. distillation unit.
The content of mobile P in the soil was determined according to the Egner-Riehm-Domingo method, colorimetrically with a Jasco V-530 UV VIS spectrophotometer.
The K content in the soil was determined according to the Egner-Riehm-Domingo method, using the flame photometer Jenway PFP-7.
Determination of heavy metals in the soil was carried out by weighing 3 g of soil and moistening it with 1 mL of deionized water, then the sample was mineralized using 21 mL of HCl and 7 mL of HNO_3, the solution obtained was then used to determine the content of heavy metals using iCE^{TM} 3000 AAS Spectrometer Thermo Fisher Scientific.

Plant analyses

Determination of heavy metals in corn cobs was carried out by drying the corn cobs in an oven at 105°C, grounded with the knife mill Grindomix GM 200, Retsch, followed by the mineralization of plant samples (1 g of plant product) which is carried out using 5 mL of HNO_3 (65%) and 4 mL H_2O_2 (35%). The solution thus obtained is prepared for the determination of the metal content of plant samples with the help of the iCE^{TM} 3000 AAS Spectrometer Thermo Fisher Scientific.

RESULTS AND DISCUSSIONS

Research was carried out on a preluvosol, stagnant, vertic, moderately pseudo-glazed, bathycalcaric with loamy/clayey texture, generated by disaggregation-alteration material consisting of medium-fine and fine material stratifications (Table 1).
A quantity of 30 t/ha sewage sludge was applied to this soil, its chemical composition being presented in Table 2.
Soil is characterized with low humus content, low to medium total nitrogen content, very high phosphorus content, high/very high mobile potassium content, loamy/clay texture, an imperfect global drainage and a strong compaction of the lower horizons.
The values obtained for the physicochemical characteristics of the soil were processed using the statistical package SPSS 17, the descriptive statistics including the minimum value, the maximum value, the average value and the standard deviation and are presented in Table 1.

Table 1. The physicochemical characteristics of the preluvosol from Varvor statistically interpreted

Physico-chemical characteristics of the soil	Minimum	Maximum	Mean	Std. Deviation
pH	5.28	5.91	5.50	0.21
Humus (%)	2.12	2.90	2.41	0.29
N total (%)	0.12	0.15	0.13	0.01
P mobile (mg·kg^{-1})	97	137	111.44	16.94
K mobile (mg·kg^{-1})	186	207	194	8.30
Clay (%)	35.70	49.80	43.70	5.70
Sand (%)	31	38.10	34.08	3.26
Silt (%)	19.2	26.2	23.33	3.03

Table 2. Characterization of sewage sludge

Parameter	Determined value
Humidity, %	263
pH	7.82
N total, %	4.80
P total, %	0.22
Ca, %	0.79
Mg, %	0.35
Cu (mg·kg^{-1})	167
Zn (mg·kg^{-1})	663
Pb (mg·kg^{-1})	62.3
Cd (mg·kg^{-1})	2.22
Co (mg·kg^{-1})	4.51
Ni (mg·kg^{-1})	94.8
Cr (mg·kg^{-1})	68.90

The soil has the following morphological characteristics:

- 0-20 cm - dark brown Ao horizon, loamy texture, subangular and small angular polyhedral structure, dry, gradual transition.
- 20-40 cm - A/By horizon, dark yellowish-brown colour, clayey texture, medium-large angular polyhedral structure, very plastic, very adhesive, moderately compacted, rare thin roots, dry, gradual transition.
- 40-74 cm - horizon Bt1w2, brown colour 20-25% stains in redox colours, clayey texture, polyhedral angular and large prismatic structure, shows clay films and oblique faces, very plastic, very adhesive, present cracks filled with very rare material that penetrate up to 80-90 cm deep, strongly compacted, gradual transition.
- 74-100 cm - Bt2w2, dark yellowish-brown colour by 25-30%, spots and dots in

oxidation-reduction colours, clay loamy texture, massive structure, strongly compacted.

According to the data presented in Table 1, the pH of the soil varied between 5.28 and 5.90, in these conditions the soil reaction was moderately acidic (pH=5.28) and weakly acidic (pH=5.91). In acidic, well-aerated soils, heavy metals are easily mobile and therefore accessible to plants (Król et al., 2020).

Humus content of the soil is between 2.12 and 2.90%, with a mean content of 2.41%, indicating a low supply state.

Regarding the total N content in the analysed samples, it varied between 0.12-0.15%, this indicating a low to medium supply state of the soil in this element.

The mobile phosphorus content varied between 97-137 mg·kg^{-1} P, with an average of 114.44 mg·kg^{-1} P. These values indicate a very good state of soil supply with phosphorus.

The potassium content recorded values between 186-207 mg·kg^{-1} K, with an average of 194 mg·kg^{-1} K, values between 186-200 mg·kg^{-1}K indicate a good state of soil supply in this element, and values that exceed 200 mg·kg^{-1} K indicate a very good supply of soil in this element.

The obtained concentrations of heavy metals in the stagnant preluvosol from Varvor locality were compared with the normal values of these metals in soils for sensitive use allowed by the legislation in force (Order 756/1997) and were processed with statistical package SPSS 17, descriptive statistics including maximum value, minimum value, arithmetic mean and standard deviation. All these data are presented in Table 3.

Table 3. Values of the content of heavy metal in the soils from Varvor (mg·kg^{-1})

Metal	Minimum	Maximum	Mean	Std. Deviation
Cd	0.07	0.27	0.13	0.06
Cu	19.1	35.8	22.95	5.67
Pb	10.0	17.7	13.21	2.59
Ni	13.6	15.5	14.51	0.66
Zn	43.1	68.1	57.88	7.02

The values of cadmium, nickel, zinc, lead concentrations are below the normal values mentioned in Order 756/1997 for soils with sensitive use, except for the values of the copper concentrations (Table 4).

The range of variation for the copper content of the analysed soils is between the minimum value of 19.1 mg·kg^{-1} and the maximum value of 35.80 mg·kg^{-1} (mean value of 22.95 mg·kg^{-1}), for 6 out of 9 samples, the normal value of 20 mg·kg^{-1} according to Order 756/1997 is exceeded but staying below the alert threshold of 100 mg·kg^{-1}. Copper is one of the microelements essential for plant nutrition, contents lower than 10 mg·kg^{-1} in soils determine the deficiency in this element in vegetation, while higher contents can be toxic.

Total copper content from the surface layer of different soil type varies between 4 and 49 mg·kg^{-1}, while the available copper content varies between 0.5 -5 mg·kg^{-1} (Radulov et al., 2011). Fulvic acids from organic matter show a preference for copper in the formation of complexes, showing a very strong affinity for the organic matter in the soil, forming very stable complexes and that is why it remains in the soil.

Regarding the heavy metal concentration values obtained for the soil samples, they had the following descending order: Zn>Cu>Pb>Ni>Cd, which is in correlation with the research of Lokeshwari and Chandrappa (2006), who concluded that zinc is a very mobile element and therefore the retention capacity of the soil is much lower.

Table 4. Reference values (mg·kg^{-1}) according to Order 756/1997 for sensitive soil

Metal	Normal values	Alert threshold	Intervention threshold
Cd	1	3	5
Cu	20	100	200
Pb	20	50	100
Ni	20	75	150
Zn	100	300	600

All the data obtained indicates that the application of biosolids shows the lack of pollution of the soil by the application of sludge, which suggests that these types of soils have the intrinsic possibility of limiting the effect of acidity on the balance of heavy metals.

The values obtained for content of heavy metals in corn cobs were processed using the statistical package SPSS 17, the descriptive statistics

including the minimum value, the maximum value, the average value and the standard deviation and are presented in Table 5.

Regarding the values of the heavy metals' concentrations obtained for corn grains samples, they had the following descending order: Zn>Cu>Ni>Pb>Cd, this being in correlation with research conducted by Sungur and his team (2014).

Table 5. The values of the content of heavy metal in corn cobs (mg·kg^{-1})

Metal	Minimum	Maximum	Mean	Std. Deviation	Maximum allowed limits *
Cd	0.03	0.15	0.08	0.04	0.20
Cu	1.23	4.39	2.49	1.31	50
Pb	0.12	0.16	0.12	0.01	0.30
Ni	0.12	0.79	0.49	0.25	67
Zn	9.21	15.31	14.41	1.96	100

* According to Codex Alimentarius Commission 2001

The highest values of heavy metal concentrations were recorded for zinc because it is more mobile and once embedded in biochemical compounds and in specific anatomical-physiological structures it can no longer be displaced from the corn cobs. This is followed by copper and then by nickel. The lowest concentrations of heavy metals were recorded for cadmium and lead.

In conclusion, it can be said that copper and zinc have much higher mobility compared to the other heavy metals analyzed.

Research has shown that when heavy metals (zinc, iron, nickel, copper, lead) are found in the soil, they will accumulate in all the vegetative organs of the plants that grow on this soil (Ibrahim, 2015).

Heavy metals content in corn were within the acceptable limits, according to Codex Alimentarius, 2001.

According to EU regulations, the maximum allowed concentrations for cadmium and lead are limited (***, Commission Regulation no. 1881/2006), the maximum allowed concentration in the case of cereals are 0.2 mg·kg^{-1} for lead and 0.10 mg·kg^{-1}for cadmium, these being much lower than those established by Codex Alimentarius. Regarding the other heavy metals studied, no maximum limits are established by Commission Regulation no. 1881/2006. According to this, in 3 of 9 corn cobs samples analyzed, the limit value for cadmium was exceeded and for lead, all the concentrations of the analyzed samples are below the limit.

All the copper concentration values do not indicate an excess of the normal content values, which is 3-15 mg·kg^{-1}, although for grains these concentrations can be even higher (Lațo et al. 2012).

The correlation coefficient (r) ranges from 0.68 - moderate correlation for copper, to 0.80-0.84 - strong correlation for lead, zinc, and to 0.90-0.91 strong-very strong for cadmium and nickel. This indicates that there is a direct correlation between the content of heavy metals in the soil and the content of metals accumulated in the corn cobs (Table 6).

Table 6. Correlation coefficients between total heavy metal content in soil and corn cobs

Metal mg·kg^{-1}	Correlation coefficient
Cd	0.90
Cu	0.68
Pb	0.80
Ni	0.91
Zn	0.84

CONCLUSIONS

Following the results, it can be concluded that all values obtained for cadmium, lead, nickel and zinc are falling below the established normal values by Order 756/1997, for sensitive soils. Only with regard to copper content of the analysed soil samples, the limit value of 20 mg kg $^{-1}$ was exceeded for 6 of the 9 samples, the variation range being between 19.1-35.8 mg kg^{1}.

Analysis of the data obtained indicates that application of biosolids specifies the lack of pollution of the soil by the application of sludge, which suggests that these types of soils have the intrinsic possibility of limiting the effect of acidity on the balance of heavy metals.

Heavy metals content in corn cobs were within the acceptable limits according to Codex Alimentarius, except for cadmium, which exceeded the limit value established by Commission Regulation no. 1881/2006. There is a direct correlation between the content of heavy

metals in the soil and the content of metals accumulated in the corn cobs. Compared to the other analysed metals in corn cobs, the highest values were registered for zinc, copper and nickel and the minimum values were registered for lead and cadmium.

REFERENCES

Andrade, V.M., Aschner, M., & Dos Santos, A.P.M. (2017). Neurotoxicity of metal mixtures. *Advances in Neurobiology, 18*, 227–265.

Ashraf, R., & Ali, T.A. (2007). Effect of heavy metals on soil microbial community and mung beans seed germination. *Pakistan Journals of Botany*, *39*(2), 629-636.

Baghaie, A.H., & Fereydoni, M. (2019). The potential risk of heavy metals on human health due to the daily consumption of vegetables. *Environmental Health Engineering and Management, 6*, 11- 16.

Banks, M.K., Schwab A.P., & Henderson C. (2006). Leaching and reduction of chromium in soil as affected by soil organic content and plants*, Chemosphere, 62*(2), 255–264.

Buzatu, G.D., & Dodocioiu, A.M. (2015). Research regarding agrochemical characteristics and heavy metals content in a vineyard soil, *Journal of Horticulture, Forestry and Biotechnology*, *19(1*), 201-206.

Buzatu, G.D., & Dodocioiu, A.M. (2017). Study to assess the presence of micro-, macroelements and heavy metals within the soil - grapevine plants system, *Journal of Horticulture, Forestry and Biotechnology, 21(2)* 97-102.

Dodocioiu, A.M., & Mocanu, R (2009). *Agrochimie*, Craiova, RO: Sitech Publishing House.

Davidescu, D., Davidescu, V. (1988). *Microelementele în agricultura*, Bucuresti, RO: Academia RSR Publishing House.

Florea, N., & Munteanu, I. (2012). *Sistemul Român de Taxonomie a Solurilor (SRTS*), Craiova, RO: Sitech Publishing.

Garrido, S., Campo, G.M.D., Esteller, M.V., Vaca, R. & Lugo, J. (2005), Heavy metals in soil treated with sewage sludge composting, their effect on yield and uptake of broad bean seeds (*Vicia faba* L.). *Water, Air, and Soil Pollution*, *166,* 303–319.

Ibrahim, K.N. (2015). Heavy metal concentration (Pb, Cu, Fe, Zn, Ni) in plant parts of *Zea mays* L. cultivated in agricultural area near Alor Gajah, Melaka, Malaysia. *American Journal of Environmental Engineering, 5 (3)*, 8-12.

Jarup, L. (2003). Hazards of heavy metal contamination. *British Medical Bulletin, 68*, 167-182.

Król, A., Mizerna, K., & Bozym, M. (2020). An assessment of pH-dependent release and mobility of heavy metals from metallurgical slag. *Journal of Hazardous Material*s, *384*, 121502, doi.org/10.1016/j.jhazmat.2019.121502

Laţo, A., Radulov, I., Berbecea, A., Laţo, K., & Crista, F. (2012). The transfer factor of metals in soil-plant system, *Research Journal of Agricultural Science, 44*(3), 67-72.

Lokeshwari, H., & Chandrappa, G.T. (2006). Impact of heavy metal contamination of Bellandur Lake on soil and cultivated vegetation. *Current Science*, *91*(5), 622-627.

Lu, Y., Yao, H., Shan, D., Jiang,Y., Zhang, S., & Yang, J. (2015). Heavy Metal Residues in Soil and Accumulation in Maize at Long-Term Wastewater Irrigation Area in Tongliao, China, *Journal of Chemistry, 2,* doi 10.1155/2015/628280.

Milačič, R., & Štupar J., (1995). Fractionation and oxidation of chromium in tannery waste-and sewage sludge-amended soils, *Environmental Science and Technology*, *29*(2), 506–514.

Rascio, N. & Izzo, F.N. (2011). Heavy metal hyperaccumulating plants: How and why do they do it? And what makes them so interesting? *Plant Science, 180*, 169–181.

Radulov, I., Laţo, A., Berbecea, A., Crista F. (2011). *Analiza chimica a solului*, Timisoara, RO: Eurobit Publishing House.

Singh, J., & Kalamdhad, Ajay S. (2011). Effects of Heavy Metals on Soil, Plants, Human Health and Aquatic Life, *International Journal of Research in Chemistry and Environment*, *1*(2),15-21.

Sungur, A., Soylak, M., & Ozcan, H. (2014). Investigation of heavy metal mobility and availability by the BCR sequential extraction procedure: relationship between soil properties and heavy metals availability, *Chemical Speciation & Bioavailability*, *26*(4), 219-230.

Thielecke, F., & Nugent, A.P. (2018). Contaminants in Grain-A Major Risk for Whole Grain Safety? *Nutrients, 10*(9), 1213, doi 10.3390/nu10091213.

Zhao, F.J., Ma, Y., Zhu, Y.G., Tang, Z., & McGrath, S.P. Soil contamination in China: Current status and mitigation strategies. (2015). *Environmental Science & Technology, 49*, 750–759.

***Commission Regulation no. 1881/2006 setting maximum levels for certain contaminants in foodstuffs

***Directive no. 86/278/CEE on the protection of the environment, and in particular of the soil, when sewage sludge is used in agriculture.

***FAO/WHO. (2001).Food Additive and Contaminants bythe Joint FAO/WHO Food Codex Alimentarius.

***Order No. 344/708 of 16 August 2004 for the approval of the Technical Norms concerning the protection of the environment and especially of the soils, when sewage sludge is used in agriculture.

***Order of the Ministry of Waters, Forests and Environmental Protection No. 756/3 November 1997, approving the regulation on the assessment of environmental pollution, Bucharest, Romania.

Scientific Papers. Series E. Land Reclamation, Earth Observation & Surveying, Environmental Engineering. Vol. XII, 2023
Print ISSN 2285-6064, CD-ROM ISSN 2285-6072, Online ISSN 2393-5138, ISSN-L 2285-6064

AIR EMISSIONS INVENTORY FROM A ROMANIAN CONSTRUCTION MATERIALS FACTORY

Patricia MOCANU, Veronica IVANESCU, Mirela Alina SANDU

University of Agronomic Sciences and Veterinary Medicine of Bucharest,
59 Marasti Blvd, District 1, Bucharest, Romania

Corresponding author email: patmocanu07@gmail.com

Abstract

The paper aimed to present the main methodologies for estimating atmospheric emissions, with an example for a construction materials factory. It is based on the statistical data provided by a pre-dosed dry mortar factory, for which both the emissions specific to the limestone quarry where the raw material comes from, as well as the emissions from the manufacturing process, were analysed. The presented method, used for the elaboration of the emission inventory and not only, requires the use of specific emission factors for each emission-generating activity in an area or in a company. The method can be used for other purposes as well, including for calculating taxes to the Environmental Fund. Sometimes, due to legislative oversights or the impossibility of including a source in the existing list, it is up to the evaluator to choose the most correct approach.

Key words*: air pollutants, emission source, emission factor, emission inventory, Environmental Found.*

INTRODUCTION

Substances emitted into the atmosphere by human activities and natural sources represents one of the main causes of many current and potential environmental problems, including acidification, eutrophication, and tropospheric ozone pollution, air quality degradation, global warming, damage of buildings and other structures, human and ecosystem exposure to hazardous substances (EMEP/EEA, 2019).

Air pollution is a major concern and impacts the quality of human life and the smooth functioning of human activities. In addition, the almost rampant industrialisation that has taken place in recent decades has visibly affected the quality of the air we breathe, with a significant proportion of the world's population suffering from pollution by various harmful substances and particulate matter in the air (Ciobanu C. et al., 2021). The rapid growth of urban complexes has increased pollution emissions from residential constructions, transportation, power generation and residential (Nastase G. et al., 2018).

For this reason, it is necessary to have quantitative information on these air emissions and their sources. And then, based on the data and information obtained, to be able to: define environmental priorities and identify the activities responsible for the problems; assess the potential environmental impacts; evaluate the costs to solve the identified problems as well for air pollution strategies and plans; establish the targets are being achieved. Air pollutant emission inventories are an essential basis for controlling and managing pollutant emissions (Xu B. et al., 2020).

Therefore, at the EU level there had to be a unified approach and a methodology for estimating atmospheric emissions from different types of sources, thus creating what is known today as an emissions inventory (Figure 1). Representative emission inventories are crucial for air quality applications as they will largely determine the accuracy of subsequent air quality modelling results (Georgiou et al., 2020).

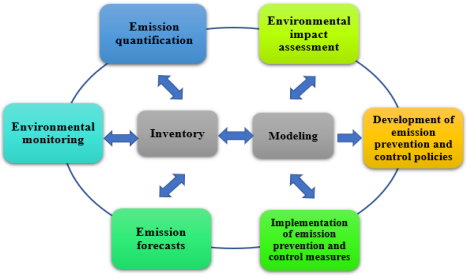

Figure 1. The role of emission inventories for air quality assessment

Emission inventories are now considered indispensable tools for a wide range of environmental measures, such as chemicals management and air pollution prevention.
The work on the original European monitoring and evaluation programme (known as CORINAIR) started in 1985. It started from the idea that it is not possible to measure air emissions from all the individual source's type. Therefore, it was elaborated a basic model based on statistic data about the main industrial activities (location, production rate, operating condition etc.), their typical sources and pollutants and emission measurements over a period.
A guidebook has since been developed and maintained by the UNECE Task Force on Emission Inventories and Projections (TFEIP) under the Convention on Long Range Transboundary Air Pollution (LRTAP Convention).
The guidebook continues to be published and updated by the European Environment Agency (EEA) and it is known as *EMEP/EEA Air Pollutant Emission Inventory Guidebook*, its latest version being the one from 2019 (EMEP = European Monitoring and Evaluation Programme). Periodically, the European Environment Agency publishes the results of the annual reports made by the member countries.

MATERIALS AND METHODS

The structure and content of local emission inventories must meet two essential criteria: to allow the use as input data in mathematical models of pollutant dispersion; to include all the sources of atmospheric pollutants existing in the area for which the inventory is drawn up. In order to develop an emission inventory for an area or company with specific activities one must:
- list the types of sources;
- determine the type of air pollutant emission from each of the listed sources;
- examine the literature to find valid emission factors for each of the pollutants of concern;
- determine the number and size of specific sources;
- calculate the total emissions (Valero D.A., 2008).

The EMEP/EEA Guidebook has two key functions: to provide procedures that enable users to develop emission inventories that meet quality criteria for transparency, consistency, comparability and accuracy; to provide estimation methods and emission factors that are applicable for various degrees of complexity.
Romania is obliged to report annually to the EEA the inventories regarding pollutant emissions into the atmosphere, in accordance with the provisions of European legislation and international conventions in the field to which it is a party. Economic operators are obliged to report the data specific to their activities, so that the environmental protection authorities can centralise them and report them in turn for the annual emission inventory.
The procedure for making local emissions inventories and the national inventory in accordance with the requirements of the EMEP/EEA Guidebook is provided in the Ministry Order no. 3299/2012 for the approval of the methodology for making and reporting the inventories regarding the emissions of pollutants into the atmosphere.
Although the guide covers a wide range of activities, for which useful information is specified, it cannot cover the millions of possible situations. Therefore, often those who are involved in reporting face difficulties regarding the framing of the activity for which they are reporting, identifying the appropriate emission factors, etc. In such situations, those interested must ensure that they make the best choice using the guide or must look for other methods proposed by countries outside the EU and justify the choice made.
An alternative solution for such situations, quite often used, is the *AP-42 Compilation of Air Pollutant Emissions Factors*, that has been published starting with 1972 as a compilation of US EPA's emissions factor information (US EPA AP-42, 2009). It contains emissions factors and process information for more than 200 air pollution source categories and is constantly updated, like the EMEP/EEA Guidebook.
On the other hand, depending on the estimates made for the emissions inventory, economic agents must also pay taxes to the Environment Fund Administration, for a few types of pollutants.

RESULTS AND DISCUSSIONS

The estimation approach is to combine information on the extent to which a human activity takes place (called activity data or AD) with coefficients that quantify the emissions or removals per unit activity, called emission factors (EF).
The basic equation is therefore:

$$\text{Emissions} = \text{AD} \times \text{EF}$$

The emission factors are given for three tiers and a tier represents a level of methodological complexity. The three tiers provided by the EMEP/EEA Guidebook (EMEP/EEA, 2019) are the follows:
- Tier 1 is the simplest method that represents a default relation between activity data and emission factor; the activity data are based on statistical information for all the sources and substances;
- Tier 2 is more advanced method that uses more specific emission factors, using country specific information on process specific conditions;
- Tier 3 is the method that uses the latest scientific knowledge in more sophisticated approaches and models; it is recommended where facility-level emission data are available and depends on the specific national circumstances.

Tier 1 is the most used and convenient method as long as there is no complete and available data for Tier 2 and Tier 3.
According to the EMEP/EEA Guidebook, the pollutant emissions estimates are divided into sectors (energy, industrial processes and product use, agriculture, waste, natural sources) and sources are divided into categories and subcategories, each one being assigned an NFR code (Nomenclature For Reporting).
The emission inventories prepared according to the Guidebook are different purposes: providing information to policymakers in the Member States of the European Union, as well as the public; defining environmental priorities; air quality assessment for current situation; development, implementation and updating of plans and programs for air quality management; estimating the specific environmental costs of different policies. Also, the national emission inventories allow to model the dispersion of pollutants at a local scale and to assess compliance by Parties with their emission obligations under the existing international protocols.
The case study presented in this paper refers to a dry mortar factory, for which data were available regarding the specifics of the activities, production capacities, etc. The factory's products are represented by mortars, gypsum- and lime-based facades renders, adhesives, plasters and other products used in construction.
Because the main raw material used in the production process is limestone, when inventorying the sources of emissions, we also considered those specific to the extraction activities from the quarry (the quarry belongs to the same company).
The main phases of the technological process in the limestone quarry are the following:
- detonation, for which nitrammonium (94.5% ammonium nitrate + 5.5% diesel) is used as an explosive;
- transportation of raw limestone by vehicle for processing;
- preliminary sorting of the raw limestone, with the aim of separating the sterile material;
- crushing with the help of jaw crushers and final sorting with the help of vibrating sieves;
- temporary storage of the resulting sorts (40 - 80 mm, 80 - 110 mm and over 110 mm).

The local transport of the granular material inside the sorting and crushing station, respectively for temporary storage is done with the help of conveyor belts.
Next, limestone with grains up to 80 mm is transported to the dry mortar factory where, before being processed, it is dried; for this purpose, a dryer is used with a drying capacity of about 50 t/h, with a maximum gas consumption of 250 mc/h. After drying, the limestone is subjected to a process of processing and fine sorting, so that various sorts with granulometry corresponding to the various types of manufactured products are obtained.
The local transport of dry limestone, the making of mixtures and the packaging of finished products are operations that take place in closed spaces, where the existed exhaust pipes are provided with batteries of filters with bags, to

limit the emission of solid particles into the atmosphere.

The emission from detonation depends on the chemical composition of explosive and on the weight of explosive used. Therefore, the main pollutant generated from explosives detonation is the carbon monoxide. In second place in terms of the quantity generated are the particulates; such large quantities of particulate are generated in the shattering of the rock and earth by the explosive that the quantity of particulates from the explosive charge are not significant and cannot be distinguished. Nitrogen and sulphur oxides are also generated, but only limited data are available on these emissions.

Emissions of particulate matter (PM), PM-10, and PM-2.5 occur from specific operations in limestone quarrying and processing. A substantial portion of these emissions consists of heavy particles that may settle out within the plant. The main variables that affect uncontrolled PM emissions are wind and material moisture content. If these are added other variables such as: crusher type, size reduction ratio, fines content etc. Therefore, the emission factors developed from the emissions data gathered at limestone processing facilities are considered representative and were established based on the processed limestone quantity. However, only the emission of particulate matter is considered to be the main type of emission.

Regarding the limestone drying in the mortars factory, are taken into account all the specific emissions from combustion process of the natural gas: black carbon (BC), methane (CH_4), carbon monoxide (CO), carbon dioxide (CO_2), nitrous oxide (N_2O), ammonia (NH_3), nitrogen and sulphur oxides, non-methane volatile organic compounds (NMVOC), heavy metals and persistent organic pollutants. The emissions are calculated based on gas consumption. In Table 1 are presented the type of sources and emissions as well as the bibliographic sources from which the emission factors were taken for the analysed case study.

Table 1. Sources of pollution and types of specific emissions

Sources categories	NFR code	Type of emissions	Emission factors
Detonation of explosive (ammonium nitrate with 5 – 8% fuel oil)		products of explosives use (CO, NO_x, SO_2)	US EPA: AP 42, Fifth Edition Compilation of Air Pollutant Emissions Factors, Volume 1: Stationary Point and Area Sources, Chap. 13.3 - Explosives Detonation, Table 13.3.1
Row limestone loading-unloading		particulate matter	US EPA: AP 42, Fifth Edition Compilation of Air Pollutant Emissions Factors, Volume 1: Stationary Point and Area Sources, Chap. 11.19.2 - Crushed Stone Processing and Pulverized Mineral Processing, Table 11.19.2-1
Processing operations (sorting, crushing, belt transportation)		particulate matter	
Non road mobile machinery (excavators, loaders, off-highway trucks, graders)	1.A.2.g.vii	exhaust emissions	EMEP/EEA Air Pollutant Emission Inventory Guidebook, 2019, Chap. 1.A.4 - Non road mobile machinery, Table 3-1
Limestone drying (gaseous fuels)	1.A.2	emission from combustion process (CO, NO_x, SO_x, particulate matter, etc.)	EMEP/EEA Air Pollutant Emission Inventory Guidebook, 2019, Chap. 1.A.2 - Manufacturing industries and construction (combustion), Table 3-3

As stated in Table 1, the methodologies proposed by the European guide and the American standard were considered.

It is important to mention that special attention must be paid to the measurement units when choosing the emission factor values, especially in situations where the sources use different measurement unit systems.

In Table 2, in which the emission factors are presented, units from the International System of Units of Measure were used.

Empty cells mean that either that type of pollutants are not generated from the respective activity, or that no emission factors are established for some pollutants (these pollutants are considered insignificant from a quantitative point of view).

Table 2. Emission factors taken into account

Source	limestone quarry							factory	
	Detonation of explosive	Row limestone loading	Row limestone unloading	Screening	Crushing	Conveyor transport	Non road mobile machinery	Limestone drying	Non road mobile machinery
Pollutant	[kg/t explosive]	[kg/t limestone]					[kg/t diesel]	[g/Gj]	[kg/t diesel]
BC							1.306	0.03	1.306
CH_4							0.083		0.083
CO	34						10.774	29	10.774
CO_2							3,160		3,160
N_2O							0.135		0.135
NH_3							0.008		0.008
NO_x	8						32.629	74	32.629
SO_2	1							0.67	
NMVOC							3.377	23	3.377
TPM		$5x10^{-5}$	$8x10^{-6}$	0.15	0.0195	0.0015	2.104	0.78	2.104
Cadmium							$0.01x10^{-3}$	$0.00091x10^{-3}$	$0.01x10^{-3}$
Copper							$1.7x10^{-3}$	$0.0026x10^{-3}$	$1.7x10^{-3}$
Chromium							$0.05x10^{-3}$	$0.013x10^{-3}$	$0.05x10^{-3}$
Nickel							$0.07x10^{-3}$	$0.013x10^{-3}$	$0.07x10^{-3}$
Mercury								$0.54x10^{-3}$	
Arsenic								$0.1x10^{-3}$	
Selenium							$0.01x10^{-3}$	$0.058x10^{-3}$	$0.01x10^{-3}$
Zinc							$1x10^{-3}$	$0.73x10^{-3}$	$1x10^{-3}$
Lead								$0.011x10^{-3}$	
POPs							$3.32x10^{-3}$	$5.8x10^{-6}$	$3.32x10^{-3}$

The air emission calculation to be presented below was developed for an average month, in which the activity data (AD) considered are the following: detonation and processing of 56,000 t limestone; using 27 t diesel for non road mobile machinery; using 32,760 mc gas for drying (assuming that around 45% of the extracted limestone is processed in the factory, the rest being sold in various forms to third parties); using 4 t diesel for non road mobile machinery. The quantities of emissions, expressed in kg, are presented in Table 3. Five decimals were kept, so that the highest values could be highlighted in comparison with the insignificant ones, almost zero.

Table 3. Emission of pollutants for an average month

Source / Pollutant	Detonation of explosive	Row limestone loading	Row limestone unloading	Screening	Crushing	Conveyor transport	Total non road mobile machinery	Limestone drying	Total emission [kg]
BC							39.5979	0.03909	39.63701
CH_4							2.5166	0.00000	2.51656
CO	262.8						326.6677	37.78309	627.20277
CO_2							95,811.2000	0.00000	95,811.20000
N_2O							4.0932	0.00000	4.09320
NH_3							0.2426	0.00000	0.24256
NO_x	61.8						989.3113	96.41202	1,147.54730
SO_2	7.7							0.87292	8.60092
NMVOC							102.3906	29.96590	132.35654
TSP		3	0.448	5880	764.4	58.8	63.7933	1.01623	6,771.25751
Cadmium							0.0003	0.00000	0.00030
Copper							0.0515	0.00000	0.05155
Chromium							0.0015	0.00002	0.00153
Nickel							0.0021	0.00002	0.00214
Mercury								0.00070	0.00070
Arsenic								0.00013	0.00013
Selenium							0.0003	0.00008	0.00038
Zinc							0.0303	0.00095	0.03127
Lead								0.00001	0.00001
POPs							0.1007	0.00001	0.10067

Analysing the figures resulting from the calculations, it can be seen (Figure 2) that the largest quantity of emissions is represented by carbon dioxide (91.65%) and total suspended particles (6.48%).

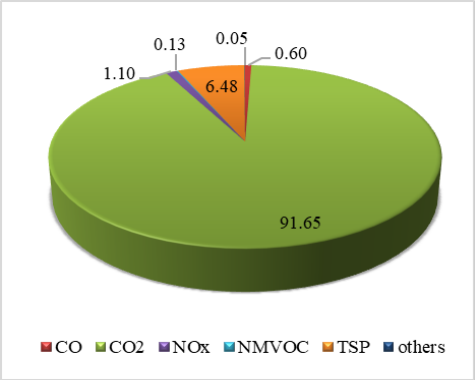

Figure 2. Main air emissions (in percentage)

The main source of CO_2 is the combustion process specific to the non road machinery, that depends on the diesel consumption. Carbon dioxide is not considered a pollutant, as it occurs naturally in the air. However, it is a greenhouse gas and the increase in greenhouse gas emissions causes warming the climate of our planet which is an actual and important environmental problem.

On the other hand, the particulates are mainly resulting from the row limestone processing steps and from the combustion processes which are taken in the engine of the non road machinery.

Also, it can be easily observed that the specific emissions from the quarry activities are significantly higher than those from the limestone drying process. It must be realised that an uncontrolled source, like crushing and sorting processes, will emit at least 10 times the number of pollutants released from one operating properly with air pollution control equipment installed (Valero Daniela A., 2008). It is true that not all the extracted limestone is processed in the factory, but even so, the sources from the quarry have a clearly higher weight.

Last but not least, it should be remembered that, according to the Romanian legislation (MO no. 578/2006), the economic operators owning stationary sources, the use of which affects environmental factors, are obliged to pay taxes to the Environmental Fund for the generated atmospheric pollutant emissions.

Stationary sources that generate pollutant emissions into the atmosphere mean constructions, machines, installations, including ventilation, other fixed works that generate or through which polluting substances are discharged into the atmosphere, as well as fixed combustion installations belonging to the same economic operator, with a power installed total greater than or equal to 1 MW. It can be observed that for the considered stationary sources the monthly amount of taxes isn't so significant, and it is mainly caused by particle emissions (Table 4).

Table 4. The amount of taxes for estimated air emissions

	Total emissions from stationary sources [kg]	Taxes [lei/kg]	Total taxes [lei]
NO_x	96.412020	0.04	3.86
SO_2	0.872920	0.04	0.03
TSP	6645.416230	0.02	132.91
Cadmium	0.000001	16	0.00
Mercury	0.000704	20	0.01
Lead	0.000014	12	0.00
POPs	0.000008	20	0.00
Total			136.81

As can be seen, the relatively small taxes that the company has to pay to the Environmental Fund, due to the atmospheric emissions generated, are not so high as to stimulate the reduction of these emissions.

CONCLUSIONS

National inventories are drawn up in order to fulfil the reporting obligations deriving from the status of a member state of the European Union, respectively, a Party to international conventions, serving, mainly, to draw up national and international policies for the protection of the environment.

The purpose of this article was not to assess the impact on the environment, nor the assessment of the impact on air quality, because of the activities specific to the production of dry mortars.

The intention of the authors was to draw attention to some difficulties encountered by environmental consultants and companies that have to choose the most suitable methods for estimating atmospheric emissions from various sources.

The use of emission factors to estimate the quantities of atmospheric pollutants can be applied in several cases: assessment of the impact on the environment in the design phase; evaluation of the effects on the environment during the operation phase, especially when

measurements cannot be made at the source; making annual reports for the emissions inventory; calculation of taxes at the Environmental Fund for atmospheric emissions. However, this method used for the emission inventory does have some errors. The other alternatives are expensive and subject to their own errors: the first alternative refers to monitoring every major source; the second method would be to monitor the imissions at many points at the limit of the property.

The use of emission factors to quantify the quantities of pollutants emitted into the atmosphere from different anthropogenic activities can be applied in different situations: environmental impact assessment, in the design phase; evaluation of the effects on the environment during the operation phase, for situations where measurements cannot be made, and when the estimated values can be used both for the emission inventory and for the fees to the Environmental Fund.

For that reason, there should be and maintain a greater concordance between the provisions of the slightly older legislation and the new requirements arising from the repeated changes of the European legislation, including the Romanian legislation.

For the national emissions inventory, the following must be ensured:

- data transparency, which requires the provision of sufficient documentation so that the method of estimating emissions for each individual source can be followed;
- consistency of the data, which assumes that the methods are in accordance with the best practices and that they are used consistently for all pollutants;
- data comparability, which implies the use of the best methodologies for estimating and reporting emissions;
- completeness of the data, respectively the inclusion in the inventory of all categories of sources/activities, from the entire national territory;
- data accuracy, which implies the use of best practices for estimating emissions according to the provisions of the latest version of the EMEP/EEA Guide.

REFERENCES

Ciobanu, C., Istrate, I.A., Tudor, P., Voicu, G. (2021). Dust Emission Monitoring in Cement Plant Mills: A Case Study in Romania. *Int J Environ Res Public Health, 28, 18*(17), 9096. doi: 10.3390/ijerph18179096. PMID: 34501682; PMCID: PMC8431024.

EMEP/EEA air pollutant emission inventory guidebook, (2019). Technical guidance to prepare national emission inventories, Retrieved in February 8 2023 from https://www.eea.europa.eu/publications/emep-eea-guidebook-2019/part-b-sectoral-guidance-chapters/1-energy/1-a-combustion/1-a-2-manufacturing-industries/view

Georgiou, G.K., Kushta, J., Christoudias, T., Proestos, Y., Lelieveld J. (2020). Air quality modelling over the eastern mediterranean: seasonal sensitivity to anthropogenic emissions. *Atmos. Environ*., 222.

MO no. 3299/2012 for the approval of the methodology for making and reporting the inventories regarding the emissions of pollutants into the atmosphere.

MO no. 578/2006 for the approval of the Methodology for calculating the contributions and taxes owed to the Environmental Fund (with subsequent additions and modifications.

Nastase, G., Șerban, A., Năstase, A.F., Dragomir, G., Brezeanu A.I. (2018). Air quality, primary air pollutants and ambient concentrations inventory for Romania, *Atmospheric Environment, 184*, 292-303, ISSN 1352-2310, https://doi.org/10.1016/j.atmosenv.2018.04.034.

US EPA AP-42 Compilation of Air Pollutant Emissions Factors (2009), Retrieved in February 16 2023 from https://www.epa.gov/air-emissions-factors-and-quantification/ap-42-compilation-air-emissions-factors#:~:text=Compilation%20of%20Air%20Pollutant%20Emissions,200%20air%20pollution%20source%20categories

Valero, D.A. (2008). Fundamentals of Air Pollution, Fourth Edition, Academic Press, 343-344. Retrieved in March 15 2023 from https://edisciplinas.usp.br/pluginfile.php/5464081/mod_book/chapter/23386/Fundamentals%20of%20Air%20Pollution.pdf

Xu, B., You, X., Zhou, Y., Dai, C., Liu, Z., Huang, S., Luo, D., Peng, H. (2020). The Study of Emission Inventory on Anthropogenic Air Pollutants and Source Apportionment of PM2.5 in the Changzhutan Urban Agglomeration, China. *Atmosphere, 11*(7), 739. https://doi.org/10.3390/atmos11070739

Scientific Papers. Series E. Land Reclamation, Earth Observation & Surveying, Environmental Engineering. Vol. XII, 2023
Print ISSN 2285-6064, CD-ROM ISSN 2285-6072, Online ISSN 2393-5138, ISSN-L 2285-6064

EVALUATION OF THE INFLUENCE OF GREEN SPACE IN THE PROCESS OF REDUCING URBAN NOISE, ON THE TRANSVERSAL PROFILES OF TRAFFIC ROADS

Marta Cristina ZAHARIA, Gabriela VOLOACA

INCD URBAN-INCERC, 266 Pantelimon Street, District 2, Bucharest, Romania

Corresponding author email: marta_cristina_zaharia@yahoo.co.uk

Abstract

A special importance in designing the urban assemblies in cities, especially the configuration of the transversal profiles of the traffic roads, from the point of view of the acoustic and vibration protection for people, has the judicious design of the green spaces that are placed between the traffic roads and building front facades construction elements. Green spaces bring with a good contribution in the process of reducing urban noise, because of acoustic absorption characteristics they have. The relationship between the profile / size of urban road arteries in correlation with the size of adjacent green spaces and/or the distance from the running area to buildings can be evaluated from several points of view, including the effect of an earthquake. There were made research, in projects PN 23 35 01 01 and PN 23 35 06 01, by calculation studies regarding the values of the equivalent noise level, Lext (f), from traffic, - which were performed for a street-study profile, considered as a standard, then for other cases of study-road profiles. It was shown that for a traffic street of technical class 1 (with 8 lanes of traffic), bordered by two fronts of buildings of at least 8 floors high, having a complex composition of traffic, the two cases: without and with green area made by trees, shrubs and grass, indicates that values of transmission noise may decrease between 1 to 5 dB, depending on the winter and summer seasons.

Key words*: absorption coefficients, acoustics, civil buildings, green spaces/areas, urban noise.*

INTRODUCTION

The *design of the urban assemblies in cities* from the point of view of the *acoustic and vibration protection for people*, must be made in order to obtain an *urban noise level* that has values that fall within the provisions specified in the *technical regulations* (norme C125:2013) in force, regarding *building acoustics and urban acoustics*.

In designing *the configuration* of the *transversal profiles of the traffic roads bordered with buildings*, a special importance has the judicious design of *the green spaces* that are *placed between* the *traffic roads* and *building front facades construction elements*. (Zaharia M.C., 1999).

Also, green areas placed on the configuration of the traffic roads gives a beautiful aesthetic view and can improve the acoustic comfort of indoor spaces (Scamoni et al., 2022) and the urban spaces (Timothy Van Renterghem et al., 2009; Hyung Suk Jang et al., 2015, Zaharia M.C., 2020). An example of a street in the center of Bucharest is shown in Figure 1.

Figure 1. Image from street in center of Bucharest (internet image)

Green spaces bring with a good contribution in the process of *reducing urban noise*, because it constitutes an *acoustic barrier* and they have *acoustic absorption characteristics*.

On the other side, *the relationship* between *the profile / size of urban road arteries* in correlation with *the size* of *adjacent green spaces* and/or *the distance* from the running area to buildings *can be evaluated* from *several points of view*, including the effect of the transmision of *vibration waves* from an *earthquake* or from *traffic road service*.

Finaly the scope is *to obtain a decrease of traffic noise propagation, by reducing the reflection of acoustic and vibration waves:*
1) *between the fronts of buildings*
and
2) *between the noise source coming from traffic, to the receiver (people) located in the building* or *in the external environment*, in *a point A of the transverse profile of the traffic artery,*
according to *green spaces acoustic absorption characteristics*, respectively *the sound absorption coefficient*.
Considering the configuration of *green areas* like *big trees, with big roots in the ground*, can have also the effect of *a barrier* in transmision of *vibration waves* from an *earthquake* or from *traffic road service* to the *bordered building* of traffic roads.
The identification of the *destructive potential of seismic events* produced *in Romania* can be *preventively and effectively correlated* with *different parameters of the urban system* such as the *relationship between the profile / size of urban road arteries* in correlation with the size of *adjacent green spaces* and/or *the distance from the running area to buildings.*
The experience of the Vrancea earthquake of March 4, 1977 (Bălan et al., 1982) highlighted the following:
- the reinforced concrete structure or the masonry mortar of buildings from older generations, located on relatively narrow streets, *may suffer degradation over time* as a *result of repeated or aggressive mechanical stresses over decades, traffic in the immediate vicinity of the buildings* may be a cause aggravating;
- such phenomena are broadly comparable to those *of fatigue at a very large number of cycles*, which can *accumulate in several decades*, in *combination with the effects of strong earthquakes* (e.g. *traffic vibrations plus the earthquakes* of 1940, 1977, 1986 and 1990) and can lead to a *decrease in the strength of some concretes from older generations*;
- *modern isolation systems*, - including *green areas* -, against *vibrations from tram or subway tracks can reduce these negative effects*.

MATERIALS AND METHODS

According to Romanian technical regulation norm no. *C125:2013 Normative regarding Acoustics in constructions and urban areas, Part IV - Protection measures against noise in urban areas* (*subchapter 2.3.2.3.(2)*), where there is a method of calculation the street exterior noise level, *Lext(f),* in one point from a transverse profile of a traffic artery, respectively *Level of noise in measurement point "A",* originated from several types of vehicles moving on multiple lane of a traffic road is in formula 1:

$$L_{ext}(f) = 10 \lg \left(\frac{1}{T} \sum_{I=1}^{n} t_I \cdot 10^{\frac{L_I^A}{10}} \right) \text{ (dB)} \qquad (1)$$

,

in which:
$\mathbf{L_I^A}$- the noise level corresponding to the action "I", (dB).
T - characteristic time period (in seconds (s)); (choose for example: 3600 s);
$\mathbf{t_I}$ - the duration of time corresponding to action "I" at the considered point;
$t_I = n_I \cdot \tau_I$, (s)
where:
$\mathbf{n_I}$ - the number of means of traffic of a certain type "I" which circulates in the characteristic period "T", for which the equivalent noise level is established;
$\boldsymbol{\tau_I}$ - the time (in seconds), in which the vehicle covers a distance L = 20 metra.
The *level of noise in measurement point "A", "L_I^A", originated from a noise source type "I",* in case of a transversal profile of traffic road which is *bourded with two fronts of buildings* and have ***green zones*,** is calculated (cf. Normative C125:2013, *Part IV, subchapter 2.3.2.3.(6)*) with the following geometrical elements from Figure 2 for determining the noise level, and the complex formula 2.

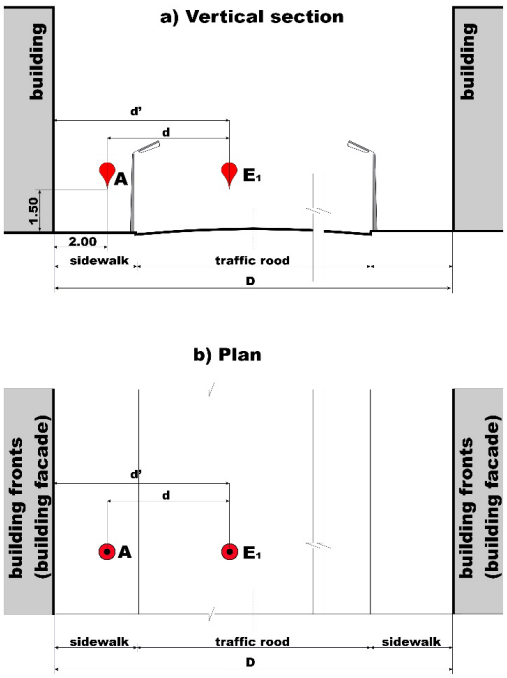

Figure 2. The geometrical elements for determining the noise level,
in case of a transversal profile of traffic road which is *bourded with two fronts of buildings*
A - measurement point (situated usually at 2.00 m distance from the building facade and at 1.50 m high distance from the ground); d - distance from noise source to the measurement point, (m); d' - distance from noise source to the building facade, beside it is made the measurement, (m);
D - distance between the buildings fronts (m); E1 - noise source

$$L_I^A = L_I^1 + 10\lg\left\{\frac{1}{\left[\left(\frac{d}{d_0}\right)^{\frac{k}{10}}\right]c_s c_{zv}} + \frac{1}{\left(\frac{d'-d}{d_0}\right)^{\frac{k'}{10}}}\left[\frac{1-\alpha_1}{\left(\frac{d'}{d_0}\right)^{\frac{k}{10}}} + \frac{(1-\alpha_1)(1-\alpha_2)}{c_s c_{zv}\left(\frac{D-d'}{d_0}\right)^{\frac{k}{10}}\left(\frac{D}{d_0}\right)^{\frac{k'}{10}}}\right]\frac{\left(\frac{D}{d_0}\right)^{\frac{k'}{5}}}{\left[\left(\frac{D}{d_0}\right)^{\frac{k'}{5}} - (1-\alpha_1)(1-\alpha_2)\right]c_s c_{zv}}\right\} \quad \text{(dB)..(2)}$$

in which:

k - directivity coefficient of the source; corresponds to the propagation of direct waves from the source to the measurement point; the direction of the waves is considered perpendicular to the front of the buildings.

k = 20, for a spherical source (example: a car);

k = 10, for a cylindrical linear source (example: usual road traffic);

k = 0, for parallel linear sources (example: road traffic continuous flow, unrealistic situation).

k' - directivity coefficient of reflected waves between building fronts.

k' = 10, on the traffic arteries bordered by a single front of buildings;

k' = 5, in the case of traffic arteries bordered by two fronts with at most 4 floors;

k' = 3, in the case of traffic arteries bordered by two fronts of buildings with max. 4 floors on one side and 4 ... 8 floors on the other side;

k' = 0, in the case of traffic arteries bordered by two fronts of buildings with at least 8 floors.

α_1 - the acoustic absorption coefficient of the facades of the buildings located on the side of the traffic artery on which the measurement point is located.

α_2 - the acoustic absorption coefficient of the building facades located on the side of the traffic artery opposite the measurement point.

The acoustic absorption coefficient, **"α_i"**, depends on the architectural configuration of the facades, represented by the coefficient **"φ"**:

$\varphi = 1$ - for flat facades;

$\varphi = 1.1$ - for facades provided with continuous balconies;

$\varphi = 1.2$ - for facades provided with continuous loggias.

The acoustic absorption coefficient, "α_i", corresponds to the area **"S_i"** made of material "i" on the facade.

The **"S_A^l"** area in the front of the buildings, related to the measurement point "A", made up of "n" acoustically different areas, "S_i".

"**L_i^l**" - the noise levels characteristic of the considered mobile sources, which are rounded, for calculation, into five noise classes: 70, 75, 80, 85, 90 dB(A); each class includes vehicles whose characteristic noise level deviates by no more than ±2 dB (A) from the class definition value.

n_1 - the number of vehicles with a noise level less than or equal to 80 dB that pass on the traffic artery, in a 1-hour time period;

n_2 - the number of vehicles with a noise level higher than 80 dB that pass on the traffic artery during the same period;

The number of means of traffic of a certain type "n_i" that circulates in the characteristic period "**T**", "**n_i/h**", is determined by measurements or established by statistical calculations, depending on: the type of means of transport, the number of vehicles per hour "n_i/h", in both directions, depending on *the technical class of the street*, the considered time period (hour).

τ_i - the time (sec), in which the vehicle covers a distance L = 20 m, specific for different types of means of traffic circulating at characteristic speeds.

"**c_s**" - coefficient depending on the nature of the road surface or the land surface; example: c_s = 0.85 for Cubic stone; c_s = 0.90 for Asphalt; c_s = 1.00 for Earth; c_s = 1.10 for Turf; c_s = 1.20 for Sand.

"**c_{zv}**" - coefficient depending on ***the type of green area***.

The green spaces in urban and / or rural areas ***can be made*** usually *with* ***different types of green plants***, such as the following:

A) the ***type of green area***: a) conifer plantations, b) deciduous plantations, c) the area with grass or earth, etc.,

B) the ***number of rows*** on which ***trees with interlaced crowns*** are planted, and if they have ***little trees*** and ***shrubs*** planted *between the stems*,

C) the ***number of rows*** on which the ***trees with uncrossed crowns*** are planted,

D) the ***area without trees***,

E) the ***season: summer*** or ***winter***.

The values of the "c_{zv}" coefficient depending on the type of green area are presented in table 1 (cf. Norm no. C125:2013, *Part IV*).

In Table 1 it is considered only the situation, most frequently found in urban areas, in which the green areas with trees are located only between the curb of the street and the fronts of the buildings (not the case of the green areas existing in the spaces provided in the middle of the traffic artery).

Researches were made in projects PN 23 35 01 01, PN 09-14.04.07 and PN 23 35 06 01, and in a doctoral thesis (Zaharia M.C., 1999), by ***calculation studies*** regarding the ***values of the equivalent noise level, Lext (f)***, from ***traffic sources***, - which were performed for ***6 Study transversal profiles of traffic roads***, considering ***many parameters*** and also ***the influence of green areas***.

Table 1. The values of the Coefficient "c_{zv}"

The type of green area	"n"	Czv - for conifer plantations	Czv - for deciduous plantations		Czv - area with grass or earth, etc.
			summer	winter	
Trees in "n" rows with intertwined crowns, with trees and shrubs planted between stems [n = 1 ...3]	n=1 n=2 n=3	1.4+0.4(n-1) 1.4 1.8 2.2	1.4+0.4(n-l) 1.4 1.8 2.2	(n-1) 1.1 1.2 1.3	-
Trees on "n" rows with crowns, not interlaced [n = 1...3]	n=1 n=2 n=3	l.25+0.25(n-l) 1.25 1.5 1.75	1.25+0.25 (n-1) 1.25 1.5 1.75	1.1+0.1(n-1) 1.1 1.2 1.3	-
Area without trees [n = 0]	n = 0	1	1	1	1

RESULTS AND DISCUSSIONS

The ***Study transversal profiles of traffic roads***, are presented, as follow, in Figures 3 to 8.
The values of *Level of noise in measurement point "A", Lext(f),* originated from several types of vehicles moving on the 6 Study profiles of streets, with multiple lanes of a traffic road, bourded with two fronts of buildings, considering different types of parameters including the ***green areas***, are presented in Table 2.

Table 2. The values of *Level of noise in measurement point "A", Lext(f),* originated from several types of vehicles moving on the 6 Study profiles of streets

No.	Name of traffic road	Technical Category of street	K'	D (m)	Number of traffic lanes	Number of traffic direc-tions	Traffic composition (no. of lines/no. of vehicles/direction)						Front of buildings		c_s		L_{ech} (dB(A))		
							passen ger cars	tram-woe silence.	trolley-bus	micro-bus	silent buses	quiet heavy traffic (trucks)	with shops	without shops	cubic stone	asphalt	winter, summer c_{zv}= 1	summer c_{zv}=1.25	summer c_{zv}=2.2
1	Street profile - Study 1	I	0	43	6	2	250	21/30	11/25	-	21/50	-	-	*	-	0.90	**78.58**	**77.15**	-
															0.85	-	**80.85**	**79.41**	
							500					200			-	0.90	**85.05**	**83.63**	
2	Street profile - Study 2	I	a) 3 b) 5	43	6	2	250	21/30	11/25	-	21/50	-	-	*	- -	0.90 0.90	**67.24** **66.50**	**66.15** **65.47**	-
															0.85	-	**68.67**	**67.65**	
3	Street profile - Study 3	I	10	43	6	2	250	21/30	11/25	-	21/50	-	-	*	-	0.90	**65.85**	**64.08**	**62.42**
															0.85	-	**68.18**	**67.21**	**64.75**
4	Street profile - Study 4	I	0	83	6	2	250	21/30	11/25	-	21/50	-	-	*	-	0.90	**75.54**	**74.11**	**70.73**
															0.85	-	77.65	**76.20**	**72.79**
							500					200			-	0.90	**81.78**	**80.35**	**76.97**
5	Street profile - Study 5	I	a) 3 b) 5	83	6	2	250	21/30	11/25	-	21/50	-	-	*	- -	0.90 0.90	**63.90** **63.22**	- **62.21**	- **59.69**
															0.85	-	**65.20**	**64.19**	**61.66**
6	Street profile - Study 6	I	10	83	6	2	250	21/30	11/25	-	21/50	-	-	*	-	0.90	**62.63**	**61.66**	**59.21**
															0.85	-	**64.77**	**63.81**	**61.35**

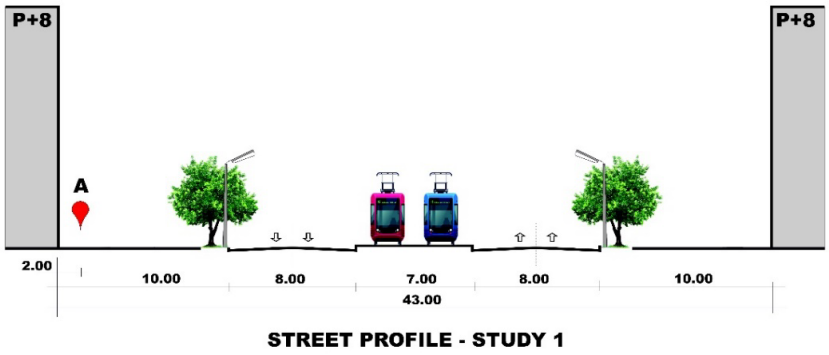

Figure 3. The geometrical elements for determining the A-point exterior noise level, *Lext(f),* on Street profile - Study 1

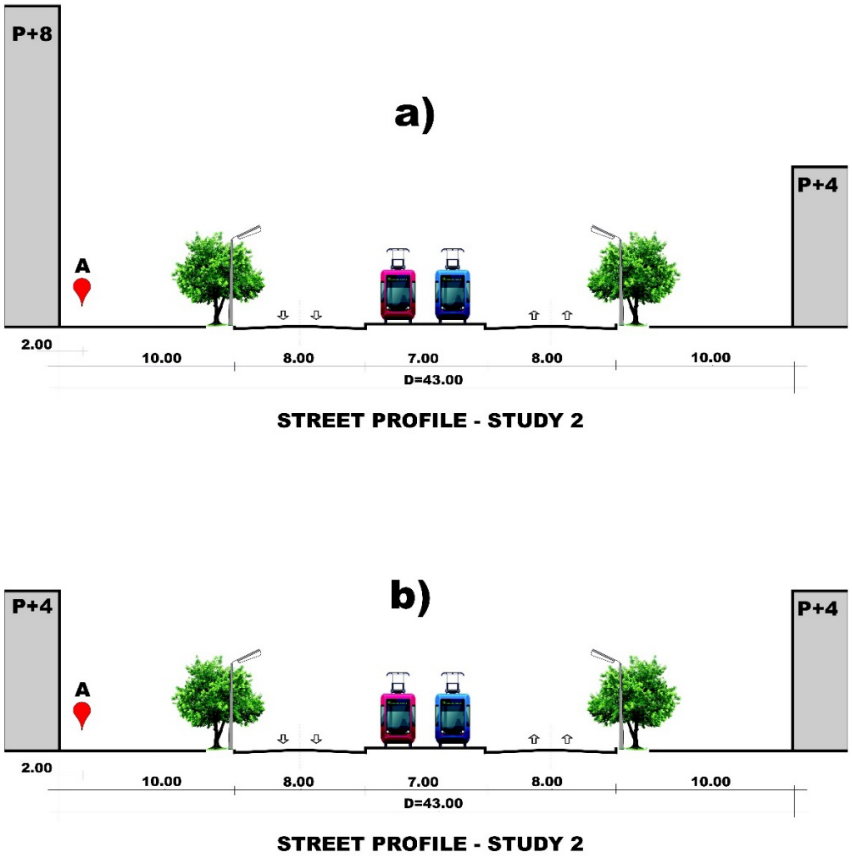

Figure 4. The geometrical elements for determining the A-point exterior noise level, *Lext(f),* on Street profile - Study 2

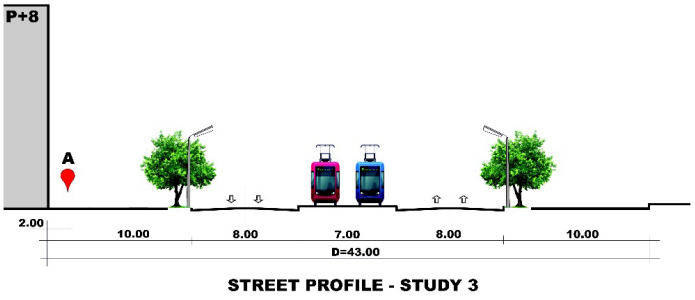

Figure 5. The geometrical elements for determining the A-point exterior noise level, *Lext(f),* on Street profile - Study 3

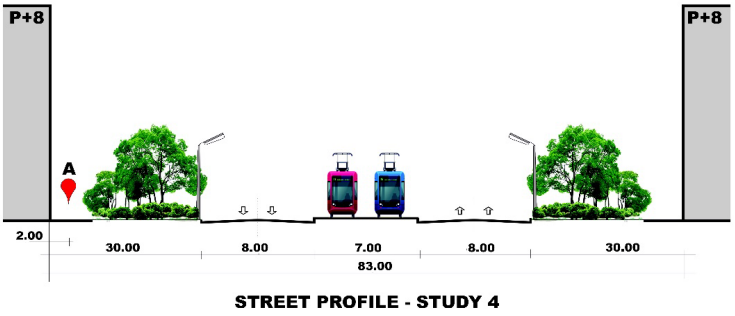

Figure 6. The geometrical elements for determining the A-point exterior noise level, *Lext(f),* on Street profile - Study 4

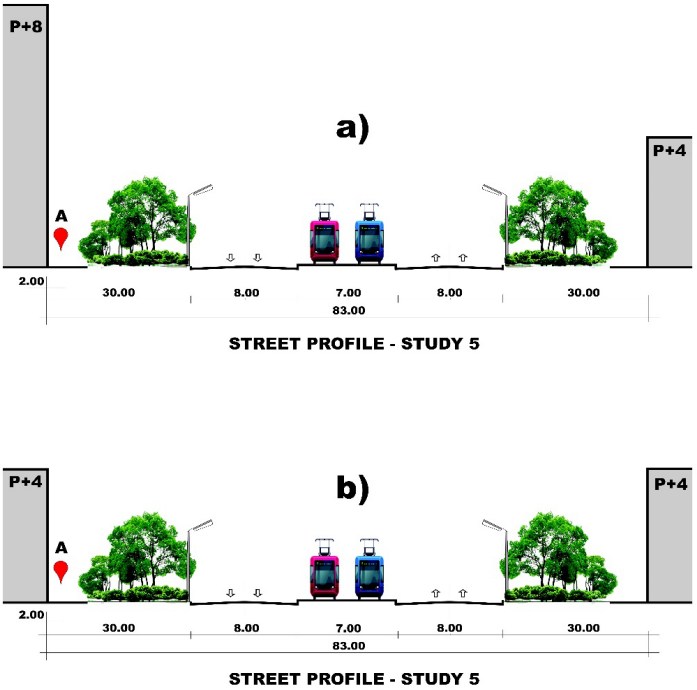

Figure 7. The geometrical elements for determining the A-point exterior noise level, *Lext(f),* on Street profile - Study 5

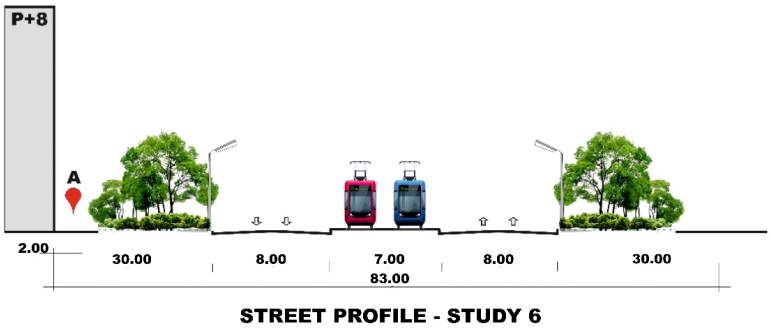

Figure 8. The geometrical elements for determining the A-point exterior noise level, *Lext(f),* on Street profile - Study 6

Analyzing the results obtained from the studies carried out, presented in table 2, for the *6 street profiles-study*, regarding the influence of the variable characteristic parameters of the traffic arteries, including the provision of ***green spaces***, the following main aspects can be highlighted:

a) Increasing the width ("D") of the transverse profile (from 43 m to 83 m) leads to noise reductions of 3 ... 5 dB(A). It should be noted that the effect of increasing the width of the profile is less than decreasing the height regime of the bordering buildings.

b) The variation of the height regime, in the case of streets bordered by two fronts of buildings, can lead to a decrease in the noise level value by up to 10 dB(A) (by moving from delimiting buildings with a height of "P + 8 floors" to buildings with the height "P + 4 floors" or less).

c) The provision of ***green spaces*** leads to a decrease in the noise level by 1...5 dB(A) compared to the case when such spaces are not provided. This difference is evident during the leafing period (summer).

d) The type of road surface also influences the noise level, in the case of asphalted arteries obtaining noise levels 2 ... 3 dB(A) lower than in the case of arteries paved with cubic stone.

e) In the case of arteries bordered only on one side by buildings, with the height "P + 8 floors", the noise level can be 12 ... 15 dB(A) lower than in the case of arteries bordered on both sides by buildings with the height "P + 8 floors".

f) In the case of a street profile of technical category I, having: - distance D = 43 m (between building fronts); - fronts of delimiting buildings, with the height "P + 8 floors"; and - traffic composition: no heavy traffic (trucks); the noise level value is approximately 77 ... 80 dB(A).

g) The influence of heavy traffic in establishing the acoustic regime is decisive, its presence can lead to increases in the noise level of more than 6 dB(A), depending on the width of the street profile and the height regime of the bordering buildings.

CONCLUSIONS

From the studies performed it was shown that for a ***traffic street of technical class 1*** (with ***6 lanes of traffic***), ***bordered*** by ***two fronts of buildings*** of ***maximum 8 floors high***, having a ***complex composition of traffic***, in case of *2 types of* ***distances (43 m*** *and* ***83 m)*** *between the fronts of buildings*, the two cases: without and with ***green area*** made by ***trees, shrubs and grass***, indicates that values of transmission noise may ***decrease between 1 to 5 dB***, depending on ***the winter*** and ***summer seasons***.

ACKNOWLEDGEMENTS

This research work was carried out from the following projects:

- PN 09-14.04.07 "Methods to combat urban noise. Analysis and multi-criteria solution of the acoustics of buildings and living areas in urban and rural areas exposed to noise".
- PN 23 35 01 01: “Integrative concept for the digital analysis of data from the large-scale seismic monitoring of the national territory and built environment, aimed for rapid identification of the destructive potential of

seismic events occurring in Romania and in the adjacent regions",
- PN 23 35 06 01: "Integrated IT & urban planning system for evaluating the green-blue infrastructure of Romanian municipalities and cities, in order to be implemented in their General Urban Plans. Case study: Râmnicu Vâlcea Municipality"; all financed by the Romanian Government founds.

REFERENCES

C125:2013. Normative regarding acoustics in buildings and urban areas,

C125:2013. Part IV - Protection measures against noise in urban areas.

Bălan, St., Cristescu, V. Cornea, I., (1982), (Coordinators): The Romanian earthquake of March 4, 1977, Ed. Academy, Bucharest, 1982. Chap. VI, pp. 238-239; Head. VI, pp. 347-348, 351.

Hyung Suk Jang, Ho Jun Kim, Jin Yong Jeon, (2015). Scale-model method for measuring noise reduction in residential buildings by vegetation, *Journal Building and Environment*, *86*, 81–88, https://www.sciencedirect.com/science/article/abs/pii/S0360132314004375

Scamoni, F., Scrosati, C., Depalma, M., Barozzi, B., (2022). Experimental evaluations of acoustic properties and long-term analysis of a novel indoor living wall, *Journal of Building Engineering*, *4*(1), 98–16. 103890, https://www.sciencedirect.com/science/article/abs/pii/S2352710221017484

Van Renterghem, T., Botteldooren, D., (2009). Reducing the acoustical façade load from road traffic with green roofs, *Journal Building and Environment*, 4(5), 1081–1087 https://www.sciencedirect.com/science/article/abs/pii/S0360132308001923

Zaharia, M.C., (1999). Contributions regarding the evaluation and combating of urban noise, Doctoral Thesis, - Faculty of Faculty of Civil Construction and Architecture, Ghe. Asachi Technical University - Iasi, Romania.

Zaharia, M.C., Delia, M.F. (2014). Chapter 21. Romania, in: Rasmussen B., Machimbarrena M. (Editori), COST Action TU0901 - Building acoustics throughout Europe Volume 2: Housing and construction types country by country, COST Office and authors, (2014), COST Action - Publisher: DiScript Preimpresion, S.L., pp. 570, e-ISBN: 978-84-697-0159-1, 352-372, www.costtu0901.eu/tu0901-e-books

Zaharia, M.C. (2020). The Influence of the Coefficient of Acoustic Absorption of the Facades of the Buildings from the Street Profiles on the Noise Level from the Urban Road Traffic, in Conference Paper Proceedings Series of the *10th Annual International Conference on Civil Engineering*, Athens, Greece, https://www.atiner.gr/presentations/CIV2020-0197.pdf, ISSN: 2529-167X.

Scientific Papers. Series E. Land Reclamation, Earth Observation & Surveying, Environmental Engineering. Vol. XII, 2023
Print ISSN 2285-6064, CD-ROM ISSN 2285-6072, Online ISSN 2393-5138, ISSN-L 2285-6064

MODERN AND PRECISE SOLUTIONS FOR MAKING ORTHOPHOTOS WITH THE TOPOGRAPHIC DRONE, NECESSARY FOR OBSTACLE STUDIES

Alin CROITORU, Nicolae Ion BABUCA, Jenica CĂLINA, Aurel CĂLINA, Gabriel BĂDESCU

University of Craiova, 19 Libertatii Street, Craiova, Romania

Corresponding author email: cristi.babuca@gmail.com

Abstract

The use of the drone offers the possibility of approaching surfaces that are difficult or even impossible to assess with the help of land surveying tools. With the help of professional drones, high-resolution images can be recorded for any type of terrain, with centimetric accuracy, regardless of whether it is an uneven surface, swamps, land where dangerous materials or substances are stored, forested areas or very large areas. Drone photogrammetry is a technique used to measure, metrically and graphically represent an area of land or other objects of interest, using aerial photographs. This photogrammetric method using drones is used to perform topographical measurements with centimetres accuracy and to make digital land models, topographic plans and many other applications for surveying and geodesy on large, drilled areas, agriculture, construction.

Key words*: topographic drone, orthophoto, precision, photogrammetry.*

INTRODUCTION

The UAV drone measurement solution presented in this study was used to perform an obstruction study for the realization of a heliport located on a construction.

For this reason, according to AACR legislation, in order to carry out this obstacle study, it is necessary to identify obstacles from both flight directions, depending on the importance class of the heliport.

These obstacles, respectively the area with all the obstacles in the area related to the proposed heliport could not be achieved in a very short time by classical methods, which is why a modern measurement method was adopted with the help of the drone to ensure a very high precision, respectively through this method to achieve an orthophoto with a resolution of 5 achieve an orthophoto with a resolution of 5 cm/pixels well adapted to identify the obstacles in the researched area.

The purpose of the obstruction study is to determine the airspace around the heliport, in such a way as to allow proper control by the authorities for helicopter operations to be carried out safely and to prevent the heliport from becoming unusable by the appearance of obstacles around it.

MATERIALS AND METHODS

The UAV (aerial vehicle without human personnel on board, a Rebel 1718 drone) technology was used for the presented study.

In the office phase before the measurement, the following steps were taken:

- the zone with the area necessary for the flight was identified (Figure 1);
- a polygon was drawn with the studied area which was loaded into the flight program.

Figure 1. Zone with the area necessary for the flight

Workflow description

The reference geodetic network represents the mathematical support for drawing up all the

plans for the entire proposed location (Băbucă et al., 2014).
The reference geodetic network will ensure the connection of all measurements in a general unitary system (the reference systems are established by the construction designers).
The proposed method - the static and RTK method is the most used method for creating geodetic networks that require very high precision (Băbucă et al., 2016).

Stages in making the ground support network:

- Land recognition;
- Making measurements;
- Processing and compensation of measurements;
- Preparation of reports on the processing and compensation of measurements.

Steps taken:

- Realization of the main network through GPS observations – static methods (Figure 2);
- Realization of the main network through GPS observations - RTK methods (Figure 3) (Băbucă et al., 2018).

Coordinate systems used:

- System1970 stereographic;
- Black Sea Altitudes in 1975.

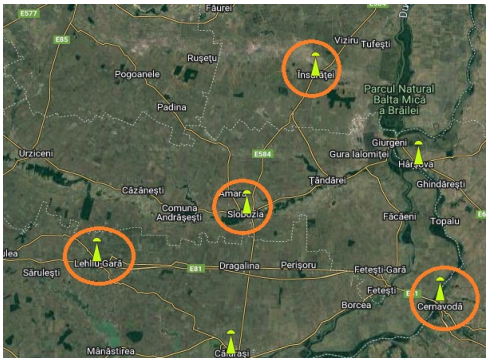

Figure 2. Rompos Network

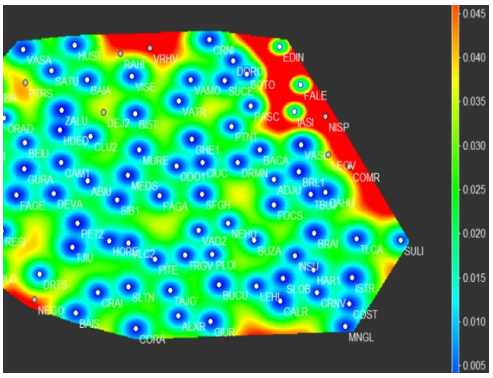

Figure 3. Residual Ionosphere (Network RTK).
The estimated residual ionospheric error for a network RTK user

GPS observations were made with the following equipment:

- Leica System GPS receivers (Figure 4);
- Data RINNEX from GPS Permanent Stations (Slobozia, Cernavodă, Lehliu, Însurăței).

Figure 4. Leica System GPS receivers

The condition for GPS observations are:

- The geometry of the satellites, in order to ensure the most accurate determination, it is necessary that at the time of observation the satellites have an optimal geometric arrangement (for example, they are not all on the same direction) (Figure 5) (Băbucă et al., 2018).

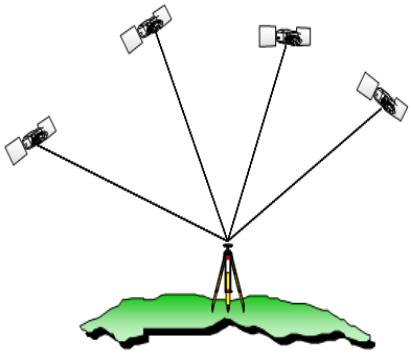

Figure 5. Geometry of the satellites

- The visibility of the signal emitted by the satellite can be distorted or even obstructed by different obstacles (vegetation, constructions, etc.) or it can be received after reflection from different surfaces, thus affecting the accuracy of the determination (Figure 6).

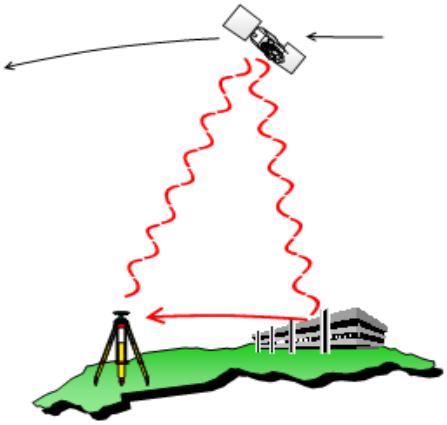

Figure 6. Visibility of the signal

Aero Scanning Methodology

To carry out measurements on the ground, a topographically specific UAV was used, with the precision of GNSS RTK - PPK Technology (Băbucă et al., 2018; https://rompos.ro).

These equipments perform topographical measurements with centimeter precision on hard-to-reach or inaccessible surfaces.

With the help of the drone, was created the digital model of the terrain in autocad format, the point cloud and the orthophoto. The achieved ground resolution is 5cm/pixel.

Presentation of the equipment used

To carry out the study it was used a Rebel 1718 drone, this is a professional airplane - type drone used in surveying and agriculture (Figure 7).

Figure 7. Rebel 1718 drone

The initial parameters are imposed by the useful mass that it must carry in stable flight conditions, but also the chassis structure that allows the placement of sensors and modules in the key points of the systems that I compose it.

Thus, the configuration of the drone exemplified in Figure 7, with the following characteristics (https://fae-drones.com):

- *Coverage:* covers extensive areas of over 1000 Ha with a resolution of 5 cm / pen and lateral coverage of 60% in two hours of flight.
- *Flight time*: 120 minutes with a load of 500 g at a speed of 60 km/h
- Wingspan: 1718 mm
- Fuselage length: 1100 mm
- Fuselage material: Elapor
- Weight in flight: 2500-3800g
- Wing surface: 60 dm ^2
- Recommended flight speed: 60 Km/h
- Maximum flight speed: 110Km/h
- Payload size: 30x13x13 cm
- Maximum flight altitude ASL: 5 Km
- Li-Po 21A/ 4S battery
- *Telemetry*, map navigation and wireless configuration through a PC system via remote control - 60 km.

The studied area

The measurements were made in the Slobozia city area, where a classic mapping mission was performed. The average altitude of the drone during the mission was about 330 m above the ground and about 350 m above the level of the Black Sea.

Purpose of the study: creating a digital elevation model (DEM) and an orthophoto image with an accuracy of 5 cm/ pixel (Figure 8).

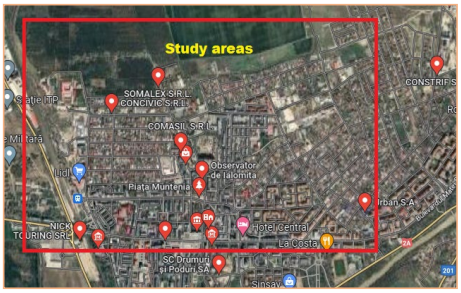

Figure 8. Study area - 300 Ha

Survey Data:

- Number of images: 867
- Flying altitude: 303 m
- Ground resolution: 4.45 cm/pix
- Coverage area: 3.21 Km^2
- Camera stations: 867
- Tie points: 2.170.535
- Projections: 5.294.514
- Reprojection error: 0.6 pix

Camera used is a model ILCE-5100 with 6000*4000 resolution. The location of camera is presentet in Figure 9 and the calibration of camera in Figure 10 and Table 1.

In Figure 11 and Tabel 2 we can see the camera locations and error estimates.

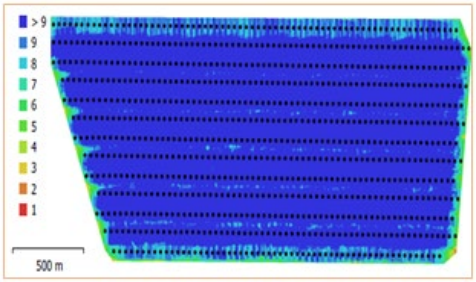

Figure 9. Camera locations and image overlap

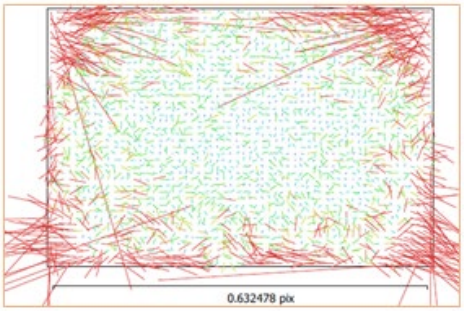

Figure 10. Image residuals for ILCE-5100

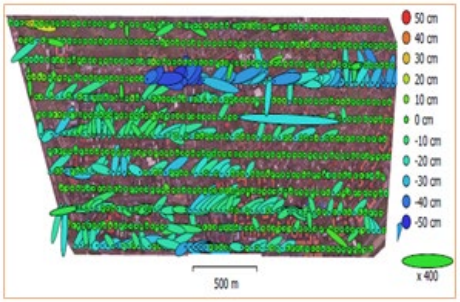

Figure 11. Camera locations and error estimates.
Z error is represented by ellipse color
X,Y errors are represented by ellipse shape
Estimated camera locations are marked with a black dot

Table 1. Calibration coefficients and correlation matrix

	Value	Error	F	Cx	Cy	B1	B2	K1	K2	K3	K4	P1	P2
F	6577.93	0.42	1.00	0.13	-0.03	-0.23	0.04	-0.89	0.87	-0.84	0.80	0.12	0.01
Cx	-63.3359	0.27		1.00	-0.06	-0.20	0.08	-0.15	0.15	-0.15	0.15	0.98	-0.06
Cy	-40.7628	0.22			1.00	-0.08	-0.26	-0.01	0.01	-0.02	0.02	-0.06	0.98
B1	-0.893444	0.028				1.00	0.01	0.32	-0.33	0.32	-0.29	-0.20	-0.05
B2	0.0789858	0.017					1.00	-0.02	0.02	-0.02	0.02	0.08	-0.26
K1	-0.13866	0.0012						1.00	-0.99	0.97	-0.93	-0.16	-0.00
K2	0.103026	0.01							1.00	-0.99	0.97	0.16	0.01
K3	0.161212	0.035								1.00	-0.99	-0.16	-0.01
K4	-0.0187057	0.047									1.00	0.15	0.01
P1	-0.00101429	1.7e-05										1.00	-0.07
P2	0.00171841	1.4e-05											1.00

Table 2. Average camera location error

X error (cm)	Y error (cm)	Z error (cm)	XY error (cm)	Total error (cm)
15.7953	7.89966	10.9639	17.6606	20.7871

X - Easting, Y - Northing, Z - Altitude

RESULTS AND DISCUSSIONS

In Figure 12 we can see the reconstructed Digital Elevation Model (DEM) with resolution: 4.45 cm/pix and point density 504 points/m².
The processing parameters are presented in Table 3 and Ortofotoplan in Figure 13.

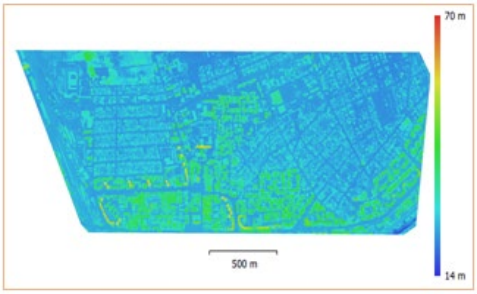

Figure 12. Reconstructed DEM

Table 3. Processing parameters

General	
Cameras	867
Aligned cameras	867
Shapes	
Polygons	1
Coordinate system	Stereo 70
Rotation angles	aw, Pitch, Roll
Point Cloud	
Points	2,170,535 of 3,305,505
RMS reprojection error	0.131075 (0.599675 pix)
Max reprojection error	0.5416 (3.98802 pix)
Mean key point size	4.29851 pix
Point colors	3 bands, uint8
Average tie point multiplicity	2.84331
Alignment parameters	
Accuracy	Highest
Generic preselection	Yes
Reference preselection	Source
Key point limit	500,000
Tie point limit	50,000
Matching time 4 hours	4 hours 25 minutes
Matching memory usage	3.65 GB
Alignment time	37 seconds
Alignment memory usage	990.07 MB
Optimization parameters	
Parameters	f,b1,b2,cx,cy,k1-k4,p1,p2
Fit additional corrections	Yes
Optimization time	2 minutes 33 seconds
Software version	1.6.5.11249
File size	274.25 MB
Depth Maps	
Count	863
Depth maps generation	
Quality	High
Filtering mode	Moderate
Processing time	5 hours 34 minutes
Memory usage	8.53 GB
Software version	1.6.5.11249
File size	24.27 GB
Dense Point Cloud	
Points	2,042,276,561
Point colors	3 bands, uint8
Depth maps generation	
Quality	Ultra High
Filtering mode	Moderate
Processing time	5 hours 34 minutes
Memory usage	8.53 GB
Dense cloud generation parameters	
Processing time	8 hours 29 minutes
Memory usage	32.84 GB
Software version	1.6.5.11249
File size	62.93 GB
DEM	
Size	90,582 x 47,572
Coordinate system	Stereo 70
Reconstruction parameters	
Source data	Dense cloud
Interpolation	Enabled
Processing time	42 minutes 51 seconds
Memory usage	704.74 MB
Software version	1.6.5.11249
File size	8.69 GB
Orthomosaic	
Size	62,776 x 28,025
Coordinate system	Stereo 70
Colors	3 bands, uint8
Reconstruction parameters	
Blending mode Mosaic	Mosaic
Surface	DEM
Enable hole filling	Yes
Processing time	25 minutes 23 seconds
Memory usage	2.88 GB
Software version	1.6.5.11249
File size	12.65 GB
System	
Software	Agisoft Metashape Pro
Software version	1.6.5 build 11249
OS Windows	64 bit
RAM	63.93 GB
CPU	Intel(R) Core, i7-9700
GPU(s)	GeForce GTX 1080 Ti

Figure 13. Ortofotoplan - Final results

The deliverables obtained from the measurements with the UAV drone, the digital elevation model of the landscape and the orthophoto image with a precision of 5cm/ pixel, allowed the realization of the study of obstacles necessary for the heliport design (Figure 14).

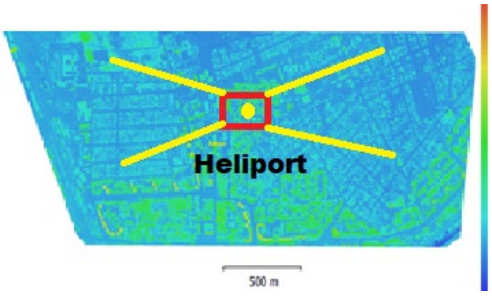

Figure 14. Obstruction study

Before starting your drone mapping here are the things you will need to consider:

- the type of drone used specific to each project will always use a high resolution camera and integrated GPS module.
- methods of investigation if you want to produce a truly accurate topographic map you will need to make measurements on the ground in the form of ground control points.
- Survey planning software and data processing software will be used for data processing that ensures increased confidence in obtaining correct results, exemple Pix4D, Drone Deploy and Precision Mapper, mapping software solutions.
- Mapping software: A 3D topographic model will allow us to visualize a lot of information that we can analyze and study.

CONCLUSIONS

At the end of the study we can make the following conclusions:

- the method proposed and used in the creation of the orthophoto image necessary for the realization of the obstruction study was successfully completed.
- the method proposed and analyzed based on the data and values obtained is confidently recommended for other types of works and engineering studies.
- after processing the images, the accuracy of the resulting orthophoto image is 5cm/ pixel
- precision of Digital Elevation Model – (resolution: 4.45 cm/pix, point density: 504 points/m²).

ACKNOWLEDGEMENTS

This research work was carried out with the support of Fae Drones, 287 Theodor Pallady Blvd, IOR2 building, 4th floor, main building. District 3, 032267, Bucharest.

REFERENCES

Băbucă, N.I. (2018). *Global Positioning Systems, Course Notes and Applications,* ISBN:978-606-14-1379-9, 228. Universitaria Publishing House, Craiova.

Băbucă, N.I., Călina, J., Călina, A., Miluț, M., Badescu, G. (2018). Using GPS RTK method in determining horizontal movement, stage 2016, of floating marks set on ash and slag dams deposit from Santaul Mic, Romania, *18th International Multidisciplinary Scientific GeoConference, 2*(18). 1123-1130.

Băbucă, N.I., Ciolac, V., Ienciu, A., Pet, I., Pet, E. (2016). Use GPS method static measurements to create the network to extend and upgrade roads, water and sewerage in Petrila, Hunedoara county, *16th International Multidisciplinary Scientific GeoConference, 2*(2). 705-712.

Băbucă, N.I., Calina, J., Calina, A. (2014). *GPS measurement methods for measurement applied in forestry,* References: *14th International Multidisciplinary Scientific GeoConference 2*(1). 621-626.

https://rompos.ro

https://fae-drones.com

Scientific Papers. Series E. Land Reclamation, Earth Observation & Surveying, Environmental Engineering. Vol. XII, 2023
Print ISSN 2285-6064, CD-ROM ISSN 2285-6072, Online ISSN 2393-5138, ISSN-L 2285-6064

COMPARATIVE STUDY ON DIGITAL IMAGE PROCESSING FOR 3D MODELING

Laurențiu BUDĂU[1], Simon PESCARI[1], Remus CHENDEȘ[1], Clara-Beatrice VÎLCEANU[2], Sorin HERBAN[2]

[1]Politehnica University Timisoara, Civil Engineer Faculty, Department of Civil Engineering and Building Services Engineering, 2 Traian Lalescu Street, Timisoara, Romania
[2]Politehnica University Timisoara, Civil Engineer Faculty, Department of Overland Communication Ways, Foundations and Cadastral Survey, 1 Ioan Curea Street, Timisoara, Romania

Corresponding author email: laurentiu.budau@student.upt.ro

Abstract

The needs of today's society for urban planning require realistic 3D representations of objects or cities for various purposes. The topicality of the study is given by the fact that digital recording of cultural heritage objects represents one of today's society preoccupation for purposes such as maintenance, reproduction multimedia tools for education and dissemination, to artefact condition monitoring. Analysis in a virtual world, using 3D models, for historic buildings or ancient fortresses is much more efficient than a classical 2D analysis. Thus, the aim of this study was to make a comparison between processing digital images to obtain a 3D model of an object using, in the first case, a specialized, widely used software, and, in the other cases, different open-source specialized software. The object studied was the statue of General Ion Dragalina located in Dragalina Park in Caransebeș municipality, western Romania. To process the digital images, four specialized programs were used: Agisoft Metashape, 3DF Zephyr Free, Regard 3D and Meshroom together with Meshlab. Finally, the advantages and disadvantages of each of the programs studied are highlighted by comparison.

Key words*: cultural heritage; 3D representations; historic buildings; 3D models; digital recording.*

INTRODUCTION

In order to carry out the documentation for the preservation of cultural heritage (Abdelhamid, 2019; Agosto & Bornaz, 2017; Balsa-Barreiro & Fritsch, 2018), a multidisciplinary approach is required, which aims to understand the heritage object itself and to collect all the information that characterizes it. Documentation for Cultural Heritage Preservation is much more than the generic term used to define the acquisition of all the information needed to understand an object for documentation in order to restore, conserve and manage it or to disseminate the results and transform them into a usable form in the future.
One of the priorities of the European Parliament's Commission on 2010 - A European Information Society for growth and employment states: "In launching the Partnership for Growth and Jobs as a new start for the Lisbon Strategy, the 2005 Spring European Council recommended knowledge and innovation as drivers of sustainable growth and stated that it is essential to build a fully inclusive information society, based on the widespread use of Information and Communication Technologies (ICT), for all areas of the economy: public services, SMEs and individuals doing business. ICT can be a powerful tool for strengthening Europe's cultural diversity and can make our cultural heritage (De Luca, 2013; Di Giulio et al., 2016; Messaoudi et al., 2018) and cultural creations available to as many citizens as possible" (https://ec.europa.eu/programmes/horizon2020/en/area/ict-research-innovation).
In this context, the needs of today's society for urban planning require realistic 3D representations of objects or cities for various purposes. Analysis in a virtual world, using 3D models, for historic buildings or ancient fortresses is much more efficient than a classical 2D analysis (Micoli et al., 2013; Soto-Martin et al., 2020; Owda et al., 2018).
This is why automated procedures based on scientific protocols are needed in an ICT-based world. 3D design software applications are a modern and much more efficient solution for the realisation (Arbace et al., 2013), management

and execution of large-scale projects where a clear vision is needed to optimise expenditure and resource allocation (Figure 1).
To carry out the study, a mobile phone was used and 26 digital images were taken, keeping the same distance from the object, with the main condition being that the image of the object must be whole in each of the 26 positions.
The timeliness of the study is due to the fact that digital recording of cultural heritage objects is one of the concerns of today's society, (Maravelakis et al, 2013; Dore & Murphy, 2012) for purposes such as maintenance (e.g., computer-aided repair), reproduction (e.g., rapid prototyping), multimedia tools for education and dissemination (e.g., virtual museums), monitoring the condition of artefacts (e.g., computer-aided inspection) and many others.

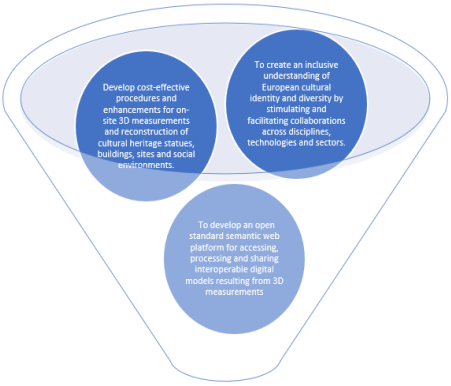

Figure 1. Objectives of using 3D models in the field of cultural heritage conservation

MATERIALS AND METHODS

Specialised 3D reconstruction software from photographs comes in many forms. Certainly, there are commercial solutions that are ideal for industrial and engineering applications. But there is also a good suite of software available online for free download. Users then only need a camera or smartphone to take photos and, if using a 3D printer afterwards, can even print the resulting models. (Guarnieri et al., 2006; Murphy et al., 2013)
The table below (Table 1) lists the best photogrammetric software, selected and sorted alphabetically. Firstly, free photogrammetric software tools are centralized. Secondly, professional software used to create 3D models is also listed. (Pepe et al., 2021; Jiménez Fernández-Palacios et al., 2015)

Table 1. Specialised photogrammetric software for digital image processing

Software name	Photogramm etry type	Operating system running	Price
COLMAP	Aerial, Short distance	Windows, macOS, Linux	Free
Meshroom	Aerial, Short distance	Windows, Linux	Free
MicMac	Aerial, Short distance	Windows, macOS, Linux	Free
Multi - View Environment	Aerial, Short distance	Windows, macOS	Free
OpenMVG	Aerial, Short distance	Linux, Windows, MacOS	Free
Regard3D	Aerial, Short distance	Windows, macOS, Linux	Free
VisualSFM	Aerial, Short distance	Windows, macOS, Linux	Free
3DF Zephyr	Aerial, Short distance	Windows	From $300/month
Autodesk ReCap	Aerial, Short distance	Windows	$340/year
Agisoft Metashape	Aerial, Short distance	Windows, macOS, Linux	Starting at $179
Bentley ContextCapture	Aerial, Short distance	Windows	On request
Correlator3D	Aerial	Windows	From $295/month
DroneDeploy	Aerial	Windows, macOS, Android, iOS	From $99/month
Elcovision 10	Aerial, Short distance	Windows	On request
iWitnessPro	Aerial, Short distance	Windows	On request
IMAGINE Photogrammetry	Aerial	Windows	On request
Photomodeler	Aerial, Short distance	Windows	From $59/month
Pix4Dmapper	Aerial	Windows, macOS, Android, iOS	From $160/month
RealityCapture	Aerial, Short distance	Windows	$10 for 3500 PPI credits or $3,750 for unlimited access
SOCET GXP	Aerial	Windows	On request
Trimble Inpho	Aerial, Short distance	Windows	On request
WebODM	Aerial	Windows, macOS	$57

Short-range photogrammetry

Short-range photogrammetry is a special case where the distance from the camera to the object does not exceed 100m. Short-range terrestrial photogrammetry is based on photographs taken with a digital camera, (Kadobayashi et al., 2004) taken manually by the operator or with the digital camera mounted on a tripod. These photos are then used to create 3D models of objects such as monuments, statues and cultural heritage buildings, traffic accident scenes or

even on film sets. It also emphasises the application of effective multidisciplinary teamwork techniques on various hierarchical levels.
Advantages of using 3D models using short-range photogrammetry (Fiorillo et al., 2013; Kuroczyński et al., 2016):

- a measurement method is without direct contact with the object under study;
- results are accurate and reliable;
- data collection is realized in a short time and at low cost;
- images are retrieved and stored and can be consulted and re-measured at any time in the future;
- in the 3D plane all measured elements have dimensions and the relative differences are real;
- cost assessment as accurate as possible (in case of rehabilitation or construction of new targets);
- planning construction phases more accurately;
- control the project in a much more rigorous manner;
- helps preserve the national historical and architectural heritage and beyond (Miles et al., 2015, Pietroni and Ferdani, 2021).

Agisoft Metashape specialized digital image processing software
(https://www.agisoft.com/)
The Metashape Agisoft PhotoScan Pro software is a 3D modeling solution based on digital images and allows the creation of photogrammetric products of type:

- orthophoto plan;
- a digital reflectance surface model;
- a digital terrain model;
- tie points (correspondences) between images;
- information on camera calibration and orientation parameters.

3DF Zephyr specialized digital image processing software (https://www.3dflow.net/3df-zephyr-photogrammetry-software/)
3DF Zephyr is a commercial 3D photogrammetry and modelling software. (Koeva, 2016) Developed and marketed by Italian software house 3DFLOW, 3DF Zephyr was first released in January 2014 and continuously updated since then. It is a complete photogrammetry software package that includes many post-processing tools for measurements, 3D modeling and content creation. It enables 3D reconstruction from both photos and videos by automatically extracting frames and selecting the most suitable ones for computation.

Regard 3D specialized digital image processing software
(https://www.regard3d.org/)
Regard3D is a free and open-source photogrammetry software that uses the Structure from Motion (SfM) method to convert photographs of an object taken from different angles into a 3D model. It offers an extensive set of tools for editing the point cloud, either with coloured spikes or a texture, before generating a 3D mesh. But it might take some time for users to get familiar with using all the settings and parameters that can be adjusted in Regard3D before getting the kind of results they want. However, even if users are new to using photogrammetry software, the Regard3D website provides all the guides and tutorials needed to get started quickly.

Meshroom and Meshlabs specialised digital image processing software
(https://alicevision.org,
https://www.meshlab.net)
Meshroom is an open-source photogrammetry software based on the AliceVision framework. With it, users can generate a 3D model using large images of an object taken from different angles. The software calculates the distance between surface points and creates a mesh.
MeshLab is an open-source solution for processing and editing 3D meshes. It provides a set of tools for editing, cleaning, inspecting, rendering, texturing and converting meshes. It provides functions for processing raw data produced by 3D digitizing tools/devices and for preparing models for 3D printing.

RESULTS AND DISCUSSIONS

The aim of this study was to make a comparison between processing digital images to obtain a 3D model of an object using, in the first case, a specialized, widely used software, available at low cost, and, in the other cases, different open-source specialized software, available online for free download.
Thus, the object under study is represented by the statue of General Ion Dragalina located in Dragalina Park in Caransebeș, western

Romania, which was photographed using a mobile phone, namely the iPhone 12 Pro.
The characteristics of the camera sensor of the phone with which the digital images were taken are shown in (Table 2).

Table 2. Camera sensor features

Main camera	12megapixels
Video Features	4K@24/30/60fps, 1080p@30/60/120/240fps, Dolby Vision HDR, stereo sound recording
Photo Features	Dual Pixel, PDAF, OIS, wide camera, ultra-wide camera, telephoto camera, 2x optical zoom, 3D LIDAR TOF sensor
Telephoto camera	12megapixels
Ultra-wide camera	12megapixels
Front Camera	12megapixels

For the study, a mobile phone was used, and 26 photographs were taken. Each of these photos was taken keeping the same distance from the object, considering, as a main condition, that the image is whole in each of the 26 positions.
To process the 26 digital images that were processed in the field, the four specialised programs described in the previous chapter were used: Agisoft Metashape, 3DF Zephyr, Regard 3D and Meshroom together with MeshLab.
The statue of General Ioan Dragalina (Figure 2) was unveiled on 3 June 1943, depicting the general in a reconnaissance with map and binoculars in hand. It is the work of the Romanian sculptor Mihail Onofrei (http://cnipt-caransebes.ro/zona-turistica/obiective-turistice-din-caransebes/statui/statuia-generalului-ioan-dragalina/)

Figure 2. The object under study: the statue of General Ion Dragalina, Dragalina Park, Caransebeș

Digital image processing and 3D modeling using Agisoft Metashape software

The data processing and modeling using the specialised software consists of the following workflow (Herban et al., 2014):
1) Importing photos via the suggestive command "Add photos" or they can be brought in via the drag&drop method".
2) Selecting the area of interest, in the sense that the program allows the processing of complete images, with the disadvantage that the point cloud obtained will be very dense and will also contain elements that are not important. Also, the processing time will be very long, so it is preferable to crop the images (eliminating the vegetation) using the "Intelligent scissors" tool. Pick points on the outline of the object, in this case points on the outline of the statue and use the "Invert selection" and "Add selection" commands to remove unnecessary parts of the images. Selecting the outline of the object is done by placing a series of points (vertex), and when closing the created polyline, the MASK image for each photo is obtained and saved. This must be repeated for each individual digital image.
3) Once the Mask images have been created, their alignment follows, i.e., the program must identify the common points in each of the positions and determine how to translate them. The result of this step is a point cloud. The joining/triangulation of the photos is done using the "Align photos" command to obtain the point cloud, choosing the high precision option.
4) Build the geometry of the point cloud using the "Build geometry" command.
5) Build Mesh.
The 3D model obtained can be seen in the image below (Figure 3).

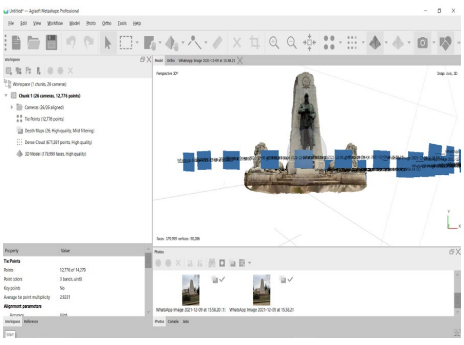

Figure 3. 3D model obtained with camera position display

Digital image processing and 3D modeling using the specialized software 3DFZephyr

Although there are notable limitations between the Free and retail versions of this software, it still gives us an overview of how to work with it. The first step is to open a new project and set its parameters. The next step is to import the digital images by using "Workflow" and "New Project" commands. The users should make sure that the following are ticked: "Compute 3D Model after project creation", "Compute Texture after Surface extraction" and "Check online for precomputed camera calibration". Once the options needed have been set, the photos can be imported by using the "Copy-Paste" command. To start modelling the digital images, the "Run" button should be used. To continue modelling, the user needs to call the commands "Point Cloud", "Dense Point Cloud" and "Meshes"(Figure 4).

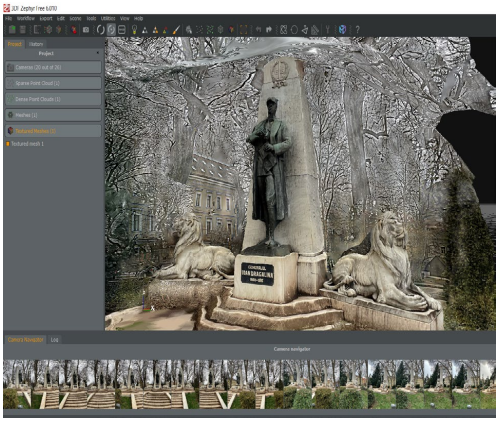

Figure 4. 3D model obtained with camera position display

In the following table (Table 3), advantages and disadvantages of the above mentioned 2 software are presented.

Table 3. Advantages and disadvantages of Agisoft Metashape and 3DFZephyr specialized software

Specialized software	PROs	CONs
Agisoft Metashape	○ Better control (manual) of selecting the subject from the background image; ○ Good quality of the obtained images;	○ The manual selection process is very time-consuming; ○ The way of interacting with the program, as well as the steps required to complete the project, are not intuitive and do not guide the user to achieve the proposed goal.
	○ For different monuments known worldwide, there is a database where mask selections are already made.	
3DF Zephyr (Free)	○ The initial interaction with the program is friendly; ○ Almost the whole process is automatic, once the desired settings are established; ○ It benefits from online databases for the type of camera used/its parameters can also be set manually.	○ The quality of the final model is weaker (in the Free version); ○ Markers cannot be added for scaling (in the Free version)

Digital image processing and 3D modeling using the specialised software Regard3D

Processing of digital images using the specialised Regard 3D software is carried out automatically after they have been inserted (Figure 5).

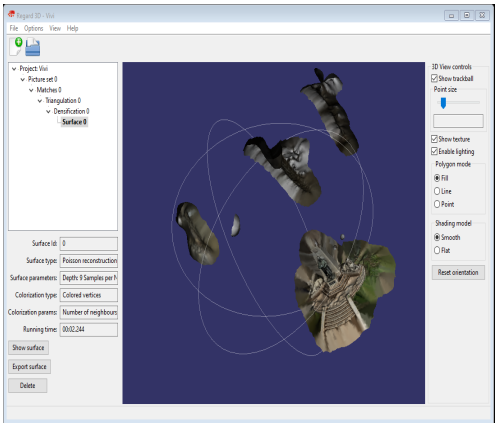

Figure 5. 3D surface obtained

Digital image processing and 3D modelling using specialised MeshRoom and MeshLab software

A disadvantage of this specialized program is that users cannot select and delete information that is extra. Thus, the created model was exported to be further processed with another specialized program, namely MeshLab (Figures 6 and 7).

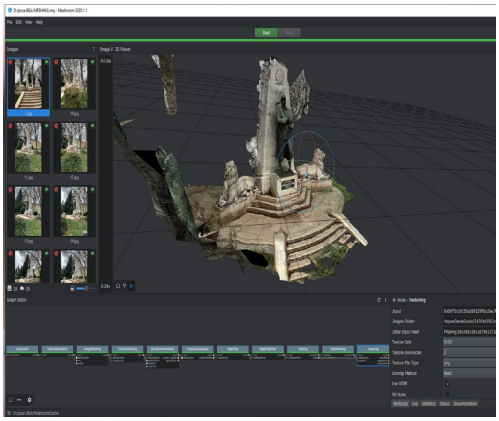

Figure 6. Result in Meshroom

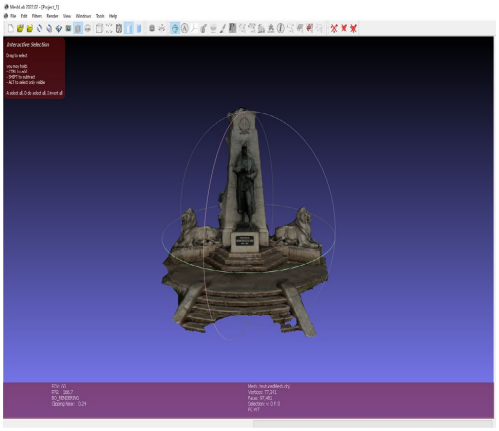

Figure 7. Result in MeshLab

CONCLUSIONS

In carrying out this study, we started from the premise that the implementation of new technologies for various industrial and socially important tasks is a way of promoting low-cost research and documentation methods. For the field of cultural heritage conservation, 3D models have many practical applications, from the implications of their online availability to academic research, conservation and other innovations to come.

Although, it can be said that the result is sensibly the same, the processing manner in the chosen specialized programs is different, mainly due to the working algorithm of each individual software. The more laborious the model creation methodology, the more faithful the representation of the models is to reality. It also comprises more steps or stages that require appropriate tools and equipment.

Agisoft Metashape is available in 2 versions: Agisoft Metashape Professional Edition and Agisoft Metashape Standard Edition. The first version, the Professional Edition costs $3499 and the Standard Edition costs $179.

In the case of 3DF Zephyr, the Free version was used. The program is fully automated, the user only contributes by pressing commands, processing digital images faster than with Agisoft.

Comparing the two models, the one realized with Agisoft Metashape software is much more accurate, the modelling is complete, whereas with 3DF Zephyr, the statue is not complete and the upper part of its head has not been modelled. Paid software may provide better accuracy.

As for the specialised programs Regard 3D and Meshroom, they have a user-friendly interface, do not require advanced knowledge of 3D modelling, the controls are intuitive, but have the disadvantage that the auxiliary surfaces cannot be deleted, requiring export for further processing in another program, in this case MeshLab. It also does not require higher performance requirements of the technical specifications of the computer on which the processing is performed.

For the processing of the 26 digital images in order to obtain the 3D model of the statue of General Ion Dragalina, a Dell laptop with an 8th generation Intel® Core™ i5-8250U processor has been used. The first 3 programs ran on this PC, but for the processing using the specialised MeshRoom program a much more powerful computer was needed. Thus, the processing was done on a gaming laptop, the Asus Rog Strix G with a 9th generation Intel Core i7 processor.

REFERENCES

Abdelhamid, T.G. (2019). Digital techniques for cultural heritage and artifacts recording. *Resourceedings*, *2*(2). 72-112.

Agosto, E., Bornaz, L. (2017). 3D models in cultural heritage: approaches for their creation and use. International *Journal of Computational Methods in Heritage Science (IJCMHS)*, *1*(1). 1-9.

Arbace, L., Sonnino, E., Callieri, M., Dellepiane, M., Fabbri, M., Idelson, A.I., Scopigno, R. (2013). Innovative uses of 3D digital technologies to assist the restoration of a fragmented terracotta statue. *Journal of Cultural Heritage*, *14*(4), 332-345.

Balsa-Barreiro, J., Fritsch, D. (2018). Generation of visually aesthetic and detailed 3D models of historical cities by using laser scanning and digital photogrammetry. *Digital applications in archaeology and cultural heritage*, *8*. 57-64.

De Luca, L. (2013). *3D Modelling and semantic enrichment in cultural heritage.* In Photogrammetric Week'13.

Di Giulio, R., Maietti, F., & Piaia, E. (2016). 3D Documentation and Semantic Aware Representation of Cultural Heritage: the INCEPTION Project. In GCH (pp. 195-198).

Dore, C., Murphy, M. (2012). Integration of Historic Building Information Modeling (HBIM) and 3D GIS for recording and managing cultural heritage sites. *18th International conference on virtual systems and multimedia*. 369-376. IEEE.

Fiorillo, F., Remondino, F., Barba, S., Santoriello, A., De Vita, C.B., Casellato, A. (2013). 3D digitization and mapping of heritage monuments and comparison with historical drawings. *ISPRS Annals of the Photogrammetry, Remote Sensing and Spatial Information Sciences*, *2*. 133-138.

Guarnieri, A., Remondino, F., Vettore, A., (2006). Digital photogrammetry and TLS data fusion applied to Cultural Heritage 3D modeling. *Int. Arch. Photogramm. Remote Sens. Spat. Inf. Sci*, *36.* 1-6.

Herban, I.S., Vîlceanu, C.B., Alionescu, A., (2014). Application of close-range photogrammetry to cultural heritage, *Rev Cad Journal of Geodesy and Cadastre*, *16*. 104 – 112, ISSN 1583-2279, Alba Iulia, Romania.

Jiménez Fernández-Palacios, B., Rizzi, A., Remondino, F. (2015). Etruscans in 3D-Surveying and 3D modeling for a better access and understanding of heritage. *Virtual Archaeology Review*, *4*(8). 85-89.

Kadobayashi, R., Kochi, N., Otani, H., Furukawa, R. (2004). Comparison and evaluation of laser scanning and photogrammetry and their combined use for digital recording of cultural heritage. *International Archives of the Photogrammetry, Remote Sensing and Spatial Information Sciences*, *35* (5). 401-406.

Koeva, M.N. (2016). 3D Modelling and interactive web-based visualization of cultural heritage objects. *International Archives of the Photogrammetry, Remote Sensing & Spatial Information Sciences, 41.*

Kuroczyński, P., Hauck, O., Dworak, D. (2016). 3D Models on Triple Paths - New Pathways for Documenting and Visualizing Virtual Reconstructions. In: Münster, S., Pfarr-Harfst, M., Kuroczyński, P., Ioannides, M. (eds) *3D Research Challenges in Cultural Heritage II. Lecture Notes in Computer Science*, *10025*. Springer, Cham. https://doi.org/10.1007/978-3-319-47647-6_8.

Maravelakis, E., Konstantaras, A., Kritsotaki, A., Angelakis, D., & Xinogalos, M. (2013). Analysing user needs for a unified 3D metadata recording and exploitation of cultural heritage monuments system. In Advances in Visual Computing: *9th International Symposium, ISVC 2013*, Rethymnon, Crete, Greece, July 29-31, 2013. Proceedings, Part II 9. 138-147. Springer Berlin Heidelberg.

Messaoudi, T., Véron, P., Halin, G., De Luca, L. (2018). An ontological model for the reality-based 3D annotation of heritage building conservation state. *Journal of Cultural Heritage*, *29*. 100-112.

Micoli, L., Guidi, G., Angheleddu, D., & Russo, M. (2013). A multidisciplinary approach to 3D survey and reconstruction of historical buildings. *Digital Heritage International Congress (Digital Heritage), 2*. 241-248. IEEE.

Miles, H.C., Wilson, A.T., Labrosse, F., Tiddeman, B., Griffiths, S., Edwards, B., Roberts, J.C. (2015). Alternative representations of 3D-reconstructed heritage data. *Journal on Computing and Cultural Heritage*, *9*(1). 1-18.

Murphy, M., McGovern, E., Pavia, S. (2013). Historic Building Information Modelling–Adding intelligence to laser and image based surveys of European classical architecture. *ISPRS journal of photogrammetry and remote sensing*, *76*. 89-102.

Owda, A., Balsa-Barreiro, J., Fritsch, D. (2018). Methodology for digital preservation of the cultural and patrimonial heritage: Generation of a 3D model of the Church St. Peter and Paul (Calw, Germany) by using laser scanning and digital photogrammetry. *Sensor Review*.

Pepe, M., Costantino, D., Alfio, V.S., Restuccia, A.G., Papalino, N.M. (2021). Scan to BIM for the digital management and representation in 3D GIS environment of cultural heritage site. *Journal of Cultural Heritage*, *50*. 115-125.

Pietroni, E., Ferdani, D. (2021). Virtual Restoration and Virtual reconstruction in Cultural Heritage: Terminology, methodologies, visual representation techniques and cognitive models. *Information*, *12*(4). 167.

Soto-Martin, O., Fuentes-Porto, A., & Martin-Gutierrez, J. (2020). A digital reconstruction of a historical building and virtual reintegration of mural paintings to create an interactive and immersive experience in virtual reality. *Applied Sciences*, *10*(2). 597.

https://ec.europa.eu/programmes/horizon2020/en/area/ict-research-innovation

https://www.agisoft.com/

https://www.3dflow.net/3df-zephyr-photogrammetry-software/

https://www.regard3d.org/

https://alicevision.org/

https://www.meshlab.net/

http://cnipt-caransebes.ro/zona-turistica/obiective-turistice-din-caransebes/statui/statuia-generalului-ioan-dragalina/

Scientific Papers. Series E. Land Reclamation, Earth Observation & Surveying, Environmental Engineering. Vol. XII, 2023
Print ISSN 2285-6064, CD-ROM ISSN 2285-6072, Online ISSN 2393-5138, ISSN-L 2285-6064

GIS FACILITIES FOR THE AUTOMATION OF CADASTRAL DOCUMENTATIONS

Cornel Cristian TEREŞNEU, Cristian Samuel TEREŞNEU

Transilvania University of Brasov, 25 Eroilor Street, Brasov, Romania

Corresponding author email: cteresneu@unitbv.ro

Abstract

This paper highlights a few ideas which lead to a significantly higher efficiency with regards to cadastral documentations. Each legislation change in the field of cadaster brings new challenges for a geodetic engineer. Although many software packages are available which partially automate the generation of various appendices of cadastral documentations, never was there an attempt to fully automate the generation of a documentation. Taking into consideration the facilities offered by GIS tools especially, an attempt was made to make a major reduction of the time necessary to create a documentation. For the appendices which involve both numerical and alpha-numerical inputs, a very cheap and simple solution was proposed - Microsoft Excel; meanwhile, for the graphical parts of the documentation, which are the most important, an alternative which uses AutoCAD Civil 3D and ArcGIS was proposed. The method was tested on a sample of 47 cadastral documentations, which highlighted that the time involved in the completion of a cadastral documentation was reduced by a factor of 8.

Key words*: cadastral documentation, GIS, automation.*

INTRODUCTION

All of us are feeling the discomfort caused by the speed at which our activities are carried out. In the conditions, it seems there is never enough time to successfully accomplish everything we aim for. In addition, the recent legislation change is added (***, ANCPI, 2023), specifically the publishing of Executive Order 600 which brings into regulation the way cadastral documentations are created. In this context, there is a need for a better organisation of the geodetic engineer's activity and an increased time efficiently for completing cadastral documentations. Such proposals have been made previously (Tereşneu & Vasilescu, 2013), but these were aimed at past legislation and were only focused on the partial automation of the generation of cadastral documentations.

Today, a very high degree of automation of all cadastral operations is achieved, from field surveys (using total stations and GNSS equipment) to steps involving office work (both in terms of numerical processing of data and creation of graphical documents - Boş and Iacobescu, 2007; Boş et al., 2015; Tămâioagă & Tămâioagă, 2007).

Additionally, previous studies have investigated achieving an inter-operability between the cadastral system and other systems dealing with land administration (like tax records, land administration, issuing construction approval documents, legalisation of building and so on) and which would also benefit from a high degree of automation (Sladic et al., 2020).

Another area in which automation has seen significant use is that which aims to monitor urban sprawl, both horizontally and vertically. Complex mechanisms are required not only to monitor but also control the degree to which established urban development reglementations are followed (Ghawana et al., 2020).

In this context, we can also mention some other challenges from the field of automation of cadastral operations, with regards to the automatic identification of land parcel boundaries, both in 2D and 3D (Larsson et al., 2020).

Since this automation process involves working data stored on-line, other papers were taken into account which, although used other kinds of data, still offered the necessary theoretical basis for the correct approach of the current problem (Díaz-Hormazábal et al., 2020).

Previous papers also looked at solving the graphical elements of the cadastral

documentation, which are the most important and difficult to complete (Tereşneu et al., 2013).
Also, there are numerous software packages which can aid and facilitate the automation of various steps in the creation of cadastral documentations (Tereşneu et al., 2009), or the automation of acquiring necessary data from the immediate vicinity (Tereşneu et al., 2016). In addition, this paper also uses techniques specific to photogrammetry and remote sensing (Herbei et al., 2021; Vorovencii 2014a; 2014b; 2015a; 2015b; 2017), as each cadastral land plot is interconnected with other land plots, with which it always has a common arc.
Not only that, but similar approaches from other countries were also taken into account (Mataraci, 2005), which aimed and ultimately managed to create cadastral land records for the whole national territory.

MATERIALS AND METHODS

The materials used for this study are a:

- Dell Latitude 5411 laptop with Intel(R) Core(TM) i7-10850H CPU @ 2.70GHz 2.71 GHz, 16GB RAM, for the processing of all numerical and graphical data;
- the Microsoft Office package, especially Microsoft Excel, which was used to automate the input of text and numerical data into the appendices, but also to reunite all appendices in a single file (using VBA facilities);
- AutoCAD Civil 3D which was used to import field survey data and for the automatic creation of polylines for each individual land parcel;
- The E-terra platform for the verification of adjaciencies of studied land parcels;
- ArcGis, which was used for automating the generation of delimitation plans for the land parcels.

In terms of research methods, various techniques of applied informatics, computer programming (Tereşneu & Ionescu, 2019; Tereşneu & Ionescu, 2016) and GIS-specific methods (spatial analysis, VBA code-sequences etc.) were used (Tereşneu & Ionescu, 2014; Tamaş & Tereşneu, 2010).

RESULTS AND DISCUSSIONS

As is well known, a cadastral documentation requires the completion of appendices 13, 14, 15 and 16. The first three appendices require numerical and alpha-numerical data which are specific for each cadastral documentation.
With regards to appendix no. 13, a template in which the specific data will be input has been created in an Excel worksheet (Figure 1).

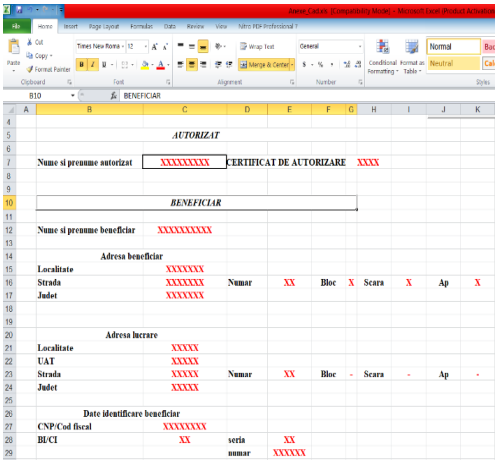

Figure 1. Input of general data

In another worksheet of the previously created Excel file (Figure 2), a template of appendix 13 is introduced, which will take the required data from the previous sheet. This can be done by a VBA code sequence which add into sheet 2 all necessary data from sheet 1 (Figure 3).
Appendix 14 is completed in a similar manner, by taking necessary data from the first sheet of the Excel registry and inserting it into the appropriate worksheet (Figure 4), also by using a VBA code sequence.
With regards to appendix no. 15 which is the technical report of the documentation, besides general information which is inserted into a distinct worksheet of the Excel registry, two types of data will be acquired from the first sheet (Figure 5): simple data and data specific to the technical report (the motivation for the documentation, data regarding adjacent parcels, data regarding old land writs of the parcel, data regarding the land survey and so on).

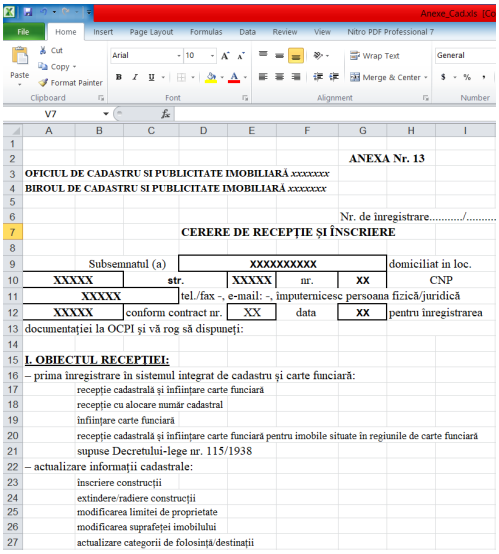

ANEXA Nr. 13

OFICIUL DE CADASTRU SI PUBLICITATE IMOBILIARĂ *xxxxxxx*
BIROUL DE CADASTRU SI PUBLICITATE IMOBILIARĂ *xxxxxxx*

Nr. de înregistrare...../.....

CERERE DE RECEPȚIE ȘI ÎNSCRIERE

Subsemnatul (a) **XXXXXXXXXX** domiciliat in loc.
XXXXX str. **XXXXX** nr. **XX** CNP
XXXXX tel./fax -, e-mail: -, imputernicesc persoana fizică/juridică
XXXXX conform contract nr. XX data **XX** pentru înregistrarea
documentației la OCPI și vă rog să dispuneți:

I. OBIECTUL RECEPȚIEI:
– prima înregistrare în sistemul integrat de cadastru și carte funciară:
recepție cadastrală și înființare carte funciară
recepție cu alocare număr cadastral
înființare carte funciară
recepție cadastrală și înființare carte funciară pentru imobile situate în regiunile de carte funciară supuse Decretului-lege nr. 115/1938
– actualizare informații cadastrale:
înscriere construcții
extindere/radiere construcții
modificarea limitei de proprietate
modificarea suprafeței imobilului
actualizare categorii de folosință/destinații

Figure 2. Template for appendix 13

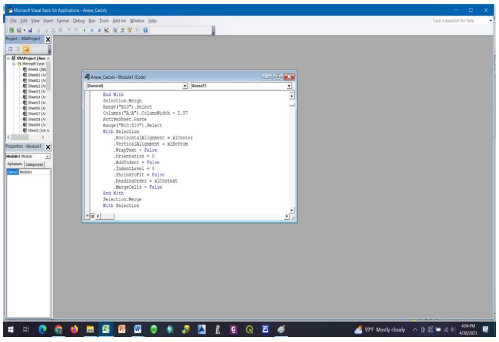

Figure 3. VBA sequence for the generation of appendix 13

The more delicate part is automating the generation of appendix 16, which is the plan of delimitation for the land parcel. This is done in multiple steps:

- The AutoCAD step; here points are imported from the *.txt file of the land survey, which was previously converted to *.csv. A crosspiece is created which automatically connects (by code) all points that define the parcel's boundary (Figure 6).

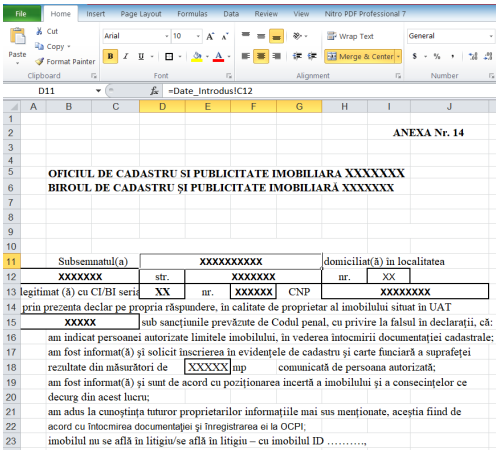

ANEXA Nr. 14

OFICIUL DE CADASTRU SI PUBLICITATE IMOBILIARA XXXXXXX
BIROUL DE CADASTRU ȘI PUBLICITATE IMOBILIARĂ XXXXXXX

Subsemnatul(a) **XXXXXXXXX** domiciliat(ă) în localitatea
XXXXXXX str. **XXXXXXX** nr. XX
legitimat (ă) cu CI/BI seria **XX** nr. **XXXXXX** CNP **XXXXXXXX**
prin prezenta declar pe propria răspundere, în calitate de proprietar al imobilului situat în UAT **XXXXX** sub sancțiunile prevăzute de Codul penal, cu privire la falsul în declarații, că:
am indicat persoanei autorizate limitele imobilului, în vederea întocmirii documentației cadastrale;
am fost informat(ă) și solicit înscrierea în evidențele de cadastru și carte funciară a suprafeței rezultate din măsurători de **XXXXX** mp comunicată de persoana autorizată;
am fost informat(ă) și sunt de acord cu poziționarea incertă a imobilului și a consecințelor ce decurg din acest lucru;
am adus la cunoștința tuturor proprietarilor informațiile mai sus menționate, aceștia fiind de acord cu întocmirea documentației și înregistrarea ei la OCPI;
imobilul nu se află în litigiu/se află în litigiu – cu imobilul ID ……,

Figure 4. Template for appendix 14

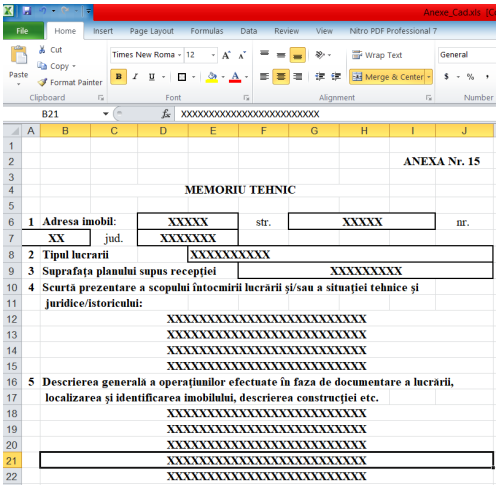

ANEXA Nr. 15

MEMORIU TEHNIC

1 **Adresa imobil:** **XXXXX** str. **XXXXX** nr.
XX jud. **XXXXXXX**
2 **Tipul lucrarii** **XXXXXXXXXX**
3 **Suprafața planului supus recepției** **XXXXXXXXX**
4 **Scurtă prezentare a scopului întocmirii lucrării și/sau a situației tehnice și juridice/istoricului:**
XXXXXXXXXXXXXXXXXXXXXXXXX
XXXXXXXXXXXXXXXXXXXXXXXXX
XXXXXXXXXXXXXXXXXXXXXXXXX
XXXXXXXXXXXXXXXXXXXXXXXXX
5 **Descrierea generală a operațiunilor efectuate în faza de documentare a lucrării, localizarea și identificarea imobilului, descrierea construcției etc.**
XXXXXXXXXXXXXXXXXXXXXXXXX
XXXXXXXXXXXXXXXXXXXXXXXXX
XXXXXXXXXXXXXXXXXXXXXXXXX
XXXXXXXXXXXXXXXXXXXXXXXXX
XXXXXXXXXXXXXXXXXXXXXXXXX

Figure 5. Template for appendix 15

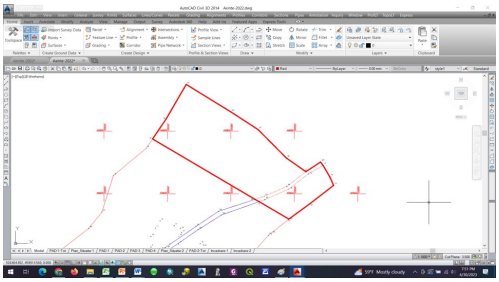

Figure 6. Automatic generation of parcel boundary

- The E-Terra step; on the E-Terra platform, a first registration job is created for the municipality where the land parcel is located and its polyline is imported. Plot adjacencies are verified; if adjacent parcels are already registered in the integrated system of cadastre and land records, their cadastral ID numbers (Figure 7) are automatically retrieved, with appropriate labels being placed on the corresponding sides at 0.5 cm (Figure 8). Also in this step, a general verification is done regarding possible boundary overlaps or gaps due to parcel misalignment. From the platform, data of interest is export in *.shp format: polygons of adjacent plot boundaries and neighboring numbers applied on adjacency arcs.
- The ArcGIS step; the AutoCAD and everything exported from E-terra is imported into ArcMap (Figure 9). Here, overlaps/gaps are checked using a VBA code sequence. The script takes into account accepted tolerances intra-urban/extra urban areas and the degree of closeness/overlap with adjacent plots. If the appropriate conditions are met, point coordinates are taken from adjacent land plots to modify the boundary of the current parcel. In this case, a warning message is shown in which the distances between polylines and the areas of overlaps/gaps are presented. Significant problems are found when there are certain spaces between the surveyed parcel and other parcels recorded in E-Terra and the coordinates of neighbouring points cannot be assumed because the land area calculated from the survey would be changed. Since this is a relatively complicated issue, it is beyond the scope of this paper. Finally, the North symbol, the coordinate grid and the tables specific to appendix 16 are added and then the appendix (Figure 10) is exported to a *.pdf file.

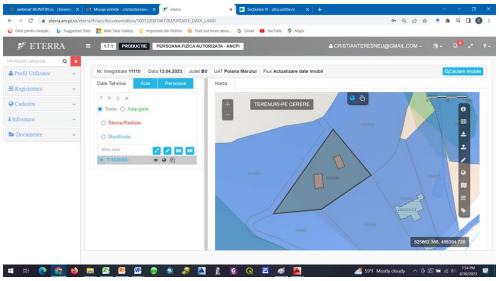

Figure 7. Studying adjacencies in E-Terra

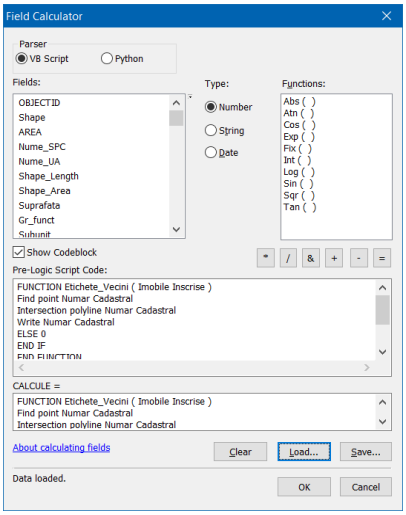

Figure 8. Automatic labelling of adjacent parcels

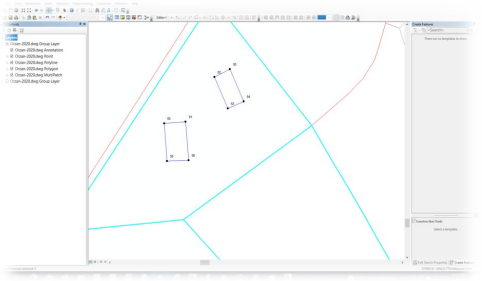
Figure 9. Importing of data into ArcMap

The last step is joining all appendices into a new worksheet of the Excel registry (Figure 11).

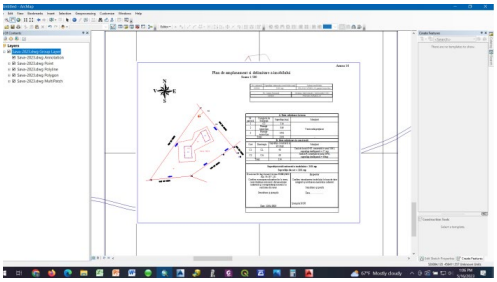

Figure 10. Plan of delimitation (PAD) generation in ArcMap.

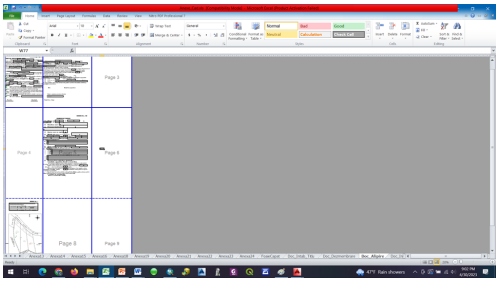

Figure 11. Completion of the cadastral documentation

CONCLUSIONS

The application of this method on 47 test cases lead to very good results both in terms of time efficiency and the correctness with which documentations were completed. With regards to time, a maximum efficiency was recorded, as working time has been shortened by a factor of 8. All 47 documentations were done by the same person in both approaches, with the effective working time being shorter in the automated approach by a factor of 7.6-8.1. Taking into account external factors (especially the degree of tiredness), we can assume that the recorded time economy is 8 times larger than in the classical approach (also considering the time necessary for an additional verification).

With regards to the correctness of the completed documentations, it has been found that this approach eliminates numerous possibilities of incorrect data input.

Evidently, the proposed approach can be improved, especially with regards to the automation of appendix 16. Besides the E-Terra step which is mandatory to be carried out under strict observation by the geodetic engineer, all other steps can be fully automated, with the most pressing issue being that of linking all pieces that are part of the same documentation.

REFERENCES

Boş, N., Iacobescu, O. (2007). *Topografie modernă*. Editura C.H. Beck, Bucureşti. pp. 542.

Boş, N., Iacobescu, O., Boş, N.C. (2015). *Topografie digitală*. Editura C.H. Beck, Bucureşti. pp. 454.

Díaz-Hormazábal, I., Valencia D., Valenzuela J. (2020). "Implementation Of Technologies in the Public Service: Geomatics in the Cloud for Monitoring Wetlands in Protected Areas," *2020 IEEE Latin American GRSS & ISPRS Remote Sensing Conference (LAGIRS)*, Santiago, Chile. 155-159

Ghawana, T., Sargent J., Bennett, R.M., Zevenbergen, J., Khandelwal, P., Rahman, S. (2020). 3D Cadastres in India: Examining the status and potential for land administration and management in Delhi. *Land Use Policy, 98*. 11.

Herbei, M.V., Bertici, R., Sala, F. (2021). Geomatic Methods for management planning of protected areas. Case study: Paniova forest, Timis County, Romania. In *Scientific paper. Series E. Land reclamation Earth observation & surveying environmental engineering*, *X*. 301-310.

Larsson, K., Paasch, M.J., Paulsson, J. (2020). Representation of 3D cadastral boundaries - From analogue to digital. *Land Use Policy 98*. 13.

Mataracı, O. (2005). "The Management of Cadastral Data in the Land Registry Information System Project", the *10th Map Meeting, Chamber of Engineers of Mapping and Cadastre*. 469-485.

Sladić, D., Radulović, A., Govedarica, M. (2020). Development of process model for Serbian cadastre, *Land Use Policy 98*. 15.

Tamaş, Şt., Tereşneu, C.C. (2010). *Concepte şi tehnici ale sistemelor de informaţii geografice.* Editura LuxLibris, Braşov. pp. 268.

Tamaş, Şt., Tereşneu, C.C. (2009). *Elemente de informatică aplicată*. Editura LuxLibris, Braşov, pp. 240.

Tămâioagă, Gh., Tămâioagă, D. (2007). *Automatizarea lucrărilor de cadastru*. Editura MatrixRom, Bucureşti, pp. 186.

Tereşneu, C.C., Ionescu, M. (2019). *Programarea calculatoarelor şi limbaje de programare.* Editura Universităţii Transilvania, Braşov, pp. 424.

Tereşneu, C.C., Ionescu, M. (2016). *Lecţii de Excel şi AutoCAD*. Editura MatrixRom, Bucureşti, pp. 238.

Tereşneu, C.C., Ionescu, M. (2014). *Auto-CAD-ul pentru topografie*. Editura MatrixRom, Bucureşti, pp. 386.

Tereşneu, C.C., Tamaş, Şt., Vasilescu, M.M., Ionescu, M., Hanzu, M., Cîrstian D.G. (2009). Possibilities of automated solving of some representative surveying-related problems by means of AutoCAD and Scilab software. În *Pădurea şi dezvoltarea durabilă*, Editura Universităţii Transilvania din Braşov, pp. 503-510.

Tereşneu, C.C., Vasilescu, M.M. (2013): Possibilities to automatize the process of elaboration the cadastral documentation. *RevCAD, 14*. 179-188.

Tereşneu, C.C., Cîrstian, D.G., Hanganu, H., Vlad-Drăghici, H.G. (2013). Using Geographical Information System for the Automatic Creation of Topographic Maps. *Pădurea şi dezvoltarea durabilă*, Editura Universităţii Transilvania din Braşov, 117-122.

Tereşneu, C.C., Clinciu, I., Vasilescu, M.M., Biali, G. (2016). Using the GIS Tools for a sustainable forest management. *Environmental Engineering and Management Journal, 15(2).* 461-472.

Vorovencii, I. (2017). Applying the change vector analysis technique to assess the desertification risk in the south-west of Romania in the period 1984-2011. *Environmental Monitoring and Assessment*, *189*(13). 524-542.

Vorovencii, I. (2015a). Quantifying landscape pattern and assessing the land cover changes in Piatra Craiului National Park and Bucegi Natural Park, Romania, using satellite imagery and landscape metrics. *Environmental Monitoring and Assessment*, *187*(11). 692-714.

Vorovencii, I. (2015b). Assessing and monitoring the risk of desertification in Dobrogea, Romania, using Landsat data and decision tree classifier. *Environmental Monitoring and Assessment*, *187*(4). 1-17.

Vorovencii, I. (2014a). A change vector analysis technique for monitoring land cover changes in Copsa Mica, Romania, in the period 1985-2011. *Environmental Monitoring and Assessment*, *186*(9). 5951-5968.

Vorovencii, I. (2014b). Detection on environmental changes due to windhrows using Landsat 7 ETM+ satellite images. *Environmental Engineering and Management Journal*, *13*(3). 565-576.

***ANCPI (2023). Ordinul 600 din 8 februarie 2023, https://legislatie.just.ro/Public/DetaliiDocument/264801.

Scientific Papers. Series E. Land Reclamation, Earth Observation & Surveying, Environmental Engineering. Vol. XII, 2023
Print ISSN 2285-6064, CD-ROM ISSN 2285-6072, Online ISSN 2393-5138, ISSN-L 2285-6064

APPLICATION OF GIS IN MANAGING THE AGGREGATE COMPOSITION OF THE SOIL WITH A NEW ACTIVE WORKING BODY FOR SURFACE TREATMENT

Petya GENKOVA, Vera STEFANOVA, Manol DALLEV

Agriculture University - Plovdiv, 12 Mendeleev Blvd, Plovdiv, Bulgaria

Corresponding author email: manol_dallev@abv.bg

Abstract

The fertility of the soil depends on its conditions, which are quantitatively expressed through its properties of porosity, density and humidity. The change in these properties is due to its structural construction and the environmental impacts. A part of the soil is damaged by heavy metals, improper fertilization and threatened by erosion. In this research proposal, innovative working bodies will be investigated for soil treatment, with the aim of managing the aggregate composition and predicting fragmentation, to protect it from erosion. The aim of the study is to application of GIS investigate innovative working bodies with active drive, to achieve a higher quality of surface tillage taking into account the existing external and controllable factors. Statistical processing of the results and optimization lead to the various operating modes of a machine to achieve the main idea and the resulting soil fragmentation regression equations are entered into a GIS environment. The Surface soil treatment is managed by GIS tools for variety visualization and presented statistically the most suitable information. The implementation of working bodies in practice will enrich the soil fragmentation data base, which leads to a greater choice of tillage bodies for soil erosion control.

Key words*: GIS, soil treatment, soil fragmentation.*

INTRODUCTION

On a global scale, agriculture has the proven potential to increase food supplies faster than the growth of the population (Davidson, 1992).

Tillage is the oldest operation in agriculture, so tillage machines have the longest development path and the greatest variety of types and types. Their main task is to bring the soil to the level of suitability for carrying out the following work processes, such as sowing, planting, fertilizing and others.

The main goals of tillage machines are saved of soil conditions, which are quantitatively expressed through its properties of porosity, density and humidity to increase crop yields and soil fertility. Therefore, the necessary tillage is determined above all by agrotechnical expedient general measures. Most importantly for the soil, if it is fertile and sufficiently enriched with nutrients, there will be a rich harvest and yield, which is the goal of every farmer (Dobrevska et al., 2015).

According to (Ksenevich, 1985; Mandrajiev, 1982) the density of the soil is essential and important, with this indicator the porosity can be determined and, accordingly, the amount of soil mass per unit volume can be determined. The conclusion is that at high density the porosity is lower.

With the advancement and improvement of the methodology, at the different stages of growing crops, it is appropriate to use and apply computerized and mechanized techniques for the evaluation and analysis of various factors that have a strong influence on the development of the cultivated plants and the evaluation of the land. Such a modern method is the use of the Geographical Information System (GIS). This approach offers structured processing of various types of data, both textual and graphical.

The combination of diverse information presupposes the analysis and arrangement of important information.

The natural conditions in Bulgaria favour the cultivation of various types of agricultural crops through a variety of soil and climatic conditions. Several authors indicate the need to develop strategies for the production and realization of agricultural production (Stoeva, 2013; Hristova & Ilieva, 2013; Toskov, 2014; Nikolova, 2013, Dobrevska et al., 2015). According to them, the developed measures should have a complex

nature, tied into a common system for effective management of agricultural holdings.
With the advancement of technology and the development of agricultural industries, more and more methods are used to analyze the purpose and usability of the land. These technologies and methods present the available information in the form of maps combining the various data (Carver, 1991; Eastman, 1997). All action related to spatial data as collecting new information, organize in groups, creating connection between them, logical links, correct and sufficient presentation and sharing can be realized by Geographical Information Systems, named GIS (Stefanova et al., 2014).
Based on the Geographical Information Systems, the methods for evaluating the multitude of factors are presented as a process combining within itself the transformation of spatial information into a process for finding solutions with optimal results.

MATERIALS AND METHODS

The surface tillage machine with which the studies were carried out combines the kinematics of a tiller with a horizontal axis of rotation and the horizontal displacement of the soil by a disc working body (Dallev, 2012). Surface active cultivation machinery soil led to a suitable condition for conducting subsequent operations sowing or planting. The experiments were carried out according to the methodology of the planned passive two-factor experiment (Mitkov, 2011).
The forward speed in the process of machine operation is changed to V1 = 1.89 km/h; V2 = 5.48 km/h; V3 = 7.97 km/h and the humidity is measured. Machine which carries out the surveys (Dallev, 2013) is equipped with a cut disc.
Studies of the aggregate composition of the different type of soil according to the speed and the moisture content are done by using a regression model. After a data-processing are derived regression equations describing fragmentation of the three fractions of soil: up to 1mm; from 1 to 25 mm and over 25 mm.
The next formulas calculated the soil fragments and grouped in 3 levels.
For aggregate composition < 1 mm is the next formula:
$Z = Aggr < 1\ mm = 8.67 + 3.2V - 0.28V^2 - 0.11V.M$ (Dallev et al., 2015);
For aggregate composition between 1 - 25 mm:
$Z = Aggr1\text{-}2mm = - 7.84V + 6.54M + 0,.61V^2$ (Dallev et al., 2015);
For aggregate composition > 25 mm:
$Z = Aggr > 25\ mm = 73.75 + 5.74V - 4.75M - 0.3V^2$ (Dallev et al., 2015), where M is soil moisture content and V is the speed.

Disk machine with R = 250 mm (Dallev, 2013)

Materials and data necessary for research:
Map of the the studied area in digital model;
Cadastre maps- The digital model formats are ZEM, CAD. Information source: the Geodesy, Cartography and Cadastre Agency.
Soil map in digital form;
Soil characteristics - Information source: The Soil Resources Agency and the Institute of Soil Science "Nikola Pushkarov";
QGIS 3.16 applications were used to visualize individual data and general analyses.

RESULTS AND DISCUSSIONS

The development of modern agriculture is unthinkable without complex mechanization of all production processes. In agriculture, mechanization and individual processes are leading to the industrialization of all branches. This is the development of new machine systems, the improvement of a given technology in growing a given crop, the provision of tillage machines with great operational reliability, and a significant increase in labor productivity. It has been established that with different types of

agricultural machinery on the same soil we have a different final appearance of the cultivated area, a different fraction of the soil. And all this again depends on all the indicators of the type of soil.

The object of the development are territories for the cultivation of various crops. The studies were carried out on the territory of the land of the village of Kaloyanovo, Plovdiv region.

The necessary data contents coordinated geographical borderlines of villages in the Municipality of Kaloyanovo.

Situated in the north part of the Upper Thracian plain, covering area of 347 sq. km., the municipality is part of the region of Plovdiv and consists of the municipal center Kaloyanovo, and 14 settlements as well - Begovo, Glavatar, Gorna Mahala, Dolna Mahala, Duvanlii, Dalgo Pole, Zhitnitsa, Ivan Vazovo, Otets Paisievo, Pesnopoy, Razhevo, Razhevo Konare, Suhozem and Chernozemen. This is the most developed agricultural region for different agricultural production. Today, Municipality of Kaloyanovo faces a number of various soil treatments and ecological innovations and yield increased challenges. The development and implementation of an environmental action plan for the valleys are associated with the strategy position and closely connection with another neighbour agricultural areas. The picture above presents the Municipality of Kaloyanovo situated in Bulgaria map (Figure 1).

Figure 1. Bulgarian map and Municipality of Kaloyanovo

In the municipality are situated 14 villages with one center city, named Kaloyanovo (Figure 2). The relief is plane to hilly and average elevation is 250 m. The climate is transcontinental, characterized with an open winter and a hot summer. These factors are essential and favorable for agricultural developing.

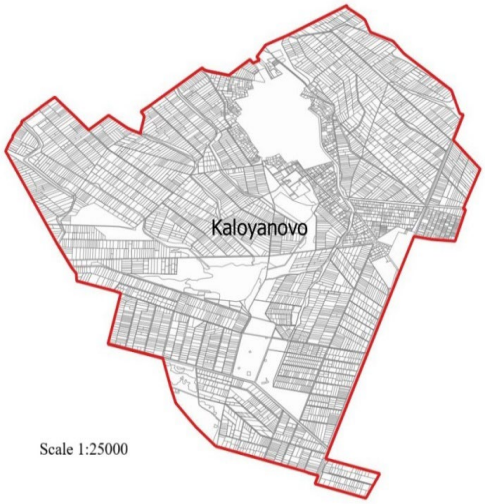

Figure 2. Map of the village Kaloyanovo

Next map (Figure 3) presents information about soil distribution in the studied area. Dominant soil types are sandy-clay and loamy, presented in the next map. These soil characteristics are useful for cultivation of various plants - both grain-legume and vegetable.

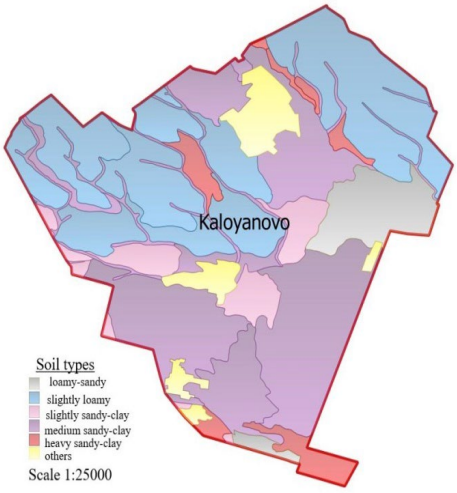

Figure 3. Map of Soil type in the studied area

Soil moisture at depth is defined as the average of all samples for a given depth (Figure 4).

When choosing a field of performing experiments with the following requirements:
The plot has a slope to the horizon is not more than 2-3°.
Surface no bumps, lumps, ridges and overthrew that provides safe operation of a machine.
The moisture content is determined by taking daily samples before and after lunch on the test area. Samples taken in airtight cups, dried at 105°C to constant weight. Measure the weight before and after drying.

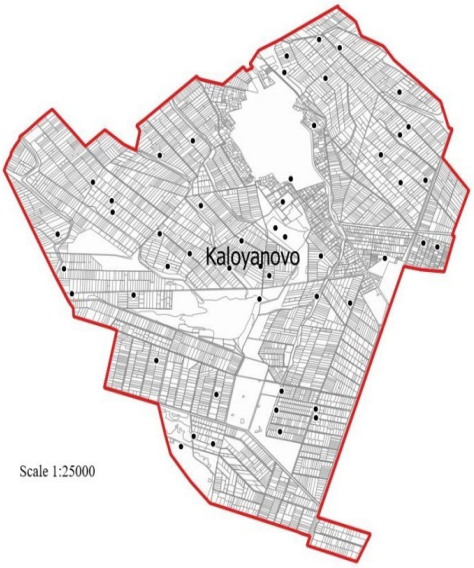

Figure 4. Map of the soil samples of moisture in the village Kaloyanovo

To visualize the results of the simulation experiments, GIS maps were created, visualizing soil fragmentation in the range of 3 levels:
- up to 1mm;
- between 1mm and 25 mm;
- more than 25mm.
With the implementation of the database in GIS, the method is developed for each property, array or the entire considered territory within one or several lands.
The soil aggregate fractions are calculated with speeds V1 = 1.89 km/h; V2 = 5.48 km/h; V3 = 7.97 km/h and respectively presented in the next three maps (Figures 5, 6, 7).

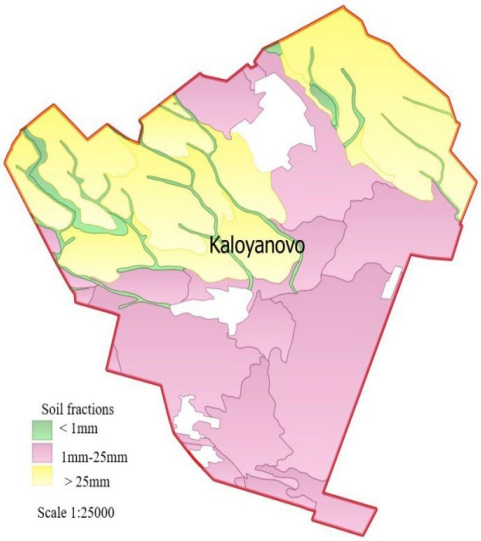

Figure 5. Map of Soil aggregate fractions with speeds V1 = 1.89 km/h

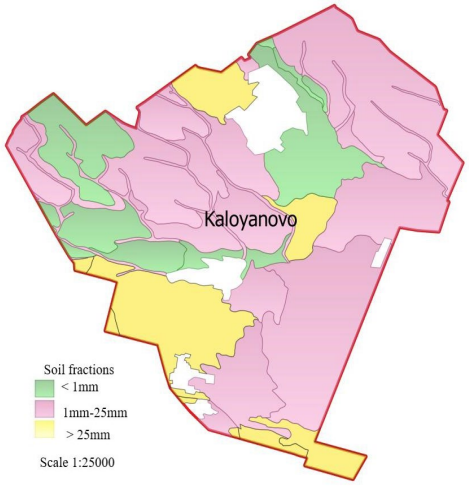

Figure 6. Map of Soil aggregate fractions with speeds V2 = 5.48 km/h

In order to observe agrotechnical requirements, units from 1 to 25 mm to be 70%, respectively, while those to 1 mm and over 25mm up to 30%, the measured values of moisture can be seen that it is impossible. Closest values to agrotechnical requirements are obtained at a speed of the unit around 5 km/h.
During this process, the following will occur aggregate composition:
- to 1 mm - 10%;

- from 1 to 25 mm - 60%;
- over 25 mm - 30%.

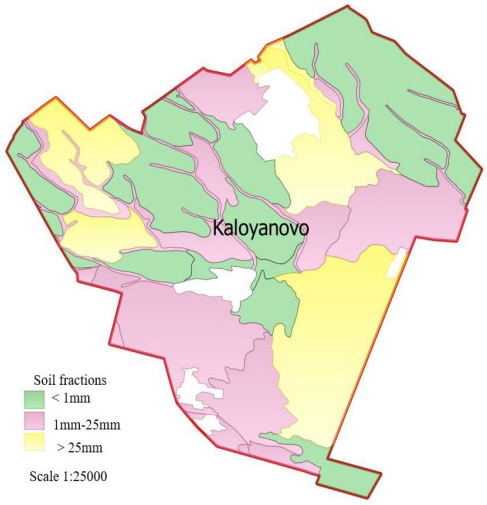

Figure 7. Map of Soil aggregate fractions with speeds V3 = 7.97 km/h

In all variants of the conducted experiments, humidity has a significant influence on the crushing of the machine under investigation.

CONCLUSIONS

This approach of presenting, harmonizing and analysing a lot of diverse information gives a clear picture for the cultivation of different types of crops in the land of the village of Kaloyanovo. When cultivating the soil, an important indicator is the achievement of a certain aggregate composition of the soil, necessary for the development of the cultivated crop. The cultivation of the soil with active working organs becomes extremely important, both from an agronomic and economic, as well as from an ecological point of view.

The indicator for the erosive dangerous condition of the soil is characterized by size fraction to 1 mm. Indicator valuable agronomic soil is determined by the fraction size of 1 to 25 mm.

Village of Kaloyanovo is good area for agricultural development. All natural factors-soil distribution, water resources and relief factors will have positive effects on crops development.

The implementation of information from real research and its transformation into a spatial database through GIS enables a modern and up-to-date analysis and summarization of the existing state of the studied territory.

ACKNOWLEDGEMENTS

This work was financed and supported by the Bulgarian Ministry of Education and Science under the National Research Programme „Smart crop production" approved by Decision of the Ministry Council № 866/ 26.11.2020 and also from Scientific Program "YOUNG SCIENTISTS AND POST-DOCTORAL STUDENTS - 2", 2022-2023, Agricultural University, Plovdiv (Bulgaria).

REFERENCES

Carver, S. (1991). Integrating multi-criteria evaluation with geographical information systems: *International Journal of Geographical Information Systems, 5*(3).

Christova, E. & Ilieva, D. (2013). Productions of vegetables and fruits – potential for increasing employment in rural Rousse district, *Proceedings of University of Ruse, vol.52*, book 1.1, pp. 122-125 (Bulgarian).

Dallev, M. (2013). Investigation of a working body surface tillage. Abstract.

Dallev, M., Ivanov, Iv. (2012). "Influence of the disk angle adjustment on the condition soil surface using surface tilling machine", *Agricultural science and technology 4*(1), 92-93.

Dallev, M. & Ivanov, I. (2015) Study of body for surface tillage in heavy soils with low humidity. *Scientific Papers. Series A. Agronomy 58:* 45-48.

Davidson, D.A. (1992). The evaluation of land resources, *Stirling University published in USA with John Wiley*, New York.

Dobrevska, G.R. Popova, H. Dzhugalov (2015). Manifestations of M9 apple rootstock in stoolbedwith different soil substrate and plants with a different origin, *"10th International Symposium on Agriculture"*, Zagreb, Croatia (16-20 February, 2015) Zbornik radova, 565-569.

Dobrevska, G.R. Popova, H. Dzhugalov (2015). Influence of plant origin and soil substrate on theBehaveour of the MM 106 rootstock in stoolbet. *10th International Symposium on Agriculture, Zagreb, Croatia* (16-20 February, 2015) Zbornik radova, 570-574.

Eastman, J.R. (1997). IDRISI for Windows, version 2.0 (Tutorial Exercises): Graduate Schoolof Geography-Clark University, Worcester, MA.

Ksenevich, I. (1985). Hodovaya sistema-pochva-urozhay., Moskve, Agroprimizdat.

Mandradzhiev, S. (1982). Izsledvane izmenenieto na teglitelnata sila i optimizirane rezhima na rabota na pochvoobrabotvashti frezi i frezi-kultivatori. Disertatsiya za obrazovatelna i nauchna stepen, Plovdiv.

Mitkov, D. & Minkov. M (1993). Statistical methods for the study of agricultural machinery part II, S., Zemizdat.

Nikolova, M. (2013). Condition and challenges for Bulgarian agriculture after accession to the EU, *Proceedings of University of Ruse, vol. 52,* book 5.1, pp. 209-214. (Bulgarian)

Stanev, S. (1968). Machinery for tillage, sowing and cultivation. "Zemizdat", Sofia.

Stefanova, V., Arnaudova, Zh., Haytova, D., Bileva, T. (2014). Multi-criteria evaluation for sustainable horticulture, *Turkish journal of agricultural and natural sciences Balkan agriculture congress special issue: 2*, 1694-1701, www.turkjans.com

Stoeva, T. (2013). "Economic effectiveness of vegetable production in Plovdiv region", *Thesis*, Agricultural university of Plovdiv, Bulgaria (Bulgarian)

Toskov, G. (2014). Strategii za upravlenieto i realizatsiyata na polskoto zelenchukoproizvodstvo-avtoreferat

Scientific Papers. Series E. Land Reclamation, Earth Observation & Surveying, Environmental Engineering. Vol. XII, 2023
Print ISSN 2285-6064, CD-ROM ISSN 2285-6072, Online ISSN 2393-5138, ISSN-L 2285-6064

EARTH OBSERVATION TECHNIQUES APPLIED FOR LAND WASTE DETECTION AND MONITORING

George BOLDEANU[1, 4], Mihaela GHEORGHE[1], Cristian MOISE[2], Iulia DANA NEGULA[2], Georgeta TUDOR[3]

[1]GMV Innovating Solutions, Calea Floreasca, District 1, Bucharest, Romania
[2]University of Agronomic Sciences and Veterinary Medicine of Bucharest, 59 Marasti Blvd, District 1, Bucharest, Romania
[3]National Institute for Research and Development in Environmental Protection, 294 Independence Embankment, District 6, Bucharest, Romania
[4]Bucharest University, Faculty of Geography, "Simion Mehedinţi" Doctoral School, 1 Nicolae Balcescu Blvd, District 1, Bucharest, Romania

Corresponding author email: george.boldeanu@gmv.com

Abstract

The dramatic increase in the amount of waste produced globally has an undeniable negative effect on the environment. The accelerated pace of urban development, the increase in consumption and the large scale of industrial activities have led to a rapid accumulation of waste in more or less proper waste dumps. All member states of the European Union are required to comply with waste management regulations, which primarily provide for the prevention of illegal dumping of any type of waste, its disposal in compliant landfills and their regular monitoring. In our ongoing project we aim to support waste management activities by proposing practical ways for Earth observation data to be used in off-site waste detection and monitoring of known landfills. Our research focuses on assessing the state of the art in earth applications techniques such as artificial intelligence/ machine learning that are currently being used for waste management and proposing approaches for building up a portfolio of scalable solutions that will support waste management not only in Romania but also at a regional, European, or global level. "This work was supported by a grant of the Ministry of Research, Innovation and Digitization, CCCDI - UEFISCDI, project number PN-III-P2-2.1-PTE-2021-0432, within PNCDI III".

Key words*: Deep Learning, Earth Observation, illegal waste dumps.*

INTRODUCTION

In the last 100 years global population increased 4 times, with 8 billion people reached in 2022 (World Population Prospects 2022: Summary of Results, n.d.). This drastic increase combined with changes in consumption and socio-economic patterns set the premise for appearance of illegal and unregulated dump waste sites. What a Waste 2.0 (Kaza, 2018) report estimates that until 2040 the global production of waste will be around 3.4 billion tons.

In Europe, in 2020 the waste production was of 4.808 kg/capita, from which 505 kg is classified as municipal waste (Eurostat, 2022). Due to strict regulations in waste management agreed at European Union level, Romania has an issue with illegal waste dumps resulting from various activities or from illegally imported waste. These dumps are a concern for human health and they also pose a threat for the environment with various risks associated with them, from air pollution to the spread of diseases transmitted by mosquitos (Environmental Center, 2021). Also, poorly managed wastes can cause infiltration of leachate in aquifers and the contamination of drinking water sources or rivers. Earth Observation (EO) data refers to continuously obtained data needed to improve the detection of illegal waste dumps that due to various factors can't be detected with traditional in field observations.

To perform more in-depth and least intrusive analysis of EO data, Deep Learning (DL) techniques were adopted to work with EO data, especially multi-spectral imagery. In the last 5-6 years a lot of progress was made in the field of DL and Computer Vision (CV). An approach to identify such waste dumps is proposed, which

uses Sentinel 2 data with a semantic segmentation model.

MATERIALS AND METHODS

Working with satellite images for Semantic Segmentation (SS) applications has one major deficit, which is the lack of already existing data masks for various tasks. Especially with a task with a very high specificity, like dump waste identification. Our approach in resolving this issue was to create masks from already existing Corine Land Cover (CLC) dataset that has a land cover class of waste dumps, containing 1727 training sites at European level (EEA, 2018). by detailed verification of dump waste sites from Romania, it was found that CLC database is vastly inaccurate, showing a lot of inconsistencies between ground truth and polygon masks. Also, the number of waste sites covering the national territory was very small (11 polygon with dump sites). To tackle this issue and have the possibility to control the quality of polygon masks corresponding to waste dumps, a manual identification and vectorization procedure was conducted. Although manual vectorization is a time-consuming task, it has a very high accuracy. Using QGIS and high-resolution imagery from Google Satellite a total number of 344 dump waste masks were created. Because the identification of waste dumps was intended to be done on 2 different datasets, Sentinel 2 and Sentinel 2 images enhanced through SuperResolution (S2 SR) techniques inhouse, the waste dumps were filtered based on their area extent. S2 SR data was created based on Super Resolution Generative Adversarial Network (SR-GAN) inspired algorithm that was trained with SPOT-6 imagery to enhance Sentinel 2 imagery. The SR-GAN algorithm uses a generator-discriminator dual scheme, where the generator uses a ResNet structure with several residual blocks. The resulting data SR S2 data have a resolution of 2.5 meters, displaying an upscale factor of 4x. For S2 SR all the waste dump masks were used; meanwhile, for S2 just the masks with an area larger than 0.2 ha were selected. S2 data was the best option due to its higher spectral and temporal resolutions and long mission time (>5 years). To deal with the fact that vector masks were created from high-resolution imagery and the data for semantic segmentation was of medium resolution, the masks were validated with the S2 data after creation, to achieve a high degree of correlation between the two. To create the training data, images from June till September 2022 with cloud coverage smaller than 10% were downloaded. The process for creating image tiles (or patches) was conducted using Python on overlaid S2 bands. The image tiles were created with dimensions of 120 x 120 pixels and 288 x 288 pixels for S2 data and with 126 x 126 pixels for S2 SR. Only 10 spectral channels out of the 13 available were used (the 60 m bands were filtered out due to lower spatial information), and all were resampled to 10 m resolution (Table 1). To increase the number of total training data, simple augmentations were implemented with the help of Albumentations (Buslaev et al., 2020). Augmentations are a set of data transformation to increase the training data when the data is scarce. Those augmentations consisted in one Vertical Flip, one Horizontal Flip and a Transposition of the original image, resulting in a total of 1376 images.

Table 1. S2 bands used for training

Sentinel 2 band	Wavelength (nm)
Band 1	442.2 - 442.7
Band 2	492.3 - 492.7
Band 3	558.9 - 559.8
Band 4	664.6 - 664.9
Band 5	703.8 - 704.1
Band 6	739.1 - 740.5
Band 7	779.7 - 782.8
Band 8	832.8 - 832.9
Band 8A	864.0 - 864.7
Band 9	943.2 - 945.1
Band 10	1373.5 - 1376.9
Band 11	1610.4 - 1613.7
Band 12	2185.7 - 2202.4

The accuracy of several SS models was assessed in the identification of waste dumps to select the best performing model: U-Net, ResUnet, PSPNet with different backbones or without. U-Net is a fast and precise convolutional network architecture for image segmentation tasks (Ronneberger et al., 2015). The U-Net architecture represents a Fully Convolutional Network (FCN) which is composed by two sides forming a U shaped network: the contracting path on the left side and the expansive path on the right side. The contracting path (also called the encoder) follows a convolutional network

architecture with 3 x 3 convolutions, followed by ReLU activation functions and 2 x 2 max pooling operations (Figure 1). The expansive path, also called the decoder, which is the symmetric part that reconstructs the precise localization of the desired features using transposed convolutions (up convolutions), ReLU activations and a final 1 x 1 convolution to reconstruct the data to the original shape of input (same height, width, number of channels).

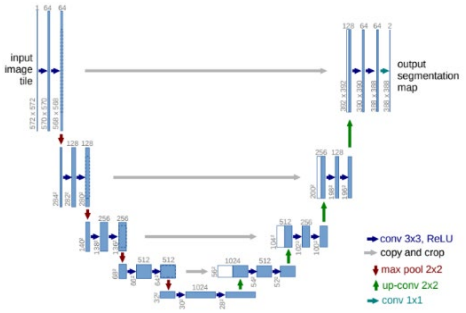

Figure 1. U-Net architecture

ResUnet is a U-net like architecture that uses residual units instead of simple neural units (convolutions followed by activation functions) to tackle the problem of vanishing gradients. Residual units are composed of 3 basic elements: BatchNormalization, ReLU activation function and convolutional layers (Figure 2). The main advantage of ResUnet is that with propagation of low level and high level information, the propagation is made without degradation, thus facilitating the design of a network with fewer parameters but comparable in performance (Zhang et al., 2017).

PSPNet or Pyramid Scene Parsing Network, is a SS model that asigns for each pixel in the image a category label using complete understanding of the scene. The main advantage of the PSPNet is that it uses dilated convolutions alongside a pyramid pooling module. The dilated convolutions are convolutions with a specified sparsity which increases the receptive field. The Pyramid Pooling Module is the central piece of the model, that captures the global context of the input image. Basically, the module upsamples and concatenates the features maps at different dimensions (1 x 1, 2 x 2, 3 x 3, 6 x 6) after which the concatenated features are convolved and lastly upsampled with a 8x bilinear upsample to create the final prediction (Zhao et al., 2016). This convolution followed by the upsampling is the decoder of the PSPNet (Figure 3).

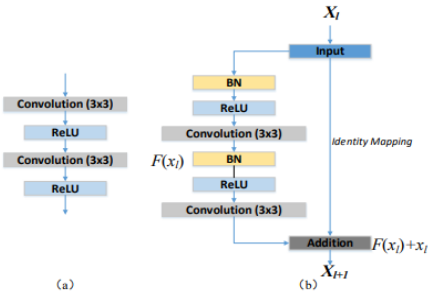

Figure 2. ResUnet residual unit

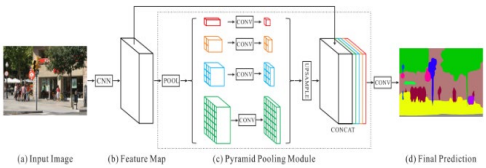

Figure 3. PSPNet architecture

For the identification of optimal hyperparameters such as: learning rate, optimizer, loss function, Optuna Framework was implemented for studying different scenarios using study/trail schema. This study/trail schema means that a study is created with all the parameters to be tested on a defined number of epochs with the desired model or models with a limited number of trials. Optuna is an automated framework that searches for the optimal hyperparameters and is not constricted by the framework where it is deployed: PyTorch, TensorFlow, Keras etc. It has an intuitive code structure and object-based orientation which makes it suitable for identifying the values to be used in finetuning the hyperparameters (Akiba et al., 2019).

RESULTS AND DISCUSIONS

Testing different approaches and sets of hyperparameters with Optuna led to the conclusion that the most important hyperparameter between the learning rate, optimizer and loss functions was the learning rate with a percentage of over 60% in most of the models tested. Testing U-Net with various

backbones based on feature extractors (ResNet and DenseNet) it is observed that IOU score values are kept at a minimum (under 0.01) (Figure 4).

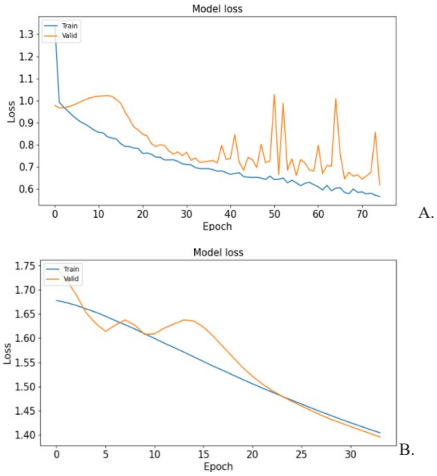

Figure 4. IOU score (A) and Loss function (B) for Unet with DenseNet 201 backbone

This fact can be explained by the lower learning rate that keeps the learning procedure at a minimum along the epochs. Even the network gradually improves this means that the learning procedure should be a longer one with too many epochs for training. Therefore, deeper networks (up to 60 million parameters to be trained on ResNet152) weren't tested. ResUnet gives the most promising results with values of IOU greater than 0.2 on a minimum of 50 epochs for training. The advantage of ResUnet is the propagation of information from low levels to high levels without degradation. Even if ResUnet has promising results, in Figure 5 a classic overfit scenario is presented, where the train metric kept increasing with the training time, but the validation metrics were stuck at a minimum level. This is a classical issue where learning rate plays a major role, with a value too small for an optimum learning procedure. The loss function that achieves the best results is a combination of a binary focal loss + Dice Loss, where binary focal loss is meant to discriminate between hard examples and easy examples, with a balance between positive and negative examples. Also, the Dice loss is a loss function adopted specially for semantic segmentation tasks, because is measures the similarity between two samples and works especially with imbalanced datasets, which is the case of binary semantic segmentation tasks. The combination of the two loss functions alongside a learning rate close to the optimum range leads to the best values for: validation IOU score, F1 (Dice) a score and Loss value (Table 2) (Figure 6).

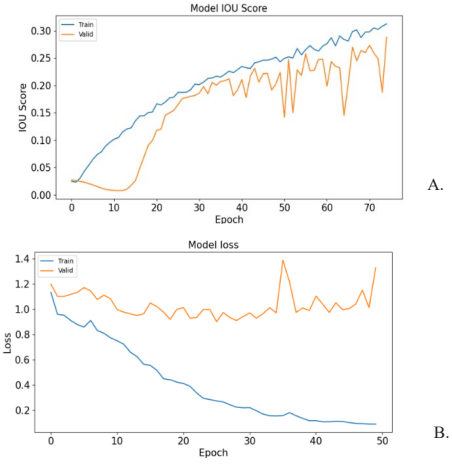

Figure 5. IOU score (A) and Loss function (B) for ResUnet with Binary Cross-Entropy + Jaccard loss

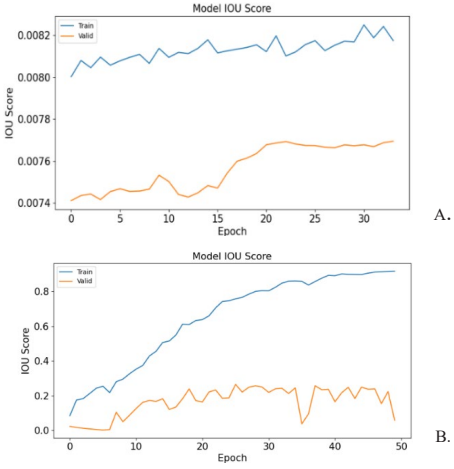

Figure 6. IOU score (A) and Loss function (B) for ResUnet with Binary Focal +Dice Loss

Table 2. Results of different models and hyperparameters

Model	Optimizer	Learning rate	Loss function	Epsilon	Epochs	IOU score (max)	Loss value (min)	Val F1 score (max)
ResUnet	Adam	0.0001	Binary Cross-Entropy + Jaccard loss	0.0000001	50	0.264	0.901	0.402
ResUnet	Adam	0.001	Binary focal + Jaccard loss	1	75	0.215	0.829	0.350
ResUnet	Adam	0.001	Jaccard loss	1	50	0.163	0.838	0.278
ResUnet	Adam	0.001	Jaccard loss	1	100	0.235	0.766	0.377
ResUnet	Adam	0.001	Binary Focal + Dice Loss	1	75	0.288	0.619	0.445
ResUnet	Adam	0.001	Dice Loss	1	75	0.238	0.619	0.382
U-Net + DenseNet 201	Adam	0.0001	Binary Cross-Entropy + Jaccard loss	1	34*	0.008	1.396	0.015
U-Net + Resnet54	Adam	0.0001	Binary Cross-Entropy + Dice Loss	1	64*	0.008	1.334	0.015
U-Net + ResNet 152	Adam	0.0001	Binary Cross-Entropy + Jaccard loss	1	38*	0.008	1.144	0.015
PSPNet	Adam	0.0005	Binary Focal + Dice Loss	1	120	0.001	1.265	0.003

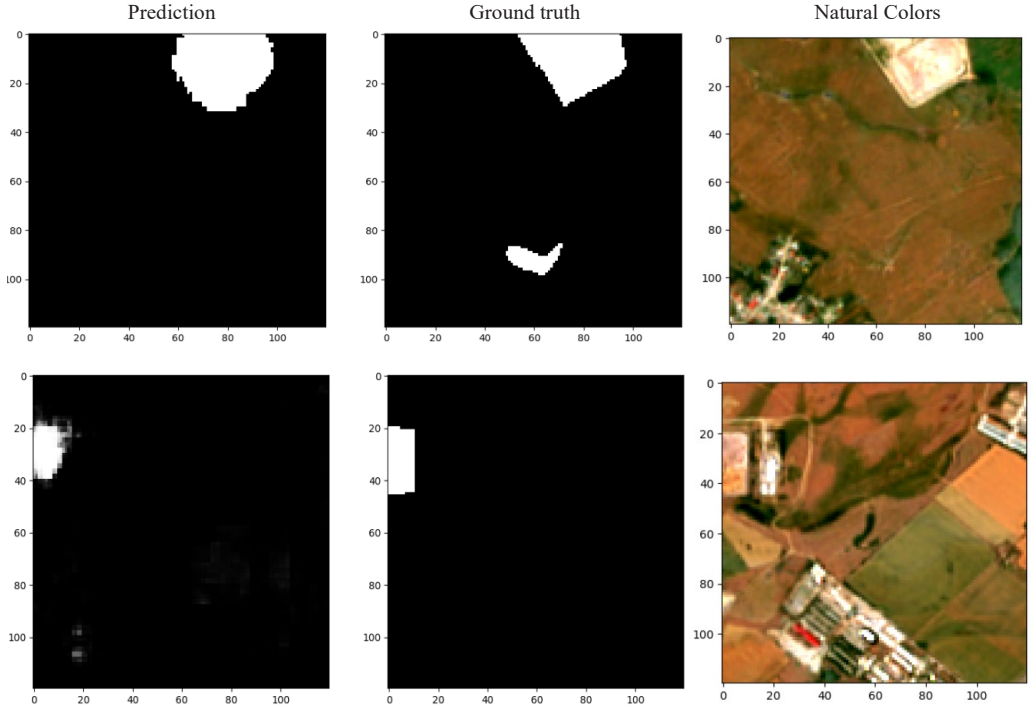

Figure 7. Inference procedure with prediction, ground truth and natural color depicted waste dump area

For the model validation task, data was derived from the initial pairs of Sentinel 2 images and dump masks. 25% percent (344 polygons) of the total data was randomly assigned for validation, Figure 7 shows an image patch in the inference step with a prediction of an administrated waste dump. The model recognizes the spectral pattern and shape of dumps that respect the norms in waste dump management and tend to have a dense material concentration. On unstructured small illegal waste dumps, the model didn't recognize the dumps from the southern part of the first image tile. This fact is due to the weak concentration of materials and therefore a weak spectral response with a lot of mixing from the surrounding area. On the second row another image tile shows how the model behaves in identifying a well-structured waste dump.

CONCLUSIONS

ResUnet is a SS model that identifies very well-structured dumps with consistent shape and spectral response. Due to the fact that the training set wasn't divided into categories of dumps, but on the criteria of area, the model was unable to differentiate between illegal waste dumps that have different properties and structure and managed waste dumps. Also, more hyperparametrization is needed for the Unet with different backbones to achieve more consistent results with higher accuracies. Even if ResUnet gives promising results, more models should be tested in the near future on a more robust training dataset that will be more rigorously created, with various approaches for limiting uncertainty. Examples of models to be tested are Mask R-CNN or DeepLabv3.

REFERENCES

Akiba, T., Sano, S., Yanase, T., Ohta, T., & Koyama, M. (2019). Optuna: A Next-generation Hyperparameter Optimization Framework. *Proceedings of the 25th ACM SIGKDD International Conference on Knowledge Discovery & Data Mining.* 2623-2631 https://doi.org/10.48550/ARXIV.1907.10902.

Buslaev, A., Iglovikov, V. I., Khvedchenya, E., Parinov, A., Druzhinin, M., & Kalinin, A.A. (2020). Albumentations: Fast and Flexible Image Augmentations. *Information*, *11*(2), 125. https://doi.org/10.3390/info11020125.

EEA (2018). *Corine Land Cover 2018*. Environmental European Agency. https://land.copernicus.eu/pan-european/corine-land-cover/clc2018?tab=metadata

Environmental Center (2021). *The Hidden Damage of Landfills* https://www.colorado.edu/ecenter/2021/04/15/hidden-damage-landfills.

Eurostat (2022). *Waste Statistics*. https://ec.europa.eu/eurostat/statistics-explained/index.php?title=Waste_statistics#Waste_generation_excluding_major_mineral_waste.

Kaza, S. (2018). *What a waste 2.0: A global snapshot of solid waste management to 2050*. Urban Development. © Washington, DC: World Bank. http://hdl.handle.net/10986/30317.

Ronneberger, O., Fischer, P., & Brox, T. (2015). *U-Net: Convolutional Networks for Biomedical Image Segmentation*. Medical Image Computing and Computer-Assisted Intervention (MICCAI), Springer, LNCS, 9351, 234-241. https://doi.org/10.48550/ARXIV.1505.04597.

World Population Prospects (2022). *Summary of Results*. (n.d.).

Zhang, Z., Liu, Q., & Wang, Y. (2017). Road Extraction by Deep Residual U-Net. IEEE *Geoscience and Remote Sensing Letters.* https://doi.org/10.48550/ARXIV.1711.10684.

Zhao, H., Shi, J., Qi, X., Wang, X., & Jia, J. (2016). Pyramid Scene Parsing Network. *IEEE Conference on Computer Vision and Pattern Recognition (CVPR).* https://doi.org/10.48550/ARXIV.1612.01105.

Scientific Papers. Series E. Land Reclamation, Earth Observation & Surveying, Environmental Engineering. Vol. XII, 2023
Print ISSN 2285-6064, CD-ROM ISSN 2285-6072, Online ISSN 2393-5138, ISSN-L 2285-6064

STUDIES OF BONITATION AND LAND EVALUATION IN MURFATLAR, CONSTANTA COUNTY, ROMANIA, USING GIS TECHNIQUES

Anca-Roxana STRUGARIU

University of Bucharest, Faculty of Geography, 4-12 Regina Elisabeta Blvd, Bucharest, Romania

Corresponding author email: anca.roxana.strugariu@gmail.com

Abstract

This paper aims to present the land quality and productivity of the administrative territorial unit of Murfatlar, Constanța County, located in south-east of Romania, an area well known for its vineyards, while used for specific purposes, such as agricultural destinations. The assessment is based on the analyses of climate (temperature and precipitation), soil (type, texture, reaction, gleization, presence of microforms and water), relief (slope), as well as other aspects of land, and their interpretation in order to determine the fertility of the site and its suitability for cultures (such as wheat, canola, corn, etc.). For the results and discussions phase, the soil bonitation note was calculated and a qualitative classification map was made to illustrate the potential productivity level. However, due to the fact that the soil evaluation is developing under both natural and human-caused environmental changes, the bonitation note needs to be revised often.

Key words*: land quality and productivity assessment, bonitation, suitability, Geographic Information System, classification.*

INTRODUCTION

Land evaluation is a complex action of examining and analysing various factors to determine the productivity level of a particular site. The process is accomplished by calculating certain elements after each of them has been given a score (between 0 and 1) beforehand. These scores represent a numerical value to indicate the amount of benefit they provide.

Among the indicators usually taken into consideration, the following were studied, as they are more significant and more precisely measurable: temperature, precipitation, soil type and texture, gleization, slope, presence of water, affected surfaces.

The bonitation note is obtained by multiplying the result of the previously mentioned indicators by 100, as following:

$X = (a*b*\ldots*n) * 100$, where X is the bonitation note, while a/b/n are the indicators' value (Biali & Popovici, 2006).

The principle which is the basis of the bonitation note is that each characteristic is appreciated under the aspect of favourability. After the bonitation note was calculated, five classes were established to express the fertility of the site.

This article suggests a way to integrate the presented information using GIS (Geographic Information System) techniques for Murfatlar (known as "Basarabi" between 1924-1965 and 1980-2007), a city in Constanța County, Dobrogea, located in south-east of Romania. The administrative territorial unit is composed of Murfatlar (the residence) and the village of Siminoc.

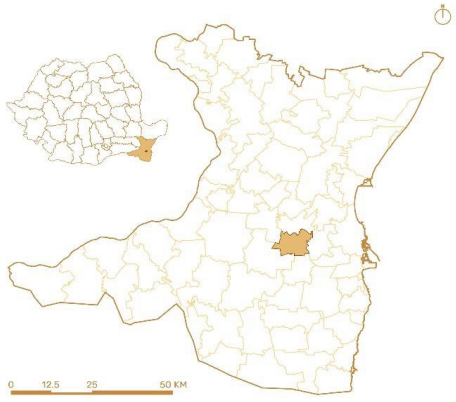

Figure 1. Map showing the location and outline of the study area. Source of vectors: geoportal.ancpi.ro

The area has an irregular shape, while the city was formed and developed in a complex natural region.

Murfatlar is very well known for its vineyards, with multiple varieties of vine, the site having certain particularities due to the geographical position. The vineyards are located between the Danube and the Black Sea, in the centre of Dobrogea Plateau, with predominantly southern and southwestern exposures.

The temperate continental climate, the diversity of the location of the vineyard plantations, the protective effect of the relief against the predominantly north-eastern cold currents, the favourable influence of excessive neighbourhood, offer the Murfatlar vineyard a particularly favourable microclimate for the production of a wide variety of wines.

The city also has a protected area of national interest corresponding to the IUCN (International Union for Conservation of Nature) category IV (floristic and faunal nature reserve). The Fântânița-Murfatlar nature reserve was placed under protection in 1932. Since 1962 the reserve has been protected by law and in 2000 was declared a protected area, identified with the site code ROSCI0083 in the Natura 2000 network.

Another attraction is represented by the monastic cave complex, one of the oldest places of worship in Romania, being excavated in a chalk hill located near the chalk quarry in Murfatlar.

For a better comprehension of the site, I realised a land use map for the administrative territorial unit which shows the variability of the functions.

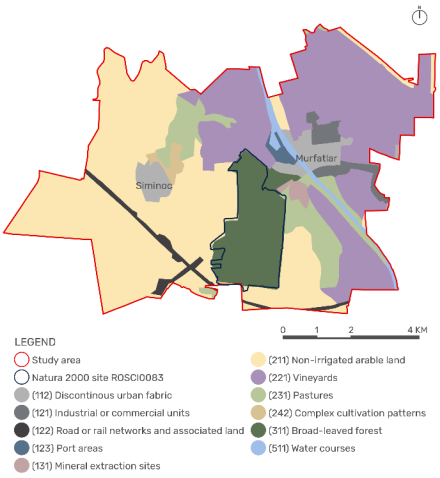

Figure 2. Land use map according to CORINE Land Cover 2018. Source of vectors: land.copernicus.eu

As shown above, the vineyards are on either side of The Danube - Black Sea Canal (represented as a "water course"), with a "port area" in vicinity. The broad-leaved forest assimilates with the Natura 2000 site. The south and south-east of the administrative territorial unit are composed of arable lands.

MATERIALS AND METHODS

Each characteristic (temperature, precipitation, soil type, texture, gleization, slope, affected surface) was analysed and received a score according to a bonitation scale (Figure 3).

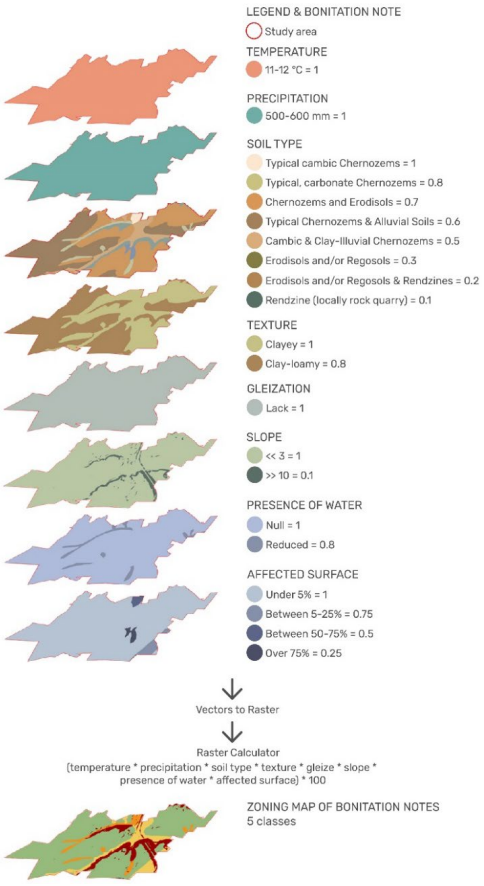

Figure 3. Diagram illustrating the map overlay process used to evaluate potential agricultural fertility

To determine the bonitation scale, multiple resources were taken into consideration, especially the methodology of pedological studies.

The study used only open-source materials (such as vectors and the EU-DEM from Land Copernicus), while the collected data was processed in QGIS and ArcMap software.
The vectors were transformed into raster in order to calculate the bonitation note and to make the qualitative classification map. Therefore, the interpretation of the results took place, to gain insights into the site's agricultural value and ecological status.
This type of information can be used for management planning or conservation strategies.
It's important to note that specific bonitation methodologies can vary depending on the purpose of the assessment and regional practices. Different countries and organizations may have their own guidelines and standards for conducting bonitation studies.

RESULTS AND DISCUSSIONS

The city's climate is part of central Dobrogea, characterised by continentality, with large diurnal and annual oscillations of air temperature, low amounts of precipitation.
The presence of The Danube - Black Sea Canal contributes to a permanent evaporation of water, ensures the humidity of the air and regulates the heating, while the relative proximity of the sea influences the circulation of air masses.
The frequent torrential nature of the rains, resulting in floods, is recorded as a specific phenomenon. However, the town benefits from a pleasant climate, determined by its geographical location and relief.

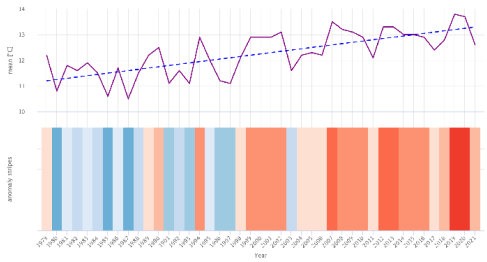

Figure 4. Mean yearly temperature in Murfatlar.
Source: meteoblue.com

The data above (Figure 4), provided by Meteoblue, show the trend and anomaly of temperature.
The blue dotted line represents the linear trend of climate change. As the trend line is upward from left to right, the temperature trend is positive and warming in Murfatlar due to climate change.
At the bottom, the graph shows the so-called anomaly stripes. Each coloured band represents the average temperature for a year, blue for colder years and red for warmer years. Thus, it is clear that in the past two decades the temperature has risen, the effects of climate change are already well visible through more frequent extreme weather events such as heat waves, drought, floods and storms.
As the average annual temperature for Murfatlar is higher than the mean for the country, with more than 11°C, it received the score 1 in the bonitation scale (Table 1).

Table 1. Bonitation scale for rating the temperature

Temperature (°C)			
11-12	10-11	9-10	8-9
1	0.9	0.8	0.7

For the precipitation, the trend (blue dotted line) is set at 533.5 mm, with clear ups and downs. As the line is horizontal, no clear trend can be determined. The below graph shows the anomaly stripes. Each coloured band represents a year's total rainfall, green for high rainfall and brown for drier years.

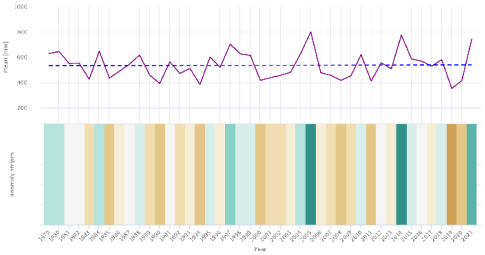

Figure 5. Mean yearly precipitation in Murfatlar
(Source: meteoblue.com)

The temperature and the precipitation are deeply correlated. In the warmer years, the rainfall registered was low, while in colder years the precipitation' quantity was higher.
As the precipitation' trend line is between 500-600 mm, and the listed values are more or less close, it got the score 1 in accordance with the bonitation scale (Table 2).

Table 2. Bonitation scale for rating the precipitation

Precipitation (mm)		
500-600	400-500	600-700
1	0.9	0.8

In Murfatlar there are numerous soil types, 11 to be precise (Figure 6).

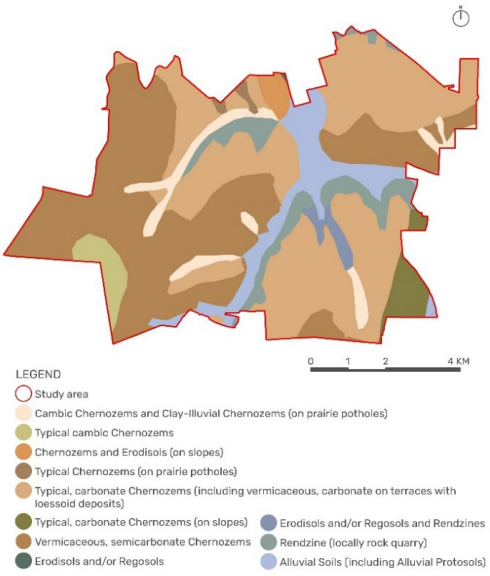

Figure 6. The soil map of the study area.
Source of vectors: geo-spatial.org

There are varieties of Chernozems, which are the most common and represent the fertility of the site. However, there are also Erodisols, Regosols and Rendzines, especially in the vicinity of the Danube - Black Sea Canal and the monastic cave complex.
The highest score of 1 in rating the soil type was received by typical cambic and vermicaceous, semicarbonate Chernozems.
The score of 0.8 was for Chernozems on slopes and on terraces. In-between (with 0.5-0.7) are the Chernozems on prairie potholes, while Erodisols and Regosols got 0.2-0.3.
The Rendzine (locally rock quarry) is the most unsuitable for agriculture, therefore it received the score 0.1 according to the bonitation scale (Table 3).

Table 3. Bonitation scale for rating the soil type

Soil type						
Chernozems	Cambic Chernozems	Brown Soils	Argilluvisols	Alluvial	Protosol	Gleic
1	1	0.8	0.7	0.7	0.5	0.1

Across the administrative territorial unit there are two main textures (Figure 7), clayey and clay-loamy.

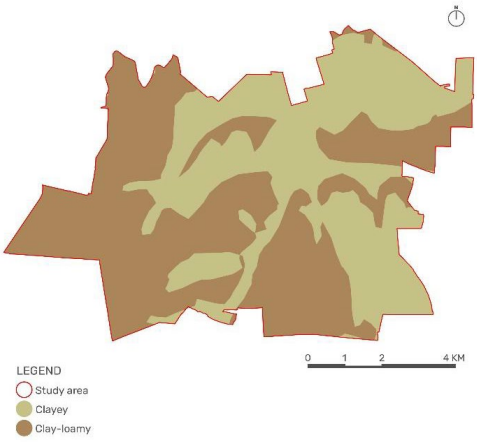

Figure 7. The texture of the study area

Conforming to the bonitation scale (Table 4) the clayey texture received a score of 1 and the clay-loamy texture received 0.8.

Table 4. Bonitation scale for rating the texture of soil

Texture					
clayey	clay-loamy	clay-sandy	loamy	sandy-loamy	sandy
1	0.8	0.7	0.6	0.5	0.4

Soil gleization represents a soil formation process which results in the development of glei horizon in the soil profile, due to poor drainage condition (depression land), impervious soil parent material, lack of aeration and more (Singh & Chandran, 2015, p. 76). This type of soil is inappropriate for agriculture.
In Murfatlar there is an absence of gleization, therefore it got the score 1 (Table 5).

Table 5. Bonitation scale for rating the gleization

Gleization				
lack	small	small -medium	medium	huge
1	0.8	0.6	0.4	0.1

The altitude in Murfatlar is low, of the plain, with values between 2.52 m and 121.40 m, as suggested by the EU-DEM, a digital surface model (DSM), shown below.

Murfatlar is located on the Pre-Balkan Dobrogean platform, the relief being formed by gentle slopes and valley confluences.
In Murfatlar, the valleys of Seacă, Basarabi, Șerpelea and Siminoc converge, all tributaries of the Danube-Black Sea Canal, with development works on the lower course and in the confluence area.
Here are three district forms of relief: hills 80-130 m (Maltezeanu), mounds 15-80 m (Siminoc), valleys (Carasu, Siminoc, Șerpelea).

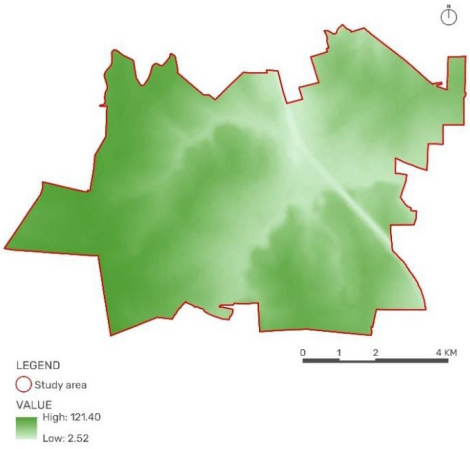

Figure 8. DSM (Digital Surface Model) of Murfatlar.
DSM source: EU-DEM - land.copernicus.eu

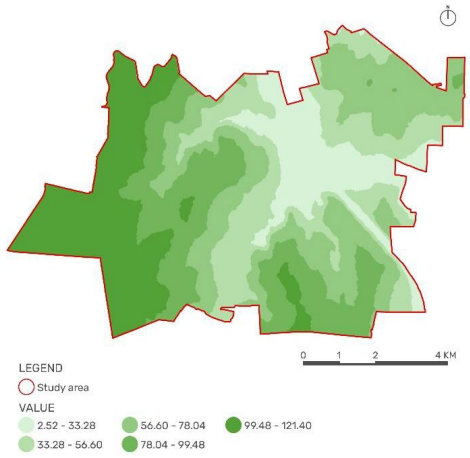

Figure 9. Classified DSM (Digital Surface Model) of Murfatlar using the ArcMap software.
DSM source: EU-DEM - land.copernicus.eu

The study area has a generally smooth slope, but it was categorized into two main classes based on the steepness of the terrain. Steeper slopes can potentially cause erosion and affect soil moisture levels.
The slope in Murfatlar (represented in Figure 10) in usually much less than 3 degrees, which means a score of 1.

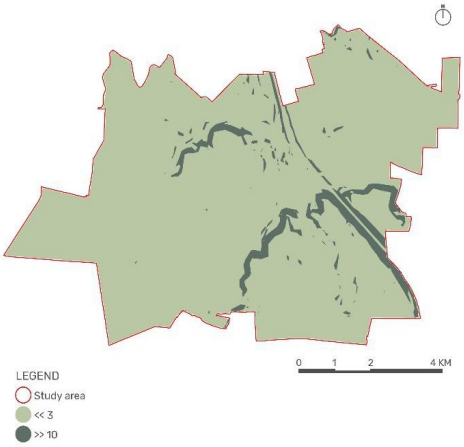

Figure 10. Slopes in the administrative territorial unit

However, along the Danube - Black Sea Canal, due to the excavations, as well as in the proximity of the chalk hills, the slope gets steep (much more than 10 degrees), meaning a score of 0.1 in accordance with the bonitation scale (Table 6).

Table 6. Bonitation scale for rating the slope

Slope (degrees)			
<< 3	3-5	5-10	>> 10
1	0.8	0.6	0.2

The presence of water (Figure 11) is mainly null, with some areas where it is reduced. These reduced zones are at the confluence of steeper altitudes and on specific Clay-Illuvial soils on prairie potholes.
The null area got the 1 score, while the reduced presence of water surfaces received the score 0.8 (Table 7).

Table 7. Bonitation scale for rating the presence of water

Presence of water			
null	reduced	big	huge
1	0.8	0.4	0.2

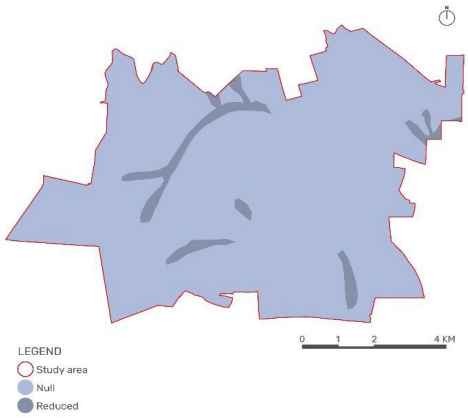

Figure 11. Presence of water in Murfatlar

The affected surface is presented below in the Figure 12.

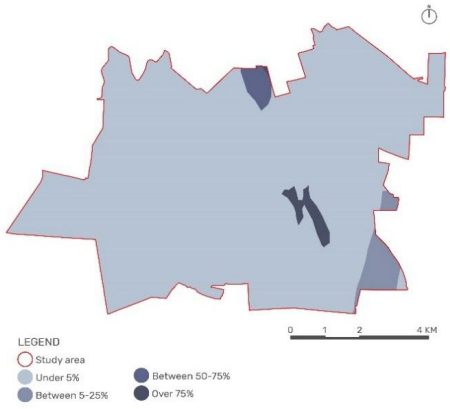

Figure 12. Affected surface around Murfatlar

The most affected surface (over 75%) is close to the chalk hills around the monastic cave complex and Murfatlar Chalk Lake, which received the lowest score of 0.25 (Table 8). In general, the study area is not affected and has 1. It is shown that the affected surfaces are on edges because of the lower altitude, between 5-25% in the south-east corner and between 50-75% in central-north (which assimilates with the Chernozems and Erodisols soil on slopes).

Table 8. Bonitation scale for rating the affected surface

Affected surface (%)			
0-5	5-20	20-50	50-70
1	0.8	0.6	0.3

After calculating the bonitation note of all the elements presented above, the next step was to use the Raster Calculator method in GIS to establish five pretability classes, colours represented from very low to very high pretability for cultures (wheat, canola, corn).
In the qualitative classification map (Figure 13) are also shown the circulations (roads and railroad), water courses and irrigation canals, for a better understanding of the surroundings.

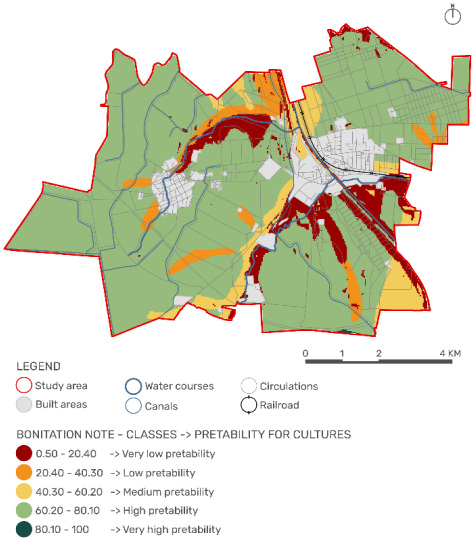

Figure 13. The qualitative classification map of Murfatlar based on the bonitation note

As graphically represented, Murfatlar has a high pretability (light green) across its surface which assimilates with the existing vineyards and arable lands. The very high pretability (dark green) is little represented in the south-east area. The in-between classes (low - orange and medium - yellow pretability) are almost equally illustrated.
The very low pretability (red) is pictured around built areas and the canal, as well as the chalk hills, which is well argumented with the slopes and anthropic surfaces.
For a more detailed interpretation, a map (Figure 14) picturing both the resulting qualitative classification layer and the CORINE land cover layer was made, to determine whether the current land use is fully exploiting the potential of the area regarding the specific crop cultivation.

The qualitative classification layer is represented with a stripped pattern to see through the land use characteristics.
It is shown that the current land cover takes advantage of the suitability of the site. For example, most of the surface of the vineyards and arable land has a high pretability, while the urban fabric shows a very low pretability.
Such analysis integrate spatial data and overlaying these layers could encourage management decisions and strategies.

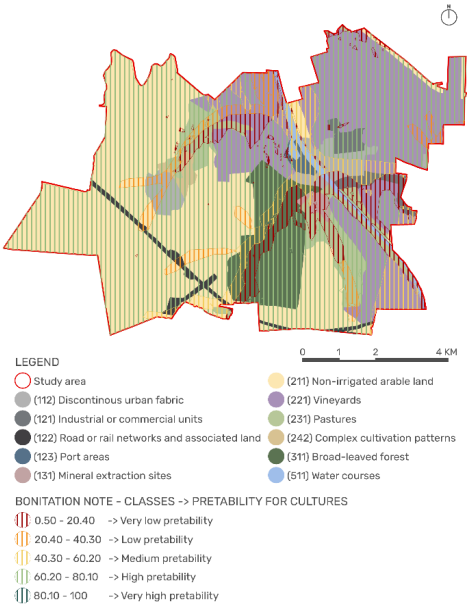

Figure 14. Map showing the overlay of land use and the qualitative classification

CONCLUSIONS

The administrative territorial unit of Murfatlar has multiple resources and benefits from the natural complex region. After making the qualitative classification map, the following step was to reclassify and convert the raster to vector (shapefile) in order to calculate the area.
The assessment of agricultural land and its suitability highlighted the classification (Figure 15), in a proportion of 10% in the first class - very low pretability, 5.3% for the second - low pretability, 9.4% in the third category with medium pretability and 74.8% with high (good) pretability, while just 0.05% has a very high (great) pretability.

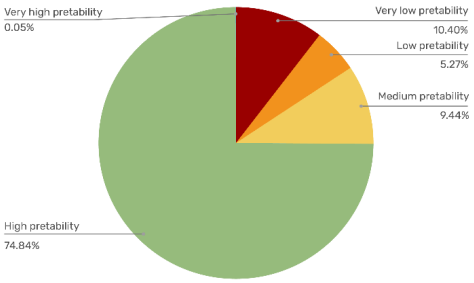

Figure 15. Statistical graphic to illustrate numerical proportion

AKNOWLEDGMENTS

This research was not conducted with the support of an institution. However, it would have not been possible to carry the study without the open-source materials used and mentioned along the paper.

REFERENCES

Biali, G. & Popovici, N. (2006). Realizarea stratului tematic/informational "poluarea solului" pentru un teren agricol, necesar acțiunii de bonitare a acestuia prin tehnice GIS. Cu referire la poluarea cu "metale grele". Lucrările Simpozionului *Sisteme informaționale geografice*, Nr. 12. Anal. St. Univ. Al. I. Cuza Iasi, Tom LII, s.IIc. Geografie.

Copernicus. CORINE Land Cover - CLC (2018). https://land.copernicus.eu/pan-european/corine-land-cover/clc2018

Copernicus. EU-DEM (2016). https://land.copernicus.eu/imagery-in-situ/eu-dem/eu-dem-v1.1

Geoportal ANCPI (Agenția Națională de Cadastru și Publicitate Imobiliară). Hărți și aplicații prezentate. https://geoportal.ancpi.ro/portal/home/

Geo-spatial.org. https://geo-spatial.org/

Meteoblue (1979-2023). Istoric și Climat. Schimbări climatice. https://www.meteoblue.com/ro/climate-change/murfatlar_rom%c3%a2nia_672620

Singh, S.K & Chandran, P. (2015). *Soil genesis and classification* "Upon this handful of soil our survival depends. Husband it and it will grow our food, our fuel and our shelter and surround us with beauty. Abuse it and the soil will collapse and die, taking humanity with it." – Vedas Sanskrit scripture-1500 BC. In book: Soil Science-An Introduction, pp.57-96. Edition: First Chapter: 3Publisher: Indian Society of Soil Science. Editors: R. K. Rattan, J. C. Katyal, B. S. Dwivedi https://www.researchgate.net/publication/314453325

Scientific Papers. Series E. Land Reclamation, Earth Observation & Surveying, Environmental Engineering. Vol. XII, 2023
Print ISSN 2285-6064, CD-ROM ISSN 2285-6072, Online ISSN 2393-5138, ISSN-L 2285-6064

AN ANALYSIS OF THE EVAPOTRANSPIRATION IN THE ARGES RIVER BASIN USING MODIS MOD16A2

Adrian FILIP[1], Stefano CASADEI[2], Nicolae PETRESCU[3], Daniel DUNEA[3]

[1]University of Agronomic Sciences and Veterinary Medicine of Bucharest,
59 Marasti Blvd, District1, Bucharest, Romania
[2]Università degli Studi di Perugia, 93 Via Duranti, Perugia, Italy
[3]Valahia University of Targoviste, 13 Sinaia Aleey, Targoviste, Romania

Corresponding author email: n_petrescu06@yahoo.com

Abstract

This work presents an analysis of the evapotranspiration in the Arges River Basin, including a riparian system located near Dragomiresti village, using MODIS Global Terrestrial Evapotranspiration 8-Day Global (MOD16A2) at 500-m pixel resolution to assess the amount of water lost from the hydrologic budget. The period of coverage is 8 days during the vegetation season of the considered period (2015-2022). The geospatial analysis of the selected riparian systems was performed with ArcGIS Desktop 10.8.1 and Google Earth Engine. Arges River supplies water for several important Romanian cities, and thus, the rationale of this work relies on the characterization of evapotranspiration for potential better management. Riparian vegetation has multiple functions and provides a wide range of ecosystem services of which yields are directly influenced by the river basin`s ecological status. Limiting anthropogenic disturbance is important for the health of lotic ecosystems. The utilization of MODIS does not provide fine-scale resolution (< 10 m), making it difficult to discriminate between phytosociological associations at a small scale and thus establish the riparian systems' typology and associated vegetation indicators. Downscaling and data fusion methods will be further explored.

Key words*: MODIS, MOD16A2, riparian grasslands, riparian systems, geospatial analysis, ecological efficiency, Google Earth Engine.*

INTRODUCTION

Performing multidisciplinary research on the dynamics of herbaceous mixed canopy growth and development (Constantinescu et al., 2019), and the multifunctional potential of grasslands located in riparian areas is required because of the agri-environmental implications and benefits of these zones (Dunea et al., 2019). Riparian vegetation is a central component of the hydrosystem (Huylenbroeck et al., 2020) providing a series of important ecosystem services such as:

- Water quality regulation and site-specific pollution mitigation (up-take of heavy metals and retention/recycling of nutrients) (Stutter et al., 2021; Dunea et al., 2020);
- Biodiversity conservation (wildlife protection near neighboring farmlands or urban areas by provisioning food and habitat);
- Goods and habitat provisioning (Source of raw materials; corridor function - enhances the movement of organisms);
- Discharge control and flooding avoidance (influence on kinetic energy and turbulence, and diminishing of the velocity of runoff reaching the riverbed) (Dingman, 2014; Sabău et al., 2023);
- Climate regulation (decrease of in-stream and local temperatures; the presence of trees modifies wind currents) (Abatzoglou et al., 2018);
- Disturbance prevention (maintenance of riverbank stability and protection from erosion) (Dingman, 2014);
- Carbon storage (restoring and reforesting of riparian zones along headwater streams would both increase carbon storage and improve water quality) (Rheinhardt et al., 2012);
- Noise dissipation from nearby traffic;
- Aesthetic and recreational use.

Farming to maximize economic performance is usually in conflict with wildlife needs (Whittingham, 2007). Most of the time, the farmlands are areas located near riparian areas, making them important shelters for wildlife. The

grasslands are usually grazed by the livestock from the neighboring villages because of their good pastoral value and enhanced floristic composition (Dunea et al., 2021a).
Establishing the relationship between the environmental factors and the dynamics of the growth and development of the canopy specific to the grasslands located in riparian areas requires more attention to the study of the availability of solar radiation resources, the seasonal fluctuations and distribution of leaf area, the evapotranspiration, and other biological factors, and the efficiency of estimation methods based on the remote sensing products and modern data processing tools (GIS software) and platforms e.g., Google Earth Engine - GEE (Dunea et al., 2021b).
One of the objectives is to highlight the efficiency and usefulness of remote sensing methods with the help of sensors equipped on vegetation monitoring satellites launched into the Earth's orbit (McShane et al., 2017).
The extraction of vegetation indices consists of establishing how the radiative properties of interest of a variable - characteristic of an entity at the level of the terrestrial surface affect the spectral reflectance to be captured and the interpreted results.
Generally, there is a good correlation between the synthetic vegetation indices and different parameters specific to the growth and development of the canopy, such as reliable yield, leaf surface, photosynthetic activity, density, and distribution of component species (Dunea & Dincă, 2014).
The increase in vegetation cover, respectively the weight of vegetation at the level of a grassland system, leads to an increase in reflectance in the near-infrared channel and a decrease in reflectance in the red channel of the visible spectrum; in this case, the reflectance values in IRa are higher than those in red, which indicates a grassland with an integral soil cover, and an increase in the biomass, without external stress factors.
Consequently, the specific objectives of the research are related to the study of dynamics of the growth and development of the herbaceous canopy of the riparian grasslands including the floristic composition and the eco-pedoclimatic conditions with an accent on availability of the solar resources. Secondly, the evaluation and improvement of the multifunctional potential of the riparian grasslands are also envisaged.
In this paper, the evapotranspiration in the Arges River Basin (R.B.), including a riparian system located near Dragomiresti village, was analyzed between 2015 and 2022 using the GEE environment for MODIS Global Terrestrial Evapotranspiration 8-Day Global (MOD16A2) at 500-m pixel resolution to assess the amount of water lost from the hydrologic budget. Other available resources from MODIS related to the Leaf Area Index (LAI), the Normalized Difference Vegetation Index (NDVI), and the Enhanced Vegetation Index (EVI) were also considered and discussed.

MATERIALS AND METHODS

Study area

Arges River is a left tributary of the Danube River with a length of 350 km and a basin area of approximately 12,550 km^2, representing 5.3% of Romania's total area (Figure 1).

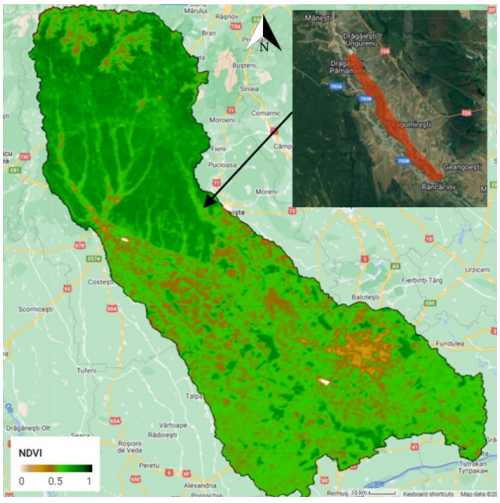

Figure 1. Arges River Basin showing an NDVI example (May-July 2022) using the 'MODIS/MCD43A4_006_NDVI' Image Collection, and the riparian system selected as a case study for evapotranspiration near Dragomiresti village on Dambovita River (processed with Google Earth Engine)

Identification and evaluation of the significant environmental impacts on the watercourses and adjacent riparian areas in the hydrographic basin of the Arges River are required either from discharges of treated or untreated waters in

surface waters (from sources of urban pollution/human settlements and/or industrial sources), or diffuse pollution, from agriculture and other sources.

The source is located in the Fagaras Mountains, and it flows into the Danube River at Oltenita. The capital Bucharest and other important cities (Pitesti, Curtea de Arges, Campulung, Gaesti, Oltenita) are supplied with water from the Arges R.B. Arges River gathers 178 codified watercourses with a length of 4579 km (5.8% of the total length of codified watercourses in Romania). The density of watercourses is 0.36 km/km^2.

Regarding the land cover, the non-irrigated arable land reaches 46% (Corine Land Cover - CLC category 211), forests 26.2% (5.2% of the national forest fund), watercourses (CLC 511) 12%, and the discontinuous urban fabric (CLC 112) 4%, respectively (Dunea, 2022). Based on these indicators, the Arges R.B. is important for agriculture and has key forest resources (approximately 3283 km^2).

The water quality of Arges River is affected by industrial and agricultural activities with point and nonpoint source pollution, including toxic contaminants (dissolved Ni, Cr, and Pb), and nutrients, which can degrade water quality, especially in the lower part of the river (Dunea, 2022).

Data processing and statistics

was performed using mainly the Google Earth Engine (GEE) platform. GEE is a catalog of satellite imagery and geospatial datasets with planetary-scale analysis capabilities for detecting changes, mapping trends, and quantifying differences on the Earth's surface. GEE is free for academic and research use. In this environment, we used specific scripts in Python for accessing and collecting the required data for the Arges R.B. between the considered periods (2015-2022) and for drawing specific maps.

We imported the basin limits and river network as layers retrieved with ArcGIS 10.8.1 and imported them in GEE as an ‘asset’. The retrieved time series were analyzed using the SPSS software (SPSS Inc., Chicago, IL, USA, 2011). The variability was determined using descriptive statistics (average, coefficient of variation, skewness, kurtosis, etc.). Because this is a preliminary screening study regarding the variability of the considered parameters within the basin, detailed time series analysis and complex statistics were not employed at this stage.

Vegetation indices and corresponding collections

***Leaf area index* (*LAI*)** is the unitless ratio of green leaf area to ground area (m^{-2} m^2). We used the LAI derived from the MCD15A3H.006 MODIS data product (Myneni et al., 2015). This algorithm derives 4-day composite LAI values at a 500 m spatial resolution from the Terra and Aqua satellites and is available from 2003 onwards.

Within this 4-day period, the most accurate pixel is selected from the MODIS sensors located on the Terra and Aqua satellite for the calculation of the LAI. The LAI calculation algorithm uses a lookup table that was generated using a 3-D radiative transfer equation (Myneni et al., 2015). MODIS LAI has a long record length, reliable and free data availability, proper spatial coverage, and adequate temporal resolution.

Enhanced Vegetation Index (EVI) and NDVI

EVI is an advanced vegetation index with higher sensitivity to biomass, atmospheric background, and soil condition. We used the MOD13A1 V6.1 product, which provides a Vegetation Index (VI) value per pixel basis. There are two primary vegetation layers.

The first one is the NDVI, which is referred to as the continuity index to the existing National Oceanic and Atmospheric Administration-Advanced Very High-Resolution Radiometer (NOAA-AVHRR) derived NDVI.

EVI is the second one and minimizes the canopy background variations and maintains sensitivity over dense vegetation conditions. The EVI also uses the blue band to remove residual atmosphere contamination caused by smoke and sub-pixel thin cloud.

The MODIS NDVI and EVI products are computed from atmospherically corrected bi-directional surface reflectance that have been masked for water, clouds, heavy aerosols, and cloud shadows. (https://doi.org/10.5067/MODIS/MOD13A1.061).

Evapotranspiration

We used the MOD16A2 Version 6 Evapotranspiration/Latent Heat Flux product, which is an 8-day composite product at 500-meter pixel resolution.

The algorithm used for the MOD16 data product collection is based on the Penman-Monteith algorithm, which includes inputs of daily meteorological reanalysis data along with MODIS remotely sensed data products (vegetation property dynamics, albedo, and land cover).

The pixel values for the two Evapotranspiration layers (ET & PET) are the sum of all eight days within the composite period (Mu et al., 2011). The pixel values for the two Latent Heat layers (LE & PLE) are the average of all eight days within the composite period (https://doi.org/10.5067/MODIS/MOD16A2.006).

RESULTS AND DISCUSSIONS

The applied tests aimed to develop a procedure that can ensure the detection of changes in vegetation and ET characteristics concerning phenology and seasonal variations in the growing season at the river basin level and a riparian system from the basin.

Moreover, the detection of changes is an important step for scaling procedures, which will be developed, if possible, by inferring high-resolution information from low-resolution variables to increase the spatial resolution of ET estimates (Singh et al., 2014).

The first step in ET calculation involves partitioning incident solar radiation into net radiation available to plants and soil. This is done by calculating the vegetation condition using the LAI parameter.

Figure 2 presents the LAI distribution at maximum development in June at the basin level and selected riparian system, and the evolution between 2015 and 2022 as a mean calculated for the river basin.

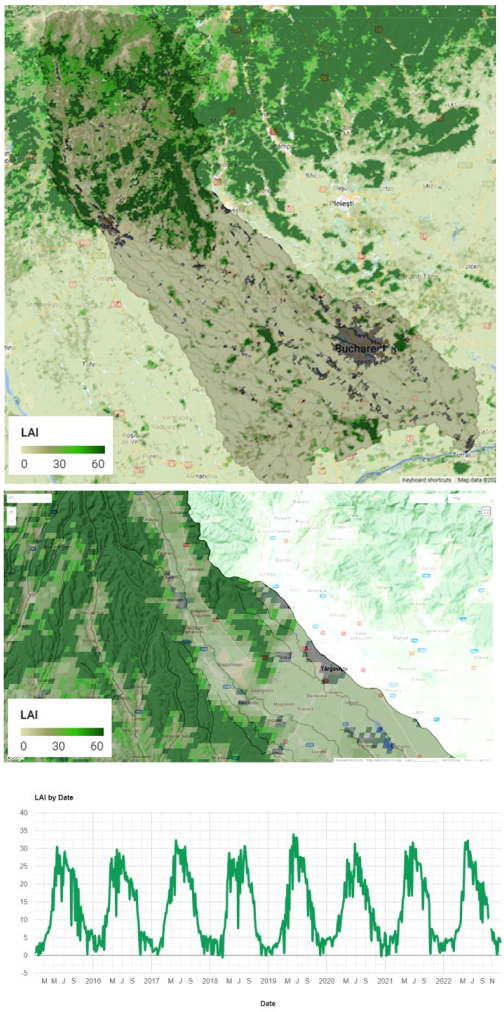

Figure 2. Leaf area index (LAI) retrieved using MCD15A3H.006 MODIS data product (Valid Range = 0-100; Scale Factor = 0.1) at basin scale, at riparian area scale, and the time series from 2015 to2022 (http://doi.org/10.5067/MODIS/MCD15A3H.006)

It can be noted that the highest LAI is usually reached in June with a maximum in the year 2019 and minimum values in 2015 and 2016 (2015 was one of the driest years in the last 50 years). EVI and NDVI are other important indices that characterize the status of vegetation (Figures 3 and 4).

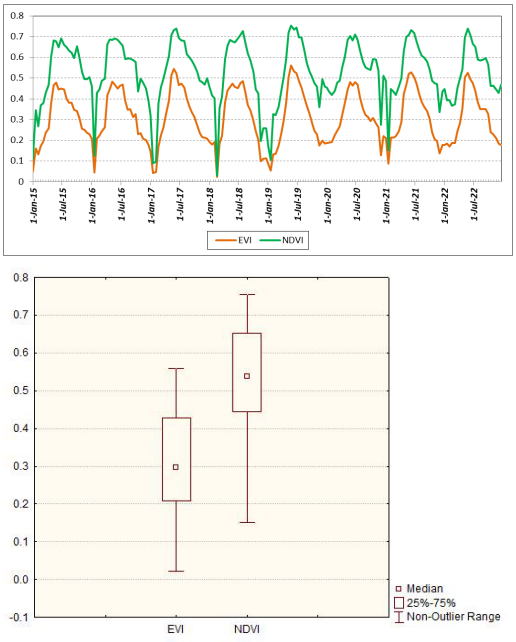

Figure 3. Average EVI and NDVI time series from January 1, 2015, to December 31, 2022, using MOD13A1.061 Terra Vegetation Indices 16-Day Global 500-m Collection for the Arges R.B. (minor ticks = 16 days); Median and percentiles of the period (box-whisker graph)

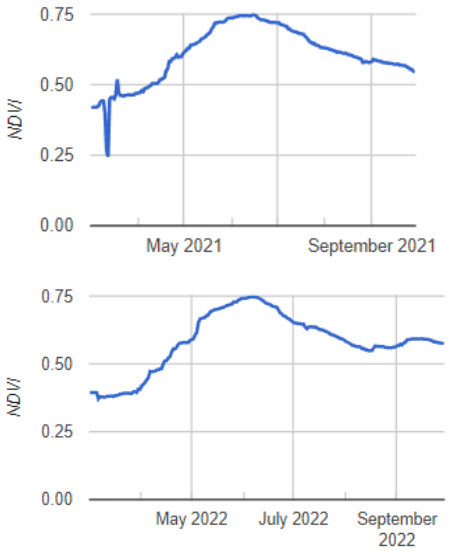

Figure 4. NDVI retrieved for the vegetation seasons of years 2021 and 2022 based on the 'MODIS/MCD43A4_006_NDVI' Collection

Table 1 presents the descriptive statistics of the analyzed time series i.e. EVI, NDVI, ET, and PET for the whole basin, and cumulative PET for the riparian system located near Dragomiresti village.

Table 1. Descriptive statistics of the time series retrieved from the MODIS Datasets (2015-2022 excepting PET for the riparian system - PET_RP for which the period is 2015-2019*); ET and PET - kg/m^2/8-day

Indicator	Valid N	Time step	Mean	Median	Minimum	Maximum	Range	Quartile	Std.Dev.	Coef. Of Var.	Skewness	Kurtosis
EVI	184	16-Day	0.31	0.30	0.02	0.56	0.54	0.22	0.13	41.97	0.04	-0.97
NDVI	184	16-Day	0.53	0.54	0.03	0.75	0.72	0.21	0.15	28.43	-0.88	0.81
LAI	729	4-Day	1.30	1.07	0.00	3.33	3.33	1.72	0.96	73.72	0.35	-1.30
ET_ARB	367	8-Day	134.76	98.92	21.62	358.85	337.23	151.65	89.70	66.57	0.69	-0.83
PET_ARB	367	8-Day	11,398,935.22	10,035,953.71	5113	30,846,772.80	30,841,659.80	15,873,096.27	8,795,739.38	77.16	0.38	-1.12
PET_RP*	230	8-Day	2003.22	1362.45	0.00	7019.25	7019.25	2657.09	1786.52	89.18	0.84	-0.49

At the river basin level, based on the statistical indicators of the time series from 2015 to 2022, EVI showed a mean of 0.31 with a maximum of 0.56 and a C.V. (coefficient of variation) = 41.97%. NDVI had a mean of 0.53 ranging between 0.03 and 0.75 and a C.V. = 28.43%, which was the lowest value from all the tested parameters. This suggests the constancy of the vegetation in the basin. The LAI reached a maximum of 3.33 with a mean of 1.3 and a C.V. = 73.72%. This denotes a higher variance of the LAI due to the influence of water availability. Cumulative PET showed a similar C.V. value (77.16%) and mean ET had also a high C.V. (66.57%) at the basin level. From 2015 to 2022, ET recorded a mean of 134.76 kg/m^2/8-day, a minimum of 21.62, and a maximum of 358.85 kg/m^2/8-day.

Figures 5 and 6 provide clear insights into the ET and PET variability at the basin level showing the lowest values in years 2015 and 2016, and the highest in 2019 and 2020.

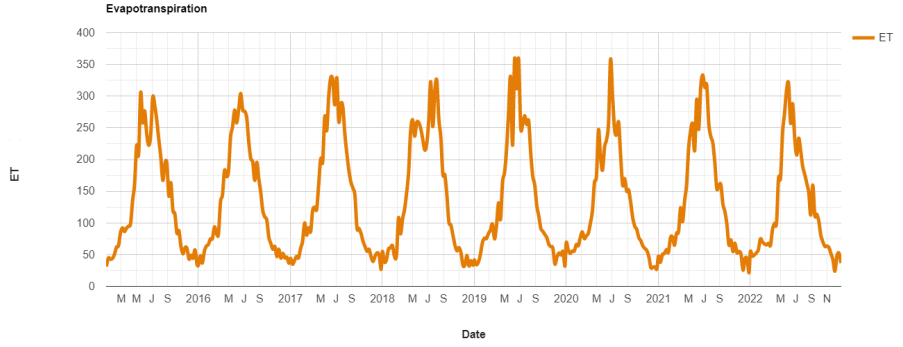

a)

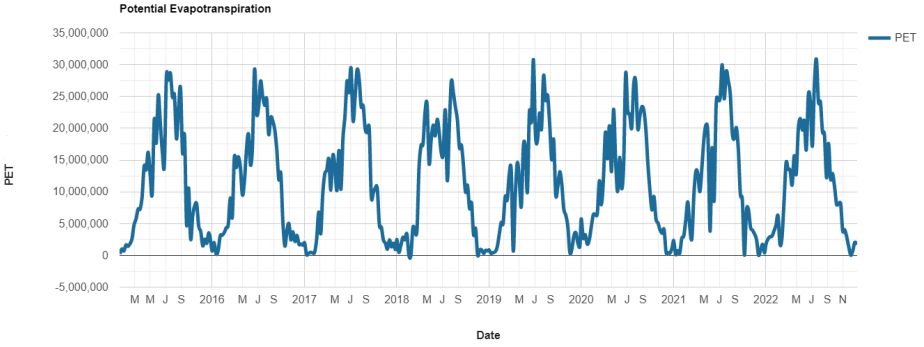

b)

c)

Figure 5. Evapotranspiration indices (kg/m^2/8-day) retrieved using MOD16A2.006: Terra Net Evapotranspiration 8-Day Global 500m (https://doi.org/10.5067/MODIS/MOD16A2.006) between 2015 and 2022: a) Actual evapotranspiration - averaged at Arges River basin level; b) potential evapotranspiration - cumulative values at basin scale; c) potential evapotranspiration - cumulative values at Dragomirești riparian system level (2015-2019 period selected)

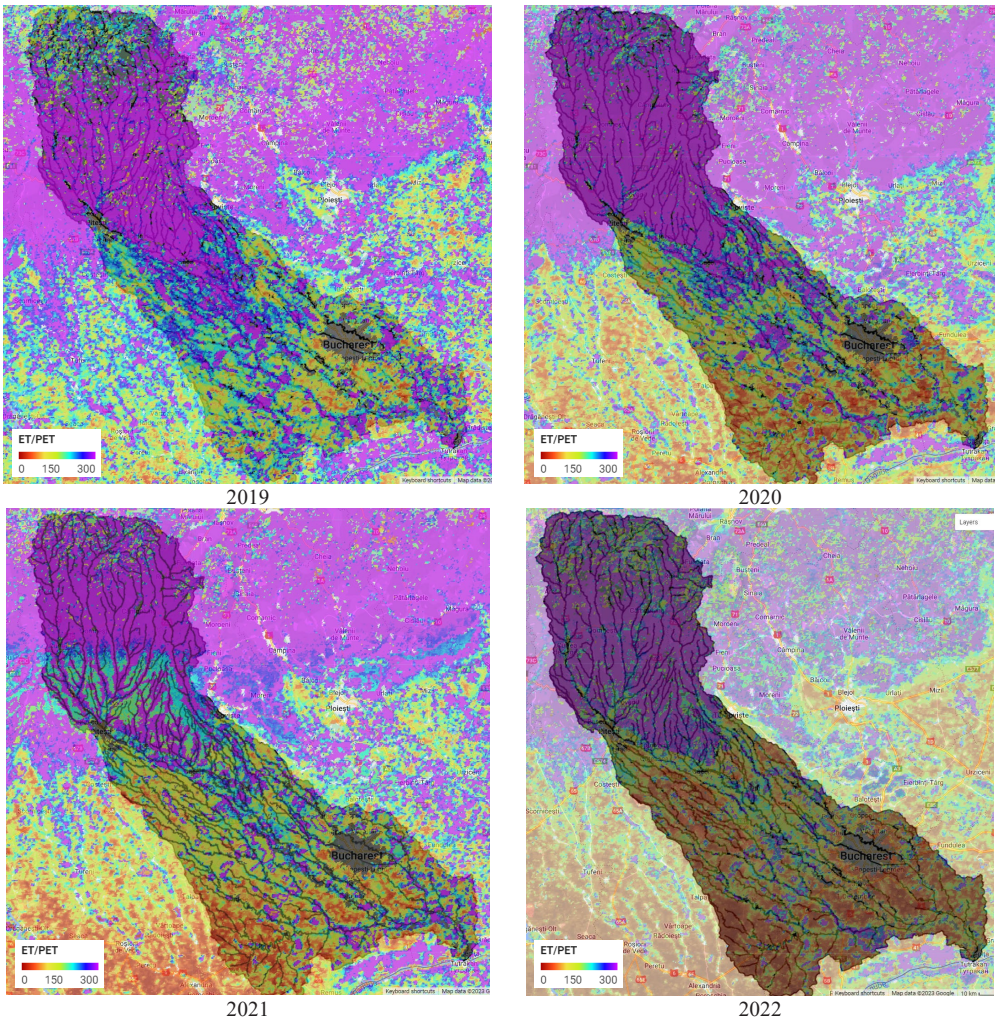

Figure 6. Maps of potential evapotranspiration - means (kg/m^2/8-day) obtained using MOD16A2.006: Terra Net Evapotranspiration 8-Day Global 500-m (https://doi.org/10.5067/MODIS/MOD16A2.006)

The potential ground-level evaporation is calculated using the Penman-Monteith algorithm based on meteorological parameters and vegetation characteristics (e.g. height, conductance factor, maximum leaf conductance, albedo, LAI). Based on the cumulative PET, the lowest values were in the year 2018, and the highest in 2019 and 2022. Regarding the riparian system, the cumulative PET was relatively constant between 2015 and 2019.

This may be related to the capacity of riparian systems to maintain a balanced hydrological feature (https://directives.sc.egov.usda.gov/18532.wba).

The Arges River from Romania and its tributaries encounter significant pressures from anthropogenic factors passing highly inhabited areas with moderate efficiency of wastewater treatment. In addition to the potentially significant pressures already presented above, other types of activities/pressures may affect the condition of water bodies such as accidental pollution, fishing, and aquaculture activities, ballast and sand extraction from minor riverbeds, forest exploitation, unidentified pressures, etc. Riparian buffer zones may diminish the negative effect, but this requires proper management. Grasslands from these areas are also of interest

and the current study gives good promises for using remote sensing in determining long-time processes that affect the floristic composition.

CONCLUSIONS

Observation of evapotranspiration (ET) processes using the existing remote sensing systems is a key element that provides up-to-date information for water resource management, weather forecasting, climate studies, agriculture, and other essential applications. Easy access to reliable ET estimates is important in these strategic areas. When ET values are successfully estimated at high resolutions, water scarcity at land surfaces can be mapped and hot spots can be better investigated. At this point, the analyzed datasets provided a good assessment of the processes related to vegetation evolution, pointing out the reductions during the drought periods. Further work will consider the utilization of downscaling and data fusion methods in combination with other high-resolution products for application in monitoring the grasslands located in the riparian systems.

ACKNOWLEDGEMENTS

This research work was carried out with the support of a Romanian Ministry of Education Grant, CNFIS-T-FDI-2023-0646.

REFERENCES

Abatzoglou, J.T., Dobrowski, S.Z., Parks, S.A., Hegewisch, K.C. (2018). Terraclimate, a high-resolution global dataset of monthly climate and climatic water balance from 1958-2015, *Scientific Data, 5*, 170191, doi:10.1038/sdata.2017.191

Constantinescu, P., Neagoe, A., Nicoară, A., Grawunder, A., Ion, S., Onete, M. et al. (2019). Implications of spatial heterogeneity of tailing material and time scale of vegetation growth processes for the design of phytostabilisation. *Sci Total Environ*., *692*, 1057-1069.

European Union, Copernicus Land Monitoring Service 2018, European Environment Agency (EEA), Corine Land Cover, https://land.copernicus.eu/user-corner/technical-library/corine-land-cover-nomenclature-guidelines/docs/pdf/CLC2018_Nomenclature_illustrated_guide_20190510.pdf

Dingman, S.L. (2014). Physical Hydrology. Waveland Press, Inc.; 3rd edition.

Dunea, D., Dincă, N. (2014). Improving land utilization using intensive grass-clover mixtures in forage production systems. *Rom. Agric. Res.*, *31*, 147-158.

Dunea, D., Iordache, Ş., Iordache, V., Purcoi, L., Predescu, L. (2019). Monitoring of the evapotranspiration processes in riparian grasslands. *Scientific Papers. Series A. Agronomy*, *62*(1), 278-285.

Dunea, D., Bretcan, P., Tanislav, D., Serban, G., Teodorescu, R., Iordache, S. et al. (2020). Evaluation of water quality in Ialomita River Basin in relationship with land cover patterns. *Water*, *12*(3), 735.

Dunea, D., Dincă, N., Stanciu, A.M., Glod-Lendvai, A.M. (2021a). Bringing forward the potential of geo-information tools for grassland studies in Romania. *Romanian Journal of Grasslands and Forage Crops*, *23*, 79-89.

Dunea, D., Bretcan, P., Purcoi, L., Tanislav, D., Serban, G., Neagoe, A. et al. (2021b). Effects of riparian vegetation on evapotranspiration processes and water quality of small plain streams. *Ecohydrology & Hydrobiology*, *21*(4), 629-640.

Dunea, D. (2022). Water Quality and Anthropogenic Pressures in a Changing Environment: The Arges River Basin, Romania. doi: 10.5772/intechopen.101790 in Dunea, D. (Ed.). Water Quality - Factors and Impacts. *IntechOpen*. doi: 10.5772/intechopen.96701

Huylenbroeck, L., Laslier, M., Dufour, S., Georges, B., Lejeune, P., Michez, A. (2020). Using remote sensing to characterize riparian vegetation: A review of available tools and perspectives for managers. *J Environ Manage.*, *267*, 110652. doi: 10.1016/j.jenvman.2020.110652.

McShane, R.R., Driscoll, K.P., Sando, R. (2017). A review of surface energy balance models for estimating actual evapotranspiration with remote sensing at high spatiotemporal resolution over large extents. *U.S. Geological Survey Scientific Investigations Report* 2017–5087, 19, https://doi.org/10.3133/sir20175087.

Mu, Q., Zhao, M., Running, S.W. (2011). Improvements to a MODIS global terrestrial evapotranspiration algorithm, *Remote Sens. Environ.*, *115* (8), 1781-1800.

Myneni, R., Knyazikhin, Y., Park, T. (2015). MCD15A3H MODIS/Terra+Aqua Leaf Area Index/FPAR 4-day L4 Global 500m SIN Grid V006. *NASA EOSDIS Land Processes DAAC*. http://doi.org/10.5067/MODIS/MCD15A3H.006

Rheinhardt, R.D., Brinson, M.M., Meyer, G.F. (2012). Carbon storage of headwater riparian zones in an agricultural landscape. *Carbon Balance Manage*, *7*(4). https://doi.org/10.1186/1750-0680-7-4

Sabău, D.A., Şerban, G., Breţcan, P., Dunea, D., Petrea, D., Rus, I., Tanislav, D. (2023). Combining radar quantitative precipitation estimates (QPEs) with distributed hydrological model for controlling transit of flash-flood upstream of crowded human habitats in Romania, *Nat Hazards*, *116,* 1209–1238. https://doi.org/10.1007/s11069-022-05718-9.

Singh, R.K., Senay, G.B., Velpuri, N.M., Bohms, S., Verdin, J.P. (2014). On the Downscaling of Actual Evapotranspiration Maps Based on Combination of

MODIS and Landsat-Based Actual Evapotranspiration Estimates. *Remote Sens.*, *6*(11), 10483-10509.

Stutter, M., Costa, F.B., Ó hUallacháin, D. (2021). The interactions of site-specific factors on riparian buffer effectiveness across multiple pollutants: A review. *Sci Total Environ*., *798*, 149238. doi: 10.1016/j.scitotenv.2021.149238.

Whittingham, M.J. (2007). Will agri-environment schemes deliver substantial biodiversity gain, and if not why not? *Journal of Applied Ecology*, *44*(1), 1-5, https://doi.org/10.1111/j.1365-2664.2006.01263.x

https://directives.sc.egov.usda.gov/18532.wba

https://doi.org/10.5067/MODIS/MOD16A2.006

https://doi.org/10.5067/MODIS/MOD13A1.061

Scientific Papers. Series E. Land Reclamation, Earth Observation & Surveying, Environmental Engineering. Vol. XII, 2023
Print ISSN 2285-6064, CD-ROM ISSN 2285-6072, Online ISSN 2393-5138, ISSN-L 2285-6064

NOISE POLLUTION: A GIS-BASED APPROACH TO MAPPING AND ASSESSMENT

Cristina Elena MIHALACHE, Bogdan ERGHELEGIU, Mirela Alina SANDU

University of Agronomic Sciences and Veterinary Medicine of Bucharest,
Faculty of Land Reclamation and Environmental Engineering,
59 Marasti Blvd, District 1, Bucharest, Romania

Corresponding author email: mihalachecristina19@gmail.com

Abstract

Monitoring noise pollution is crucial for protecting public health and the environment. It provides data and information needed to understand the sources and distribution of noise levels. This paper presents a GIS-based study of noise pollution for an area located in the southwest part of Bucharest, between Mihail Sebastian, Calea 13 Septembrie and Drumul Sării streets. The values of noise have been recorded by using the Sound Level Meter Lutron - Model SL-4012, in September 2022, for 3 different moments: in the morning, at midday, and in the evening. The results of the analysis have been then used to produce noise maps for each of the three locations. The results showed significant differences in noise levels across different times of the day, with peak levels occurring during daytime hours and early evening in different locations. The study's noise maps provided a clear visual representation of the distribution of noise levels, highlighting areas of concern. The study presents the importance of considering temporal factors in noise mapping and assessment, and the benefits of using GIS tools for this type of analysis.

Key words*: GIS-based mapping, noise pollution, road traffic noise, SLM-Sound Level Meter.*

INTRODUCTION

Noise pollution refers to excessive or annoying sound that can have an adverse effect on human health and the environment. Noise pollution is a growing concern in many urban areas, affecting the physical and mental health of millions of people worldwide (Ertugrul E. & Sercan E., 2021).

Sources of noise pollution can include traffic, construction sites, industrial machinery, loud music, and other human activities.

Even though noise is a consequence of numerous human activities, the main source of environmental noise is urban traffic. Urban traffic noise is regarded as the 2nd most important environmental source of health concerns in Europe, after fine particle pollution (Hänninen et al., 2014). Ambient noise levels in a large city tend to be higher when traffic is heavier (Alves, J.A. et al., 2015).

Despite new vehicle models becoming quieter, the increasing volume of road traffic increases the noise emitted. Many central city streets have reached traffic saturation, congested almost daily and with lower speeds throughout the day (Fan S., 2022).

Urbanization generates significant environmental issues like air pollution (Yuan Song et al., 2014), loss of biodiversity (Cardinale et al., 2012), soil pollution (Sandu, 2013) and noise levels exceeding permissible limits (Halonen et al., 2016).

EEA (2019) & ETC/ATNI (2019) shows that most countries have more than 50% of urban dwellers exposed to road noise levels of 55 dB Lden or higher during the day-evening-night period. Excessive exposure to noise pollution can lead to heart disease, high blood pressure, hearing loss and even cognitive impairment (Cueto et al., 2017; Majidi & Khosravi, 2016; WHO, 2018).

Environmental noise is one of the issues that is attracting more and more attention worldwide and is regulated by an increasingly demanding legal framework, because its effects on the population are really worrying (Titu et al., 2022). Noise pollution remains a major environmental health problem in Europe (EEA, 2017). Romania also has a considerable number of urban areas within territories, with a high percentage of people exposed to noise levels above the Environmental Noise Directive in Europe thresholds (Table 1).

Tabel 1. Number of people exposed in Romania to high levels of noise above the EU reporting thresholds (https://www.eea.europa.eu/themes/human/noise/noise-fact-sheets/noise-country-fact-sheets-2021/romania)

	Lden > = 55 dB			**Lnight > = 50 dB**		
	2007	**2012**	**2017**	**2007**	**2012**	**2017**
Road	2.897.000	2.511.100	2.752.700	2.056.500	2.090.900	1.956.700
Rail	273.100	275.400	96.700	206.000	241.600	93.500
Air	25.800	44.300	3.500	27.700	27.400	13.300
Industry	90.400	230.700	15.800	50.400	64.000	7.100

A Geographic Information System (GIS) - based approach for noise monitoring can address several problems associated with traditional noise monitoring methods, providing a more comprehensive and spatially explicit understanding of noise pollution. GIS allows the collection, storage, manipulation, and analysis of spatial data, providing a comprehensive understanding of the distribution and intensity of noise pollution.

Traditional noise monitoring methods often provide only point measurements of noise levels, which do not capture the spatial distribution of noise pollution. GIS-based approaches, on the other hand, can provide a spatially explicit understanding of noise pollution by mapping noise levels across different locations.

On the other hand, by combining GIS with noise measurement devices, it is possible to create accurate noise maps that can help identify high-risk areas and inform urban planning and environmental policies.

While the use of GIS for noise mapping is a relatively new field, researchers have made significant strides in understanding the complexities of noise pollution and developing effective solutions using GIS techniques (Alvarado, R.A. & Parra, C.M., 2019; Baskaran, R. & Ravindran, D., 2018; Castillo-Salazar, J.A. et al., 2020; Cheng, M., Lu, X. & Du, W., 2017; Eftekhari, M. et al., 2020).

In their studies, the specialists have found that the use of GIS-based noise monitoring can provide a more accurate and comprehensive picture of noise pollution levels in each area. The researchers, including L. Maffei and A. Zambon, conducted their study in the city of Padua, Italy and concluded that GIS-based noise monitoring can help identify noise hotspots and support effective noise control strategies (Maffei, L. & Zambon, A., 2012). Another study focused on the use of GIS and noise modeling to assess the impact of urbanization on noise pollution in the city of Chandigarh, India. The researchers, including S. K. Saha and S. Kumar, found that GIS-based noise modeling can provide valuable insights into the sources and levels of noise pollution in urban areas, as well as help identify areas where noise reduction measures are needed (Saha, S. K. & Kumar, S., 2019).

E. McKeogh and D. Robinson, examined the use of GIS-based noise mapping to support urban planning and land-use management in the city of Dublin, Ireland. The researchers found in their study that a GIS-based noise mapping can help identify areas with high noise pollution levels and inform decisions on land-use planning and development (McKeogh, E. & Robinson, D., 2004).

GIS-based noise monitoring is an important tool for this task as it allows for a more accurate and comprehensive assessment of noise pollution levels in each area. GIS technology enables the integration of different types of data, including noise measurements, land use patterns, and demographic information, which can be used to identify noise hotspots and develop targeted noise control strategies.

In summary, the use of GIS-based noise monitoring is essential for effective noise pollution management and can help improve the quality of life in urban areas. It is therefore important for policymakers and urban planners to consider the benefits of this technology when developing noise control policies and strategies.

MATERIALS AND METHODS

Bucharest, Romania's capital city, is facing a growing problem with noise pollution (Albu, C. et al., 2019; Boboc, M.C. et al., 2018; Chiriac, C.R. et al., 2017; Deaconu, S. & Cioca, L.I., 2019; Rusu, C.M. et al., 2015; Soreanu, G., & Dumitru, D., 2015; Tăranu, N. & Ioniță, I., 2019; WHO, 2018). The city's rapid urbanization, increasing population, and high levels of traffic are some of the main causes of noise pollution in the area. The effects of noise pollution in Bucharest can be particularly harmful to public health, including hearing loss, cardiovascular disease, and sleep disturbances. Noise pollution can also negatively impact the environment and quality of life in urban areas.

Some places in Bucharest that are particularly noisy include busy intersections, construction sites, and public transportation hubs. The city's nightlife scene, which includes numerous bars and nightclubs, can also contribute to high levels of noise pollution in certain areas. The paper "Assessment of urban noise pollution in Bucharest, Romania", published in the Journal of Environmental Protection and Ecology in 2015, found that noise pollution levels in Bucharest exceed World Health Organization guidelines and pose a significant health risk to residents. This study provides an assessment of urban noise pollution in Bucharest, with a focus on traffic noise. The authors used measurements from 48 monitoring stations throughout the city to assess noise levels and found that levels exceeded World Health Organization guidelines in many areas. The study also highlights the health risks associated with high levels of noise pollution, including hearing loss, cardiovascular disease, and sleep disturbances (Rusu, C.M. et al., 2015).

The study "Mapping noise pollution in Bucharest using GIS technology", published in the Environmental Engineering and Management Journal in 2019, conducted by Nicoleta Tăranu and Ion Ioniță aimed to map the noise pollution levels in Bucharest, using GIS technology. The authors collected noise data from 34 measurement points across the city over a 24-hour period. They also collected data on various noise sources, such as road traffic, trains, and planes.

The noise pollution thresholds in Bucharest vary depending on the location and time of day. According to a study published in the Environmental Engineering and Management Journal in 2019 (Tăranu, N. & Ioniță, I., 2019), the average noise level in Bucharest is estimated at 70 decibels (dB). However, in congested areas with heavy traffic or in the vicinity of airports and train stations, noise levels can reach over 80 dB.

Furthermore, the study found that noise levels in residential areas during the day ranged between 55-70 dB, which is above the recommended threshold by the World Health Organization - WHO (WHO, 2018) of 55 dB. At night, the noise levels in residential areas ranged between 45-60 dB, which is also above the recommended threshold by the WHO (2018) of 40 dB. Overall, the study highlights the need for effective noise reduction strategies and policies to address the significant impact of noise pollution on public health and well-being in Bucharest.

Using GIS technology, the authors created noise pollution maps of Bucharest, showing the noise levels in different areas of the city. They found that the noise pollution levels were highest in areas with heavy road traffic and in areas close to airports and train stations. The authors also analyzed the impact of noise pollution on human health and found that prolonged exposure to high levels of noise can lead to various health problems, including hearing loss, cardiovascular diseases, and stress.

The study concluded that GIS technology is an effective tool for mapping noise pollution in urban areas and can be used to develop noise reduction strategies and policies to improve public health and well-being.

To address the issue of noise pollution, policymakers and urban planners in Bucharest can use GIS-based noise monitoring to identify areas with high levels of noise pollution and implement targeted noise reduction measures. These may include noise barriers, traffic management strategies, and building design modifications. By taking proactive steps to reduce noise pollution levels, Bucharest can protect public health and improve the quality of life for its residents.

The studied area is located in the southwest part of Bucharest, between Mihail Sebastian, Calea 13 Septembrie and Drumul Sarii streets.
It is a mixed area consisting of residential buildings, both blocks of flats and houses, shops, commercial spaces, restaurants, playgrounds for children, office buildings, the Ion Barbu theoretical high school, various institutions, as well as thoroughfares with heavy traffic as well as pedestrian streets and alleys. It is a very crowded area in the city with a high level of noise pollution due to heavy traffic, proximity to office buildings and other areas of activity.
The period chosen for the analysis is 2022 September month. This month is the moment when economic activity resumes, and road traffic is more intense in the area. This could lead to an increase in noise levels and makes this period relevant for noise pollution analysis.
The measurements the measurements were carried out in September 2022, three times a day at 07:00 A.M., 12:00 P.M and 9:00 P.M.
The data were taken from the sidewalk in the immediate vicinity of the mentioned intersections, at a height of 1 meter above the ground. The temperatures on the date of the measurements were on average between 15 and 28 degrees Celsius, the wind speed was generally between 1 and 30 km/h, generally clear sky and with a low level of precipitation, between 0 and 8 mm.
GPS coordinates were recorded for each analyzed location. These are represented in Figure 1.

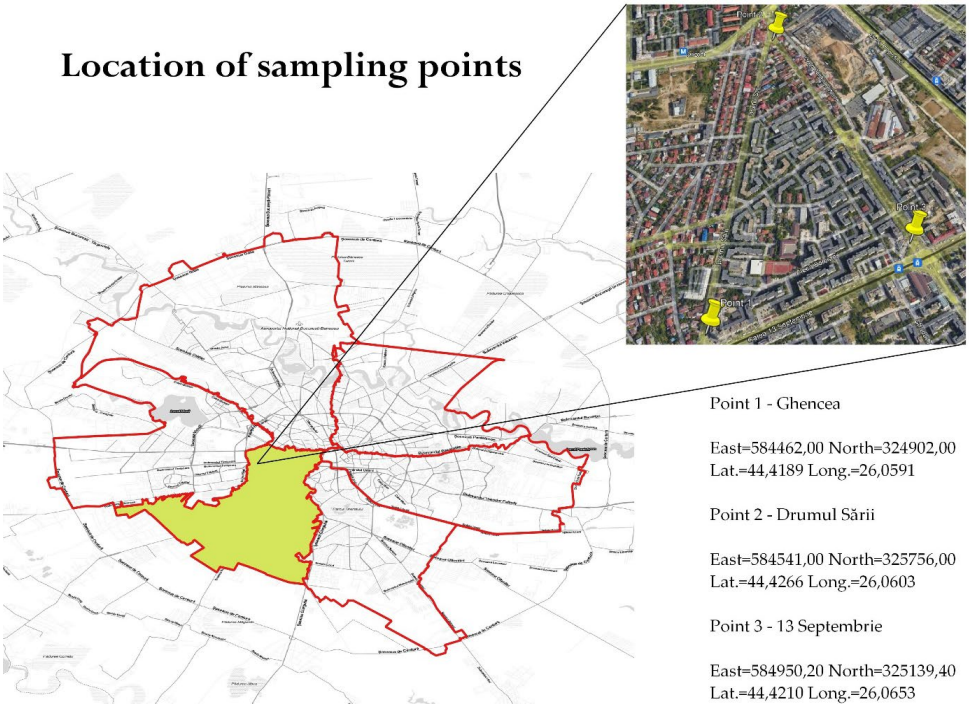

Figure 1. Sampling points locations map

The first location, named generically "Ghencea" is located at the intersection of Calea 13 Septembrie and Drumul Sării; the measurements were made from the sidewalk related to the intersection located approximately 30 m away from the Calea 13 Septembrie road and approximately 2 m from the Drumul Sării road. The coordinates in the 1970 Stereographic System are: East = 584462.00 and North = 324902.00 (Latitude = 44.4189 and Longitude = 26.0591).
The second site named generically "Drumul Sării" is located at the intersection between Drumul Sării and Mihail Sebastian Street; the

measurements were made from the sidewalk related to the intersection, located approximately 5 m from Drumul Sării road and approximately 5 m from Mihail Sebastian Street Road. The coordinates in the 1970 Stereographic System are: East = 584541.00 and North = 325756.00 (Latitude = 44.4266 and Longitude = 26.0603).

The third and last location named generically "13 Septembrie" was established at the intersection between Mihail Sebastian Street and Calea 13 Septembrie; the measurements were carried out from the sidewalk related to the intersection, located approximately 30 m away from the Calea 13 Septembrie road and approximately 5 m from the Mihail Sebastian Street Road. The coordinates in the 1970 Stereographic System are: East = 584950.20 and North = 325139.40 (Latitude = 44.4210 and Longitude = 26.0653).

The sound values were recorded using the sound level meter Lutron - Model SL-4012 (Figure 2). This is a high-precision digital sound-level meter, accuracy class 2 according to IEC 61672, A & C frequency weighting, high accuracy condenser microphone and measurement range from 30 to 130 dB.

Figure 2. Sound Level Meter Lutron - Model SL-4012 used for measurements

The device is designed for neighborhoods noise monitoring, construction site noise control and road traffic noise monitoring.

The measurements are carried out according to specific requirements for the road noise measurements in the immediate vicinity of the currents of vehicles from the intersections with the microphone pointing toward the main noise source (SR ISO 1996-1 regulation).

In many cases, noise data can only be collected at a few locations, making it difficult to estimate noise levels at unknown locations. In such cases, data interpolation can be used to estimate noise values at these unknown locations.

Interpolation is an important process in spatial data analysis that involves estimating values at unknown locations based on known values from adjacent or neighboring locations.

In this paper, we used the interpolation tool from QGIS software to determine values for the entire area of interest.

We chose to apply the IDW (Inverse Distance Weighting) method, which considers the values of the three points to estimate the unknown value. Thus, we obtained maps of the interpolation results, which shows the distribution of noise around interest. We checked and adjusted the interpolation settings to obtain the best possible result.

This analysis contributes to a better-informed decision regarding the impact of noise on the area and can aid in the development of effective strategies to mitigate or manage noise levels in the affected areas.

RESULTS AND DISCUSSIONS

This preliminary study was conducted in a small area to provide an initial assessment of noise pollution levels and distribution. By conducting this preliminary study, we have identified key areas where noise pollution is particularly high, which can be targeted for further research and intervention.

The noise pollution maps, generated by using the calculated average noise values of the measurements taken during September month, is given in Figures 3, 4 and 5.

In the maps the red color indicates the higher noise level, yellow indicate medium level of noise while the blue color indicates the lowest values of noise.

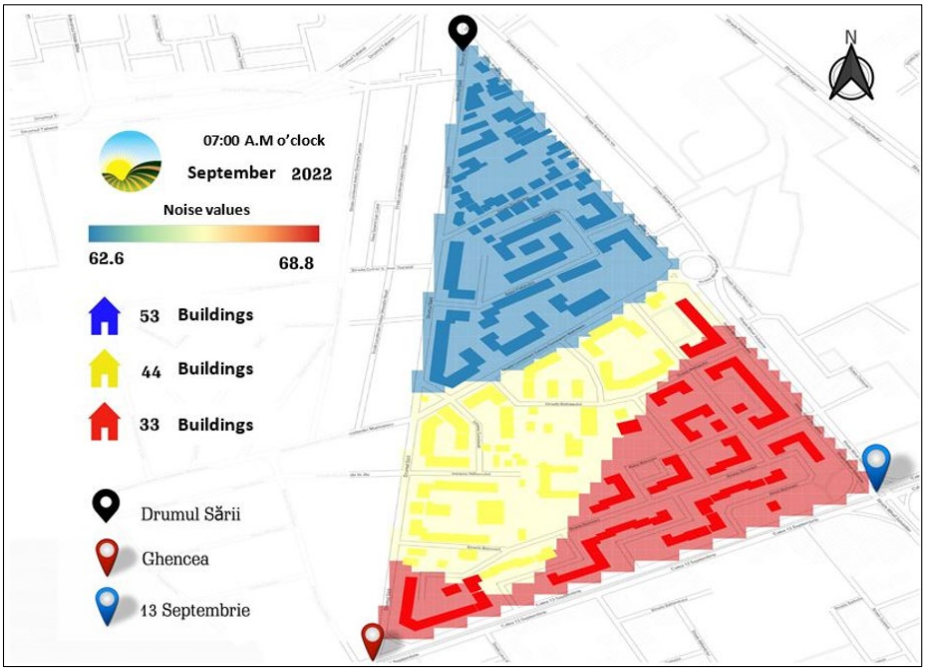

Figure 3. Interpolation of average values of noise at 07:00 A.M o'clock

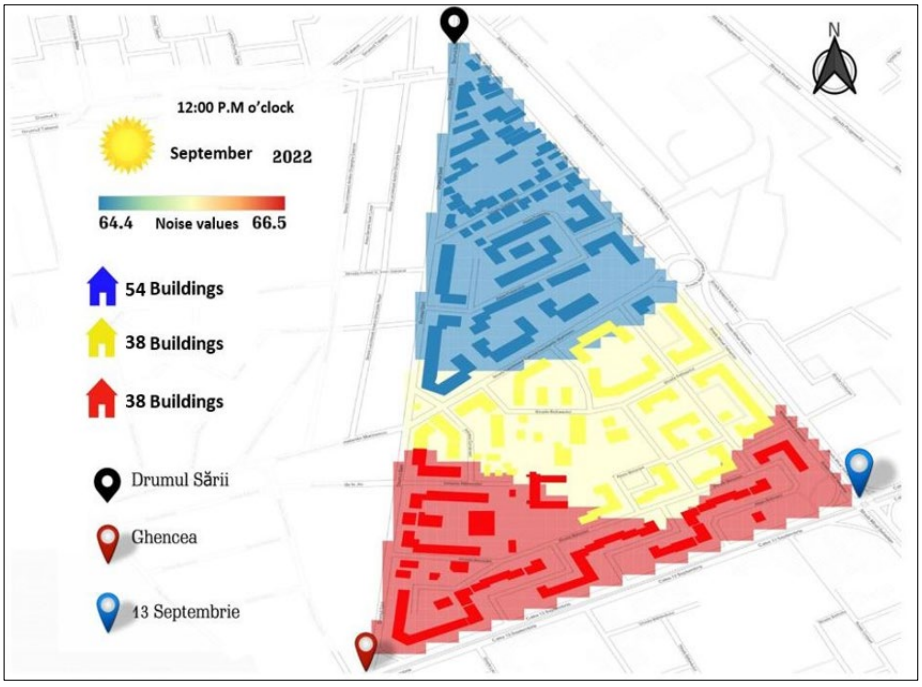

Figure 4. Interpolation of average values of noise at 12:00 P.M o'clock

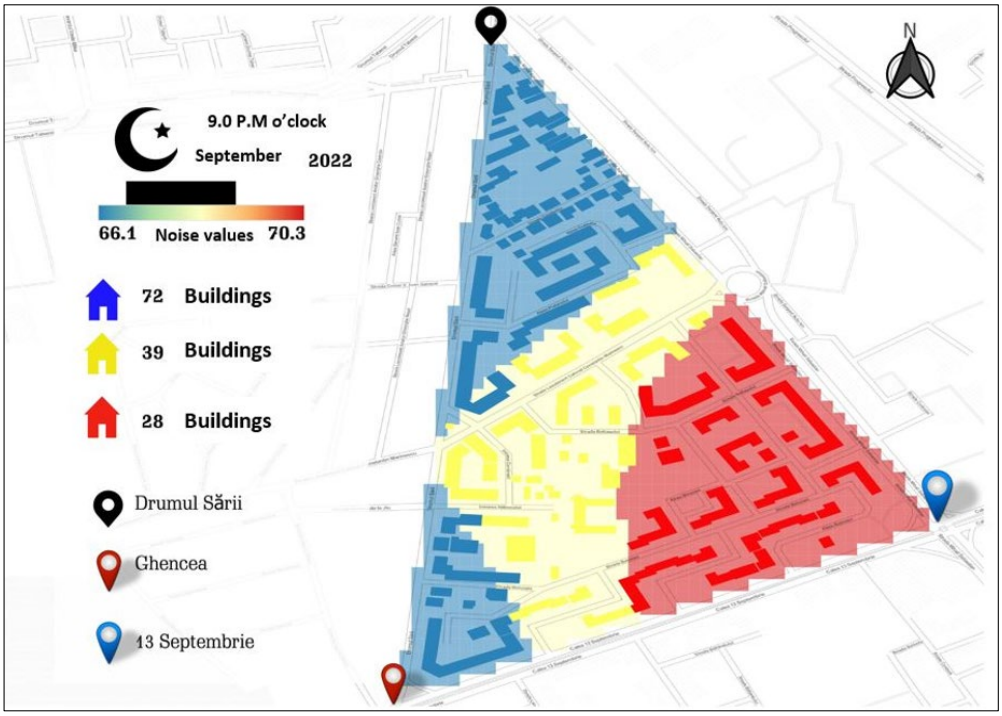

Figure 5. Interpolation of average values of noise at 09:00 P.M o'clock

The GIS-based mapping and assessment of noise pollution revealed that the recorded noise values varied in the three locations depending on the time of day.

According to the Figures 3, 4 and 5, the higher levels of noise pollution have been recorded in the Point 1 - Ghencea and in the Point 3 - 13 Septembrie while the lowest noise values are recorded in the Point 2 - Drumul Sării.

By analyzing the noise values recorded in September, Figures 6, 7 and 8 the following classifications were made:

By time, in the morning, at 07:AM, the lowest noise values were recorded in Point 2 - Drumul Sării, with values between 56.9 dB and 70.4 dB, while the highest values were recorded in Point 3 - 13 Septembrie with values between 65.5 dB and 71.5 dB.

At the midday, at 12:00 P.M the lowest noise values were recorded in Point 2 - Drumul Sării, with values between 55.7 dB and 70.2 dB. At the same time, the Point 1 - Ghencea recorded the highest noise trend with values between 62.9 dB and 70.2 dB.

In the evening, a trend like the one recorded in the morning was registered, namely, the trend with the lowest noise values was recorded in the location Drumul Sării with values between 60.1 dB and 70.1 dB. At the same time, the trend with the highest noise values was recorded in the location 13 Septembrie, with values between 68.9 dB and 72.5 dB.

The lowest value recorded for the entire analyzed period was 55.7 dB (recorded in Drumul Sării location) while the highest value was 71.5 dB (recorded in 13 Septembrie location).

Furthermore, from the analysis of the collected values, it was observed that there are some gaps in the noise values recorded on weekend days. This observation suggests that noise levels may be lower on weekend days, which may be explained by a reduced road traffic.

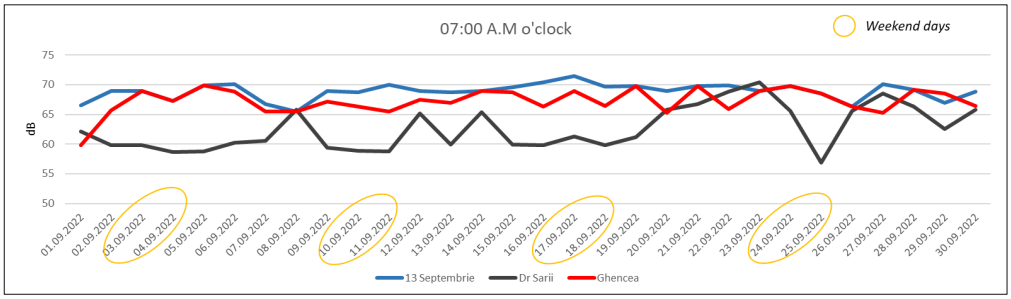

Figure 6. Distribution of the Noise Values Recorded in the three locations at 07:00 A.M o'clock

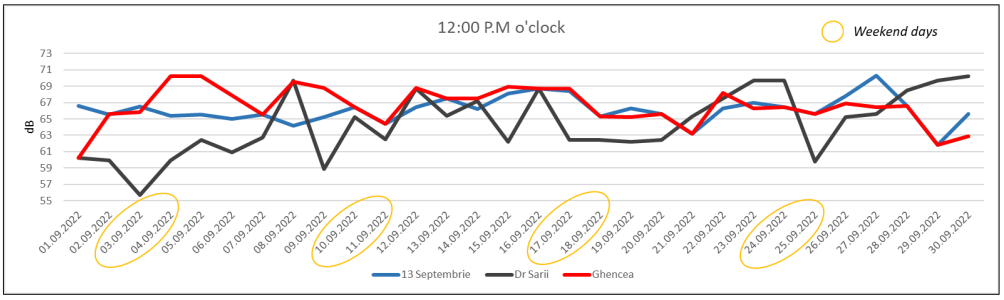

Figure 7. Distribution of the Noise Values Recorded in the three locations at 12:00 P.M o'clock

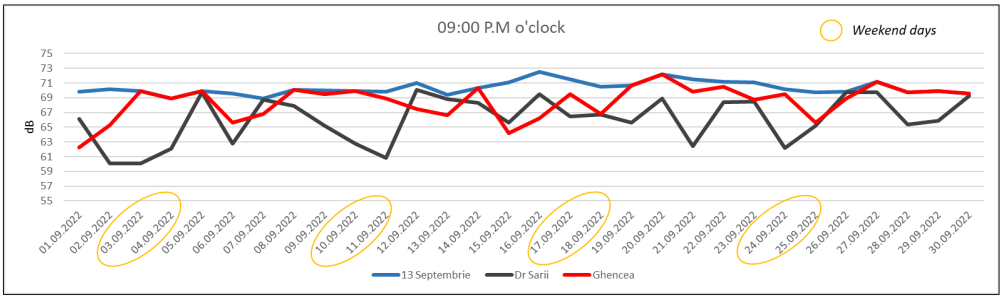

Figure 8. Distribution of the Noise Values Recorded in the three locations at 09:00 P.M o'clock

CONCLUSIONS

Noise pollution is a widespread problem in urban areas, with high levels of noise exposure affecting large numbers of people. In conclusion, the tested GIS interpolation variant has shown promising results in the analysis of noise values during the preliminary study. Conclusions that can be drawn from this study include the effectiveness of interpolation, the establishment of a noise value analysis methodology, the need for further research, and the importance of using GIS in noise value analysis.

The distribution of noise pollution is not uniform, with certain areas experiencing higher levels of noise than others. GIS-based noise pollution analysis is proper to identify areas with diverse levels of noise pollution. Interpolation in GIS is extremely useful, especially where there is no noise data, it can be said that its use allows making estimates of the noise level in areas without data, by extrapolating existing values in adjacent areas. Interpolation can also create a coherent picture of the distribution of noise levels. Therefore, interpolation in GIS is an effective method to estimate the noise level in areas where no noise data exists, making it a valuable technique for

assessing the impact of noise in the urban environment.

In Bucharest, the ambient noise limit values are set by Government Decision No. 944/2003 regarding the noise produced by fixed and mobile sources, with subsequent amendments and additions. This decision was issued in accordance with the provisions of Law no. 349/2002 regarding the prevention and combating of pollution.

According to this decision, for mixed-use areas, the limit values for noise produced by fixed sources are 70 dB during the day and 60 dB during the night. After our analysis, the average values recorded in September 2022 in the three locations fall within the official limits.

Of the four possible sources of environmental noise - road traffic, rail traffic, air traffic and industrial activity - the only cause of exceeding the limit values in Bucharest can be road traffic, as there is no industry in residential areas, the railway and the airport are far from residential areas. Therefore, given that the only source of noise exceeding the limit levels set by European legislation (ECD, 2002/49/EC; Xu, H. & Zhao, G., 2021) is road traffic, reducing environmental noise can only be achieved by reducing road noise, both at the source (emitted noise) and at the receiver (mixed noise-perceived by residents).

It is important to note that this preliminary study was conducted in a limited area, which may limit the ability to draw clear conclusions. There is also the opportunity to continue the study, expanding the analyzed area and applying various analysis methods and techniques, integrating noise data in the context of other geospatial data, such as land use, traffic, transportation, population density maps and others. So that a more detailed and accurate understanding of the noise level and the factors that influence it in those areas can be obtained.

REFERENCES

Albu, C., Olaru, M., & Gavrilă, A.G. (2019). Noise pollution in Bucharest: A case study. In Proceedings of the International Conference on Noise and Vibration Engineering (pp. 1969-1976).

Alvarado, R.A., & Parra, C.M. (2019). Noise pollution mapping and modelling using GIS and mobile monitoring devices: a case study in a Colombian city. *Applied Acoustics*, 149, 212-222.

Alves, J.A.; Silva, L.T.; Remoaldo, P.C.C. (2015). The Influence of Low-Frequency Noise Pollution on the Quality of Life and Place in Sustainable Cities: A Case Study from Northern Portugal. *Sustainability,* 7, 13920–13946.

Baskaran, R., & Ravindran, D. (2018). Spatial mapping and analysis of noise pollution using GIS: A case study of Chennai city, India. *Sustainable Cities and Society*, 38, 413-424.

Boboc, M.C., Ionel, I., & Ene, A. (2018). Environmental noise pollution in Bucharest, Romania. *Journal of Environmental Protection and Ecology*, 19(3), 1228-1236.

Cardinale, B. J., Duffy, J. E., Gonzalez, A., Hooper, D. U., Perrings, C., Venail, P. (2012). Biodiversity loss and its impact on humanity. Nature, 486, 59–67.

Castillo-Salazar, J.A., Cañete-Medinilla, A., & Vidal-Barrero, F. (2020). Noise pollution modeling and mapping in urban areas using GIS and regression analysis. *Journal of Environmental Management*, 257, 109976.

Cheng, M., Lu, X., & Du, W. (2017). Spatial mapping and analysis of noise pollution in urban areas: A case study in Harbin, China. *Applied Geography*, 79, 89-98.

Chiriac, C.R., Chiriac, A.E., & Popa, V. (2017). Environmental noise monitoring in Bucharest using GIS technology. Energy Procedia, 111, 553-562.

Cueto, J. L., Petrovici, A. M., Hernández, R., & Fernández, F. (2017). Analysis of the impact of bus signal priority on urban noise. *Acta Acustica United Acustica*, 103(4), 561–573. https://doi.org/10.3813/AAA.919085.

Deaconu, S., & Cioca, L.I. (2019). Noise pollution and urban planning in Bucharest, Romania. In Proceedings of the 16th International Multidisciplinary Scientific GeoConference SGEM, pp. 63-70.

EEA Report (2019). Environmental noise in Europe - 2020, No 22/2019, ISBN 978-92-9480-209-5, ISSN 1977-8449, doi:10.2800/686249

EEA (2017). Managing exposure to noise in Europe. EEA_briefing 2017-blue.pdf

EEA (2019). 'Reported data on noise exposure covered by Directive 2002/49/EC', European Environment Agency. Available online: https://www.eea.europa.eu/data-and-maps/data/data-on-noise-exposure-7

Eftekhari, M., Sarafi, M., Akhavan, S., Motlagh, M. M. (2020). Noise pollution mapping in the city of Tehran, Iran: Application of GIS and machine learning techniques. *Environmental Pollution*, 259, 113862.

Ertugrul E., Sercan E. (2021). GIS-based mapping and assessment of noise pollution in Safranbolu, Karabuk, Turkey. Environment, Development and *Sustainability* 23:15413–15431

ETC/ATNI (2019). Noise indicators under the Environmental Noise Directive. Methodology for estimating missing data, Eionet Report ETC/ATNI No 1/2019, European Topic Centre on Air Pollution, Transport, Noise and Industrial Pollution. Available online: https://www.eionet.europa.eu/etcs/etc-

atni/products/etc-atni-reports/noise-indicators-under-the-environmental-noise directive methodology-for-estimating-missing-data.

European Commission Directive 2002/49/EC of the European Parliament and of the Council of 25 June 2002 Relating to the Assessment and Management of Environmental Noise. Available online: https://publications.europa.eu/en/publication-detail/-/publication/27d1a64e-08f0-4665-a258-96f16c7af072/language-en

Fan, S., Li, J., Li, L., Chu, Z. (2022). Noise Annoyance Prediction of Urban Substation Based on Transfer Learning and Convolutional Neural Network. *Energies*, 15, 749.

Halonen, J. I., Dehbi, H. M., Hansell, A. L., Gulliver, J., Fecht, D., Blangiardo, M. (2016). Associations of night-time road traffic noise with carotid intima-media thickness and blood pressure: The Whitehall II and SABRE study cohorts. *Environment International*, 98, 54.

Hänninen, O. (2014). Environmental burden of disease in Europe: assessing nine risk factors in six countries, *Environmental Health Perspectives* 122(5), pp. 439-446 DOI: https://doi.org/10.1289/ehp.1206154.

https://www.eea.europa.eu/themes/human/noise/noise-fact-sheets/noise-country-fact-sheets-2021/romania

Maffei, L. and Zambon, A. (2012). GIS-based noise monitoring: a case study in Padua, Italy. *International Journal of Environmental Research and Public Health*, 9(9), 3247–3265.

Majidi, F., & Khosravi, Y. (2016). Noise pollution evaluation of City Center of Zanjan by geographic information system (GIS). *Iranian Journal of Health and Environment*, 9(1), 91–102.

McKeogh, E. and Robinson, D. (2004). GIS-based noise mapping as a tool for implementing European environmental noise directive in Dublin, Ireland. *Applied Acoustics*, 65(9), 887-904.

Rusu, C.M., Roșu, E., & Georgescu, L.P. (2015). Assessment of urban noise pollution in Bucharest, Romania. *Journal of Environmental Protection and Ecology*, 16(3), 1293-1303.

Saha, S.K. and Kumar, S. (2019). GIS-based noise modeling to assess the impact of urbanization on noise pollution: a case study of Chandigarh, India. *Environmental Monitoring and Assessment*, 191(5), 293.

Sandu M.A., Bica I., Virsta A., Preda M. (2013). Human health risk of contamination by polychlorinated biphenyls in the area of Bucharest city International Multidisciplinary Scientific GeoConference SGEM; Sofia: 545-552. Sofia: Surveying Geology & Mining Ecology Management (SGEM).

Soreanu, G., & Dumitru, D. (2015). Noise pollution in Bucharest, Romania. *Revista de Chimie*, 66(9), 1373-1377.

Sound Level Meter - Model: SL-4012. Technical Reference Manual. Available online: http://lutron1976.myqnapcloud.com/database/pdf/SL-4012.PDF

SR 10009:2017 Acoustics. Permissible limits of ambient noise level, www.asro.ro

Tăranu, N., & Ioniță, I., (2019). Mapping noise pollution in Bucharest using GIS technology. *Environmental Engineering and Management Journal*, 18(11), 2593-2601.

Titu, A.M., Boroiu, A.A., Mihailescu, S., Pop, A.B., Boroiu, A. (2022). Assessment of Road Noise Pollution in Urban Residential Areas - A Case Study in Pitesti, Romania. *Appl. Sci.*, 12, 4053. https://doi.org/ 10.3390/app12084053.

World Health Organization - WHO (2018). Environmental noise guidelines for the European region, WHO Regional Office for Europe, Copenhagen, Available online: http://www.euro.who.int/en/health-topics/environment-and-health/noise/publications/2018/environmental-noise-guidelines-for the-european-region-2018.

Xu, H. & Zhao, G. (2021). Assessing the Value of Urban Green Infrastructure Ecosystem Services for High-Density Urban Management and Development: Case from the Capital Core Area of Beijing, China. *Sustainability*, 13, 12115.

Yuan, M., Song, Y., Huang, Y., Hong, S., Huang, L. (2017). Exploring the association between urban form and air quality in China. *Journal of Planning Education and Research* 0739456X1771151.

Scientific Papers. Series E. Land Reclamation, Earth Observation & Surveying, Environmental Engineering. Vol. XII, 2023
Print ISSN 2285-6064, CD-ROM ISSN 2285-6072, Online ISSN 2393-5138, ISSN-L 2285-6064

SUPERIOR PHOTOGRAMMETRIC PRODUCTS USING DIRECT GEOREFERENCING, LIDAR DATA AND PRECISE TRANSFORMATIONS

Daniel ILIE[1, 2, 3], Constantin MOLDOVEANU[1], Octavian Laurentiu BALOTA[2, 4]

[1]Technical University of Civil Engineering of Bucharest,
112-124 Lacul Tei Blvd, District 2, Bucharest, Romania
[2]Romanian Society of Photogrammetry and Remote Sensing,
124 Lacul Tei Blvd, District 2, Bucharest, Romania
[3]Terra Advanced Technologies SRL, 149 Bahluiului Street, Ploiesti, Romania
[4]University of Agronomic Sciences and Veterinary Medicine of Bucharest,
59 Marasti Blvd, District 1, Bucharest, Romania

Corresponding author email: danielilie17@yahoo.com

Abstract

The current research presents the way to obtain direct georeferencing of photogrammetric imagery and to obtain rigorously georeferenced orthophoto plans without using ground control points. The direct georeferencing procedure is studied in Romania`s atypical coordinate systems (planimetric system based on an ellipsoid different than GRS80 and a vertical system of normal elevations, different than the ellipsoidal elevations used in GNSS technology), but it can also be applied to other systems of coordinates. To generate superior photogrammetric products, an innovative orthorectification methodology based on LIDAR data acquired simultaneously with photogrammetric images is presented. LIDAR data is also acquired by a direct georeferencing procedure and transformed with high precision using an application designed for this purpose. Therefore, a much faster way to generate orthophoto plans is presented, with lower production costs, without a substantial loss of the positional quality of the final product. Finally, there is presented the first stereo restitution project in Romania using small size images, acquired with a UAV system by direct georeferencing. The focus on the atypical case of Romania underlines the innovative features of this research.

Key words*: direct georeferencing, orthorectification, LIDAR, UAV stereo restitution.*

INTRODUCTION

The accelerated development of unmanned aerial vehicle (UAV) photogrammetric systems in recent years and their widespread distribution demonstrate the usefulness of research in this area. Current research reveals how superior photogrammetric products can be obtained through direct georeferencing (DG) orthorectification based on Light Detection and Ranging (LIDAR) data, and precise transformations.

Direct georeferencing (DG) in the field of photogrammetry has been one of the topics that has concerned many geodetic researchers in the last decades (Chiang et al., 2012). A comprehensive presentation of this subject was made in the review article published by Correia et al. (2022). The problem of accurate georeferencing of photogrammetric products is currently solved indirectly by using ground control points (GCP) and the bundle block adjustment (BBA) method in aerotriangulation. The development of in-flight positioning sensors (Global Navigation Satellite System (GNSS) antennas, Inertial Measurement Unit (IMU) sensors, Inertial Navigation System (INS), Synchronized Position Attitude Navigation (SPAN) system, etc.) has opened the possibility to identify better positioning solutions than indirect georeferencing through GCPs. The development of the SPAN system paved the way for direct georeferencing, and the first tests were carried out on the photogrammetric airplanes as early as 2007 by the company that invented this system, NovAtel (Development Team of NovAtel, 2007).

Currently, there are several studies carried out recently in the field of direct georeferencing, but also comparisons between the various methods approached (Gómez-Gutiérrez, 2022), which showed that low-cost photogrammetric systems cannot achieve satisfactory results for geodetic works (Essel et al., 2022). In the field of UAV

systems, several studies on direct georeferencing are known. However, most of them have a much poorer final positioning accuracy than that pursued in the current research (Salas López et al., 2022; Teppati Losè et al., 2020; Thiab & Seker, 2022). Even for UAV systems with built-in Real Time Kinematics (RTK) technology, the direct georeferencing error relative to the unit pixel is approximately ten times greater (Przybilla et al., 2020). There are also studies that propose a hybrid approach to DG by using a reduced number of GCPs (Liu et al., 2022). Rigorous calibration of imaging systems for DG is another topic of current research (Kordić et al., 2020). A part of the principles required for DG, such as camera calibration based on images acquired in a grid pattern, are presented in some research articles (Hutton et al., 2020). Another type of hybrid DG is based on the acquisition of highly accurate LIDAR data alongside the optical data. Finally, the optical data is georeferenced by correlation with the LIDAR data, but the LIDAR data is georeferenced with the help of ground targets, resulting in an indirect georeferencing (Haala et al., 2022).

Another field where similar research has not been identified is the realization of directly georeferenced stereo restitution projects, with small-sized images taken from low altitudes.

The aim of this research was to obtain directly georeferenced orthophoto for stereo restitution and rigorously georeferenced orthophoto plans without using GCP. The assumed goal was to obtain a maximum error of 1-2 GSD (Ground Sample Distance) for DG products.

The DG procedure will be studied mainly in the national coordinate systems of Romania (the 1970 Stereographic planimetric system and the Black Sea 1975 altimetric system), but it can be reproduced in any other coordinate systems.

The procedure for obtaining direct georeferencing, through its method of implementation, is itself an innovative element. The focus on the atypical case of Romania (planimetric system based on a different ellipsoid and a system of normal heights, different from those used according to the GNSS technology) underlines the innovative feature of this research. Thereby, the aim is to obtain orthophoto plans much faster, with production costs as low as possible, without a substantial loss of the positional quality of the final product. In conclusion, no research is known about direct georeferencing achieved within the assumed accuracy limit. Moreover, there are no known direct georeferencing studies carried out in Romania's national coordinate systems. It should be noted that there are implications of local systems in which direct georeferencing is carried out. These implications will be developed in current research. There is also no global research on orthorectification based on directly georeferenced LIDAR data, and even less in Romania's coordinate systems. The lack of methods for accurately transforming LIDAR data files makes this a difficult topic to approach. In practice, in the best case scenario, LIDAR data files are transformed with an error of 0.1-0.5m in 3D (Ilie et al., 2022).

All these aspects lead to the usefulness of this research with direct applicability to photogrammetric works in Romania. However, the principles that will be stated can be adapted for other photogrammetric systems, respectively for other coordinate systems.

MATERIALS AND METHODS

1. Equipment used

In terms of georeferencing, the integrator of the equipment used, UAV-M600-VLP32c-SonyA7RII, Phoenix LiDAR Systems LLC (PLS), proposes the use of 10 GCPs for a flight area of approximately 1 km^2 (100 ha) (Development Team of PLS, 2018). Also in the cited report, it is mentioned that the number of points on the ground increases in the context where more flights are used on the surface of 1 km^2. In the case of the UAV-M600-VLP32c-SonyA7RII system, for a height of up to 120m, the surface of 1 km^2 can be covered by at least 4 flight missions. In this case, the number of GCPs would increase exponentially, in the context in which they would also be needed in connecting areas between flights.

As a result of the experiments carried out, several essential elements were found for obtaining a system capable of DG. The main elements that have an important role in direct georeferencing and the minimum requirements regarding their technical capacity will be highlighted. The present study was carried out with the help of an integrated system for

simultaneous acquisition of LIDAR and optical data. The system is composed of a Velodyne UltraPuck LIDAR sensor (VLP 32c), nadiral oriented (Field Of View 40°/360°), with a maximum recording capacity of 1.2 mil. points/s, a maximum range of 200 m and an internal accuracy of ± 3 cm. The optical sensor is a Sony A7RII camera, nadiral oriented, with a resolution of 42 MB pixels and a focal length of approximately 20.79 mm.

2. Technical requirements

The system used must have an IMU dedicated to photogrammetric sensors with an update rate of at least 125Hz. The SPAN INS technology developed by NovAtel (Hexagon), which combines GNSS data and INS data, is also an essential element for a DG system (Development Team of NovAtel, 2020).

Complementarily, the scanning system must have its own GNSS receiver, capable of receiving satellite data from NAVSTAR (L1/L2/L2C/L5), GLONASS (L1/L2), Galileo (E1/E5a/E5b) and BeiDou (B1/B2). For accurate georeferencing it is important that the GNSS antenna to be equipped with multipath error filtering technology (*choke rings*) (Development Team of NovAtel, 2022).

The essential element to have a DG system consist of a rigid mounting of sensors to the IMU unit, but also of their precise calibration. To assure the quality of the LIDAR data, it is necessary that the vibrations generated by the engines and propellers are attenuated by rubber dampers, and thus transformed into vibrations that can be recorded by IMU.

For a correct georeferencing it is necessary that the flight platform is stable during the flight in order not to induce errors in the georeferencing. In this case, the aerial platform is the DJI Matrice M600 PRO, a hexacopter with a weight of 13.5 kg (including the onboard sensors), which ensures a smooth flight, without sudden movements generated by wind gusts. Affecting the flight attitude of the UAV by more than about 8° (especially the κ angle) can lead to the appearance of parallax in stereo restitution projects. Other additional systems that have been used to improve the positioning of the system: the professional flight control system, DJI A3 Pro (consisting of three GNSS antennas and three IMU units, which work as a redundant and mutual control system) and the D-RTK positioning system for precise autonomous flights that works on the RTK Base-Rover principle. These additional systems bring a considerable contribution to the flight attitude of the aircraft and mitigates the effects of wind gusts. Thereby, smooth flights are obtained, without sudden movements, without incidents even in the event of errors in the IMU/GNSS sensors (Development Team of DJI, 2018a).

3. Technology for obtaining DG

The proposed technology consists of combining the best calibration methods, acquisition procedures, processing processes, as well as software solutions. Along with these elements, innovative research elements are also added that together lead to obtaining the orthophoto plane by DG and rectified based on LIDAR data.

Pre-calibration of the LIDAR-Optic system

The first phase of rigorous calibration involved accurately determining the offsets between the IMU sensor and the GNSS antenna, respectively the LIDAR and optical sensors. Calibration was performed by geometric measurement methods after a thorough research of the coordinate systems and their origins, with a maximum error of ±1-2 mm.

Pre-calibration of the IMU-GNSS assembly consisted in determining the offsets between the IMU system and the GNSS antenna, and was performed along the axes of the IMU system (body frame). The determination of the offsets was made from the center of the system to the phase center of the GNSS antenna, by summing the measured segments (Table 1). In addition, transition rotations between theoretical systems that are involved in post-processing have been introduced in Table 1.

Pre-calibration of the IMU-Camera assembly (Sony A7RII) involved the determination of offsets to the perspective center of the camera, considering the lens focal length of approximately 21 mm. The offsets and their determination errors are consolidated in Table 2. Table 2 also centralized the initial rotations between the IMU and the camera coordinate system, which are to be rigorously calibrated.

Pre-calibration of the IMU-LIDAR assembly (Velodyne Ultra Puck VLP 32c) involved determining the offsets to the optical center of

the LIDAR sensor. The determined offsets were centralized in Table 3, alongside the initial rotations between the PLS systems (LIDAR) and the IMU sensor. They will be rigorously calibrated through specialized procedures and software for each individual laser head.

Air data enhancement

To obtain photogrammetric products through DG, it is necessary to take into account a multitude of factors that affect accuracy throughout the entire data acquisition process. In addition to rigorous system calibration, it is necessary to use best practices in photogrammetric data acquisition. Along with these, there are other principles and methods that can help eliminate certain errors and consequently improve aerial data.

Ensuring smooth flight is a basic requirement in obtaining quality photogrammetric data. Although the UAV system uses a precise positioning system (D-RTK GNSS system), the flight assurance is given by the integration of several data. Thus, along with GNSS data, the IMU sensors and the magnetic compass play an important role in the stability and uniformity of a flight. The IMU sensors are calibrated whenever large differences are found between the three modules installed on the flight platform. The IMU calibration should be performed in an area with flat terrain (Development Team of PLS, 2019). Magnetic compass calibration is performed much more often, basically every time the flight location is more than 30 km away from the last calibration performed (Development Team of PLS, 2019). The variation of gravity from one area to another, but also electromagnetic interference led to the need to calibrate this sensor quite often. In the absence of this calibration, chaotic movements can be encountered in the flight of the drone (Development Team of DJI, 2018b).

The optimal scanning method is based on autopilot flight, based on a flight design that has been conceived using the stated principles. One of the most versatile autonomous flight applications, Litchi, was used in this regard. In the case of LIDAR data acquisition, it is very important that the scan is performed on straight trajectories, as errors occur in the case of curves or sudden changes in direction.

The optimal method of aerial photography in the case of DG is defined by a side coverage of more than 55% and a forward overlap of more than 80% (Ma et al., 2020). This coverage generates accurate image correlation with a major impact on DG accuracy, even for classical photogrammetry (Gruber et al., 2022).

Table 1. IMU-GNSS offsets and rotations between theoretical coordinate systems

The coordinate system	X axis	Y axis	Z axis	RMS_X	RMS_Y	RMS_Z	Mentions
Offsets in Coordinate System of IMU to GNSS	-0.019m	0.050m	0.369m	0.002m	0.002m	0.001m	Used in post-processing (PP) (Inertial Explorer)
IMU Body Frame Rotations -> Vehicle Body F.	-90°	0°	0°	-	-	-	Used in post-processing (PP) (Inertial Explorer)

Table 2. IMU-Camera Sony A7RII offsets and initial rotations between IMU-Camera systems

The coordinate system	X axis	Y axis	Z axis	RMS_X	RMS_Y	RMS_Z	Mentions
Offsets in the IMU Coordinate System to Camera	-0.019m	0.141m	0.042m	0.002m	0.002m	0.003m	Used in post-processing (PP) (Inertial Explorer)
IMU Body Frame Rotations -> Camera Frame	0°	0°	0°	-	-	-	Used in PP. Extrinsic rot. X, Y, Z (Inertial Explorer)

Table 3. IMU-LIDAR VLP 32c offsets and initial rotations between systems

The coordinate system	X axis	Y axis	Z axis	RMS_X	RMS_Y	RMS_Z	Mentions
Offsets from IMU Coordinate System to the PLS System (LIDAR)	-0.019m	0.046m	0.043m	0.001m	0.001m	0.001m	Used in PP and real-time (Spatial Explorer)
SPAN IMU Body Frame Rotations -> LIDAR Frame	-45°	90°	90°	-	-	-	Used in PP and real-time. Extr. rot. Z, X, Y (Spatial Explorer)

Atmospheric influences are another important aspect in DG. The most important elements that can negatively affect flight missions are represented by wind gust speed (>5 m/s) and the *Kp* index of geomagnetic storms (>3). The geomagnetic storms that induce significant errors in the magnetic field of the planet, and in the waves that cross the ionosphere fall within the 4-9 *Kp* range (Matzka, 2023). The index of geomagnetic storms on the surface of the planet, *Kp*, is of particular importance because it induces errors in GNSS positioning, in radio transmissions, in any electronic sensor, and consequently in the UAV flight attitude (Development Team of NOAA, 2023).

The RTK corrections provided a priori PPK (Post Processing Kinematics) generated improved results in terms of the quality of the flight trajectories.

Trajectory calibration is accomplished in two stages: *static* and *kinematic* alignment (Development Team of NovAtel, 2019b). The *static alignment* was achieved by two sessions of static satellite measurements, one at the beginning of the flight and one after its completion. Static sessions required the drone to remain stationary for at least 10 minutes, clear of obstacles and with the engines off, during which satellite data was recorded every second (Development Team of PLS, 2021).

For systems equipped with only a GPS antenna, the IMU calibration procedure is completed by *kinematic alignment*. The first part of the calibration was performed through a straight flight, at a speed of over 6m/s, carried out in the direction of the wind, in the opposite direction. The second part of the airborne calibration consisted of calibrating the IMU with the GNSS data. IMU sensors are affected by drift errors, directly proportional to time passed from initial calibration (Development Team of NovAtel, 2020), therefore they are correlated with the position of the GNSS antenna. This calibration consisted of performing movements in the air (infinity shaped movements ∞), that involves large variations on each of the three components: *yaw*, *pitch*, *roll*. A minimum of 3 infinity shapes are required, until a relative calibration of the data recorded by the IMU sensor is achieved in the arcsecond range (Development Team of PLS, 2023). Since the PPK is performed in *forward*/*reverse* mode, all these procedures must be done in the mirror at the end of the flight mission. IMU calibration deteriorates over time in straight flights, even when it is correlated with precise GNSS positioning and corrected by the intelligent SPAN system (Development Team of NovAtel, 2019a). For this reason, it is recommended to limit the acquisition of photogrammetric data to strips of approximately 1 km, with block flights being preferable, not strips. The IMU sensor will recalibrate with each turn to the next lane due to the large variations in the three components: *yaw*, *pitch* and *roll*.

4. Experimental data: Isaccea Port

Based on the flight realised in the new Isaccea Port, both the rigorous calibration procedure and the obtaining of DG data were accomplished. The flight performed in Isaccea port was designed for the calibration of the LIDAR and camera sensors. The design of the flight assumed the creation of several sets of flight lines (in both directions), perpendicular to each other and with a 55% side coverage and 85% forward coverage (Terrasolid Ltd, 2022). After the flight, 23 GCPs were measured for the orthophoto plan and 29 points for the LIDAR data. The 23 GCPs will be exploited to calibrate the camera used, but also to check the DG.

PPK of the flight trajectory

Flight trajectory post-processing (PPK) was performed with the Inertial Explorer software solution, developed by NovAtel. As the GNSS and IMU data were of high quality, they were *tightly coupled* in the PPK process. Data processing was performed using a fixed base, with satellite records at one-second, using the European Terrestrial Reference System 1989 (ETRS89) datum the ETRS2000 frame, at epoch 2000. Accurate satellite ephemerides were used, trajectory quality being critical for DG. As results after PPK, differences between *forward*/*reverse* solutions of less than 3 mm in the horizontal plane and less than 12 mm in the vertical plane were obtained. From the point of view of the angles that define the attitude of the UAV, the differences between the *forward*/*reverse* solutions were a maximum of 0.6 arcminutes on each component. Finally, the two solutions were combined, resulting the final trajectory. The application was configured to

export the external orientation angles ω, φ, κ of the images relative to the national coordinate system, Stereographic 1970 (Zhao et al., 2014). The coordinates were adjusted with the offsets determined in Table 2 and then transformed into the national coordinate systems of Romania, with the TransDatRo v4.06 application.

Internal camera calibration

Image processing was done with the PIX4D Mapper software solution. The procedure used for internal camera calibration is BBA, using Automatic AeroTriangulation (AAT) techniques and GCP (Christian Heipke, 2002). The BBA was performed with an accuracy of 6 mm on X and Y axes, and of 17 mm on the Z axis. For a correct analysis, it should be noted that the average value of the GSD is 15.4 mm. Interchangeable lenses of non-metric cameras are not precisely calibrated in terms of focal length, optical center, radial or tangential distortions. Internal orientation parameters are sensitive to exposure from the acquisition environment, to extreme temperatures, pressure or vibrations (Oniga & Maximilian, 2013). Furthermore, a rigorous calibration done in the laboratory does not deliver the best results (Yodono Garcia et al., 2020), even less in a DG process. The distortions produced by lens aberrations (radial, tangential), also prevent the use of images in stereo restitution projects. Taking images with UAV systems from low altitude, amplifies parallax due to distortions and prevents the creation of stereoscopic models. This is the reason why non-metric cameras must be calibrated in the environment where are used, and then easily recalibrated within each mission. The laboratory calibration was used as a priori data, resulting the calibrated interior orientation parameters (Figure 1).

In order to verify the previously stated principles, the 23 GCPs were used as CPs (Check Points). DG processing was performed both with the laboratory calibrated camera and with the camera calibrated through the AAT and BBA process. The errors obtained in this first phase of DG are presented in Table 4. The analysis of Table 4 reveals that a laboratory camera calibration can be used to obtain orthophoto plans with average accuracy, relative to GSD. The visible difference between the obtained results demonstrates the high quality of the calibration achieved by the BBA process.

Camera boresight calibration

The rotations between the IMU sensor and the Sony A7RII camera determined in Table 2 must be rigorously calibrated. Uncalibrated orientations can be automatically corrected by the AAT process. However, a rigorously calibrated optical sensor with the IMU sensor translates into much more accurate image orientation data in the AAT process. The main effect of this rigorous calibration is to reduce the time to identify the tie points between the images, and to mitigate the risk of them being incorrectly identified (Ciobanu et al., 2022). Starting from the ω, φ, κ angles calculated in the BBA process, the correction angles (boresight) were calculated with NovAtel Inertial Explorer.

	Focal Length	Principal Point x	Principal Point y	R1	R2	R3	T1	T2
Initial Values	4723.510 [pixel] 20.790 [mm]	3990.200 [pixel] 17.563 [mm]	2648.330 [pixel] 11.656 [mm]	-0.013	0.013	-0.005	0.000	0.000
Optimized Values	4715.848 [pixel] 20.756 [mm]	4010.424 [pixel] 17.652 [mm]	2651.175 [pixel] 11.669 [mm]	-0.014	0.013	-0.005	-0.000	0.001
Uncertainties (Sigma)	0.279 [pixel] 0.001 [mm]	0.073 [pixel] 0.000 [mm]	0.073 [pixel] 0.000 [mm]	0.000	0.000	0.000	0.000	0.000

Figure 1. Capture from BBA report (PIX4D Mapper) - Sony A7RII internal orientation parameters calibration

Table 4. DG comparison using internal orientation parameters calibrated in laboratory or by BBA

Statistical Indicator	LABORATORY CALIBRATION			BBA CALIBRATION		
	Error X [m]	Error Y [m]	Error Z [m]	Error X [m]	Error Y [m]	Error Z [m]
Mean [m]	0.0125	0.0125	0.1171	0.0023	-0.0078	0.0060
Sigma [m]	0.0241	0.0215	0.0321	0.0084	0.0076	0.0192
RMS Error [m]	0.0271	0.0249	0.1214	0.0087	0.0108	0.0201

The algorithm for boresight calibration is based on the rotation equation from the image to the terrain coordinate system. The calculation of the corrections was realized in accordance with the definition of the Stereographic 1970 coordinate system. After the boresight calibration, the whole process of AAT was repeated. Figure 2 shows a graphical comparison between the quality of the BBA performed before and after the boresight calibration.

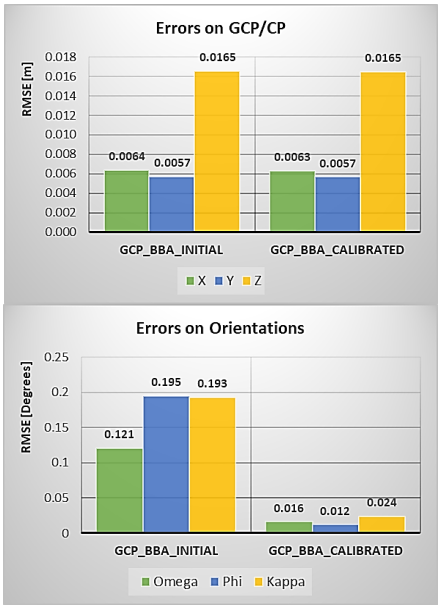

Figure 2. The influence of boresight calibration of the Sony A7RII camera in the BBA process

From the analysis of the graphs in Figure 2, it can be seen that the positioning errors on GCPs remain approximately identical. The errors obtained on the orientations after the rigorous calibration of camera are ten times smaller. This translates into an efficiency in the AAT process.

Rigorous calibration of the LIDAR sensor

Orthorectification of photogrammetric data using LIDAR data requires a high quality of these data. In the case of the present study, the flight was designed in an area with roads, platforms, concrete walls, beams, etc., for a better calibration of the LIDAR data. The software solution used to determine the correction angles for each laser heads was the TerraScan and TerraMatch application developed by Terrasolid Ltd. Starting from the rotations determined in Table 3, LIDAR data was exported for each individual laser head. The final objective of the calibration involves the calculation of the correction angles on all three axes: *heading* (*-yaw*), *pitch*, *roll*. The LIDAR point cloud was noise filtered and then classified into object classes on each strip and laser head. After classifying the LIDAR data, matching lines were identified in each set, lines that approximate very well certain areas on the ground, buildings, or walls. Matching lines are used to calculate corrections on each rotation axis (Terrasolid Ltd, 2022). A total of approximately one hundred thousand cross-sections with matching lines were used in the calibration process. As previously specified, laser head calibration for the IMU-Velodyne VLP 32c system was initially performed in a work-specific environment by the system integrator Phoenix LiDAR Systems LLC. Following the current calibration, the analysis of the corrections obtained on the three angles shows a good initial calibration, with the corrections having insignificant values. Checking the statistical parameters before and after calibrating the laser heads reveals only a small improvement in the quality of LIDAR data (Table 5). It should be pointed out that these calibrations are also limited by the constructive accuracy of the LIDAR sensor (±3cm, under optimal conditions).

In the case of the LIDAR calibration, the data were used in the ETRS89 coordinate system, using the Universal Transverse Mercator (UTM) 35N projection. In addition to the LIDAR point cloud, PPK trajectories were also used, with the obtained accuracies. Because flight trajectories have atypical formats, they are difficult to convert to other coordinate systems which are not based on GRS80, without a loss of accuracy.

Table 5. Verification of statistical parameters before and after LIDAR data calibration

LIDAR Verified	Check on GCP [m]					Check on strips [m]
	Average dZ	Min. dZ	Max. dZ	1 Sigma	RMSE	Avg. Magnitude
INITIAL	0.017	-0.012	0.047	0.015	0.022	0.0229
CALIBRATED	0.017	-0.016	0.042	0.013	0.022	0.0223

Therefore, in the case of LIDAR data, the export is first done in the UTM system and after calibration the LIDAR data is transformed in others systems.

Preliminary results of DG

The photogrammetric data were reprocessed, using the calibrated interior and exterior orientation elements. The data were processed using the principle of DG. Thus, GCPs were used only as CPs to be able to evaluate the final quality of the obtained data. The obtained accuracies were compared with the classical way of generating orthophoto plans (BBA), but also with the accuracy of DG obtained with PPK trajectory, but uncalibrated sensors (DG PPK). From the analysis of Figure 3, it can be concluded that satisfactory accuracy can be obtained through DG if the stated principles and working method detailed in this study are followed. If the sensors are rigorously calibrated, then with DG accuracies similar to the BBA technology can be achieved.

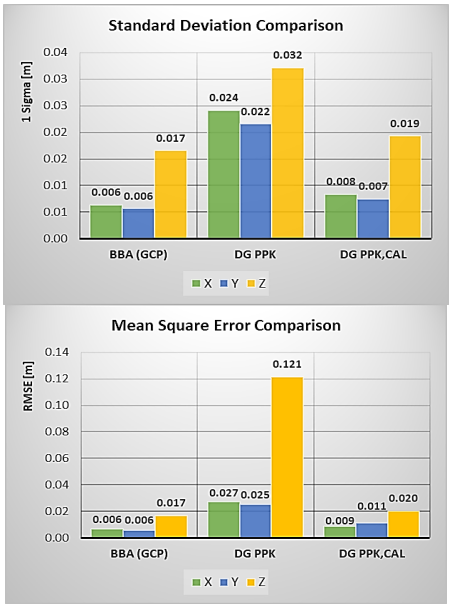

Figure 3. Comparison of the quality of Direct Georeferencing obtained after rigorous calibration

It should be emphasized that the accuracies obtained in BBA are substantially improved by using images with high overlap: over 50% side overlap, respectively over 85% forward overlap.

5. Precise transformation of LIDAR data

Orthorectification is currently performed based on the tie points dense cloud generated through the AAT process. Until now, there was no possibility to use LIDAR data to orthorectify images, with the aim of obtaining orthophoto plans in the National Projection System, Stereographic 1970. One of the impediments was the lack of precision of the LIDAR data obtained by DG, but which can be solved by rigorous calibration and the stated principles. The second significant impediment in the specific case of Romania consists in the lack of a precise transformation of the LIDAR data in the national coordinate systems. The problem of transformation from the ETRS89 geodetic system (based on GRS80 ellipsoid) to the Stereographic 1970 oblique azimuthal projection system (having associated Krasovski datum 1942 and Krasovski 1940 ellipsoid) has been solved for point transformations (Avramiuc et al., 2009), but it is difficult to apply for atypical data formats. The situation becomes even more complicated when the transformation of ellipsoidal heights into normal heights, referred to the Black Sea 1975, is performed. This system of normal heights is based on a continuously developing quasi-geoid (Avramiuc et al., 2019), which further complicates matters by periodically releasing new transformation parameters (The National Center for Cartography, 2020).

The errors obtained by transforming the LIDAR data with the generic software range from decimeters to meters, both planimetrically and in elevation. In this context, together with other researchers, we developed the RoTLAS APP v1.62 for high-precision transformation of LIDAR data into LAS format. Consequently, the acquired LIDAR data were transformed into national coordinate systems with an accuracy identical to the TransDatRo v4.06 application. The differences between a point transformation performed with the official app and RoTLAS APP v1.62 are sub-millimeter and essentially represent residual errors (Ilie et al., 2022).

RESULTS AND DISCUSSIONS

1. DG orthophoto plan, rectified on LIDAR data: Isaccea Port

The calibrated and precisely transformed LIDAR point cloud in the Stereographic 1970 system, respectively Black Sea 1975, was used as a substitute for the dense cloud of tie points. The orthophoto mosaic made by DG is presented in Figure 4, superimposed with the GCPs (R4 and R6 are detailed).

The accuracy obtained by direct georeferencing is presented in Figure 3 (section DG PPK, CAL). The quality of the orthorectification is presented by comparison in Figure 5. No discrepancies were identified between the georeferencing of the optical data and the LIDAR data, a fact also demonstrated by the correct orthorectification.

Improvements in orthorectification are found in areas shaded by vegetation and in the case of atypical structures such as communication antennas, where classical orthorectification fails. For projects where both optical and LIDAR data are required, a considerable time saving of approximately 54% can be achieved using LIDAR data. The time saved multiplies by the number of flights involved in the project, to which is added the time saved that would have been necessary for determining the GCP.

2. Validation of DG: Turnu Magurele Port

The validation of the DG was carried out based on two new flights performed in Turnu Magurele Port. The calibrated internal orientation parameters of the camera (Figure 1) were easily recalibrated to the new environmental conditions of the current project (as close as possible to the initially calibrated data). The internal orientation parameters of DSLR cameras are sensitive to exposure from the acquisition environment, to extreme temperatures, pressure or vibration (Yodono Garcia et al., 2020), which is why slight corrections are required. To fully validate the proposed procedure, the quasi-geoid model used has also changed: TransDatRo version v4.07 (Bagherbandi et al., 2022).

Validation of DG accuracy on CP

To check the DG against the classical method, 17 GCPs were determined. Also, 132 RTK points were determined in the normal working mode, to verify the stereo restitution projects realised with DG. In a first step, the accuracies obtained by the two BBA and DG methods were compared (Figure 6).

Figure 4. Direct georeferenced orthophoto plan, orthorectified based on LIDAR data

Figure 5. Comparison between classical (left) and on LIDAR data (right) orthorectification

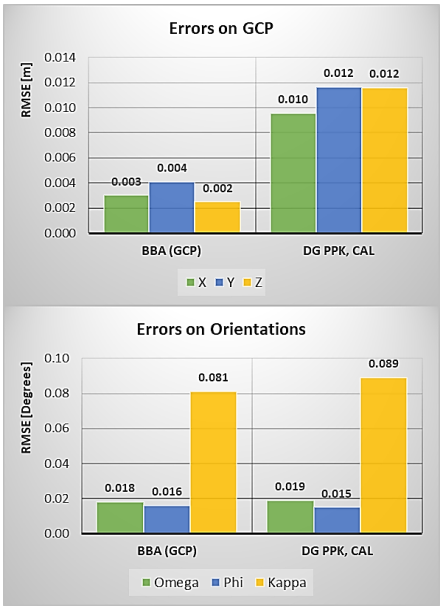

Figure 6. Validation of DG based on statistical data

The inputs to the BBA process were the high-coverage images (taken as for DG) and the calibrated camera. Thereby, the accuracies obtained by BBA were also improved. The DG was carried out in a similar way to the one presented in case of Isaccea Port.
The data in Figure 6 highlights the fact that the errors on each axis were below the value of 1 GSD of 14.4 mm. From the point of view of errors on the orientations, a slight systematic influence of the wind (the value of the angle κ) is found. This error has no influence on the georeferencing accuracy for photogrammetric data, due to the AAT process present in both processing modes (BBA/GD). In conclusion, it can be noticed that the goal of obtaining directly georeferenced products within the accuracy limit of 1-2 GSD has been achieved.

Validation of orthorectification on LIDAR

In order to validate the orthorectification mode, the orthophoto plan made in the classical way (BBA) was compared with the orthophoto plan made based on the LIDAR point cloud. The verification was carried out on several classes of objects. The first check was carried out on buildings, with an emphasis on areas covered by vegetation. In Figure 7 two types of buildings were chosen: with roof in two waters (extended to the walls) and respectively with a terrace roof. In the classic process carried out by AAT, orthorectification errors were identified, especially in areas covered by vegetation, but also in the case of buildings with terraced roofs. Using orthorectification based on LIDAR data, these errors were eliminated. Moreover, the LIDAR orthorectification of building edges was found to be less jagged and closer to the reality.

Figure 7. Buildings and vegetation: the improvement brought by orthorectification based on LIDAR data

The second way of validating DG with LIDAR orthorectification, was performed on a telecommunications antenna. Orthorectification based on the dense point cloud generated by AAT completely fails for atypical structures (Figure 5, left). Significant improvements are found in antenna orthorectification on LIDAR data, but some residual image mosaicking errors remain (Figure 8, right).

Figure 8. Telecommunication antennas: differences between classical and LIDAR orthorectification

For suspended buildings, better results were found on the edges of orthorectified buildings using LIDAR data. In the case of conveyor belts, orthorectification errors were identified with the AAT method, the largest being found in the case of uncovered conveyor belts (Figure 9).

Figure 9. Suspended buildings: differences between classical and LIDAR orthorectification

Industrial machines are also difficult to orthorectify, because they are composed of atypical structures, partially suspended in the air (Figure 10).

Figure 10. Industrial machinery: differences between classical and LIDAR orthorectification

Through the classic orthorectification technology (Figure 10, left) the results are completely unusable. Figure 10 exemplified the case of a wharf crane, which is substantially better orthorectified by the DG procedure on LIDAR data (right image). Also, in this case there are small mosaic errors that can be rectified by manual editing of the orthophoto plane. Better results can be achieved if these

atypical machines are scanned from four different directions. Usually, their rectification is not of great interest. If the project is carried out in areas such as refineries, mining excavations, chemical plants, then the rectification of atypical objects is necessary.
Classic orthorectification was positively influenced by the high coverage between the acquired images. The good results obtained based on LIDAR data rectification are also due to the high density of points per square meter, with an average of over 550 points/m^2.

3D validation of DG by stereo restitution

The final part of the validation was performed by stereo restitution, to verify the accuracy of the DG process in a three-dimensional system. In order to be able to perform stereo restitution projects, the images were rectified from the influence of radial and tangential distortions using the internal orientation calibrated parameters. The DG stereo restitution project was verified with the help of the 17 GCPs through stereoscopic measurements (Table 6).
Following the precisions obtained and in accordance with GSD, respectively with the precisions presented for the classical case (Figure 6), the stereo restitution made by the DG process is validated. The orthophoto plane made through DG was also checked with the 3D vector data from the stereo restitution by BBA (Figure 11) and with RTK data from the field.

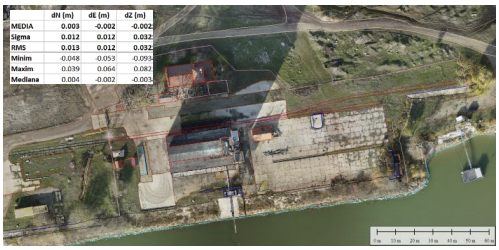

Figure 11. Orthophoto plan verification based on vector data from stereo restitution

To compute the stereoscopic accuracy over the entire validation area from Turnu Magurele Port, 132 points were determined by RTK technology. CPs were chosen on the railways or on the crane's tracks. This type of points is considered to be the most difficult to measure in a stereoscopic model. Figure 11 shows the error statistics of the differences found on the 132 CP. After normalizing the observed differences, they were represented graphically in order to analyze their distribution (Figure 12).

Table 6. Direct georeferencing verification by GCP reading through stereo restitution

No. PTS	PTS NAME	Coordinate systems: Stereographic 1970, Black Sea 1975, Ed. 1990 - RTK MEASUREMENTS			Coordinate systems: Stereographic 1970, Black Sea 1975, Ed. 1990 - DG STEREORESTITUTION			Measurement Differences RTK-DG		
		North (m)	East (m)	Elev. (m)	North (m)	East (m)	Elev. (m)	dN	dE	dH
1	CB1	246204.109	491995.281	25.823	246204.082	491995.283	25.805	0.027	-0.002	0.018
2	CB2	246033.325	491553.281	25.689	246033.327	491553.277	25.680	-0.002	0.004	0.009
3	CB3	246130.565	492074.477	26.265	246130.572	492074.474	26.252	-0.007	0.003	0.013
4	CM1	246046.764	491256.538	27.417	246046.747	491256.554	27.397	0.017	-0.016	0.020
5	R1	246098.203	492004.645	25.654	246098.201	492004.641	25.637	0.002	0.004	0.017
6	R10	245897.748	491324.338	22.459	245897.751	491324.338	22.433	-0.003	0.000	0.026
7	R11	245999.607	491241.164	26.996	245999.605	491241.158	26.987	0.002	0.006	0.009
8	R12	245982.928	491314.693	27.109	245982.917	491314.692	27.091	0.011	0.001	0.018
9	R13	246046.433	491586.885	25.404	246046.428	491586.870	25.392	0.005	0.015	0.012
10	R2	246139.846	492073.387	26.342	246139.841	492073.384	26.328	0.005	0.003	0.014
11	R4	246188.000	492329.869	23.848	246187.994	492329.864	23.844	0.006	0.005	0.004
12	R5	246294.850	492178.513	26.827	246294.848	492178.530	26.812	0.002	-0.017	0.015
13	R6	246193.761	492106.337	25.983	246193.736	492106.341	25.987	0.025	-0.004	-0.004
14	R7	246062.406	491770.006	26.279	246062.403	491769.989	26.281	0.003	0.017	-0.002
15	R8	246119.681	491684.352	26.551	246119.668	491684.346	26.554	0.013	0.006	-0.003
16	R9	245947.838	491498.857	25.576	245947.845	491498.838	25.572	-0.007	0.019	0.004
17	TM1	246066.428	491780.939	26.249	246066.432	491780.917	26.229	-0.004	0.022	0.020
							Media	**0.006**	**0.004**	**0.011**
							Sigma	**0.010**	**0.010**	**0.009**
							RMS	**0.011**	**0.011**	**0.014**

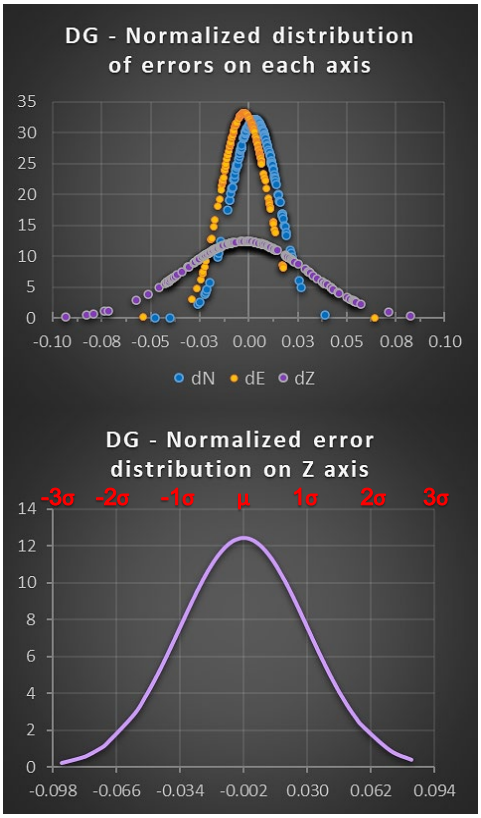

Figure 12. Normalized distribution of errors on 132 CP

Most planimetric differences fall within ±36 mm, which is close to the error of the RTK point determination method. In terms of the differences identified on hight, they are larger, but evenly distributed. The dispersion of errors on the Z-axis is in contrast with the dispersion of errors obtained on the Z-axis from GCP. From the point of view of stereo restitution, the only major difference between the checkpoints is the ease with which they can be scored in the stereoscopic model. In conclusion, an influence generated by the human eye is found, which manifests itself equally in both directions. Thus, the human eye can limit the accuracy of data acquired by stereo restitution, despite the very small size of the GSD.

CONCLUSIONS

The research carried out in the field of DG in the coordinate systems of Romania brings with it several benefits. The most important benefits are production time efficiency and cost reduction associated with photogrammetric products. Orthorectification based on LIDAR DG data is performed much more accurately in many situations and brings more efficiency in the creation of orthophoto plans. As a result of this research, it was found that the creation of topographic plans by UAV stereo restitution is much faster than classic measurements.

The validation of the DG was carried out on two different versions of the quasi-geoid (version 4.06, respectively version 4.07), the results being similar. The verification of the correctness of the DG was realised by several methods, resulting in a heterogeneous validation. The generated orthophoto plan and the vector plan made by stereo restitution were mutually verified demonstrating the reliability of the procedure. The statistics of these checks highlight the quality of the products made by direct georeferencing.

An aspect that can be improved in future research is the residual mosaicking errors that appear after the rectification based on LIDAR data. This happens especially in the areas of atypical objects. However, orthorectification is performed much more correctly than by classical methods, leaving only mosaic errors to be rectified.

Despite the results obtained, the DG method should be applied with caution. During the production process, random errors may occur that are difficult to identify. For this reason, it is recommended to use 2-3 GCPs to ensure the verification of the entire process.

ACKNOWLEDGEMENTS

The validation by stereoscopic measurements was performed independently with the help of several professional stereo restitutors from the Tehnogis Grup SRL company. The applications used were provided by Tehnogis Grup SRL, Prosig Expert SRL and the Technical University of Civil Engineering of Bucharest. Finally, we thank all those who directly or indirectly supported this research.

REFERENCES

Avramiuc, N., Dragomir, P. I., Rus, T. (2009). Algorithm for direct and inverse coordinate transformation

between ETRS89 CRS and S-42 CRS. *RevCAD Journal of Geodesy and Cadastre*, 105-114.

Avramiuc, N., Erhan, C., Spiroiu, I., Crişan, R.-D.-N., & Flueraş, M. (2019). Determination of a new gravimetric quasigeoid for Romania. *Journal of Geodesy, Cartography and Cadastre*.

Bagherbandi, M., Jouybari, A., Nilfouroushan, F., & Ågren, J. (2022). Importance of Precise Gravity Field Modeling in Direct Georeferencing and Aerial Photogrammetry: a Case Study for Sweden. *The International Archives of the Photogrammetry, Remote Sensing and Spatial Information Sciences, XLIII-B2-2022*, 15-20. doi:10.5194/isprs-archives-XLIII-B2-2022-15-2022

Chiang, K.-W., Tsai, M.-L., & Chu, C.-H. (2012). The Development of an UAV Borne Direct Georeferenced Photogrammetric Platform for Ground Control Point Free Applications. *12*(7), 9161-9180.

Christian Heipke, K. J. a. H. W. (2002). *Integrated Sensor Orientation - Test Report and Workshop Proceedings*. European Organization for Experimental Photogrammetric Research, Vol. Official Publication No 43. (pp. 302).

Ciobanu, D., Kemper, G., Ilie, D., Răducanu, D., & Balotă, O. L. (2022). Using the Open Skies multi sensor system for military observation missions and civilian applications. *Int. Arch. Photogramm. Remote Sens. Spatial Inf. Sci., XLIII-B1-2022*, 301-308. doi:10.5194/isprs-archives-XLIII-B1-2022-301-2022

Correia, C. A. M., Andrade, F. A. A., Sivertsen, A., Guedes, I. P., Pinto, M. F., Manhães, A. G., & Haddad, D. B. (2022). Comprehensive Direct Georeferencing of Aerial Images for Unmanned Aerial Systems Applications. *22*(2), 604.

Development Team of DJI. (2018a). A3 Flight Controller. Retrieved from https://www.dji.com/a3

Development Team of DJI. (2018b). Matrice M600 PRO User Manual. Retrieved from https://dl.djicdn.com/downloads/m600%20pro/1208EN/Matrice_600_Pro_User_Manual_v1.0_EN_1208.pdf

Development Team of NOAA. (2023). Planetary K-Index. Retrieved from https://www.swpc.noaa.gov/products/planetary-k-index

Development Team of NovAtel. (2007). NovAtel SPAN Aerial Photogrammetry Test Flights Results.

Development Team of NovAtel. (2019a). OEM7 on SPAN Installation and Operation User Manual.

Development Team of NovAtel. (2019b). Waypoint Products Group - A NovAtel Precise Prositioning Product [User Manual v8.80]: Hexagon, NovAtel Inc.

Development Team of NovAtel. (2020). SPAN - Tightly coupled GNSS+INS technology for exceptional continuous 3D position, velocity & attitude performance. Calgary, Alberta, Canada: Hexagon, NovAtel Inc.

Development Team of NovAtel. (2022). Antennas Pinwheel OEM. Retrieved from https://hexagondownloads.blob.core.windows.net/public/Novatel/assets/Documents/Papers/Pinwheel_OEM/Pinwheel_OEM.pdf

Development Team of PLS. (2018). Ground Control Recommendation for Phoenix Clients.

Development Team of PLS. (2019). LiDAR Mapping Systems - Drone Pilot Training.

Development Team of PLS. (2021). Post Processing - Workflow with Inertial Explorer and TerraSolid.

Development Team of PLS. (2023, January 19, 2023). Phoenix LiDAR Systems User Manual. Retrieved from https://docs.phoenixlidar.com/

Essel, B., McDonald, J., Bolger, M., & Cahalane, C. (2022). Initial Study Assessing the Suitability of Drones With Low-Cost GNSS And IMU for Mapping Over Featureless Terrain Using Direct Georeferencing. *The International Archives of the Photogrammetry, Remote Sensing and Spatial Information Sciences, XLIII-B2-2022*, 37-44. doi:10.5194/isprs-archives-XLIII-B2-2022-37-2022

Gómez-Gutiérrez, Á., Sánchez-Fernández, M., and de Sanjosé-Blasco. (2022). Performance of Different UAS Platforms, Techniques (LIDAR and photogrammetry) and Referencing Approaches (RTK, PPK or GCP-based) to Acquire 3D Data in Coastal Cliffs. *EGU General Assembly 2022, Vienna, Austria*. doi: https://doi.org/10.5194/egusphere-egu22-9881

Gruber, M., Schachinger, B., & Mostafa, M. (2022). The Next Generation Vexcel Imaging 3D City Modelling Using Directly Georeferenced Data. *The International Archives of the Photogrammetry, Remote Sensing and Spatial Information Sciences, XLIII-B1-2022*, 309-316. doi:10.5194/isprs-archives-XLIII-B1-2022-309-2022

Haala, N., Kölle, M., Cramer, M., Laupheimer, D., & Zimmermann, F. (2022). Hybrid Georeferencing of Images and LiDAR Data for UAV-based Point Cloud Collection at Millimetre Accuracy. *ISPRS Open Journal of Photogrammetry and Remote Sensing, 4*, 100014. doi:https://doi.org/10.1016/j.ophoto.2022.100014

Hutton, J., Lipa, G., Baustian, D., Sulik, J., & Bruce, R. (2020). High Accuracy Direct Georeferencing of the Altum Multi-Spectral UAV Camera and its Application to High Throughput Plant Phenotyping. *ISPRS - International Archives of the Photogrammetry, Remote Sensing and Spatial Information Sciences, XLIII-B1-2020*, 451-456. doi:10.5194/isprs-archives-XLIII-B1-2020-451-2020

Ilie, D., Balotă, O. L., Iordan, D., & Nicoară, P. S. (2022). Algorithm and application development for precise and accurate transformation of LIDAR point clouds into national coordinate systems of Romania using official equations and quasigeoid model. *ISPRS Ann. Photogramm. Remote Sens. Spatial Inf. Sci., V-4-2022*, 181-188. doi:10.5194/isprs-annals-V-4-2022-181-2022

Kordić, B., Gašparović, M., Lužar Oberiter, B., Đapo, A., & Vlastelica, G. (2020). Spatial Data Performance Test of Mid-cost UAS with Direct Georeferencing. *Periodica Polytechnica Civil Engineering, 64*(3), 859-868. doi:10.3311/PPci.15619

Liu, X., Lian, X., Yang, W., Wang, F., Han, Y., & Zhang, Y. (2022). Accuracy Assessment of a UAV Direct Georeferencing Method and Impact of the Configuration of Ground Control Points. *6*(2), 30.

Ma, H., Ma, H., Liu, K., Luo, W., & Zhang, L. (2020). Direct Georeferencing for the Images in an Airborne

LiDAR System by Automatic Boresight Misalignments Calibration. *20*(18), 5056.

Matzka, J. (2023). Indices of Global Geomagnetic Activity. Retrieved from https://www.gfz-potsdam.de/en/section/geomagnetism/data-products-services/geomagnetic-kp-index

Oniga, E., & Maximilian, D. (2013). Metric and Non-Metric Cameras Calibration for the Improvement of Real-Time Monitoring Process Results. *Environmental Engineering and Management Journal, 12*, 719-726. doi:10.30638/eemj.2013.088

Przybilla, H.-J., Bäumker, M., Luhmann, T., Hastedt, H., & Eilers, M. (2020). Interaction Between Direct Georeferencing, Control Point Configuration and Camera Self-Calibration for RTK-Based UAV Photogrammetry. *ISPRS - International Archives of the Photogrammetry, Remote Sensing and Spatial Information Sciences, XLIII-B1-2020*, 485-492. doi:10.5194/isprs-archives-XLIII-B1-2020-485-2020

Salas López, R., Terrones Murga, R. E., Silva-López, J. O., Rojas-Briceño, N. B., Gómez Fernández, D., Oliva-Cruz, M., & Taddia, Y. (2022). Accuracy Assessment of Direct Georeferencing for Photogrammetric Applications Based on UAS-GNSS for High Andean Urban Environments. *6*(12), 388.

Teppati Losè, L., Chiabrando, F., & Giulio Tonolo, F. (2020). Boosting the Timeliness of UAV Large Scale Mapping. Direct Georeferencing Approaches: Operational Strategies and Best Practices. *9*(10), 578.

Terrasolid Ltd, Arttu S. (2022). *TerraMatch User's Guide*.

The National Center for Cartography. (2020). Determination of a quasigeoid for the area of Romania. Retrieved from https://www.cngcft.ro/index.php/ro/portofoliu/proiecte-in-lucru/determinarea-unui-cvasigeoid-pentru-zona-romaniei

Thiab, W., & Seker, D. (2022). *Direct and Indirect Georeferencing with a Light-Weight UAV and an RTK UAV*.

Yodono Garcia, M., Oliveira, H., Fernandes, R., & Costa, D. (2020). Evaluation of Different Methods for Non-Metric Camera Calibration. *Anuario do Instituto de Geociencias, 43*, 266-272. doi:10.11137/2020_1_266_272

Zhao, H., Zhang, B., Wu, C., Zuo, Z., Chen, Z., & Bi, J. (2014). Direct georeferencing of oblique and vertical imagery in different coordinate systems. *ISPRS Journal of Photogrammetry and Remote Sensing, 95*, 122-133. doi:https://doi.org/10.1016/j.isprsjprs.2014.06.001

Scientific Papers. Series E. Land Reclamation, Earth Observation & Surveying, Environmental Engineering. Vol. XII, 2023
Print ISSN 2285-6064, CD-ROM ISSN 2285-6072, Online ISSN 2393-5138, ISSN-L 2285-6064

DIGITAL CONSERVATION OF HERITAGE BUILDINGS USING A UAV SYSTEM CONFIGURED FOR LATERAL SCANNING AND IMAGES, COMBINED WITH A HYBRID PROCESSING METHOD

Daniel ILIE[1, 2, 3], Constantin MOLDOVEANU[1], Octavian Laurentiu BALOTA[2, 4]

[1]Technical University of Civil Engineering of Bucharest, 122-124 Lacul Tei Blvd, District 2, Bucharest, Romania
[2]Romanian Society of Photogrammetry and Remote Sensing, 124 Lacul Tei Blvd, District 2, Bucharest, Romania
[3]Terra Advanced Technologies SRL, 149 Bahluiului Street, Ploiesti, Romania
[4]University of Agronomic Sciences and Veterinary Medicine of Bucharest, 59 Marasti Blvd, District 1, Bucharest, Romania

Corresponding author email: danielilie17@yahoo.com

Abstract

The preservation of heritage buildings is essential in a modern society that understands the importance of architecture, culture, and history. The lack of reconstruction funds or the vision of the decision-makers can delay the realization of the works to protect these buildings. The digital conservation of these buildings can be a solution for a later reconstruction or for the creation of a realistic virtual museum. The article presents the rigorous setup and calibration of an airborne side scanner mounted on a UAV platform. Acquiring fine architectural details involves the use of more precise scanning sensors, with substantially higher costs, leading to delays. The present study shows that medium precision scanning sensors can also be used for digitizing architectural details. The side scan solution can be applied successfully in the digital preservation of buildings with a medium degree of detail, but it can also be useful in complex cases. Using optimal processing methods greatly improves the internal accuracy of the modelling with little loss in accuracy. The proposed methodology can be applied even when using superior sensors, leading to exceptional results.

Key words*: digital modelling, lateral scanning, UAV, LIDAR, heritage, hybrid processing.*

INTRODUCTION

Digital preservation of heritage buildings can be achieved through terrestrial scanning (Mentzer, 2021) or through image-based photogrammetric modelling. The present research paper aims to bring to the forefront a new method of achieving numerical modelling of heritage buildings. This new method involves setting up an airborne lateral scanning system and taking images for the reconstruction of historic building facades. The configuration of this system is based on an existing Unmanned Aerial Vehicle (UAV) system with vertical acquisition for optical imagery and a Light Detection and Ranging (LIDAR) sensor. To produce realistic models, a hybrid method is proposed, combining LIDAR data with images acquired from facades.

Setting up such a system will bring a degree of practical novelty, adapted to atypical situations where vertical or tilted scanning did not produce satisfactory results. The usefulness of this system will not only be in the field of heritage buildings but also in other areas such as: monitoring of cliffs, scanning of bridges (including the lower structure), scanning of communication towers and equipment installed on them, complementing scans carried out in industrial areas, etc.

Furthermore, a hybrid method of processing the scanned LIDAR data to obtain superior digital modelling of the sensor construction parameters is presented. The purpose was to develop a methodology that, by processing medium quality data, would generate a high-quality digital model that would approximate as closely as possible the architectural details of the building. The methodology requires the creative combination of calibration methods, acquisition processes, processing methods and known software solutions.

The implementation of this innovative procedure will effectively contribute to the digital preservation of heritage buildings,

memorial houses, historical ruins, or archaeological sites.

One of the largest digital reconstructions based on LIDAR scanning was Notre-Dame Cathedral in Paris after the fire in April 2019. Terrestrial LIDAR scanning was used to preserve the lateral architectural details, ensuring high precision on the detail elements. This technology has also been used for the digital reconstruction of other heritage buildings such as the Statue of Liberty in New York, the Royal Palace in Madrid, the Opera House in Rhode Island (Development Team of Leica GeoS, 2020) or the Saigon Opera House - one of Ho Chi Minh City's most elegant and historic cultural assets (Nuron, 2021). Research using this method of reconstruction has also been carried out in Romania, the interest growing with Timișoara winning the title of European Capital of Culture in 2021 (Alionescu et al., 2019). Globally, the importance of the need to preserve heritage buildings has increased after the Paris tragedy (Buczkowski, 2019), but it has always been a subject of interest for researchers (Paul-Martin, 2020).

Terrestrial scanning provides high accuracy and represents a good solution for scanning heritage buildings (Carber-White, 2021). For even higher accuracy of digital reconstruction for correlation of multiple terrestrial scans, classical geodetic methods were used (Baik et al., 2021). However, in certain situations, this method of heritage conservation has several disadvantages that can hardly be eliminated or resolved. The most well-known disadvantage arises from the fact that scanning is done from ground level, thus generating areas that are only partially scanned, these being shadowed by other architectural elements (Almukhtar et al., 2021; Boardman et al., 2018). Among the most popular technologies to eliminate these disadvantages are reconstruction from aerial imagery (Desa et al., 2021; Ehtemami et al., 2021) or LIDAR scanning reconstruction using UAV platforms (Alessandra et al., 2020; Maté-González et al., 2022). Reconstruction using aerial photogrammetric imagery often does not give a satisfactory degree of accuracy (Hu et al., 2021). Much better results have been obtained by combining various types of imagery (satellite, nadir aerial photograms, oblique or low-altitude, as well as imagery acquired from the ground) to obtain a complex three-dimensional model (Choi et al., 2021). One of the methods used to improve accuracy is the integration of terrestrial scanning with photogrammetric modelling based on nadir or oblique aerial imagery (Alessandra et al., 2020; Costantino et al., 2021; Lerones et al., 2021).

Another method is to acquire images at the same time as aerial LIDAR scanning, thus considerably improving the geometric accuracy of the 3D model and the visual quality of the details (Development Team of Hexagon, 2020). The reconstruction of heritage buildings through this technology is done by vertical scanning and thus there are areas of the walls that are only partially scanned (Boardman et al., 2018).

In other cases, various fewer common methods have been used to eliminate these shortcomings of terrestrial laser scanning. One example is the installation of the scanner on the boom of a crane for scanning the floors of the Mores Bell Tower at various heights (Vacca et al., 2012).

Precise handheld scanners are also a solution to complement three-dimensional models obtained by terrestrial laser scanning (Ramsey, 2020). Newer technologies are LIDAR scanners based on the GeoSLAM principle (Fowkes, 2020). This operating principle has been implemented in handheld or airborne scanners which can operate both outdoors and indoors (Development Team of GeoSLAM, 2021), but have a much larger operating range than precise handheld scanners. For indoor scanning, research has also been performed in GeoSLAM scanning technology using Unmanned Ground Vehicle (UGV) (Wei et al., 2021).

Another method of scanning the 3D model of a heritage building is automated mobile (Wang et al., 2019) or pedestrian scanning with backpack-type systems (Erdal et al., 2021). In this case, some of the areas hidden behind other architectural details are scanned in detail at scanner level only.

In terms of research on side-scanners installed on UAV platforms, a lateral LIDAR system tested for scanning the interior of a forest to measure forest biomass has been identified (Hyyppä et al., 2020). However, this system does not have RGB (integrated optical camera) information and has not been used in reconstructions of heritage buildings or historical sites. Another system that could also

scan sideways is Zenmuse L1, designed by DJI. This is mounted on a gimbal that can scan sideways, but its scanning accuracy is not feasible for architectural reconstructions (horizontal 10 cm @ 50 m, vertical 5 cm @ 50 m - achieved under optimal laboratory conditions) (Development Team of DJI, 2021). There are also no known applications of this system in the field of conservation of heritage buildings. Moreover, the setup of this new system is part of a whole innovative procedure for acquiring and processing LIDAR data for digital modelling of heritage building facades.
The potential of LIDAR-UAV platforms is still unexploited to its true value (Kadhim et al., 2021). This is why it is necessary to deepen new methods of acquiring, processing but also configuring new systems for the reconstruction of heritage buildings or historical sites.

MATERIALS AND METHODS

1. Equipment used

The configuration of the lateral scanning system was done by physical methods, making a system to attach the reconfigured system to the drone body. The center of gravity of the scanning system was balanced with the entire UAV assembly. This new scanning system will be calibrated in terms of coordinate axis systems for each component (Global Navigation Satellite System or GNSS, LIDAR, Camera). The following equipment was used for this procedure: UAV drone DJI MATRICE M600 with LIDAR VLP 16 Puck Lite sensor, Sony α6000 camera, CPU (central processing unit) with Inertial Measurement Unit (IMU) ADIS 16488 sensor, SPAN OEM6 receiver, DJI Dual D-RTK GNSS (rover) antennas, CHC GPS X900 (or similar) reference (base) station. Tools such as screwdrivers, calliper compasses, square with the toric level, physical coordinate axis systems, etc. were used to set up and physically calibrate the system. Software solutions used for data acquisition and processing: Phoenix Spatial Explorer, Phoenix LightHouse, Novatel Inertial Explorer, Terra Scan, Terra Match, Terra Modeler, Pix4D Mapper, Potree-Prosig, etc.

2. Test area: Little Trianon Palace

To highlight the scanning capacity of the new system, a heritage building in urgent need of digital preservation was chosen. The Little Trianon Palace is a building in a strong state of decay, but still has many architectural elements that are well worth preserving or even restoring. Also known as the Cantacuzino Palace in Florești (Prahova County, Romania), it was designed by the famous architect Ion D. Berindey (who also designed the Cantacuzino Palace in Bucharest, the current "George Enescu" National Museum). The origin of this project is inspired by the architecture of the Petit Trianon and Grand Trianon Palaces, which are found in the gardens of the Palace of Versailles in France. The building was built in the *Mavros* style and is dominated by *rococo* and *neoclassical* architectural elements. The facades were made of white Albești limestone, where several bas-reliefs are carved. Although almost completed in 1913, this heritage building has suffered numerous destructions over the years. After the 1977 earthquake, the inner walls of the palace and its ceiling collapsed. Today only the outer walls of the palace remain, which are still witnesses of the architectural beauty.

3. Preliminary sensor calibration

In order to acquire qualitative data, the newly configured system had to be rigorously calibrated. The reference system that defines the entire assembly is the IMU coordinate system (also called the "navigation center"). For this reason, all sensors of the scanning system must be calibrated relative to the coordinate system of the IMU. The IMU sensor was mounted with X Vehicle-Left, Y Vehicle-backward and Z Vehicle-up axis relative to the UAV orientation. The first stage of the calibration involved determining the translations from the IMU to each sensor in the IMU coordinate system. Along with these translations, the rotation angles to be applied to each sensor to bring it into the IMU coordinate system were also determined. The rotations on each axis are determined in an approximate way, and in the second step they are calibrated in a rigorous way. For the determination of translations and rotations, the definition of coordinate systems for each sensor, the definition of coordinate vehicles and other auxiliary systems were considered, depending on the software applications in which the processing was performed. The preliminary calibration of the

optical sensor with respect to the IMU Body Frame is shown in Table 1

The orientation parameters of the LIDAR sensor in relation to the IMU sensor, determined in the preliminary calibration step, are centralized in Table 2. From these parameters the correction angles on each laser head were determined.

4. Calibration of the navigational system

After mounting the IMU-LIDAR-Camera sub-assembly on the UAV platform, the calibration of the navigation system was performed. Correlation of the IMU Body Frame with the coordinate system of the UAV, Vehicle Frame (X Vehicle-Right, Y Vehicle-backward and Z Vehicle-up) is necessary for processing the flight trajectory relative to the UAV orientation. Thus, to bring the aircraft into the IMU system requires a rotation around the Z-axis of 180° (direction is not relevant), the origin of the system being identical to that of the IMU. The second component of this system is the correlation of the positioning system (the two DJI Dual D-RTK GNSS antennas) by determining the translations in the Vehicle Frame system (Table 3).

The input of offsets into the data acquisition application was done in the IMU coordinate system (Spatial Explorer).

5. Precise calibration of the side scan system

Lateral scans of the three accessible facades were made with the preliminary calibrated system, as well as a vertical scan with the UAV-M600-VLP32c-SonyA7RII system. Lateral scans differ from nadir scans primarily by lower accuracy. The facade of the scanned building, as well as other obstructions that are in its vicinity, can significantly limit the satellite signal. In the present study, there were additional obstructions on all facades, which resulted in a significant decrease in the accuracy of the trajectory recorded by the GNSS antennas. A static ground calibration of the IMU sensor was performed at both the beginning and end of each flight mission. The calibration procedures of the inertial data with GNSS measurements were carried out in the air, through a straight flight line and three infinity-shaped figures (Development Team of NovAtel, 2019). Scanning was done by performing vertical scan lines at a very low speed (less than 1 m/s). In the case of vertical trajectories executed at low speed, the accuracy of the inertial data degrades rapidly. Obstructions and poor satellite data amplify this effect as the inertial sensor recalibrates with each UAV positioning.

Table 1. Preliminary calibration of the optical sensor, Sony α6000 Camera

Operation	X axis	Y axis	Z axis	RMS_X	RMS_Y	RMS_Z	Remarks
Offsets from Vehicle Frame -> Camera Sys.	-0.023m	0.123m	0.063m	0.002m	0.002m	0.002m	Used in post-processing (PP) Used for OPK Export, Extrinsic Rotations X Y Z (Inertial Explorer)
Vehicle Frame rotations -> Camera Sys.	90°	0°	180°	-	-	-	
Offsets from IMU Frame -> PLS Camera Sys.	-0.023m	0.063m	-0.123m	0.002m	0.002m	0.002m	Used in PP, RT, LAS Export in UTM, Extrinsic Rotations Z X Y (Spatial Explorer)
IMU Body Frame Rotations -> PLS Camera Sys	0°	0°	180°	-	-	-	

Table 2. Preliminary calibration of the VLP16 LIDAR

Operation	X axis	Y axis	Z axis	RMS_X	RMS_Y	RMS_Z	Remarks
Offsets from IMU -> PLS LIDAR System	-0.023m	-0.047m	0.004m	0.001m	0.001m	0.001m	Used in PP, Real-Time (RT), LAS export LAS in UTM. Extrinsic Rotations Z X Y (Spatial Explorer)
IMU Body Frame Rotations -> LIDAR Frame	0°	-135°	180°	-	-	-	

Table 3. Calibration of the Dual D-RTK GNSS system

Offsets from IMU to	X axis	Y axis	Z axis	RMS_X	RMS_Y	RMS_Z	Remarks
GNSS 1	-0.182m	0.021m	0.452m	0.001m	0.001m	0.001m	Used in post-processing PPK (Inertial Explorer)
GNSS 2	0.138m	0.021m	0.452m	0.001m	0.001m	0.001m	

Table 4. Calibration values of the Sony α6000 camera

Operation	X axis	Y axis	Z axis	RMS_X	RMS_Y	RMS_Z	Remarks
Vehicle Frame rotations -> Camera Sys. (ST70)	90.9226°	0.0648°	-179.8502°	0.0191°	0.0617°	0.0286°	Used in PP in ST70. Extrinsic Rotations X, Y, Z (Inertial Explorer)
Vehicle Frame rotations -> Camera Sys. (UTM)	90.9081°	0.0522°	-179.8581°	0.0182°	0.0617°	0.0289°	Used in PP in UTM. Extrinsic Rotations X, Y, Z (Inertial Explorer)
IMU Body Frame Rotations -> PLS Camera Sys	-0.9081°	-0.0522°	0.1419°	0.0191°	0.0617°	0.0286°	Corrections for extrinsic rotations. Used in PP, RT, LAS Export (Spatial Explorer)

Thus, the poor quality of the inertial and positioning data is also reflected in the accuracy of the trajectory, as well as in the quality of the acquired data. Consequently, it was decided to make additional calibration figures (∞) every two flightlines. However, the low accuracy of the flight path makes it necessary to identify new processing procedures to improve the accuracy of LIDAR data.

Trajectory kinematic post-processing (PPK)

To counteract the effect of satellite obstructions, the flight paths were post-processed with at least two fixed ground stations. The base network of all flights was made using the static GNSS method, to reduce the accumulation of as many errors as possible.

The post-processing kinematics of the trajectory was realised in the NovAtel Inertial Explorer application, using the best method for data processing, according to the circumstances of each flight. For trajectories with good positioning and low accuracy of the IMU data, post-processing was performed using the loosely correlated method. In case the satellite data presented multiple obstructions and the number of satellites was low, tightly correlation between GNSS and the IMU data was chosen, to obtain a trajectory estimate as close as possible to the reality. The configuration of the processing mode differed from one flight to another, depending on the context, the number of satellites, as well as their distribution.

Rigorous camera calibration

The calibration of the interior orientation parameters of the camera was carried out with the help of the PIX4D Mapper application based on a flight specially designed for this purpose on the southern facade. A hybrid calibration flight was designed, based on the principles of calibration from classical photogrammetry, as well as from terrestrial photogrammetry taken from mobile platforms. Thus, vertical and longitudinal flight strips were made, as well as strips from a different scanning distance. Longitudinal coverage ranged from 90% to 100%, and transverse coverage was at least 60%. As a result, each tie point was identified on dozens of images helping to better calibrate the internal parameters of the camera, the external orientation angles of the images, as well as the IMU sensor. These principles of flight realization helped to calibrate the focal length and internal orientation parameters without using control points on the building facade.

The determination of the boresight corrections on the three axes of rotation was achieved through a combined process between the PIX4D Mapper and NovAtel Inertial Explorer applications. Therefore, starting from the angles ω, φ, κ obtained from the Automatic Aero Triangulation (AAT) process, the angular corrections on each axis were calculated for the rigorous calibration of the optical sensor at the IMU. Since LIDAR data processing is performed in the Universal Transverse Mercator (UTM) system, it was also necessary to calibrate the camera in this coordinate system for points fusion with the optical data. The rigorous calibration of the camera in relation to the IMU sensor was carried out both in the UTM system and in the Stereographic 1970 system, with small differences in the angles ω, φ, κ depending on the coordinate system used. The calibrated values of the initial rotations (Table 1) are centralized in Table 4.

Following the calibration, the angular errors on the three external orientation angles of the images decreased significantly compared to the initial errors (Figure 1).

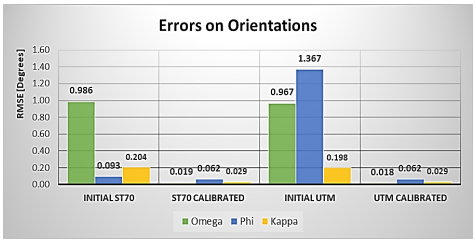

Figure 1. External Orientation Errors - before and after camera calibration with respect to the IMU sensor

After calibration, the LIDAR data was exported in LAS format (UTM system) for rigorous calibration in the TerraScan and TerraMatch applications, respectively. The transformation of LIDAR data into the national systems of Romania (Stereographic 1970) was realised at the final stage, due to considerations related to accuracy and the software applications used.

Rigorous calibration of laser heads

Correction angles on each laser head were determined using the TerraMatch application. To be able to perform the calibration, a hybrid calibration method was used, using both principles from the calibration of aerial scans and from mobile (terrestrial) scans. To calibrate the correction angles for each laser head it was decided to use two perpendicular facades as in the case of mobile scans. But with lateral scans, horizontal surfaces (such as the ground surface) are affected by much larger errors due to the large incident scan angles. Additionally, hard horizontal surfaces are required for mobile scanner calibrations. In the present study there are no such surfaces, the land around the palace being lawn type. Therefore, a hybrid way of calibration was identified, using the facades of two perpendicular walls, but also the horizontal surfaces, as well as the inclined ones that are part of these facades (sills, windowsills, beams, ceilings, columns, etc.).

Scans made on the southern and eastern facade were used. A total of 12 vertical strips, 3 detail strips and one horizontal strip on each side were used.

The LIDAR points were classified by object classes for each strip and for each laser head (16 heads). The facades that were used in the calibration of the LIDAR heads were classified in a separate class of objects. The calibration was made based on the corresponding lines (tie lines) identified on each strip, generated by the 16 laser heads.

The TerraMatch application was not designed for calibrations based on side scans. However, if one forces the parameterization contrary to the user manual, very good results can be obtained. Normally, horizontal lines (perpendicular or along the flight) as well as lines of constant slope are searched on the ground class, where in theory there must be scans of hard surfaces (roads, platforms). In the current study there is no such class on which to generate reliable results. Consequently, the application was forced to identify the corresponding horizontal and oblique lines in the object class in which the two facades were classified. More than six thousand sections of corresponding lines were identified between the laser data of each head, in the coverage areas. The lines identified on the south facade, as well as working process in TerraMatch, are exemplified in Figure 2.

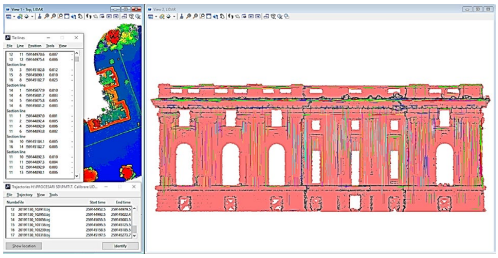

Figure 2. Identifying the corresponding tie lines on the Southern facade - TerraMatch

The length of the sections where the corresponding lines were searched was established according to the average density of points on the facades, generated by each individual laser head. Therefore, corresponding lines were searched in sections that varied from 0.8 m to 5.0 m. Using the corresponding lines from each section, but also the post-processed flight paths, the three correction angles on each laser head were determined (Figure 3).

In order for the obtained data to be reliable, corresponding lines that have a direct impact (on their direction) in solving each angle (yaw, pitch, roll) must be used. Another important point is that this calibration does not adjust the flight bands to each other. By calibrating the laser heads, only the internal accuracy on each band is improved. This is an internal strips calibration and not a calibration between strips.

Theoretically, through this type of calibration, we want to get as close as possible to the internal accuracy of the sensor used, VLP16 (± 3 cm) on each strip (Development Team of Velodyne, 2016). In order to obtain qualitative data for the preservation of the architectural details, in the next step the LIDAR strips will be calibrated, using the data corrected with the angular values from Figure 3.

	Translation X/right	Translation Y/up	Translation Z/rear	Rotation X/pitch	Rotation Y/yaw	Rotation Z/roll	Rotation
1	0.000 m	0.000 m	0.000 m	0.1358 °	0.0259 °	-0.0319 °	0.14°
2	0.000 m	0.000 m	0.000 m	0.0921 °	-0.0488 °	0.0099 °	0.10°
3	0.000 m	0.000 m	0.000 m	0.1810 °	0.0190 °	-0.1262 °	0.22°
4	0.000 m	0.000 m	0.000 m	0.0982 °	-0.0134 °	0.0154 °	0.10°
5	0.000 m	0.000 m	0.000 m	0.1236 °	-0.0072 °	-0.0212 °	0.13°
6	0.000 m	0.000 m	0.000 m	0.0990 °	-0.0347 °	0.0039 °	0.10°
7	0.000 m	0.000 m	0.000 m	0.1233 °	-0.0194 °	-0.0214 °	0.13°
8	0.000 m	0.000 m	0.000 m	0.1131 °	-0.0268 °	0.0059 °	0.12°
9	0.000 m	0.000 m	0.000 m	0.1109 °	-0.0178 °	-0.0177 °	0.11°
10	0.000 m	0.000 m	0.000 m	0.0919 °	-0.0189 °	0.0033 °	0.09°
11	0.000 m	0.000 m	0.000 m	0.1240 °	-0.0232 °	-0.0121 °	0.13°
12	0.000 m	0.000 m	0.000 m	0.0904 °	-0.0343 °	0.0024 °	0.10°
13	0.000 m	0.000 m	0.000 m	0.1008 °	-0.0041 °	0.0103 °	0.10°
14	0.000 m	0.000 m	0.000 m	0.0965 °	-0.0097 °	0.0035 °	0.10°
15	0.000 m	0.000 m	0.000 m	0.0919 °	-0.0356 °	0.0081 °	0.10°
16	0.000 m	0.000 m	0.000 m	0.1119 °	-0.0216 °	0.0052 °	0.11°

Figure 3. Applying determined corrections for each laser head - Phoenix Spatial Explorer

6. Hybrid procedure for side scan processing

As previously shown, the quality of side scans is much lower than that of nadir scans. To improve the quality of the scanned data, it is necessary to perform a data calibration based on correlation algorithms. As in the case of the calibration of the laser heads, the corresponding lines will be used to calibrate the LIDAR strips. This time the corresponding lines are searched between the strips and will be used for angular corrections, but also for fine positioning corrections (determined by fluctuating positioning errors of the trajectory).

Correction of systematic errors

In the case of lateral LIDAR scans, the systematic errors are defined by angular rotations (*yaw*, *pitch*, *roll*) and three-dimensional translations (*north*, *east*, *elevation*) which are constant on each scan strip.

In Figure 4 a cross-section on the western facade is exemplified where the influence of systematic errors can be seen (the points in the section have different colours for each overlapping strips).

Corresponding lines were searched for each strip separately, using all the data from the 16 laser heads. Therefore, the point density is very high compared to the previous calibration procedure.

In this context, the search sections of the corresponding lines varied between 0.4 m and 5.0 m. As with the laser heads, horizontal and inclined lines were also searched on the facades, being the only hard surfaces in this case study. To limit errors due to the incident scanning angle, the LIDAR data were filtered at an angle of 80°, perpendicular to the scanning direction (building facades). The inconsistency between scan bands is generated equally by the poor quality of positioning and attitude. Therefore, an iterative method for block determination of angular rotations (*yaw*, *pitch*, *roll*) and of three-dimensional translations (*north*, *east*, *elevation*), related to each scan strip will be addressed.

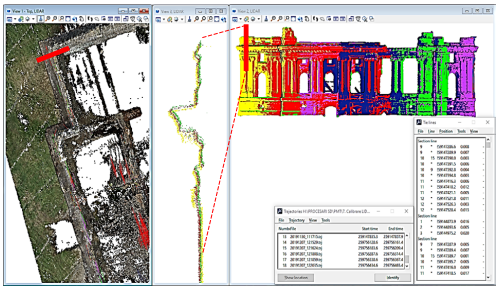

Figure 4. Calibration of LIDAR data on strips using only building facades - TerraMatch

Systematic error calibration was performed on all three facades in two iterations, using over 2500 sections in each iteration. After determining the corrections in iteration 1, they were applied to each individual strip. After applying the corrections, the quality of the LIDAR data was verified by survey with the help of cross-sections, but also with the help of statistical reports on the average magnitude on the data of the building facades (0.043 m).

In the second iteration, the process of identifying the corresponding lines between the strips was resumed on the corrected data set. After determining and applying systematic corrections (significantly smaller in this iteration) an average magnitude of 0.031 m was obtained.

This value is very close to the theoretical scanning capability of the VLP16 sensor (± 3 cm), which is why another iteration would not significantly improve the internal accuracy of the LIDAR data.

Correction of random errors

Visual verification of LIDAR data through cross-sections and longitudinal sections is absolutely necessary and cannot be replaced by statistical reports generated by processing applications (TerraMatch in this case). Random errors can hide behind a statistical report that appears to confirm the high quality of a dataset. In the case of the present study, under the circumstances outlined above, it is erroneous to assume that the scan strips are not also affected by significant random errors in some areas. Following visual checks, several such areas were identified, which confirmed the above hypothesis. As in the case of data strip calibration, random errors were considered to be caused by angular rotations (*yaw*, *pitch*, *roll*) as well as three-dimensional translations (*north*, *east*, *elevation*), affecting small portions or in different proportions a LIDAR data strip.

To correct these random errors, the procedure described above was used, but using small working sections (between 0.3 m and 1.5 m). Their density was much higher than in the previous cases, searching for corresponding lines at distances of up to 0.1 m between them. The underlying principle is to cover the entire scanning duration with corresponding lines. Corrections can therefore be calculated for each scanning second, in relation to the time position on the scan line. Since calibration processes are themselves affected by errors in identifying correlation lines, it was considered that a correct application is one that is also correlated with the a priori flight trajectory accuracy determined for each second. Therefore, the identified corrections were weighted according to the trajectory errors at that time position (Figure 5).

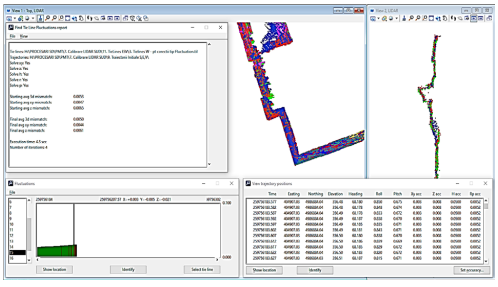

Figure 5. Determination and application of random errors in correlation with flight trajectory accuracy, TerraMatch

More than 7000 sections with corresponding lines were used to determine random corrections. In most cases, the position corrections were in the order of millimetres. Following the visual checks undertaken, no further random errors were identified on the facades of the Little Trianon Palace. However, the average amplitude remains around 3 cm.

Improvement of lateral scanning accuracy

Even if the data has been calibrated close to the maximum scanning potential of the LIDAR sensor, a dispersion of about ± 3 cm is not desirable when scanning architectural details such as stucco, bas-reliefs, blazons, pattern columns, etc. In this case, the theoretically best solution is to use a scanning sensor with a much higher internal accuracy. But this is not always feasible, mainly because of high costs.

At the end of the calibration procedure, it is proposed to improve the internal accuracy of the current data.

With accurately calibrated data, but also with a very high density of points (over 90 points/dm^2), it is possible to use the average of the dispersion over the scanned area. Three-dimensional segmentation based on a value that fits the magnitude of the data and does not affect the scanned details is used to make this adjustment. The adjustment of the maximum magnitude of the data was performed iteratively, using a 6 cm segmentation and then a 3 cm segmentation. Thus, the internal accuracy of the scanning performed was optimised to 5-10 mm, with little loss of data accuracy. Surface averaging requires LIDAR data free of noise points and well calibrated between strips.

In areas affected by such errors, surface averaging improves the internal accuracy of the LIDAR data but can also leave noise points behind. This can be removed by a statistical filtering algorithm in TerraScan.

Figure 6 shows a section on the eastern facade with the sequential calibration between strips 5, 6 and 7.

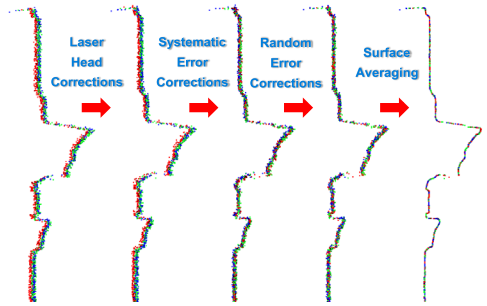

Figure 6. Example of sequential calibration performed between strips 5, 6, 7 (East)

The quality of the final data is also highlighted in Figure 7 using the visualization in the Potree-Prosig application (Schuetz, 2016).

Figure 7. Viewing calibrated LIDAR data in the Potree-Prosig web application

The aim of this research is to highlight the quality optimizations that can be achieved by various processing methods. This does not mean that fine architectural details can be reconstructed by average quality sensors. The recommendation is that scans should be performed with sensors of the highest accuracy, which through calibration and processing can produce truly stunning results.

RESULTS AND DISCUSSIONS

1. Digital model of the Little Trianon Palace

In order to obtain the digital model of the scanned facades, the final data was filtered for vegetation near the facades as well as vegetation growing on the walls or in the window area. The LIDAR scan was also filtered by the supporting scaffolding of degraded columns on the west side of the ruins (Figure 8). The digital model of the facades was classified into a separate object class for ease of use.

2. Integration of lateral and vertical scans

In order to have a complete model of the ruins of the Little Trianon Palace, the lateral scan was enriched with data from the nadir scan. The completion was done for the inner areas of the ruin and for the upper parts where the data from the lateral scans were insufficient. The ground control points (base network), the post-processed trajectory and the rigorous calibration ensured the accuracy required to combine the two data sets. The selection of data from the vertical flight was performed with the TerraScan application, using selection procedures in the vertical plane as well as on sections. The final digital model was highlighted with the Potree-Prosig web application in Figure 9.

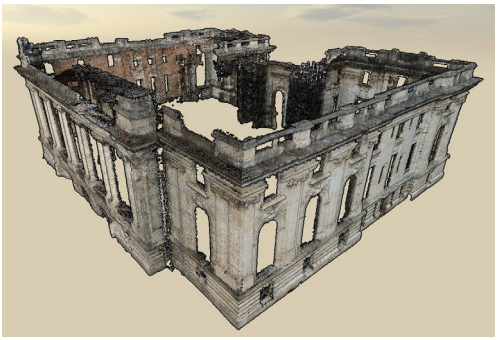

Figure 8. The digital model of the facades - visualization in the Potree-Prosig web application

Figure 9. The complete digital model of the Little Trianon Palace - Potree-Prosig visualization

In the end, the data were accurately transformed into national coordinate systems using RoTLAS APP v1.62 (Ilie et al., 2022). The accurate model transformation can be useful in the design and execution of the rehabilitation of this heritage building.

3. Creating the realistic 3D model

The flights performed did not have the primary purpose of three-dimensional modelling based on the images taken. However, the images taken laterally can be combined with those taken nadiral to obtain a realistic 3D model.

Realistic modelling based on optical data

The following data were used to obtain this model: calibrated interior orientation parameters and exterior orientation data with corrected rotation angles in national coordinate systems. The application used for the realistic modelling of the whole Little Trianon Palace was PIX4D Mapper. It generates optimal results that can be used later in various digital projects such as those based on virtual reality (VR), digital twins or augmented reality (AR). The model obtained preserves quite a lot of the architectural details of the facades (Figure 10), but for precision details it is necessary to use another software solution.

Figure 10. 3D modelling of the Little Trianon Palace based on lateral and vertical images - PIX4D Mapper

However, quite a lot of errors are found in the mesh surface, in areas with noise points. The result can be improved by a manual and laborious filtering of the points in the dense cloud. Using LIDAR scans in combination with optical data can bring more accuracy for realistic modelling.

For the finest modelling, the 3DF Zephyr software solution was used. This application generates qualitative results using only images, as can be seen from the 3D bas-relief generated on the Eastern facade shown in Figure 11.

Figure 11. 3D detail of the bas-relief of the Eastern gate - image based model - 3DF Zephyr

Hybrid modelling of the heritage building

In order to eliminate the deficiencies generated by three-dimensional image-based models (scale errors, noise points, non-conforming textures, voids, etc.) a hybrid modelling based on LIDAR data was chosen. Using the imagery taken on the southern facade, the reconstruction of the model was performed. The dense cloud was aligned and scaled to the LIDAR cloud, calibrated and transformed to national coordinate systems. This georeferencing helped to correlate the images with the LIDAR point cloud. Finally, a qualitative three-dimensional model was produced using the LIDAR data and the images correlated with it (Figure 12).

Figure 12. Hybrid 3D model - LIDAR and optical data - 3DF Zephyr

For a rigorous analysis of the obtained hybrid model, it was compared with the classical realistic model obtained from the images and the dense point cloud. A detailed comparison is

shown on the bas-relief on the south facade in Figure 13.

Figure 13. Modelling the bas-relief on the southern facade: based on images (left) and based on LIDAR and Images (right) - 3DF Zephyr

This application is an excellent solution for realistic qualitative models, optical or hybrid generated. Although the application is optimized for big data management, the major disadvantage is that 3D models cannot be easily used in generic visualization applications due to the huge amount of data.

CONCLUSIONS

Scanning fine architectural details involves using the most accurate scanning sensors possible. High accuracy usually brings with it substantially higher costs, so the digitisation of heritage buildings is often delayed. This study has shown that medium accuracy scanning sensors can also be used to preserve architectural details through digitisation. The lateral scanning solution can be successfully used in the digital reconstruction of buildings with a medium degree of detail (such as memorial houses) but can also be useful in more complex cases. The solution does not offer the quality of a high-precision sensor, but optimal processing methods greatly improve the internal accuracy of the modelling, with little loss of accuracy. Therefore, the proposed methodology can be applied even when using superior sensors, leading to exceptional results.

Rigorous calibration of a side scanning system is essential and increases data accuracy. Systematic errors and most of the random errors can be corrected by correlation methods between scanning strips. Most of the time this process is iterative and requires a lot of processing time. Consequently, it is desirable to avoid the accumulation of such errors by using the best LIDAR data acquisition procedures. This is not always possible, which is why the proposed hybrid method for calibration and processing is an optimal solution.

Surface averaging by segmentation must be done with caution so not to lose too much of the accuracy of the scanned shapes. Using it at the same time as preserving fine detail can lead to noise points in certain areas of the scan.

Calibration of the optical sensor to the IMU, and calibration of the LIDAR to the IMU, are essential to obtain LIDAR data with correct RGB information. Calibration of LIDAR data is necessary if hybrid 3D modelling desired.

Digital models are much easier to visualise and to use than realistic 3D models. Three-dimensional realistic models can be produced using both side images and a combination of LIDAR and optical data. The quality of the models produced by the two methods is approximately similar (Figure 13), but an increase in the quality of detail is observed in the image-based model. It should be noted that this accuracy was also ensured due to the very high resolution of the images (the pixel on the building facade being of the order of 3-5 mm). Moreover, the quality of the image pattern is determined by the use of images with a longitudinal coverage of about 90%. In the context of images with lower coverage, the quality of the resulting model would be poorer and would include shape and scale deformations. Therefore, the use of a hybrid method is a very correct option to generate 3D models. In this sense, the LIDAR data cloud can be used for scaling and constraining the dense point cloud or it can be used to make the digital twin models (Ćosović et al., 2022). The digital model of the Little Trianon Palace has been made available to the private owner via the Potree-Prosig web application. This will be launched on the official website to offer the possibility of virtual tours of the Little Trianon Palace or to implement a digital twin model.

Even though the internal accuracy of the LIDAR sensor is not very suitable for scanning heritage buildings with complex architectural details, the side scanner can be useful in many other types of work. These include scanning sea cliffs, scanning surface mining operations, scanning bridge infrastructure, scanning towers or power poles, etc. The boresight camera calibration and the LIDAR sensor calibration, both performed in relation to the IMU, determine a calibration

between the two acquisition sensors as well. As a result, LIDAR data can be accurately fused with optical data. Hybrid methods of calibrating and enhancing LIDAR data can also be successfully applied to mobile scans.
The calibration and configuration of this system opens up similar new research opportunities. In this regard, the configuration of a shore scanning system that can be used from a boat or an autonomous system is being considered.

ACKNOWLEDGEMENTS

The applications used were provided by Tehnogis Grup SRL, Prosig Expert SRL and the Technical University of Civil Engineering of Bucharest. A demo license was used for 3DF Zephyr. Finally, we thank to all those who directly or indirectly supported this research.

REFERENCES

Alessandra, C., Antonino, M., Mirko, S., & Domenica, C. (2020). *Integration of terrestrial laser scanning and UAV-SFM technique to generate a detailed 3D textured model of a heritage building.* Paper presented at the Proc.SPIE.

Alionescu, A., Herban, S., & Vilceanu, C. B. (2019). *3D modelling of cultural heritage objective in Timisoara using precise LiDAR* (Vol. 2116).

Almukhtar, A., Saeed, Z. O., & Tah, H. A. a. J. H. M. (2021). Reality Capture of Buildings Using 3D Laser Scanners. *MDPI, CivilEng*. doi:10.3390/civileng2010012

Baik, A., Almaimani, A., Al-Amodi, M., & Rahaman, K. R. (2021). Applying digital methods for documenting heritage building in Old Jeddah: A case study of Hazzazi House. *Digital Applications in Archaeology and Cultural Heritage, 21*, e00189. doi:https://doi.org/10.1016/j.daach.2021.e00189

Boardman, C., Bryan, P., McDougall, L., Reuter, T., Payne, E., Moitinho, V., Rodgers, T., Honkova, J., O'Connor, L., Blockley, C., Andrews, D., Bedford, J., Sawdon, S., Hook, L., Green, R., Price, K., Klÿn, N., & Abbott, M. (2018). *3D Laser Scanning for Heritage. Advice and Guidance on the Use of Laser Scanning in Archaeology and Architecture*.

Buczkowski, A. (2019). *How the tragic fire at Notre Dame will accelerate the adoption of laser scanning of historic architecture. Retrieved from* https://geoawesomeness.com/how-the-tragic-fire-at-notre-dame-will-accelerate-the-adoption-of-laser-scanning-of-historic-architecture/

Carber-White, K. (2021). 3D Scanning Technology Plays Key Role in Historic Preservation Project. Retrieved from https://www.directionsmag.com/article/10645

Choi, Y., Yang, Y.-J., & Sohn, H.-G. (2021). Resilient cultural heritage through digital cultural heritage cube: Two cases in South Korea. *Journal of Cultural Heritage, 48*. doi:10.1016/j.culher.2021.01.007

Ćosović, M., & Maksimović, M. (2022). Application of the digital twin concept in cultural heritage. *VIPERC2022: 1st International Virtual Conference on Visual Pattern Extraction and Recognition for Cultural Heritage Understanding*.

Costantino, D., Pepe, M., & Restuccia, A. G. (2021). Scan-to-HBIM for conservation and preservation of Cultural Heritage building: the case study of San Nicola in Montedoro church (Italy). *Applied Geomatics*. doi:10.1007/s12518-021-00359-2

Desa, H., Azizan, M. A., Zulkepli, N. N., & Romeli, N. (2021). Heritage Building Modelling: Photogrammetry Challenges in Producing an As Built Drawing (ABD) Using Unmanned Aerial System (UAS). *Atlantis Press, Journal of Robotics, Networking and Artificial Life*. doi:10.2991/jrnal.k.201215.003

Development Team of DJI. (2021, 05.2021). *ZENMUSE L1 User Manual*. User Manual. China.

Development Team of GeoSLAM. (2021). Meet the ZEB Horizon: The Ultimate Mobile Mapping Tool. Retrieved from https://geoslam.com/solutions/zeb-horizon/

Development Team of Hexagon. (2020). Reporter - Geosystems Division. *REPORTER,* 88.

Development Team of Leica GeoS. (2020,19.07.2020). The Vital Role of Laser Scanning in Heritage Conservation. *Survey & Construction Technology.* Retrieved from https://globalsurvey.co.nz/surveying-gis-news/the-vital-role-of-laser-scanning-in-heritage-conservation/

Development Team of NovAtel. (2019). Waypoint Products Group - A NovAtel Precise Prositioning Product [User Manual v8.80]: Hexagon, NovAtel Inc.

Development Team of Velodyne. (2016). Velodyne LIDAR Puck Light - Light weight real-time 3D LiDAR sensor. Retrieved from https://velodynelidar.com/wp-content/uploads/2019/12/63-9378_Rev-F_Ultra-Puck_Datasheet_Web.pdf

Ehtemami, A., Park, S., Bernadin, S., Lescop, L., & Chin, A. (2021). Review of Visualizing Historical Architectural Knowledge through Virtual Reality. *HAL*.

Erdal, K., & Makineci, H. (2021). Documentation of Cultural Heritage with Backpack Lidar Usage on Photogrammetric Purpose. *Turkey Lidar Journal*. doi:10.51946/melid.921032

Fowkes, D. (2020). Bringing the past to life: 3D mapping historic sites for restoration. Retrieved from https://www.pbctoday.co.uk/news/bim-news/historic-sites-mapping/78863/

Hu, Y., Chen, X., Tang, Z., Yu, J., Chen, Y., Wu, Z., Yang, D., & Chen, Y. (2021). Collaborative 3D real modeling by multi-view images photogrammetry and laser scanning: The case study of Tangwei Village, China. *Digital Applications in Archaeology and Cultural Heritage, 21*, e00185. doi:https://doi.org/10.1016/j.daach.2021.e00185

Hyyppä, E., Hyyppä, J., Hakala, T., Kukko, A., Wulder, M. A., White, J. C., Pyörälä, J., Yu, X., Wang, Y.,

Virtanen, J.-P., Pohjavirta, O., Liang, X., Holopainen, M., & Kaartinen, H. (2020). Under-canopy UAV laser scanning for accurate forest field measurements. *ISPRS Journal of Photogrammetry and Remote Sensing, 164*, 41-60. doi:https://doi.org/10.1016/j.isprsjprs.2020.03.021

Ilie, D., Balotă, O. L., Iordan, D., & Nicoară, P. S. (2022). Algorithm and application development for precise and accurate transformation of LIDAR point clouds into national coordinate systems of Romania using official equations and quasigeoid model. *ISPRS Ann. Photogramm. Remote Sens. Spatial Inf. Sci., V-4-2022*, 181-188. doi:10.5194/isprs-annals-V-4-2022-181-2022

Kadhim, I., & Abed, F. M. (2021). The Potential of LiDAR and UAV-Photogrammetric Data Analysis to Interpret Archaeological Sites: A Case Study of Chun Castle in South-West England. *ISPRS - International Journal of Geo-Information*.

Lerones, P. M., David Olmedo, Ana López-Vidal, Gómez-García-Bermejo, J., & Zalama, E. (2021). BIM Supported Surveying and Imaging Combination for Heritage Conservation. *MDPI, Remote Sensing*. doi:10.3390/rs13081584

Maté-González, M. Á., Di Pietra, V., & Piras, M. (2022). Evaluation of Different LiDAR Technologies for the Documentation of Forgotten Cultural Heritage under Forest Environments. *22*(16), 6314.

Mentzer, R. (2021). 3D Scans Will Allow Historic Building Slated For Demolition To Be Rebuilt In Virtual Reality. Retrieved from https://www.wpr.org/3d-scans-will-allow-historic-building-slated-demolition-be-rebuilt-virtual-reality

Nuron, H. M. (2021). Heritage-BIM model to future proof an Opera House. Retrieved from https://leica-geosystems.com/case-studies/reality-capture/heritage-bim-model-to-future-proof-an-opera-house

Paul-Martin, R. (2020,1.07.2020). Preserving our world's heritage with advanced laser scanning. Retrieved from https://hxgnspotlight.com/preserving-worlds-heritage-advanced-laser-scanning/

Ramsey, D. (2020). Using 3D Scanning for Heritage Preservation. 3D Scanning. Retrieved from https://blog.trimech.com/using-3d-scanning-for-heritage-preservation

Schuetz, M. (2016). *Potree: Rendering Large Point Clouds in Web Browsers* (Engineer Bachelor Thesis), Vienna University of Technology, Vienna. (0825723)

Vacca, G., Deidda, M., Dessi, A., & Marras, M. (2012). Laser scanner survey to cultural heritage conservation and restoration. *ISPRS - International Archives of the Photogrammetry, Remote Sensing and Spatial Information Sciences, XXXIX-B5*, 589-594. doi:10.5194/isprsarchives-XXXIX-B5-589-2012

Wang, Y., Chen, Q., Zhu, Q., Liu, L., Li, C., & Zheng, D. (2019). A Survey of Mobile Laser Scanning Applications and Key Techniques over Urban Areas. *Remote Sensing*.

Wei, W., Shirinzadeh, B., Nowell, R., Ghafarian, M., Ammar, M. M. A., & Shen, T. (2021). Enhancing Solid State LiDAR Mapping with a 2D Spinning LiDAR in Urban Scenario SLAM on Ground Vehicles. *MDPI, Sensors*. doi:10.3390/s21051773

Scientific Papers. Series E. Land Reclamation, Earth Observation & Surveying, Environmental Engineering. Vol. XII, 2023
Print ISSN 2285-6064, CD-ROM ISSN 2285-6072, Online ISSN 2393-5138, ISSN-L 2285-6064

SAR-BASED SUBSIDENCE MONITORING IN URBAN AREAS DUE TO GROUNDWATER WITHDRAWAL FOR AGRICULTURE: A REVIEW WITH DEMOGRAFIC INDICATORS ASSESSMENT

Alina RĂDUȚU, Maria-Ioana VLAD-ȘANDRU

Romanian Space Agency, 21-25 Mendeleev Street, District 1, Bucharest, Romania

Corresponding author email: alina.radutu@rosa.ro

Abstract

Intensive groundwater withdrawal is one of the main causes leading to land subsidence in the natural and urban environments. The overexploitation of groundwater in urban areas comes mainly in the context of rapid urbanization, expansion of industrial and agricultural activities, and in some cases, climatic changes. Sustainable urban planning and detection of potential hazards involve the use of adequate instruments such as the continuous monitoring of land subsidence. The satellite remote sensing Synthetic Aperture Radar Interferometry (InSAR) techniques offer the opportunity for early detection and continuous monitoring of land subsidence for wide areas, including urban centres. Considering various aspects, a review of scientific contributions where urban subsidence due to the intensive groundwater withdrawal for agricultural purposes is monitored based on InSAR techniques, is presented. As land subsidence in urban areas has a direct impact on the quality of life, the review is completed with demographic indicators assessment, followed by analysis on the dynamics of the population in some urban areas affected by land subsidence.

Key words*: InSAR, groundwater-related subsidence, urban, agriculture, demographic indicators.*

INTRODUCTION

One of the main degradation forms affecting land surface and having a variety of effects on the natural and anthropogenic environments is represented by land subsidence (Ahmad et al., 2017; Bawden et al., 2003; Burkett et al., 2003; Sneed et al., 2014; Bitelli et al., 2015). As a result of various natural or anthropogenic factors (Orellana et al., 2022), this phenomenon is characterized by sinking or settling of the land surface (Allaby, 2013).

Intensive groundwater withdrawal is one of the anthropogenic factors leading to subsidence in urban areas (Galloway & Burbey, 2011). This comes in the context of rapid urbanization and industrial development (Poland, 1984; Ruiz-Constan et al., 2016), leading to the progressive use of groundwater resources in industry, various urban needs and activities, and agriculture (Ezquerro et al., 2020).

Globally, agriculture is using almost 70% of all groundwater withdrawals, reaching in some developing countries up to 95% (Meza-Gastelum et al., 2022). Unless in many cases the groundwater withdrawal for agricultural purposes is not the main cause of land subsidence in urban environment, this phenomenon was or it is still present in significant urban centres. Some urban areas may be prone to subsidence due to the presence of some geological and hydrogeological particularities as well as climatic aspects (Ahmad et al., 2022).

As the land subsidence due to groundwater withdrawal is often a slow process not prominent until its effects are visible (Orellana et al., 2022), measuring and monitoring of this phenomenon is necessary for a sustainable urban planning and for the disclosure of potential hazards (Chen et al., 2016). In this context, various methods and techniques are being used for measuring land subsidence (Galloway & Burbey, 2011), since the beginning of the 20th century, when the subsidence phenomena due to groundwater withdrawal was identified in U.S.A. (USGS, 2017).

Precise levelling and extensometry are the most accurate subsidence monitoring methods, reaching sub-millimetre accuracies (Radutu & Gogu, 2018). Following the technological evolution, since the 1980s, the GNSS techniques started to be used, reaching millimetre accuracy (Bitelli et al., 2015). In the last decades, considering different constraints of each of these methods (Karila et al., 2013), the evolution of

the remote sensing techniques and of the radar satellite missions, the Synthetic Aperture Radar Interferometry (InSAR) techniques started to be used successfully for the continuous land subsidence monitoring and for early detection over wide areas (Raucoules et al., 2007). The complementarity use of different monitoring methods may have the best results.

In this context, the paper presents an analysis of urban areas worldwide, where InSAR techniques are used for monitoring land subsidence due to groundwater withdrawal for agriculture purposes. Different aspects, such as benefits, limitations, particularities are highlighted, considering this type of specific area of interest.

As human resources are vital for the development of each economic sector including agriculture and at the same time land subsidence in urban areas can have a great impact on the quality of life, some demographic characteristics are highlighted having in mind the dynamics of the population for two urban centres from Spain.

MATERIALS AND METHODS

Scientific contributions investigating urban subsidence due to the groundwater pumping for agriculture purposes are analysed.

Different parameters are taken into account, such as history, monitoring methods, geology, climatic conditions and demographic characteristics.

This section presents the InSAR techniques applied for monitoring different areas affected by subsidence, followed by the description of the demographic indicators.

InSAR techniques for monitoring urban subsidence due to groundwater pumping for agriculture

InSAR techniques became popular at the beginning of 1990s when the ERS-1 (European Remote-Sensing Satellite-1) mission was launched (ESA, 2023), providing data with enough high spatial and temporal resolution for generating interferograms. The displacements are encoded in the phase difference between the two coregistered SAR images used for computing the interferogram (Galloway & Hoffman, 2006) along the Line of Sight (LOS) of the satellite (Colesanti & Wasowski, 2006). The day and night operational capabilities regardless the weather conditions of InSAR techniques (Ferretti et al., 2007), the ability to measure the subsidence with a relative low cost and to perform precise ground monitoring (Chaabani & Deffontaines, 2020) are some of the advantages of these techniques, addressing the limitations of the classical methods.

Two classes of InSAR techniques are being used over time:

- the conventional approach, using single interferometric processing, known as **conventional InSAR** (Bamler & Hartl, 1998), and
- the differential approach, or **conventional DInSAR** (Crossetto et al., 2016; Ruiz-Constan et al., 2015), when multiple SAR scenes with the same geometry are used over the same study area at different time moments (Ferreti et al., 2007). As DInSAR technique might be affected by atmospheric influences and temporal and spatial decorrelations when measuring ground displacements (Chaabani & Deffontaines, 2020; Chen et al., 2016; Cianflone et al., 2022), more advanced DInSAR techniques are being developed, named the Multi-Temporal Interferometry techniques (**MTI**) or Advanced-Differential SAR Interferometry techniques (**A-DInSAR**), such as Persistent-Scaterrer Interferometry (**PSI**) (Ferretti et al., 2001; Crossetto et al., 2016; Espiritu et al., 2022) and Small Baseline Intereferometry (**SBAS**) (Berardino et al., 2002).

Further, to compensate some of the MTI techniques' limitations, the temporal decorellation on vegetated or bare soil areas (Galloway & Burbey, 2011), new MTI techniques from the PSI and SBAS families, or combinations of the two techniques were proposed, such as Wavelet Based InSAR (**WabInSAR**) (Miller & Shirzaei, 2015), Parallel Small Baseline Subset (**P-SBAS**) (Cigna & Tapete, 2022; Orellana, et al., 2022), **SqueeSAR** (Ezquerro et al., 2020), Coherence Pixel Technique (**CPT**) (Ezquerro et al., 2020), **StaMPS-MTI** (Ruiz-Constan et al., 2016).

Demographic assessment

Human beings have a powerful effect on the environment quantified in demographic factors regarded as one of the primarily global drivers

of human-induced environmental change, in addition to biophysical, economic, socio-political, technological factors (Boberg, 2005). Demographics variability and effects on the environment are emphasised by the population growth and the natural increase rate, information which can be used in many ways to discover the generalities of a particular population.
The natural increase rate in the total population refers to the difference between the number birth rate and the death rate occurring in a year, divided by the mid-year population of that year, multiplied by a factor (usually 1,000) (Dumitrache & Erdeli, 2009). For birth rate evaluation it is considered the number of people born in a population in a given amount of time, while the death rate is represented by the number of deaths, per year, varying, due to differences in living standards and economic conditions.
The natural increase rate indicator is determined for Murcia and Madrid, two regions from Spain where groundwater usage is contributing significantly to Spanish agricultural and regional development.

RESULTS AND DISCUSSIONS

The current review, based on an extensive scientific literature inquiry on the urban areas affected by land subsidence due to groundwater withdrawal for agriculture, are taking into consideration different aspects, considering the domain of interest. Therefore climate, geology, hydrogeology, InSAR monitoring techniques, satellite SAR missions, management of hydrological resources, demographic dynamics, or urbanisation might give a glimpse on where and how overexploitation of groundwater resources for agriculture purposes might affect urban areas.

History of groundwater pumping for agriculture in urban areas

- First half of 20th century

U.S.A.

Looking on the history aspect, groundwater pumping for agriculture has enabled the San Joaquin Valley of California, U.S.A. to become one of the world's most productive agricultural regions (Galloway & Riley, 1999).
For Santa Clara Valley, Coachella Valley, San Joaquin Valley, California, agriculture was the predominant activity in the first half of the 20th century, with a rapid urban and industrial development after the World War II (Galloway & Hoffman, 2006; Sneed et al., 2014; Galloway & Riley, 1999), and the extraction rate of groundwater continuing to increase (Schmidt & Burgman, 2003). Same situation is specific for Phoenix, Arizona (Miller & Shirzaei, 2015). Therefore, since 1970s, the water in many wells declined from 15 m (Sneed et al., 2014) up to 90 m in the deep confined aquifers, while large areas from these regions were affected by land subsidence reaching up to 8 m subsidence (Galloway & Riley, 1999). For Santa Clara Valley, the decrease of rainfalls in the first part of the 20th century contributed to the increase of groundwater needs for agriculture (Schmidt & Burgman, 2003).
As a consequence of the water increase demand, the necessity to preserve the groundwater resources and to prevent severe damages, various measures were taken in the U.S.A. Thus, in the Coachella Valley, California, in 1949 water from Colorado River started to be imported, a recovery of the groundwater levels being registered until 1970. However, since late 1970s, the water demand increased leading to the increase of groundwater pumping (Sneed et al., 2014). As a consequence, the subsidence process continued until today, in the 2000s, in Palm Desert a 4 cm/year subsidence being registered (Sneed et al., 2014).
The import of surface-water has been used also in Santa Clara valley for supplementing the water demand and to recharge the declining groundwater system (Galloway & Hoffmann, 2006). Favourable rainfalls contributed to the recovery, so that in the 1990s InSAR measurements indicated up to 6.4 mm/year uplift North to Sunnyvale (Schmidt & Burgman, 2003). Unless highly urbanised, these areas are still major agriculture regions in the U.S.A, relying heavily on the groundwater resources. Therefore, in San Joaquin Valley, a long-term land subsidence is present, due to the compaction of fine-grained aquitard layers within the aquifer system, reaching in the 2000s up to 25 cm/year subsidence (Liu et al., 2019). As a consequence, aqueducts, levees, bridges and roads are at risk of damage (NASA, 2017), potentially affecting the quality of life of the population from the region.

China

Found on a different continent, land-subsidence due to groundwater over-exploitation is present in Beijing, China, since 1935 (Chen et al., 2016). As groundwater is the main water source for industry, agriculture and domestic use in the area, and considering the great impact of the land subsidence, more than 25 studies on this subject are available for Beijing (Hu et al., 2019; Bai et al., 2022). Nowadays, the values of land-subsidence are greater than 10 cm/year (Chen et al., 2016).

- Second half of 20th century

Mexico

Unless land-subsidence due to groundwater extraction was observed in Mexico City since 1920, it was in the 1980s when subsidence started to be observed and monitored in other cities from central Mexico, such as Morelia or Celaya (Suarez et al., 2018), where agriculture is one of the important activities for which groundwater exploitation is necessary (Cigna et al., 2022; Chaussard et al., 2014). In the Metropolitan Area of Morelia, 47% of the groundwater wells are for agriculture, the yearly subsidence rate between 2014 and 2021 reaching up to 9 cm. Celaya, Silao and Leon cities are characterised by a rapid, local-scale subsidence due to groundwater withdrawal for agriculture, reaching up to 8 cm/year from a SAR subsidence monitoring conducted between 2007 and 2011 (Chaussard et al., 2014).

Spain

Alto Guadalentin Basin from Southeast Spain, is a fertile basin cultivated since the Arabic ages (800 B.C.), agriculture being traditionally the most important economic activity in the area (Ezquerro et al., 2017). However, in the 1960s the agricultural development involved the use of groundwater resources, helping to the revitalization of this economic sector in the 1980s, but leading to temporally overexploitation in 1987 (Boni et al., 2015; Ezquerro et al., 2017). After this moment, the transfer of water resources from Tajo River and Segura River helped the recovery of the aquifer system, but the droughts periods from 1990 to 1995 and from 2005 to 2007 led again to the intensive use of groundwater resources (Boni et al., 2015). Unless urban and touristic activities progressively entered the economic activity, agriculture still has an important impact over groundwater resources, studies using SAR data revealing a continuous deformation pattern with greatest values in Europe, higher than 10 cm/year (Gonzales & Fernandez, 2011). This dynamics comes in the context of continuous increase of population, in Lorca and Puerto Lumbreras cities reaching more than 100,000 inhabitants in 2012, an increase of almost 50% from 1960. Land subsidence and the increase of population make the structures and infrastructures from the area vulnerable, considering also the important geological risk of the region (Ezquerro et al., 2017).

City of Murcia, found in the neighbouring of Alto Guadalentin valley, is also part of the South-Eastern regions of Spain known and being monitored due to the over-exploitation of groundwater for domestic, agricultural and industrial needs (Rigo et al., 2013). The drought period from the 1990s led to the groundwater overexploitation that generated land-subsidence accompanied by damages to over 150 buildings and other structures. During the drought period from 2004 to 2008, new wells were drilled for maintaining water supply for population and agriculture needs (Tessitore et al., 2016).

Unless not having the same importance as in Alto Guadalentin Basin, agriculture and groundwater pumping for agriculture are present also in the Metropolitan area of Madrid, 32% of the land-use from this region being arable for annual crops (Copernicus, 2018). Agriculture is more important here for the smaller municipalities, correlation coefficients between displacements and piezometric time series having values higher than 85% for all the wells, for a cumulated value of subsidence over almost 20 years of 8 cm (Ezquerro et al., 2014).

Montellano, Spain, is another town where land subsidence is present due to intensive exploitation of groundwater for agricultural and urban purposes, the particularity of this area being that aquifer was not exploited before 1990s the use of water from river being more common.

The changes in agricultural practices from non-irrigated to irrigated land and the severe droughts since 1990s favoured intensive groundwater exploitation and a cumulated value of 33 mm subsidence for almost 20 years, since 1992 (Ruiz-Constan et al., 2016).

Italy

The economic boom of Italy after the World War II led to extensive exploitation of groundwater for agricultural and industrial use in the Plain of Po River Delta, making it a historically land-subsidence affected area (Solari et al., 2018). This resulted in a territory very difficult to be managed, as large areas were part of the land reclamation projects from the end of 19th century, when the territory was largely increased for usable crop production (Corbau et al., 2019). Unless this is a poorly urbanised area, this is an example of successful policies applied since the 1950s, as subsidence was estimated to 300 mm/year in the period from 1950 to 1957. Therefore, since 1960, anthropogenic withdrawals were suspended and other specific works have been done, leading to the decrease of land subsidence to values of 4.5 mm/year nowadays (Fabris et al., 2022), which are mainly related to the natural consolidation of the compressible Holocene deposits (Corbau et al., 2019).

In Gioia Tauro Plain, an important urban industrialised and coastal agricultural area from the Southern part of Italy, the groundwater pumping for agricultural purposes is present since the 1970s. A significant drop of the piezometric level of the shallow aquifer was registered between that period and 2021 (Cianflone et al., 2021). Unless the main towns of the plain (Gioia Tauro, Rosarno, Nicotera, Taurianova, and Citanova) are stable, an increasing subsidence rate of up to -5mm/year was observed in the town of Polistena (Cianflone et al., 2022). The farming system from the area with hundreds of individual small plots, despite the public water supply network, leads to the presence of uncontrolled drilled water wells (Raspini et al., 2012). Another particularity of the area is related to the land use changes in the last two decades, with intensive and ongoing kiwifruit farming, requiring a high-water supply, almost doubled, compared to the previous citrus and olive crops (Cianflone et al., 2022).

Part of the Firenze-Prato-Pistoia plain, Pistoia is a city with instability phenomena documented since the 1960s (Ceccatelli, 2020). From the early 1990s, Ezquerro et al. (2020), states that land subsidence is occurring in the Firenze-Prato-Pistoia basin, due to intensive groundwater withdrawal for agriculture. More specifically, Pistoia is known for the tree nursery activities, and the presence of soft sediments subsiding due to groundwater withdrawal (Del Soldato et al., 2018), the maximum deformation measured during 2014-2018 being of 1.7 cm/year (Ezquerro et al., 2020).

Using SAR interferometry, severe land subsidence was detected in the last two decades in the Sele and Volturno Plain, being stated that land subsidence is present due to groundwater overexploitation for agricultural use, inducing coastal inundation (Solari et al., 2018). The plain is characterised by an increased concentration of infrastructure and inhabited areas, such as Castelvolturno, Mondragone, or Capua cities, with known farming, agricultural and cheese production activities (Matano et al., 2018).

Turkey

Konya Plain, with its urban areas Konya, Ismil, Cumra, Hotamis, or Eregli, it is a known area in Turkey for intensive groundwater pumping for covering the agricultural, urban and industrial needs (Calo et al., 2017). The rapid groundwater withdrawal and vertical displacements have been observed during the last 3-4 decades, with an intensification of the groundwater pumping in the last years (Ustun et al., 2018), in the context of an increase of irrigated land, for crops as sugar beet and corn. Water needs for irrigation led to uncontrolled groundwater withdrawal, and as a consequence of groundwater withdrawal, sinkholes appeared, leading to damages to infrastructures and of some villages. Vertical deformation of up to 10 cm during 8 years of monitoring were detected in the area (Calo et al., 2017).

Iran

At the Iran country level, 90% of the groundwater consumption is used for agricultural purposes (Haghshenas Haghighi & Motagh, 2021). The old and inefficient farming methods are one of the factors prone to higher need for groundwater (Pirouzi & Eslami, 2017). Shariar area, situated in the west of Tehran plain, faced over-exploitation of groundwater resources few years after the construction of a dam in the area in the 1960 (Khodapanah et al., 2011). In the Kerman Province, subsidence due to extensive groundwater withdrawal is present since the 1980s (Toufigh et al., 2004). As agricultural regions are spread all over the

country, many urban areas, or neighbouring of urban areas are affected by land subsidence, such as Tehran city (Pirouzi & Eslami, 2017), Neyshabour City (Dehghani et al., 2009), Rafsanjan and Anar cities situated in the Iran's center of Pistachio plantation, Mashhad city (Haghshenas Haghighi & Motagh, 2021), Ardabil, Khalilabad, and Araloyebozorg (Ghorbani et al., 2022), Ashkane city (Rafiei et al., 2022). In many areas affected by land subsidence, the vertical displacements have values higher than 10 cm/year, which can lead in the near future to significant economic losses such as structural damage and high maintenance costs for roads, railways, dikes, pipelines, and buildings (Rajabi Baniani et al., 2020). Several roads located in the agricultural area to the southwest of Tehran are already affected by land subsidence (Haghshenas Haghighi & Motagh, 2021), while field research in the city of Ashkhane and neighbouring areas showed the presence of damages such as cracks in the walls (Rafiei et al., 2022).

Philippines

Subsidence due to groundwater withdrawal in East Asia has as one of the main cause the expanding of coastal aquaculture and the presence large crops of rice, especially for Manila Bay, where the biggest crops of rice across the East Asia are found. Subsidence due to groundwater use is known since 1965 (Rodolfo & Siringan, 2006). The Metropolitan Manila, including Manila, Caloocan, Malabon, Navotas and Valenzuela cities, is affected by land subsidence with rates between 1 and 2 cm/ year, studies showing that subsidence is the cause of floods worsening in the recent years. This comes in the context of an area exposed to multiple natural hazards, such as earthquakes, landslides, volcano eruptions, and typhoons, endangering buildings, houses and underground facilities (Espiritu et al., 2022).

- The 21st century

Pakistan

Pakistan has at the moment the highest speed of urbanization in South Asia. As an example, the urban area of Lahore city doubled between years 1999 to 2011 (Ahmad et al., 2021). As the only source of water for the city, due to the uncontrolled urbanization, the intensive groundwater extraction led to land subsidence (Farhat et al., 2018; Hussain et al., 2022), with values up to 11 cm/year (Ahmad et al., 2022). Although the highest rate of groundwater pumping is for the domestic use, agriculture still has an important role and impact in the groundwater balance of Lahore city, 23% of the discharge being for agricultural purposes, more than for the industrial and commercial use (Ahmad et al., 2022). Field surveys confirmed the results of the InSAR analyses, damages of buildings and other infrastructures taking place in areas affected by subsidence (Ahmad et al., 2022; Hussain et al., 2022). In the actual context, for a sustainable development, proper strategies of urban planning considering the land use and land cover classes, including agricultural lands, should be developed (Farhat et al., 2018).

Chile

Found in a vulnerable area with the most seismically active subduction zones in the world, the Metropolitan Area of Santiago de Chile is affected by ground instability due to natural factors and anthropic factors, such as the groundwater overexploitation. As a result of climate changes and influenced by the intensive agriculture, Paine city, part of Grater Santiago, experienced in the recent years more noticeable deformations, considering the exploitation and compaction of the aquifer (Orellana et al., 2022).

Tunisia

Situated in North Africa, Tunisia is one of the Mediterranean countries which relies on deep aquifers for fulfilling the water needs for agriculture, domestic use and industry, as surface waters are scarce and irregular (Mokadem et al., 2018). Since the 1960s, a significant agricultural and industrial boom was registered in the coastal northern Tunisia. Therefore, the groundwater exploitation speed from the unconfined aquifer increased from 280 l/s in 1971, to 600 l/s in 1999 (Charef et al., 2012).

As a consequence, in the last two decades land subsidence is producing in Tunis City and the Mornag plain with values up to 19 mm/ year, leading to numerous failures of buildings, considering also the highly compressive deposits from the area. Also, due to agricultural and industrial activities, in the peri-urban area of Mornag plain, drinking water resources is under substantial pressure (Chaabani & Deffontaines, 2020).

Indonesia

Indonesia is one of the countries with rapid increasing of population in urban areas, followed by increasing of water and land needs, considering mainly the industrial needs, followed by the agricultural and housing activities, causing land subsidence (Sidiq et al., 2019). Groundwater exploitation is documented in Indonesia since the first half of 20th century, and it could be revealed the massive increase of groundwater exploitation since 1970, concomitantly with the manufacturing industry development, and the massive urbanisation, consequently. Due to industrial pumpers, the total groundwater abstractions in Bandung basin grew from 18% to 83% during 1950-1990 time period (Braadbaart & Braadbaart, 1997). However, the presence of land subsidence is mentioned since year 2000, when the GPS surveys started to be used for ground motion monitoring (Abidin et al., 2009). As for the SAR monitoring, from 2007 to 2011, for two agricultural areas from Bandung, the land subsidence rate was as high as 5 cm/year (Sidiq et al., 2019). Similar values are registered for two other urban areas, Blanakan and Pekalongan cities, where agriculture has a significant impact on groundwater withdrawal (Chaussard et al., 2013).

SAR techniques and SAR data used for land subsidence monitoring

The capability of SBAS technique of improving conventional InSAR monitoring over agricultural areas (Galloway & Burbey, 2011) is proved by the high number of scientific contributions where SBAS (Chaussard et al., 2013; Sidiq et al., 2019; Chaabani & Deffontaines, 2020; Chen et al., 2016; Calo et al., 2017; Haghighi & Motagh, 2021; Dehghani et al., 2009; Farr & Liu, 2015; Cianflone et al., 2022; Ezquerro et al., 2017) is used as SAR processing technique for subsidence monitoring in the urban areas where agricultural activities have a great importance. This is highlighted in Figure 1, where a statistic of the SAR monitoring techniques is made, considering the consulted scientific contributions available on the topic of this paper. Thus, in 36% of the contributions, the SBAS techniques is used, followed by the PSI technique (Baniani et al., 2021; Fabris et al., 2022; Ezquerro et al., 2014; Espiritu et al., 2022; Ahmad et al., 2022; Boni et al., 2015) with 21% and other InSAR (Galloway & Hoffmann, 2006; Sneed et al., 2014) and A-DInSAR techniques such as P-SBAS (Orellana et al., 2022; Cigna & Tapete, 2022), DInSAR (Liu et al., 2019; Rafiei et al., 2022), InSAR-SB (Chaussard et al., 2014), LiCSBAS (Ghorbani et al., 2022), WabInSAR (Miller & Shirzaei, 2015), SqueeSAR (Ezquerro et al., 2020), or STAMPS-MTI (Ruiz-Constan et al., 2016). If we take into consideration all the techniques which are part of the SBAS family, more than half of the scientific contributions are using an approach based on SBAS technique.

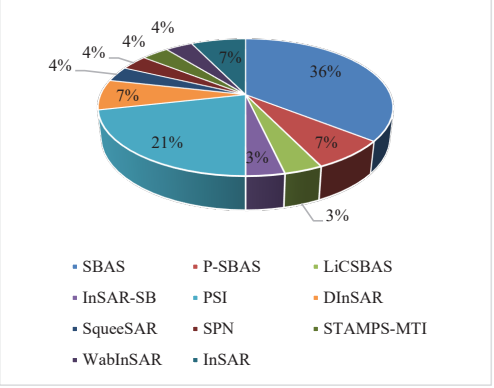

Figure 1. SAR monitoring techniques used in the scientific contributions

Figure 2 presents a statistics on the data sets used in the scientific contributions on the topic of this paper, considering the past and actual launched SAR missions. The figure highlights at a first sight the high number of studies using data from European SAR missions.

This comes in the context of free and open access of the European SAR missions, starting with ERS 1& 2 in the 1990s, the ENVISAT ASAR in the 2000s and the actual European SAR mission, Sentinel-1 mission since 2014. Therefore, almost 80% of the used SAR data are from European missions: the greatest percentage is registered for Sentinel-1 data sets, with 35%, followed by ENVISAT datasets with 24%, and ERS 1&2 with 19%. Other data sets are from the TerraSAR-X mission which was available during the gap period between the retirement of ENVISAT mission in 2012 and the launch of Sentinel-1 in 2014 (Romero, et al., 2020), from ALOS PALSAR and CosmoSkyMed.

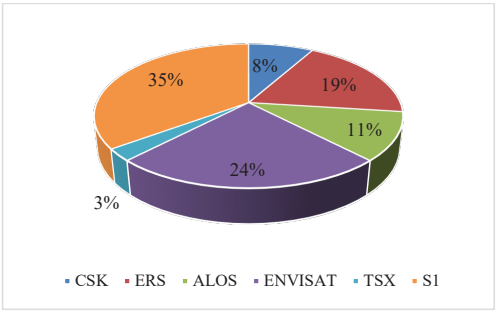

Figure 2. SAR data sets from different SAR missions used in the scientific contributions

Datasets from the different SAR missions covers time intervals starting with the 1990s until the present day. Figure 3 presents the percentages of datasets used in each decade from 1990s, followed by the 2000s and all the datasets since 2010s.

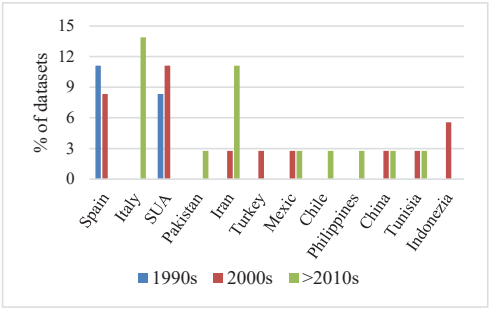

Figure 3. Percentages of SAR data sets used for land subsidence monitoring in different countries

Looking on the graph, the highest percentages of datasets from the 1990s and from the 2000s are used for urban areas from Spain and U.S.A, both countries with long history on groundwater pumping for agricultural activities. For the time interval covering the last decade, Italy has the highest percentage of SAR datasets used for land subsidence monitoring, followed by Iran, one of the countries with high land subsidence problems nowadays. The lack of studies covering the 1990s in some countries where land subsidence is present for more than half of a century, might be explained by the use of other land subsidence monitoring methods, such as precise levelling or GNSS surveillance.
Different numbers of SAR data sets are used in in the consulted scientific contributions for the land subsidence monitoring, the maximum number of data sets from different missions being three. Therefore, Figure 4 presents the percentages of scientific contributions which used data sets from one, two or three SAR missions for land subsidence monitoring.
Most contributions used a SAR data set from a single SAR mission (65%), followed by contributions where data sets from two SAR missions were used (31%). Only 4% of contributions used data sets from three SAR missions.

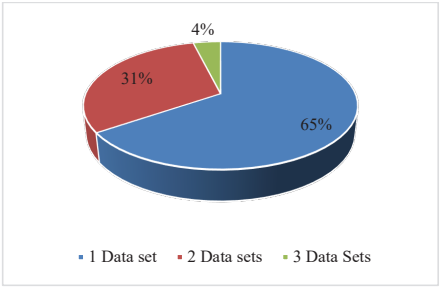

Figure 4. Percentages of scientific contributions using data sets from one or more SAR missions

As for the land subsidence measured using SAR techniques, there were registered values between 1.4 cm/year in Lahore City, Pakistan (Ahmad et al., 2022) and 25 cm/year in San Joaquin, U.S.A. (Liu et al., 2019).
Figure 5 presents the percentages of urban areas from different countries affected by land subsidence due to groundwater withdrawal for agricultural purposes, considering different deformation intervals. It includes areas with land subsidence rates: under 5 cm/year, between 5 and 10 cm/year, between 10 and 20 cm/year and higher than 20 cm/year.
Urban areas where land subsidence has values lower than 5 cm/year are present in Tunisia, Philippines, Iran, U.S.A., Italy and Spain. On the other side, as mentioned above, in U.S.A. is registered also the highest subsidence rate, higher than 20 cm/year. Displacement values between 5 and 10 cm/year are measured by InSAR techniques in Indonesia, Mexic, and Spain, while displacements values between 10-20 cm/year are measured in urban areas from China, Chile, Turkey, Iran, Pakistan, U.S.A., and Spain.

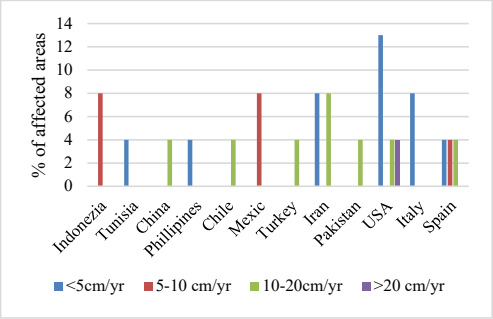

Figure 5. Percentages of urban areas affected by land subsidence due to groundwater withdrawal for agricultural activities, considering different intervals of displacements

Climatic, hydrogeological, geological aspects of the studied areas

Most urban areas affected by land subsidence due to groundwater withdrawal for agricultural purposes are located in arid and semi-arid regions worldwide, from Western U.S.A., Mexico, Middle East, Southern Asia, North Africa, or Mediterranean basin. As rivers and surface water sources are poor or unavailable in some periods of the year in the arid and semi-arid regions, groundwater is the main water source (Pirouzi & Eslami, 2017; Espiritu et al., 2022; Cigna et al., 2022; Ustun et al., 2010; Baniani et al., 2021; Dehghani et al., 2009; Haghighi & Motagh, 2021), or the only water source (Ahmad et al., 2022).

In many cases, severe droughts (Ruiz-Constan et al., 2016; Tessitore et al., 2016; Boni et al., 2015) and climatic changes (Ahmad et al., 2022) contributed to the groundwater overexploitation, unless the anthropic factors are the most pregnant.

The presence of the alluvial compressible deposits with variable thicknesses (Galloway & Hoffmann, 2006; Ahmad et al., 2022; Baniani et al., 2021; Ghorbani et al., 2022; Calo et al., 2017; Chen et al., 2016; Chaussard et al., 2013) and of aquifer systems with highly compressible fine-grained interbeds (Fabris et al., 2022; Dehghani et al., 2009; Chaussard et al., 2014; Chaabani & Deffontaines, 2020) are also part of the factors that favour the occurrence of land subsidence when important quantities of groundwater are pumped.

Demographic indicator assessment for Murcia and Madrid regions

Spain is between the most arid countries in Europe having a massive hydrogeological potential, groundwater usage development contributing significantly to Spanish agricultural and regional development. Spain's current total water use is distributed between irrigation (67%), urban needs and industry (14%) and independent industrial use and cooling (19%) (Llmas & Garrido, 2007). As a consequence on the difficulties in the planning and control of groundwater use, ecological and socio-economic impacts arisen.

The Regulation for the Public Water Domain says that "an aquifer is overexploited when the continuation of existing uses is in immediate threat as a consequence of abstraction being greater or very close to the mean annual volume of renewable resources, or when it may produce a serious water quality deterioration". This is due to the dramatic increase usage of groundwater by thousands of individual farmers, industries in different regions with very limited public involvement.

Comprehensive research on groundwater use and resources in Spain are introduced in the Groundwater White Book (MIE & MOPTM, 1995), the Water White Book (MMA, 2000) and the book by Llamas et al. (2001).

Based on other related research (Richey et al., 2015) which employ satellite measurement of Earth's gravity, it is proved that a third of big groundwater basins are in distress endangering water security and resilience at regional level. In densely populated areas from arid and semi-arid regions, this problem is intensified by climate change and rapid increase of population (Bejar-Pizarro et al., 2017).

With regard to the social analysis of the groundwater monitoring, focusing on the evolution of demographic indicators, two regions in Spain are laid out, adjoining Urban Atlas (Copernicus, 2018) statistical figures.

Murcia is located in the southeast of the Iberian peninsula, at the very centre of the peninsular Mediterranean arc with a semiarid climate, which determines a high rate of erosion, has a total surface of 11,314 km^2 (2.2% of the Spanish surface). The region has an increasingly population number in the period from 2006 to 2018 (Figure 6), having decreasing features in

2013, continued by a rise to 2018. The rural area takes up to 83% of the regional territory with 36% of Murcia's population living there (RDP, 2010).

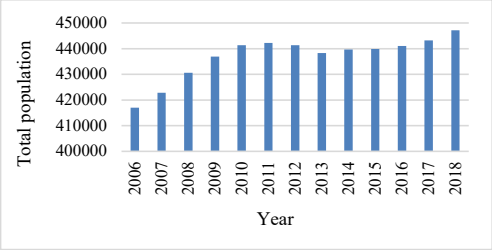

Figure 6. Total population number in Murcia region, Data source: Spanish Institute of Statistics (INE, 2023)

The economic crisis occurred in Spain since 2008, led to unemployment, which causes changes in the demographic trend (Moya Ortega & Garcia Marin, 2015). The highest percentage of the natural increase rate is registered in 2008 (Figure 7), determined by highest birth rate in the analysed time series (2006-2018). The natural increase rate and birth rate values of the data series are decreasing from 2008, while the death rate was continually increasing (Figure 7). The population employed in agriculture has increased from 1999 to 2006. The region presents great agricultural potential, one of the most intensive in Europe, with crops such as almond tree and cereals in dry lands, and vegetables as potatoes, cabbage and pepper, irrigated fruit trees such as the lemon tree, orange tree, peach and plum tree (Andrade-Limas et al., 2007), due to the favourable environmental conditions in the area, such as high temperatures all over the year, and fertile soils. Lately, Murcia has become one of the main producers of fruits and vegetables in Spain. As the region covers 4.3% of the Spanish population, having the power of the country's export for between 20 and 30%, in this segment, it consequently incur a considerable part of its economic productivity to the agricultural sector (Murcia Today, 2017).

CHS is the Segura River Basin Authority in the Region of Murcia, in charge of the general management of water resources, including the aquifers in the Basin (Mamais et al., 2020). As Murcia Region is one of the most water-stressed regions in the Mediterranean basin with frequent extreme meteorological events, such as multi-annual droughts (Calatrava & Martinez-Granados, 2017), the structural water deficit is the biggest challenge faced by CHS in the area. As a consequence, the various water users in the basin through a long history, gained a strong expertise in water culture, aiming at balancing groundwater use for both drinking and irrigation purposes (Mamais et al., 2020).

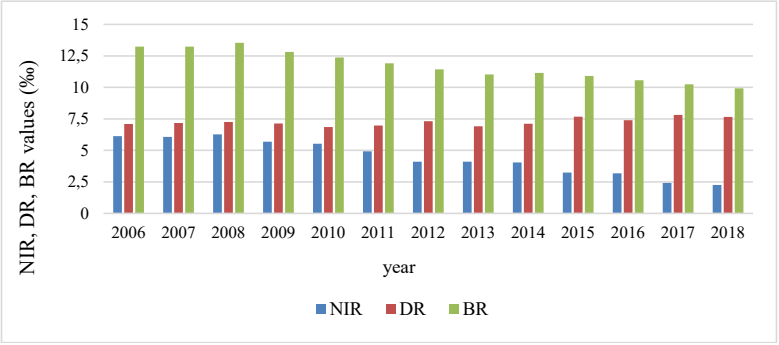

Figure 7. NIR, DR, BR evolution in Murcia region during 2006 and 2018 Data source: Spanish Institute of Statistics (INE, 2023)

Construction of illegal wells and of canals, followed by illegal groundwater use, have become an increasing phenomenon in the region, due to the implementation of a restrictive policy in terms of access to groundwater and an increasing agricultural cultivation. The high rate of illegal groundwater abstraction is explained by the huge profits that encourage farmers to expand their farmland despite ineffective controls by public authorities. As a consequence, river basin authorities are continuously under both, political and economic

pressure, which involve restrictions on their efforts to deal with illegal water use and aquifer exploitation (WWF, 2006).

Another Spanish urban area to be mentioned, is Madrid, as one of the best documented Spanish example (De Stefano et al., 2015), where groundwater is a critical resource to prevent failures in the urban supply system, especially during droughts.

Madrid, the most populated region in Spain, generates 17% of the country's gross domestic product and is the second most important industrial centre of the country, currently ranking second among the cities of the European Union behind Berlin, and the third place among the largest urban agglomeration in Europe, behind Île-de-France, and Greater London.

Madrid's population has experienced growth since 2008 due to significant number of foreign immigrants settling in the city (Observatorio Economico, 2010) due to the strength of Madrid's economy, the main economic hub and decision making centre in Spain.

During the demographic data series assessment (Figure 8), the highest number of the population in 2010 starts to decrease, recording the lowest people number in 2015, followed by an increased trend in the number of populations till 2018.

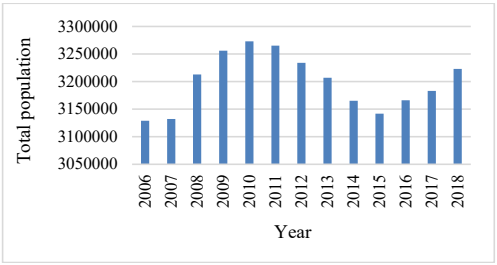

Figure 8. Total population number in Madrid during 2006 and 2018. Data source: Spanish Institute of Statistics (INE, 2023)

The natural increase rate has positive values during the analysed period, given the highest birth rate than the death rate. The birth rate is slightly decreasing since 2006, while the death rate has an annually increasing rate until 2018. Based on this, the natural increase rate register decreasing values frequency, the lowest value being recorded in 2018 (Figure 9).

Concerning the monitoring availability of several European urban regions which can increase groundwater development and management solutions, the Copernicus Land Monitoring Service step into action (Copernicus, 2023). It provides geographical information on land cover/land use and on variables related to vegetation state and the water cycle.

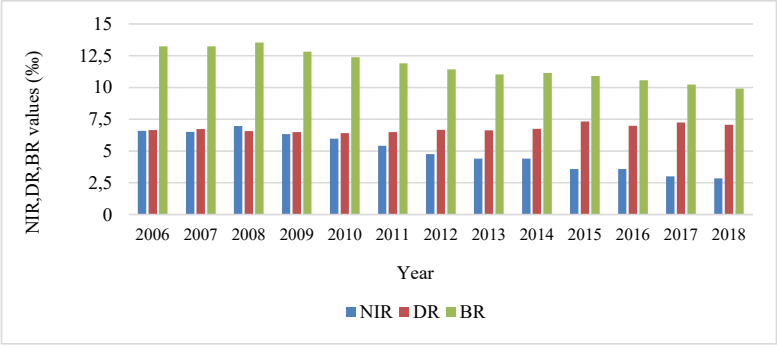

Figure 9. NIR, DR, BR evolution in Madrid region during 2006 and 2018
Data source: Spanish Institute of Statistics (INE, 2023)

It supports applications in a variety of domains, such as spatial planning, forest management, water management and agriculture.

Urban Atlas is focused on FUAs (Functional Urban Area), which include core cities and their commuting zones, providing reliable, inter-comparable, high-resolution land use maps for 2006, 2012, and 2018 (Copernicus, 2023). In total, the Urban Atlas includes 27 land cover classes, of which 17 are urban classes and 10 are rural classes.

The agriculture segment of Murcia and Madrid regions (Figure 10), determined from Urban Atlas classes (within the three available

databases, in 2006, 2012 and 2018) cover nearly 76% of the total functional urban area, including arable land, herbaceous vegetation associations, pastures, permanent crops (vineyards, fruit trees, olive groves), open space with little vegetation, wetlands. No major changes are registered between the different time periods. Looking only at the surface occupied by arable, pastures and permanent crops, the percent is around 40% for Murcia and 44% for Madrid, with a higher percent of permanent crops for Murcia (24%) and of arable land for Madrid (33%).

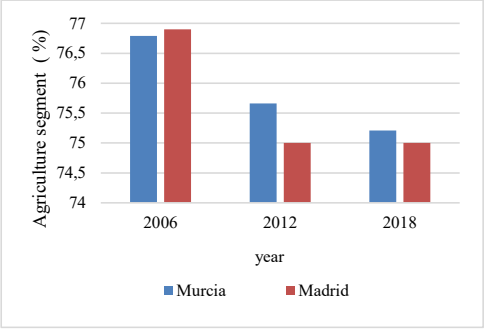

Figure 10. The evolution of Urban Atlas agriculture land class in 2006, 2012 and 2018 for Murcia and Madrid, including arable land, herbaceous vegetation, pastures, permanent crops, open space with little vegetation, wetlands. Data source: Urban Atlas (Copernicus, 2018)

CONCLUSIONS

Land subsidence is mainly caused by human activities, as highlighted in the present review, mainly due to groundwater pumping for anthropogenic activities.

Groundwater withdrawal for agricultural purposes in urban areas, is encountered mainly in arid and semiarid regions, where surface waters are very limited. Considering also the presence of the alluvial compressible deposits and of aquifer systems with highly compressible fine-grained interbeds, these areas are prone to the occurrence of land subsidence. The major impacts of land subsidence include direct damages with the loss of functionality and/or integrity of the structures such as buildings, roads, subways and underground utility networks (infrastructures). The most usual indirect effects are related to changes in relative surface and groundwater levels. In this context, a method of continuous monitoring of subsidence is of great importance. InSAR techniques represent a feasible subsidence monitoring method for urban areas with agricultural activities. From the consulted scientific literature, it could be noticed that the techniques from SBAS family are the most suitable for subsidence monitoring in urban areas with agricultural activities, as some InSAR limitations related to vegetation are mitigated. For the still remaining limitations, a combination between an InSAR technique and an in-situ technique is the most feasible monitoring approach.

In order to manage land subsidence's both consequences and exposed elements, there is a need to have human component assessment, through demographic indicators evaluation.

Following a statistical data evaluation, during 2006 – 2018, Murcia and Madrid regions present a positive natural increase rate due to a balanced population change (the birth rate higher than the death rate).

Both land subsidence monitoring and demographic indicators evaluation represent valuable instruments for decision making for urban planning, in the context of sustainable development.

REFERENCES

Abidin, H., Andreas, H., Gumilar, I., Wangsaatmaja, S., Fukuda, Y., & Deguchi, T. (2009). *Land subsidence and groundwater extraction in Bandung Basin, Indonesia*. In Trends and Sustainability of Groundwater in Highly Stressed Aquifers, IAHS Publ. 329, IAHS Press 2009, UK.

Ahmad, A., Wang, C., Tang, Y., Sultan, M., Falak, A., Duan, W., & Wang, J. (2022). Subsidence Monitoring and Assessment of the Factors Involved in the Occurrence of Subsidence, Lahore City. *Journal of Resources and Ecology*, *13*(5), 826-841. doi: 10.5814/j.issn.1674-764x.2022.05.007

Ahmad, A., Sultan, M., & Falak, A. (2021). *Urban subsidence monitoring by PSInSAR and its causes in Lahore, Pakistan*. SAR in Big Data Era (BIGSARDATA), Nanjing, China, 2021, pp. 1-4, doi: 10.1109/BIGSARDATA53212.2021.9574414.

Allaby, M. (2013). *A Dictionary of Geology and Earth Sciences* (4th ed.). Oxford University Press. 10.1093/acref/9780199653065.001.0001

Andrade-Limas, E., Faz-Cano, A., García-Fernández, G., & Arnaldos-Lozano, R. (2007). *Farmer classification. An approach to soil quality in Murcia, SE of Spain* (Research report no.7). European Soil Bureau. Retrieved from url: https://esdac.jrc.ec.europa.eu/ESDB_Archive/eusoils

_docs/esb_rr/n07_ESBResRep07/407Andrade.pdf on 14.03.2023

Bai, Z., Wang, Y., & Balz, T. (2022). Beijing Land Subsidence Revealed Using PS-InSAR with Long Time Series TerraSAR-X SAR Data. *Remote Sens. 14*(11), 2529. https://doi.org/10.3390/rs14112529

Bamler, R., & Hartl, P. (1998). Synthetic aperture radar interferometry. *Inverse Problems, 14*, R1–R54.

Bawden, G., Sneed, M., Stork, S., & Galloway, D. (2003). *Measuring Human-Induced Land Subsidence from Space.* Reston, VA: U.S. Geological Survey. doi:https://doi.org/10.3133/fs06903.

Bejar-Pizarro, M., Ezquerro, P., Herrera, G., Tomas, R., Guardiola-Albert, C., Ruiz Hernandez, J., Fernandez Merodo, J., Marchamalo, M. & Martinez, R. (2017). Mapping groundwater level and aquifer storage variations from InSAR measurements in the Madrid aquifer, Central Spain. *Journal of Hydrology*, *547*, pp. 678-689, doi: 10.1016/j.jhydrol.2017.02.011

Berardino, P., Fornaro, G., & Lanari, R. (2002). A New Algorithm for Surface Deformation Monitoring Based on Small Baseline Differential SAR Interferograms. *IEEE Transactions on geoscience and remote sensing, 40*(11), 2375-2383. doi:10.1109/TGRS.2002.803792

Bitelli, G., Bonsignore, F., Pellegrino, I., & Vittuari, L. (2015). Evolution of the techniques for subsidence monitoring at regional scale: the case of Emilia-Romagna region (Italy). *Proc. IAHS, 372*, 315-321. doi:10.5194/piahs-372-315-2015

Boberg, J. (2005). *Liquid Assests: How Demographic Changes and Water Management Policies Affect Freshwater Resources*. Santa Monica, CA: RAND Corporation. Retrived from URL: https://www.rand.org/content/dam/rand/pubs/monographs/2005/RAND_MG358.pdf, on 14.03.2023

Boni, R., Herrera, G., Meisina, C., Notti, D., Béjar-Pizarro, M., Zucca, F., Gonzales, P., Palano, M., Tomas, R., Fernandez, J., Fernández-Merodo, J.A., Mulas, J., Aragon, R., Guardiola-Albert, C., & Mora, O. (2015). Twenty-year advanced DInSAR analysis of severe land subsidence: The Alto Guadalentín Basin (Spain) case study. *Engineeering Geology, 198,* 40-52. https://doi.org/10.1016/j.enggeo.2015.08.014

Braadbaart, O., & Braadbart, F. (1997). Policing the Urban Pumping Race: Industrial Groundwater Overexploitation in Indonesia. *World Development*, *25*(2), 199-210. doi:10.1016/S0305-750X(96)00102-7

Burkett, V. R., Zilkoski, D. B., & Hart, D. A. (2003). Sea-Level Rise and Subsidence: Implications for Flooding in New Orleans, Louisiana. In *U.S. Geological Survey Subsidence Interest Group Conference: Proceedings of the Technical Meeting, Galveston, Texas, November 27-29, 2001* (pp. 63-70). U.S. Geological Survey.

Calatrava, J., & Martínez-Granados, D. (2018). The limited success of formal water markets in the Segura River basin, Spain. *International Journal of Water Resources Development*, *34*(6), 961-981, doi: 10.1080/07900627.2017.1378628.

Calo, F., Notti, D., Galve, J.P., Abdikan, S., Gorum, T., Pepe, A., & Sanli, F.B. (2017). DInSAR-Based Detection of Land Subsidence and Correlation with Groundwater Depletion in Konya Plain, Turkey, *Remote Sens., 9*, 83, doi:10.3390/rs9010083

Ceccatelli, M., Del Soldato, M., Solari, L., Fanti, R., Mannori, G., & Castelli, F. (2020). Numerical modelling of land subsidence related to groundwater withdrawal in the Firenze-Prato-Pistoia basin (central Italy), *Hydrogeology Journal, 29*, 629-649, https://doi.org/10.1007/s10040-020-02255-2.

Chaabani, A. & Deffontaines, B. (2020). Application of the SBAS-DInSAR technique for deformation monitoring in Tunis City and Mornag plain, *Geomatics, Natural Hazards and Risk, 11*(1), 1346-1377, doi: 10.1080/19475705.2020.1788654

Charef, A., Ayed, L., & Azzouzi, R. (2012). Impact of natural and human processes on the hydrochemical evolution of overexploited coastal groundwater: Case study of the Mornag aquifer refill (South-East Tunis, Tunisia). *Chemie der Erde*, *72*, 61-69. doi:10.1016/j.chemer.2011.11.005

Chaussard, E., Amelung, F., Abidin, H., & Hong, S-H. (2013). Sinking cities in Indonesia: ALOS PALSAR detects rapid subsidence due to groundwater and gas extraction. *Remote Sensing of Environment, 128*, 150-161. https://doi.org/10.1016/j.rse.2012.10.015

Chaussard, E., Wdowinski, S., Cabral-Cano, E., & Amelung, F. (2014). Land subsidence in central Mexico detected by ALOS InSAR time-series. *Remote Sensing of Environment, 140*, 94-106. http://dx.doi.org/10.1016/j.rse.2013.08.038

Chen, M., Tomás, R., Li, Z., Motagh, M., Li, T., Hu, L., Gong, H., Li, X., Yu, J., & Gong, X. (2016). Imaging Land Subsidence Induced by Groundwater Extraction in Beijing (China) Using Satellite Radar Interferometry. *Remote Sensing, 8*, 468. https://doi.org/10.3390/rs8060468

Cianflone, G., Vespasiano, G., De Rosa, R, Rocco, D., Apollaro, C., Vaselli, O., Pizzino, L., Tolomei, C., Capecchiacci, F., & Polemio, M. (2021). Hydrostratigraphic Framework and Physicochemical Status of Groundwater in the Gioia Tauro Coastal Plain (Calabria - Southern Italy). *Water, 13*, 3279. doi.org/10.3390/w13223279

Cianflone, G., Vespasiano, G., Tolomei, C., De Rosa, R., Dominici, R., Apollaro, C., Walraevens, K., & Polemio, M. (2022). Different Ground Subsidence Contributions Revealed by Integrated Discussion of Sentinel-1 Datasets,Well Discharge, Stratigraphical and Geomorphological Data: The Case of the Gioia Tauro Coastal Plain (Southern Italy). *Sustainability, 14*, 2926. https://doi.org/10.3390/su14052926

Cigna, F. & Tapete, D. (2022). Urban growth and land subsidence: Multi-decadal investigation using human settlement data and satellite InSAR in Morelia, Mexico. *Science of the Total Environment 811,* 152211. http://dx.doi.org/10.1016/j.scitotenv.2021.152211

Colesanti C & Wasowski J. (2006). Investigated landslide with space-borne Synthetic Aperture Radar (SAR) interferometry. *Eng Geol. 88*(3-4), 173–199.

Copernicus (2018). Urban Atlas. Retrieved from URL: https://land.copernicus.eu/local/urban-atlas/urban-atlas-2018, on 27.02.2023.

Copernicus (2023). Copernicus Land Monitoring Service at a glance. Retrieved from URL: https://land.copernicus.eu/, on 14.03.2023

Corbau, C., Simeoni, U., Zoccarato, C., Mantovani, G., & Teatini, P. (2019). Coupling land use evolution and subsidence in the Po Delta, Italy: Revising the past occurrence and prospecting the future management challenges. *Science of the Total Environment. 654*, 1196–1208. https://doi.org/10.1016/j.scitotenv.2018.11.104

Crossetto, M., Monserrat, O., Cuevas-Gonzalez, M., Devanthery, N., & Crippa B. (2016). Persistent Scatterer Interferometry: a review. *ISPRS J Photogramm Remote Sens. 115*, 78–89.

De Stefano, L., Fornés, J.M., López-Geta, J.A. & Villarroya, F. (2015). Groundwater use in Spain: an overview in light of the EU Water Framework Directive. *International Journal of Water Resources Development, 31*(4), 640-656. doi: 10.1080/07900627.2014.938260.

Del Soldato, M., Farolfi, G., Rosi, A., Raspini, F., & Casagli, N. (2018). Subsidence Evolution of the Firenze–Prato–Pistoia Plain (Central Italy) Combining PSI and GNSS Data. *Remote Sens. 10*, 1146. doi:10.3390/rs10071146

Dehghani, M., Zoej, M.J.V., Entezam, I., Mansourian, A., & Saatchi, S. (2009). InSAR monitoring of progressive land subsidence in Neyshabour, northeast Iran. *Geophys. J. Int*. *178*, 47-56. doi: 10.1111/j.1365-246X.2009.04135.x

Dumitrache, L., Erdeli, G. (2009). *Geografia populatiei mondiale*. Bucharest, RO: Editura Universitara.

ESA (2023). *ERS Overview*. Retrieved from URL: https://earth.esa.int/eogateway/missions/ers/description, on 27.02.2023.

Espiritu, K.W., Reyes, C.J., Benitez, T.M., Tokita, R.C., Galvez, L.J., & Ramirez, R. (2022). Sentinel-1 Interferometric Synthetic Aperture Radar (InSAR) reveals continued ground deformation in and around Metro Manila, Philippines, associated with groundwater exploitation. *Natural Hazards, 114*, 3139-3161. https://doi.org/10.1007/s11069-022-05509-2

Ezquerro, P., Del Soldato, M., Solari, L., Tomás, R., Raspini, F., Ceccatelli, M., Fernández-Merodo, J.A., Casagli, N., & Herrera, G. (2020). Vulnerability Assessment of Buildings due to Land Subsidence Using InSAR Data in the Ancient Historical City of Pistoia (Italy). *Sensors, 20,* 2749. https://doi.org/10.3390/s20102749

Ezquerro, P., Guardiola-Albert, C., Herrera, G., Fernández-Merodo, J.A., Béjar-Pizarro, M., & Boni, R. (2017). Groundwater and Subsidence Modeling Combining Geological and Multi-Satellite SAR Data over the Alto Guadalentín Aquifer (SE Spain). *Geofluids, 2017,* 1359325. https://doi.org/10.1155/2017/1359325

Ezquerro, P., Herrera, G., Marchamalo, M., Tomas, R., Béjar-Pizarro, M., & Martinez, R. (2014). A quasi-elastic aquifer deformational behavior: Madrid aquifer case study. *Journal of Hydrology, 519,* 1192-1204. http://dx.doi.org/10.1016/j.jhydrol.2014.08.040

Fabris, M., Battaglia, M., Chen, X., Menin, A., Monego, M., & Floris, M. (2022). An Integrated InSAR and GNSS Approach to Monitor Land Subsidence in the Po River Delta (Italy). *Remote Sens., 14*, 5578. https://doi.org/10.3390/rs14215578

Farhat, K., Waseem, L., Khan, A., & Baig, S. (2018). Spatiotemporal Demographic Trends and Land Use Dynamics of Metropolitan Lahore. *Journal of History Culture and Art Research*, *7*(5), 92-102. doi:http://dx.doi.org/10.7596/taksad.v7i5.1774

Farr, T., & Liu, Z. (2015). *Monitoring Subsidence Associated with Groundwater Dynamics in the Central Valley of California Using Interferometric Radar*. In Remote Sensing of the Terrestrial Water Cycle, (eds V. Lakshmi, D. Alsdorf, M. Anderson, S. Biancamaria, M. Cosh, J. Entin, G. Huffman, W. Kustas, P. van Oevelen, T. Painter, J. Parajka, M. Rodell and C. Rüdiger). https://doi.org/10.1002/9781118872086.ch24

Ferretti, A., Monti-Guarnieri, A., Prati, C., Rocca, F., & Massonnet, D. (2007). *InSAR Principles: Guidelines for SAR Interferometry Processing and Interpretation (TM-19, February 2007).* ESA Publications

Ferretti, A., Prati, C., & Rocca, F. (2001). Permanent Scatterers in SAR Interferometry. *IEEE TRANSACTIONS ON GEOSCIENCE AND REMOTE SENSING, 39*(1), 8-20.

Galloway, D. L., & Burbey, T. L. (2011). Review: Regional land subsidence accompanying groundwater extraction. *Hydrogeology Journal, 19*, 1459-1486. doi:10.1007/s10040-011-0775-5.

Galloway, D. L., & Hoffmann, J. (2006). The application of satellite differential SAR interferometry-derived ground displacements in hydrogeology. *Hydrogeology Journal, 15*(1), 133–154. doi: 10.1007/s10040-006-0121-5.

Galloway, D. & Riley, F.S. (1999). *San Joaquin Valley: California Largest Human Alteration of the Earth's Surface. Land Subsidence in the United States*, U.S. Geological Survey Circular, 1182, 23-34.

Ghorbani, Z., Khosravi, A., Maghsoudi, Y., Mojtahedi, F. F., Javadnia, E. & Nazari, A. (2022). Use of InSAR data for measuring land subsidence induced by groundwater withdrawal and climate change in Ardabil Plain, Iran. *Sci Rep, 12,* 13998. https://doi.org/10.1038/s41598-022-17438-y

Gonzales, P., & Fernandez, J. (2011). Drought-driven transient aquifer compaction imaged using multitemporal satellite radar interferometry. *Geology 39*(6), 551-554. https://doi.org/10.1130/G31900.1

Haghshenas Haghighi, M. & Motagh, M. (2021). Land subsidence hazard in iran revealed by country-scale analysis OF Sentinel-1 INSAR. *Int. Arch. Photogramm. Remote Sens. Spatial Inf. Sci., XLIII-B3-2021,* 155–161. https://doi.org/10.5194/isprs-archives-XLIII-B3-2021-155-2021

Hu, L., Dai, K., Xing, C., Li, Z., Tomas, R., Clark, B., Shi, X., Chen, M., Zhang, R., Qiu, Q., & Lu, Y. (2019). Land subsidence in Beijing and its relationship with geological faults revealed by Sentinel-1 InSAR observations. *International Journal of Applied Earth Observation and Geoinformation 82,* 101886. https://doi.org/10.1016/j.jag.2019.05.019

Hussain, M.A., Chen, Z., Zheng, Y., Shoaib, M., Ma, J., Ahmad, I., Asghar, A., & Khan, J. (2022). PS-InSAR Based Monitoring of Land Subsidence by

Groundwater Extraction for Lahore Metropolitan City, Pakistan. *Remote Sens.*, *14*, 3950. https://doi.org/10.3390/rs14163950

INE (Instituto Nacional de Estadistica). 2023. Retrieved from URL: https://www.ine.es, on 14.03.2023.

Karila, K., Karjalainen, M., Hyyppä, J., Koskinen, J., Saaranen, V., & Rouhiainen, P. (2013). A Comparison of Precise Leveling and Persistent Scatterer SAR Interferometry for Building Subsidence Rate Measurement. *ISPRS Int. J. Geo-Inf., 2*, 797-816. doi:10.3390/ijgi2030797

Khodapanah, L., Sulaiman, W.N.A., Hyyppä, J., & Nassery, H.R. (2011). Hydrogeological Framework and Groundwater Balance of a Semi-Arid Aquifer, a Case Study from Iran. *Journal of Water Resource and Protection, 3*, 513-521. doi:10.4236/jwarp.2011.37061

Liu, Z., Liu, P-W., Masooud, E., Farr, T., Lundgren, P., & Famiglietti, J. (2019). Monitoring Groundwater Change in California's Central Valley Using Sentinel-1 and GRACE Observations. *Geosciences, 9*, 436. doi:10.3390/geosciences9100436

Llmas, R., Fornes, J., Hernandez-Mora, N. & Martinez Cortina, L. (2001). Aguas subterráneas: retos y oportunidades [Groundwater: Challenges and opportunities]. Madrid, USpain: Mundi-Prensa, ISBN 92-9220-016-X.

Llmas, R. & Garrido, A. (2007). Lessons from Intensive Groundwater Use in Spain: economic and social benefits and conflicts. In Giordano M. & Villholth (Eds.). *The agricultural groundwater revolution: opportunities and threats to development*. pp 266-295. Wallingford, UK: CABI.

Mamais, L., Oligschläger, C., & Khabarov, N. (2020). *A case study: Aquifer Management in Spain* (Sentinels Benefits Study SeBS-CR-009). European Association of Remote Sensing Companies (EARSC), Funded by the EU and ESA – ESA Contract Number: 4000119743/17/I-SBo. Retrieved from URL: https://earsc.org/sebs/wp-content/uploads/2020/10/Aquifer-Management-in-Spain_vf.pdf on 14 March 2023.

Matano, F., Sacchi, M., Vigliotti, M., & Ruberti, D. (2018). Subsidence Trends of Volturno River Coastal Plain (Northern Campania, Southern Italy) Inferred by SAR Interferometry Data. *Geosciences, 8*, 8. doi:10.3390/geosciences8010008

Meza-Gastelum, M.A., Campos-Gaytán, J.R., Ramírez-Hernández, J., Herrera-Oliva, C.S., Villegas-León, J.J., & Figueroa-Núñez, A. (2022). Review of Groundwater Withdrawal Estimation Methods. *Water, 14*, 2762. https://doi.org/10.3390/w14172762

MIE (Ministerio de Industria y Energia) & MOPTM (Ministerio de Obras Publicas, Transportes y Medio Ambiente) (1995). *Libro Blanco de las Aguas Subterráneas [Groundwater White Book]*. Retrieved online from URL: https://hispagua.cedex.es/en/node/66985 on 14.03.2023

Miller, M. M., & Shirzaei, M., (2015). Spatiotemporal characterization of land subsidence and uplift in Phoenix using InSAR time series and wavelet transforms, J. *Geophys. Res. Solid Earth, 120*, 5822–5842, doi:10.1002/2015JB012017.

Mokadem, N., Redhaounia, B., Besser, H., Ayadi, Y., Khelifi, F., Hamad, A., Hamed, Y., & Bouri, S. (2018). Impact of climate change on groundwater and the extinction of ancient "Foggara" and springs systems in arid lands in North Africa: a case study in Gafsa basin (Central of Tunisia), *Euro-Mediterranean Journal for Environmental Integration, 3*, 28, https://doi.org/10.1007/s41207-018-0070-0.

Moya Ortega, C. & Garcia Marin, R. (2015). Population aging in Murcia Region: causes and consequences. *Geography papers*, *61*. doi: http://dx.doi.org/10.6018/geografia/2015/213901

MMA (Ministerio de Medio Ambiente) (2000). *Libro Blanco del Agua en España [White Book of Water in Spain]*. Retrieved online from URL: https://faolex.fao.org/docs/pdf/spa192539.pdf, on 14.03.2023

Murcia Today (2017). Understanding water and the drought in Murcia and the Segura basin. Retrieved from URL: https://murciatoday.com/understanding-water-and-the-drought-in-murcia-and-the-segura-basin_171862-a.html on 14.03.2023.

NASA. (2017). *NASA Data Show California's San Joaquin Valley Still Sinking*. Retrieved from URL: https://www.nasa.gov/feature/jpl/nasa-data-show-californias-san-joaquin-valley-still-sinking, on 27.02.2023.

Observatorio Economico. (2010). *Madrid Economy 2010*. Area de Gobierno de Economia, Madrid. Retrieved from URL: https://www.madrid.es/UnidadesDescentralizadas/UDCObservEconomico/MadridEconomia/Ficheros/MadridEconomia2010Ingles.pdf

Orellana, F., Moreno, M., & Yáñez, G. (2022). High-Resolution Deformation Monitoring from DInSAR: Implications for Geohazards and Ground Stability in the Metropolitan Area of Santiago, Chile. *Remote Sens.*, *14*, 6115.https://doi.org/10.3390/rs14236115

Pirouzi, A. & Eslami, A. (2017). Ground subsidence in plains around Tehran: site survey, records compilation and analysis, *Geo-Engineering, 8*, 30. https://doi.org/10.1186/s40703-017-0069-4

Poland, J. S. (1984). *Guidebook to studies of land subsidence due to ground-water withdrawal.* UNESCO.

Radutu, A. &Gogu, R.C. (2018). *Chronological reflection on monitoring urban areas subsidence due to groundwater extraction*. In E3S Web of Conferences, Volume 85, Proceedings of the EENVIRO 2018 Conference: Sustainable Solutions for Energy and Environment, Cluj Napoca, Romania, 9–13 October 2018; Balan, M.C., Bode, F., Croitoru, C., Dogeanu, A., Georgescu, A., Georgescu, C., Nastase, I., Sandu, M., Eds.; EDP Sciences: Paris, France, 2019; pp. 07015.

Rafiei, F., Gharechelou, S., Golian, S., & Johnson, B.A. (2022). Aquifer and Land Subsidence Interaction Assessment Using Sentinel-1 Data and DInSAR Technique. *ISPRS Int. J. Geo-Inf.*, *11*, 495. https://doi.org/10.3390/ijgi11090495

Rajabi Baniani, S., Chang, L., & Maghsoudi, Y. (2021). *Mapping and analyzing land subsidence for Tehran using Sentinel-1 SAR and GPS and geological data*. EGU General Assembly 2021, online, 19–30 Apr 2021, EGU21-295, https://doi.org/10.5194/egusphere-egu21-295, 2020.

Raspini, F., Cigna, F., & Moretti, S. (2012). Multitemporal mapping of land subsidence at basin scale exploiting Persistent Scatterer Interferometry: case study of Gioia Tauro plain (Italy), *Journal of Maps, 8*(4), 514–524. 10.1080/17445647.2012.743440

Raucoules, D., Colesanti, C., & Carnec, C. (2007). Use of SAR interferometry for detecting and assessing ground subsidence, *C. R. Geoscience, 339*, 289–302. https://doi.org/10.1016/j.crte.2007.02.002

Rickey, S., Thomas, B., Lo, M-H., Famiglietti, J., Swenson, S., Rodell, M. (2015). Uncertainty in Global Groundwater storage estimates in a total groundwater stress framework. *Water Resources Research*. *51*(7), 5189-5216. DOI: 10.1002/2015WR017351

Rigo, A., Bejar-Pizzaro, M., & Martinez-Diac, J. (2013). Monitoring of Guadalentín valley (southern Spain) through a fast SAR Interferometry method, *Journal of Applied Geophysics, 91*, 39-48. http://dx.doi.org/10.1016/j.jappgeo.2013.02.001

RDP, 2010, *Rural Development Programme of Murcia – Spain, European Network for Rural Development*. Retrieved from URL: https://enrd.ec.europa.eu/sites/default/files/fms/documents/RDP/RDP_Murcia%20_Spain.pdf, on 14.03.2023

Rodolfo, K., & Siringan, F. (2006). Global sea-level rise is recognised, but flooding from anthropogenic land subsidence is ignored around northern Manila Bay, Philippines, *Disasters, 30*(1), 118-139. https://doi.org/10.1111/j.1467-9523.2006.00310.x

Ruiz-Constan, A., Ruiz-Armenteros, A., Lamas-Fernandez, F., Martos-Rosillo, S., Delgado, J., Bekaert, D., Sousa, J., Gil, A., Cuenca, M., Hanssen, R., Galindo-Zaldivar, J., & de Galdeano, C. (2016). Multi-temporal InSAR evidence of ground subsidence induced by groundwater withdrawal: the Montellano aquifer (SW Spain). *Environ Earth Sci, 75*(242), 1-16. doi:10.1007/s12665-015-5051-x

Schmidt, D. A., & Burgmann, R. (2003). Time-dependent land uplift and subsidence in the Santa Clara valley, California, from a large interferometric synthetic aperture radar data set. *Journal of geophysical research, 108*(B9). doi:10.1029/2002JB002267

Sidiq, T.P., Gumilar, I., Abidin, H.Z., & Gamal, M. (2019). Land subsidence induced by agriculture activity in Bandung, West Java Indonesia. *IOP Conf. Ser.: Earth Environ. Sci., 389*(012024). doi: 10.1088/1755-1315/389/1/012024

Sneed, M., Brandt, J. T., & Solt, M. (2014). *Land Subsidence, Groundwater Levels, and Geology in the Coachella Valley, California, 1993–2010: US Geological Survey.* Scientific Investigations Report 2014–5075. http://dx.doi.org/10.3133/sir20145075

Solari, L., Del Soldato, M., Bianchini, S., Ciampalini, A., Ezquerro, P., Montalti, R., Raspini, F., & Moretti, S. (2018). From ERS 1/2 to Sentinel-1: Subsidence Monitoring in Italy in the Last Two Decades. *Front. Earth Sci. 6*, 149. doi: 10.3389/feart.2018.00149

Suarez, G., Jaramillo, S., López-Quiroz, P., & Sánchez-Zamora, O. (2018). Estimation of ground subsidence in the city of Morelia, Mexico using Satellite Interferometry (INSAR)s. *Geofísica Internacional 57*(1), 41-60.

Tessitore, S., Fernández-Merodo, J.A., Herrera, G., Tomas, R., Ramondini, R., Sanabria, M., Duro, J., Mulas, J., & Calcaterra, D. (2016). Comparison of water-level, extensometric, DInSAR and simulation data for quantification of subsidence in Murcia City (SE Spain). *Hydrogeol J, 24*, 727-747. doi 10.1007/s10040-015-1349-8

Toufigh, M., Tabatabaei Aghda, S.T., Fahmi, A. & Mortazavi, S.M. (2004). *Land subsidence and its consequences of large groundwater withdrawal in Rafsanjan, Iran*. Conference: Management of Aquifer Recharge and Water Harvesting in Arid and Semi-arid Regions of Asia. At: International Center of Qanat, Yazd, Iran.

USGS. (2017). *California Water Science Center*. Retrieved from URL: https://ca.water.usgs.gov/land_subsidence/california-subsidence-cause-effect.html on 27.02.2023.

Ustun, A., Tusat, E., & Yalvac, S. (2010). Preliminary results of land subsidence monitoring project in Konya Closed Basin between 2006–2009 by means of GNSS observations. *Nat. Hazards Earth Syst. Sci.,10*, 1151-1157. doi:10.5194/nhess-10-1151-2010

WWF (2006). *Illegal water use in Spain. Causes, effects and solutions*. Madrid, Spain: WWF/Adena. Retrieved from URL: https://wwfeu.awsassets.panda.org/downloads/illegal_water_use_in_spain_may06.pdf on 14.03.2023

Scientific Papers. Series E. Land Reclamation, Earth Observation & Surveying, Environmental Engineering. Vol. XII, 2023
Print ISSN 2285-6064, CD-ROM ISSN 2285-6072, Online ISSN 2393-5138, ISSN-L 2285-6064

MONITORING THE VEGETATION STATE IN OLTENIA PLAIN, USING COPERNICUS LAND PRODUCTS

Denis MIHAILESCU[1, 2], Sorin Mihai CIMPEANU[2]

[1]National Meteorological Administration, 97 Bucharest-Ploiesti Street, District 1, Bucharest, Romania
[2]University of Agronomic Sciences and Veterinary Medicine of Bucharest, 59 Marasti Blvd, District 1, Bucharest, Romania

Corresponding author email: denis.mihailescu@meteoromania.ro

Abstract

The development of Earth Observation Systems in Europe began since the 1970s. France, through the National Center for Space Studies (CNES) together with partners from Belgium and Sweden and later through the establishment of Spot Image, laid the foundations of the SPOT space program. The year 1998 brings the first steps of a new common space program of the EU countries by the appearance of the GMES (Global Monitoring for Environment and Security) initiative. In 2014 GMES changed its name to Copernicus and is coordinated and managed by the European Commission, in collaboration with European Space Agency for the space component, European Environment Agency and Member States for the in-situ component. An important step in the study of vegetation was made with the emergence of the SPOT-VEGETATION program based on SPOT 4 and 5 from 1998 to 2013, followed by Proba-V from 2013 until 2020 and continued today by Sentinel-3. Vegetation indices are widely used for assessment of green biomass, crop production, plant health and stress to water scarcity, extreme weather conditions, and diseases.

Key words*: Copernicus, CGLS, Proba-V, Vegetation state.*

INTRODUCTION

The Copernicus program is the European Earth observation system, using both satellite and in-situ data. It is coordinated and managed by the European Commission and implemented in partnership with Member States, ESA, EUMETSAT, ECMWF (European Center for Medium-Range Weather Forecasts), EU Agencies and Mercator Océan (copernicus.eu).
To meet all user's needs and requirements in all areas of interest, Copernicus has been divided into 6 services: atmosphere, marine, land, climate change, security and emergency. Copernicus Global Land Service (CGLS) is the global component of the land monitoring service, which produces a series of medium and low-resolution bio-physical indices. In the initial phase of operation (2013-2016), CGLS developed 13 products (variables), based on observations made by VEGETATION instruments on board SPOT (Arnaud et al., 1991; Pulitini et al., 1994; Kurtis et al., 1998; Maisongrande et al., 2003), MetOp-ASCAT (Eumetsat, 2014) and other geostationary meteorological satellites. In 2016, new products were made available from PROBA-V (Dierckx et al., 2013), with improved spatial resolution of 300 m. From January 2017, other products with the same spatial resolution of 300 m were added. In the last phase of development (2016-2019), the number of bio-physical variables with global coverage was increased. Products from the cryosphere area have been added, as well as new products in existing areas. After the retirement of PROBA-V in 2020, the coverage is provided by OLCI instrument on board of Sentinel-3. The products are used for vegetation monitoring, water circuit, solar energy and cryosphere, being complemented by the existence of multi-temporal data series (land.copernicus.eu). All datasets can be accessed through several services: interactive notebooks, web, virtual machine desktop, manifest files, regular FTP, legacy portal and GEONETCast. For visualization there are 4 services: Global Land Cover Viewer, Africa demo Land Cover Viewer, Hot Spot Land Cover Change Explorer and Tiled map viewing service. There is also a multi-temporal analysis

service, for several variables. Analyzes can be made starting with 1998 at the level of administrative region (predefined) but also on customized points and polygons.

MATERIALS AND METHODS

Due to the position in southwestern Romania, the generally smooth landscape with average altitudes of approx. 100 m, the aspect of steppe and forest-steppe, the climatic influences and particularities, the Oltenia Plain has mainly an agricultural feature. It represents the plain area of Mehedinți and Dolj counties and almost 2/3 of the plain area of Olt County. The main cultivated crops are wheat, rye, barley, oats, corn, sunflower and rapeseed. In addition to these, potatoes, melons, vegetables and various types of fodder plants are also grown. Cumulated in the 3 counties, between 1990 and 2018, areas cultivated with wheat and rye increased by 110.000 ha, sunflower by 77.000 ha and rapeseed crops from 2000 ha to 63.000 ha. Instead, the areas occupied by corn decreased by 88,000 ha and those with barley and oats by almost 30,000 ha (Figure 1).

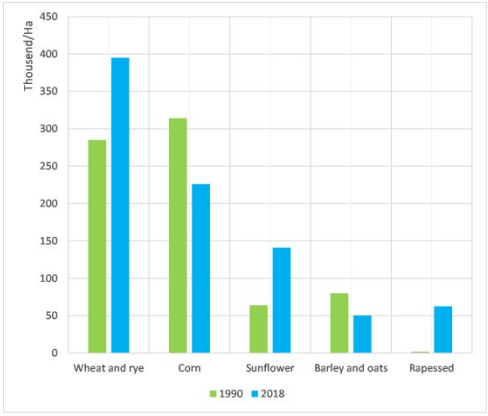

Figure 1. Cumulated areas occupied by the main crops in Mehedinți, Dolj and Olt counties for 1990 and 2018 (Source INS)

From the area of the Oltenia Plain, approximately 800.000 ha, 82% is used as agricultural land, and the arable land represents 70% (560.000 ha) of the total unit area. Between 1990 and 2018, the largest changes in land cover were recorded by arable land, which gains 50.000 ha taking over vineyards and pastures (Mihailescu & Cimpeanu, 2019). The most cultivated plant type is wheat, which together with barley, oats and rye can cover almost 60% of the total arable land. Next are corn, sunflower, rapeseed that have gained ground in recent years, and watermelon, especially in the Dabuleni-Sadova area.

Figure 2 show the density of the main crops in 2010, for the plots with an area of at least 10 ha and 10 km x 10 km grid. The data are acquired in the Farm Structure Survey (FSS), carried out by all Member States, following a common methodology to have comparative and representative results and statistics in time and space. The study is performed with a complete set of observations at an interval of 10 years (the last agricultural census and at 3-4 years on certain test areas - Eurostat).

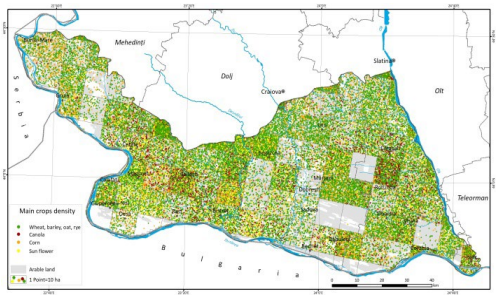

Figure 2. Main crops density in Oltenia Plain (Source: EC/Eurostat)

Wheat crops are covering areas of approx. 280.000 ha and together with barley, oats and rye exceed 320.000 ha. Maize exceeds 100.000 ha, sunflower 80.000 ha and rapeseed over 50.000 ha. Considering the data from 2018, it is foreseen that for the next FSS study, the values will remain constant for the crops over Oltenia Plain. The map above clearly shows three distinct areas: north of Dabuleni, Desa and east of Gruia in Blahniței Plain, where the crop density is low or almost non-existent. This is due to the presence of sandy soil and the phenomena of aridization and desertification associated with pedological drought.

With the launch of the NOAA AVHRR satellites and continuing with the NASA ERTS-Landsat program, the Earth's surface was also scanned into the red and infrared bands of the electromagnetic spectrum. The notion of "vegetation index" was first used by American researchers Donald Deering and Dr.

Robert Hass. Together with mathematician Dr. John Schell, they studied the biophysical characteristics of vegetation in the Great Plains region, using spectral signals from satellites. The first study to use NDVI, "Monitoring Vegetation Systems in the Great Plains with ERTS" was published in 1974 by Dr. J. W. Rouse. In the following period it was introduced in more studies on vegetation, remaining even today the most known and used vegetation index. NDVI is an indicator of presence, density and greenness state of biomass, thus having a close link with other vegetation proprieties indicator Fraction of Absorbed Photosynthetically Active Radiation (FAPAR). Even if it is not a physical property of vegetation, the use in the calculation algorithm of spectral bands in red and near infrared, makes NDVI to be widely used in ecosystem monitoring.

$$\text{NDVI}=\frac{(NIR-Red)}{(NIR+Red)} \quad (1)$$

The normalized values of the pixels are between -1 and 1. The spectral signature of the vegetation shows a reflection increase around 0.7 μm, while the land without vegetation, depending on the type of surface, has a more linear spectral signature. The negative values (-1; 0) of NDVI can be associated with water, snow, clouds, land without vegetation (or dead vegetation). The positive values increase the more active the chlorophyll is, which makes the level of infrared reflection (0.78-1 μm) very high. Between 0 and 0.33, sparse vegetation and unhealthy plants occur, up to 0.66, moderately healthy and denser vegetation. The high values of NDVI, over 0.6, show healthy and high-density vegetation, as in the case of forests (0.7-1).

The Fraction of Absorbed Photosynthetically Active Radiation (FAPAR) is defined as the fraction of active radiation absorbed by the process of photosynthesis (PAR) by the canopy. PAR is the solar radiation that reaches the leaves with a wavelength between 0.4-0.7μm. FAPAR quantifies the fraction of solar radiation absorbed by healthy leaves, necessary for the process of photosynthesis and depends on the structure of the canopy, the optical properties of vegetation, atmospheric conditions and angular configuration. FAPAR plays a crucial role in the energy balance of ecosystems and in estimating the carbon balance. It is one of the surface parameters that can be used to quantify CO_2 assimilated by plants and water released by evapotranspiration. The continuous observation of FAPAR is indicated for the monitoring of the seasonal and inter-annual cycle of the variability of the photosynthesis activity of the terrestrial vegetation. FAPAR is used as an input parameter in primary productivity models, based on considerations of light use efficiency. There is a relationship between FAPAR and NDVI. The increase in values depends on land cover and leaf area, with a similar response to leaf orientation, zenithal solar angle, and the coefficient of attenuation of solar radiation by the atmosphere (Myneni et al., 1994). FAPAR is recognized by the Global Climate Observing System (GCOS) as an Essential Climate Variable (ECV) and is a good indicator of drought.

The Leaf Area Index (LAI) is defined as half of the total area of the green elements of the vegetation canopy per horizontal ground surface (Chen & Black, 1992). The values derived from the satellite correspond to the total green leaf area in all layers of the canopy, including the first layer at ground level, which can be a significant contribution, in particular, for forests. LAI varies depending on several factors including seasonal climate change, the presence of water and nitrogen, the distribution of carbon dioxide vertically (Cowling et al., 2003). LAI can be estimated by in-situ measurements but also by remote sensing with the specification that this includes all green vegetation, such as in the case of forests, the lower layer of vegetation on the ground. With the exception of directional observations (Chen et al., 2005), LAI is not directly accessible through remote sensing observations due to the possible existence of heterogeneity in leaf distribution relative to canopy volume (Baret et al., 2016). Therefore, remote sensing observations are rather sensitive to the "effective" leaf surface index, thus the value that provides the same diffuse difference fraction, assuming a random distribution of leaves (Baret et al., 2016). The difference between the current and the actual leaf surface index can be quantified by the vegetation

agglomeration index (Chen et al., 2005) which varies approximately between 0.5 (dense canopy) and 1 (randomly distributed leaves). The measured LAI actually corresponds to the green elements, being rather a greenness indicator.

Soil moisture (SM) dynamics is important in understanding environmental but also socio-economic processes, such as its impact on vegetation vitality, crop yields, droughts or flood risk exposure. SM is a key factor in the exchange of water and heat between soil and atmosphere, regulating air temperature and humidity (Bauer-Marschallinger et al., 2018). Soil Water Index (SWI) quantifies the state of humidity starting from the soil surface to a depth of 1m. It is mainly conditioned by precipitation through the infiltration process. Soil moisture is a very heterogeneous variable and varies on small scales depending on soil properties and drainage patterns. Satellite determinations are integrated over relatively large areas, with the presence of vegetation which adds complexity to the interpretation (land.copernicus.eu). SWI is produce in 2 forms: at European level, with 1 km spatial resolution, based on daily measurements from Sentinel-1 (C band SAR) and Metop ASCAT and at global level, with 12.5 km spatial resolution, from Metop ASCAT, daily and 10 days synthesis (SWI10). The quality of the SWI 1 km product was evaluated in the period 2015-2019 by comparing with the in-situ measurements provided by International Soil Moisture Network (ISMN), to which Romania also contributes with its own measurement network (RSMN) composed of 20 automatic stations. The analysis includes an examination of the temporary dynamics of SWI and how it correlates with field reference data. The SWI retrieval method does not consider the soil texture, which determines the relationship between T-value (time length) and soil depth (de Lange et al., 2008), and evapotranspiration. Eight T-values are provided to give more possibility to the user for selecting the best matching data (CGLS Product user manual, 2018). Currently is not possible to associate a T-value to a certain soil depth since this depends strongly on the application and the soil composition of the area of interest (Paulik et al., 2014). The quality of the SWI and SWI10 was evaluated by comparing different T-values to different layers of the global GLADS Noah model (higher T-values represent deeper soil layer) and in situ data from ISMN (GIO-GL Quality assessment report, 2015).

For validation, Pearson correlation coefficient (R) with a $p\ value < 0.01$ and root mean square difference (RMSD) were used. The accuracy assessment is performed every year using the latest *in situ* measured reference data.

RESULTS AND DISCUSSIONS

Knowing the soil moisture values is very important as the occurrence of drought and associated phenomena of aridization and desertification are increasingly frequent in Oltenia Plain given that the agricultural area occupies 82% of the total unit. Soil moisture is graphically represented in Figure 3, through the Soil Water Index (SWI), over entire plain at various soil depths (T-values = 5.40 and 100) for 2019 and 2020. The temporal resolution is 10 days.

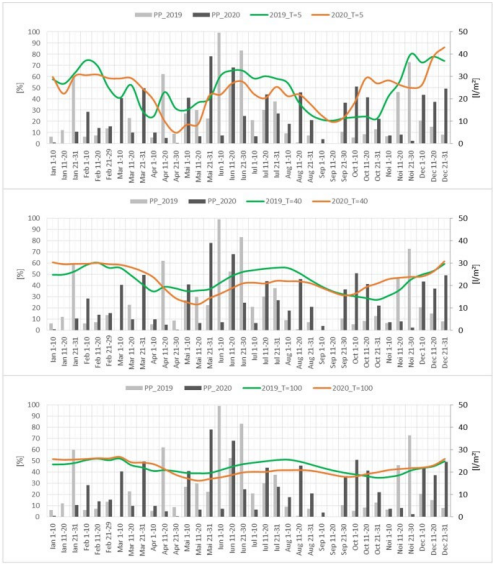

Figure 3. Soil Water Index and rainfalls for 2019 and 2020

An accentuated dynamics can be observed for T = 5 where the humidity is strongly correlated with rainfalls. SWI reacts immediately, naturally, to the appearance of water but also to small and insufficient amounts for plant

development. In spring 2019, due to low amounts of rainfall, the relative value of humidity reaches a minimum of 24% in the first decade of April. There is a period of growth until mid-July, after which the values fall sharply in August, September and October, following an increase and a maximum of 80% in the last decade of November. In 2020, starting with the second decade of March, soil humidity is decreasing from 59% to under 10% in the last decade of April and stay under 2019 values until late August. For T = 40 and T = 100, the humidity is more linear and similar, a lower dynamic due to the ability of water to infiltrate into the soil depending on its texture. The SWI 2019-2020, March to September average is presented in Table 1.

Table 1. SWI average 2019 vs. 2020

Year	SWI T = 5	SWI T = 40	SWI T = 100
2019	48%	45%	45%
2020	46%	45%	43%
1.03-30.09.2019	42%	44%	45%
1.03-30.09.2020	38%	40%	41%

In spring, when moisture intake is necessary for plant development, soil moisture for T = 40 and T = 100 is 50-60% in the first decade of March, then rapidly dropping to a minimum of 23-35% in the second decade of May. In August and September (droughty months), even if the SWI values at depth are on average 40%, they remain higher than the surface values of 30%, thus ensuring a certain degree of humidity in the soil. The occurrence of drought in May 2020 is observed by comparing the values recorded in the second decade of the month in 2019 and 2020 (Figure 4). During May 11-20, 2019, on the largest surface of the Oltenia Plain, the average value of relative humidity is approx. 40%, except for two areas. In the center of Bailestilor Plain, for T = 5 and T = 40, the values were lower, between 20% and 30%, and east of Jiu River (Romanatilor Plane), the SWI values were higher, between 40% and 50%. Between 11 and 20 May 2020, the relative humidity for T = 5 was 10-20% on most of the unit, even below 10% in the south, in the Lake Bistret are and maximum 30% in the center and north of the Romanatilor Plain.

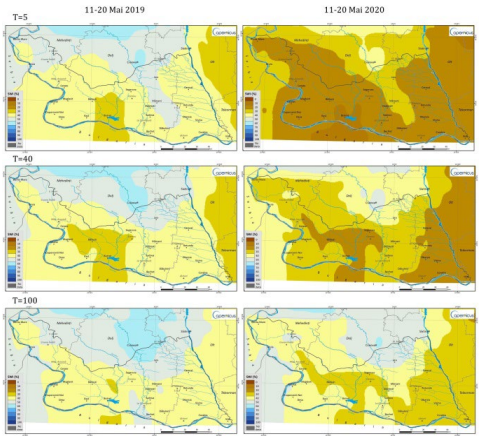

Figure 4. SWI10 in the second decade of May 2019 and 2020 (T = 5, 40 and 100), highlights the occurrence of drought in late spring 2020

For T = 40 the average is 30%, but on two areas, in the center and east, the values are lower, from 10% to 20%. For T = 100, the situation is slightly better, with values of 20-40% and over 40% in the north of the Romanatilor Plain.

The amounts of rainfalls measured at 5 meteorological stations, Bailesti, Bechet, Calafat, Caracal and Craiova (Figure 5), confirm the lack of soil moisture recorded by satellite sensors. From May 7, 2020 until May 19 (13 consecutive days) three of the five stations do not record rainfall values (Bechet, Calafat and Caracal) and the other two, only at the end of period, registered low quantities.

On May 18, 2020, at Craiova station there are very low amounts of rainfalls, of only 0.5 mm, and on May 19 in Bailesti 8.4 mm.

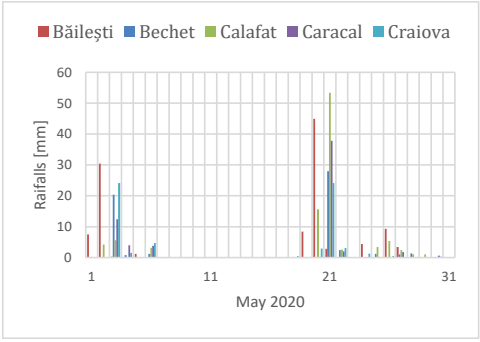

Figure 5. Rainfall amount in May 2020 at five meteorological stations

After two days of rain, with quantities that even exceeded 50 mm in Calafat, follows a period with very low or even non-existent quantities at some stations. These quantities may not be enough for the affected plants to return, moreover, a new period with moisture deficit can occur.

What is important to emphasize is that May is one of the months with the richest rainfall recorded at the 5 weather stations, compared to the climatic average. In addition, even if they all approach the value of the climatological average or even exceed it, the drought occurs. This is possible because rainfalls were recorded practically only in 2 periods of the month: at the beginning of the first and third decade. The uneven distribution of rainfalls and the deficit of humidity in winter due to an almost non-existent layer of snow, led to the appearance of drought.

The evolution of vegetation and in particular of crops depends to a very large extent on the amount of water (from rainfall or irrigation) that provides the necessary soil moisture. The temporary extension of rainfalls during the most important phenological phases of crops is also important. Even if the norm is met at an average/month level, it is important to be evenly divided during the entire period. The response of the vegetation to the presence or scarcity of water is reflected in the NDVI values with a delay of several days. The beginning of 2019 came with a higher amount of water from rainfalls but with NDVI values smaller than 2020. This happened because of an extensive layer of snow that persisted until the end of February. In the first 10 days of May 2020, NDVI drops suddenly as consequence of an April almost without rain. Following this period, the values remain lower than same period of 2019, highlighting a drought phenomenon in May 2020 (Figure 6).

The graph pointed out the agricultural characteristics of the plain and the type of crops. Winter crops, especially wheat, give higher NDVI values in the first half of the year, so that in the second half, spring crops, which occupy smaller areas, together with the moisture deficit, give lower NDVI values.

The first 3 months of the year are part of the last phase of the rooting stage of wheat (beginning in September-October), when the twining of the shoots and the elongation of the stem takes place.

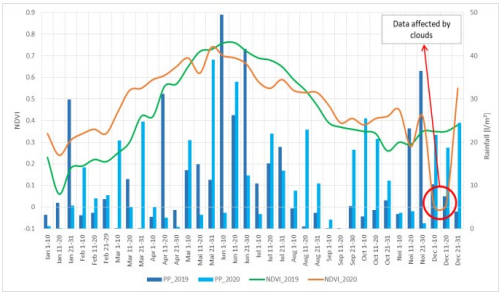

Figure 6. NDVI evolution in 2019 and 2020

The growth depends during this period on temperature, the number of sunny days, and the presence of a protective snow layer. In April and May follows the establishment stage, a critical period in the plant's development, as the elongation of the stem continues, the roots deepen, the first detectable node appears, the inflorescences and spike formation appear. This is a period in which the presence of water plays an important role, on which the productivity of the plant depends. The production stage begins in June, after flowering, when the number of grains/m^2 and their weight can be determined.

With the maturation and gradual loss of greenness, starting in mid-June, the NDVI values begin to decrease. This cycle can be observed annually, with slight differences depending on environmental conditions and possible image errors (Figure 7).

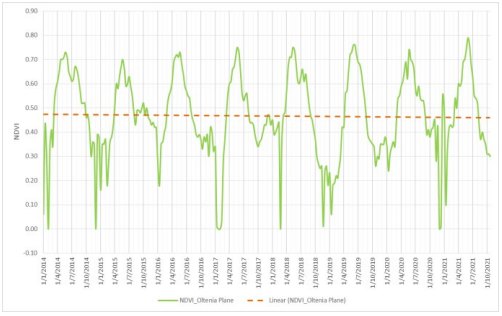

Figure 7. NDVI multitemporal cycle and trend from 2014 until 2021

The NDVI trend shows a slight decrease of values from 2014 until 2021, which can be caused by a low amount of water from rainfalls

at the times when the plant needs it the most, the lack of irrigation especially in the months when the phenomenon of drought occurs and possible diseases that affect the plant condition. Given that NDVI is considered a vegetation index and FAPAR represents vegetation properties, the response to soil reflectance and vegetation optical properties are different. Depending on the type of vegetation, the canopy can cover ground. Higher soil reflectance negatively influences NDVI but increases FAPAR values. The canopy of summer crops like corn and sunflower decrease soil reflectance. The diminishing of photosynthesis process occurs when the plants are mature and close to harvest. When canopy is losing his greenness becoming browned, FAPAR begins to decrease. This can be observed starting May when NDVI continues to increase until June and FAPAR reaches its maximum in the last decade of May. From June, the differences increase due to the harvesting of winter crops and the appearance of the panicle and corn silk, when part of the leaves at the base may turn yellow and dry. With the ripening of the grain and the reaching of physiological maturity in the months of July and August, adding a lack of rainfalls, FAPAR registers a steep drop on arable land, reaching values of 0.2 at the end of September, which means low health or no vegetation. If in the first decades of May 2019, the average value of FAPAR for arable land was 0.64, in the similar period of 2020, the value is 0.57. In Figure 8, orange-red areas from 2019 highlight a greater absorption of solar radiation, therefore, more active photosynthesis process compared to 2020.

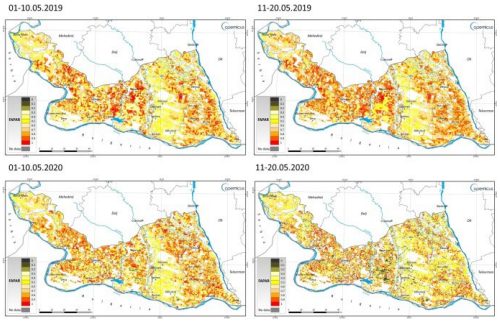

Figure 8. FAPAR evolution in the first two decades on May 2019-2020

In the decade 10-20 May 2020, with the intensification of the drought, dark areas appear in the central part of the plain, which indicate a decrease of the crop's health and withering.

A large variety of models used in agriculture, ecology, carbon cycle, climate or other studies use LAI to quantify the number of leaves present in each environment to correctly represent radiation, heat, water and various gas exchanges with the atmosphere and soil.

The main uses are in the soil-vegetation-atmosphere transfer scheme, in models of biogeochemical cycles, in agrometeorology for crop evaluation, which usually require long time series at a certain spatial scale. Together with the variation of FAPAR and soil moisture, LAI can highlight the increase or decrease of green mass in agricultural area. For arable land in the plain area, the maximum annual value of LAI is usually reached at the end of May or the beginning of June. In the Oltenia Plain, during this period, the values are around 3, in the years favorable for the development of crops reaching the value of 3.4-3.5 and in the deficit years around the value of 2.2-2.4. Moreover, the multi-temporal average over a period of 20 years is slightly above the value of 2.2 in the last decade of May. If in the first decade of May 2020, the LAI had a slightly higher value compared to the same period in 2019, in the second decade, the LAI value is lower and continues to decrease in the last decade as well (Table 2).

Table 2. LAI values in May 2019-2020

Decade	2019	2020
01-10 May	2.65	2.67
11-20 May	2.94	2.69
21-31 May	3.15	2.52

Figure 9 shows the differences that appear in the second decade, more pronounced in the center, south of Segarcea, between Desnățui and Jiu rivers, continuing in the last decade of May. Due to the 2 weeks without rainfall, the soil moisture decreased on the surface, while at depth (root zone), the water reserve managed to ensure a small amount, however, insufficient for further development of the crops. The LAI values started to decrease in the second and third decade of the month, compared to 2019 when the development continues and the LAI reaches the maximum value of 3.15. These

decreases are equivalent to the reduction of the percentage of green mass, which can lead to a lower agricultural production. Since, in general, the maximum LAI values are at the end of May, even with the contribution of rainfall that fell in the last decade of the month, it is impossible to return to values close to 3, resulting in a period affected by drought.

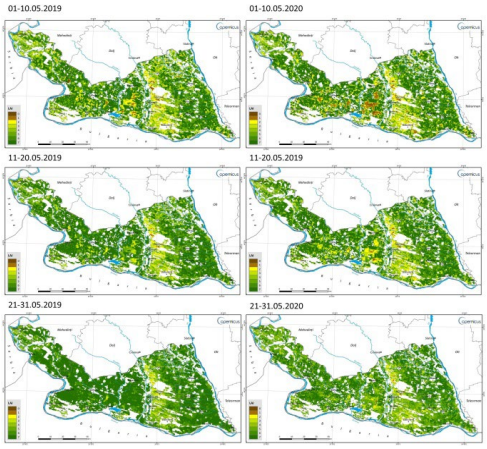

Figure 9. Leaf Area Index in May 2019-2020

What stands out is the lack of vegetation on the eastern side of the Jiu River, from south of Craiova to the contact with the Danube valley. This strip, which can reach a width of 30 km in the southern part, is known as an area dominated by sandy soils on which sand dunes have developed. Land fragmentation, active processes of desertification and aridization, lack of land reclamation especially irrigation and sand-stabilizing plants, will lead to an increase of affected areas by climate change.

CONCLUSIONS

The satellite products for land monitoring are increasingly used because they are non-invasive means of measurement, ensure the observation of any area with global coverage, daily temporal resolutions and 10-day synthesis, delivery of products in less than 24 hours and consolidated after 3 days. In this case, only a small part of what is called vegetation thematic area was described and used (products with medium spatial resolution of 300m, 1km and coarser at 12.5km), useful for monitoring larger areas, such as plains. For detailed analysis, vegetation indices derived from higher spatial resolution satellite images such as Sentinel-2 can be produced. With the archiving of older products, time series of data can be created that help to develop new indices such as VCI (Vegetation Condition Index) or VPI (Vegetation Productivity Index), which evaluate the current state of vegetation with the help of long-term statistics. Together with the data acquired in-situ, with the help of specific devices, from meteorological stations in the national system or from mini-stations located right in the cultivated land, the satellite data provide a picture of what happened in the recent past, for at least 24 hours, thus being able to make forecasts or act punctually in the field, for the best possible management of material and human resources. In the evolution of the vegetation indices (NDVI, FAPAR, LAI) can be observed the effects of climate change that affect the evolution of the phenological phases. This effects together with poor land reclamation actions will lead to a decrease in crop productivity.

REFERENCES

Arnaud, M., Leroy, M. (1991). SPOT4: a new Generation of SPOT satellites. *ISPRS Journal of Photogrammetry and Remote Sensing, 46*, 205-215.

Baret, F., Weiss, M., Verger, A., Smets, B. (2016). *ATBD for LAI, FAPAR and FCOVER from PROBA-V products at 300m resolution (GEOV3)*. Imagine S, FP7-Space-2012-1.

Bauer-Marschallinger, B., Paulik, C., Hochstoger, S., Mistelbauer, T., Modanesi, S., Ciabatta L., MASSARI C., Brocca, L., Wagner, W. (2018). Soil Moisture from fusion of scatterometer and SAR: Closing the scale gap with temporal filtering. *Remote Sensing 1019*, 1030. http://doi.org/10.3390/rs10071030

Chen, J.M., Black, T.A. (1992). Defining leaf area index for non-flat leaves. *Plant Cell Environ, 15*, 421–429.

Chen, J.M., Menges, C.H., Leblanc, S.G. (2005). Global mapping of foliage clumping index using multi-angular satellite data. *Remote Sensing of Environment, 97*(4), 447-457. https://doi.org/10.1016/j.rse.2005.05.003

Copernicus https://www.copernicus.eu/en

Copernicus Land Monitoring Service https://land.copernicus.eu/

Copernicus GIO-GL "Operations of the Global Land Component". (2015). SWI Quality Assessment Report (Validation Report). https://land.copernicus.eu/global/products/swi

Copernicus Global Land Operations "Vegetation and Energy". (2018). Soil Water Index, Product User

Manual. https://land.copernicus.eu/global/products/swi

Cowling, S.A., Field, C.B. (2003). Environmental control of leaf area production: Implications for vegetation and land-surface modeling. *Global Biogeochemical Cycles*, *7*(1), 7-1-7-14. https://doi.org/10.1029/2002GB001915

de Lange, R., Beck, R., van de Giesen, N., Friesen, J., De Wilt, A., Wagner, W. (2008). Scatterometer-derived soil moisture calibrated for soil texture with a one-dimensional water flow model. *Geoscience and Remote sensing, IEEE Transactions on, 46*, 4041-4049. https://doi.org/10.1109/TGRS.2008.2000796

Dierckx, W., Benhadj, I. (2013). Proba-V Belgian Mission Satellite Global Products for Vegetation Monitoring. Geoinfor Geostat: An Overview. s1. doi:10.4172/2327-4581.S1-018.

EUMETSAT (2014). *ASCAT Level 1 SZF Climate Data Record Release 2 - Metop, European Organisation for the Exploitation of Meteorological Satellites*, doi: 10.15770/EUM_SEC_CLM_0041. http://doi.org/10.15770/EUM_SEC_CLM_0041

EUROSTAT https://ec.europa.eu/eurostat/web/microdata/farm-structure-survey

Kurtis, J.T., LaMarr, J.H., Scott, K., Gustafson-Bold, C. (1998). Methods for the calibration of SPOT4 HRVIR and vegetation. *Proc. SPIE Int. Soc. Opt. Eng., 3439*, 439-449.

Maisongrande, P., Duchemin, B., Dedieu, G. (2003). *VEGETATION/SPOT* - An Operational Mission for the Earth Monitoring: Presentation of New Standard Products. *International Journal of Remote Sensing, 25*(1), 9-14, doi:10.1080/0143116031000115265.

Mihailescu, D., Cimpeanu, S.M. (2019). Multi-temporal analysis of land cover changes in Oltenia Plain, using Terrset Land Change Modeler. *Agrolife Scientific Journal, 8*(2), 82-91, ISSN 2285-5718.

Myneni, R.B., Williams, D.L. (1994). On the relationship between FAPAR and NDVI. *Remote Sensing of Environment, 49(*3), 200-211. https://doi.org/10.1016/0034-4257(94)90016-7

Paulik, C., Dorigo, W., Wagner, W., Kidd, R. (2014). Validation of the ASCAT Soil Water Index using in situ data from the International Soil Moisture Network. *International Journal of Applied Earth Observation and Georinformation, 30*, 1-8. https://doi.org/10.1016/j.jag.2014.01.007

Pulitini, P., Barillot, M., Gentet, T., Reulet, J.F. (1994). Vegetation payload. In Proceedings of the International Society for Optical Engineering (SPIE) 2209, Garmisch-Partenkirchen, Germany, pp. 126.

Rouse, J.W., Haas, R.H., Schell, J.A., Deering, D.W. (1974). Monitoring Vegetation System in the Great Plains with Erts. Third Earth Resources Technology Satellite-1 Symposium- Volume I: Technical Presentations. NASA SP-351, compiled and edited by Stanley C. Freden, Enrico P. Mercanti, and Margaret A. Becker, 1994, published by NASA, Washington, D.C., 1974, pp.309.

Scientific Papers. Series E. Land Reclamation, Earth Observation & Surveying, Environmental Engineering. Vol. XII, 2023
Print ISSN 2285-6064, CD-ROM ISSN 2285-6072, Online ISSN 2393-5138, ISSN-L 2285-6064

EXTREME AGROCLIMATIC INDICATORS PROJECTION UNDER CLIMATE CHANGE IN OLTENIA PLANE

Denis MIHAILESCU[1, 2], Mihaela CAIAN[1], Sorin Mihai CIMPEANU[2]

[1]National Meteorological Administration, 97 Bucharest-Ploiesti Street, District 1, Bucharest, Romania
[2]University of Agronomic Sciences and Veterinary Medicine of Bucharest, 59 Marasti Blvd, District 1, Bucharest, Romania

Corresponding author email: denis.mihailescu@meteoromania.ro

Abstract

The warming of the climate system is a reality, with observations indicating increases in global average water and ocean temperatures, extensive melting of snow and ice, and global average sea level rise. It is highly likely that much of the warming can be attributed to human-caused greenhouse gas (GHG) emissions. Over the past 150 years, the average global surface temperature has risen by almost 0.8ºC overall and by 1ºC in Europe. The average global temperature in 2020 was almost identical with 2016, considered the warmest year on record. Continuing the planet's long-term warming trend, the 2020 annual average temperature was 1.02ºC higher than 1951-1980 reference average, according to NASA. 2020 slightly exceeded 2016 values, which were within the error boundaries of the analysis, making the two years the warmest on record in modern history. Here we analyse projected changes over one of the most important agricultural areas for Romania with focus on extreme agroclimatic indicators analysis.

Key words*: climate change, C3S, extreme agroclimatic indicators, climate projection.*

INTRODUCTION

Climate change is a significant change in long-term average weather conditions, so a region can become warmer, wetter or drier over several decades. A trend of change lasting a large number of years makes the difference between climate change and weather variability in its natural dynamics. Throughout its existence, the Earth has gone through periods of warming and cooling, driven by solar intensity, volcanic eruptions, and natural changes in greenhouse gas concentrations. These climate changes are considered natural. However, records show that climate change is occurring much more rapidly than in the past, especially since the mid-20th century, and cannot be explained as having natural causes alone (Turrentine et al., 2021). According to Riebeek, 2010 "These natural causes are still active today, but their influence is too small or too slow to explain the rapid warming observed in recent decades." The anthropogenic causes of climate change or more specifically the greenhouse gas emissions (GHG) they generate are the main cause of climate change at global level. Normally, greenhouse gases play an important and beneficial role in keeping the planet warm enough to be habitable. However, in recent decades, the amount of these gases in the Earth's atmosphere has increased greatly. The Intergovernmental Panel on Climate Change (IPCC, 2021) claims that concentrations of carbon dioxide, methane and nitrogen oxides are not seen in the last 800,000 years. The main contributor to climate change, carbon dioxide in the atmosphere, has increased by 40% since the beginning of the pre-industrial era. The burning of fossil fuels (oil, coal, gas) and transport represent the main source of anthropogenic emissions. Another important source is deforestation, which can come in various forms: logging, clear-cutting, fires and other forms of forest degradation. As a result, carbon is released into the air, with an estimated contribution of 20% of the total global carbon emissions. Other human activities that generate pollution are: the use of fertilizers based on nitrogen oxides, animal farms that leave behind massive emissions of methane and certain industrial activities that release fluorinated gases. And other activities that affect the land cover (agriculture, construction) can change the reflectivity of the

land surface, leading to warming or cooling (Turrentine et al., 2021). Even though forests and oceans absorb greenhouse gases from the atmosphere through photosynthesis and other processes, they cannot keep up with increasing human emissions. As a result of rapid climate change, the global temperature is increasing by about 1.18ºC since the late 19th century, with most of the warming occurring in the last 40 years. In Figure 1 is highlighted the evolution of carbon dioxide and temperature anomaly in the last 1000 years.

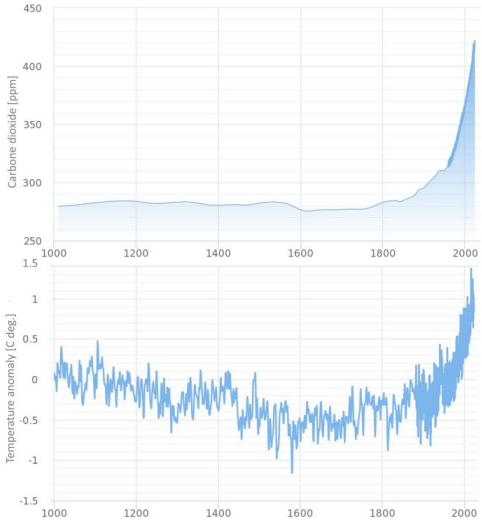

Figure 1. Carbone dioxide and temperature anomaly evolution in the last 1000 years
(source: 2degreeinstitute)

MATERIALS AND METHODS

Copernicus is the Earth observation program managed by the European Commission (copernicus.eu). It provides information acquired from satellites and in-situ data. The program is implemented
in partnership with the Member States, European Space Agency (ESA), European Organization for the Exploitation of Meteorological Satellites (EUMETSAT), European Center for Long-Range Meteorological Forecasts (ECMWF), Mercator Océan and other agencies of the European Union. All data and measurements from sensors installed on satellites, planes, ships, help service providers, public authorities and other international organizations, to make decisions to improve the quality of life at European and global level. All information made available by Copernicus services is free, open and accessible to users. The Copernicus program consists of six services, which have become operational in stages since 2012. The service, which aims at climate change, started operating in July 2018 and supports society by making available authoritative information about the past, present and future of the climate in Europe but also globally. Copernicus Climate Change Service (C3S) is based on research carried out by the World Climate Research Programme (WCRP) and responds to user requirements defined by the Global Climate Observing System (GCOS) and is an important resource for the Global Framework for Climate Services (GFCS). C3S is implemented by the European Centre for Long-Range Weather Forecasts (ECMWF) on behalf of the European Commission. The service provides data and information on the impact of climate change, for a wide range of topics and sectors of activity (water resource management, agriculture, energy, infrastructure and transport, disaster reduction, health, biodiversity, etc.), through the climate database (Copernicus Climate Data Store. C3S complements the weather and environmental services that every European country already has in place.

Climate projections are simulations of the Earth's climate in the coming decades, usually until the year 2100. They are based on possible scenarios of the evolution of concentrations of greenhouse gases, aerosols and other constituents of the atmosphere that affect the radiative balance of the planet (Climate Change Service). Climate projections are obtained by running mathematical models that can cover the entire globe or just regions. These models are known as Global Climate Models (GCM) or General Circulation Models, respectively Regional Climate Models (RCM). Most climate projections made by GCMs were part of the Coupled Model Intercomparison Project, phase 5 (CMIP5). The simulations and projections by RCM followed protocols established by the Coordinated Regional Climate Downscaling Experiment (CORDEX). C3S through CDS provides access to an important part of climate projections run under CMIP5 and CORDEX for the European domain. Climate models are

one of the main means for scientists to understand how the climate has changed in the past and might change in the future. These models simulate in detail the physics, chemistry and biology of the atmosphere, land and oceans and require some of the world's largest supercomputers to generate the climate projections (CarbonBrief, 2023). These models are continuously updated by increasing the spatial resolution, mainly, but also by adding new physical and biogeochemical processes. To make climate projections for the future, climate forcing is set to change in accordance with possible future scenarios. Scenarios represent possibilities for population growth and how quickly it will happen, how land will be used, how economies and atmospheric conditions will evolve. Before the year 1750, the Earth's average radiative forcing (net incoming minus outgoing radiation at the top of the atmosphere, [W/m^2]) was relatively constant. Human-made changes after this period in land use and greenhouse gas emissions led to an increase of radiative forcing, from 0 Wm^{-2} in 1750 to 3.18 W/m^{-2} in 2020, according to NOAA. Climatologists have defined four possible scenarios of radiative forcing (2.6, 4.5, 6.0, 8.5 W/m^2 in year 2100) that are used as input in calculating future climate. Each scenario is based on a plausible future that takes into account global greenhouse gas emissions. The scenarios, known as Representative Concentration Pathways (RCP), specify an amount of radiative forcing for the year 2100 relative to the year 1750. Unlike weather forecasts, which describe a detailed picture of conditions for the next few hours or days from now, climate models are probabilistic, indicating areas that are more likely to be warmer or colder and wetter or drier than usually. Climate models are based on global ocean and atmosphere physics and records of weather patterns that have occurred in similar ways in the past (NOAA-Climate).

Regarding actual data, **ERA-interim from ECMWF** it was initiated in 2006 to create a link between the data originally reanalysed in the ERA-40 project (1957-2002) and the next extended generation of reanalysis envisaged by ECMWF. The main objective was to improve aspects related to the representation of the hydrological cycle, the quality of the stratospheric circulation, and the management of bias and changes in the observing system. These goals were achieved largely as a result of a combination of factors, including the improvement of several parameterizations, the use of 4D variation analyses, the revised moisture analysis, the use of a variational bias correction for satellite data, and other improvements in data handling (Berrisford et al., 2011). **ERA5** is the successor to the ERA-Interim reanalysis as of 31 August 2019. It provides hourly estimates for a large number of atmospheric, oceanic and terrestrial climate variables. The data cover a global grid of 30 km and 137 atmospheric levels, from the surface to 80 km altitude. Compared to ERA-Interim, the ERA5 analysis comes with a high spatial and temporal resolution, information on quality variation in time and space, a better global balance for precipitation and evapotranspiration, an improvement in soil moisture, etc.

Climate models used in this study are from state-of the art ensemble models in CMIP5 Project that were specifically developed to overcome biases in the previous CMIP3 experiments, and are briefly described in the following (GFDL, HadGEM, MIROC, IPS, NorESM).

To better understand how Earth's biogeochemical cycles, including human actions, interact with climate, the Geophysical Fluid Dynamics Laboratory (**GFDL**) built the first NOAA-Earth System Models (**ESM**) (Dunne et al, 2012). The ESM2.1 prototype model evolved directly from the CM2.1 climate model (Delwort et al., 2006), which in turn spawned two new models representing ocean physics with alternative numerical frameworks to explore the implications of fundamental assumptions (**ESM2M** and ESM2G). The differences between the two are generally made in the physics component of the ocean. In ESM2M pressure-based vertical coordinates are used along the GFDL modular ocean model version 4.1 development path. GFDL performed all integrations with ESM2M and ESM2G for the CMIP5 protocol (Taylor et al., 2012). **HadGEM-ES** from Met Office is part of the second generation of climate models configured by the Hadley Center Global Environment Model, with new features

including a more accurate stratosphere and land system components. The individual components were successfully tuned and combined into the fully coupled model (Collins et al., 2008). The model represents interactive land and ocean carbon cycles and vegetation dynamics, with the option to prescribe either atmospheric CO_2 concentrations or anthropogenic CO_2 emissions and simulate CO_2 concentrations (Jones et al., 2011). **MIROC-ESM-CHEM** (JAMSTEC) is based on the global climate model MIROC (Model for Interdisciplinary Research on Climate), developed in partnership with the University of Tokyo, NIES and JAMSTEC. It is composed of a general atmospheric circulation model (MIROC-AGCM 2010) that includes an on-line aerosol component (SPRINTARS 5.00), an ocean model (COCO 3.4) and a land surface model (MATSIRO), all of which being coupled in MIROC (Watanabe et al., 2011). MIROC-ESM additionally comes with an atmospheric chemistry component (CHASER 4.1), an ocean nutrient-phytoplankton-zooplankton-detritus (NPZD) component, and a terrestrial ecosystem (vegetation dynamics) component (SEIB-DGVM). **IPSL-CM5A-LR** is the 5th version of the model developed by the Institut Pierre Simon Laplace (IPSL). In addition to the atmosphere-ocean-land-surface-ice components, it also includes a representation of the carbon cycle, stratospheric and tropospheric aerosol chemistry. The IPSL-CM5A-LR model incorporates an ORCHIDEE surface model into the LMDZ5A atmospheric component. It is coupled with the NEMOv3.2 ocean module which includes the LIM-2 ice model and the PISCES biogeochemistry model. The coupling between the two models (atmospheric and oceanic) is done using the OASIS3 software (Valcke, 2006). Includes 31 vertical levels with the best resolution in the first 150 m at the top (Peresechino et al., 2013). **NorESM1-M** is mostly based on CCSM4 (Community Climate System Model, version 4), but differs by using an isopycnic ocean module and replacing the CAM4 atmospheric mode with CAM4-Oslo (Bentsen et al., 2013). The CCSM4 components are coupled through CPL7 (Craig et al., 2012) which manages overall control of model execution and information exchange between components. Inside the coupling is a top-level driver that organizes the coupled model into a single executable and issues calls to the initialization, run, and completion routines for each component of the model (Bentsen et al., 2013).

Focuses of this work, the agroclimatic indicators are useful because they "translate" climate variability and changes into useful terms for the agricultural sector (Agroclimatic Indicators, 2019). They are often used in species distribution modeling to study plant phenological evolutions under varied climatic conditions. For many users in the agricultural community, crop development assessments for current or future crop seasons are particularly important. This is especially true for agricultural policy and business environments, as early indications of production anomalies are of critical importance for taxes/subsidies and price volatility. The provision of pre-processed agroclimatic indicators facilitates availability to the user and will facilitate the use of climate data by the agricultural community. Agroclimatic indicators are based on formulas that measure factors and climatic conditions that can affect vegetation positively or negatively and can correlate with the main type of vegetation of an area. They are used in agriculture to reconstruct climate and environmental changes such as: climate-induced phases in plant growth, amount of moisture and heat, drought, etc. (Agroclimatic Indicators, 2019). There are two main categories of indicators calculated directly from climate variables, which C3S makes available pre-calculated, along with the workflow for on-demand generation of specific indicators:

- Generic Agroclimatic Indicators: represent aggregations, accumulations or frequencies calculated according to a certain atmospheric variable (temperature and precipitation);
- Crop-specific indicators: require information on the date of sowing and harvesting, the growing range of minimum and maximum temperatures, etc. to produce products specific to the culture of interest.

C3S produces a total of 26 indicators with global coverage calculated from daily data, derived from two essential climate variables (ECVs):

- Surface air temperature: daily minimum air temperature at 2 m (TN), daily maximum air temperature at 2 m (TX) and daily mean air temperature at 2 m (TG);
- Precipitation: daily total (RR).

The indicators were adapted from the collection of the European Climate Assessment & Dataset (ECA & D) project, for their relevance in agriculture but not oriented towards a certain type of culture. Data description is presented in Table 1.

Table 1. Spatial and temporal characteristics (source: CDS Service)

Data type	Gridded
Projection	Regular latitude-longitude grid
Horizontal coverage	Global
Horizontal resolution	0.5° x 0.5°
Vertical coverage	Surface
Vertical resolution	Single level
Temporal coverage	1951-2099
Temporal resolution	10-day, Seasonal, Annual
File format	netCDF-4

To generate historical and future agroclimatic indicators, climate data with bias corrections made available through the ISIMIP project (Inter-Sectoral Impact Model Intercomparison Project) were used. Bias correction is a process of scaling climate model outputs to account for systematic errors in order to improve correlation with observed data (Soriano et al., 2019). ISIMIP was organized into 3 main simulation rounds, from which the ISIMIP Fast Track products formed the basis of the current set of indicators. For each simulation run a set of gridded and corrected climate variables were produced to be used as input data in running the impact models. These climate datasets contain bias correction for climate data from 5 CMIP5 models covering the period 1950-2099, daily temporal resolution and downscaling to 0.5° x 0.5° lat-lon globally. For historical observations, the WFDEI - Watch Forcing data methodology applied to ERA-Interim dataset (Weedon et al., 2014) was used to generate agroclimatic indicators from the climatological period 1981-2010. The temperature bias correction algorithm preserves GCM monthly mean values by adding a compensation constant for each grid point and month. In this way, the absolute temperature changes are not modified by the bias correction, but the reference level is adjusted to the level of observations over the period of 40 years. The minimum and maximum temperature (Tmin. and Tmax.) are also corrected for systematic bias. The algorithm ensures that for the historical period, the average distance between the maximum (or minimum) daily temperature value and the average daily temperature (T) is maintained. This is achieved by calculating a factor for the historical period:

$$K = \text{mean}\,[\text{Tmin. (max.)}_{Watch} - T_{Watch}] / \text{mean}\,[\text{Tmin. (max.)}_{GCM} - T_{GCM}] \quad (1)$$

and the corrected bias for the maximum (minimum) temperature is given by the relation:

$$\text{Tmin. (max.)}_{BC} = k\,[\text{Tmin. (max.)}_{GCM} - T_{GCM}] + T_{GCM} \quad (2)$$

The daily variability of the temperature data is adjusted to reproduce the variability of the observed data. The data is processed by:

- subtracting the monthly averages from both sets of data;
- multiplying the daily residual variations with a monthly constant and specific factor per grid point, thus correlating the variations of the simulations with observations;
- the daily variation with bias correction is subsequently added to the corrected monthly averages provided by the GCM.

For the precipitation data, a multiplicative correction was used to adjust the historical monthly mean values to the observed climatological monthly mean values. This ensures that the monthly precipitation values are kept up to a constant multiplier factor. Monthly averages are multiplied by a grid point and a constant monthly correction factor (one for each month). It therefore ensures that the relative change in precipitation, as described by the original GCM data, is preserved. In combination with the temperature correction, the hydrological sensitivity of the GCM (relative change in precipitation per degree of warming) was preserved. To adjust the daily variability of precipitation, a multiplicative method was also adopted that adjusts the relative variability. The data is processed as follows:

- normalization of daily precipitation data from GCM and observed (Watch) data by dividing by their monthly mean values. The daily variability of months without precipitation, specified by a certain threshold, is not changed;
- after normalizing wet months, the distribution of simulated data is correlated to the distribution of observed daily data using a transfer function (Piani et al., 2010). This function corrects both the frequency of dry days and the distribution of precipitation intensity to the observed statistics;
- for the projections, the transfer function is applied to the normalized daily precipitation for wet months;
- multiplying the transferred data with monthly average values with bias correction. By ensuring that the mean values of the normalized daily data transferred is equal to one (by dividing by the associated mean value), it ensures that the corrected monthly mean values are preserved when daily variability is taken into account.

For the other variables (monthly and daily) the same multiplicative approach as for precipitation was used. In the case of the monthly variables, the only exception is the wind, its magnitude being corrected using a multiplicative algorithm, its individual components being then derived by preserving the direction from the original GCM data.

From 26 indicators, 6 were selected with a temporally resolution of 10 days. Thus, each processed indicator contains 1080 time steps for each period of 30 years. Data processing was done with Climate Data Operators (CDO) and cartographic representations in ArcGIS. The historical climatological period includes the interval 1981-2010 and the projections were made for 2 periods, 2011-2040 (near future) and 2041-2070 (near-medium future). The scenarios for which simulations were made are: RCP4.5 (medium radiative forcing) and RCP8.5 (high radiative forcing). Data from all 5 models were used in assembled format from which the historical period was subtracted. The cartographic products are made for the fields over Romania and represent time averages (30 years) of each indicator for the 2011-2040 (P1) and 2041-2070 (P2) projections. The graphic products are made strictly on the Oltenia Plain and represent the estimates of expected long-term variability under climate change. The location of Oltenia Plain, in the south-western Romania, the overlapping of the Danube terraces, the sandy soils and other topoclimatic features, make drought and associated phenomena occur annually in this area. The multi-model ensemble was used in order to cover the inherent modeling uncertainty. To create the graphs, the moving average was calculated with a period of 150 time steps (one time step = 10 days), thus eliminating waves with a period of less than approximately 4 years. Finally, the data were averaged for the entire surface of the Oltenia Plain and represented.

RESULTS AND DISCUSSIONS

Heavy precipitation days (R 10 mm)

It represents the number of days in which at least 10 mm of precipitation was recorded over a period of 10 days (Figure 2). It provides useful information for possible crop damage and losses due to runoff. The trend of the R 10 mm indicator is to migrate to the north and northwest of the country, a fact that is best observed in P2. In Oltenia Plain, the change values are low, between 0-0.024 days/10 days in P1 (compared with Hist), but also in the RCP4.5 scenario in P2 (compared with Hist). Note the eastern part of the plain, which overlaps the areas where sand dunes have developed, where the R 10 mm changes are minimal in both scenarios and periods. In the first part of P2, the heavy precipitation has an increasing tendency and higher values than Hist especially in western part of Oltenia Plain, in both scenarios (mainly RCP8.5) but after 2060 they will decrease quickly to negative differences compared to Hist (making an overall negative trend of differences over the whole period) (Figure 3).

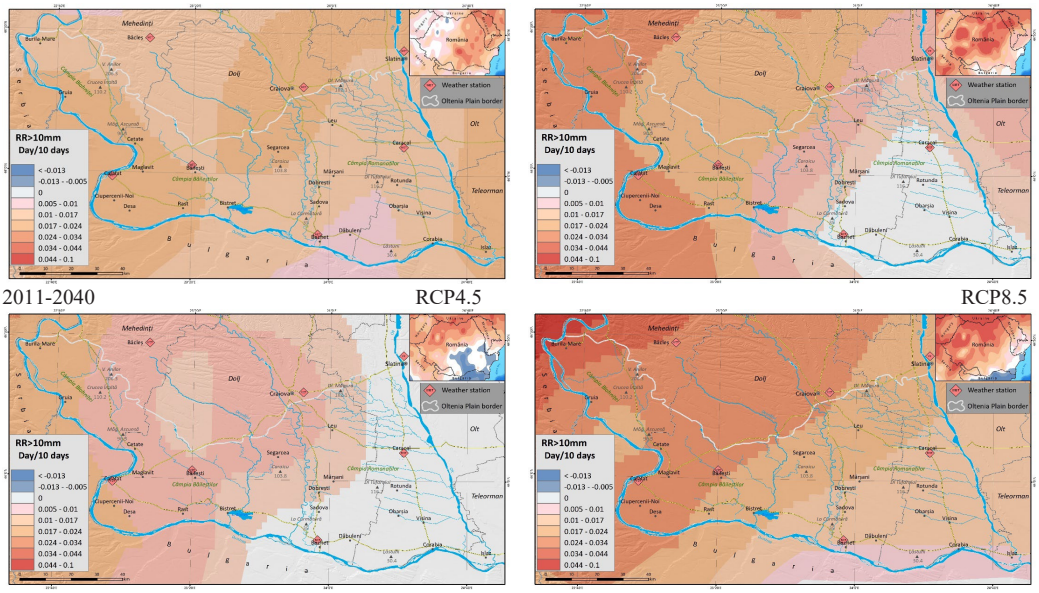

Figure 2. Heavy precipitation days projected changes in scenarios compared with Hist

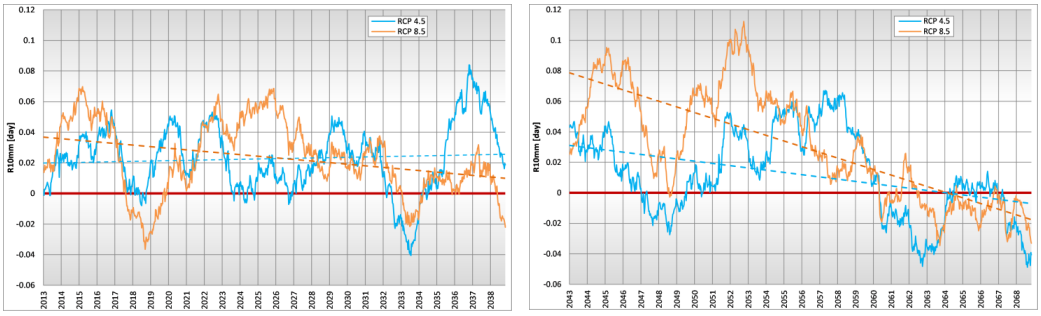

Figure 3. Heavy precipitation days trend for P1-Hist (left 2011-2040) and P2-Hist (right 2041-2070)

Very heavy precipitation days (R 20 mm)

It represents the number of days in which at least 20 mm of precipitation was recorded over a period of 10 days (Figure 4). It provides information on extreme possible crop damage and losses due to runoff. The R 20 mm indicator differences (scenarios minus Hist), follows the R 10 mm trends, with values very slightly above 0 for both scenarios until the year 2034. Quite similar to R10mm, after this year and continuing in P2, the values oscillate between 0 and 0.017 days/10 days, generally being a period of increasing values (Figure 5). Due to the global warming trend, warm air holds more water vapor in the atmosphere, which in turn can produce extreme events in the form of precipitation. Dynamical changes have also a contribution to regional changes in these extremes. Increasing R 20 mm values does not always also lead to increased accumulated precipitation, but the amounts that fall during extreme events can increase, which is already observed during the latest decades.

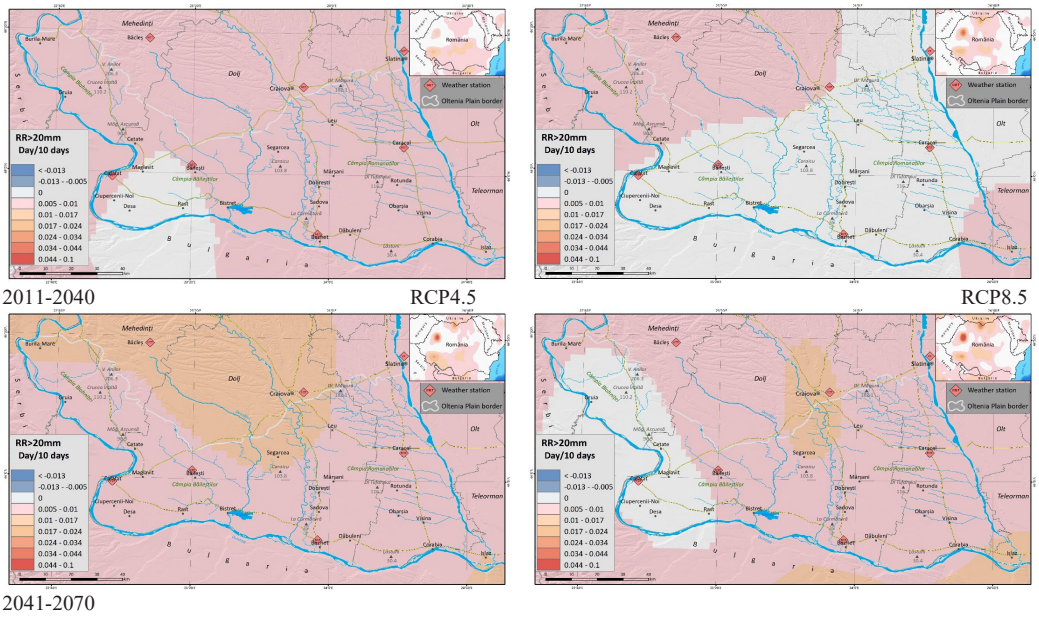

Figure 4. Very heavy precipitation days projected changes in scenarios compared with Hist

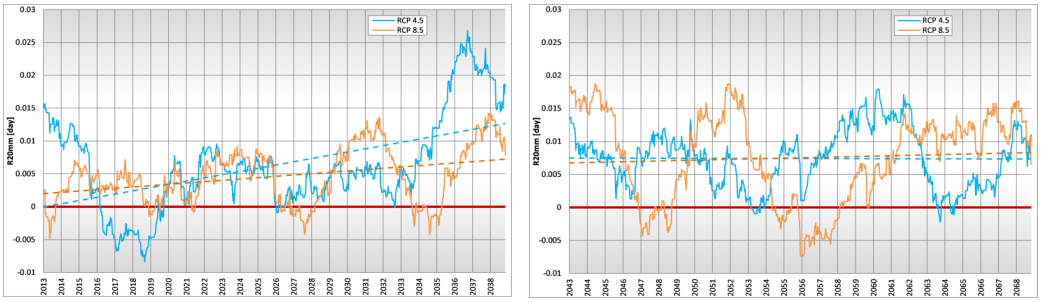

Figure 5. Very heavy precipitation days trend in P1-Hist (left 2011-2040) and P2-Hist (right 2041-2070)

Precipitation sum (RR)

RR is the sum of accumulated precipitation in 10 days. The indicator provides information about the excess or reduction of the water reserve. A wet day has RR = 1 mm while a dry day has RR<1 mm (Figure 6). In P1, both scenarios indicate positive RR differences values compared with Hist and slightly higher in RCP8.5. Towards the end of the period, the difference values (relative to Hist) become clearly negative in average for both scenarios (but however later in P2 with some still increase in P2 in the first part, more in RCP8.5). Even though extreme precipitation tends to increase, moderate precipitation is decreasing in P2, having the effect of reducing cumulative precipitation. RR drops strongly in the second half of P2, its negative values indicating periods of dryness for very long periods of time (Figure 7).

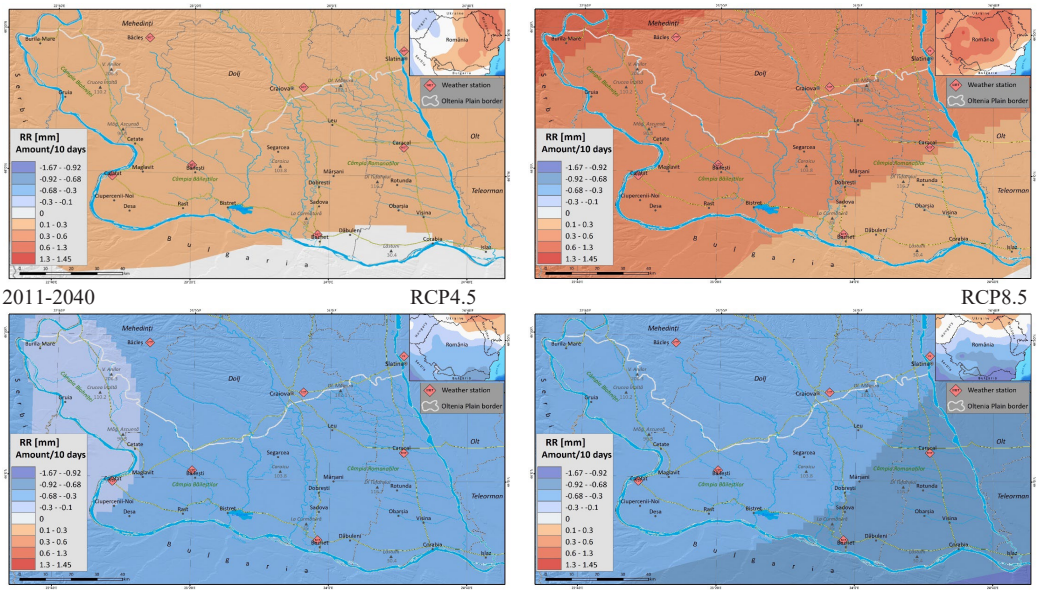

Figure 6. Precipitation sums projected changes in scenarios compared with Hist

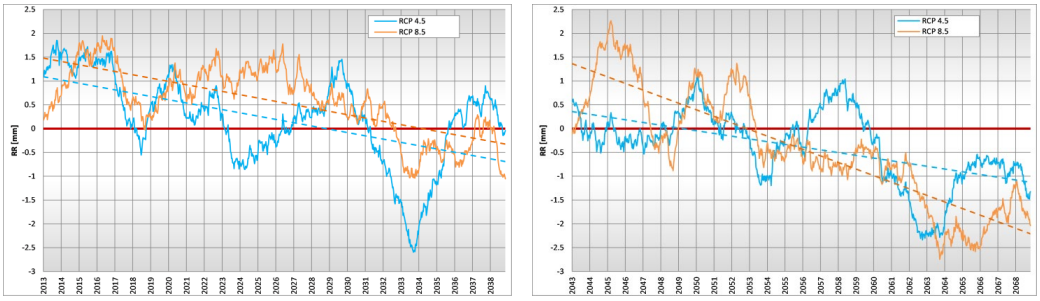

Figure 7. Precipitation sum trend in P1-Hist (left 2011-2040) and P2-Hist (right 2041-2070)

Mean of daily mean temperature (TG)

Average TG values for a 10-day interval where TG represents the average daily temperatures (Figure 8). It provides information on long-term climate variability and change. In P1, the TG values indicate an increase compared to the historical period with an average of approximately 1.2ºC in the RCP4.5 scenario and nearly 1.5ºC in the RCP8.5.

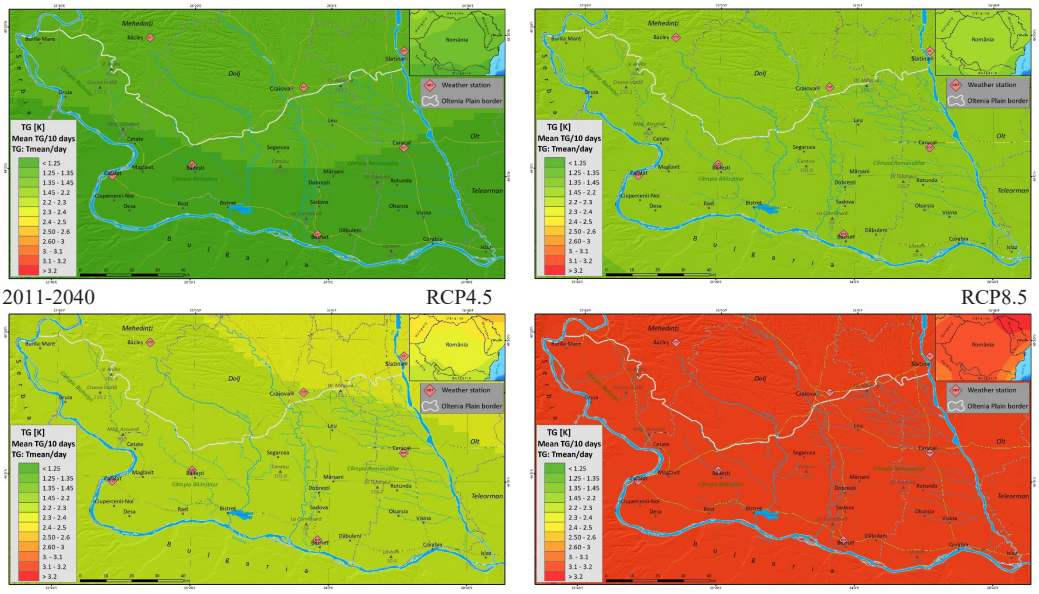

Figure 8. Mean of daily mean temperature projected changes in scenarios compared with Hist

In P2 both scenarios indicate almost double TG increases (relative to Hist) compared to P1, starting in 2050. If over 4-year period RCP4.5 stabilizes at an average value of about 2ºC, RCP8.5 forecasts a TG increase of average 3ºC, punctually even exceeding the value of 3.5ºC (after 2053) and frequently after 2060 (Figure 9).

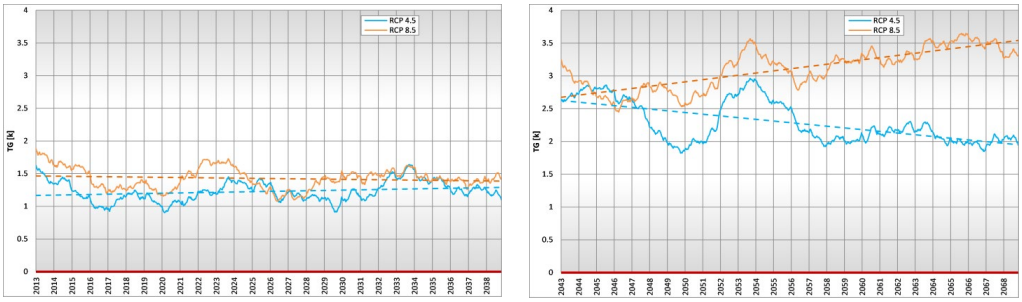

Figure 9. Mean of daily mean temperature trend in P1-Hist (left 2011-2040) and P2-Hist (right 2041-2070)

Summer days (SU)

The number of days relative to a 10-day period in which the maximum daily temperature TX >25ºC (Figure 10). It provides indications of the occurrence of heat stress and is useful for specific crop variants for heat/cold stress (above/below optimal temperature thresholds). SU fluctuates quite a lot over periods of about 10 years, an aspect that stands out in both periods. However, the general trend is to increase the number of days with temperatures higher than 25ºC compared to Hist. In P2, SU differences reaches double values compared to P1, after 2050 (Figure 11).

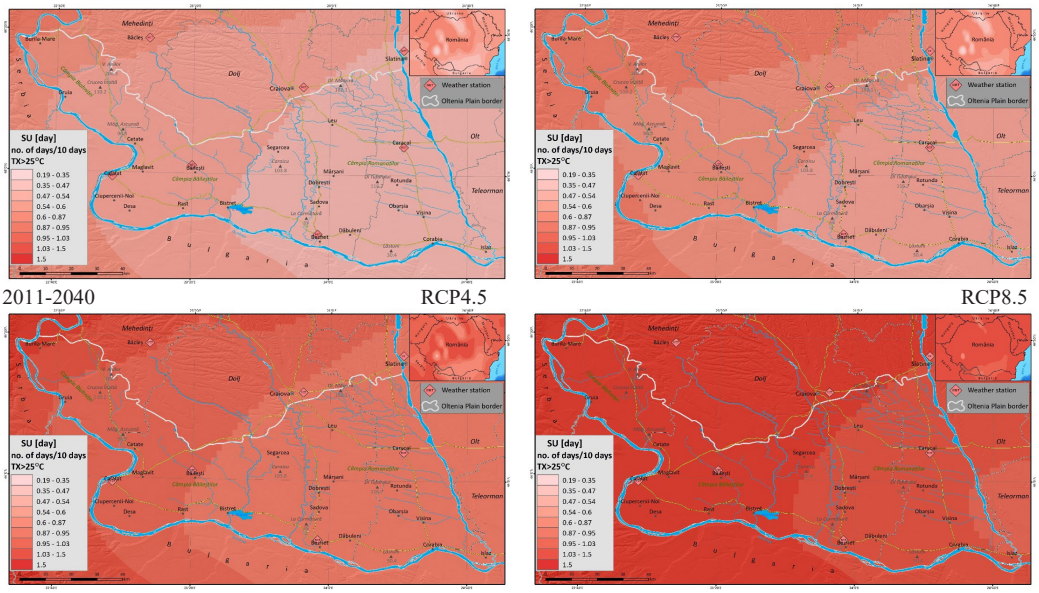

Figure 10. Summer days projected changes in scenarios compared with Hist

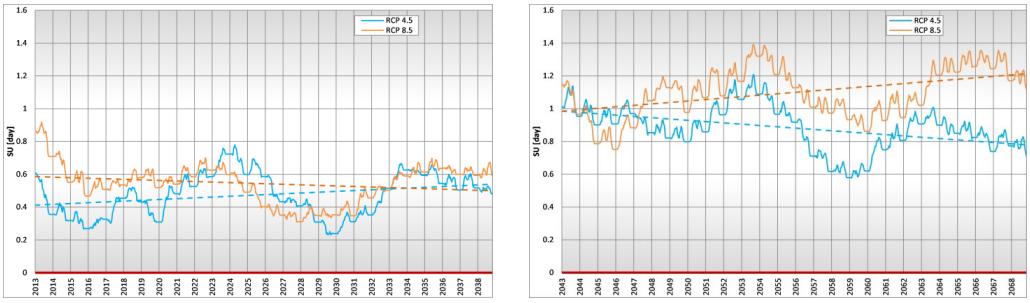

Figure 11. Summer days trend in P1-Hist (left 2011-2040) and P2-Hist (right 2041-2070)

CONCLUSIONS

The current context requires an accelerated effort at the international and national level in terms of monitoring and understanding the mechanisms of the evolution of climatic and environmental parameters in the context of climate change, in order to be able to develop methods to counter their effects in a timely manner. Unfortunately, the time scale and speed with which these events become more intense and accelerated is short, many times shorter than the time in which such mitigation measures can be developed. However, current climate scenarios project important changes both at the country and regional level. Agroclimatic indices analysed for the Oltenia Plain, very clearly forecast the increase in temperatures (averages, minimums, daily maximums) and the increase in extreme precipitation (in spite of overall RR mean decrease) that lead to the destruction of crops due to thermal stress and water runoff from precipitation. At the same time, soil fertility decreases due to surface washing. In the context where the Oltenia Plain is already affected by drought (especially agricultural) and its associated phenomena (aridization and desertification), the increase in temperatures above the thresholds of 1.5°C and 2°C can lead to catastrophic effects for specific agricultural crops. Because of this, changes can occur in the pattern of crops that can be replaced by other species resistant to heat stress, such as exotic

cultures. These projected values should be a warning and the decision-makers should get involved in the development of environmental policies that reduce the effect of climate change in Romania and in particular in the Oltenia Plain.

REFERENCES

2degree Institute. Retrieved from https://www.2degreesinstitute.org/

Agroclimatic indicators - Product User Guide and Specification (2019). C3S Global Agriculture SIS, Issued by Telespazio VEGA, UK.

Bentsen, M., Bethke, I., Debernard, J. B., Iversen, T., Kirkevåg, A., Seland, Ø., Drange, H., Roelandt, C., Seierstad, I. A., Hoose, C., and Kristjánsson, J. E. (2013). The Norwegian Earth System Model, NorESM1-M - Part 1: Description and basic evaluation of the physical climate. *Geosci. Model Dev., 6,* 687-720, doi.org/10.5194/gmd-6-687-2013

Berrisford, P., Dee, D., Poli, P., Brugge, R., Fielding. K., Fuentes, M., Kalberg, P., Kobayashi, S., Uppala, S., Simmons, A. (2011). *ERA report series, The ERA-Interim archive, Version 2.0*. ECMWF Publications, Reading, UK.

CarbonBrief. Retrieved from https://www.carbonbrief.org/

Climate Data Operators (CDO). Retrieved from https://code.mpimet.mpg.de/projects/cdo/

Collins, W.J., Bellouin, N., Doutriaux-Boucher, M., Gedney, N., Hinton, T., Jones, C.D., Liddicoat, S., Martin, G., O'Connor, F., Rae, J., Senior, C., Totterdell, I., Woodward. S. (2008). *Evaluation of the HadGEM2 model*. Met Office Hadley Centre, Exter, UK.

Copernicus. Retrieved from https://www.copernicus.eu/

Copernicus Climate Change Service. Retrieved from https://climate.copernicus.eu/

Copernicus Climate Data Store. Retrieved from https://cds.climate.copernicus.eu/

Craig, A., Vertenstein, M., Jacob, R. (2021). A new flexible coupler for earth system modeling developed for CCSM4 and CESM1. *Int. J. High Perform. Comput. Appl., 26*, 31–42, doi.org/10.1177/109434201142814

Delworth, T., Broccoli, A., Rosati, A., Ronald, S., Balaji, V., Beesley, J., Cooke, W., Dixon, K., Dunne, J., Dunne, K.A., Durachta, J., Findell, K., Ginoux, P., Gnanadesikan, A., Gordon, C., Griffies, S., Gudgel, R., Harrison, M., Held, I., Zhang, R. (2006). GFDL's CM2 Global Coupled Climate Models. Part I: Formulation and Simulation Characteristics. *Journal of Climate, 19*. 643-674. 10.1175/JCLI3629.1.

Intergovernmental Panel on Climate Change (2021). *Climate Change 2021, The physical Science Basis. Summary for policymakers*. ISBN 978-92-9169-158-6

Jones, C. D., Hughes, J. K., Bellouin, N., Hardiman, S. C., Jones, G. S., Knight, J., Liddicoat, S., O'Connor, F. M., Andres, R. J., Bell, C., Boo, K.-O., Bozzo, A., Butchart, N., Cadule, P., Corbin, K. D., Doutriaux-Boucher, M., Friedlingstein, P., Gornall, J., Gray, L., Halloran, P. R., Hurtt, G., Ingram, W. J., Lamarque, J.-F., Law, R. M., Meinshausen, M., Osprey, S., Palin, E. J., Parsons Chini, L., Raddatz, T., Sanderson, M. G., Sellar, A. A., Schurer, A., Valdes, P., Wood, N., Woodward, S., Yoshioka, M., and Zerroukat, M. (2011). The HadGEM2-ES implementation of CMIP5 centennial simulations, *Geosci. Model Dev.*, 4, 543–570, https://doi.org/10.5194/gmd-4-543-2011

National Aeronautics and Space Administration (NASA). Retrieved from https://www.nasa.gov/

Natural Resources Defense Council (NRDC). Retrieved from https://www.nrdc.org/

National Oceanic and Atmospheric Administration (NOAA). Retrieved from
https://www.noaa.gov/; noaa.gov/climate

Peresechino, A., Mignot, J., Swingedouw, D., Labetoulle, S., Guilyardi, E. (2012). Decadal predictability of the Atlantic meridional overturning circulation and climate in the IPSL-CM5A-LR model. *Clim Dyn 40*, 2359-2380, doi.org/10.1007/s00382-012-1466-1

Piani, C., Weedon, P.G., Best, M., Gomes, S., Viterbo, P., Hagemann, S., Haerter, J.O. (2010). Statistical bias correction of global simulated daily precipitation and temperature for the application of hydrological models. *J. Hydrol., 395*, 199–215.

Riebeek, H. (2010). *Global Warming*. NASA Earth Observatory. Retrieved from https://earthobservatory.nasa.gov/features/GlobalWarming

Soriano, E., Medeiro, L., Garijo, C. (2019). Selection of bias correction methods to assess the impact of climate change on flood frequency curves. MDPI *Water, 11*, 2266, doi.org/10.3390/w11112266

Taylor, K.E., Stouffer, R.J., Meehl, G.A. (2012*).* An overview of CMIP5 and experiment design. *Bull. Amer. Meteor. Soc., 93*, 485-498, https://doi.org/10.1175/BAMS-D-11-00094.1

Turrentine, J., Denchak, M. (2021). *What is climate change?* National Resources Defence Coincil. Retrieved from https://www.nrdc.org/

Valcke, S. (2006). *OASIS3 user guide (prism_2-5), technical report TR/CMGC/06/73, PRISM Report No 2*. P 60, CERFACS, Toulouse, France.

Watanabe, S., Hajima, T., Sudo, K., Nagashima, T., Takemura, T., Okajima, H., Nozawa, T., Kawase, H., Abe, M., Yokohata, T., Ise, T., Sato, H., Kato, E., Takata, K., Emori, S., and Kawamiya, M. (2011). MIROC-ESM 2010: model description and basic results of CMIP5-20c3m experiments, *Geosci. Model Dev., 4*, 845–872, https://doi.org/10.5194/gmd-4-845-2011.

Weedon, P.G., Balsamo, G., Bellouin, N., Gomes, S., Best, J.M., Viterbo, P. (2014). The WFDEI meteorological forcing data set: WATCH Forcing Data methodology applied to ERA-Interim reanalysis data. *Water Resources Research, 50*(9), doi.org/10.1002/2014WR015638

Scientific Papers. Series E. Land Reclamation, Earth Observation & Surveying, Environmental Engineering. Vol. XII, 2023
Print ISSN 2285-6064, CD-ROM ISSN 2285-6072, Online ISSN 2393-5138, ISSN-L 2285-6064

ASSESSMENT OF THE EUROPEAN GROUND MOTION SERVICE ORTHO PRODUCTS FOR LANDFILL SYSTEMATIC OBSERVATION

Iulia DANA NEGULA[1, 2*], Cristian MOISE[1, 2*], Florina DEDIU[1, 2], Mihaela GHEORGHE[3], Georgeta TUDOR[4], Umut Güneș SEFERCIK[5]

[1]University of Agronomic Sciences and Veterinary Medicine of Bucharest,
59 Marasti Blvd, District 1, Bucharest, Romania
[2]Romanian Space Agency, 21-25 Mendeleev Street, District 1, Bucharest, Romania
[3]GMV Innovating Solutions, 246C Calea Floreasca, District 1, Bucharest, Romania
[4]National Institute for Research and Development in Environmental Protection,
294 Splaiul Independenței, District 6, Bucharest, Romania
[5]Gebze Technical University, 41400 Gebze/Kocaeli, Turkey

Corresponding author email: iulia.dana@fifim.ro
*These authors contributed equally to this work and share first authorship.

Abstract

The European Ground Motion Service (EGMS) is a new, open and freely available addition to the pan-European component of the core Copernicus Land Management Service (CLMS). The service offers very accurate and consistent information regarding the ground motion velocity that might be correlated with a wide range of circumstances, such as landslides, subsidence, volcanic activity and many others. The products (i.e., basic, calibrated and ortho) delivered by EGMS were generated based on Sentinel-1 time-series acquired between 2016 and 2020, using advanced Differential Synthetic Aperture Radar Interferometry (A-DInSAR) techniques. The present study addresses the suitability of the EGMS ortho products for the monitoring of 15 solid waste landfills located across the territory of Romania. The vertical displacements extracted for each selected landfill were analysed and correlated with the available background information (e.g., exploitation duration, the quantity of waste disposal per year, etc.). The study proved that EGMS might be an important tool for waste management since it enables the continued monitoring of the landfill settlement process.

Key words*: Advanced Differential Synthetic Aperture Radar Interferometry (A-DInSAR), European Ground Motion Service (EGMS), landfill monitoring, landfill settlement, Sentinel-1.*

INTRODUCTION

Landfills have complex structures that enable the storage of waste without contaminating the environment. Landfills have several layers that prevent the leachate to reach groundwater. Soil is frequently added to cover the waste for odour reduction and keep the trash inside the disposal site. Landfill settlement represents a process in which the ground or surface of a landfill lowers over time. The magnitude and duration of this process is influenced by various factors such as the volume of the stored waste as well as the mechanisms that are developing in the lower layers of the structure (Chabuk et al., 2018). According to He et al. (2021), the settlement process usually takes place over a period of 20 to 30 years and may reach 50% of the initial landfill depth, therefore continuous monitoring is of high importance for effective waste management that results in reduced impact on the environment (Virsta et al., 2020).

The monitoring of landfills can be successfully performed based on satellite data, especially when a synergistic use of different data types and methods is employed (Papale et al., 2023). The use of synthetic aperture radar (SAR) and interferometric techniques is also demonstrated by several studies (Du et al., 2021; Zhang et al., 2021; Tabish et al., 2022). EGMS provides products generated based on Advanced Differential SAR Interferometry (A-DInSAR) techniques (Crosetto et al., 2020). These are based on time series of SAR images, examples including Persistent Scatterers Interferometry (PS-InSAR) and Small Baseline Subset Interferometry (SBAS-InSAR). The present study aims to assess the suitability of the EGMS products for landfill systematic observation, using 15 test sites located in Romania.

MATERIALS AND METHODS

EGMS functions within the Land Management Service (CLMS) of the Copernicus Programme and provides accurate information about the ground and infrastructure displacements, expressed in mm/year for each identified stable point named persistent scatterer. The service is covering the territory of the European countries that are committed to Copernicus Programme and the United Kingdom (Kotzerke, 2022).

The information provided by EGMS is derived based on multitemporal series of Sentinel-1 data acquired between Feb 2015 and Dec 2021, using Persistent and Distributed Scatterers (Crosetto et al., 2020). EGMS offers three types of open and free products, namely: Basic (relative displacements measured on the Line-of-Sight, derived from ascending and descending orbits, having 20 x 5 m spatial resolution), Calibrated (also derived from combined ascending and descending orbits, with absolute displacements measured on the Line-of-Sight, at 20 m x 5 m spatial resolution) and Ortho (reference geodetic model, horizontal/east -west and vertical/up-down displacements, 100 m spatial resolution, data derived from both ascending and descending orbits). In case of the latter product, the north-south component of motion is compensated using calibration based on Global Navigation Satellite System (GNSS) data. Due to the SAR acquisition geometry, the detection of motion on this direction is less sensitive (Kotzerke, 2022).

The EGMS products are quality controlled (Kotzerke, 2022) and validated (Crosetto et al., 2021). For each product, mean velocity standard deviation is 0.7 mm/year (Kotzerke, 2022).

The EGMS products can be used in a large number of applications, such as the study of geohazards (e.g., subsidence, volcanic activity, earthquakes, landslides, etc.), civil engineering and infrastructure (e.g., buildings, roads, ports, railways, tunnels, bridges, airports, etc.), energy and natural resources (e.g., oil and gas, power plants, wind farms, power lines, dams, mining, etc.) and cultural heritage (Kotzerke, 2022). In addition, other applications, such as landfill monitoring, are acknowledged as being suitable for benefiting from the products provided by this service (EGMS, 2023). For the present study, the EGMS Ortho product (Jan 2016 - Dec 2021, vertical displacements) covering the territory of Romania (Figure 1) was used.

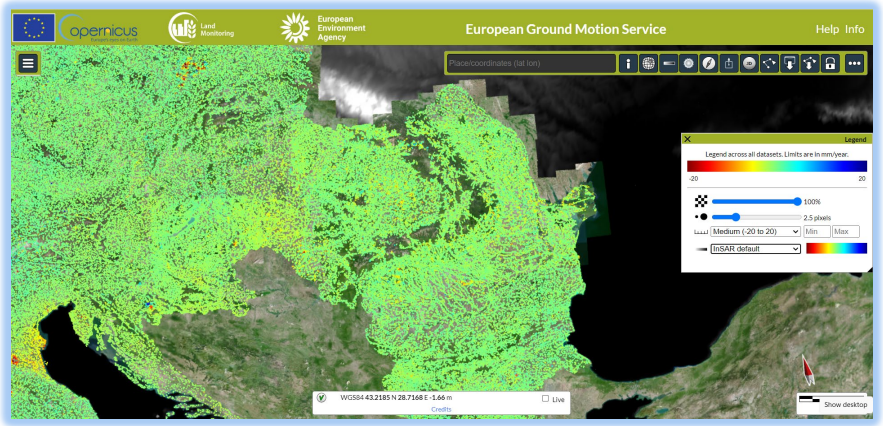

Figure 1. EGMS Explorer view (centre of the picture: dataset covering Romania)

Data regarding the studied waste disposal areas were provided by the National Institute for Research and Development in Environmental Protection. These data consist of: date when the landfill became operative, closure date, landfill structure (e.g., total number of cells, number of operational cells, number of projected cells), status (usually at the level of 2021), history and evolution, quantity of waste stored (in tons/year) and any other useful information (quality of the surrounding construction works, such as roads, dams; known issues regarding the leachate, the condition of the geotextile layer, etc.).

The selected landfills are illustrated in Figure 2.

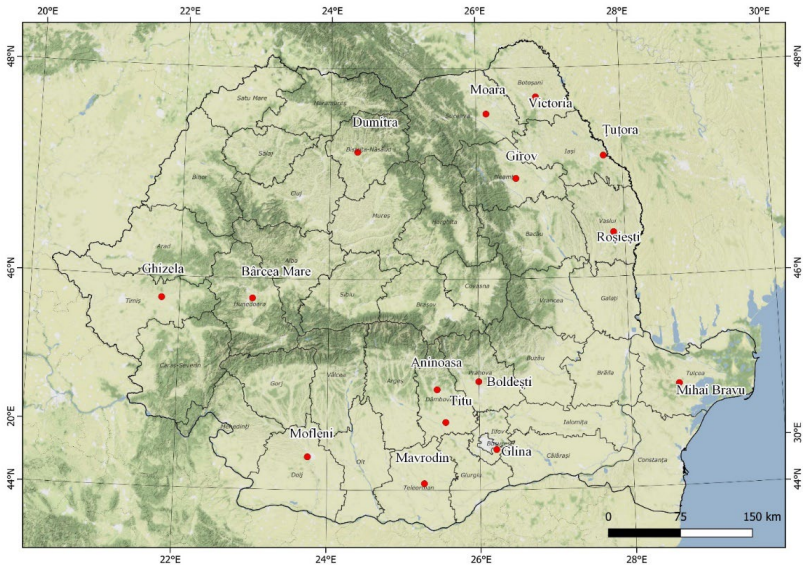

Figure 2. Location of the selected landfills within the territory of Romania

The methodology is presented in Figure 3 and it consists of 5 main phases. In the first phase, the EGMS dataset was downloaded from the CLMS site (https://egms.land.copernicus.eu/). Regions of interest were defined in order to obtain a complete coverage of the Romanian territory. The dataset was downloaded in .CSV format at grid level. Next, the .CSV format was converted into the OGC (Open Geospatial Consortium) GeoPackage format for further processing in QGIS, an open-source Geographic Information System (GIS). For each landfill, a selection of relevant persistent scatterers was performed. The information regarding the boundaries of the landfills was not available, hence the choice of suitable persistent scatterers was made manually using very high-resolution satellite data. In the following phase, the data were analysed in order to determine the evolution of each landfill in what concerns the detection of the settlement process (a negative subsidence trend, with high displacement values, reveals the lowering of the landfill over time). Firstly, the extracted EGMS data required preparation, meaning that the displacement values (in mm/year) available for all the persistent scatterers located within a landfill were averaged for each acquisition date; next, the mean values obtained before were averaged at quarter level; hence, for each landfill 24 displacement values were computed for the 6-year monitoring window. Since the average values are not entirely revealing the amplitude of subsidence, 3 persistent scatterers displaying the most significant displacement rates were selected for each test site. For these points, the actual displacement values measured at the beginning of each quarter were analysed. Hence, the displacement trend was investigated also using 24 values, for each selected persistent scatterer. In the last phase, the results were evaluated based on the available information. For example, the start and closure dates are essential knowledge in this context, as well as the information regarding the number of landfill cells and their status (currently operational or non-operational, covered or not covered, the quantity of waste disposal stored each year etc.) during the observation period.

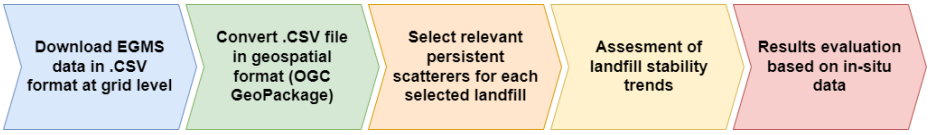

Figure 3. Workflow for the identification of potential landfill settlement process

RESULTS AND DISCUSSION

The overall mean displacement velocity (in mm/year) was computed for each landfill (Figure 4), based on the EGMS dataset covering a time interval of 6 years (January 2016 - December 2021). EGMS enables a detailed analysis of the displacement process by providing vertical shift rates every 6 days, thus resulting more than 360 records for each persistent scatterer (Figure 5).

Next, the most significant displacement values were investigated (Figures 6-8). Overall, the results indicate that Glina landfill presents the most significant negative displacement rates that might be associated with the evolution of the settlement process. A clear negative trend is also observed for Victoria, Aninoasa, Titu, Ghizela, and Mofleni; the negative trend in less pronounced for Dumitra and Mavrodin landfills. On the contrary, Bârcea Mare is the only solid waste landfill showing positive displacement velocities that suggest an uplift process. Landfill stability or slight negative displacement rates are specific to Roșiești, Boldești, Girov, Moara, Țuțora and Mihai Bravu disposal sites. Further, a more detailed analysis in presented.

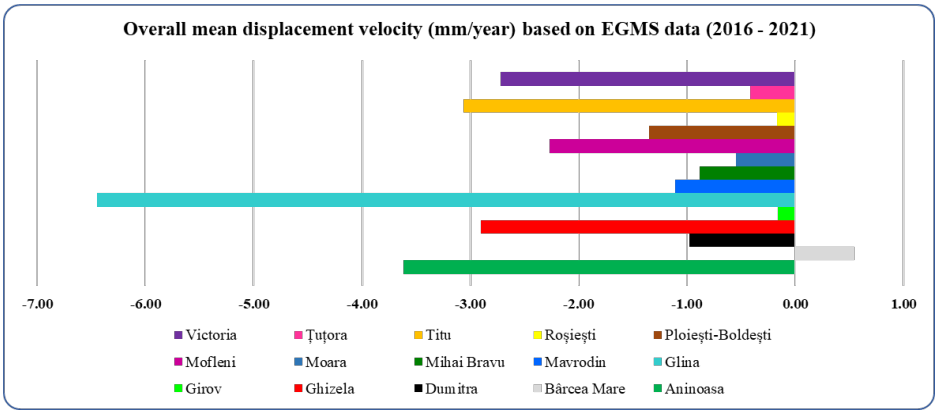

Figure 4. EGMS-derived overall mean displacement rate

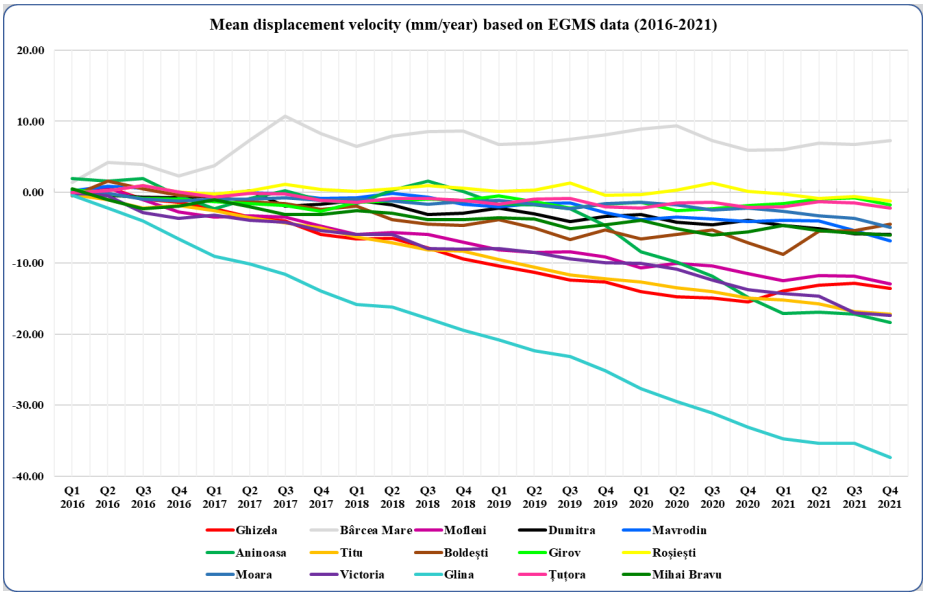

Figure 5. EGMS-derived displacement rate for each quarter of the investigated time frame - all landfills

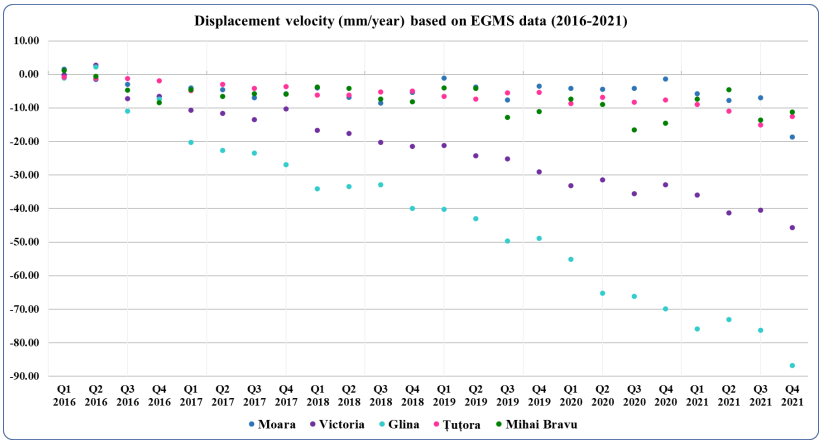

Figure 6. EGMS-derived displacement rate for each quarter of the investigated time frame - batch 1

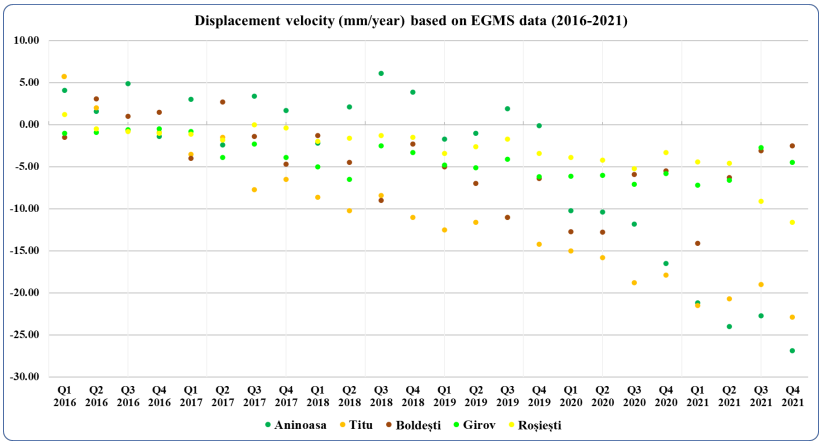

Figure 7. EGMS-derived displacement rate for each quarter of the investigated time frame - batch 2

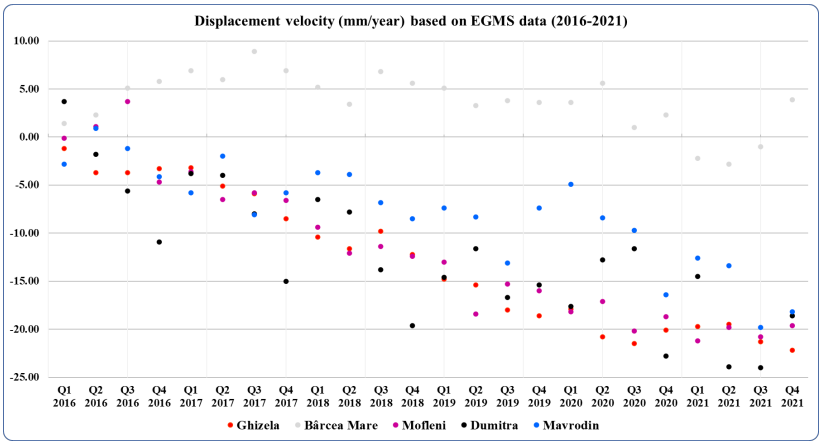

Figure 8. EGMS-derived displacement rate for each quarter of the investigated time frame - batch 3

Batch 1 of the selected sites (Figure 6) contains 3 rather stable landfills, namely Moara, Țuțora and Mihai Bravu. Moara is an ecological waste disposal site that is operational starting with July 2019. At the level of 2021, the landfill was receiving waste collected from the entire Suceava County, the first cell having a projected lifetime of 10 years. A subsidence process is not clearly observable within the EGMS dataset, primarily because the exploitation time frame and the EGMS time coverage are overlapping for a rather short interval (i.e., July 2019 - December 2021). Having a similar evolution, Țuțora is also an ecological landfill that will be composed of 4 main cells, covering a 30-year time span. The first cell is in service since 2012 and it is receiving all the waste that accumulates within the Iași County. Starting with 2013, the landfill stored more than 125,000 tons/year, reaching almost 181,000 tons/year in 2019. Even though some technical and maintenance issues have been present (i.e., with leachate and geotextile layer) and the disposal site is in use for a rather large number of years, a clear subsidence process was not detected based on the EGMS data. With regard to the Mihai Bravu landfill, it is functional since 2020, hence the analysis period is of only 2 years. Similar to the previous examples, a subsidence process is not observable yet for this waste disposal site.

Victoria landfill (Botoșani County) is in use since September 2016. Starting with the first quarter of 2018, a subsidence process is noticeable (Figure 6), with subsidence rates reaching almost -50 mm/year at the end of 2021, based on the several persistent scatterers (Figure 9) that are present within the waste disposal site.

The Glina landfill (Ilfov County) was officially operational from 2008 until 2017. However, the site was used for waste disposal since 1977, when large quantities of construction debris generated by the 7.2 magnitude earthquake were stored there. For this landfill, the EGMS contains the greatest number of persistent scatterers and the most significant displacement values (Figure 10). The analysis shows that the settlement process started even before the closing of the landfill and continued on a steady basis until the end of the monitoring window. In the latest observation years, for some persistent scatterers, the vertical displacements reached almost -90 mm/year, hence the amplitude of the landfill settlement process is considerable. Figure 11 illustrates the surrounding area of Glina landfill, where the mean displacement velocities of the persistent scatterers located within a buffer of 1,000 m to 2,000 m around the landfill are approximately 6 times lower than the mean values corresponding to the landfill.

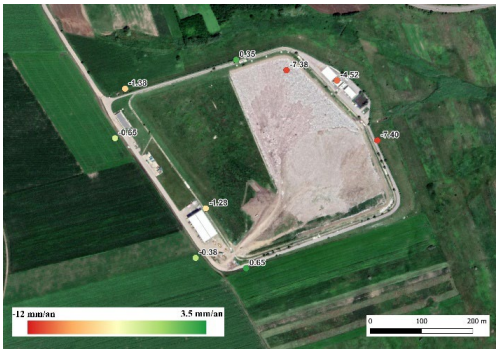

Figure 9. Overall mean displacement velocities (2016-2021) for the persistent scatterers of the Victoria landfill

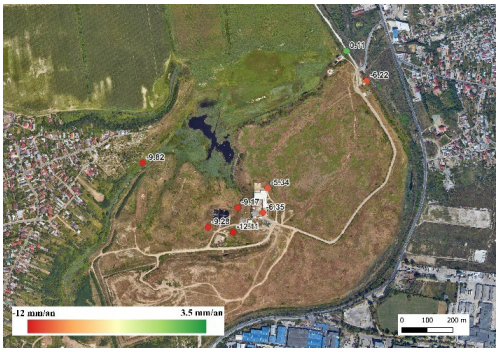

Figure 10. Overall mean displacement velocities (2016-2021) for the persistent scatterers of the Glina landfill

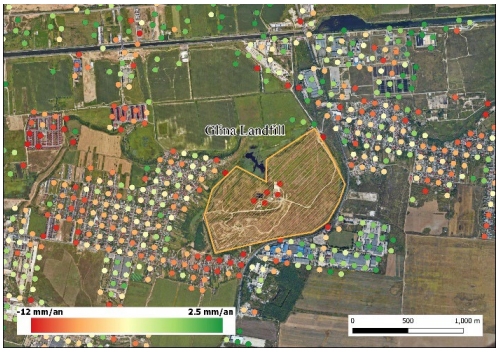

Figure 11. Displacement map (2016-2021) for the surrounding area of Glina landfill

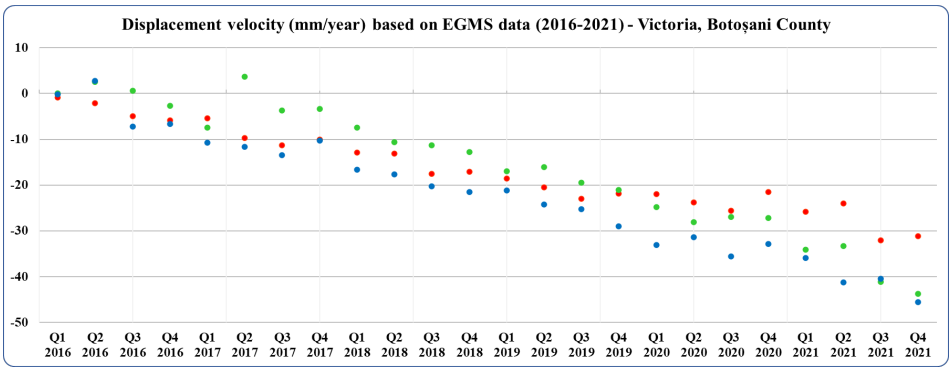

Figure 12. Persistent scatterers displaying the most significant displacement rates (2016-2021) - Victoria

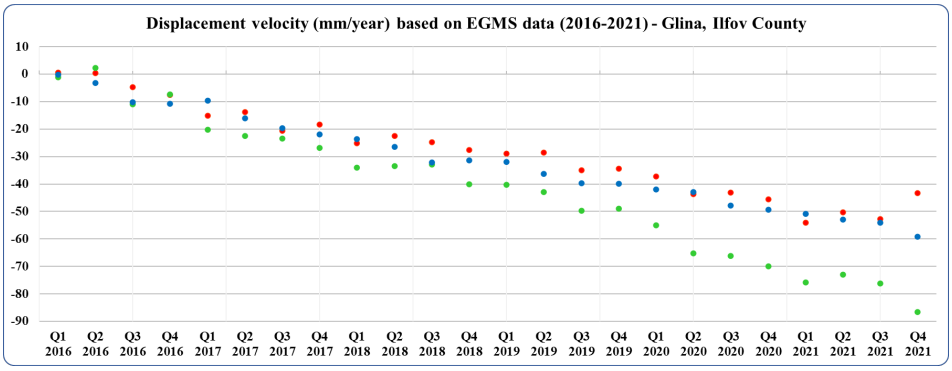

Figure 13. Persistent scatterers displaying the most significant displacement rates (2016-2021) - Glina

Figures 12 and 13 present the evolution of the 3 persistent scatterers that present the most significant displacement values for Victoria and Glina, respectively. The subsidence trend is definite in both cases, for the points considered. The second batch of the selected test sites (Figure 7) includes two landfills that are stable, namely Girov and Roșiești. The first one (Girov) is located in Neamț County and it is operational since 2015. The landfill is designed to have a lifespan of 21 years, while the first of the 3 projected cells will be functional for 5 years. The second landfill (Roșiești) represents the only landfill of Vaslui County, being functional since 2018 and storing more than 70,000 tons in 2019. Further, the Boldești landfill (located in Boldești -Scăieni, near Ploiești, Prahova County) became operational in 2001 and it is still currently in use. In this case, although the operational framework is considerably long (approximately 20 years), a pronounced landfill settlement process was not detected based on EGMS data. Some possible explanations include: (1) the settlement process ended before the monitoring window started, thus indicating a relatively stable area; (2) the quality and number of persistent scatterers are not satisfactory (Figure 14).

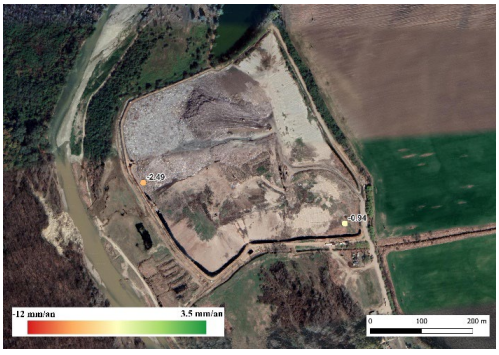

Figure 14. Overall mean displacement velocities (2016-2021) for the persistent scatterers of the Boldești landfill

Titu and Aninoasa landfills are both located in Dâmbovița County. These waste disposal sites present a similar displacement trend, although in

case of the latter the values are slightly higher (Figure 7). The Titu landfill (Figure 15) is in service since 2010; the first cell functioned until 2018, whereas the second one was operational between 2018 and November 2019. Almost the same trend is impacting a small part of the near-by city of Titu (i.e., the area located in a buffer of 1,000-2,000 m around the landfill). In this case, the displacement rates are equalling almost 60% of the numeric values corresponding to the waste disposal site (Figure 16).

Figure 15. Overall mean displacement velocities (2016-2021) for the persistent scatterers of the Titu landfill

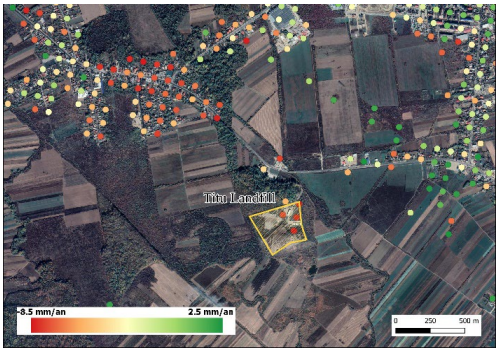

Figure 16. Displacement map (2016-2021) for the surrounding area of Titu landfill

The Aninoasa landfill is operational since 2010; first cell reached maximum capacity in 2018, while the second cell is still in service. Based on the EGMS data (Figure 17), a clear subsidence process can be identified for the first cell a few months after its closure (beginning of 2019). In addition, the surrounding areas of the landfill (including a part of Aninoasa city) also have relatively high subsidence values (Figure 18), following the same displacement trend. In this case, the persistent scatterers located in the buffer of 1,000-2,000 m around the waste disposal site have mean displacement values that are reaching almost 50% of the figures detected for the Aninoasa landfill.

Figure 17. Overall mean displacement velocities (2016-2021) for the persistent scatterers of Aninoasa landfill

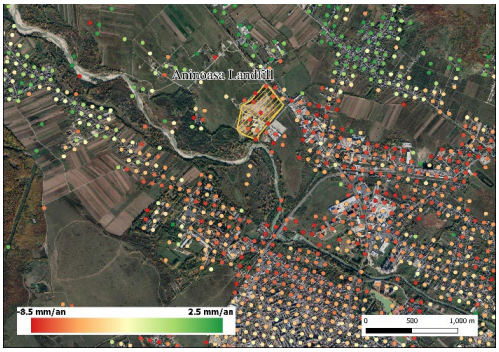

Figure 18. Displacement map (2016-2021) of the surrounding areas of Aninoasa landfill

For both Titu and Aninoasa waste disposal sites, the persistent scatterers that display the most significant subsidence values are revealing a clear subsidence process (Figures 19 and 20).
The last batch of selected sites (Figure 8) contains Dumitra (Tărpiu, Bistrița-Năsăud) and Mavrodin (Teleorman), two landfills with a similar pattern that suggests a less evident subsidence trend due to the presence of also stable persistent scatterers. The first one is operational since 2014, with cell 1 reaching full capacity at the end of 2020 and cell 2 being in service starting with 2021. Mavrodin serves as a landfill since 2013. The waste quantities decreased from almost 85,000 tons in 2014 to approximately 50,000 tons in 2019.

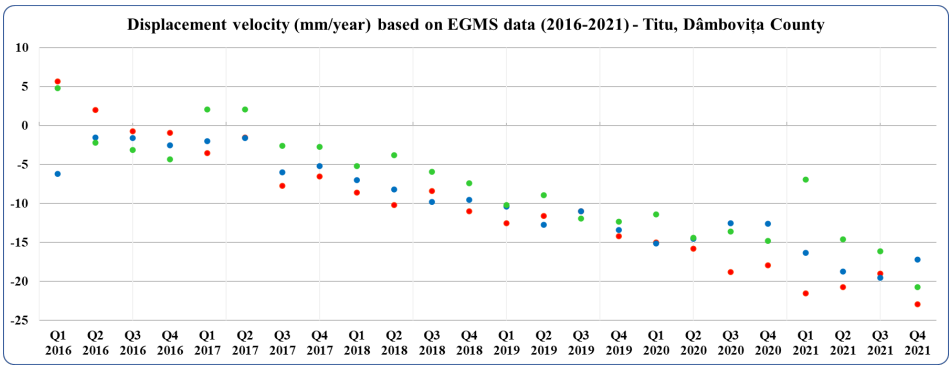

Figure 19. Persistent scatterers displaying the most significant displacement rates (2016-2021) - Titu

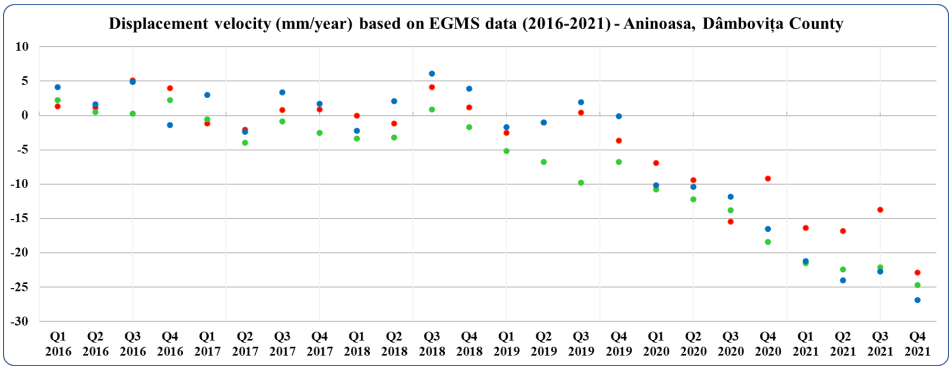

Figure 20. Persistent scatterers displaying the most significant displacement rates (2016-2021) - Aninoasa

Bârcea Mare (located in Hunedoara County) is a landfill that is in use since 2017. Only the first cell is built, the second one will be functional starting with 2028. Based on the analysis of the EGMS data, this landfill presents positive displacement values that are specific to land uplift, with mean values in the range of 5-10 mm/year. The mean displacement values were computed based on only 4 persistent scatterers identified within the test site, hence the landfill necessitates systematic monitoring for a longer time frame due to the atypical values measured. However, a possible explanation might be that the landfill does not have any closed cells within the monitoring interval, therefore the proper identification of persistent scatterers in the multitemporal series of satellite data could have been hindered.

Ghizela and Mofleni landfills (Figure 8) have a similar displacement evolution. Ghizela (Timiș County) is operational since 2012; its first cell functioned until November 2019; currently, the second cell is in service. The volumes deposited during 2019 were significantly higher than the ones stored between 2014 and 2018. A clear negative displacement trend is observed starting with the third quarter of 2018. In what concerns Mofleni landfill, it is operational starting with 2006 and collects waste from the entire Dolj County. Between 1970 and 2005, a non-compliant waste disposal site functioned in the same place. At the level of 2021, the first cell of the Mofleni landfill was closed, cells 2, 3, 4 and 5 were temporarily covered and cell 6 was operational. In this case, subsidence is observed starting with the end of 2017, reaching more significant displacement values at the end of the monitoring window. The 3 persistent scatterers that exhibit the most considerable subsidence values have values in the range of -15 mm/year ± -20 mm/year, in December 2021 (Figure 21). Their progression in time is comparable.

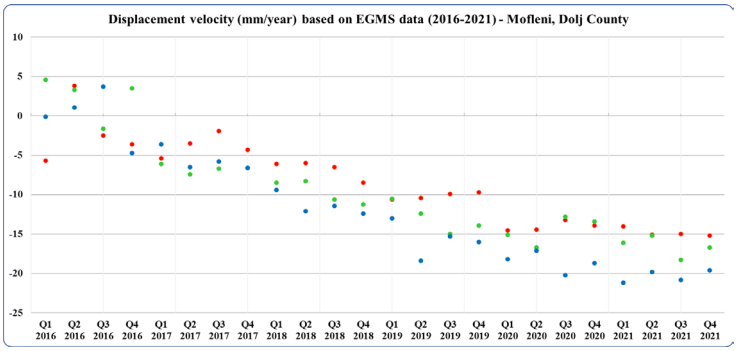

Figure 21. Persistent scatterers displaying the most significant displacement rates (2016-2021) - Mofleni

CONCLUSIONS

The analysis revealed that EGMS dataset offers good results in the identification of subsidence, considering that for 8 out of the 15 investigated landfills, the phenomenon could be identified and accurately monitored within the specific time frame. The rest of the monitored landfills present trends that relatively indicate stability. However, it should be kept in mind that a proper monitoring interval for the landfill settlement process is much longer. Therefore, the EGMS dataset might represent an important tool for landfill management since it enables both the detection and long-term, systematic monitoring of land subsidence, that could be correlated with the landfill settlement process. This aspect is of particular importance for environmental risk assessment. In addition, the EGMS dataset provides insights also about the surrounding areas, over large regions, hence the estimation of the landfill impact or the detection of other potential threats may be accomplished as well.

ACKNOWLEDGEMENTS

This work was supported by a grant from the Romanian Ministry of Research, Innovation and Digitalisation, CCCDI—UEFISCDI, project number PN-III-P2-2.1-PTE-2021-0432/contract number 82PTE, within PNCDI III.

REFERENCES

Chabuk, A.; Al-Ansari, N.; Ezz-Aldeen, M.; Laue, J.; Pusch, R.; Hussain, H.M.; Knutsson, S. (2018). Two Scenarios for Landfills Design in Special Conditions Using the HELP Model: A Case Study in Babylon Governorate, Iraq. *Sustainability*, *10*, 125.

Crosetto, M.; Solari, L.; Mróz, M.; Balasis-Levinsen, J.; Casagli, N.; Frei, M.; Oyen, A.; Moldestad, D.A.; Bateson, L.; Guerrieri, L.; et al. (2020). The Evolution of Wide-Area DInSAR: From Regional and National Services to the European Ground Motion Service. *Remote Sens.*, *12*, 2043.

Crosetto, M., Solari, L., Frei, M., Balasis-Levinsen, J., Moldestad, D.A., Oyen, A., Casagli, N., Bateson, L., Guerrieri, L., Comerci, V., Mróz, M. (2021). *Validation of the EGMS Product Portfolio*.

Du, Y.; Fu, H.; Liu, L.; Feng, G.; Wen, D.; Peng, X.; Ding, H. (2021). Continued Monitoring and Modeling of Xingfeng Solid Waste Landfill Settlement, China, Based on Multiplatform SAR Images. *Remote Sens.*, *13*.

EGMS (2023). *Webinar "EGMS, a General Introduction" - Questions and Answers.* https://land.copernicus.eu/user-corner/events/q-a-1st-egms-webinar-2023.

He, H.; Wu, T.; Wang, X.; Qiu, Z.; Lan, J. (2021). Study on Compressibility and Settlement of a Landfill with Aged Municipal Solid Waste: A Case Study in Taizhou. *Sustainability*, *13*, 4831.

Kotzerke, P., Siegmund, R., Langenwalter. J. (2022). *End-to-end implementation and operation of the European Ground Motion Service (EGMS) - Product User Manual.* ORIGINAL Consortium.

Papale, L.G., Guerrisi, G., De Santis, D., Schiavon, G., Del Frate, F. (2023). Satellite Data Potentialities in Solid Waste Landfill Monitoring: Review and Case Studies. *Sensors (Basel)*. 2023 Apr 12; 23(8):3917. doi: 10.3390/s23083917. PMID: 37112260.

Tabish, R., Yang, Z., Wu, L., Xu, Z., Cao, Z., Zheng, K. and Zhang, Y. (2022). Predicting the Settlement of Mine Waste Dump Using Multi-Source Remote Sensing and a Secondary Consolidation Model. *Front. Environ. Sci.* 10:885346.

Virsta, A., Sandu, M.A., Daraban, A.E. (2020). Dealing with the Transition from In Line Economy to Circular Economy - Public Awareness Investigation in Bucharest. *AgroLife Scientific Journal*, *9(1)*.

Zhang, S.; Lv, Y.; Yang, H.; Han, Y.; Peng, J.; Lan, J.; Zhan, L.; Chen, Y.; Bate, B. (2021). Monitoring and Quantitative Human Risk Assessment of Municipal Solid Waste Landfill Using Integrated Satellite–UAV–Ground Survey Approach. *Remote Sens. 13*, 4496.

Scientific Papers. Series E. Land Reclamation, Earth Observation & Surveying, Environmental Engineering. Vol. XII, 2023
Print ISSN 2285-6064, CD-ROM ISSN 2285-6072, Online ISSN 2393-5138, ISSN-L 2285-6064

AN OPTIMIZATION MODEL FOR THE DELIVERY OF PLANTS TO NURSERIES

Velika KUNEVA, Manol DALLEV

Agricultural University - Plovdic, 12 Mendeleev Blvd, Plovdiv, Bulgaria

Corresponding author email: kuneva@au-plovdiv.bg

Abstract

The purpose of the development is to present an option for reducing costs in the delivery of ornamental plants to nurseries. The nursery is located in the town of Parvomai and is located in the eastern part of the Plovdiv region, in the Thracian plain, at about 134 meters above sea level. Different varieties of flowers are produced in it – petunias, violets, verbena, tagetis, sakezets and other species. The nursery stocks and delivers goods to 5 small sites in the surrounding area To achieve the goal, the following tasks must be solved: to characterize the used vehicles; to optimize transport costs by solving a transport task under certain conditions. By using MS Excel Solver, proposed algorithm for describing a transport task and its subsequent solution, significantly speeds up the calculation procedures and helps to reduce costs when making deliveries.

Key words*: optimization model, transport task, Solver.*

INTRODUCTION

Decorative plants are one of the main details of the interior of the house or the landscape of the garden. The beginning of the nursery production of decorative planting materials in our country is connected with the construction of the parks at the residences Evksinograd - Varna, Krichim and Vrana - Sofia. The creation of green systems in cities and other settlements, the landscaping of various objects (enterprises, schools, hospitals, etc.), knowledge of the stages in the production and cultivation of ornamental trees and shrubs in nurseries, planting in the green areas and their successful further cultivation are the main tasks for specialists in this field.

The cultivation of ornamental plants falls under floriculture, which is a major branch of horticulture. They are seen not so much for practical purposes as for decoration and comfort. Decorative indoor plants perfect house design. The assortment of plants is large. Ornamental plants have quite exotic species. A nursery is a place where plants are propagated and grown to the desired size. Some nurseries specialize in certain areas. Nurseries can also specialize in one type of plant.

Some produce stock seasonally, ready in the spring for export to colder regions where breeding could not begin as early, or to regions where seasonal pests prevent early season cultivation. (Dobrevska G. et al., 2015). Nurseries grow plants outdoors, in container fields, tunnels and greenhouses. There should be a minimum time gap between removing the material from the nursery and planting in the desired location. To avoid exposure to the sun, the planting material should be removed from the nursery in the evening and planted the next day.

The aim of the development is to load more sites with minimal fuel costs. To achieve it, the following task must be solved: to optimize transport costs by solving a transport task under certain conditions. Such an approach was developed in the publication (Dallev, 2021) to optimize the transport costs of fertilizing on a farmer's farm. Thus, we have already created a program for optimization problem solving. This approach was use in the research study of (Ivanova et al., 2018; Marinov, 2016; Atanasov et al., 2020; Blagoeva et al., 2021; Georgieva et al., 2019; Yordanova et al., 2020).

MATERIALS AND METHODS

The nursery is located in the town of Parvomai and is located in the eastern part of the Plovdiv region, in the Thracian plain, at about 134 meters above sea level. The terrain is predominantly hilly and flat. The climate is transitional-continental with pronounced

temperature contrasts. The soils are chernozem (smolny, cinnamon-forest, meadow-alluvial). (Dobrevska et al., 2015). Different varieties of flowers are produced in it – petunias, violets, verbena, tagetis, sakezets and other species (Figure 1).

The nursery supplies and delivers goods to 5 small sites in the vicinity. The first site is located in the village of Gradina, the distance is 6 km from our base. The second object is located again in the village of Gradina, but it is at a distance of 8 km. Object 1 and object 2 are at a distance of 2 km from each other. Site three is located in the village of Byala Reka and is 10 km away from the nursery. Site four is located in the village of Dragoynovo and is 15 km away. The two sites are 5 km away from each other. The last site we charge is located in the village of Patriarch Evtimovo and is 20 km away from the nursery.

From the calculations, it can be seen that the sites are not close to the nursery.

The transport is carried out with two vehicles, each of which has an additional construction made of shelves in order to maximize the use of space and ensure a larger delivery of goods. We have the following equipment:

Fiat Scudo 2005-

Characteristics: Length - 4,805 m, Width -1,895 m, Height -1,980 m

Fuel consumption - urban 8.4/100 km, extra-urban 6.8/100 km, combined - 7.2/100 km.

Fuel type - diesel

We load the sites with seedlings in trays, dimensions of the trays - 48 nests, length 52.5 cm, width 37.5 cm. The number of boards in the Renault Master with the additional 3 shelves is:

Width includes 55 pcs. boards, i.e. 55 x 3 = 165 pcs. boards, there are 13 boards in length - 13 x 3 = 39 pcs., the total capacity is 165 + 39 = 204 pcs. boards.

Which makes 204 pcs. boards with 48 nests, a total of 9792 plants.

In order to keep the fuel costs to a minimum, we proposed to site 1 and site 2 to make their delivery of plants on the same day, the delivery is made by Renault Master due to the large requests (Monday and Wednesday).

On Monday we deliver 72 boards for Site 1 and 100 boards for Site 2.

On Wednesday we deliver 90 boards to site 1 and 110 boards to site 2.

We deliver 17,856 plants per week.

After that, we offered the same option to site 3 and 4, with which their delivery takes place (Tuesday and Friday).

Tuesday we deliver 50 boards to site 3 and 130 boards to site 4.

Friday we deliver 160 boards to site 3 and 43 boards to site 4.

A total of 9744 plants. Again, delivery is made by Renault Master.

At sites 1, 2, 3 and 4, delivery is made with a Renault Master bus, due to its large size and the possibility of more goods.

Object 5 - delivery is made (Monday and Thursday), due to the small amount of sales, delivery is made with Fiat Scudo.

We deliver 18 boards on Monday and 25 boards on Thursday.

In total for the two days we deliver 2064 plants.

Figure 1. The nursery varieties of flowers

Algorithm used for the transport problem solving via the instruments of MS Excel Solver (MS EXCEL 2010)

One of the tools in MS Excel is a module for optimization task solving called Solver (Figure 2). It can be found under the Data menu. It must be activated before its first use taking the following steps:

• launch MS Excel;
• select Options from the File menu;
• the Excel Option dialog box appears;
• click on the submenu Add-Ins (Additions) → Manage (Management) and select Excel Add-ins (additions in Excel);
• close the dialog box with OK.

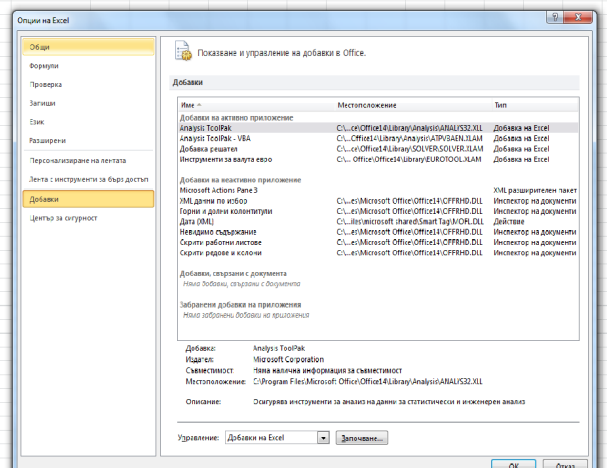

Figure 2. Solver activation dialog box

In this way, we now have the program for solving optimization tasks.

The transport task is formulated as it follows:

Consider the following task. At the points $A_1, A_2, ...A_m$ (which we will call producers) is produced output in quantity, respectively a_1, a_2,…..a_m. Points $B_1, B_2, ...B_n$ (we will call them users) need the same output in quantities respectively b_1, b_2,……, b_n. There is a balance between production and consumption i.e. $\sum_{i=1}^{m} a_i = \sum_{j=1}^{n} b_j$.

The transport costs per unit from point $A_i (i = 1,2,..., m)$ to point $B_j (j = 1,2,..., n)$ are c_{ij}.

To devise up a plan for the procurement of points $B_1, B_2, ...B_n$ of production from the points $A_1, A_2, ...A_m$, so that the needs of consumers are met, the goods of the producers to be disposed of and the total transport costs to be minimal.

RESULTS AND DISCUSSIONS

Assignment to optimize transportation costs for delivery to five sites:

To carry out the delivery operation with two vehicles to the following sites (Figure 3):

1. Site 1 - 162 boards at a distance of 6 km from the nursery;
2. Site 2 - 210 boards at a distance of 8 km from the nursery;
3. Site 3 - 210 boards at a distance of 10 km from the nursery;
4. Site 4 - 173 boards at a distance of 15 km from the nursery;
5. Site 5 - 43 boards at a distance of 20 km from the nursery.

The data on the average fuel consumption during transport has been determined empirically - 0.244 L/km and the calculations are made at an average fuel price of BGN 3.25.

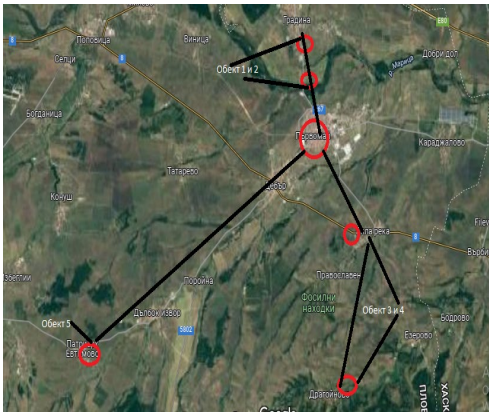

Figure 3. The sites

Task. To solve the following transport problem

B_j / A_i	B_1	B_2	B_3	B_4	B_5	a_i
A_1	0.05	0.12	0.05	0	0.1	755
A_2	0.02	0	0	0.02	0	43
b_j	162	210	210	173	43	798

Solution. The transportation problem is closed because a balance between production and consumption is observed, i.e.

$$\sum_{i=1}^{2} a_i = \sum_{j=1}^{4} b_j = 798$$

MS Excel (Solver) is used for solving the resulting closed (balanced) transport problem. Figure 4 presents a spreadsheet with the mathematical model of the specified task.

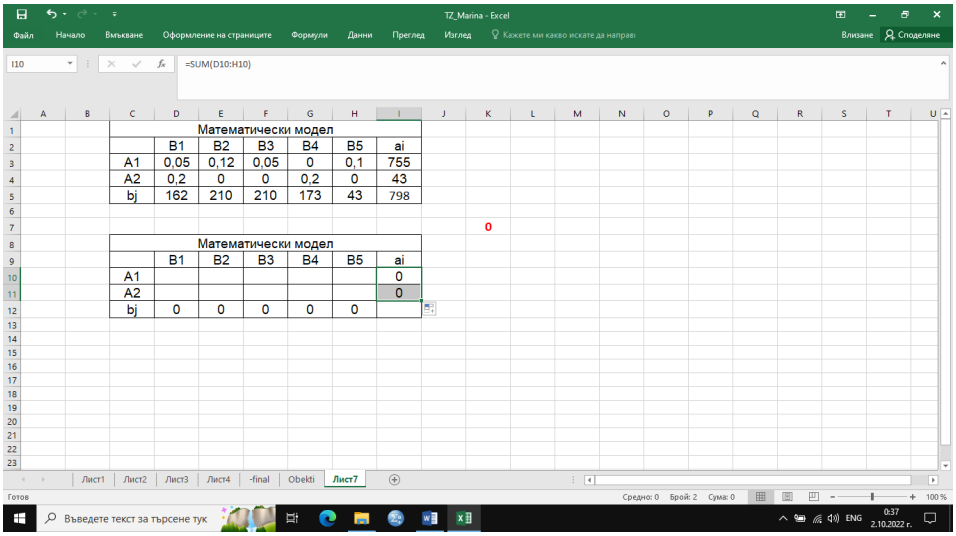

Figure 4. Task model spreadsheet

Completing the worksheet:

1. In cells $D$3:$H$4 we enter the values of transport costs, in cells $I$3:$I$4 - the constants from matrix A(ai), and in cells $D$5:$H$5 - the constants from matrix B (bi).
2. In cell $K$7, we enter the formula used for calculating the value of the objective function, i.e. = SUM PRODUCT(D3:H4; D109:H11).
3. In the second table, in cell $C$11, formula = SUM (D10:D11) is entered and zero appears after clicking the mouse.

And then it is copied to the remaining cells $D$12:$F$12. A null value also comes out.

In the same way, a formula is entered for cell $I$10 and copied to cell I 11.

When composing the formula, one can use absolute addressing of the cells that contain the variables of the task (the $ sign is placed in front of the column name and/or row number).

When solving large-scale problems, it is suitable to use the built-in function, SUMPRODUCT, which calculates the scalar product of two vectors of the same dimension.

We enter the input data and activate the formula from the menu Data (Data) → Solver, after that We open an empty dialog box named Solver Parameters, which shows the formula for the value of the objective function (Figure 5).

It is recommended that before calling Solver, the cell with the target function should be current - in this case, cell $K$7.

With Equal To, select the radio button corresponding to the criteria of the model, in the specific task, select Min.

The By Changing Cells box shows the entered cells, which contain the values of the problem`s variables. In the present task, these cells are $D$12:$H$12 on which the objective function is minimized.

When we click on the Subject to the Constraints field, we use the buttons next to it in order to enter the restrictive conditions - in this case we can add, or change using the Change button and delete existing constraints using the Delete button. After the entry of the current limit is finished, we select the Add button if we must enter a new limit, or the OK button if the entry is completed.

The Make Unconstrained Variables Non-Negative option is checked.

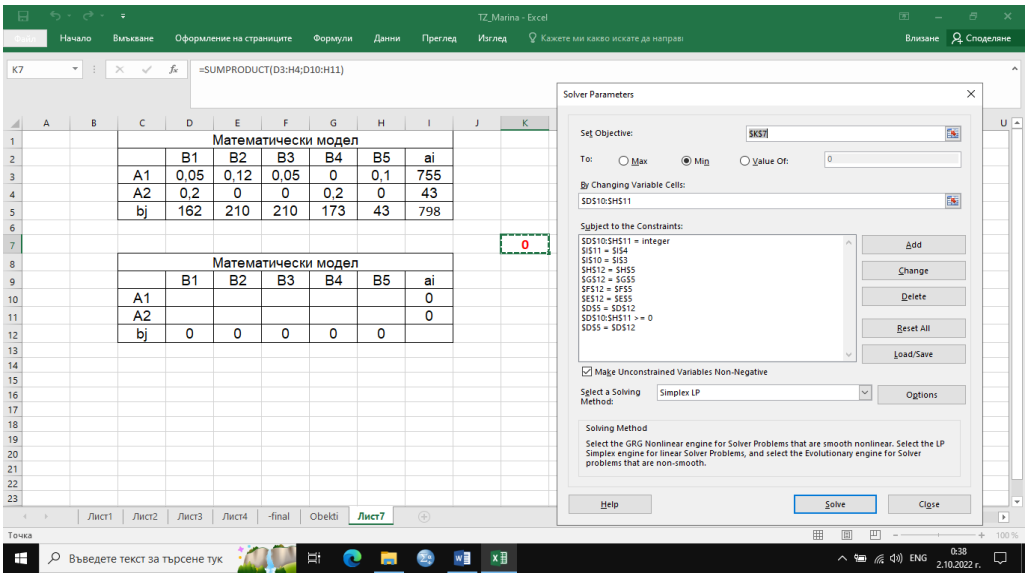

Figure 5. "Solver Parameters" dialog box

The other items in the dialog box are not recommended for a change. Finally, when we click the OK button, we return to the Solver Parameters dialog box.

Figure 5 shows the Solver Parameters dialog box. The Solver button is selected from the Solver Parameters dialog box to solve the problem. The solution is presented in Figure 6.

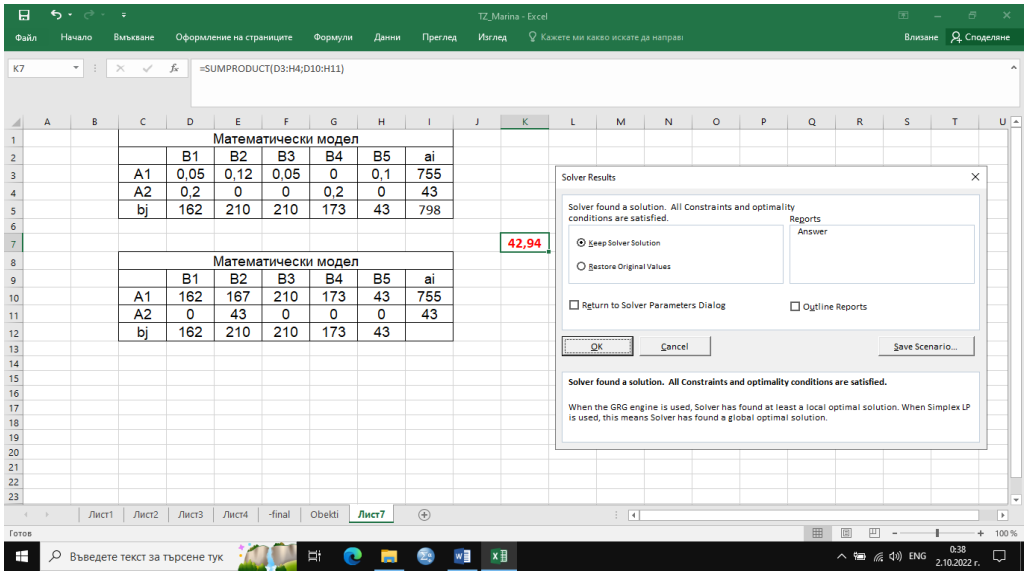

Figure 6. The spreadsheet and dialog box

Solver Results

The results obtained by the performed optimization are provided in the Solver Results dialog box. In the specific case, it is established that all restrictive conditions and conditions for optimality are satisfied regarding the given solution. Cells $D$10:$H$11 show the optimal solutions and an optimal plan is obtained.

We can save the found optimal solution in the Solver Results dialog box (clicking the Keep Solver Solution button) or we can restore the original worksheet (clicking the Restore Original Values radio button).
It is possible to make a reference to the problem`s solution from this dialog box (Answer Report).
Taking into account the proposed description, as well as the presented solution of a transport problem in MS Excel environment using the capabilities of the MS Excel Solver, we can conclude the following:
The proposed algorithm is easily applicable regarding the description of a transport task and its subsequent solution using MS Excel Solver;
Software applications use significantly quickens the calculation procedures;
"Solver" add-on tool is established as a functional one as it can be used both, for transport-type problems, as well as for problems in other areas.
The model of the transported problem is suitable for the correct and optimal solution of the problem under consideration.

CONCLUSIONS

The following conclusions can be drawn from the present research study:
• The used algorithm proposed for describing a transport problem and its subsequent solution by means of software applications significantly accelerates the calculation procedures and is an easily applicable optimization method.
• Thanks to the optimization, the transport costs for charging 5 objects have been minimized to BGN 42.94.

ACKNOWLEDGEMENTS

This research work was carried out with the support of Agricultural university- Plovdiv and also was financed from Project National Scientific Program - Intelligent Plant Breeding.

REFERENCES

Atanasov, D., Dobrevska, G., Dallev, M. (2020). Economic assessment of an optimised model of apple rootstock production. *Bulgarian Journal of Agricultural Science, 26*(6), 1166-1170.
Blagoeva, N., Georgieva, V., (2021). Tax expenditures as an incentive for the agriculture in bulgaria. *Scientific Papers Series Management, Economic Engineering in Agriculture and Rural Development, 21*(1).
Dallev, M., Kuneva, V. (2021). Optimization model for fertilization operations. *Scientific Papers. Series A. Agronomy, 10.* 85-88.
Dobrevska, G., Popova, R., Dzhugalov, H. (2015). Manifestations of M9 apple rootstock in stoolbedwith different soil substrate and plants with a different origin, "10th International Symposium on Agriculture", Zagreb, Croatia (16-20 February 2015) Zbornik radova, 565-569.
Dobrevska, G., Popova, R., Dzhugalov, H. (2015). Influence of plant origin and soil substrate on theBehaveour of the MM 106 rootstock in stoolbet. "10th International Symposium on Agriculture", Zagreb, Croatia (16-20 February 2015) Zbornik radova, 570-574.
Ivanova, I., Kuneva, V. (2018). Handbook on Optimization Methods. Plovdiv: Academic Press AU (In Bulgarian).
Marinov, M., Marinova, L. (2016). Algorithm for calculating the transportation problem and its solution in Excel, Russe, Scientific Works in Rousse University, 55(3). 19-24 (In Bulgarian).
Yordanova, A., Kulina, H. (2020). Random forest models of 305 - Days Milk Yield for Holstein Cows in Bulgaria, AIP Conference Proceedings 2302, 060020

Scientific Papers. Series E. Land Reclamation, Earth Observation & Surveying, Environmental Engineering. Vol. XII, 2023
Print ISSN 2285-6064, CD-ROM ISSN 2285-6072, Online ISSN 2393-5138, ISSN-L 2285-6064

SCENARIO-BASED ON LEARNING ACTIVITIES DESIGNED TO PROVIDE INTERACTIVE EXPERIMENTAL LAB AT SCIENCE DISCIPLINES

Mirela Alina SANDU, Ana VIRSTA, Roxana Maria MADJAR, Gina VASILE SCĂEȚEANU

University of Agronomic Sciences and Veterinary Medicine of Bucharest, 59 Marasti Blvd, District 1, Bucharest, Romania

Corresponding author email: gina.scaeteanu@agro-bucuresti.ro

Abstract

Even if online and distance learning options were accessible before COVID-19 it wasn't appreciated and incorporated properly within educational process. The unwelcomed situation created by COVID-19 pandemic it has brought a lot of uncertainties, challenges and set a milestone for online educational process. In the context of suspended face-to-face activities, teachers had to solve a great challenge: to teach online experimental activities at science disciplines. Hence, everyone had to adapt and to found in a short period of time the best solutions. If delivering theoretical aspects was easier to implement, experimental activities became quite provocative at that moment. This paper presents solutions that we found and implemented in our science classes during COVID-19 pandemic period and the new perspectives that arose from this experience. Considering that online learning represents a powerful educational solution and having in view possible future emerging situations (pandemic, extreme climatic conditions etc) that may affect face to face learning, we intend to develop and implement in our science disciplines a virtual laboratory under the name "Hybrid Environmental Engineering Laboratory for exercising practical skills".

Key words*: education; online learning; virtual laboratories (VLs).*

INTRODUCTION

On 11th of March 2020, the World Health Organization officially declared COVID-19 a global pandemic, due to the rapid increase in the number of cases and the high risk of spreading the infection globally (Cucinotta & Vanelli, 2020). As a reaction, the European Union and the authorities of the Member States, including Romania, have taken a series of measures to protect the population from the Coronavirus: movement and travel restrictions, quarantine of localities, strict hygiene measures, the distribution of medical and protective equipment, and even the temporary stoppage of certain economic activities.

Among all these, the education sector was one of the worst affected, as more so as online teaching was not implemented before. Universities, including those from Romania, have been forced to switch to online education and to reconfigure all educational practices from face-to-face interaction to online environment. The sudden and unplanned transition to online learning has created a number of challenges for students and for faculty academic staff, this being the new standard teaching method for almost an entire academic year (Merill, 2020; De Witt, 2020) and the only available manner to continue educational process in this given situation (Kee & Zhang, 2022).

The closure of all educational institutions worldwide marked the beginning of a period full of challenges for the entire education system.

The COVID-19 pandemic has significantly accelerated the digital transformation of our societies and these processes, once triggered, are expected to gain more and more speed.

This paper highlights the challenges of the rapid transition to online and distance education, the identified solutions to surpass the educational crisis and to sustain at acceptable standard the educational process.

CHALLENGES

When educational activities were suspended in the third week of the second semester of University of Agronomic Sciences and Veterinary Medicine Bucharest (USAMV of Bucharest) studies until the end of the academic year (June 2020), appeared the necessity to reorganize "on the fly" the modality of operation, educational resources, pedagogical techniques and the interaction between teaching staff, students and colleagues.

The transition was characterized by a short but intense period of reorganization and regrouping of the educational process. Learning and teaching has been structured to effectively meet the challenges of fulfilling the most important university's mission: providing education. Empowering teachers to deliver distance education while ensuring and engaging students was vital in managing the transition and successfully completing the academic year. Having a strong instructional design team working closely with academic staff has proven to be essential to the effective transition to online and distance learning (Hodges et al., 2020).

The most prominent and impactful change was the necessity of rapid adaptation to provide education by finding the best solutions at that time. While all disciplines were affected by this sudden change, science teaching was particularly disrupted due to the hands-on and research-based nature of laboratory activities.

Linking theory and practice has always represented a manner that helped students to develop their logical reasoning, thinking skills, to understand many processes and concepts, but before year 2020 this was not a challenge.

In this crisis situation, difficulties arose with some courses that required laboratory training of students.

Theory classes were held online using e-learning platforms and videoconferencing applications, meanwhile for experimental disciplines were used virtual labs (VLs) existing on different platforms at that moment (Table 1).

During the COVID-19 pandemic period, the VLs were adopted as the only possible manner to experiment scientific concepts which otherwise were presented satisfactorily in the real laboratories.

In addition, after pandemic period in universities all over the world the challenge accepted by scientists, informaticians and teachers was to develop VLs suitable to provide education in all circumstances and to integrate technology into the traditional learning environment.

VIRTUAL LABS (VLs)

Literature studies have indicated VLs as an education platform for improving education through the dissemination of laboratory education (Radhamani et al., 2021). These are the digital tools that can be used to provide distance learning for laboratory sessions (Radhamani et al., 2021) without affecting the quality of learning (Toma et al., 2022).

In addition, Vary (2000) defines VLs as "*an electronic workspace designed for remote collaboration and experimentation, or carries out other creative activities, and disseminate results using information and communication technologies*".

During the quarantine and after, due to restrictions, VLs played a crucial role in the higher education sector, this being the only route to continue teaching and learning. Most teachers supported the role of VLs in improving their teaching skills and supporting students to complete laboratory practices without affecting the quality of learning (Raman et al., 2021a; 2021b; 2021c).

VLs cannot completely replace the physical experiments in traditional laboratories. However, in academic environments, virtual and physical laboratories can work together (Achuthan et al., 2017; Vasiliadou, 2020). Furthermore, there are authors that sustain that the best results are obtained when virtual labs and traditional methods are combined (Chan et al., 2021).

Especially during the COVID-19 pandemic, students performed online experiments without time limitations, received instant feedback, familiarized themselves with health and safety regulations, repeated experiments and self-evaluated (Vasiliadou, 2020). Also, by using VLs, they are engaged with technology and prepare more productively for their physical laboratories (Breakey et al., 2008). Moreover, studies (Hawkins & Phelps, 2013; Usman & Huda, 2021) provide evidence that VLs enhance comprehension and motivation, students being more interested by this approach.

Even if before the pandemic there were many concerns regarding the VLs and the efficiency of this approach regarding learning (Tatli & Ayas, 2010; Mikropoulos & Natsis, 2011; Herga & Dinevski, 2012; Hawkins & Phelps, 2013; Ratamun & Osman, 2018; Nais et al., 2019) the real value of this study method was found when access to university laboratories was restricted due to the quarantine and the pandemic of COVID-19.

In Romania, before COVID-19 period were reported several VLs for university studies and their effectiveness was evaluated on the basis of students' attitudes and results (Nedelcu and Saru, 2003; Trifan, 2011; Craifaleanu et al., 2014; Popescu, 2015; Marusteri et al., 2019). After pandemic period, because of difficult situations that occurred during educational process and had to be surpassed, VLs were developed by different teams (Craifaleanu & Craifaleanu, 2022; Vergara et al., 2022; Schneider et al., 2022).

1. Benefits of Using Virtual Labs

In the following section are summarized the main advantages of VLs.

- ***Availability***

The great advantage is that worldwide students who learn remotely or are restricted due to pandemic situations or other emerging cases may access the virtual experiments any time they need from all places. Virtual experiments are very effective in the learning process since application of certain scientific concepts is possible from places all over the the world.

- ***Accessibility*** for people those are not able to participate at classes because of health issues or incapacity (Heradio et al., 2016).
- ***Personal experience***

In VLs, experiments are performed individually or in small groups, similar to real-world labs.

- ***Better student safety***

Some experiments that are dangerous or difficult to perform in real laboratory are possible to be conducted in VLs. Using virtual experiments, disappear the deal with toxic or radioactive chemicals and other hazards and in this approach, laboratory accidents are totally avoided (Heradio et al., 2016; Chan et al., 2021).

- ***Flexibility in learning process***

Students can access VLs from different types of devices from any location whenever they want.

- ***Quick feed-back***

Due to rapid feed-back, students can repeat the experiments so many times as it is necessary to understand the scientific concepts.

- ***Better immersion***

Difficult to understand concepts are more easily presented in the VLs by using animations and simulations (Tüysüz, 2010); some processes that may unfold during a long period of time in real life may take minutes using simulations.

- ***Reduced economic and time costs***

VLs alleviate the space, time and cost constraints associated with traditional labs and are an effective teaching aid. Planning the experiments, the preparation of solutions used in the experimental protocols is time consuming and, in some cases, the lack of instrumentation or worse in the laboratory strongly limits the development of experiments (Tüysüz, 2010).

2. Cons of Using Virtual Labs

Beside advantages, there are some negative aspects associated with VLs.

- ***Difficult development of VLs***

Development of virtual experiments requires a multidisciplinary team made of subjects with different expertise areas, and the optimization of the resulted product is associated with the harmonization of the ideas provided by each team member, which in many cases is time consuming. Consequently, the design and implementation of a certain scientific concept into a virtual laboratory experiment is difficult, time consuming, suppose high costs but the advantage is that the end product it will be used by many students and if it is necessary, it may be updated easily.

- ***Reduced direct human interaction***

One of the main negative effects of VLs is that it reduces direct student-student as well as student-teacher interaction, given that most of the time, communication between them is done electronically.

- ***Student may behave like a viewer without implication, with lack of responsibility and seriousness*** (Potkonjak et al., 2016; Salmeron-Manzano & Manzano Agugliaro, 2018). Immediate feedback improves student engagement.
- ***Student insensitivity***

Student may become insensitive to failures and danger in certain real situations.

- ***Danger of excessive individualism of students and teamwork skills decrease*** (Salmeron-Manzano & Manzano Agugliaro, 2018).
- ***Limited sensory experience***

In a real laboratory, during experiments students may observe some unusual smells, noises that could influence their perception and contribute to scientific knowledge. Tactile experiences are completely missing.

IMPLEMENTED SOLUTIONS

1. Virtual simulation provided by different platforms

During academic year 2020-2021, as attempt to find a solution to the impossibility to attend physically to experimental activities associated with environmental disciplines it was used different virtual substitutions.

In Table 1 is presented an analysis of virtual simulations found on different platforms that are suitable to be aligned to environmental courses.

After evaluation of all found resources (Table 1) for environmental disciplines, precisely for course "Polluting sources, processes and products" most appropriate was found the "Labster Virtual Lab Experiments" because it offers virtual immersive laboratories, besides a complete set of teaching resources and allowed to enroll students.

Labster is a company dedicated to developing virtual laboratory simulations designed to stimulate students' natural curiosity and highlight the connection between science and the real world. Labster gave us the opportunity to explore virtually for a month without cost the desired experiments without problems of access and especially of danger.

Regarding students' opinion related to interactivity provided by Labster, they appreciated immersive nature, 3D reality and application. They found it to be a suitable substitute for experiments in the physical laboratory and considered that in a critical situation as COVID-19 created, this was the best manner to achieve educational goals.

Table 1. Simulations suitable for environmental sciences

No	Site name	Attributes and characteristics	Disciplines	Free/Subscription
1.	**Amrita Vishwa Vidyapeetham**	- suitable for students, high-school students, engineering scientists; - simulations-based experiments can be accessed remotely via internet; - each virtual lab is composed from sections: theory, procedure, self-evaluation, animation, assignment, reference, feed-back.	Electronics&Communications; Computer Science & Engineering; Electrical Engineering; Mechanical Engineering; Chemical Engineering; Biotechnology and Biomedical Engineering; Physical Sciences; Chemical Sciences.	- open access; - user must create a free account
	https://vlab.amrita.edu/index.php; https://www.vlab.co.in/			
2.	**eduMedia**	- interactive resources for learning science; - available in 8 languages; - suitable for teachers, students (elementary and secondary levels), libraries and individuals, publishers; - interactive simulations, quizzes and videos sorted by subject and by grade; - easy to access.	Life Sciences; Environment; Technology; Math; Physics; Astronomy; Chemistry.	- free of charge without registering; - subscription to secured access authorize projections in classroom/public.
	https://www.edumedia-sciences.com/en/			
3.	**Gizmos**	- interactive math and science lab simulations; - suitable for grades 3-12; - library with over 500 simulations where students can graph, measure and compare; - contain STEM* cases where students assume the role of scientist which must solve a situation.	Mathematics; Science	- 30 days free trial account with full access to all labs and simulations
	https://gizmos.explorelearning.com/			
4.	**HHMI BioInteractive**	- case studies, high quality videos, interactive media; - suitable for high school and undergraduate students; - available in English and Spanish.	Science	- free
	https://www.biointeractive.org/			

5.	**Labster**	- suitable for universities and high school; - interactive experiments, quizzes, supplemental resources (manuals, videos etc); - educators can track student performance from their gradebooks, and students can stay on top of their work; - easy to access by everyone; - easy to obtain support from Labster experts.	Analytical Chemistry, Anatomy & Physiology, Animal Physiology, Biochemistry, Biology, Biotechnology, Botany, Cellular and Molecular Biology; Chemistry; Civil Engineering & Material Science; Classical Mechanics; Demo; Developmental Biology; Earth and Space Science; Earth Science; Ecology; Electricity; Engineering; Environmental engineering; Evolution and Biodiversity; Forces and Motion; Foundation Concepts in Science; General Biology; General Chemistry; General Physics; General Science; Genetics; Inorganic Chemistry; Lab Safety; Microbiology; Modern Physics; Nutrition; Organic Chemistry; Oscillations; Pharmacology; Physics; Physiology; Universal Scientific Skills; Waves	- 30 days free trial full access; - institutional subscription (cost: $49 -$99).
	https://www.labster.com/			
6.	**LabXchange**	- free online platform for science education created at Harvard University with support from de Amgen Foundation; - available in 14 languages; - contains videos, simulations, case studies, question tests, textbooks.	Biological sciences; Health science; Physics; Chemistry: Science & Society; Mathematics	- free account
	https://www.labxchange.org			
7.	**Merlot**	- a database with animations, case studies, on-line courses, textbooks, presentations, quizzes, simulations; - suitable for all levels starting with pre-K up to professional.	Art; Business; Education; Mathematics and Statistics; Science and Technology	- free membership
	https://www.merlot.org/merlot/			
8.	**NMSU**	- eight modules that help students learn basic laboratory techniques and practice methods used by lab technicians and researchers in a variety of careers, using specific food science lab processes.	Science; Food Safety	- free
	https://virtuallabs.nmsu.edu/index.php			
9.	**NOVA Labs**	- a digital platform that engages teens and lifelong learners in games and interactives that foster authentic scientific exploration; - on the basis of an account, students will be able to track and save their progress, achieve goals in the games and interactives.	Science	- free
	https://www.pbs.org/wgbh/nova/labs/			

10.	**OLabs**	- a platform that hosts experiments for students from classes 9 to 12; - contain theory, procedures, animations, videos, simulations, self-evaluation, resources.	Physics; Chemistry; Biology; Maths; English	- free upon registration
	https://www.olabs.edu.in/			
11.	**PhET Interactive simulations**	- interactive simulations; - PhET sims are based on extensive education research and engage students through an intuitive, game-like environment where students learn through exploration and discovery; -PhET has received a lot of awards (https://phet.colorado.edu/en/about)	Physics; Chemistry; Math; Earth Sciences	- free and open source
	https://phet.colorado.edu/			
12.	**PNX Labs**	- virtual labs for companies and education institutions (college, university); - virtual labs are suitable to train students to operate complex industrial equipment; - virtual labs for STEM* education.	Physics; Chemistry; Biology; Materials Science; Engineering Mechanics; Manufacturing; Nanotechnology	- demos are for free
	https://pnxlabs.com/			
13.	**PraxiLabs**	- suitable for students and educators; - unlimited access to STEM* simulations; - highly interactive and immersive 3D simulations that mimic real-life labs.	Biology; Chemistry; Physics	- free account; - PraxiLabs free plan offers 20 fixed experiments in the fields of science; - in paid plans, the user can go through all the simulations portfolio available and select what he needs.
	https://praxilabs.com/en/virtual-labs			
14.	**The Concord Consortium - Molecular Workbench** -	- software for designing and conducting computational experiments across science; - visual, interactive simulations for teaching and learning science.	Physics; Chemistry; Biology; Biotechnology; Nanotechnology.	- free and open source
	http://mw.concord.org/modeler/			
15.	**The Concord Consortium – online resources**	- scientific accurate virtual labs; - based on STEM* education (merging science, technology, engineering, mathematics); - accessible from elementary level to higher education; - registration as a student; - registration as a teacher to access several key features (creating classes, assigning activities, saving work, tracking student progress); - easy to access.	Chemistry; Earth&Space; Engineering; Life Science; Mathematics; Physics	- free registration
	https://learn.concord.org/about			

***STEM** = Science, Technology, Engineering, and Mathematics.

2. Developing environmental engineering laboratory education: hybrid virtual lab for exercising practical skills

There are significant educational advantages that can be achieved when high quality virtual tools are fully integrated next to traditional laboratory sessions within curricula, each complementing and consolidating learning from the other. In engineering education, there are still many areas waiting to be digitized and to

offer hybrid interactions with users in meaningful manners.

Therefore, transferring traditional labs to the hybrid of real and virtual forms are urgent and timely, particularly in the current situation of post-pandemic recovery.

In order to develop digital competences and surpass the similar crisis situations as pandemic, in 2022 USAMV of Bucharest financed project Hybrid lab of Environmental Engineering for practical skills (HybridPraxisLab) which will be implemented by our team and which consists in creating virtual laboratory (environmental sciences) with experiments that can be mapped successfully with environmental disciplines.

The main aim of the project is to facilitate and improve laboratory education by implementing new technical and pedagogical models of laboratory conduct through the development of a new model of virtual access laboratory.

The project is intended to cover mainly but not only the thematic area of the course "Pollutant Sources, Processes and Products" and covers 28 hours of practical lessons in which students develop experiments to apply the theoretical concepts acquired during the course. Experiments developed on the HybridPraxisLab will be used in these lab hours during the second semester of the academic course 2022/2023.

With the help of simulations from the virtual laboratory HybridPraxisLab, students will:

- work with real-life case studies;
- use laboratory equipment;
- conduct experiments;
- understand and deepen different scientific concepts with the help of experiments.

HybridPraxisLab will be an interactive, immersive learning environment designed to prepare students for real-life experiments, supplement and complement the practical experience by “teleporting” the physical “Environmental Engineering Laboratory” into the virtual environment. Students will practice and become confident in handling equipment before entering the real lab. It is very important for relating theory to practice, so that the students can develop engineering judgment and understand how process behavior can be captured using mathematical models and interesting graphical user interfaces.

The specific objectives of the project are to:

- **develop** graduates prepared for the demands of the future by experiencing a real working environment through virtual training;
- **delivery** of a complete learning management system around the virtual lab where students can use the various tools for learning, including additional web resources, lab manual, step-by-step procedures, animated demonstrations and self-assessment;
- **increase** student engagement in learning practical techniques and understanding of key concepts through a blended approach that complements real, face-to-face lab experiences with virtual lab experiences;
- **determine** the impact of integrating components of the hybrid approach on students' learning experience using educational research methods and modern pedagogical theories.

Water quality testing is the module developed for now from HybridPraxisLab.

Learning outcomes include:

- **gaining** knowledge of the parameters used to determine water quality;
- **mastering** laboratory methods;
- **acquiring** specific water quality testing skills;
- **acquisition of** practical experience in collecting and analysing water samples;
- **understanding** how human activities affect
- **water quality and watersheds**.

A representation of the virtual lab interface is shown in the Figure 1.

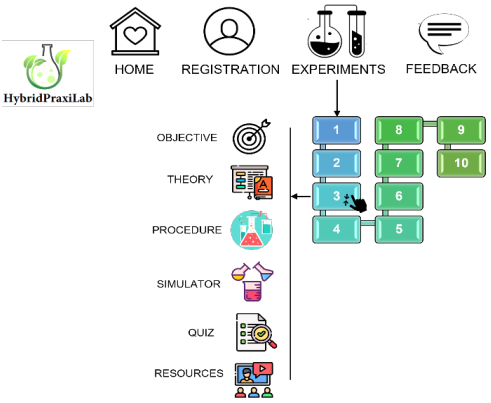

Figure 1. Virtual lab interface

Access to HybridPraxisLab is free for students upon registration with email and password.

The protocol that a student may follow to access any of the ten **Experiments** is presented below:

- student has to choose from a number of topics related to laboratory practice;
- the aim and significance of experiment is found in **Objective** section;
- the experiment description and theoretical aspects are depicted in **Theory**;
- the experimental part is detailed step-by-step in **Procedure** section;
- the simulation of the chosen experiment is found in **Simulator** area;
- evaluation of the acquired information after simulation into virtual laboratory is achieved using an assessment test from **Quiz** section;
- supplemental information (lists of books, videos, links) are found in the **Bibliographic resources** area (Figure 1, Figure 2).

The experiments that are virtualized into HybridPraxisLab laboratory are:

1. Lab safety virtual lab.
2. Protocol for sampling and transport of water samples.
3. Pipetting: selecting and using micropipettes virtual lab.
4. Acids and bases.
5. Determination of pH for different water samples.
6. Preparation of solution: from salt to solution.
7. Determination of turbidity for different water samples.
8. Determination of chlorides in different water samples.
9. Determination of dissolved oxygen in water.
10. Mass spectrometry virtual lab: exploring the instrument.

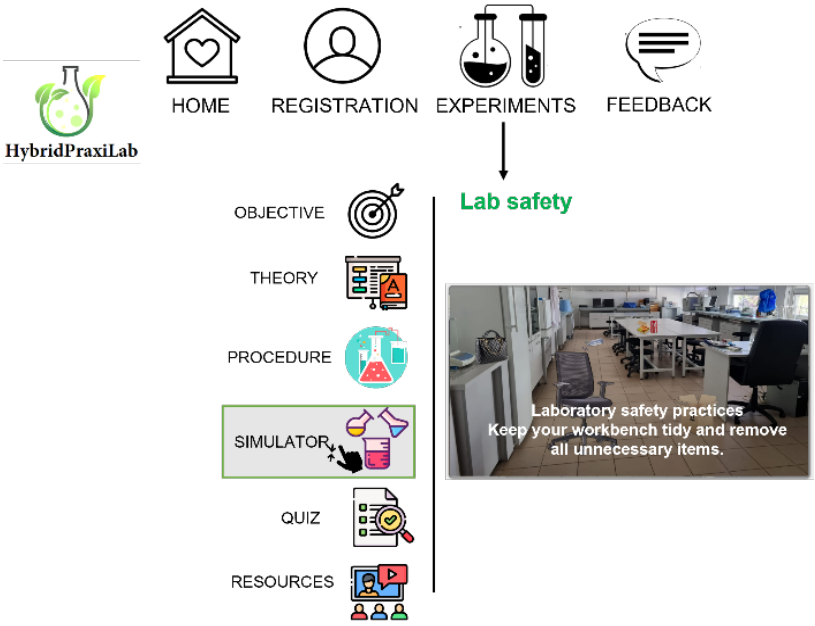

Figure 2. Laboratory safety simulation

The potential benefits of the virtual experiments from HybridPraxisLab are:

- improved understanding, knowledge retention and transfer of learning through visualization;
- active learning using interaction;
- continuous testing of learning outcomes;
- delivery of continuous feedback;
- providing self-paced instruction;
- provide feedback to the instructor on concepts that are not well understood so that remedial action can be taken;
- integrating basic concepts with virtual labs.

The efficacy of the virtual experiments from HybridPraxisLab and feed-back from students will be evaluated after second semester of the academic year 2022/2023 on the basis of questionnaires/surveys and considering the

obtained results at exams, this information being disseminated in a future paper.

CONCLUSIONS

The "digital impulse" of the educational area was facilitated by the COVID-19 pandemic and it is an action now considered unstoppable. Having in view the unexpected and until now, unique situation created by COVID-19 it is mandatory for all educational staff to find new solutions to provide education on all circumstances (quarantine, extreme climatic conditions etc).

Today's students are "the digital generation" and nowadays, the request for engineers with employability skills and digital competences has increased. Using VLs gives students the chance to develop critical, innovative thinking, digital enrichment, teamwork, communication and key employability skills, all of which are highly valued in today's job market.

After pandemic period, everyone has understood that VLs are a part of the future in learning and it will used as a supplement to hand-on laboratories and traditional teaching manner. Universities has realized that distance is not a problem to continue the educational process and not only in special situations and emergencies.

It has been accepted that online education is here to stay and the implementation of VLs into education is a fact that provide its evolution. HybridPraxisLab, a virtual lab created as a necessity to overcome the critical situations, will be easy to use and can be accessed by students and teachers 24/7, 365 days a year, removing all geographical, mobility and time barriers. It will provide a more efficient learning experience for students and make more resources and technology available. Therefore, students can improve their STEM education skills in a safe virtual lab, no matter where they are.

ACKNOWLEDGEMENTS

This research work was carried out with the support of University of Agronomic Sciences and Veterinary Medicine of Bucharest – Romania, Research Project 1059/15.06.2022, acronym HybridPraxisLab in the competition IPC 2022.

REFERENCES

Achuthan, K., Francis, S.P., & Diwakar, S. (2017). Augmented reflective learning and knowledge retention perceived among students in classrooms involving virtual laboratories. *Education and Information Technologies, 22*(6), 2825–2855.

Breakey, K.M., Levin, D., Miller, I. & Hentges, K.E. (2008). The use of scenario-based-learning interactive software to create custom virtual laboratory scenarios for teaching genetics. *Genetics, 179*(3), 1151–1155.

Chan, P., Van Gerven, T., Dubois, J.-L. & Bernaerts, K. (2021). Virtual chemical laboratories: a systematic literature review of research, technologies and instructional design. *Computers and Education Open, 2*, 100053, https://doi.org/10.1016/j.caeo.2021.100053.

Craifaleanu, A. & Craifaleanu, I.G. (2022). A co-creation experiment for virtual laboratories of mechanics in engineering education. *Computer Applications in Engineering Education*, *30*(4), 991-1008.

Craifaleanu, A., Dragomirescu, C. & Craifaleanu, I.G. (2014). Virtual laboratory of dynamics. *EDULEARN14 Proceedings*, 4612-4619.

Cucinotta, D. & Vanelli, M. (2020). WHO declares COVID-19 a pandemic. *Acta Biomedica, 91*(1), 157-160.

De Witt, P. (2020). 6 reasons students aren't showing up for virtual learning. Education Week. Available at: https://www.edweek.org/leadership/opinion-6-reasons-students-arent-showing-up-for-virtual-learning/2020/04. [Accessed: 18.02.2023].

Hawkins, I. & Phelps, A. (2013). Virtual laboratory vs. traditional laboratory: which is more effective for teaching electrochemistry? *Chemistry Education Research and Practice*, *14*, 516-523.

Heradio, R., de la Torre, L., Galan, D., Cabrerizo, F.J., Herrera-Viedma, E. & Dormido, S. (2016). Virtual and remote labs in education: a bibliometric analysis. *Computers&Education, 98*, 14-38.

Herga, N.R. & Dinevski, D. (2012). Virtual laboratory in chemistry – experimental study of understanding, reproduction and application of acquired knowledge of subject's chemical content. *Organizacija, 45*(3), 108-116.

Hodges, C., Moore, S., Lockee, B., Trust, T. & Bond, A. (2020). The difference between emergency remote teaching and online learning. Available at: https://er.educause.edu/articles/2020/3/the-difference-between-emergency-remote-teaching-and-online-learning. [Accessed: 18.02.2023].

Kee, T. & Zhang, H. (2022). Digital Experiential Learning for Sustainable Horticulture and Landscape Management Education. *Sustainability*, 14, 9116. https://doi.org/10.3390/su14159116

Marusteri, M., Bacarea. V. & Brinzaniuc, K. (2019). Next generation 3D virtual human anatomy laboratory, using off-the-shelf hardware and software. *Applied Medical Informatics, 41*(1), 4.

Merrill, S. (2020). Teaching through a pandemic: A mindset for this moment. Edutopia. Available at:

https://www.edutopia.org/article/teaching-through-pandemic-mindset-moment. [Accessed: 18.02.2023].

Mikropoulos, T. & Natsis, A. (2011). Educational virtual environments: a ten-year review of empirical research (1999-2009). *Computers & Education, 56*, 769-780.

Nais, M.K., Sugiyarto, K.H. & Ikhsan, J. (2019). Virtual chemistry laboratory (virtual chem-lab): potential experimental media in hybrid learning. *Journal of Physics: Conference Series*, 1156, 012028, doi:10.1088/1742-6596/1156/1/012028

Nedelcu, M. & Saru, D. (2003). Multipurpose virtual laboratory for long distance learning. *Romanian Journal of Information Technology and Automatic Control*, 13(1), 18-27.

Popescu, G. (2015). Virtual laboratory for marine structures. *Annals of "Dunărea de Jos" University of Galati, Fascicle XI - Shipbuilding*, 183-188.

Potkonjak, V., Gardner, M., Callaghan, V., Mattila, P., Guetl, C., Petrovic, V. & Jovanovic, K. (2016). Virtual laboratories for education in science, technology and engineering: a review. *Computers & Education, 95*, 309-327.

Radhamani, R., Kumar, D., Nizar, N., Achuthan, K., Nair, B. & Diwakar, S. (2021). What virtual laboratory usage tells us about laboratory skill education pre- and post-COVID-19: Focus on usage, behavior, intention and adoption. *Education and Information Technologies*, *26*(6), 7477-7495.

Raman, R., Sairam, B., Veena, G., Vachharajani, H., & Nedungadi, P. (2021a). Adoption of online proctored examinations by university students during COVID-19: Innovation difusion study. *Education and Information Technologies*, *26*(6), 1–20.

Raman, R., Vinuesa, R. & Nedungadi, P. (2021b). Acquisition and user behavior in online science laboratories before and during the COVID-19 pandemic. *Multimodal Technologies and Interaction, 5*(8), 46.

Raman, R., Vinuesa, R. & Nedungadi, P. (2021c). Bibliometric analysis of SARS, MERS, and COVID-19 studies from India and connection to sustainable development goals. *Sustainability, 13*(14), 7555.

Ratamun, M.M. & Osman, K. (2018). The effectiveness of virtual lab compared to physical lab in the mastery of science proves skills for chemistry experiment. *Problems of Education in the 21th Century*, *76*(4), 544-560.

Salmeron-Manzano, E. & Manzano-Agugliaro, F. (2018). The higher education sustainability through virtual laboratories: the Spanish university as case of study. *Sustainability, 10*, 4040, doi:10.3390/su10114040.

Schneider, J., Felkai, C. & Munro, I. (2022). A Comparison of Real and Virtual Laboratories for Pharmacy Teaching. *Pharmacy*, *10*, 133. https://doi.org/10.3390/pharmacy10050133.

Tatli, Z. & Ayas, A. (2010). Virtual laboratory applications in chemistry education. *Procedia Social and Behavioral Sciences, 9*, 938-942.

Toma, R.C., Diguță, C.F., Boiu-Sicuia, O.A., Frîncu, M. & Cornea, C. P. (2022). Digital application for remote control of bacterial endophytes growth in bioreactor via INTERNET as a design solution to a virtual laboratory. *Scientific Papers. Series E. Land Reclamation, Earth Observation & Surveying, Environmental Engineering,* XI, 517-524.

Trifan, D. (2011). Using virtual laboratories in teaching of agricultural sciences. *The 7th International Scientific Conferences e-Learning and Software Education*, Bucharest, April 28-29.

Tüysüz, C. (2010). The effect of the virtual laboratory on students' achievement and attitude in chemistry. *International Online Journal of Educational Sciences, 2*(1), 37-53.

Usman, M. & Huda, K. (2021). Virtual lab as distance learning media to enhance student's science process skill during the COVID-19 pandemic. *Journal of Physics: Conference Series, 1882*, 012126. doi:0.1088/1742-6596/1882/1/012126.

Vary, J. (2000). Report of the expert meeting on virtual laboratories organized by the International Institute of Theoretical and Applied Physics (IITAP) Ames, Iowa, 10-12 May 1999.

Vasiliadou, R. (2020). Virtual laboratories during coronavirus (COVID-19) pandemic. *Biochemistry and Molecular Biology Education, 48*, 482-483.

Vergara, D., Fernandez-Arias, P., Extremera, J., Davila, L. & Rubio, M. (2022). Educational trends post COVID-19 in engineering: virtual laboratories. *Materials Today: Proceedings, 49*, 155-160.

Scientific Papers. Series E. Land Reclamation, Earth Observation & Surveying, Environmental Engineering. Vol. XII, 2023
Print ISSN 2285-6064, CD-ROM ISSN 2285-6072, Online ISSN 2393-5138, ISSN-L 2285-6064

COMPARISON STUDY BETWEEN A CONCRETE FRAME STRUCTURE AND A MASONRY STRUCTURE FOR A FIVE-STOREY BUILDING

Mircea Răzvan MEREA, Simon Alexandru PESCARI, Valeriu-Augustin STOIAN, Clara-Beatrice VÎLCEANU

Politehnica University Timisoara, 2 Piata Victoriei Street, Timisoara, Romania

Corresponding author email: mircea.merea@student.upt.ro

Abstract

The current study focuses on the structure cost and the energy efficiency for a five-storey building located in Timisoara, Romania. A cost comparison and the energy demand between two types of structures was concluded, namely a concrete structure and a masonry structure. The study focuses only on the building's structure because the building's finishes and the installation are the same for both cases. Regarding the energy efficiency, the difference appears for the exterior walls, in the first case, for the concrete structure building the walls are realized with autoclaved cellular concrete (ACC) and in the second case for the masonry structure the exterior walls are realized with brick masonry. The walls insulation is the same in both cases.

Key words: *cost comparison, frame structure, masonry structure.*

INTRODUCTION

The current study focuses on the decision factors when choosing a structural solution for a building. The analyzed building has five floors, which is the maxim number of floors for a masonry structure building in Romania, according to the National Normative. The two factors are the economic factor and the energy efficiency factor, which are combined in a life cycle cost analysis.

There are two structural cases chosen for this study, the first one, using reinforced concrete frames, and the second one using a masonry structure. In the case when the structure is realized using reinforced concrete, the design is made using beams and columns. A more cost-efficient design would be using flat slabs and columns, but considering the irregularity of the building this solution is not considered because of the seismic instability (Sahab et al., 2005). In the case when the structure is realized with masonry, a cost-reduction solution for the building, would be the reduction of the wall thickness, but this would reduce the shear strength of the building, and in terms of efficiency this would not be beneficial (Min Jiang, 2020).

The concrete class used in both cases of the study is C25. A higher class would increase significant the building cost, and the reduction of the element would be subtle (Khan I.K. & Abbas H., 2011).

In each case, the structural conformation is attentively designed, so that the building does not collapse, in the first case, and secondly, in case of a seismic impact, the damages should be subtle. The cost would be overwhelming if the building suffers a big damage (Roque et al., 2021).

In terms of sustainability, a more suitable material would be timber. But in Romania, because of the high deforestation and the low level of regenerating the forests, this solution is not suitable (Ahmed Shafayet & Arocho Ingrid, 2021).

Regarding energy efficiency, the major difference between the chosen solutions, is the material used for the exterior walls. In the first case the walls are realized of autoclaved cellular concrete (ACC) and in the second case the walls are realized using bricks with gaps. Considering the two types of exterior walls used, even though the ACC has a higher thermal resistance than bricks with gaps, the masonry walls with bricks have a higher

thermal inertia, that offers a better interior comfort (Uroš, M. et al., 2023).
The life cycle cost analysis consists of the initial investment, the future cost for a chosen period. The actualization factor and the waste value at the end of the analyzed period. The initial investment deducted, may differ to the real cost of the building with 2-4%, as shown in a study. This difference is due to the loss of concrete during the implementation phase, which may be even higher depending on the experience of the builder (Kanit Recep et al., 2007). The cost is affected by factors like the construction level, the coordination ability between different type of work, the preparation rate and assembly rate (Linkevicius, E. et al., 2023).
An important role in the life cycle cost analysis is assigned to the location of the building, pricing may vary depending on the location. All the financial parameters may differ, including material price, manufacturer price and energy price (Samani P. et al., 2015).
The LCC analysis is suitable for every investment to determine the profitability of the project. The cost-effectiveness is an important matter, especially nowadays in a crisis period, and a small reduction counts even more for a large surface building (Mwafy A. et al., 2015).

MATERIALS AND METHODS

The analyzed building is in the design phase now, and it will be in the city of Timisoara, Romania. The building developer wants to get the best cost-efficiency for the building, so a study is required. The building has five floors, and it is a collective building with 20 apartments, and it has no basement.
There are two solutions considered. The first one is by using reinforced concrete frames for the structure, and the walls are realized with autoclaved cellular concrete (ACC). The second solution is chosen to be with masonry walls for the structure, and the walls are realized using bricks with gaps. The building is designed in both cases using the Romanian normative, especially the normative for building design in seismic zones, P100-1/2013.
The comparison between the two solutions follows the life cycle cost of the building. For realizing the life cycle cost analysis, it is required the cost of the building, but it is considered only the cost of the structure, the cost for the rest of the building is not considered, because it is the same for both cases, regarding the thermal insulation, the finish, and installations. Another element required for the life cycle cost analysis is the energy cost for the building.
The building cost is realized using the prices on the current market, and by using medium quality materials, used in most cases.
The energy cost for the building is determined using the current prices for the used energy (gas, electricity) and multiplying it with the energy demand deduced using the energetic stationary method. For this study a local program is used.
The life cycle cost is determined by using an excel program developed by the research team, that considers, the initial cost, the annual cost, the actualization factor and the waste value at the end of the analysis period.

Structural solutions

In the first case when using reinforced concrete frames, the main elements are the beams and the columns. The beams have the cross-section dimension 30x60 cm, and there are two types of columns, one with the cross-section dimension 40x40 cm, and the other one with variable cross-section, having the dimension 50x50 cm at the ground floor, and the dimension for the rest of the floors is 40 x 40 cm (Figure 1).

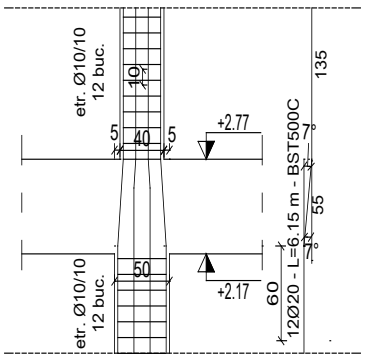

Figure 1. Vertical section of the beam with variable dimensions

The foundation of the building is realised using isolated foundations for each column, and

coupling beams, elements that stiffen the foundation.

The roof for both cases is realised using wooden frames.

In the second case when using masonry walls for the structure, the thickness of the walls remains the same as in the first case, the difference is the material used, instead of ACC it is used bricks with gaps. Instead of the beams used in the first case, there are used smaller beams on each wall that have only 25 cm heigh. (Figure 2). Instead of the columns used in the first case, there are used smaller columns at the intersection of the walls (Figure 3). The beams and columns used in the second case have only the role to link the walls to each other, and not structural role.

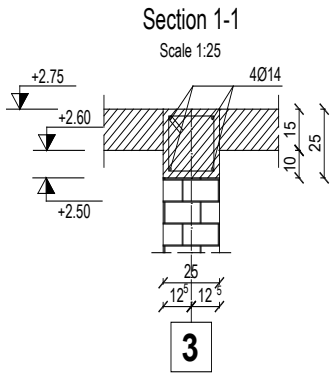

Figure 2. Beam on top of the wall

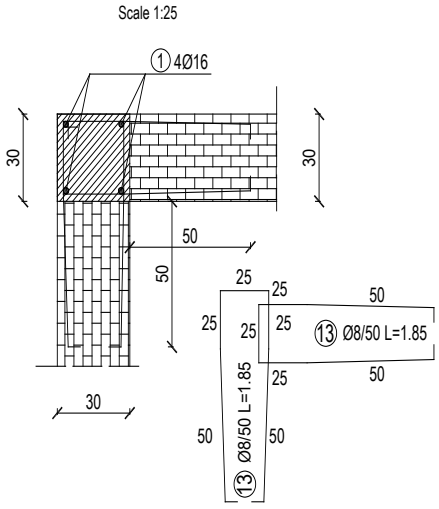

Figure 3. Columns at the intersection of the walls

RESULTS AND DISCUSSIONS

Building cost

The building cost is the initial cost for the life cycle cost analysis, but it is taken into consideration only the cost for the structure of the building, without finish and installation. This choice is because, the only difference when calculating the cost, is the type of structure. The total cost consists of the material price, the workforce, and the transportation. Also, VAT is included in the sum, and it is 19% for Romania. Table 1 displays the results for the total structure cost in the two considered cases.

Table 1. The cost differences between the two cases

Case	Total cost (including V.A.T) [euro]	Price / built square meter [euro/sqm]	Price / useful square meter [euro/sqm]
I	484448.36	347	384.21
II	450854.43	322.93	357.57

As shown, the initial cost is 7% higher for the first case, when the structure is realised with reinforced concrete frames. The difference may not be significant, but it can be a decision-making factor when choosing the solution. The surface is the same for both cases, so an important element when comparing the two solutions is the price per square meter, which is a very important indicator when developing a high surface building.

Energy demand

The building envelope differs only for the exterior walls. For this element the different layer is the masonry, which in the first case consist of ACC and in the second case consists of bricks with gaps. The thermal conductivity for ACC is 0.1 W/mK and for bricks with gaps it is 0.207 W/mK. The lower the thermal conductivity is, the higher is the value of the thermal resistance. The thermal insulation for the exterior wall is the same in both cases, and it consist of 10 cm of expanded polystyrene. The thermal insulation of the slab under the roof is insulated using 15 cm of mineral wool and the ground slab is insulated using 10 cm of extruded polystyrene. The installation is the same for both cases. The heating is realised using local heating units that use gas as fuel,

the same system being used for domestic hot water preparation. The cooling is not considered, and the ventilation is done naturally.
Internal gains are considered, from the building's residents. The building is occupied 24 hours per day. The stationary method considers a constant occupancy for the specified period. The energy demand is determined using the stationary energetic method, using the monthly method, according to the Romanian Methodology Mc 001-2006.
The envelope area of each element is presented in Table 2. The exterior walls represent over 50% of the building's envelope, so it has a high intake.

Table 2. Envelope elements surface

Element	Surface	Unit
Ground slab	252.4	m²
Slab under roof	252.4	m²
North wall	139.42	m²
West wall	226.47	m²
East wall	224.77	m²
South wall	139.42	m²
North window/door	19.66	m²
West window/door	66.01	m²
East window/door	67.71	m²
South Window/wall	19.66	m²
Volume	2895.03	m³

The data described is used for obtaining the energy demand for heating, domestic hot water, lightning, and the total energy consumption. The data obtained for the two cases is shown in Table 3.
The consumption of domestic hot water and lightning remain the same in both cases because the envelope affects only the heating consumption.

Table 3. Energy demand

	Case I	Case II	Measuring unit
Heating	80,6	81,5	kWh/m²year
Domestic hot water	28,8	28,8	kWh/m²year
Lightning	2,6	2,6	kWh/m²year
Total energy consumption	112,0	112,9	kWh/m²year

Life cycle cost

Life cycle cost is an economical method used to determine the cost efficiency of an investment. The method is useful for higher investments.
The global cost for the analysed period contains data regarding the initial investment cost, the maintenance cost, the actualisation factor, and the waste value of the investment at the end of the analysed period. The maintenance cost contains the energy prices, consisting of natural gas and electricity. The prices considered were 0.067 Euro/Kw for natural gas and 0.16 Euro/kW for electricity, being the current energy prices in Romania.
For realising the calculus, and excel program was used developed by the research team. The results are presented in Figure 4 and show the investment cost over the chosen period, which in this case was chosen to be 20 years, even if the period for a radical rehabilitation is higher. The period was chosen considering the building as an investment.
The life cycle cost chart is presented in Figure 4. The chart shows that when using the case 1 structure, with a higher initial cost, the investment is not recovered in a 20-year period. This situation is because the difference between the energy consumptions is insignificant and using AAC walls does not bring such a big benefit.

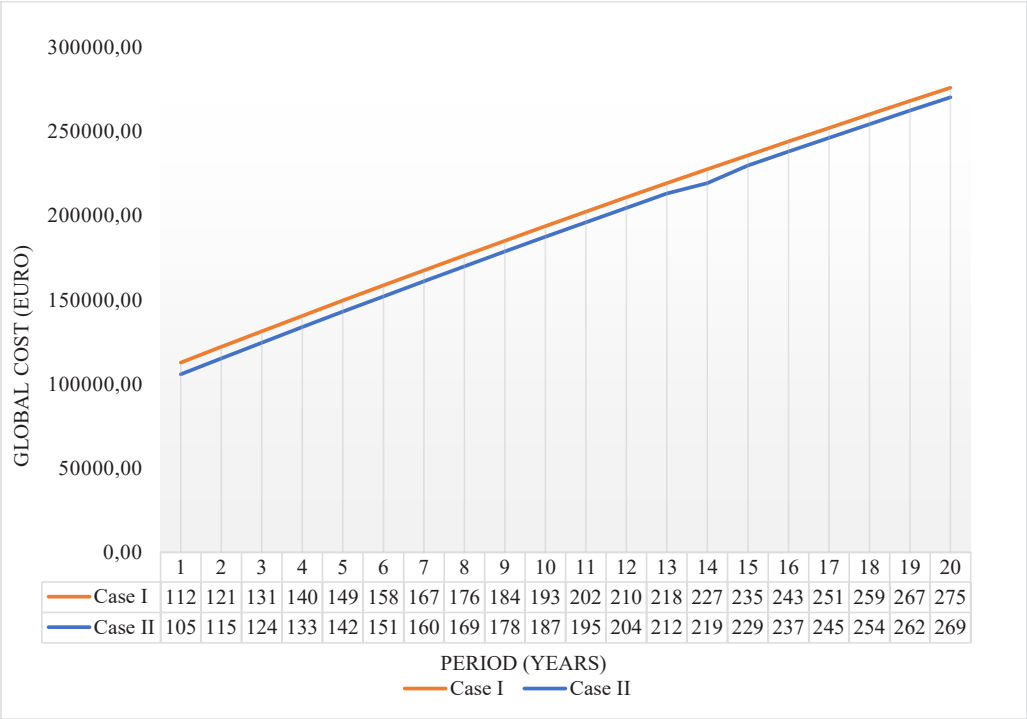

	1	2	3	4	5	6	7	8	9	10	11	12	13	14	15	16	17	18	19	20
Case I	112	121	131	140	149	158	167	176	184	193	202	210	218	227	235	243	251	259	267	275
Case II	105	115	124	133	142	151	160	169	178	187	195	204	212	219	229	237	245	254	262	269

Figure 4. Life cycle cost analysis

CONCLUSIONS

Considering the price increases in all sectors, the spendings should be reduced for every investment.

The life cycle cost presents a viable tool for determining which investment is useful and profitable.

The study presents a cost comparison between two structural solutions for a residential building, the first one is by using reinforced concrete frames for the structure, and the walls are realized with autoclaved cellular concrete (ACC) and the second solution is by using masonry walls for the structure, and the walls are realized using bricks with gaps.

The study shows that when choosing a reinforced concrete frame structure, the cost is significantly higher that a masonry wall structure and the investment does not pay off after a 20-year period.

The study is realized for a four-floor building, which is the maximum number of floors for the chosen zone in Romania, according to the national Normative.

When designing a higher building, in Timisoara, a reinforced concrete structure is necessary.

ACKNOWLEDGEMENTS

This research did not receive any specific grant from funding agencies in the public, commercial, or not-for-profit sectors.

REFERENCES

Ahmed, S., Arocho, I. (2021). Analysis of cost comparison and effects of change orders during construction: Study of a mass timber and a concrete building project. *Journal of Building Engineering, 33.* 101856.

Kanit, R., Ozkan, O., Gunduz, M. (2007). Cost assessment of concrete and steel types for office buildings: An exploratory study. *Building and Environment, 42*(9). 3404–3409.

Khan I.K., Abbas H. (2011). Static and dynamic response of cost-effective unreinforced brick masonry buildings. doi: 10.1016/s1644-9665(12)60087-9.

Linkevicius, E., Žemaitis, P., Aleinikovas, M. (2023). Sustainability Impacts of Wood- and Concrete-Based Frame Buildings. *Sustainability, 15.* 1560. https://doi.org/10.3390/su15021560.

Min Jiang. Building cost control of assembly construction project using analytic hierarchy process. (2020). 5th International Conference on Smart Grid and Electrical Automation (ICSGEA)

Mwafy A., Hussain N., El-Sawy K. (2015). Seismic performance and cost-effectiveness of high-rise buildings with increasing concrete strength. 2015-03-04. doi: 10.1002/tal.1165.

Roque, E., Vicente, R., Almeida, Ricardo M.S.F., Ferreira, Victor M. (2021). Energy Romeu consumption in intermittently heated residential buildings: Light Steel Framing vs hollow brick masonry constructive system. *Journal of Building Engineering,* 43, 103024.

Sahab M.G., Ashour A.F., Toropov V.V. (2005). Cost optimisation of reinforced concrete flat slab buildings. *Engineering Structures, 27.* 313–322.

Samani P., Gregory J., Leal V., Mendes A., Correia N. (2018). Lifecycle cost analysis of prefabricated composite and masonry buildings: Comparative study. 2018-12-28. doi: 10.1061/(ASCE)AE.1943-5568.0000288.

Uroš, M.; Demšic, M., Banicek, M., Pilipovic, A. (2023). Seismic Retrofitting of Dual Structural Systems-A Case Study of an Educational Building in Croatia. *Buildings, 13.* 292. https://doi.org/10.3390/buildings13020292

Scientific Papers. Series E. Land Reclamation, Earth Observation & Surveying, Environmental Engineering. Vol. XII, 2023
Print ISSN 2285-6064, CD-ROM ISSN 2285-6072, Online ISSN 2393-5138, ISSN-L 2285-6064

COMPARISON STUDY BETWEEN A PITCHED ROOF AND A FLAT ROOF FOR A 2-STOREY HOUSE

Alexandru Florin PITROACA, Simon Alexandru PESCARI, Valeriu-Augustin STOIAN, Clara-Beatrice VÎLCEANU

Politehnica University Timisoara, 2 Piata Victoriei Street, Timisoara, Romania

Corresponding author email: alexandru.pitroaca@upt.ro

Abstract

The purpose of this study is to see the differences between the investment costs and the energy efficiency for two types of roofs for a 2-storey house located in Timisoara, Romania. The paper contains a comparison of the costs and energy demand between a pitched roof and a flat roof. The energy demand will be calculated using the stationary method with a modeling program. The study focuses only on the effects of choosing between the two types of buildings roofs, so the dimensions of buildings, characteristics of the buildings envelope (exterior walls, windows and doors, ground floor slab) and the installation systems remain the same.

Key words*: energy efficiency, pitched, flat, roof.*

INTRODUCTION

The building sector energy consumption is in a continuous increase (Loukaidou et al., 2017). Buildings are responsible for about 40% of global energy use and for 36% of greenhouse gas emissions in the EU and from the total amount of energy involved in buildings, a total of 60% is used for heating and cooling them (Qiong et al., 2019; Maduta et al., 2022; Pescari et al., 2022).

In this context, there is a need to decrease the energy consumption of buildings, according to actual Regulations (Zhang et al., 2022).

One of the main elements of a building in terms of energy consumption, is the building envelope (Zhang et al., 2022). The building envelope is defined as the totality of the surfaces of the perimeter construction elements, which delimit the interior (heated) volume of a building, from the outside environment or unheated spaces outside the building.

Considering the roles of envelope, the proper design and selection of materials are an efficient way to reduce the thermal transfer between a building and the environment (Kaynakli, 2012; Stachera et al., 2022).

The buildings roofs are an important element of envelope in energy efficiency because thru them a significant amount of heat is lost and a significant amount of solar radiation is absorbed (Abuseif, 2018).

In this context, the paper presents a study between two types of roofs for a two-storey house located in Timișoara, Romania. The purpose of this paper is to highlight if there is an important difference in terms of energy reduction between two types of buildings roofs.

MATERIALS AND METHODS

It is proposed to conduct a case study on a residential building. The analysed building is a single-family house with two apartments, located in the municipality of Timișoara, having a height regime of Gf+1F (Figures 1 and 2). It was started to be built in august 2022, the resistance structure being made of masonry walls. The building is moderately sheltered and has more than one exposed façade.

The study involves the calculation of the energy required for heating the house using, in turn, the two types of roofs. The calculation of the energy required for heating was performed using the monthly calculation method with steady state.

The steady state is a conventional thermotechnical calculation hypothesis, within which assume that temperatures do not vary with time. The building was examined in climate zone II using a steady state simulation software.

The study also presents the differences between the investment costs of the house with both type of roofs. The construction costs of the house are real, not estimated, because the house is already in construction and the roof is realised in the "flat roof" manner.

The study focuses only on the effects of choosing between the two types of roofs, so the dimensions of buildings, characteristics of the buildings envelope and the installation systems remain the same. The envelope elements were designed so that the thermal transmittance fulfils the minimum requirements of the Romanian Regulations (Charisi, 2017).

As already stated, the analysed building is a two-storey residential house with the resistance structure made of masonry walls. Heating is realized by means of two local thermal plants that use natural gas as fuel.

The ground floor is almost identical for both apartments and consists of an access hall, living + dining room, a corridor to access the bathroom, a kitchen with pantry, the stairs to access the first floor and an outside terrace.

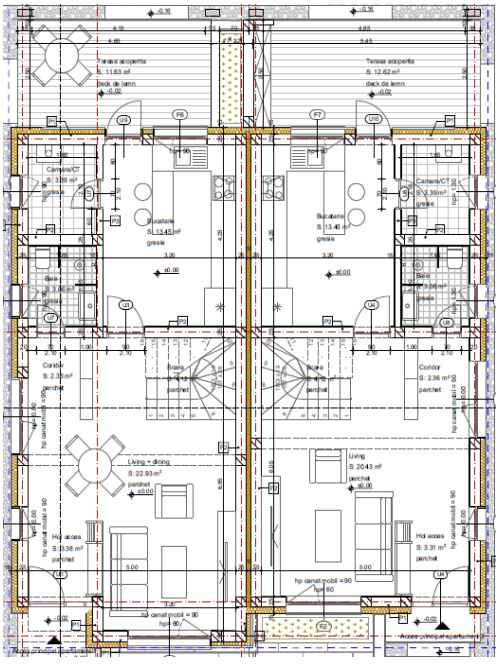

Figure 1. Ground floor

The first floor is also identical for both apartments and consists of 2 bedrooms with 2 dressings, a hall and a bathroom.

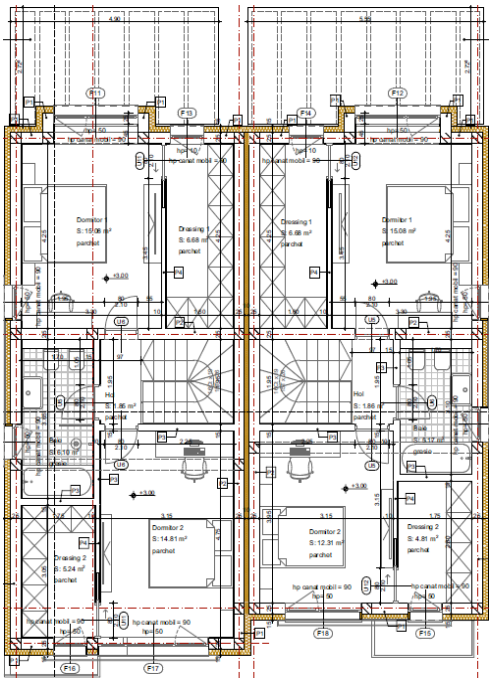

Figure 2. First floor

In order to realize the energy simulation, the two types of roofs need to be defined.

The first one is the flat roof (Figure 3). This type of roof has started to be used quite often in recent years in Romania because it offers the house a modern look. The component layers of this type of roof are (in order from inside to outside as well as heat transfer is realised):

- washable paint;
- lime-based plaster 1 cm;
- reinforced concrete floor 13 cm;
- bituminous vapor barrier with integrated diffusion layer;
- expanded polystyrene - EPS 120 20 cm;
- separating film - polyethylene film;
- slope extruded polystyrene 0.5-1.8% EPS 120 min. 3 cm;
- polymeric membrane for ballasted roof waterproofing;
- separation layer, geotextile, 200 g/m^2;
- protective layer - gravel 8-16 mm, min. 8 cm.

Even if it has an impact on the thermal transmittance, the slope extruded polystyrene it is not used as a thermal insulation, its purpose is technological, to achieve the necessary slope.

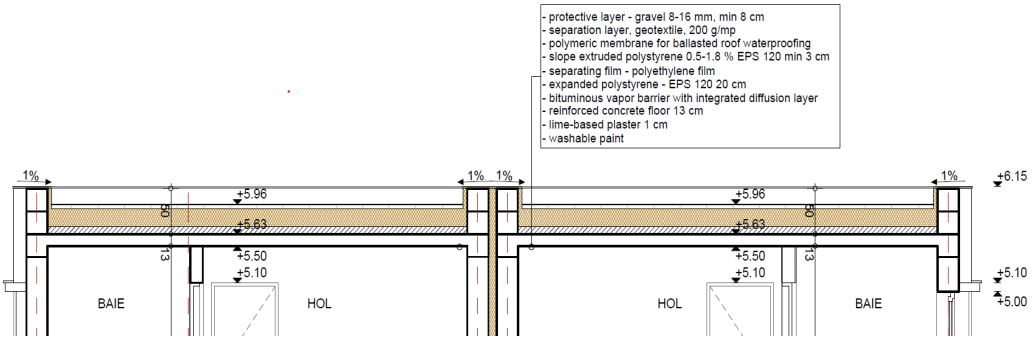

Figure 3. Section from flat roof

The second one is the pitched roof (Figure 4). This type of roof is the classic one and was used to build houses for centuries. The component layers of this type of roof are (in order from inside to outside as well as heat transfer is realised):

- rafters 10 x 15 cm;
- wooden board 2.5 cm;
- anti-condensation foil;
- longitudinal bar 3 x 5 cm;
- transverse bar 3 x 5 cm;
- ceramic tile.

Even if this are the components of the pitched roof, when the energy simulation is realized, we will consider the floor above the last level with its component layers (in order from inside to outside as well as heat transfer is realised):

- washable paint;
- lime-based plaster 1 cm;
- reinforced concrete floor 13 cm;
- polystyrene 20 cm.

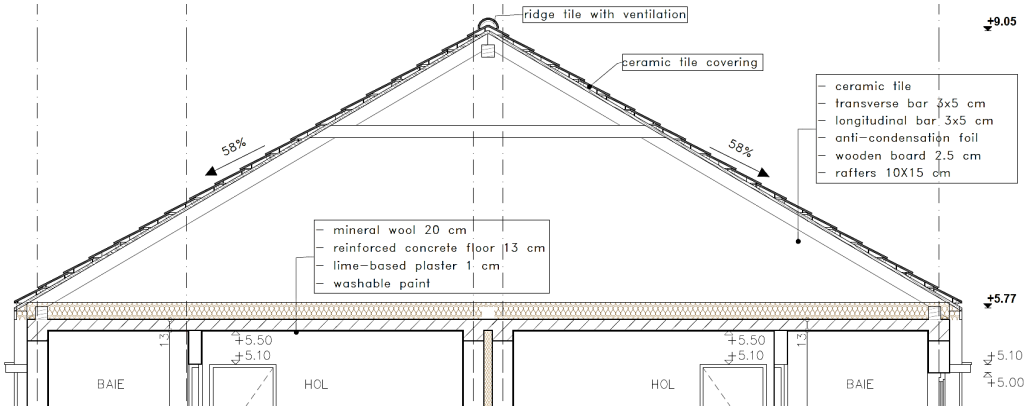

Figure 4. Section from pitched roof

RESULTS AND DISCUSSIONS

The aim of the current study is to do determine if there is a difference for heating energy demand and investment cost between the two types of roofs. Using the simulation software, the calculation for the heating energy demand of the building for each type of roof was realized.

The only difference between the two cases is the thermal transmittance for the last floor slab (lower is better).

The building envelope is described in the Table 1. The surface of each element calculated for every cardinal orientation and the material of each component layer with its thickness are presented.

Table 1. Building envelope components

	Description		Area [m²]	Layers (i-o)	
				Material	Thickness [m]
Exterior walls	N-V	Masonry walls	53.99	Lime-based plaster	0.01
	N-E		44.265	Masonry	0.25
	S-V		44.31	Mineral wool	0.15
	S-E		52.185	Lime-based plaster	0.005
Ground floor slab	-	Reinforced concrete slab	117.38	Floor tiles	0.01
				Cement mortar	0.05
				Polystyrene	0.05
				Reinforced concrete	0.1
				Polystyrene	0.1
Exterior w/d	N-V	PVC windows/doors with 3 glass layers and gas	11.46	PVC and glass	-
	N-E		17.06		
	S-V		21.14		
	S-E		9.14		
Last floor slab flat roof	-	Reinforced concrete slab	118.66	Lime-based plaster	0.01
				Reinforced concrete	0.13
				Polystyrene	0.2
				Slope polystyrene	0.03-0.20
				Gravel	0.08
Last floor slab pitched roof	-	Reinforced concrete slab	118.66	Lime-based plaster	0.01
				Reinforced concrete	0.13
				Polystyrene	0.2

To make the calculation of the energy required for heating the house, the thermal conductivity of envelope materials needs to be known. The thermal conductivity of component materials is presented in the Table 2.

Table 2. Thermal conductivity of last floor slab

	Description	Material	Thickness [m]	Thermal conductivity [W/mK]	Thermal transmittance [W/m²K]
Last floor slab flat roof	Reinforced concrete slab	Cement mortar	0.01	0.6	0.11
		Reinforced concrete	0.13	1.7	
		Polystyrene	0.2	0.029	
		Slope polystyrene	0.03-0.20	0.029	
		Gravel	0.08	0.8	
Last floor slab pitched roof	Reinforced concrete slab	Cement mortar	0.01	0.6	0.2
		Reinforced concrete	0.13	1.7	
		Polystyrene	0.2	0.029	

As we can see, the last floor slab represents 24% of the total area of building envelope. This means that it has a major effect on heating energy demand. The thermal transmittance of last floor slab for flat roof is 0.11 W/m^{2}K and for pitched roof is 0.20, so a difference of 83%. Even if between the thermal transmittances the difference is almost double, the heating energy demand in case of flat roof is 71.10 kWh/m^{2}year and in case of pitched roof is 76.04 kWh/m^{2}year (Table 3).

Table 3. Heating energy demand

Roof type	Thermal transmittance [W/m^{2}K]	Heating energy demand [kWh/m^{2}year]
Flat	0.11	71.10
Pitched	0.20	76.04

So, for heating energy demand there is only a difference of 7% between the two types of roofs. This is due to the fact that in case of pitched roof, the last floor slab is not in direct contact with the outside because between the roof itself and last floor slab a buffer zone is created. Apart from the heating energy demand, the investment costs must be considered. To highlight the difference between the roofs we will compare only the cost for the roof itself, not for the entire building. The total costs for the roofs are composed of:

- materials for roof structure;
- materials for thermal insulation;
- materials for waterproofing;
- materials for roof covering;
- labour costs.

The costs are not estimated, they are current market costs. For the flat roof, the investment cost is 12.900 euro. For the pitched roof, the investment cost is 19.130 euro. So, there is a difference between the two types of roofs of 48%. This means that the pitched roof is with 6230 euro more expensive than the flat roof.

CONCLUSIONS

A very important aspect of future sustainability is that buildings are in need to meet higher performance requirements, for reaching a positive balance between the produced and required energy (Economidou et al., 2020).

With the help of an energy simulation that we made for the building, we showed that the heating energy demand differ only for 7% between the flat roof and pitched roof.

In terms of investment costs, things are a little different. The financial analysis shows that the flat roof is more economical.

So, the flat roof has a better impact on the heating energy demand of the building and is also cheaper to be developed. But it is not all about costs, because in case of buildings roofs the architectural factor also plays an important role.

Thus, the decision to choose the type of roof is not always based on energy considerations.

REFERENCES

Abuseif, M., & Gou, Z. (2018). A review of roofing methods: Construction features, heat reduction, payback period and climatic responsiveness. *Energies, 11*(11). 3196.

Charisi, S. (2017). The role of the building envelope in achieving nearly-zero energy buildings (nZEBs). *Procedia Environmental Sciences, 38.* 115-120.

Economidou, M., Todeschi, V., Bertoldi, P., D'Agostino, D., Zangheri, P., & Castellazzi, L. (2020). Review of 50 years of EU energy efficiency policies for buildings. *Energy and Buildings, 225*. 110322.

He, Q., Ng, S. T., Hossain, M. U., & Skitmore, M. (2019). Energy-efficient window retrofit for high-rise residential buildings in different climatic zones of China. *Sustainability, 11*(22). 6473.

Kaynakli, O. (2012). A review of the economical and optimum thermal insulation thickness for building applications. *Renewable and Sustainable Energy Reviews, 16*(1). 415-425.

Loukaidou, K., Michopoulos, A., & Zachariadis, T. (2017). Nearly-zero energy buildings: Cost-optimal analysis of building envelope characteristics. *Procedia Environmental Sciences, 38*. 20-27.

Maduta, C., Giulia, M., & Paolo, B. (2022). Towards a decarbonised building stock by 2050: The meaning and the role of zero emission buildings (ZEBs) in Europe. *Energy Strategy Reviews, 44*. 101009.

Pescari, S., Stoian, V. A., Merea, M., & Pitroaca, A. (2022). Comparison Study of the Heating Energy Demand for a Multi-Storey Residential Building in Romania Using Steady-State and Dynamic Methods. *Buildings, 12*(8). 124.

Stachera, A., Stolarski, A., Owczarek, M., & Telejko, M. (2023). A Method of Multi-Criteria Assessment of the Building Energy Consumption. *Energies, 16*(1). 183.

Zhang, S., Sun, P., & Sun, E.P. (2022). Research on energy saving of small public building envelope system. *Energy Reports, 8*. 559-565.

Zhang, D., Ding, Y., Wang, Y., & Fan, L. (2022). Towards ultra-low energy consumption buildings: Implementation path strategy based on practical effects in China. *Energy for Sustainable Development, 70*. 537-548.

Scientific Papers. Series E. Land Reclamation, Earth Observation & Surveying, Environmental Engineering. Vol. XII, 2023
Print ISSN 2285-6064, CD-ROM ISSN 2285-6072, Online ISSN 2393-5138, ISSN-L 2285-6064

DIFFERENTIALS AND APPLICATIONS TO FUNCTION APPROXIMATIONS

Cosmin-Constantin NIȚU

University of Agronomic Sciences and Veterinary Medicine of Bucharest, Faculty of Land Reclamation and Environmental Engineering, 59 Marasti Blvd, District 1, Bucharest, Romania

Corresponding author email: cosmin.nitu@fifim.ro

Abstract

In mathematics, the term "differential" refers to several related notions derived from the early days of mathematical analysis, which became rigorous later, such as infinitesimal differences and the derivatives of functions. The notion is used in various areas of mathematics such as algebraic geometry, algebraic topology, calculus, differential geometry etc. The term differential is used non rigorously in calculus referring to an infinitely small ("infinitesimal") variation change in a quantity. For example, if one considers x as a variable, then a "bigger" change in the value of x is often denoted by Δx. The differential dx is an infinitesimal change of the variable x. The concept of an infinitely small or infinitely slow change is very useful, and there are several of mathematical tools to make it precise. Using calculus, it is possible to relate the infinitesimal changes of several variables to each other using function derivatives. In this article we present the notions of Gateaux and Fréchet differentials of a multivariable function with their properties, geometric interpretation and applications to function approximations.

Key words*: differential, multivariable function, function approximation.*

INTRODUCTION

The derivative of a one variable function

Definition 1. A function $f: I \to \mathbb{R}$ is derivable at a point $a \in I$ if the following limit exists:

$$\lim_{h\to 0} \frac{f(a+h)-f(a)}{h} = f'(a) \in \mathbb{R} \qquad (1)$$

In this case, we also denote $f'(a) = \frac{df}{dx}(a)$.

Remark 1. If f is derivable at the point $a \in I$ then f is continuous at a, because:

$$\lim_{h\to 0} f(a+h) - f(a) = 0$$

implies that:

$$\lim_{x\to a} f(x) = f(a).$$

Geometric interpretation of the first order derivative of a single variable real function is presentet in Figure 1.

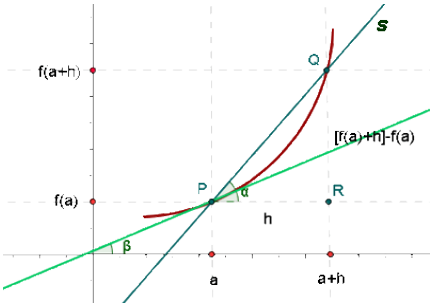

Figure 1. Geometric interpretation of the first order derivative of a single variable real function (https://www.superprof.co.uk/resources/academic/maths/calculus/derivatives/physical-interpretation-of-the-derivative.html)

The graph of f has a tangent at the point $(a, f(a))$

$$y - f(a) = f'(a)(x-a) \qquad (2)$$

Also we can define the linear application $T: \mathbb{R} \to \mathbb{R}$, $T(h) = f'(a)h$, which in a vicinity of the point a represents an approximation of the $f(a+h) - f(a)$, because:

$$\lim_{h\to 0}\frac{f(a+h)-f(a)}{h}-f'(a)=0$$

implies that:

$$\lim_{h\to 0}\frac{f(a+h)-f(a)-T(h)}{h}=0$$

Thus

$$\lim_{h\to 0} f(a+h)-f(a)-T(h)=0,$$

which implies that:

$$f(a+h)-f(a)=T(h)+o(h) \quad (3)$$

where: $o(h)$ is a function with the property

$$\lim_{h\to 0} o(h)=0$$

Remark 2

$f(a+h)-f(a)\approx T(h)$, when $h\to 0$

Remark 3. The notation $\Delta x := h$ is mainly used in practice for approximations, being asimilated with an increase of x. With this one can write:

$$f(a+\Delta x)-f(a)\approx f'(a)\Delta x, \text{ when } \Delta x\to 0 \quad (4)$$

And, even further

$$\Delta f(a)\approx f'(a)\Delta x, \text{ when } \Delta x\to 0 \quad (5)$$

which means that:

$$f(x)\approx f(a)+f'(a)(x-a), \text{ when } x\to a \quad (6)$$

MATERIALS AND METHODS

In this paper we will consider $x=(x_1,x_2,\dots,x_n)$ and $f=f(x)=f(x_1,x_2,\dots,x_n)$

Definition 2 (Colojoară, 1983; Gateux differentiation) Let $U\subset\mathbb{R}^n$ be an open set, $f: U\to\mathbb{R}$ a function and $u\in U$. We say that *f is derivable on the direction a* if the following limit exists:

$$\lim_{h\to 0}\frac{f(x+hu)-f(x)}{h}:=\frac{\partial f}{\partial u}(x) \quad (7)$$

If $u=e_i=(0,0,\dots 0,1,0\dots 0)$, where 1 lies on the *i*-th position, then we denote for simplicity

$$\frac{\partial f}{\partial x_i}:=\frac{\partial f}{\partial e_i}, \qquad i=\overline{1,n} \quad (8)$$

Definition 2. We say that $T:\mathbb{R}^n\to\mathbb{R}^m$ is a *linear application* (or a *functional, or a morphism* of $\mathbb{R}$ vectorial spaces) if it has the property:

$$T(\alpha x+\beta y)=\alpha f(x)+\beta f(y), \quad \forall x,y\in\mathbb{R}^n,\alpha,\beta\in\mathbb{R} \quad (9)$$

We denote by $L(\mathbb{R}^n,\mathbb{R}^m)$ the space of all such functionals.

Definition 3. (Nicolescu, et al., 1971; Fréchet differentiation) Let $U\subset\mathbb{R}^n$ be an open set, $f: U\to\mathbb{R}$ a function and $a\in U$. We say that *f is differentiable at the point a* if there exists a continuous functional $T\in L(\mathbb{R}^n,\mathbb{R}^m)$ such that

$$\lim_{h\to 0}\frac{f(x+ha)-f(x)-hT(a)}{h}=0 \quad (10)$$

In case of existence, we denote

$$T(a):=df(a) \quad (11)$$

Remark 4. If $T\in L(\mathbb{R}^n,\mathbb{R}^m)$, then:

$$dT(a)=T(a) \quad (12)$$

because:

$$\lim_{h\to 0}\frac{T(x+ha)-T(x)-T(a)}{h}=\lim_{h\to 0}\frac{T(x)+hT(a)-T(x)-T(a)}{h}$$

Remark 5. If *f* is differentiable then there exists $\varphi: U\to\mathbb{R}^m$ such that

$$f(x)=f(a)+T(x-a)+\|x-a\|\varphi(x), \quad \forall x\in U \quad (13)$$

and

$$\lim_{x\to a}\varphi(x)=0 \quad (14)$$

Lema 1. In the conditions from above the application *T* is uniquely determined.

Proof. We assume the existence of another linear application $T\in L(\mathbb{R}^n,\mathbb{R}^m)$ such that

$$f(x)=f(a)+T_1(x-a)+\|x-a\|\psi(x),\forall x\in U$$

where

$$\lim_{x\to a}\psi(x)=0.$$

By denoting

$$T - T_1 = T_2 \in L(\mathbb{R}^n, \mathbb{R}^m),$$

and

$$\alpha(x) = \varphi(x) - \psi(x)$$

we have

$$T_2(x-a) = \|x-a\|\alpha(x), \qquad \forall x \in U$$

where:

$$\lim_{x \to a} \alpha(x) = 0.$$

For $h \in \mathbb{R}^n$, fixed, and $t > 0$ sufficiently small, taking $x = a + th$ we get

$$T_2(th) = \|th\|\ \alpha(a+th)$$

And due to liniarity one has

$$T_2(h) = \|h\|\ \alpha(a+th)$$

Thus, for $t \to 0$ it results

$$T_2(h) = 0, \forall\ h \in \mathbb{R}^n$$

Therefore

$$T_2 = 0,$$

which shows that

$$T = T_1$$

and the unicity is proved.

Theorem 1. (Stănășilă, O. (1981), Boboc, N. (1999), the connexion between Gateaux and Fréchet differentiation) Let $f: U \to \mathbb{R}$ be a function defined on an open set $\subset \mathbb{R}^n$.

i) If f is differentiable at a point $a \in U$ then f is continuous in a. Furthermore, there exists $\frac{df}{ds}(a)$ for every versor $s \in \mathbb{R}^n$(i.e. vector with the norm equal to 1). In particular, there exist all the first order partial derivatives

$$\frac{df}{ds}(a) = df(a)(s) \tag{15}$$

and

$$\frac{\partial f}{\partial x_i}(a) = df(a)(e_i), i = \overline{1,n} \tag{16}$$

where: $E = \{e_i |\ i = \overline{1,n}\}$ is the canonic base of $\mathbb{R}^n$.

ii) If $f \in C^1(U)$ (i.e. the space of derivable functions defined on U, with all the partial derivatives continuous) then f is differentiable on U. Particularly, every elementary function is differentiable.

Proof.

i) On one hand, for any convergent sequence $(x_n) \subset U, x_n \to a$, we have

$$f(x_n) = f(a) + df(a)(x_n - a) + \|x_n - a\|\varphi(x_n), \forall n \in \mathbb{N}$$

Therefore, if $n \to \infty$, it results

$$f(x_n) \to f(a).$$

Thus, f is continuous in a.

On the other hand, choosing $r > 0$ with the property that $B(a,r) \subset U$, then for any $t \neq 0, |t| < r$, one has $d(a+ts, a) < r$, so

$$a + ts \in U,\ \forall\ k = \overline{1,n}.$$

Furthermore

$$\frac{f(a+ts) - f(a)}{t} = \frac{df(a)(ts) + \|ts\|\varphi(a+ts)}{t} = df(a)(s) + \frac{|t|}{t}\varphi(a+ts)$$

Thus,

$$\lim_{t \to 0} \frac{f(a+ts) - f(a)}{t} = df(a)(s)$$

which means that

$$\frac{df}{ds}(a) = df(a)(s), \qquad for\ s = e_i, \quad i = \overline{1,n}$$

As a result:

$$\frac{\partial f}{\partial x_i}(a) = df(a)(e_i), i = \overline{1,n}$$

ii) One has

$$\begin{aligned} f(x) - f(a) = {} & [f(x_1, x_2, \dots, x_n) - f(a_1, x_2, x_3, \dots, x_n)] \\ & + [f(a_1, x_2, x_3, \dots, x_n) - f(a_1, a_2, x_3, \dots, x_n)] + \cdots \\ & + [f(a_1, a_2, \dots a_{n-1}, x_n) - f(a_1, a_2, a_3, \dots, a_n)] \\ = {} & (x_1 - a_1)\frac{\partial f}{\partial x_1}(\xi_1, x_2, x_3, \dots, x_n) \\ & + (x_2 - a_2)\frac{\partial f}{\partial x_2}(x_1, \xi_2, x_3, \dots, x_n) \\ & + \cdots \\ & + (x_n - a_n)\frac{\partial f}{\partial x_n}(x_1, x_2, x_3, \dots, \xi_n) \end{aligned}$$

(we applied Lagrange's theorem for finite increases for each term, finding ξ_i between a_i and $x_i, i = \overline{1,n}$).

Now, we define the liniar application

$$T: \mathbb{R}^n \to \mathbb{R},$$

$$T(x) = \sum_{i=1}^{n} \frac{\partial f}{\partial x_i}(a) x_i$$

From here

$$T(x-a) = \sum_{i=1}^{n} \frac{\partial f}{\partial x_i}(a)(x_i - a)$$

thus,

$$\lim_{x\to a}\frac{f(x)-f(a)-T(x-a)}{\|x-a\|}$$
$$=\lim_{x\to a}\frac{(x_1-a_1)\left[\frac{\partial f}{\partial x_1}(\xi_1,x_2,x_3,\dots,x_n)-\frac{\partial f}{\partial x_1}(a)\right]}{\|x-a\|}$$
$$+\lim_{x\to a}\frac{(x_2-a_2)\left[\frac{\partial f}{\partial x_2}(a_1,\xi_2,x_3,\dots,x_n)-\frac{\partial f}{\partial x_2}(a)\right]}{\|x-a\|}+\cdots$$
$$+\lim_{x\to a}\frac{(x_n-a_n)\left[\frac{\partial f}{\partial x_n}(a_1,x_2,x_3,\dots,a_{n-1},\xi_n)-\frac{\partial f}{\partial x_n}(a)\right]}{\|x-a\|}$$

Every limit from above is equal to 0, as the quotients

$$\left|\frac{x_i-a_i}{\|x-a\|}\right|\le 1,\qquad i=\overline{1,n}$$

and because $f\in C^1$, its partial derivatives are continuous and the straight brackets tend to 0, $x\to a$ (which means that $x_i\to a_i,\ ,\ i=\overline{1,n}$).
In conclusion,

$$\lim_{x\to a}\frac{f(x)-f(a)-T(x-a)}{\|x-a\|}=0$$

which shows that f is differentiable at any point $a\in U$.

Theorem 2. (The formula for computing the differential) Let $f: U\to\mathbb{R}$ be a function defined on an open set $U\subset\mathbb{R}^n$, differentiable at a point $a\in U$. Then the following formula takes place:

$$df(a)=\sum_{i=1}^{n}\frac{\partial f}{\partial x_i}(a)pr_i \qquad (17)$$

(equality of liniar applications)
Proof.
Two liniar applications are equal if and only if they coincide on the canonic base $E=\{e_i|\ i=\overline{1,n}\}$. Applying this property, the desired relation is proven from the fact that

$$pr_i(e_j)=\delta_{ij}$$

where

$$\delta_{ij}=\begin{cases}1, & if\ i=j\\ 0, & if\ i\neq j\end{cases}$$

is the Kronecker symbol.
Thus, for any $h=(h_1,h_2,\dots,h_n)\in\mathbb{R}^n$ one can write

$$df(a)(h_1,h_2,\dots,h_n)=\sum_{i=1}^{n}\frac{\partial f}{\partial x_i}(a)h_i \qquad (18)$$

We can write this relation more conveniently in the following way: we observe that the projections $pr_i:\mathbb{R}^n\to\mathbb{R}$, defined by

$$pr_i(x)=x_i$$

are liniar applications, so

$$d(pr_i)(a)=pr_i.$$

Thus

$$dx_i(a)=pr_i$$

And the desired formula can be written:

$$df(a)=\sum_{i=1}^{n}\frac{\partial f}{\partial x_i}(a)dx_i(a) \qquad (19)$$

Remark 6. The function $f:\mathbb{R}^2\to\mathbb{R}$,

$$f(x,y)=\begin{cases}\frac{x^2y}{x^6+y^2}, & if\ (x,y)\neq(0,0)\\ 0, & if\ (x,y)=(0,0)\end{cases} \qquad (20)$$

is not continuous in (0,0), because

$$\lim_{\substack{x\to0^+\\ y=x^3}}f(x,y)=\lim_{x\to0^+}\frac{1}{x}=+\infty$$

but it has partial derivatives at (0,0), as

$$\frac{\partial f}{\partial x}(0,0)=\lim_{t\to0}\frac{f(t,0)-f(0,0)}{t}=0$$

and

$$\frac{\partial f}{\partial y}(0,0)=\lim_{t\to0}\frac{f(0,t)-f(0,0)}{t}=0$$

Remark 7. In practice, one may denote the increase of the variables x_i , resp. of the function f at the point a, with Δx_i, resp. $\Delta f(a)$ and one may write:

$$\Delta f(a)\approx\sum_{i=1}^{n}\frac{\partial f}{\partial x_i}(a)\Delta x_i\ \text{, when } \Delta x_i\to0,\quad i=\overline{1,n} \qquad (21)$$

which means that

$f(x) \approx f(a) + df(a)(x-a)$, when $x \to a$ (22)

Remark 8.

$$|\Delta f(a)| \approx \left|\sum_{i=1}^{n} \frac{\partial f}{\partial x_i}(a)\Delta x_i\right|$$

and using module inequality we obtain

$$|\Delta f(a)| \leq \sum_{i=1}^{n} \left|\frac{\partial f}{\partial x_i}(a)\right| |\Delta x_i| \quad (23)$$

when $\Delta x_i \to 0$

Remark 9. The vector

$$grad_a f = \left(\frac{\partial f}{\partial x_1}(a), \frac{\partial f}{\partial x_2}(a), \dots, \frac{\partial f}{\partial x_n}(a)\right) \in \mathbb{R}^n \quad (24)$$

is called the *gradient* of f at the point a and the set

$$T_a f = \{x \in \mathbb{R}^n | \, df(a)(x) = 0\} \quad (25)$$

is called the *hyperplane tangent* at a at the hypersurface of equation

$$f(x) = f(a)$$

Geometric interpetation of the differential is presentet in Figure 2.

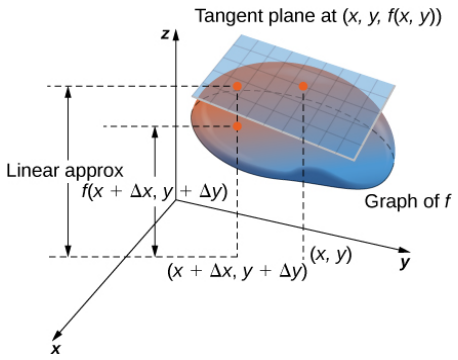

Figure 2. Geometric interpretation of the differential of multivariable function (https://math.libretexts.org/Bookshelves/Calculus/Map%3A_University_Calculus_(Hass_et_al)/13%3A_Partial_Derivatives/13.6%3A_Tangent_Planes_and_Differentials)

Exemple. $f: \mathbb{R}^3 \to \mathbb{R}, f(x,y,z) = x^3 + xyz$

The differential of f at the current point is:

$$df = \frac{\partial f}{\partial x}dx + \frac{\partial f}{\partial y}dy + \frac{\partial f}{\partial z}dz$$
$$= (3x^2 + yz)dx + xzdy + xydz$$

In particular, for every $a = (a_1, a_2, a_3)$ and $h = (h_1, h_2, h_3) \in \mathbb{R}^3$ one has

$$df(a)(h_1, h_2, h_3) = (3a_1^2 + a_2a_3)h_1 + a_1a_3h_2 + a_1a_2h_3$$

Also the increase of f is:

$$\Delta f \approx (3x^2 + yz)\Delta x + xz\Delta y + xy\Delta z$$

APPLICATIONS

For more details and applications see Martin, O. (2008), Șerban S et al., (2015) and Tudor, H. (2008).

Practical example 1: Aproximate $\cos 61^\circ$ using differentials.

Solution:

Considering the function $y = \cos x$

$$\Rightarrow dy = -sinx\, dx$$
$$\Rightarrow \Delta y \approx -sinx\, \Delta x$$
$$x = 60^\circ = \frac{\pi}{3}\, rad$$
$$\Delta x = 61^\circ - 60^\circ = 1^\circ = \frac{\pi}{180}\, rad$$
$$\cos 61^\circ = \cos 60^\circ + \Delta y \approx \frac{1}{2} - \frac{\sqrt{3}\pi}{360} \approx 0.484$$

Practical example 2: Consider a sphere with the radius R=10 m. Determine the aproximative increase of the volume, if the radius increases with $\Delta R = 1\, m$.

Solution:

$$V = \frac{4\pi R^3}{3} dV = 4 \Rightarrow \pi R^2 dR \Rightarrow \Delta V \approx 4\pi R^2 \Delta R \approx 1256\, m^3$$

Practical example 3: The radius and the height of a right-circular cylinder are measured with an error of at most 2%. Approximate the maximum percentage error in the volume.

Solution:

$$V = \pi r^2 h \Rightarrow \begin{cases} \frac{\partial V}{\partial r} = 2\pi rh \\ \frac{\partial V}{\partial h} = \pi r^2 \end{cases}$$

$$dV = \frac{\partial V}{\partial r}\, dr + \frac{\partial V}{\partial h} dh$$
$$\Rightarrow dV = 2\pi rh\, dr + \pi r^2 dh$$
$$\Rightarrow \Delta V \approx 2\pi rh\, \Delta r + \pi r^2 \Delta h$$
$$\Rightarrow \frac{\Delta V}{V} \approx 2\,\frac{\Delta r}{r} + \frac{\Delta h}{h} = 6\%$$

Practical example 4: The lengths of a rectangle are measured with an error 1%. Estimate the maximum percentage error in the area.

Solution:

$$A = L \cdot l$$
$$\Rightarrow \begin{cases} \frac{\partial A}{\partial L} = l \\ \frac{\partial A}{\partial l} = L \end{cases} \Rightarrow dA = \frac{\partial A}{\partial L} dL + \frac{\partial A}{\partial l} dl$$
$$\Rightarrow \Delta A \approx l\, \Delta L + L \Delta l$$
$$\Rightarrow \frac{\Delta A}{A} \approx \frac{\Delta L}{L} + \frac{\Delta l}{l} = 1\% + 1\% = 2\%$$

Practical example 5: The lengths of a triangle are measured with an error 1%, and the angles are measured with a precision of 2%. Estimate the maximum percentage error in the area.

Solution:

Considering a triangle MPQ the area is given by the formula: $A = \frac{mq\, sinP}{2}$

(we measure the sides $m = PQ, q = MP$ and the angle P, where P is the widest acute angle)

$$\Rightarrow \begin{cases} \frac{\partial A}{\partial m} = \frac{q\, sinP}{2} \\ \frac{\partial A}{\partial q} = \frac{m\, sinP}{2} \\ \frac{\partial A}{\partial P} = \frac{mq\, cosP}{2} \end{cases}$$
$$\Rightarrow dA = \frac{\partial A}{\partial m} dm + \frac{\partial A}{\partial q} dq + \frac{\partial A}{\partial P} dP$$
$$\Rightarrow \Delta\, A \approx \frac{\partial A}{\partial m} \Delta m + \frac{\partial A}{\partial q} \Delta q + \frac{\partial A}{\partial P} \Delta P$$
$$\Rightarrow \frac{\Delta A}{A} \approx \frac{\Delta m}{m} + \frac{\Delta q}{q} + Pctg(P)\frac{\Delta P}{P}$$
$$= 0{,}02(1 + Pctg(P)) \leq 0.04$$

Practical example 6: $\rho = \frac{m}{V}$,

$\Delta m =$ the error on the scale,

$\Delta V =$ volume′s measurement error, $\Delta \rho =$?

Solution:

The differential of ρ is:

$$d\rho = \frac{\partial \rho}{\partial m} dm + \frac{\partial \rho}{\partial V} dV$$
$$d\rho = \frac{1}{V} dm - \frac{m}{V^2} dV$$

The increase of ρ is:

$$\Delta\rho \approx \frac{1}{V} \Delta m - \frac{m}{V^2} \Delta V$$

If needed:

$$|\Delta\rho| \leq \frac{1}{V} |\Delta m| + \frac{m}{V^2} |\Delta V|$$

CONCLUSIONS

Differentials are a powerful and useful instrument to study function approximations. This technique is universal and can be applied to any formula that involves elementary mathematical functions, and for any scientific field, from pure mathematics to engineering. Differentials, in general, have wide applications in science: deduction of different formulas and equations, motion description, calculation of profit and losses in economics, differential equations and partial differential equations, mathematical modelling etc.

REFERENCES

Boboc, N. (1999). *Mathematical Analysis*, 2 volumes, pp. 260, 226. Publishing house Universitatii din Bucuresti. ISBN 973-575-285-9 (in romanian).

Colojoară, I. (1983). *Mathematical Analysis*, pp. 486. Publishing house E.D.P., Bucharest (in romanian).

Martin, O. (2008). *Differential and integral calculation in engineering*, pp. 333. Publishing house Politehnica Press, Bucharest (in romanian).

Nicolescu, M., Dinculeanu, N., Marcus, S. (1971). *Mathematical Analysis*, 2 volumes, pp. 783, 400. Publishing house E.D.P., Bucharest (in romanian).

Stănășilă, O. (1981). *Mathematical Analysis*, pp. 478. Publishing house E.D.P., Bucharest (in romanian).

Șerban S., Ijacu D., Mircea I. (2015). *Algebra and mathematical analysis. Theory and applications*. Pp. 319. Publishing house Corint, Bucharest. ISBN 9786068723327 (in romanian).

Tudor, H. (2008). *Analiză Matematică. Curs practic pentru ingineri*, pp. 219. Publishing house Albastra (in romanian).

https://www.superprof.co.uk/resources/academic/maths/calculus/derivatives/physical-interpretation-of-the-derivative.html

https://math.libretexts.org/Bookshelves/Calculus/Map%3A_University_Calculus_(Hass_et_al)/13%3A_Partial_Derivatives/13.6%3A_Tangent_Planes_and_Differentials

Scientific Papers. Series E. Land Reclamation, Earth Observation & Surveying, Environmental Engineering. Vol. XII, 2023
Print ISSN 2285-6064, CD-ROM ISSN 2285-6072, Online ISSN 2393-5138, ISSN-L 2285-6064

ASSESSING CHARACTERISTICS OF MICROBIAL COMMUNITIES IN SOILS FROM HIGH NATURAL VALUE AGRICULTURAL SYSTEMS FROM CARAS-SEVERIN COUNTY

Gabi Mirela MATEI, Sorin MATEI, Monica DUMITRASCU, Victoria MOCANU

National Research-Development Institute for Soil Science, Agrochemistry and Environment, Bucharest, 61 Marasti Blvd, District 1, Bucharest, Romania

Corresponding author email: so_matei602003@yahoo.com

Abstract

Romania owns important areas with High Natural Value (HNV) agriculture systems. The aim of the paper was to assess the biodiversity aspects of microbial communities in two soils from the areal selected for HNV payments, that belongs to the Pilot Zone II in Lupac, Caras-Severin County: P3-cultivated in conventional system with maize for forage and P4-under HNV agriculture system with forage plants, mainly leguminous, between abandoned orchard trees. Microbial counts and taxonomy of bacteria and fungi have been determined (by dilution plate method). Diversity index of Shannon and similarity index between the habitats have been calculated, as well as soil respiration potential (estimated by substrate-induced respiration method). Microbial diversity varied from 3 to 9 species. Dominant species included Pseudomonas fluorescent, Bacillus spp. and cosmopolitan genera Penicillium and Trichoderma, with role in improving the control of phytopathogens in rhizosphere and nutrients uptake by plants, aggregation of soil, cellulose decomposition and carbon sequestration. Circular paper chromatograms provided information on biological quality of studied soils.

Key words*: HNV agriculture system, biodiversity, bacteria, fungi, paper chromatograms.*

INTRODUCTION

Various agricultural practices target the reduction of CO_2 and greenhouse gases accumulation in atmosphere by increasing the sequestration of carbon in soil, thus mitigating the effects of climate change and preventing the global change (Alidoust et al., 2018).

Land-management practices including organic matter amendments proved their beneficial effect on carbon and nitrogen dynamics in grassland soils (Ryals et al., 2014), resulting in improvement of carbon sequestration, plant nutrition and preventing soil degradation. Recent studies underlined the importance of land use and agronomic practices on carbon sequestration mediated by soil microbiota and the influence of edaphic microbial diversity on preventing soil loss caused by various types of degradation (Guo et al., 2014; Lal et al., 2015; Raducu et al., 2017; Lalichetti & Sultan, 2020), as well as the beneficial role of microflora in sustaining soil fertility (Valensa et al., 2017).

Houghton & Nassikas (2017) reported that global and regional fluxes of carbon were affected by land use and land cover change. Research reports from China evidenced the beneficial effects of long-term application of manure and other fertilizers on the fractions of soil organic matter and microorganisms under a cropping system with wheat-maize rotation (Gong et al., 2009).

Results from a long-term field experiment in Sweden evidenced quantitative changes in organic carbon and the structure and taxonomy of microbial communities caused to repeated treatments with organic and N fertilizers (Katterer et al., 2014).

Soil microorganisms play an important role in organic matter cycling, regulation of gas exchange, carbon sequestration, improving plant growth by increasing nutrients availability and uptake, suppression of pathogens or by eliciting of plants immune response, all these activities contributing to soil services in ecosystem (Aislabie & Deslippe, 2013; Matei et al., 2020; Yan et al, 2021).

Studies on soils from areas with high natural value (HNV) agriculture systems underlined their importance in preservation of vegetal and microbial biodiversity, because they are the source of valuable species which intervene in

the main processes influencing ecosystem dynamics (Matei et al., 2018; Dumitrascu et al., 2020).
This paper presents the results of research in order to evaluate the biodiversity aspects of microbial communities in two soils from a selected areal, eligible for HNV payments, that belongs to Pilot Zone II, Caras-Severin County from South-West region of Romania.

MATERIALS AND METHODS

Soils have been collected from a selected areal belonging to Pilot Zone II, in Caraş-Severin County, eligible for HNV payments.
P3-Lupac (Clocotici) (arable in conventional system)
Profile no. 3 is situated nearby village Clocotici and the road towards locality Lupac, (Longitude: 21.823421°E, Latitude: 45.244880°N), at 232 m altitude, slope 10%, on an arable terrain, cultivated in conventional system.
Culture sowed is maize for forage. It belongs to a landscape of mosaic type, characteristic for the type 2 of HNV terrain. The terrain was fertilized with manure (Figure 1).
Soil Type: Endostagnic Luvisol (WRB, 2014).
Soil presented medium texture; loose in surface layer; medium permeability; acid reaction in surface (pH - 4.95), oligomesobasic; medium humus content (4.59%), medium organic matter reserve in the first 50 cm (132 t/ha); medium nitrogen content (Nt - 0.238%), low and very low available phosphorus and potassium contents P_{AL} - 5 mg x kg^{-1} and K_{AL} - 180 mg x kg^{-1}.

Figure 1. Soil profile P3 in arable (conventional system) - Lupac (Clocotici)

P 4 - Lupac (Clocotici) (abandoned orchard, in HNV system) Soil profile no. 4 is located at 50 m distance from Profile no. 3 nearby village Clocotici and on the left side of road towards locality Lupac (Longitude: 21.824058°E, Latitude: 45. 244671°N), at 234 m altitude.
The terrain is covered with natural and semi-natural vegetation, in mosaic, characteristic to the type 2 of HNV terrain. The vegetal cover between species of trees from abandoned orchard (plum and cherry) consists in forage plants, the majority belonging to leguminous plants (Figure 2). Fibrous roots of plants are present in surface soil layer (0–20 cm).
Soil Type: Endostagnic Luvisol (WRB, 2014).
Soil presented medium texture; loose in surface layer; medium permeability; moderate acid reaction (pH - 5.61), mesobasic; medium humus content (3.63%), medium organic matter reserve in the first 50 cm (160 t/ha); medium nitrogen content (Nt - 0.343%), very low and low available phosphorus and potassium contents P_{AL} - 7 mg x kg^{-1} and K_{AL} - 262 mg x kg^{-1}.

Figure 2. Soil profile P4 in abandoned orchard (HNV system) - Lupac (Clocotici)

Surface samples (0-20 cm) from soils under conventional (P3) and HNV (P4) agriculture systems have been analysed using microbial indicators of biodiversity and microbiological activity of bacterial and fungal communities, as well as image forming methods for evidencing the specific aspects concerning the biological quality.
Microbiological analysis was performed according to soil serial dilution method. Specific culture media have been utilised: Nutrient Agar (NA) purchased by Difco, USA for bacteria and potato - dextrose agar (PDA) purchased by Merck, Germany. Colonies developed after 7 days incubation were counted and results expressed as Total Number of Bacteria - TNB and Total Number of Fungi reported to 1gram of dry soil (Dumitru & Manea, 2011). Taxonomy study utilised the morphologic criteria by optical microscope

(MC 5. A) examination and measurements according to determinative manuals: Bergey & Holt (1994) for bacteria and Domsch & Gams (1970) and Watanabe (2002) for fungi. In order to evaluate microbial diversity of bacterial and fungal communities, total number of species (S), Relative abundance (A%), Species richness (SR_2 index) and Diversity index of Shannon (H') have been utilised for soils under conventional and HNV agriculture systems (Mohan & Ardelean, 1993). According to Morris et al. (2014), a high value of H' index is registered when the number of species is high and have a high homogeneity. The homogeneity (evenness) or equitability (ε) was calculated according to Stugren (1982) and Similarity index (SI%) between the lists of species from the two soils (according to Tiwari et al., 1994).

The global physiological activities of edaphic communities were determined by substrate induced respiration method (SIR) and expressed as mg CO_2 x 100 g^{-1} soil (Matei, 2011).

Soil biological quality was assessed by interpreting the characteristics of images of circular chromatograms obtained as a result of migration of soil extracts on filter paper previously impregnated with developing substance, accordingly to procedure recommended by Pfeiffer (1984).

All data are the mean of three replicates. The results were interpreted by one-way analysis of variance (ANOVA) and the value $p<0.05$ was considered statistically significant (Student test).

RESULTS AND DISCUSSIONS

Analysis of results revealed significant differences between the microbial characteristics of soils from areas under arable (conventional) and forage plants in abandoned orchard (HNV) agriculture systems concerning both total counts of bacteria, fungi and global physiological activities (Table 1).

P3- Soil from P3 Lupac, in conventional system of agriculture presented moderate to low total counts of heterotrophic bacteria (11.892 x 10^6 viable cells x g^{-1} dry soil), a high number of fungi (148.914 x 10^3 cfu x g^{-1} dry soil) and, as a consequence, a more intense global activity of microbial community (39.436 mg CO_2 x 100 g^{-1} soil, value considered to characterize a moderate potential of soil respiration) as compared to microflora from P4.

Table 1. Total counts and global physiological activity of soil bacterial and fungal communities in HNV and conventional agriculture systems

Soil profile location and land use	TNB (x 10^6 viable cells x g^{-1} d. s.)	TNF (x 10^3 cfu x g^{-1} d. s.)	Soil respiration (mg CO_2 x 100 g^{-1} soil)
LUPAC P3 (Conventional)	11.892a[1]	148.914a	39.436a
LUPAC P4 (HNV)	5.905b	46.316b	24.785b

[1]The values in a column followed by the same letter are not significantly different for P<0.05 (Student test)

Fungal microflora (Figure 3) presented the highest diversity (9 species), characterized by the dominance of antagonists *Trichoderma viride* and *Penicillium chrysogenum*, able to control, in conditions from this soil, the development of some potential phytopathogens represented by species of genera *Fusarium* and *Pythium*.

These species were accompanied by accessory or accidental species (less abundant in community from genera *Penicillium, Paecilomyces, Mucor*) well-known for their diverse enzyme equipment (cellulase, pectinase, chitinase), very efficient in degradation of various materials of vegetal origin.

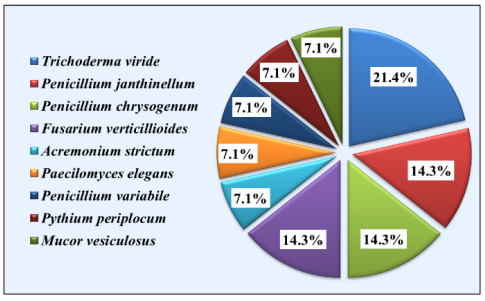

Figure 3. Relative abundance of fungal species in soil from P3 under arable (in conventional system)

The population of heterotrophic bacteria was dominated by fluorescent and non-fluorescent representatives of genus *Pseudomonas* and various bacillaceae, both with role in suppressing pathogens and carbon sequestration in stable forms (humus) (Figure 4).

P4 - Soil from P4 Lupac (HNV system) situated in abandoned orchard was populated with low numbers of heterotrophic bacteria (5.905 x10^6 viable cells x g^{-1} dry soil) and fungi (46.316 x 10^3 cfu x g^{-1} dry soil), low values being also registered for the level of global physiological activities of microbiota (24.785 mg CO_2 x 100 g^{-1} soil).

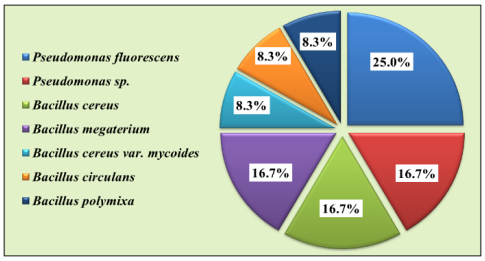

Figure 4. Relative abundance of bacterial species in soil from P3 under arable (in conventional system)

Species diversity of fungal microflora from this soil was low (only 3 species identified). Dominant species was potential phytopathogen from genus *Fusarium* (*F. culmorum* var. *roseum*), its development being stimulated by supplementary nitrogen fixed from atmosphere by leguminous plants between the rows of trees, accompanied by representatives of two cosmopolitan, cellulolytic genera (*Penicillium* and *Aspergillus* (Figure 5).

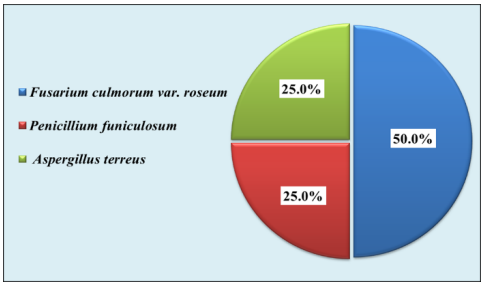

Figure 5. Relative abundance of fungal species in soil from P4 under arable (in conventional system)

The community of heterotrophic bacteria from P4 (Figure 6) consisted of 8 species as compared with 7 species in the case of nearby soil from P3, representatives of genus *Arthrobacter* accompanying the bacilli and pseudomonads (fluorescent, non-fluorescent).
Other results in literature (Attitalla et al., 2001; Weller et al., 2002) attribute the soil suppressiveness to the presence of a population of fluorescent bacteria from genus *Pseudomonas*, able to control the development of phytopathogens (species from genus *Fusarium*). According to results of Ahmed & Holstrom (2014), the suppressiveness is also influenced by the siderophores, exometabolites released by various microbial species in the soil (e. g. pseudomonads, bacilli, fungi from genera *Trichoderma*, *Penicillium*, *Aspergillus*, *Paecilomyces*), that inhibit the proliferation of phytopathogenic bacteria and fungi, species also found in both Endostagnic Luvisols from Lupac (Clocotici).

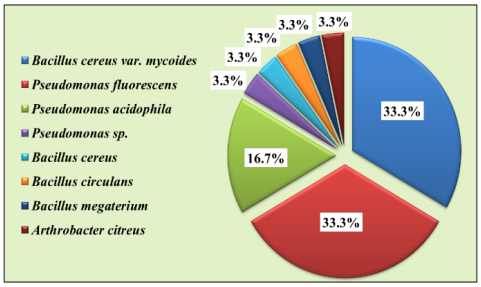

Figure 6. Relative abundance of bacterial microflora in soil from P4 under abandoned orchard (HNV system)

Present data evidencing the beneficial microorganisms from both bacterial and fungal populations with role in biocontrol of pathogens, organic matter recycling and humification are in concordance with previous results on edaphic microflora from HNV agriculture systems in Suceava county, North-East Romania (Matei et al., 2022) and South-Eastern Transylvania (Dumitrascu et al., 2019).
Comparative analysis of lists with taxonomic composition of bacterial communities showed that 80% of species were common (present in both soils) and two species were unique, *Bacillus polymixa* only for P3 (conventional) and *Arthrobacter citreus* only for P4 (HNV).
Each soil owns a specific taxonomic composition and structure of fungal community and there are no common species (SI = 0).
Authors of a study in grassland soils reported that composition and structure of microbial communities from rhizosphere were influenced by soil type and grass plant species (Singh et al., 2007).
On the other hand, the interactions between plants, microorganisms and soil were

considered by Reynolds et al. (2003) as drivers of the structure and dynamics of grass plants community.

The values of all diversity indices calculated for bacterial and fungal communities from Endostagnic Luvisols from Lupac (Clocotici) under arable and abandoned orchard are presented in Table 2.

According to the value of biodiversity index (S), microbial communities in studied soils consisted in minimum 3 and maximum 9 species. An increased value of diversity index of Shannon was found for bacterial community in soil from P3, under maize for forage cultivated in conventional system and fertilized with manure (H' = 1.864 bits and evenness ε = 0.737), higher than those from P4 (with H' = 1.598 bits and lower evenness value ε = 0.558). The highest diversity of fungi was also found in soil from P3 conventional system (H' = 2.107 bits and the highest evenness ε = 0.756).

Accordingly, other research presented the use of manure and compost as a practice for restoring the functions of most soils, particularly those with low levels of organic matter and poor structure by improving the soil microbial activity, nutritional status and physical characteristics (Tavali, 2021).

Table 2. Taxonomic composition and biodiversity indices of microbial communities in soils under conventional and HNV agriculture systems from Lupac (Clocotici)

Soil profile location and land use	**Fungal species**	**Bacterial species**
Lupac (Clocotici) P3 Arable (Conventional)	*Trichoderma viride* *Penicillium janthinellum* *Penicillium chrysogenum* *Fusarium verticillioides* *Acremonium strictum* *Paecilomyces elegans* *Penicillium variable* *Pythium periplocum* *Mucor vesiculosus*	*Pseudomonas fluorescens* *Pseudomonas* sp. *Bacillus cereus* *Bacillus megaterium* *Bacillus cereus* var. *mycoides* *Bacillus circulans* *Bacillus polymixa*
	S = 9; SR_2 = 0.642 Shannon H' = 2.107; ε = 0.756 Hmax = 2.197; H1' = 1.662 var(H') = 0.069	S = 7; SR_2 = 0.583 Shannon H' = 1.864; ε = 0.737 Hmax = 1.946; H1' = 1.435 var(H') = 0.084
Lupac (Clocotici) P4 Abandoned orchard (HNV)	*Fusarium culmorumm* var. *roseum* *Penicillium funiculosum* *Aspergillus terreus*	*Bacillus cereus* var. *mycoides* *Pseudomonas fluorescens* *Pseudomonas acidophila* *Pseudomonas* sp. *Bacillus cereus* *Bacillus circulans* *Bacillus megaterium* *Arthrobacter citreus*
	S = 3; SR_2 = 0.750 Shannon H' = 1.040; ε = 0.643 Hmax = 1.099; H1' = 0.706 var(H') = 0.737	S = 8; SR_2 = 1.333 Shannon H'=1.598; ε = 0.558 Hmax = 2.079; H1' = 1.160 var(H') = 0.144
	Similarity index SI = 0	Similarity index SI = 80%

Circular paper chromatograms provided information on biological quality of the soils, by image analysis concerning the general aspect and harmony, color, shape and size, useful for evaluation of vitality, fertility, the complexity of organic matter, the stable humus or the intensity of biologic activity in soils (Figure 7).

There are no evidences of unfavorable soil conditions for plant growth.

Generally, the chromatograms of the two soils reveal some problems of integration of mineral compounds, low mineral diversity, abiotic conditions preponderant, relatively weak conditions for organic aggregation and floculation.

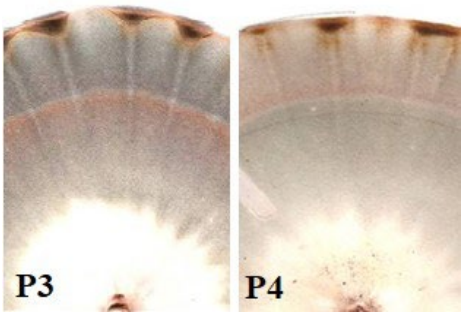

Figure 7. Sections of circular chromatograms of soils under arable (P3) and abandoned orchard (P4) from Lupac (Clocotici)

The aspect, color and radius of internal zone of both chromatograms are characteristic for increased contents in non-accessible minerals.
Low accessibility of mineral contents is more evident on chromatogram from P4 but a higher accessibility is evidenced on chromatogram from P3.
Analysis of external zone of chromatograms reveals a weak enzymatic activity. Yet, the level of enzymatic activity is higher in P3 soil than in P4.
Functional diversity is better evidenced in chromatogram from P3 as compared to P4, where a weaker microbial activity and a lower functional diversity is evidenced in image of external zone, in concordance with the values presented in Tables 1 and 2.
Studies on image forming methods sustain the use of circular chromatograms for rapid characterization of quality, applicable to various soil types and land management (More et al., 2014). Our results on microbial diversity and quality of soils from HNV areas are similar to studies from literature (Gomez et al., 200; Fritz et al., 2011) and underline the influence of land use on soil organic status that in turn, induces modifications of density and genetic structure of microbial communities (Lejon et al., 2007), as well as the role of soil heterotrophic respiration patterns in terrestrial ecosystems for global carbon dynamics (Tang et al., 2020; Matei et al., 2023).
Present research findings are in concordance with results confirming that land use shapes the resistance of soil microbiota and the carbon cycling response to global warming, contributing to preventing the effects of climate changes (Moreno et al., 2019).

CONCLUSIONS

Soil from P3 cultivated with maize for forage in conventional system presented significantly higher values of total counts of both bacteria, fungi and CO_2 released by global physiological activities as compared with P4 (HNV) from abandoned orchard.
Biodiversity index (S) of microbial communities in studied soils consisted in minimum 3 and maximum 9 species.
Bacterial community from soil cultivated with maize for forage in conventional system presented the highest value of diversity index (H' = 1.864 bits and evenness $\varepsilon = 0.737$).
Biodiversity of fungal community was higher in soil from conventional system P3 (H' = 2.107 bits and the highest evenness $\varepsilon = 0.756$).
Dominance of fluorescent pseudomonads, bacilli and fungi from cosmopolitan genera *Penicillium* and *Trichoderma* presented importance in improving nutrients availability, uptake and the control of pathogens in plants rhizosphere, soil aggregation, cellulose decomposition and carbon sequestration processes.
Circular paper chromatograms provided useful evidences on biological quality of soils.
Areas with HNV agriculture practices contribute to protection and preservation of microbial diversity in soils, sustaining its important functions and services for ecosystem.

ACKNOWLEDGEMENTS

This work was supported by two grants of the Romanian Ministry of Research, Innovation and Digitization, Project number PN 23 29 03 01/2023 and Project number 44PFE/2021, Program 1 – Development of national research-developing system, Subprogramme 1.2 - Institutional performance - RDI Excellence Financing Projects.

REFERENCES

Ahmed, E., & Holmström, S.J.M. (2014). Siderophores in environmental research: roles and applications, *Microbial Biotechnolgy, 7*(3). 196–208.

Aislabie, J., & Deslippe, J. (2013). Soil microbes and their contribution to soil services. In: Dymond JR (Ed.), *Ecosystem services in New Zeeland–conditions and trends*. Lincoln, New Zeeland: Manaaki Whenua Press.

Alidoust, E., Afyuni, M., Hajabbasi, M.A., & Mosaddeghi, M.R. (2018). Soil carbon sequestration potential as affected by soil physical and climatic factors under different land uses in a semiarid region. *Catena, 171*, 62–71.

Attitalla I., Johanson, P.M., Brishammar, S., & Gerhardsson, B. (2001). *Pseudomonas* sp., strain MF30 suppresses fusarium wilt of tomato in vivo. *Phytopathologia Mediterranea, 40*, 234–239.

Bergey, D.H., & Holt, J.G. (1994). *Bergey's manual of determinative bacteriology* 9, vol.2. Baltimore, US: Williams & Wilkins (Eds.).

Domsch, K.H., & Gams, W. (1970). *Fungi in agricultural soils*, Edinburg, London, GB: T&A Constable Ltd. Publishing House.

Dumitrascu, M., Anghel, V.A., Matei, S., Sirbu, C.E., & Cioroianu, T.M. (2020). Agriculture with high natural value in Romania; soil quality and socio-economic impact in the context of crisis. *Annals of the University of Craiova Series Environmental Engineering, XXV(LXI*), 352–357.

Dumitrascu, M., Lungu, M., Stefănescu, S.L., Mocanu, V., Matei, G.M., & Lazar, R. (2019). Soil fertility assessment of an high natural value eligible area in South-Eastern Transylvania. *Journal of Present and Sustainable Development, 13*(1), 57–67.

Dumitru, M. & Manea, A.(coord.). (2011). *Methods of chemical and microbiological analysis (utilized in monitoring system)*, (in Romanian) (pp. 271–283). Craiova, RO: SITECH Publishing House.

Fritz, J., Athmann, M., Kautz, T., & Köpke, U. (2011). Grouping and classification of wheat from organic and conventional production systems by combining three image forming methods, *Biological Agriculture & Horticulture, 27(*3-4), 320–336.

Gomez, E., Ferreras, L., & Toresani, S. (2006). Soil bacterial functional diversity as influenced by organic amendment application. *Bioresources Technology, 97*, 1484–1489.

Gong, W., Yan, X., Wang, J., Hu, T., & Gong, Y. (2009). Long-term manure and fertilizer effects on soil organic matter fractions and microbes under a wheat-maize cropping system in northern China. *Geoderma, 149*, 318–324.

Guo, L.J., Zhang, Z.S., Wang, D.D., Fang, C.L., & Cao, C.G. (2014). Effects of short-term conservation management practices on soil organic carbon fractions and microbial community composition under a rice-wheat rotation system. *Biology and Fertility of Soils, 51*(1), 65–75.

Houghton, R.A. & Nassikas, A.A. (2017). Global and regional fluxes of carbon from land use and land cover change. 1850–2015. *Global Biogeochemistry Cycles, 31*(3), 456–472.

Kätterer, T., Börjesson, G., & Kirchmann, H. (2014). Changes in organic carbon in topsoil and subsoil and microbial community composition caused by repeated additions of organic amendments and N fertilisation in a long-term field experiment in Sweden. *Agriculture, Ecosystems and Environment, 189*, 110–118.

Lal, R. (2015). Restoring soil quality to mitigate soil degradation. *Sustainability, 7*, 5875– 5895.

Lalichetti, S. & Sultan, S. (2020). Impact of agronomic practices on soil organic carbon dynamics: A review. International *Journal of Chemical Studies, 8*(4), 2173–2178.

Lejon, D.P., Sebastia, J., Lamy, I., Chaussod, R., & Ranjard, L. (2007). Relationships between soil organic status and microbial community density and genetic structure in two agricultural soils submitted to various types of organic management. *Microbial Ecology, 53*, 650–663.

Matei, G.M., Matei, S., & Dumitrascu, M. (2022). Microbial diversity in soils from high natural value agricultural systems with pastures and natural meadow in Suceava county. *Scientific papers, Series E. Land Reclamation, Earth Observation & Surveying, Environmental Engineering, XI*, 210–217.

Matei, G.M., Matei, S., & Mocanu, V. (2020). Assessing the role of soil microbial communities of natural forest ecosystem. *The EuroBiotech Journal, 4*(1), 1–7.

Matei, S. (2011). Determination of soil respiration and microbial biomass. In: Dumitru, M. & Manea, A.(coord.). *Methods of chemical and microbiological analysis (utilized in soil monitoring system*), (in Romanian) (pp. 283–288). Craiova, RO: SITECH Publishing House.

Matei, S., Matei, G.M., & Dumitrascu, M. (2018). Soils from HNV Agriculture Systems as Source of Microorganisms with Antifungal Activity. *The EuroBiotech Journal, 2*(4), 196–199.

Matei, S., Matei, G.M., Dumitru, S., & Mocanu, V. (2023). Soil respiration as microbial response to the endogen input of bio-synhesized organic matter and its implication in C sequestration. *Carpathian Journal of Earth and Environmental Sciences, 18*(1), 51–64.

Mohan, G. & Ardelean, I. (1993). *Ecology and environment protection* (in Romanian). Bucharest, RO: Scaiul Publishing House.

More, S., Khan, M.A., & Agrawal, P. (2014). Soil nutrient detection through image processing in chromatogram image. *International Journal of Pure and Applied Research in Engineering and Technology, 2*(8), 360–364.

Moreno, J.L., Torres, I.F., Garcia, C., Lopez-Mondejar, R., & Bastida, F. (2019). Land use shapes the resistance of the soil microbial community and the C cycling response to drought in a semi-arid area. *Science of the Total Environment, 648*, 1018–1030.

Morris, E.K., Caruso, T., Buscot, F., Fischer, M., Hancock, C., Maier, T.S., Meiners, T., Müller, C., Obermaier, E., Prati, D., Socher, S.A., Sonnemann, I., Wäschke, N., Wubet, T., Wurst, S., & Rillig, M.C. (2014). Choosing and using diversity indices: insights for ecological applications from the German Biodiversity exploratories. *Ecology and Evolution, 4*(18), 3514–3524.

Pfeiffer, E. (1984). *Chromatography applied to quality testing*. Bio-dynamic literature, Wyoming, USA.

Raducu, D., Lazar, R., Dumitrascu, M., Manea, A., & Eftene, A. (2017). An agricultural soil between tillage and pasture. *Proceedings of Geography Workshop Dimitrie Cantemir, 45*, 221–227.

Reynolds, H.L., Packer, A., Bever, J.D., & Clay, K. (2003). Grassroots ecology: plant-microbe-soil interactions as drivers of plant community structure and dynamics. *Ecology, 84*, 2281–2291.

Ryals, R., Kaiser, M., Torn, M.S., Berhe, A.A., & Silver, W.L. (2014). Impacts of organic matter amendments on carbon and nitrogen dynamics in grassland soils. *Soil Biology and Biochemistry, 68*, 52–61.

Singh, B.K., Munro, S., Potts, J.M., & Millard, P. (2007). Influence of grass species and soil type on rhizosphere microbial community structure in grassland soils. *Applied Soil Ecology, 36*, 147–155.

Stugren, B. (1982). *Bases of general ecology* (in Romanian). Bucharest, RO: Scientific and Encyclopedic Publishing House.

Tang, X., Fan, S., Du, M., Zhang, W., Gao, S., Liu, S., Chen, G., Yu, Z. & Yang, W. (2020). Spatial and temporal patterns of global soil heterotrophic respiration in terrestrial ecosystems. *Earth System Science Data, 12*(2), 1037–1051.

Tavali, I.E. (2021). Short-term effect of compost amendment on the fertility of calcareous soil and basil growth. *Communications in Soil Science and Plant Analysis, 52*, 172–182.

Tiwari, S.C., Tiwari, B.K., & Mishra, R.R. (1994) Succession of microfungi associated with the decomposing litters of pineapple (Ananas comosus). *Pedobiologia, 38*, 185–192.

Valenca, A.W., Vanek, S.J., Meza, K., Canto, R., Oliveira, E., Scurrah, M., Lantinga, E.A., & Fonte, S. J. (2017). Land use as driver of soil fertility and biodiversity across an agricultural landscape in the Central Peruvian Andes. *Ecological Application, 27*(4), 1138–1154.

Watanabe, T. (2002). *Pictorial Atlas of Soil and Seed Fungi: Morphologies of Cultured Fungi and Key to Species* 2nd ed. London, New York, Washington D.C., USA: CRC PRESS, Boca Raton Publishing House.

Weller, D.M., Raaijmakers, J.M., McSpadden Gardener, B.B., & Thomashow, L.S. (2002). Microbial populations responsible for specific soil suppressiveness to plant pathogens. *Annual Review of Phytopathology, 40*, 309–348.

World reference base for soil resources - WRB (2014). International soil classification system for naming soils and creating legends for soil maps. Update 2015. Rome, Italy: Food and Agriculture Organization of the United Nations.

Yan, Y.R., Mao, Q., Wang, Y.Q., Zhao, J.J., Fu, Y.L., Yang, Z.K., Peng, X.H., Zhang, M.K., Bai, B., Liu, A.R., Chen, H.L. & Golam, J.A. (2021). *Trichoderma harzianum* induces resistance to root-knot nematodes by increasing secondary metabolite synthesis and defense-related enzyme activity in *Solanum lycopersicum* L. *Biological Control, 158*. 104609. Retrieved February 28, 2021 from https://www.sciencedirect.com/science/article/pii/S1049964421000797.

ISSN 2285 – 6064
ISSN-L 2285 – 6064